Wind –induced Pressure Quantification on Gable Roof Flush-Mounted Solar Panels Systems

By

Haisam Yakoub

Thesis submitted in partial
fulfilment of the requirements for the
Doctorate in Philosophy degree in
Civil Engineering

Department of Civil Engineering
Faculty of Engineering
University of Ottawa



uOttawa

© Haisam Yakoub, Ottawa, Canada, 2019

Abstract

Photovoltaic (PV) solar panels are solar energy collection systems with increasing terrestrial and roof applications reported worldwide. If the terrestrial mounting does not require specific wind resistance verifications, installing them on top of flat and gable roofs implies a drastic change of the roofing systems geometry, thus a re-evaluation of the wind-induced pressure is necessary. Among the roof top applications, provisions exist for the flat roofs mounted solar panels, however, design recommendations for wind-induced loadings on PV solar panels arrays flush-mounted on gable roofs are not fully developed in current wind loading standards (SEAOC PV2-2012) and building codes (ASCE 07, NBCC 2015), in spite of the numerous applications on residential and agricultural buildings, primarily due to the limited research investigating this topic.

The current dissertation employs CFD k-ε and LE (Large Eddy) simulations for analyzing the effects of wind acting on solar panels flush-mounted on gable roofs, considering the influence of several parameters such as: the slope of the gable roof, the wind directions, the spaces between the adjacent solar panel arrays and the clearance between the roof surface and the solar panels. A comprehensive database of solar panels with different installation parameters subjected to wind speeds were developed under the current research project. The database includes detailed distribution of wind-induced pressure coefficients for the three parallel surfaces constituting the roof-solar panels systems: the top and bottom surfaces of the panels, and the roof surface under the panels, which represents a novel approach in investigating and clarifying the wind effects on solar panels. This approach also provides in detail the variation of the pressure coefficients on the three surfaces, due to the change of installation conditions (roof slope, arrays spacing, roof clearance) and wind parameters (wind speed and wind direction).

As an original contribution to the existing knowledge, this thesis found that the installation of solar arrays on gable roofs, redistributes the wind-induced pressure on both sides of the roof windward and leeward, resulting in total horizontal wind-induced pressures on the entire roof lower than that registered on the corresponding roof without solar panels. In addition, dominant resultant pressure coefficients on solar panels concluded

to be lower than for the roof without panels. When the roof clearance increases, total average pressure coefficients on the roof supporting the panels decreases on both, windward and leeward sides of the roof. Moreover, when the roof clearance increases, the pressures in the cavity decrease significantly on both windward and leeward sides of the roof, which could impact the requirements for installing and fixing such panels on gable roofs. For example, for 10" clearance the flush-mounted solar panels were subject to pressure instead of suction. Similarly, when panel array spacing increases, the magnitude of the net mean pressure coefficients on the roof surface under the solar panels further decreases for all wind directions investigated.

Dedication

To my parents, beloved wife and wonderful children.

Acknowledgement

My genuine appreciation and greatest thankfulness are due to my research supervisors Dr. Elena Dragomirescu. and Dr. Ghasan Doudak, their deep knowledge, continuous encouragement, inspiring ideas and keen supervision extremely helped me achieve this work.

I would like to express my sincere love and warmest gratitude to my beloved wife, Rima, for her love and never-ending support she gave me throughout all these years, which were not always so easy.

Finally, my love is always due to my wonderful children, Grace, Larissa and Elias.

TABLE OF CONTENT

ABSTRACT …….II
DEDICATION ……..……..IV
ACKNOWLEDGEMENT……..….....V
TABLE OF CONTENT……...VI
LIST OF FIGURES……XVIII
LIST OF TABLES……...XXXIV

Contents

CHAPTER 1: Introduction 1
1.1 Wind effects on roofs and PV solar panels 1
1.2 Installation methods for PV solar panels..... 4
1.3. Research motivation..... 6
1.4. Research objectives and scope 7
1.5. Research methodology 9
CHAPTER 2 Literature review 10
2.1. Mean wind speed profiles logarithmic and power laws..... 10
2.2. Turbulence intensity..... 11
2.3. Code development for wind load effect on roofs..... 11
2.3.1. Pressure coefficient..... 12
2.4. Wind effects on solar panels..... 13
2.4.1. CFD and wind tunnel studies for gable roof mounted solar panels..... 13
2.4.2. CFD and wind tunnel studies for flat roof mounted solar panels 18
2.4.3. CFD and wind tunnel studies for ground roof mounted solar panels 23
2.5. Pressure equalization phenomenon..... 29
2.5. Conclusions..... 31
CHAPTER 3: CFD Modeling and simulations 32
3.1. CFD Modeling validation..... 33

3.1.1. Mesh details and model's geometry validation 33
3.1.2. Boundary conditions and mesh details for building model and building model with solar panels 36
3.1.3. Mesh sensitivity analysis 40
3.1.4. Validation case 1: Canopy structure, modeled using les algorithms 43
3.1.5. Validation case 2: Residential building modeled using k-ε algorithm 47
3.1.6. Validation case 3: Residential building using les algorithm 51
3.1.7. Validation case 4: CFD model validation for gable roofs 56
a) Bare gable roof (45º) and ratio of height to depth h/d =1 56
b) Bare gable roof (45º), ratio height to depth h/d =0.40 59
c) Bare gable roof (30º), ratio height to depth h/d = 1 62
d) Bare roof (30º) and ratio of height to depth h/d =0.4 65
3.1.8. Wind effects on singular solar panels mounted on open versus enclosed /solid bases 68
3.2. CONCLUSIONS 80

CHAPTER 4 82
Wind-induced pressure on gable roof mounted solar panels: the effect of wind directions and roof slopes 82
4.1. Introduction 82
4.1.1. Wind loads and relation to pressure coefficient factors 83
4.2. Effects of wind directions on solar panel arrays for 2″ spacing and 3″ roof clearance, mounted on 35º gable roofs 84
4.2.1. Pressure contours distributions for wind direction 45º 84
4.2.2. Pressure contour distributions for wind direction 90º 86
4.2.3. Pressure contours distributions for wind direction 0º 88
4.2.4. Pressure coefficients for roof mounted solar panels and roof without solar panels for windward side of the roof 90

4.2.4.1.Pressure coefficients on the bottom surface of the solar panels vs. roof surface under the solar panels 91

4.2.4.2.Pressure coefficients on roof surface under the solar panels vs. roofs without solar panels 94

4.2.4.3.Pressure coefficients on roof without solar panels vs. total pressure coefficients on the roof surface due to installation of solar panels 97

4.2.4.4.Pressure coefficients on roof without solar panels vs. top of the panels 100

4.2.4.5.Wind flow characteristics for gable roofs with solar panels for 90º wind direction 103

103

4.2.4.6.Pressure coefficients and velocity profiles in the cavity and above the solar panels for wind direction 90º, windward side of the roof 108

4.2.5. Pressure coefficients for roof mounted solar panels and roof without solar panels for leeward side of the roof 120

4.2.5.1.Pressure coefficient on roof under solar panels vs. roofs without solar panels 120

4.2.5.2.Pressure coefficient on bottom surface of the solar panels vs. roof surface under solar panels 122

4.2.5.3.Pressure coefficients for roof without solar panels vs. pressure coefficients on top surface of solar panels 124

4.2.5.4.Pressure coefficients for roof without solar panels vs. resultant of pressure coefficient on the roof – solar panels system 126

4.2.6. Net pressure coefficients on roof-solar panels system for slope 35º, wind directions 90º, 45º, 0º 128

4.2.7. Conclusions 134

4.3. Effects of wind directions on solar panel array with 2″ spacing and 3″ roof-panels clearance installed on 27º inclined roofs 134

4.3.1. Pressure contour distribution for wind direction 90º 134

4.3.2. Pressure coefficient for roof mounted solar panels and roofs with no panels, windward surface of the roof 138

4.3.2.1.Pressure coefficients on the roof under the solar panels vs. the roofs without solar panels 138

4.3.2.2.Pressure coefficients on bottom surface of the solar panels vs. roof surface under solar panels 141

4.3.2.3.Pressure coefficients on roof surface without solar panels vs. pressure coefficients on top of the panels 144

4.3.3. Pressure coefficients for roof mounted solar panels and roofs without panels, leeward side of the roof..... 146

4.3.3.1.Pressure coefficients on the roof under solar panels vs. roofs without solar panels 147

4.3.3.2. Pressure coefficient on bottom surface of the solar panels vs. roof surface under solar panels 149

4.3.3.3.Pressure coefficients roof without solar panels vs. pressure coefficient on top of panels 151

4.3.3.4.Wind flow characteristics for gable roofs with solar solar panels for wind direction 90º 153

4.3.3.5.Pressure coefficients and velocity profiles in the cavity and above the solar panels for wind direction 90º, windward side of the roof 160

4.3.4. Wind flow characteristics and three-dimensional vortex formations for gable roofs without solar panels for wind direction 90º..... 172

4.3.4.1.Pressure coefficients observations on the building. 172

4.3.4.2.Pressure coefficients and velocity profiles for roof without solar panels, wind direction 90º, windward side of the roof 174

4.3.5. Pressure coefficients on a vertical cross section 182

4.3.6. Net pressure coefficients on roof-solar panels system for slope 27º, for wind directions 90º, 45º and 0º, clearance 3" and spacing 2" 187

4.3.7. Conclusions 193

4.4. Effects of wind directions on solar panel arrays, 2" spacing and 3" roof clearance installed on 15º inclined roofs 193

4.4.1. Pressure contours distributions for wind direction 90º 193

4.4.2. Net pressure coefficients roof-solar panels system for slope 15º, wind directions 90º, 45º, 0º 195

4.4.3. Conclusions 200

4.5. Conclusions on wind effects on roof mounted solar panels, due to change in slopes and wind directions..... 201

4.6. Pressure coefficients comparison for using constant versus boundary layer wind profiles at the inlet 202

CHAPTER 5 208

Wind-induced pressure on gable roof mounted solar panels: the effect of roof clearance and array spacing 208

5.1. Effect of roof clearance 10” and array spacing 2” on roof mounted solar panels for roof slope 27º, wind directions 90º and 45º and wind speed 40m/s..... 209

5.1.1. Pressure contour distributions for wind direction 90º 209

5.1.2. Pressure coefficients for roof mounted solar panels and roof without solar panels for windward side of the roof..... 212

5.1.2.1. Pressure coefficients on bottom surface of the solar panels vs. roof surface under solar panels 213

5.1.2.2. Pressure coefficients on roof without solar panels vs. roof surface under solar panels 215

5.1.2.3. Pressure coefficients on roof without solar panels vs. top surface of solar panels217

5.1.3. Pressure coefficients for roof mounted solar panels and roof without solar panels for leeward side of the roof 219

5.1.3.1. Pressure coefficients on bottom surface of the solar panels vs. roof surface under solar panels 220

5.1.3.2. Pressure coefficients on roof surface under the solar panels vs. roof surface without solar panels 222

5.1.3.3. Pressure coefficients on top surface of the solar panels vs. roof surface without solar panels 224

5.1.4. Wind flow characteristics for gable roofs with solar panels for 90º wind direction 226

5.1.5. Wind flow characteristics for gable roofs with solar panels for 45º wind direction, windward side of the roof..... 232

5.1.6. Three-dimensional vortex flow formations around gable roofs with flush-mounted solar panels for 90º wind direction..... 237

5.1.7. Three-dimensional vortex flow formations around gable roofs with flush-mounted solar panels for 45º wind direction..... 240

5.1.8. Pressure coefficients and velocity profiles in the cavity and above the solar panels for wind direction 90º, windward side of the roof 243

5.1.9. Wind flow characteristics and three-dimensional vortex formations for gable roofs without solar panels for wind direction 90º..... 254

5.1.10.Net pressure coefficients on roof with and without solar panels array for wind directions 90º and 45º, clearance 10" and spacing 2" 259

5.2. Effects of roof clearance 3" and array spacing 2" on roof mounted solar panels, inclined roof 27º, wind direction 90º, 45º and 0º 268

5.3. Conclusions 269

5.4. Effects of roof clearance 3" and array spacing 8" on roof mounted solar panels, inclined roof 27º, wind directions 90º, 45º, and 0º 270

5.4.1. Pressure contour distributions, wind direction 90º 270

5.4.2. Pressure coefficient distributions for roof mounted solar panels and roof without solar panels for windward side of the roof 273

5.4.2.1. Pressure coefficients on bottom surface of the solar panels vs. roof surface under solar panels 274

5.4.2.2. Pressure coefficients on roof surface without solar panels vs. roof surface under solar panels 276

5.4.2.3. Pressure coefficients on bottom surface of the solar panels vs. roof surface without solar panels 278

5.4.2.4. Pressure coefficients on top surface of the solar panels vs. roof without solar panels 280

5.4.3. Pressure coefficient distributions for roof mounted solar panels and for roof without panels for the leeward side of the roof 283

5.4.3.1. Pressure coefficients on bottom surface of the solar panels vs. roof surface under solar panels 283

Fig. 5. 86. Pressure coefficients on bottom surface of solar panels vs. on roof under the panels, slope 27º, leeward, wind direction 90º 284

Fig. 5. 87. Pressure coefficients on bottom surface of solar panels vs. on roof under the panels, slope 27º, leeward, wind direction 45º 285

5.4.3.2. Pressure coefficients on roof surface without solar panels vs. roof surface under solar panels 285

5.4.3.3. Pressure coefficients on bottom surface of the solar panels vs. roof surface without solar panels 287

5.4.3.4. Pressure coefficients on top surface of the solar panels vs. roof surface without solar panels 289

5.4.4. Wind flow characteristics for gable roofs with solar panels for 90º wind direction 291

5.4.5. Wind flow characteristics and three-dimensional vortex formations for gable roofs without solar panels for wind direction 90º 298

5.4.6. Wind flow characteristics for gable roofs with solar panels for 45º wind direction, windward side of the roof 301
5.4.7. Detailed distribution of vortex cores on roof with solar panels 308
5.4.8. Wind pressure coefficient and flow distributions along 6 lines 310
5.4.9. Integration of pressure coefficients on surfaces of roof mounted solar panels in comparison with roof without solar panels, slope 27º, wind directions 90º and 45º, clearance 3", spacing 8" 322
5.4.10.CONCLUSIONS 327

CHAPTER 6 329
Discussion and results 329
6.1. Summary of the research 329
6.2. Contribution and novelty of the current research 329
6.3. Correlation between pressure coefficients on the roof, panel surfaces, and roof without solar panels 331
6.3.1. Correlation between pressure coefficients on top and bottom surfaces of roof tiles/pavers 331
6.3.2. Correlations between pressure coefficients on top, bottom of the panels, roof surface, 2" spacing, 3" clearance, 35º roof slope and roof without solar panels 334
6.3.3. Correlations between pressure coefficients on top, bottom of the panels and roof surface, 2" spacing, 10" clearance, 35º roof slope and roof without solar panels 342
6.4. Pressure coefficients correlations summary 351
6.5. Pressure equalization classification on solar panels and in the roof-panel cavity 352
6.6. Implication on the design code 356
6.6.1. Comparison with NBC 2010 for gable roofs with no panels 357
6.6.2. Comparison with SEAOC PV2 2012 and common practice 357
6.7.Conclusions 365

CHAPTER 7 367
7.1 Summary 367
7.2 Limitations of the research 367
7.3 General findings 368
7.4 Wind effects on roof mounted solar panels, due changes in wind directions or /and roof slopes 369
7.5 Wind effects on roof mounted solar panels due to change in roof clearance 369
7.6 Wind effects on roof mounted solar panels due to change in array spacing 370
7.7 Implication on the design codes 370
7.8 Main contributions and conclusions 371
7.8 Further researches on wind effects on gable roof mounted solar panels 373

REFERENCES 374

Appendix A 381
A-I- Turbulence intensities 381
A-II- Integral Scale of Turbulence 384
A-III- Power Spectral Density of Velocity 384
A-IV- Validation case 4: residential building modeled with CFD and LES algorithm 387
A-V- Demonstration of Wind effects on singular solar panels mounted on open bases, ... 389

APPENDIX B 392
B-I- Pressure coefficients for slope 27º, wind direction 45º, spacing 2", clearance 3" 392
B-II- Pressure coefficients for slope 27º, wind direction 0.0º, spacing 2", clearance 3" 400
Wind Pressure Coefficient and Flow Distributions under and above the solar panels, Windward side, 90º Wind Direction, 2" Spacing, 3" Roof Clearance, Slope 35º 407
B-IV- Wind Pressure Coefficient and Flow Distributions under and above the solar panels, Windward side, 90º Wind Direction, 2" Spacing, 3" Roof Clearance, Slope 27º 413
B-V- Wind Pressure Coefficient and Flow Distributions, along same 6 Perpendicular Lines, Windwards, Bare Roof, Wind Direction 90º 419

B-VI- Wind Pressure Coefficient and Flow Distributions under and above the solar panels, Windward side, 90º Wind Direction, 2" Spacing, 3" Roof Clearance, Slope 15º 423
B-VII- Pressure contours for solar panels on 15º inclined roofs for wind direction 45º 429
B-VIII- Pressure contours for solar panels mounted on 15º inclined roofs for wind direction 0.0º..... 430
B-IX- Comparison of pressure coefficient distribution on roof mounted solar panels and on roof without solar panels, slope 15º 432
B-IX-i Pressure coefficients on bottom surface of the solar panels Vs. roof surface under solar panels, for 15º inclined roofs and 90º, 45º and 0º wind directions, windward 432
B-IX-ii- Pressure coefficient on roof under panels vs. roof without panels, for 15º inclined roofs and 90º, 45º and 0º wind directions, windward 435
B-IX-iii Pressure coefficients on bottom surface of the solar panels Vs. roof without panels, for 15º inclined roofs and 90º, 45º and 0º wind directions, windward..... 438
B-IX-iv Pressure coefficients on top surface of the solar panels vs. roof without panels, for 15º inclined roofs and 90º, 45º and 0º wind directions, windward..... 440
B-X- Flow-structure interaction for the roof mounted solar panels for wind direction 90º and slope 15º 443
B-XI- ºWind pressure coefficient and flow distributions along 6 lines perpendicular to panels under and above the panels, windward side, slope 15º, wind direction 90º, wind speeds 40m/s and 10m/s..... 451 451
B-XII- Detailed distribution of wind pressure on roof mounted solar panels in comparison with roof without solar panels, leeward..... 464
B-XII-i Pressure coefficient on bottom surface of the solar panels Vs. roof surface under solar panels, for 15º inclined roofs and 90º, 45º and 0º wind directions, leeward 464
B-XII- ii Pressure coefficient on roof without panels Vs. roof surface under solar panels, for 15º inclined roofs and 90º, 45º and 0º wind directions, leeward 466
B-XII-iii Pressure coefficient on roof without panels vs. bottom of the panels surface, for 15º inclined roofs and 90º, 45º and 0º wind directions, Leeward..... 468
B-XII-iv Pressure coefficient on roof without panels vs. top of the panels surface, for 15º inclined roofs and 90º, 45º and 0º wind directions, leeward 469
B-XIV- Pressure coefficient distribution on roof mounted solar panels and on roofs with no panels, for wind directions 90º, 45º and 0º wind, windward surface 472
XIV.1. Pressure coefficients on bottom surface of solar panels vs. roofs without solar panels, roof slope 35º 472
XIV.2. Pressure coefficient on bottom surface of solar panels vs. roofs without solar panels, roof slope 35º 474

XIV.3. Pressure coefficients on the bottom surface of the solar panels vs. roofs without solar panels, roof slope 27º 477

XIV.4. Pressure coefficients on bottom of solar panels vs. roofs without solar panels, roof slope 27º 480

APPENDIX C 483

C.1 Slope 35º, ... 483

1.1. 2” Spacing, 10” Clearance 483

1.1.2. WIND DIRECTION 90º 485

1.1.3. WIND DIRECTION 0.0º 487

1.1.4. Detailed Distribution of Wind Pressure on roof mounted solar panels in comparison with bare roofs, Windward, 2” apart, 10” roof space 488

1.1.5. Detailed Distribution of Wind Pressure on roof mounted solar panels in comparison with roof under panels and bare roofs, Leeward, 2” spacing , 10” roof clearance 496

1.1.6. Detailed Distribution of Wind Pressure, and flow on roof mounted solar panels, 2” apart, 10” roof space, 504

1.1.7. Calculation of resultant Cp of the three surfaces of roof mounted solar panels in comparison with bare roofs, Leeward, 2” apart, 10” roof space 517

Tabulated results of the integration, ... 517

1.2. 8” Spacing, 3” Clearance 521

1.2.2. WIND DIRECTION 90º 524

1.2.3. WIND DIRECTION 0.0º 529

1.2.4. Detailed Distribution of Wind Pressure on roof mounted solar panels in comparison with bare roofs, Windward, 2” apart, 10” roof space 530

1.2.5. Detailed Distribution of Wind Pressure on roof mounted solar panels in comparison with roof under panels and bare roofs, Leeward, 2” spacing , 10” roof clearance 533

1.2.6. Detailed Distribution of Wind Pressure, and flow on roof mounted solar panels, 2” apart, 10” roof space, 538

1.2.7. Calculation of resultant Cp of the three surfaces of roof mounted solar panels in comparison with bare roofs, Leeward, 2” apart, 10” roof space 551

Tabulated results of the integration, ... 551

1.3. 8” Spacing, 10” Clearance 554

1.3.2. WIND DIRECTION 90º 558

1.3.3. WIND DIRECTION 0.0º 561

1.3.4. Detailed Distribution of Wind Pressure on roof mounted solar panels in comparison with bare roofs, Windward, S8" , C10" 564

1.3.5. Detailed Distribution of Wind Pressure, and flow on roof mounted solar panels, S 8", C10" . 566

1.3.6. Calculation of resultant Cp of the three surfaces of roof mounted solar panels in comparison with bare roofs, Leeward, 2" apart, 10" roof space..... 583

Tabulated results of the integration, 583

APPENDIX D..... 586

D.1. Slope 27º, ... 586

1.1. 8" Spacing, 10" Clearance 586

1.1.2. WIND DIRECTION 90º 591

1.1.3. WIND DIRECTION 0º 594

1.1.4. Detailed Distribution of Wind Pressure and Wind Speed on Roof Mounted Solar Panels In Comparison with Bare Roofs, Windward, S8" , C10"..... 597

1.1.5. Detailed Distribution Of Wind Pressure and Speed, and Flow on Roof Mounted Solar Panels, S 8", C10" 600

1.1.6. Integration of Cp on the three surfaces and Cp resultant of roof mounted solar panels in comparison with bare roofs, S8" C 10" 621

Tabulated results of the integration,..... 621

APPENDIX E 627

E.1. Slope 15º, ... 627

1.1. 2" Spacing, 10" Clearance 627

1.1.2. WIND DIRECTION 90º 635

1.1.3. WIND DIRECTION 0º 637

1.1.4. Detailed Distribution of Wind Pressure and Speed on Roof Mounted Solar Panels, S2"C10" 643

1.1.5. Integration of Cp on The Three Surfaces and the Resultant of CP on Roof Mounted Solar Panels in Comparison with Bare Roof, S2"C10" 670

Tabulated results of the integration,..... 670

1.2. 8" Spacing, 3" Clearance 676

1.2.2. WIND DIRECTION 90º 685
1.2.3. WIND DIRECTION 0º 687
1.2.4. Detailed Distribution of Wind Pressure and Speed on Roof Mounted Solar Panels, S8" C3" . 696
1.2.5. Integration of Cp on The Three Surfaces and the Resultant of CP on Roof Mounted Solar Panels in Comparison with Bare Roof, S8"C3" 724
Tabulated results of the integration, ... 724
1.3. 8" Spacing, 10" Clearance 730
1.3.2. WIND DIRECTION 90º 746
1.3.3. WIND DIRECTION 0º 748
1.3.4. Detailed Distribution of Wind Pressure and speed on Roof Mounted Solar Panels in Comparison with Bare Roof, S8"C10" 759
1.3.5. Integration of Cp on The Three Surfaces and Resultant Cp of Roof Mounted Solar Panels in Comparison with Bare Roof,S8"C10" 790
Tabulated results of the integration, 790

APPENDIX F 797
F.1. Correlations between pressure coefficients on top, bottom of the panels and roof surface, 2" spacing, 10" clearance, 35º roof slope and roof without solar panels 797
F.2. Correlations between pressure coefficients on top, bottom of the panels, and roof surface, 8" spacing, 3" clearance, 35º roof slope, and roof without solar panels 806
F.3. Correlations between pressure coefficients on top, bottom of the panels and roof surface, 8" spacing, 10" clearance, 35º roof slope and roof without solar panels 817
F.4. Correlation between pressure coefficients on top and bottom surfaces of roof tiles/pavers 827
F.5. External pressure on gable roofs as per ASCE 7-10 830

LIST OF FIGURES

Fig. 1.1. Wind loading components, (Holmes et al, 2001). 1
Fig. 1.2. Wind typical flow around a bluff and streamlined objects (Holmes, 2001)..... 2
Fig. 1.3. Generation of eddies, typical bluff structure (Mendis et al, 2007). 3
Fig. 1.4. Wind flow around a low-rise building with pitched roof, (Holmes, 2001) 3
Fig. 1.5. Conical vortices for oblique wind directions, (Holmes, 2001)..... 4
Fig. 1.6. Typical rail-foot attachments for solar panels, (UNIRAC, 2014) 5
Fig. 1. 7. PV solar panels connection to roofs a) With brackets, b) With standoffs (Unirac, 2014) 5
Fig. 1. 8. Examples of PV solar panels failures (IEA-PVPS T13-01, 2014) 6
Fig.1.9. Examples of PV solar panels and the installation system failures (http://runonsun.com/~runons5/blogs/blog1.php/solworks/safety/solar-trumps-windstorm-part-2) 6

Fig. 2.1. Two Laws to Calculate Mean Wind Speed at Different Heights (m) for exposure "C" Open Terrain or Grass Land or Land with Few Trees. 11
Fig. 2. 2 Wind tunnel velocity (a) mean wind speed profile; (b) turbulence intensity profile; (c) integral length scale; Bitsuamlak et al (2014)..... 14
Fig. 2. 3. (a) Maximum and minimum pressure coefficients and comparison with external pressure on roof without panels in the ASCE 7-2010 (ASCE 2010) (7° < slope <27°); (b) solar panel modules (H1) mounted on gable roofs with slopes 3:12 (14°) or 4/12 (22.6°), Bitsuamlak et al (2014). 14
Fig. 2. 4. Mean wind speed and turbulence intensity profiles (Stenabaugh, 2015) 15
Fig. 2. 5. Sloped roof model (Stenabaugh, 2015). 16
Fig. 2. 6. (a) Wind velocity profiles. Dots represent the experimental data; solid lines are the CFD profiles. (b) Turbulence intensity profiles. (Chowdhury et al, 2018)..... 17
Fig. 2. 7. (a) turbulence intensity (b) profiles at 2H from the exit of the blowers, (Aly et al, 2017) 18
Fig. 2. 8. Computational domain, (Geurts et al, 2010) 18
Fig. 2. 9. Peak uplift contours, with vortex identifier labels, (a) Wind direction 50°and (b) Wind direction 140° (Banks, 2013). 19
Fig. 2. 10. (a) CFD inlet velocity mean wind speed profile and experimental wind speeds (b) Computational domain, boundary conditions of stand-alone solar panel (Bitsuamlak et al, 2010) 23
Fig. 2. 11. Computational domain size and boundary conditions in the CFD (Shademan et al, 2009) 24
Fig. 2. 12. Computational domain, (Reina et al, 2017)..... 25
Fig. 2. 13. Computational domain, (Chowdhury et al, 2016) 26
Fig. 2. 14. Computational domain, (Aly M. A., 2016) 26
Fig. 2. 15. CFD wind speed profiles and measured BLWT profiles for open terrain: (a) mean velocity profile and (b) turbulence intensity profile(Aly M. A., 2016). 27
Fig. 2. 16. Free vibration test, (a) Test setup, and (b) Damped response (Schellenberg et al, 2013). 28

Fig. 3.1. Dimensions (m) of the simulation domain surrounding Zisis (2011) Doudak et al (2011) building model 34
Fig. 3.2. Zisis (2011) and Doudak et al (2011) building model mesh detail in CFD analysis 34
Fig. 3. 3, Dimensions (m) of the simulation domain surrounding Holmes (2001) building models 35
Fig. 3. 4, Holmes (2001) model mesh detail used for the CFD analysis 35
Fig. 3. 5, Dimensions (m) of the simulation domain surrounding Robertson et al (1985) canopy model..... 35
Fig. 3.6. Canopy model mesh detail used for the CFD analysis..... 36
Fig. 3.7.Minimum computational domain dimensions as recommended by Franke (2006) and COST (2007) for a single building, as reported by Dagnew and Bitsumlak (2013) and Dagnew (2012). 37
Fig. 3. 8. Computational domain in this study. 37
Fig. 3. 9. Residential building model (12m x 8m x 7.40 m) mesh details used for the CFD analysis, 90° wind direction, slope 35°..... 37
Fig. 3. 10. Dimensions (m) of the simulation domain surrounding a typical residential building model..... 38
Fig. 3. 11. Building model mesh detail used for the CFD analysis 38
Fig. 3. 12. Building model mesh detail, top of the roof with panels, 10" clearance, 2" spacing. 39
Fig. 3. 13. Building model mesh detail, under the panels, 10" clearance, 2" spacing..... 39
Fig. 3. 14. Building model mesh detail, top of the roof with panels, 10" clearance, 8" spacing.. 39
Fig. 3. 15. Building model mesh detail, under the panels, 10" clearance, 8" spacing..... 40
Fig. 3. 16. Different size meshes used for mesh sensitivity analysis..... 41
Fig. 3. 17. Cp contours on the building with solar panels for the corresponding meshes 41
Fig. 3. 18. Wind velocity profiles along the computational domain for the building with solar panels for the corresponding meshes 42
Fig. 3. 19. Agricultural canopy geometry investigated by Robertson et al, (1985)..... 44
Fig. 3. 20. Wind directions and monitored points for the agricultural canopy (Robertson et al, 1985) 44
Fig. 3. 21. a) Average pressure coefficients along the middle cross-section of the corrugated roof canopy for 0° wind direction; b) Location of the canopy middle cross-section and surface pressure coefficient distribution 45
Fig. 3. 22 a) Average pressure coefficients along the smooth canopy middle cross-section for 0°; b) Location of the canopy middle cross-section and surface pressure coefficient distribution 45
Fig. 3. 23. CFD pressure coefficients for the canopy with corrugated roof - longitudinal and transversal monitored sections..... 46
Fig. 3. 24. Pressure coefficients comparison CFD and full-scale measurements (Robertson et al, (1985) and CFD simulations for 90°, a) Longitudinal sections b) Transversal sections 46
Fig. 3. 25. Mean pressure coefficients on the lateral wall of a residential building Doudak et al (2011)..... 47
Fig. 3. 26. Mean pressure coefficients on the roof of a residential building Doudak et al, (2011) 48

Fig. 3. 27. CFD Mean pressure coefficients for the residential building for a) 0° wind direction, b) 180° wind direction, (This Research) 49
Fig. 3. 28. Mean pressure coefficients for the residential building for 0° and 180° for a) Roof tap location, b) Wall tap location..... 49
Fig. 3. 29. CFD Mean pressure coefficients for the residential building for a) 265.5° wind direction, b) 333.5° wind direction 50
Fig. 3. 30. Mean pressure coefficients for the residential building for 265.5° and 333.5° for a) Roof tap location, b) Wall tap location..... 51
Fig. 3. 31. a) Residential building, (Zisis, 2011) b) Instrumented frames, full-scale, (Zisis, 2011) 51
Fig. 3. 32 Mean pressure coefficients for frame 14. (zisis, 2011)..... 52
Fig. 3. 33. Contour of pressure coefficients for residential building, tested by Zisis, (2011) Wind direction is 240 °, Frame 2 (ww), Frame 14 (middle) and Frame 28 (lw)..... 52
Fig. 3. 34. Mean pressure coefficients on Frame 14 of the residential building, Zisis (2011) full-scale with CFD analysis-Current study, wind direction 240°..... 53
Fig. 3. 35. Mean pressure coefficients for Frame 2, wind direction 240° (Zisis, 2011). 54
Fig. 3. 36. Mean pressure coefficients on Frame 2 of residential building, Zisis (2011) full-scale with CFD analysis-Current study, wind direction 240°..... 54
Fig. 3. 37. Mean pressure coefficients for Frame 28, wind direction 240° (Zisis, 2011). 55
Fig. 3. 38. Mean pressure coefficients on Frame 28 of residential building, Zisis (2011) full-scale with CFD of this study, wind direction 240° 55
Fig. 3. 39. Pressure Coefficient distribution on the roof middle cross-line, roof slope (45º), h/d=1, d=8m: 57
Fig. 3. 40. CFD model, Slope (45º), middle line, h/d=1, d=8m..... 57
Fig. 3. 41. Pressure Coefficient distribution on the roof side lines 46 and 47, roof slope (45º), h/d=1, d=8m..... 58
Fig. 3. 42. CFD model, Slope (45º), h/d=1, d=8m..... 58
Fig. 3. 43. Swirling strength, CFD model, Slope 45º, Fig. 3. 44.Swirling strength, CFD model, Slope 45º 59
Fig. 3. 45. Pressure coefficient distribution on the roof middle cross-line, roof slope 45º, h/d=0.4, d=8m: 60
Fig. 3. 46. Holmes model for (45º), h/d=0.4, d=8m 61
Fig. 3. 47. Pressure coefficient distribution on the Lines 46 and 47, roof slope (45º), h/d=1, d=8m. 61
Fig. 3. 48. CFD model, Swirling strength, Fig. 3. 49. CFD model, Swirling strength, . 62
Fig. 3. 50. Pressure Coefficient distribution on the roof middle cross-line, roof slope (30º), h/d=1, d=8m: 63
Fig. 3. 51. Pressure coefficient distribution on the Lines 46 and 47, CFD, Slope (30º), h/d=1, d=8m. 64
Fig. 3. 52. Holmes model, Slope (30º), 5 lines, h/d=1, d=8m 64
Fig. 3. 53. Swirling strength CFD model, Slope 30º, Fig. 3. 54. Swirling strength CFD model, Slope 30º, ... 65
Fig. 3. 55. Pressure Coefficient distribution on the roof middle cross-line, roof slope (30º), h/d=0.4, d=8m: a) Adapted from Holmes (2001) b) Current CFD study 66
Fig. 3. 56 Pressure coefficient distribution on Lines 46 and 47, CFD, Slope (30º), h/d=0.4, d=8m. 66

Fig. 3. 57. Holmes model, Slope (30º), h/d=0.4, d=8m 67
Fig. 3. 58. CFD model, Slope 30º Fig. 3. 59. CFD model, Slope 30º 68
Fig. 3. 60. Single panels on solid bases, Mesh of the model, slopes (a) 0°, (b) 15°, (c) 35°, (c) -15° 69
Fig. 3. 61. Double panels on roofs with open bases, Mesh of the model, slopes, (a) 0°, (b) 15°, (c) 35°, (c) -15° 70
Fig. 3. 62. Single panels mounted on open bases, Mesh of the model, slopes (a) 0°, (b) 15°, (c) 35°, (c) -15° 71
Fig. 3. 63. Single panels on solid bases, Top of panels WD (45º) 71
Fig. 3. 64 Single panel on solid base, (35º) slope, top of the panel. 72
Fig. 3. 65. Single panel on a solid base, (35º) slope, roof top under the panel. 73
Fig. 3. 66. Single panel on a solid base, (35º) slope, bottom of the panel. 73
Fig. 3. 67. Single panel on solid base, (15º) slope, top of the panel. 74
Fig. 3. 68.. Single panel on a solid base, (15º) slope, roof top under the panel. 75
Fig. 3. 69. Single panel on a solid base, (15º) slope, bottom of the panel. 75
Fig. 3. 70. Single panel on solid base, (0º) slope, top of the panel. 76
Fig. 3. 71. Single panel on a solid base, (0º) slope, roof top under the panel. 76
Fig. 3. 72. Single panel on a solid base, (0º) slope, bottom of the panel. 77
Fig. 3. 73. Single panel on solid base, (-15º) slope, top of the panel. 78
Fig. 3. 74. Single panel on a solid base, (-15º) slope, roof top under the panel 78
Fig. 3. 75. Single panel on a solid base, (-15º) slope, bottom of the panel. 78
Fig. 3. 76. Panel on roof 3” gap, solid base, 0 º S, 45 º WD Fig. 3. 77. Panel on roof 3” gap, solid base, 15º S, 45 º WD 79
Fig. 3. 78. With panels 3” gap, solid base, 35º S, 45º WD Fig. 3. 79. With panels 3” gap, solid base, -15º S, 45º WD 80

Fig. 4. 1. Pressure coefficient distribution on a) Bottom surface of the solar panels, and b) Top surface of the solar panel for roof slope 35º and wind direction 45º, windward side 84
Fig. 4. 2. Pressure coefficients on roof under the solar panels, wind direction 45º, windward side 85
Fig. 4. 3. Pressure coefficient distribution on the house model with solar panels installed on the roof, for roof slope 35º and wind direction 45º 86
Fig. 4. 4. Pressure coefficient distribution on roof surface underneath the solar panels, roof slope 35º and wind direction 90º, windward side 87
Fig. 4. 5. Pressure coefficient distribution on a) Bottom surface of the solar panels, and b) Top surface of the solar panel, for roof slope 35º and wind direction 90º, windward side 87
Fig. 4. 6. Pressure coefficient distribution on the house model with solar panels installed on the roof, with main polylines for roof slope 35º and wind direction 90º 88
Fig. 4. 7. Pressure coefficient distribution on roof surface underneath the solar panels, for roof slope 35º and wind direction 0º, side of the building 89
Fig. 4. 8. Pressure coefficient distribution on a) Bottom of the solar panels, and b) Top of the solar panel, for roof slope 35º and wind direction 0º 89
Fig. 4. 9. Pressure coefficient distribution on the house model with solar panels installed on the roof for roof slope 35º and wind direction 0º 90

Fig. 4. 10. Pressure coefficient distribution on the bottom surface of the solar panels and on the roof surface under the panels, for roof slope 35º, and wind direction 90º, windward side 92
Fig. 4. 11. Pressure coefficient distribution on the bottom surface of the solar panels and on the roof surface under the panels, for roof slope 35º, and wind direction 45º, windward side 92
Fig. 4. 12. Pressure coefficient distribution on the bottom surface of the solar panels and on the roof surface under the panels, for roof slope 35º, and wind direction 0º, windward side. 93
Fig. 4. 13. Pressure coefficient distribution on the roof surface under the panels and on roof surface without mounted panels, slope 35º, and wind direction 90º, windward side..... 94
Fig. 4. 14. Pressure coefficient distribution on the roof surface under the panels and on roof surface without mounted panels, slope 35º, and wind direction 45º, windward side..... 95
Fig. 4. 15. Pressure coefficient distribution on the roof surface under the panels and on roof surface without mounted panels, slope 35º, and wind direction 0º 95
Fig. 4. 16. Pressure coefficient distribution on roof surface without mounted panels and resultant of pressure coefficients on roof surface due to panel installation, slope 35º, and wind direction 90º, windward side 98
Fig. 4. 17. Pressure coefficient distribution on roof surface without mounted panels and resultant of pressure coefficients on roof surface due to panel installation, windward side, slope 35º, and wind direction 45º 99
Fig. 4. 18. Pressure coefficient distribution on roof surface without mounted panels, and resultant of pressure coefficients on roof surface due to panel installation, slope 35º, and wind direction 0º 99
Fig. 4. 19. Pressure coefficient distribution on the roof surface without solar panels and on top of the solar panels, for roof slope 35º, and wind direction 90º, windward side..... 101
Fig. 4. 20. Pressure coefficient distribution on the roof surface without solar panels and on top of the solar panels, for roof slope 35º, and wind direction 45º, windward side..... 102
Fig. 4. 21. Pressure coefficient distribution on the roof surface without solar panels and on top of the solar panels, for roof slope 35º, and wind direction 0º 102
Fig. 4. 22.Close view of pressure coefficients..... 103
Fig. 4. 23. Close view of pressure coefficients and panel gaps, windward wind direction 45º. 103
Fig. 4. 24. Close view of pressure coefficients and panel gaps, near edge A wind direction 90º 104
Fig. 4. 25. Pressure coefficients on a perpendicular plane under the panels, wind direction 90º 104
Fig. 4. 26. Pressure coefficient on a perpendicular plane and bottom surface of panels, wind direction 90º 104
Fig. 4. 27. Pressure coefficient on a plane perpendicular on the house ridge, wind direction 90º 105
Fig. 4. 28. Lines configuration for monitoring the velocity and pressure, wind direction 90º .. 105
Fig. 4. 29. Velocity streamlines at middle cross section plane, wind direction 90º..... 106
Fig. 4. 30. Vortex core distribution on bottom of the panels, windward, wind direction 90º ..107
Fig. 4. 31. Vortex core distribution on top of the panels windward, wind direction 90º ……107
Fig. 4. 32. Vortex core distribution, on roof under the panels, and around the house..... 108
Fig. 4. 33. Velocity and Cp changes between panels, and above roof, Line 1, 40 m/s, windward, wind direction 90º 109
Fig. 4. 34. Velocity and Cp changes between panels, and above roof, Line 2, 40m/s, windward, wind direction 90º 110

Fig. 4. 35. Velocity changes between panels, and above roof, Line 3, 40m/s, windward, wind direction 90º 112
Fig. 4. 36. Velocity between panels, and above roof, Line 4, 40m/s, windward, wind direction 90º 113
Fig. 4. 37. Cp changes between panels, and above roof, Line 5, 40 m/s, windward, wind direction 90º 115
Fig. 4. 38. Pressure coefficients and velocity changes between panels, and above roof, Line 6, 40 m/s, windward, wind direction 90º 116
Fig. 4. 39. Pressure coefficient and velocity between panels and roof, and above the panels, Lines 1 to 6, 40 m/s, windward, wind direction 90º 118
Fig. 4. 40. Cp and velocity changes between panels and roof, and above the panels, Lines 1-6, 40 m/s, windward, wind direction 90º, Zoom into space between panels and roof..... 118
Fig. 4. 41. Cp and velocity changes between panels and roof, and above the panels, Lines 1-6, 10 m/s, windward, wind direction 90º 119
Fig. 4. 42. Cp and velocity changes between panels and roof, and above the panels, Lines 1-6, 10 m/s, windward, wind direction 90º Zoom into space between panels and roof..... 119
Fig. 4. 43. Pressure coefficient distribution on the roof surface under the solar panels and on the roof surface without panels, for roof slope 35º, and wind direction 90º, leeward side 121
Fig. 4. 44. Pressure coefficient distribution on the roof surface under the solar panels and on the roof surface without panels, for roof slope 35º, and wind direction 45º, leeward side 121
Fig. 4. 45. Pressure coefficient distribution on the roof surface under the solar panels and on bottom of the panels, for roof slope 35º, and wind direction 90º, leeward side 123
Fig. 4. 46. Pressure coefficient distribution on the roof surface under the solar panels and on bottom of the panels, for roof slope 35º, and wind direction 45º, leeward side 123
Fig. 4. 47. Pressure coefficient distribution on the bottom surface of the solar panels and on top of panels, for roof slope 35º, and wind direction 90º, leeward side..... 125
Fig. 4. 48. Pressure coefficient distribution on the bottom surface of the solar panels and on top of panels, for roof slope 35º, and wind direction 45º, leeward side..... 126
Fig. 4. 49. Pressure coefficient distribution on roof surface without mounted panels and resultant of pressure coefficients on roof surface due to panel installation, slope 35º, and wind direction 90º, leeward side 127
Fig. 4.50. Pressure coefficient distribution on roof surface without mounted panels and resultant of pressure coefficients on roof surface due to panel installation, slope 35º, and wind direction 45º, leeward side 128
Fig. 4. 51. Pressure coefficient contours of roof with solar panels, slope 27º, windward, wind direction 90º, ... 135
Fig. 4. 52. Pressure coefficient on top of solar panels with lines, slope 27º, windward, wind direction 90º 135
Fig. 4. 53. Pressure coefficient distribution on a) Top of the solar panels, and b) Bottom of the solar panel, for roof slope 27º and wind direction 0º..... 136
Fig. 4. 54. Pressure coefficient on roof under solar panels, slope 27º, windward, wind direction 90º 136
Fig. 4. 55. Pressure coefficient on (a) bottom of the panel array, and (b) top of solar panels, slope 27º, Leeward, wind direction 90º..... 137
Fig. 4. 56. Pressure coefficient on roof under solar panels, slope 27º, Leeward, wind direction 90º 137

Fig. 4. 57. Pressure coefficient distribution on the roof surface under the solar panels and on the roof surface without mounted solar panels, for roof slope 27º, and wind direction 90º, windward side 139
Fig. 4. 58. Pressure coefficient distribution on the roof surface under the solar panels and on the roof surface without mounted solar panels, for roof slope 27º, and wind direction 45º, windward side 140
Fig. 4. 59. Pressure coefficient distribution on the roof surface under the solar panels and on the roof surface without mounted solar panels, for roof slope 27º, and wind direction 0º..... 140
Fig. 4. 60. Pressure coefficient distribution on the bottom surface of the solar panels and on the roof surface under the panels, for roof slope 27º, and wind direction 90º, windward side 142
Fig. 4. 61. Pressure coefficient distribution on the bottom surface of the solar panels and on the roof surface under the panels, for roof slope 27º, and wind direction 45º, windward side 143
Fig. 4. 62. Pressure coefficient distribution on the bottom surface of the solar panels and on the roof surface under the panels, for roof slope 27º, and wind direction 0º,..... 143
Fig. 4. 63. Pressure coefficient distribution on top surface of the solar panels and on the roof surface without mounted solar panels, for roof slope 27º, and wind direction 90º, windward side 144
Fig. 4. 64. Pressure coefficient distribution on top surface of the solar panels and on the roof surface without mounted solar panels, for roof slope 27º, and wind direction 45º, windward side 145
Fig. 4. 65. Pressure coefficient distribution on top surface of the solar panels and on the roof surface without mounted solar panels, for roof slope 27º, and wind direction 0º 146
Fig. 4. 66. Pressure coefficient distribution on roof surface under the solar panels and on the roof without mounted solar panels, for roof slope 27º, and wind direction 90º, leeward side..... 148
Fig. 4. 67. Pressure coefficient distribution on roof surface under the solar panels and on the roof without mounted solar panels, for roof slope 27º, and wind direction 45º, leeward side..... 149
Fig. 4. 68. Pressure coefficient distribution on bottom surface of the solar panels and on the roof under solar panels, for roof slope 27º, and wind direction 90º, leeward side 150
Fig. 4. 69. Pressure coefficient distribution on bottom surface of the solar panels and on the roof under solar panels, for roof slope 27º, and wind direction 45º, leeward side 151
Fig. 4. 70. Pressure coefficient distribution on top surface of the solar panels and on the roof without mounted 152
Fig. 4. 71. Pressure coefficient distribution on top surface of the solar panels and on the roof without mounted solar panels, for roof slope 27º, and wind direction 45º, leeward side..... 153
Fig. 4. 72. Pressure coefficient on a perpendicular Longitudinal plane, roof under panels, wind direction 90º, windward, slope 27º 154
Fig. 4. 73. Pressure coefficient on a perpendicular transversal plane, roof under panels, wind direction 90º, leeward, slope 27º..... 154
Fig. 4. 74. Pressure coefficient on a transversal plane perpendicular to the house ridge 155
Fig. 4. 75. Lines used to track velocity and pressure coefficient changes..... 156
Fig. 4. 76. Velocity streamlines at middle cross section plane, windward view 156
Fig. 4. 77. Velocity stream lines at middle cross section plane, Leeward view 157
Fig. 4. 78. Vortex core distribution on roof with panels installed, and around the structure. ... 157
Fig. 4. 79. Vortex core distribution on roof under panels, windward, and leeward with panels, No Contours, and on the building structure..... 158
Fig. 4. 80. Vortex core distribution on top of the panels, windward 159

Fig. 4. 81. Vortex core distribution, on bottom of the panels, windward 159
Fig. 4. 82. Vortex core distribution on top of the panels, Leeward 159
Fig. 4. 83. Vortex core distribution on bottom of the panels, Leeward 160
Fig. 4. 84. Velocity and Cp changes between panels, and above roof, Line 1, 40m/s, windward, wind direction 90º 161
Fig. 4. 85. Velocity and Cp changes between panels, and above roof, Line 2, 40m/s, windward, wind direction 90º 162
Fig. 4. 86. Velocity changes between panels, and above roof, Line 3, 40m/s, windward, wind direction 90º 164
Fig. 4. 87. Pressure coefficient and velocity changes between panels, and above roof, Line 4, 40m/s, windward, wind direction 90º 165
Fig. 4. 88. Pressure coefficient and velocity changes between panels, and above roof, Line 5, 40m/s, windward, wind direction 90º 167
Fig. 4. 89. Pressure coefficient and velocity changes between panels, and above roof, Line 6, 40m/s, windward, wind direction 90º 168
Fig. 4. 90. Pressure coefficient and velocity changes between panels and roof, and above the panels, Lines 1-6, 10 m/s, windward, wind direction 90º 170
Fig. 4. 91. Pressure coefficient and velocity changes between panels and roof, and above the panels, Lines 1-6, 40 m/s, windward, wind direction 90º 170
Fig. 4. 92. Pressure coefficient and velocity changes between panels and roof, and above the panels, Lines 1-6, 10 m/s, windward, wind direction 90º Zoom into space between panels and roof 171
Fig. 4. 93. Pressure coefficient and velocity changes between panels and roof, and above the panels, Lines 1-6, 40 m/s, windward, wind direction 90º Zoom into space between panels and roof 171
Fig. 4. 94. Pressure coefficient contours top view, windward, slope 27º, wind direction 90º. 172
Fig. 4. 95. Pressure coefficients, Vortex core windward, slope27º, wind direction 90º 173
Fig. 4. 98. Pressure coefficient and velocity streamlines at middle of the roof, line 4, slope27º, wind direction 90º 173
Fig. 4. 99. Pressure coefficient and velocity streamlines at middle of the roof, line 4, slope27º, wind direction 90º, leeward view 174
Fig. 4. 100. Pressure coefficient and velocity change along Line1, wind direction 90º, 40m/s, windward, wind direction 90º 175
Fig. 4. 101. Pressure coefficient and velocity change along Line2, wind direction 90º, 40m/s, windward, wind direction 90º 176
Fig. 4. 102. Pressure coefficient and velocity change along Line3, wind direction 90º, 40m/s, windward, wind direction 90º 177
Fig. 4. 103. Pressure coefficient and velocity change along Line4, wind direction 90º, 40m/s, windward, wind direction 90º 178
Fig. 4. 104. Pressure coefficient and velocity change along Line5, wind direction 90º, 40m/s, windward, wind direction 90º 179
Fig. 4. 105. Pressure coefficient and velocity change along Line6, wind direction 90º, 40m/s, windward, wind direction 90º 179
Fig. 4. 106. Pressure coefficient and velocity change along all Lines, wind direction 90º, 10m/s, windward, wind direction 90º 181

Fig. 4. 107. Pressure coefficient and velocity change along all Lines, wind direction 90º, 40m/s, windward, wind direction 90º 181
Fig. 4. 108. Pressure coefficient on transverse plane crosses middle of the building, slope 27º, wind direction 90º 182
Fig. 4. 109. Pressure coefficient on roof with no panels with transverse 5 lines, slope27º, windward, wind direction 182
Fig. 4. 110. Pressure coefficient on roof without panels, 5 transverse lines, slope 27º, wind direction 90º, ... 183
Fig. 4. 111. Pressure coefficient on roof with panels, 5 transverse Lines, slope 27º, wind direction 90º 183
Fig. 4. 112. slope 27º, wind direction 90º, ... 184
Fig. 4. 113. Pressure coefficient distributions all polylines on windward, roof without solar panels, slope 27º, wind direction 90º 185
Fig. 4. 114. Pressure coefficient distribution on windward side of roof, all polylines, roof with panels, ... 185
Fig. 4. 115. Pressure coefficient distributions all polylines on leeward, roof without solar panels, slope 27º, wind direction 90º 186
Fig. 4. 116. Pressure coefficient distributions all polylines on leeward, roof with solar panels, slope 27º, wind direction 90º 186
Fig. 4. 117**.** Pressure coefficients on (a) Bottom of the solar panels, (b) Top of the solar panels, windward, slope 15º, wind direction 90º 194
Fig. 4. 118. Depicts pressure coefficients on top surface of the solar panels in the windward direction, windward, slope 15º, wind direction 90º 194
Fig. 4. 119. A cut off shows pressure coefficients on roof under solar panels, windward, slope 15º, wind direction 90º 195
Fig. 4. 120. Constant wind velocity profile at inlet…….. ……204
Fig. 4. 121. Boundary layer wind velocity profile at inlet 204
Fig. 4. 122. Pressure coefficients on the building for a) constant velocity profile at inlet and b) boundary layer at inlet 205
Fig. 4. 123. Comparison between the pressure coefficients on top of the panels, representative lines, windwards, for constant velocity profile at inlet and boundary layer at inlet. 206

Fig. 5. 1. Pressure coefficients contours of roof with solar panels, slope 27º, windward, wind direction 90º 210
Fig. 5. 2. Pressure coefficients on bottom of solar panels**,** slope 27º, windward, wind direction 90º 210
Fig. 5. 3. Pressure coefficients on roof under solar panels, slope 27º, windward, wind direction 90º 211
Fig. 5. 4. Pressure coefficients on roof under solar panels, slope 27º, leeward, wind direction 90º 211

Fig. 5. 5. Pressure coefficients on bottom of solar panels, slope 27º, leeward, wind direction 90º 211
Fig. 5. 6. Pressure coefficients on top of solar panels, slope 27º, wind direction 90º a) Leeward side of the roof b) Windward side of the roof..... 212
Fig. 5. 7. Pressure coefficients on bottom of solar panels vs. on roof under the panels, slope 27º, windward, wind direction 90 º 214
Fig. 5. 8. Pressure coefficients on bottom of solar panels vs. on roof under the panels, slope 27º, windward, wind direction 45 º 214
Fig. 5. 9. Pressure coefficients on roof without solar panels vs. on roof under the panels, slope 27º, windward, wind direction 90º 216
Fig. 5. 10. Pressure coefficients on roof without solar panels vs. on roof under the panels, slope 27º, windward, wind direction 45º 217
Fig. 5. 11. Pressure coefficients of roof without solar panels vs. top of solar panels, slope 27º, windward, wind direction 90º 218
Fig. 5. 12. Pressure coefficients of roof without solar panels vs. top of solar panels, slope 27º, windward, wind direction 45º 219
Fig. 5. 13. Pressure coefficients on bottom of solar panels vs. on roof under the panels, slope 27º, leeward side wind direction 90º 221
Fig. 5. 14. Pressure coefficients on bottom of solar panels vs. on roof under the panels, slope 27º, leeward, wind direction 45º 221
Fig. 5. 15. Pressure coefficients on roof without solar panels vs. on roof under the panels, slope 27º, leeward, wind direction 90º 223
Fig. 5. 16. Pressure coefficients on roof without solar panels vs. on roof under the panels, slope 27º, leeward, wind direction 45º 223
Fig. 5. 17. Pressure coefficients of roof without solar panels vs. top of solar panels, slope 27º, leeward, wind direction 90º 225
Fig. 5. 18. Pressure coefficients of roof without solar panels vs. top of solar panels, slope 27º, leeward, wind direction 45º 225
Fig. 5. 19. Wind velocity on a perpendicular plane under panels, with pressure coefficients contour on the structure, windward, slope 27º, clearance 10”, spacing 2”, wind speeds a) 10 m/s and b) 40 m/s..... 226
Fig. 5. 20. Pressure coefficients on a perpendicular plane under panels, windward, slope 27º, clearance 10”, spacing 2”, wind speeds a) 10 m/s and b) 40 m/s 227
Fig. 5. 21. Wind velocity distribution on a perpendicular plane and pressure coefficients on the structure, , slope 2 7º, clearance 10”, spacing 2”, wind speeds a) 10 m/s and b) 40 m/s..... 228
Fig. 5. 22. Wind velocity on a perpendicular plane under panels with pressure coefficient contours on the structure, leeward, slope 27º, clearance 10”, spacing 2”, wind speeds a) 10 m/s and b) 40 m/s..... 228
Fig. 5. 23. Pressure coefficients on a perpendicular plane under panels, leeward, slope 27º, clearance 10”, spacing 2”, wind speeds a) 10 m/s and b) 40 m/s 228
Fig. 5. 24. Pressure coefficients on a perpendicular plane and pressure coefficients on the structure, whole view from west side, slope 27º, clearance 10”, spacing 2”, wind speeds a) 10 m/s and b) 40 m/s..... 229
Fig. 5. 25. Pressure coefficients on a perpendicular plane under the solar panels, windward, and pressure coefficients on the structure, slope 27º, clearance 10”, spacing 2”, wind speeds a) 10 m/s and b) 40 m/s..... 230

Fig. 5. 26. Lines for velocity and pressure changes 230
Fig. 5. 27. Velocity streamlines at middle and west cross-section planes, slope 27º, clearance 10", spacing 2", wind speeds a) 10 m/s and b) 40 m/s 231
Fig. 5. 28. Pressure coefficients for wind direction 45º, on windward side of the roof a) Bottom surface of the panels, b) Top surface of the panels 232
Fig. 5. 29. Pressure coefficients on roof under panels, wind direction 45º, windward side 233
Fig. 5. 30. Pressure coefficients on roof, panels and building, wind direction 45º 234
Fig. 5. 31. Pressure coefficients on: a) bottom surface of the panels, b) top of the panels, wind direction 45º, leeward 234
Fig. 5. 32. Pressure coefficients on roof under panels, wind direction 45º, leeward 235
Fig. 5. 33. Velocity distribution around the panels and building along with pressure coefficients on roof, panels and building, wind direction 45º 236
Fig. 5. 34. Velocity distribution under the panels along with pressure coefficients on the bottom surface of the panels, wind direction 45º, windward side 236
Fig. 5. 35. Velocity distribution under the panels along with pressure coefficients on the bottom surface of the panels, wind direction 45º, leeward side 236
Fig. 5. 36. Vortex core distribution on roof with panels installed and around the structure, windward side 238
Fig. 5. 37. Vortex core distribution on roof with panels installed and around the structure, back view, leeward side 238
Fig. 5. 38. Vortex core distribution, on roof surface under of the panels 238
Fig. 5. 39. Vortex core distribution on top surface of the panels, windward 239
Fig. 5. 40. Vortex core distribution on bottom surface of the panels, windward 239
Fig. 5. 41. Vortex core distribution on roof with panels installed and around the structure, windward 240
Fig. 5. 42. Vortex core distribution on roof with panels installed and around the structure, back view, leeward 241
Fig. 5. 43. Vortex core distribution on roof surface under the panels, windward 241
Fig. 5. 44. Vortex core distribution on top surface of the panels, windward 242
Fig. 5. 45. Vortex core distribution on bottom surface of the panels, windward, ... 242
Fig. 5. 46. Vortex core distribution on top surface of the panels, leeward side 243
Fig. 5. 47. Vortex core distribution on bottom surface of the panels, leeward side 243
Fig. 5. 48. Wind velocity profile in the cavity and above roof along Line 1 244
Fig. 5. 49. Pressure coefficient variation in the cavity and above the panels along Line 1 244
Fig. 5. 50. Wind velocity profile in the cavity and above roof along Line 2 246
Fig. 5. 51. Pressure coefficient variation in the cavity and above the panels along Line 2 246
Fig. 5. 52. Wind velocity profile in the cavity and above roof along Line 3 247
Fig. 5. 53. Pressure coefficient variation in the cavity and above the panels along Line 3 248
Fig. 5. 54. Wind velocity profile in the cavity and above roof along Line 4 249
Fig. 5. 55. Pressure coefficient variation in the cavity and above the panels along Line 4 249
Fig. 5. 56. Wind velocity profile in the cavity and above roof along Line 5 250
Fig. 5. 57. Pressure coefficient variation in the cavity and above the panels along Line 5 251
Fig. 5. 58. Wind velocity profile in the cavity and above roof along Line 6 252
Fig. 5. 59. Pressure coefficient variation in the cavity and above the panels along Line 6 252
Fig. 5. 60. Wind velocity profile in the cavity and above roof along all 6 lines 253
Fig. 5. 61. Pressure coefficient variation in the cavity and above the panels along all 6 lines 254

Fig. 5. 62. Pressure coefficient contours top view, windward, slope 27º, wind direction 90º.... 255
Fig. 5. 63. Pressure coefficient contours top view, leeward, slope 27º, wind direction 90º 255
Fig. 5. 64. Vortex core representation for windward side of the roof, slope 27 º, wind direction 90º 256
Fig. 5. 65. Vortex core representation for leeward side of the roof, slope 27 º, wind direction 90º 256
Fig. 5. 66. Vortex core representation, isometric view, slope 27 º, wind direction 90º..... 257
Fig. 5. 67. Streamlines on middle of roof, Line 4, slope 27 º, wind direction 90º, wind speeds 10 and 40 m/s 258
Fig. 5. 68. Pressure coefficients on transverse plane on the middle of the building, slope 27 º, wind direction 90º 258
Fig. 5. 69. Roof without solar panels, slope 27 º, wind direction 90º..... 259
Fig. 5. 70. Pressure coefficients, windward and leeward sides for the roof with solar panels, slope 27 º, wind direction 90º..... 261
Fig. 5. 71. Pressure coefficients, windward and leeward sides for the roof without solar panels, slope 27 º, wind direction 90º 262
Fig. 5.72, Pressure coefficient contours of roof with solar panels, slope 27º, windward, wind direction 90º 271
Fig. 5. 73. Pressure coefficients on top of solar panels with Plines, slope 27º, windward, wind direction 90º 271
Fig. 5. 74. Pressure coefficients on a) Bottom surface of the solar panels, b) Top surface of the solar panels for slope 27º wind direction 90º, windward side 272
Fig. 5. 75. Pressure coefficients on roof under solar panels, slope 27º, windward, wind direction 90º 272
Fig. 5. 76. Pressure coefficients on roof under solar panels, slope 27º, leeward, wind direction 90º 273
Fig. 5. 77. Pressure coefficients a) Bottom surface of the solar panels, b) Top surface of the solar panels, slope 27º, leeward side, wind direction 90º 273
Fig. 5. 78. Pressure coefficients on bottom surface of solar panels vs. on roof under the panels, slope 27º, windward, wind direction 90º 275
Fig. 5. 79. Pressure coefficients on bottom surface of solar panels vs. on roof under the panels, slope 27º, windward, wind direction 45º 275
Fig. 5. 80. Pressure coefficients on roof without solar panels vs. on roof under the panels, slope 27º, windward, wind direction 90º..... 277
Fig. 5. 81. Pressure coefficients on roof without solar panels vs. on roof under the panels, slope 27º, windward, wind direction 45º..... 278
Fig. 5. 82. Pressure coefficients on bottom surface of solar panels vs. on roof without solar panels, slope 27º, windward, wind direction 90º 280
Fig. 5. 83. Pressure coefficients on bottom surface of solar panels vs. on roof without solar panels, slope 27º, windward, wind direction 45º 280
Fig. 5. 84. Pressure coefficients of roof without solar panels vs. top of solar panels, slope 27º, windward, wind direction 90º..... 282
Fig. 5. 85. Pressure coefficients of roof without solar panels vs. top of solar panels, slope 27º, windward, wind direction 45º..... 282
Fig. 5. 86. Pressure coefficients on bottom surface of solar panels vs. on roof under the panels, slope 27º, leeward, wind direction 90º..... 284

Fig. 5. 87. Pressure coefficients on bottom surface of solar panels vs. on roof under the panels, slope 27º, leeward, wind direction 45º 285
Fig. 5. 88. Pressure coefficients on roof without solar panels vs. on roof under the panels, slope 27º, leeward, wind direction 90º 286
Fig. 5. 89. Pressure coefficients on roof without solar panels vs. on roof under the panels, slope 27º, leeward, wind direction 45º 287
Fig. 5. 90. Pressure coefficients on bottom surface of solar panels vs. on roof without solar panels, slope 27º, leeward, wind direction 90º 288
Fig. 5. 91. Pressure coefficients on bottom surface of solar panels vs. on roof without solar panels, slope 27º, leeward, wind direction 45º 289
Fig. 5. 92. Pressure coefficients on roof without solar panels vs. top of solar panels, slope 27º, leeward, wind direction 90º 290
Fig. 5. 93. Pressure coefficients on roof without solar panels vs. top of solar panels, slope 27º, leeward, wind direction 45º 291
Fig. 5. 94. Velocity on a perpendicular plane under panels, wind speeds a) 10 m/s and b) 40 m/s, windward, wind direction 90º 292
Fig. 5. 95. Pressure coefficients on a perpendicular plane under panels, wind speeds a) 10 m/s and b) 40 m/s, windward, wind direction 90º 292
Fig. 5. 96. Pressure coefficients and velocity on a perpendicular plane under panels, leeward, wind direction 90º, wind speed 40 m/s 292
Fig. 5. 97. a) Pressure coefficients and b) velocity distribution on a perpendicular plane, wind speed 10m/s, wind direction 90º 293
Fig. 5. 98. a) Velocity and b) pressure coefficients on perpendicular planes, wind speed 40 m/s, wind direction 90º 293
Fig. 5. 99. Velocity on a perpendicular plane under the solar panels, wind speeds a) 10 m/s and b) 40 m/s, wind direction 90º 295
Fig. 5. 100. Pressure coefficients on a perpendicular plane under the solar panels, windward, wind speeds a) 10 m/s and b) 40 m/s, wind direction 90º 295
Fig. 5. 101. Pressure coefficients and velocity on a perpendicular plane under the solar panels, leeward, wind speed 40m/s, wind direction 90º 296
Fig. 5. 102. Velocity and pressure coefficients on a perpendicular plane under the solar panels, wind speed 40m/s wind direction 90º 297
Fig. 5. 103. a) Lines for the cavity velocity and b) streamlines, windward, wind direction 90º, wind speed 40 m/s 297
Fig. 5. 104. Velocity stream lines at middle and west cross-section planes, wind speeds a) 10 m/s and b) 40 m/s, windward, wind direction 90º 298
Fig. 5. 105. Vortex core distribution on roof with panels installed and around the structure; no building is shown 299
Fig. 5. 106. Vortex core distribution on roof under panels and around the structure, windward, wind direction 90º 299
Fig. 5. 107. Vortex core distribution on top of the panels, windward 300
Fig. 5. 108. Vortex core distribution on bottom surface of the panels, windward 300
Fig. 5. 109. Vortex core distribution on top of the panels, leeward 301
Fig. 5. 110. Vortex core distribution on bottom surface of the panels, leeward 301

Fig. 5. 111. Velocity on a perpendicular plane under panels, low wind speed, windward, wind direction 45º 302
Fig. 5. 112. Velocity on a perpendicular plane under panels, low wind speed, leeward, wind direction 45º 302
Fig. 5. 113. Velocity on a perpendicular plane above panels, low wind speed, windward, wind direction 45º 303
Fig. 5. 114. Velocity on a perpendicular plane above panels, low wind speed, leeward, wind direction 45º 303
Fig. 5. 115. Pressure coefficients on a perpendicular plane, wind direction 45º 304
Fig. 5. 116. Velocity on perpendicular plane, wind direction 45º 304
Fig. 5. 117. Pressure coefficients on whole building, roof with solar panels, slope 27º, windward, wind direction 45º 305
Fig. 5. 118. Pressure coefficients on whole building, roof with solar panels, slope 27º, leeward, wind direction 45º 305
Fig. 5. 119. Pressure coefficients on: a) bottom surface of the panels, b) top of the panels, slope 27º, windward, wind direction 45º 306
Fig. 5. 120. Pressure coefficients on: a) bottom surface of the panels, b) top of the panels, slope 27º, leeward, wind direction 45º 306
Fig. 5. 121. Pressure coefficients on roof surface under the panels, slope 27º, windward, wind direction 45º 307
Fig. 5. 122. Pressure coefficients on roof surface under the panels, slope 27º, leeward, wind direction 45º 307
Fig. 5. 123. Pressure coefficients on roof surface along with distribution of the polylines used to calculate the pressure coefficients along the 3 surfaces, slope 27º, leeward, wind direction 45º308
Fig. 5. 124. Vortex core distributions on: a) top of the panels, b) bottom surface of the panels, slope 27º, windward, wind direction 45º 308
Fig. 5. 125. Vortex core distributions on: a) top of the panels, b) bottom surface of the panels, slope 27º, leeward, wind direction 45º 309
Fig. 5. 126. Vortex core distributions on roof with panels, slope 27º, windward, wind direction 45º 309
Fig. 5. 127. Vortex core distributions on roof with panels, slope 27º, leeward, wind direction 45º 309
Fig. 5. 128. Vortex core distributions on roof under panels, slope 27º, windward, wind direction 45º 310
Fig. 5. 129. Vortex core distributions on roof under panels, slope 27º, leeward, wind direction 45º 310
Fig. 5. 130. Pressure coefficient variation in the cavity and above the panels along Line 1 311
Fig. 5. 131. Wind velocity profile in the cavity and above roof along Line 1 312
Fig. 5. 132. Wind velocity profile in the cavity and above roof along Line 2 313
Fig. 5. 133. Pressure coefficient variation in the cavity and above the panels along Line 2 313
Fig. 5. 134. Wind velocity profile in the cavity and above roof along Line 3 314
Fig. 5. 135. Pressure coefficient variation in the cavity and above the panels along Line 3 315
Fig. 5. 136. Wind velocity profile in the cavity and above roof along Line 4 316
Fig. 5. 137. Pressure coefficient variation in the cavity and above the panels along Line 4 316
Fig. 5. 138. Wind velocity profile in the cavity and above roof along Line 5 317
Fig. 5. 139. Pressure coefficient variation in the cavity and above the panels along Line 5 318

Fig. 5. 140. Wind velocity profile in the cavity and above roof along Line 6 319
Fig. 5. 141. Pressure coefficient variation in the cavity and above the panels along Line 6 319
Fig. 5. 142. Wind velocity profile in the cavity and above roof along all 6 lines 320
Fig. 5. 143. Pressure coefficient variation in the cavity and above the panels along all 6 lines. 321
Fig. 5. 144. Pressure coefficients, windward and leeward, slope 27º, wind direction 90º 322
Fig. 5. 145. Pressure coefficients, windward and leeward, slope 27º, leeward Direction 45º 322

Fig.6. 1. External and net $\boldsymbol{Cpmean}$ on the tiles on the long side of a half-cut hip roof (Habte et al., 2017) 332
Fig.6. 2. Correlation between Cp on top surface of the tiles and in the cavity Cp under tiles of a half-cut hip roof, for roof slope 18.5º (Drawn based on Habte et al., 2017) 333
Fig.6. 3. Correlation between pressure coefficients for the three pairs of surfaces, for leeward and windward sides, S2"C 3" and roof slope 35º a) Correlation values b) Location of correlation coefficients 335
Fig.6. 4. Cp as a function of one surface Cp of the other, 2" spacing, 3" clearance, slope 35º, wind direction 45º, leeward side a) Bottom of panels Vs roof surface under the panels, b) Bottom of panels Vs top of the panels c) Roof without panels Vs top of the panels 337
Fig.6. 5. Cp as a function of one surface Cp of the other, 2" spacing, 3" clearance, slope 35º, wind direction 45º, windward a) Point B, Bottom of panels Vs roof surface under the panels b) Point I, Bottom Vs top of the panels c) Point M, Roof without panels Vs top of the panels 338
Fig.6.6. Cp as a function of one surface Cp of the other, 2" spacing, 3" clearance, slope 35º, wind direction 90º, leeward side a) Point E, Bottom Vs Roof surface under the panels b) Point H, Bottom Vs Top of the panels c) Point P, Roof without panels Vs Top of the panels 339
Fig.6. 7. Cp as a function of one surface Cp of the other, 2" spacing, 3" clearance, slope 35º, wind direction 90º, windward a) Point C, Bottom of panels Vs roof surface under the panels b) Point K, bottom Vs top of the panels c) Point N, Roof without panels Vs top of the panels 340
Fig.6. 8. Cp as a function of one surface Cp of the other, 2" spacing, 3" clearance, slope 35º, wind direction 0º a) Point F, bottom Vs top of the panels, b) Point A, bottom Vs roof surface under the panels, c) Point L, Roof without panels Vs top of the panels. 341
Fig.6. 9. Correlation between pressure coefficients of the surfaces, 2" spacing, 10" clearance, slope 35º , a) Correlation values b) Location of correlation coefficients 343
Fig.6. 10. Cp as a function of one surface Cp on the other, 2" spacing, 10" clearance, slope 35º, wind direction 45º, leeward a) Point B, Bottom of the panels Vs roof surface b) Point B, Bottom Vs top of the panels c)Point L, Top of the panels Vs Roof without panels 346
Fig.6. 11. Cp as a function of one surface Cp on the other, 2" spacing, 10" clearance, slope 35º, wind direction 45º, windward a) Point D, Bottom of the panels Vs roof surface b) Point G, Bottom Vs Top of the panels (45º,WW) c) Point N, Top of the panels Vs Roof without panels 347
Fig.6. 12. Cp as a function of one surface Cp on the other, 2" spacing, 10" clearance, slope 35º, wind direction 90º, leeward a) Point C Bottom of panel Vs roof surface b) Point J Bottom Vs Top of the panels c) Point M, Top of the panels Vs Roof without panels 348

Fig.6. 13. Cp as a function of one surface Cp of the other, 2" spacing, 10" clearance, slope 35º, wind direction 90º, windward a) point E, Bottom of panel Vs roof surface b) Point H, Bottom Vs Top of the panels c) Point O Top of the panels Vs Roof Without panels..... 349
Fig.6. 14. Cp as a function of one surface Cp on the other, 2" spacing, 10" clearance, slope 35º, wind direction 0.0º a) Point A, Bottom of panel Vs roof surface b) Point K, Top of the panels Vs Without panels Roof c) Point F Roof without panels Vs Top of the panels..... 350
Fig.6. 15. Section view of double-layer system and sketch of pressure equalization (Oh, PhD thesis, 2014). 353
Fig.6. 16. Schematics of pressure equalization mechanism a) Pressure equalization on the panels, b) Pressure equalization in the cavity 354
Fig.6. 17. Nominal Net Pressure Coefficients, for Low-Profile Solar Photovoltaic Arrays on Flat Roofs (SEAOC PV2-2012)..... 359
Fig.6. 18. Area based Net Cp on solar panels, this research, spacing 2”, clearance 3”..... 361
Fig.6. 19. Normalized Area based Net Cp on solar panels, this research, spacing 2”, clearance 3” 362
Fig.6. 20. External peak composite pressure-gust coefficients, CpCg, on single-span gabled and hipped roofs, slope of 7° or greater for the design of structural components and cladding (NBC Structural Commentaries, 2015, Part 4 of Division B). 363
Fig.6. 21. Area based total Cp, this research, spacing 2”, C 3”..... 364
Fig.6. 22. Total Cp, Normalized area, (m^2) based, this research, spacing 2”, clearance 3” 364

LIST OF TABLES

Table 1. 1. Analysis matrix and the simulation cases to be performed 9

Table 3. 1. Characteristics of different fine and coarse meshes used in the simulations..... 43
Table 3. 2. Pressure coefficients comparison on four points on the PL19, top of the panels, windward side, for different meshes. 43
Table 3. 3. Comparison between Holmes (2001) full scale and Current CFD study 68

Table 4. 1 . Pressure coefficients on roof without panels vs. resultant pressure coefficients on roof under solar panels, slope 35º, wind direction 45º, windward side..... 129
Table 4. 2 . Pressure coefficients on roof without panels vs. total resultant pressure coefficients on roof under solar panels, slope 35º, wind direction 45º, Leeward side 130
Table 4. 3 . Pressure coefficients on roof without panels vs. total resultant pressure coefficients on roof under solar panels, slope 35º, wind direction 90º, windward side 131
Table 4. 4 . Pressure coefficients on roof without panels vs. total resultant pressure coefficients on roof under solar panels, slope 35º, wind direction 90º, Leeward side 132
Table 4. 5 . Pressure coefficients on roof without panels vs. total resultant pressure coefficients on roof under solar panels, slope 35º, wind direction 0º..... 133
Table 4. 6 . Pressure coefficients on roof without panels vs. total resultant pressure coefficients on roof under solar panels, slope 27º, wind direction 90º, windward side 188
Table 4. 7 . Pressure coefficients on roof without panels vs. total resultant pressure coefficients on roof under solar panels, slope 27º, wind direction 90º, Leeward side 189
Table 4. 8 . Pressure coefficients on roof without panels vs. total resultant pressure coefficients on roof under solar panels, slope 27º, wind direction 45º, windward side 190
Table 4. 9 . Pressure coefficients on roof without panels vs. total resultant pressure coefficients on roof under solar panels, slope 27º, wind direction 45º, leeward side 191
Table 4. 10 . Pressure coefficients on roof without panels vs. total resultant pressure coefficients on roof under solar panels, slope 27º, wind direction 0º..... 192
Table 4. 11 . Pressure coefficients on roof without panels vs. total resultant pressure coefficients on roof under solar panels, slope 15º, wind direction 90º, windward side 196
Table 4. 12 . Pressure coefficients on roof without panels vs. total resultant pressure coefficients on roof under solar panels, slope 15º, wind direction 90º, leeward side 197
Table 4. 13 . Pressure coefficients on roof without panels vs. total resultant pressure coefficients on roof under solar panels, slope 15º, wind direction 45º, windward side 198
Table 4. 14 . Pressure coefficients on roof without panels vs. total resultant pressure coefficients on roof under solar panels, slope 15º, wind direction 45º, leeward side 198
Table 4. 15 . Pressure coefficients on roof without panels vs. total resultant pressure coefficients on roof under solar panels, slope 15º, wind direction 0º..... 199
Table 4. 16. Velocity value along height at inlet based on power law, open terrain, mean wind speed 40 m/s..... 204

Table 4. 17. Effects of BL and constant velocity profiles applied at inlet, on solar panel surfaces, roof surface, net Cp and total Cp, windward, 90° WD, 35° slope, 2" spacing and 3" clearance. 207

Table 5. 1. Pressure coefficients for roof without solar panels vs. net pressure coefficients for the roof-panels system, slope 27º, 90º, windward side 263
Table 5. 2. Pressure coefficients for roof without solar panels vs. net pressure coefficients for the roof-panels system, slope 27º, wind direction 90º, leeward side 263
Table 5. 3. Pressure coefficients for roof without solar panels vs. net pressure coefficients for the roof-panels system, slope 27º, wind direction º45, windward side 264
Table 5. 4. Pressure coefficients for roof without solar panels vs. net pressure coefficients for the roof-panels system, slope 27º, wind direction 45º, leeward 265
Table 5. 5. Pressure coefficients for roof without solar panels vs. net pressure coefficients for the roof-panels system, slope 27º, wind direction 0º 266
Table 5. 6. Pressure coefficients for roof without solar panels vs. total pressure coefficients, slope 27º, wind direction 90º, windward 323
Table 5. 7. Pressure coefficients for roof without solar panels vs. total pressure coefficients, slope 27º, wind direction 90º, leeward 324
Table 5. 8. Pressure coefficients for roof without solar panels vs. total pressure coefficients, slope 27º, wind direction 45º, windward 324
Table 5. 9. Pressure coefficients for roof without solar panels vs. total pressure coefficients, slope 27º, wind direction 45º, leeward 325
Table 5. 10. Pressure coefficients for roof without solar panels vs. total pressure coefficients, slope 27º, wind direction 0º 326

Table 6. 1. Derived Cp values from Fig. 1.6 of Habte et al. (2017) 333
Table 6. 2. Cp on top and bottom surfaces of solar panels, and on the roof surface under the panels, for clearance 10", spacing 2" 344

CHAPTER 1: Introduction

1.1 Wind effects on roofs and PV solar panels

Photovoltaic (PV) solar panels are solar energy collection systems, which nowadays are widely used and can be found on numerous residential and agricultural buildings. The PV panels can be installed on the ground, or on buildings' rooftops, as either singular panels or as part of multi-panel array systems. Usually, the panels are inclined such that a better exposure to sunlight can be achieved; and as such they can have different azimuth inclination angles with respect to the sunlight and wind directions. Design recommendations for wind-induced loadings on PV solar panels arrays are not fully developed in current wind loading standards (SEAOC PV2-2012) and building codes (ASCE 07, NBCC 2015), primarily due to the limited research activities investigating this topic. To reduce cost and overall gravity loads on roofs, PV solar panels are designed and manufactured to be as light as possible. The structural system consisting of PV solar panels and support frames must be adequately anchored to the roof structure in order to resist the wind loads imparted on the building.

When estimating the wind effects on structures, it is generally agreed that forces and responses in the along-wind (drag) and cross-wind (lift) directions (Fig.1) are of primary interest (Holmes et al, 2001).

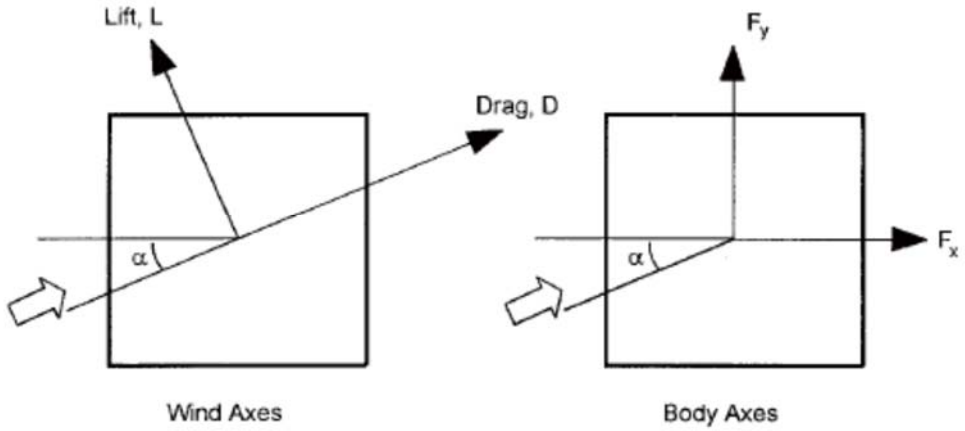


Fig. 1.1. Wind loading components, (Holmes et al, 2001).

Dynamic effects of the wind-induced forces on structures are caused by the fluctuation in the air flow, also referred to as gustiness, and their interaction with the structure (Höffer et al, 2007). Gustiness in wind may increase considerably by natural topography and human made obstacles (Holmes, 2001). The large wind flow eddies formed by interaction with a structural system (such as whole building, or roof) envelope the structure and generate correlated wind-induced pressures around the structure (Mendis et al, 2007). Small eddies affect small parts of the structure and result in uncorrelated pressures (Mendis et al, 2007). When a flat roof support solar panels, turbulence may increase on the entire roof (Radu et al, 1986). Furthermore, an increase in the tilt angle of solar panels or distance between rows of panels mounted on flat roofs increases, the panel-generated turbulences intensify, causing larger wind loads (Kopp et al, 2012, Cao et al, 2013).

For a better visualisation of the wind-structure interaction and vortex formations, typical wind flow around bluff (rectangular) and streamlined (air foil) objects are presented in Figures 1.2 and 1.3, respectively (Holmes, 2001). At the windward edge of the object, where the flow approaches the structure, a stagnation point, consisting of constant pressure of high magnitude, is formed.

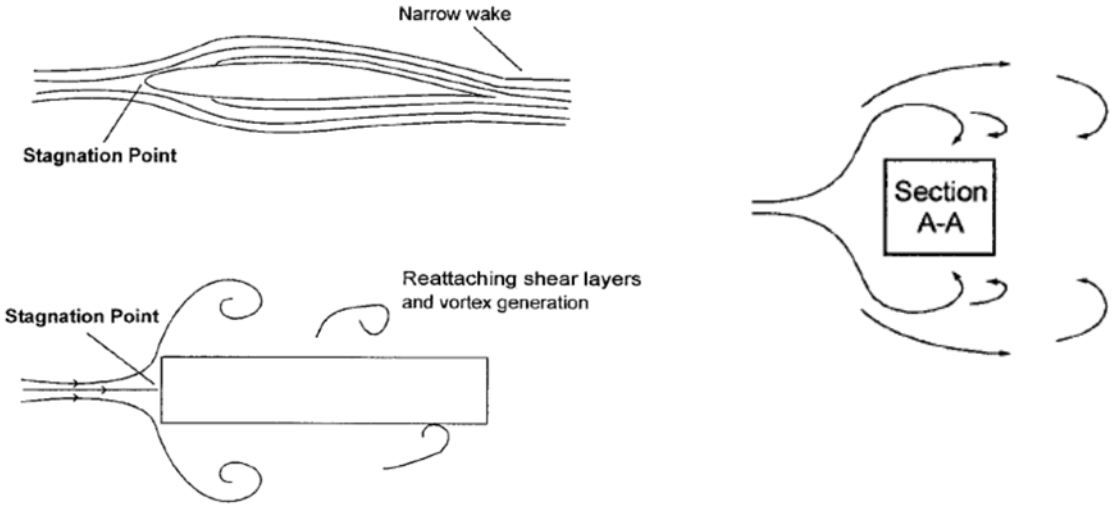


Fig. 1.2. Wind typical flow around a bluff and streamlined objects (Holmes, 2001)

For streamlined objects, uniform shear layers are formed close to the foil contour, separated from free stream by a thin layer of air, and a narrow wake is developed at the leeward tail. However, for bluff bodies (representative of most buildings), a flow separation occurs at the leading edges (Holmes, 2001).

In case of a typical structure exposed to a uniform streamlined flow, the separated shear layers are close to the object's surface. These layers will detach from the corners of the structure or at the rear side of the building, forming a trail of vortices, as can be seen in Fig. 1.3.

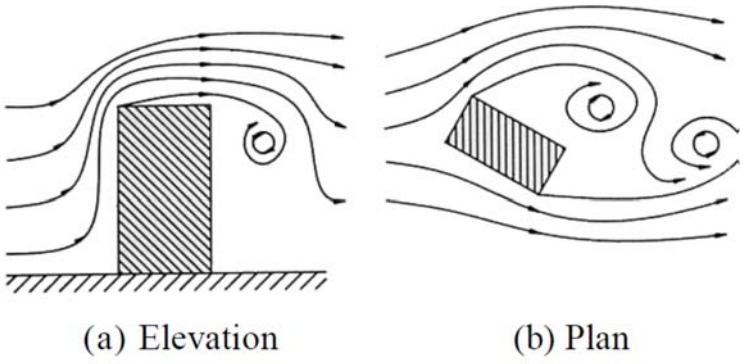


Fig. 1.3. Generation of eddies, typical bluff structure (Mendis et al, 2007).

Figure 1.4 shows the main features of the wind flow around low-rise buildings with an inclined roof. The flow separates at the windward edge of the roof and may re-attach to the roof surface at a certain distance, creating a separation "bubble" where a suction region is formed. For roof slopes greater than 20°, positive mean pressures can be recorded on the windward roof surface, and fully separated shear layers without re-attachment can occur on the leeward surface of the roof, which results in negative mean pressures (Holmes, 2001).

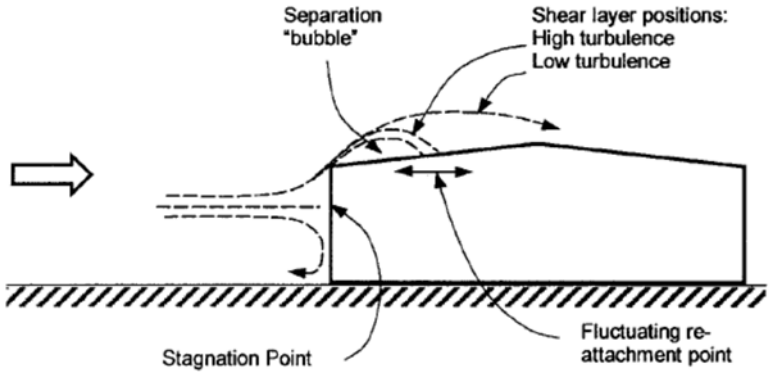


Fig. 1.4. Wind flow around a low-rise building with pitched roof, (Holmes, 2001)

In the cross-wind direction, the vortex shedding develops at the corner of the roof and travels along its edges (Fig. 1.5), potentially causing additional wind loads (Holmes, 2001).

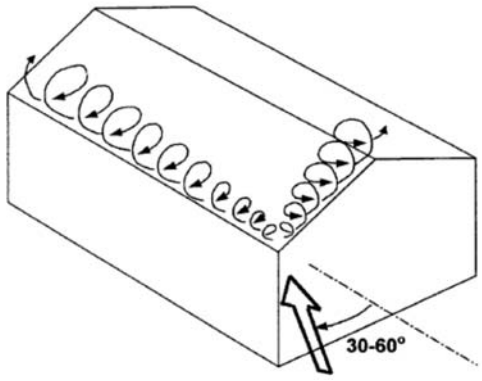


Fig. 1.5. Conical vortices for oblique wind directions, (Holmes, 2001)

1.2 Installation methods for PV solar panels

The installation method and geometry of the PV panels can have a significant effect on the wind flow formations on the roof surface and thereby implicitly affect the wind-induced pressure on both the roof surface as well as the solar panels. PV solar panels installed on flat roofs typically have inclination angles of up to 35° (SEAOC, 2012), however this can vary with the geographical location. For PV solar panels mounted on inclined roofs flush-mounted panels, which are generally parallel to the roof surface, are used. Panels mounted on flat roofs are installed either with fixed or adjustable tilts varying their inclination with the season in order to achieve optimum exposure to sunlight. The flush-mounted PV solar panels are limited by the roof slopes and thus their orientation and efficiency are dictated by the geometry of the roof. Flush-mounted PV panels are the most commonly encountered solar energy systems for inclined roof, due to convenience in application and design.

PV solar panel arrays mounted on inclined roofs are installed on supporting rails, which are fixed to the roofs using footings (Fig. 1.6). The footings are fixed directly to the inclined roof rafters or to the roof truss top chords (UNIRAC, 2014). The height of the mounting rails and of the footings typically ranges between 3” and 10” (76 mm to 254 mm) as shown in Figs. 1.7. Since the height of the panels is typically about 2”, the total height of the system measured from top surface of the panels to the pitched roof surface usually varies between 5” and 12”.

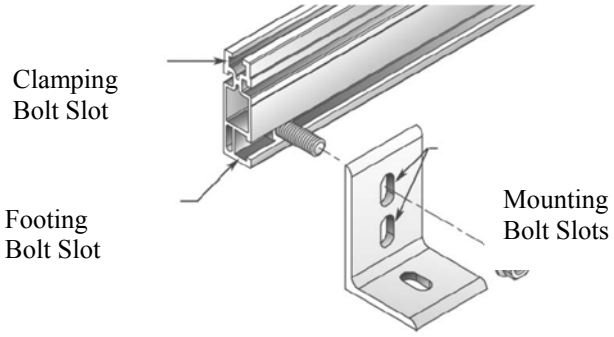
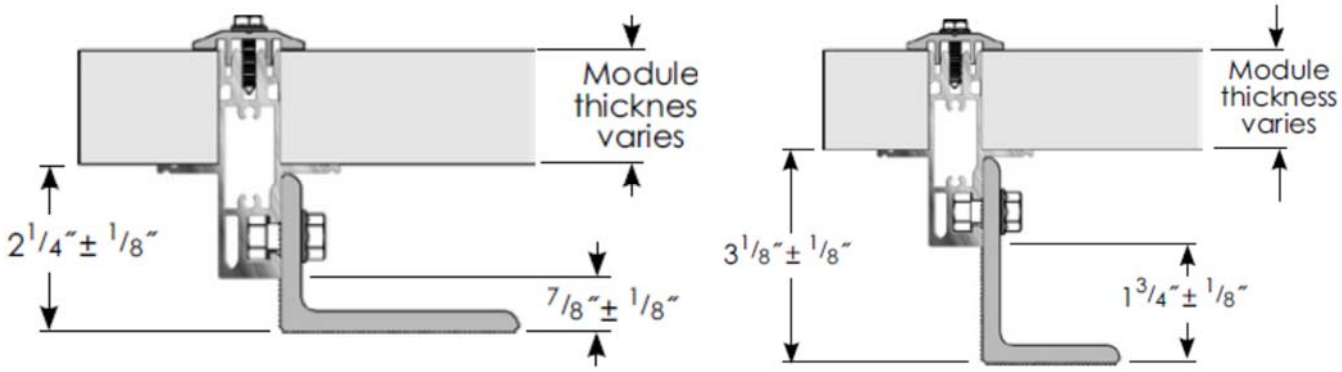
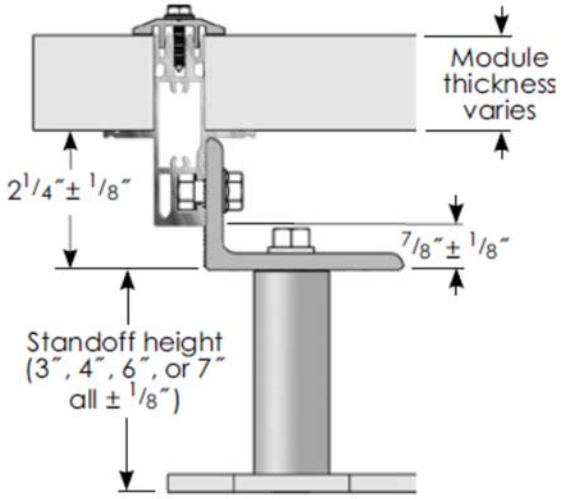


Fig. 1.6. Typical rail-foot attachments for solar panels, (UNIRAC, 2014)



(a)



(b)

Fig. 1. 7. PV solar panels connection to roofs a) With brackets, b) With standoffs (Unirac, 2014)

Incorrect installation or wrong design and application of the brackets and connecting fasteners could lead to cracking of the PV solar panel surface, as shown in Fig. 1.9, while a faulty installation rack would lead to partial or total dislocation of the PV solar panels, especially under the effect of strong winds (Fig. 1.10). Developing a full and accurate understanding of the wind flow around the solar panels is crucial to avoid such costly damage.

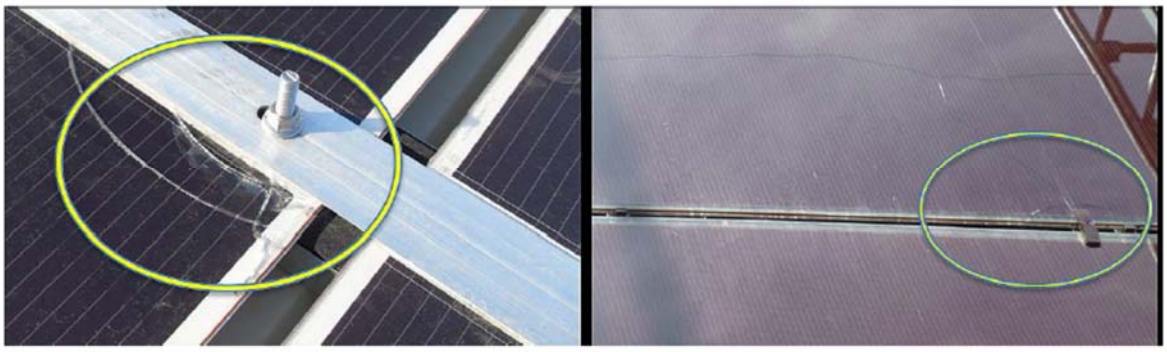


Fig. 1. 8. Examples of PV solar panels failures (IEA-PVPS T13-01, 2014)



Fig.1.9. Examples of PV solar panels and the installation system failures (http://runonsun.com/~runons5/blogs/blog1.php/solworks/safety/solar-trumps-windstorm-part-2)

1.3. Research motivation

PV solar panels on flat roofs have been widely investigated in the literature, and numerous wind tunnels experiments have studied different orientations and boundary conditions of solar panels (e.g. Banks, 2013; Geurts et al, 2007, 2008, 2009, and 2013; Kopp et al, 2013; Cao et al, 2013). However, only scarce experimental and numerical research exist for the PV solar panels mounted on gable roofs (Kopp et al, 2012). In addition, none of the existing wind tunnel and numerical studies have addressed the effect on the wind-induced pressures caused by the change in the mounting system parameters. From a design point of view, it is important to note that guidelines

for PV solar panels installed on building roofs currently require that the same design procedure as that applicable to bare roofs are implemented, (e.g. Solar Ready 2013), and (TPIC 2012). The assumption that the pressure distribution on the roof is unaffected by the presence of the solar panels has not yet been verified and may lead to significant underestimation of the design loads. Current common practice is that PV solar panels installed on inclined roofs are parallel to the roof surfaces, in order to eliminate shading effects from adjacent panels, and to increase exposure to sunlight. From a wind design perspective, similar pressure coefficients are used for the PV solar panels, as the ones recommended by design codes for the inclined roof structures (e.g. NBCC, 2015). Such assumption implies that the flush-mounted panels (parallel to roof surface) behave as the roof itself under wind loading, ignoring the arrangements of the PV solar panels arrays, inclinations and distance between the roof and the panels. There is a need to investigate the wind effects on PV solar panels in order to achieve a safe and economical design which will allow for wider use these solar systems on inclined roofs especially for low-rise residential buildings.

The majority of research studies have been investigating the wind effects on PV solar panels on reduced models, scaled by 1:50, 1:100, and 1:200. However, for solar panels mounted on ground, wind tunnel model scales of 1:20 to 1:30 were recommended by Bitsuamlak et al (2013). Discrepancies were reported between wind tunnel experiments conducted on small scales of 1:50 to 1:500 (Stathopoulos et al, 1983). Only a limited number of studies reporting full scale results for wind effects on solar panels are available; however, these were conducted only for one or two solar panels, due to the wind tunnel dimensions limitations. The current study aims to bridge the gap by considering on the effects of rows of full-scale solar panels with different configurations and layouts on inclined room systems. Detailed objectives are discussed in the next section.

1.4. Research objectives and scope

The main goal of the current research is to determine the pressure coefficients on gable roof mounted solar panels, and their supporting roofs with different slopes and wind directions. In order to achieve this goal the following objectives were identified :

1. Determine the effects of slope, and wind directions, on the Cp of the solar panels and the supporting roofs and identify the critical slope and wind direction combinations.

2. Determine the effects of mounting parameters using the critical combinations of roof slope and wind direction determined in objective 1.
3. Compare the net Cp on the solar panels, and total pressure on the supporting roof with Cp on roofs without solar panels of similar slopes, and investigate the effects of mounting parameters on the Cp.

The current research project did not consider the wind effects on tilted solar panels mounted on gable roofs; only the flush mounted solar panels on gable roofs were investigated. Also, another limitation was related to the computational efficiency offered by the desktop DELL i7 which was used for the current simulations. Thus, only the CFD algorithms which achieved convergence on this desktop, could be employed for the solar panels on gable roofs models.

A comprehensive database of pressure coefficients on the PV solar panels with different installation parameters and subjected to wind loading will be developed under the current research project. A total of 90 simulation cases will be generated, including 72 cases for roof mounted solar panels, and 18 cases performed on inclined roofs without solar panels. Other parameters considered include different combinations of roof slope, wind directions, spaces between panels and distances from roofs, and wind speed magnitudes. Inclination of the solar panels with respect to the inclined roof surface, and the effects of tilting the solar panels (rotation of panels around an axis perpendicular to the roof surfaces) are considered beyond the scope of the current study. The omission is mainly due to these cases being uncommon in practice.

Performing experimental work to fully investigate the wind pressure distribution on solar panels mounted on inclined roofs would be impractical when considering the time and cost associated with such endeavour. Employing Computational Fluid Dynamics (CFD) modelling would significantly reduce the cost and the time for obtaining very similar results, if the appropriate CFD model for PV solar panels is developed. The study therefore aims to develop and validate a CFD model for the inclined roofs of different configurations, using the results reported in the literature from full-scale measurements, as well as from the wind tunnel experiments, prior to conducting the detailed parametric analysis CFD models.

1.5. Research methodology

CFD simulations will be carried out for inclined gable roofs and the results will be compared with those reported in the literature. CFD models and simulations will be performed for solar panel arrays mounted on different inclined gable roofs, in order to capture the effect on pressure due to changes with the roof slopes and different installation methods of the PV solar panels. This involves varying the mounting distance between the solar panels and the roof surface as well as roof inclination, while employing different turbulent flow algorithms.

The current research will compare the average peak wind pressure coefficients obtained from the CFD analyses with those obtained from full-scale experiments on buildings with inclined roofs reported in the literature, in order to validate the developed CFD model. Once validated, the CFD model will be used to generate pressure coefficients developed specifically for inclined roofs with PV solar panels. CFD analyses will be carried out for solar panels mounted on roofs with slopes of 15˚, 27˚and 35°. Wind directions of 45˚and 90˚will be considered, and the effect of the space between the solar panels' rows will be investigated for the assumed distances of 2" (51 mm) and 8" (203 mm). Solar panels installed on standoffs are also considered in the current study, and the effect of the clearance height defined as the distances between the solar panels and the roof surface will be analyzed, for the standard spacing of 3" (76 mm), and 10" (254 mm). Applied wind speeds will be 40 m/s, and 10 m/s. Table 1.1 summarizes the analysis matrix which will be followed in the current research study.

Table 1. 1. Analysis matrix and the simulation cases to be performed

Roof Slope Angle	Wind directions	PV panels rows spacing	Clearance between PV panels - Roof	Inclination angle PV panel - Roof	Wind speed
15˚	0º, 45º, 90º	2", 8"	3", 10"	0°	10, 40 m/s
27˚	0º, 45º, 90º	2", 8"	3",10"	0°	10, 40 m/s
35˚	0º, 45º, 90º	2", 8"	3", 10"	0°	10, 40 m/s

CHAPTER 2 Literature review

2.1. Mean wind speed profiles logarithmic and power laws

The rate of change of the average wind speed, U, can be described as a function of the boundary layer height above ground, Z, the surface shear stresses, τ_0 , and the air density, ρ_a. τ_0 is the friction stress between ground surface and the flow. Equation (1) represents the Logarithmic Law for the wind speed profile as described by Holmes, (2001):

$$\frac{\partial U}{\partial Z} Z \sqrt{\frac{\rho_a}{\tau_0}} = constant = \frac{1}{k} \Rightarrow U_Z = \frac{u^*}{k}(\log Z - \log Z_0) = \frac{u^*}{k}\log(\frac{Z}{Z_0}) \quad (1)$$

$$where \quad u^* = \sqrt{\frac{\tau_0}{\rho_a}} \text{ is friction velocity,} \quad (2)$$

Z_0 is the integration constant with the length dimension, also known as the roughness length of the ground surface. K is the Von Karman's constant. ρ_a is air density.

The wind speed profile can also be approximated by the Power Law (Holmes, 2001), as given in Eq. (3). α in Eq. 3 is the exponential coefficient of the Power Law and is defined in Eq. (4):

$$\frac{U_Z}{U_{10}} = \left(\frac{Z}{10}\right)^{\alpha} \quad (3)$$

$$\alpha = \frac{1}{\log\left(\frac{Z_{ref}}{Z_0}\right)} \quad (4)$$

Where $U_z \; and \; U_{10}$, are the velocities at height Z near ground and at $Z_{ref} = 10\ m$ above ground, respectively.

Fig. 2.1 illustrates the wind speed profile calculated using the Logarithmic and Power Laws and shows a slight difference between the two approaches. In Fig. 2.1, Z_{ref} is assumed to be 10 m and $U_z \; and \; U_{10}$, are explained above.

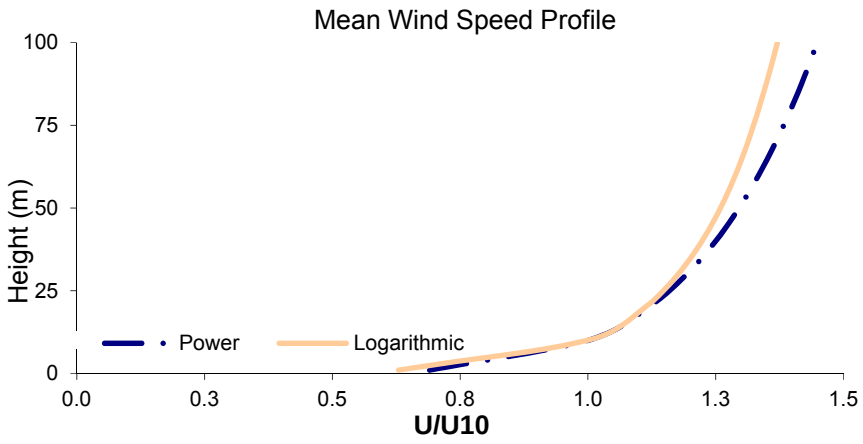


Fig. 2.1. Two Laws to Calculate Mean Wind Speed at Different Heights (m) for exposure "C" Open Terrain or Grass Land or Land with Few Trees.

2.2. Turbulence intensity

A parameter characterizing gustiness in the wind flow is the turbulence intensity I_u which is defined as the ratio between the standard deviation, σ_u of the wind speed and the mean wind speed for a given direction:

$$I_u = \frac{\sigma_u}{\overline{U}} \tag{5}$$

Where $\overline{U}$ is the mean velocity in the longitudinal direction.

σ_u is standard deviation of wind speed as defined in Eq. (6),

$$\sigma_u = \frac{1}{T}\left(\int_0^T \left[U_t - \overline{U}\right]^2\right)^{\frac{1}{2}} \tag{6}$$

Where U_t is the velocity total component in direction of mean wind, $\overline{U}$, $U_t = \overline{U} + u(t)$ where u(t) is the fluctuating velocity component along longitudinal axis u (Holmes, 2001).

2.3. Code development for wind load effect on roofs

Investigating along-wind response of roofs started with a study performed by Davenport (1961), where the mean value of the maximum along-wind displacement was expressed by estimating

the product of the mean static displacement with a non-dimensional constant coefficient, defined as the Gust Response Factor (GRF). Davenport (1961) also defined the Equivalent Static Force (ESF) as a wind-induced force which produces a corresponding maximum along-wind displacement in the structure. This approach became the basis for most of the wind design codes (e.g. NBCC 2015, ASCE 2010, and SEAOC 2012).

The National Building Code of Canada (2015) details the wind design for gable roofs by dividing them into three groups according to the slope: first group addresses quasi-flat slopes with pitch of $0° < \propto \leq 7°$, second group includes intermediate slopes of $7° < \propto \leq 27°$ and the third group includes high pitched roofs of $27° < \propto \leq 45°$. For each of the groups, the NBCC (2015) recommends wind-induced pressures coefficients on the roof surface, as an external peak coefficient combined with the pressure-gust coefficients ($C_p C_g$). Charts and graphical representations for $C_p C_g$ coefficients are provided for different roof regions: edges, corners and internal surface of the roof. At the time of writing of this thesis, the NBCC did not contain any provisions related to the design of PV solar panels.
The Structural Engineers Association of California (SEAOC) contains pressure coefficient charts, compatible with the ASCE- 07 provisions, which can be used for the wind design of solar panels installed on rooftops (SEAOC, 2012). The code stipulates that the minimum distance between the solar panels and the edge of the roof is to be taken as 4ft or $2(h_2 - h_{pt})$ whichever is greater, where h_2 is the height of the solar array above the roof surface, for roofs without parapets, and h_{pt} is the mean height of the parapet, measured from the roof surface. In general, wind pressure coefficients on edges and at the corners of the roofs are higher than in middle of the roofs, which is consistent with pressure coefficients for roofs with no solar panels incurrent design codes (e.g. ASCE 7-10, NBCC 2015).

2.3.1. Pressure coefficient

NBC 2015 defines the pressure coefficient as follows:

"Pressure coefficients are the non-dimensional ratios of actual wind –induced pressures on a building surface to the velocity pressure of the wind at the reference height. They account for the

effects of aerodynamic shape of the building, orientation of the surface with respect to the wind flow, and profile of the wind velocity." (NBC 2015)

That is expressed as $C_p = \frac{p-p_0}{1/2 \rho_a U_0^2}$ (Holmes 2011).

Where $p-p_0 = p_t$ is wind induced pressure on the surface and

U_0 is reference velocity.

Then pressure calculated as $qC_e(C_gC_p)$ NBC (2015)

Where

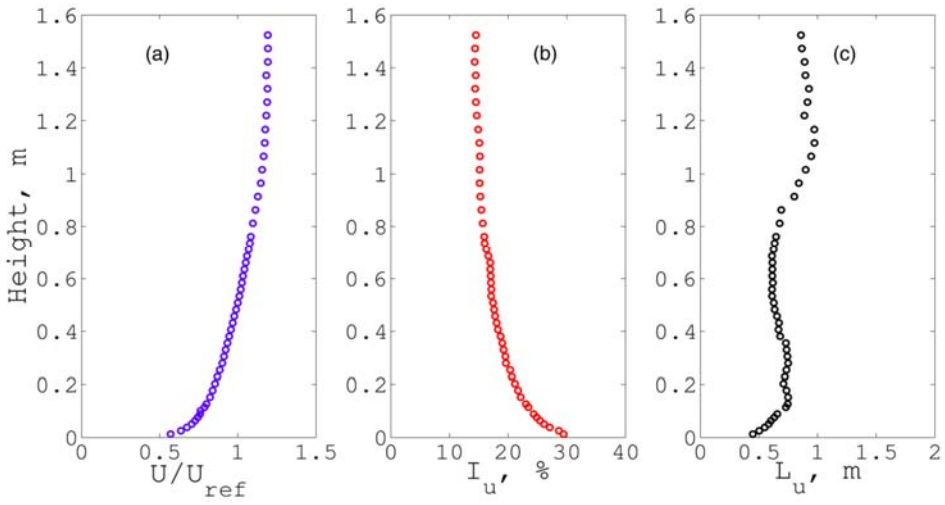
$$q = \frac{1}{2}\rho V^2$$

"The reference wind speeds are nominal one-hour averages of wind speeds representative of the 10 m height in flat open terrain" NBC (2015). The primary records are compilation of hourly averaged wind speeds, 10 minutes average (surface stations) and 2 minutes average wind speeds. Peak wind gusts recorded for 3-7 seconds and used to supplement the primary records.
The records should be adjusted to have 1% probability of being exceeded in 50 years.
The pressure coefficient formula above is the one used in the current study.

2.4. Wind effects on solar panels

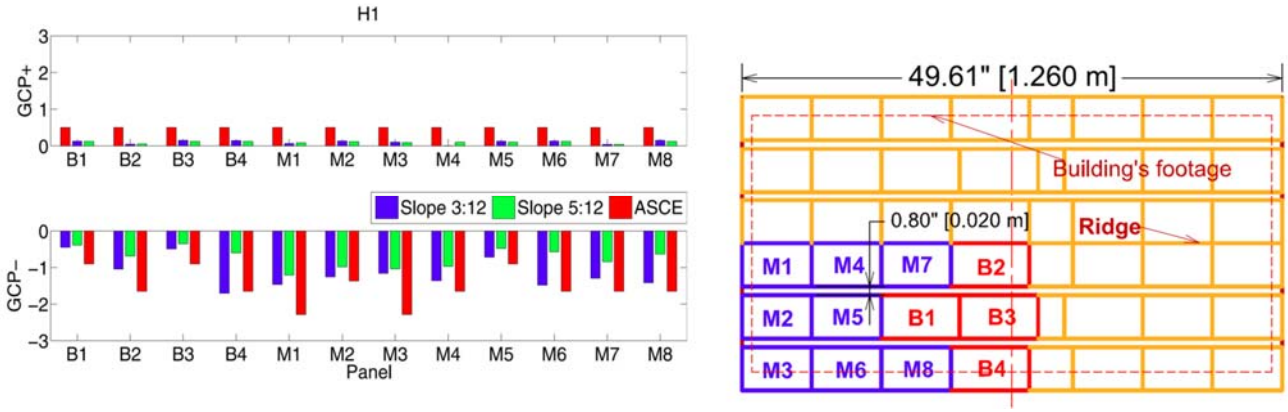
2.4.1. CFD and wind tunnel studies for gable roof mounted solar panels

Bitsuamlak et al. (2014) conducted boundary layer (Fig. 2.2) wind tunnel tests on solar panels mounted on gable roofs with 14° and 22.6° slopes. The distances between panel arrays were 20% of the panel width, while clearance from the roof was 6" (150 mm). Two vertical and two horizontal configurations were investigated. The pressure taps were installed on part of the roof, as shown in Fig. 2.3. b and no pressure data measurements were available for the rest of the roof. Also, the study did not investigate the roof surface under the panels. The authors concluded that there was 25 - 47 % reduction in net pressure on the panels mounted in zone 1, in comparison with the external pressure on roof without panels as presented in ASCE 7-2010 for slopes between 7° and 27°, Fig. 2.3 a.



(a) (b) (c)

Fig. 2. 2 Wind tunnel velocity (a) mean wind speed profile; (b) turbulence intensity profile; (c) integral length scale; Bitsuamlak et al (2014).



(a) (b)

Fig. 2. 3. (a) Maximum and minimum pressure coefficients and comparison with external pressure on roof without panels in the ASCE 7-2010 (ASCE 2010) (7° < slope <27°); (b) solar panel modules (H1) mounted on gable roofs with slopes 3:12 (14°) or 4/12 (22.6°), Bitsuamlak et al (2014).

Stenabaugh (2015) conducted an experimental boundary layer, (Fig. 2.4) wind tunnel study on 30° gable roof, where solar panels were installed on a corner of the leeward side (1/6 roof area) of the roof, Fig. 2.5. The study used shrouds around the solar panel array to prevent outside airflow from directly entering the cavity between the solar panels and the roof. This study focused on the

pressure induced at the top surface of the panels and cavity pressure. The author concluded that net pressure on the panels has smaller magnitude than the external pressure, with proportional distribution to that of the external pressure. It was also found that increasing the spacing between panel rows resulted in higher pressure equalization than increasing the height of the clearance between the panels and roof.

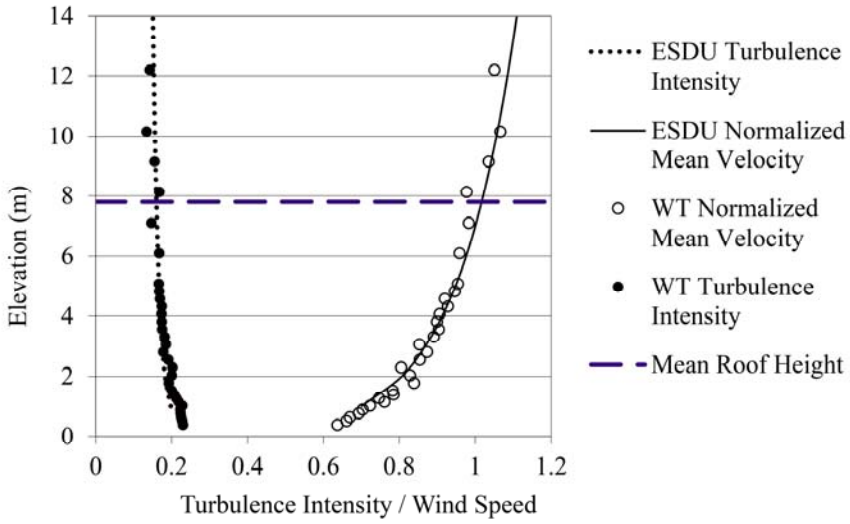


Fig. 2. 4. Mean wind speed and turbulence intensity profiles (Stenabaugh, 2015)

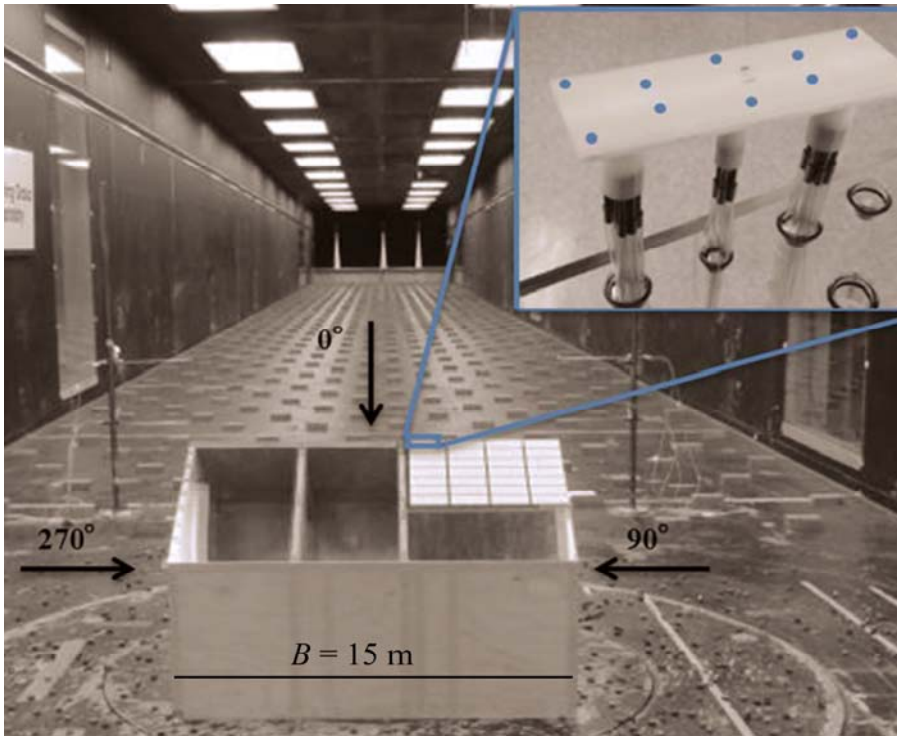


Fig. 2. 5. Sloped roof model (Stenabaugh, 2015).

A CFD investigation, conducted by Chowdhury et al, (2018) focused on clarifying the effects of gaps between the wind speed near solar panels and roofs, and the effect of the support structure side walls on the wind flow pattern on the top and back of the solar panels mounted on the mono-sloped roof . In addition, the study analyzed the effects of irregularities of the solar panels on the wind speeds around the models. The study used RANS (K-ε) for the CFD simulation and the results were verified by wind tunnel tests and a satisfactory agreement was found between the CFD simulations and the wind tunnel tests results. The study used the boundary layer profile and turbulence intensity as shown in Fig.2.6 (a) and (b) for five different wind speeds.

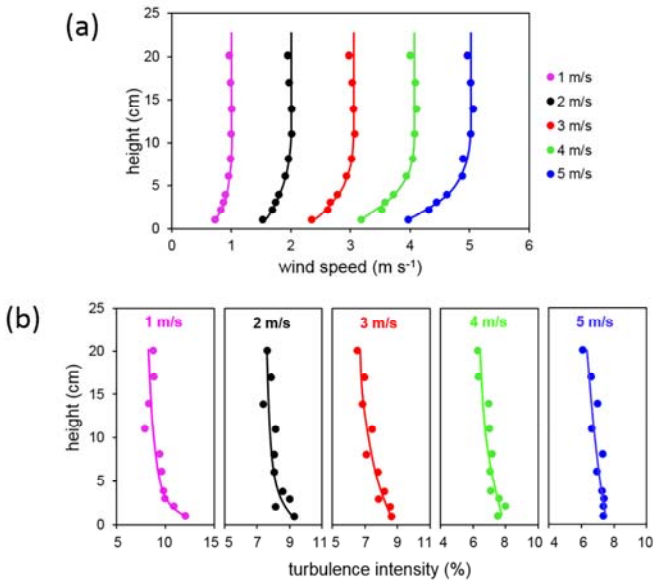


Fig. 2. 6. (a) Wind velocity profiles. Dots represent the experimental data; solid lines are the CFD profiles. (b) Turbulence intensity profiles. (Chowdhury et al, 2018)

Chowdhury et al, (2018) found that narrow gaps, between the roof and bottom of the solar panels, reduce the velocities near top and bottom of the panels. The study showed that the CFD simulations should include the irregularities in the solar panels in order to have more reliable results. The spacing between the solar panels was not investigated in this study.

A CFD study investigating the possibility of retrofitting building roofs with aerodynamic features and solar panels to reduce hurricane damage, was performed by Aly et al, (2017). The study

investigated the effect of parapets, circular edges, inclined edges, airfoil edges and installation of solar panels on the interior areas of the flat and gable roofs. The study found that the installation of solar panels away from the edges of the roofs reduced the uplift forces on the entire roofs and on the solar panels themselves. The boundary layer velocity profiles and turbulence intensity shown in the Fig. 2.7.

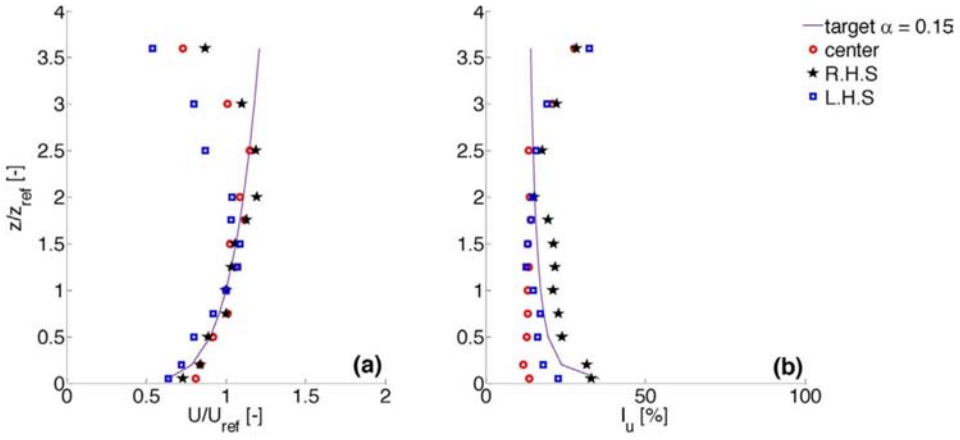


Fig. 2. 7. (a) turbulence intensity (b) profiles at 2H from the exit of the blowers, (Aly et al, 2017)

2.4.2. CFD and wind tunnel studies for flat roof mounted solar panels

Geurts et al (2010) conducted a wind tunnel study and CFD modelling of wind pressures on solar energy systems mounted on flat roofs. The CFD used RANS algorithm, constant velocity and turbulence quantities at the top of the boundary were derived from mean reference velocity and experimental surface roughness. The authors concluded that in comparison with the wind tunnel experiments performed for all turbulence models, the pressure distribution is predicted well by the CFD simulations. In addition, the effects of solar panels installed in different locations, and their orientations are well reproduced in the CFD model. The largest differences between the CFD and the wind tunnel tests performed for all models, were in the wake side of the systems that have a large spacing.

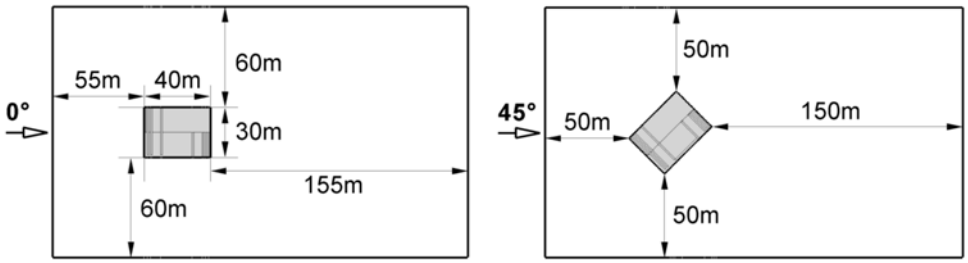


Fig. 2. 8. Computational domain, (Geurts et al, 2010)

Banks (2013) performed tests on a model representing a 10 m high building with a roof area of 60m by 60 m, on which PV solar panel arrays of 20 m x 20 m were installed. The roof had 1.0 m high parapet on the edge. Nine different configurations were investigated, and they showed that the corner vortices dictate the peak wind loads on inclined solar panels (0°-20°). The author varied the direction of wind with respect to the tested solar panel array in a wind tunnel, from 0° to 180°. Fig. 2.9 illustrates the peak uplift contours that resulted from the corner vortices at dark and sunny regions of the array. Capital letters indicate regions initiated at dark or sunny sides and small letters indicate whether vortices are strong or weak. The peak uplift forces represented in Fig. 2.9. were obtained for along wind vortices formed along the 50° direction, while many solar panels that were situated farther from the vortex corner, were not affected by the high uplift. The study also found that the peak uplift is dictated by the direction of the panels' inclination relative to the vortex swirl, the position of the panel relative to the vortex reattachment, and the proximity of the panel to the vortex-generating corner of the array.

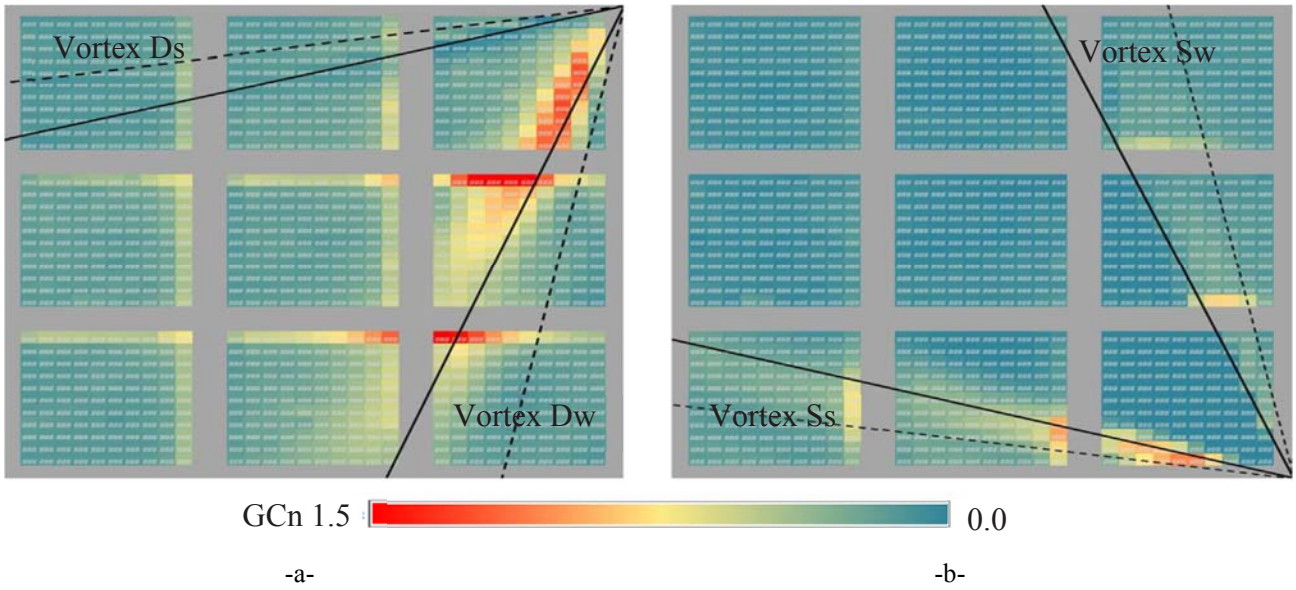


Fig. 2. 9. Peak uplift contours, with vortex identifier labels, (a) Wind direction 50°and (b) Wind direction 140° (Banks, 2013).

Alrawashdeh and Stathopoulos (2016) conducted a comprehensive literature review comparing the latest results reported for flat roof mounted solar panels under the effect of wind loads. They reviewed eleven wind tunnel test results for different building sizes, roof slopes, array inclinations, as well as size and spacing of the solar panels rows. The authors pointed out large discrepancies, up to a factor of 2, between the results and highlighted the presence of contradictory statements among the reported studies. Furthermore, the authors emphasized the need for further studies on the effects geometric test scale on the results of wind pressures recorded on solar panels in wind tunnels. It was also noted that studies on the wind effects on roof mounted solar panels are lacking.

Pratt and Kopp (2013) studied the wind flow velocity profiles formed over and around flat roof mounted PV solar panels, tilted at 2° and 20°, and using a model scale of 1:30. The actual building height was 7.3 m, and the solar panel arrays consisted of 12 rows, each containing 12 solar panels. The reference wind speed in the wind tunnel was approximately 15 m/s. The authors noted that no fundamental changes in mean wind speed occurred due to the installation of the inclined PV solar panel arrays, compared to the bare roof. It was also reported that for small tilt angle (2°) arrays, peak uplift was generated mainly by the same vortices that caused the peak uplift on bare roofs.

However, for larger tilt angle (20°) arrays, separated shear layers generated by the building geometry, reattached near the solar panels and caused local flows.

Cao et. al. (2013) investigated PV solar arrays mounted on flat roofs to establish the effect of the panel tilt angle, distance between arrays, location of the panels on the roof, roof depth and parapet height. The model scale was 1:50 for a medium-rise building with a flat roof of full-scale dimensions of 25 m (B) x 25 m (D) x 20 m (H). Only two instrumented arrays, of dimensions 7 m x 2 m, were installed while the remaining ones were without pressure taps. The authors found that the suction measured for one single panel located in the middle of the roof, were larger than those located on corners and edges of the roof. The authors also noted that the pressure coefficients decreased with the distance from the roof edges for a flat roof mounted multi-array solar panels. Increasing the tilt angles of the solar panels, increased the panel-generated turbulence, and consequently the suction acting on the panel arrays also increased. In addition, increasing the space between the arrays, consolidated the panel-generated turbulence, leading to an increase in the wind-induced forces. The study also reported that the effects of the roof depth on the force coefficient on the panels could be negligible.

Geurts and Blackmore (2008) conducted wind tunnel tests on a 1:100 scaled model of solar panel arrays mounted on flat roof of a low-rise building. The authors found that when the spacing between the panels and the roof were changed from 3.0 mm to 0.25 mm, the net wind pressure coefficients on the panels changed from 0.24 to -0.31. This pressure variation, from positive to negative values, revealed the significance of the spacing between the mounted solar panels and the roof surface. The effect of the spacing between the solar panels and the roof will also be investigated in the current study based on CFD models developed for solar panels on inclined roofs.

Geurts and Steenbergen (2009) conducted a full-scale study on two PV solar panels equipped with 12 pressure taps. Each panel had dimensions of 1.6 m (length) x 0.8 m (width) x 0.018 m (thickness) and was placed 0.15 m away from the roof surface. The panels were mounted on the roof with inclination of 42°. One panel was attached to southern side (150°) and the second panel

was mounted on western side (240°) of the roof. The authors noted that the absolute values of minima and maxima pressure coefficients measured on the same panel were slightly reduced when the period increased. However, mean pressure coefficients remain nearly constant for both panels and wind directions. The authors concluded that when comparison is made between full-scale and wind tunnels or CFD analyses, the mean pressure obtained for different periods is expected to be almost constant for specific average wind speed.

Stathopoulos et al, (2014 and 2015) conducted a wind tunnel study in order to examine the wind-induced loads on solar panel systems mounted on flat roofs. The aim of the work was to better understand the wind pressure distribution on stand-alone panel surfaces and panels attached to flat building roofs. The authors evaluated the most critical net effect through investigating the top and bottom pressure time histories obtained from the pressure taps. The study also examined the effects of panel inclination, panel location and building height. The author concluded that the wind direction of 135 degrees experienced the highest peak pressure coefficients. The panel inclination was found to affect the pressure coefficient. It was reported that for panels located at the ground level, increasing panel inclination results in greater suction. This was also observed for panels attached to 7 m and 16 m high buildings, located at the back of the roof. For front-located panels attached to 7 m and 16 m high building roofs, suction was reported to be smaller with increasing panel inclination. In general, back located panels suffered higher suction than front located panels.

Kopp et al (2012) performed a wind-tunnel study on 12 rows of solar panels array model, scaled by 1:30. Arrays were placed on ground as well as flat roof in order to distinguish array generated aerodynamic effects from building generated effects. The study emphasized that the wind-induced pressure is affected by two different mechanisms, namely, turbulence generated by the solar panel, and the pressure equalization between top and bottom of the panels. The study showed that for higher tilt angles (20º), the turbulence increased the net wind loads on roof, while for low tilt angles (2º), pressure equalization seemed to dominate. The presence of building was investigated, and the results showed that the building cause significant changes to the aerodynamic loads compared to ground-mounted systems. The interaction was found to be dependent by several parameters, mainly the building height, and the setback of the array from the roof edge. The author noted that

for cornering winds, there is a complex interaction between the flow generated at the array edge and the building-generated corner vortices, so that larger array setbacks can have very high loads, as for arrays with narrower setbacks. This observation was contrary to that found for the same array placed on the ground. It was therefore concluded that array zoning would be different for roof-mounted arrays bare roofs, and ground-mounted array fields. It was also found that the net roof loading was not significantly altered by the presence of arrays. It was found that uplift loads on the roof were slightly reduced for larger areas because of

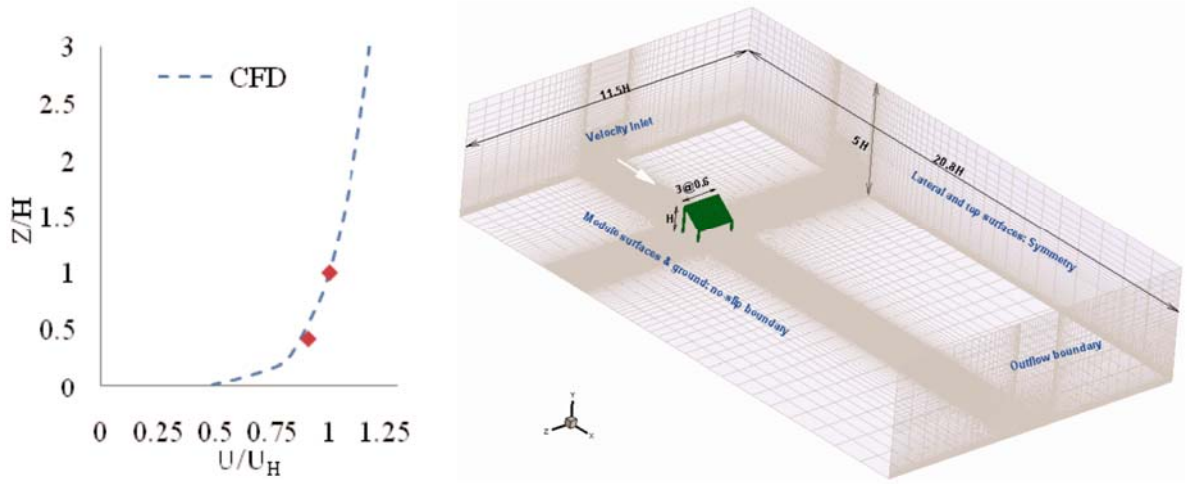
Kopp et al (2013) investigated the wind field around solar arrays mounted on flat roofs, in order to better understand the flow structures and aerodynamic mechanisms. The study was focused on wind directions that would result in critical loads on panels within the separation bubble. Two panel tilt angles, 2º and 20º, were examined. The authors reported that the mean flow was not significantly different between a building with and without solar panels installed on the roof. It was found that the 2º array shortened the mean reattachment length slightly in comparison with the bare roof. For the 20º array experienced a reattachment at approximately the same location as the bare roof. Contrarily, it was reported that the array had a significant effect on the turbulence above and around the panels. For small tilt angle arrays this local flow is established by large-scale building generated vortices, while for the larger tilt angle arrays the instantaneous reattachment of the building generated separated shear layer sets up the local flow.

2.4.3. CFD and wind tunnel studies for ground roof mounted solar panels

CFD and full-scale tests on two stand-alone solar panels mounted on ground and inclined at 40° were conducted by Bitsuamlak et al (2010) to evaluate wind loads on the solar panel modules.

The study compared mean Cp on the solar panels obtained from CFD simulations, employing the LES algorithm and the mean pressures measured from the Wind of Wall (WoW) experiment. The study found that panels were subjected to highest Cp, when wind blew from the back of the panels (180°). When the solar panels were arranged in tandem, the sheltering effect influenced the pressure coefficients, when wind approached from the front (0°), thus the Cp reduced substantially

on the panels surface. The boundary layer wind profile used in the CFD model in this study are shown below in Fig. 2.10.



(a) **(b)**

Fig. 2. 10. (a) CFD inlet velocity mean wind speed profile and experimental wind speeds (b) Computational domain, boundary conditions of stand-alone solar panel (Bitsuamlak et al, 2010)

Irtaza et al (2018) conducted a CFD simulation of turbulent wind effect on an array of ground-mounted solar PV panels, using RNG and RANS K-ε algorithms. The simulated wind velocity profile had a power law coefficient (α) of 0.15, longitudinal turbulence intensity of 15% used for inlet boundary condition. The study found the highest pressure was in the wind direction 90° and -90° (perpendicular to the rows) and that the net pressure increases with increasing the array tilt angle.

Shademan et al (2009), studied wind loading on solar panels mounted on ground at different inclination angles. The study used CFD-RANS simulations with the boundary layer wind profile and 0.16 turbulence intensity, applied in the computational domain shown in the Fig. 2.11. The study shows that the sheltering effects are highest when the gap between two subsequent panels in tandem is equal to the length of the panel.

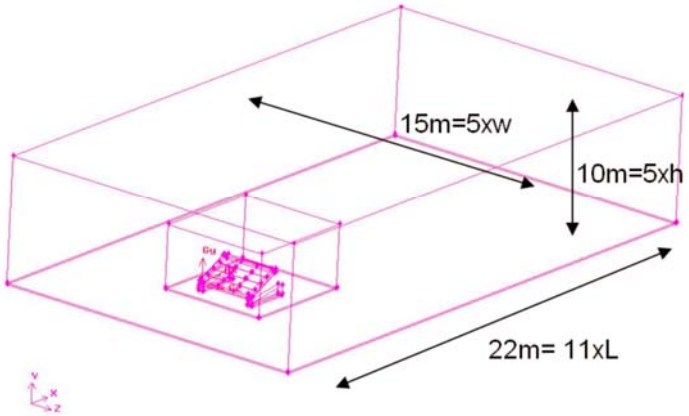


Fig. 2. 11. Computational domain size and boundary conditions in the CFD (Shademan et al, 2009)

Reina et al (2017), studied the computational evaluation of mean wind loads on sun-tracking ground-mounted photovoltaic panel array. The CFD study uses 26 m/s reference wind speed at 10 m height and the logarithmic law boundary layer velocity profile at the inlet. In addition, this study used the computational domain shown in Fig. 2.12 and the RANS algorithm to simulate the cases.

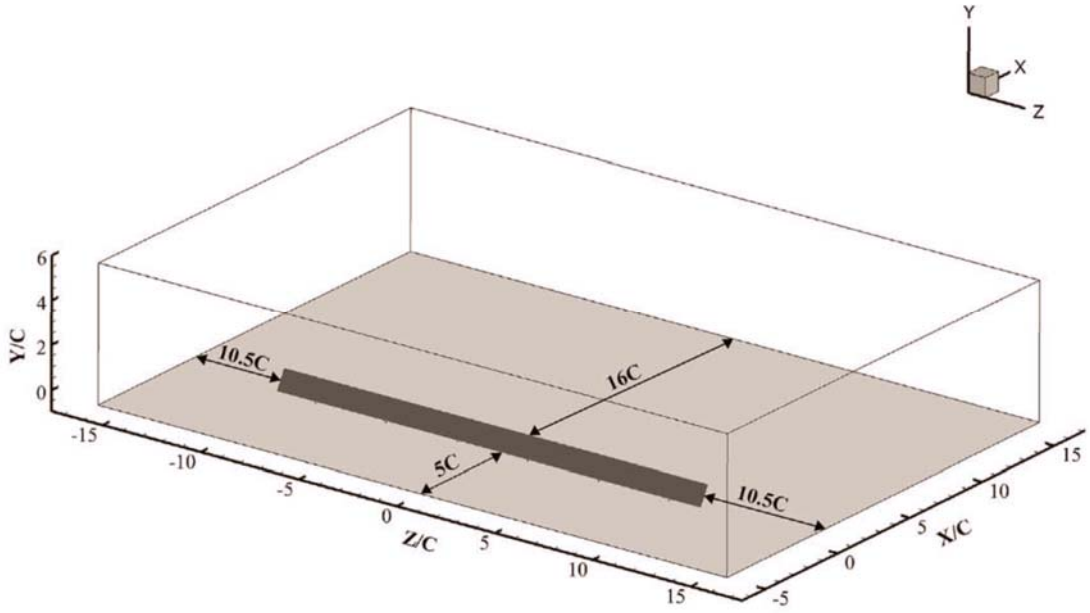


Fig. 2. 12. Computational domain, (Reina et al, 2017)

The study found that dynamic meshing technique could determine the history of aerodynamic loads on the panels due to sun-tracking movement around the horizontal axis. Also the results of

the mean aerodynamic loads are in good agreement with the static simulation results for corresponding tilt angle.

Chowdhury et al, (2016) investigated wind loading on an array of ground mounted solar photovoltaic (PV) panels using numerical approach. RANS, k-ε algorithm is used for the analysis, using boundary layer wind speed at the inlet in the computational domain shown in Fig. 2.13. The study concluded that the first row for the windward side is subjected to the highest loads for all wind directions (0°, 45°, 135° and 180°), while the middle rows are subjected to higher loads for the oblique wind directions (45° and 135°). The highest wind loads registered on the first row were for the wind directions 0° and 180°. In addition, corner vortices were observed on the leeward sides of all five rows for the oblique wind directions 45° and 135°.

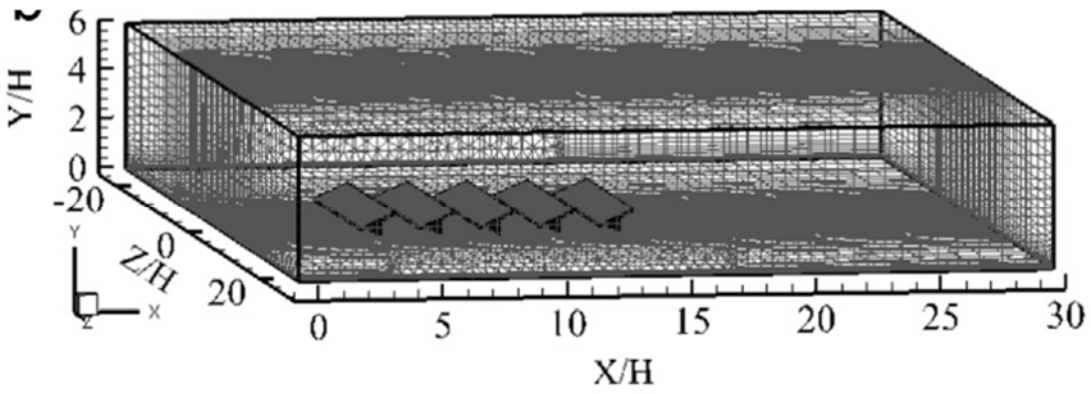


Fig. 2. 13. Computational domain, (Chowdhury et al, 2016)

Aly M. A. (2016), conducted a CFD study to evaluate the wind loads on ground mounted solar panels by modelling a CFD virtual wind tunnel which has exact size of the physical one. The study used a virtual wind tunnel (26 m x 2.4 m x 2.15 m , near the outlet) while the height of the gap above the model to the boundary of the computational domain is 7.5*H* (*H* is the maximum height of the full-scale ground mounted solar panel), Fig. 2.14. Lateral boundary distance is 3.3*W* (where *W* is the crosswind dimension of the solar panel). The inflow boundary was 6.8H, and the

outflow boundary was at 13.6H downstream the panel. The study used boundary layer velocity profile and Reynolds Stress Model algorithm to obtain the main loads on the ground-mounted solar panels while LES algorithm was used for the peak loads, Fig. 2.15.

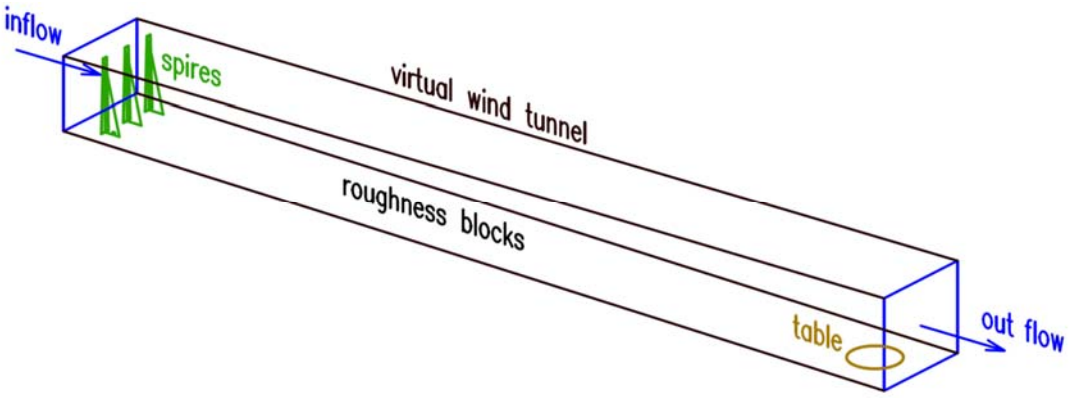


Fig. 2. 14. Computational domain, (Aly M. A., 2016)

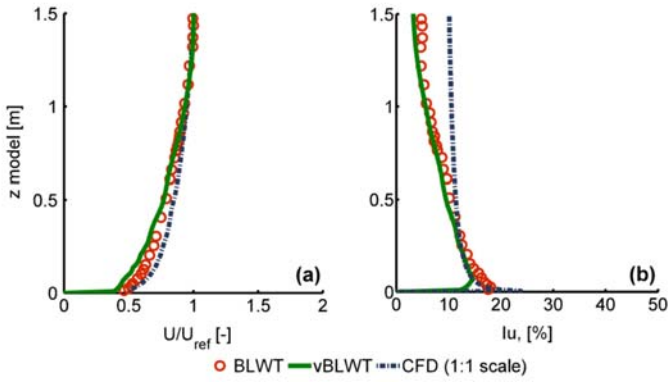


Fig. 2. 15. CFD wind speed profiles and measured BLWT profiles for open terrain: (a) mean velocity profile and (b) turbulence intensity profile(Aly M. A., 2016).

The author concluded that the mean pressure coefficients are not significantly affected by the model size (1:50, 1:30, 1:20, and 1:10) with excellent agreement between the CFD simulations and the experimental results. However, the peak pressures were affected by both geometric scale and inflow turbulence. In addition, the peak pressures recorded in BLWT testing were low

compared to the LES generated peak pressures. The study proposed using 3-sec data analysis approach to minimize discrepancies in estimating the peak loads.

While it is generaly assumed that flush-mounted solar panels are subjected to wind loads of similar magnitude and pattern as those on the supporting roofs with no panels (Radu et al, 1986), no comprehensive investigaiton has studied whether the gaps between the PV solar panels rows and between the panels and the roof surface have any effect on such assumption. Also, although numerouse studies have been undertaken on panels inclined with respect to flat surface, the literature on flush-mounted PV solar panels on inclined roofs is scarce. Schellenberg, et al, (2013) conducted dynamic analyses and tests on PV solar panels arrays of 12 rows with 12 panels on each row. The PV solar panels were inclined at 20° with respect to the surface they were installed on. The authors conducted free vibration tests to estimate the equivalent viscous damping ratios and the periods of vibrations caused by small initial displacements, as shown in Fig. 2.16. The authors estimated the equivalent damping ratio for slippage by conducting large displacement tests. The first 1.5 loading cycle was used to calculate the damping during the slippage, while the next four cycles were used to calculate the overall damping during the free vibration test. As a result, the authors determined that the damping of the PV solar panels array for small vibrations was 1%- 4% and for large vibrations was 8%-12% (Schellenberg, et al, 2013).

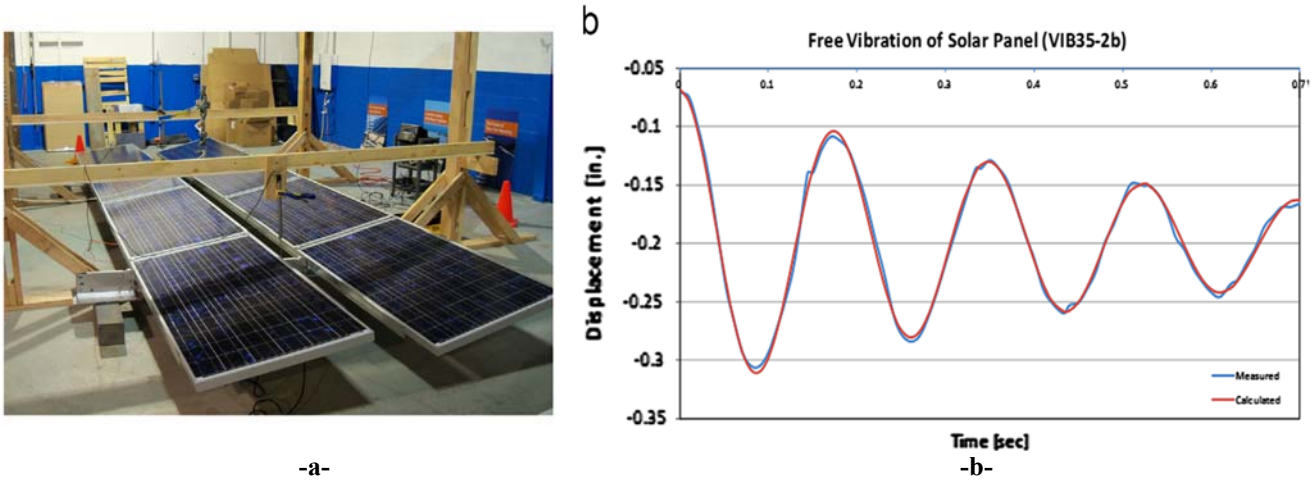


Fig. 2. 16. Free vibration test, (a) Test setup, and (b) Damped response (Schellenberg et al, 2013).

The experimental tests estimated the first mode frequency as 4.0 Hz, which was close to 3.94 Hz value determined from the FE model. Moreover, the study noted that dynamic analysis, which

incorporates damping ratios, provided more realistic values of displacement and forces. From a static analysis, higher displacements were obtained when compared with the dynamic analysis.

A full-scale experimental study was performed by Samani (2016) on 2 ground mounted solar panels inclined at 25º from horizontal. Several wind directions were considered between 0º and 180º. Sensitivity analyses were also performed on both pressure and force measurements. The authors also developed a Finite element model of the solar panels and the wind obtained from the experimental testing was applied in the model. The rack design was also evaluated, and the internal stresses of the rack elements were determined.

The results from the study showed symmetry in the pressure distribution on the model at 0º and 180º wind angles about the center line, where most critical positive and negative values were obtained in these two directions. For oblique angles the mean pressure distribution showed a separated region for both 45º and 135º wind angles of attack which confirmed possible existence of corner vortices. However, the suction pressures at the top panel for 135º was found to be more critical.

The author emphasized that the mean pressure cannot solely represent the critical wind angle of attack, and maximum and minimum Cp contour plots are also required for general conclusions.

The study also compared the experimental result with the ASCE-7 provisions and showed that the code requirements offer a good estimation for the drag force applied on a solar panel if the parameter are correctly chosen.

The FEA analysis showed that the reaction forces directly obtained from force balances were more reliable compared to those obtained from the pressure taps.

2.5. Pressure equalization phenomenon

Pressure equalization is a phenomenon that occurs in multi-layer systems, where existing gaps in those layers permit the external wind pressures to be transmitted to interior layers, which leads to reduction of the net loads.

Bienkiewicz and Sun (1992) conducted an experimental study on the effects of wind loading on loose laid paver system. The system was installed on a flat roof of a low-rise building. The focus of the study was on the distribution of correlation of external and underneath pressures. The effects of a void space under pavers on the pressure distribution and the pressure correlation was also investigated. The study found that generally the underneath pressure distribution for pavers without spacers was similar to the external pressure distribution. The authors also noted that the underneath pressure distribution was significantly altered when a void space was introduced underneath pavers. The correlation between the external and underneath pressures was high along the roof edges except for the pavers near the roof corner. It was also found that the time history of the underneath pressure was very similar to that of the external pressure.

Choi et. al. (1998) developed a numerical model capable of predicting the cavity pressure in curtain wall systems. The model includes a front-panel (rain screen) and back-panel (air barrier) based on Helmholtz resonator theory. The study showed that there was an increase in cavity pressure when the vent area increased for all pressure frequencies and for any material of back panels, whether flexible or rigid. The study also showed that the material stiffness of the back panel largely affects the cavity pressure ratio, where rigid material resonates at high pressure frequencies and at much higher values than flexible material.

The effects of vent area on pressure ratio indicates that a proportional relationship exist between change in vent area and pressure ratio (cavity pressure to external pressure). The findings also demonstrate significant changes in pressure ratio when vent factor (ratio of opening in rain screen to void volume) changes slightly in the low frequency domain which implies a significant impact of vent area on pressure equalization.

Geurts et al, 2013 performed full scale and wind tunnel experiments to determine the net uplift loads on stand-off PV systems. The study investigated the effect of distance between panel and roof through an experimental study in the wind-tunnel. The authors reported that the effect of distance between PV system and roof surface is relatively small and that the loads on the underlying roof are not significantly higher or lower compared to the case without system. The results from both the wind-tunnel and full-scale measurements showed

that there is a high level of correlation between the wind pressures on the top and bottom surfaces of the PV modules. It was noted that differences between panels were found in the full-scale measurements and the distribution of the loads with respect to the angle of attack differed in full scale and wind tunnel experiment. The maximum and minimum values for the net loads were found to be in the same order of magnitude.
Form a design perspective, the net pressure coefficients were found to be considerably smaller than the values recommended for use in design in current guidance.

Kopp et al (2015) studied the pressure distributions on the external and internal surfaces of the outer layer of an air-permeable, double-layer roof system. The study aimed to investigate the effects of the gaps between panels, cavity depth between layers, and the panel size on the pressures and panel loads. Wind tunnel-based experimental data from the model of a low-rise building in an open country terrain were used. Several configurations were examined and it was found that the cavity pressure distributions were significantly affected by the geometric parameters. The study found that the mean pressure distribution on the internal surfaces of the cavity was significantly affected by geometric parameters of the multi-layer system. It was also found that cavity pressures were uniform for smaller gap to cavity depth ratios but vary approximately linearly within the cavity for larger ratios. The authors noted that larger models or increased wind tunnel speeds could be used to improve the match to full-scale.

Stenabaugh (2015) studied effects of change in height of panels (clearance) and in gaps (spacing) between panels mounted on flat or inclined (30 º) mono-sloped roofs.
The author noted that the mean net pressure decreased when the panel height decreases. This finding is consistent with that reported by Kopp et al, (2015). In addition, when gaps increased beyond 2 cm, the mean net pressure decreases (and pressure equalization increases) very slightly for all cavity heights. Contrarily, the study found that when the gap decreased, the mean net pressure increased.

2.5. Conclusions

The literature review performed in this chapter presented several wind tunnel experiments performed on solar panels mounted on gable and flat roofs. In addition, one full-scale experiment

on individual solar panels mounted on inclined roof was also reported. A brief introduction of the wind design recommendations for building roof was presented along with the current design guidelines used for solar panels mounted on building roofs, focusing on medium and low-rise buildings. The published experimental studies performed on solar panels acknowledged the existence of scale effect for the solar panels. Only very few studies conducted full-scale studies for wind effects on solar panels, reporting results for layouts limited to only one or two solar panels. Almost all existing literature which dealt with pressure equalization addressed flat roofs using either experimental, CFD or both. However, these studies did not investigate the pressure on roof surface under the panels, nor the resultant pressure on both top and bottom faces of panels, as well as on the roof surface beneath the panels.

CHAPTER 3: CFD Modeling and simulations

In order to simulate the wind effects on roofs with PV solar panels, Computational Fluid Dynamics (CFD) simulations were employed and pressure coefficients were determined for different wind speeds and geometry conditions. Reynolds-Averaged Navier-Stokes (RANS) models help provide a reasonable approach to solving these complex, turbulent flows by modeling turbulence as fluctuations within a steady, average velocity field (ANSYS Users Guide, 2015). In addition, the RANS are accurate near the surfaces (Bitsuamlak et al , 2013) which is the case in the simulations of this research. The turbulent specifications of 5% intensity and 10% viscosity assumed in the model to represent medium-turbulence intensity flow (ANSYS Users Guide 2015) were deemed appropriate for this application.

Large Eddy Simulation (LES) is commonly used due to their accuracy in describing the flow in the separation bubbles. LES is largely used by the academic community, but has limited application in industrial simulations (where RANS are widely used). The reason is excessive computational effort.

Limitations: Desktop DELL I7 with 16 GB RAM was used successfully to run the CFD analyses with K-ε algorithm, especially for the models with solar panels, which presented a more complicated geometry. The CFD simulation employing LES algorithm was attempted on the same desktop, however these did not converge for the roofs with solar panels cases, due to the complicated geometry. The corresponding cases of roofs without solar panels were modeled with same RANS, k-ε for consistency and in order to minimize errors.

For low-rise buildings, the separation region is small, and CFD using $k-\varepsilon$ model shows good agreement with the experimental data (Staphopoulos et al, 1995). On the other hand, installation of solar array on flat roofs initiates local turbulences above and around the panels in the separation bubbles and that reduces the turbulence intensity around those panels.

The turbulence models of Reynolds-Averaged Navier Stokes, RANS, have been developed to estimate the mean flow field with the introduction of eddy viscosity to the simulation to mimic the effect of turbulence (ANSYS Users Guide, 2015).Subsequently, in this study, RANS is considered as appropriate for calculating mean values of pressure and velocity of the flow, and to capture the turbulence characteristics throughout the models. That is in compliance with NBC 2015 which calculates the average reference velocities based on average one-hour records.

To validate the CFD model and the k-ε algorithm, three models consisting of a full-scale test on a canopy (Robertson et al 2010), a full scale and wind tunnel experiment on a residential building (Doudak 2011) and an existing residential building by (Holmes 2001) were investigated and compared. Verification of LES algorithm was done on a full scale on a residential by Zisis (2011) and another full scale on a residential building by Apperley et al, (1979). After validating the CFD models additional 40 analyses cases were investigated for the model residential building with PV solar panels mounted on the roof under different configurations. For comparison purpose, other corresponding 12 cases for roofs without solar panels were investigated.

3.1. CFD Modeling validation

3.1.1. Mesh details and model's geometry validation

For each of the investigated cases, computational domains were developed as closed rectangular prism fields with dimensions of 41L x 41B x (H+50) m, where L, B and H are length, width and height of the modeled building respectively. Thus, the computational domains for the building investigated by Zisis (2011), and Doudak (2011) was 17.2 m x 8.6 m x 4.8 m which resulted in total computational domain dimensions of 705m x 355m x 54.8m (Fig. 3.1). Typical model mesh used 735,058 tetrahedral cells, 1,448,971 triangular faces connected to 133,578 nodes. Minimum cell edge length varied for each model but was, in general, approximately 0.0092 m in the model representing the building investigated by Zisis (2011) and Doudak et al (2011), as shown in Fig.3.2. Similarly, computational domain for the model representing the buildings tested by Holmes (2011) consisted of 12m x 8m x 7.9m. The domain was developed as a closed rectangular prism field with dimensions of 492 m x 328 m x 57.9 m, as shown in Fig. 3.3. Typical model mesh used 594.172 tetrahedral cells, 1,178,316 triangular faces connected to 104,698 nodes. Minimum cell edge length varied for each model but was in general approximately 0.1 m in the model representing the building investigated by Holmes (2011) (Fig.3.4).

The computational domain for the canopy structure investigated by Robertson et al (1985) was developed as a closed rectangular prism field with dimensions of 21L x 21B x (H+50) m which is different from the computational domains of the other two structures. The reason for this

discrepancy is that the canopy is an open wall structure that generates significantly less turbulence than the aforementioned structures. This yields a computational domain size of 510.3m x 210m x 57.2m based on a canopy model size of 24.3 m length × 11.0 m width × 7.52 m height (Fig.3.5). Typical model mesh used 4,230,809 tetrahedral cells, 8,253,581 triangular faces connected to 809,422 nodes. Minimum cell edge length varied for each model but was in general approximately 0.0034 m in the model representing the building investigated by Robertson et al (1985) (Fig. 3.6).

The k-ε and LES algorithms were used, as part of the commercial software Fluent ANSYS. Several cases were considered for wind flow angles of attack of 0°, 45°, and 90° relative to the ridge of the building models, and for three different roof slopes of 15°, 27° and 35°. The wind speeds considered in the simulation were 10 m/s and 40 m/sec. Wind profile is assumed constant at the inlet, see 4.6 for comparison with boundary layer wind profile.

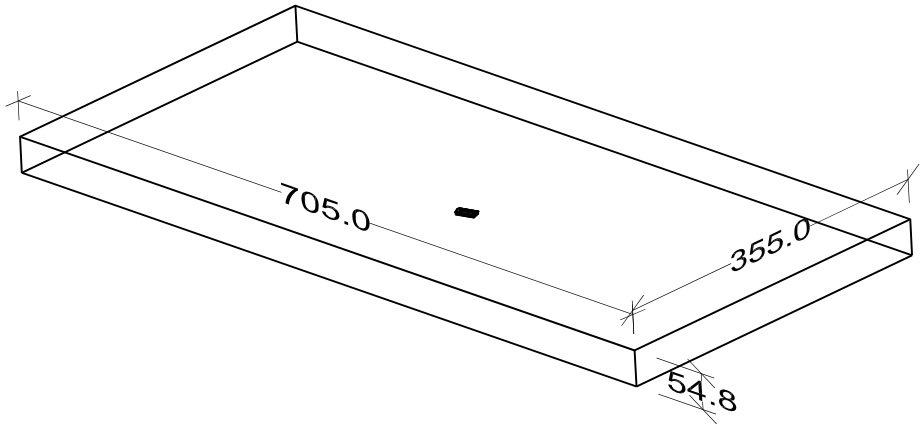


Fig. 3.1. Dimensions (m) of the simulation domain surrounding Zisis (2011) Doudak et al (2011) building model

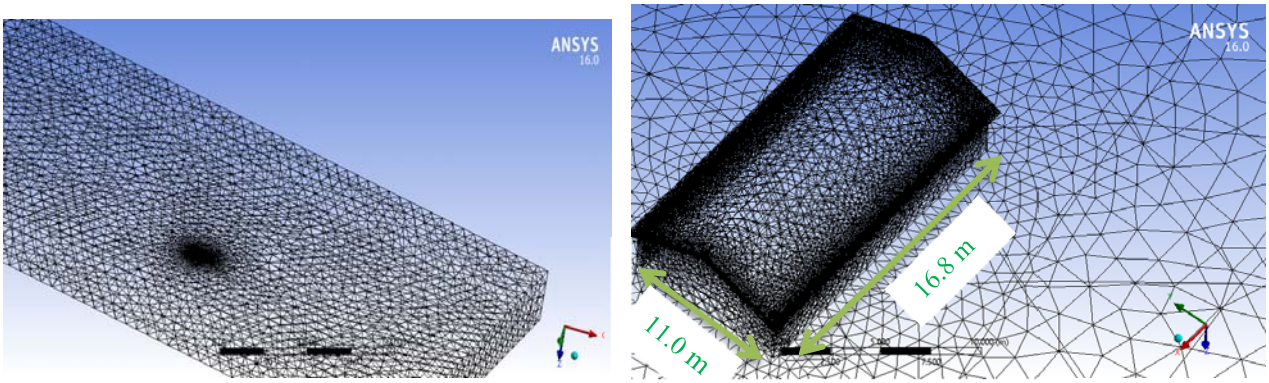


Fig. 3.2. Zisis (2011) and Doudak et al (2011) building model mesh detail in CFD analysis

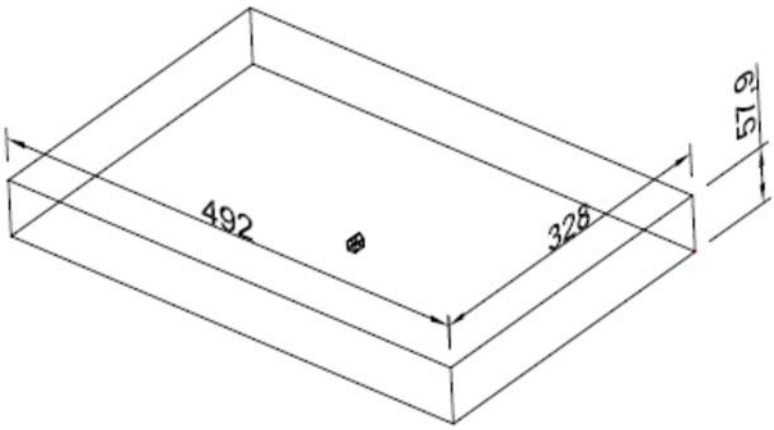


Fig. 3. 3, Dimensions (m) of the simulation domain surrounding Holmes (2001) building models

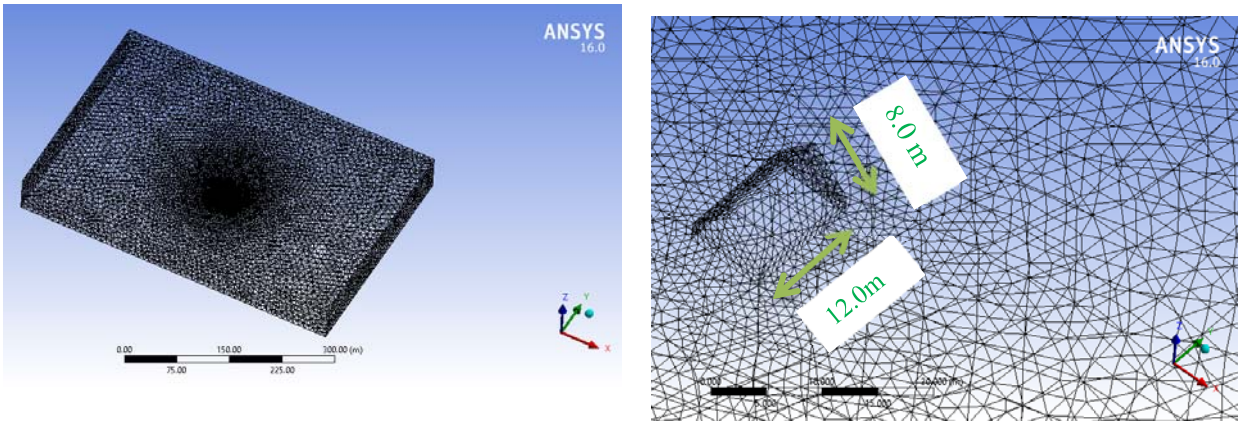


Fig. 3. 4, Holmes (2001) model mesh detail used for the CFD analysis

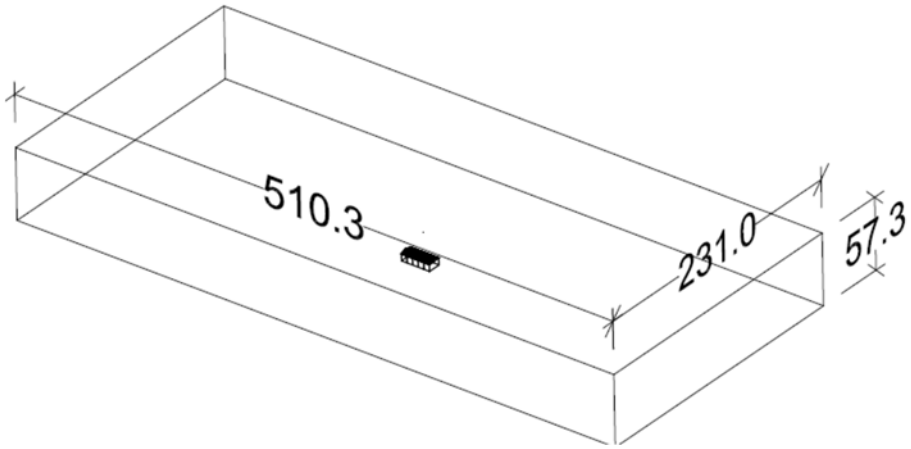


Fig. 3. 5, Dimensions (m) of the simulation domain surrounding Robertson et al (1985) canopy model

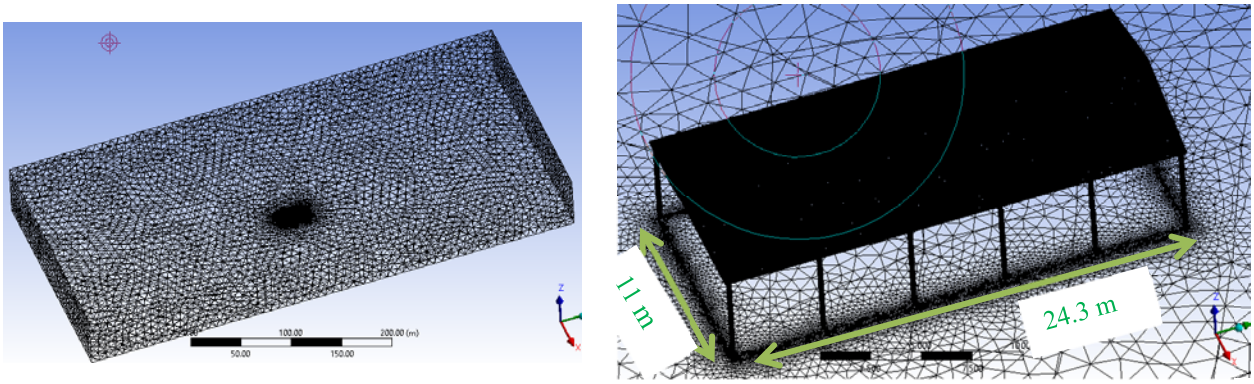


Fig. 3.6. Canopy model mesh detail used for the CFD analysis

3.1.2. Boundary conditions and mesh details for building model and building model with solar panels

The computational domain in the boundary conditions, has dimensions of 492 m x 328 m x 57.9 m high, surrounding the residential building model, which has the dimensions of 12 m x 8m x 7.40 m and has 0.60 m overhang, as it can be noticed in Fig. 3.7 and Fig. 3.8. The minimum computational domain surrounding dimensions as recommended by Franke (2006) and Cost (2007) for a single building and reported by Dagnew and Bitsumlak (2013) and Dagnew (2012) is of 15h x 5h x 5h x 4h for the downstream field, side field, upstream and ceiling distance respectively (Fig. 3.7). The computational domains used in the current research varied slightly from case to case, however the minimum dimensions of 240 m (32 h) downstream field, 158 m (21h), sideways field, 240 m (32h) upstream field and 50 m (6.75h) distance to ceiling, were bigger than the minimum recommended computational domain represented in Fig. 3.8.

The computational domain has velocity inlet, outlet and four other walls (no penetration no slip conditions), Fig. 3.9. Wind velocity was constant; however it was assumed to have 5% turbulence intensity and 10 % turbulence viscosity at the inlet, in order to develop a medium turbulent flow as described in the Ansys Users Guide (2015). The outlet was considered as velocity outlet where flow exits the computational domain. RANS, k-ε realizable or k-ε standard with enhanced wall treatment was used for all solar panel cases, while the LES algorithm was used in the verification of the residential building models of Apperley (1979) and Zisis (2011).

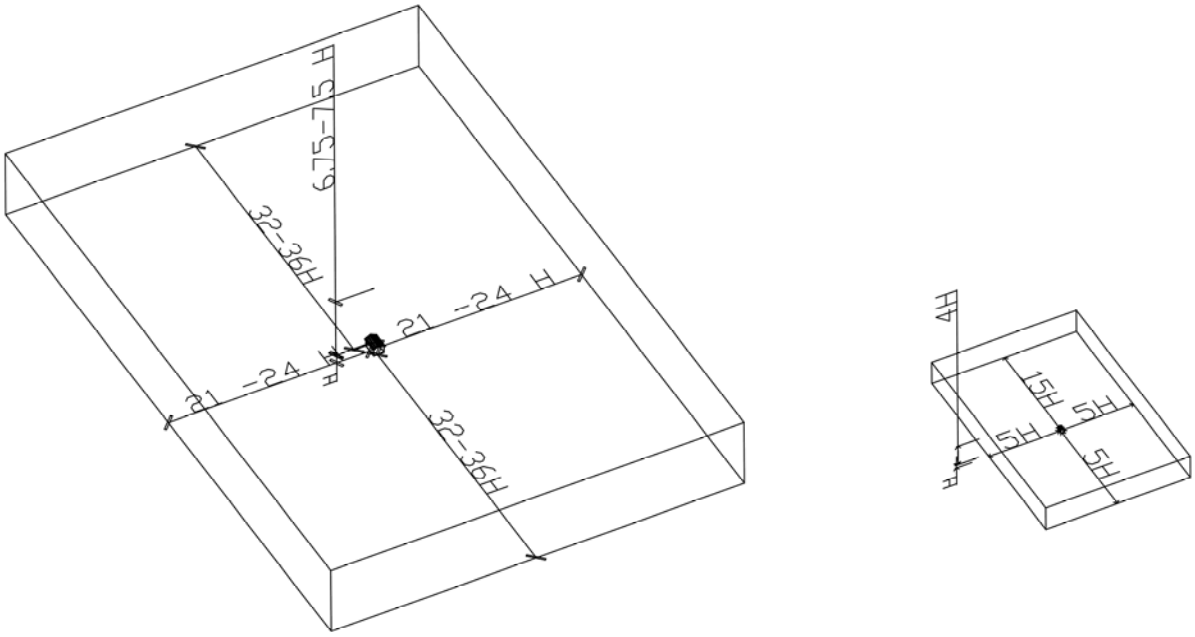


Fig. 3. 8. Computational domain in this study.
(492 x 328 x 57.9 m) for the model is much higher than minimum recommended by Franke (2006) and COST (2007) for a single building, as reported by Dagnew and Bitsumlak (2013), and Dagnew (2012).

Fig. 3.7.Minimum computational domain dimensions as recommended by Franke (2006) and COST (2007) for a single building, as reported by Dagnew and Bitsumlak (2013) and Dagnew (2012).

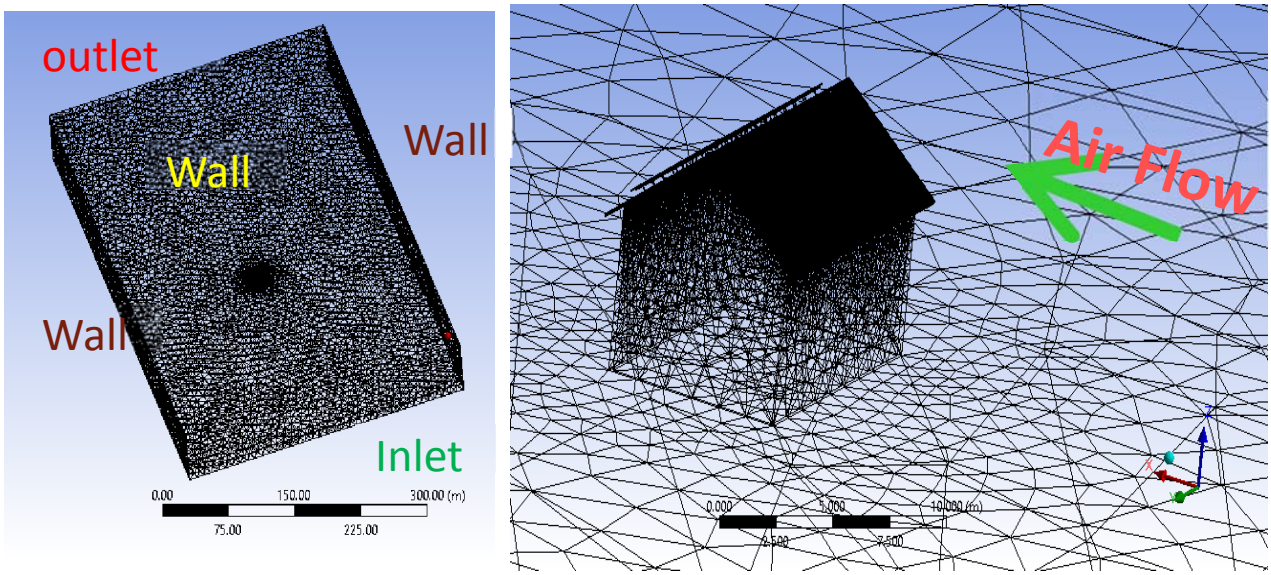


Fig. 3. 9. Residential building model (12m x 8m x 7.40 m) mesh details used for the CFD analysis, 90° wind direction, slope 35°. Boundary conditions, CD domain is 492x328x57.9 m high, wind velocity profile assumed 5% turbulence intensity at the inlet. Turbulent viscosity ratio 10%. Model: RANS, K-epsilon realizable or K-epsilon standard with enhanced wall treatment. Overhangs are 0.60 m wide.

The residential building model with dimensions of 12.0 m in length, 8.0 m in width and 6.0 m in height was analyzed in this study.

Figures 3.11 to 3.15 show the mesh details for the residential building model. Typical model mesh, without panels, used 767,851 tetrahedral cells, 3,960 hexahedral cells, 1,573,350 triangular faces, 15,733 quadrilateral faces, and 142,338 nodes. Minimum cell edge length varied slightly between models, but in general this was approximately 0.04 m. A typical model with panels (10" clearance, 2" spacing) had 551,284 nodes, 2,844,274 cells, 296,878 triangular wall faces, 5,533,760 triangular interior faces, as shown in Figs. 3.8 to 3.12.

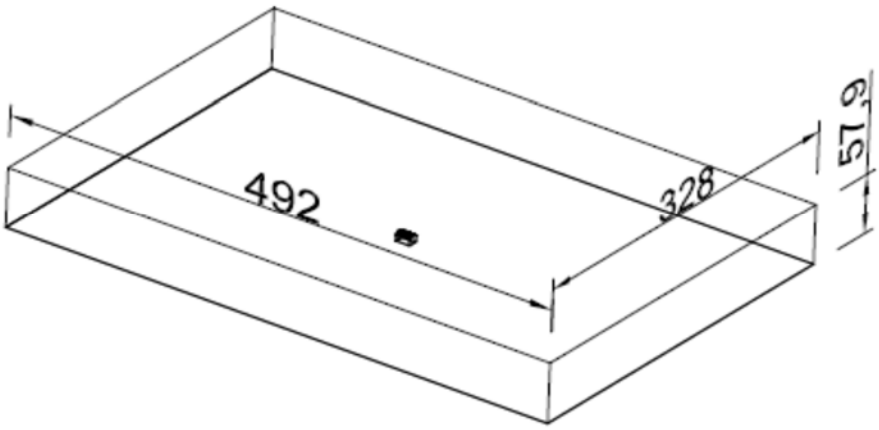


Fig. 3. 10. Dimensions (m) of the simulation domain surrounding a typical residential building model

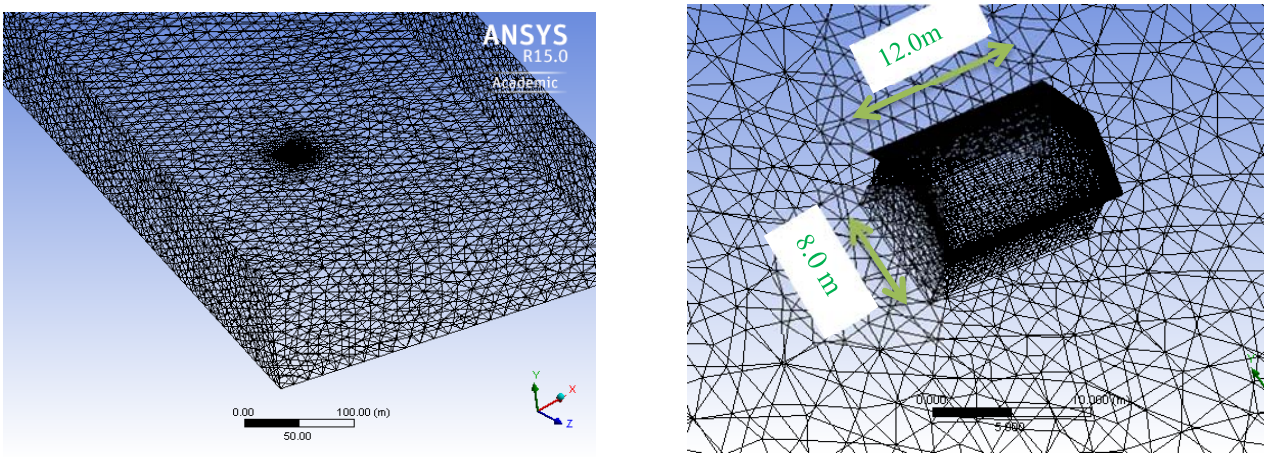


Fig. 3. 11. Building model mesh detail used for the CFD analysis

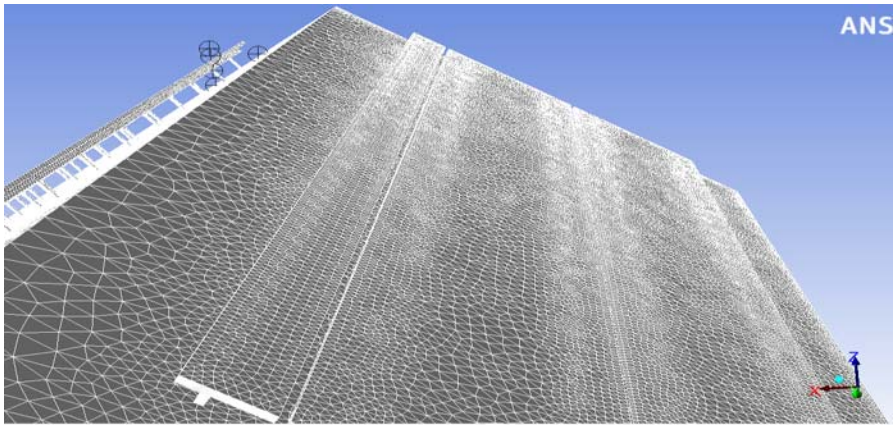


Fig. 3. 12. Building model mesh detail, top of the roof with panels, 10” clearance, 2” spacing

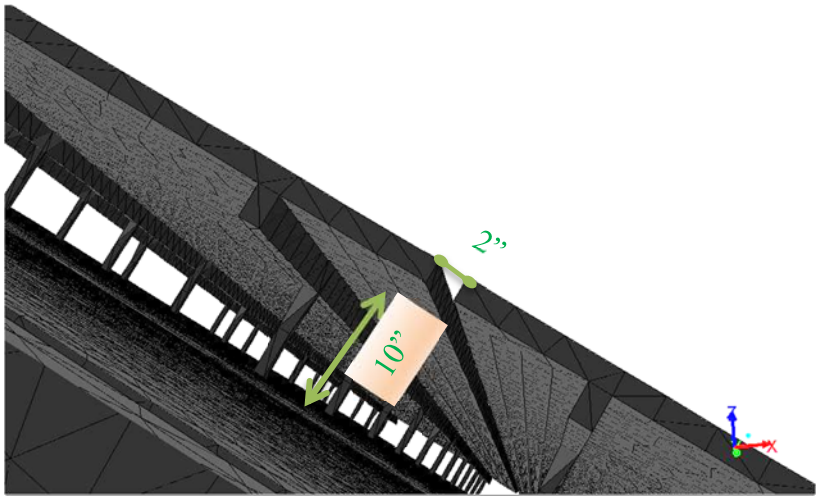


Fig. 3. 13. Building model mesh detail, under the panels, 10” clearance, 2” spacing

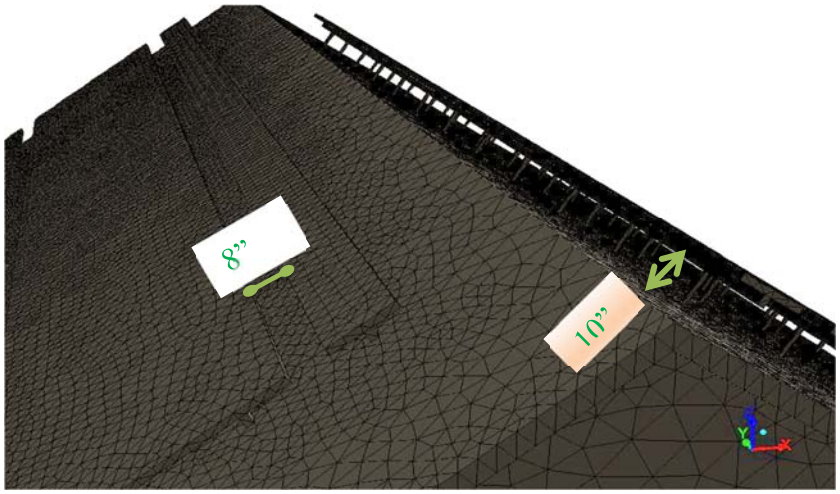


Fig. 3. 14. Building model mesh detail, top of the roof with panels, 10” clearance, 8” spacing

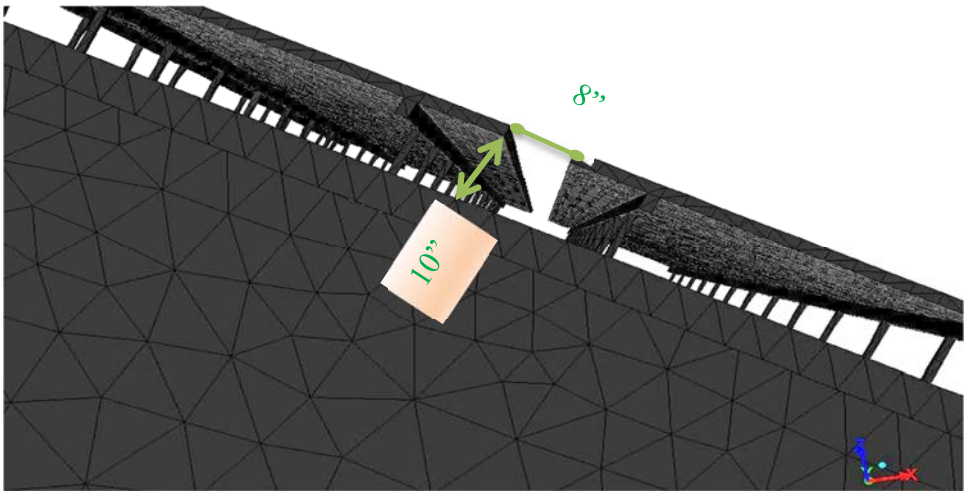
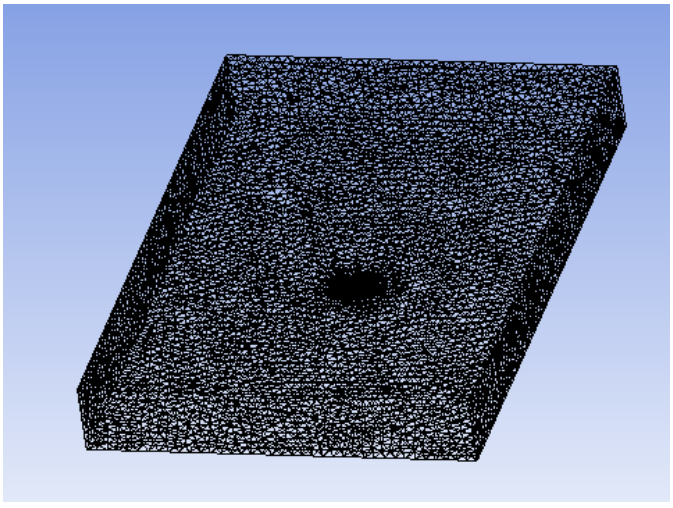


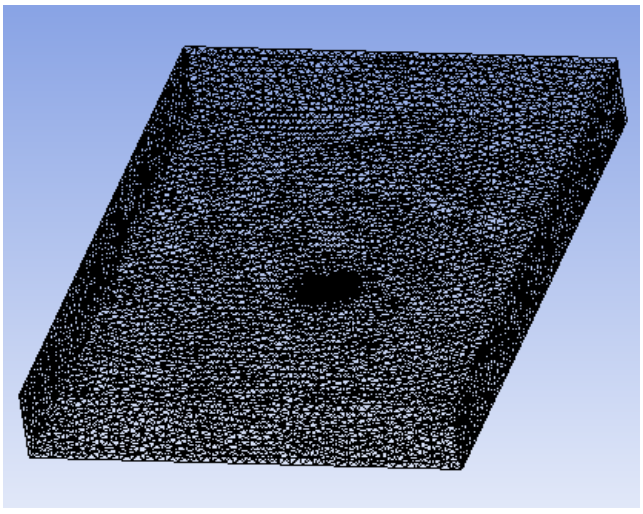
Fig. 3. 15. Building model mesh detail, under the panels, 10” clearance, 8” spacing

3.1.3. Mesh sensitivity analysis

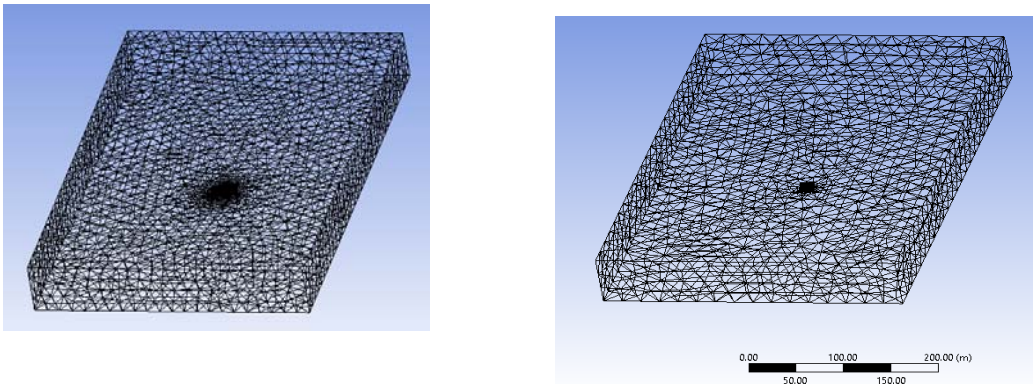
A mesh sensitivity was conducted for four different mesh sizes, Fig. 3.16, as identified in Table 3.1. The results show that the mesh size used in the thesis strikes the right balance between computational effort and accuracy. It can be seen that creating the model with a finer mesh than that used in the thesis yields no significant difference when comparing the CP values and velocity profiles over the computational domain, as demonstrated in Fig. 3.17, Fig. 3.18 and Tables 3.1 and 3.2. Using coarser meshes would have yielded results that are significantly different than those obtained in this study.



(a) Very fine mesh

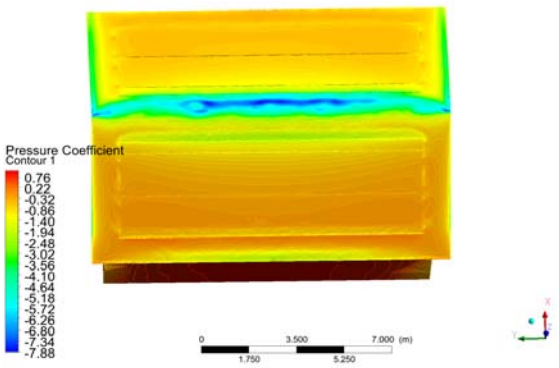


(b) Fine mesh used in the simulations (current mesh)

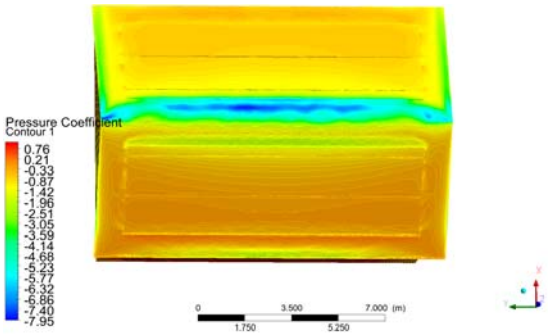


(c) Medium mesh (d) Coarse mesh

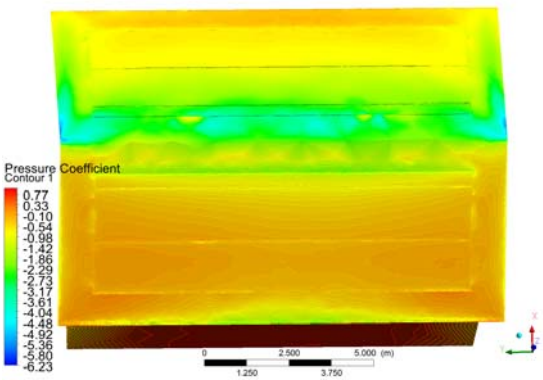
Fig. 3. 16. Different size meshes used for mesh sensitivity analysis



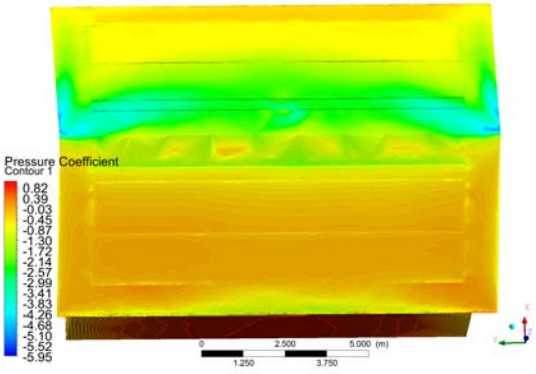
(a) Cp for very fine mesh



(b) Cp for fine mesh (current mesh)

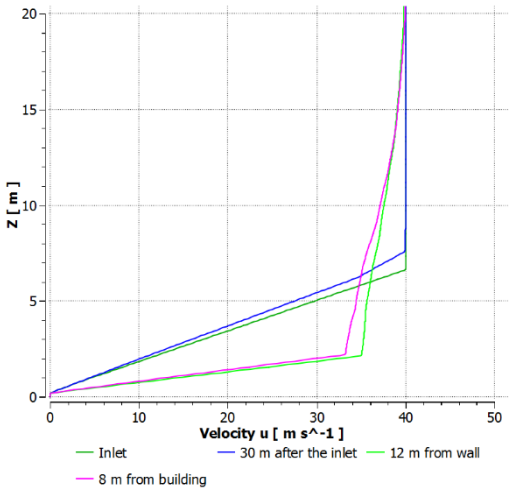


(c) Cp for medium mesh

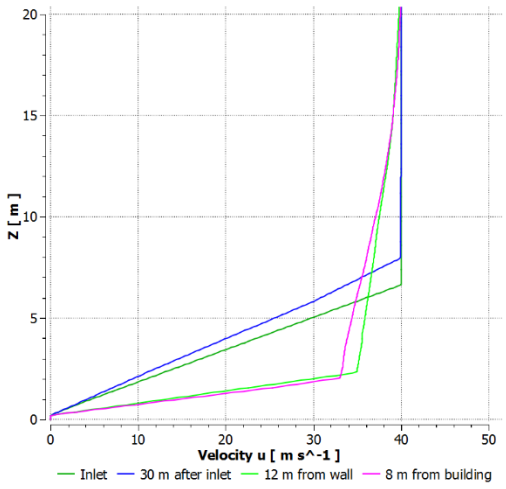


d) Cp for coarse mesh

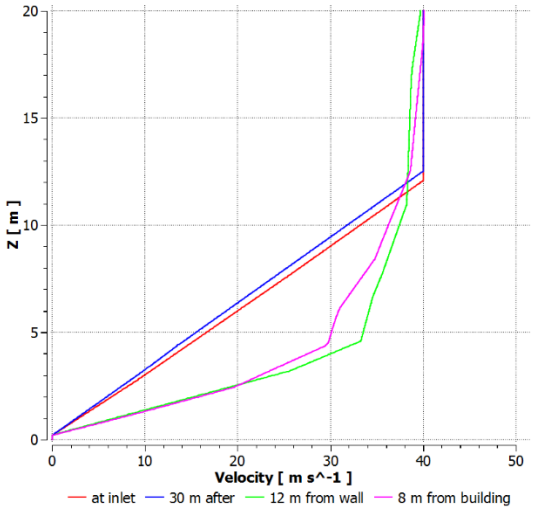
Fig. 3. 17. Cp contours on the building with solar panels for the corresponding meshes



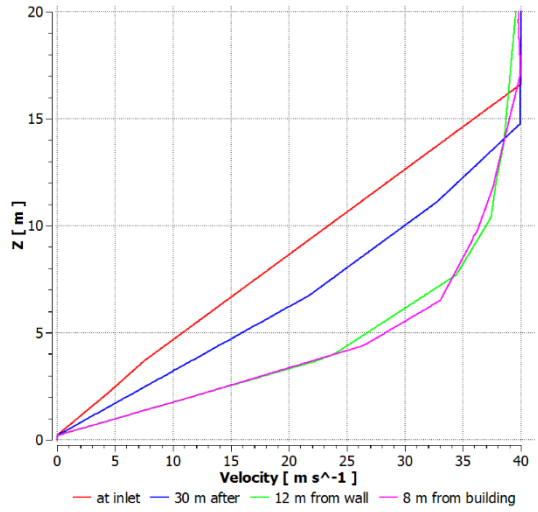
(a) Wind velocity profiles along computational domain very fine mesh



(b) Wind velocity profiles along computational domain, fine mesh (current mesh)



(c) Wind velocity profiles along computational domain medium mesh



(b) Wind velocity profiles along computational domain, coarse mesh.

Fig. 3. 18. Wind velocity profiles along the computational domain for the building with solar panels for the corresponding meshes

Table 3. 1. Characteristics of different fine and coarse meshes used in the simulations

Mesh	Statistics	Relevance center, smoothing, transition, span angle center
Very fine	3,707,909 tetrahedral cells, , 724,808 nodes	Fine, high, slow, fine with smaller min size and proximity size
Fine	2,719,816 tetrahedral cells, 529,167 nodes	Fine, high, slow, fine
Medium	1,552,950 tetrahedral cells, 302,465 nodes	Medium, medium, fast, medium
Coarse	792,140 tetrahedral cells, 188,833 nodes	Coarse, low, fast, coarse

Table 3. 2. Pressure coefficients comparison on four points on the PL19, top of the panels, windward side, for different meshes.

Y(m)	0	2	4	5.6	Average difference in regard to fine mesh, %
Very fine mesh	-1.45	-1.36	-1.17	-1.05	3.25
Fine (current mesh)	-1.48	-1.4	-1.2	-1.08	0
Medium mesh	-2.05	-1.75	-1.6	-1.35	39.75
Coarse mesh	-2.35	-2.05	-1.85	-1.6	67.25

3.1.4. Validation case 1: Canopy structure, modeled using les algorithms

Validation of the CFD models was performed by comparing the analysis results with full-scale field test measurements recorded on an agricultural canopy structure with a corrugated steel gable roof with 16.7° inclination (Robertson et al 1985). Pressure coefficients were measured for several canopy configurations, including empty canopy, closed canopy, windward wall closed canopy and leeward wall closed canopy (Fig. 3.19). In the current study, only the open canopy was investigated. The canopy dimensions and the corrugated steel geometry were modeled to be consistent with the details reported by Robertson et al (1985). Additionally, a model with a smooth roof surface was developed to investigate the effect of the roof geometry on the wind flow developed around its surface.

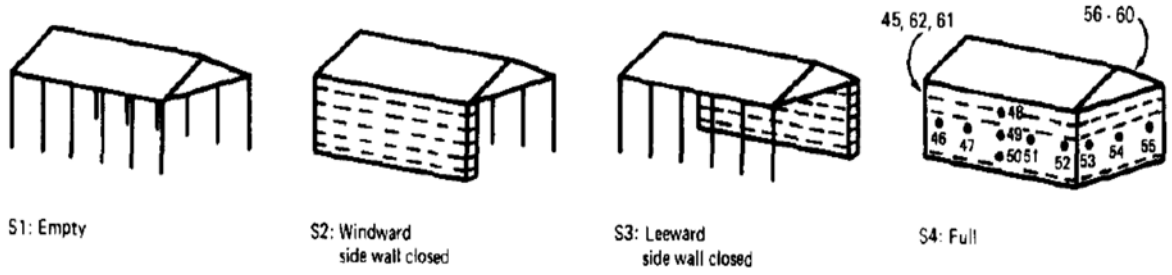


Fig. 3. 19. Agricultural canopy geometry investigated by Robertson et al, (1985)

Wind speed of 8.0 m/s and two wind directions, 0° and 90°, were simulated for the canopy structure. The 0° and 90° wind simulate the perpendicular and parallel to canopy ridge directions, respectively, as shown in Fig. 3.20.

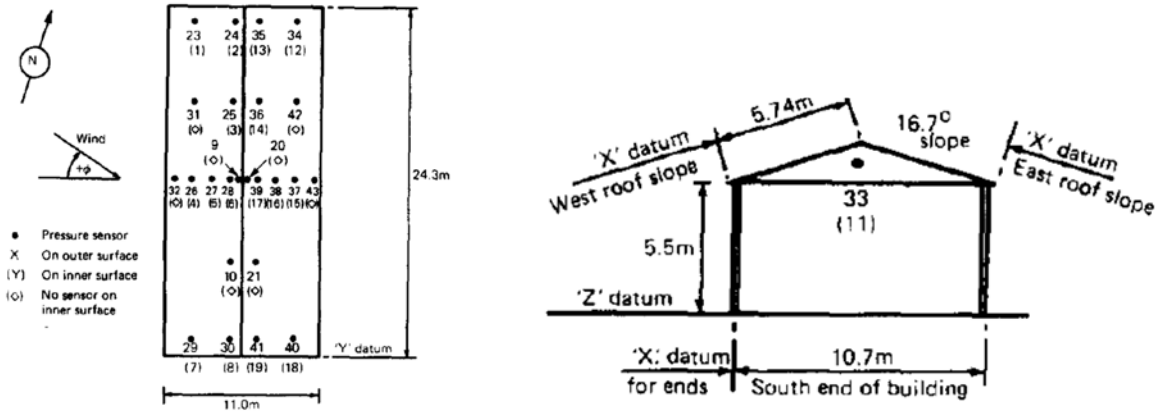
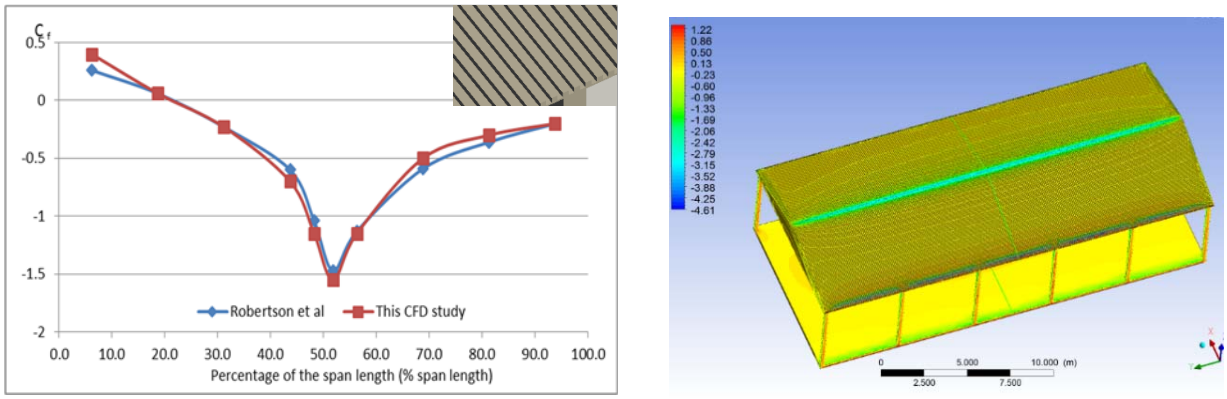


Fig. 3. 20. Wind directions and monitored points for the agricultural canopy (Robertson et al, 1985)

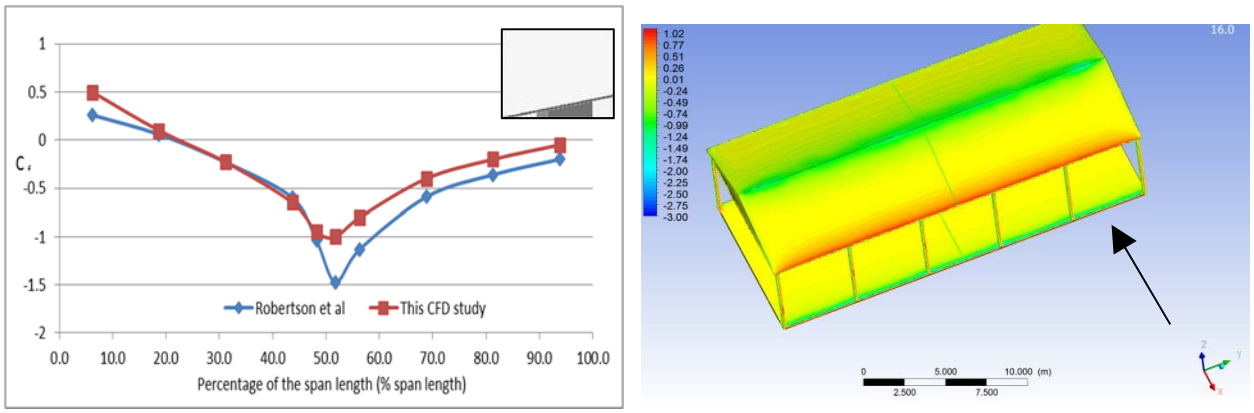
The time averaged wind pressure coefficients reported by Robertson et al, (1985) and the ones obtained in the current CFD investigation are compared in Figs. 3.15 to 3.18. In general, a very good agreement between the CFD model and the full-scale measurements can be observed when considering corrugated steel roof. Figure 3.15 a) shows comparison between the average pressure coefficients on the cross-section running at the middle of the roof in the length direction (See Figure 3.15 b) for wind perpendicular to the ridge (0°).



-a- **-b-**

Fig. 3. 21. a) Average pressure coefficients along the middle cross-section of the corrugated roof canopy for 0° wind direction; b) Location of the canopy middle cross-section and surface pressure coefficient distribution

In the case of smooth roof surface, it was observed that the average pressure coefficients were slightly lower in the CFD simulations than those reported in the full-scale measurements (Robertson et al, 1985). This was particularly the case for the ridge region and leeward side of the roof (Fig. 3.22 a). This shows that ignoring the geometry roughness details by using a smooth surface for the roof of the canopy could alter the pressure distribution, and as shown in this case underestimated the pressure coefficients. This could be attributed to local flows generated by the geometry of the corrugated steel roof.



-a- **-b-**

Fig. 3. 22 a) Average pressure coefficients along the smooth canopy middle cross-section for 0°; b) Location of the canopy middle cross-section and surface pressure coefficient distribution

Pressure coefficients were also compared for the wind direction parallel to the ridge of the canopy (90°). Observations were made for two longitudinal lines on the leeward side of the roof, one near the ridge and another near the edge of the roof. Furthermore, two cross sectional lines, one in

middle of the roof and another near the front edge of the empty canopy, were considered as shown in Fig. 3.23. Only the case with corrugated roof geometry was investigated.

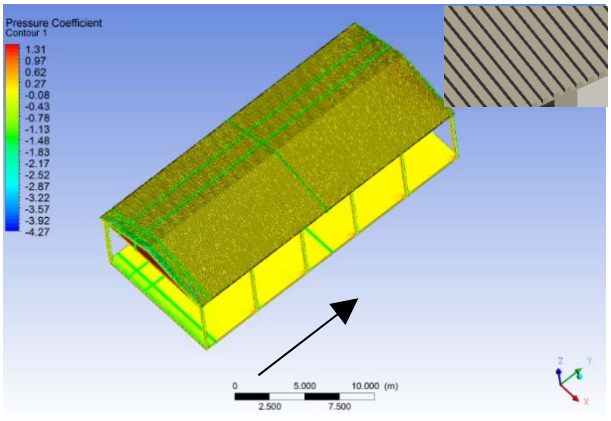


Fig. 3. 23. CFD pressure coefficients for the canopy with corrugated roof - longitudinal and transversal monitored sections

Figs. 3.24 a) and b) show the pressure coefficients for the wind parallel to the canopy ridge along the four sections described in Figure 3.23 for both the full-scale measurements and those obtained from the CFD simulations. It can be observed that the differences between the pressure coefficients were very small (Cp=0.01 to 0.03). The results highlight the level of accuracy that can be obtained in calculating the pressure coefficients along the entire roof surface using the CFD modelling techniques.

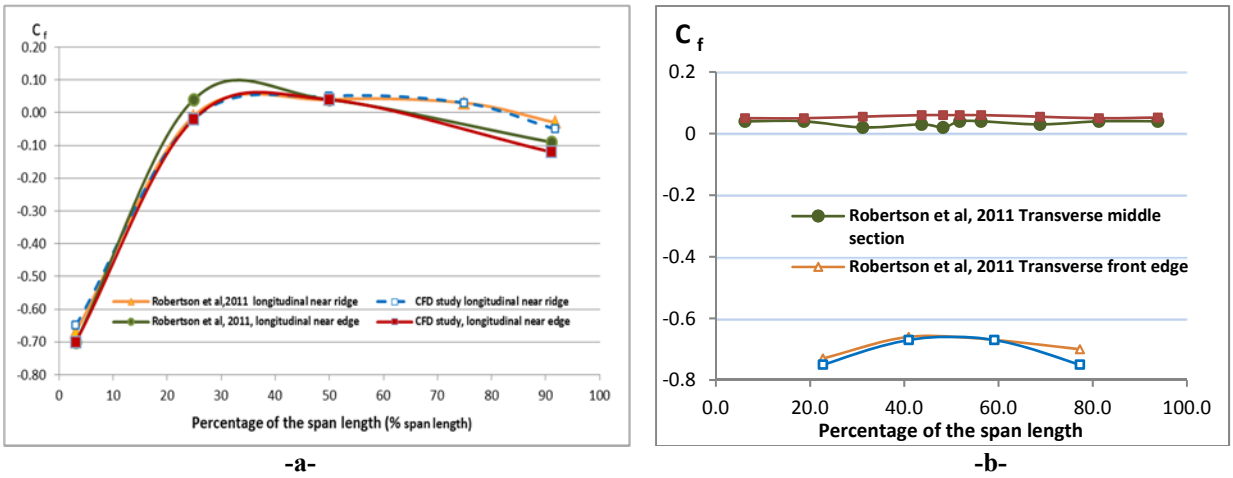


Fig. 3. 24. Pressure coefficients comparison CFD and full-scale measurements (Robertson et al, (1985) and CFD simulations for 90°, a) Longitudinal sections b) Transversal sections

3.1.5. Validation case 2: Residential building modeled using k-ε algorithm

Full-scale measurements of wind-induced pressure coefficients were reported by Doudak et al, (2011), for a residential building located in Fredericton, New Brunswick. The building had dimensions of 8.6 m × 17.2 m × 5.6 m (width × length × height) and a gable roof with a 4/12 (19.5°) slope. Mean pressure coefficients were determined for two pressure taps located at the middle of the windward wall and in the middle of the windward roof section of the building, as shown in Figs. 3.25 and 3.26. The full-scale test was performed for wind directions between 230° and 335°, and for different $\propto$= 0.16, 0.22 and 0.28, where $\propto$ is the exponent coefficient used in profile formulation of the wind speed. The mean, maximum and minimum pressure coefficients were compared with the wind tunnel results obtained for a scaled model (scale 1:200) of the same residential building (Doudak et al, 2011). The wind tunnel tests were carried out for wind directions between 0° and 360° (Figs. 3.25 and 3.26).

A CFD model employing the k-ε algorithm was developed to simulate the full-scale residential building with the same geometrical dimensions as reported by Doudak et al, (2011). Simulations were performed for 13.5 m/s, which is consistent with the experimental observations, but only for four wind directions. The directions were 0° and 180°, to obtain comparable results with the wind tunnel experiments (Fig. 3.25), as well as 333.5° and 265.5°, to compare with both full-scale and wind tunnel experiments (Fig. 3.30).

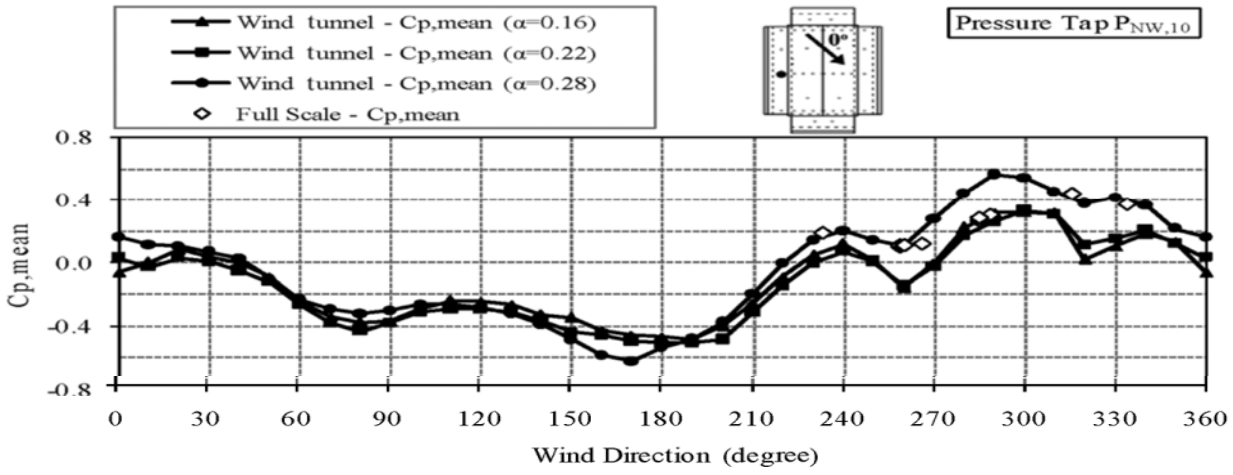


Fig. 3. 25. Mean pressure coefficients on the lateral wall of a residential building Doudak et al (2011)

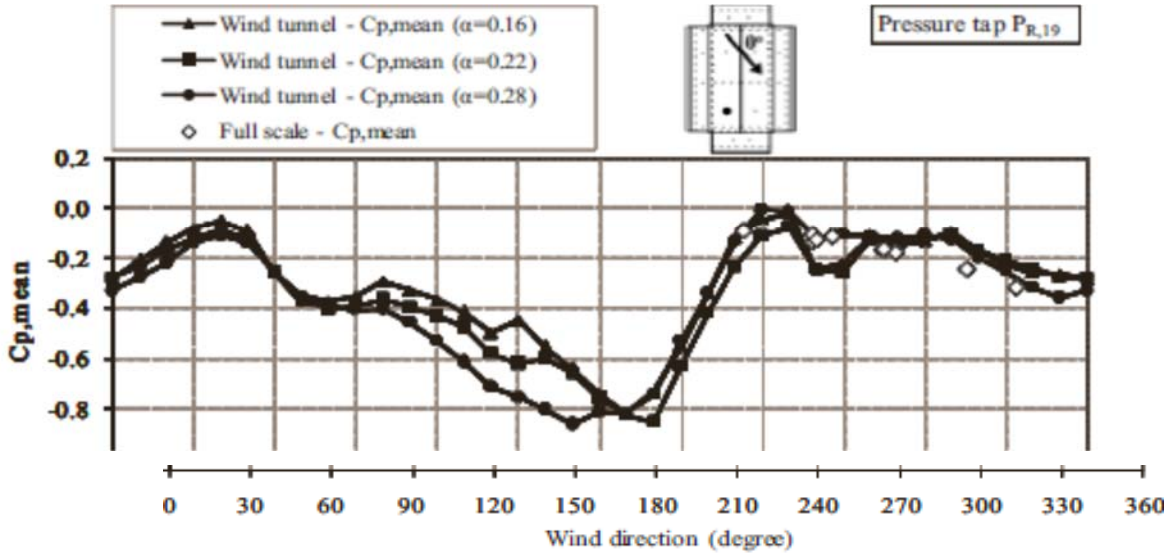
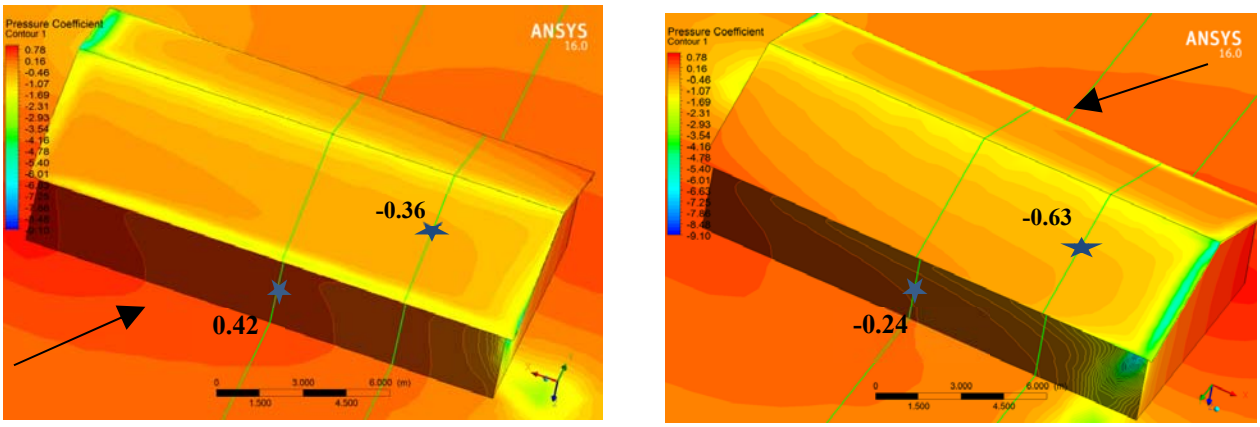


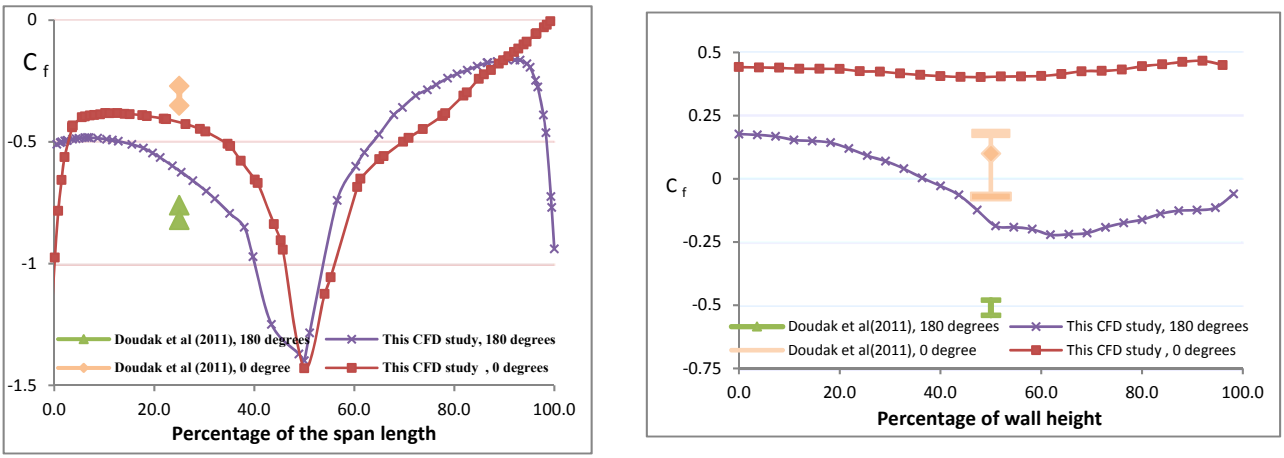
Fig. 3. 26. Mean pressure coefficients on the roof of a residential building Doudak et al, (2011)

Figures 3.27 and 3.28 represent the distribution of the average pressure coefficient at the surface of the residential building, along with the two monitored points corresponding to the locations reported by Doudak et al (2011). For the 0° wind direction, the CFD simulations yielded an average pressure coefficient of (Cp=0.42) on the wall and (Cp=-0.36) on the roof of the building. These results are comparable to those obtained from the wind tunnel experiments, where values between (Cp=-0.07) and (Cp=0.18) were reported for the windward wall, and values between (Cp=-0.27) and (Cp=-0.35) were reported for the roof (Fig. 3.25) (Fig. 3.26). For the 180° wind direction, the CFD simulations showed average pressure coefficients of (Cp=-0.24) on the wall and (Cp=-0.63) for the roof (Fig. 3.27 b), where for the same locations Doudak et al, (2011) reported ranges between (Cp=-0.45) and (Cp=-0.51) (Fig. 3.25) and (Cp=-0.76) and (Cp=-0.82) (Fig. 3.26), respectively. Both cases were found to be in good agreement with the CFD simulations results performed in the current research.



-a- -b-

Fig. 3. 27. CFD Mean pressure coefficients for the residential building for a) 0° wind direction, b) 180° wind direction, (This Research)



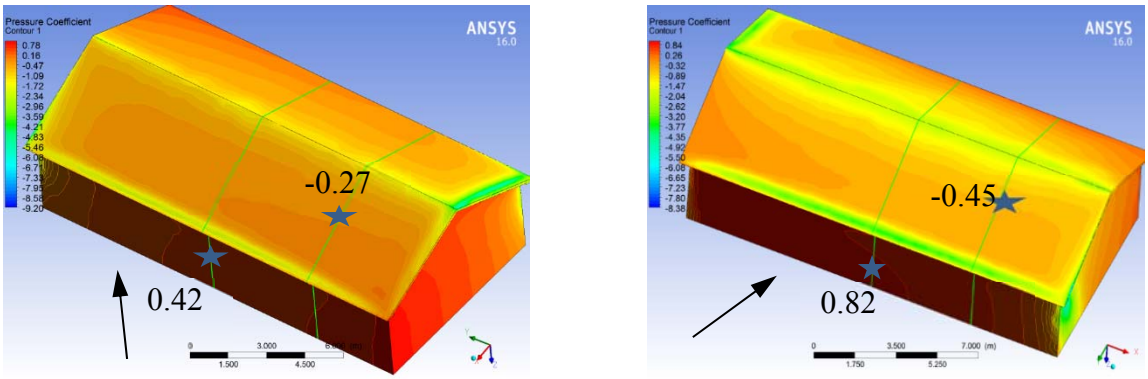
-a- -b-

Fig. 3. 28. Mean pressure coefficients for the residential building for 0° and 180° for a) Roof tap location, b) Wall tap location

Figure 3.28 (b) represents the pressure distribution at the wall tap location considered in the full-scale study performed by Doudak et al (2011). In this case, the wind pressure coefficients on windward wall for 0° wind direction case was almost constant, at around 0.4, while for the wind tunnel study the pressure coefficients were in the range of (Cp=-0.07) to (Cp=0.18). The difference might be attributed to the scale effect, as the scaled model used by Doudak et al (2011) in the wind tunnel was 1/200, while the current CFD simulation is at full-scale (1:1). For 180° wind direction, the pressure coefficient recorded at the wall tap location started at 0.18 at bottom of the wall, and decreased, reaching a negative value of (Cp=-0.24) towards the middle height of the wall, and increased again towards the upper height of the wall, up to (Cp=-0.10). At the tap location the CFD

simulations showed pressure coefficients of about -0.24, while Doudak et al (2011) measured values between (Cp=-0.47) and (Cp=-0.54) in the wind tunnel experiments.

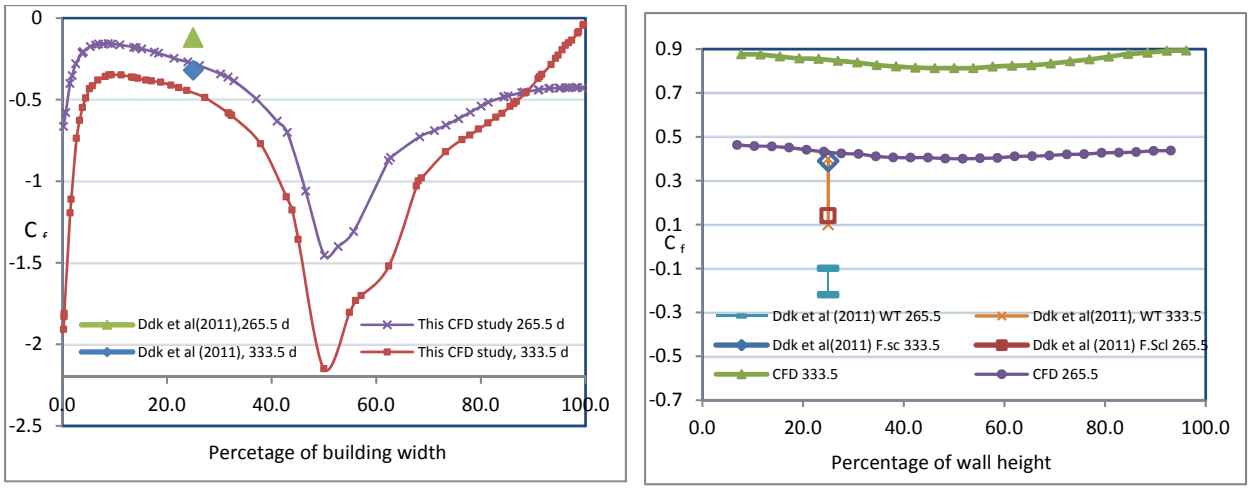
For the 265.5° wind direction, the pressure coefficient obtained from the CFD simulations was (Cp=0.42) for the wall pressure tap location, whereas Doudak et al, (2011) reported pressure coefficients of (Cp=-0.1) to (Cp=-0.22) in the wind tunnel, and (Cp=0.14) in the full-scale tests. This difference might be explained in part by neglecting the roughness length of the ground surface in the analysis, as well as the turbulent k-ε algorithm used in the CFD simulation, which creates turbulent wind formations at contact with the wall surface. For the roof pressure tap location, the CFD simulations indicated a pressure coefficient of (Cp=-0.27) (Fig. 3.29 a)), while the wind tunnel tests yielded values for the pressure coefficients between (Cp=-0.11) and (Cp=-0.25), and a value of (Cp=-0.12) was obtained from the full-scale measurements.



-a- -b-

Fig. 3. 29. CFD Mean pressure coefficients for the residential building for a) 265.5° wind direction, b) 333.5° wind direction

For the 333.5° wind direction, the wind-induced pressure coefficient was 0.82 for the wall pressure tap location and (Cp=-0.45) for the roof pressure tap location. The reported pressure coefficients on the wall was between (Cp=0.1 to 0.4), for the wind tunnel tests and (Cp=0.39) in the full-scale tests. The roof taps registered pressure coefficient values for the wind tunnel between (Cp=-0.25) and (Cp=-0.30), and from the full-scale measurements value of (Cp=-0.32) was reported by Doudak et al (2011).

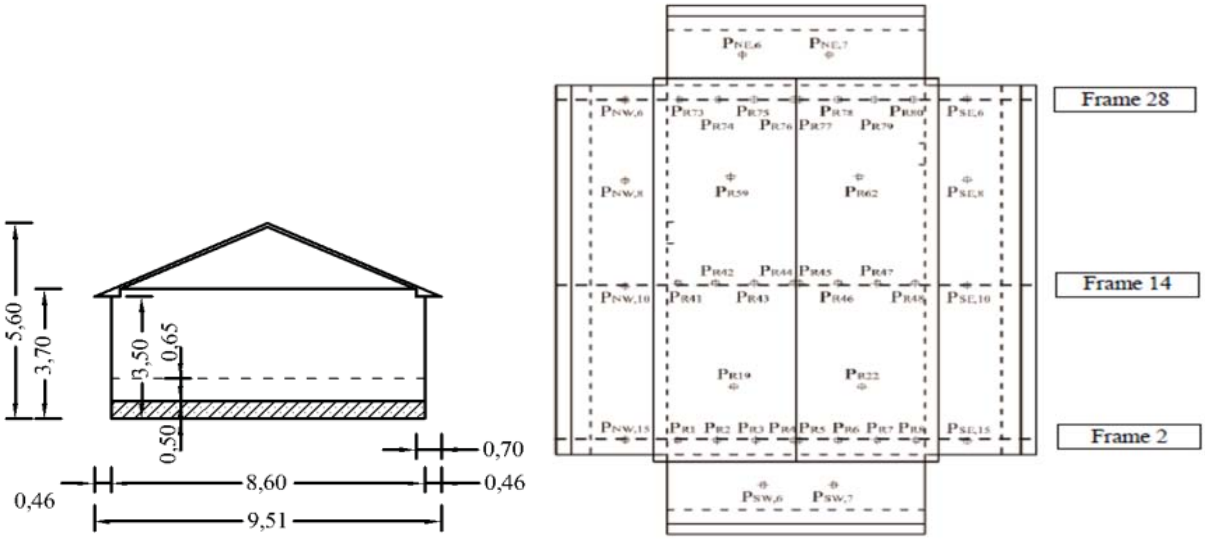


-a- -b-

Fig. 3. 30. Mean pressure coefficients for the residential building for 265.5° and 333.5° for a) Roof tap location, b) Wall tap location

3.1.6. Validation case 3: Residential building using les algorithm

Validation of CFD models was performed in this case by comparing modeling analysis results of a residential building with measurements reported in a full-scale experiment conducted by Zisis (2011). The building is the same as that studied by Doudak et al, (2011).



-a- - b-

Fig. 3. 31. a) Residential building, (Zisis, 2011) b) Instrumented frames, full-scale, (Zisis, 2011)

Distribution of the pressure taps, used in the full-scale test is shown Fig. 3.31, however, the comparison was made with pressure taps records located on Frame 14. Full-scale records of the

pressure taps on Frame 14 are shown in Fig. 3.32. Wind direction in the full-scale test was 240° from assumed reference zero point (43° counter clockwise from geometric North) which corresponds to 17° wind direction with ridge as shown in Fig. 3.33. The same average wind speed as in the full-scale test (15.6 m/s) was used in the CFD analysis.

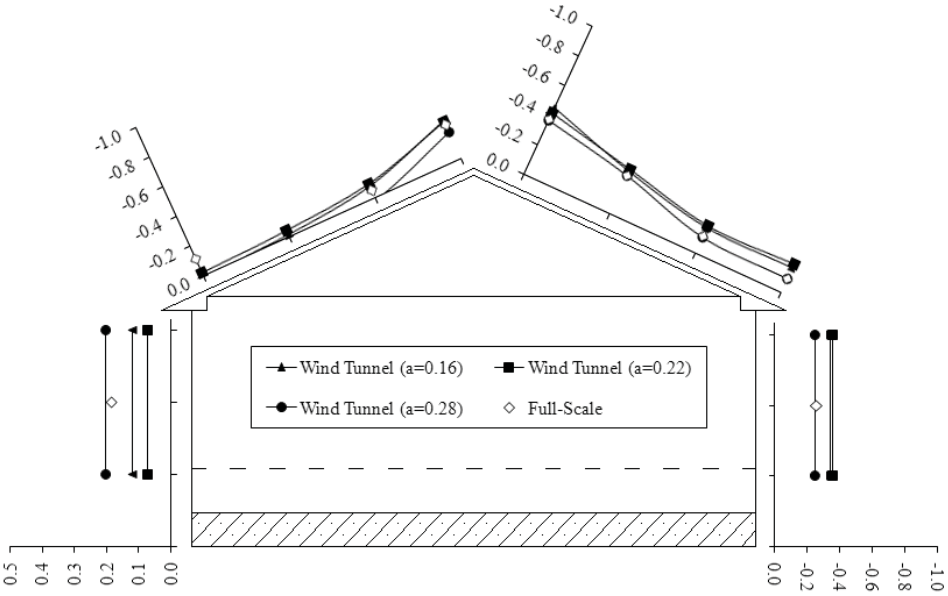


Fig. 3. 32 Mean pressure coefficients for frame 14. (zisis, 2011)

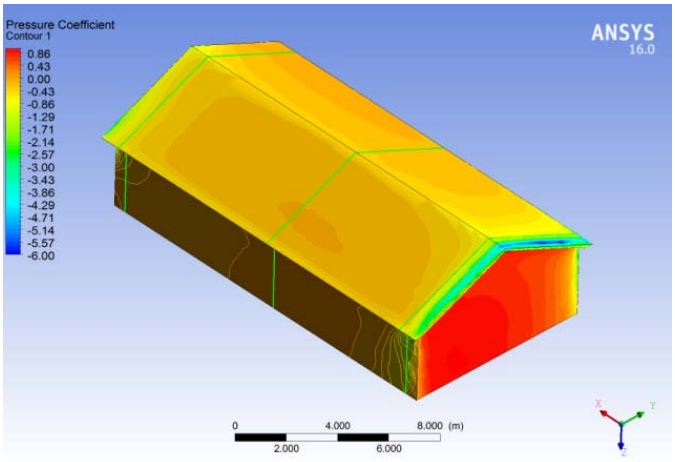


Fig. 3. 33. Contour of pressure coefficients for residential building, tested by Zisis, (2011) Wind direction is 240 °, Frame 2 (ww), Frame 14 (middle) and Frame 28 (lw).

Figures 3.34, 3.36 and 3.38 show very good agreement between pressure coefficients results from CFD model for frames 14, 2 and 28, respectively, and mean pressure coefficients recorded by Zisis (2011).

For frame 14 (Fig. 3.34), the pressure coefficients varied between (Cp=-0.16) at the windward edge of the roof, gradually decreasing to (Cp=-0.35) at the ridge of the roof and increasing again on the other side of the building reaching (Cp=-0.15) at the base of the leeward edge. The trend of the pressure coefficient was very similar when compared with the full-scale experiments reported by Zisis (2011), however, slightly higher pressure coefficients for the roof edges of the instrumented building were observed.

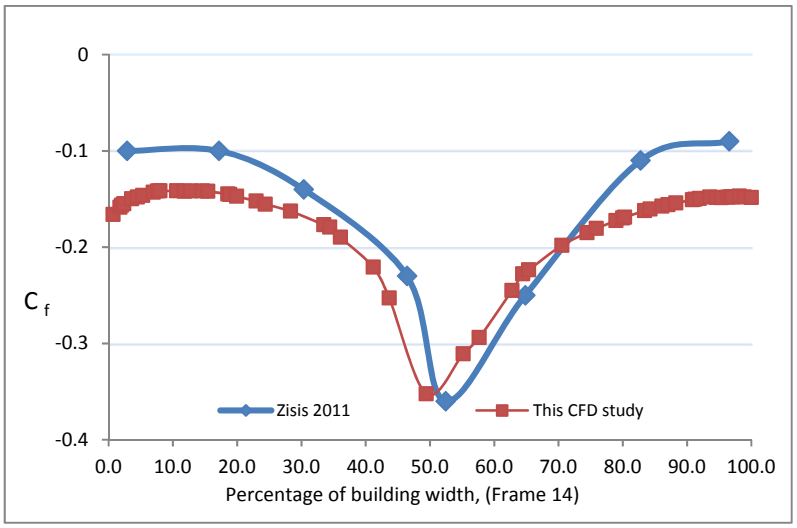


Fig. 3. 34. Mean pressure coefficients on Frame 14 of the residential building, Zisis (2011) full-scale with CFD analysis-Current study, wind direction 240°.

Along frame 2 (Figs. 3.35 and 3.36), very good agreement was observed for the pressure coefficients obtained from the CFD simulation, for the windward taps of the roof, where the recorded values varied between (Cp=-0.4) at the base of the edge to (Cp=-1.19) at the ridge of the roof. For the leeward edge, the CFD simulation yielded higher pressure coefficients of -1.2, when compared with the (Cp=-0.9) reported by the full-scale measurements. However, near the ridge, both CFD and full-scale measurement provide the same value of (Cp=-1.19), and all pressure coefficients were very similar.

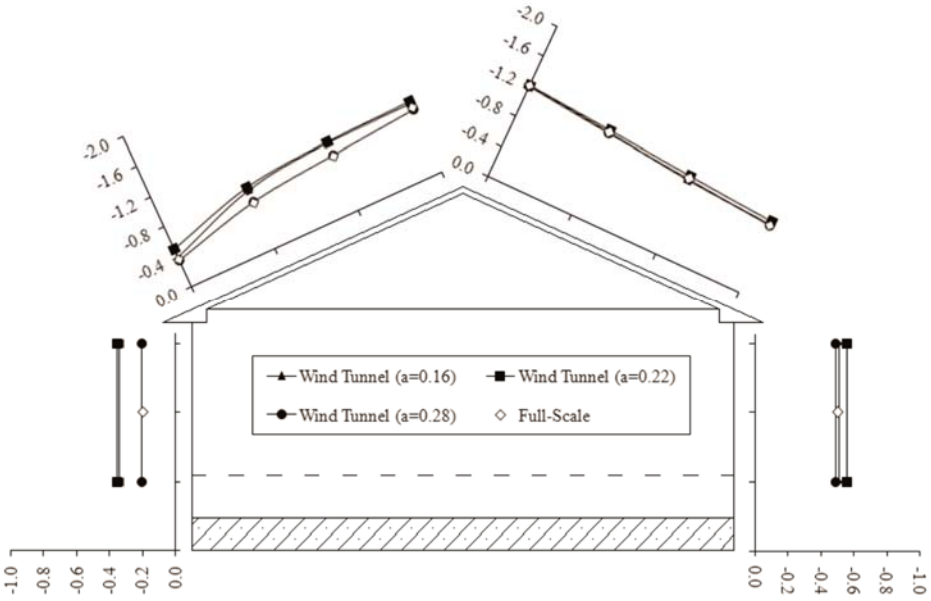


Fig. 3. 35. Mean pressure coefficients for Frame 2, wind direction 240° (Zisis, 2011).

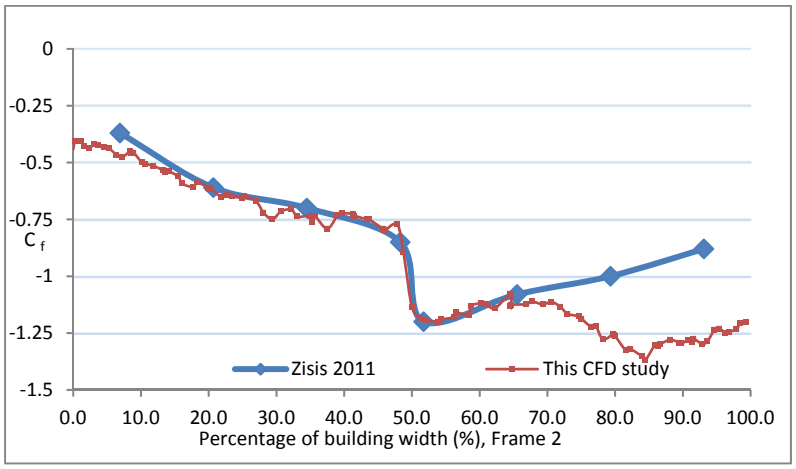


Fig. 3. 36. Mean pressure coefficients on Frame 2 of residential building, Zisis (2011) full-scale with CFD analysis-Current study, wind direction 240°.

The large eddies formed on the leeward side of the roof in the LES model might have caused this overestimation, which indicates that longer simulation times should be employed for allowing the turbulent flow to dissipate.

Also, the CFD simulation is overestimating the pressure coefficients on the windward edge (frame 28), which is the closest to the impact point with the incoming wind flow.

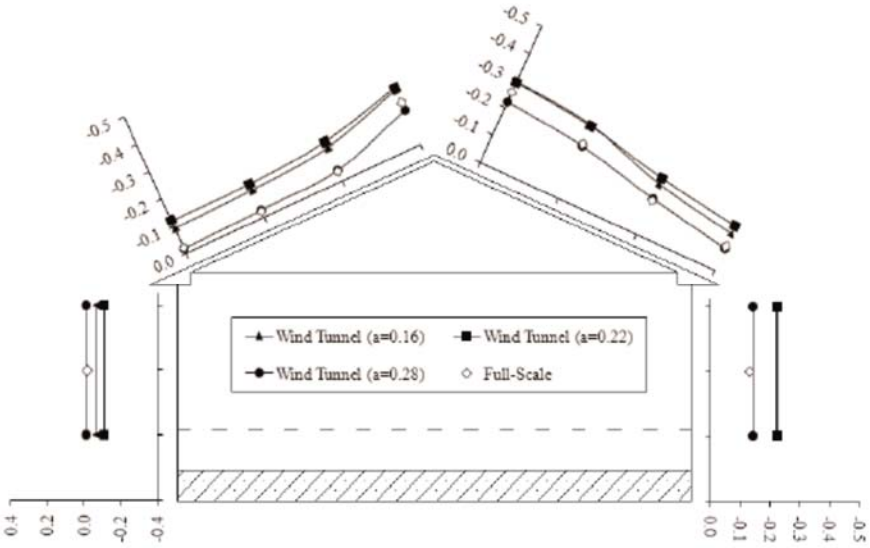


Fig. 3. 37. Mean pressure coefficients for Frame 28, wind direction 240° (Zisis, 2011).

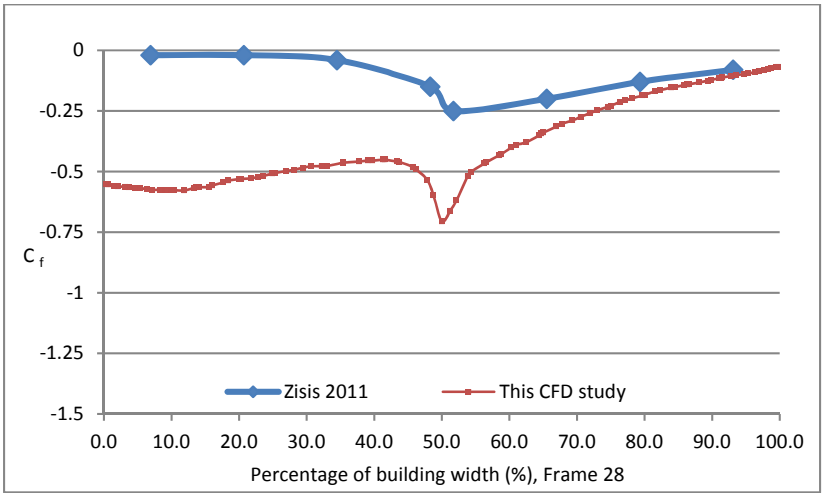


Fig. 3. 38. Mean pressure coefficients on Frame 28 of residential building, Zisis (2011) full-scale with CFD of this study, wind direction 240°

In general, a good agreement was obtained between the full-scale experiments and the current CFD simulations, for the pressure coefficient measured along the three frames specified above. However, pressure coefficients reported on the windward and leeward edges of the roof were influenced by the edge and corner vortices simulated by the CFD LES model and therefore higher pressure coefficient values were obtained.

3.1.7. Validation case 4: CFD model validation for gable roofs

In this section, the validation is done on four cases, two cases for (45º) roof slope and the other two cases for (30º) roof slope. For each slope case roof height to depth ratios of $\frac{h}{d} = 1.0 - 0.4$ were considered. It should be noted that all values reported in the figures below were obtained from the original graphs, however with scales adopted to the current study. This change was necessary because the original values were not available.

a) Bare gable roof (45º) and ratio of height to depth h/d =1

Figure 3.39 shows wind tunnel results conducted by Holmes (2001) on a gable roof sloped at (45º) and ratio of height to depth h/d =1. Fig. 3.40 displays corresponding CFD contours of pressure coefficients of the same model. The evolution of the pressure coefficient over the roof and the corresponding values were in good agreement, except for the pressure coefficients obtained from the CFD model on the windward edge of the roof. Also, the pressure coefficient from the CFD model recorded on the leeward edges of the roof of (Cp=-0.76) was slightly higher than the value of (Cp=-0.71) reported by Holmes (2011).

It should be mentioned that the values of the pressure coefficient near the ridge of the roof were not reported in the wind tunnel tests (Holmes, 2001), where the pressure coefficient changes from 0 on the windward roof to -0.56 on the leeward roof.

The CFD model includes the transitional pressure change near the ridge and reports pressure coefficients from -0.10 on the windward side to -0.56 on leeward side, thus showing a good agreement with the results provided by Holmes (2001). Pressure coefficients from the CFD model were selected along the middle line of the roof surface, starting from the windward edge of the roof, and extending until the edge of the leeward side of the roof, as illustrated by Fig. 3.39.

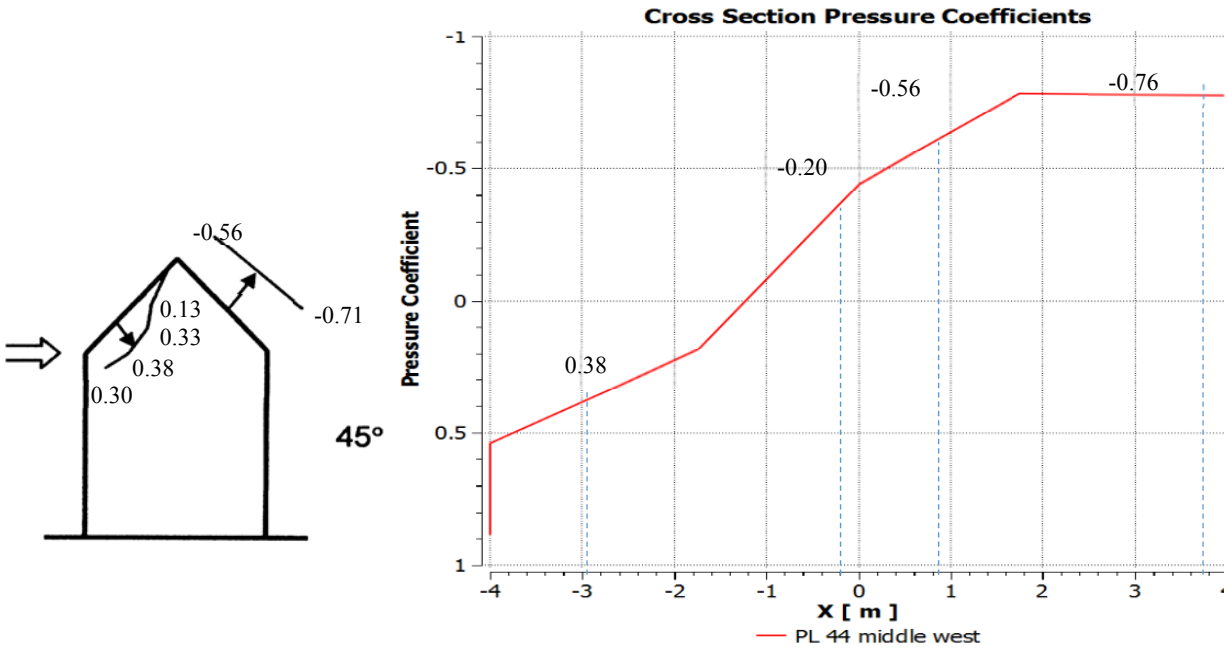


Fig. 3. 39. Pressure Coefficient distribution on the roof middle cross-line, roof slope (45º), h/d=1, d=8m: a) Adapted from Holmes (2001) b) Current CFD study

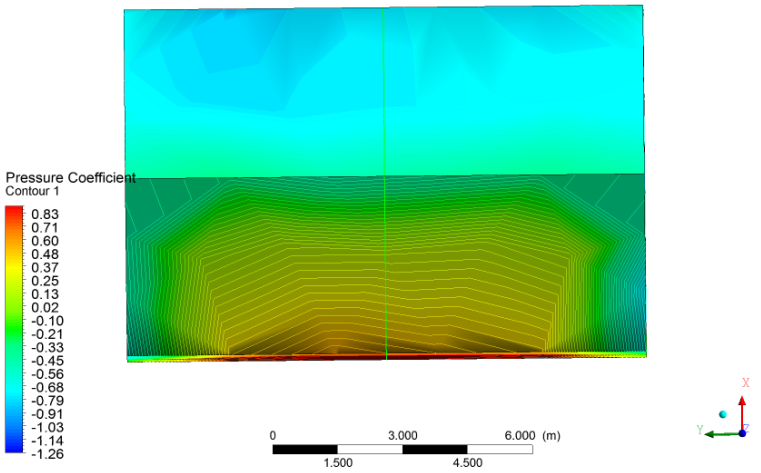


Fig. 3. 40. CFD model, Slope (45º), middle line, h/d=1, d=8m

Also Fig. 3.40 depicts the pressure coefficient contour for the entire surface of the roof. As the wind is perpendicular to the ridge direction, a higher-pressure coefficient can be observed on the windward side of the roof, which changes gradually into suction for the leeward side of the roof. Since this transition is not uniform along the roof surface, and it was not addressed in the study

performed by Holmes (2011), the current study provides two other cross lines, line 46 and line 47, which are situated at 2.0 m and 0.5 m from the east roof edge, respectively (Fig. 3.41).

The pressure coefficient for the other two symmetrical lines corresponding to the west edge were nearly identical to those of the two east lines, for the (90º) wind direction, and thus they were not reported here.

Figure 3.41 indicates that the pressure coefficients on the leeward side of the roof are in good agreement with those on the middle crossline as evolution and magnitude are similar to the pressure coefficients reported in Fig. 3.39. However, the pressure coefficient on the windward side of the roof decreased proportionally with the distance from the middle line of the roof.

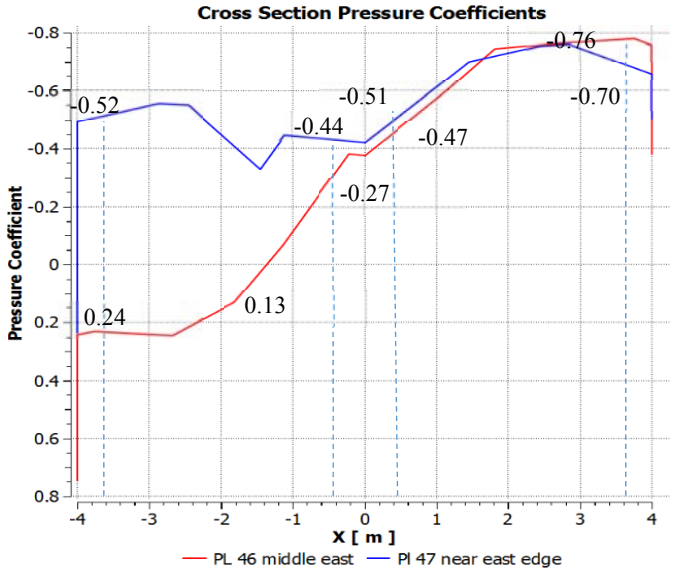


Fig. 3. 41. Pressure Coefficient distribution on the roof side lines 46 and 47, roof slope (45º), h/d=1, d=8m

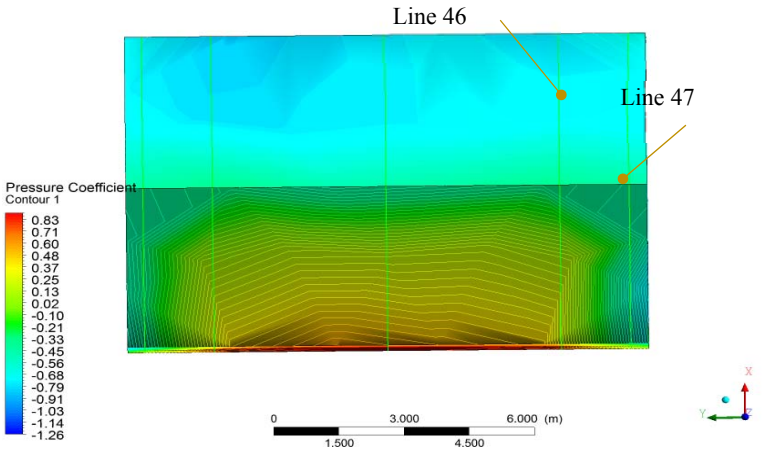


Fig. 3. 42. CFD model, Slope (45º), h/d=1, d=8m

The decrease in wind induced pressure coefficient on the windward side is greater for line 47 (Fig. 3.41), which indicates a change in the local flow formation around the edge of the roof. However, pressure coefficients on the leeward side, are very similar along the 3 lines (45, 46 and 47) as shown in Figs. 3.39 and 3.42. Strength of swirling is shown in Figs. 3.43 and 3.44 and reveals a large vortex similar in shape to the horseshoe vortices. This engulfs not only the windward edges of the roof, but it extends beyond the ridge, influencing the turbulences on the leeward and east and west edges of the roof, as indicated by the negative pressure coefficients in Figs. 3.39 and 3.42.

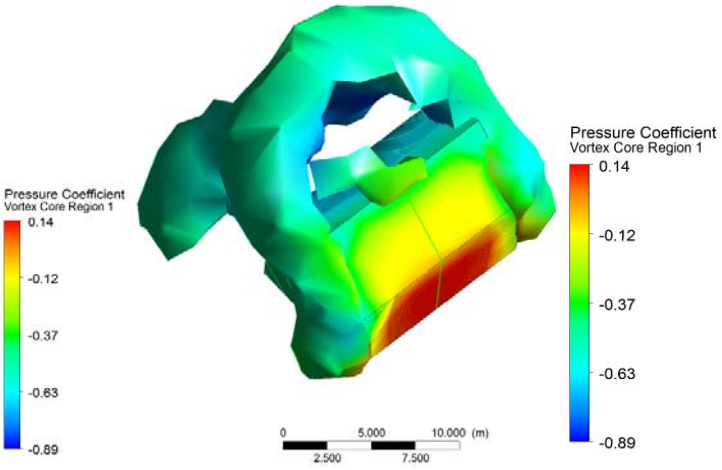


Fig. 3. 43. Swirling strength, CFD model, Slope 45º, isometric view, h/d=1, d=8m,

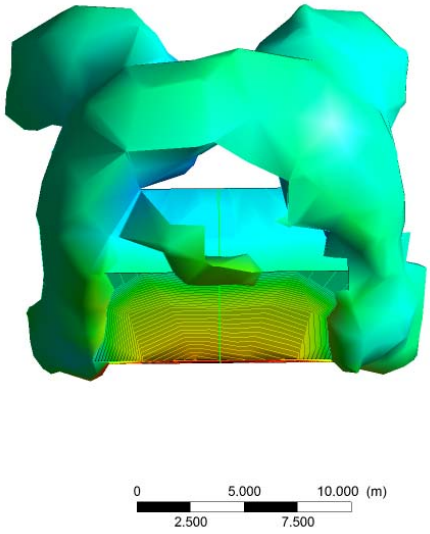


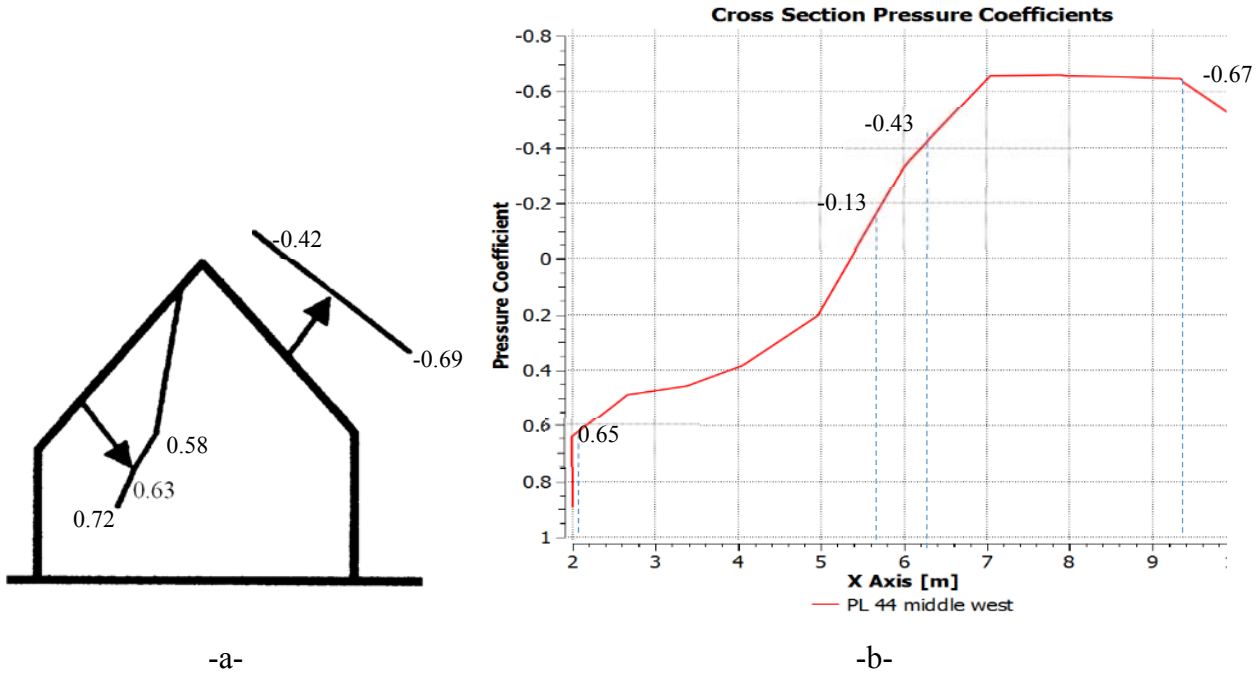
Fig. 3. 44.Swirling strength, CFD model, Slope 45º top view, h/d=1, d=8 m,

b) Bare gable roof (45º), ratio height to depth h/d =0.40

Figure 3.46 a) shows the wind tunnel results obtained by Holmes (2001) on a gable roof sloped at 45º using ratio of height to depth equal to 0.4, while Fig. 3.46 b) displays the pressure coefficients for the corresponding building model, obtained from the CFD simulations.

In general, good agreement can be observed between the current CFD study and the results by Holmes, (2011). The pressure coefficient on the windward roof edge (Cp = 0.65) in the CFD study was lower than the wind tunnel results (0.72) reported by Holmes (2001). Also, a slightly higher pressure coefficient was recorded by the CFD model at the leeward edges (Cp = - 0.62) compared

to that reported by Holmes (2001) (Cp = - 0.69). However, the average of the negative pressure coefficients obtained for the leeward side of the roof by CFD model was (Cp mean = -0.60), which is slightly higher than the average (Cp=-0.56) calculated from the wind tunnel results by Holmes (2001). Similar to the previous case, the pressure coefficients adjacent to ridge were not reported in the wind tunnel study performed by Holmes (2001) and they can only be interpreted from Fig. 3.46 as an abrupt change from (Cp= 0) on the windward side, to (Cp = -0.42) on the leeward side. The dashed vertical lines in Fig. 3.46 correspond to the location of the first and last monitored points on the windward and leeward side of the roof, as reported by Holmes (2001).



-a- -b-

Fig. 3. 45. Pressure coefficient distribution on the roof middle cross-line, roof slope 45º, h/d=0.4, d=8m: a) Adapted from Holmes (2001); b) Current CFD study.

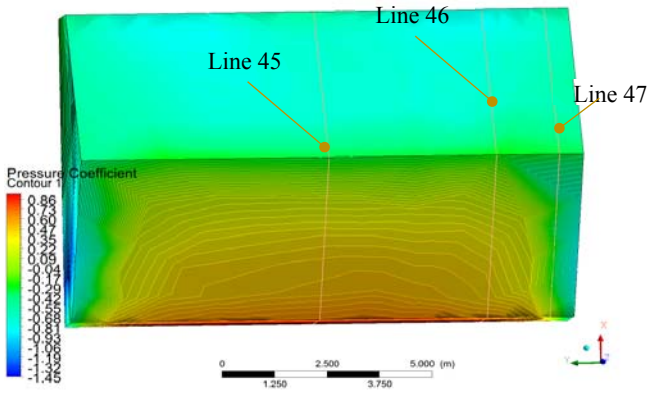


Fig. 3. 46. Holmes model for (45º), h/d=0.4, d=8m

Figure 3.47 indicates that the pressure coefficient on the leeward side of the roof remains in good agreement with Cp on the middle crossline, in terms of evolution and magnitude (Fig. 3.45 a). However, the pressure coefficient on the windward side of the roof, decreased proportional with the distance from the middle cross line of the roof, reaching value of (Cp = -0.5) in top quarter of the windward line 47. This indicates an increase in the suction along line 47, when compared with the line 46 (Fig. 3.47).

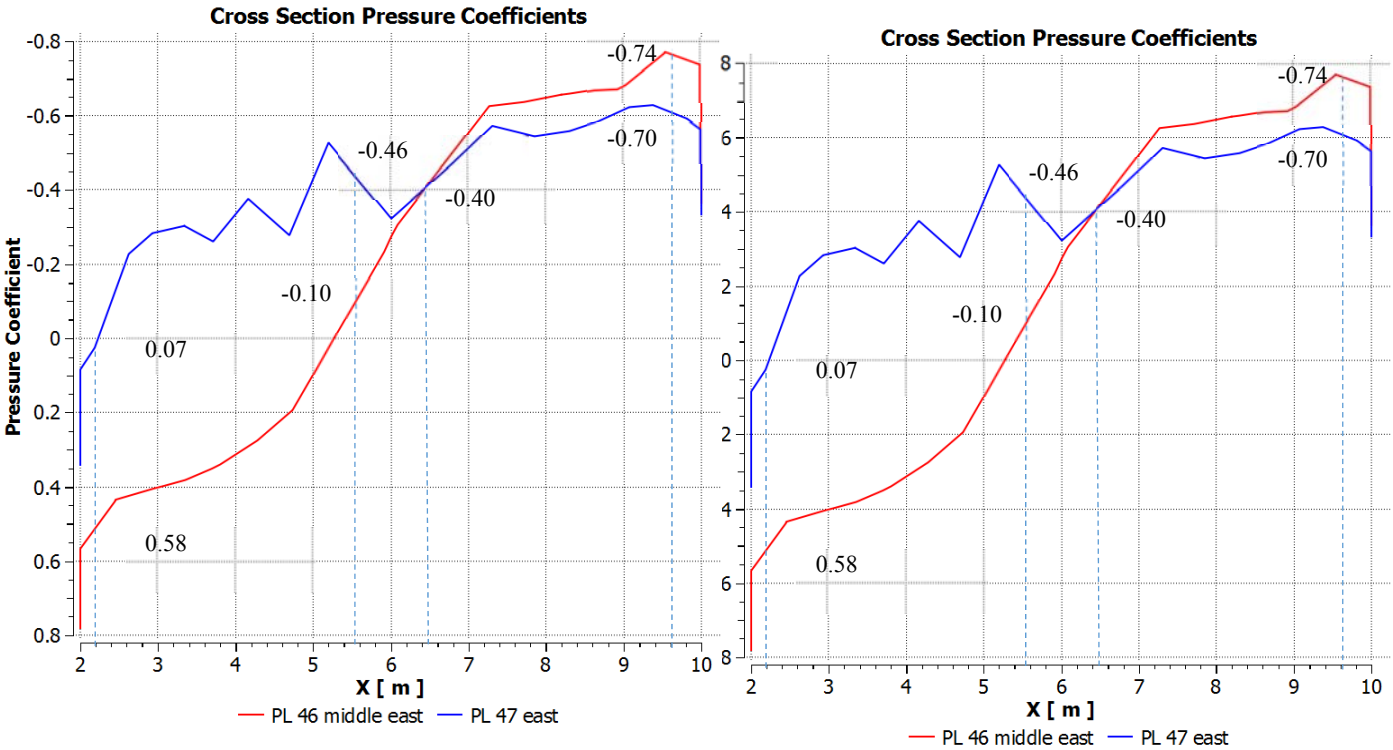


Fig. 3. 47. Pressure coefficient distribution on the Lines 46 and 47, roof slope (45º), h/d=1, d=8m.

The swirl strength reveals the formation of longitudinal vortices along each lateral edge of the windward side of the roof, as shown in Figs. 3.48 and 3.49. A swirl formation can be noticed along the longitudinal direction, in the vicinity of the ridge, which justifies the sudden decrease in pressure coefficients over the ridge area, as reported by Holmes (2001) and by the current CFD study (Figs. 3.45 and 3.47).

This turbulent flow formation swiped part of the leeward surface of the roof and detached downstream, as indicated by the Fig. 3.45 and Fig. 3.47, thus justifying the pressure coefficient values of (Cp=-0.67, -0.74 and -0.70) recorded by the CFD and (Cp=-0.69) recoded by Holmes 2011.

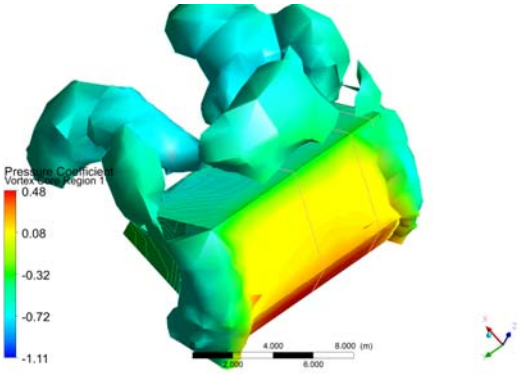


Fig. 3. 48. CFD model, Swirling strength, Lateral view, h/d=0.4, d=8m, slope 45º

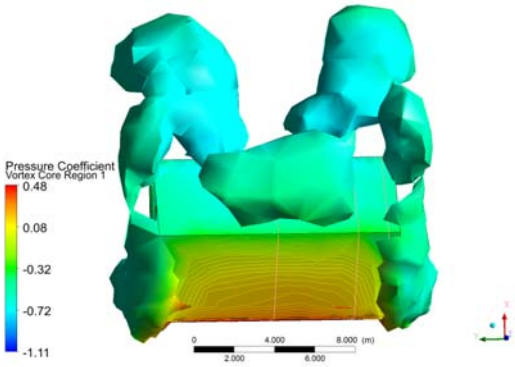
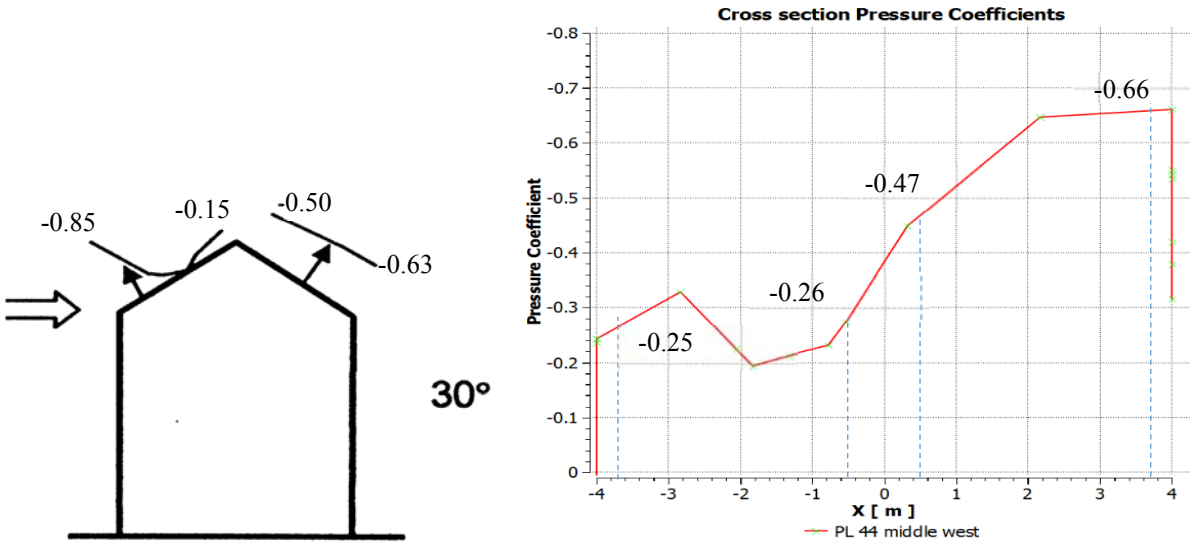


Fig. 3. 49. CFD model, Swirling strength, Front view, top view, h/d=0.4, d=8m, slope 45º

c) Bare gable roof (30º), ratio height to depth h/d = 1

Figure 3.50, a) shows the wind tunnel results reported by Holmes (2001) for a gable roof inclined at (30º) for a building model with height to depth ratio of 1, while Fig. 3.50, b) displays the pressure coefficients obtained from the current CFD simulations for a building and roof model. For the pressure coefficients monitored on the middle cross-line of the roof, a good agreement was obtained.

The pressure coefficients for the windward surface of the roof started at a value of (Cp = -0.25), when compared with the (Cp = -0.85) reported by Holmes (2001), however, after encountering a sudden drop around the middle region of the windward surface, the pressure coefficients increased near the ridge until (Cp = -0.26), which is lower than the wind tunnel result of (Cp = -0.15). The CFD model exhibited a transitional pressure change over the ridge of the roof, from (Cp = -0.26) on the windward side to (Cp = -0.47) on the leeward surface. The leeward side of the roof experienced a gradual decrease of pressure coefficients from (Cp = -0.5 to Cp = -0.63) in the wind tunnel test (Holmes, 2001) and slightly more accentuated decrease, from (Cp = -0.47 to -0.66) as reported in the current CFD study.



-a- -b-

Fig. 3. 50. Pressure Coefficient distribution on the roof middle cross-line, roof slope (30º), h/d=1, d=8m: a) Adapted from Holmes (2001), b) Current CFD study.

Moreover, the pressure coefficients for lines 46 and 47 (Fig. 3.51) showed a good agreement with the pressure coefficient values reported for the middle crossline. However slightly lower suction on the windward side of the roof and higher suction on the leeward side was observed for line 46, while the line 47 much higher suction or negative pressures for both windward and leeward sides of the roof was observed (Fig. 3.52).

Swirling flow strength are presented as a function of pressure coefficient in Figs. 3.53 and 3.54. On the windward edge of the roof, a longitudinal vortex formation was noticed, which detaches

from the roof, before the ridge and travels upstream with the flow. Lower pressure coefficients were induced by the longitudinal vortex.

On the leeward surface of the roof, the swirl formations were stronger but detached on the main region of the roof and remain attached only along the lateral edges and on the lower corners (Fig. 3.54).

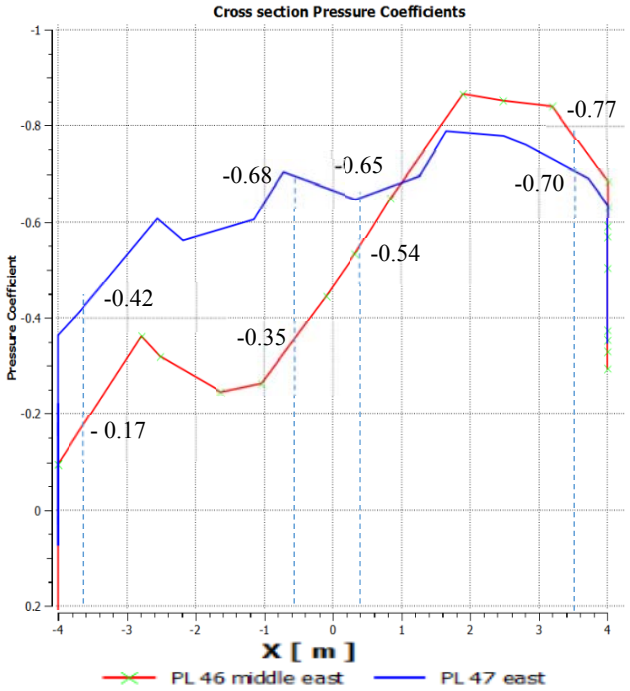


Fig. 3. 51. Pressure coefficient distribution on the Lines 46 and 47, CFD, Slope (30º), h/d=1, d=8m.

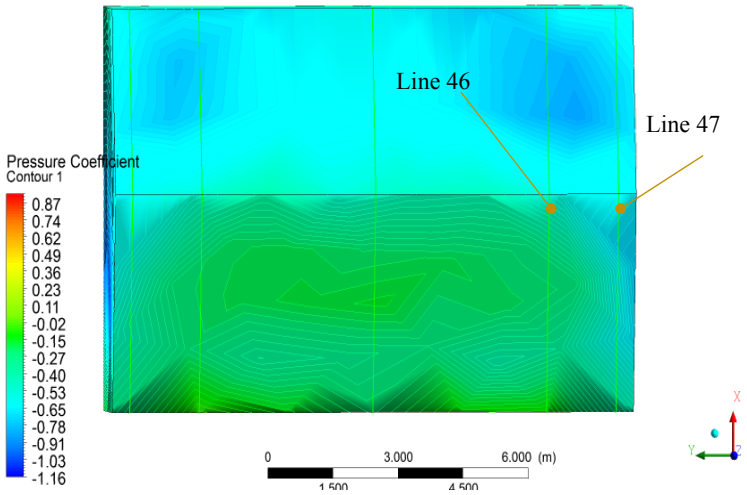


Fig. 3. 52. Holmes model, Slope (30º), 5 lines, h/d=1, d=8m

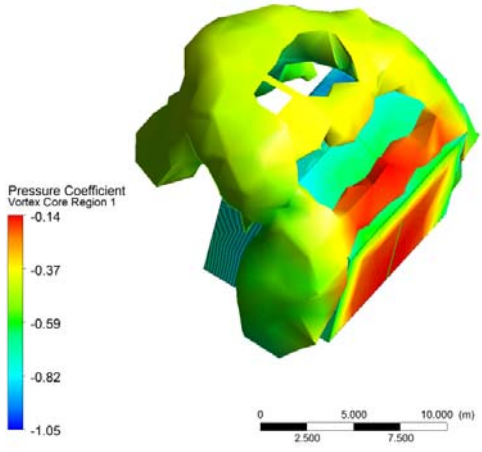


Fig. 3. 53. Swirling strength CFD model, Slope 30º, isometric view h/d=1, d=8m.

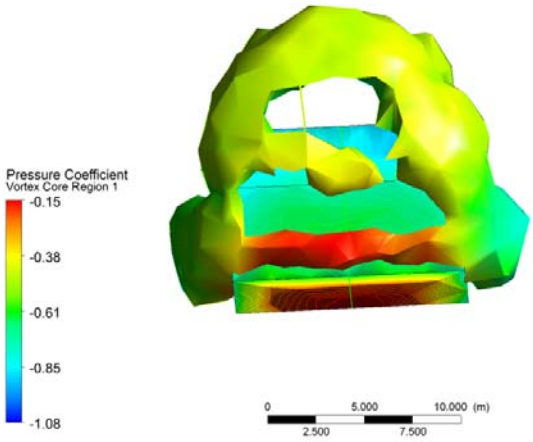


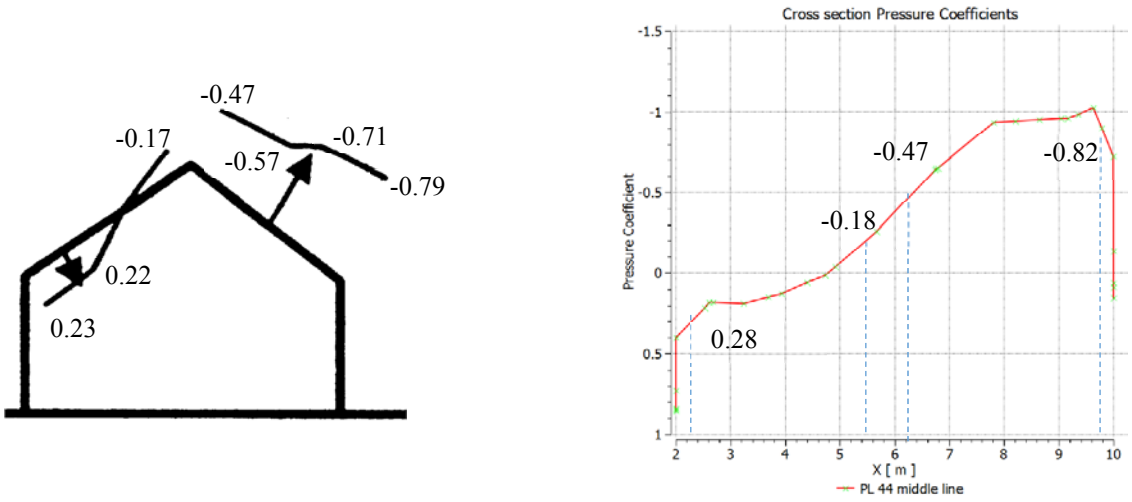
Fig. 3. 54. Swirling strength CFD model, Slope 30º, Front view, h/d=1, d=8m.

d) Bare roof (30º) and ratio of height to depth h/d =0.4

For the final validation case, the wind tunnel results reported by Holmes (2001) on a gable roof inclined at 30º and for a building model with height to depth ratio of 0.4 (3.49), were compared with the pressure coefficients obtained from the CFD simulations performed on corresponding building and roof model.

Good agreement was obtained between Holmes (2001) and current CFD study as it can be noticed in Figs. 3.55 a) and b). However, the pressure coefficient near the north leeward edge of the roof in the CFD study showed slightly higher negative pressures of (Cp = -0.82), than (Cp = -0.79) as reported by Holmes (2001).

Also, over the ridge of the roof, the transitional pressure changed from (Cp = -0.17) on windward side to (Cp = -0.47) on leeward side, compared to values obtained in the current CFD of (Cp = -0.18 to -0.47).



-a- -b-

Fig. 3. 55. Pressure Coefficient distribution on the roof middle cross-line, roof slope (30º), h/d=0.4, d=8m: a) Adapted from Holmes (2001) b) Current CFD study

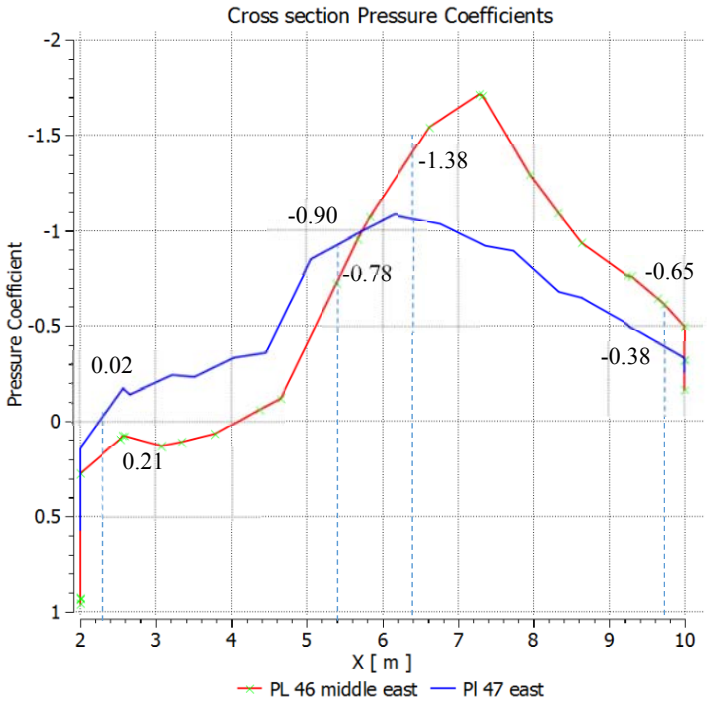


Fig. 3. 56 Pressure coefficient distribution on Lines 46 and 47, CFD, Slope (30º), h/d=0.4, d=8m.

Similar to the previous validation cases, additional transversal lines 46 and 47 located at 2.0 m and 0.5 m from the east edge of the roof were investigated and the pressure coefficients were reported in Fig. 3.56.

Figure 3.56 indicates that pressure coefficient is lowest on the leeward side, nearly 1.50m away from the ridge. Values of Cp = -1.70 was recorded on line 46, while lowest Cp along line 47 was Cp = -1.08, located on the leeward surface of the roof.

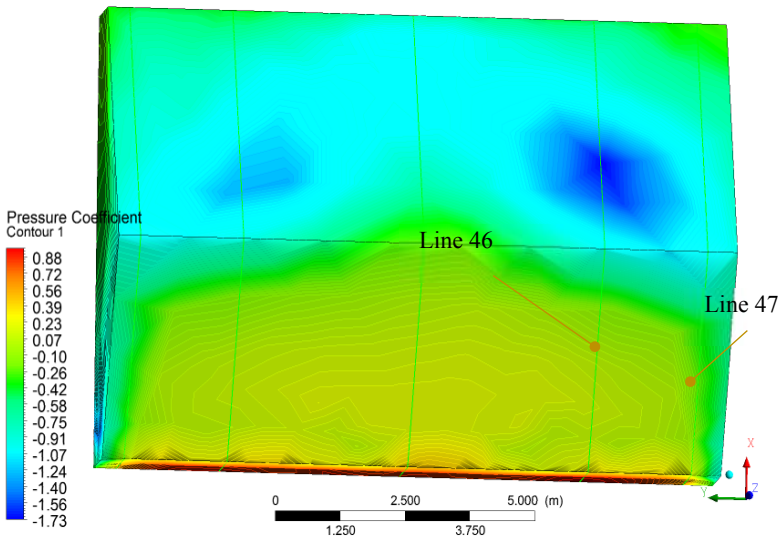


Fig. 3. 57. Holmes model, Slope (30º), h/d=0.4, d=8m

The swirling strength formed by the flow exhibited, as presented in Figs. 3.58 and 3.59, show a major vortex formation shedding on the leeward side of the roof and from the two lateral corners in the vicinity of the ridge, but no other significant swirl formations were noticed on the roof region.

The swirl flow formation detaching from the leeward side of the roof confirms the sudden decrease of pressure coefficient for lines 46 and 47. The consistent pressure coefficient evolution for the middle cross-line, where no vortex detachment, was also noticed (Figs. 3.59 and 3.59).

The two flow formations shedding from the windward corners of the building, do not influence the pressure coefficients on the edges of the roof, as can be confirmed by the positive pressure coefficients reported for this region on both line 46 and line 47.

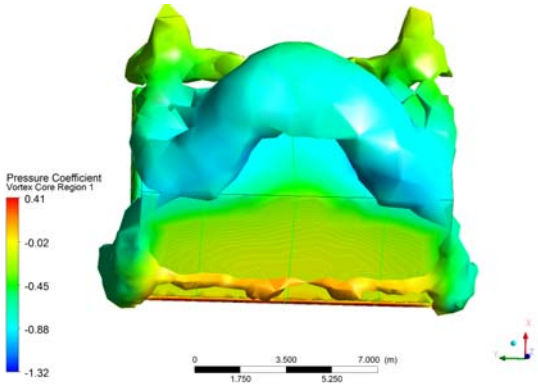


Fig. 3. 58. CFD model, Slope 30º
Swirling strength, h/d=0.4, d=8m,

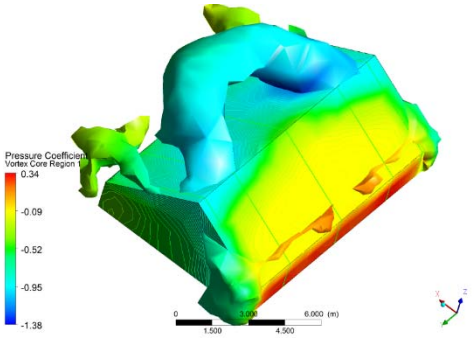


Fig. 3. 59. CFD model, Slope 30º
Swirling strength, lateral, h/d=0.4, d=8m,

Table 3. 3. Comparison between Holmes (2001) full scale and Current CFD study

Slope	45º											
H/d	1						0.4					
Roof Side	Leeward		Windwards				Leeward		Windwards			
Holmes	-0.71	-0.56	0.13	0.33	0.38	0.3	-0.69	-0.42	0.01	0.58	0.63	0.72
Current Study	-0.76	-0.56	0.13	0.3	0.38	0.5	-0.67	-0.43	0.01	0.49	0.55	0.65
Ratio	1.07	1.00	1.00	0.91	1.00	1.67	0.97	1.02	1.00	0.84	0.87	0.90

Slope	30º												
H/d	1						0.4						
Roof Side	Leeward		Windwards				Leeward				Windwards		
Holmes	-0.63	-0.5	-0.15	-0.1	-0.05	-0.85	-0.79	-0.71	-0.57	-0.47	-0.17	0.22	0.23
Current Study	-0.66	-0.47	-0.26	-0.21	-0.22	-0.25	-0.82	-0.9	-0.75	-0.47	-0.18	0.19	0.28
Ratio	1.05	0.94	1.73	2.10	4.40	0.29	1.04	1.27	1.32	1.00	1.06	0.86	1.22

From the simulation of Holmes (2001) full scale cases above, Table 3. 3, it can be concluded that current CFD simulation match very well the Holmes results, for both slopes and heights of the roof, except for the windward side to the slope 30 and h/d =1.

3.1.8. Wind effects on singular solar panels mounted on open versus enclosed /solid bases

The following presents CFD analysis on the effects of wind on singular panels with dimensions of 2m x 1m mounted on solid (with wall all around) or open bases. The analysis considers panels inclines of -15º, 0º, 15º and 35º, for a panel height of 1m above ground.

For solid bases, a clearance of 3” was selected between the roof base and the bottom of the panels. All single panels and their bases were arranged with gaps of 3m between adjacent panels.

The panel with 0º inclination is presented in Figs. 60 (a) to 63 (a), while the panel with (15º) inclination is shown in Figs. 60(b), to 63 (b). Panels with (35º) and (-15º) are presented in the same figures with designations (c) and (d) respectively.

The model mesh consisted of 84,693 nodes and 459,125 elements for all the solid bases, which are placed at the center of a 60m x 60m x 20m (length, width and height) box. Figure 3.60 shows single solar panels mounted on solid bases, while Fig. 3.61 and Fig. 3.62 depict double and single solar panels mounted on open bases.

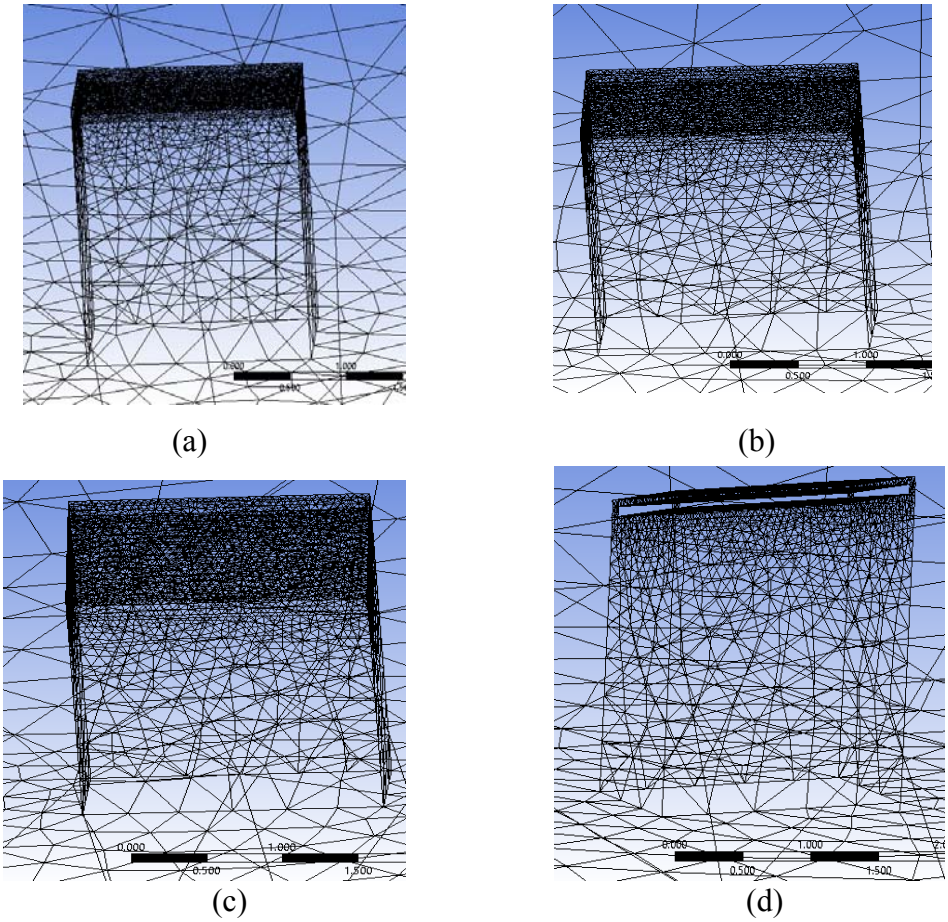


Fig. 3. 60. Single panels on solid bases, Mesh of the model, slopes (a) 0°, (b) 15°, (c) 35°, (c) -15°

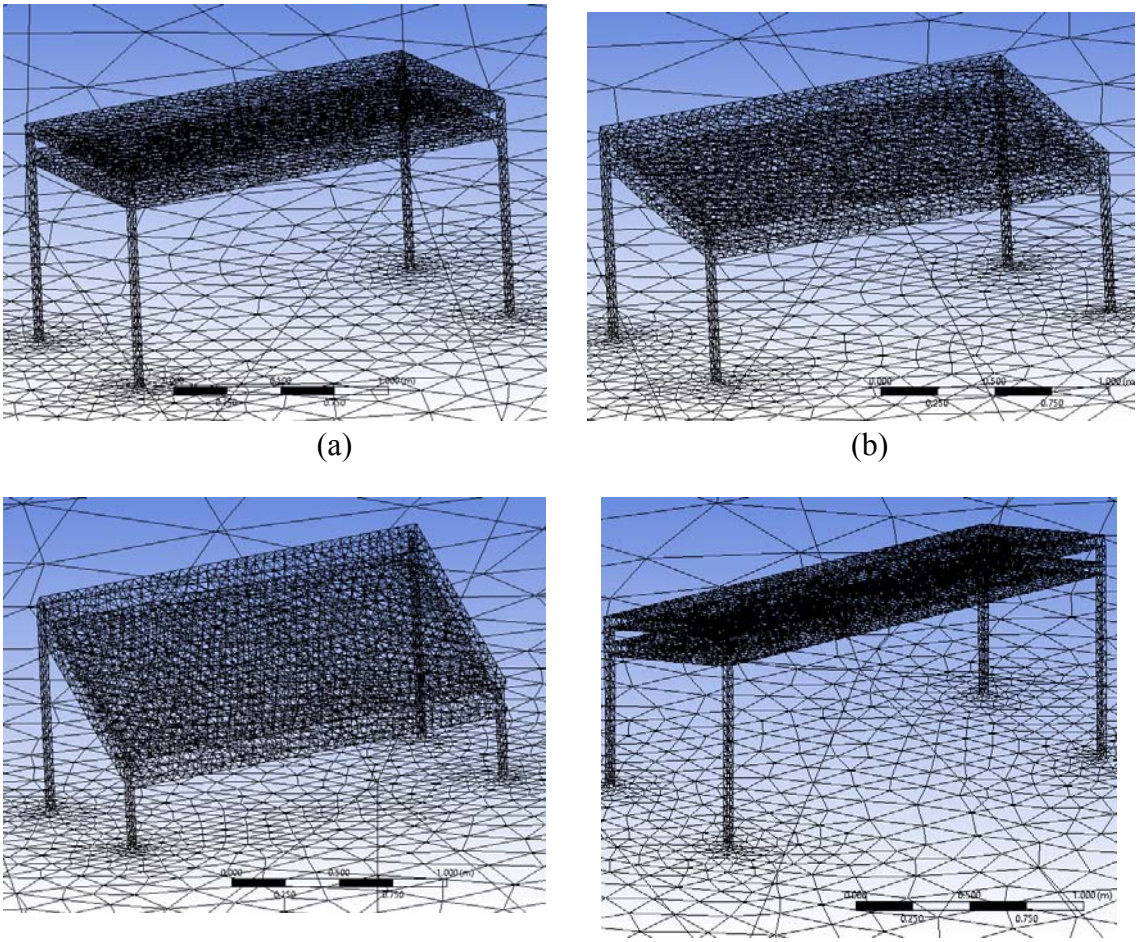
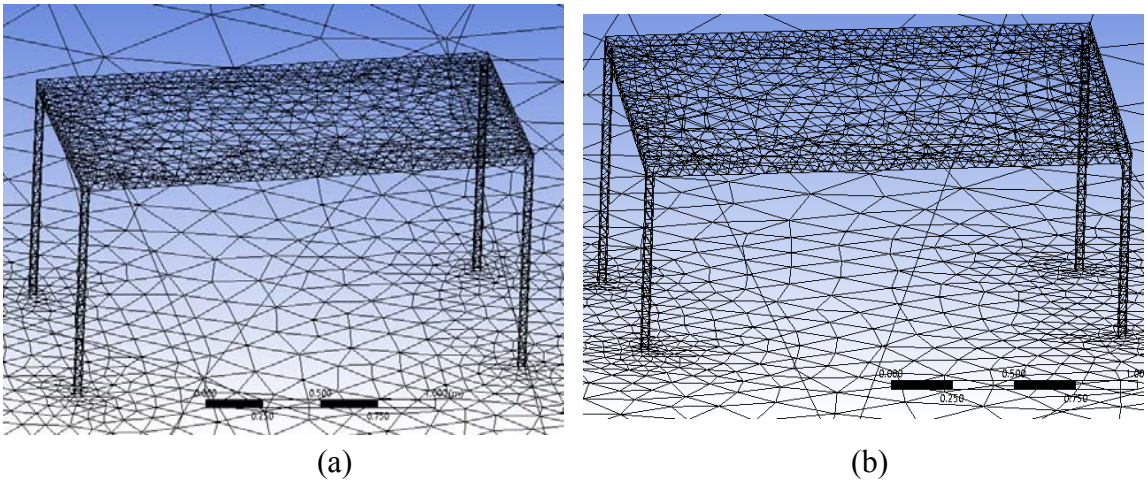
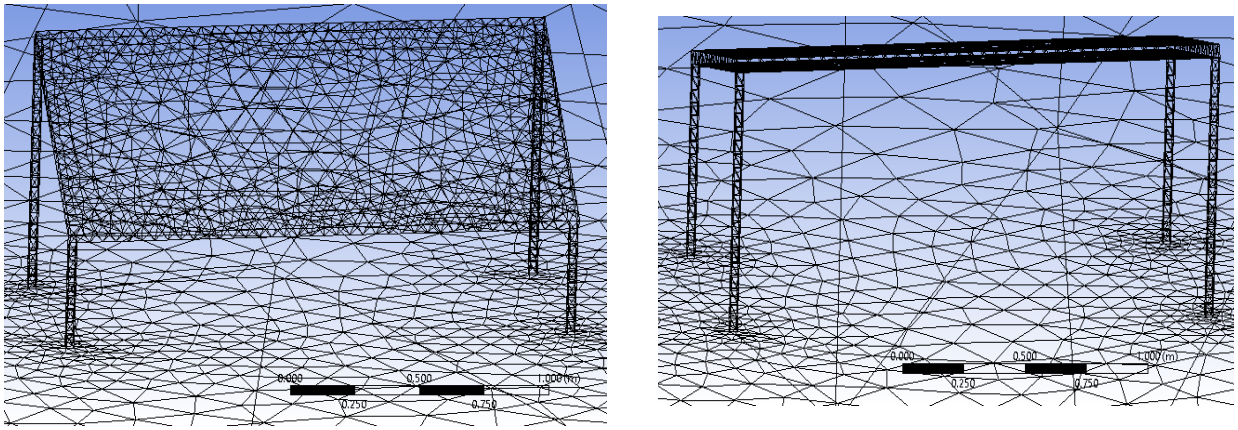


Fig. 3. 61. Double panels on roofs with open bases, Mesh of the model, slopes, (a) 0°, (b) 15°, (c) 35°, (c) -15°





(c) (d)

Fig. 3. 62. Single panels mounted on open bases, Mesh of the model, slopes (a) 0°, (b) 15°, (c) 35°, (c) -15°

Although the (0.0º) inclined panels, causes similar range of pressure like (15º) inclined panel; however, the areas on south and west edges of the panels, subject to very high pressure (-1.11 to -2.41) on the flat panel, Fig. 3.63, are much larger than that areas on (15º) inclined panel, Fig. 3.63. Figure 3.63 illustrates 4 single solar panels, each mounted on a mono sloped solid bases 1 m high above ground. The slopes are (0 º, 15 º, 35 º and -15 º).

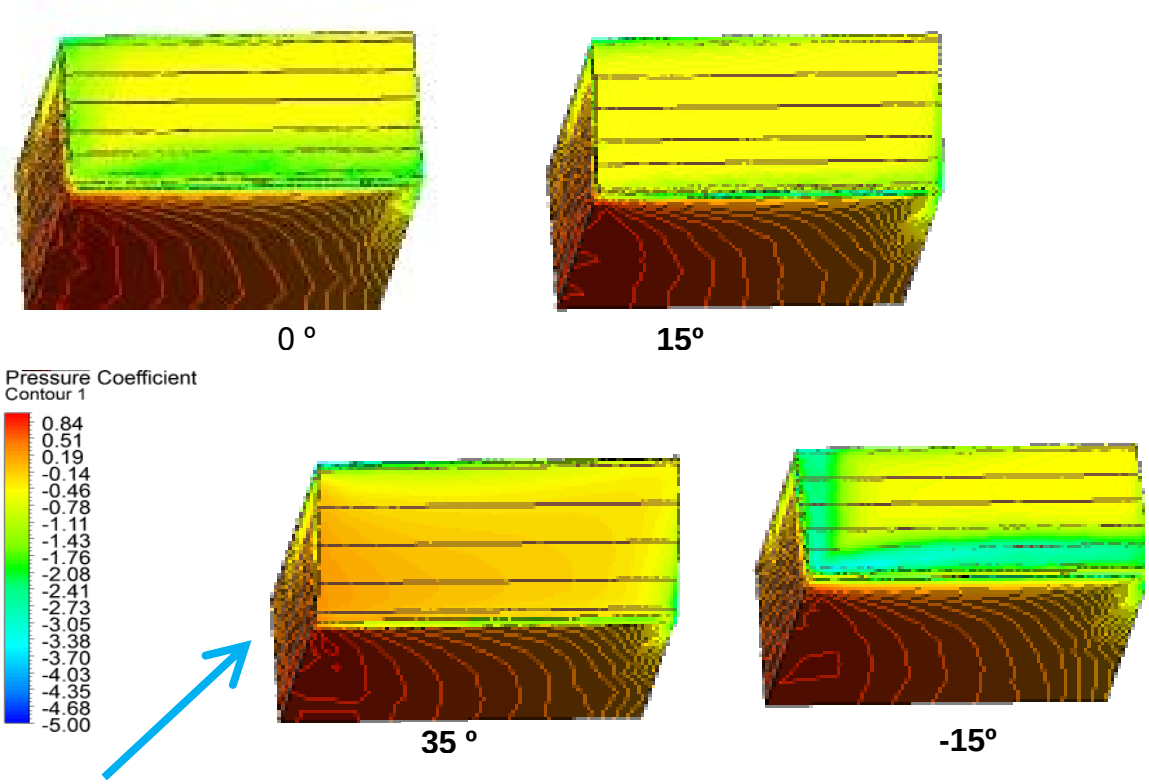


Fig. 3. 63. Single panels on solid bases, Top of panels WD (45º)

In comparison with same solar panels mounted on 4 legs with open space underneath, (Appendix B) it is noted that pressure coefficients are much higher on the panels with solid bases. Figs. 3.64 to 3.70.

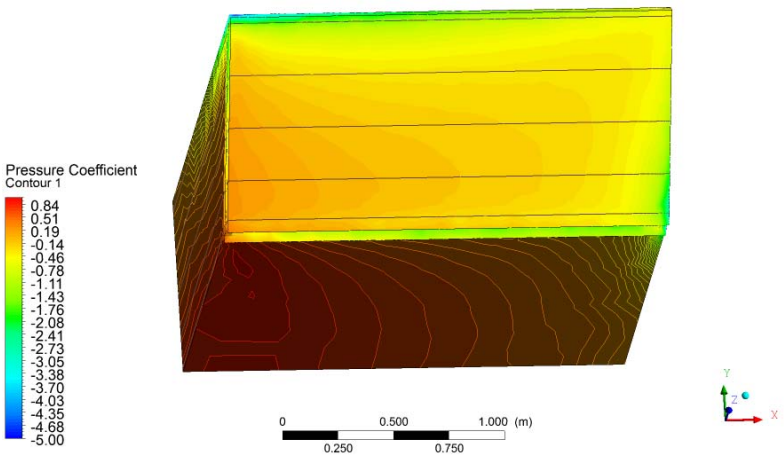


Fig. 3. 64 Single panel on solid base, (35º) slope, top of the panel.

Figures 3.65, 3.66, and 3.67 demonstrate wind pressure coefficients on the panel inclined (35º) and mounted on a closed base. As it appears from Fig. 3.66 for roof under the solar panel and Fig. 3.67 for the bottom of the solar panel, the pressure coefficient diagrams on roof under solar panels and bottom of the solar panels, are very close to identical which means that total pressure coefficients on the roof in presence of solar panels mounted flush to roofs with 3" gap, can be approximated to wind pressure coefficients on top of the panels which are illustrated on Fig. 3.65

The pressure coefficients on top and bottom of the solar panels seem to be close in values and opposite in directions. This observation can be generalized to all panel slopes reported herein.
However, top of the panel in Fig. 4.65 is subjected to very different pressure coefficients range from large on the edges, (Cp=-3.05 to -2.08), to smaller suction in the middle, (Cp=0 to -0.78), and slight pressure, (Cp=0 to 0.51) on the south corner. However, the bottom surface of this panels subject to high suction, (Cp=-4.68 to -2.08), which means that resultant pressure coefficient on this panel might be towards the roof.

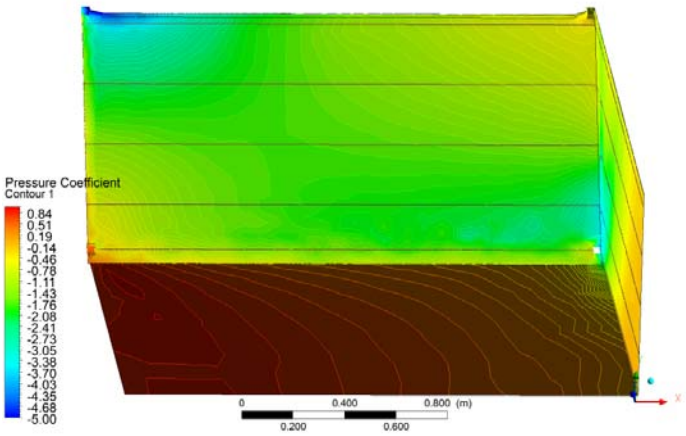


Fig. 3. 65. Single panel on a solid base, (35º) slope, roof top under the panel.

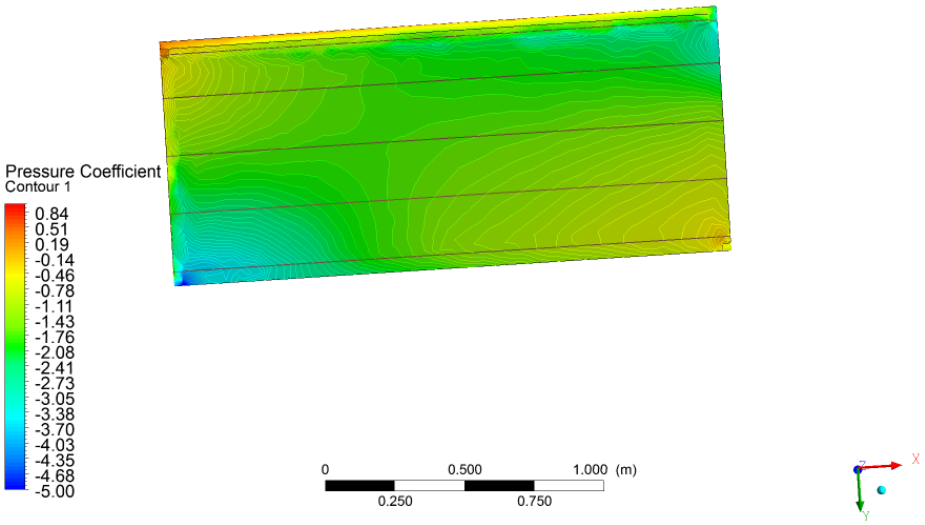


Fig. 3. 66. Single panel on a solid base, (35º) slope, bottom of the panel.

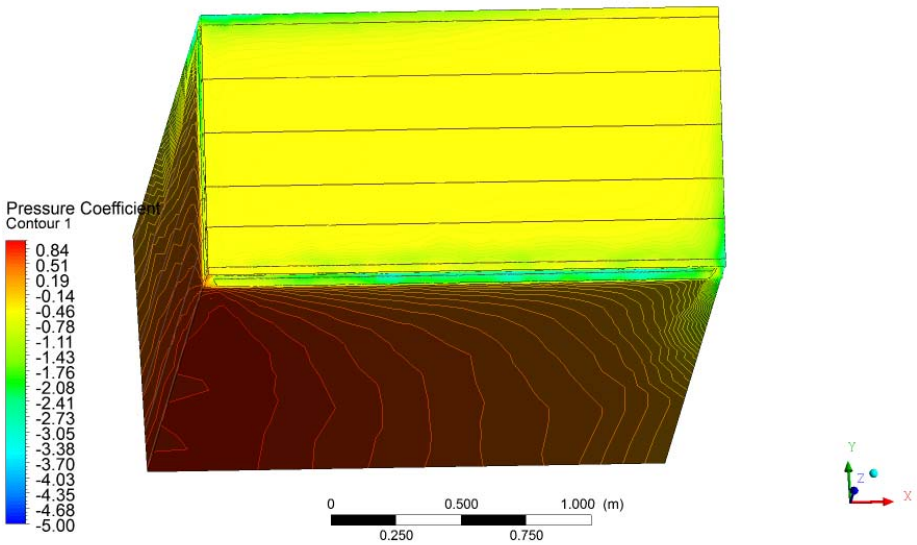


Fig. 3. 67. Single panel on solid base, (15º) slope, top of the panel.

Figures 3.67, 3.68 and 3.69 display wind pressure coefficients on top of a panel, roof under the panel and bottom of the panel which inclines 15º and mounted on a closed base.

Figs. 3.68 and 3.69 exhibit very similar pressure coefficient diagrams on roof under solar panels and on bottom of the solar panels, which look like mirroring of one surface Cp of another. That means that resultant pressure coefficients on the roof can be approximated to wind pressure coefficients on top of the panel which is presented in Fig.3.62.

Top of the panel in Fig. 4.67 subjects to very different pressure coefficients range from large suction on the edges, -3.05 to -2.08, to smaller suction in the middle, 0 to -0.46. However, bottom surface of this panels subject to high suction, -4.03 to -1.76, which means that resultant pressure coefficient on this panel is probably towards the roof.

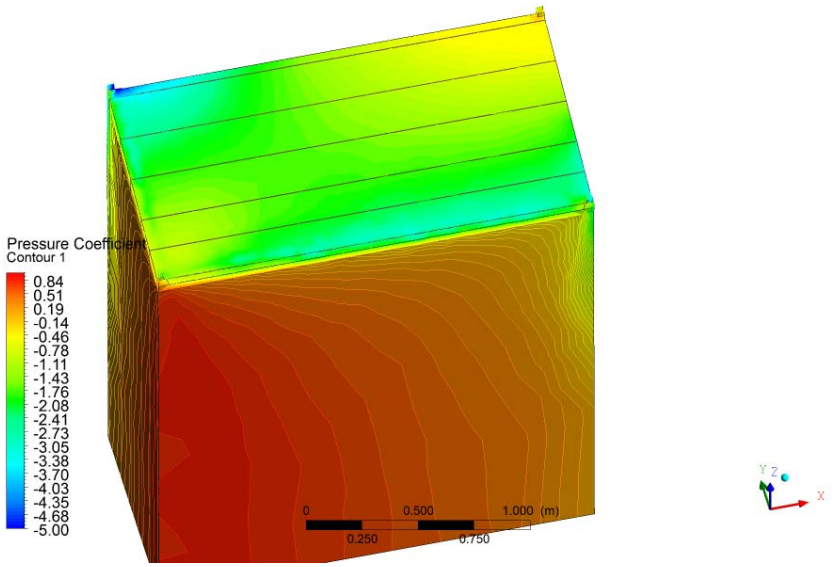


Fig. 3. 68.. Single panel on a solid base, (15º) slope, roof top under the panel.

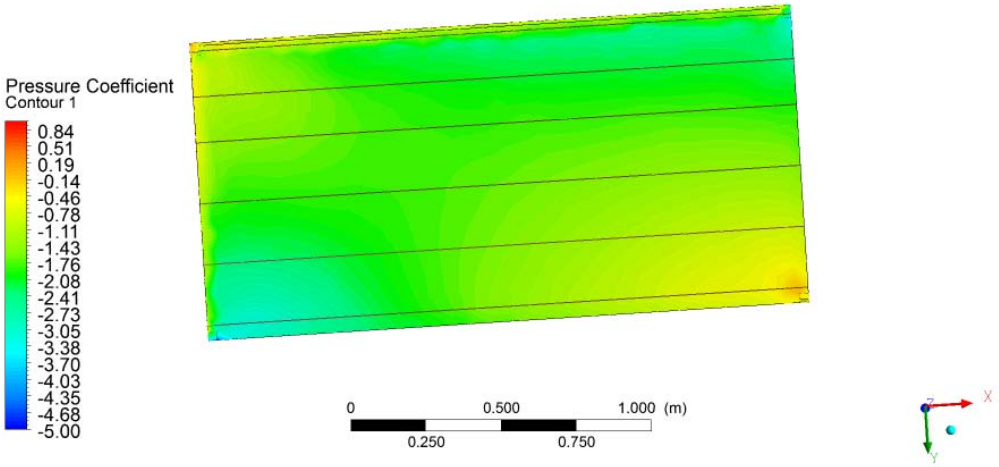


Fig. 3. 69. Single panel on a solid base, (15º) slope, bottom of the panel.

Figures 3.70, 3.71, and 3.72 display wind pressure coefficients on the panel inclined 0º and mounted on a closed base. Different from what noticed panels slopped (35º) and (15º), it is noticed from figures 3.70 and 3.72 that pressure coefficient diagrams on top and bottom of the panels are very similar which indicates that total pressure coefficients on the roof can be approximated to wind pressure coefficients on roof under the panel. In addition, the roof surface under the panels subject to much higher suction, -0.46 to -4.35 than either top or bottom of the panels, -0.46 to -2.73. In other words, for solar panels mounted on (0º) flat roofs, the solar panels might just need to minimum connections with roofs. However, the roof itself might subject to higher suction due the installation of solar panels on the flat roofs. This result seems to be specific to (0º) slopped panels and is different from other slopes (15º, 35º and -15º).

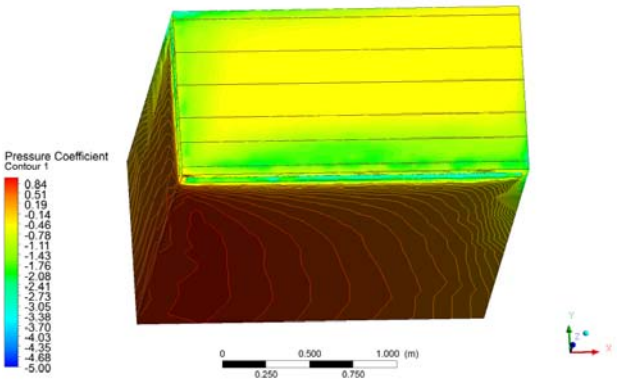


Fig. 3. 70. Single panel on solid base, (0º) slope, top of the panel.

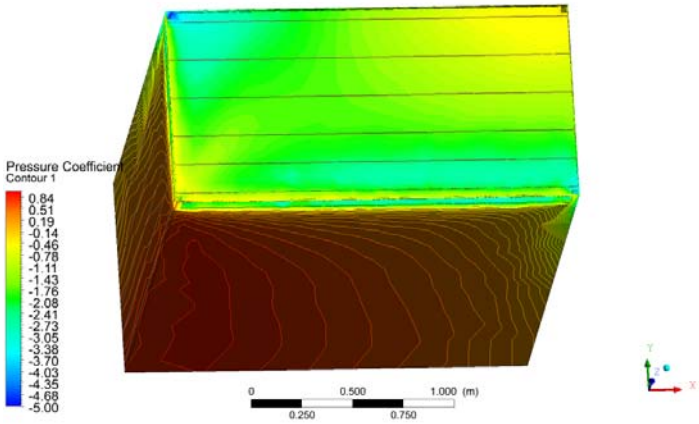


Fig. 3. 71. Single panel on a solid base, (0º) slope, roof top under the panel.

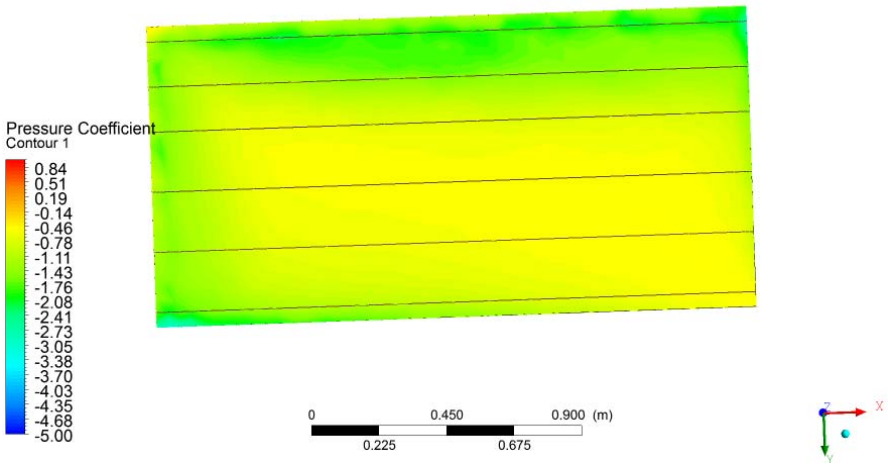


Fig. 3. 72. Single panel on a solid base, (0º) slope, bottom of the panel.

Figures 3.73, 3.74 and 3.75 show wind pressure coefficients on top of panels, roof under the panels and bottom of the panels mounted on roof inclined (-15º) and mounted on a closed base. As it stands out from figures 3.74 and 3.75, pressure coefficient diagrams on roof under panels and on bottom of the panels, are very similar, which might be considered as Cp on one surface is a mirroring of Cp of the other. That results in that total pressure coefficients on the roof can be approximated by wind pressure coefficients on top of the panel which is illustrated in Fig.3.73, which is like the conclusions on the slopes (15º), and (35º) and different from the effects of flat roof, (0º) slope.

Top of the panels in Fig. 4.73 subjects to pressure coefficients range from large suction spread along large areas near the south and west edges, -3.38 to – 17.6, and to much smaller suction in over smaller areas in the middle towards north east corner, 0 to -0.46.

However, roof surface of this panel, Fig. 3.74 subject to much higher suction, -4.35 to -1.76 where the lowest Cp are near the north-west and south-east corners and along the edge while highest spread all over most of the panel. Nonetheless, bottom of the panels, are very similar to surface under the panel, with less intense suction near the corners. That results in the resultant pressure coefficient on this panel might be towards the roof, (pressure not suction), and that resultant Cp on the roof surface due installation of the panels, can be estimated, roughly by the Cp of top of the panels. The estimation might not be conservative because roof surface subject to higher suction than the bottom of the panel.

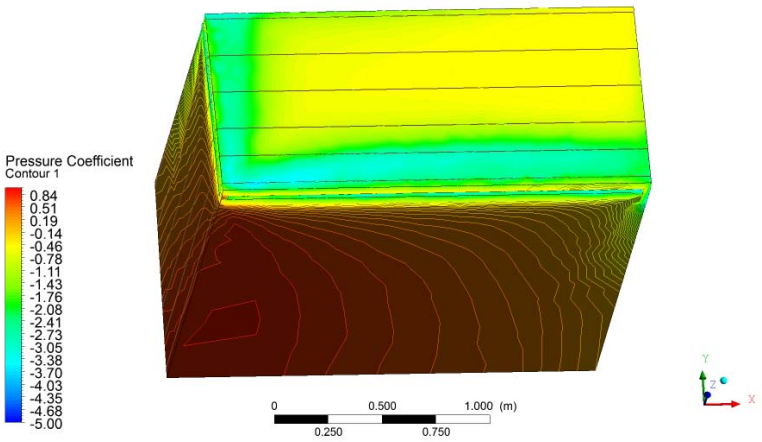


Fig. 3. 73. Single panel on solid base, (-15º) slope, top of the panel.

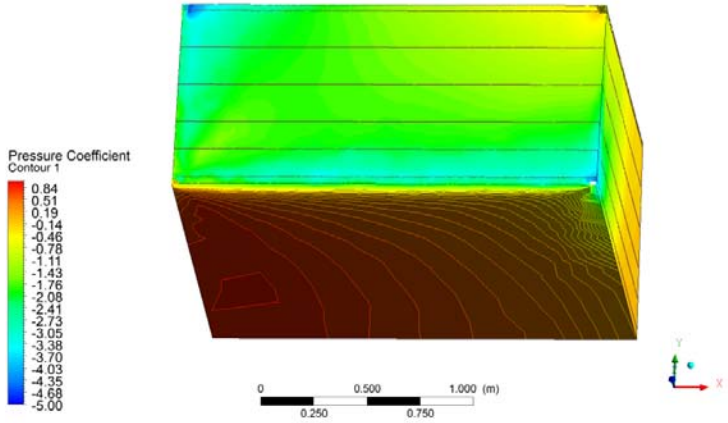


Fig. 3. 74**.** Single panel on a solid base, (-15º) slope, roof top under the panel.

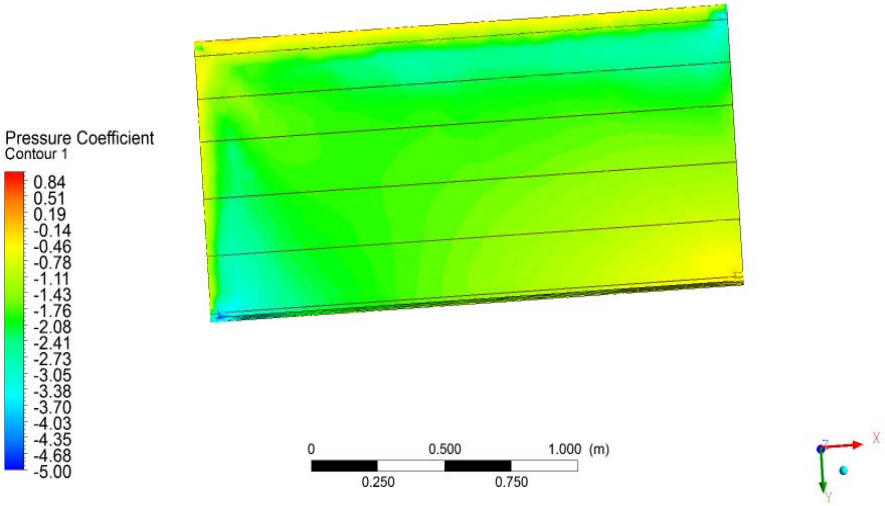


Fig. 3. 75. Single panel on a solid base, (-15º) slope, bottom of the panel.

Moreover, Figs. 3.76 to 3.79 illustrate pressure coefficients detailed along 5 polylines on top, bottom and roof surfaces under the single panels mounted on solid bases, where the clearance between the bottom of the panels and the roof is 3". The polylines are 5- 6 multi level polylines, each of which surrounds each of the panels, and goes along the roof surface underneath that panel. The polylines are shown in Figs. 3.63 to 3.75. Each polyline is mainly a set of 3 parallel lines are located in one plane perpendicular to roof surface.

One main observation in all those graphs (including those in Appendix B), is that pressure coefficients on panels mounted on solid bases, are 1.5 -6 times higher than the pressure coefficients on panels mounted on open bases, largest numbers are for smallest slopes.

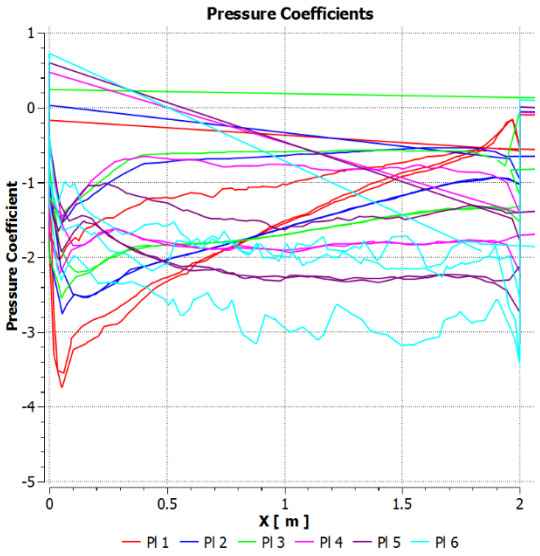


Fig. 3. 76. Panel on roof 3" gap, solid base, 0 º S, 45 º WD

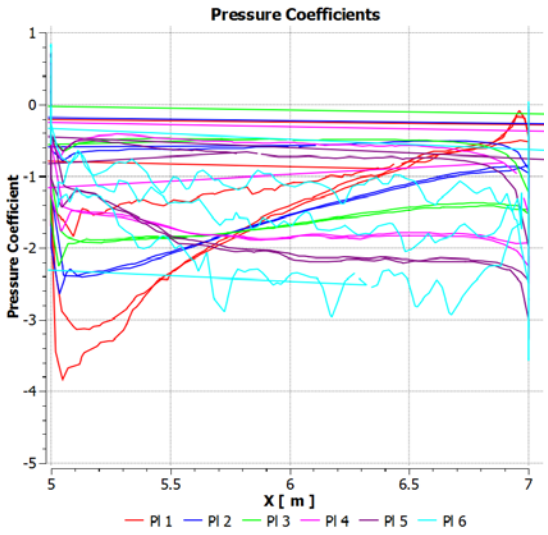


Fig. 3. 77. Panel on roof 3" gap, solid base, 15º S, 45 º WD

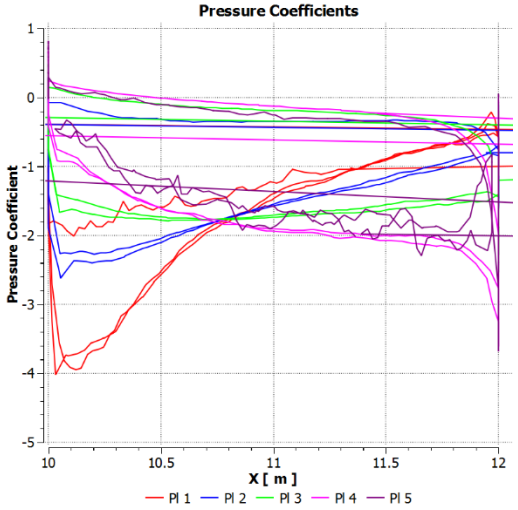


Fig. 3. 78. With panels 3" gap, solid base, 35º S, 45º WD

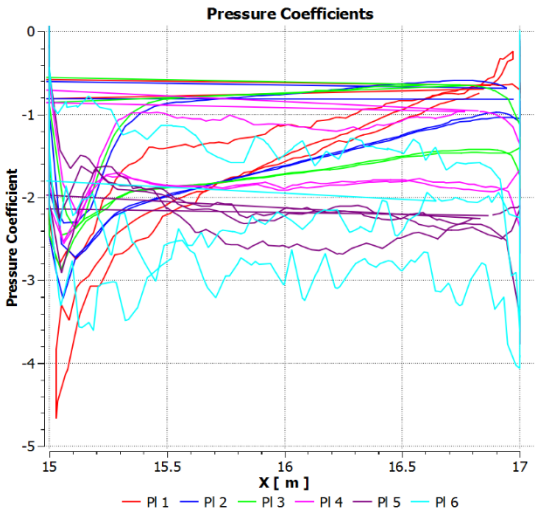


Fig. 3. 79. With panels 3" gap, solid base, -15º S, 45º WD

3.2. CONCLUSIONS

The current research verified averaged maximum pressure coefficients on a canopy structure along two wind directions, and compared results obtained from the CFD analysis performed with the corresponding field measurements.

Good agreement was found between the CFD model analysis and the full-scale measurements of Robertson et al (1985), thus the CFD modeling developed was validated for the structures with large openings.

Other two verifications were performed on a residential building model, and results were compared with the wind tunnel and field experiments performed by Doduak et al (2011) and Zisis (2011). Good agreement was found in both cases; however closer results to the full-scale measurements were noticed for both cases.

The last validation is done on a gable roofed building, which was conducted in wind tunnel, by Holmes 2001. Good agreement was found, in evolution and values, which sometimes were identical.

Then preliminary CFD analysis was applied to analyze wind effects on a single panel mounted on a solid or open base 1 m high above ground. In comparison with same solar panels mounted on a roof with an open base, it was noted that pressure coefficients are much higher for the panels with solid bases.

On the other hand, the pressure coefficient diagrams on roof under solar panels and bottom of the solar panels, are very close to identical which means that total pressure coefficients on the roof in presence of solar panels mounted flush to roofs with 3" gap, can be approximated to wind pressure coefficients on top of the panels. That seems to be true for the panels mounted on roofs inclined (15 º, 35 º and -15 º) but that is not true for panels on flat roofs.

In addition, pressure coefficients on top and bottom of the solar panels seem to be close in values and opposite in directions, which means much smaller resultant forces act on the panels and then on the connections between the solar panels and roofs.

However, different from panels mounted on roofs inclined (35º) and (15º), it is noticed that pressure coefficient diagrams on top and bottom of the panels mounted on flat base, (0 º), are very similar which indicates that total pressure coefficients on the roof can be approximated by wind pressure coefficients on roof under the panel.

That means there is pressure equalization, (cavity equalization) between roof top and bottom of the panels for inclined panels at (15 º, 35 º and -15 º), while pressure equalization is exist between bottom and top of the panels for single panel inclined on flat base (0 º).

CHAPTER 4

Wind-induced pressure on gable roof mounted solar panels: the effect of wind directions and roof slopes

4.1. Introduction

The results of the CFD analyses performed to estimate the wind effects on roof mounted solar panels with solar panels array spacing of 2″ (50 mm) and roof clearance of 3″ (76 mm) are presented in this chapter. The selection of the 2″ (50 mm) spacing and 3″ (76 mm) roof clearance is attributed to the common use of such spacing dimensions in solar panels installation and construction industry. The current study investigates a variety of roof slopes and wind directions including: 35º, 27º and 15º roof slopes, and 0º, 90º and 45º wind directions. Wind directions 0º and 90º are used in this research since they represent the directions for which the design codes recommend maximum and minimum wind-induced pressure coefficients on the roof, without solar panels, respectively (NBCC, 2015, ASCE/SAE07-10). Moreover, 45º wind direction was selected because several studies reported that the 45º wind direction may present a critical case for flat roof mounted solar panels (Samani (2016), Xypnitou, et al. (2012) and Stathopoulos et al, (2015)). The CFD simulation were performed for an extensive number of cases, but due to space limitations, results for all the additional investigated cases of spacing, clearance, slope and wind directions are presented in the Appendices C, D, and E. The wind effects induced on roof mounted solar panels are presented and compared in this chapter in order to investigate the variation of pressure coefficients and the evolution of the wind speed profiles due to the change in roof slopes and wind directions. Also, 19 longitudinal polylines were created along each of the two inclined surfaces of the gable roof. The pressure coefficients were integrated along the roof surfaces, as well as on the bottom and top surfaces of the solar panels. Six vertical polylines were also identified at the two corners of the solar array, as well as in the middle and on the side edge of the roof, in order to study the variation of wind velocity and pressure coefficient profiles above and underneath the solar panels.

The net pressure coefficient is obtained as an algebraic summation of Cp on the top and bottom surfaces of the panels, as well as on the roof surface under the panels. Only the Cp values on the roof surface are obtained from the CFD analysis, while the summation of top and bottom of the panels is transferred to the roof surface via the railing supports (standoffs), which are fixed to the roof surface. This approach allows the distinction between the Cp on the panels and on the roof and facilitate the design pressures for each component of these systems.

4.1.1. Wind loads and relation to pressure coefficient factors

In order to be able to interpret and discuss the wind design recommendations for solar panels installed on roofs, the relation between the pressure induced by wind on the exposed surfaces and the design wind load must be introduced, as formulated in the NBCC (2015) design code. The external pressure or suction, P [Pa], due to wind acting on a surface of a building can be calculated using the following formula, (NBC, 2015)

$$P = I_w q C_e C_g C_p \ (P_a) \qquad (1)$$

Where I_w is the importance factor,

$q\ (P_a)$ is the reference velocity pressure for a certain region

C_e is the exposure factor,

C_g is the gust factor, and

C_p is the external pressure coefficient averaged over the area of the surface considered.

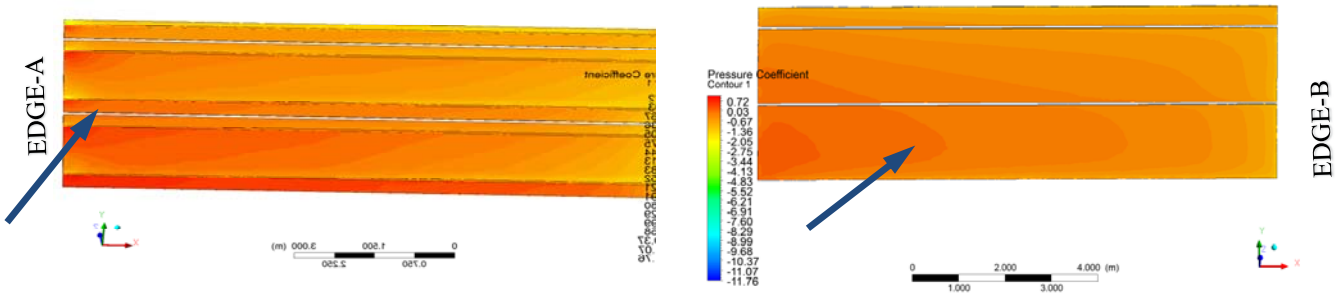
Only the external pressure coefficient, C_p, depends on the geometry of a structure and it can be approximated from the code. Values for C_p can be obtained from experiments or through CFD modeling. Therefore, it seems appropriate to express the wind effects on roofs and roof-mounted solar panels in terms of pressure coefficients.

4.2. Effects of wind directions on solar panel arrays for 2″ spacing and 3″ roof clearance, mounted on 35º gable roofs

In order to investigate the effects of the roof slopes on the pressure coefficients, roof slopes 35º, 27º and 15º were investigated herewith for 40 m/s wind speed and 0º, 45º and 90º wind directions. Wind speeds of 10 m/s were also investigated for the same roof slopes and wind directions, and results are included in Appendices B and C. Roof slope and wind direction cases which resulted in the largest total pressure coefficients are further investigated for different spacing and clearance values in Chapter 5. The case with spacing between the rows of panels of 2″ and clearance between the roof and the panels of 3″ were used in this chapter, for panels installed in the interior region of the gable roof, as designated by the design code (NBCC, 2015).

4.2.1. Pressure contours distributions for wind direction 45º

The pressure coefficients distributions for solar panels mounted on a 35° inclined gable roof subjected to wind speed of 40 m/s and wind direction of 45º, are detailed in the current section. Figures 4.1, 4.2. and 4.3 show the pressure coefficient distributions on the bottom and top surfaces of the solar panels and roof surface, respectively, for the windward side of the structure. The two side edges of the roof were denoted as edge A and edge B, as represented in Fig. 4.1.



a) **b)**

Fig. 4. 1. Pressure coefficient distribution on a) Bottom surface of the solar panels, and b) Top surface of the solar panel for roof slope 35º and wind direction 45º, windward side

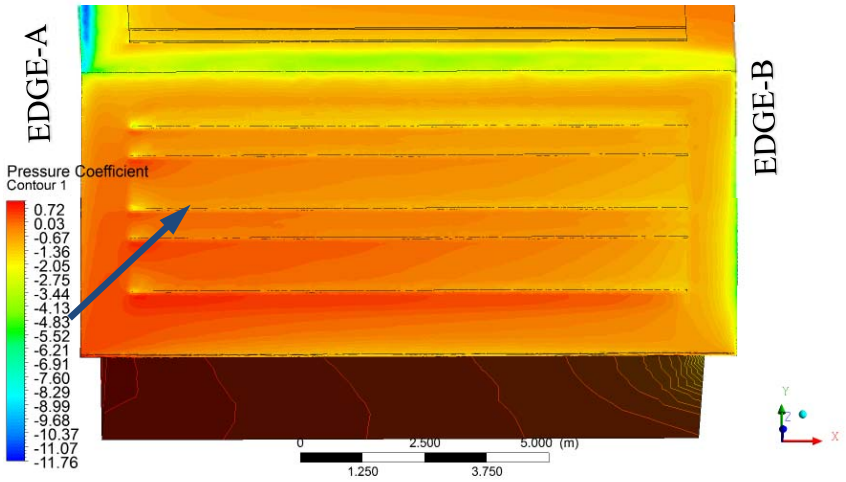


Fig. 4. 2. Pressure coefficients on roof under the solar panels, wind direction 45º, windward side

In general, pressure coefficients, of up to Cp = 0.72, were obtained on the windward corner of edge A of the roof. Such pressure coefficients were higher than those obtained for the rest of the roof surface under the panels. The top of the panels on the leeward side of the roof were subjected to slightly higher suctions than the top surface of the panels on the windward side of the roof. The highest suction value Cp = -11.0 was obtained at edge A on the leeward surface of the roof. However, it should be noted that these values were obtained from points located on the roof surface, but outside the area were solar panel were installed. When comparing figures 4.1 and 4.2, it can be observed that the distribution of the pressure coefficients on the bottom surface of the panels (Fig. 4.1a) is very similar to that obtained on the roof surface under the panels (Fig. 4.2). Positive pressure coefficients (Cp = 0.72) can be found towards the edge A near the windward corner of the roof, they gradually changed into negative pressures (Cp = -1.36) near the edge B. The pressure coefficient distribution on the top surface of the panels is slightly different from the bottom surface, showing similar distribution but different values for the pressure coefficients (Figs. 4.1a and 4.1b).

The overall distribution of the pressure coefficients on the house model with roof mounted solar panels is depicted in Fig. 4.3, where very high negative coefficients can be noticed along the ridge of the roof, while the largest suction is on the roof near the edge A. However, no solar panels are installed in these regions of very high suction, because the panels are mounted at 1.0 m away from the edges of the roof. The 1.0 m distance from the edge was selected according to the definition of

the end zone, Z, in NBCC (2015), where this is defined as the lesser of 10% of the width of the building (0.8 m) or 40% of the building height (2.5 m), but not less than 4% of the width (0.32 m) of the building or 1.0 m.

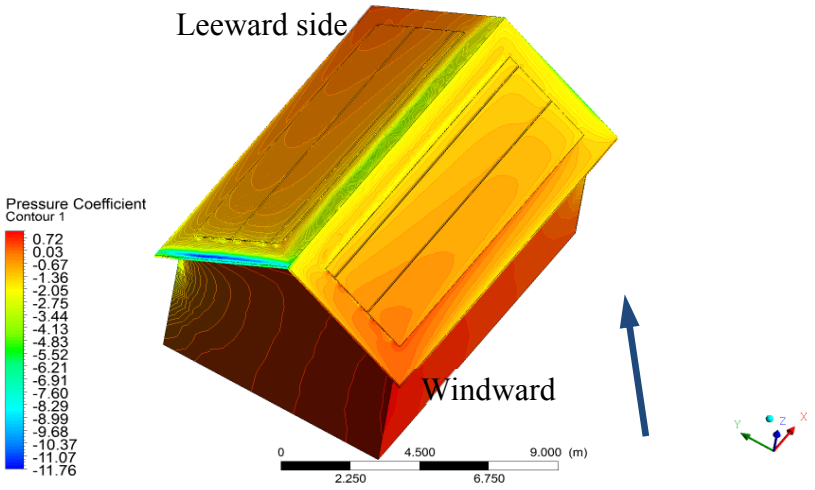


Fig. 4. 3. Pressure coefficient distribution on the house model with solar panels installed on the roof, for roof slope 35º and wind direction 45º

4.2.2. Pressure contour distributions for wind direction 90º

For the gable roof subjected to wind speed of 40 m/s for wind direction of 90º, which is perpendicular to the ridge of the roof, similar to the previous case (Section 4.2.1.), the pressure coefficients distributions on the roof surface and on top and the bottom surfaces of the solar panels are illustrated in figures 4.4, and 4.5, respectively. The distribution of pressure coefficients on the bottom surface of the solar panels (Fig. 4.5 a) is very similar to that on the roof surface underneath the panels (Fig. 4.4); however, the pressure distribution on top surface of the solar panels has a slightly different pattern of pressure coefficients (Fig. 4.5 b). The highest-pressure coefficient was Cp = 0.84 and it was recorded on the windward edge of the roof and the windward edge of the bottom surface of the solar panels, in front of the rails closest to the windward edge. Beyond the first row of solar panels however, the pressure coefficients decreased until negative values of around Cp = -1.48. Near the ridge, a region of high suction was observed beyond the last row of panels, where the pressure coefficients reached values of Cp = -3.5.

The overall pressure coefficients distribution on the roof and on the solar panels is depicted in Fig. 4.6, which shows that the highest suction registered on the roof is concentrated at the middle

section of the ridge, where negative values of Cp = -8.44 were obtained. However, in this study, as pointed out in the previous section, no solar panels were installed in these very high suction areas.

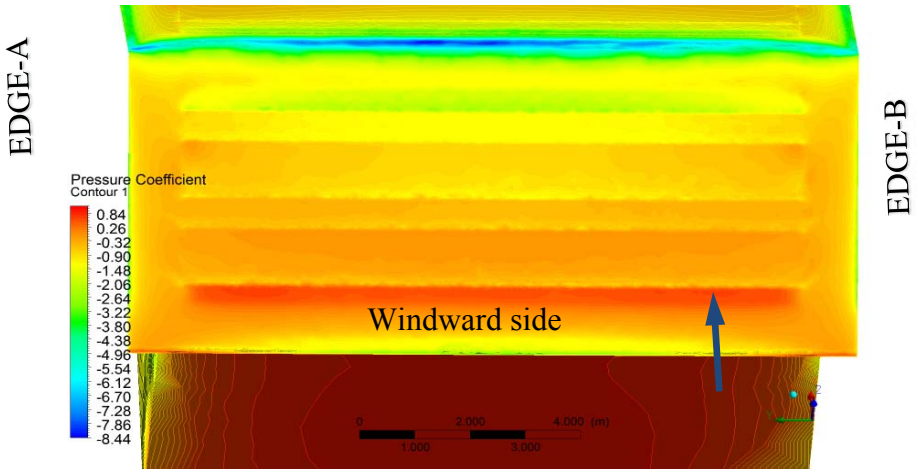
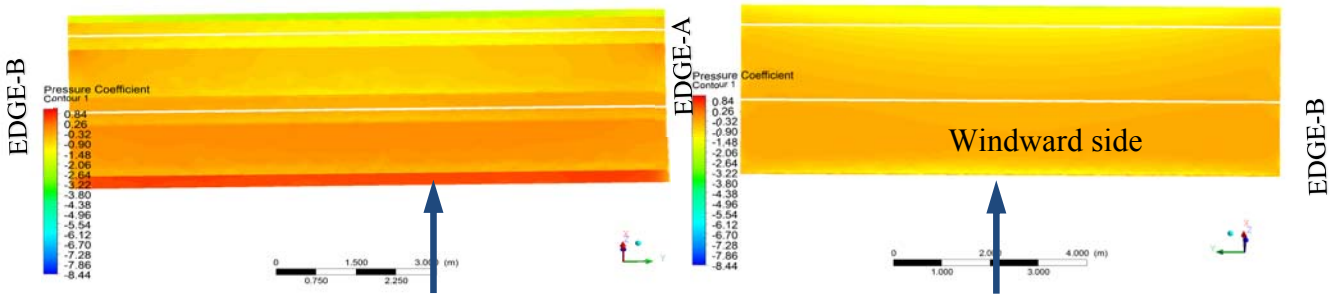


Fig. 4. 4. Pressure coefficient distribution on roof surface underneath the solar panels, roof slope 35º and wind direction 90º, windward side



a) **b)**

Fig. 4. 5. Pressure coefficient distribution on a) Bottom surface of the solar panels, and b) Top surface of the solar panel, for roof slope 35º and wind direction 90º, windward side

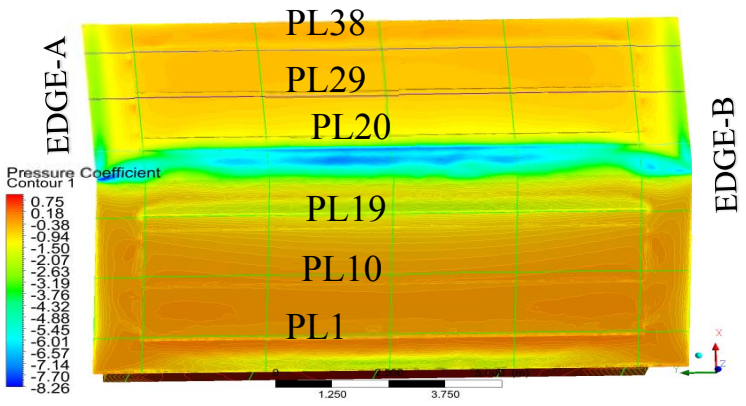


Fig. 4. 6. Pressure coefficient distribution on the house model with solar panels installed on the roof, with main polylines for roof slope 35º and wind direction 90º

Figure 4.6 shows the location of the along-wind (transversal) and cross-wind (longitudinal) polylines which are used in this study for sampling data used for further comparisons and interpretations.

4.2.3. Pressure contours distributions for wind direction 0º

The detailed distributions of the pressure coefficients on the roof for wind direction 0° are presented in figures Figs. 4.7 to 4.9. The two long edges of the roof were denoted as edge C and edge D, as represented in Fig. 4.7. Similar to the previous cases (Sections 4.2.1. and 4.2.2.), it was observed that the pressure coefficients distribution on the roof underneath the solar panels (Fig. 4.7) was very similar to the one obtained on the bottom surface of the solar panels (Fig. 4.8 a). Also, similar suction values of pressure coefficients of Cp = -2.4 was observed towards the windward edge, while a value of (Cp = -0.5) is obtained in the middle section for both surfaces. Therefore, considering also the similar conclusions drawn for the 0° and 90° wind directions, (Sections 4.2.1. and 4.2.2.), the idea of a pressure equalization between the roof surface underneath the panels and the bottom surface of the panels can be formulated. Such concept is vastly documented by Kopp et al. (2015) for solar panels installed on flat roofs, described as double-layers systems; however, the pressure equalization defined by Kopp et al. (2015) referred to the balance of pressure acting on the top surface and bottom surface of the solar panels. For the currently investigated cases of solar panels installed on inclined roofs, the pressure equalization was noticed between the roof surface and bottom surface of the panels. For the top surface of the solar panels (Fig. 4.8b) it can be observed that the pressure in the middle section is similar to the

one obtained underneath the panels. However, towards the leeward (B) and windward (A) edges, suction was considerably smaller reaching values of about Cp = -1.0 to -2.0 on the leeward versus Cp=-0.5 to -1.0 on the windward, for bottom and top of the solar panels, respectively.

The overall distribution of the pressure coefficients on the roof with solar panels is presented in Fig. 4.9 from which it can be concluded that the highest suction on the roof of the building was concentrated at the windward edge A (Cp = -5.0), while the rest of the roof was subjected to lower suction (Cp = -0.2).

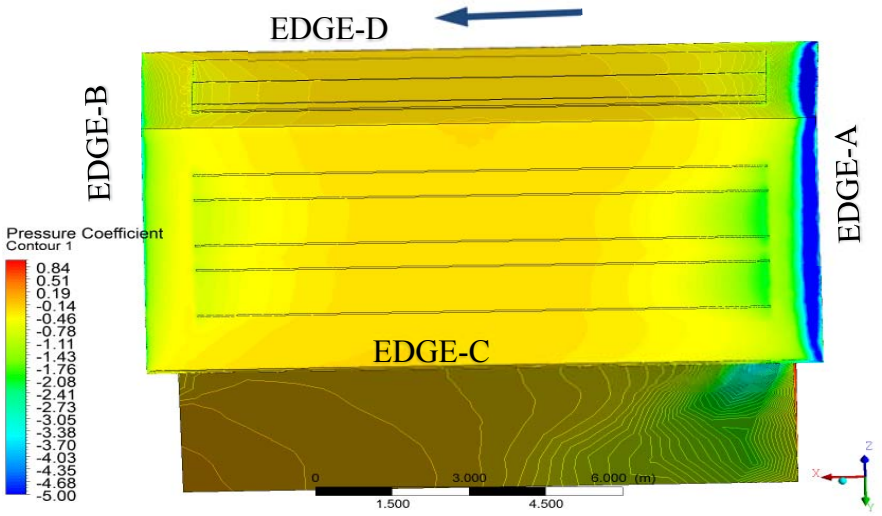


Fig. 4. 7. Pressure coefficient distribution on roof surface underneath the solar panels, for roof slope 35º and wind direction 0º, side of the building

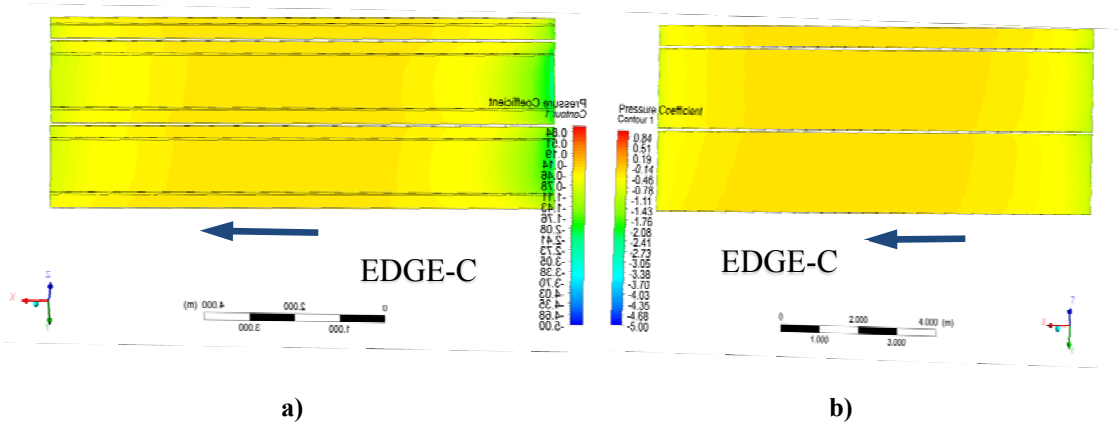


Fig. 4. 8. Pressure coefficient distribution on a) Bottom of the solar panels, and b) Top of the solar panel, for roof slope 35º and wind direction 0º

For a better comparison between the cases, pressure coefficients were represented across the roof and across the solar panels for a total of 38 longitudinal polylines. Figure 4.9 shows all the longitudinal polylines, which were also used to integrate the pressure coefficients in this study. The segments of the polylines crossing the overhangs and the walls of the house model were removed when data analysis was performed.

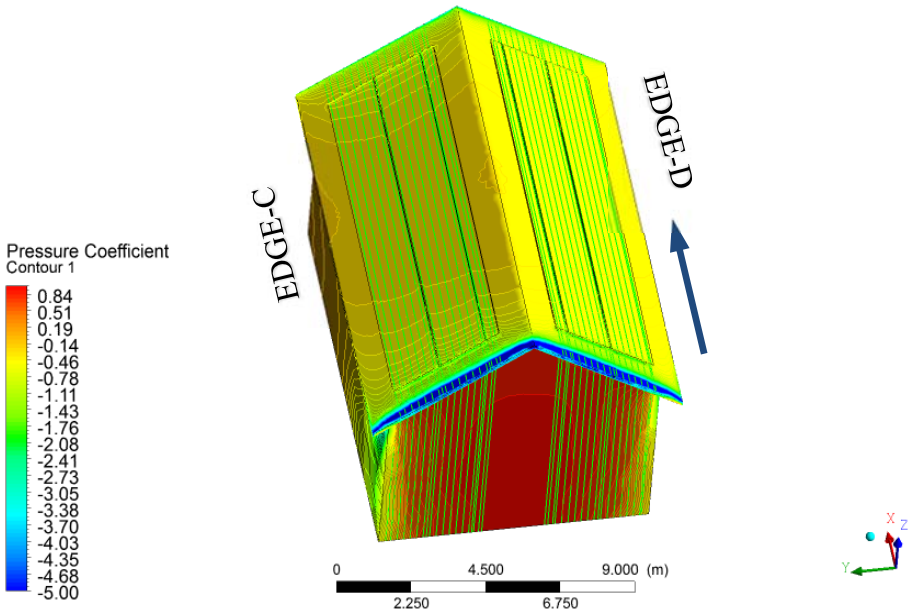


Fig. 4. 9. Pressure coefficient distribution on the house model with solar panels installed on the roof for roof slope 35º and wind direction 0º

4.2.4. Pressure coefficients for roof mounted solar panels and roof without solar panels for windward side of the roof

To establish the effects solar panels, have on the wind flow–structure interaction, several simulation cases were performed on the house model with and without solar panels installed on the roof. Wind-induced pressure was analyzed on four surfaces, namely: roof surface under the solar panels, bottom and top surfaces of the solar panels, and roof surface for the building model without solar panels. The total pressure on the windward side of the roof is calculated by summation of pressure coefficients sampled along 19 longitudinal lines crossing the top and bottom surfaces of the solar panels and the roof surface under the solar panels. The transferred net

pressure on the panels was averaged over the entire roof area under the panels, to better understand the contribution of the pressure on the panels to the pressure registered on the roof under the panels.

4.2.4.1. Pressure coefficients on the bottom surface of the solar panels vs. roof surface under the solar panels

Figures 4.10, 4.11 and 4.12 show the wind pressure coefficients obtained on the bottom surface of the solar panels and on the roof surface under the solar panels, for wind directions 90º, 45º and 0º, respectively. From these figures, it can be observed that for most of the surface covered by panels, the difference between the Cp values on the bottom surface of the panels and on the roof surface under the panels was very small, ranging from Cp= 0 to 0.15. For the 90° case, the Cp coefficients along the lines PL1 and PL10 representing the roof surface under the panels and on the bottom surface of the panels seem consistent throughout the length of the polylines. The pressure coefficients were observed to have values ranging between 0.5 to 0.6, and -0.28 to -0.34 along polylines PL1 and PL10, respectively. However, Cp decreased sharply to Cp=-0.30 on PL1, near the edges A and B of the windward surface of the solar panels array.

The pressure coefficient values on the PL19 on the two surfaces, bottom surface of the solar panels and the roof surface under the panels, show slight differences, for the three wind directions, however, always the Cp coefficient on roof under the panels was lower than Cp on the bottom surface of the panel, along the line PL19.

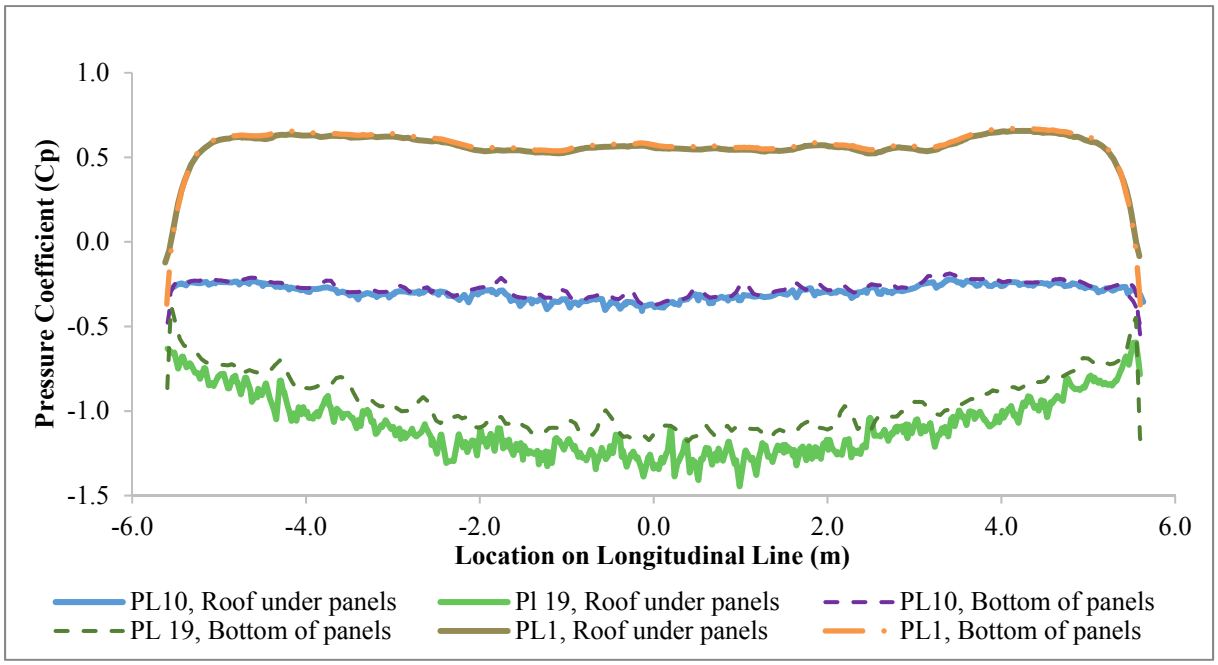


Fig. 4. 10. Pressure coefficient distribution on the bottom surface of the solar panels and on the roof surface under the panels, for roof slope 35º, and wind direction 90º, windward side

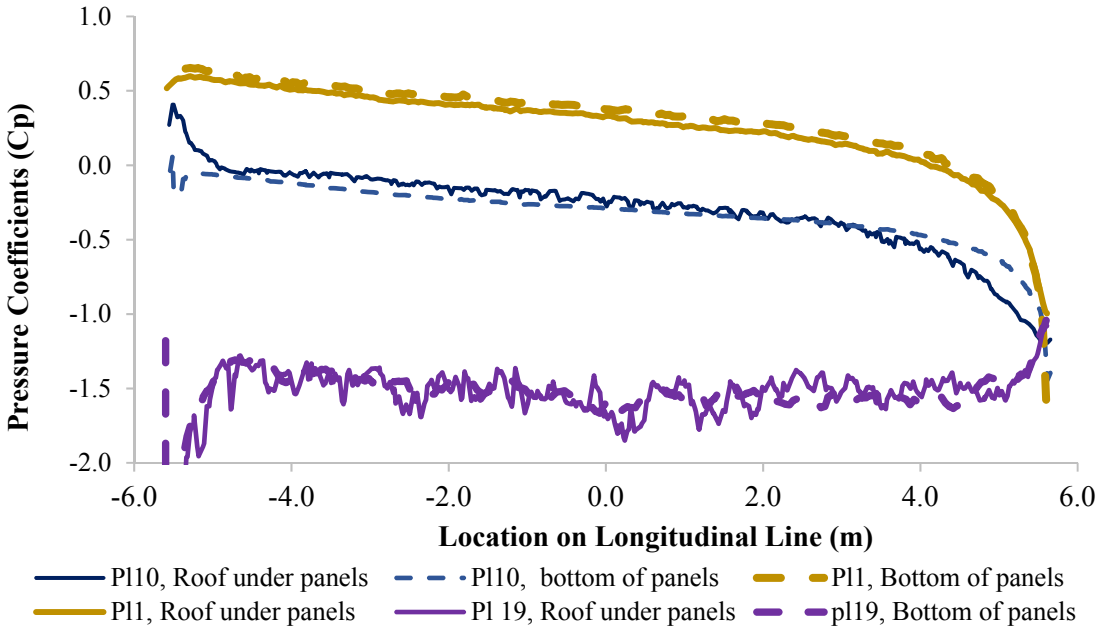


Fig. 4. 11. Pressure coefficient distribution on the bottom surface of the solar panels and on the roof surface under the panels, for roof slope 35º, and wind direction 45º, windward side

The Cp suction coefficient along PL19 increased in the middle of the panel array to -1.35, from -0.7 at the edges of the solar array, which is contrary to the trends observed for the lines PL1 and

PL10 on the bottom surface of the solar panels and on the roof surface under the panels, for 90° wind direction (Fig. 4.10). For the case of 45° wind direction, the Cp along all three lines PL1, PL10 and PL19 demonstrated a good agreement throughout their length, except for the slight differences of Cp near the beginning and end of PL10. For wind direction of 90º, the pressure coefficients increased from Cp =0.6 and 0, to Cp =-1.0 towards the B edge of lines PL1 and PL10, respectively. However, Cp remained constant for line PL19 at a value of Cp= -1.6 (Fig. 4.11).
For wind direction 0º, the pressure coefficients along the PL1, PL10 and PL19 lines on the roof surface under the panels and on the bottom surface of the panels, were similar, except for the A and B edges where Cp coefficients along PL10 were lower than those on the bottom surface of the panels (Fig. 4.12).

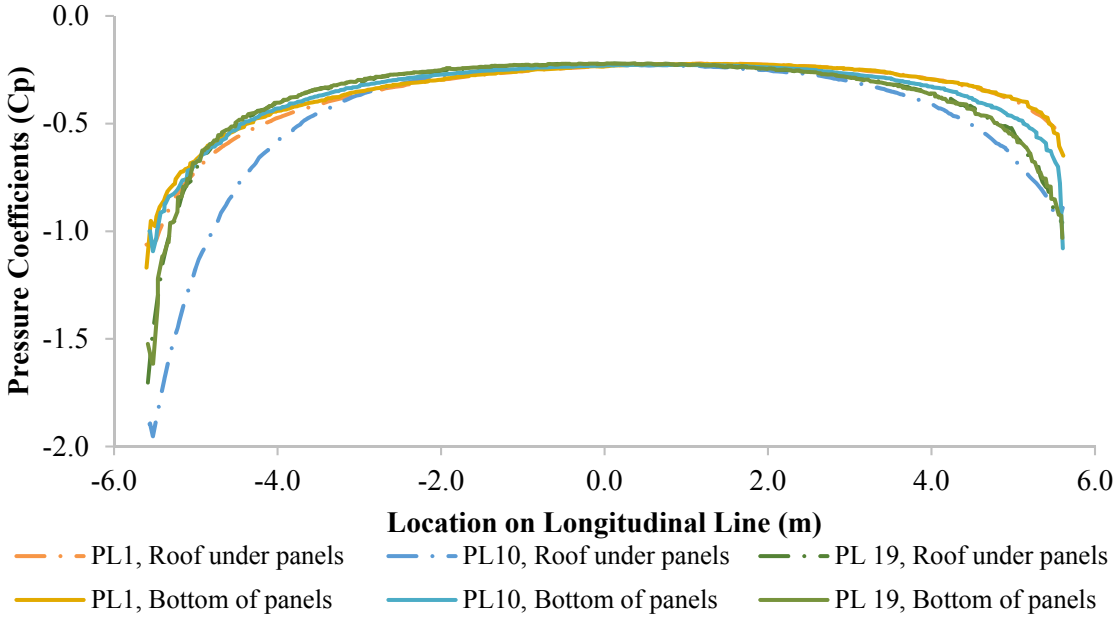


Fig. 4. 12. Pressure coefficient distribution on the bottom surface of the solar panels and on the roof surface under the panels, for roof slope 35º, and wind direction 0º, windward side.

The good agreement between the pressure coefficients on the roof surface under the panels and on the bottom surface of the panels, registered for 0°, 45° and 90° wind directions, for each set of lines, reiterate the occurrence of pressure equalization between these two surfaces.

4.2.4.2. Pressure coefficients on roof surface under the solar panels vs. roofs without solar panels

Comparisons of the wind-induced pressure coefficients on the roof surface without solar panels and on the roof surface under the solar panels, for wind directions 45º, 90º and 0º, are shown in Figs. 4.13, 4.14 and 4.15, respectively. For the 90° wind direction, the line PL1 shows significantly higher pressure coefficients on the roof surface under the solar panels (Cp = 0.6) compared to the same line on the roof without panels (Cp = 0.02). Also, it can be observed that the pressure coefficients on PL10 on roof surface under the panels (Cp = -0.25 to -0.35) are higher than the pressure coefficients along the same line on the roof surface without panels (Cp = 0 to -0.15).

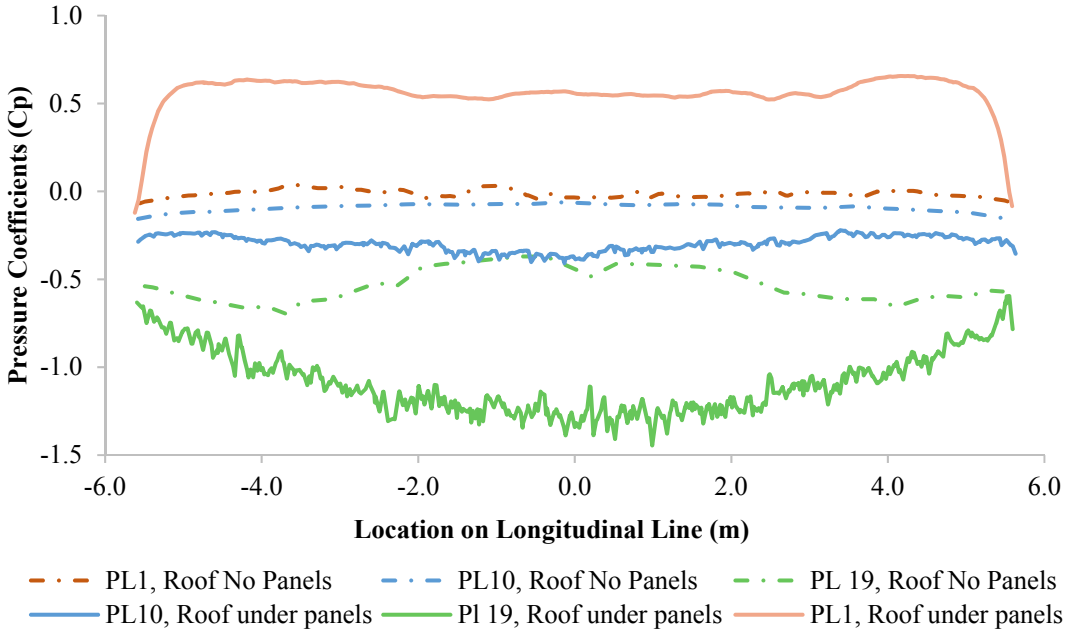


Fig. 4. 13. Pressure coefficient distribution on the roof surface under the panels and on roof surface without mounted panels, slope 35º, and wind direction 90º, windward side

The PL19 line crossing the roof surface under the installed panels shows higher suction (Cp=-0.7 to -1.3) than the corresponding line on the roof without panels, (Cp= -0.3 to -0.7). Also, it can be observed that for all the lines the Cp values registered for the 90° wind direction are symmetric around the middle of the roof, for both roof surface under the panels and roof surface without solar panels (Fig. 4.13).

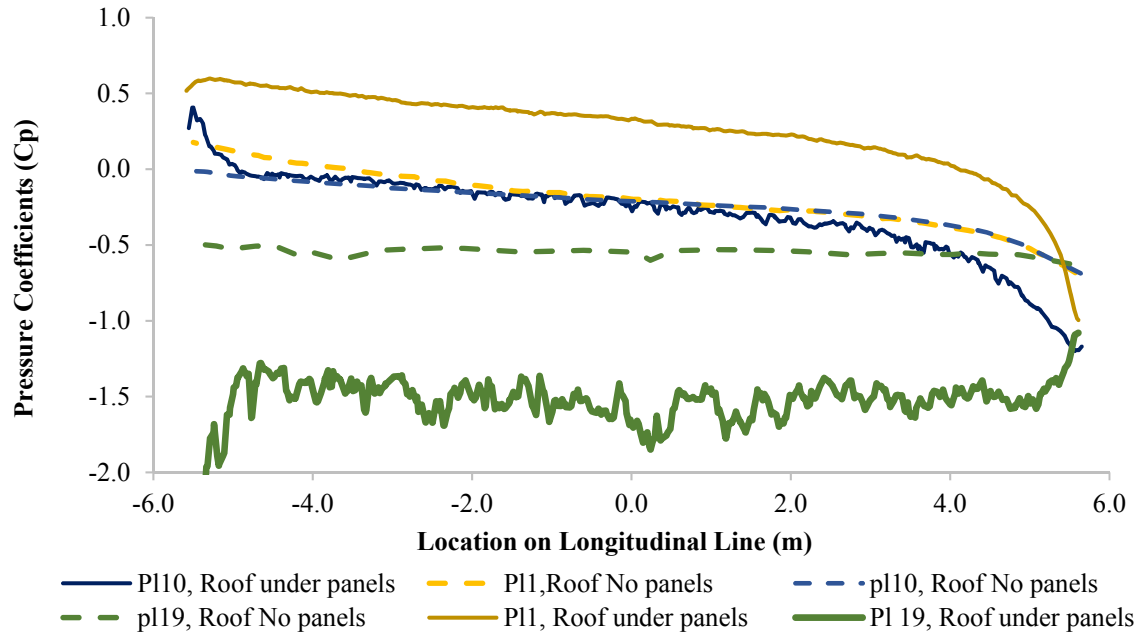


Fig. 4. 14. Pressure coefficient distribution on the roof surface under the panels and on roof surface without mounted panels, slope 35º, and wind direction 45º, windward side

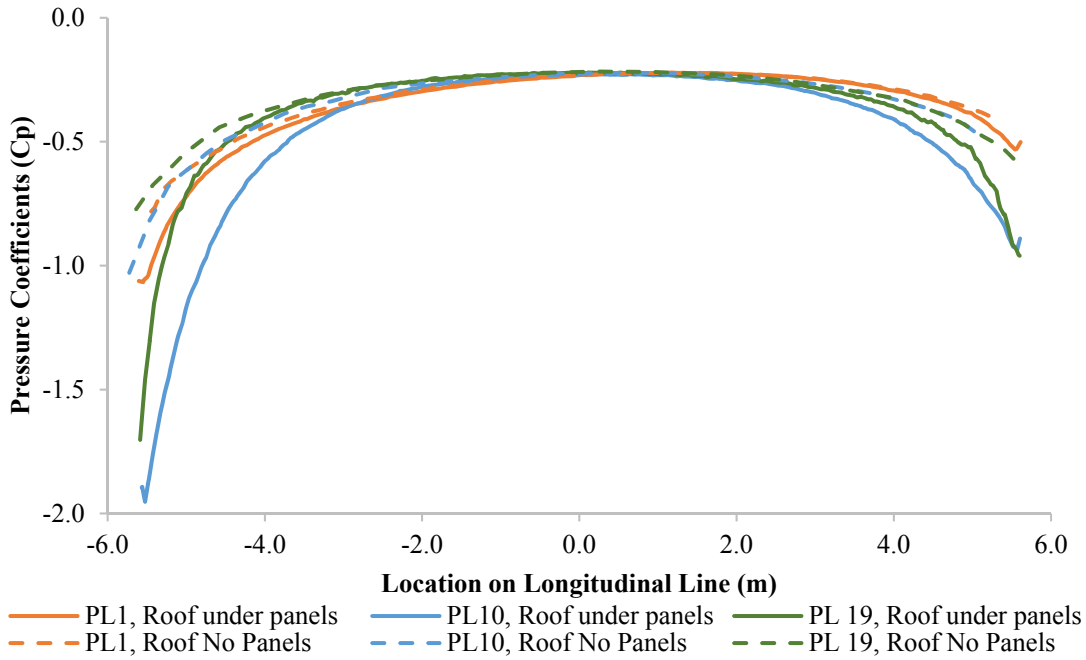


Fig. 4. 15. Pressure coefficient distribution on the roof surface under the panels and on roof surface without mounted panels, slope 35º, and wind direction 0º

For the case of 45° wind direction (Fig. 4.14) it was noticed that the pressure coefficients have very similar trends on the roof surface with and without solar panels. For line PL1 (Fig. 4.14) located near the windward A edge of the solar array, the pressure coefficients on the roof under the panels are higher (Cp = 0.55 to -0.6) than corresponding line on the roof with no panels (Cp = 0.2 to -0.6). For PL19 located near the ridge (Fig.4.6), the suction coefficients are much higher (Cp = -1.5), than the corresponding line on the roof with no panels (Cp = -0.5). On the contrary, the middle line (PL 10) shows slightly different pressure coefficients from the corresponding line on the roof without panels, in comparison to PL1 and PL19.

For wind direction 0º, the pressure coefficients along the lines PL1 and PL19 on the roof surface under the panels are slightly higher than those on the roof without panels. However, suction coefficients along PL10 on the roof under the panels are comparatively higher than those on the roof without panels, as shown in Fig. 4.15. The largest differences between the Cp values on PL19 can be found within the first 4.0 m of the array on the windward side, and at last 2.0 m on the leeward side. In addition, the values of suction coefficients along all three lines increased significantly from Cp=-0.25 in the middle of the array to Cp=-0.5 to -1.0 on the leeward B edge, and to Cp=-0.75 to -1.95 on the windward A edge, where these differences are near the ends of the lines, while remain nearly constant in the middle parts of these lines. In conclusion, the pressure coefficients on the roof surface under the panels had higher magnitudes than for the case when no panels are installed on the roof. This might be the effect of the wind flow passing through the cavity formed between the panels and the roof, thus brings the necessity of performing a detailed analysis of the velocities and pressures recorded in this region, as presented in later sections. Moreover, the current comparison does not reflect the total pressure acting on the roof, but only the pressure on the roof surface underneath the panels. For a complete estimation, the net pressure acting on the solar panels-roof system (resultant pressure on the top, bottom surfaces of the solar panel and the roof under the panels) should be compared with the pressure acting on the roof without solar panels installed. However, the current comparison of the instantaneous Cp values measured for the roof surface with and without panels was required, in order to verify the potential critical pressures which might occur for the roof surface in both mentioned cases.

4.2.4.3. Pressure coefficients on roof without solar panels vs. total pressure coefficients on the roof surface due to installation of solar panels

Detailed graphs for the wind pressure coefficients acting on a roof surface without solar panels compared with the resultant of the pressure coefficients estimated on the roof-panels system formed by the three surfaces: roof surface under the solar panels, top and bottom surfaces of the panels, are shown in Figs. 4.16, 4.17 and 4.18 for wind direction 45º, 90º and 0º, respectively. The net pressure coefficient resultant is the algebraic summation of the Cp coefficients on top and bottom surface of the panels as well as on the roof surface under the panels.

For wind direction 90°, the resultant Cp along PL1 for the roof-panels system shows higher magnitude of negative pressure coefficients, (Cp= -0.2 to -0.8) than the pressure coefficients along the corresponding line on roof without panels, which were around 0.02 (Fig. 4.16). In addition, the resultant Cp on PL19 shows much larger suction, (Cp=-1.0 to -1.6) on the roof-panels system than the net Cp on the corresponding line on the roof without panels, (Cp = -0.3 to -0.7). Resultant pressure coefficients on PL10 on roof with panels are slightly lower near the middle of the array, (Cp=-0.25 to -0.40), than the pressure coefficients registered on the roof without panels, (Cp = -0.05 to -0.15) for the same line. On the other hand, the Cp coefficients for all three lines are symmetric around the middle of the roof, including both Cp resultant of the three surfaces of roof with solar panels, and for roof without solar panels (Fig. 4.16).

For the wind direction 45° (Fig. 4.17) it was noticed that all pressure coefficients have similar trends especially for the middle region of the roof. However, the Cp resultant coefficients on line PL1, located near the windward edge of the solar array (Fig. 4.6), are higher, (Cp=0.02 to -0.8) for the roof-panels system than the Cp coefficients registered on the corresponding line on the roof with no panels, (Cp = 0.2 to -0.6). Nonetheless, for PL19 located near the ridge (Fig. 4.6), the pressure coefficient resultants for the roof-panels system are much higher, (Cp = -1.6) than those for the corresponding line on the roof with no panels, (Cp=-0.5). Contrary, Cp resultant coefficient the roof-panels system on the middle line PL10 shows different pressure values than those recorded on the corresponding line on the roof without panels. The resultant pressure coefficients along PL1 and PL10 increased towards the leeward edge B of the roof, to Cp=-1.25 to -1.4 for roof with panels, versus Cp=-0.55 to -0.6 on the roof without panels, as it can be noticed in Fig 4.17. Moreover, for wind direction 0º, the resultant of pressure coefficients on the roof with solar panels are slightly higher along PL1 and PL19 than the pressure coefficients on the roof without panels

for the same lines. However, the resultant of the pressure coefficients, for the roof-panels system, along the PL 10 middle line on the roof with solar panels are much higher than those on the roof without panels (Fig. 4.18). The largest differences between the Cp coefficients on PL19 on either surface, are located in first 4.0 m of the array on the windward side, and on the last 2.0 m from the leeward side. In addition, resultant Cp along all the three lines increased sharply, from -0.25 in the middle of the array, to Cp=-0.75 to -3.0 on the windward edge, and to Cp= -0.5 to -1.6 on the leeward edge, while remaining nearly constant in the middle parts of those lines.

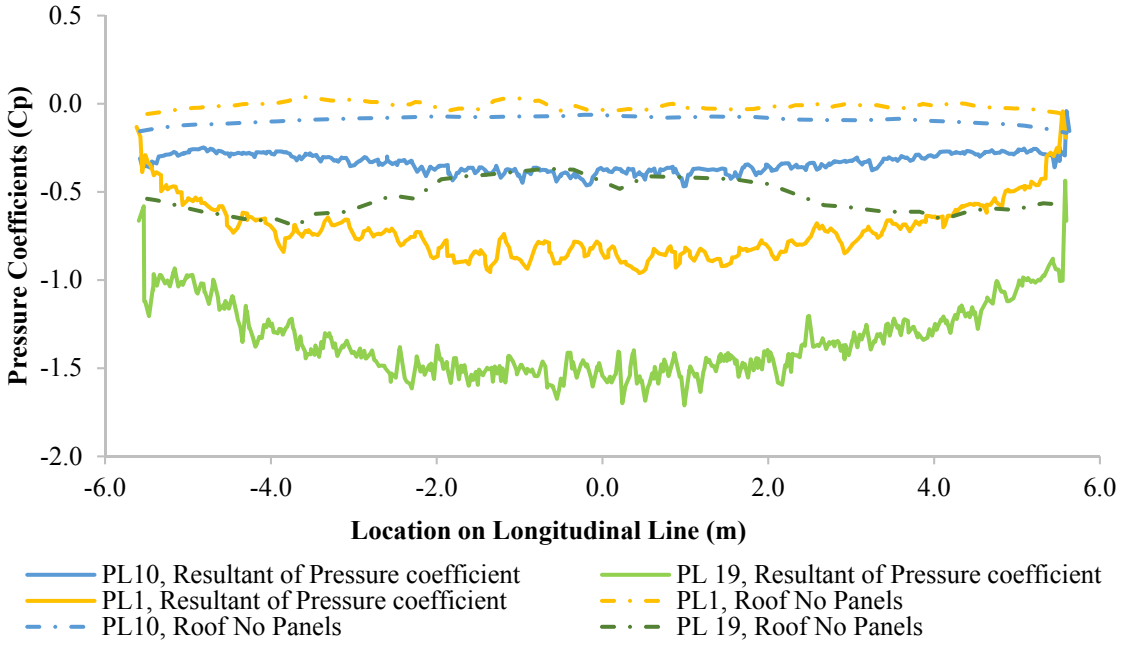


Fig. 4. 16. Pressure coefficient distribution on roof surface without mounted panels and resultant of pressure coefficients on roof surface due to panel installation, slope 35º, and wind direction 90º, windward side

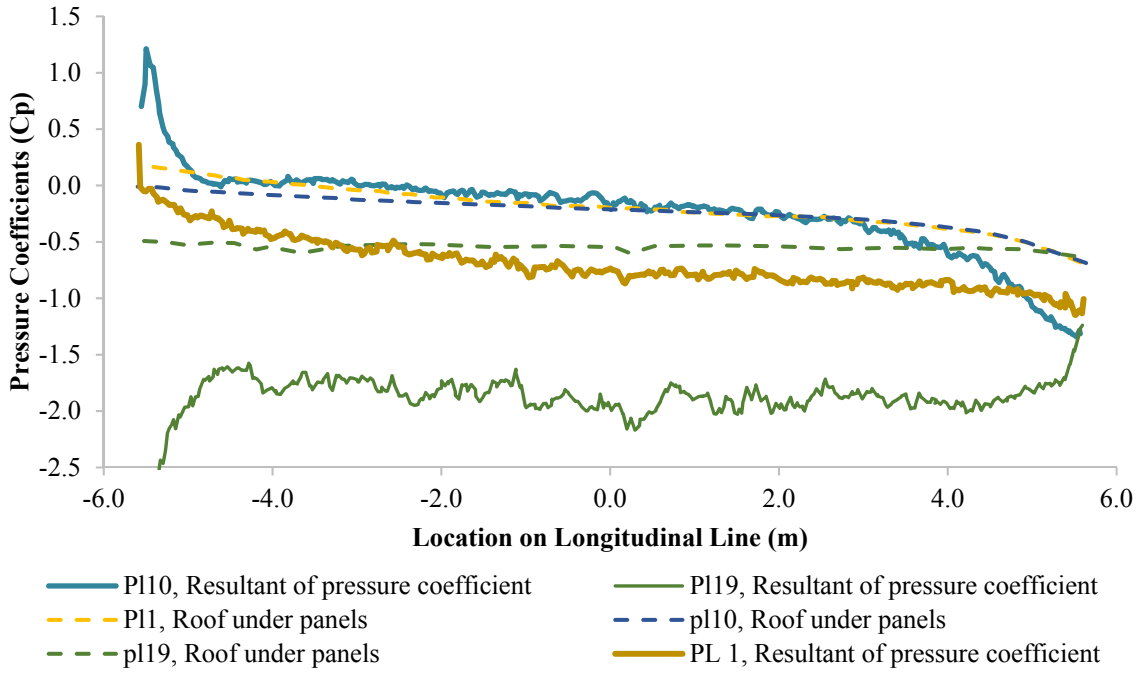


Fig. 4. 17. Pressure coefficient distribution on roof surface without mounted panels and resultant of pressure coefficients on roof surface due to panel installation, windward side, slope 35º, and wind direction 45º

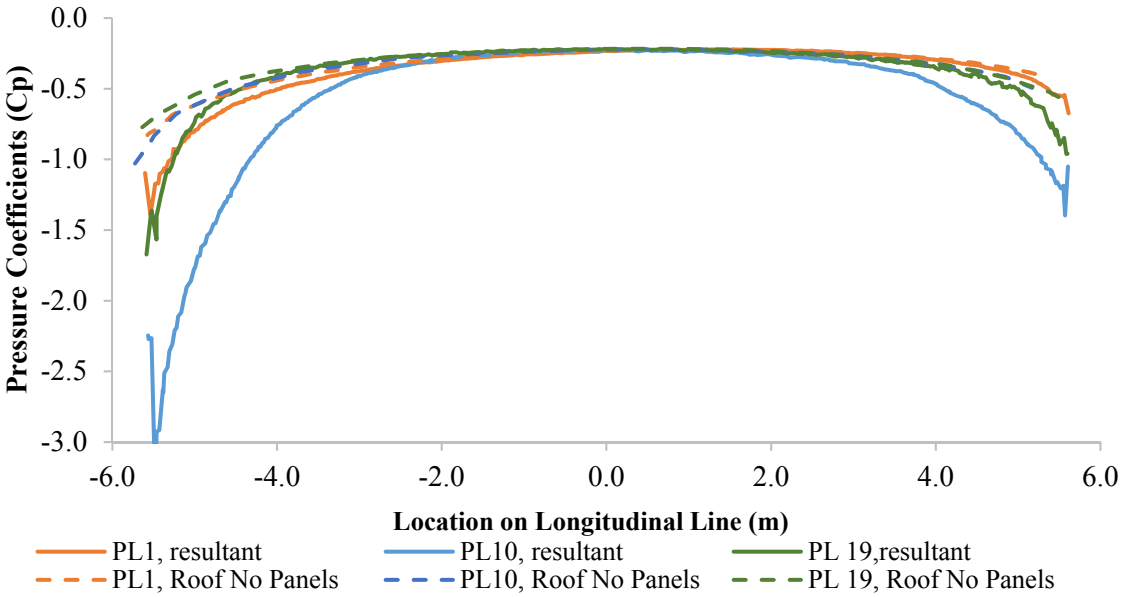


Fig. 4. 18. Pressure coefficient distribution on roof surface without mounted panels, and resultant of pressure coefficients on roof surface due to panel installation, slope 35º, and wind direction 0º

In conclusion, it can be noticed that for the cruelty studied case, of roof slope 35º the resultant pressure coefficients determined for the roof-panels systems, for the panels installed at 2″ (50 mm) spacing and 3″ (76 mm) roof clearance, were higher than for the case when no solar panels are

installed, for wind directions 0º, 45º and 90º. Other roof slopes and other combinations of solar panels spacing/roof clearance dimensions will be investigated in the following sections in order to establish if this conclusion can be generalized or it applies to the current case in particular. However, in order to understand how the pressure coefficients, vary and the reason for which the pressures are higher for the roof-panels systems, the Cp comparisons between the other surfaces composing the system will be performed first.

4.2.4.4.Pressure coefficients on roof without solar panels vs. top of the panels

Representation of wind pressure coefficients on the roof surface without solar panels versus the pressure coefficients on the top surface of the solar panels, for wind direction 45º, 90º and 0º, are shown on Figs. 4.19, 4.20 and 4.21 respectively. For wind flow along direction 90°, Cp on PL1 shows higher pressure coefficients, on the top surface of the panel (Cp= -0.4 to -0.7) than the corresponding line on the roof without panels, (Cp=0.02). In addition, Cp on PL19 shows much higher suction on the top surface of the panel, (Cp= -0.8 to -1.35), than the corresponding line on roof without panels, (Cp= -0.3 to -0.7). The pressure coefficients on PL10 line on top and middle of the panels, are slightly higher for the same top surface of the panel, (Cp=-0.25 to -0.3), than the pressure coefficients along PL10 on the roof without panels, (Cp=-0.05 to -0.15). On the other hand, all Cp graphs for all three lines are symmetric around the middle of the roof, for both, top surface of the solar panels, and for roof without solar panels (Fig. 4.19). When the wind direction is 45° (Fig. 4.20) it was noticed that all pressure coefficients have similar trends especially for the inner region of the roof. However, for Cp on line PL1 located near the windward edge of the solar array (Fig.4.6), pressure coefficients are higher, (Cp = 0.02 to -1.1) than the Cp of the corresponding line on the roof with no panels, (Cp=0.2 to -0.6). Similarly, for PL19 pressure coefficients on top surface of the panel, (Cp= -1.1), are higher than the Cp on corresponding line on roof with no panels, (Cp= -0.5). The pressure coefficients on the middle line PL 10 shows slightly different pressure coefficients, for the two surfaces, the roof without panels and the top surface of the panels. Moreover, pressure coefficients along PL1 and PL10 increase from Cp=0.5 on leeward side, to (Cp=-1.1) towards the leeward edge of the roof, and to (Cp=-0.6) toward the leeward side of the roof without panels. (Fig 4.20).

When wind direction 0º is investigated, pressure coefficients along PL1 and PL19 on top of the panels are slightly higher than those on the roof without panels. Similarly, pressure coefficients along PL 10 on roof with solar panels are slightly higher than those on the roof without panels (Fig. 4.21). In addition, Cp along all lines increased sharply from Cp=-0.25 in the middle of the array to Cp=-0.75 to -2.0 on the windward side, and Cp=-0.5 to -1.6 on the leeward side, while remaining nearly constant in the middle parts of these lines.

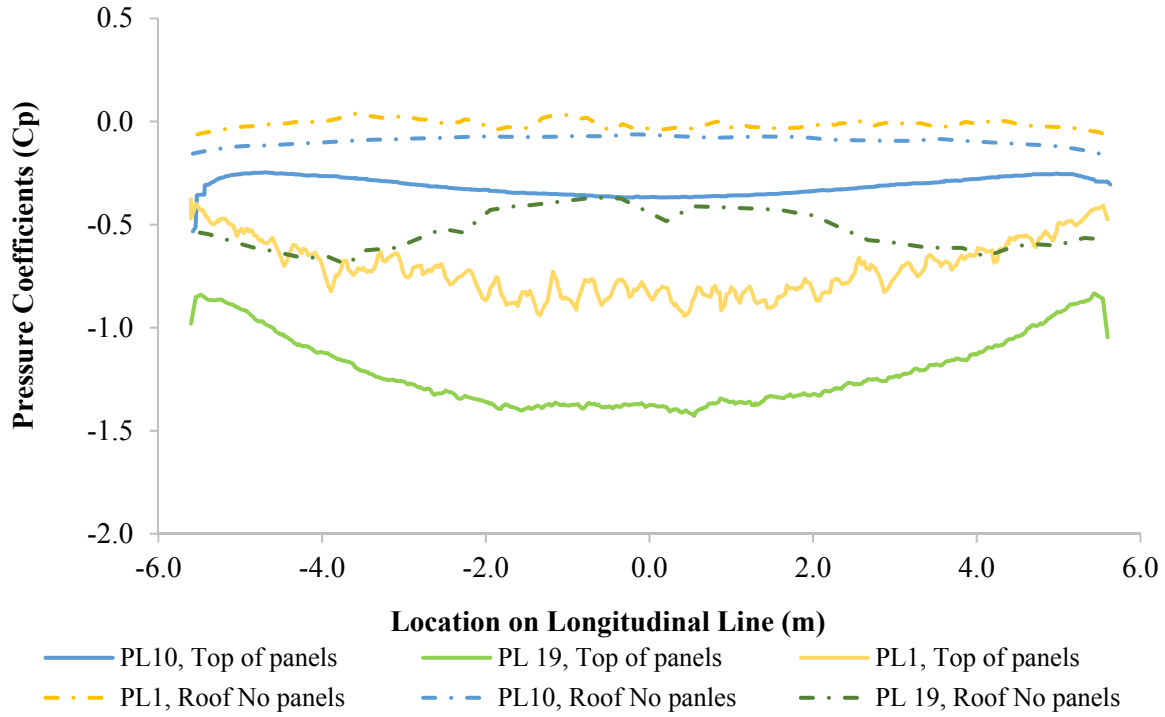


Fig. 4. 19. Pressure coefficient distribution on the roof surface without solar panels and on top of the solar panels, for roof slope 35º, and wind direction 90º, windward side

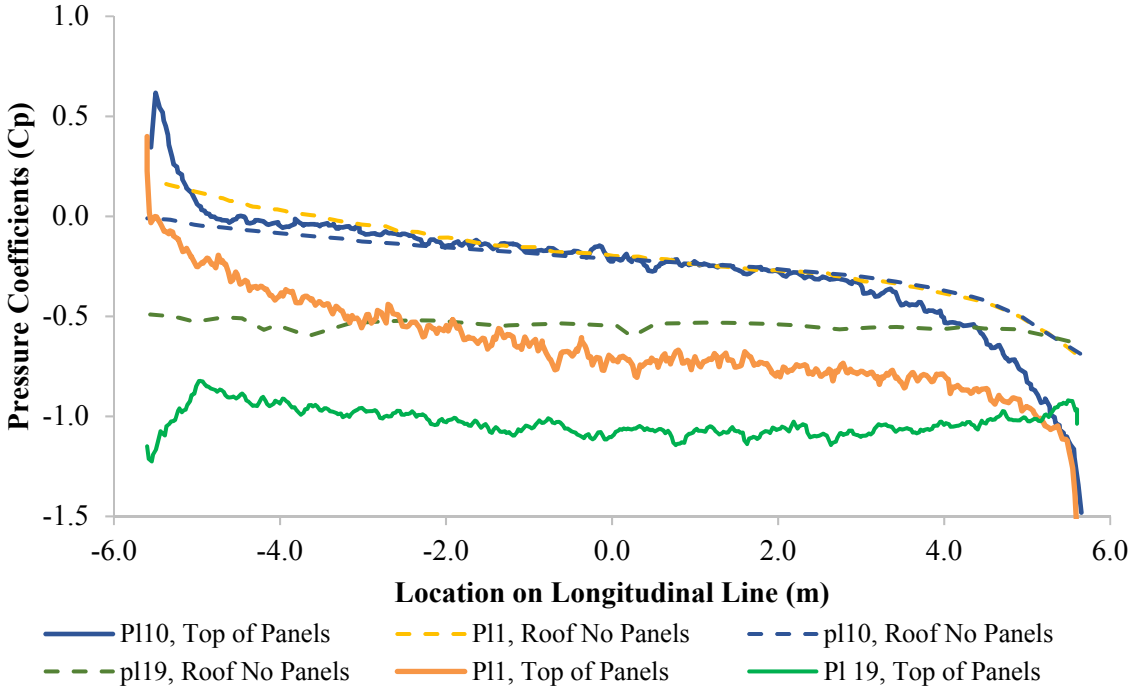


Fig. 4. 20. Pressure coefficient distribution on the roof surface without solar panels and on top of the solar panels, for roof slope 35º, and wind direction 45º, windward side

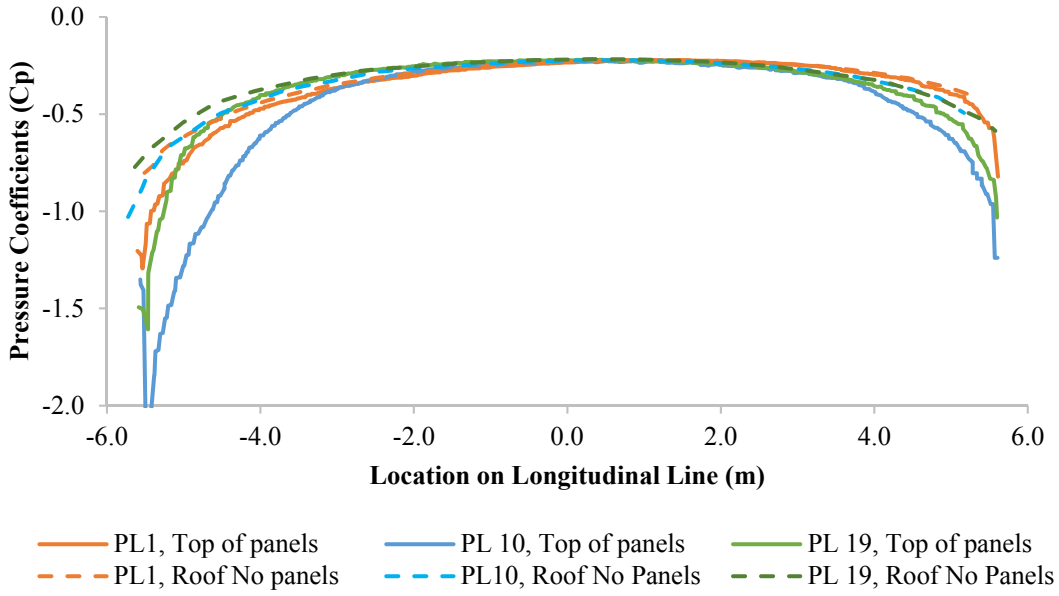


Fig. 4. 21. Pressure coefficient distribution on the roof surface without solar panels and on top of the solar panels, for roof slope 35º, and wind direction 0º

In conclusion, except for a small region near the edge A of the roof, for wind direction 45 º, the pressure coefficients were negative for the investigated lines, therefore suction predominates for both surfaces. However, always the suction on the top surface of the solar panels was higher than suction registered on the roof surface, for the case when no panels are installed.

4.2.4.5. Wind flow characteristics for gable roofs with solar panels for 90º wind direction

The flow-structure interaction was investigated to clarify the evolution of the pressure coefficients and to better understand the wind-induced pressure in the cavity region between the solar panels and the roof surface. Figures 4.22, 4.23 and 4.24 illustrate detailed representation of the pressure coefficients on solar panels and their rail supports for wind directions 0º, 45º and 90º, respectively. Figures 4.25 and 4.26 show the distribution of Cp below and above the solar panels, for wind direction 90º. The graphs illustrate that the Cp in the cavity formed between the solar panels and the roof surface, increased from Cp= 0.14 at the windward edge to Cp= -3.0 at the leeward edge of the roof. In addition, Figs. 4.25 and 4.26 indicate a slight decreased in the Cp along the entire length of the roof surface, measured parallel to the ridge.

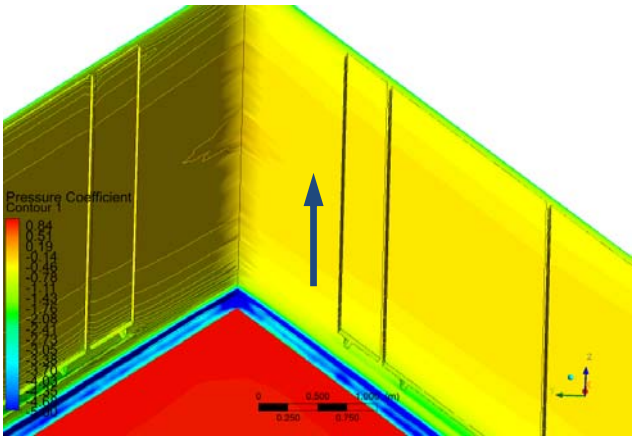


Fig. 4. 22.Close view of pressure coefficients and panel gaps, windward, wind direction 0. 0º.

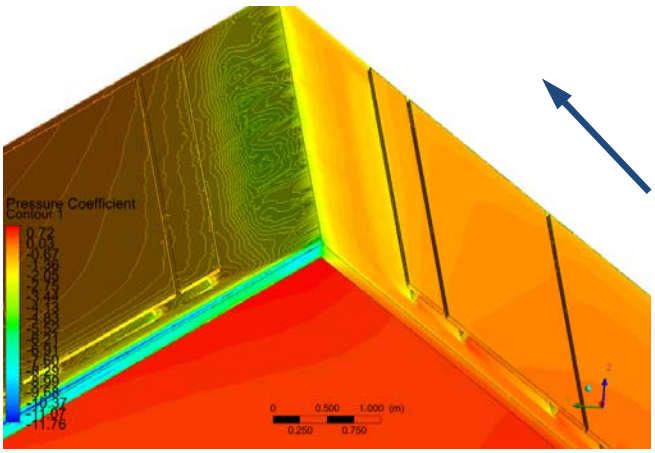


Fig. 4. 23. Close view of pressure coefficients and panel gaps, windward wind direction 45º

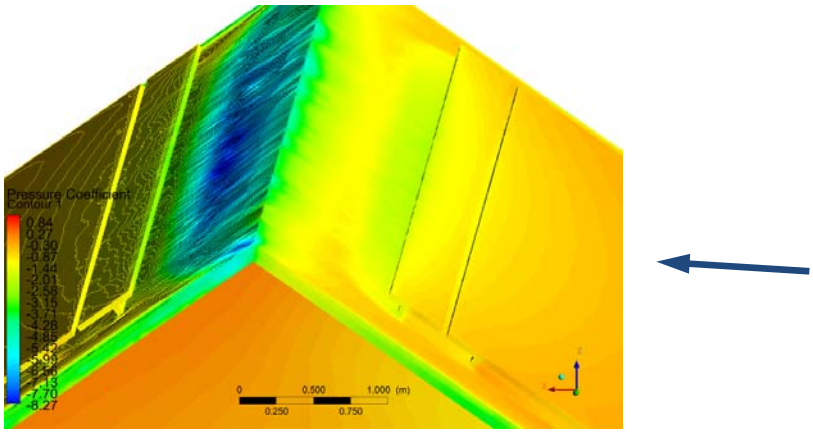


Fig. 4. 24. Close view of pressure coefficients and panel gaps, near edge A wind direction 90º

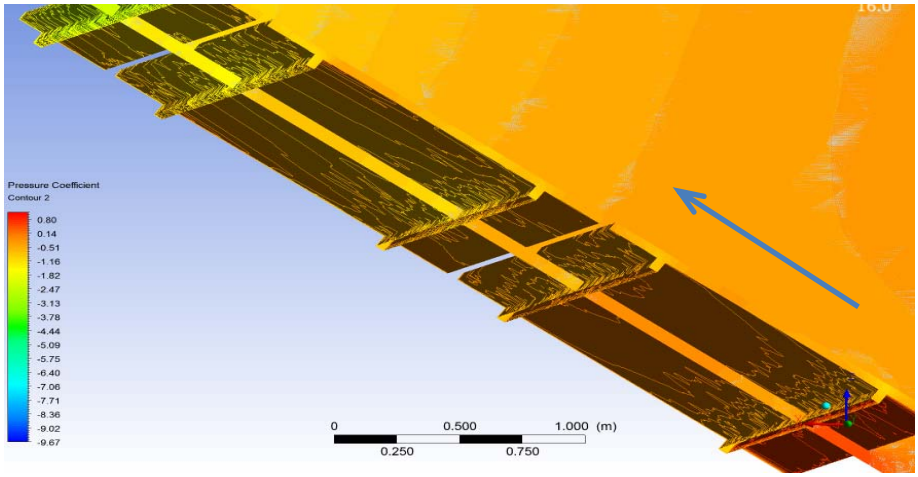


Fig. 4. 25. Pressure coefficients on a perpendicular plane under the panels, wind direction 90º

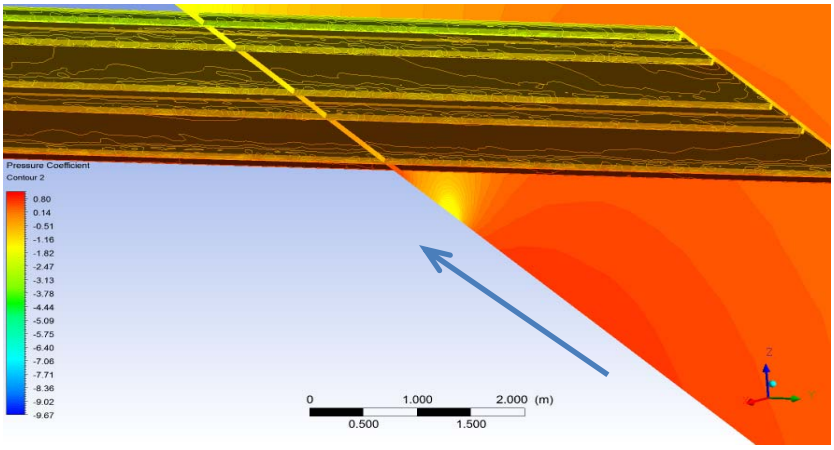


Fig. 4. 26. Pressure coefficient on a perpendicular plane and bottom surface of panels, wind direction 90º

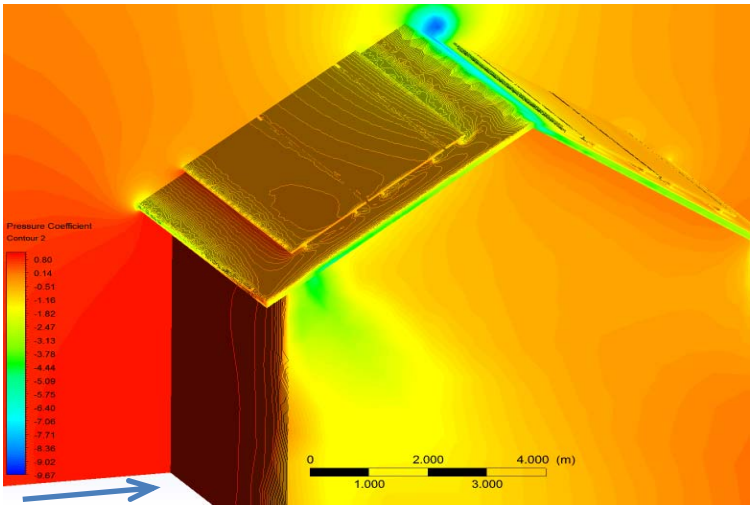


Fig. 4. 27. Pressure coefficient on a plane perpendicular on the house ridge, wind direction 90º

The pressure coefficient obtained on the solar panels and on the roof surface is determined by the flow formations created on the roof-panels model. The Cp distributions and the flow vortex core ratios were investigated for a plane perpendicular to the ridge, along the flow direction and in the regions adjacent to the model. The distribution of the wind-induced pressure coefficients along the central vertical plane perpendicular on the model (Figure 4.27) aids in interpreting the pressure coefficient on the roof and on the solar panels. The vertical plane shows that the lowest pressure was concentrated near the ridge on the leeward side of the roof. However, Cp increased gradually from the lowest values near the ridge, fanning upwards, and towards windward and leeward, on the vertical plane.

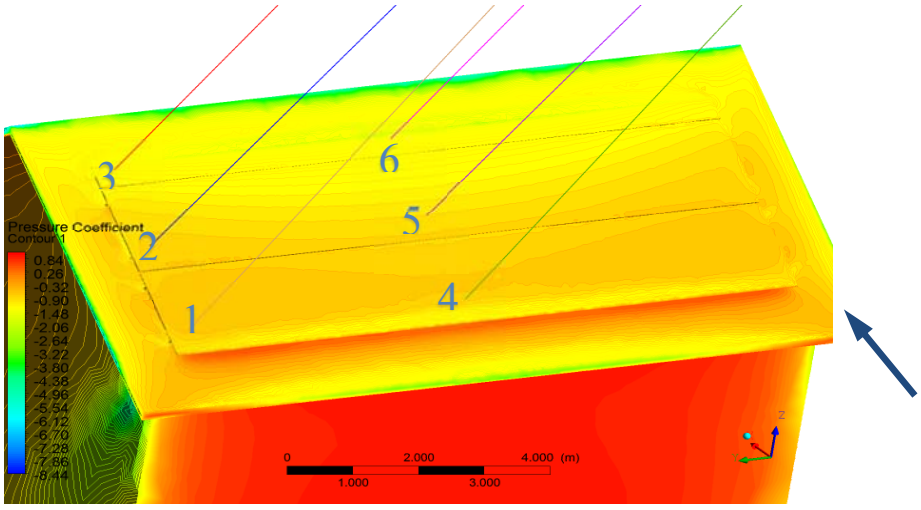


Fig. 4. 28. Lines configuration for monitoring the velocity and pressure, wind direction 90º

Figure 4.28 shows the lines perpendicular to the roof surface, which are used to monitor the velocity and pressure changes starting from the roof surface, crossing the cavity between the roof and the solar panels and continuing above the solar panels, for a height of 15 to 30 m above ground. The locations of the lines were on the solar array near the edge A and near the middle cross-section of the array.

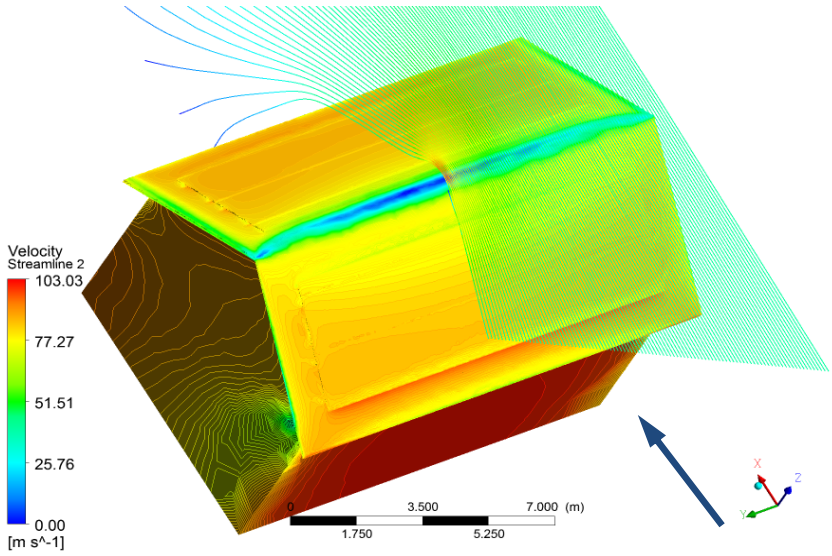


Fig. 4. 29. Velocity streamlines at middle cross section plane, wind direction 90º

Figure 4.29 shows the wind flow velocity pattern above the roof, on both windward and leeward sides of the roof, by illustrating the velocity streamlines at a central vertical plane for the 90° wind direction. Wind speeds higher than the free stream speed of 40 m/s, were noticed when the wind flow approaches the ridge; thus, the highest speed was noticed on the leeward side of the ridge of 103 m/s, also corresponding to the highest Cp = -8.27. Thereafter the wind speed deaccelerates steeply to near 50 m/s shortly after the ridge and above the panels, while it further reduced to 40 m/s at 15 m above the roof.

It can be observed that the Cp values are lower on the leeward side than those registered on the windward side. The highest suction coefficients are concentrated near the ridge, on the leeward side of the roof, where these reached values of up to Cp=-8.27, along a narrow long strip, of nearly 7.5 m × 0.25 m wide. Then the pressure coefficients decrease sharply to Cp= -2.06 in the immediate vicinity of the narrow strip near the ridge, on the leeward side and at the roof surface under the panels. The description of the flow-structure interaction can be completed by investigating the

rotational flows formed around the structure. Two types of vortex core formations were noticed: the largest vortex cores located at the corners on the leeward, and on the sides of the building. These are longitudinal vortex cores formed due to the flow detaching from the sharp edges and from the corners of the structure. The second type of vortex cores were the transversal vortex cores which were noticed as smaller flow formations located on the roof, and near the ridge, on the leeward side. Further transversal smaller vortex cores are located around the edges of the solar panels, and smallest vortex cores are located on the surfaces of the solar panels, as seen in Figs. 4.30 and Fig. 4.31.

In comparison with the distribution of vortex cores on top surface of the solar panels array, the vortex cores of the bottom surface of the solar panels exhibit higher pressure coefficients at the windward side, than the corresponding area on top surface of the panels, despite the similar transversal vortex core flows.

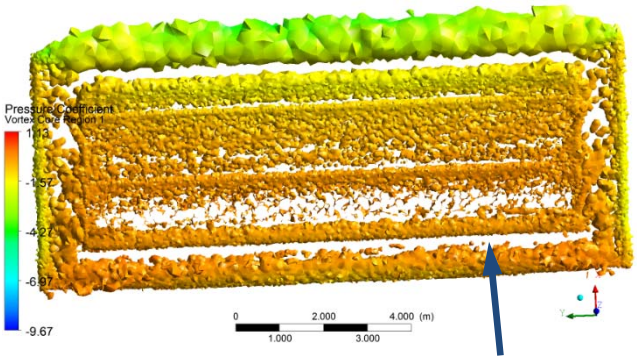


Fig. 4. 30. Vortex core distribution on bottom of the panels windward, wind direction 90º

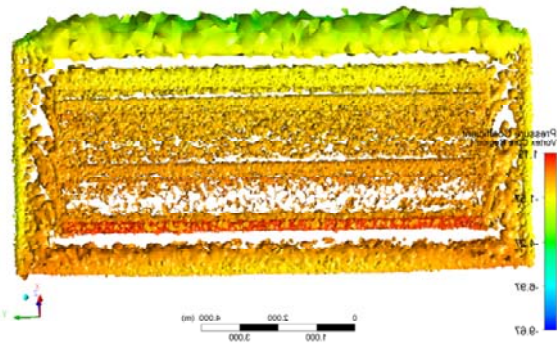


Fig. 4. 31. Vortex core distribution on top of the windward, wind direction 90º

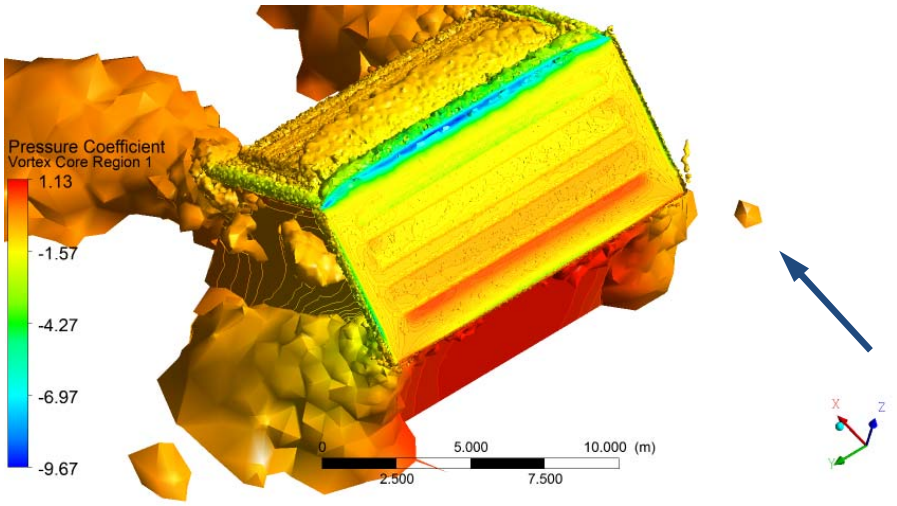


Fig. 4. 32. Vortex core distribution, on roof under the panels, and around the house

4.2.4.6. Pressure coefficients and velocity profiles in the cavity and above the solar panels for wind direction 90º, windward side of the roof

The cavity between the surface of the roof and the bottom surface of the solar panels has proved to play an important role in the evolution of the wind flow and the induced pressure coefficients. Thus, the current section is dedicated to a detailed investigation of the velocities and pressures within the cavity region. Distribution of the velocities and pressure coefficients along lines 1 to 6 are depicted in Fig. 4.33 to Fig. 4.42, for 90° wind direction and 40 m/s incoming wind speed. For each line, two separate graphs are presented, the first one for the wind speed inside the gap between the roof surface and the bottom surface of the solar panels, and the second one for the upper surface of the solar panels and up to 15 m - 20 m above their surfaces. Near the corner of the solar panel array (line 1), the wind velocity profile is shown for the gap between the roof surface and the bottom of the panels (Fig. 4.33 a)). The velocity changes from 0 m/s on the surface of the roof to 2.2 m/s at 1″ (0.025m) from the roof surface, then remained constant for 0.02 m; thereafter it returns back to 0 m/s at the top of this space, on the bottom surface of the panel. Moreover, along line 1, above the solar panel surfaces velocity increased to 44 m/s in the first 0.102 m (4″) above the top of the panel surface, then it decreased to 40 m/s at 5.5 m above the roof surface (Fig.4.33 b)).

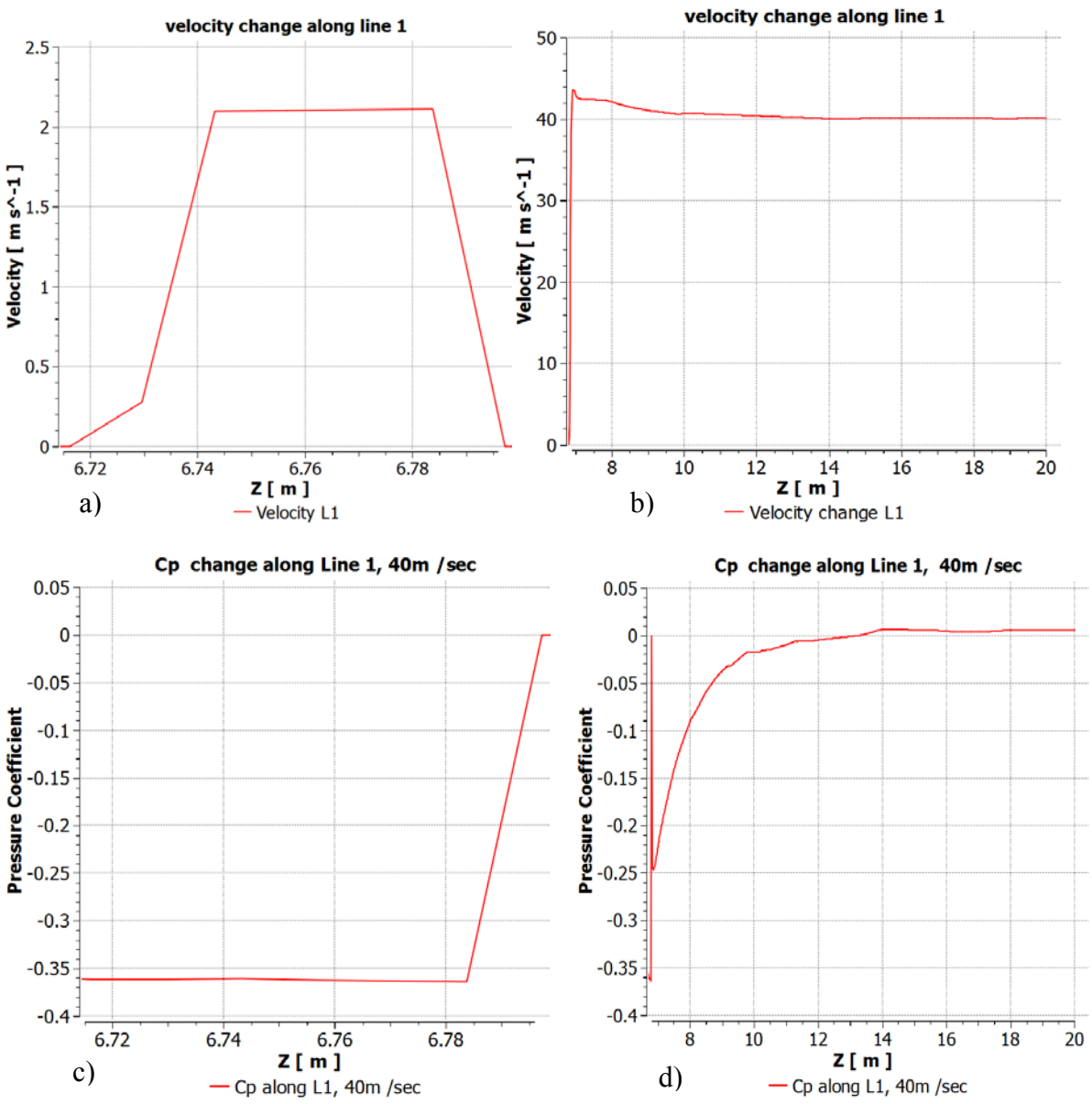


Fig. 4. 33. Velocity and Cp changes between panels, and above roof, Line 1, 40 m/s, windward, wind direction 90º

Figs. 4.33 c) and d) show the pressure coefficient profile between the roof surface and the bottom of the panels. The pressure coefficient in this region remained constant at Cp=-0.36 for the entire cavity between roof surface under the panels and bottom of the panels. Then the pressure coefficient decreased to 0 when it reached the bottom surface of the panel. At the panel top surface, Cp decreased to Cp=-0.25, then it increased gradually to 0 at 5.5 m above the roof surface.

For line 2 located in the middle of edge A of the panel array, Fig. 4.34 a) shows the velocity profile in the cavity between the roof surface and the bottom of the panels. Similar to line 1, the velocity

increased from 0 m/s on the roof surface to 1.0 m/s at 0.013 m above the surface, and it reduced slightly to 0.8 m/s in the next 0.015 m, then increased sharply to 3.1 m/s at 0.042 m above the roof surface, only to reduce again sharply to 0 m/s at the bottom surface of the panels.

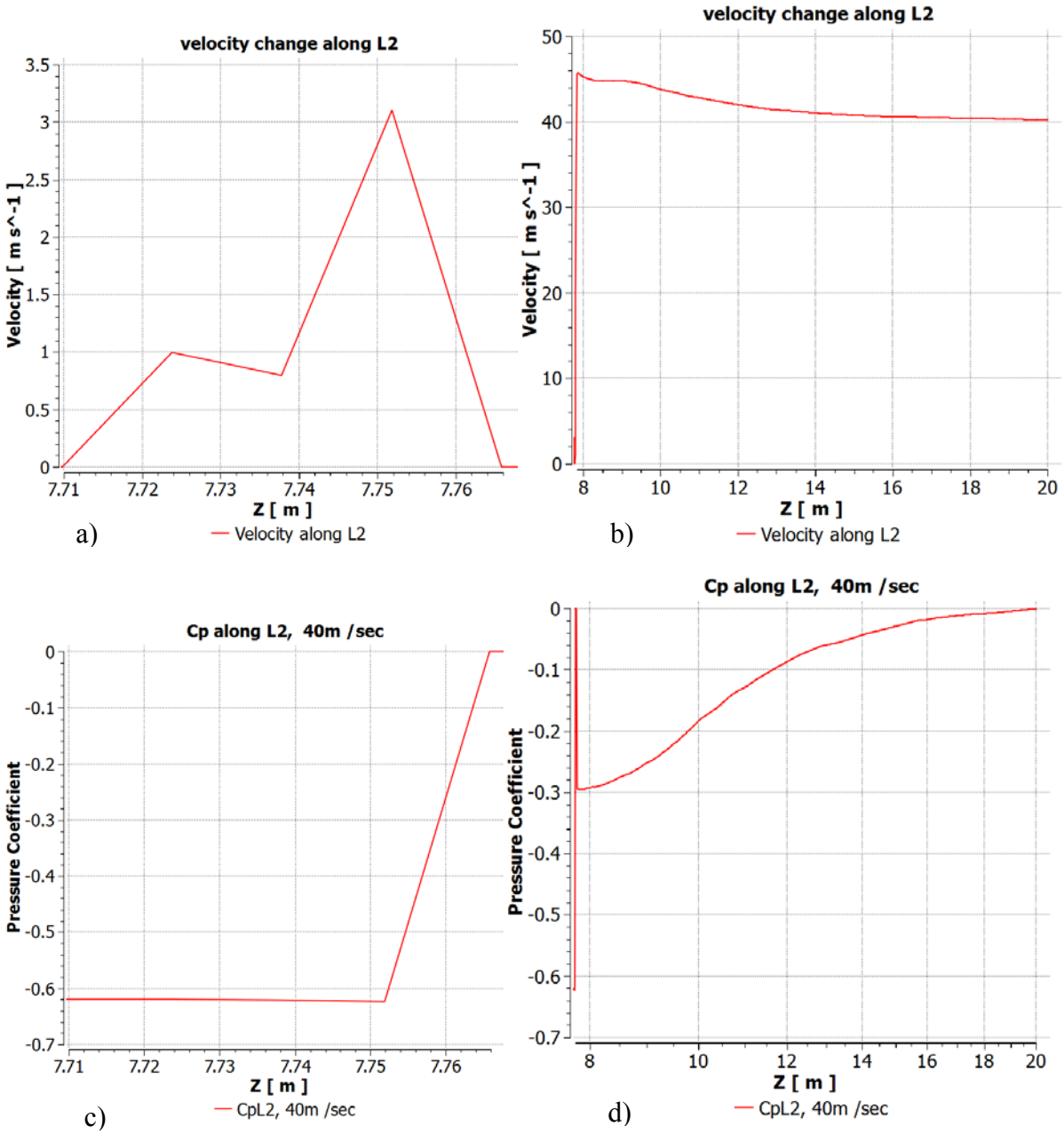


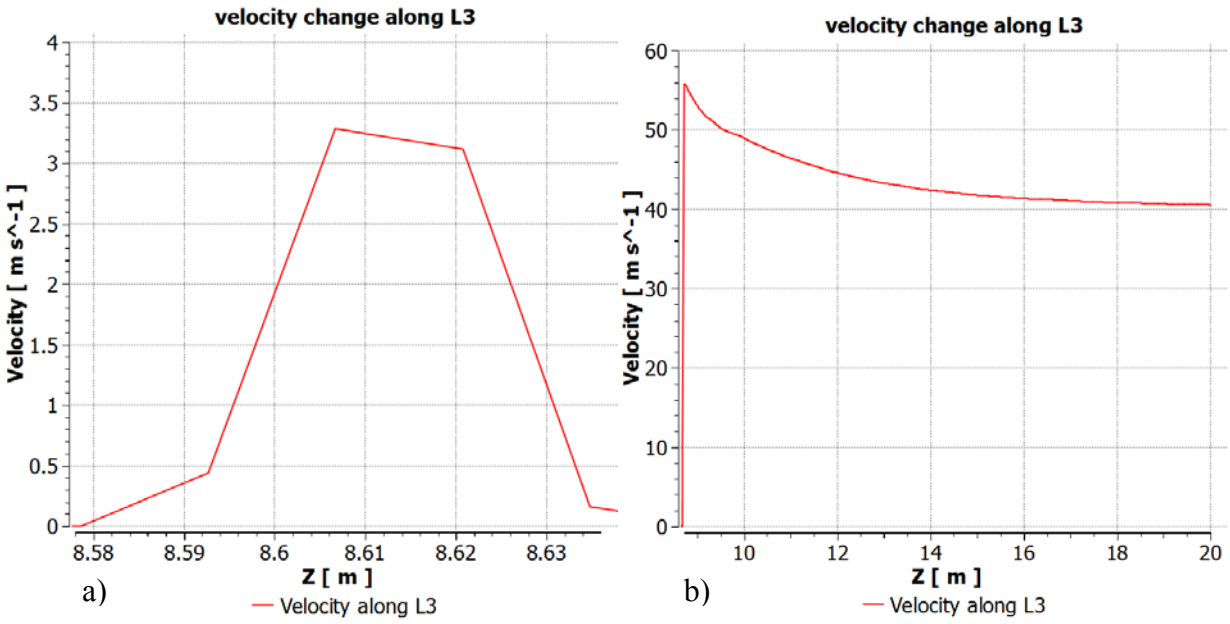
Fig. 4. 34. Velocity and Cp changes between panels, and above roof, Line 2, 40m/s, windward, wind direction 90º

Above the solar panel surface, the velocity increased to 46 m/s at 0.102 m (4″) above the roof surface then decreased to 40 m/s at 8.25 m above the roof surface (Fig. 4.34 b)). Fig. 4.34 c) shows

the pressure coefficient profile between the roof surface and the bottom surface of the panels. It can be observed that the pressure coefficient remained constant at Cp = -0.62 over 0.042 m from the roof surface, then increased to Cp close to 0 at the bottom of the panels. Directly above the top surface of the panels, Cp is -0.29, which then reduced gradually to Cp = 0 at 12.5 m above roof surface (Fig. 34 d)).

When comparing the pressure coefficients for wind speed 40 m/s, with 10 m/s (reported in Appendix B), it is observed that there are slight differences in values and trends. That might be because of the proportional wind speeds at the objects to the free stream wind speed.

This can be explained theoretically as follows from the expression of the pressure coefficient $C_p = \frac{P-P_0}{1/2 \rho_a U_0^2}$ (Holmes, 2001), which can be written as $C_p = 1 - \frac{U^2}{U_0^2}$ when Bernoulli theory holds. Then if the ratio of $\frac{U^2}{U_0^2}$ is constant or $\frac{U}{U_0}$ is constant, that would lead to C_p being constant as well, for two different wind speeds. Where P_0, U_0, ρ_a are pressure, mean velocity and air density at a reference point at a proper height, respectively; $P, U,$ are pressure, velocity and air density at the point where pressure coefficient is measured/calculated. This result is confirmed to be valid for all the lines 1 to 6, and for all the roof slopes, 35º, 27º and 15º.



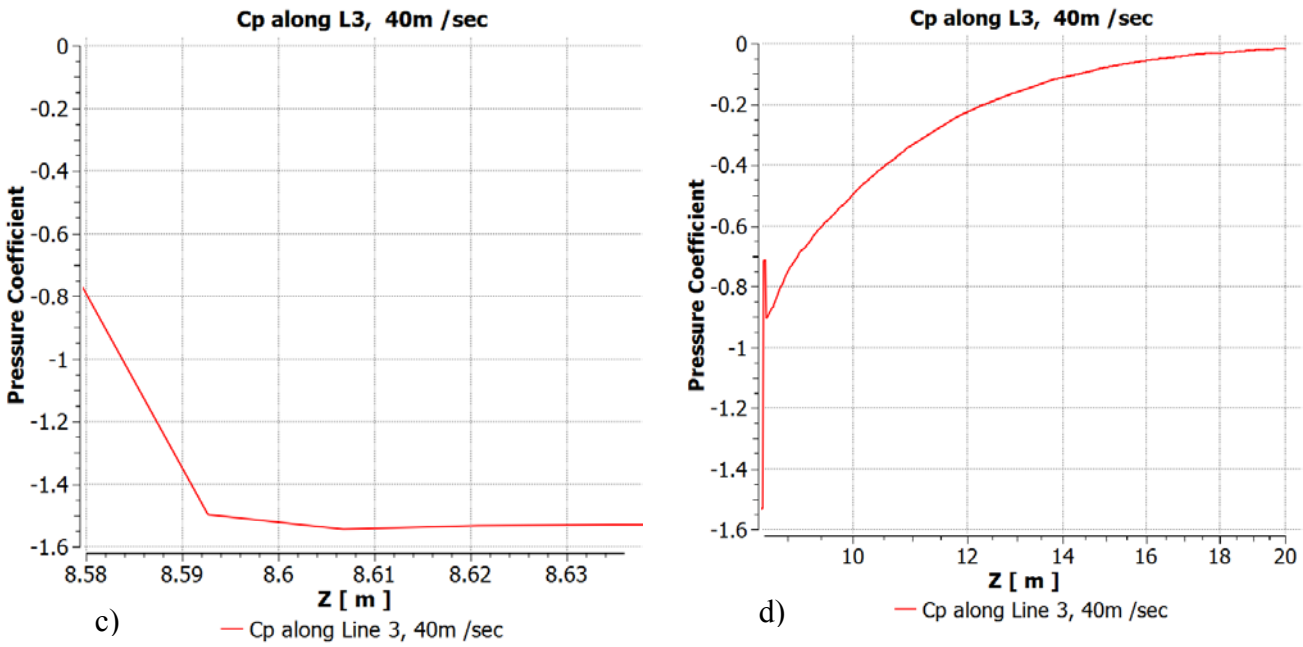


Fig. 4. 35. Velocity changes between panels, and above roof, Line 3, 40m/s, windward, wind direction 90º

Along the line 3, located at the top corner of the panels near edge A, Figure 4.35 a) shows the velocity profile between the roof surface and bottom of the panels, wherein velocity increased from 0 m/s on surfaces to 3.3 m/s in the middle of the space and remained constant for 0.015m then reduced again to 0 at the bottom of the panels. Above the solar panel surfaces, the velocity increased to 46 m/s near the surface then decreased to 40 m/s at 11.5m above the roof surface (Fig. 4.35 b)).

Figure 4.35 c) shows the pressure coefficient profile between the roof surface and bottom of the panels. The pressure coefficient is Cp=-0.72 on roof surface then increased to Cp=-1.49 at 0.015 m above the roof surface, then slightly increased to Cp= -1.53 for the remaining height of the space, while decreased again to Cp=-0.90 at the top surface of the panels then increased further to 0 at 20 m height above ground (Fig. 4.35 d)).

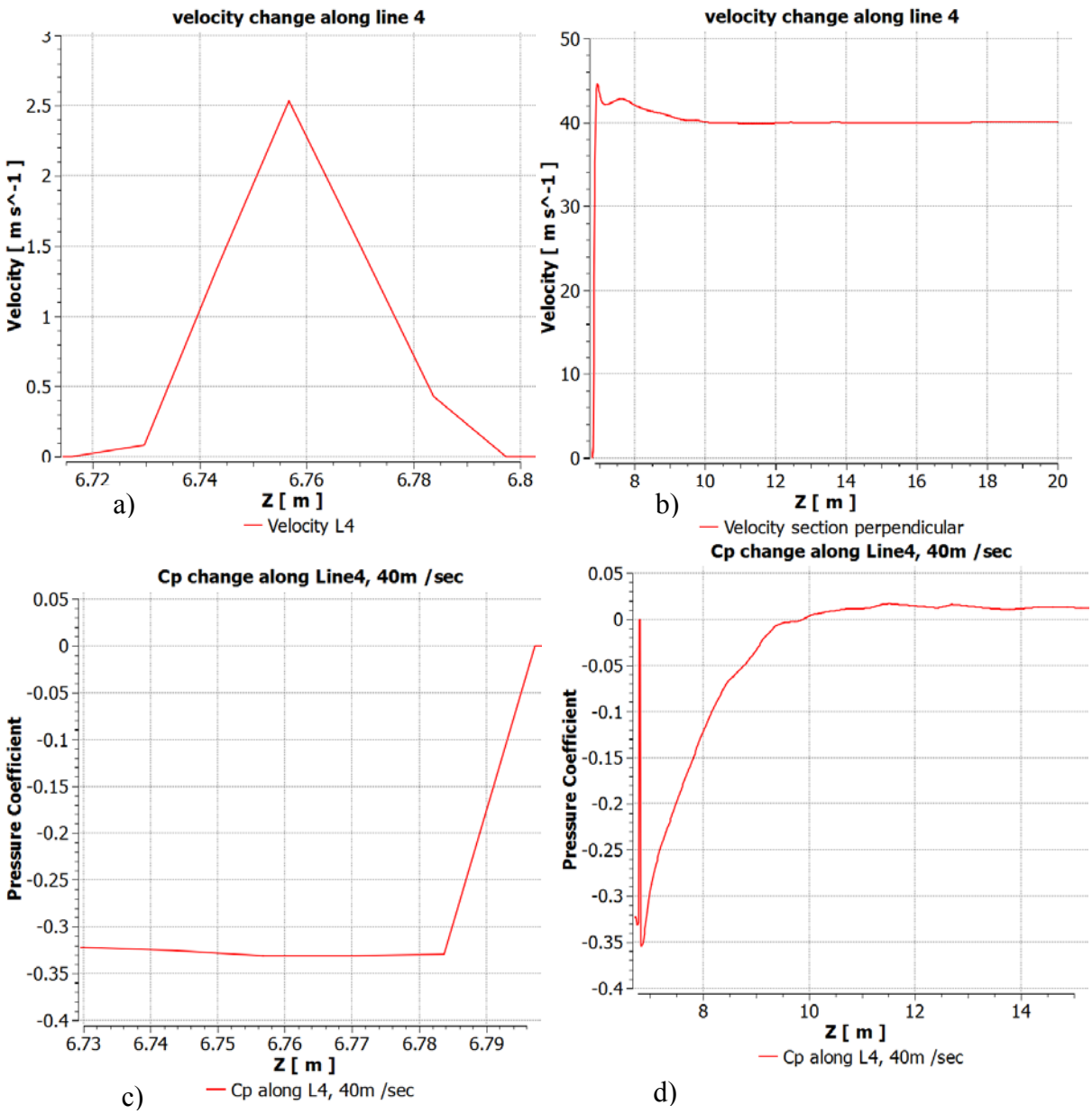


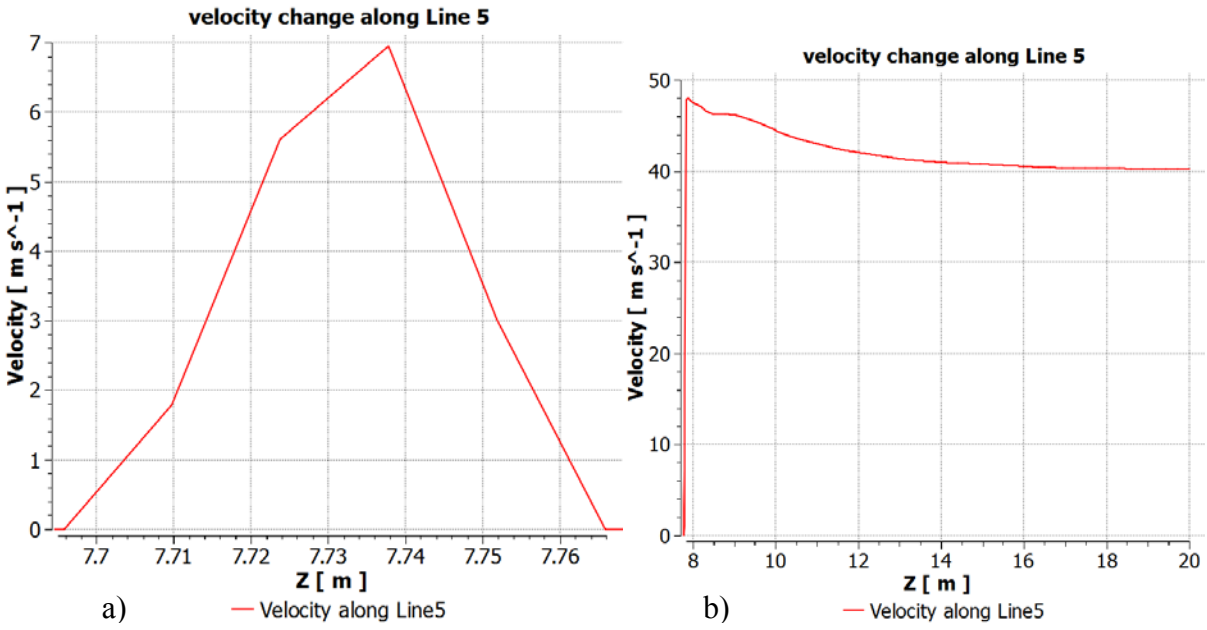
Fig. 4. 36. Velocity between panels, and above roof, Line 4, 40m/s, windward, wind direction 90º

Along the line 4, in the middle of the windward edge of the panels, Figure 4.36 a) shows velocity profile between the roof surface and bottom of the panels, where the velocity increased from 0 m/s on surfaces to 2.5 m/s at the middle of the space then reduced again to 0 at the bottom of the panels. Above the solar panel surfaces, the velocity increased to 45.5 m/s near the panel surface then decreased to 40 m/s at 3.5m above the roof surface (Fig. 4.36 b)). The last two graphs in Fig. 4.36 (c) and d)) show the pressure coefficients for the cavity between the roof surface and bottom surface of the panels along the line 4. For this case, the pressure coefficient is Cp= -0.32 and it

remained nearly constant until 0.5″ (12.5 mm) below the bottom surface of the panels. On top of the panels, the pressure coefficient started from Cp=0 and it decreased abruptly to Cp=-0.36 at a height of 0.102 m (4″) from the top panel surface; thereafter it increased gradually to 0, at 10 m height above ground surface.

Near the center of solar panel arrays, along the line 5, the velocity profile in the gap region between roof surface and the bottom surface of the panels shows that the velocity increased from 0 m/s near the roof surface, to 6.9 m/s in the middle of the space, then it reduced again to 0 m/s at the bottom surface of the panels (Fig. 4.37 a) and b)). Above the solar panel surface velocity increased to 48 m/s near the surface then it decreased to 40 m/s at 18 m height above the ground surface.

The last two graphs in Fig. 4.37 (c) and d)) show the pressure coefficient evolution for the gap region between the roof surface and bottom surface of the panels, where the pressure coefficient at the roof surface is -0.78 and it remained constant in the most gap region until 12mm (1/2″) under the bottom surface of the panels. At the top surface of the panels Cp increased to -0.42 then it increased gradually to 0 at 18 m height above ground surface.



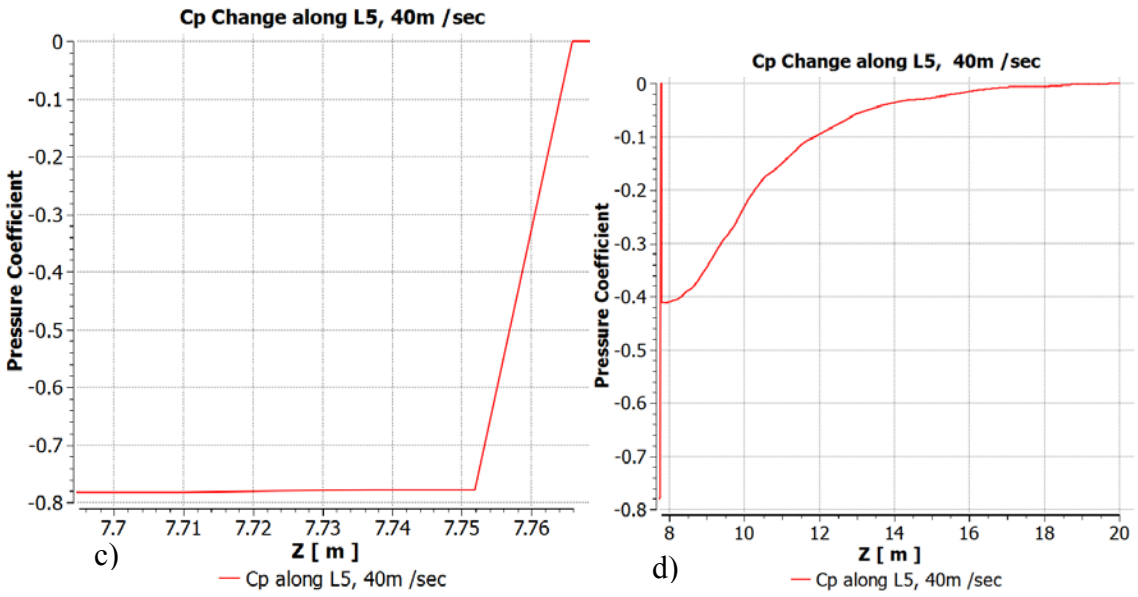
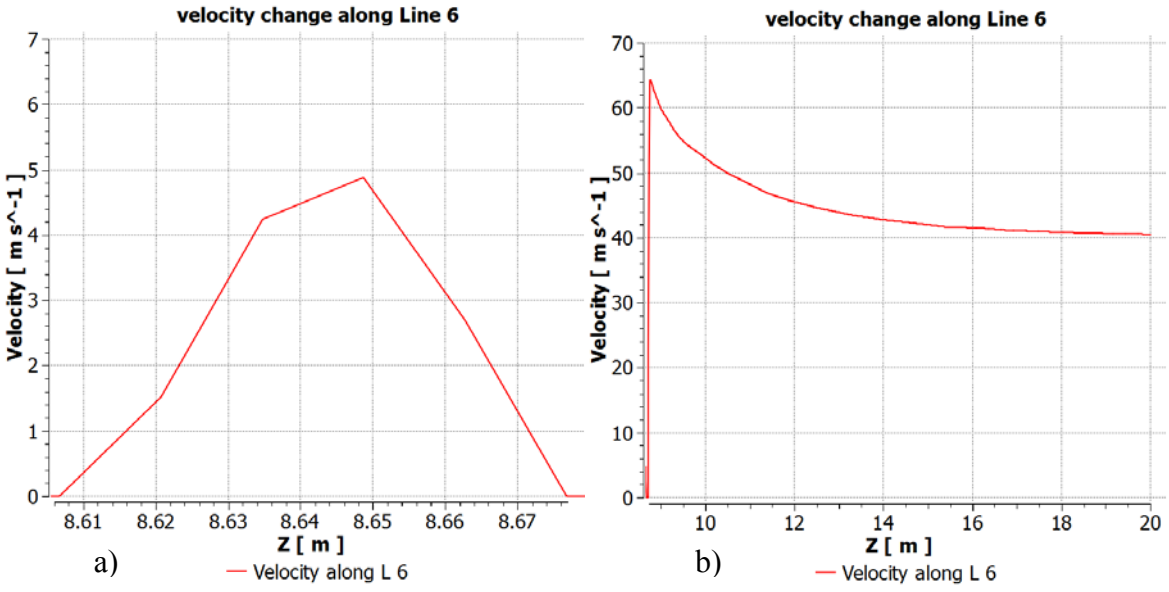


Fig. 4. 37. Cp changes between panels, and above roof, Line 5, 40 m/s, windward, wind direction 90º

Fig. 4.38 a) shows the velocity profile for the gap region between the roof surface and the bottom of the panels for line 6. Similar to the cases described above, the velocity increased from 0 m/s at the roof surface, to 4.8 m/s, slightly beyond the middle of the gap space, then it reduced to 0 m/s at the bottom surface of the panels.



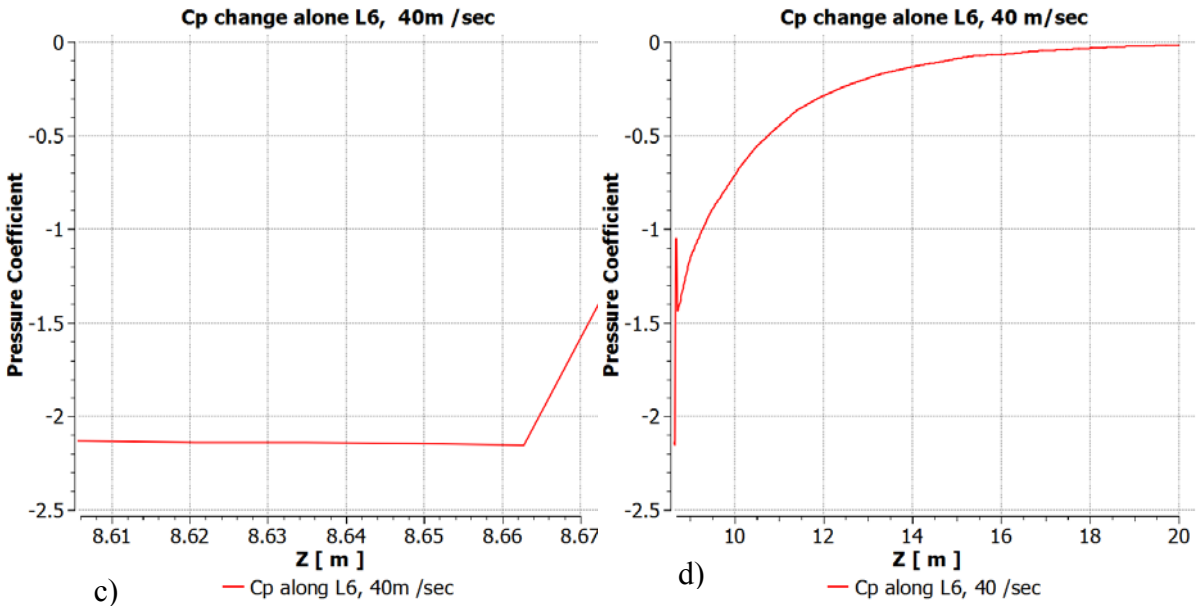


Fig. 4. 38. Pressure coefficients and velocity changes between panels, and above roof, Line 6, 40 m/s, windward, wind direction 90º

In the immediate vicinity of the upper solar panel surface, the velocity increased to 64 m/s, along the line 6, then it decreased gradually to 40 m/s at about 20 m height above the ground surface. The last two graphs in Fig. 4.38 (c) and d)) show the pressure coefficient evolution along line 6, for the same two regions: for the gap between the roof and the panels, and above the solar panels. The pressure coefficient in the cavity started from Cp=– 2.21 at roof surface which is the lowest among the lines 4, 5 and 6, located in the middle of the solar panel array. Thereafter the Cp remained constant until nearly 12 mm below the bottom surface of the panels; above the top surface of the panels this increased up to Cp=-1.42 then continues to increase gradually to 0, at 20 m height above ground surface.

Figures 4.39 and 4.40 show the pressure coefficients and the velocity profiles for all lines, 1 to 6, for an incoming flow of 40 m/s. It is evident that the pressure coefficients and the velocities for the investigated lines, situated at the same horizontal level locations were consistent, e.g.: lines 1 and 4, lines 2 and 5 and lines 3 and 6. Pressure coefficients for the gap region between the roof and the solar panels reached values of Cp=-0.33 to -0.36 for the lower two lines L1 and L4. Along the middle lines, L2 and L5, the pressure coefficients under the solar panels decreased to Cp=-0.62 and -0.78, while the Cp decreased to Cp=-1.53 and -2.15 along the top two lines L3 and L6 and under the panels. The corresponding velocities along the lower, middle, and top lines range between 2.2 to 2.5 m/s, 3.3 to 6.8 m/s and 3.2 to 4.9 m/s, respectively. In addition, wind speed

above the panels range between 44 to 44.8 m/s, 46 m/s to 48 m/s and 56 m/s to 64 m/s for the lower, middle and top lines, respectively. Therefore, it can be noticed that for all the lines, except line 1, the suction in the gap region increased with increasing wind speed. That is evident for the wind field domain above the solar panels, where it was noticed that the suction at all the lines above the panels is proportional to wind speeds in those points.

Figures 4.41 and 4.42 show the pressure coefficients and velocities in the gap region between the roof and the panels and on top of the panels, due to an incoming wind speed of 10 m/s. Pressure coefficients for 10 m/s are very similar to the ones obtained for 40 m/s (Fig. 4.39 and 4.40), for the space under and above the panels. As it can be noticed, the Cp for the gap region is nearly (Cp=-0.33 to -0.36), for the lower two lines L1 and L4. Along the middle lines, L2 and L5 the pressure coefficients decrease to Cp=-0.62 to -0.78, while the Cp decreased to Cp=-1.50 and -2.15 along the top two lines L3 and L6 (Fig. 4.39). The corresponding velocities along the bottom, middle, and top lines range between 0.52 m/s to 0.66 m/s, 0.72 m/s to 1.63 m/s and 0.82 m/s to 1.25 m/s, respectively. In addition, wind speed above the panels range between 11.01 m/s to 11.19 m/s, 11.52 m/s to 12.10 m/s and 13.95 m/s to 16.10 m/s for the lower, middle and top lines, respectively. Thus, it can be concluded that the pressure coefficients for 10 m/s and 40 m/s were very similar, for the gap region and for the region above the solar panels, despite the different values of the wind speed recorded. Moreover, the recorded wind speeds are proportional to the free stream wind speed, the ratios of recorded wind speeds to free stream speeds are similar for the same configuration of solar panels over the gable roof.

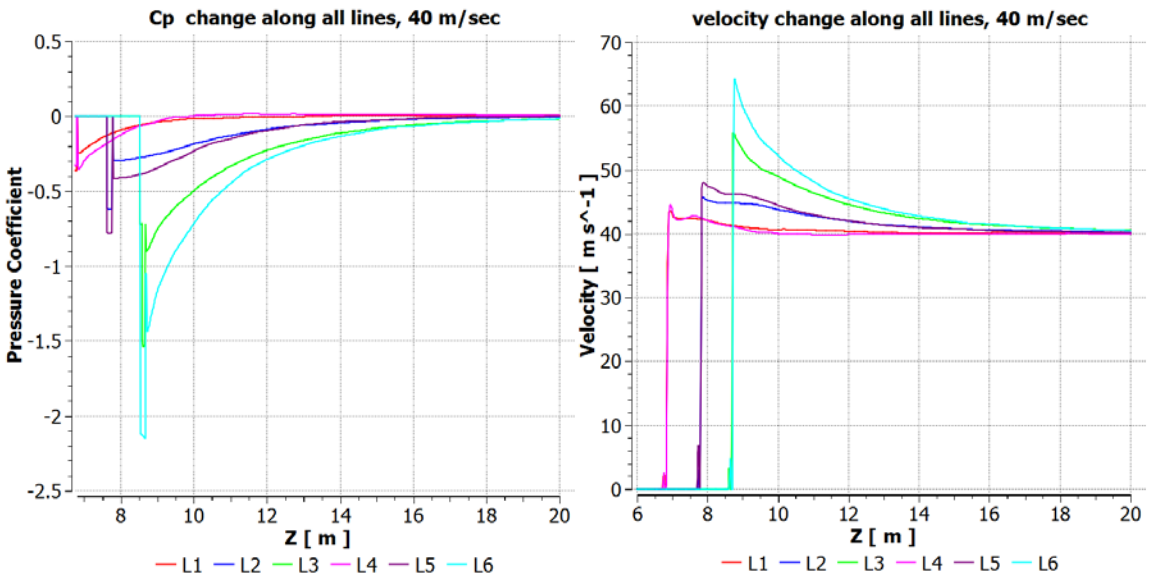


Fig. 4. 39. Pressure coefficient and velocity between panels and roof, and above the panels, Lines 1 to 6, 40 m/s, windward, wind direction 90º

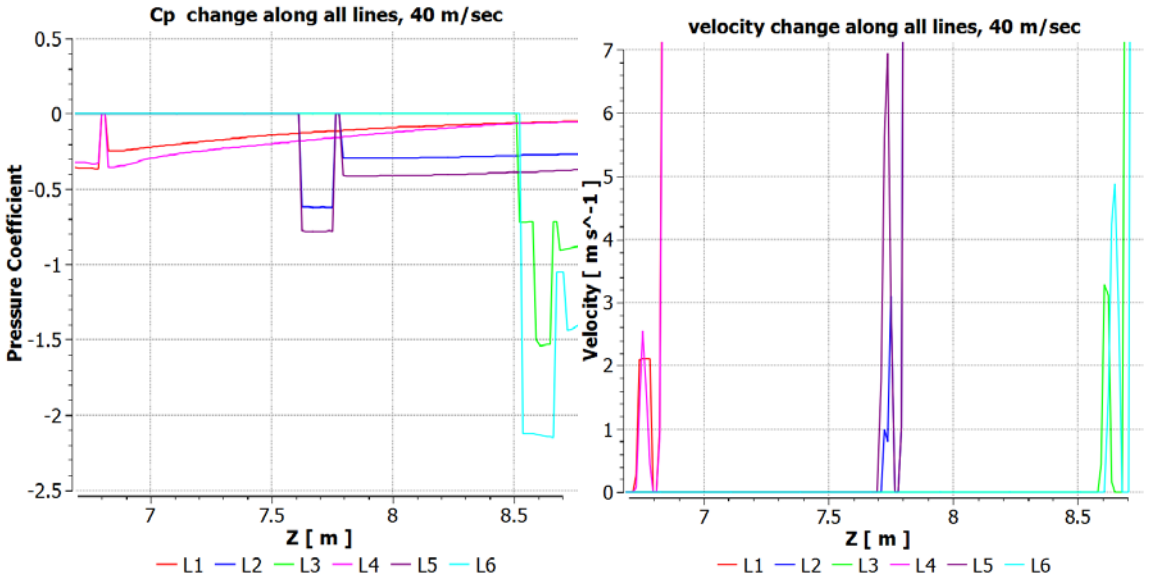


Fig. 4. 40. Cp and velocity changes between panels and roof, and above the panels, Lines 1-6, 40 m/s, windward, wind direction 90º, Zoom into space between panels and roof

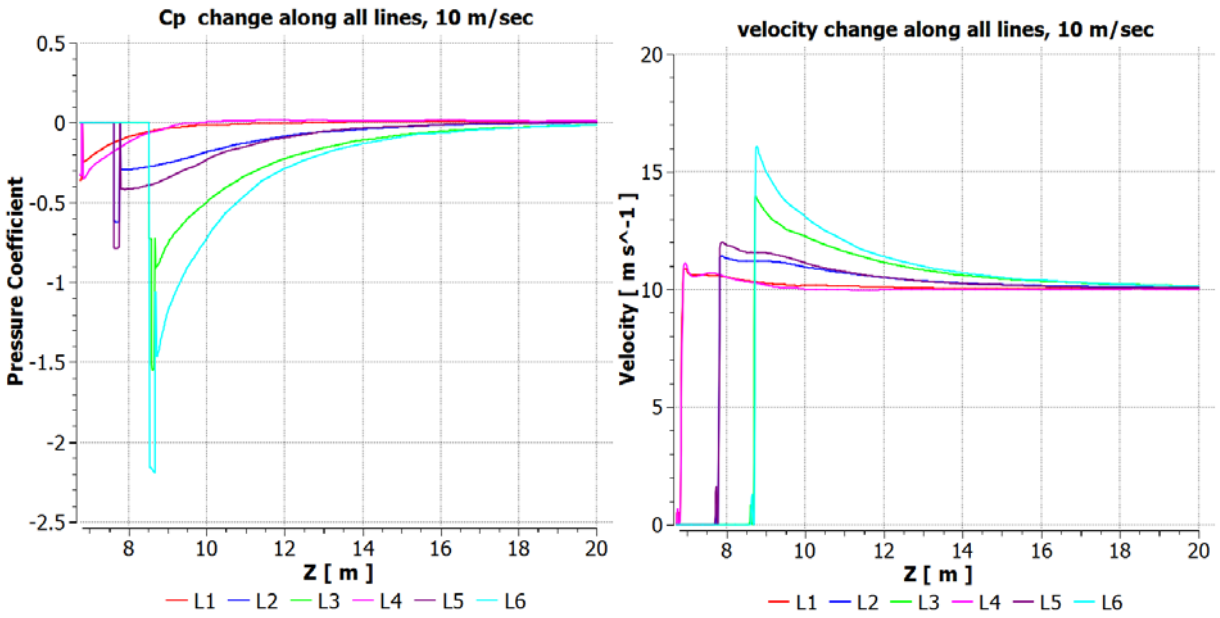


Fig. 4. 41. Cp and velocity changes between panels and roof, and above the panels, Lines 1-6, 10 m/s, windward, wind direction 90º

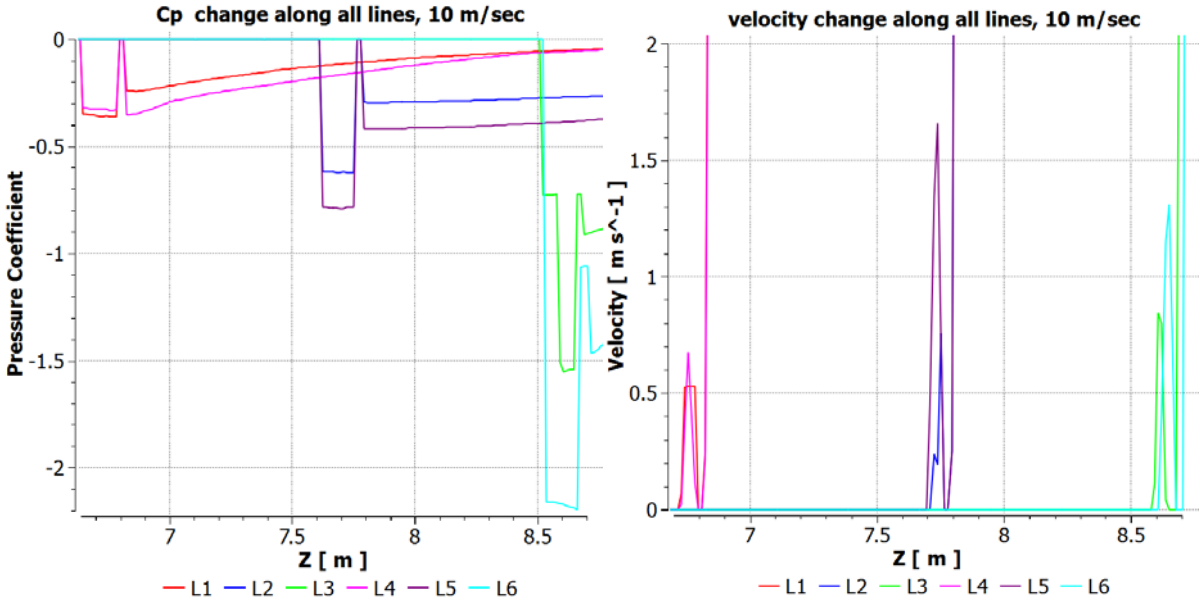


Fig. 4. 42. Cp and velocity changes between panels and roof, and above the panels, Lines 1-6, 10 m/s, windward, wind direction 90º Zoom into space between panels and roof

4.2.5. Pressure coefficients for roof mounted solar panels and roof without solar panels for leeward side of the roof

The previous sections focused on the wind-induced pressure coefficients on the roof surface and the solar panels installed on the windward side of the roof. The data analysis presented in the current section will reveal the fact that the leeward surface of the roof without panels is subjected to higher suction than the windward surface of the roof without panels. Thus, it is very important to detail the changes of wind pressure distribution on the leeward side, when solar panels are installed on the roof as described in the following subsections.

4.2.5.1. Pressure coefficient on roof under solar panels vs. roofs without solar panels

Comparisons between the wind-induced pressure coefficients on the roof surface without solar panels and on the roof surface under the solar panels for wind directions 45º, 90º and 0º are shown in Figs. 4.46, 4.47 and 4.15 respectively. Three lines PL20, PL29 and PL38, located on the leeward side of the roof, at same distances from the ridge as the windward side lines PL1, PL10 and PL19, were used for reporting the results.

For the 90° wind direction, Cp along PL20 shows higher pressure coefficients, 0.1 to 2.0, than the corresponding line on the roof without panels, where two symmetric drops were noticed near the edges A and B of the roof. In addition, PL29 shows higher negative pressure coefficients of up to Cp= -1.3, than the corresponding line on the roof without panels. However, pressure coefficients on PL38 on the roof under the panels, are lower Cp=0.1 to 0.30 than the pressure coefficients on the roof without panels. On the other hand, Cp for all the lines are symmetric around the middle of the roof, for both roof surface under the panels and roof surface without solar panels (Fig. 4.43). When wind direction is 45° (Fig. 4.44) it was noticed that pressure coefficients have similar trends for the roof surface with solar panels installed and without solar panels. For line PL20 located at the edge of the solar array near the ridge at the leeward side, the pressure coefficients are lower, by up to Cp =0.6 than the corresponding line on the roof with no panels. Nonetheless, for line PL29 located in middle of the array, the pressure coefficients are higher by Cp=0.6 than corresponding line on the roof with no panels. The pressure coefficients along line PL38 on the

roof under the panels is lower for most of the line length than the corresponding line on roof without panels.

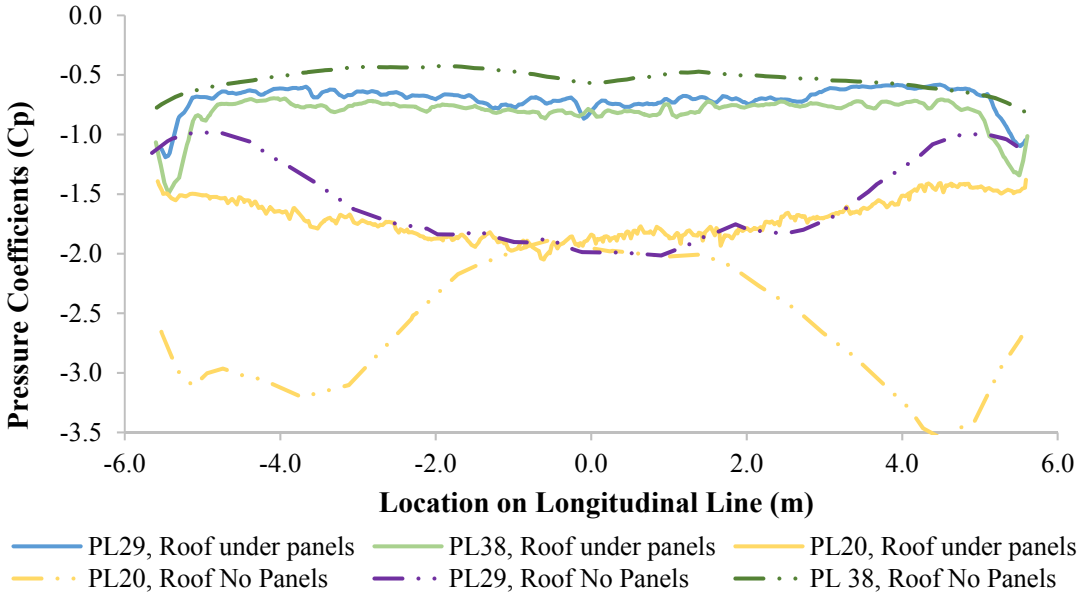


Fig. 4. 43. Pressure coefficient distribution on the roof surface under the solar panels and on the roof surface without panels, for roof slope 35º, and wind direction 90º, leeward side

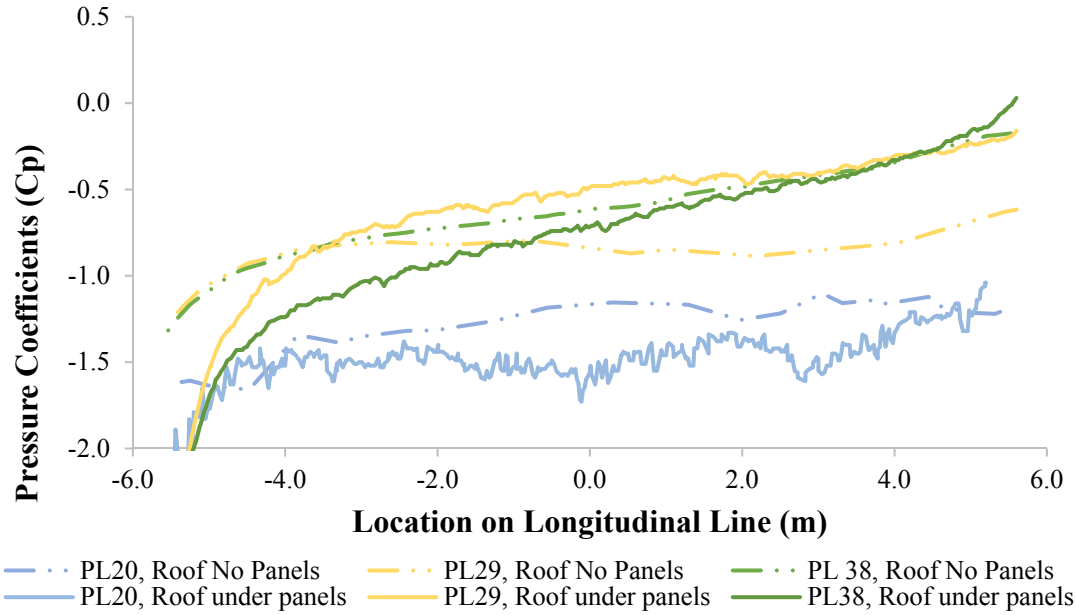


Fig. 4. 44. Pressure coefficient distribution on the roof surface under the solar panels and on the roof surface without panels, for roof slope 35º, and wind direction 45º, leeward side

For wind direction 0º due to the symmetry of the wind flow and the roof-solar panels system, Cp is the same on both windward and leeward sides of the gable roof surfaces. Consequently, the graphs and description are the same as those shown in Fig. 4.15.

4.2.5.2. Pressure coefficient on bottom surface of the solar panels vs. roof surface under solar panels

Graphical representation of wind pressure coefficients obtained for the bottom surface of the solar panels and on the roof surface under the solar panels, for wind directions 90º, 45º and 0º angles with ridge, are shown in Figs. 4.45, 4.46 and 4.12, respectively. For 0º wind direction the pressure coefficient distribution is identical on the windward and leeward sides, therefore there is no need to duplicate Fig. 4.12 introduced in the previous section. The pressure coefficients were reported for three longitudinal lines situated on the leeward side of the roof as follows: line PL20 near the ridge of the roof, line PL29 in the middle of the roof and solar panel array surface and PL38 situated near the lower edge C of the solar panel array. Overall, from Figures 4.45 , 4.46 and 4.12, it can be observed that for most of the solar panels area, the difference between the Cp on the bottom surface of the panels, and on the roof surface under the panels, are very small in the range of 0 to 0.2. This indicates the occurrence of the pressure equalization between the roof surface and the bottom surface of the panels. Moreover, on lines PL20, PL29 and PL38, all pressure coefficients had negative values, which shows that the entire roof-panels system is under suction.

For 90° wind direction, the Cp along the longitudinal line PL29 located on the roof surface under the panels and on the bottom surface of the panels, depict high similarity throughout the entire length of the line. The pressure coefficients for the middle section of the PL29 line, approach the values of Cp =0.65 to 0.70, however, this decreased sharply to -1.20 at the edges A and B of the leeward surface of the array. Pressure coefficient Cp along line PL20 on the roof surface under the panels is slightly higher than the Cp along the bottom surface of the panel. Nonetheless, for the solar panels located near the lower edge of the roof (line PL38), the difference between the Cp coefficients on the roof surface under the panels and Cp on the bottom surface of the panels was higher than for the previous two lines. It is also noteworthy to mention that the suction was higher on the roof under the solar panels.

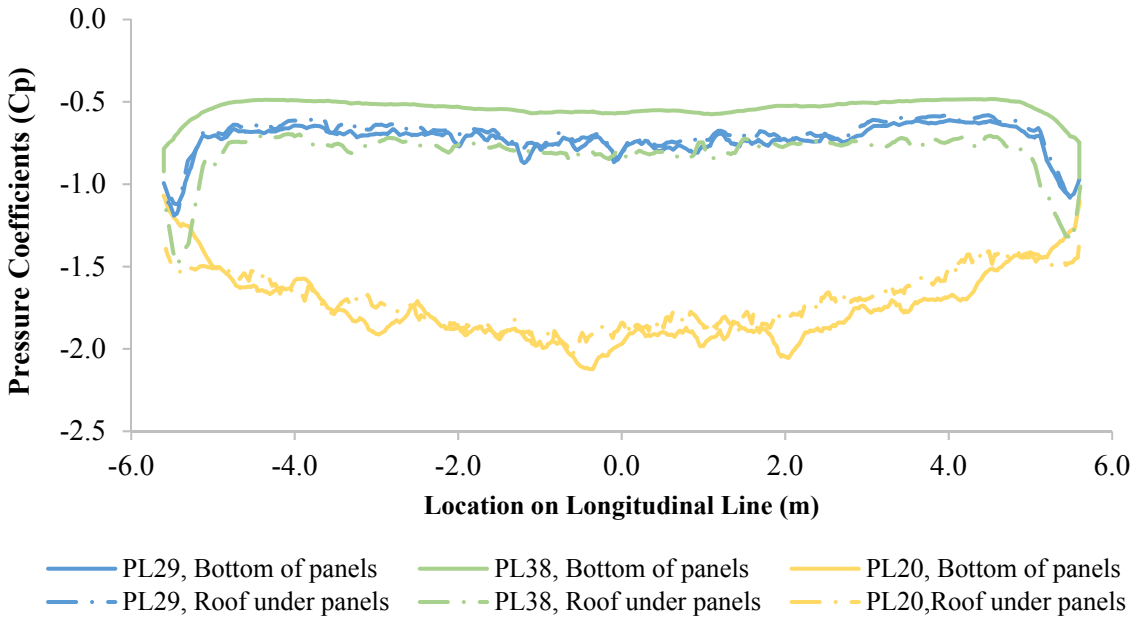


Fig. 4. 45. Pressure coefficient distribution on the roof surface under the solar panels and on bottom of the panels, for roof slope 35º, and wind direction 90º, leeward side

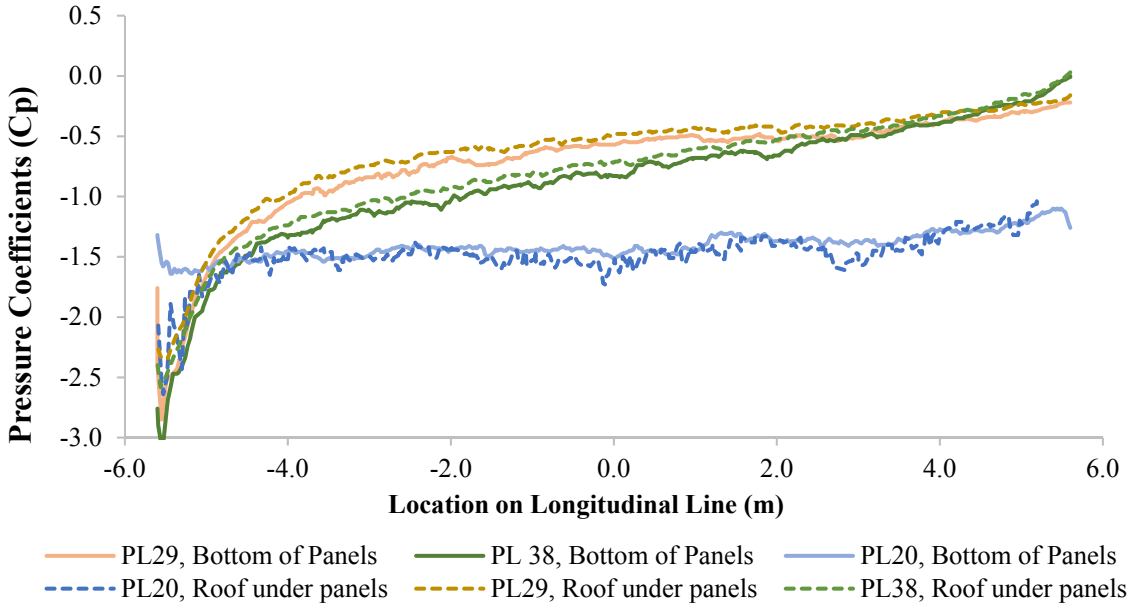


Fig. 4. 46. Pressure coefficient distribution on the roof surface under the solar panels and on bottom of the panels, for roof slope 35º, and wind direction 45º, leeward side

In addition, the suction, represented by negative Cp coefficients, along PL20 on both surfaces increased moderately in the middle of the panel array to Cp=-1.9 from Cp=-1.25 at the edges of the solar array, which is contrary to the trends followed by Cp for lines PL29 and PL38 (Fig. 4.45).

For the case of 45° wind direction, the Cp values along the three lines PL20, PL29 and PL38, on the roof surface under the panels and on the bottom surface of the panels, demonstrate high similarity throughout the entire length of the three lines. Contrary to the 90º wind direction case, the pressure coefficients for 45° increased gradually from edge A to edge B of the roof, for PL29 and PL 38. However, near edge A, the pressure coefficient magnitudes decreased sharply on the leeward side of the array, from Cp=-2.7 to about 0. For line PL 20, Cp remained in the range of Cp=-1.5 to -1.3 for the bottom of the panels but drops to Cp=-2.6 for the roof under the panels, as it can be seen in Fig. 4.46.

For wind direction 0º, the pressure coefficients were identical for both leeward and windward sides of the roof, for all the investigated lines. This can be attributed to the flow and structure symmetry. Consequently, the graphs and the interpretation are the same as in Fig. 4.12 and section 4.1.4.1 above. In comparison with the 45º and 90 º wind directions, it can be noticed that for 0º case, evolution of the pressure coefficients is symmetric about the middle of the solar panel array while the bottom surface of the panels and the roof surface under the panels had consistent pressure coefficients. Sharper drop in Cp was noticed near edges A and B of the solar panel array, for all the three lines.

4.2.5.3. Pressure coefficients for roof without solar panels vs. pressure coefficients on top surface of solar panels

For 90°, Cp along the line PL20 shows lower suction coefficients, (Cp= -1.1 to -2.1), for top surface of the panels, than the corresponding line on the roof without panels, which changes from -2.0 to -3.5. Similarly, PL29 shows lower suction for the top surface of the panels, of Cp=-0.7 to -0.9, than the corresponding line on the roof surface without panels, (Cp=-1.2 to -2.0). However, pressure coefficients for most length of the line PL38 on the top surface of the panels are slightly lower (with 0.3), than the pressure coefficients along PL38 on the roof without panels. In addition, Cp along PL29 and PL38, on the top surface of the panels change slightly along the length of these lines, in comparison with PL 20. On the other hand, Cp on all three lines are symmetrical around the middle of the roof, for both roof surfaces under the panels and roof surface without solar panels (Fig. 4.47).

For the case of 45° wind direction (Fig. 4.48) it was noticed that all pressure coefficients on either surface have similar trends. Pressure coefficients on line PL20 of the solar array edge located near

the ridge (Fig.6), are moderately lower, -0.9 to -1.6 for most of the line length than the Cp of the corresponding line on the roof with no panels, (Cp =-1.3 to -1.7). Nonetheless, for PL38 located near leeward edge of the array, pressure coefficients on top surface of the panel are in the range, of 0 to -2.0, thus are slightly higher, than those on the corresponding line on the roof with no panels, (Cp=-0.2 to -1.3), for most of the line length starting from leeward panel edge.

However, Cp on middle line PL 29 shows much higher pressure coefficients, -0.3 to -1.75, on the top surface of the panels, than the Cp on the corresponding line on the roof without panels, which were in the range of -0.7 to -1.25. Moreover, pressure coefficients along the lines PL29 and PL38 on the top surfaces of the panels, decrease sharply from Cp= 0 and -0.3 on leeward edge B, to Cp =-2.0 and -1.7 respectively, at the windward edge A of the roof, as shown in Fig 4.48.

For wind direction 0º, Cp is the same on both sides, of the gable roof surfaces, for both cases with or without solar panels installed, due to the symmetry of the structure geometry and the flow. However, these symmetries in addition, that flow in this wind direction run parallel to roof surfaces, are not exist in the other wind directions . Consequently, graphs and description reporting the pressure coefficients for this case are as shown in Fig. 4.24 and section 4.1.4.5 above.

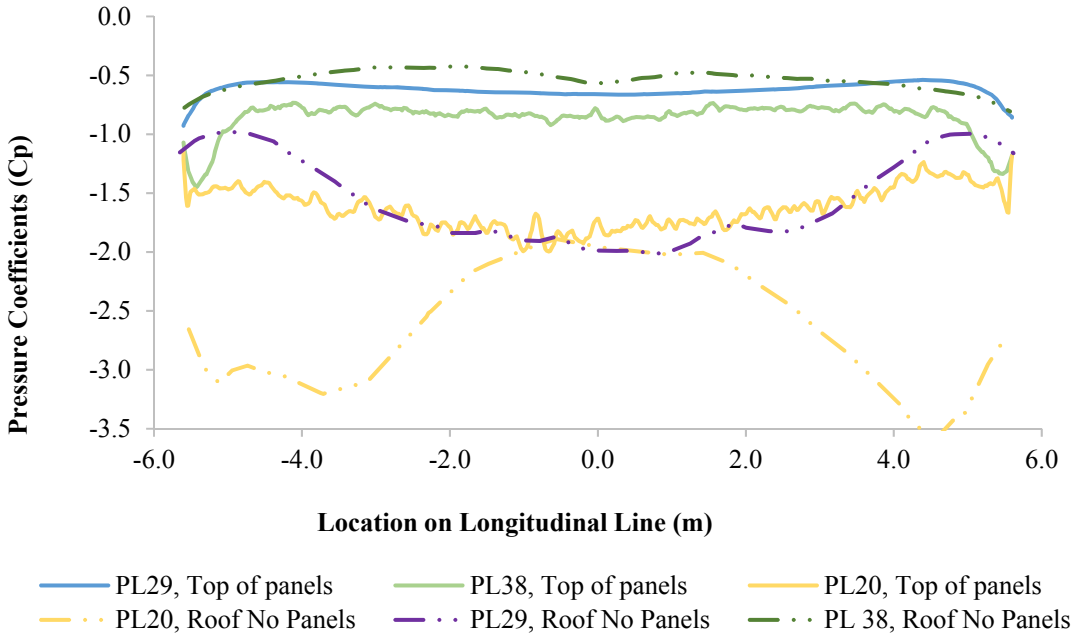


Fig. 4. 47. Pressure coefficient distribution on the bottom surface of the solar panels and on top of panels, for roof slope 35º, and wind direction 90º, leeward side

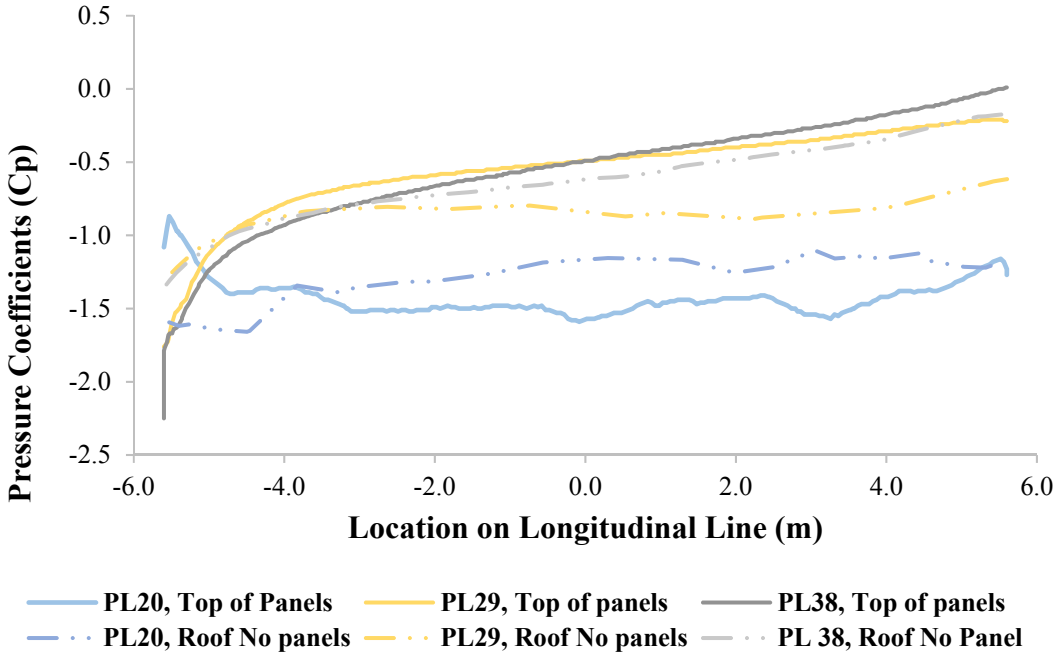


Fig. 4. 48. Pressure coefficient distribution on the bottom surface of the solar panels and on top of panels, for roof slope 35º, and wind direction 45º, leeward side

4.2.5.4. Pressure coefficients for roof without solar panels vs. resultant of pressure coefficient on the roof – solar panels system

Wind pressure coefficients on the roof surface without panels is compared with the resultant of the wind pressure coefficients on the entire system: roof surface under the panels, bottom surface of the panels and top surface of the panels, for wind directions 90º, 45º, and 0º and the results are shown in Figs. 4.49, 4.50 and 4.21 respectively.

Lower resultant pressure coefficients were registered for 90° wind direction, along the line PL20 (-1.4 to -2.1), than the corresponding line on roof without panels, which changes from Cp=-2.0 to -3.5. Similarly, on line PL29 resultant pressure coefficients for the entire roof-solar panels system indicate lower suction, of Cp=-0.5 to -1.0 than the corresponding line on the roof without panels, (Cp= -1.2 to -2.0). On contrary, resultant pressure coefficients on most length of the line PL38, are up to 0.6 higher than the pressure coefficients along PL38 on the roof without panels. The resultant Cp along PL29 and PL38, change slightly along the length of these lines, except for the two extremities, edges A and B of the roof, in comparison with pressure coefficients on PL 20. Moreover, Fig. 4.49. shows that the pressure coefficients Cp on all the lines investigated are

symmetric around the middle of the roof, for both cases: roof surface without solar panels and the system roof - panels.

For the case of 45° wind direction (Fig. 4.50) it was noticed that the resultant pressure coefficients and those on the roof with no panels, have similar trends. Resultant pressure coefficients on line PL20 of the solar array edge located near the ridge (Fig.6), are higher, (Cp=-1.0 to -2.5) for most of the length of this line, than the Cp of the corresponding line on the roof with no panels, (Cp=-1.3 to -1.7). Nonetheless, for PL38 located near the lower edge of the array (Fig.6) resultant pressure coefficients on the panel and roof surfaces, are in the range of (Cp = 0 to -2.0), which are moderately higher, than those on the corresponding line on the roof with no panels, (Cp= -0.3 to -1.3), for most of the line length starting 1.0 m from the windward edge A, towards the leeward array edge B. However, resultant Cp on the middle line PL 29 shows higher pressure coefficients, (Cp = -0.3 to -2.5), than the Cp on the corresponding line on the roof without panels, (Cp=-0.7 to -1.25). Resultant pressure coefficients along PL29 and PL38 for the roof-solar panels system, increased sharply from (Cp=0 and -0.3) on leeward side to (Cp= -2.5) at the windward side of the roof (Fig 4.50).

For wind direction 0º, the resultant Cp is the same on both sides of the gable roof surfaces, for the entire system and for the roof without panels. Consequently, the graphs and description are exactly

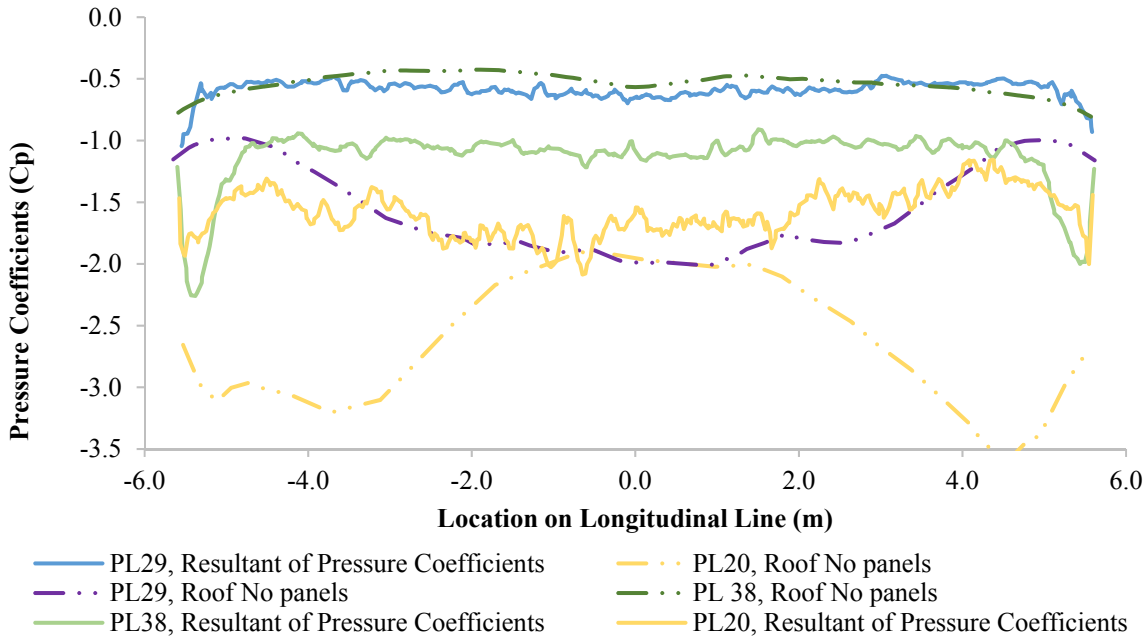


Fig. 4. 49. Pressure coefficient distribution on roof surface without mounted panels and resultant of pressure coefficients on roof surface due to panel installation, slope 35º, and wind direction 90º, leeward side

as in Fig. 4.21 and section 4.1.4.4 above. Moreover, for wind direction 0º, wind flows parallel to the roof and panel surfaces, which results in less turbulences, lower wind speed around the roof and then smaller suctions. That is evident in the small suction in 0º wind direction stays nearly constant, at around -0.3, along the middle of the surfaces, while significantly decreasing near the front /windward and leeward edges. However, suction is larger for cases 45º and 90º wind directions, where suction reached (Cp=-3.5), Figs. 4.49 to 4.50.

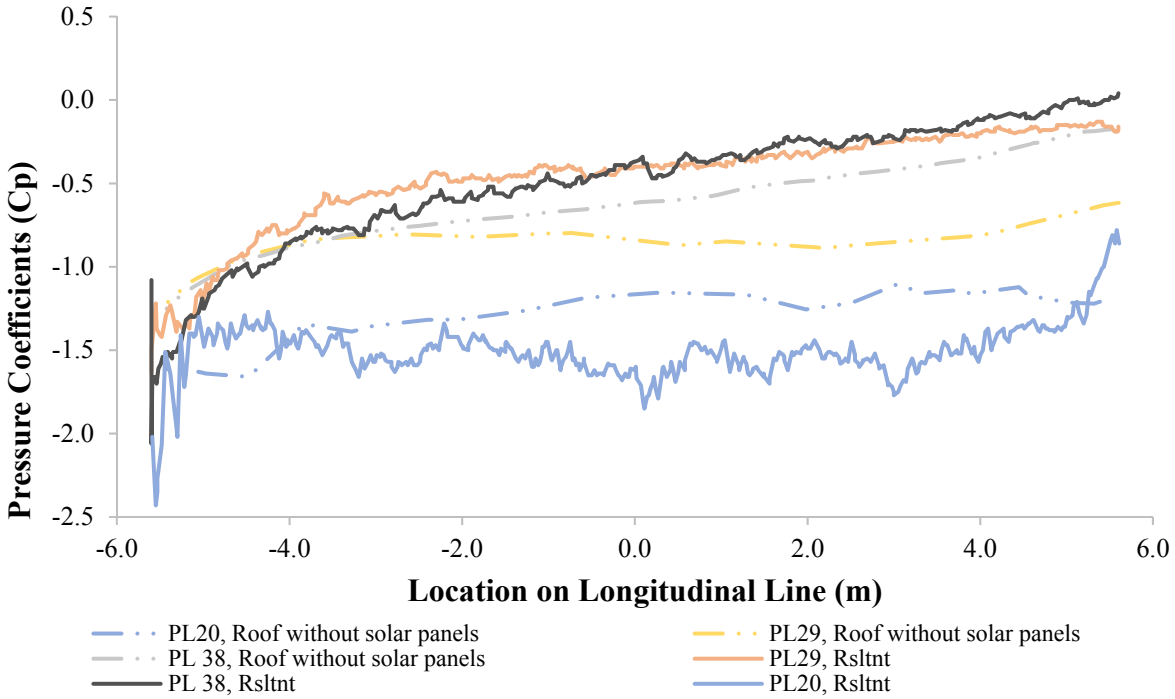


Fig. 4.50. Pressure coefficient distribution on roof surface without mounted panels and resultant of pressure coefficients on roof surface due to panel installation, slope 35º, and wind direction 45º, leeward side

4.2.6. Net pressure coefficients on roof-solar panels system for slope 35º, wind directions 90º, 45º, 0º

Pressure coefficients for three representative lines were discussed in the previous sections in order to describe the evolution and trends of the pressure coefficient for various conditions. The total pressure coefficients on the roof and on the solar panels' areas, are provided for the comparison with the corresponding pressure coefficients on roof without solar panels. A suitable method to evaluate the effects of wind-induced pressure on the roof mounted solar panels is to integrate the

pressure coefficients sampled over all the 38 polylines, and then to take the average over the areas of interest.

Tables 4.1 and 4.2 show the integrated and averaged pressure coefficients along all 38 polylines on top surface of the solar panels' arrays, for the wind direction 45º, for windward and leeward sides of the roof, respectively. In the same manner, the detailed results for the integrated and averaged total pressure coefficients for the entire roof-solar panels system, for wind direction 90º, are presented in Table 4.3 and 4.4.

Table 4. 1 . Pressure coefficients on roof without panels vs. resultant pressure coefficients on roof under solar panels, slope 35º, wind direction 45º, windward side

Polylines	Cp for roof without panels	Cp on top surface of the panels	Cp for roof under the panels	CP for bottom surface of the panels	Cp difference top – bottom surfaces of the panels	Net Cp for the system roof-panels	Ratio of net Cp on system roof-panels / roof without solar panels
Pl1	-0.17	-0.59	0.25	0.31	-0.90	-0.65	3.82
Pl2	-0.18	-0.33	0.32	0.37	-0.70	-0.38	2.11
Pl3	-0.18	-0.25	-0.41	-0.52	0.27	-0.14	0.78
Pl4	-0.19	-0.25	-0.3	-0.29	0.04	-0.26	1.37
Pl5	-0.2	-0.25	-0.23	-0.22	-0.03	-0.26	1.30
Pl6	-0.21	-0.25	-0.16	-0.15	-0.10	-0.26	1.24
Pl7	-0.24	-0.27	-0.54	-0.53	0.26	-0.28	1.17
Pl8	-0.25	-0.35	-0.45	-0.37	0.02	-0.43	1.72
Pl9	-0.27	-0.32	-0.37	-0.39	0.07	-0.3	1.11
Pl10	-0.29	-0.31	-0.29	-0.31	00	-0.29	1.00
Pl11	-0.31	-0.35	-0.76	-0.86	0.51	-0.25	0.81
Pl12	-0.34	-0.39	-0.65	-0.67	0.28	-0.37	1.09
Pl13	-0.37	-0.46	-0.58	-0.59	0.13	-0.45	1.22
Pl14	-0.42	-0.5	-0.50	-0.51	0.01	-0.49	1.17
Pl15	-0.48	-0.59	-0.91	-0.90	0.31	-0.6	1.25
Pl16	-0.50	-0.65	-0.85	-0.75	0.10	-0.75	1.79
Pl17	-0.54	-0.61	-0.67	-0.66	0.05	-0.62	1.29
Pl18	-0.64	-0.67	-0.64	-0.63	-0.04	-0.68	1.06
Pl19	-0.68	-1.02	-1.53	-1.50	0.48	-1.05	1.54
Cp	-0.34	-0.44	-0.49	-0.48	0.04	-0.45	1.32
SD	0.16	0.20	0.41	0.42	0.34	0.23	0.67
COV	0.47	0.46	0.84	0.87	8.59	0.51	0.47

Table 4. 2 . Pressure coefficients on roof without panels vs. total resultant pressure coefficients on roof under solar panels, slope 35º, wind direction 45º, Leeward side

Polylines	Cp for roof without panels	Cp on top surface of the panels	Cp for roof under the panels	CP for bottom surface of the panels	Cp difference top – bottom surfaces of the panels	Net Cp for the system roof-panels	Ratio of net Cp on system roof-panels / roof without solar panels
Pl20	-1.50	-1.19	-1.3	-1.29	0.10	-1.2	0.80
Pl21	-1.45	-1.13	-1.09	-1.08	-0.05	-1.14	0.79
Pl22	-1.41	-1.03	-1.04	-1.04	0.01	-1.03	0.73
Pl23	-1.38	-0.99	-1.03	-1.03	0.04	-0.99	0.72
Pl24	-1.33	-0.78	-1.08	-1.08	0.30	-0.78	0.59
Pl25	-1.26	-0.71	-0.95	-0.95	0.24	-0.71	0.56
Pl26	-1.18	-0.66	-0.78	-0.78	0.12	-0.66	0.56
Pl27	-1.08	-0.63	-0.66	-0.66	0.03	-0.63	0.58
Pl28	-1.00	-0.62	-0.76	-0.57	-0.05	-0.81	0.81
Pl29	-0.92	-0.6	-0.73	-0.68	0.08	-0.65	0.71
Pl30	-0.88	-0.6	-0.64	-0.63	0.03	-0.61	0.69
Pl31	-0.85	-0.68	-0.61	-0.60	-0.08	-0.69	0.81
Pl32	-0.78	-0.69	-0.98	-0.97	0.28	-0.7	0.90
Pl33	-0.72	-0.68	-0.82	-0.82	0.14	-0.68	0.94
Pl34	-0.66	-0.68	-0.75	-0.74	0.06	-0.69	1.05
Pl35	-0.61	-0.68	-0.63	-0.62	-0.06	-0.69	1.13
Pl36	-0.58	-0.69	-0.97	-0.58	-0.11	-1.08	1.86
Pl37	-0.57	-0.71	-0.96	-0.89	0.18	-0.78	1.37
PL38	-0.56	-0.73	-0.88	-0.85	0.12	-0.76	1.36
Cp	-0.99	-0.76	-0.88	-0.83	0.07	-0.80	0.89
SD	0.33	0.18	0.19	0.21	0.12	0.19	0.34
COV	0.34	0.24	0.22	0.25	1.65	0.23	0.38

Tables 4.1 and 4.2 above, summarize the results for wind direction 45º, where average suction on the leeward, -0.99 (Table 4.2) is much higher than that on the windward side of the roof without panels, -0.34 (Table 4.1). However, for the roof with panels, the suction increased on top of the panels for the windward side to Cp=-0.44 and the resultant to Cp=-0.45 (Table 4.1). Nonetheless, the suction decreased on top of panels for the leeward side to Cp=-0.76 and the resultant to Cp=-

0.8 (Table 4.2). In this case, the resultants of pressure coefficients on both windward and leeward sides of roof with solar panels, are very close to the pressure coefficients on top surface of the panels.

Table 4. 3 . Pressure coefficients on roof without panels vs. total resultant pressure coefficients on roof under solar panels, slope 35º, wind direction 90º, windward side

Polylines	Cp for roof without panels	Cp on top surface of the panels	Cp for roof under the panels	CP for bottom surface of the panels	Cp difference top – bottom surfaces of the panels	Net Cp for the system roof-panels	Ratio of net Cp on system roof-panels / roof without solar panels
Pl1	-0.02	-0.71	0.58	0.58	-1.29	-0.71	35.50
Pl2	0.02	-0.45	0.47	0.47	-0.92	-0.45	-22.50
Pl3	0.02	-0.2	-0.24	-0.15	-0.05	-0.29	-14.50
Pl4	0.01	-0.18	-0.08	-0.07	-0.11	-0.19	-19.00
Pl5	-0.02	-0.2	-0.03	-0.02	-0.18	-0.21	10.50
Pl6	-0.04	-0.23	0	0	-0.23	-0.23	5.75
Pl7	-0.06	-0.27	-0.49	-0.47	0.20	-0.29	4.83
Pl8	-0.06	-0.3	-0.42	-0.37	0.07	-0.35	5.83
Pl9	-0.07	-0.24	-0.34	-0.30	0.06	-0.28	4.00
Pl10	-0.09	-0.32	-0.30	-0.28	-0.04	-0.34	3.78
Pl11	-0.12	-0.37	-0.79	-0.73	0.36	-0.43	3.58
Pl12	-0.16	-0.42	-0.68	-0.67	0.25	-0.43	2.69
Pl13	-0.20	-0.49	-0.54	-0.54	0.05	-0.49	2.45
Pl14	-0.25	-0.61	-0.56	-0.56	-0.05	-0.61	2.44
Pl15	-0.32	-0.75	-1.16	-1.18	0.43	-0.73	2.28
Pl16	-0.36	-1.02	-1.06	-1.08	0.06	-1.0	4.00
Pl17	-0.39	-0.86	-0.96	-0.95	0.09	-0.87	2.72
Pl18	-0.36	-1.15	-0.95	-0.91	-0.24	-1.19	3.31
Pl19	-0.39	-1.42	-2.09	-2.05	0.63	-1.46	3.74
Cp	-0.15	-0.54	-0.51	-0.49	-0.05	-0.56	3.69
SD	0.15	0.36	0.61	0.61	0.44	0.36	11.94
COV	0.99	0.67	1.20	1.25	9.16	0.64	3.24

Table 4.3 and 4.4 describe the results for wind direction 90º, where average suction on the leeward side of the roof without solar panels, Cp=-1.62, (Table 4.4) is significantly higher than that on the windward side, (Cp=-0.15) (Table 4.3). However, for the roof with panels, the suction increased considerably on the windward side, on top of the panels to Cp = -0.54 and the total Cp on roof surface to Cp = -0.56, (Table 4.3). In comparison with the roof without solar panels, the suction

decreased at the leeward side on top of panels to Cp=-0.88, while the total Cp on roof surface decreased to Cp= -0.91 (Table 4.4).

Table 4. 4 . Pressure coefficients on roof without panels vs. total resultant pressure coefficients on roof under solar panels, slope 35º, wind direction 90º, Leeward side

Polylines	Cp for roof without panels	Cp on top surface of the panels	Cp for roof under the panels	CP for bottom surface of the panels	Cp difference top – bottom surfaces of the panels	Net Cp for the system roof-panels	Ratio of net Cp on system roof-panels / roof without solar panels
Pl20	-2.60	-2.78	-2.24	-1.9	-0.88	-3.12	1.20
Pl21	-2.56	-1.61	-1.63	-1.65	0.04	-1.59	0.62
Pl22	-2.52	-1.49	-1.51	-1.53	0.04	-1.47	0.58
Pl23	-2.48	-1.13	-1.38	-1.42	0.29	-1.09	0.44
Pl24	-2.37	-1.05	-1.22	-1.24	0.19	-1.03	0.43
Pl25	-2.25	-0.92	-1.12	-1.14	0.22	-0.9	0.40
Pl26	-2.11	-0.78	-1.00	-1.02	0.24	-0.76	0.36
Pl27	-1.96	-0.68	-0.90	-0.92	0.24	-0.66	0.34
Pl28	-1.78	-0.65	-0.91	-0.86	0.21	-0.7	0.39
Pl29	-1.59	-0.6	-0.65	-0.66	0.06	-0.59	0.37
Pl30	-1.45	-0.63	-0.64	-0.64	0.01	-0.63	0.43
Pl31	-1.38	-0.61	-0.61	-0.61	0.00	-0.61	0.44
Pl32	-1.20	-0.56	-0.74	-0.74	0.18	-0.56	0.47
Pl33	-1.04	-0.53	-0.68	-0.68	0.15	-0.53	0.51
Pl34	-0.90	-0.5	-0.61	-0.61	0.11	-0.5	0.56
Pl35	-0.78	-0.5	-0.57	-0.58	0.08	-0.49	0.63
Pl36	-0.68	-0.5	-0.82	-0.45	-0.05	-0.87	1.28
Pl37	-0.60	-0.54	-0.82	-0.79	0.25	-0.57	0.95
PL38	-0.60	-0.58	-0.75	-0.73	0.15	-0.6	1.00
Cp	-1.62	-0.88	-0.99	-0.96	0.08	-0.91	0.60
SD	0.73	0.57	0.44	0.41	0.25	0.62	0.29
COV	0.45	0.65	0.44	0.43	3.13	0.68	0.48

For wind direction 0º, shown in Table 4.5, the average suction remained constant for most of the roof without panels, to Cp=-0.36 (Table 4.5), and to Cp=-0.38 for roof with solar panels on top of panels, (Table 4.5); the resultant of wind pressure coefficient on the roof with solar panels was around Cp = -0.39, (Table 4.5).

Table 4. 5 . Pressure coefficients on roof without panels vs. total resultant pressure coefficients on roof under solar panels, slope 35º, wind direction 0º

Polylines	Cp for roof without panels	Cp on top surface of the panels	Cp for roof under the panels	CP for bottom surface of the panels	Cp difference top – bottom surfaces of the panels	Net Cp for the system roof-panels	Ratio of net Cp on system roof-panels / roof without solar panels
Pl1	-0.35	-0.38	-0.41	-0.4	0.02	-0.39	1.11
Pl2	-0.35	-0.38	-0.43	-0.42	0.04	-0.39	1.11
Pl3	-0.35	-0.39	-0.49	-0.48	0.09	-0.4	1.14
Pl4	-0.36	-0.39	-0.5	-0.49	0.10	-0.4	1.11
Pl5	-0.36	-0.39	-0.5	-0.49	0.10	-0.4	1.11
Pl6	-0.36	-0.39	-0.5	-0.49	0.10	-0.4	1.11
Pl7	-0.37	-0.38	-0.48	-0.47	0.09	-0.39	1.05
Pl8	-0.37	-0.39	-0.47	-0.46	0.07	-0.4	1.08
Pl9	-0.37	-0.38	-0.47	-0.46	0.08	-0.39	1.05
Pl10	-0.37	-0.38	-0.48	-0.47	0.09	-0.39	1.05
Pl11	-0.37	-0.38	-0.52	-0.52	0.14	-0.38	1.03
Pl12	-0.36	-0.38	-0.52	-0.52	0.14	-0.38	1.06
Pl13	-0.36	-0.38	-0.52	-0.52	0.14	-0.38	1.06
Pl14	-0.36	-0.38	-0.52	-0.51	0.13	-0.39	1.08
Pl15	-0.36	-0.38	-0.46	-0.45	0.07	-0.39	1.08
Pl16	-0.35	-0.4	-0.44	-0.43	0.03	-0.41	1.17
Pl17	-0.35	-0.4	-0.43	-0.41	0.01	-0.42	1.20
Pl18	-0.35	-0.38	-0.43	-0.43	0.05	-0.38	1.09
Pl19	-0.35	-0.38	-0.43	-0.43	0.05	-0.38	1.09
Cp	-0.36	-0.38	-0.47	-0.47	0.08	-0.39	1.09
SD	0.01	0.01	0.04	0.04	0.04	0.01	0.04
COV	0.02	0.02	0.08	0.08	0.50	0.03	0.04

Similar tables for nine other cases for roof slope 35º and wind directions 45º, 90º and 0º for roof mounted solar panels arrays with 8″ S (spacing), 3″ C (clearance), 8″ S, 10″ C, and 2″ S, 10″C are reported in the Appendix C. These tables include the resultant Cp coefficients obtained by integration and averaging over the lines over the entire roof-solar panels system, on the three surfaces of roof under the panels, top and bottom of the panels. The Cp coefficients on roof without solar panels are also reported in the tables for comparison.

4.2.7. Conclusions

- Total suction on gable roofs with solar panels, increased considerably (especially for 90º wind direction) on windward side of the roof with solar from those on roofs without solar panels, except for the wind direction 0º, for which the suction hardly increased on the windward side. Nonetheless, this large increase in suction on the windward side, registered for 45º and 90º wind directions, did not increase the pressure coefficients on the windward side on the inclined 35º gable roofs with solar panels.
- In comparison with the pressure coefficients on roofs without solar panels, the total suction decreased considerably for 90º wind direction on leeward surfaces of the roof mounted solar panels, while this suction decreased moderately for wind direction 45º, and hardly decreased for wind direction 0º.
- The increase in suction on the windward side and the decrease in suction on the leeward side of the roof with solar panels, result in redistribution of wind pressure towards higher balance of wind pressure on gable roof with solar panels. In other words, resultant horizontal wind pressure on roof became smaller, and the pressure reduction was highest for wind direction 90º, and smallest for wind direction 0º; the reductions can be calculated from the Tables 4.1 to 4.5 above, for these three wind directions.

4.3. Effects of wind directions on solar panel array with 2″ spacing and 3″ roof-panels clearance installed on 27º inclined roofs

4.3.1. Pressure contour distribution for wind direction 90º

This section examines the distribution of pressure coefficient for the 27º roof slope for 90º, 45º and 0º wind directions for roofs with and without solar panels, and for 2” row spacing and 3” roof mounting clearance. The discussion on pressure coefficient contours illustrated in graphs reported herein is limited to the 90º wind direction case, since this is a critical case. Similar analysis results for the other wind directions (45º and 0º) are reported in the Appendix B.

Figure 4.51 shows the pressure coefficient contours. In general, the figure shows higher pressure coefficients on the windward side, in comparison with the case of 35º roof slope. This is demonstrated near the ridge and at the front edge, C, of the windward side of the roof.

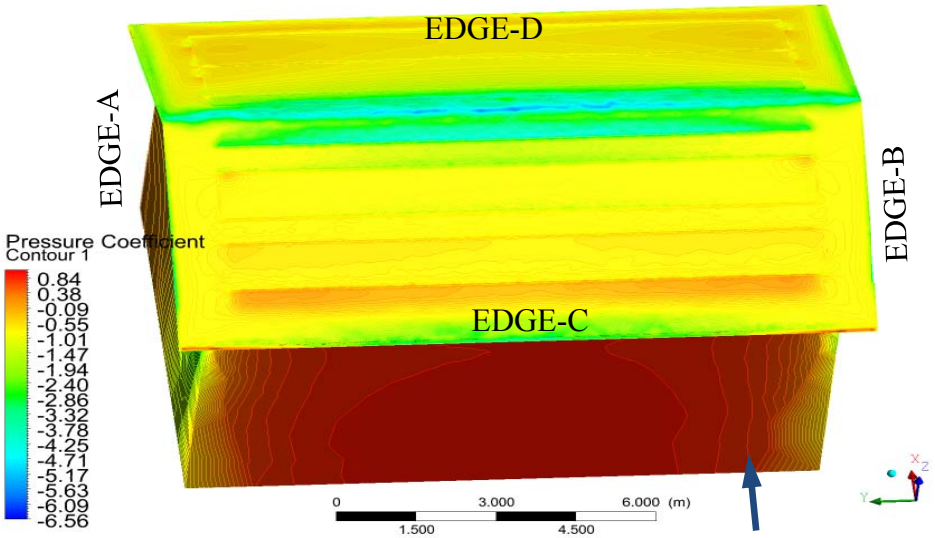


Fig. 4. 51. Pressure coefficient contours of roof with solar panels, slope 27º, windward, wind direction 90º,

Fig. 4.52, illustrates the Cp values on both sides of the 27º inclined roof along with all the polylines used for integrating the pressure coefficients along the entire roof and panels surfaces for 90º wind direction.

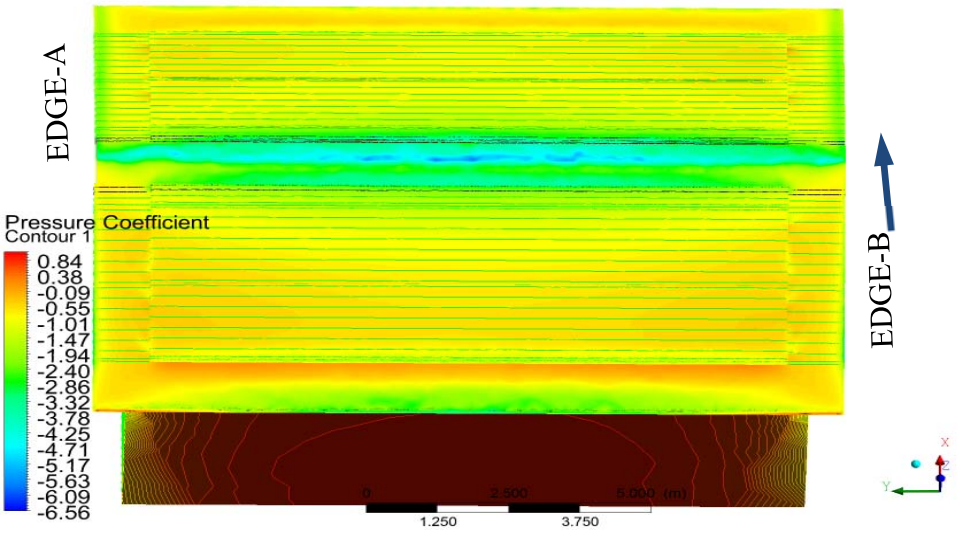


Fig. 4. 52. Pressure coefficient on top of solar panels with lines, slope 27º, windward, wind direction 90º

The following results show the pressure coefficients details on the windward side of the gable roof surface. Figs. 4.53 a) and b) show the distribution of the pressure coefficients on the bottom and top surfaces of the solar panels and on roof surface under the solar panels, respectively. The bottom surface of the solar panels is oriented such that both graphs in Fig. 4.53 have the same axes directions.

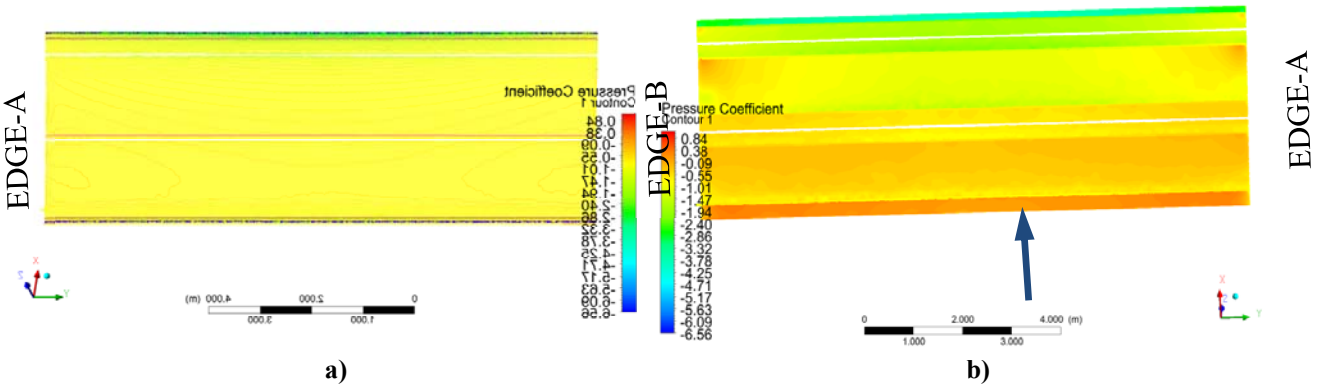


Fig. 4. 53. Pressure coefficient distribution on a) Top of the solar panels, and b) Bottom of the solar panel, for roof slope 27º and wind direction 0º

It can be observed that the distribution of pressure coefficients on the bottom surface of the panels (Fig. 4.53.b) is very similar to that on the roof under the panels (Fig. 4.54). Similarly, the pressure distribution on the bottom surface of the panels exhibit the same trends as that on the roof under the panels. However, the pressure distribution on the top surface of the panels is slightly different. The polylines used for pressure coefficient sampling are shown on both sides of the roof, where PL1, PL10 and PL19 are shown on the windward side, and PL20, PL29 and PL38 are shown on the leeward side.

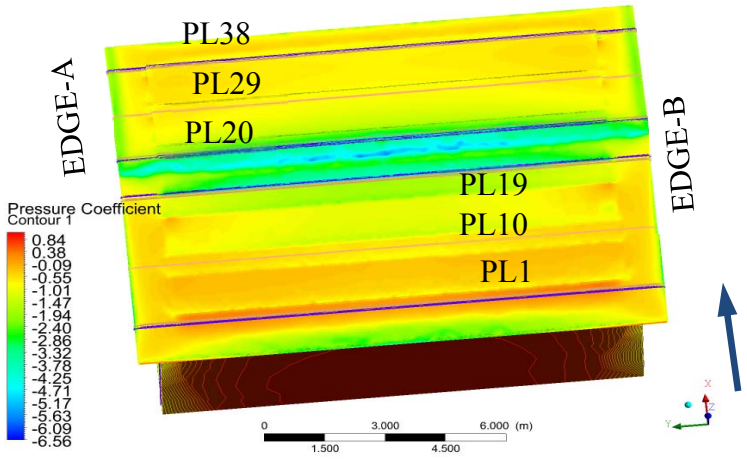


Fig. 4. 54. Pressure coefficient on roof under solar panels, slope 27º, windward, wind direction 90º

Similarly, when comparing the three graphs in Figs. 4.55 and 4.56, it can be noticed that the distribution of pressure coefficients on the bottom surface of the panels (Fig. 4.55.a) is very similar to that on the roof under the panels (Fig. 4.56). The pressure distribution on top surface of the panels (Fig. 4.55 b) is different than that on roof surface, (Fig.4.56) where pressure coefficient is slightly lower than roof under panels, in areas near the roof ridge, and near the leeward edge, D.

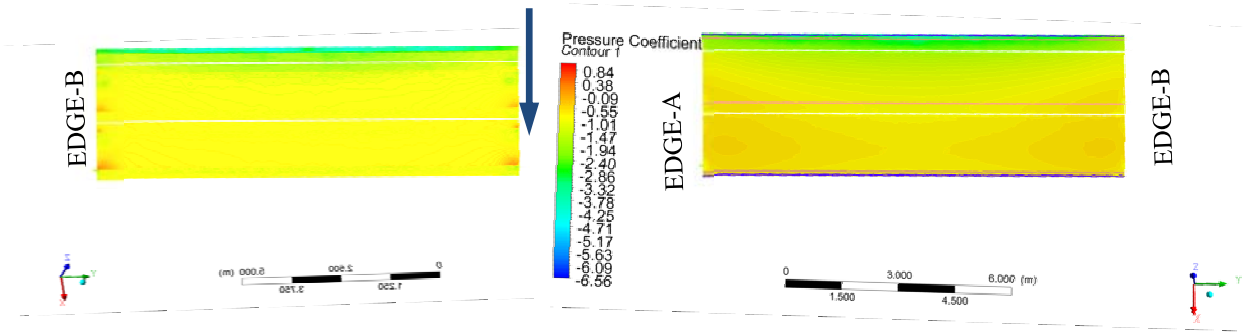


Fig. 4. 55. Pressure coefficient on (a) bottom of the panel array, and (b) top of solar panels, slope 27º, Leeward, wind direction 90º

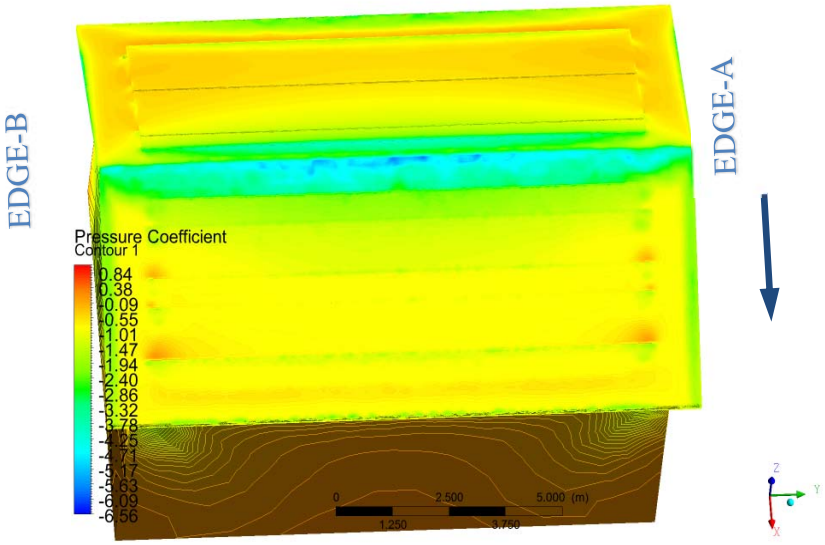


Fig. 4. 56. Pressure coefficient on roof under solar panels, slope 27º, Leeward, wind direction 90º

The overall distribution of pressure coefficients on the house, depicted in Figs. 4.55 and 4.56 reveal that the lowest pressure on the roof is located at the ridge on the leeward side. It should be noted that no panels are placed in these high suction areas. It can be observed that the leeward surface is subject to higher pressure than windward side.

4.3.2. Pressure coefficient for roof mounted solar panels and roofs with no panels, windward surface of the roof

4.3.2.1. Pressure coefficients on the roof under the solar panels vs. the roofs without solar panels

Comparisons of the wind-induced pressure coefficients on the roof surface with no panels and on the roof surface under the solar panels, for wind directions 45º, 90º and 0º, are shown in Figs. 4.57, 4.58 and 4.59, respectively. When the wind direction is 90°, the Cp coefficients along line PL1 on roof surface under the panels show positive pressure values Cp =0 to 0.3 in most of the lines, while Cp on the corresponding line on the roof surface without panels exposes suction in the range between Cp=-0.3 and -0.4. Moreover, for line PL19, Cp shows much higher suction, of CP= -1.4 to -2.7, than the corresponding line on the roof surface without panels, (CP= -0.9 to -1.25). However, suction along PL10 on the roof surface under the panels, near the middle of the array, is slightly higher (CP= -0.5 to -0.75), than the suction along line PL10 on the roof surface without panels which was Cp=-0.40. Cp on all polylines are symmetric around the middle of the roof for both roof surfaces under the panels and roof surface without solar panels (Fig. 4.57). The pressure coefficients Cp encounter a higher fluctuation on the surface of the roof, when the solar panels are installed, and for the middle line PL10 and the line near the ridge PL19, the suction on the roof surface is higher, when solar panels are installed.

In case of 45° wind direction (Fig. 4.58), it is shown that the pressure coefficients have similar general trends for the roof surface with and without solar panels. However, for line PL1 located near the windward edge, C, of the solar array (Fig.4.52), the pressure coefficients are much higher in the range of (CP= 0.50 to -1.0) than the coefficients on the corresponding line on the roof with no panels, which are (CP= 0 to -0.75). PL19, located nearest to the ridge (Fig.4.52), shows much higher pressure coefficients of (CP= -1.5 to -3.0) than the coefficients on the corresponding line on the roof with no panels, which are nearly constant at about (CP= -1.0). On the contrary, the middle line PL 10 shows slightly higher pressure coefficients, (CP= -0.25 to -1.2), than the corresponding line on the roof without panels, (CP= -0.25 to -0.75). In addition, pressure coefficients along PL1 and PL10 on both surfaces increase towards the leeward edge B of the roof. For the middle line PL10, the pressure coefficients are consistent for the roof surface with or without solar panels, however for the lines PL1 and PL19, larger discrepancies were noticed, when

the solar panels are placed on the roof surface. The Cp coefficients on line PL19 registered higher fluctuating negative values for the roof surface when the solar panels are installed. For wind direction 0º, the pressure coefficients along PL1 and PL19 on roof surface under the panels are slightly different from those on the roof without panels. However, the pressure coefficients along PL10 on the roof under the panels are moderately higher than those obtained on roof surface without panels, by nearly 0.04 (Fig. 4.59). Cp along all three lines reduced significantly from (CP= -0.25), in the middle of the array to (CP= -0.75 to -1.30) on the windward edge A, and to (CP= -0.50 to -0.85) on the leeward edge B, while it remained nearly constant in the middle parts of these lines. On the PL19 line, periodic drops in pressure coefficient are observed where the connections between panel rails and roof are located. For the 0º wind direction, the gap height does not seem to have a noticeable impact on the evolution of the pressure coefficients for the three monitored lines.

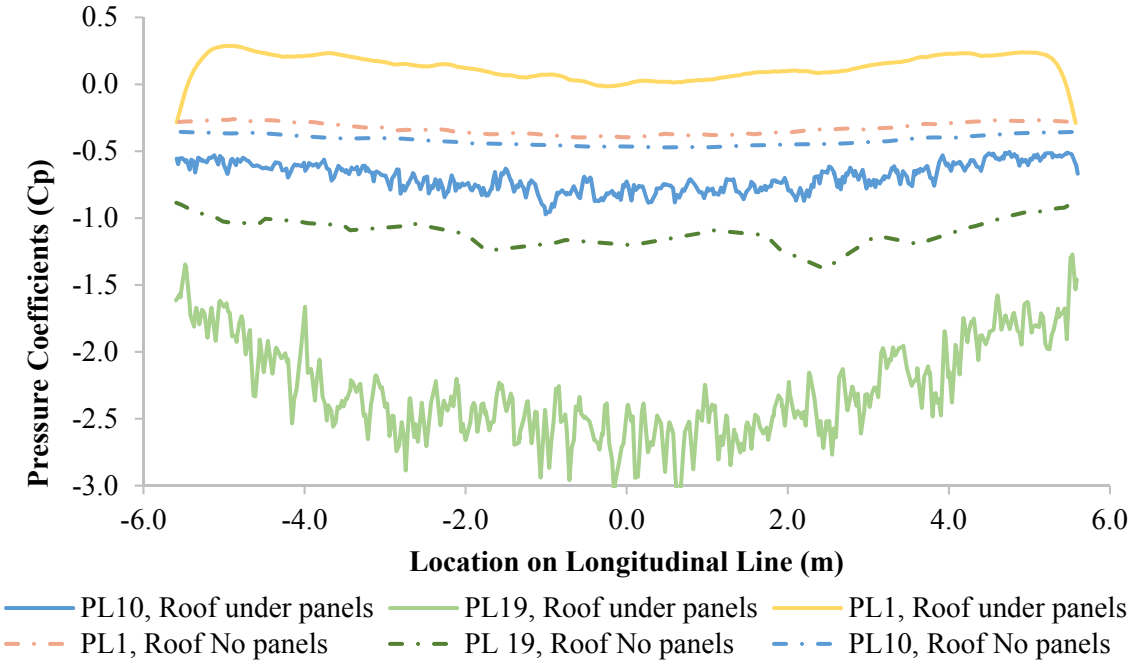


Fig. 4. 57. Pressure coefficient distribution on the roof surface under the solar panels and on the roof surface without mounted solar panels, for roof slope 27º, and wind direction 90º, windward side

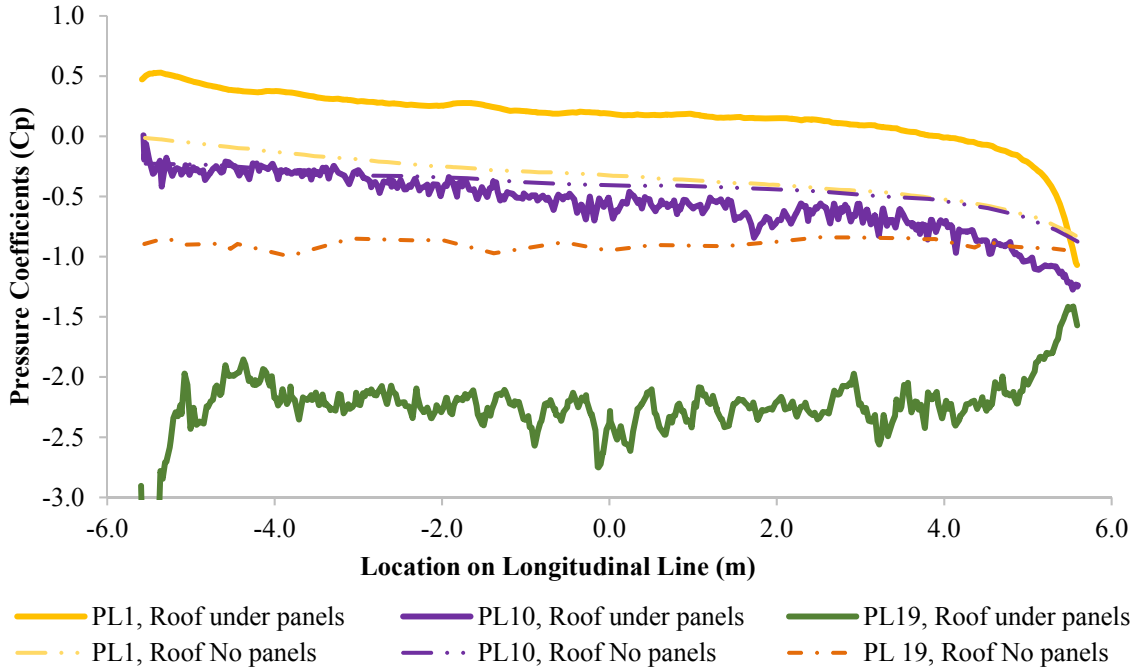


Fig. 4. 58. Pressure coefficient distribution on the roof surface under the solar panels and on the roof surface without mounted solar panels, for roof slope 27º, and wind direction 45º, windward side

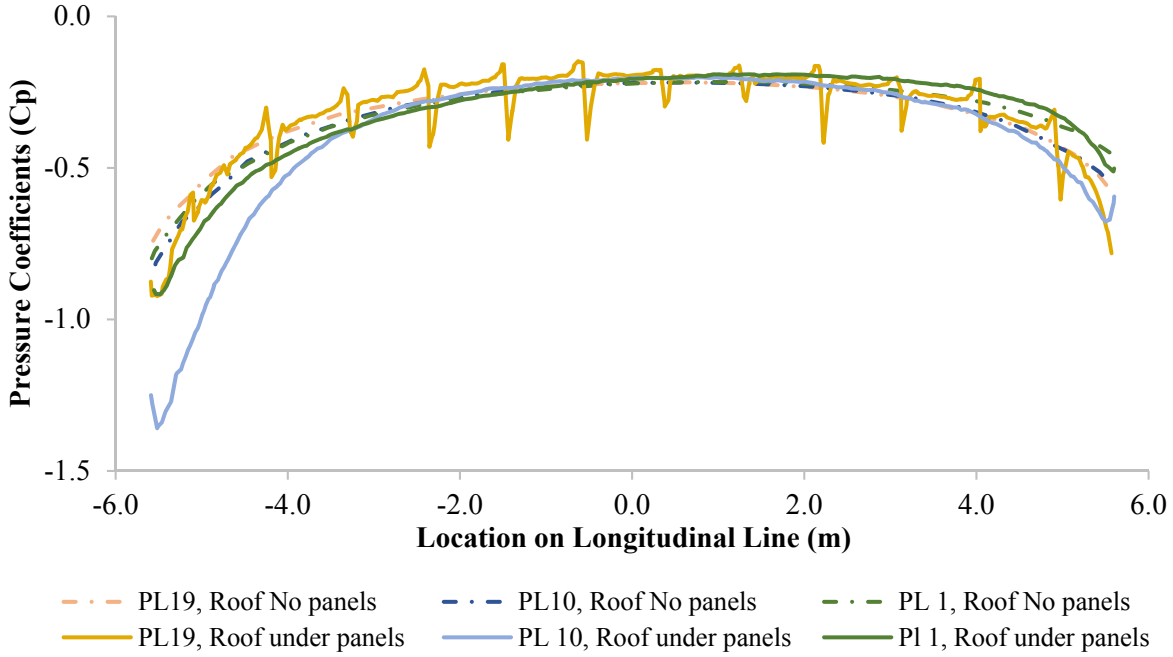


Fig. 4. 59. Pressure coefficient distribution on the roof surface under the solar panels and on the roof surface without mounted solar panels, for roof slope 27º, and wind direction 0º

4.3.2.2. Pressure coefficients on bottom surface of the solar panels vs. roof surface under solar panels

The results of wind pressure coefficients obtained on the bottom surface of the solar panels and on the roof surface under the solar panels, for wind directions 90º, 45º and 0º are presented in Figs. 4.60, 4.61 and 4.62, respectively. From Figs 4.60 and 4.61, it can be observed that for most of the panel area, the difference between Cp on bottom surface of the panels, and on the roof surface under the panels, is very small, in the range of 0 to 0.25. For wind direction 90°, the Cp coefficient along the line PL1 on the roof surface under the panels seems to be very similar to the Cp on the bottom surface of the panels throughout the length of the lines. However, Cp along the PL10 line reveals slight differences in the range of Cp = 0 to 0.10. The Cp value decreased sharply from Cp=0.25 to -0.3 on PL1 near the A and B edges of the windward surface of the array. The pressure coefficient on line PL19 show moderate differences between the roof surface under the panels and that on the bottom surface of the panel. The further the location from the windward edge of the panel array is, the larger the difference between Cp on roof surface and on the bottom surface of the panels becomes.

For the case of 45° wind direction, the Cp along the two lines, PL1 and PL19 on the roof under the panels and on the bottom surface of the panels, demonstrates very high similarity throughout the entire length of the lines. Different from the case of wind direction 90º, the pressure coefficients on both PL1 and PL10 decrease moderately, from Cp=0.5 to -1.25 towards the leeward edge B of the panels. Cp remained constant on PL19 at Cp=-2.25 for most of the line length, and it increased sharply to Cp= -1.2 near the leeward edge B and decreased steeply to Cp= -3.0 near the windward edge A of the roof (Fig. 4.61). Cp on PL10 presents values of Cp= 0.5 to -1.2 on the roof under the panels and is thus slightly higher than the Cp values along the PL10 line on the bottom surface of panels, which are in the range of Cp= 0.5 to -1.05. It can be observed that Cp along PL 19 and PL10, in both wind directions 45º and 90º, fluctuate along the lines, which can be attributed to the transversal vortex cores created adjacent to one of the railings near the roof surface. That barrier imposed by the railings does not exist on PL1, which results in a smoother Cp graph; also, higher Cp fluctuation is observed on PL 19 near the edge.

For wind direction 0º, the pressure coefficients along PL1 and PL19 lines, on both roof surfaces under the panels and on the bottom surface of the panels, are very similar. However, Cp along PL10 on the roof surface under the panels is in the range of CP= -0.25 to -1.30 and is slightly lower

than Cp on bottom surface of the panels. The largest differences between the Cp on PL10 on the two surfaces are located along the first 3 m of the array on the windward side. Cp along all the three lines increased steadily from Cp= -0.25 in the middle of the array to Cp= -1.3 on the windward side, and to Cp=-0.9 on the leeward side, while it remained nearly constant in the middle parts of these lines. On the other hand, for 0º wind direction, sudden drops in the Cp values were noticed on PL 19, which are attributed to the locations of the standoffs, or vertical supports of the rails (Fig. 4.62).

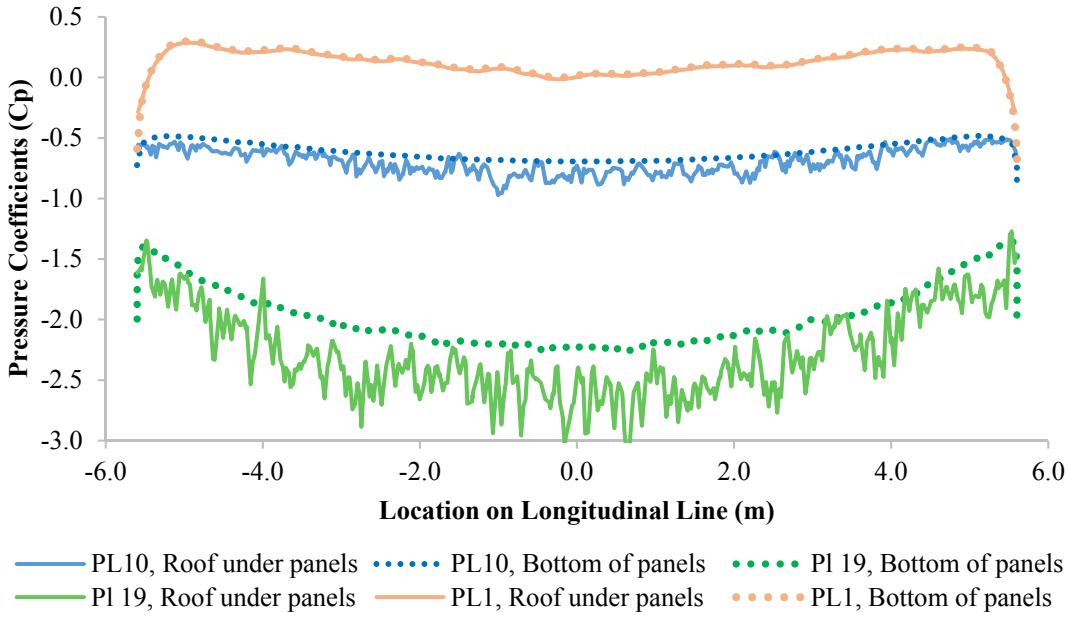


Fig. 4. 60. Pressure coefficient distribution on the bottom surface of the solar panels and on the roof surface under the panels, for roof slope 27º, and wind direction 90º, windward side

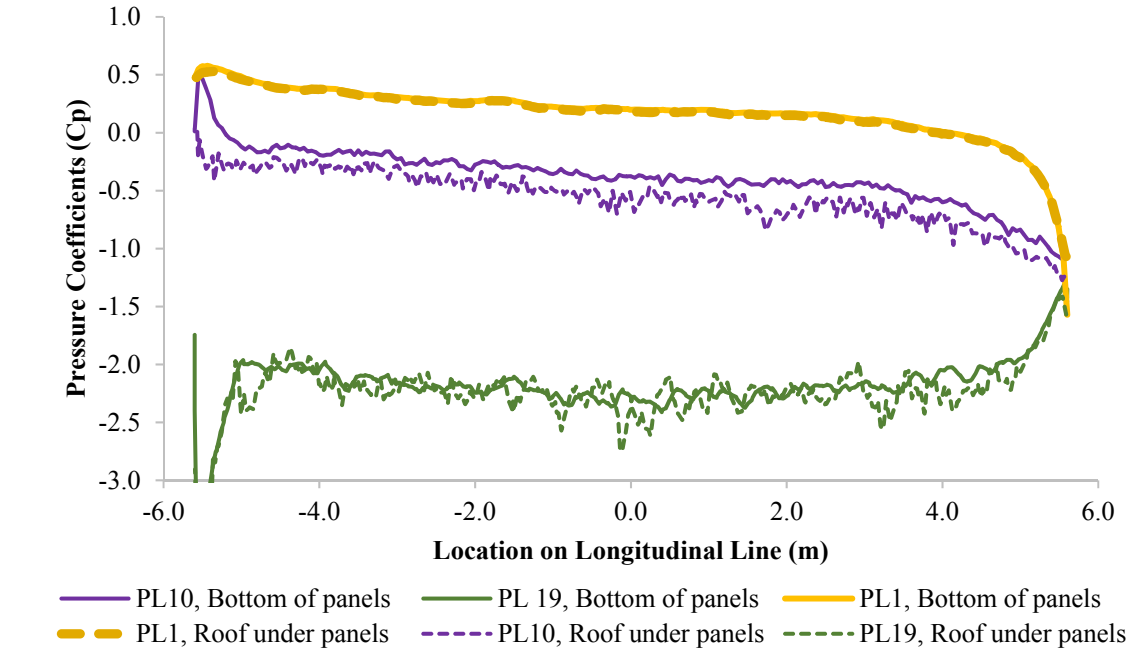


Fig. 4. 61. Pressure coefficient distribution on the bottom surface of the solar panels and on the roof surface under the panels, for roof slope 27º, and wind direction 45º, windward side

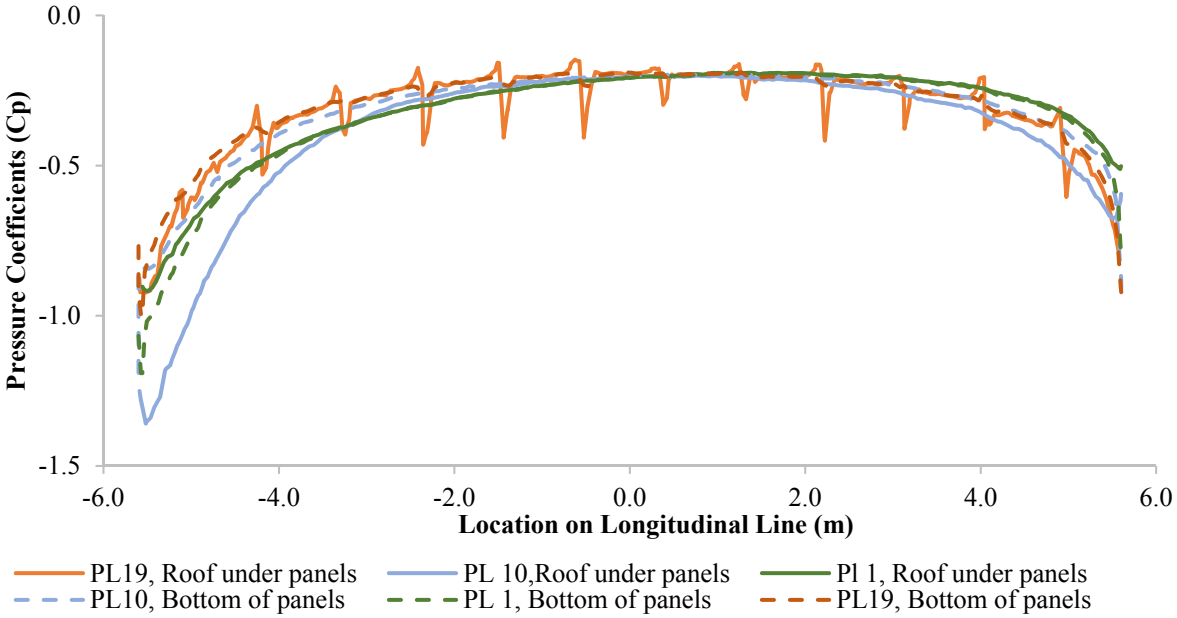


Fig. 4. 62. Pressure coefficient distribution on the bottom surface of the solar panels and on the roof surface under the panels, for roof slope 27º, and wind direction 0º,

4.3.2.3. Pressure coefficients on roof surface without solar panels vs. pressure coefficients on top of the panels

Detailed comparisons of the wind-induced pressure coefficients on the roof surface with no panels installed and on the top surface of the solar panels, for wind direction 45º, 90º and 0º, are shown in Figs. 4.63, 4.64 and 4.65, respectively.

In the case of 90° wind direction, Cp along the line PL1 on the top surface of the panels, shows pressure coefficients of Cp=-0.7 to -1.25, which are much higher than the Cp on corresponding line on roof without panels, of Cp=-0.3. Similarly, for line PL19 on top of the panels, the pressure coefficients show suction of Cp=-0.7 to -2.0, which is higher than the corresponding line on the roof without panels, Cp=-0.85 to -1.25. The pressure coefficients on line PL10 on top surface of the panels, near the middle of the array are in the range of Cp=-0.5 to -0.70, which are moderately higher than the pressure coefficients along PL10 on the roof without panels, Cp=-0.40, (Fig. 4.63). For the case of 45° wind direction (Fig. 4.64) it was noticed that pressure coefficients have similar trends for the top of the panels surface and roof surface without solar panels, especially for the middle line PL10. For line PL1 located near the windward edge of the top surface of the solar array (Fig.4.52), the pressure coefficients are much higher with values of Cp=0.30 to -1.5 than the

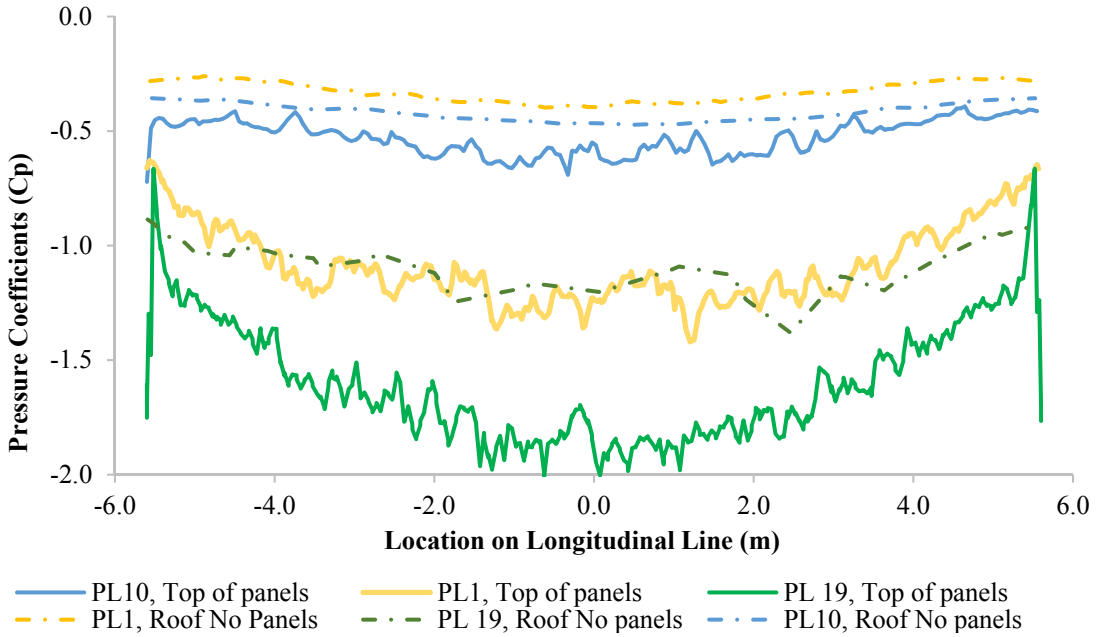


Fig. 4. 63. Pressure coefficient distribution on top surface of the solar panels and on the roof surface without mounted solar panels, for roof slope 27º, and wind direction 90º, windward side

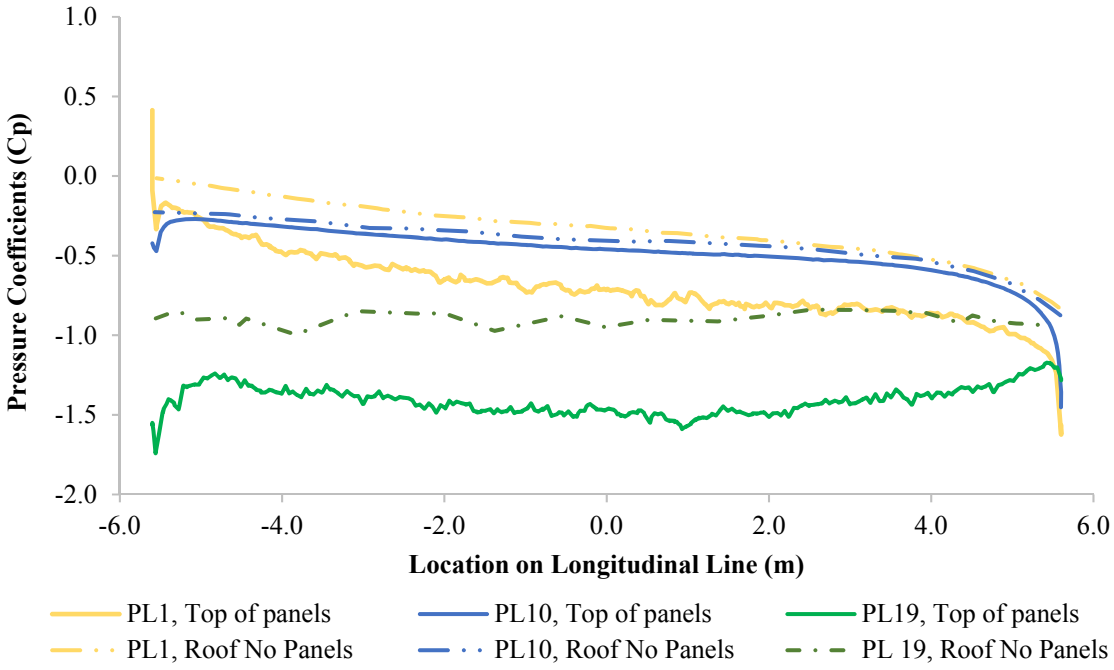


Fig. 4. 64. Pressure coefficient distribution on top surface of the solar panels and on the roof surface without mounted solar panels, for roof slope 27º, and wind direction 45º, windward side

coefficients on the corresponding line on the roof with no panels, Cp=0 to -0.75. Similarly, for PL19 located nearest to the ridge of the top surface of the panels (Fig.4.52), the pressure coefficients are much higher, Cp=-1.3 to -1.7 than corresponding line on the roof with no panels, which is nearly constant about Cp=-1.0. The Cp registered on the middle line, PL 10 on top surface of the panels, is slightly higher along the entire length of the line, (Cp=-0.3 to -1.5), than the corresponding line on the roof without panels, (Cp=-0.25 to -0.75), except near the leeward edge of the top surface of the solar panels. The pressure coefficients along PL1 and PL10 lines, decreased towards the leeward edge of the roof, for both surfaces, while the Cp on the PL19 line was relatively constant.

For wind direction 0º, the pressure coefficients along PL1 and PL10 on the top surface of the panels are slightly different than those on the roof without panels (Fig. 4.65); Cp on top surface of the panels, along the line PL19 was slightly lower, by 0.04, than the corresponding Cp on the roof surface without panels. Wind flows parallel to the roof and to the panels' surfaces, create less turbulence, smaller wind – structure interaction and therefore smaller suctions were registered for 0º wind direction than for the 45º and 90º wind directions.

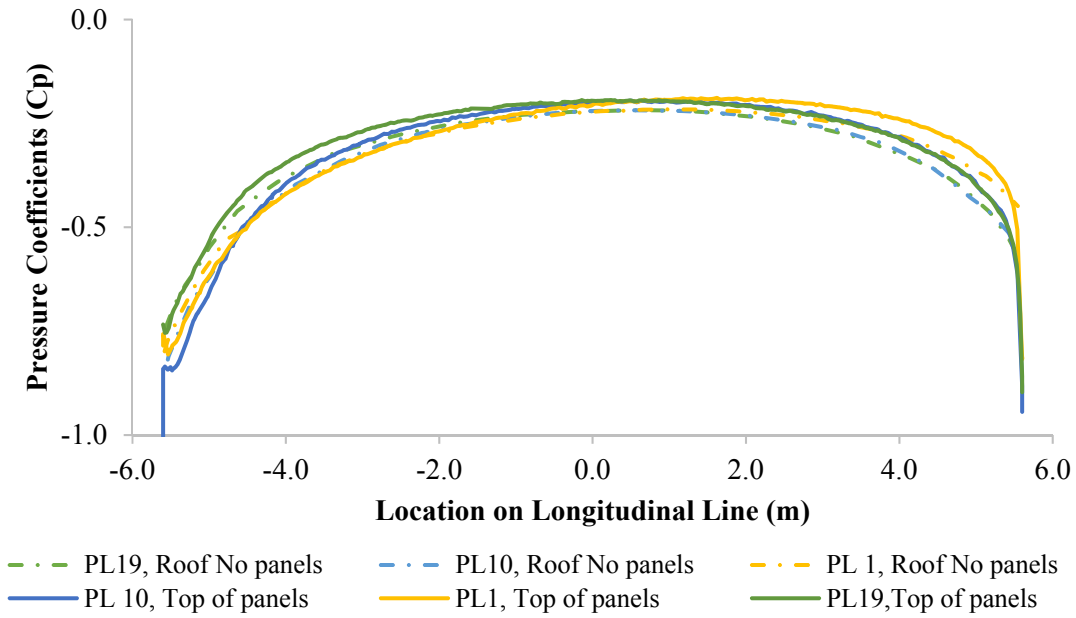


Fig. 4. 65. Pressure coefficient distribution on top surface of the solar panels and on the roof surface without mounted solar panels, for roof slope 27º, and wind direction 0º

Estimation of total pressure coefficients on the roof surface under the panels is obtained by integrations of the pressure coefficients along all 19 polylines created on the windward side of the roof, from PL 1 to PL19, for both cases of roof with solar panels and roofs without solar panels, as presented in section 4.3.6.

4.3.3. Pressure coefficients for roof mounted solar panels and roofs without panels, leeward side of the roof

In the current section, the pressure coefficients on the three surfaces on the leeward side of the roof, were considered. The values of pressure coefficients corresponding to the top and bottom surfaces of the panels and to the roof surface under the panels, are represented graphically.

Leeward side of the roof is the surface where highest section is developed for the roof without solar panels, and as such it is important to investigate the changes in the pressure coefficients on the leeward side of the roof with solar panels installed.

4.3.3.1.Pressure coefficients on the roof under solar panels vs. roofs without solar panels

Comparisons between wind-induced pressure coefficients along the three main polylines on the roof surface with no panels and on the roof surface under the solar panels, for wind directions 45º, 90º and 0º, are shown in Figs. 4.66, 4.67 and 4.68 respectively.

The first wind direction to be investigated is 90°, which is perpendicular to the ridge, where Cp along PL29 line on roof surface under panels shows much higher pressure coefficients by nearly Cp=0.6 than the Cp on the corresponding line on the roof without panels, which recorded values of Cp=-0.9 to -1.75. However, Cp on the line PL38 on roof surface shows higher suction, (Cp=-1.0 to -1.1), than the Cp on the corresponding line on roof without panels, (Cp=-0.6 to -0.75). On the other hand, pressure coefficients on PL20 near the ridge, on roof under panels, are moderately higher in the middle 6m of the line, than the pressure coefficients along PL20 on the roof without panels. However, Cp near the edges of the PL20 on roof under the panels, became higher at 2.5 m from either edges A or B of the solar panels array. Moreover, adding the solar panels on the surface of the roof brings the pressure coefficients to more consistent values for the lines PL29 and PL38, when compared with the roof surface without solar panels. Whilst, for the first line near the ridge, PL20, the influence of the transversal vortex incoming from the windward side of the roof, resulted in fluctuating pressure coefficients for the roof surface under the solar panels, as it can be noticed in Fig. 4.66.

When analyzing the other case of 45° wind direction (Fig. 4.67) it was noticed that the pressure coefficients registered on the leeward side of the roof, have similar trends, for the roof surface with solar panels installed and roof without solar panels. However, for Cp on line PL20 located near the windward edge of the solar array, on roof under panels (Fig. 6), pressure coefficients are much higher by up to 0.6 than the Cp on the corresponding line on the roof with no panels which range from Cp=-1.3 to -1.6. Nonetheless, Cp on PL38 line located near the D edge of the leeward array, on roof under panels, (Fig. 4.52), are higher reaching values up to 0.40, than the Cp on the corresponding line on the roof with no panels. On contrary, Cp on the middle line PL 29, on the roof under panels, started at Cp=-2.5 at the windward side, which is higher by about 0.6 than the Cp on the corresponding line on the roof without panels, until midpoint of the array, and it becomes higher afterwards by nearly 0.1, until the end of the array. All Cp coefficients along the lines PL29 and PL38 on both surfaces increase towards the leeward edge D of the roof, starting at much higher

pressure coefficient at the windward side. The region near the ridge of the roof is affected by the transversal vortex formation, thus only for the line PL20 a more accentuated fluctuation of Cp coefficients was noticed for the case of the roof with solar panels.

As the flow and the geometry of the structure are symmetric for wind direction 0º, Cp is the same on both sides of the gable roof surfaces. Consequently, the graphs and description are as presented in Fig. 4.59 and section 4.3.2.1 above.

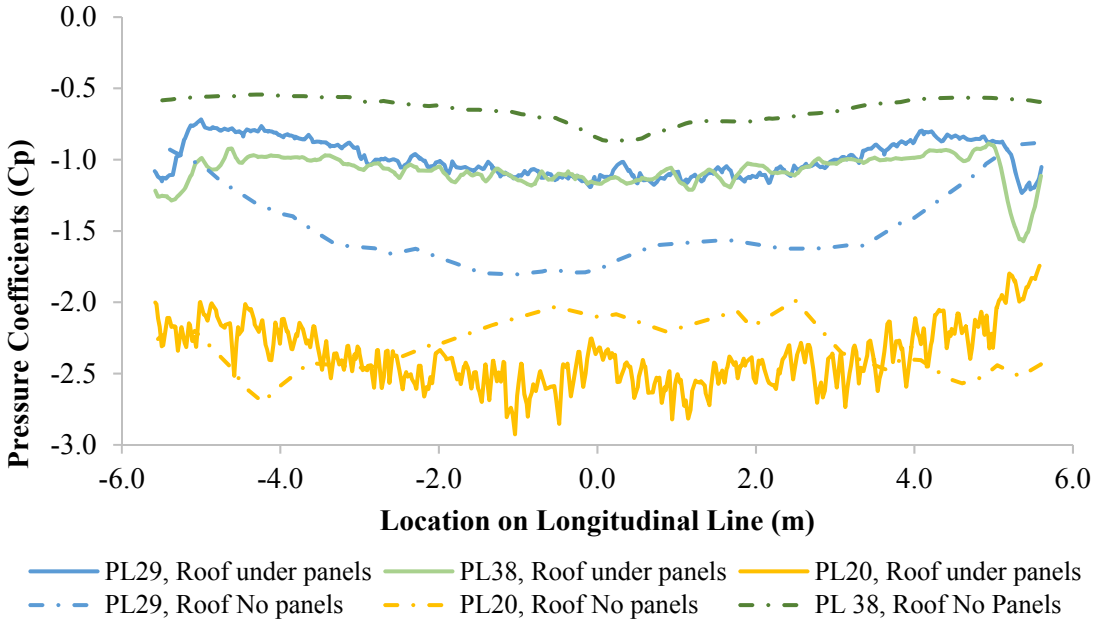


Fig. 4. 66. Pressure coefficient distribution on roof surface under the solar panels and on the roof without mounted solar panels, for roof slope 27º, and wind direction 90º, leeward side

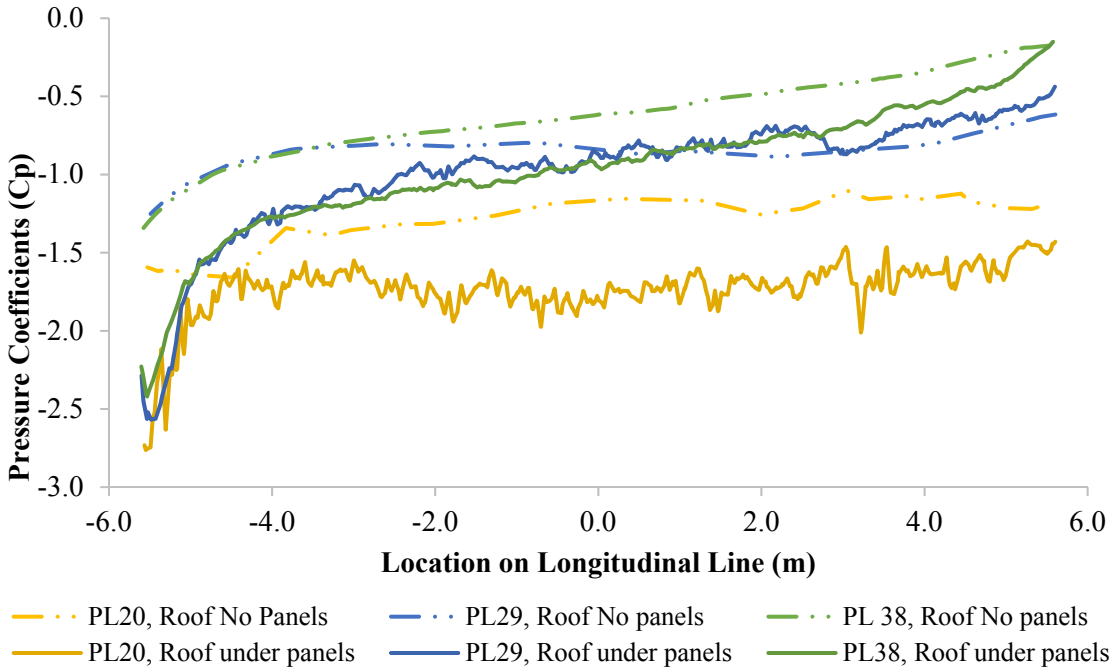


Fig. 4. 67. Pressure coefficient distribution on roof surface under the solar panels and on the roof without mounted solar panels, for roof slope 27º, and wind direction 45º, leeward side

4.3.3.2. Pressure coefficient on bottom surface of the solar panels vs. roof surface under solar panels

Figures. 4.68, 4.69 and 4.62 illustrate the wind pressure coefficients obtained on the bottom surface of the solar panels and on the roof surface under the solar panels, located at the leeward surface of the roof, when wind flows at 90º, 45º and 0º angles with ridge, respectively.

From Fig.4.68, which represents the pressure coefficients for wind direction 90°, it can be observed that the pressure coefficients along the three lines PL38 and PL29, and PL20 on roof under panels and on the bottom surface of the panels, depict similar Cp trends and values, throughout the length of the lines. Cp along the three lines on the roof under panels are moderately higher than Cp along those three lines on the bottom surface of the panels. The Cp coefficients on the two surfaces show moderate differences, where Cp along the three lines on roof under panels are higher by up to 0.25 compared to Cp along the corresponding lines on the bottom of the panels. The pressure coefficients on PL38 changes slightly, from Cp=-1.0 to -1.15, for most of the length while decreased sharply to Cp=-1.25 and -1.50 near the edge A and edge B of the leeward surface of the array. Pressure coefficients decreased moderately along PL20 in the middle of the panel array to Cp= -2.5 reaching lower suction, (Cp=-2.0), at the edges of the solar array (Fig. 4.68).

For wind direction of 45°, the Cp along all the three lines PL20, PL29 and PL38 on the roof surface under the panels and on the bottom of the panels, demonstrates high similarity throughout the entire length of the lines. The differences between Cp on each couple of corresponding lines are nearly zero. Different from symmetric Cp graphs registered for the wind direction 90º, the pressure coefficients on both PL29 and PL38 increased moderately for most of the lines length and sharply near the windward edge, A, of the array, from Cp=-0.50 to -0.20) at the leeward edge B, to (Cp=-3.0) at the windward edge A of the lines PL29 and PL38 respectively. However, Cp remained nearly constant on line PL20 at Cp=-1.5 to -1.75, (Fig. 4.69).

Because of the symmetry of the flow and the structure for wind direction 0º, Cp is the same on both sides of the gable roof surfaces. Consequently, the graphs are as presented in Fig. 4.62 in section 4.3.2.1.

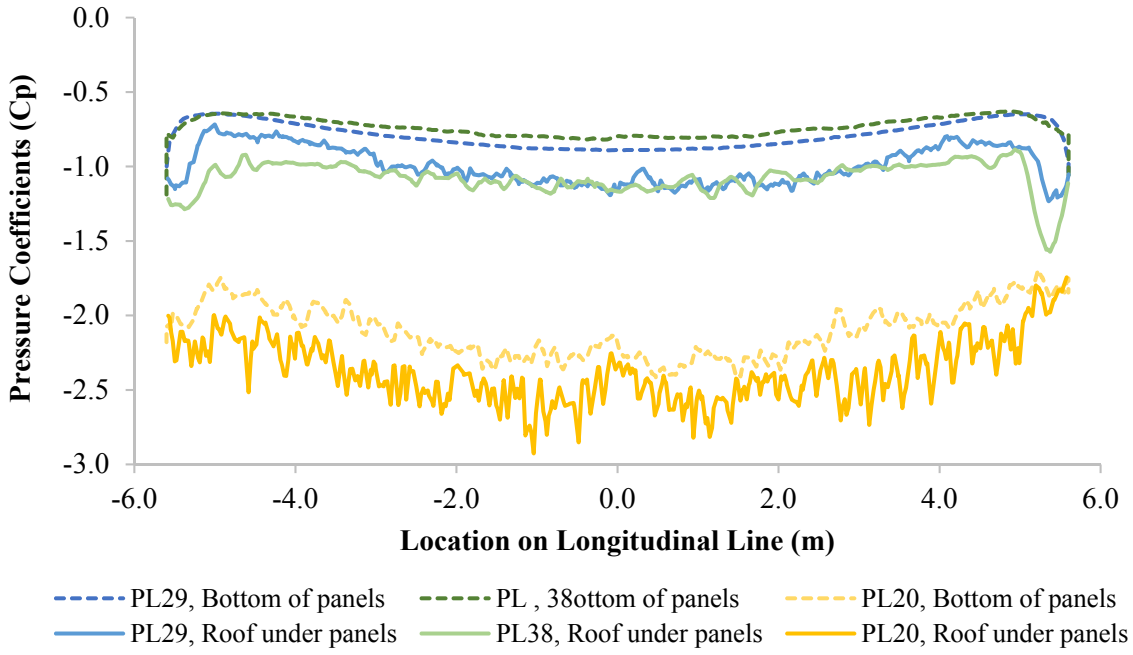


Fig. 4. 68. Pressure coefficient distribution on bottom surface of the solar panels and on the roof under solar panels, for roof slope 27º, and wind direction 90º, leeward side

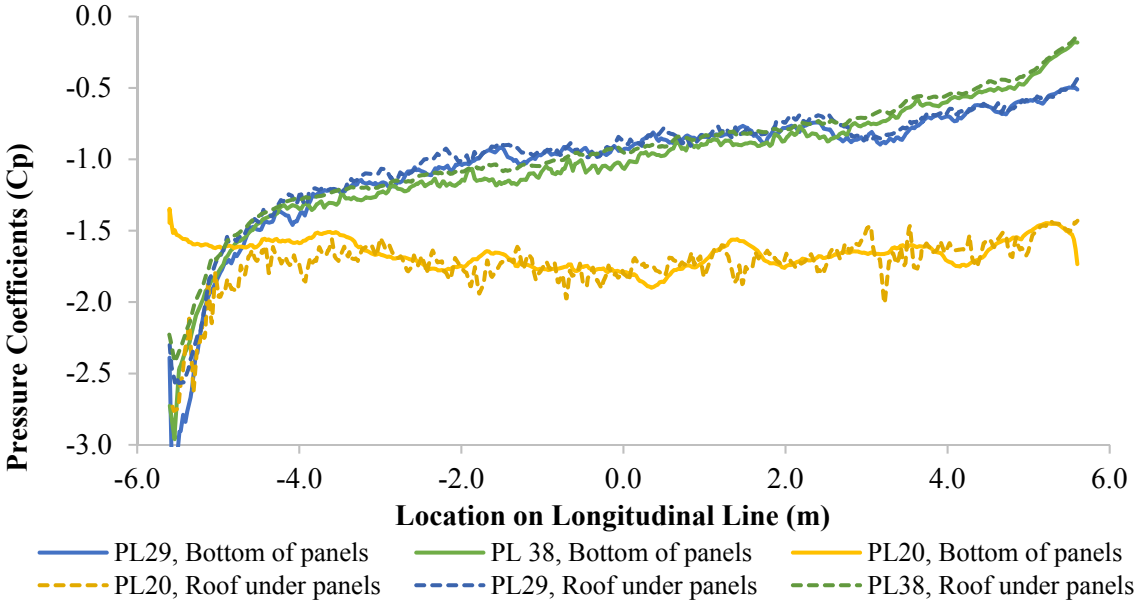


Fig. 4. 69. Pressure coefficient distribution on bottom surface of the solar panels and on the roof under solar panels, for roof slope 27º, and wind direction 45º, leeward side

4.3.3.3. Pressure coefficients roof without solar panels vs. pressure coefficient on top of panels

The pressure coefficients obtained for top surface of the solar panels and on the roof without solar panels, are provided hereafter to elucidate the effect of the roof-panels system on the wind-induced pressure. Perspicuous comparisons of the wind-induced pressure coefficients on the bottom surface of the panels, with the coefficients on the roof without panels, are shown in Figs. 4.70, 4.71 and 4.65 for wind direction 90º, 45º, and 0º, respectively.

To start with 90° wind direction, which blows perpendicular to the ridge, the Cp coefficient along the line PL38 located on top surface of the panels near leeward edge D, shows pressure coefficients of Cp=-1.0 to -1.5, which are moderately higher than the Cp on the corresponding line on the roof without panels, (Cp=-0.6 to -0.75). Similarly, PL20, which is near the ridge on top surface of the panels, shows much higher suction, (Cp=-2.0 to -3.25), than the corresponding line on the roof without panels, (Cp=-2.0 to -2.70). However, pressure coefficients on the middle of the array, on the line PL29 for the top surface of the panels, , (Cp=-0.7 to -1.2), are moderately higher, than the pressure coefficients on the roof without panels, (Cp=-0.90 to -1.65), for the same line. On the

other hand, Cp for all the investigated lines are symmetric around the middle of the roof, for both top surface of the panels and for the roof surface without solar panels, Fig. 4.70.

When discussing the case of 45° wind direction (Fig. 4.71) it was noticed that the pressure coefficients have very similar trends for the top surface of the panels and roof surface without solar panels. However, for line PL20 located near the ridge, (Fig. 6) the pressure coefficients on the top surface of the solar array are (Cp=-1.6 to -2.0) which are much higher, than Cp on the corresponding line on the roof with no panels, (Cp=-1.2 to -1.70).

Pressure coefficients, Cp on the middle line PL 29 on top surface of the panels, (Cp=-0.65 to -1.5) are moderately higher than the Cp on the corresponding line on the roof without panels, (Cp=-0.70 to -1.35). The pressure coefficients along PL29 and PL38 on both surfaces decreased towards the windward edge of the roof, while Cp on PL20 on both surfaces is relatively constant.

Pressure coefficients for wind direction 0º, on both surfaces of the roof, the top surface of the panels and on the roof without panels, are the same, therefore the graphs in Fig. 4.71 and the discussions from section 4.3.2.4 apply to this section as well.

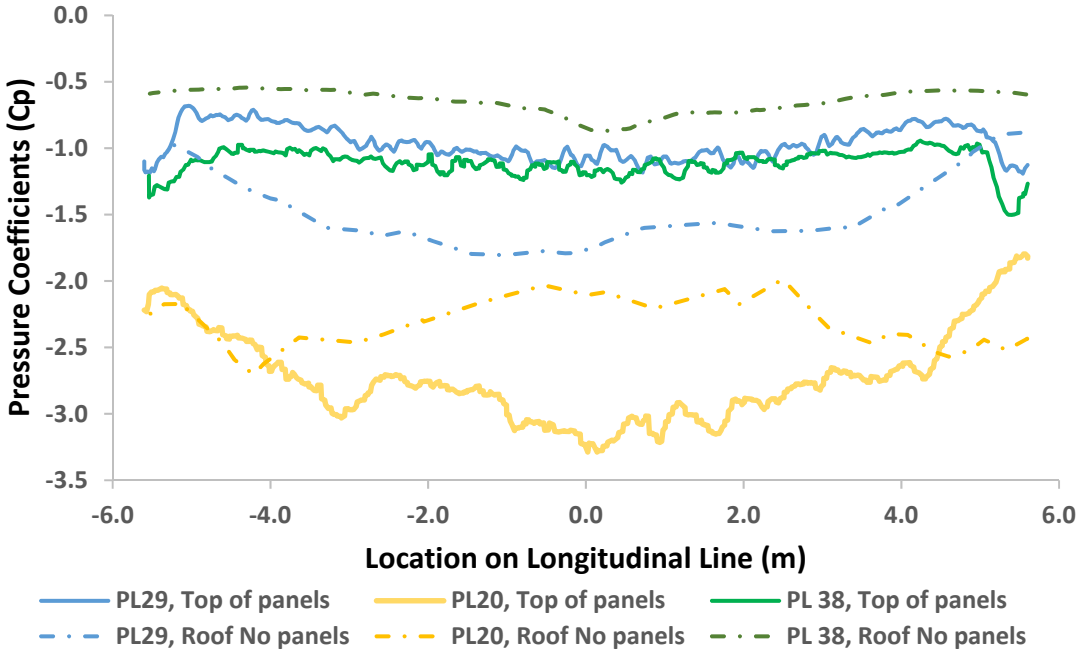


Fig. 4. 70. Pressure coefficient distribution on top surface of the solar panels and on the roof without mounted solar panels, for roof slope 27º, and wind direction 90º, leeward side

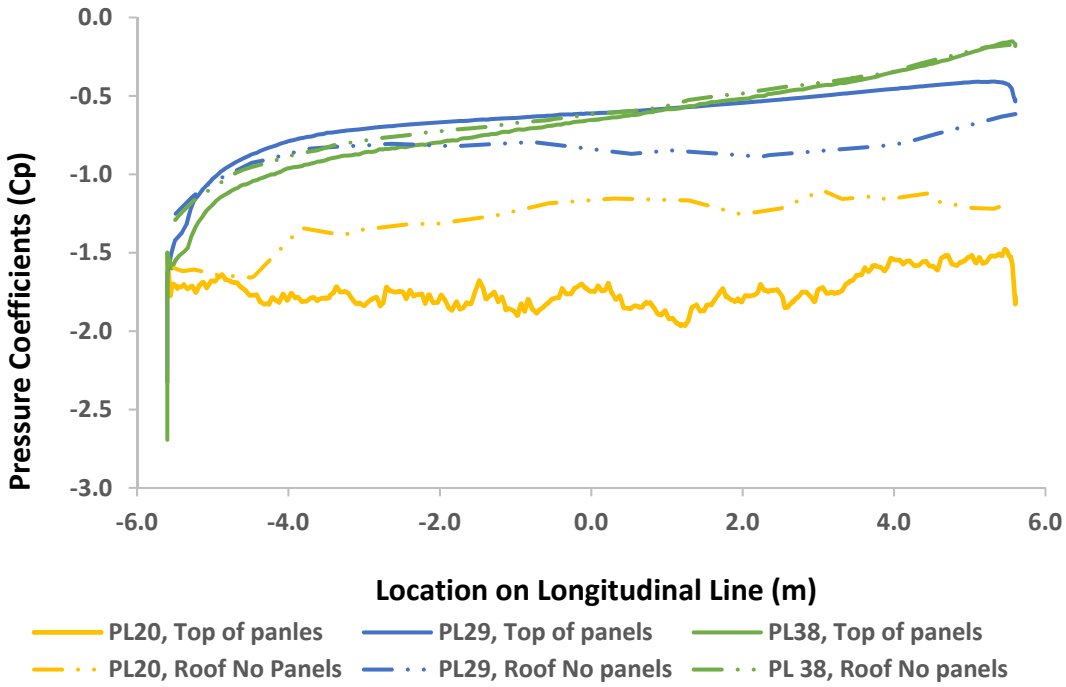


Fig. 4. 71. Pressure coefficient distribution on top surface of the solar panels and on the roof without mounted solar panels, for roof slope 27º, and wind direction 45º, leeward side

4.3.3.4. Wind flow characteristics for gable roofs with solar solar panels for wind direction 90º

Figure 4.72 illustrates the pressure coefficients distribution under the solar panels, where lowest value was registered as (Cp=-0.02), and it increased until (Cp= – 2.76). Lower pressure coefficients up to (Cp=0.23) are observed where the incoming wind flow encounters the rail of the solar panels. Figure 4.73 presents the pressure coefficients on the roof surface under the panels, and longitudinal plane parallel to the ridge of the roof. Comparison between Cp on the roof surface under the panels in Fig. 4.77 and Cp on the bottom surface of the panels, Fig.4.73, reveals that both change from (Cp=0.38 to -3.64) with similar distributions of Cp along the corresponding areas.

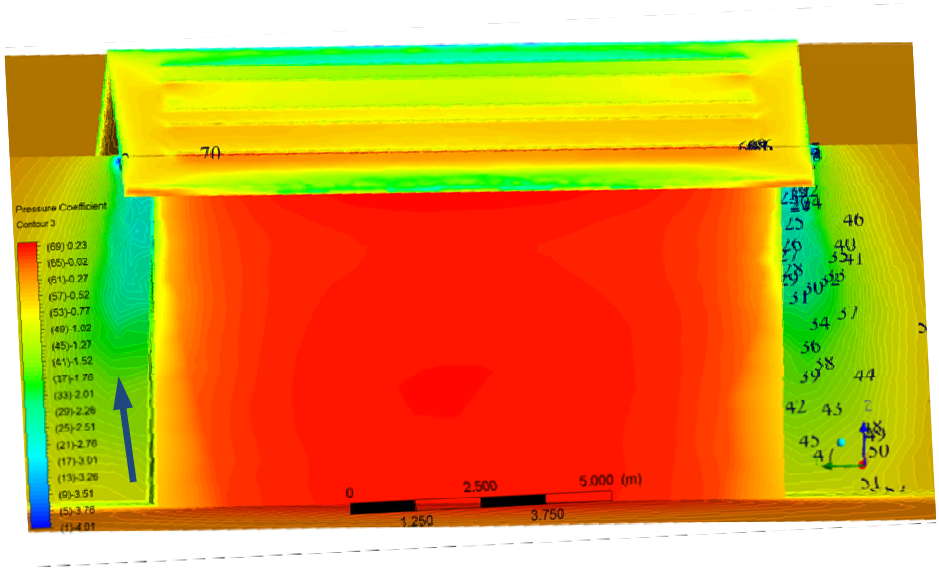


Fig. 4. 72. Pressure coefficient on a perpendicular Longitudinal plane, roof under panels, wind direction 90º, windward, slope 27º

Figure 4.72 shows high suction coefficients regions near the roof overhangs, after which the Cp increased gradually towards the ground and away from the side walls.

Figure 4.73 shows pressure coefficients contours on the bottom surface of the solar panels located on the leeward side of the roof, and part of vertical plane in the space under the panels. On the bottom of the panels, and on the vertical plane, the pressure coefficients varied from slightly positive (Cp=0.38) at the end of the leeward side of the panel array, to very high negative (Cp=-3.64) at the end of the array near the ridge.

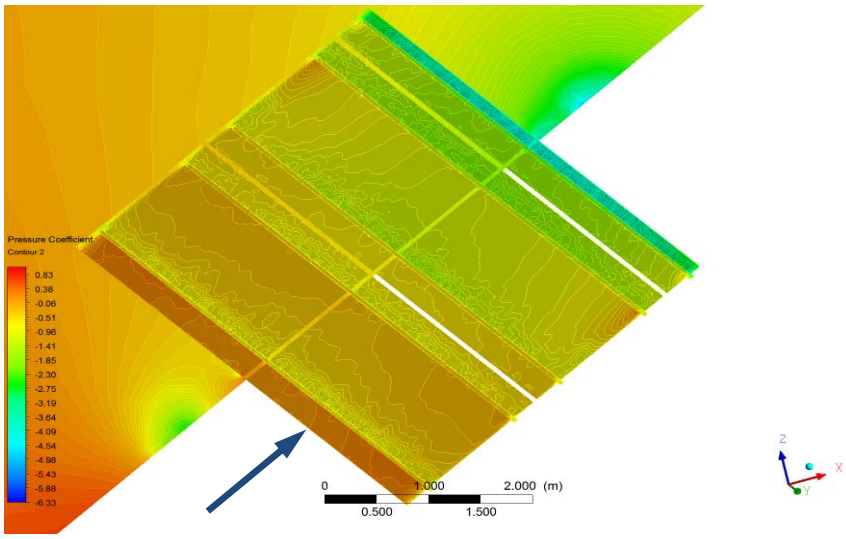


Fig. 4. 73. Pressure coefficient on a perpendicular transversal plane, roof under panels, wind direction 90º, leeward, slope 27º

Pressure coefficients are shown on the building roof with solar panels and on a transversal plane crossing the middle of the building, in Fig. 4.74. Positive pressure coefficients, (Cp=0.38) are observed on roof under the array's edge close to edge C of the roof, (on the windward side) and high suction coefficients, (Cp=-1.94) are shown at the top of the south edge of the array, and north edge of the panel array on the windward side. Very high pressure, (Cp=-4.25 to -5.63) is observed on the ridge of the building, where no panels are installed.

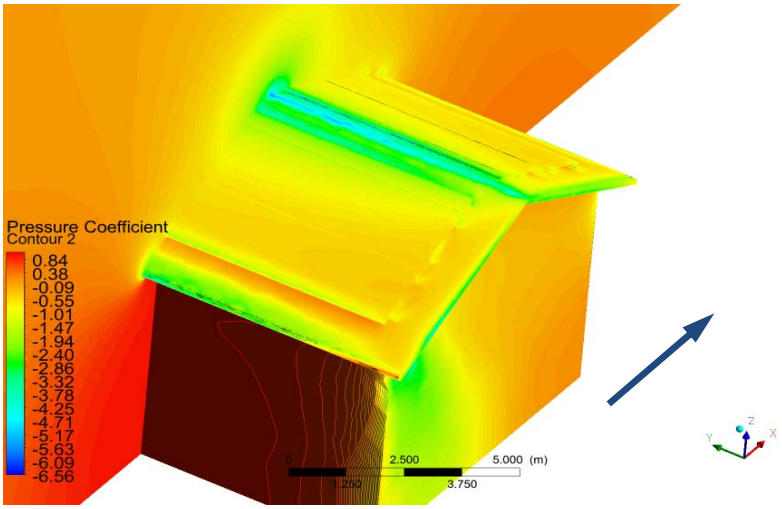


Fig. 4. 74. Pressure coefficient on a transversal plane perpendicular to the house ridge

The suction coefficient is very high (Cp=-5.63) at the intersection with the ridge; thereafter the pressure coefficients increased with the distance from the ridge.

Figure 4.75 shows the six perpendicular lines on roof and crossing through the panel arrays, which are used to track the velocity and pressure coefficients variation. Each of these lines start just below the roof surface under the panels and extends to nearly 20 m above ground or 12 m above the panels. The lines are placed on six different points distributed near the A edge of the solar panel array and near middle cross section of the array.

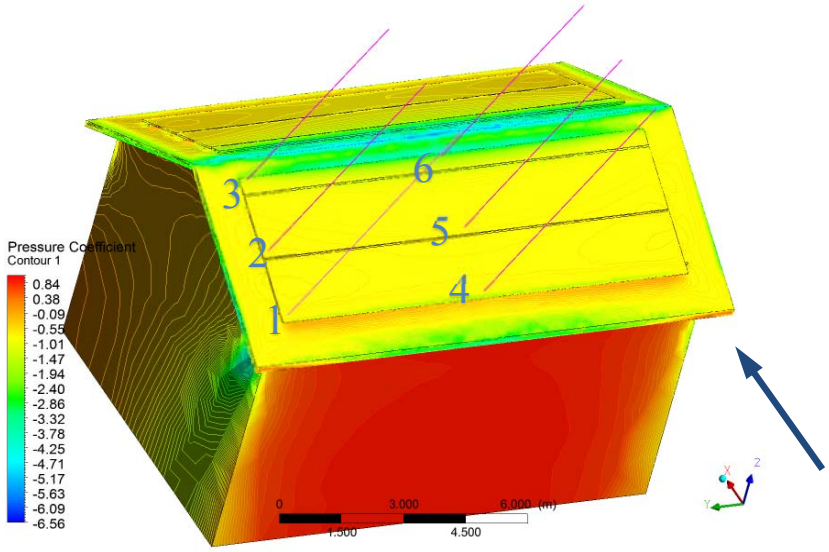


Fig. 4. 75. Lines used to track velocity and pressure coefficient changes

Figure 4.76 shows the velocity flow above the roof on both the windward and leeward sides of the roof, where the wind speed is nearly 0m/s at 0.05 m near the panel surfaces, on the windward side, and increased sharply to 40m/sec at 0.10m above the panel surface. The flow close to the panels, had an increased speed of up to 69.2m/s, as it approaches the ridge at the end of the array, then increased to 92.20 m/s at the ridge area which has no panels. The wind speed reduced from 92.2m/s at the ridge surface to 69.2 m/s at 1.0m height above the ridge.

The speed of the wind flow reduced at the leeward of the building, to less than free stream speed, from ground to nearly the height of the ridge (Fig. 4.77).

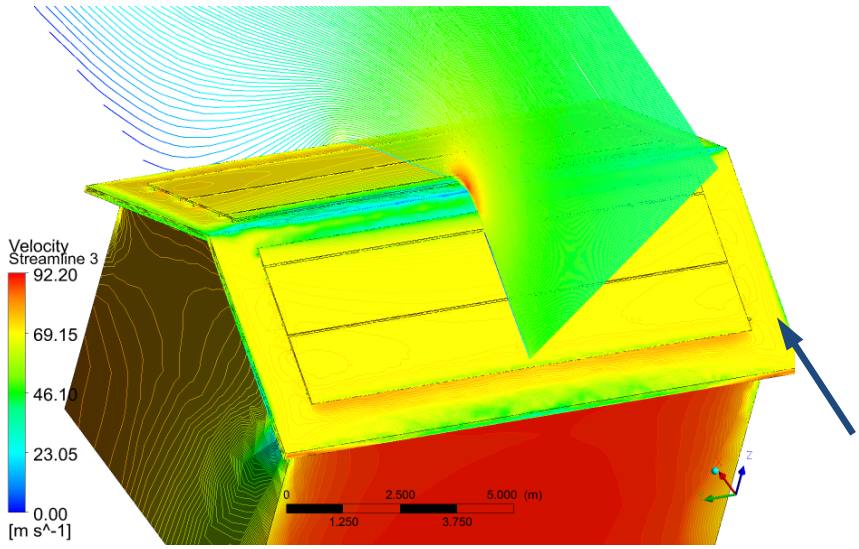


Fig. 4. 76. Velocity streamlines at middle cross section plane, windward view

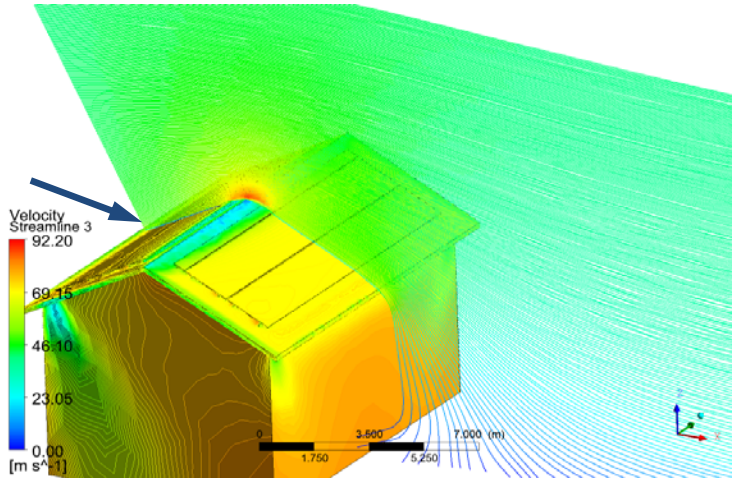


Fig. 4. 77. Velocity stream lines at middle cross section plane, Leeward view

Figures 4.78 to 4.85 show the vortex core distributions on top, underneath solar panel arrays, and around the building.

Figure 4.78 represents the main vortex cores on the entire building, on top of the panel arrays and on the roof surrounding the arrays, on the windward and leeward sides of the roof. The vortex cores around the building are larger by an order of magnitude compared to the roof vortex cores. Largest building vortex cores are shedding from the corners behind the building. Roof vortex cores are the largest on the ridge of the roof, between the windward and leeward panel arrays. However, moderate size roof vortices are shown along the edges of the panel arrays and along the roof edges.

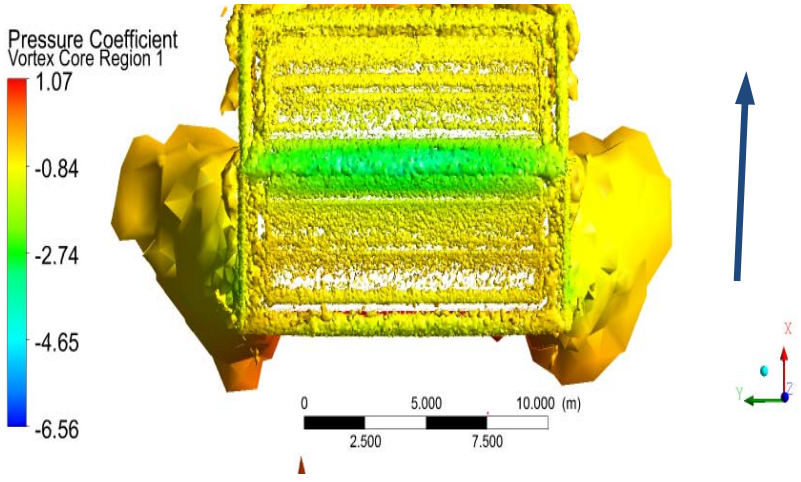


Fig. 4. 78. Vortex core distribution on roof with panels installed, and around the structure.

Figure 4.79 shows pressure coefficients only in the turbulent areas of the vortex cores, as there is no building shown in this figure. Large suction at the ridge area associated with moderate vortex core sizes, which are much smaller than the building vortex cores at much larger suction coefficients. In addition, there are two types of vortex core formations noticed in Figs 4.79 to 4.91: the largest vortex cores located at the corners on the leeward side, followed by smaller one on the sides of the building. The large vortex cores are longitudinal formed due to separation of at the edges and corners of the building. The subsequent smaller type of vortex cores were the transversal vortex cores, which are near the ridge on the leeward side. Then further transversal smaller vortex cores are located around the edges of the solar panels. However, the smallest vortex cores are located on the roof under panels and the surface of the solar panels (Figs. 4.79 to 4.85). Figure 4.79 shows vortex cores under the panels at the windward side, which are much smaller and less frequent than those on top of the panels. Figure 4.79 shows a side view of the vortex cores around the building and on the roof, where the side vortex cores are slightly smaller than the leeward vortex cores.

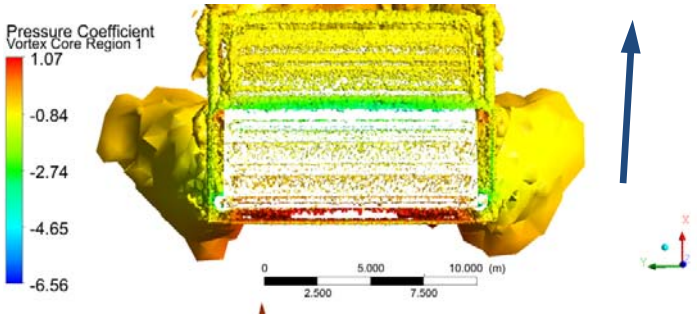


Fig. 4. 79. Vortex core distribution on roof under panels, windward, and leeward with panels, No Contours, and on the building structure

Closer view of the vortex cores on top of the panels and on the windward side of the roof, is shown in Fig. 4.80. Figure 4.81 shows vortex core distribution on the bottom of the panels, on the windward side. It can be observed that the size of the vortex cores and their distribution are similar between top and bottom of the panels.

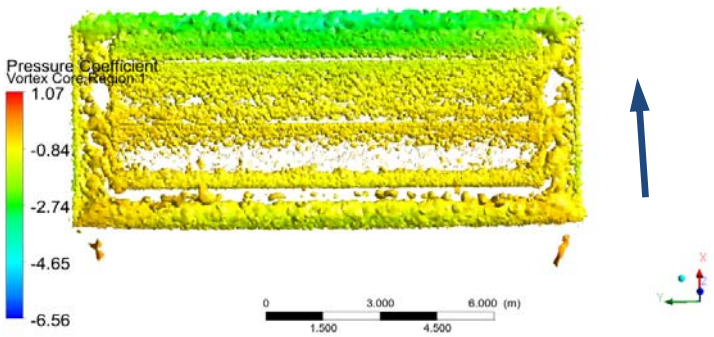


Fig. 4. 80. Vortex core distribution on top of the panels, windward

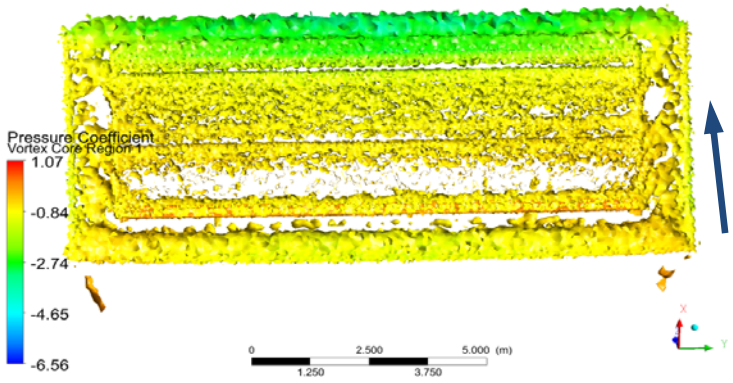


Fig. 4. 81. Vortex core distribution, on bottom of the panels, windward

Fig. 4.82 and Fig. 4. 83 illustrate close-up views of the vortex cores on top and bottom of the leeward solar arrays respectively. The distribution of vortex cores and their sizes shown in the last two figures are similar. However, size of vortex cores on top of panels or on bottom of the planes, are slightly larger than their sizes on the top and bottom of the panels mounted on the windward.

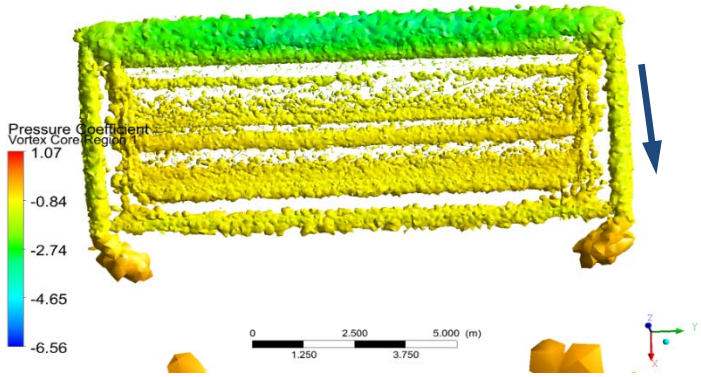


Fig. 4. 82. Vortex core distribution on top of the panels, Leeward

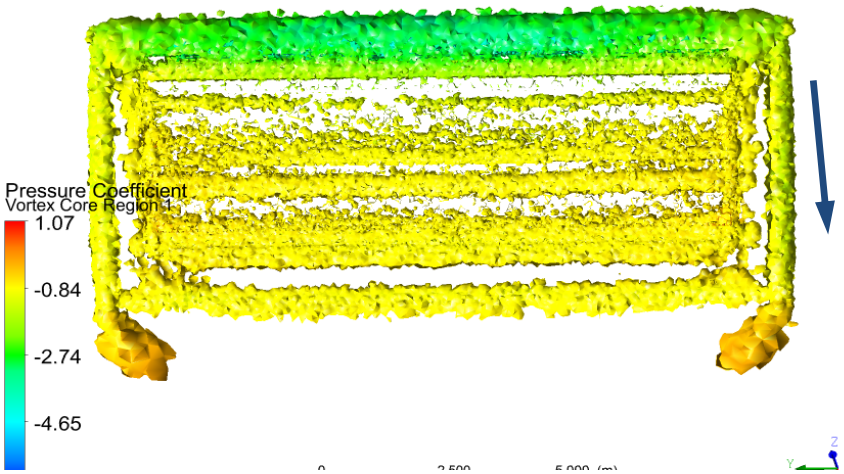


Fig. 4. 83. Vortex core distribution on bottom of the panels, Leeward

4.3.3.5. Pressure coefficients and velocity profiles in the cavity and above the solar panels for wind direction 90º, windward side of the roof

To investigate the changes in velocities and pressure coefficients across the gaps underneath the panels, and above the panel, six lines perpendicular to roof surface were chosen, on the side of the roof, windward side, and in middle of the windward side of the roof (Fig. 4.78). The results are presented in the Figs. 4.84 to 4.93, for 90° wind direction, windward side of the roof surface and 40 m/s incoming wind speed.

Along line 1, Fig. 4.84 a) and b) show the change in velocity through the gap between the roof surface and bottom of the panels, for 3" (0.075 m) gap height, wherein velocity changes from 0m/s on the surface of the roof to 25 m/s near middle of the cavity, then decreased gradually to 0 at the bottom surface of the panel.

In addition, above the solar panel, the surfaces velocity increased to 50 m/s in the first 6" (0.15m) above the top of the panel surface, then decreased to 40 m/s at 15 m and greater height above the ground surfaces.

Figures 4.84 c) and d) show that the pressure coefficient profile between the roof surface and bottom of the panels remained constant at (Cp=0.08) until middle of the space between roof surface under panels and the bottom of the panels. Then the pressure coefficient increased to (Cp=0.13) at

the bottom of the panels. At top of panel surface, the pressure coefficient reached (Cp=-0.64), then increased gradually to 0 at nearly 16 m above ground.

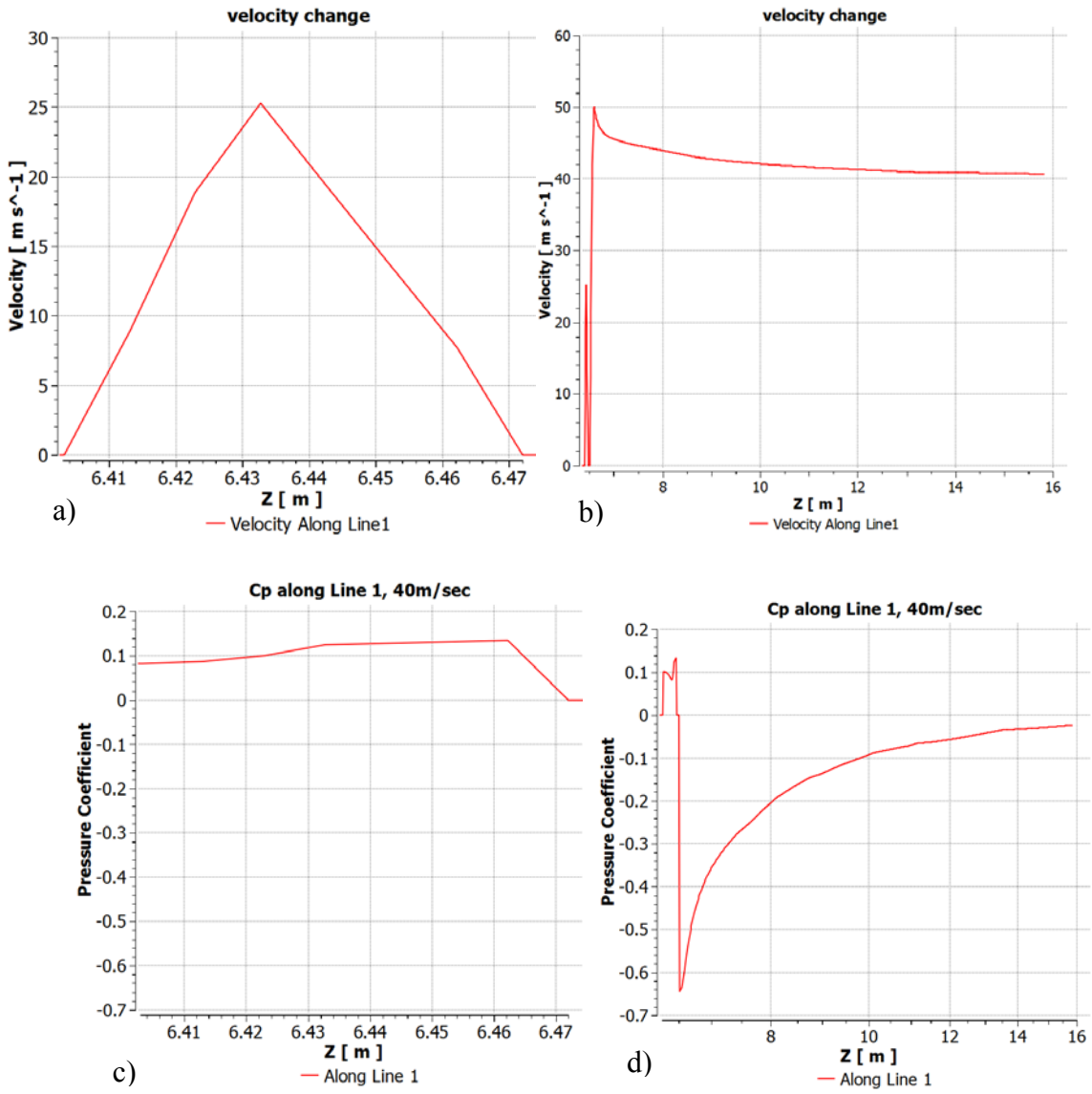


Fig. 4. 84. Velocity and Cp changes between panels, and above roof, Line 1, 40m/s, windward, wind direction 90º

In the middle of the west edge, A, along line 2, Fig. 4.85 a) and b) shows that velocity between the roof surface and bottom of the panels for 3" (0.076m) space height, increased from 0 m/s on roof surface to 10.5 m/s at the middle height of the space, then reduced to again to 0m/s at the bottom of the panels. Then velocity increased to 48 m/s at 4" (0.102m) above the solar panels, while

decreased afterwards to 40 m/s at 20 m height above the ground surfaces, which corresponds to 12.5m above the roof surface.

Pressure coefficient changes between the roof surface and bottom of the panels for 3" (0.076m) space height, from (Cp=-0.41 to -0.40) respectively. Then directly over the panels, Cp reduced to (Cp=-0.48) which then increased gradually to 0 at 20m height above ground, which corresponds to 12.5 m above roof surface, Fig. 4.85 c) and d).

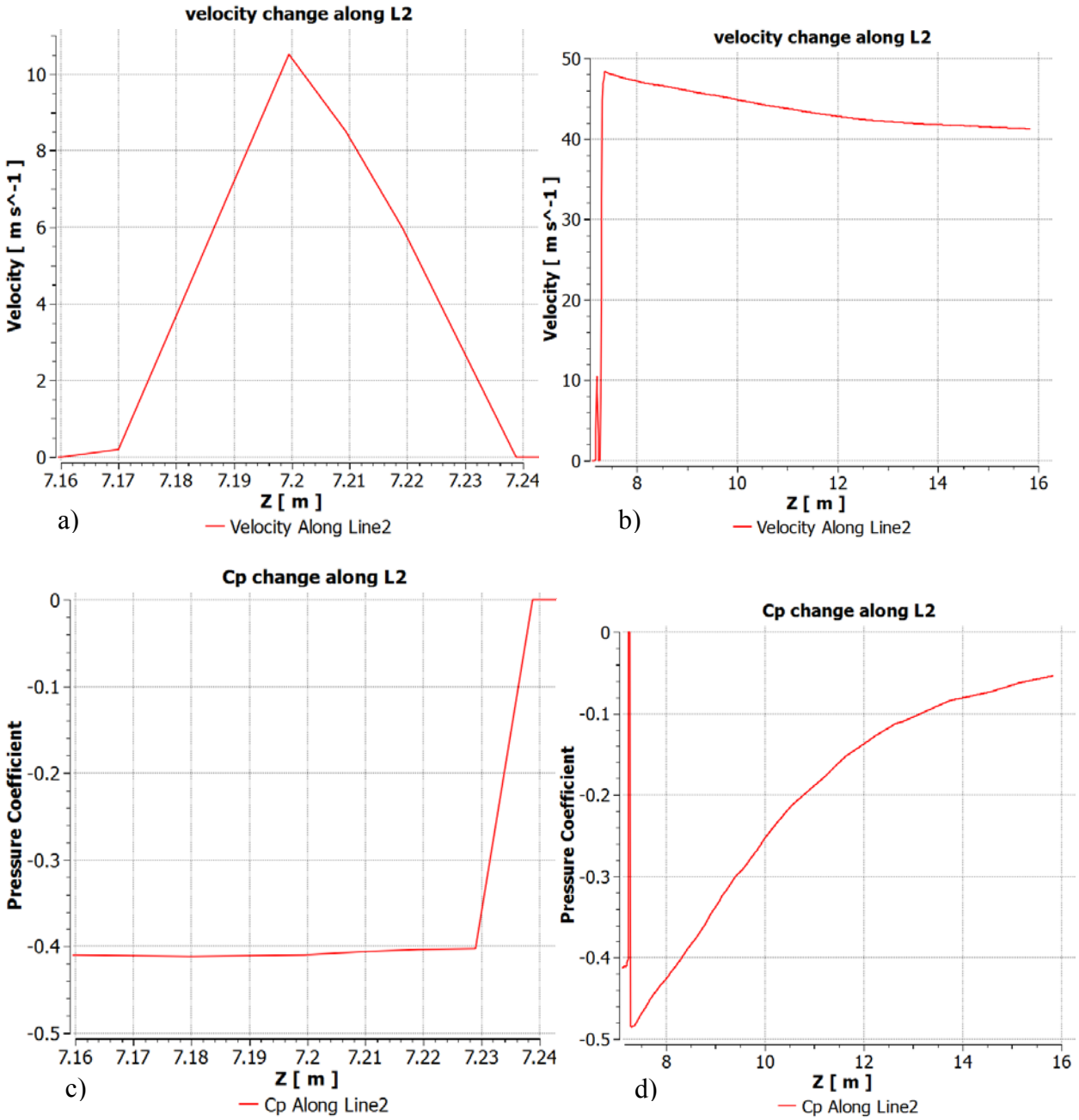
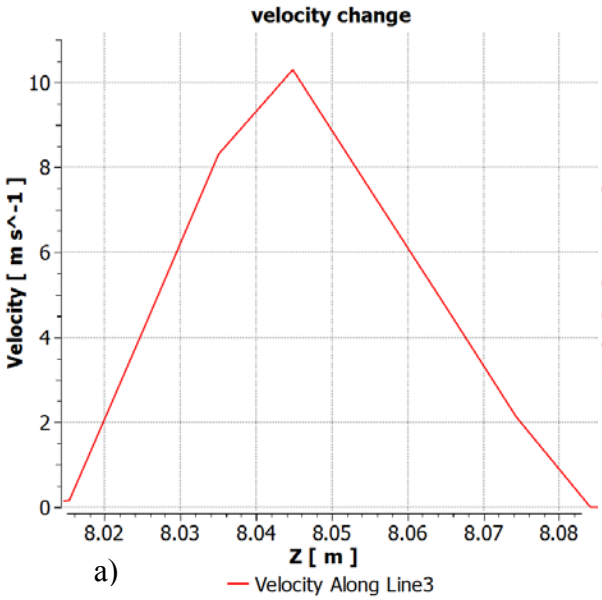
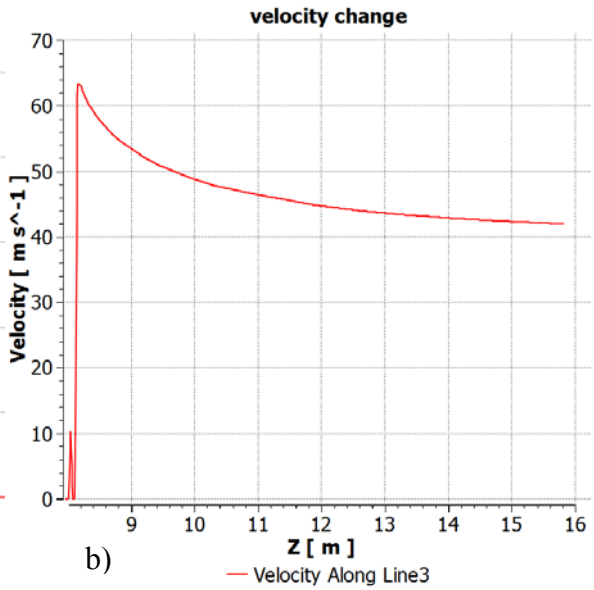


Fig. 4. 85. Velocity and Cp changes between panels, and above roof, Line 2, 40m/s, windward, wind direction 90º

Figure 4.86 a) and b), illustrates that velocity changes between roof surface and bottom of the panels along line 3, located on top corner of edge A, from 0 at the roof surface under the panels, to 10.2 m/s just below the middle of the space then decreased back to 0 at bottom of the panels.
In the same Fig. 4.86 c) and d), velocity above the panels, along line3, increased sharply from 0 m/s, on panel surface to 63 m/s at nearly 4" (0.102m) above the panels then decreased back to 40 m/s, the free current speed, at 20 m above the ground surface or 12.0 m above the roof surface.
The same Fig. 4.86 shows that pressure coefficient is (Cp=– 2.75) at roof surface and remained constant throughout the space height.
However, Cp reduced to (Cp=-1.55) on top of the panels, and then increased gradually to 0 at height 25 m above the ground, or 17 m above roof surface.



a)



b)

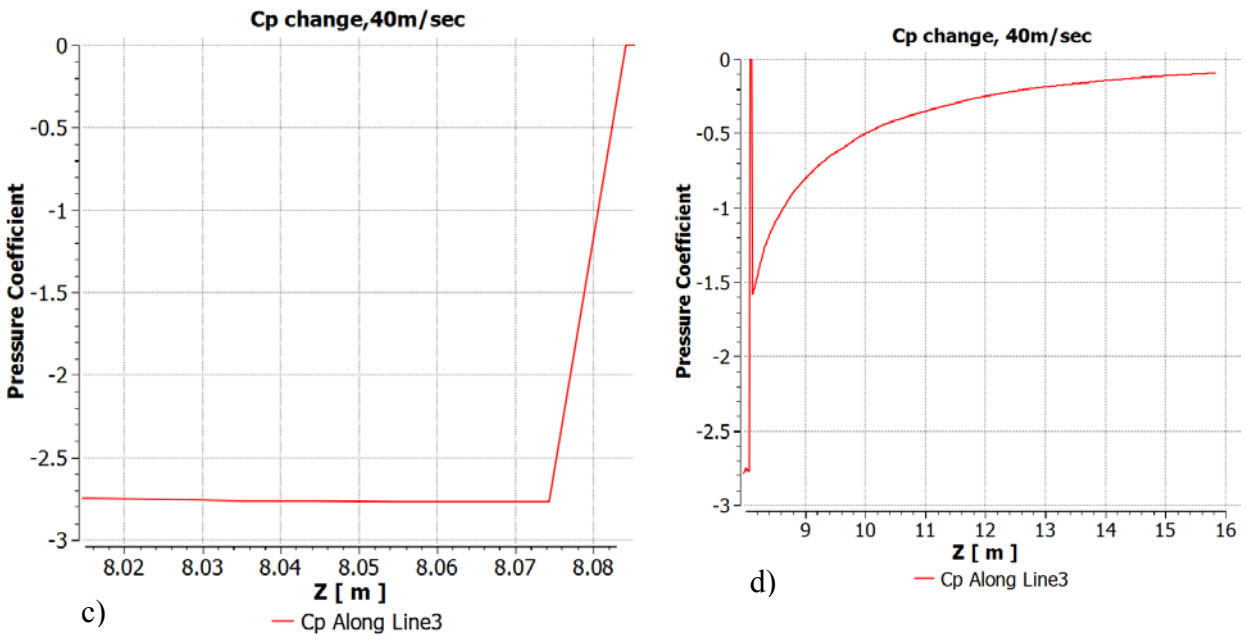


Fig. 4. 86. Velocity changes between panels, and above roof, Line 3, 40m/s, windward, wind direction 90º

Monitoring velocity along line 4, located in the middle of the windward edge, of the windward array, (Fig. 75), reveals that velocity increased from 0 at the roof surface under the panels, to 6.1 m/s in the middle of the space then decreased back to 0 at bottom of the panels, Fig.4.86 a).

In addition, velocity above the panels, increased sharply from 0 on top of the panels, m/s, to 53.5 m/s at nearly 4" above the panels then decreased back to 40 m/s, or the free current speed, at 20 m above the ground surface, or 14.5 m above the roof surface, Fig. 4.86 a) and b).

On the other hand, monitoring the pressure coefficients, in the gap between roof surface and panels, along line 4, reveals that that pressure coefficient at the roof surface is (Cp=0.03) then remained constant the whole height of the space where afterwards, above the panels, Cp decreased to (Cp=-1.0) at the panel surface, then decreased slightly to (Cp=-1.10) nearly 2" above the panels, then increased to 0 at height 20 m above the ground, or 14.50 m above the roof surface, Fig. 4.87 c) and d).

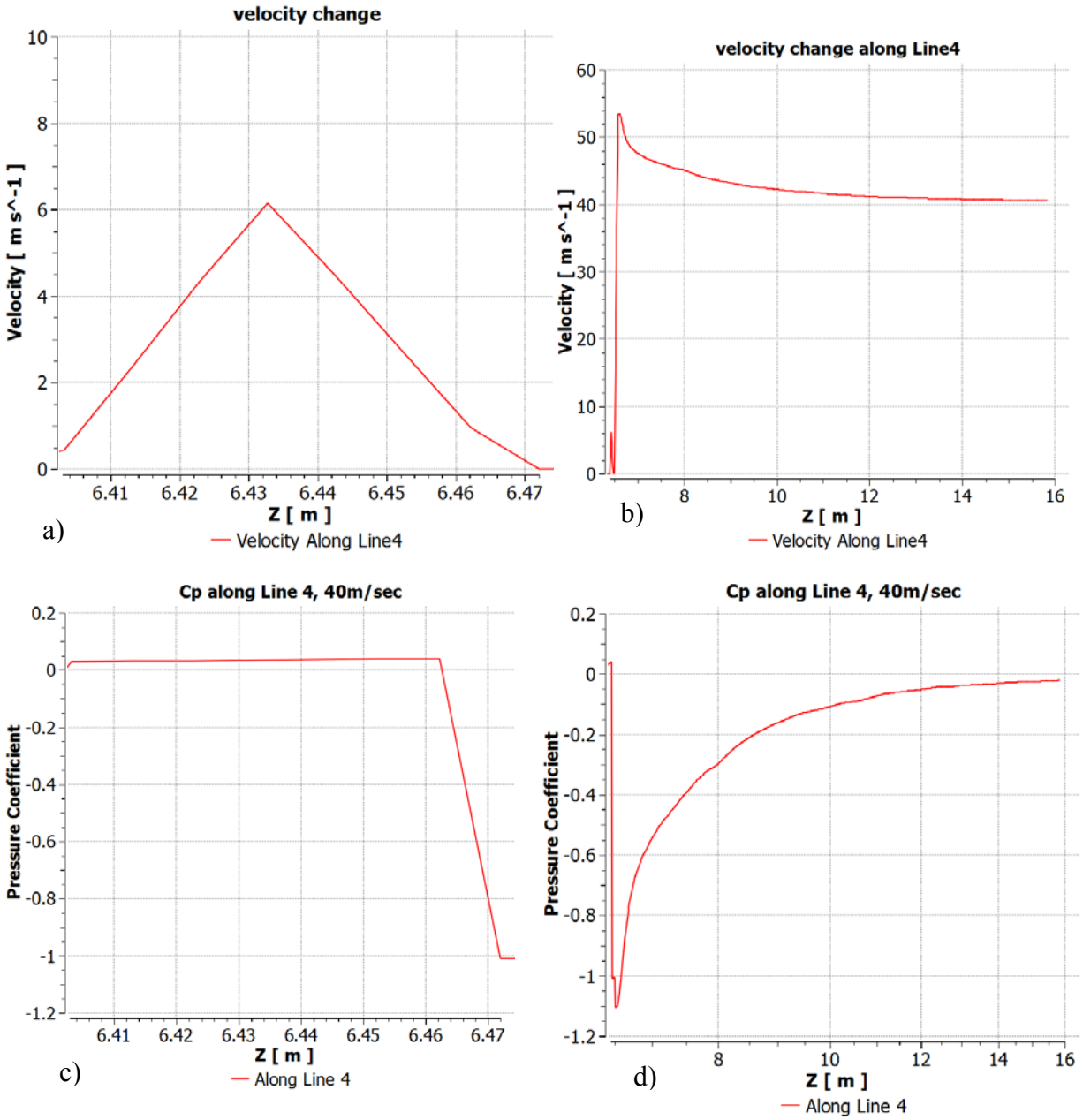


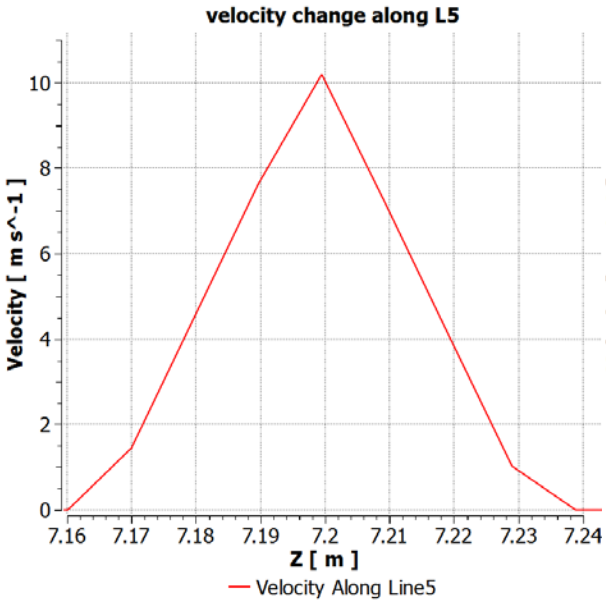
Fig. 4. 87. Pressure coefficient and velocity changes between panels, and above roof, Line 4, 40m/s, windward, wind direction 90º

In the following Fig. 4.88 a) and b), velocity and pressure coefficients are recorded along in 5, in the gap and above the panels. Velocity in the gap increased from 0 at the roof surface under the panels, to 10.1 m/s at the middle of the space then decreased back to 0 at bottom of the panels. Afterwards, velocity above the panels, increased sharply from 0 m/s, to 51 m/s at 4" (0.102m)

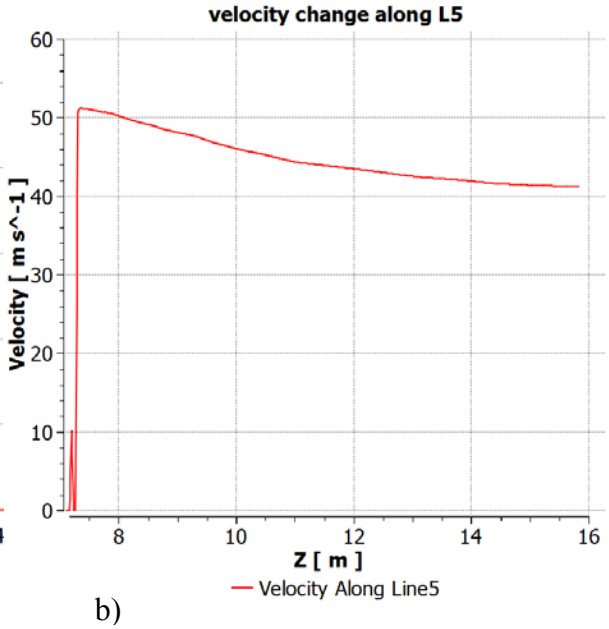
above the panels then decreased back to 40 m/s, the free steam speed, at 20 m above the ground surface, or 17.0 m above the roof surface.

On the other hand, in the Fig. 4.88 c) and d), pressure coefficient is recorded (Cp=-0.65) at roof surface, and then changes very slightly along the space between panels to (Cp=-0.61) at middle of the space then remained constant until bottom of the panel.

Then pressure coefficient reduced slightly to (Cp=-0.63) directly above the panels, which then reduced slightly to (Cp=-0.65) at 20" (0.50 m) above the panels, then increased to 0 at height 35 m above the ground, or 27.50m above the roof surface.



a)



b)

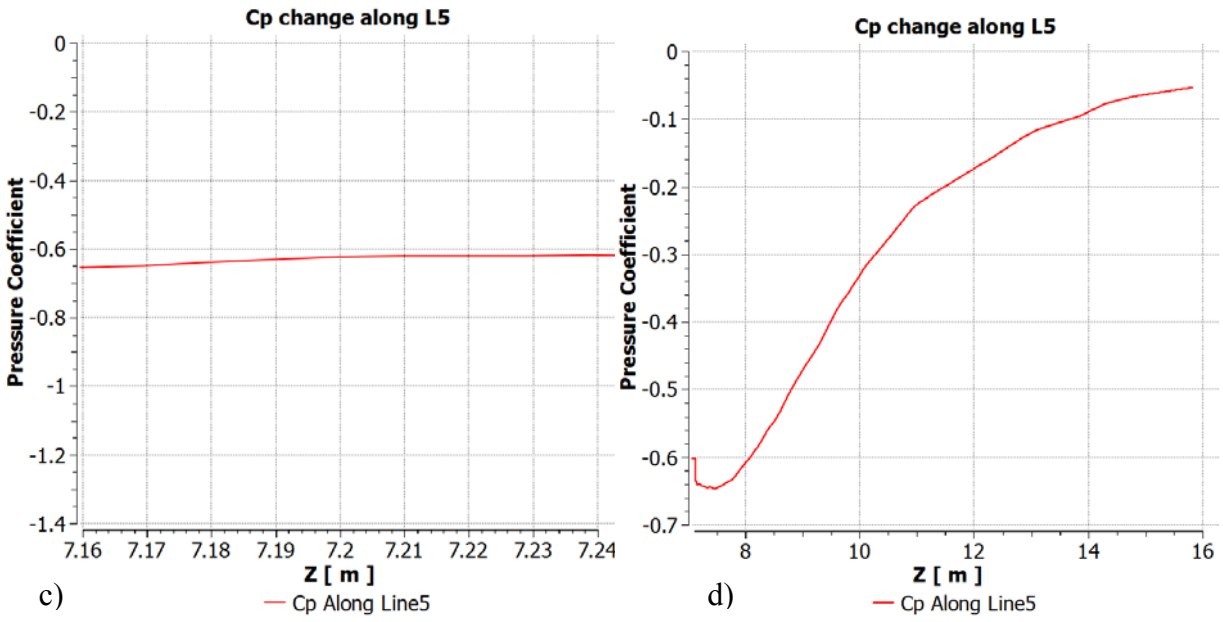


Fig. 4. 88. Pressure coefficient and velocity changes between panels, and above roof, Line 5, 40m/s, windward, wind direction 90º

Observing velocity and pressure coefficients, changes along line 6, (Fig. 75), was recorded in Fig. 4.89, which shows that velocity increased from 0 at the roof surface under the panels, to 10.80 m/s in the middle of the space then decreased back to 0 at bottom of the panels.

Afterwards on top of the panels, velocity increased sharply from 0 m/s, to 74 m/s a few inches above the panels then decreased back to 40 m/s, the free current speed, at 35 m above the ground surface or 27.0 above roof surface, Fig. 4.88 a) and b).

Moreover, Fig. 4.89 c) and d) illustrates that pressure coefficient is (Cp=-3.80) at roof surface, then remained constant for the whole height of the space between roof and panels, then increased to (Cp=-2.4) on top of the panels. Afterwards, Cp decreased abruptly in the first 1" (0.025m) above the panels, to (Cp=-2.45), then increased gradually to 0 at height 35 m above the ground, or 27.0 m above the roof.

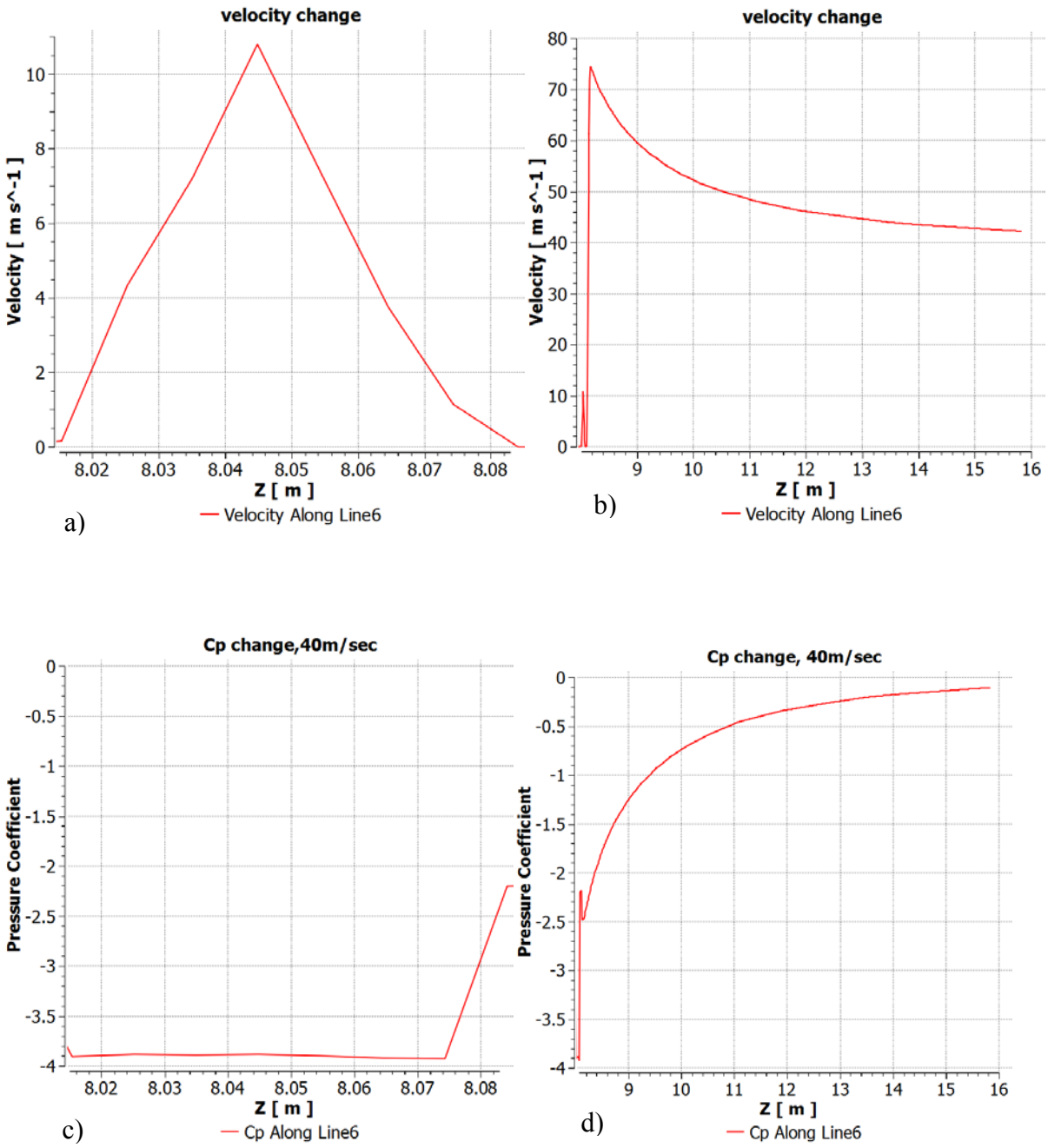


Fig. 4. 89. Pressure coefficient and velocity changes between panels, and above roof, Line 6, 40m/s, windward, wind direction 90º

The following four Figs. 4.90 to 4.91, present all the velocity profiles with each other, in addition to the Cp profiles in the gaps and above the panels, and to verify the effects of wind speed changes on the velocity and Cp in gaps and on top of panels. Figures 4.91 and 4.93 show pressure coefficients and velocity along the 6 lines perpendicular to the roof and panels, under 40 m/s wind

flow speed. While Figs. 4.90 and 4.92 show pressure coefficients and velocity along the 6 lines perpendicular to the roof and panels, due to 10 m/s wind flow.
From those collective figures, pressure coefficients for 10 m/s and 40 m/s seem to be very close to each other, as illustrated in both close views in Fig. 4.90 and Fig. 4.92, and in whole graphs depicted in Fig. 4.91 and Fig.4.93.

The pressure coefficients on L1 under panels is 0.10, reduced to (Cp=-0.03) at L4 under panels. Similarly, Cp is (Cp=-0.41) at L2 reduced to (Cp=-0.62) at L5under panels, and Cp is (Cp=-2.75) along L3 which decreased to (Cp=-3.8) along L6 under the panels.
The same trends observed above the panels, where Cp decreased at L1 to (Cp=-0.64) from that under the panels in the gap and decreased to (Cp=-1.10) at L4 above the panels. However, Cp reduced slightly along L2 above panels from that under panels, to (Cp=-0.48) and similarly Cp reduced slightly along L5 above panels from that under panels to (Cp=-0.65).
Nonetheless, Cp along L3 and L6 above the panels increase considerably from those under the panels, where Cp increased from (Cp=-2.75 to -1.60) along L3and increased from (Cp=-3.8 to -2.50) at L6 at the top of the panels.

These pressure coefficients values recorded at 40 m/s and 10 m/s wind flows are very similar to each other. However, wind speeds under and above the panels, are proportional to the free stream flow, where it was noticed that all velocities recorded under and on top of the panels for 40 m/s flow are scaled by 4 from those corresponding velocities under 10m/s wind flow.
For example, velocities under panels along L1 and L4 recorded under the panels 25.2 and 6.12 m/s, and recorded 50 and 53.2 m/s above the panels respectively, which correspond to 6.30 and 1.53 m/s under the panels and 12.50 and 13.3 m/s above the panels when wind flow is 10m/s.
Similarly, velocities under panels along L3 and L6 recorded 10.2 and 10.8 m/s under the panels respectively, while recorded 63 and 74.5 m/s above the panels respectively, which correspond to 2.55 and 2.7 m/s under panels respectively and 15.75 and 18.63 m/s above panels respectively under 10m/s flow.

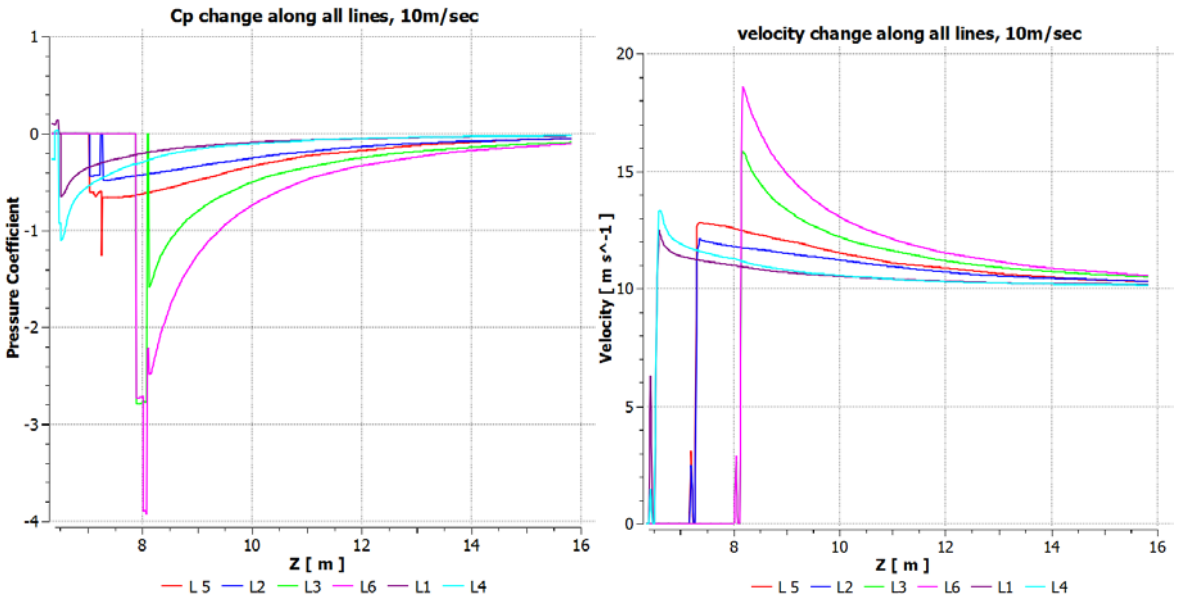


Fig. 4. 90. Pressure coefficient and velocity changes between panels and roof, and above the panels, Lines 1-6, 10 m/s, windward, wind direction 90º

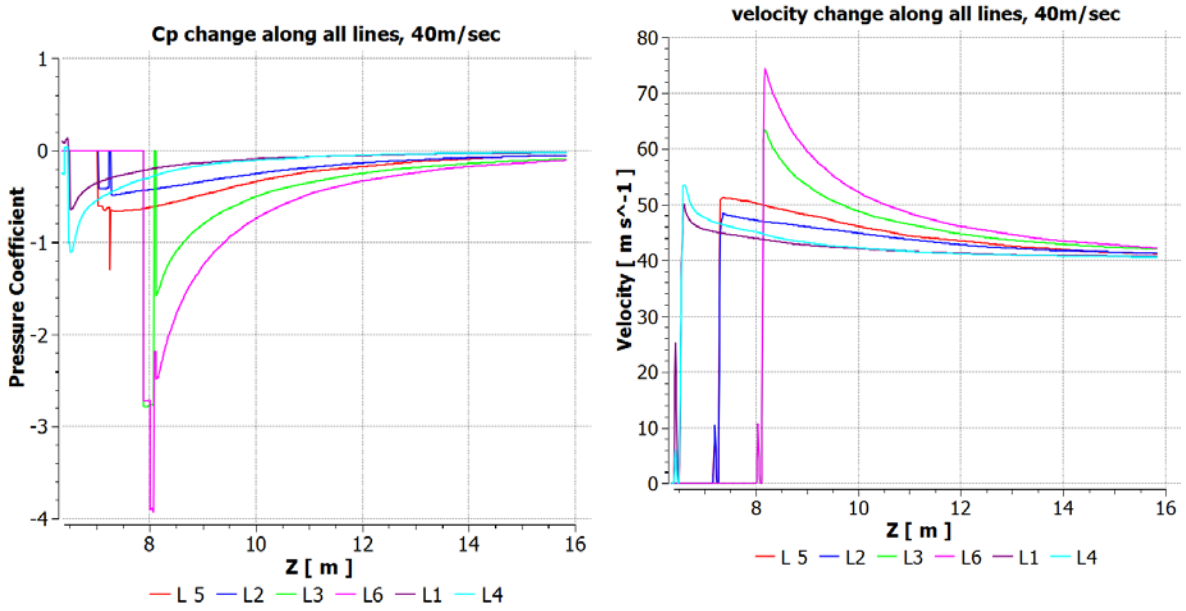


Fig. 4. 91. Pressure coefficient and velocity changes between panels and roof, and above the panels, Lines 1-6, 40 m/s, windward, wind direction 90º

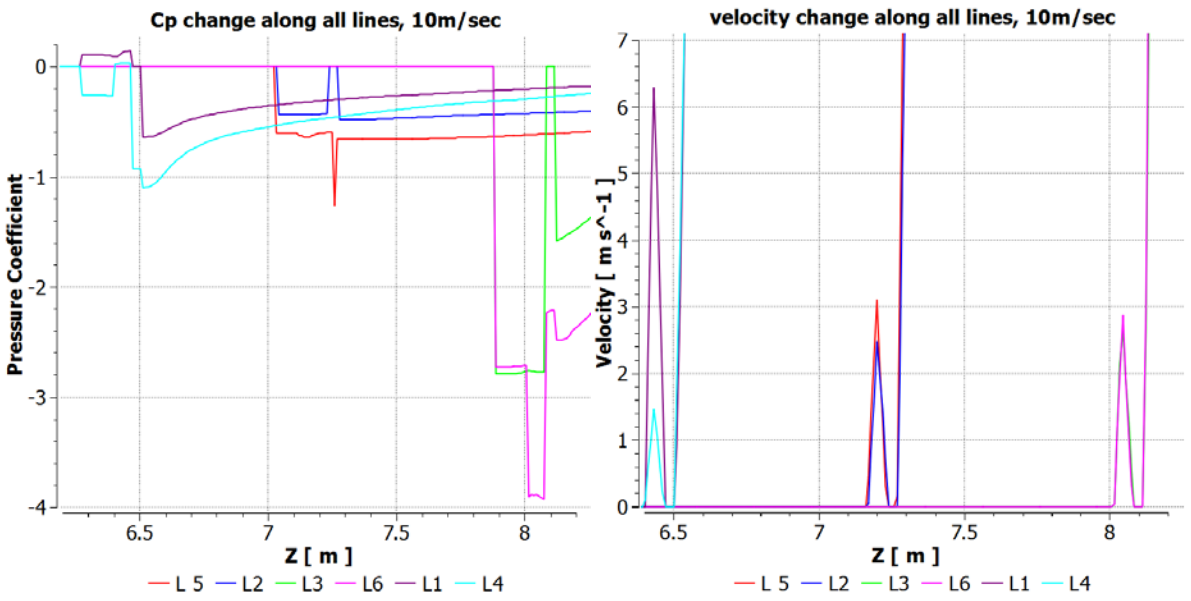


Fig. 4. 92. Pressure coefficient and velocity changes between panels and roof, and above the panels, Lines 1-6, 10 m/s, windward, wind direction 90º Zoom into space between panels and roof

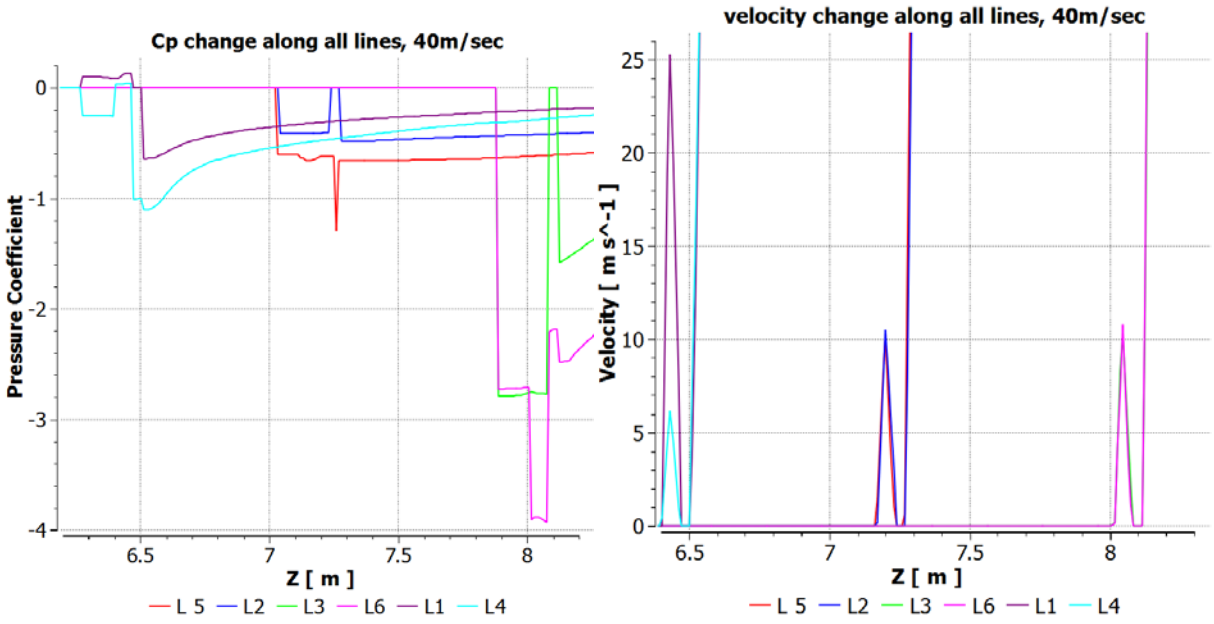


Fig. 4. 93. Pressure coefficient and velocity changes between panels and roof, and above the panels, Lines 1-6, 40 m/s, windward, wind direction 90º Zoom into space between panels and roof

4.3.4. Wind flow characteristics and three-dimensional vortex formations for gable roofs without solar panels for wind direction 90º

4.3.4.1. Pressure coefficients observations on the building.

Fig. 4.94 depicts the pressure coefficients on both sides of a 27º inclined roof with no panels. The windward side seems to be subjected to lower pressure, (Cp=0.40 to -1.86), than leeward side, (Cp=-0.51 to -3.21) and considerable low pressure is built near the ridge on the leeward side.

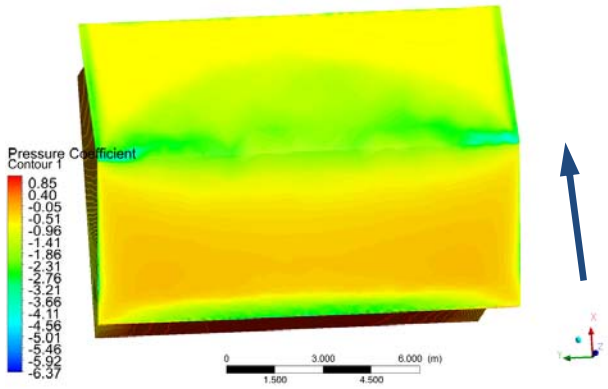


Fig. 4. 94. Pressure coefficient contours top view, windward, slope 27º, wind direction 90º

The following Figure 4.95 shows vortex cores created on the roof, and around the building. The largest vortex cores are longitudinal and are located at the corners on the leeward, and on sides of the building, and formed by flow detaching from the sharp edges and corners of the building. Another type of vortex cores were the transversal vortex cores which are nearly the same size as the first type and formed near the ridge on the leeward side. While the smallest transversal vortex cores are located around the edges of the roof overhangs.

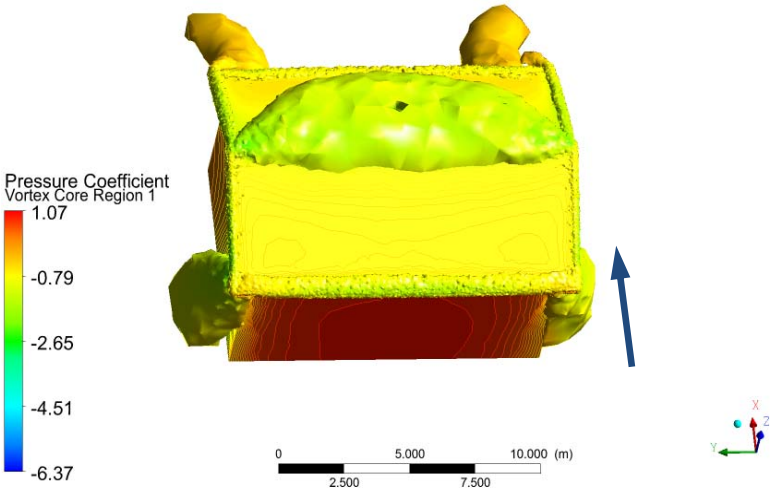


Fig. 4. 95. Pressure coefficients, Vortex core windward, slope27º, wind direction 90º

Figure 4.96 shows velocity streamlines above the roof with no panels. Velocity is close to 0 m/s at the roof surface and increased to 67.6m/s at 0.10 to 0.20 m above the ridge area and leeward side, where lowest distance corresponds to area near windward edge, and larger distance corresponds to near ridge areas. In addition, streamline velocity increased as flow approaches the ridge of the building, where the velocity increased to nearly 75 m/s before the ridge at windward side, and then fans out while passing the ridge where it reduced gradually until the free stream speed near the middle of the leeward surface.

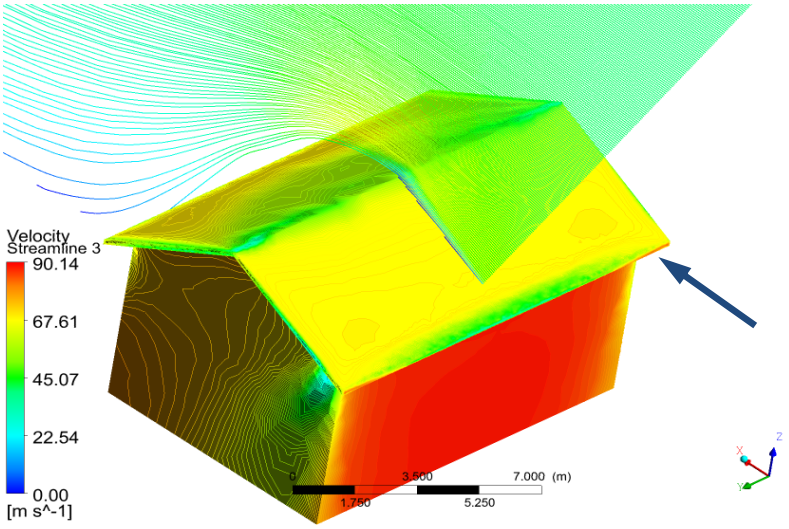


Fig. 4. 96. Pressure coefficient and velocity streamlines at middle of the roof, line 4, slope27º, wind direction 90º

Figure 4.99, shows decrease in flow speed from roof level towards the ground, after passing the leeward north edge where the flow speed gradually decreases from 40 m/s at 8.0 m above ground to 0 m/s on ground.

In comparison with Fig. 4.76 and 4.77, where panels are installed on the roof, it was noticed that wind speed above the ridge is much higher on roof with panels. However, the area of high speed is much larger in the roof with no panels.

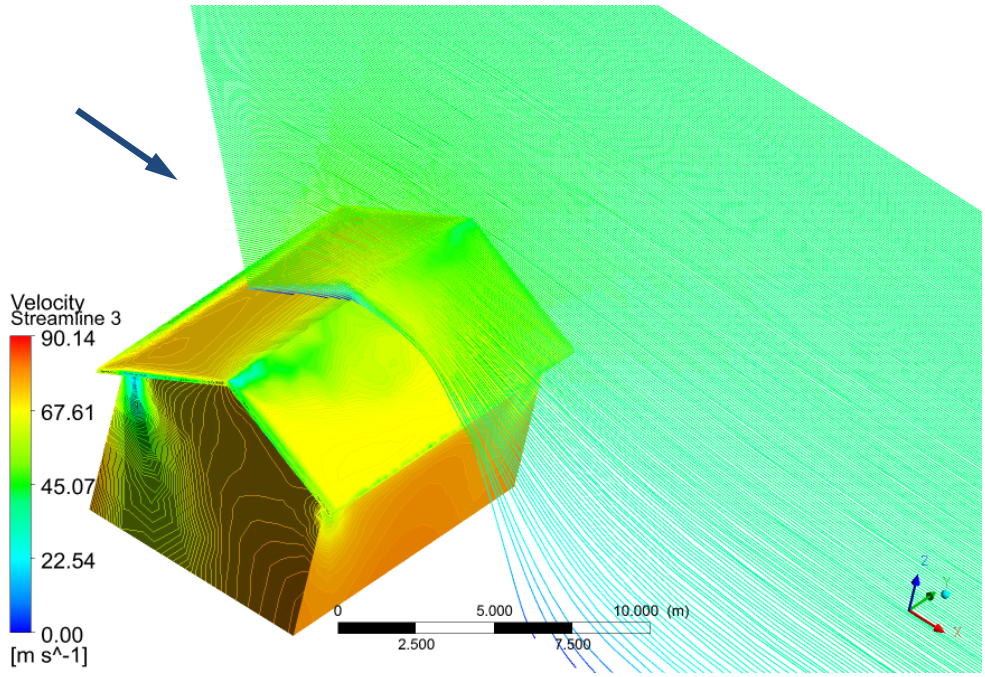


Fig. 4. 97. Pressure coefficient and velocity streamlines at middle of the roof, line 4, slope27º, wind direction 90º, leeward view

4.3.4.2. Pressure coefficients and velocity profiles for roof without solar panels, wind direction 90º, windward side of the roof

The following figures from Fig. 4.100 to Fig. 4.107 illustrate the changes of velocity, and pressure coefficients along each of the 6 lines perpendicular to the windward roof surface, for 90° wind

direction and 40 m/s incoming wind speed. Those can be compared with corresponding figures for roofs with panels illustrated herein before. In each figure, two separate graphs were presented, the first one for pressure coefficient and the other for wind speed, both continue for nearly 20 m above the roof surface.

Each line of the 6 lines is placed in the location coordinates which it has on the roof with solar panels. Figure 4.102 a) portrays Cp and velocities along line 1, whereon velocity changes from 0 on the surface of the roof to 44.0 m/s in the first 20" (0.50m) above roof surface, (which is less than 50 m/s recorded at top of the panels on a roof with panels) then decreased to 40 m/s at 25 m and greater above the ground surfaces, which corresponds to 18.5 m above the roof surface.

In addition, Fig. 4.100 b) shows pressure coefficient profile which records (Cp=-0.28) at the roof surface, which is higher than corresponding point on top of the panel, (Cp=0.08). Then decreased gradually to 0 at nearly 25 m above ground (18.5 m above the roof surface).

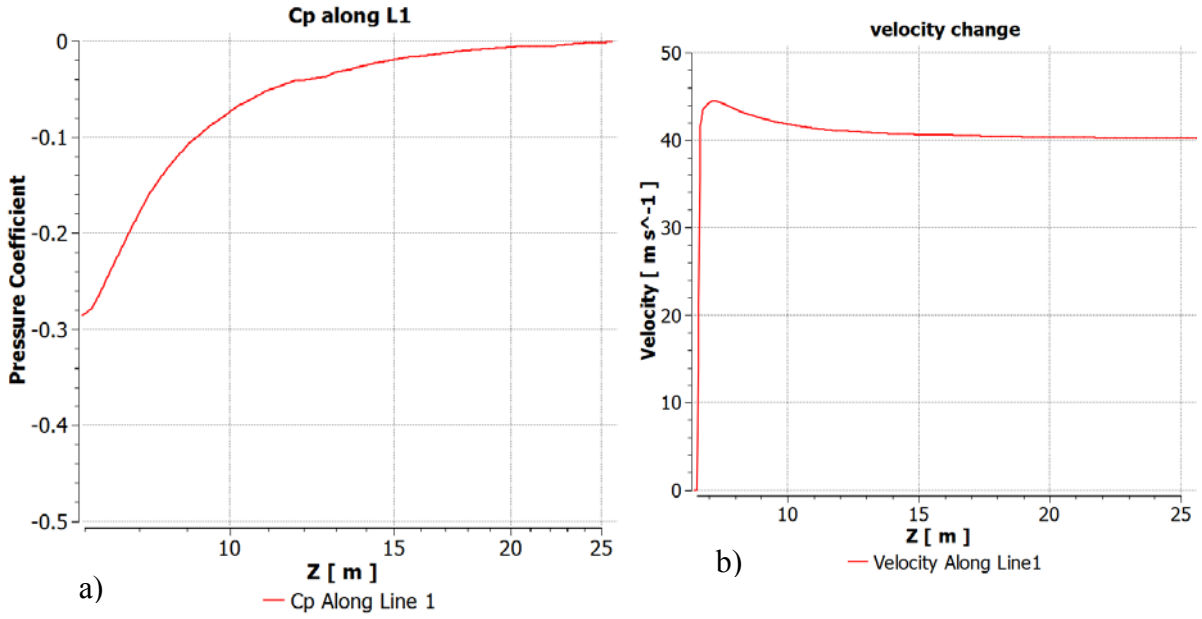


Fig. 4. 98. Pressure coefficient and velocity change along Line1, wind direction 90º, 40m/s, windward, wind direction 90º

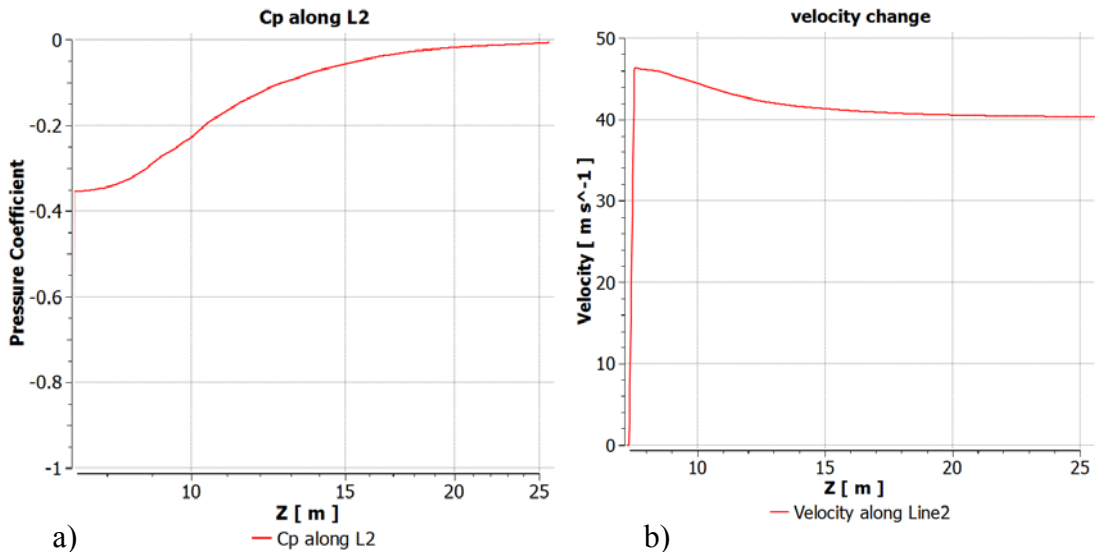


Fig. 4. 99. Pressure coefficient and velocity change along Line2, wind direction 90º, 40m/s, windward, wind direction 90º

For line 2, Fig. 4.101 b) shows that velocity increased from 0 at the roof surface to 46 m/s (which is less than 48m/s recorded at top of the panels on roof with panels) 0.30m above the roof surface then decreased to 40 m/s at 25 m height above the ground surfaces, which corresponds to 17.9m above the roof surface.

In addition, Figure 4.103 a) shows that pressure coefficient above the roof surface is (Cp= -0.35) (which is lightly higher than corresponding Cp on top of panels) which then increased gradually to 0 at 25m height above ground, which corresponds to 17.9 m above roof surface.

Considering line 3 near the ridge and edge A, the velocity increased sharply from 0 m/s, to 50.6 m/sum/sat 0.40 m above the roof, (which is much less than 63 m/s recorder on top of the panels), then decreased back to 40 m/sec, the free current speed, at 25 m above the ground surface or 17 m above the roof surface, Fig. 4.102 b).

Moreover, Fig. 4.102 a), shows that pressure coefficient is (Cp=-0.6) at roof surface (which is much higher than Cp on top of panels, (Cp=-2.75) then reduced gradually to 0 at height 25 m above the ground, or 17 m above roof surface.

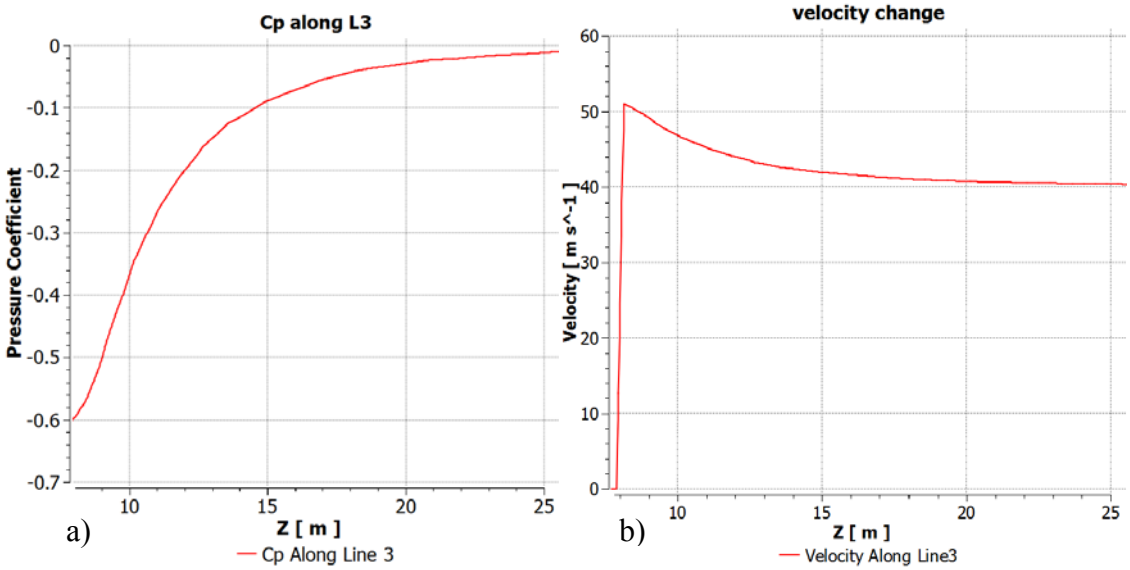


Fig. 4. 100. Pressure coefficient and velocity change along Line3, wind direction 90º, 40m/s, windward, wind direction 90º

When observing the velocity along line 4, it, the velocity increased sharply from 0 at the roof surface to 45.8 m/s (which is much less than corresponding wind speed on top of panels, 53.5 m/s), at 0.5 m above the roof surface, then decreased back to 40 m/sec, the free current speed, at 25 m above the ground surface, or 18.5 m above the roof surface, Fig. 4.103 b).

In addition, Fig. 4.103 a) shows that pressure coefficient at the roof surface is (Cp=-0.4) (which is much higher than (Cp=-1.10) at the corresponding pint on panel surface), then increased to 0 at height 25 m above the ground, or 18.50 m above the roof surface.

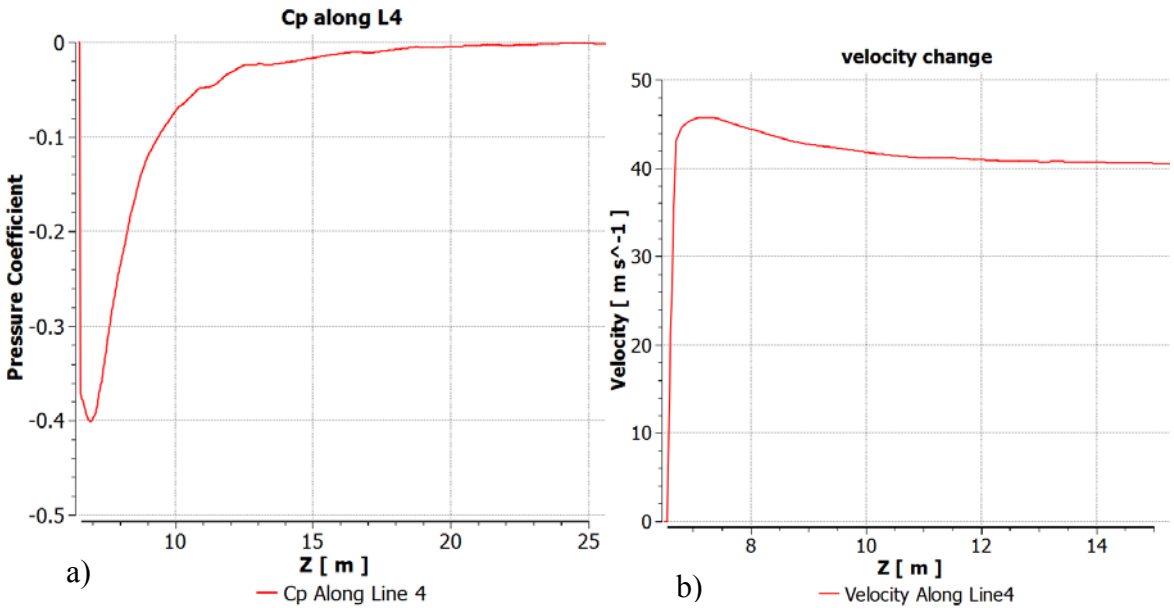


Fig. 4. 101. Pressure coefficient and velocity change along Line4, wind direction 90º, 40m/s, windward, wind direction 90º

For the line in middle of the roof, line 5, velocity profile above the roof surface increased sharply from 0 m/sec, at the roof surface to 48m/s at 0.4 m above surface (which is less than 51 m/s recorded on the corresponding point on top of the panels), then decreased back to 40 m/sec, the free steam speed, at 25 m above the ground surface, or 17.9 m above the roof surface, Fig. 4.104 b).

In the same Fig. 4.104 a), pressure coefficient along line 5, recorded (Cp=-0.46) at the roof surface, (which is moderately less than Cp recorded on top of the panels at the corresponding point, (Cp=-0.65) and then increased to 0 at height 25 m above the ground, or 179 m above the roof surface.

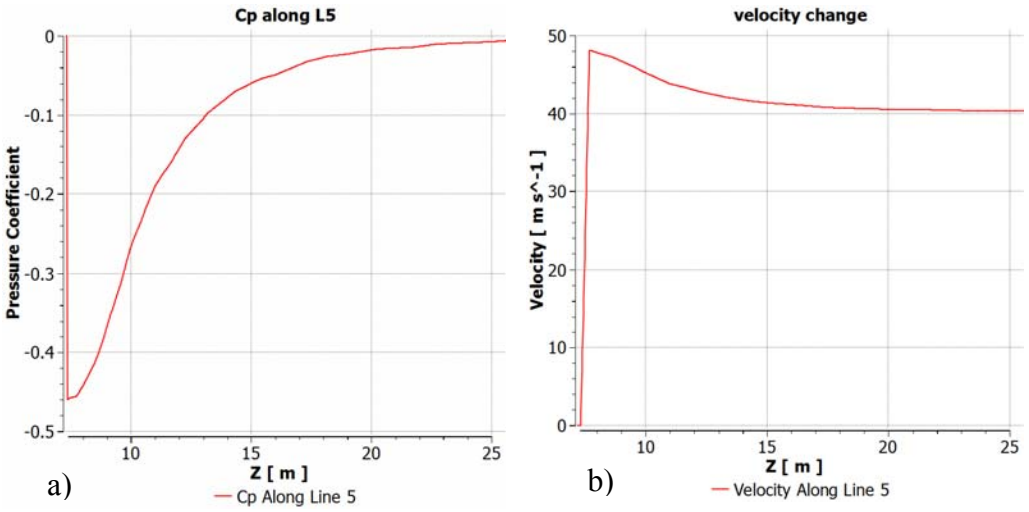


Fig. 4. 102. Pressure coefficient and velocity change along Line5, wind direction 90º, 40m/s, windward, wind direction 90º

Finally, near the ridge and on middle of the roof, along line 6, the velocity increased sharply from 0 m/sec, to 54 m/sat nearly 0.4 m above the roof surface, (which is much less than the corresponding wind speed above the panel, 74 m/sec) then decreased back to 40 m/sec, the free current speed, at 25 m above the ground surface or 17.0 above roof surface, Fig. 4.105 b).

In addition, Fig. 4.105 a), shows, that pressure coefficient above roof surface on line 6 is (Cp=-0.86) (which is way lower than corresponding Cp on top of the panels, (Cp=-2.20)) and then decreased gradually to 0 at height 25 m above the ground, or 17.0 m above the roof.

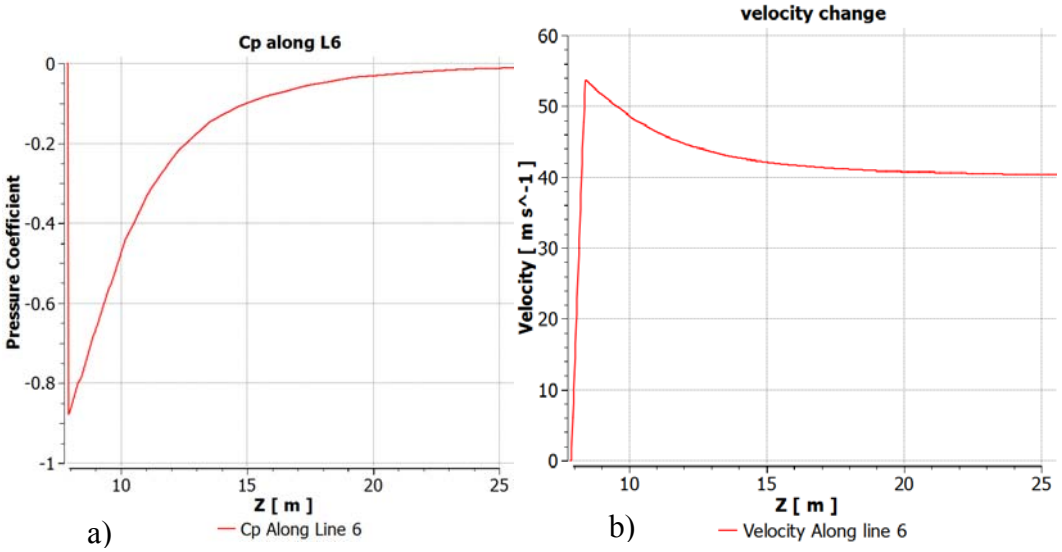


Fig. 4. 103. Pressure coefficient and velocity change along Line6, wind direction 90º, 40m/s, windward, wind direction 90º

The pressure coefficients and velocity are depicted in Figs. 4.108 and 4.109 for all the 6 lines perpendicular to the roof, for flow wind speeds 40 and 10 m/s respectively. That to compare those profiles more effectively.
From those collective graphs, pressure coefficients for 10 m/s and 40 m/s seem to be very similar. However, it was noticed that all velocities recorded for 40 m/s flow are scaled by 4 from those corresponding velocities under 10m/s wind flow.

For example, velocities along L1 and L4 recorded on roof surface are 44 and 45.8 m/s (compare with 50 and 53.2 m/s above the panels) which correspond to 11 and 11.45 m/s above the panels respectively under 10m/s flow.
Similarly, velocities along L3 and L6 recorded 50.6 and 54 m/sec on roof without panels, (compare with 63 and 74.5 m/s above the panels) which correspond to 12.65 and 13.5 m/s respectively under flow speed 10 m/s.

On the other hand, Fig. 4.106, and 4.107 illustrated that Cp decreased while approaching the ridge, where the lowest suction is at L1 and L4, (Cp= -0.28, -0.4), the moderate suction is observed at L2 and L5 (Cp= -0.35, -0.46) then largest suction is found at top lines L3 and L6 ((Cp=-0.6. -0.86). These recorded Cp reveals decrease of pressure coefficient with distance from edge A as well.

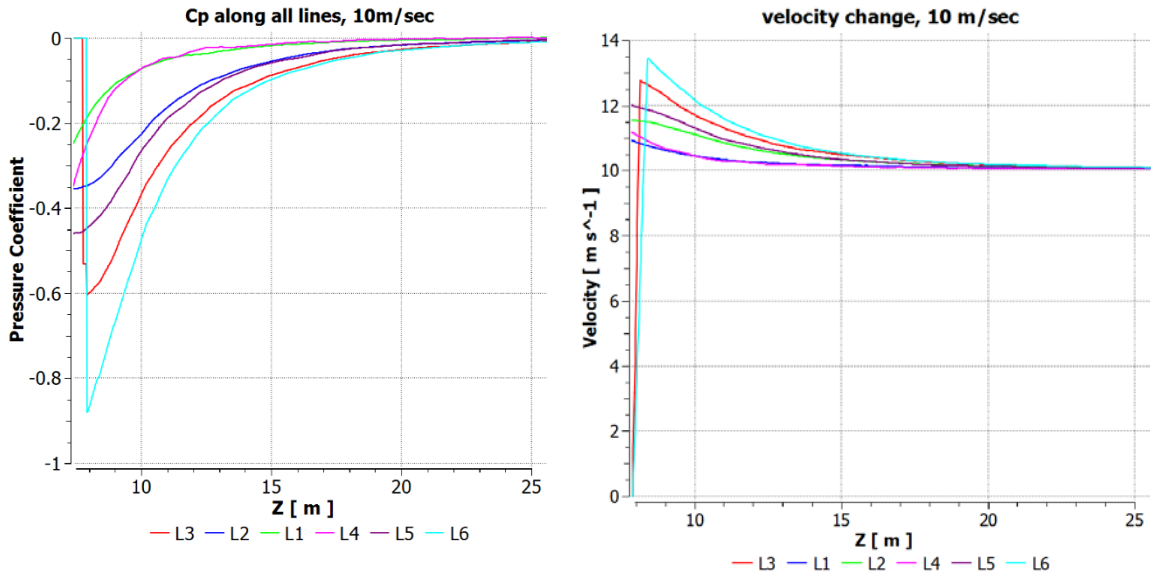


Fig. 4. 104. Pressure coefficient and velocity change along all Lines, wind direction 90º, 10m/s, windward, wind direction 90º

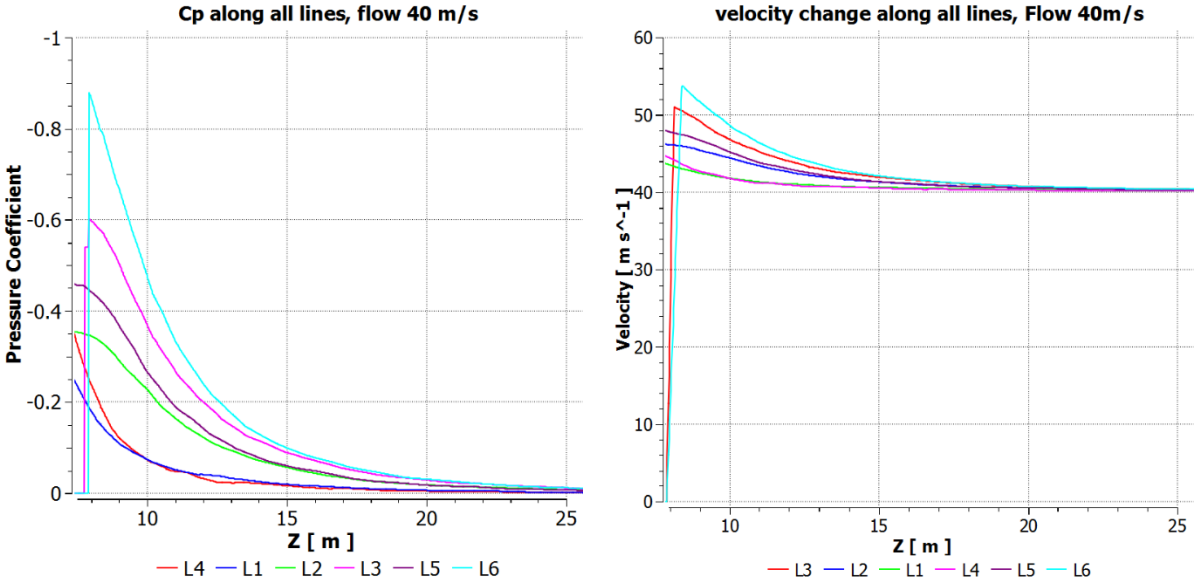


Fig. 4. 105. Pressure coefficient and velocity change along all Lines, wind direction 90º, 40m/s, windward, wind direction 90º

4.3.5. Pressure coefficients on a vertical cross section

Figure 4.110 illustrates the pressure coefficients on a cross sectional perpendicular plane on middle of the roof. Pressure coefficients are lowest (highest suction) on front overhang, on ridge and on right edge of the windward side, B. In addition, cross section plane shows highest suction, (Cp=-2.76), on the leeward side of the plane.

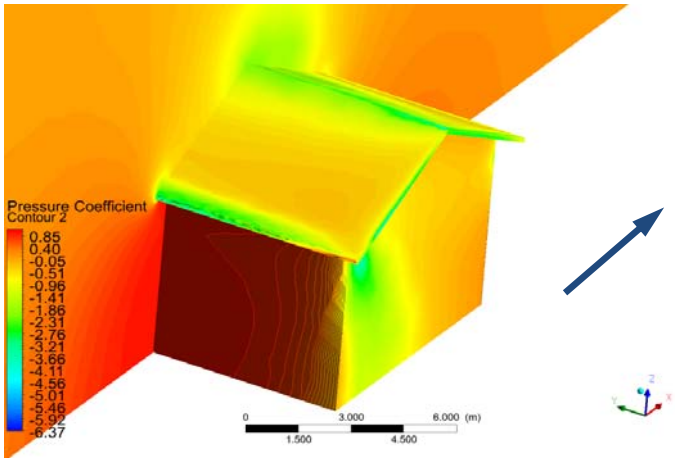


Fig. 4. 106. Pressure coefficient on transverse plane crosses middle of the building, slope 27º, wind direction 90º

To explore pressure coefficients changes across the sections of the building, five cross polylines 43 to 47, were created, Fig. 4.109.

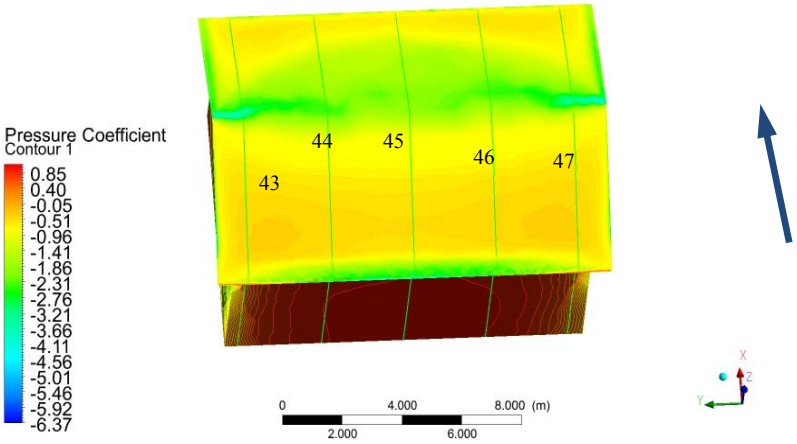


Fig. 4. 107. Pressure coefficient on roof with no panels with transverse 5 lines, slope27º, windward, wind direction 90º

It can be observed from Fig. 4.109 and 4.110 that pressure coefficients are similar on lines that have equal distance to the middle of the house. That applies for both roof without panels and roof with panels. As it can be deduced from the graphs in Figure 4.111, the pressure coefficients are decreasing on the windward side (negative coordinates) and are increasing on the leeward side (positive coordinates) in comparison with graphs on Figure 4.111 for roof without panels.

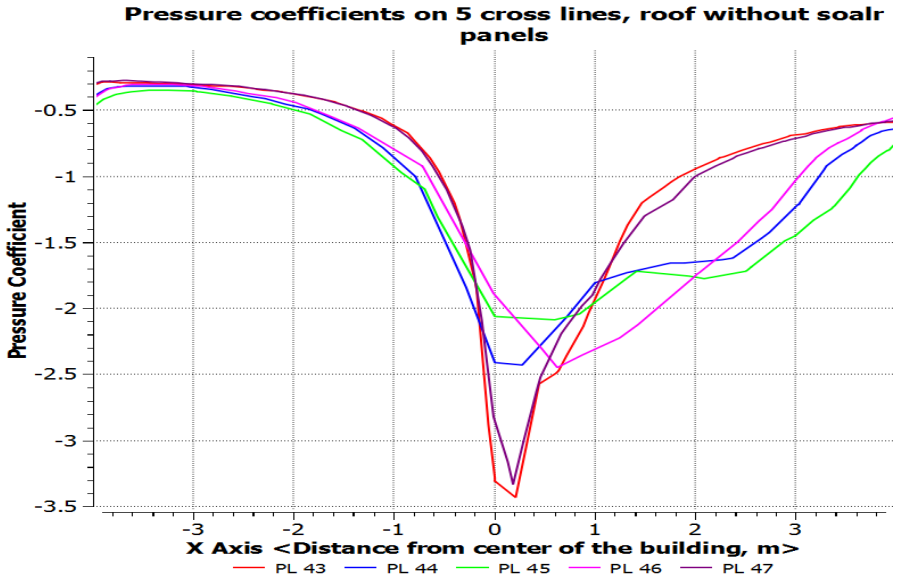


Fig. 4. 108. Pressure coefficient on roof without panels, 5 transverse lines, slope 27º, wind direction 90º,

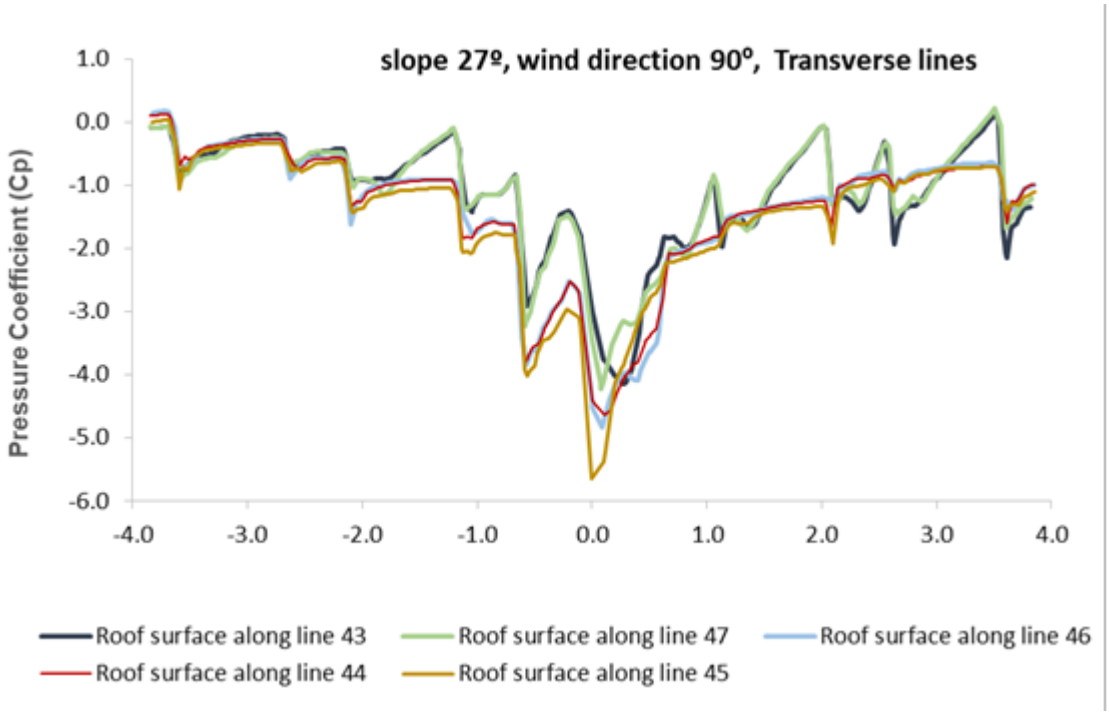


Fig. 4. 109. Pressure coefficient on roof with panels, 5 transverse Lines, slope 27º, wind direction 90º

Figure 4.112 shows the locations of polylines 1 and 19 on the windward side of the roof, used in the integration of pressure coefficients in the next windward tabulated results. Similar number are existing on the leeward side of the roof.

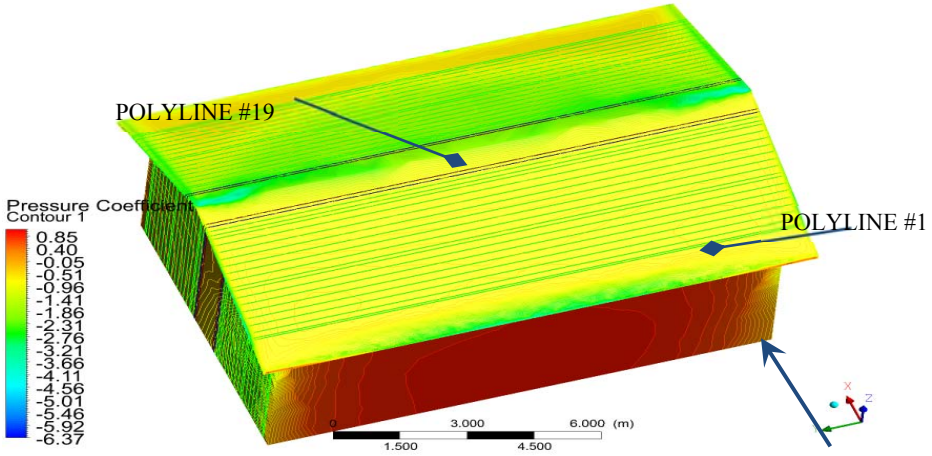


Fig. 4. 110. slope 27º, wind direction 90º,

A complete set of pressure coefficients recorded on the 38 polylines on roof with and without solar panels are represented in the Figs. 4.113 to Fig. 4.116 below. A review of these figures illustrate pressure coefficients on the windward side of the paneled roof and correspondent side on roof without panels, may deduce again that there is decrease in wind pressure on the windward side (Fig.4.113 and Fig. 4.114) and increase on the leeward (Fig.4.115 and Fig. 4.116). That is because the suction in Fig. 4.114 is much larger than the correspond side of roof without panels, Fig. 4.113, and nearly half of the lines have very small suction on roof without solar panels, versus moderated suction in Fig. 4.114.

Similar argument can be made for Fig. 4.115, which illustrates Cp on roof without solar panels, where most of the lines have moderate suction, versus lower suction on roof with panels.

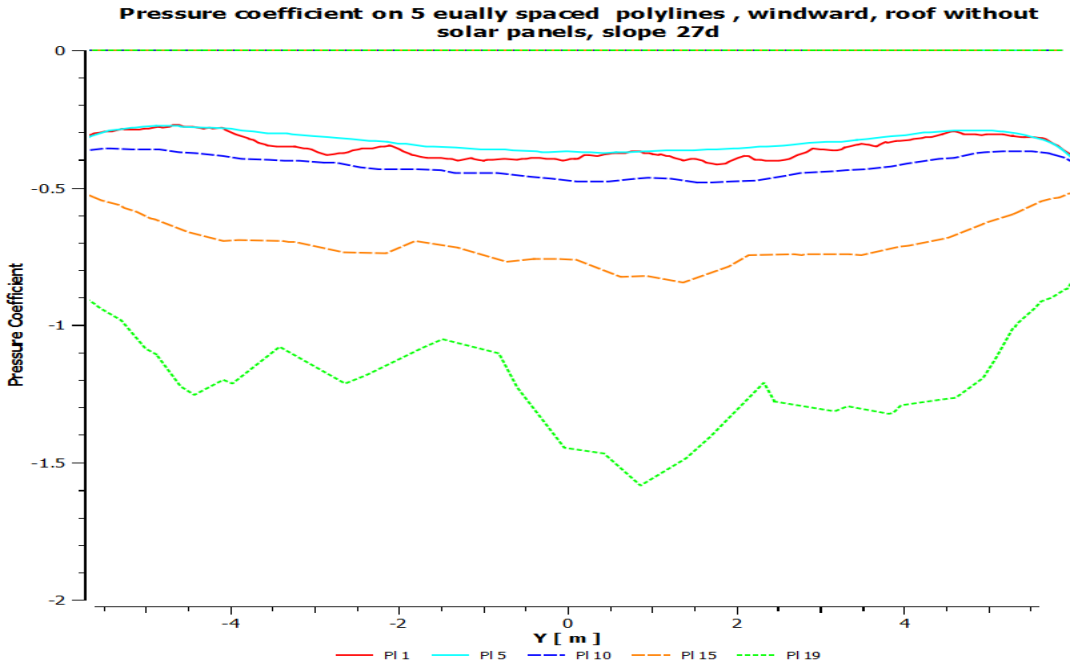


Fig. 4. 111. Pressure coefficient distributions all polylines on windward, roof without solar panels, slope 27º, wind direction 90º

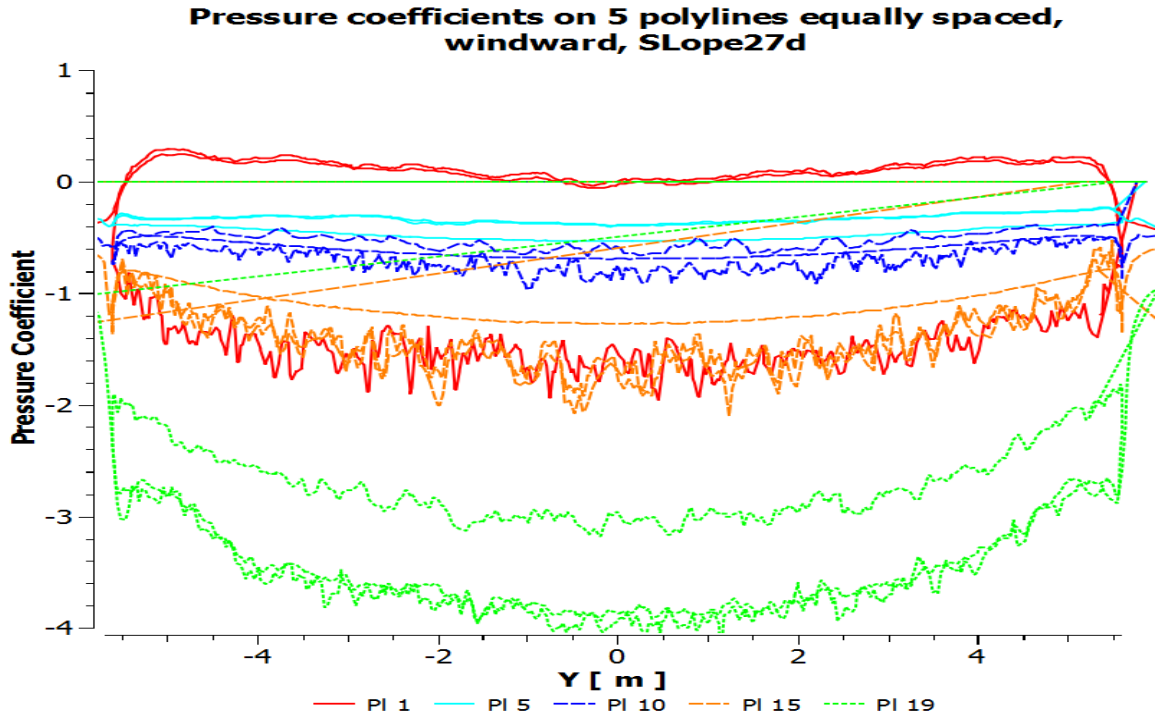


Fig. 4. 112. Pressure coefficient distribution on windward side of roof, all polylines, roof with panels, slope 27º, wind direction 90º

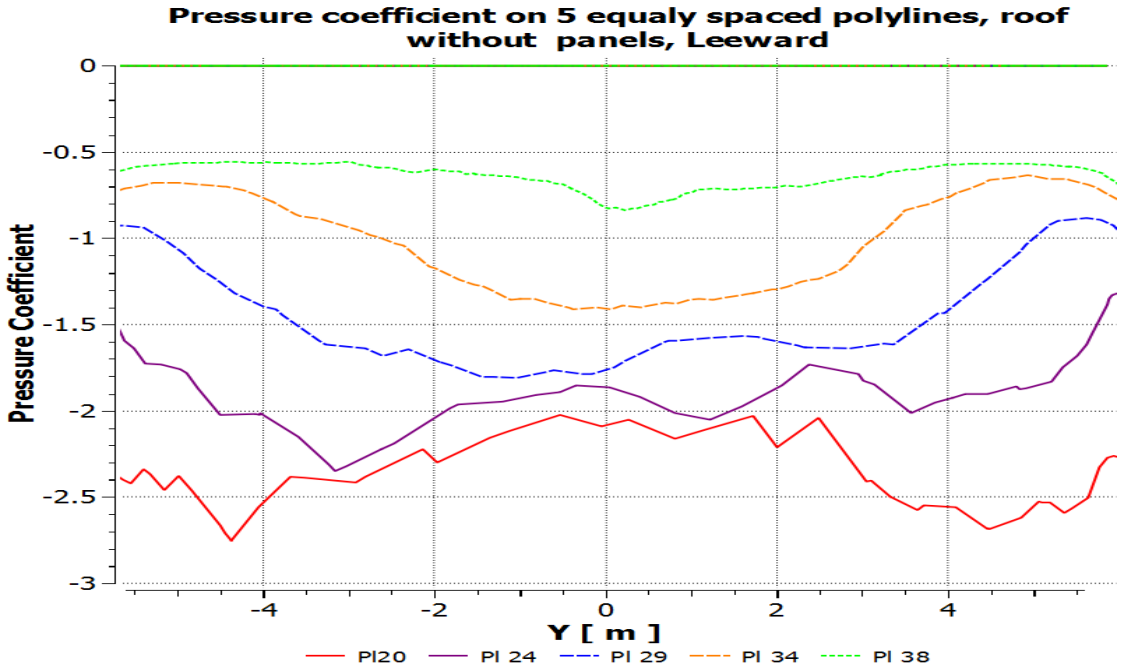


Fig. 4. 113. Pressure coefficient distributions all polylines on leeward, roof without solar panels, slope 27º, wind direction 90º

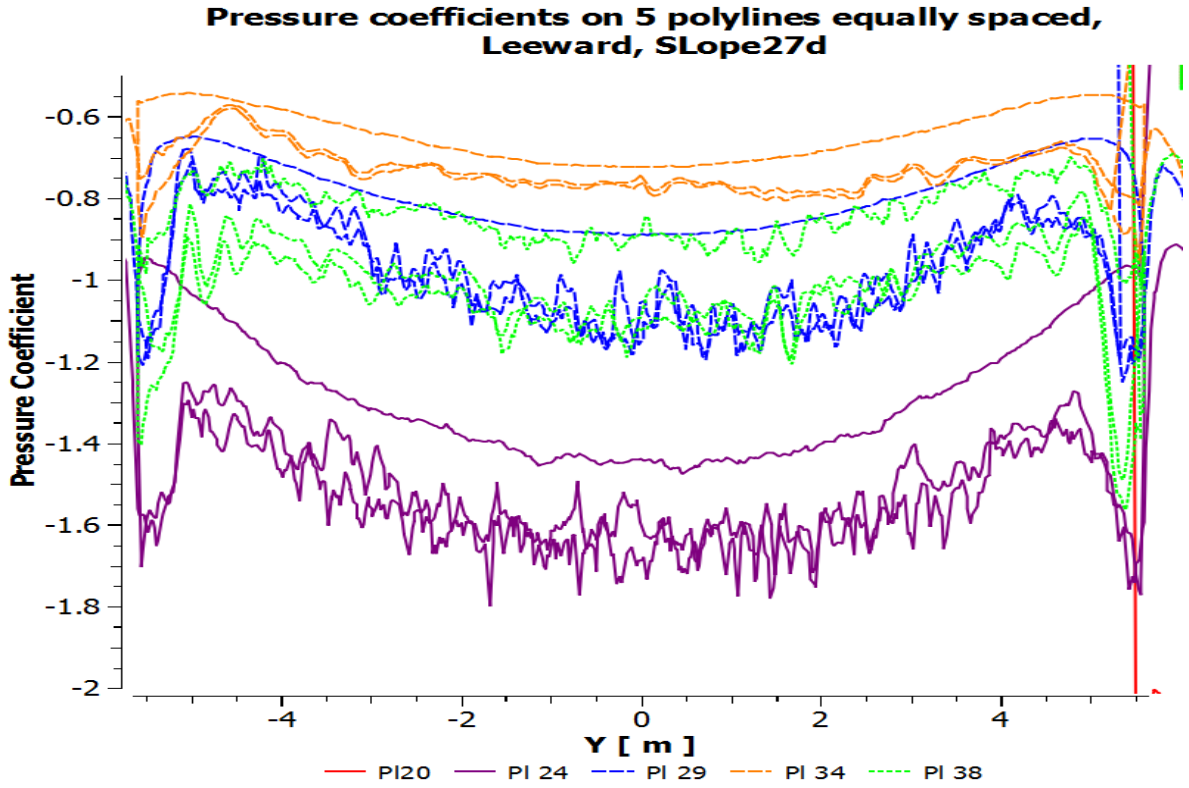


Fig. 4. 114. Pressure coefficient distributions all polylines on leeward, roof with solar panels, slope 27º, wind direction 90º

These results of integration of all these lines in Figs. 4.113 to 4.116 are illustrated in tables 4.6 to 4.10 below.

4.3.6. Net pressure coefficients on roof-solar panels system for slope 27º, for wind directions 90º, 45º and 0º, clearance 3" and spacing 2"

All the Cp values along all the polylines were integrated and presented in the tables 4.6 to 4.10 below. The integration is done for total pressure coefficients of the three surfaces which are top and bottom of the panels and the roof surface under the panels. The result of integrations on roof with panels can be compared with the results of integrations on corresponding lines on same slope and geometry bare roof.

Detailed results on the average pressure on top, bottom of panels, total pressure coefficients on roof under table and roof without panels, are reported for the three wind directions 90º, 45º and 0º.

The results show higher suction coefficient (Cp=-0.94) in windward for 90º wind direction for the roof with solar panels, versus (Cp=-0.51) for the roof without solar panels. However, for the leeward side surface, the pressure coefficients are higher on the roof with panels, (Cp=-1.14) than roof without solar panels, (Cp=-1.43). That means redistribution of wind pressure on either side of the roof, results in less resultant horizontal forces on the whole structure, and then more balanced structure, (Horizontal forces on either side of the roof, are closer to equilibrium).

In addition, the integration of Cp on all the polyline and the three surfaces in 45º wind direction and windward side gives moderately higher suction coefficient (Cp=-0.64) than roof without solar panels, (Cp=-0.54). However, in the leeward, the resultant Cp on the three surfaces is (Cp=-0.80) which is slightly lower than Cp on roof without solar panels (Cp=-0.92).

For 0º wind direction, the resultant of pressure coefficients gives (Cp=-0.40) which is lower than (Cp=-0.58) average pressure coefficients on roof without solar panels.

Table 4.6 and 4.7 present the results for wind direction 90º. The average suction on leeward side of roof without solar panels, (Cp=-1.43) (Table 4.7) is significantly larger than that on the windward side on roof without panels, (Cp=-0.51) (Table 4.6). However, for roof with panels, suction increased greatly on top of panels in windward side to(Cp= -0.93) which is very close to

the resultant (Cp=-0.94) (Table 4.6), while suction decreased on top of panels on the leeward side to (Cp=-1.13) which is very close to the resultant, (Cp=-1.14) (Table 4.7), as well, in this case. The very close value of pressure coefficients between top of the panels, and the resultant on roof, resulted from very close values between the bottom of the panels and roof surface under the panels, (Table 4.6 and Table 4.7).

Table 4. 6 . Pressure coefficients on roof without panels vs. total resultant pressure coefficients on roof under solar panels, slope 27º, wind direction 90º, windward side

Polylines	Cp Roof without solar panels	Cp Bottom of panels	Cp Roof under panels	Cp Top of panels	Cp Difference Top - Bottom	Cp Resultant	Resultant /Roof without solar panels
Pl1	-0.85	0.15	0.15	-1.09	-1.24	-1.09	1.28
Pl2	-0.37	-0.17	-0.08	-0.72	-0.89	-0.97	2.62
Pl3	-0.24	-0.43	-0.46	-0.47	-0.04	-0.5	2.08
Pl4	-0.23	-0.36	-0.46	-0.36	0	-0.46	2.00
Pl5	-0.25	-0.32	-0.47	-0.32	0	-0.47	1.88
Pl6	-0.28	-0.31	-0.48	-0.31	0	-0.48	1.71
Pl7	-0.32	-0.67	-0.50	-0.71	-0.04	-0.54	1.69
Pl8	-0.34	-0.60	-0.62	-0.65	-0.05	-0.67	1.97
P9	-0.36	-0.59	-0.58	-0.59	0	-0.58	1.61
Pl10	-0.39	-0.54	-0.60	-0.69	-0.15	-0.75	1.92
Pl11	-0.43	-1.05	-0.67	-1.08	-0.03	-0.7	1.63
Pl12	-0.48	-0.99	-0.75	-0.99	0	-0.75	1.56
Pl13	-0.53	-0.90	-0.85	-0.90	0	-0.85	1.60
Pl14	-0.58	-0.88	-0.96	-0.88	0	-0.96	1.66
Pl15	-0.66	-1.35	-1.13	-1.37	-0.02	-1.15	1.74
Pl16	-0.74	-1.53	-1.40	-1.55	-0.02	-1.42	1.92
Pl17	-0.79	-1.49	-1.35	-1.51	-0.02	-1.37	1.73
Pl18	-0.87	-1.49	-1.58	-1.51	-0.02	-1.6	1.84
Pl19	-0.92	-1.56	-2.15	-1.89	-0.33	-2.48	2.70
Ave	-0.51	-0.78	-0.79	-0.93	-0.15	-0.94	1.84
STD	0.23	0.54	0.54	0.46	0.34	0.51	2.22
COV	46	70	69	50	225	54	18

Tables 4.6 to 4.6 show the calculated total pressure coefficients on the three surfaces (top and bottom of the panels and the roof surface under the panels), in comparison with the Cp on a

corresponding roof without solar panels by taking ratios of total pressure coefficient over the corresponding pressure coefficients on the roof without solar panels.

Table 4. 7 . Pressure coefficients on roof without panels vs. total resultant pressure coefficients on roof under solar panels, slope 27º, wind direction 90º, Leeward side

Polyline	Cp Roof without solar panels	Cp Bottom of panels	Cp Roof under panels	Cp Top of panels	Cp Difference Top - Bottom	Cp Resultant	Resultant /Roof without solar panels
Pl20	-1.80	-2.1	-2.35	-2.77	-0.67	-3.02	1.68
Pl21	-1.78	-2.07	-2.08	-2.54	-0.47	-2.55	1.43
Pl22	-1.74	-2.01	-2.03	-1.98	0.03	-2	1.15
Pl23	-1.70	-1.89	-1.9	-1.69	0.2	-1.7	1.00
Pl24	-1.66	-1.4	-1.43	-1.23	0.17	-1.26	0.76
Pl25	-1.63	-1.36	-1.36	-1.08	0.28	-1.08	0.66
Pl26	-1.60	-1.25	-1.24	-0.96	0.29	-0.95	0.59
Pl27	-1.56	-1.16	-1.15	-0.92	0.24	-0.91	0.58
Pl28	-1.53	-1.11	-1.11	-0.87	0.24	-0.87	0.57
Pl29	-1.50	-0.97	-0.97	-0.81	0.16	-0.81	0.54
Pl30	-1.46	-0.85	-0.85	-0.81	0.04	-0.81	0.55
Pl31	-1.42	-0.81	-0.82	-0.79	0.02	-0.8	0.56
Pl32	-1.35	-0.99	-0.99	-0.79	0.2	-0.79	0.59
Pl33	-1.33	-0.88	-0.88	-0.78	0.1	-0.78	0.59
Pl34	-1.31	-0.93	-0.93	-0.77	0.16	-0.77	0.59
Pl35	-1.14	-0.77	-0.77	-0.77	0	-0.77	0.68
Pl36	-1.08	-0.74	-0.73	-0.7	0.04	-0.69	0.64
Pl37	-1.01	-1.27	-1.27	-0.72	0.55	-0.72	0.71
PL38	-0.97	-1	-1	-0.82	0.18	-0.82	0.85
Ave	-1.43	-1.23	-1.25	-1.13	0.11	-1.14	0.78
STD	0.28	0.44	0.48	0.62	0.27	0.66	0.31
COV	0.19	0.36	0.38	0.55	2.53	0.58	0.40

Tables 8 and 9 summarize the pressure coefficients for wind direction 45º. The average suction on the leeward, (Cp=-0.92) (Table 4.9) is much larger than that on windward on roof without panels, (Cp=-0.53) (Table 4.8). However, for roof with panels, suction increased on top of panels in windward side to (Cp=-0.63) and in resultant to (Cp=-0.67) (Table 4.8). Nonetheless, the suction reduced on top of panels in leeward side to (Cp=-0.82) and in resultant, (Cp=-0.83) (Table 4.9).

Table 4. 8 . Pressure coefficients on roof without panels vs. total resultant pressure coefficients on roof under solar panels, slope 27º, wind direction 45º, windward side

Polylines	Cp No panels	Pressure coefficients top of panels	Pressure coefficients roof under panels	Pressure coefficients bottom of panels	Pressure coefficients difference top -bottom	Total pressure coefficients on roof	Ratio of total pressure coefficients on roof / roof without solar panels
Pl1	-0.36	-0.68	0.22	0.22	-0.90	-0.68	1.89
Pl2	-0.36	-0.46	-0.82	-0.8	0.34	-0.48	1.33
Pl3	-0.37	-0.4	-0.52	-0.5	0.10	-0.42	1.14
Pl4	-0.38	-0.4	-0.44	-0.43	0.03	-0.41	1.08
Pl5	-0.4	-0.4	-0.34	-0.33	-0.07	-0.41	1.03
Pl6	-0.42	-0.41	-0.26	-0.25	-0.16	-0.42	1.00
Pl7	-0.43	-0.43	-0.74	-0.73	0.30	-0.44	1.02
Pl8	-0.45	-0.46	-0.65	-0.57	0.11	-0.54	1.20
P9	-0.45	-0.42	-0.48	-0.48	0.06	-0.42	0.93
Pl10	-0.46	-0.46	-0.54	-0.38	-0.08	-0.62	1.35
Pl11	-0.48	-0.5	-1.03	-0.97	0.47	-0.56	1.17
Pl12	-0.49	-0.55	-0.85	-0.84	0.29	-0.56	1.14
Pl13	-0.51	-0.61	-0.75	-0.74	0.13	-0.62	1.22
Pl14	-0.57	-0.66	-0.66	-0.65	-0.01	-0.67	1.18
Pl15	-0.65	-0.75	-0.97	-0.96	0.21	-0.76	1.17
Pl16	-0.69	-0.86	-1.14	-1.06	0.20	-0.94	1.36
Pl17	-0.77	-0.89	-0.95	-0.94	0.05	-0.9	1.17
Pl18	-0.85	-1.15	-1.10	-0.84	-0.31	-1.41	1.66
Pl19	-0.9	-1.41	-2.21	-2.19	0.78	-1.43	1.59
Ave	-0.53	-0.63	-0.75	-0.71	0.08	-0.67	1.26
STD	0.17	0.28	0.48	0.48	0.34	0.31	0.24
COV	-0.32	0.45	0.65	0.67	4.18	0.46	0.12

Table 4. 9 . Pressure coefficients on roof without panels vs. total resultant pressure coefficients on roof under solar panels, slope 27º, wind direction 45º, leeward side

Polyline	Cp roof No panels	Pressure coefficients top of panels	Pressure coefficients roof under panels	Pressure coefficients bottom of panels	Pressure coefficients difference top -bottom	Total pressure coefficients on roof	Ratio of total pressure coefficients on roof / roof without solar panels
Pl20	-1.33	-1.72	-1.73	-1.75	0.03	-1.7	1.28
Pl21	-1.31	-1.56	-1.53	-1.51	-0.05	-1.58	1.21
Pl22	-1.23	-1.22	-1.24	-1.26	0.04	-1.2	0.98
Pl23	-1.17	-1	-1.14	-1.13	0.13	-1.01	0.86
Pl24	-1.08	-0.9	-1.33	-1.32	0.42	-0.91	0.84
Pl25	-1.04	-0.81	-1.06	-1.05	0.24	-0.82	0.79
Pl26	-0.98	-0.73	-0.94	-0.93	0.20	-0.74	0.76
Pl27	-0.94	-0.7	-0.81	-0.80	0.10	-0.71	0.76
Pl28	-0.90	-0.67	-0.66	-0.65	-0.02	-0.68	0.76
Pl29	-0.87	-0.65	-1.01	-0.97	0.32	-0.69	0.79
Pl30	-0.84	-0.64	-0.65	-0.64	0	-0.65	0.77
Pl31	-0.83	-0.65	-0.61	-0.60	-0.05	-0.66	0.80
Pl32	-0.80	-0.62	-1.02	-0.99	0.37	-0.65	0.81
Pl33	-0.76	-0.61	-0.85	-0.84	0.23	-0.62	0.82
Pl34	-0.72	-0.61	-0.75	-0.74	0.13	-0.62	0.86
Pl35	-0.69	-0.61	-0.65	-0.64	0.03	-0.62	0.90
Pl36	-0.67	-0.63	-0.56	-0.55	-0.08	-0.64	0.96
Pl37	-0.65	-0.65	-1.22	-1.21	0.56	-0.66	1.02
PL38	-0.65	-0.68	-1.03	-1.02	0.34	-0.69	1.06
Ave	-0.92	-0.82	-0.99	-0.98	0.15	-0.83	0.90
STD	0.22	0.33	0.32	0.33	0.18	0.32	0.15
COV	-0.24	0.40	0.33	0.33	1.18	0.39	0.17

For direction 0º, shown in Table 4.10, the average suction nearly remained the same for all roof without panels, (Cp=-0.34) (Table 4.10), on roof with solar panels on top of panels, (Cp=-0.35), (Table 4.10) which is the same as resultant of wind pressure coefficients, (Cp=-0.35), (Table 4.10).

Table 4. 10 . Pressure coefficients on roof without panels vs. total resultant pressure coefficients on roof under solar panels, slope 27º, wind direction 0º

Polylines	Cp roof No panels	Pressure coefficients top of panels	Pressure coefficients on roof under panels	Pressure coefficients bottom of panels	Pressure coefficients difference top -bottom	Total pressure coefficients on roof	Ratio of total pressure coefficients on roof / roof without panels
Pl1	-0.33	-0.33	-0.35	-0.35	0.02	-0.33	1.00
Pl2	-0.33	-0.33	-0.37	-0.37	0.04	-0.33	1.00
Pl3	-0.33	-0.33	-0.42	-0.42	0.09	-0.33	1.00
Pl4	-0.36	-0.34	-0.42	-0.42	0.08	-0.34	0.94
Pl5	-0.36	-0.34	-0.42	-0.42	0.08	-0.34	0.94
Pl6	-0.36	-0.34	-0.42	-0.42	0.08	-0.34	0.94
Pl7	-0.36	-0.35	-0.42	-0.42	0.07	-0.35	0.97
Pl8	-0.35	-0.35	-0.38	-0.38	0.03	-0.35	1.00
P9	-0.35	-0.35	-0.38	-0.38	0.03	-0.35	1.00
Pl10	-0.35	-0.35	-0.39	-0.39	0.04	-0.35	1.00
Pl11	-0.35	-0.35	-0.43	-0.43	0.08	-0.35	1.00
Pl12	-0.35	-0.35	-0.43	-0.43	0.08	-0.35	1.00
Pl13	-0.34	-0.35	-0.43	-0.43	0.08	-0.35	1.03
Pl14	-0.34	-0.35	-0.43	-0.43	0.08	-0.35	1.03
Pl15	-0.34	-0.35	-0.42	-0.42	0.07	-0.35	1.03
Pl16	-0.34	-0.35	-0.39	-0.39	0.04	-0.35	1.03
Pl17	-0.34	-0.35	-0.38	-0.38	0.03	-0.35	1.03
Pl18	-0.34	-0.35	-0.38	-0.38	0.03	-0.35	1.03
Pl19	-0.33	-0.36	-0.37	-0.37	0.01	-0.36	1.09
Ave	-0.34	-0.35	-0.40	-0.40	0.06	-0.35	1.00
STD	0.01	0.01	0.03	0.03	0.03	0.01	0.03
COV	-0.03	-0.02	-0.06	-0.06	0.46	-0.02	0.03

4.3.7. Conclusions

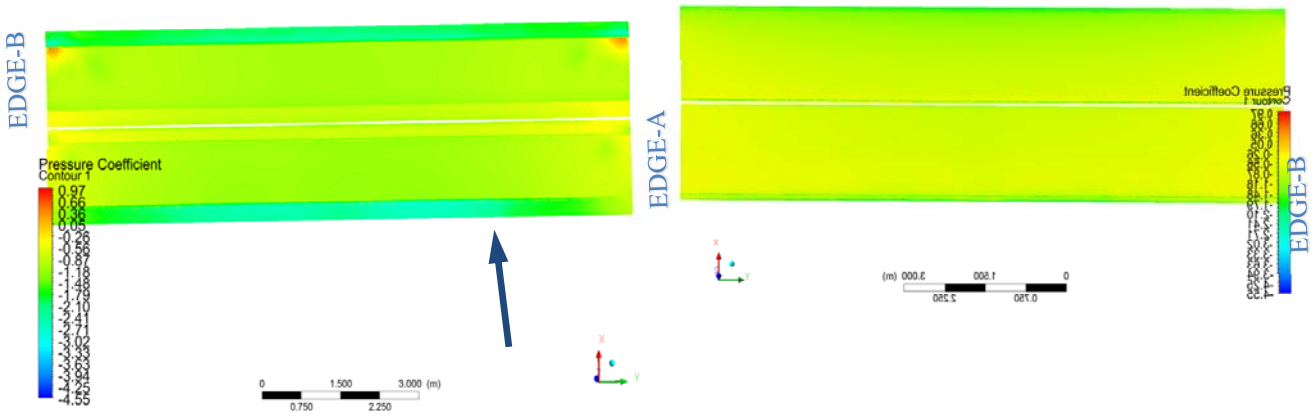
- Like 35º slope, there the total suction on gable roofs with solar panels, increased greatly for wind direction 90º on the windward side from that on roofs without solar panels. while increase much less for wind direction 45º. Nonetheless, suction increase very slightly on the windward in wind direction 0º. On the other hand, the increase of suction for this slope, 27º, is less that for 35º slope when comparing the increase with corresponding suction on similar slope roof without solar panels.
- Like the 35º roof slope, there is large decrease in the total suction (or wind load) for 90º wind direction on leeward surfaces of the roof mounted solar panels, while this suction decreased moderately for wind direction 45º, and slightly decreased for wind direction 0º.

- In the same manner as for slope 35º, the increase in suction on windward and the decrease in suction on the leeward surfaces of the roofs with solar panels, result in redistribution of wind pressure coefficients where greater balance of wind pressure (wind forces) is achieved on the gable roof with solar panels. In other words, horizontal resultant wind forces on these roofs become smaller, and the force reduction in suction is highest for wind direction 90º, while the smallest suction is for wind direction 0º, and the reductions can be calculated from the tables above, 4.6 to 4.10, for these three wind directions.

4.4. Effects of wind directions on solar panel arrays, 2” spacing and 3” roof clearance installed on 15º inclined roofs

4.4.1. Pressure contours distributions for wind direction 90º

The effect of wind on pressure coefficients evaluation on the 3 surfaces are presented hereafter. The following three figures Fig. 4.117, Fig. 4.118 and Fig. 4.119 show distribution of pressure coefficients on bottom and top of the solar panel arrays, on top of the roof with solar panels and on roof under the solar panels respectively. Bottom of the solar panels is flipped upside down with keeping the axes directions in exact similar direction.



(a) **(b)**

Fig. 4. 115. Pressure coefficients on (a) Bottom of the solar panels, (b) Top of the solar panels, windward, slope 15º, wind direction 90º

When comparing the two Cp contours in Figs. 4.117 (a) and (b), it was noticed that the pressure distribution on top of the panels, is a quite different from that on bottom of the panels, where suction coefficients under the panels are much higher, (Cp=-3.33 to -0.26), than top of the panels, (Cp=-1.45 to -0.26). However, when comparing, Fig. 4.117 (a) and Fig. 4.119 windward, it can be noticed easily that distribution of pressure coefficients on bottom of the panels, and on the roof under panels are very similar.

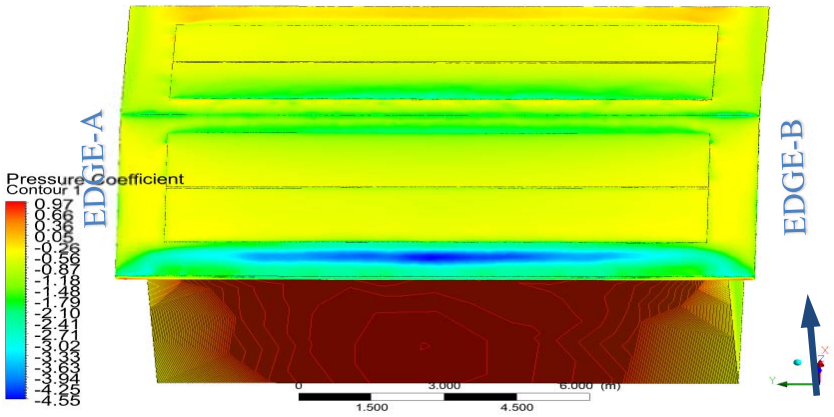


Fig. 4. 116. Depicts pressure coefficients on top surface of the solar panels in the windward direction, windward, slope 15º, wind direction 90º

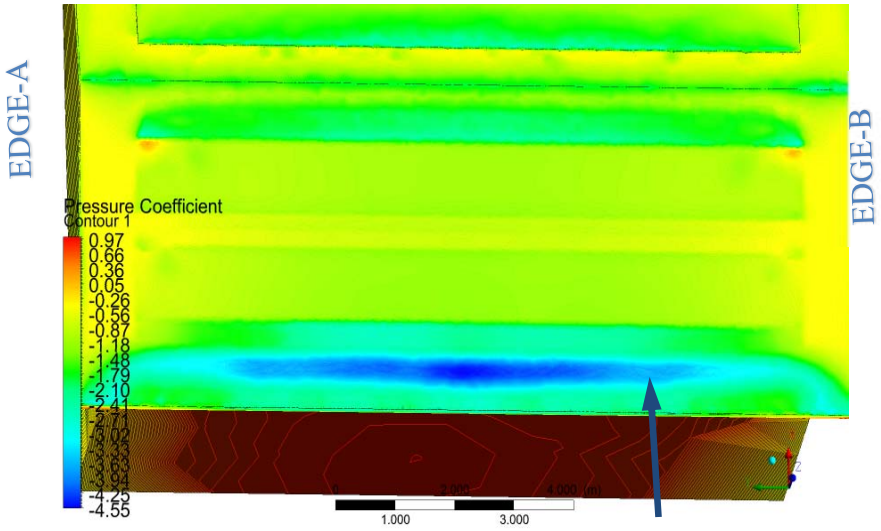


Fig. 4. 117. A cut off shows pressure coefficients on roof under solar panels, windward, slope 15º, wind direction 90º

On the other hand, to reduce length of this chapter and to avoid repeating similar steps for the wind direction 15, all the associated paragraphs and explanations, from 4.4.3 to 4.4.5. were moved to the appendix C. That includes all graphs, pressure coefficients distribution, flow-interaction, and flow distribution on the 6 perpendicular lines.

4.4.2. Net pressure coefficients roof-solar panels system for slope 15º, wind directions 90º, 45º, 0º

A very accurate way to evaluate the effects of wind pressure on roof mounted solar panels for the roof slope 15º, and 3 wind directions 0º, 45º and 90º, is to calculate total pressure coefficients on the 3 surfaces which are top and bottom of the panels and the roof surface under the panels, then find out the summation of Cp on those 3 surfaces and compare the results with Cp on a corresponding roof without solar panels.

Tables 4.11 to 4. 15 show calculated total pressure coefficients on the 3 surfaces (top and bottom of the panels and the roof surface under the panels), and those total pressure coefficients are compared with Cp on a corresponding roof without solar panels by taking ratios of total pressure coefficient over the corresponding pressure coefficients on the roof without solar panels.

Tables 4.11 and 4.12 illustrate the results for wind direction 90º where average suction on leeward side of roof without solar panels, (Cp=-0.68) (Table 4.12) is lower than on windward on roof without panels, (Cp=-0.72) (Table 4.11). However, for roof with panels, suction increased slightly on top of panels in windward side to (Cp=-0.78) and the same (Cp=-0.78) in resultant (Table 4.10). Similarly, suction increased on top of panels in leeward side to (Cp=-0.88) and the same in resultant, (Cp=-0.88) (Table 4.4).

Table 4. 11 . Pressure coefficients on roof without panels vs. total resultant pressure coefficients on roof under solar panels, slope 15º, wind direction 90º, windward side

Polylines	Cp Roof without solar panels	Cp Top of panels	Cp Roof under panels	Cp Bottom of panels	Cp Difference Top -Bottom	Cp Resultant	Resultant /Roof without solar panels
Pl1	-1.38	-0.81	-1.95	-1.95	1.14	-0.81	0.59
Pl2	-0.82	-0.58	-1.9	-1.9	1.32	-0.58	0.71
Pl3	-0.61	-0.58	-1.21	-1.21	0.63	-0.58	0.95
Pl4	-0.54	-0.61	-1.2	-1.2	0.59	-0.61	1.13
Pl5	-0.53	-0.66	-1.19	-1.19	0.53	-0.66	1.25
Pl6	-0.53	-0.67	-1.18	-1.18	0.51	-0.67	1.26
Pl7	-0.57	-0.66	-1.18	-1.18	0.52	-0.66	1.16
Pl8	-0.54	-0.73	-0.94	-0.94	0.21	-0.73	1.35
Pl9	-0.57	-0.57	-1.02	-0.96	0.39	-0.63	1.11
Pl10	-0.60	-0.64	-1.03	-1.01	0.37	-0.66	1.16
Pl11	-0.63	-0.7	-1.18	-1.18	0.48	-0.7	1.17
Pl12	-0.66	-0.73	-1.23	-1.23	0.50	-0.73	1.16
Pl13	-0.71	-0.79	-1.24	-1.24	0.45	-0.79	1.20
Pl14	-0.77	-0.88	-1.23	-1.23	0.35	-0.88	1.24
Pl15	-0.84	-1.01	-1.16	-1.17	0.16	-1	1.30
Pl16	-0.92	-1.2	-1.92	-1.92	0.72	-1.2	1.43
Pl17	-0.96	-1.41	-2.05	-2.05	0.64	-1.41	1.53
Cp	-0.72	-0.78	-1.30	-1.30	0.52	-0.78	1.09
STD	0.22	0.23	0.36	0.37	0.29	0.23	0.23
Cove	0.31	0.30	0.28	0.28	0.56	0.29	0.21

Table 4. 12 . Pressure coefficients on roof without panels vs. total resultant pressure coefficients on roof under solar panels, slope 15º, wind direction 90º, leeward side

Polylines	Cp Roof without solar panels	Cp Top of panels	Cp Roof under panels	Cp Bottom of panels	Cp Difference Top - Bottom	Cp Resultant	Resultant /Roof without solar panels
Pl20	-1.10	-2.21	-0.56	-0.57	-1.64	-2.2	2.00
Pl21	-0.98	-1.8	-0.62	-0.63	-1.17	-1.79	1.83
Pl22	-0.90	-1.6	-0.59	-0.6	-1.00	-1.59	1.77
Pl23	-0.85	-1.41	-0.58	-0.59	-0.82	-1.4	1.65
Pl24	-0.77	-1.07	-0.6	-0.6	-0.47	-1.07	1.39
Pl25	-0.72	-0.82	-0.6	-0.6	-0.22	-0.82	1.14
Pl26	-0.68	-0.7	-0.56	-0.55	-0.15	-0.71	1.04
Pl27	-0.66	-0.64	-0.55	-0.55	-0.09	-0.64	0.97
Pl28	-0.64	-0.6	-0.59	-0.59	-0.01	-0.6	0.94
Pl29	-0.62	-0.64	-0.55	-0.55	-0.09	-0.64	1.03
Pl30	-0.61	-0.55	-0.57	-0.57	0.02	-0.55	0.90
Pl31	-0.58	-0.49	-0.56	-0.56	0.07	-0.49	0.84
Pl32	-0.56	-0.49	-0.57	-0.57	0.08	-0.49	0.88
Pl33	-0.55	-0.49	-0.59	-0.59	0.10	-0.49	0.89
Pl34	-0.53	-0.49	-0.55	-0.55	0.06	-0.49	0.92
Pl35	-0.52	-0.55	-0.56	-0.51	-0.04	-0.6	1.15
Pl36	-0.49	-0.59	-0.74	-0.74	0.15	-0.59	1.20
Pl37	-0.48	-0.61	-0.73	-0.73	0.12	-0.61	1.27
Cp	-0.68	-0.88	-0.59	-0.59	-0.28	-0.88	1.29
STD	0.18	0.52	0.06	0.06	0.52	0.52	0.36
COV	0.26	0.60	0.09	0.10	1.84	0.59	0.28

Tables 4.13 and 4.14 summarize the results for wind direction 45º. The average suction on the leeward, (Cp=-0.67) (Table 4.14) is larger than that on windward on roof without panels, (Cp=-0.55) (Table 4.13). However, suction increased on top of panels in windward side to (Cp=-0.61) and the same in resultant to (Cp=-0.61) (Table 4.13). Similarly, the suction on top of panels in leeward side increased to (Cp=-0.78) and in resultant, (Cp=-0.81) (Table 4.14).

Table 4. 13 . Pressure coefficients on roof without panels vs. total resultant pressure coefficients on roof under solar panels, slope 15º, wind direction 45º, windward side

Polylines	Cp Roof without solar panels	Cp Top of panels	Cp Roof under panels	Cp Bottom of panels	Cp Difference Top - Bottom	Cp Resultant	Resultant /Roof without solar panels
Pl1	-0.57	-0.9	-0.34	-0.34	-0.56	-0.90	1.58
Pl2	-0.53	-0.72	-0.7	-0.70	-0.02	-0.72	1.36
Pl3	-0.51	-0.58	-0.73	-0.73	0.15	-0.58	1.14
Pl4	-0.5	-0.5	-0.67	-0.67	0.17	-0.50	1.00
Pl5	-0.5	-0.5	-0.6	-0.60	0.10	-0.50	1.00
Pl6	-0.5	-0.5	-0.53	-0.53	0.03	-0.50	1.00
Pl7	-0.48	-0.51	-0.51	-0.49	-0.02	-0.53	1.10
Pl8	-0.49	-0.49	0.72	0.73	-1.22	-0.50	1.02
Pl9	-0.5	-0.46	-0.64	-0.64	0.18	-0.46	0.92
Pl10	-0.50	-0.45	-0.53	-0.56	0.11	-0.42	0.84
Pl11	-0.50	-0.48	-1.12	-1.12	0.64	-0.48	0.96
Pl12	-0.52	-0.52	-1.04	-1.04	0.52	-0.52	1.00
Pl13	-0.55	-0.56	-1	-1	0.44	-0.56	1.02
Pl14	-0.58	-0.61	-0.96	-0.96	0.35	-0.61	1.05
Pl15	-0.63	-0.67	-0.92	-0.92	0.25	-0.67	1.06
Pl16	-0.68	-0.9	-1.45	-1.45	0.55	-0.90	1.32
Pl17	-0.74	-1.02	-1.38	-1.38	0.36	-1.02	1.38
Cp	-0.55	-0.61	-0.73	-0.73	0.12	-0.61	1.11
STD	0.07	0.17	0.48	0.49	0.44	0.18	0.19
COV	-0.13	-0.29	-0.66	-0.67	3.72	-0.29	0.17

Table 4. 14 . Pressure coefficients on roof without panels vs. total resultant pressure coefficients on roof under solar panels, slope 15º, wind direction 45º, leeward side

Polylines	Cp Roof without solar panels	Cp Top of panels	Cp Roof under panels	Cp Bottom of panels	Cp Difference Top - Bottom	Cp Resultant	Resultant /Roof without solar panels
Pl20	-0.98	-1.65	-0.38	-0.38	-1.27	-1.65	1.68
Pl21	-0.89	-1.16	-0.84	-0.84	-0.32	-1.16	1.3
Pl22	-0.81	-0.9	-0.67	-0.67	-0.23	-0.9	1.11
Pl23	-0.74	-0.75	-0.63	-0.63	-0.12	-0.75	1.01

Pl24	-0.68	-0.71	-0.59	-0.59	-0.12	-0.71	1.04
Pl25	-0.65	-0.69	-0.55	-0.55	-0.14	-0.69	1.06
Pl26	-0.63	-0.67	-0.7	-0.52	-0.15	-0.85	1.35
Pl27	-0.62	-0.66	-0.76	-0.76	0.1	-0.66	1.06
Pl28	-0.61	-0.66	-0.69	-0.69	0.03	-0.66	1.08
Pl29	-0.62	-0.65	-0.65	-0.65	0	-0.65	1.05
Pl30	-0.61	-0.66	-1.06	-1.06	0.4	-0.66	1.08
Pl31	-0.61	-0.66	-0.94	-0.94	0.28	-0.66	1.08
Pl32	-0.61	-0.66	-0.89	-0.89	0.23	-0.66	1.08
Pl33	-0.61	-0.67	-0.84	-0.84	0.17	-0.67	1.1
Pl34	-0.61	-0.69	-0.79	-0.79	0.1	-0.69	1.13
Pl35	-0.62	-0.7	-1.03	-0.73	0.03	-1	1.61
Pl36	-0.62	-0.75	-1.06	-1.06	0.31	-0.75	1.21
Pl37	-0.62	-0.78	-1.1	-1.1	0.32	-0.78	1.26
Cp	-0.67	-0.78	-0.79	-0.76	-0.02	-0.81	1.68
STD	0.10	0.24	0.19	0.19	0.35	0.24	0.21
COV	-0.15	-0.30	-0.24	-0.25	-17.66	-0.29	0.13

However, for direction 0º, shown in Table 4.15, average suction remained quite the same for all roof without panels, (Cp=-0.32) (Table 4.15), top of panels, (Cp=-0.30), (Table 4.15) and resultant of wind pressure on roof with solar panels, (Cp=-0.30), (Table 4.15).

Table 4. 15 . Pressure coefficients on roof without panels vs. total resultant pressure coefficients on roof under solar panels, slope 15º, wind direction 0º

Polylines	Cp roof without solar panels	Cp Top of panels	Cp Roof under panels	Cp Bottom of panels	Cp Difference Top - Bottom	Cp Resultant	Ratio of resultant / roof without solar panels
Pl1	-0.31	-0.31	-0.34	-0.34	0.03	-0.31	1.00
Pl2	-0.31	-0.31	-0.41	-0.40	0.09	-0.32	1.03
Pl3	-0.31	-0.31	-0.42	-0.42	0.11	-0.31	1.00
Pl4	-0.32	-0.31	-0.42	-0.42	0.11	-0.31	0.97
Pl5	-0.32	-0.31	-0.43	-0.42	0.11	-0.32	1.00
Pl6	-0.32	-0.31	-0.43	-0.42	0.11	-0.32	1.00
Pl7	-0.32	-0.31	-0.42	-0.42	0.11	-0.31	0.97
Pl8	-0.32	-0.29	-0.38	-0.38	0.09	-0.29	0.91
Pl9	-0.33	-0.29	-0.39	-0.39	0.10	-0.29	0.88
Pl10	-0.33	-0.29	-0.41	-0.41	0.12	-0.29	0.88

Pl11	-0.33	-0.29	-0.46	-0.46	0.17	-0.29	0.88
Pl12	-0.33	-0.27	-0.47	-0.47	0.20	-0.27	0.82
Pl13	-0.33	-0.29	-0.45	-0.45	0.16	-0.29	0.88
Pl14	-0.33	-0.29	-0.45	-0.45	0.16	-0.29	0.88
Pl15	-0.34	-0.29	-0.45	-0.45	0.16	-0.29	0.85
Pl16	-0.34	-0.33	-0.37	-0.37	0.04	-0.33	0.97
Cp	-0.32	-0.30	-0.42	-0.42	0.12	-0.30	0.93
SD	0.01	0.01	0.04	0.04	0.05	0.02	0.07
COV	0.03	0.05	0.08	0.08	0.39	0.05	0.07

4.4.3. Conclusions

- Different from the other 2 slopes, suction (or wind load) increased on the leeward of the roof with solar panels, for both wind directions 45º and 90º. This increase in suction makes the total suction on the leeward, the largest on either side of the roof, for both wind directions, 45º and 90º.

- Unlike the other 2 slopes, the total suction increased slightly on windward side of the roof (much less than on the leeward side in comparison with the roof without panels) with solar panels, from those on roof without solar panel, for both wind directions 45º and 90º.

- On the other hand, dislike the other two slopes, the largest suction on roof without panels is on the windward side for wind direction 45º. However, when panels are installed on the roof, the total suction increased faster on the leeward side of the roof, and the suction becomes largest on the leeward side. Nonetheless, the largest suction on roof without panels is on the leeward side for wind direction 90º. However, when panels are installed on the roof, the total suction on the roof increased faster on the leeward side of the roof, and the total suction remained the larger on the leeward side.

- Nevertheless, like the other 2 slopes; there is very slight decrease in suction from on roof with solar panels for 0º wind direction, from that on roof without solar panels. However,

wind pressure coefficients (wind loads) on the gable roof for wind direction 0º is the least between the 3 studied directions.

- Subsequently, the larger increase in suction on the leeward of roofs with solar panels, results in higher total horizontal wind forces on the whole roof and then less balance of the roof, for slope 15º.

4.5. Conclusions on wind effects on roof mounted solar panels, due to change in slopes and wind directions

According to the analyses above on different slopes, 15º, 27º and 35º and different wind directions, 0 º, 45 º and 90 º, the following is concluded,

- There are large reductions in suction (wind pressure or load) on the gable roofs due installation of solar panels, in comparison with roof without solar panels, for both slopes 27º and 35º slopes. The largest reduction in suction happens in wind direction 90º and slope 35º, while less reduction in suction happens on 27º inclined roof for wind direction 90º. Because of these suctions decrease, the total suction on roof inclined 27º, with solar panels, becomes larger than total suction on roof inclined 35º, with solar panels. However, the suction on 35º inclined roof without solar panel, is larger than suction on 27º inclined roof without solar panels. In other words, although suction on leeward surface of roof inclined 35º without panels is larger than that on leeward surface of roof inclined 27º without panels; however, the total suction on corresponding roof surfaces with solar panels for slope 35º, becomes smaller than suction on roofs inclined 27 º with solar panels.

- However, for roof slope 15º, suction (or wind load) increased on the leeward of the roof with solar panels, for both wind directions 45º and 90º. This increase in suction, shifts the largest suction for this slope, from windward at wind direction 45º to the leeward for same wind direction. However, this increased suction for this slope, still much less that the suction on roof inclined 27º with solar panels.

- On the other hand, the greatest suction on roofs inclined 35º and 27º happened for wind direction 90º. That is true for both roof with and without solar panels. However, for slope 15º, the maximum suction happens in wind direction 45º, in both roof with and without solar panels, although this largest suction shifts from windward on roof without solar panels to leeward when the roof has solar panels installed.

- The pressure coefficients on roof under panels, is generally equal to pressure coefficients on bottom of the panels. As a result, pressure coefficients on roof with solar panels can be approximated by pressure coefficients applied on top of the solar panels. However, the largest errors in such estimations are 3.5%, 1% and 0.5 % of the Cp on top of the panels mounted on roof inclined 35º, 27º, and 15º respectively, calculated for wind direction 90º.

- Solar panels mounted on 27º to 35º inclined gable roofs, increase total suction on windward surface of the roof and decrease it on leeward surface of the roof. In other words, solar panels cause redistribution of pressure coefficients, towards balancing of pressure coefficients on windward and leeward, where those become closer than they are on roof without solar panels. This changes in suction leads to much less total horizontal suction (wind forces) on the whole roof, which means more stability of the roofs with solar panels.

- However, solar panels mounted on 15º inclined gable roofs, increase total suction on both windward and leeward surfaces of the roof. In other words, installation of solar panels on 15º inclined gable roofs, leads to much higher total horizontal suction (wind forces) on the whole roof, which means less stability of the roofs with solar panels.

4.6. Pressure coefficients comparison for using constant versus boundary layer wind profiles at the inlet

The wind speed used in the analyses is constant at the inlet with turbulence intensity of 5% and turbulence viscosity ratio of 10 %. The selection of these values are done in order to model a medium - turbulence wind flow, following the guidance provided in the Ansys Fluent User's Guide (ANSYS 2015). The program calculates a linear wind profile along the computational domain, starting from zero wind speed at the surface of the ground and increasing up to the assigned inlet

reference wind speed at the mid height . Thus, after performing several flow steps the wind flow develops into a profile resembling the power law wind profile (Fig 4.123), used to describe the common boundary layer profile. The software calculated profiles become constant near the mid-height of the roof, Fig. 4.120, while velocity changes considerably at the roof as shown in the detailed graphs represented in Figs. 4.33 to 4.42, and Figs. 4.86 to 4.95, where the flow becomes unsteady. Unsteady flow is generated as well by the body itself, by phenomena such as separations, re-attachments and vortex shedding (Holmes 2001).

In order to compare the results based on constant wind speed and boundary layer (BL) velocity profiles at the inlet. For wind direction 90° and roof slope of 35° a case with bare roof and another with 2" spacing and 3" clearance were analyzed.

The wind speed profile used in the BL case is the Power Law (Holmes, 2001), as provided in Eq. (3).

$$\frac{\mathrm{U_Z}}{\mathrm{U_{ref}}} = \left(\frac{\mathrm{Z}}{\mathrm{Zref}}\right)^{\alpha} \quad (3)$$

Where

U_z is the velocity at height Z from ground and U_{ref} is the reference mean velocity 40 m /sec .

Zref is considered at the mid-height of the roof.

α in Eq. (3) is the exponential coefficient of the Power Law and is defined in Eq. (4):

$$\alpha = \frac{1}{log\left(\frac{Z_{ref}}{Z_0}\right)} \quad (4)$$

Z_0 is the roughness length (0.02 for an open terrain).

α can then be obtained as follows

$$\alpha = \frac{1}{ln\left(\frac{7.4}{0.02}\right)} = \frac{1}{ln\left(\frac{7.4}{0.02}\right)} = 0.1691$$

This, Eq. (3) takes on the following form:

$$\frac{\mathrm{U_Z}}{40} = \left(\frac{\mathrm{Z}}{7.4}\right)^{0.1691}$$

The values of the wind speed profile corresponding to the power law are calculated along the current domain height 57.9 m at discrete locations and presented in Table 4.16 . This boundary

layer (BL) wind profile was used as inflow wind condition in the CFD simulations, as illustrated in Fig. 4.123 printed from ANSYS Fluent software.

Table 4. 16. Velocity value along height at inlet based on power law, open terrain, mean wind speed 40 m/s.

Z (m)	0.01	0.10	0.20	0.40	0.60	0.80	1.00	1.50	1.80	2.00	2.50	3.00
V (m/sec)	13.1	19.3	21.7	24.4	26.2	27.5	28.5	30.5	31.5	32.1	33.3	34.3
Z (m)	3.50	4.00	4.50	5.00	6.00	7.40	10.00	20.00	30.00	40.00	50.00	57.90
V (m/sec)	35.2	36.0	36.8	37.40	38.6	40.00	42.1	47.3	50.7	53.2	55.3	56.6

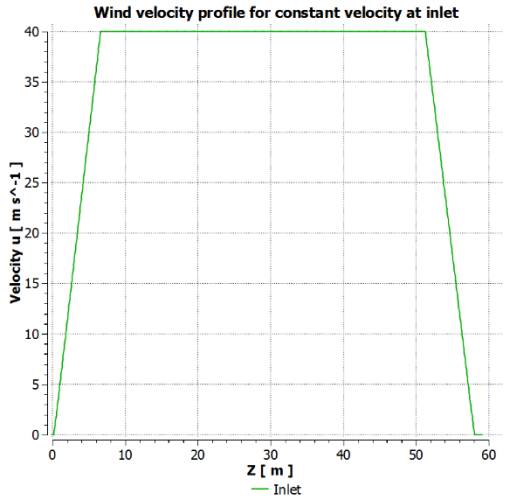


Fig. 4. 118. Constant wind velocity profile at inlet Snapshot from ANSYS

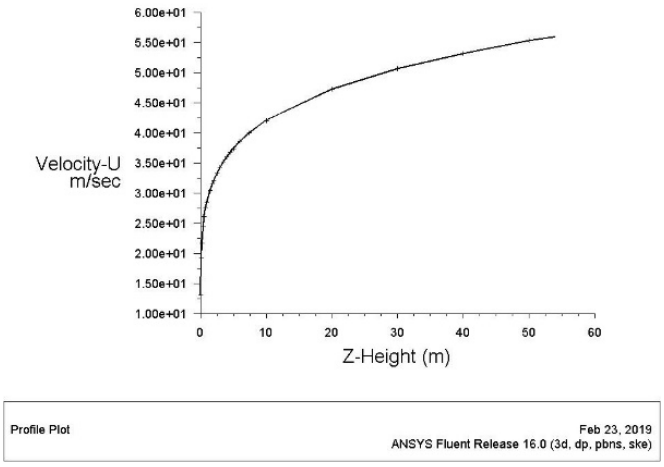
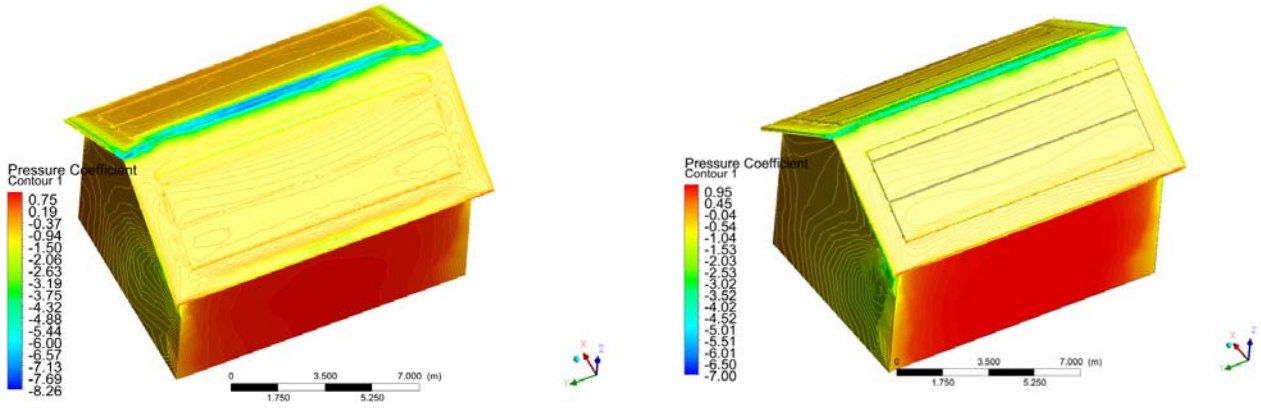


Fig. 4. 119. Boundary layer wind velocity profile at inlet Snapshot from ANSYS.

Comparison between wind velocity profiles for the constant and BL velocity at inlets are presented in Fig. 4.120 and Fig. 4.121. Illustration of the Cp contours obtained by using the BL wind profile and a constant wind profile, for the residential house model with solar panels are shown in the Fig.122. The case of 90° direction of the incoming flow in regard to the ridge of the roof was considered .



(a) (b)

Fig. 4. 120. Pressure coefficients on the building for a) constant velocity profile at inlet and b) boundary layer at inlet

By tracing the Cp changes along the representative lines Pl1, Pl10 and Pl 19, for the BL and constant velocity profile cases, it can be seen that the pressure coefficients are very similar along the representative lines Pl1, Pl 10, and Pl 19 on the windward side of the roof, Fig. 123.

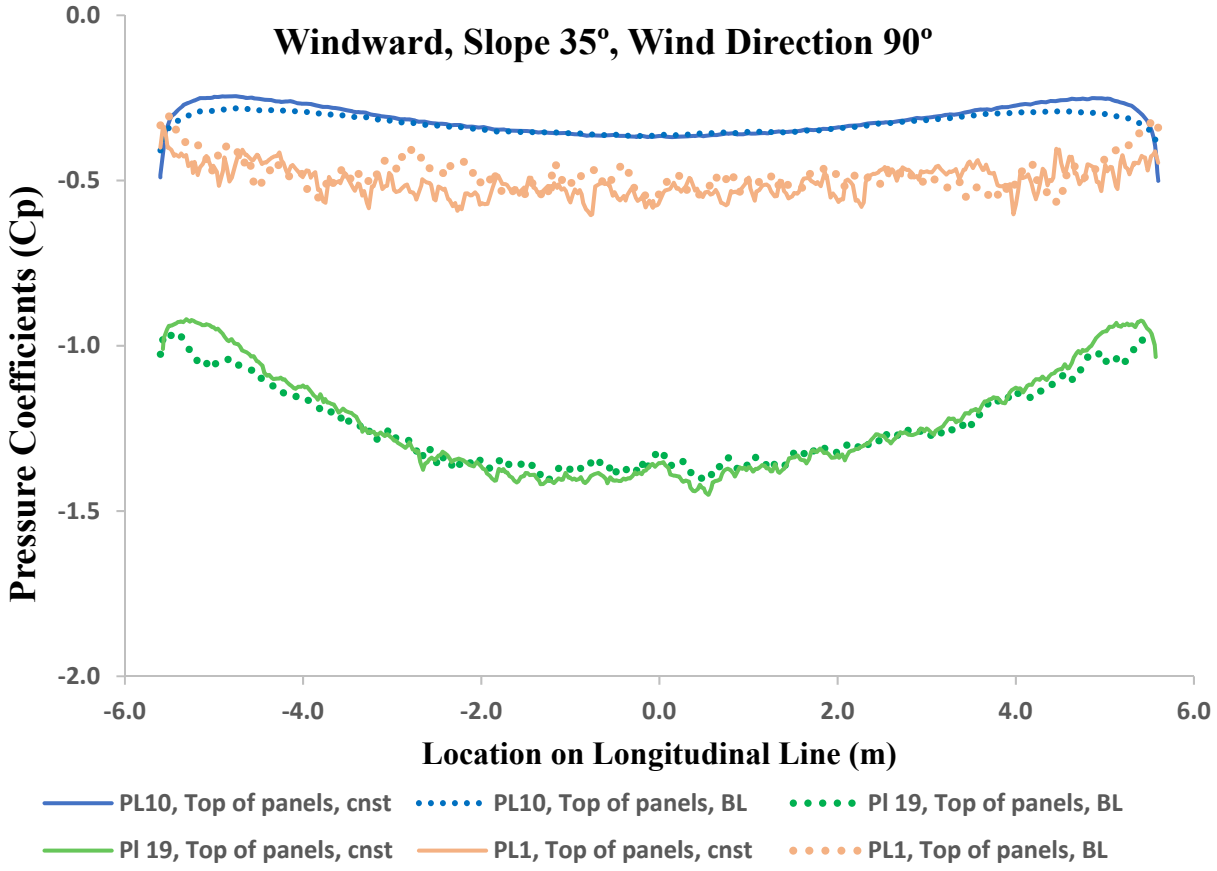


Fig. 4. 121. Comparison between the pressure coefficients on top of the panels, representative lines, windwards, for constant velocity profile at inlet and boundary layer at inlet.

The net Cp on the solar panels and total Cp on the roof-panels assembly were determined for the two types of wind profiles applied, i.e. constant wind speed with turbulence intensity 5% and turbulence viscosity 10% as well as the boundary layer wind profile, and the results are presented in Table 4.17. Also, the average Cp on the roof without solar panels is included.

Table 4. 17. Effects of BL and constant velocity profiles applied at inlet, on solar panel surfaces, roof surface, net Cp and total Cp, windward, 90° WD, 35° slope, 2" spacing and 3" clearance.

Profile / Cp	Top of the panels	Bottom of the panels	Roof surface	Total on the roof surface	Net on solar panels	Bare Roof
Power BL applied at inlet	-0.51	-0.46	-0.48	-0.53	-0.05	-0.17
Constant velocity at inlet	-0.54	-0.48	-0.51	-0.56	-0.05	-0.15
Ratios of Cp change from constant to BL profiles Cp BL/ Cp Cnst	0.94	0.96	0.94	0.95	1.00	1.13

The results show a close proximity in the CP values between the two cases. It can be observed that the pressure coefficients obtained when applying BL velocity profile at the inlet was nearly 5% less than the pressure coefficients obtained when using a constant wind velocity profiles at the inlet. However, the net pressure remains the same without change.

CHAPTER 5

Wind-induced pressure on gable roof mounted solar panels: the effect of roof clearance and array spacing

The effects of roof clearance (i.e., the distance from the bottom surface of the panels to the roof surface) and the spacing between solar panels array rows on the pressure coefficients registered for the three surfaces (top and bottom of the panels and the roof surface under the panels) will be discussed in this chapter.

The most common configuration of currently installed solar panels (as already presented in Chapter 4) is 3" roof clearance in combination with 2" array spacing therefore in the current study the results obtained for this configuration will be compared with the following cases:

1. 10" roof clearance and 2" array spacing, to investigate the effects of roof clearance change on pressure coefficients
2. 3" roof clearance and 8" array spacing to investigate the effects of spacing change on pressure coefficients
3. 10" roof clearance and 8" array spacing, to investigate the effects of either roof clearance or spacing on the pressure coefficients. The analysis results are reported in Appendix D in order to reduce the volume of this chapter, however, the net pressure coefficients obtained for these configurations are discussed in the conclusions.

The configurations above were analyzed for wind directions of 90º and 45º, because these are the wind directions with dominant effect on the pressure coefficients, as concluded in Chapter 4. Furthermore, the 0º wind direction results was found to produce much lower pressure coefficients magnitudes, in comparison with the wind directions 90º and 45º (Tables 5.1 to 5.5). The net pressure coefficients were presented in this chapter as well as in chapter 4, for all the directions investigated so that these can be compared. The roof slope of 27º was used for all the simulations discussed in this chapter, because it was concluded that this slope generates the largest suction on the roof and on the solar panels. Furthermore, the wind speed used in the current simulations was

40 m/s, which is slightly higher than the 3 second gust in the US (ASCE 7-10) and higher than the hourly design wind speed in Canada (NBC 2015).

5.1. Effect of roof clearance 10” and array spacing 2” on roof mounted solar panels for roof slope 27º, wind directions 90º and 45º and wind speed 40m/s

The solar panels investigated for all the cases are installed in the interior region of the gable roof, away from edges and corners, as designated by the roof zones for wind-induced pressure in NBC (2015).

5.1.1. Pressure contour distributions for wind direction 90º

The distribution of the pressure coefficients on the top of solar panels, bottom surface of the solar panels, and the roof surface under the solar panels, are represented in the figures below (Fig. 5.1, Fig. 5.2, Fig.5.4 and Fig. 5.5) for the windward and leeward sides of the roof.

In general, low pressure coefficients of up to Cp = -0.78 were observed at edge A of the windward panel array. However, the highest pressure, Cp = -1.95, was determined at the narrow strip at the B edge of the windward panel array. On the leeward side of the roof, higher suction of Cp = -6.09 was noticed, especially on the panel array edge near the ridge and on the leeward surface of the roof. The highest pressure coefficient was Cp = -3.58, on the leeward side of the roof located at the A edge (windward edge) of the solar panel array, while lower pressure coefficients of up to -0.78 dominated the B edge (leeward edge) of the array.

For the overall pressure distribution on the roof and on the mounted solar panels, the highest pressure coefficients were concentrated in a narrow strip near the ridge, on the leeward side of the roof and registered values as high as Cp = -5.61. However, this region of very low-pressure coefficients is located outside the surface used for mounting solar panels arrays on gable roofs.

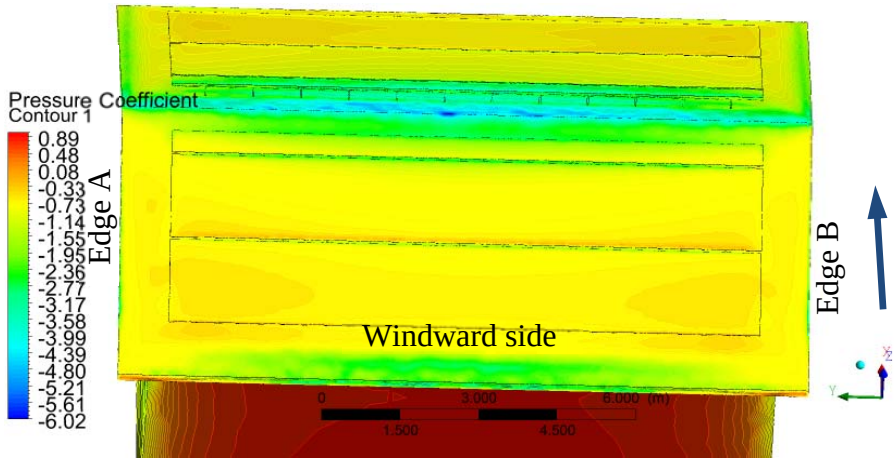


Fig. 5. 1. Pressure coefficients contours of roof with solar panels, slope 27º, windward, wind direction 90º

Figure 5.2 depicts the pressure coefficients on the bottom surface of the solar panels on the windward side of the roof, for wind direction 90º. It can be noticed that the Fig. 5.2 shows a high similarity for the distribution and values of the Cp coefficients with those reported in Fig. 5.3, for the roof surface under the solar panels. In these figures, the Cp changes from -3.40 near the B edge of the windward solar array, to -0.08 for most of the A edge of this array.

Similarly, Figs. 5.4 and 5.4 represent the Cp distribution on the leeward roof surface, under the panels and on the bottom of the leeward panel arrays, respectively. In these two figures, the Cp changes from -3.99 near the A edge of the leeward solar array to -0.08 near the B edge of this array on both the bottom surface of the panels and the roof surface under the panels.

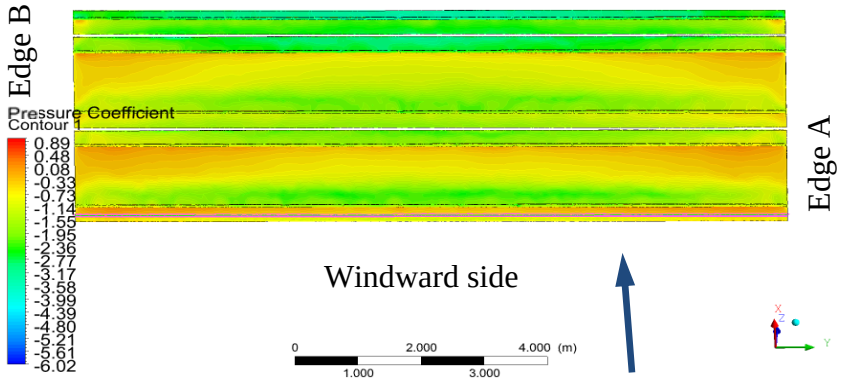


Fig. 5. 2. Pressure coefficients on bottom of solar panels**,** slope 27º, windward, wind direction 90º

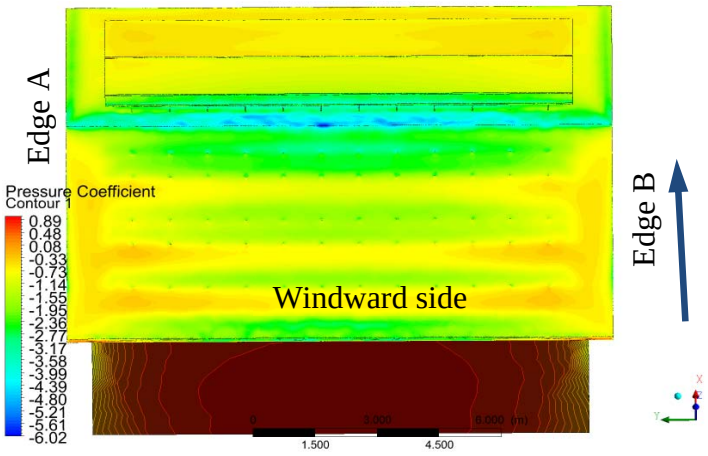


Fig. 5. 3. Pressure coefficients on roof under solar panels, slope 27º, windward, wind direction 90º

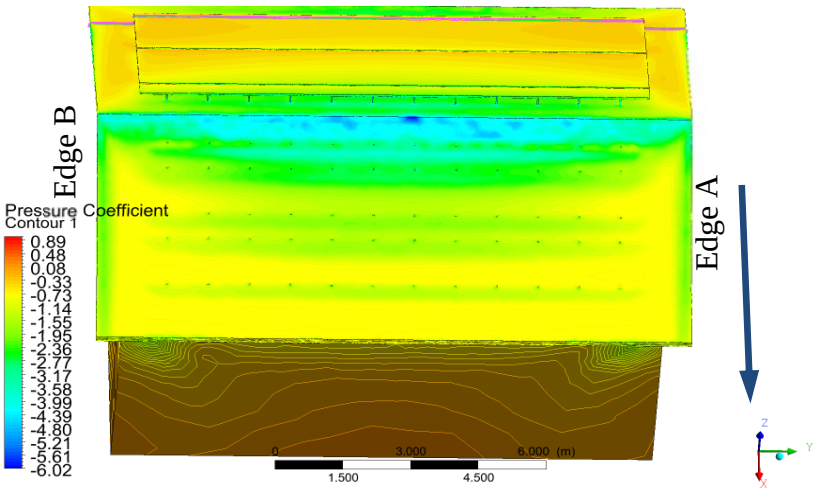


Fig. 5. 4. Pressure coefficients on roof under solar panels, slope 27º, leeward, wind direction 90º

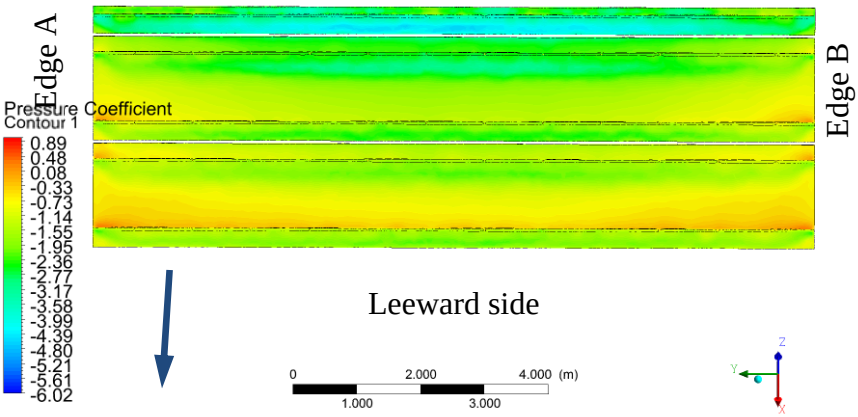


Fig. 5. 5. Pressure coefficients on bottom of solar panels, slope 27º, leeward, wind direction 90º

However, the distribution and magnitudes of the Cp on top surface of the panels on both windward (Fig. 5.6.b) and leeward (Fig. 5.6.a) sides of the roof, are different from those on the bottom of the panels and on the roof surface under the panels. On the other hand, the pressure coefficients on the bottom of the panels on the leeward side of the roof (Fig. 5.5) are considerably higher than those on top of the panels on the leeward side of the roof (Fig. 5.6.a). Similarly, the pressure coefficients on bottom surface of the panels on the windward side of the roof (Fig. 5.2) are noticeably higher than those on the top surface of the panels on the same side of the roof (Fig. 5.6.b). This means that in general a pressure equalization is present in the cavity between the roof surface and the bottom surface of the panel, while the pressure on top surface of the panels was lower than the one reported for the cavity for both windward and leeward sides of the roof.

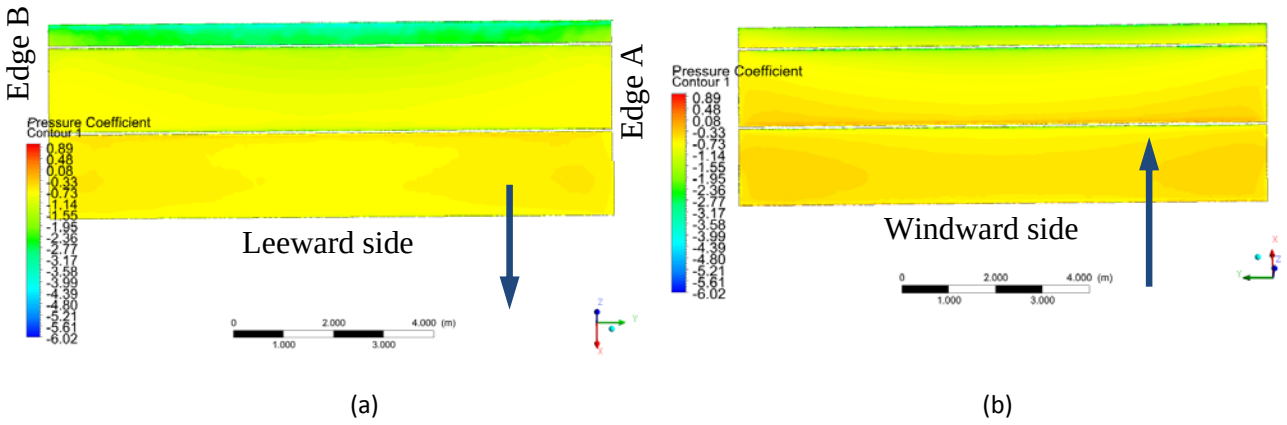


Fig. 5. 6. Pressure coefficients on top of solar panels, slope 27º, wind direction 90º a) Leeward side of the roof b) Windward side of the roof

5.1.2. Pressure coefficients for roof mounted solar panels and roof without solar panels for windward side of the roof

To determine the net pressure coefficients, in this section, the wind-induced pressure coefficients are analyzed in detail for four surfaces: the roof surface under the solar panels, the bottom and top surfaces of the solar panels, the roof surface under the panels and the roof surface without solar panels. The total pressure on the roof is calculated by summing the pressure coefficients sampled along 19 longitudinal lines crossing the top and bottom surfaces of the solar panels and of the roof surface under the solar panels. For determining the net pressure coefficient it is assumed that the

pressure at any point on the roof is obtained by adding the pressure coefficients corresponding to the three points located on the three surfaces (bottom, top of the panels, and roof surface under the panels). The three points are located on lines perpendicular to those surfaces, thus each set of three relevant points is located on one line perpendicular to the roof.

5.1.2.1. Pressure coefficients on bottom surface of the solar panels vs. roof surface under solar panels

To investigate if a similar assumption can be made for other cases, graphs representing the wind-induced pressure coefficients registered on the top and bottom surfaces of the solar panels and on the roof surface under the solar panels, for wind directions 90º and 45º with regard to ridge, are shown in Fig. 5.7 to Fig 5.12.

For wind direction 90°, the Cp along lines PL1, PL10 and PL 19 on roof under the panels and on bottom of the panels, depict high similarity throughout the entire length of the lines. On the other hand, the pressure coefficients on both PL19 and PL10 decreased moderately (in comparison with the other 2 lines) from -1.4 and -0.75 on the east and west edges to -2.6 and -1.8 in the middle of the lines PL19 and PL10, respectively. However, the pressure coefficients on PL1 increased slightly from -0.4 on the A and B edges to -0.6 in the middle of the lines. On the other hand, the largest differences of up to - 0.15, between the Cp on bottom surface of the panels and on the roof surfaces were noted along PL 19. Nonetheless, the smallest differences of 0 to 0.05, between the Cp on the three surfaces were noted along PL1 in Fig. 5.7.

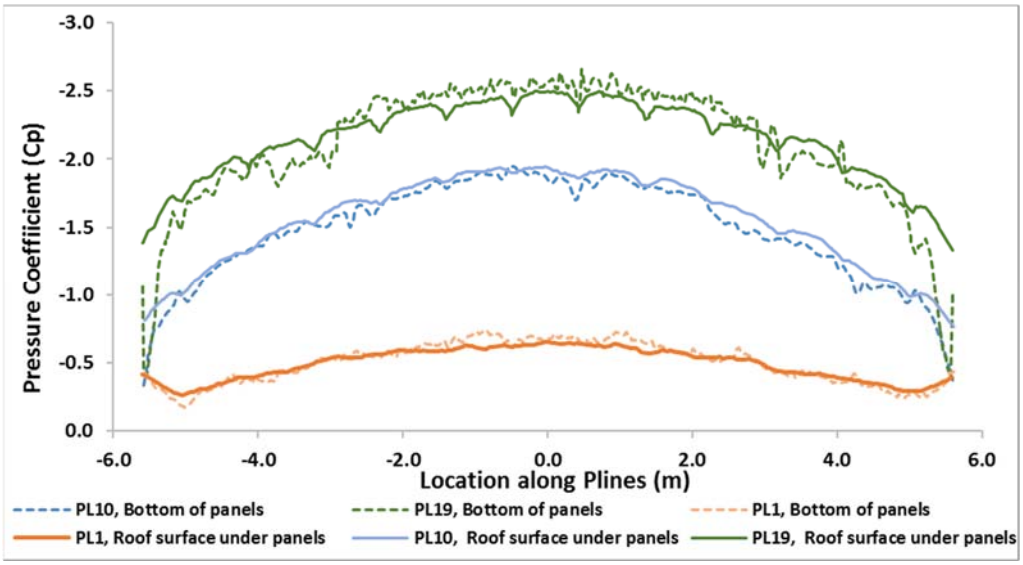


Fig. 5. 7. Pressure coefficients on bottom of solar panels vs. on roof under the panels, slope 27º, windward, wind direction 90 º

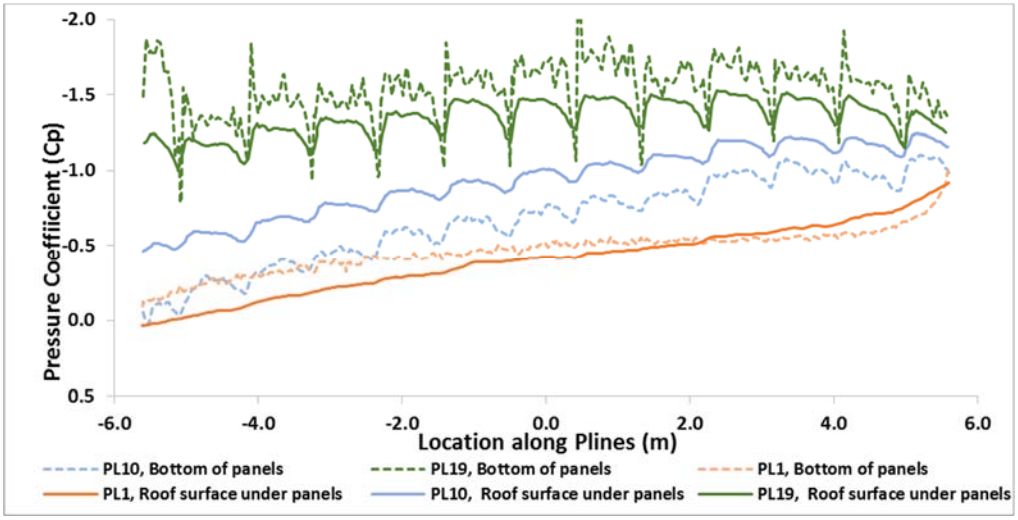


Fig. 5. 8. Pressure coefficients on bottom of solar panels vs. on roof under the panels, slope 27º, windward, wind direction 45 º

For the case of the 45° wind direction, the Cp along all the three lines (PL1, PL10 and PL19) on the roof under the panels and on the bottom of the panels demonstrate high similarity in trends throughout the entire length of the line, gradually increasing towards edge B of the roof. The pressure drop induced by the supports underneath the solar panels array is more obvious, especially

for lines PL10 and PL19, which are crossing the array at the support regions. The smallest pressure coefficients differences were noted for line PL1 (Fig.5.8).

5.1.2.2.Pressure coefficients on roof without solar panels vs. roof surface under solar panels

The current design code provides recommendations for the wind-induced pressure coefficients on gable roofs and no adjustments are provided for the practical situations when the solar panels are installed on gable roofs. Therefore it is very important to investigate the difference between the wind-induce pressures on roof surfaces before and after the solar panels are installed. The Cp coefficients on roof surface without solar panels installed and for roof surface underneath the panels, when solar panels are installed, are analyzed in the current section for different wind directions. For wind direction 90°, negative pressure coefficients were observed, (Fig. 5.9) associated with wind-induced uplift. Moreover the Cp along lines PL10 and PL 19 on the roof surface under the panels were much lower than the Cp on the roof surface with no panels installed, which means that a higher wind-induced suction is registered on the roof surface when solar panels are installed. In comparison with the other two lines (PL10 and PL19) the pressure coefficients on PL1 located on the roof surface without panels is slightly higher than the Cp coefficients on PL1 for the roof surface under the panels. This indicates that the installation of solar panels on gable roofs can induce different effects on Cp, for different locations of the roof. On the other hand, the Cp along all three lines on the roof surface have a symmetric distribution for both cases investigated: roof with and without panels. In addition, although the Cp coefficients on the roof without panels seem nearly constant, ranging from -0.3 along PL 10 to -0.8 along PL19, the Cp coefficients on the roof surface under the panels registered several drops from (-0.25, -0.75 and -1.40) at the east and west edges of the panel array, to (-0.6, -1.80 and -2.60) in the middle of lines PL1, PL10 and PL19, respectively. The regular drops on line PL19 represent the spaces between adjacent panels, where the pressure changes due to the air release through the gaps.

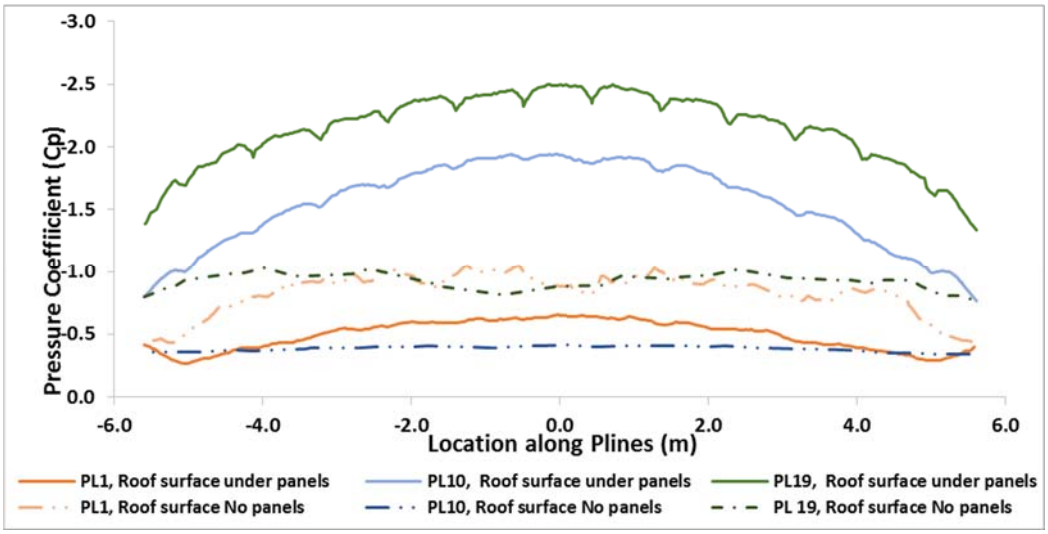


Fig. 5. 9. Pressure coefficients on roof without solar panels vs. on roof under the panels, slope 27º, windward, wind direction 90º

Similarly, for the case of 45° wind direction (Fig. 5.10), the Cp coefficients along same three lines PL1, PL10 and PL19 were monitored and it was noticed that on the roof surface under the panels the Cp coefficients were higher than those on the corresponding lines for the roof without panels. However, the smallest increase in Cp was along PL1 and the largest was along PL10, while a moderate increase in Cp was noticed along PL19. The pressure coefficients along PL1 on the roof without panels increase from 0 on edge A to -0.75 on edge B, while the Cp along PL1 on the roof under the solar panels increased from 0.05 on edge A to -0.8 on edge B, and remained slightly higher than the corresponding line on the roof without panels for most of the line. However, the pressure coefficients along PL10 on the roof without panels increased from -0.20 on the A edge to -0.75 on the B edge of the solar panel array, while the Cp along PL10 on the roof under the solar panels increases from -0.48 on the A edge to -1.20 on the B edge, and remained much higher than the coefficients on the corresponding line for the roof without panels for the entire line length. The pressure coefficients on PL19 for the roof without panels were nearly constant registering a slight increase from -0.90 on the A edge to -0.92 on the B edge of the solar array. However, the Cp on PL19 for the roof under the solar panels increased from -1.20 on the A edge to -1.30 on the B edge. The effect of the standoff supports of the panels is reflected by regular Cp coefficients drops registered along the lines PL10 and PL 19 lines

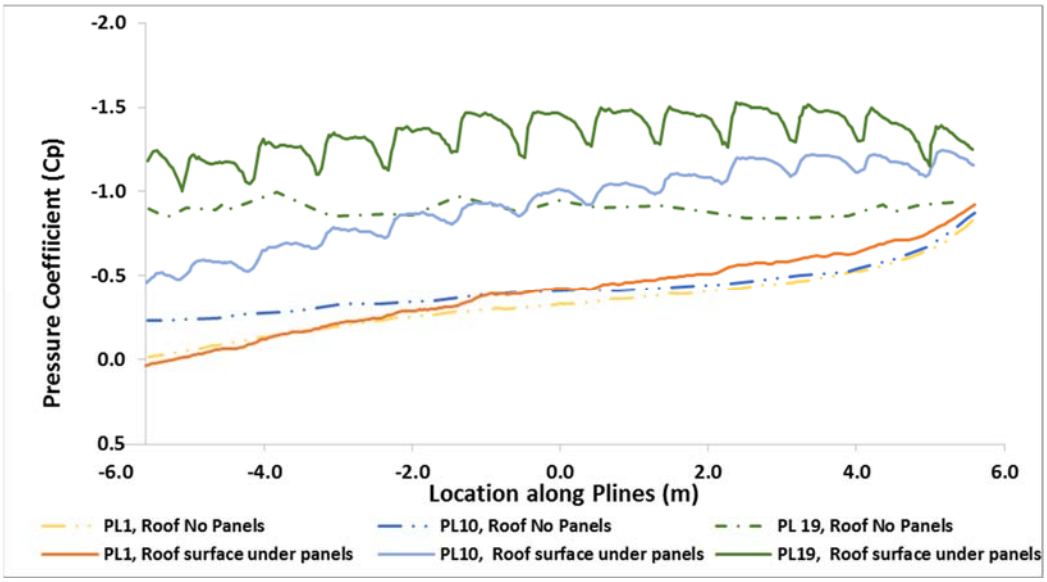


Fig. 5. 10. Pressure coefficients on roof without solar panels vs. on roof under the panels, slope 27º, windward, wind direction 45º

5.1.2.3. Pressure coefficients on roof without solar panels vs. top surface of solar panels

The surface directly exposed to wind action is the roof surface, when no solar panels are installed, and the top surface of the panels, when these are mounted on the roof. Thus, comparing the pressure coefficients for these two surfaces (Figs. 5.11 and 5.12) would provide useful information regarding the wind effect on gable roofs with and without solar panels installed. For wind direction 90° (Fig. 5.11), the Cp coefficients along line PL 19 on top surface of the panels were much higher than the Cp on the roof surface with no panels installed. However, for the line PL1, which is located near edge A of the roof, the Cp coefficients on the top surface of the panels were lower than the Cp on the roof surface without panels, while for line PL10, located in the middle of the roof, the Cp coefficients on top surface of the panels were slightly lower than the Cp on the roof surface without panels. This indicates that the discrepancy between the wind-induced pressure on the top surface of the panel and the roof surface without panels, increased with the distance from edge of the roof directly exposed to wind flow. As in the previous case, the Cp coefficients along all the three lines on the top surface of the panels and on the roof without panels were symmetric, varying from -0.3 along line PL10 to -0.8 along PL19. Also it was noticed that the Cp along the three lines increased from the lowest values of -0.25, -0.40, and -1.25 at the lateral edges of the panel array

to the highest values of -0.5, -0.48 and -1.80 for the middle of the lines PL1, PL10 and PL19 lines respectively.

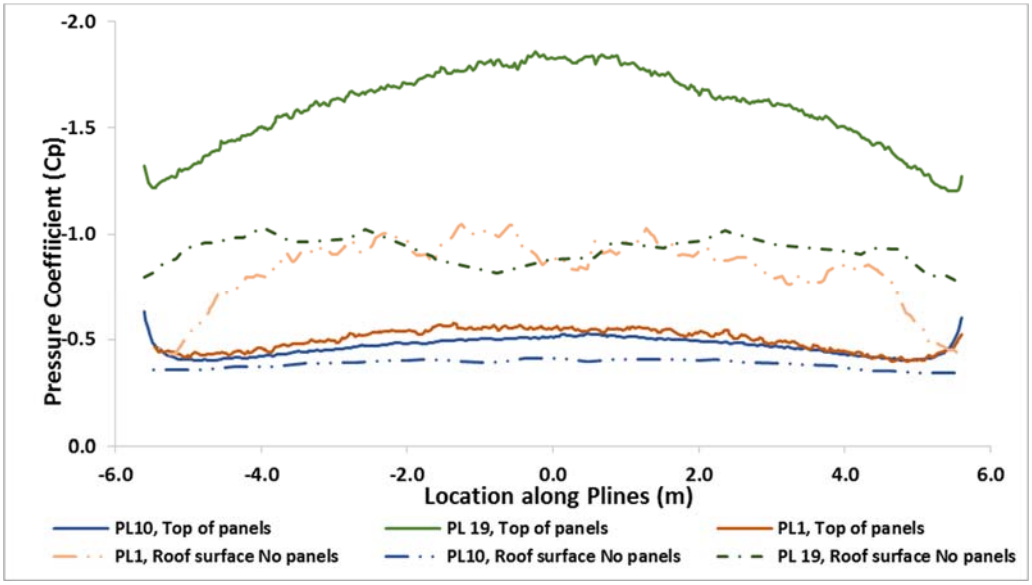


Fig. 5. 11. Pressure coefficients of roof without solar panels vs. top of solar panels, slope 27º, windward, wind direction 90º

Figure 5.12 illustrates the case of 45° wind direction, for which the Cp coefficients along the three lines (PL1, PL10 and PL19) on the top surface of the panels were lower than the Cp on the corresponding lines on the roof without panels. However, the lowest decrease in Cp was near the middle of the roof (PL10), and the largest was along PL19 and PL 1, which had similar reduction in pressure. The pressure coefficients along PL1 on top of the panels increases from -0.15 on edge A to -1.25 on edge B, while the Cp along the corresponding PL1 line on the roof without solar panels increased from -0.05 on edge A to -0.8 on edge B, while remaining much higher than the corresponding line on top surface of the panels. The pressure coefficients on PL10 also increased for the roof without panels, from -0.25 to -0.85 on the array edges A and B respectively, which was very similar to the Cp along PL10 on top of the solar panels. Contrary to Cp on PL1 and PL10, which increased gradually, the pressure coefficients along PL19 on the roof without panels remain mostly constant, and increased slightly from -0.90 to -0.92 between the two edges of the roof. On the top surface of the solar panels, however, the Cp along the line PL19 increased slightly from -1.00 to -1.10 between the array edges A and B respectively, while remaining much lower than the corresponding line on the roof without panels.

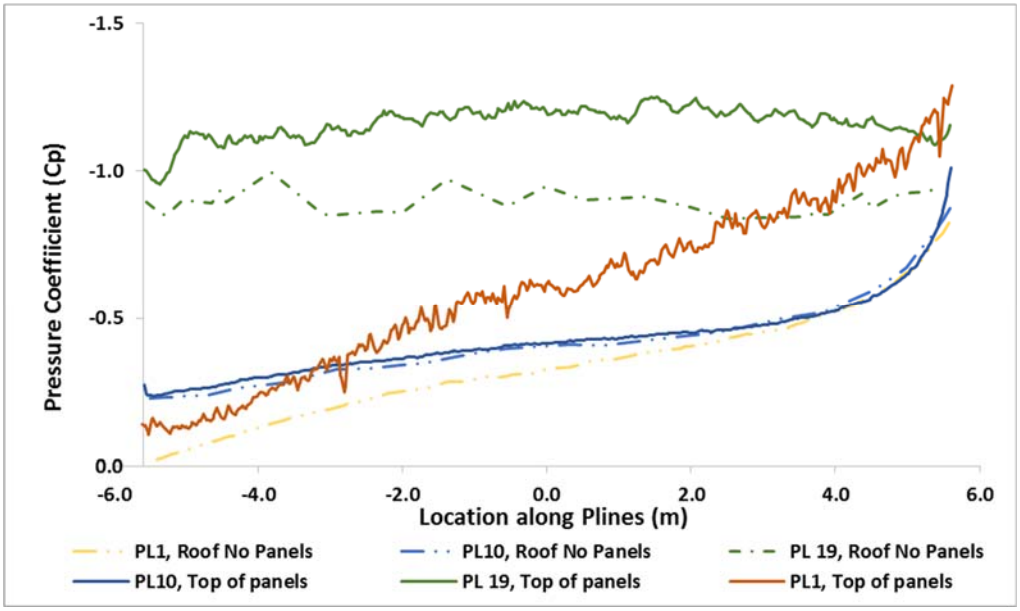


Fig. 5. 12. Pressure coefficients of roof without solar panels vs. top of solar panels, slope 27º, windward, wind direction 45º

5.1.3. Pressure coefficients for roof mounted solar panels and roof without solar panels for leeward side of the roof

The wind-induced pressures on the windward and leeward sides of the roof are different, because of the direct and indirect exposure to wind flow. For a simple roof surface the windward side is expected to show a dominant pressure, however when the solar panels are installed, due to the complex flow–structure interaction, the pressure distribution might change. Detailed investigation of pressure distribution for the leeward side of the roof with and without solar panels is described in this section. The wind-induced pressure is analyzed for four surfaces: the roof surface under the solar panels, the bottom and top surfaces of the solar panels, and the roof surface without the solar panels installed. The same convention is used for calculating the total pressure coefficients by summing the pressure coefficients sampled along 19 longitudinal lines, monitored on the top and bottom surfaces of the solar panels and separately on the roof surface under the solar panels.

5.1.3.1. Pressure coefficients on bottom surface of the solar panels vs. roof surface under solar panels

Detailed representation of the wind-induced pressure coefficients registered on the top and bottom surfaces of the solar panels and on the roof surface under the solar panels mounted on the leeward side of the roof, for wind directions 90º and 45º are shown in Figs. 5.13 to Fig 5.18. Figure 5.13 depicts the wind pressure coefficients on the roof under solar panels versus the Cp on the bottom of the solar panels. Figure 5.13 clearly shows that the differences between the Cp coefficients monitored for the corresponding points on lines PL20, PL 29 and PL 38 were very small, from 0.30 to 0 for the investigated surfaces. However, near the array edges A and B, the Cp differences increased along the top line PL20 from 0.10 at 0.50 m from edges, to 1.00 on these edges. A good agreement was noticed between the pressure coefficients on the bottom surface of the panels and on the roof surface under the panels for each of the three polylines, as shown in Fig. 5.13. As these surfaces encapsulate the cavity between the roof and the panels, and face each other, this Cp coefficients similarity results in a pressure equalization in the cavity, whereas the Cp on the top surface of the panels will describe the resultant pressure coefficient on the roof-solar panels system, as detailed in later sections. The pressure equalization can be assumed, because the Cp on the bottom surface of the panels and on the roof surface under the panels act on opposite directions and have close values. For the middle part of the roof, along line PL29, the Cp coefficients were very similar, for the two surfaces, the bottom of the panels and the roof surface under the panel, with the exception of the extremities, where the Cp for the bottom surface of the panels increased suddenly near edges of the array. The pressure coefficients on PL35 were consistent for both surfaces, however these were higher for the surface of the roof, when compared with the bottom surface of the panels, thus indicating a higher suction in this region, when the panels are not installed. On the other hand, differences of 0-0.40 were noted between Cp on bottom of the panels and on roof surfaces along lines PL 38 and PL20. The very close values of pressure coefficients between the bottom of the panels and the roof surface under the panels, means that the total pressure on the roof surface might be approximated by the pressure on top of the panels in the leeward direction. This estimation is very accurate for PL29 between -5.20m and 5.20 m, while it is slightly conservative for PL20 and slightly underestimated for PL35.

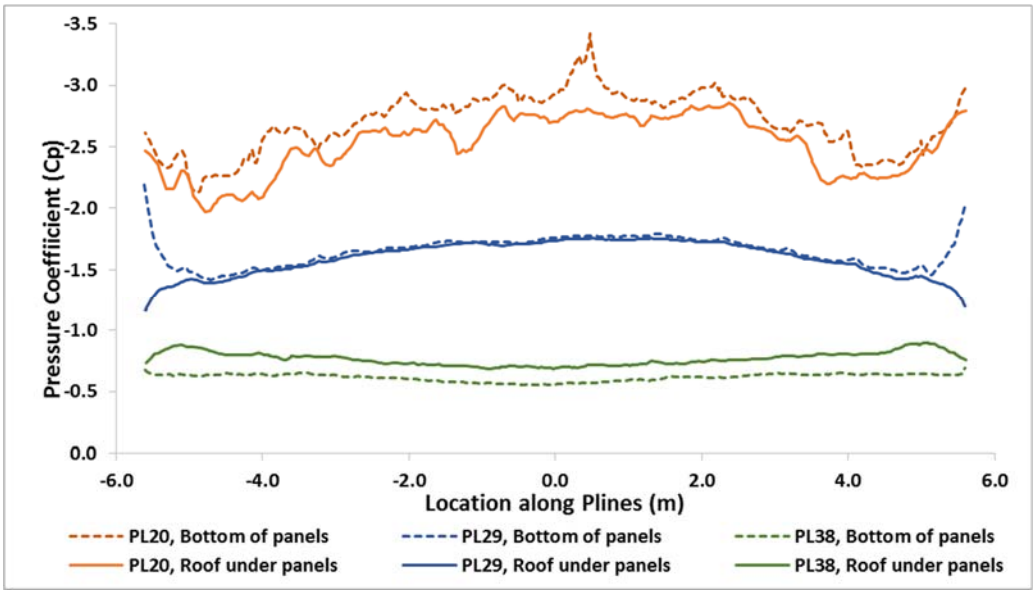


Fig. 5. 13. Pressure coefficients on bottom of solar panels vs. on roof under the panels, slope 27º, leeward side wind direction 90º

Figure 5.14 presents the wind-induced pressure coefficients for 45° wind direction, along the three lines PL20, PL29 and PL35, on the roof surface under the panels and on the bottom surface of the panels. The Cp coefficients demonstrated similarity in trend throughout the entire lengths of the lines, however the differences in values between the two surfaces were higher than the ones reported for the previous case.

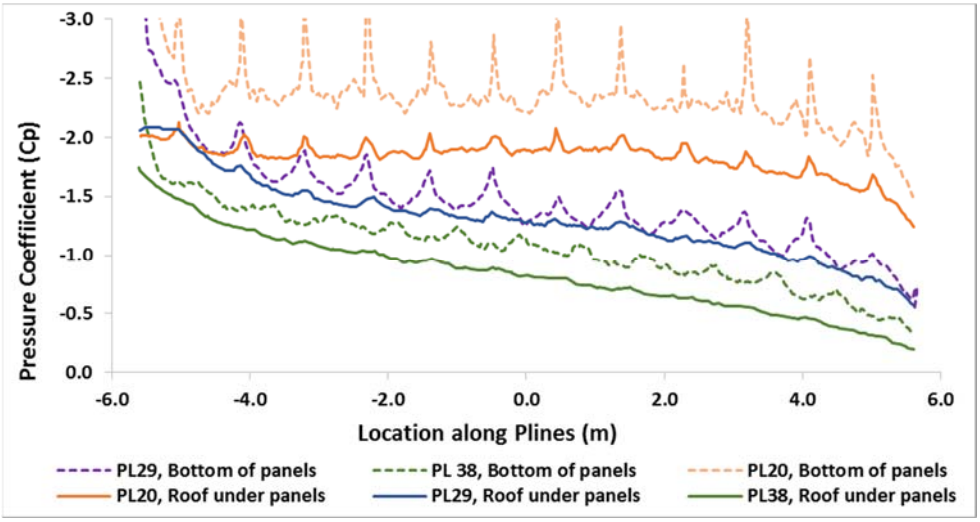


Fig. 5. 14. Pressure coefficients on bottom of solar panels vs. on roof under the panels, slope 27º, leeward, wind direction 45º

5.1.3.2. Pressure coefficients on roof surface under the solar panels vs. roof surface without solar panels

For the leeward side of the roof, the Cp coefficients along the top line, PL15 on the roof surface under the panels were much lower than the Cp on the roof surface with no panels installed, for 90° wind direction (Fig. 5.215). This implies that the wind flow incoming from the windward side of the roof, creates a higher suction near the ridge of the roof, when solar panels are installed. However, the pressure coefficients on line PL29, located in the middle of the roof surface under the panels, is just slightly lower than the Cp on PL29 on the roof without panels. Also these differences (between the effects of the solar panels on the Cp distribution on the roof surface underneath the panels) signify that the wind-induced pressure on the roof surface under the panels depend greatly on the location of the panels on the roof. Near the ridge the suction was higher for the case with solar panels, while on the lower edge, for the roof case without solar panels the suction was higher.

The Cp along the three corresponding lines on the roof surface under the panels fluctuated from -0.75 to -0.60 along PL35, from -1.20 to -1.70 along PL29, and between -2.0 to -3.0 along PL20.

Figure 5.16 represents the Cp coefficients for the case of a 45° wind direction, along the same three lines, PL20, PL29 and PL35. For the roof surface under the panels the Cp coefficients were lower than those on the corresponding lines on the roof without panels. For the current case, the Cp differences between the values for the roof surface under the panels and the roof without panels are higher on the windward edge (edge A) of the array and decrease to nearly zero at the leeward edge (edge B) of the panels.

The pressure coefficients along the top line, PL20 on the roof without panels decreased from -1.60 on the A edge to -1.25 on the A edge, while the Cp along PL20 on the roof under solar panels decreased from -2.0 on the A edge, to -1.25 on the B edge, while remaining much higher than the Cp coefficients on the corresponding line on the roof without panels, for most of the line length. On the middle line, PL29 for the roof without panels the Cp coefficients decreased from -1.30 on the A edge to -0.70 on the B edge of the solar array, while the Cp along the line PL29 on the roof

under solar panels decreased from -2.10 on the windward edge (A) to -0.70 on the leeward edge (B). Similarly, the pressure coefficients along edge line PL35 decreased moderately for the roof without panels (in comparison to the other 2 lines), from -1.30 on A edge to -0.22 on the B edge of the solar panels array. However, the Cp along PL35 on the roof under the solar panels decreased considerably, from -1.75 on the A edge, to -0.25 on the B edge of the array. The effect of the gaps between the panels is reflected by the regular jumps in Cp coefficients observed along PL20 and PL 29, for the roof surface under the panels .

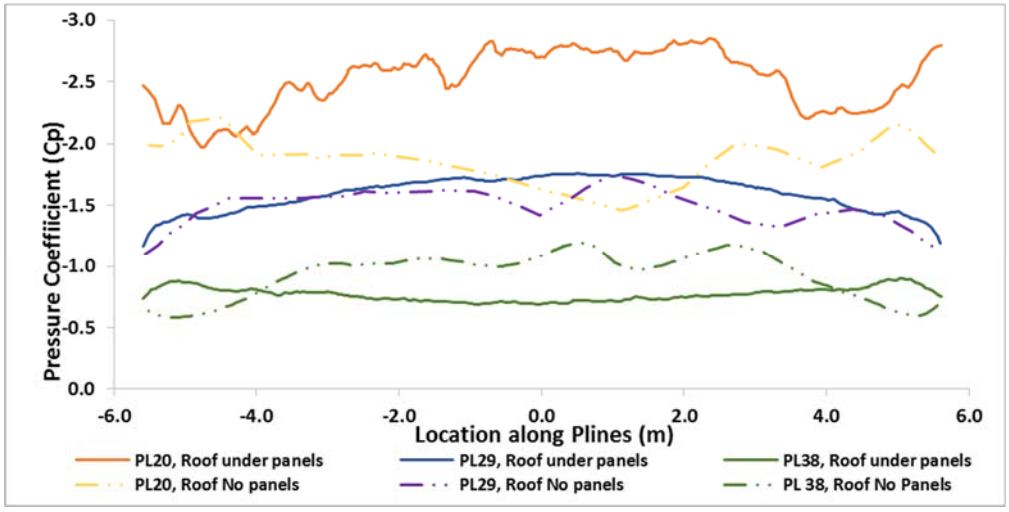


Fig. 5. 15. Pressure coefficients on roof without solar panels vs. on roof under the panels, slope 27º, leeward, wind direction 90º

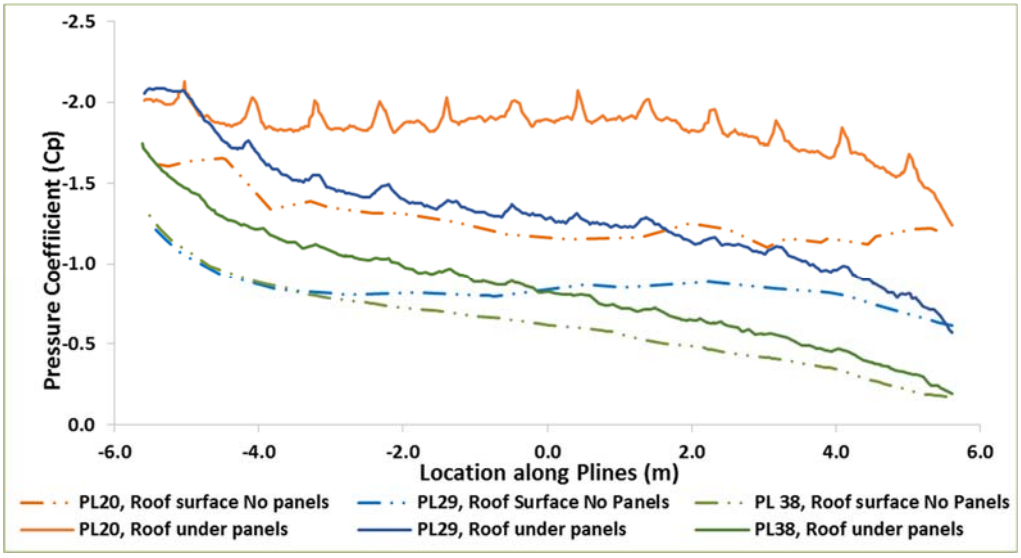


Fig. 5. 16. Pressure coefficients on roof without solar panels vs. on roof under the panels, slope 27º, leeward, wind direction 45º

5.1.3.3. Pressure coefficients on top surface of the solar panels vs. roof surface without solar panels

For the 90° wind direction (Fig. 5.17), the Cp coefficients along line PL20 on top surface of the panels were much higher than the Cp on the roof surface with no panels, however, for the middle line PL29 the Cp coefficient for the roof surface on top of the panels was moderately lower than those on the roof surface without panels. Similar to the previous case the order changed for the lower line PL 38, thus the Cp coefficients for top of the panels were lower than the Cp coefficients on the roof surface without panels. The Cp coefficients are consistent throughout the length of the lines, registering only small differences, in the range of -1.10 and -1.60 along PL 29, between -0.55 and -1.20 along line P38, and between -2.20 and -1.50 along line PL20 for the roof surface without panels. The Cp coefficients along the same three lines, but for the top surface of the panels, changed from -0.65 to -0.50 along PL35, from -1.80 to -2.20 along PL29, and from -2.20 to -3.50 along PL20.

In the case of the 45° wind direction (Fig. 5.18) , the Cp along lines PL20 and PL35 on top of the panels are higher than the Cp on the corresponding lines on the roof without panels. However, the Cp along line PL29 on top of the panels on the same windward side is moderately lower than Cp on PL29 for roof without solar panels. For the middle line PL20 on the roof surface without panels decreased from -1.60 on the A edge to -1.25 on the B edge. In addition, the Cp coefficients along the top line PL20 for the top surface of the solar panels decreased from -1.75 on the A edge to -1.50 on the B edge, while remaining much higher than the corresponding line on the roof without panels for most of the line length.

However, the pressure coefficients along PL29, for the roof surface without panels, decreased from -1.36 on the A edge to -0.61 on the B edge of the solar panels array. Moreover, the Cp along PL29 on top of the solar panels decreased from -1.38 on the A edge to -0.55 on the B edge. Similarly, the pressure coefficients along PL35 on the roof surface without panels decreased moderately from -1.26 on the A edge, to -0.18 on the B edge of the solar array. However, the Cp coefficients along PL35 decreased considerably from -1.73 on the A edge to -0.22 on the B edge for the top surface of the solar panels, while remaining lower than the Cp coefficients along the corresponding line on the roof surface without panels for all of the line.

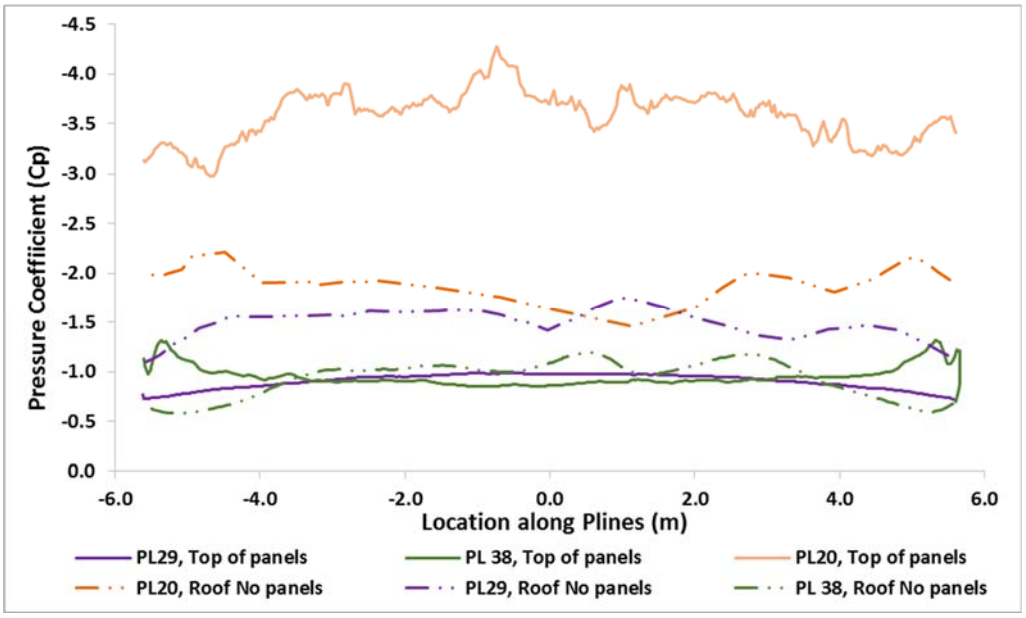


Fig. 5. 17. Pressure coefficients of roof without solar panels vs. top of solar panels, slope 27º, leeward, wind direction 90º

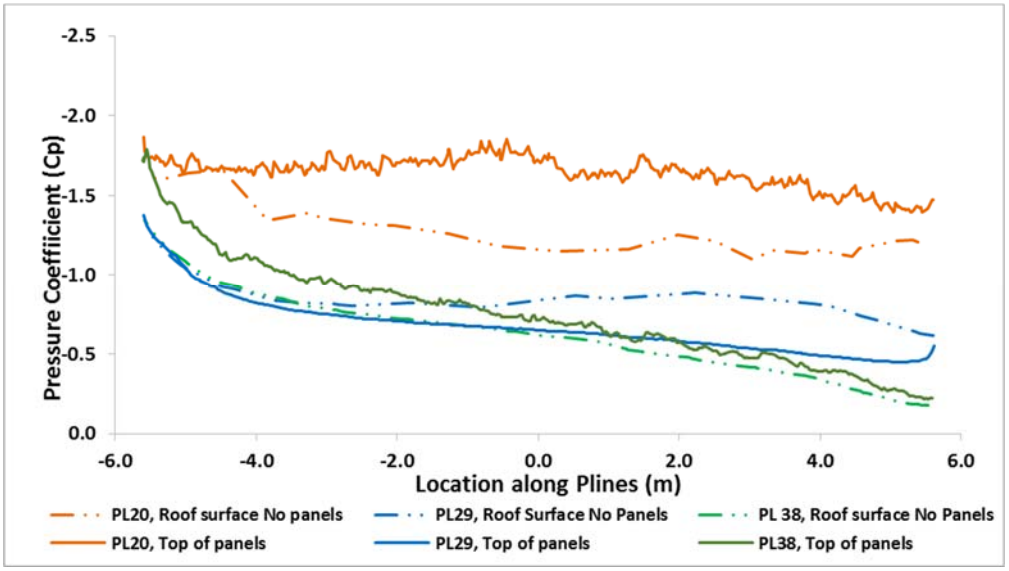


Fig. 5. 18. Pressure coefficients of roof without solar panels vs. top of solar panels, slope 27º, leeward, wind direction 45º

5.1.4. Wind flow characteristics for gable roofs with solar panels for 90º wind direction

The wind-induced pressure coefficients registered at the surface of the solar panels or on the surface of the roof underneath the solar panels, are closely related to the wind flow characteristics around and on top of the solar panels, thus the wind speed and pressure variation in the flow domain in the vicinity of the roof was studied. This section illustrates the wind velocity and pressure coefficient changes along a middle plane perpendicular to the building. For wind direction 90º, the plane was chosen in the middle of the roof, because the lowest pressure coefficients for all the roof areas investigated in the sections above, were located at the middle of the ridge. Moreover, for this wind direction, the middle section of the roof and panels surfaces were exposed to the lowest pressures. Two wind speeds were investigated, 10 m/s which is closer to the commonly encountered wind speeds, for which the design guidelines provide exemplification (SEAOC, 2012) and for 40 m/s which is considered an extreme wind speed, corresponding to a hurricane F1 intensity.

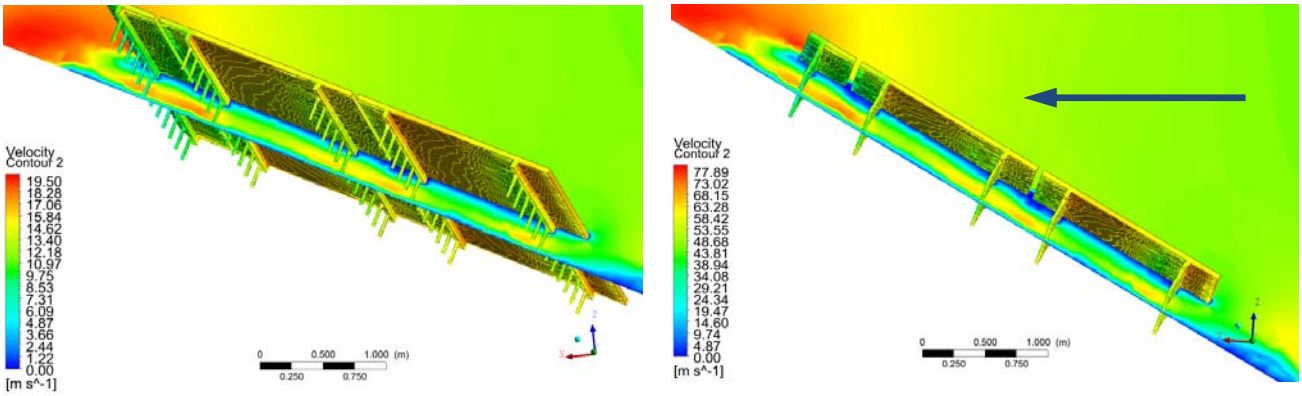
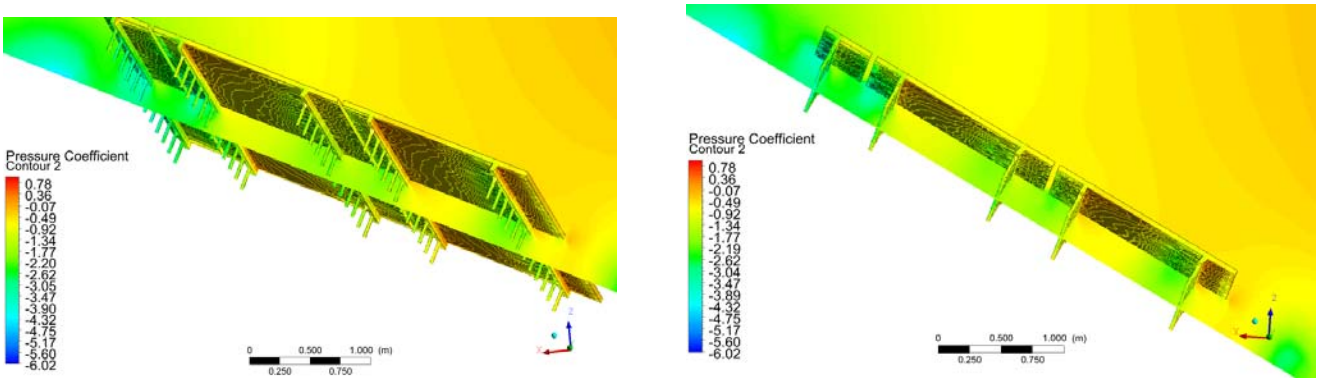


Fig. 5. 19. Wind velocity on a perpendicular plane under panels, with pressure coefficients contour on the structure, windward, slope 27º, clearance 10", spacing 2", wind speeds a) 10 m/s and b) 40 m/s

Figures 5.19, 5.21 and 5.22 show the velocity distributions, for wind speeds of 40 m/s and 10 m/s, in a plane crossing the gap between the roof and the panel array and extending upwards in the space around the panel arrays, on a plane perpendicular to the roof. The distributions showed that the maximum wind speeds in the cavity between the panels and the roof surface are higher than the free stream velocities located near the middle of this space (Fig. 5.19). The wind speed in the

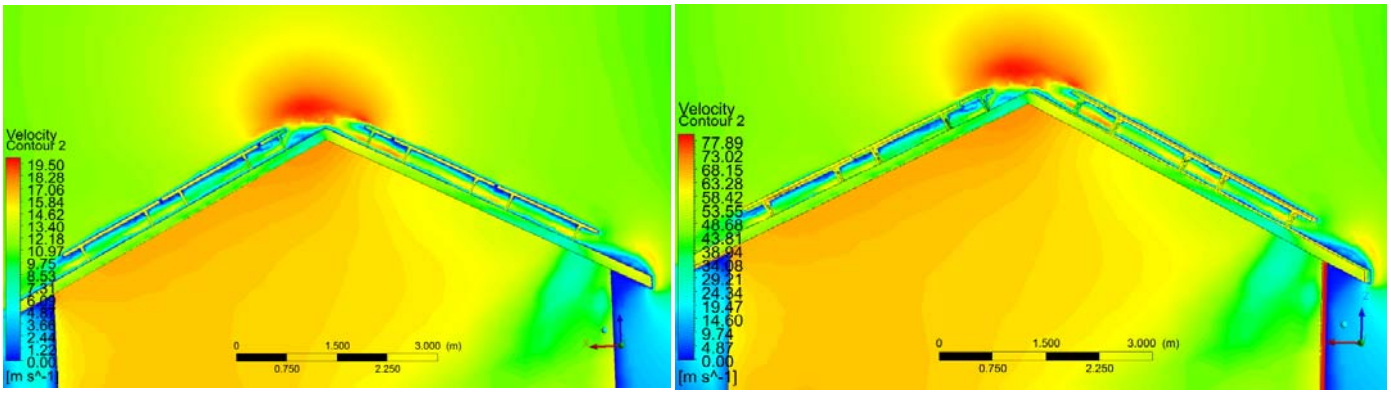
middle of the gap under the panels ranged from 40 m/s, at the impact point to 75 m/s downstream the panels (Fig. 5.19b), and from 10 m/s at the impact to 19 m/s downstream the panels for 40 m/s and 10 m/s incoming wind speeds, (Fig. 19 a) respectively. Figure 5.219 shows no difference between the relative velocity distributions with regard to free inlet wind speeds between 10 m/s and 40 m/s. Thus it can be noticed that the 27° roof slope and the solar panels arrangement can accelerate the wind flow significantly towards the ridge of the roof, thereby inducing a suction towards this region, as shown in Fig. 5.20.



a) b)

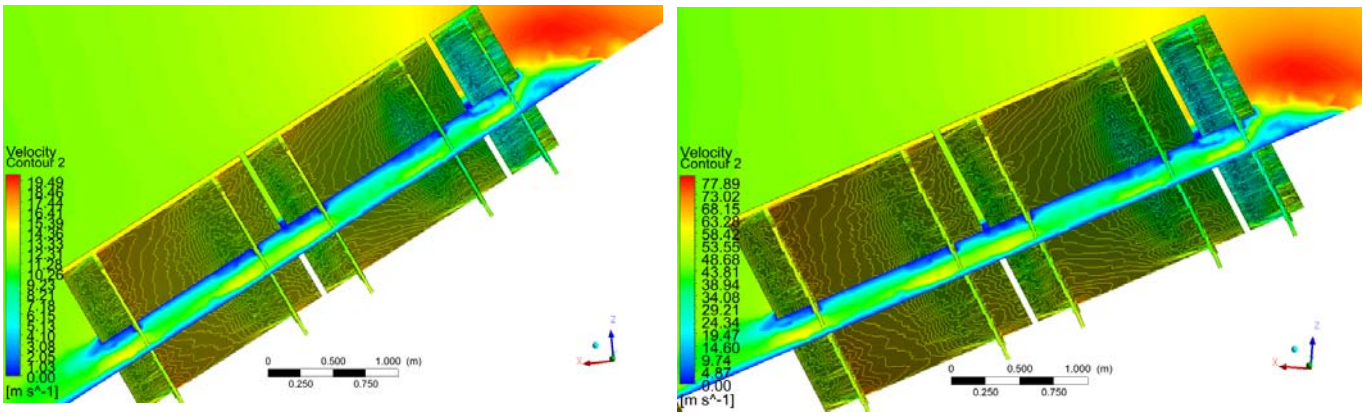
Fig. 5. 20. Pressure coefficients on a perpendicular plane under panels, windward, slope 27°, clearance 10", spacing 2", wind speeds a) 10 m/s and b) 40 m/s

Similarly, Figs. 5.21 and 5.22 show the velocity distributions under the panel arrays on a perpendicular plane. In these figures, the maximum velocities on the panels near the ridge were much higher than the inlet wind speed selected, and the wind speed increased towards the middle of the gap between the roof and the bottom surface of the panels (Fig. 5.21). Fig. 5.22 shows the detailed wind velocity distribution underneath the panels installed on the leeward side of the roof. Figure 5.22 indicates that the wind speeds between the roof surface and the bottom of the panels on the leeward side are much lower than the wind speeds in the corresponding space in the windward side.



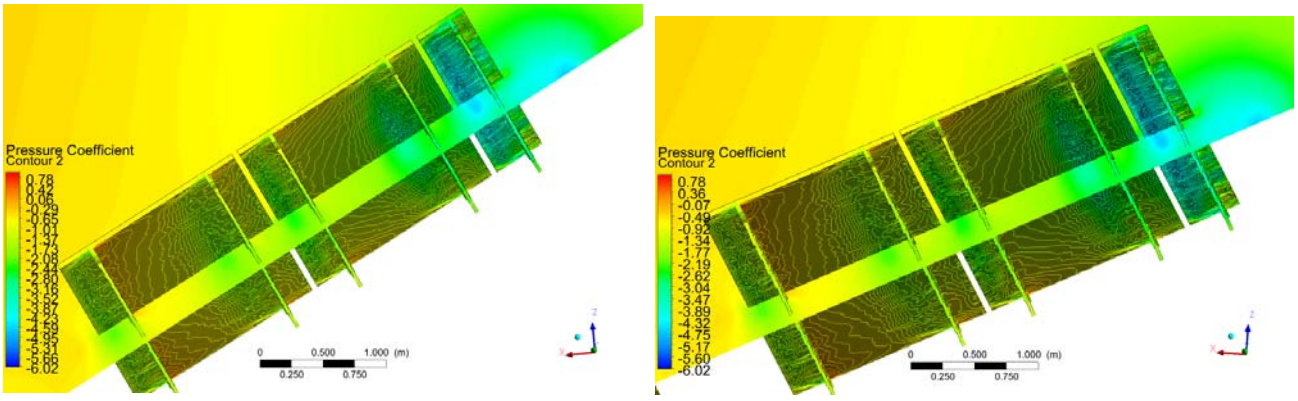
a) b)

Fig. 5. 21. Wind velocity distribution on a perpendicular plane and pressure coefficients on the structure, , slope 2 7º, clearance 10", spacing 2", wind speeds a) 10 m/s and b) 40 m/s



a) b)

Fig. 5. 22. Wind velocity on a perpendicular plane under panels with pressure coefficient contours on the structure, leeward, slope 27º, clearance 10", spacing 2", wind speeds a) 10 m/s and b) 40 m/s

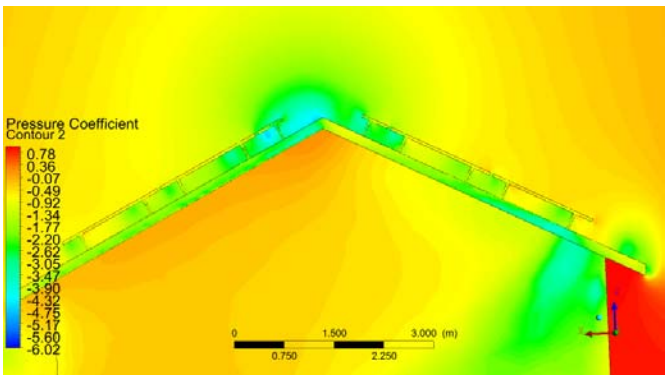


a) b)

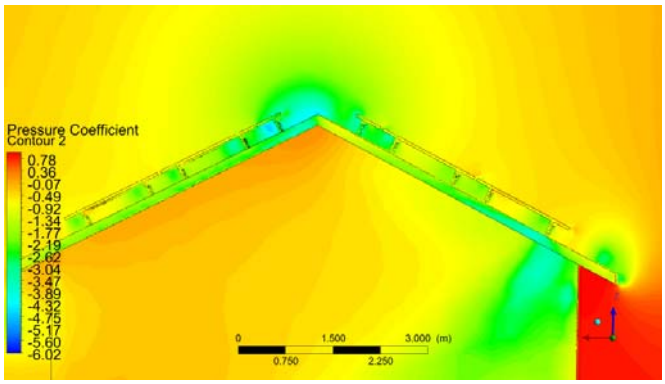
Fig. 5. 23. Pressure coefficients on a perpendicular plane under panels, leeward, slope 27º, clearance 10", spacing 2", wind speeds a) 10 m/s and b) 40 m/s

On the other hand, Fig.5.22 and Fig. 23 indicate very similar pressure coefficients under different incoming wind speeds of 10 m/s and 40 m/s. The pressure coefficients Cp registered in the windward region of the roof-panels cavity ranged between -0.49 at the A edge of the windward array and -4.32 at the B edge of the panels array (Fig. 5.23). However, the Cp in the leeward region of the roof-panels gap varied from -4.75 at the A edge near the ridge to -2.19 at the B edge, while the Cp decreased under the upper half of the array to -0.49. Nevertheless, the Cp in the gap under the leeward array is higher than that under the windward array.

The pressure coefficients for the roof under the panels and in the cavity between the roof and the bottom surface of the panels on the vertical plane are shown in Fig. 5.24. Similar Cp coefficients trends were noted between the roof surface and the bottom surface of the panels, which confirms the pressure equalization reported in subsections 5.1.2.1. and 5.1.3.1., for both leeward and windward sides of the roof. The highest Cp was observed near the ridge of the roof, near the south overhang, and for a distance of approximately 20” (0.50m) around edges A and B of the array; however, no solar panels are installed on these areas.

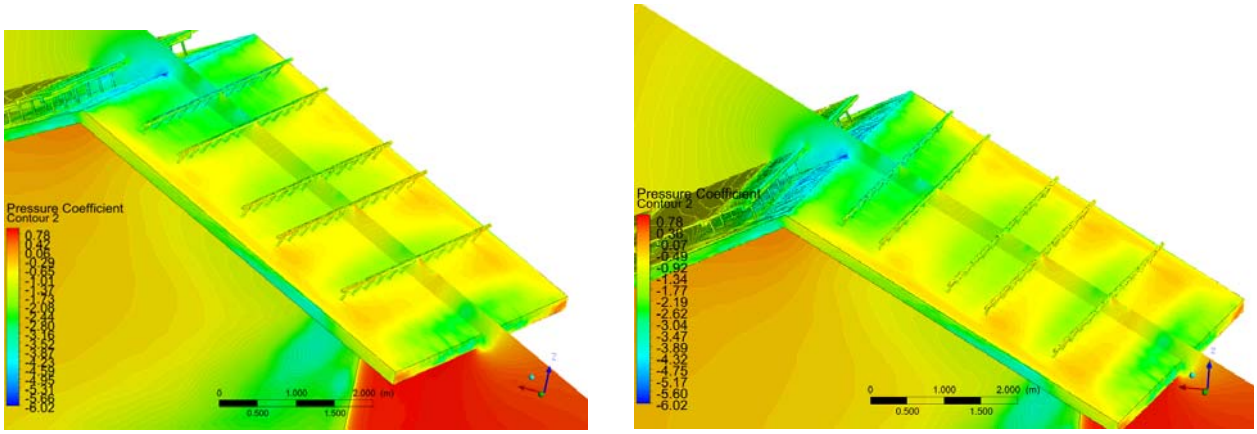


a)



b)

Fig. 5. 24. Pressure coefficients on a perpendicular plane and pressure coefficients on the structure, whole view from west side, slope 27º, clearance 10”, spacing 2”, wind speeds a) 10 m/s and b) 40 m/s



a) b)

Fig. 5. 25. Pressure coefficients on a perpendicular plane under the solar panels, windward, and pressure coefficients on the structure, slope 27º, clearance 10", spacing 2", wind speeds a) 10 m/s and b) 40 m/s

When comparing Fig. 5.23 and Fig. 5.25, it can be seen that the pressure coefficients on the bottom of the panels (Fig. 5.23) are very similar to the pressure coefficients on the roof surface under the solar panels (Fig. 5.25). Moreover, Fig. 5.325 shows very low pressure coefficients in the range of -1.0 to -2.0 in the space between the roof and the bottom of the solar panels.

For determining the wind speed profiles on top of the roof and on top of the installed solar panels, wind velocity was sampled on six lines perpendicular on the roof at different locations, as shown in Figure 5.26; also pressure coefficients variation was monitored along the six lines and complete results are provided in Appendix D. Three lines are located near the A edge of the solar panels array, and the other three lines are at the middle cross-section of the array.

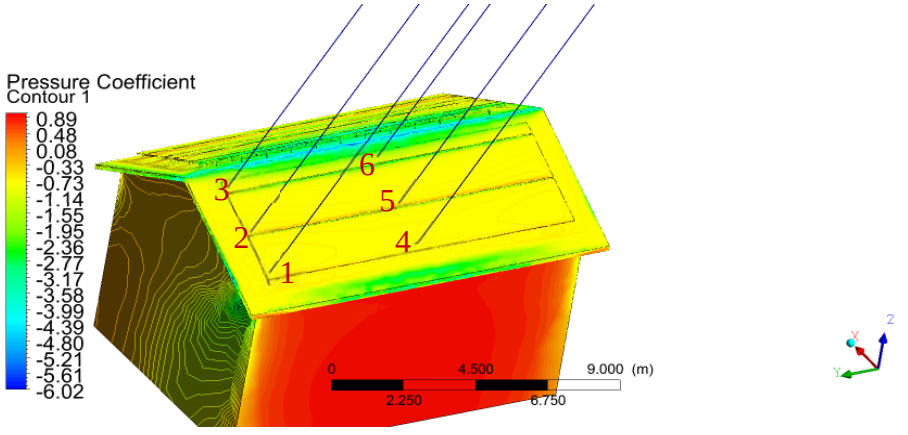
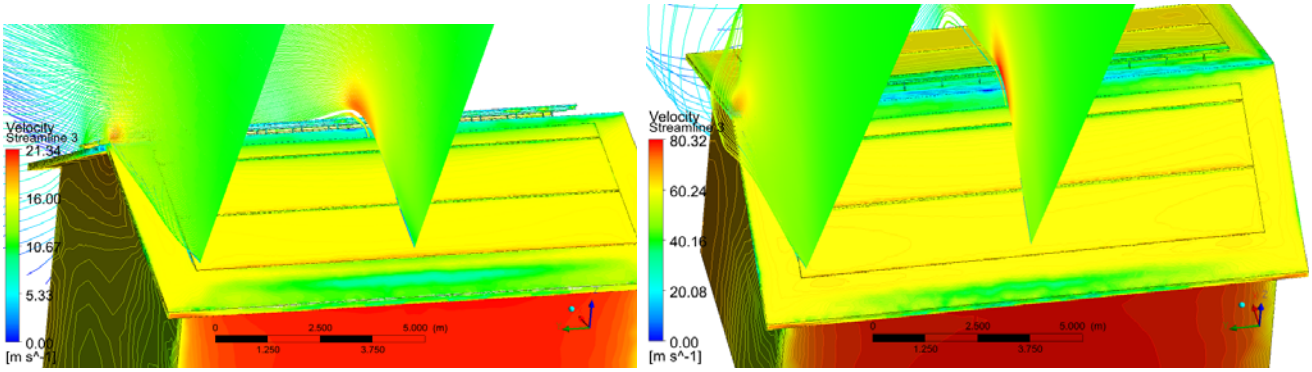


Fig. 5. 26. Lines for velocity and pressure changes

Confirming the velocity distributions described above, Figure 5.27 shows the velocity variation over two planes perpendicular to the roof surface, one at the middle of the building and the other near edge of the solar array. For both wind speeds investigated, 10 m/s and 40 m/s, the wind velocity patterns were similar, approaching values slightly higher than the incoming wind speeds at the level of the panels and increasing significantly near the ridge, especially in the middle region of the roof. Above the panels, the wind velocity decreased with the distance from the roof surface. The velocity was highest in the middle plane near the roof surface and reached 78 m/s and 19.5 m/s at the ridge area for 40m/s and 10m/s the incoming wind speeds, respectively.



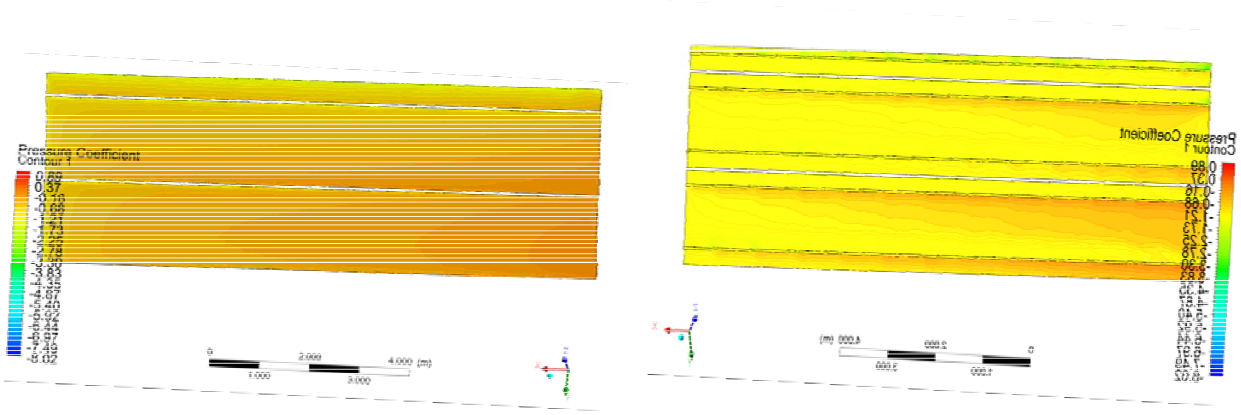
a) b)

Fig. 5. 27. Velocity streamlines at middle and west cross-section planes, slope 27º, clearance 10”, spacing 2”, wind speeds a) 10 m/s and b) 40 m/s

The wind flow characteristics studied in this section showed that, after the incoming flow encountered the roof and the solar panels system, it accelerated and it created higher wind speeds in the flow, especially near the ridge of the roof. The higher wind speed induced higher suction at the surface of the roof and the panels. The wind speed in the cavity between the roof and the solar panels array maintained values closer to the incoming wind flow selected, with slight increases near the supports of the solar panels array, where also the pressure in the cavity has increased, in spite of the pressure balance between the two surfaces limiting the cavity: the roof surface and the bottom surface of the panel. This behaviour, of increased wind speed associated with an increase of suction occurs for most of the studied cases.

5.1.5. Wind flow characteristics for gable roofs with solar panels for 45º wind direction, windward side of the roof

The 90º wind direction was expected to have the most significant effect on the wind-induced pressure for roof-solar panels system, however a milder effect is considered when the wind is approaching from the corner of the roof, at 45º wind direction. Figures 5.28 a) and b) show the pressure coefficients on the bottom and top surfaces of the panels array on the windward side of the roof, respectively, subjected to 40 m/s wind speed, for 45º wind direction. On the bottom surface of the panels, the Cp ranged from -0.16 to -1.21, which was lower than the Cp on top surface of the array which was between 0.37 and -1.21; in general, lower pressure coefficients, starting from positive values, were noticed on top surface of the panels when compared with the coefficients on the bottom surface of the array. As in the previous case of 90°, the pressure coefficients on the roof surface underneath the solar panels were investigated, as shown in Fig. 5.29, and it was noticed that there is a considerable similarity between these and the Cp on the bottom surface of the panels (Fig. 5.28 b), in terms of magnitude and distribution. This can be attributed to the pressure equalization in the cavity between the roof and the solar panels arrays.



a) b)

Fig. 5. 28. Pressure coefficients for wind direction 45º, on windward side of the roof a) Bottom surface of the panels, b) Top surface of the panels

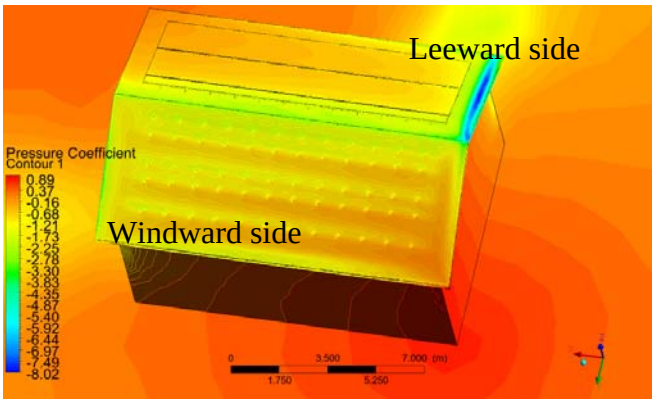


Fig. 5. 29. Pressure coefficients on roof under panels, wind direction 45º, windward side

The overall distribution of the pressure coefficients Cp on the house model with solar panels arrays installed, is depicted in Fig. 5.30, which shows highest pressure coefficients (-7.49 to -4.35) located at the east leeward edge (B) of the roof, and -3.30 to -1.73 at the ridge. Also, Fig. 5.30 indicates positive pressure coefficients 0.37 at C edge of the roof, and a general increase in Cp moving diagonally from the C to the F edge of the roof. It is noteworthy to mention that the solar panels are not installed in these areas of very high-pressure, as recommended by the design codes (SEAOC, 2012) . Also for determining the high-suction regions, NBCC 2015 defines the setback distance from edge according to the end zone, Z, where this is defined as the lower value between 10% of the width of the building (0.8 m) or 40% of the height H (~ 2.5 m), but not lower than 4% of the width of the building, or 1.0 m. However, for the current case the setback distance near the ridge is 0.60 m, which is smaller than 1.0 m.

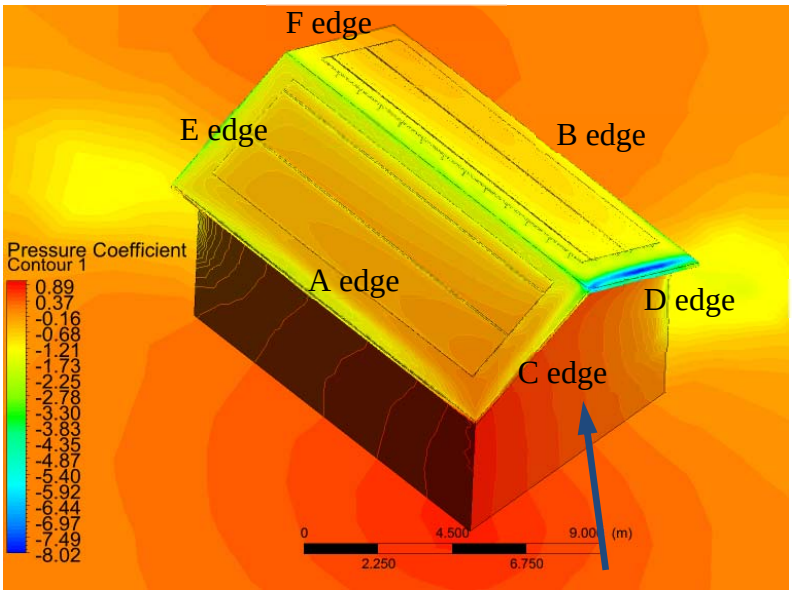
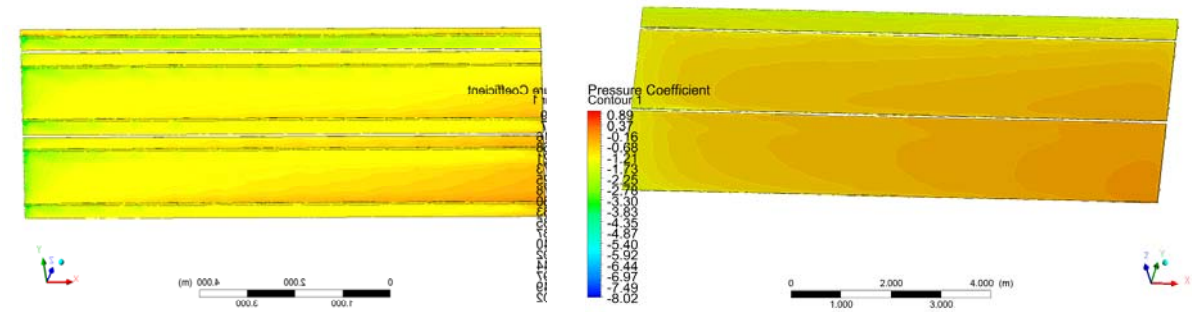


Fig. 5. 30. Pressure coefficients on roof, panels and building, wind direction 45º



a) b)

Fig. 5. 31. Pressure coefficients on: a) bottom surface of the panels, b) top of the panels, wind direction 45º, leeward

For the leeward side of the roof, the pressure coefficients on the bottom and top surfaces of the panel array are depicted in Fig.5.31; it was noticed that the Cp on the bottom surface of the panels ranged from -3.83 to -0.68 and was much higher than the top of the panels, -0.16 to -0.68 (Figs. 5.31 a and b). However, both top and bottom surfaces of the panel array on edge D of the leeward side of the roof and near the ridge registered very low values (-1.73 to -2.78).

In Fig. 5.32, the panels arrays were removed from the leeward side of the roof to represent the Cp coefficients on the roof surface under the panels and it was noticed that as for the windward side of the roof, the magnitude and distribution of these coefficients are very similar to the Cp coefficients recorded on the bottom surface of the panels, for the same leeward region of the roof.

Thus, for the case of 45°, it can be concluded that the pressure equalization in the cavity between the roof and the solar panels array persists on both leeward and windward sides of the roof.

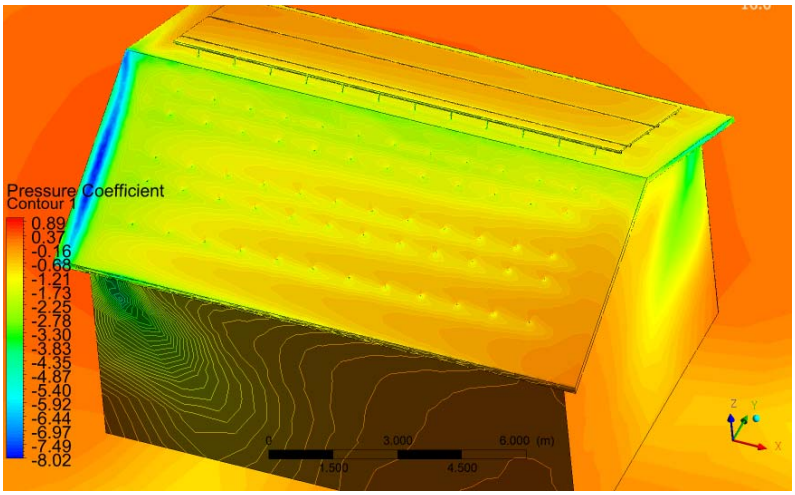


Fig. 5. 32. Pressure coefficients on roof under panels, wind direction 45º, leeward

To better understand the pressure induced by wind to the roof-solar panels array, the velocity distribution in a plane perpendicular to the middle of the building is represented in Fig. 5.33. In spite of the incoming velocity which was set at 40 m/s at the inlet of the domain, the highest wind speed of 69 m/s was near the ridge and near the windward overhang. Also, the general tendency of the wind speed profile is to show an increase from the surface of the roof and building walls, where velocity is always null, and up to 69 m/s at about 0.40m above the ridge.

The wind velocity distribution in the cavity under the panels is shown in Fig. 5.34, where it reaches 63 m/s in three regions along the width of the panels array, at the A edge, the middle of the windward array and the end of the array near the ridge.

The distribution of flow velocities under the leeward panel array is represented in Fig. 5. 35, and it was noticed that this is similar to the flow velocity distribution under the panels array on the windward side, showing a maximum of 63 m/s for the same three regions, near the B and ridge edges and in the middle region of the array. Both cavity velocity distributions are different from the velocity distribution under the panels registered for the 90º wind direction, for which the regions of maximum velocity were before the top array near the ridge.

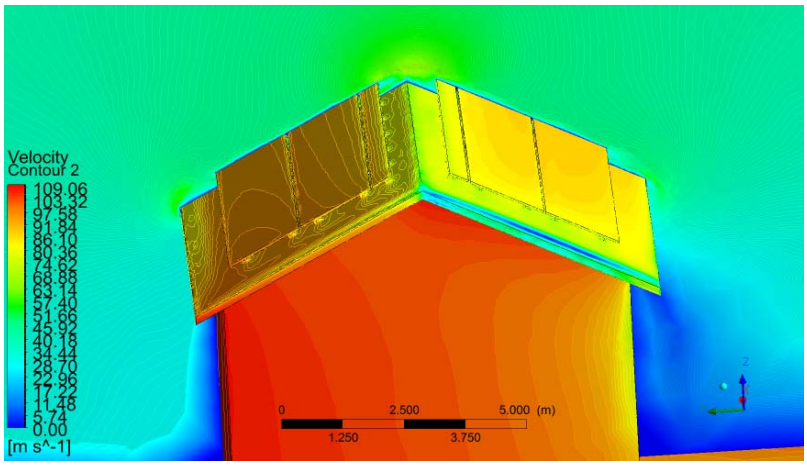


Fig. 5. 33. Velocity distribution around the panels and building along with pressure coefficients on roof, panels and building, wind direction 45º

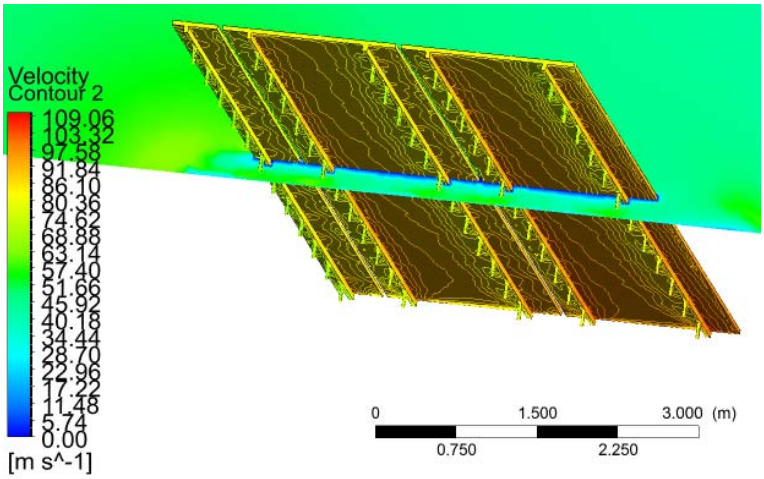


Fig. 5. 34. Velocity distribution under the panels along with pressure coefficients on the bottom surface of the panels, wind direction 45º, windward side

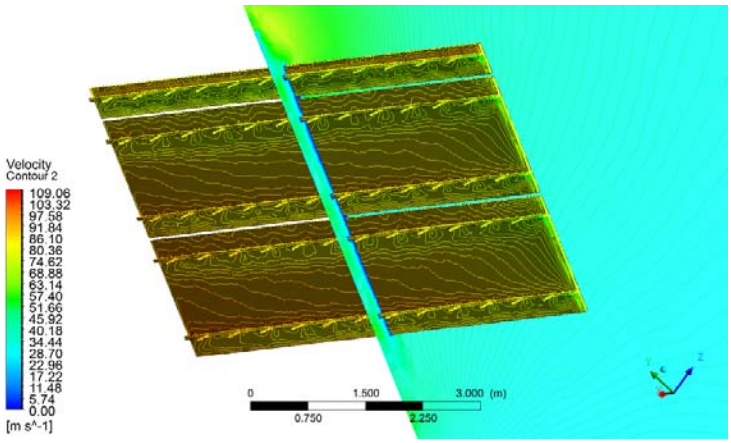


Fig. 5. 35. Velocity distribution under the panels along with pressure coefficients on the bottom surface of the panels, wind direction 45º, leeward side

5.1.6. Three-dimensional vortex flow formations around gable roofs with flush-mounted solar panels for 90º wind direction

The wind-induced pressure at the surface of a structure is caused not only by flow formations around the structure but by the small formations of wind flow around the panels as well. Figures 5.36 to 5.47 illustrate the vortex core jets formed around the building and the roof with solar panels, for the windward side and leeward side of the building, for 90° wind direction. It was noticed that the size of the vortex core jets formed around the building were larger by an order of magnitude than the sizes of those generated on the roof and panels. Where the wind is approaching the building and the roof, no major vortices were noticed, however several types of flow formations were generated when flow sheds from the corners and edges of the structure.

The overall vortex cores formations on the entire building are shown on Fig. 5.36, from the windward side, and in Fig. 5.37 from the leeward side. The largest vortex cores were located on the leeward and sides of the building. Smaller flow formations were generated on the roof near the ridge on the leeward side. Furthermore, smaller vortex cores were located around edges of the solar panels, and the smallest vortex cores were located on the surface of the solar panels.

For the surface of the roof, underneath the panels, mostly turbulent flow without a defined structure, as illustrated in Figure 5.38, for the windward and leeward sides of the roof. This figure also shows the largest vortex cores formation along the ridge, smaller vortex cores around edges A and B of the roof and the outer edges C, D, E and F of the panel array. Smaller vortices can also be found on the interior edges between the panel rows of the array. However, the vortex cores on the roof surface under the panels (Fig. 5.40) are smaller than the vortex cores on the panel surfaces (Fig. 5.39).

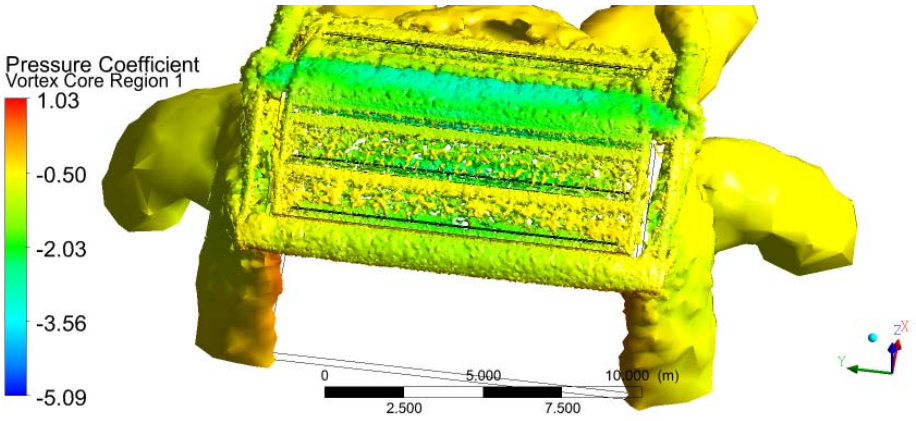


Fig. 5. 36. Vortex core distribution on roof with panels installed and around the structure, windward side

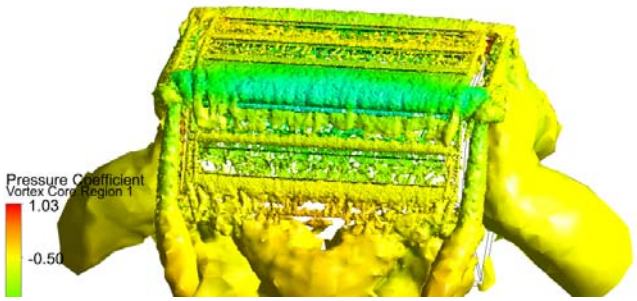


Fig. 5. 37. Vortex core distribution on roof with panels installed and around the structure, back view, leeward side

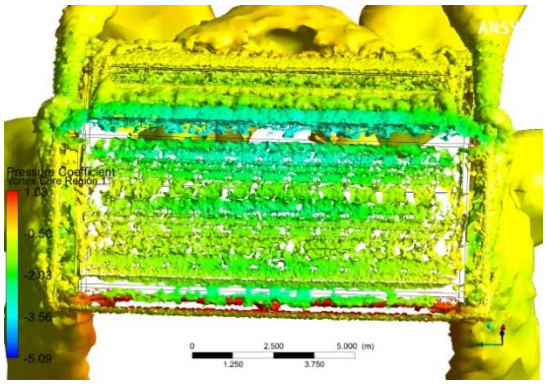


Fig. 5. 38. Vortex core distribution, on roof surface under of the panels

Figure 5.39 illustrates the vortex cores on top surface of the panels and on the roof edge A, for the windward side, where the size of these vortex cores was much higher at the ridge and near the A edge of the roof. Moderate sizes of vortex cores were generated in the spacing between the rows. Similarly, Fig. 5.40 illustrates the vortex cores on the bottom surface of the panels and on the roof edge A for the windward side of the roof, for which smaller turbulent formations were noticed at on the panels, but significant size vortex cores were signaled on the A edge of the roof and near the ridge. The vortex core near the ridge covered most of the top solar panel array, on both lower and top surfaces. In general, at the A edge of the roof and near the ridge, higher suctions were noticed on the surface of the roof, thus, such negative pressures can be associated with larger vortex core formations.

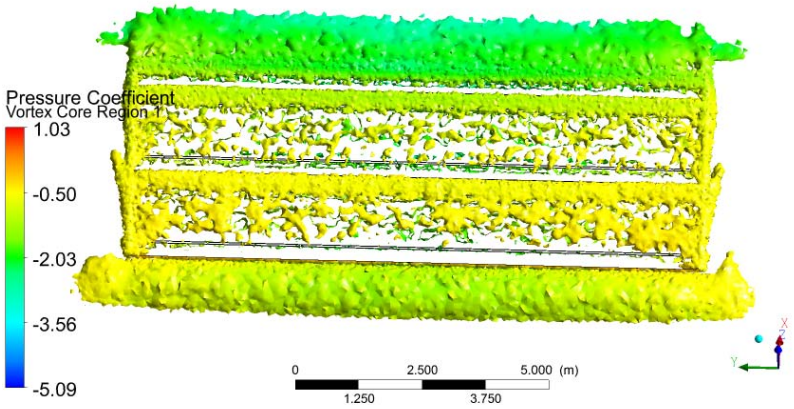


Fig. 5. 39. Vortex core distribution on top surface of the panels, windward

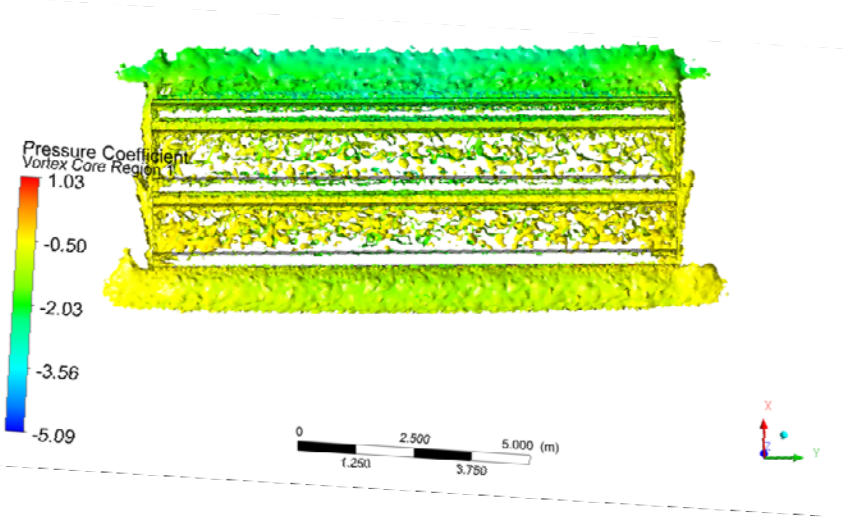


Fig. 5. 40. Vortex core distribution on bottom surface of the panels, windward

5.1.7. Three-dimensional vortex flow formations around gable roofs with flush-mounted solar panels for 45° wind direction

For the 45° wind direction, the vortices generated by the building and the roof-panels system are represented in Figures 5.41 to 4.43 for the windward, leeward, and on the roof surface under the panels, respectively. As for the previous case, it was noticed that vortex cores generated from the corners of the building are much bigger than the magnitude of the vortex formations generated by the roof edges and the by edges of the panels. On the other hand, the vortex cores on the roof surface (Fig. 5.41) are much smaller than those on top of the panels (Fig. 5.44), for both sides windward and leeward. In general, the main characteristics for the three-dimensional flow formations generated for 45° case, are the same ridge vortex core formation, however the vortices around edges of the roof A and B are smaller. This is due to the fact that the incoming wind is approaching the structure from its corner, thus breaking the wind flow formations. Moreover, instead of four major vortex core formations noticed at edges of the building only two vortex cores are present for the current case, at the building corners from where the wind detaches

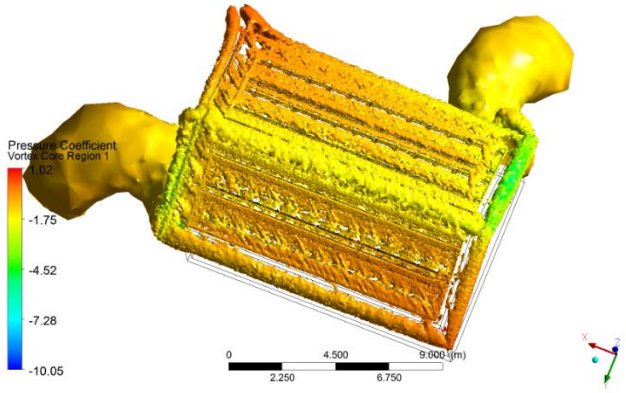


Fig. 5. 41. Vortex core distribution on roof with panels installed and around the structure, windward

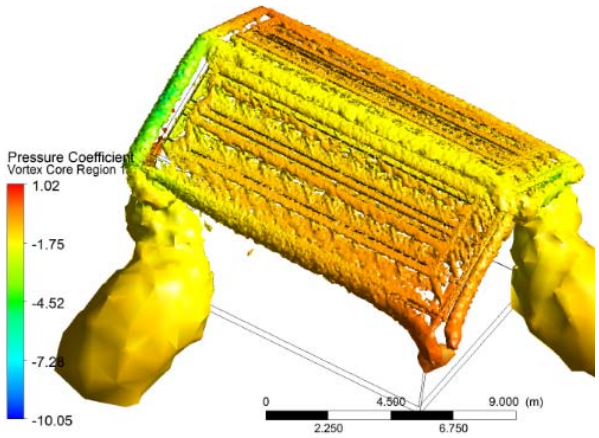


Fig. 5. 42. Vortex core distribution on roof with panels installed and around the structure, back view, leeward

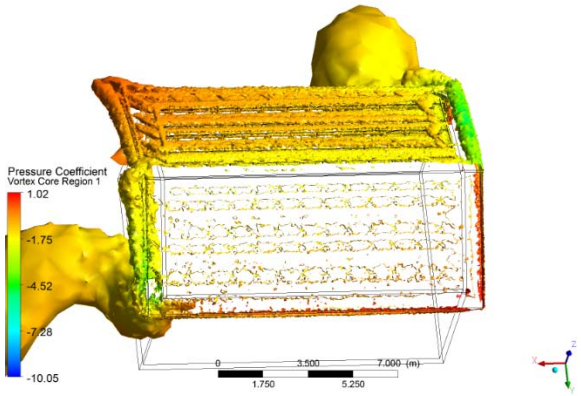


Fig. 5. 43. Vortex core distribution on roof surface under the panels, windward

When comparing the vortex cores on the bottom and top surfaces of the panels (Figs. 5.44 and 5.45), it was noticed that they are similar to each other and also that they have similar patters with the previous case of 90° wind direction, namely the bigger vortex cores around the roof edge A and around the ridge are bigger in size then the rest of the vortices.

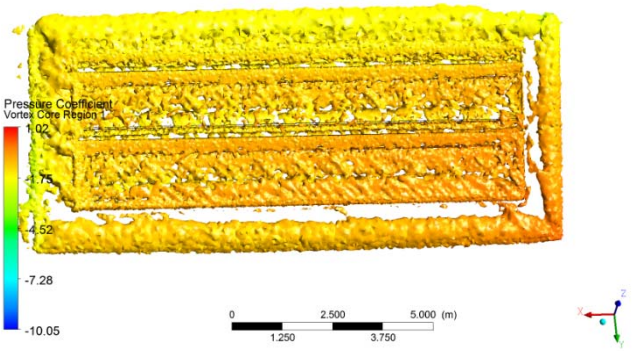


Fig. 5. 44. Vortex core distribution on top surface of the panels, windward

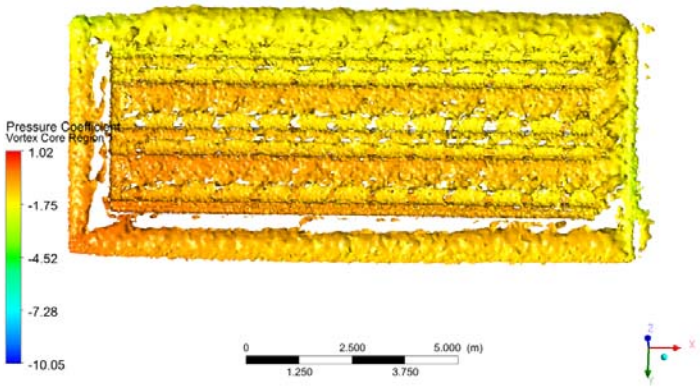


Fig. 5. 45. Vortex core distribution on bottom surface of the panels, windward,

For the leeward side of the roof, Figures 5.46 and 5.47 illustrate the vortex cores on top and bottom surfaces of the panels, respectively. Figures 5.48 to 5.49 reveal that the sizes of the building vortex cores seem larger by an order of magnitude than the sizes of those on the roof generated by the roof edges and edges of the panels. On the other hand, the vortex cores on roof surface (Fig. 5.543) are much smaller than those on top of the panels (Fig. 5.46) and on the bottom surface of the panels (Fig. 5.47). Moreover, the vortex cores on the bottom surface of the panels (Fig. 5.46) are similar to those on top surface of the panels (Fig. 5.47).

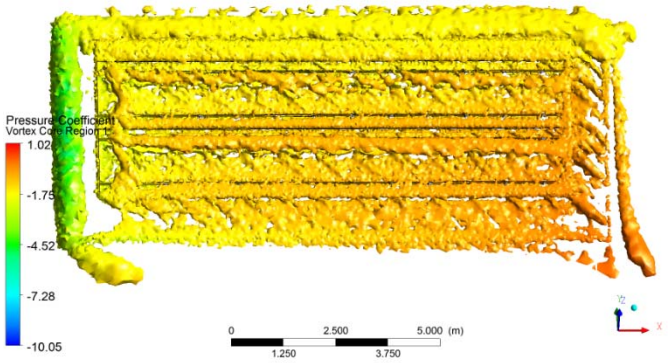


Fig. 5. 46. Vortex core distribution on top surface of the panels, leeward side

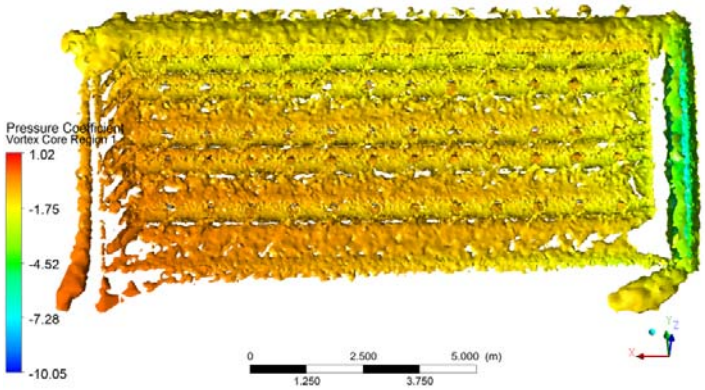


Fig. 5. 47. Vortex core distribution on bottom surface of the panels, leeward side

5.1.8. Pressure coefficients and velocity profiles in the cavity and above the solar panels for wind direction 90º, windward side of the roof

The same lines 1 to 6, perpendicular to the roof surface (Fig. 5.26) were used for sampling the distribution of wind velocities and pressure coefficients in the cavity formed between the roof and the panels and above the panels, for the 90° wind direction and 40 m/s wind speed. For each line, two separate graphs are presented: one for the wind speed inside the cavity between the roof surface and the solar panels, and a second graph for the wind speed profile from the roof surface up to 13 to 33 m above the panel surfaces. Near the corner of the solar panel array along line 1, the velocity distribution profile in the cavity is shown in Fig. 5.26, for the panel clearance of 10" (0.254 m). The wind velocity changed from 0 on the surface of the roof, to 46 m/s in the middle of the gap between the panels and the roof, and then returned to 0 m/s at the bottom surface of the panel. Moreover, along Line 1 and above the solar panel surfaces, the velocity increased to 46 m/s

again in the first 4” (0.102m) then gradually decreased to 40 m/s at 13.5 m above the roof surface and above (Fig. 5.48).

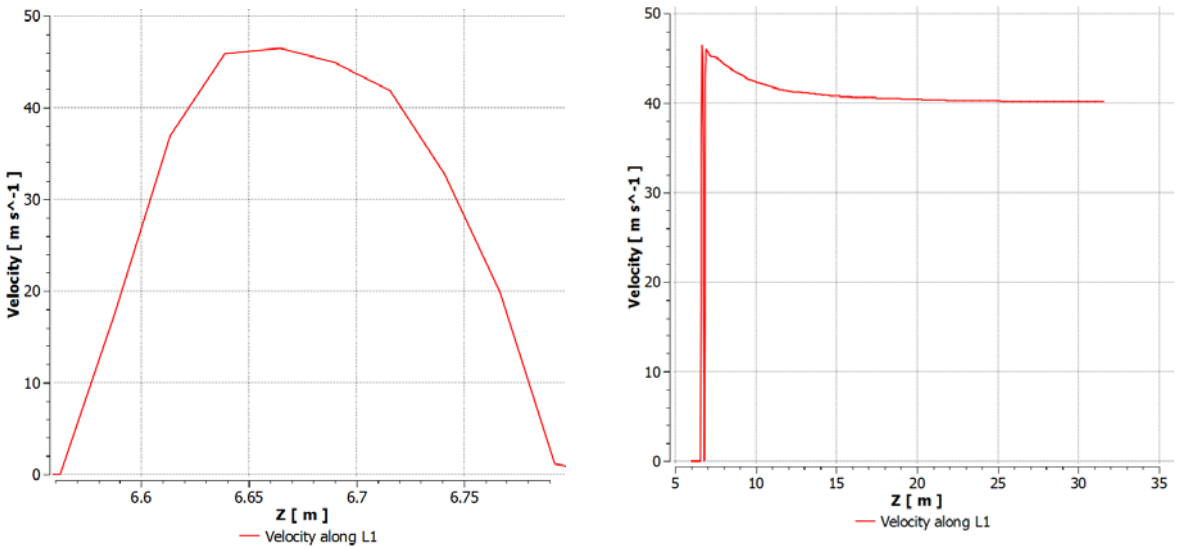


Fig. 5. 48. Wind velocity profile in the cavity and above roof along Line 1

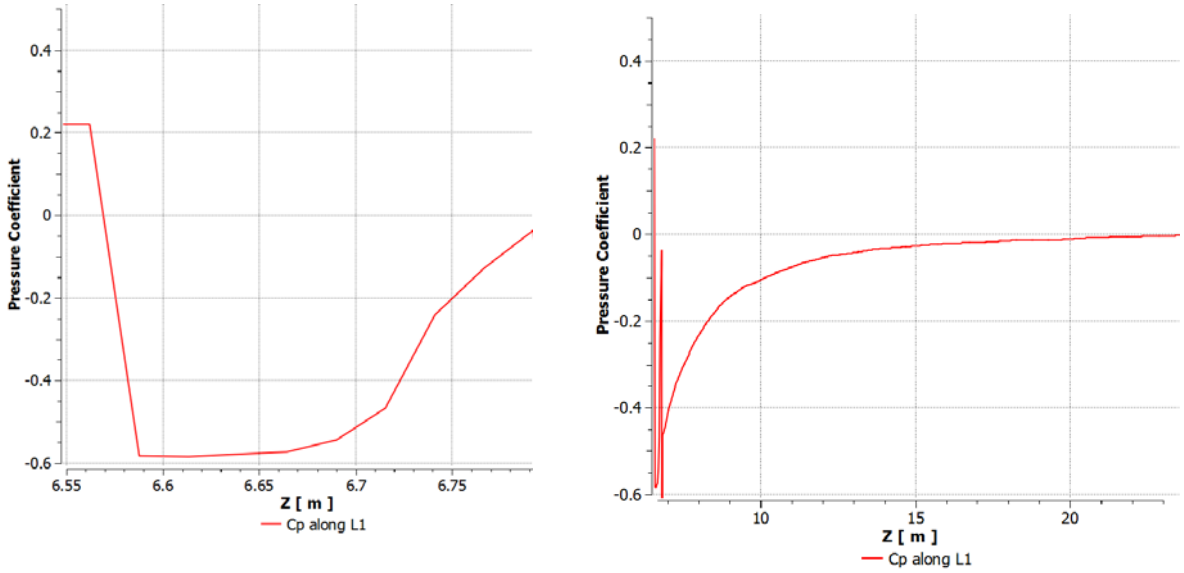


Fig. 5. 49. Pressure coefficient variation in the cavity and above the panels along Line 1

Figure 5.49 shows the variation of pressure coefficient Cp for the same two locations: in the cavity between the roof surface and the panels, and up to 13.5 m above the roof. This is important to analyze because it provides information about the pressure within the wind domain formed in the gap, and not at the limiting surfaces, as described in previous sections. Initially the pressure

coefficient decreased in the cavity, from 0.2 to -0.55 in the first half inch (0.015 m) above the roof surface, then it decreased slightly to -0.52 in the middle of the gap, finally reaching the value of -0.05 at the bottom surface of the panels. This variation proves that even if the pressure equalization occurs between the two limiting surfaces of the cavity, as it was shown in the subsections above (the roof surface and bottom surface of the panel have equal values and opposite signs), the pressure transition in the gap is not uniform. On the top surface of the panels, the Cp decreased to -0.60 and it suddenly decreased to -0.50 at 4" (0.10 m) above the panels; thereafter it decreased gradually to 0 at 13.5 m above the roof surface (Fig. 5.49).

For Line 2, located in the middle of the C edge of the panel array, Fig. 5.50 shows the velocity profile in the cavity between the roof surface and bottom surface of the panels for 10" (0.254m) space height. For this line, the velocity profile was slightly skewed towards the roof surface, with velocity increasing from 0 m/s on the roof surface to a high of 45m/s at 3" (0.076 m) in the cavity, and then decreases gradually to 0 m/s on the bottom surface of the panels. Above the solar panel surfaces, the velocity increased to 47.8 m/s at 4" (0.102m) above the roof surface, and then decreased to 40 m/s at 23.5 m above the roof surface. Figure 5.51 shows the pressure coefficient profile in the roof-panels cavity, where the pressure coefficient increases from 0 to -0.87 in the first region above the roof surface, of up to 1" (0.025m), then decreased slightly to -0.83 in the middle of the gap, followed by a decrease to -0.75 on the bottom surface of the panels. On top surface of the panels, the Cp decreased to -0.45at up to 4" (0.10m) above the panels, and afterwards decreased gradually to 0 at 23.5 m above the roof surface.

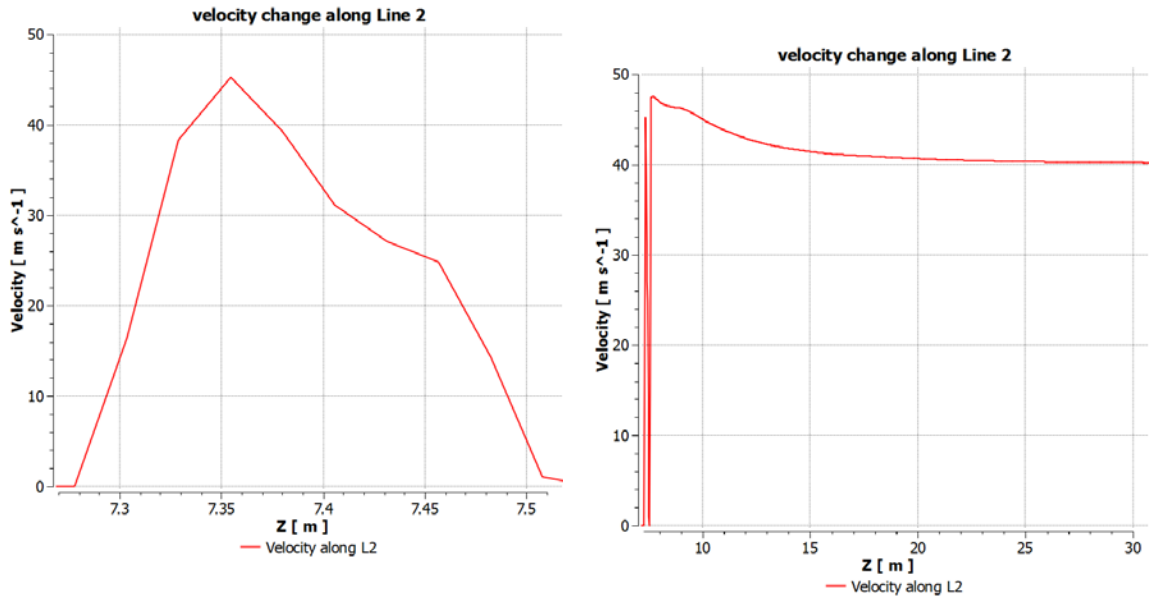


Fig. 5. 50. Wind velocity profile in the cavity and above roof along Line 2

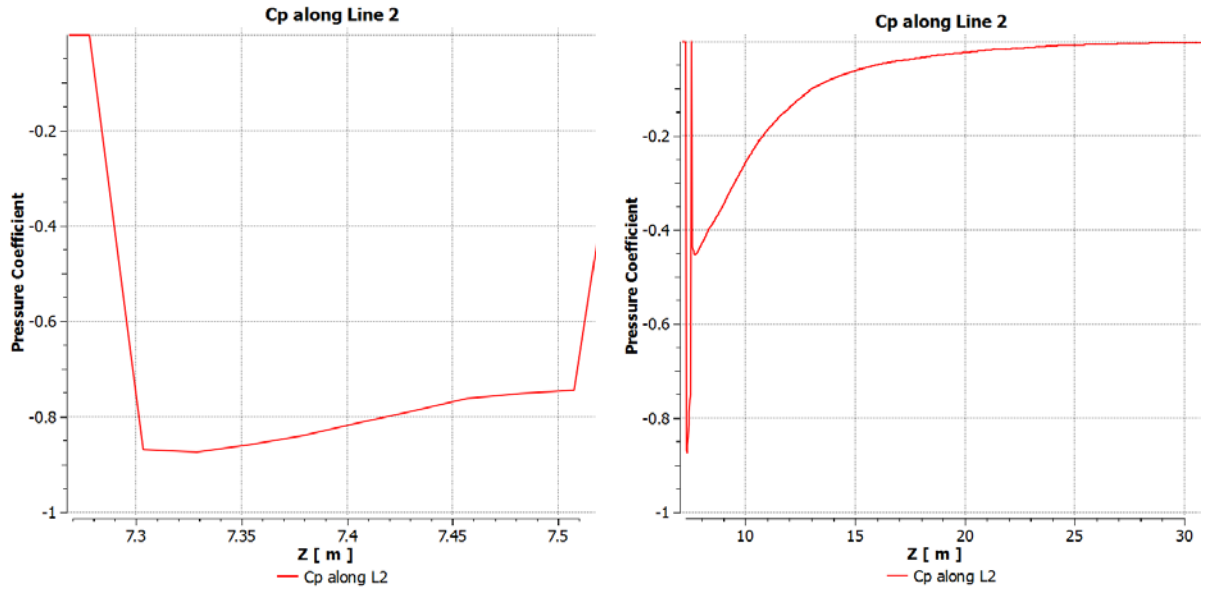


Fig. 5. 51. Pressure coefficient variation in the cavity and above the panels along Line 2

On the C edge of the panels array but near the ridge, along the Line 3, Figure 5.52 shows the velocity profile between the roof surface and the bottom surface where the velocity increased from 0 m/s to 57.80 m/s at 2" (0.51m) into the cavity, decreasing thereafter to 0 m/s on the bottom surface of the panels.

Above the solar panel surfaces, the velocity increased sharply to 57.0 m/s near the top surface of the panel, and then decreases to 40 m/s at 30 m above the ground surface, or 23.50 m above the

panels. Figure 5.53 illustrates the pressure coefficient profile between the roof surface and the bottom surface of the panels for 10" clearance, where the pressure coefficient is -1.40 at roof surface, then decreases gradually in the first half of the gap to -1.27, and then decreased sharply to -0.40 on the bottom surface of the panels. On top of the panels, the pressure coefficient starts at -1.0 near the top surface of the panels, and then decreased gradually to 0 at 30 m above the ground, or 23.5 m above the roof. It is noted that the very high decrease of wind speed, in the very close vicinity of the surfaces, both on roof and on the top of the panel, was expected as the three-dimensional flow formations showed an accelerated flow near the ridge. More important is the high pressure coefficient observed in the vicinity of the surfaces subjected to the sudden velocity increase. From a practical point of view a structural failure could be indicated for these cases, however such analysis was not included in the purpose of the current thesis.

Sudden increase of velocity up to significant values, associated with high pressure coefficients in the vicinity of the exposed surfaces, were encountered for other lines as well, as described below.

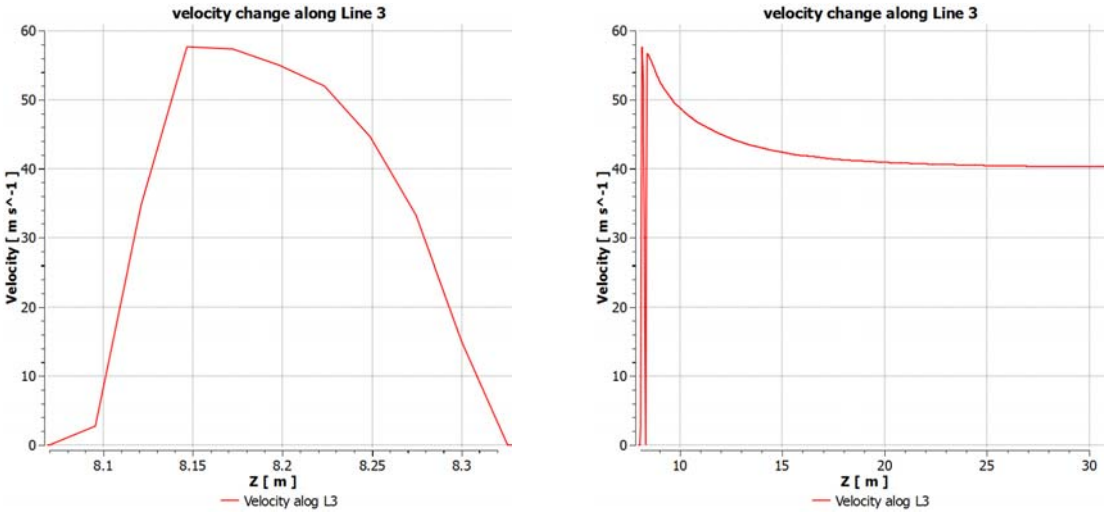


Fig. 5. 52. Wind velocity profile in the cavity and above roof along Line 3

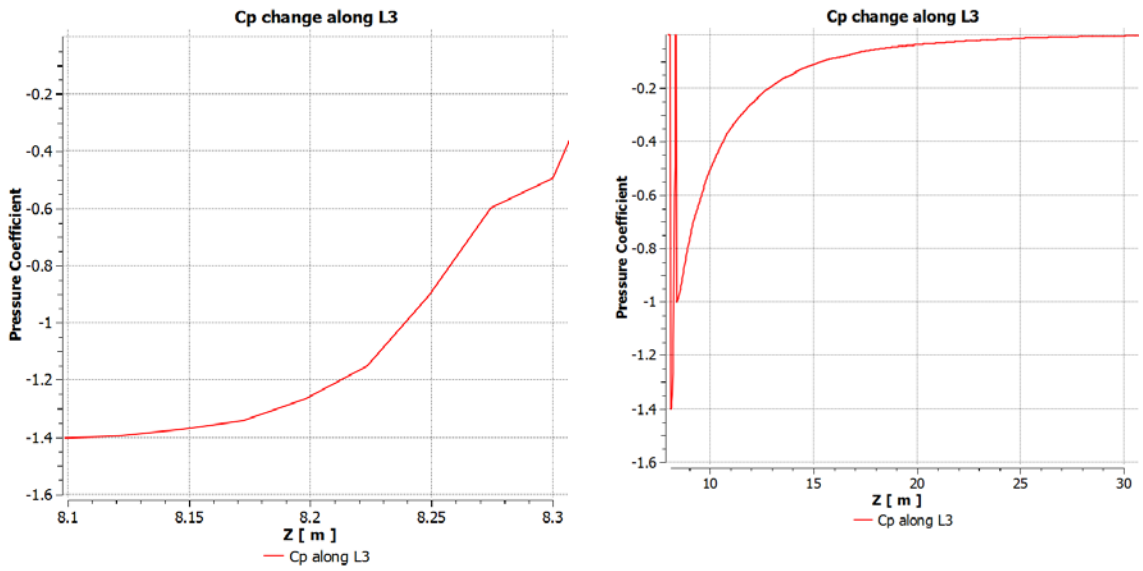


Fig. 5. 53. Pressure coefficient variation in the cavity and above the panels along Line 3

In the middle of the A edge of the panels, along Line 4, Fig. 5.54 shows the velocity profile between the roof surface and the bottom surface of the panels, where similar to the line 3 velocity evolution described above, the wind velocity increased from 0 m/s at the roof level, to 56.2 m/s in the middle of the cavity, then decreased again to 0 m/s on the bottom surface of the panels. Above the solar panel surfaces, a velocity increase was also noticed, however the values were slightly lower, reaching 46 m/s at 4" (0.103) above the panel surface, then decreased gradually to 40 m/s at 13.5m above the roof.

The pressure coefficient profiles in the cavity and above the solar panels are represented in Figure 5.55 where the pressure coefficient is -1.68 at the roof surface under the panels, then it increased to -1.87 at 1" (0.025m) above the middle of the gap, and before increasing slightly to -1.78 at 1.5" (0.037 m) below the panel surface, this dropped until -2.25 on the bottom surface of the panels. On top of the panels, the pressure coefficient is much lower than under the panels. It starts at -0.51 at top of the panels, then decreased gradually above the panels to 0 at 13.5m above the roof surface.

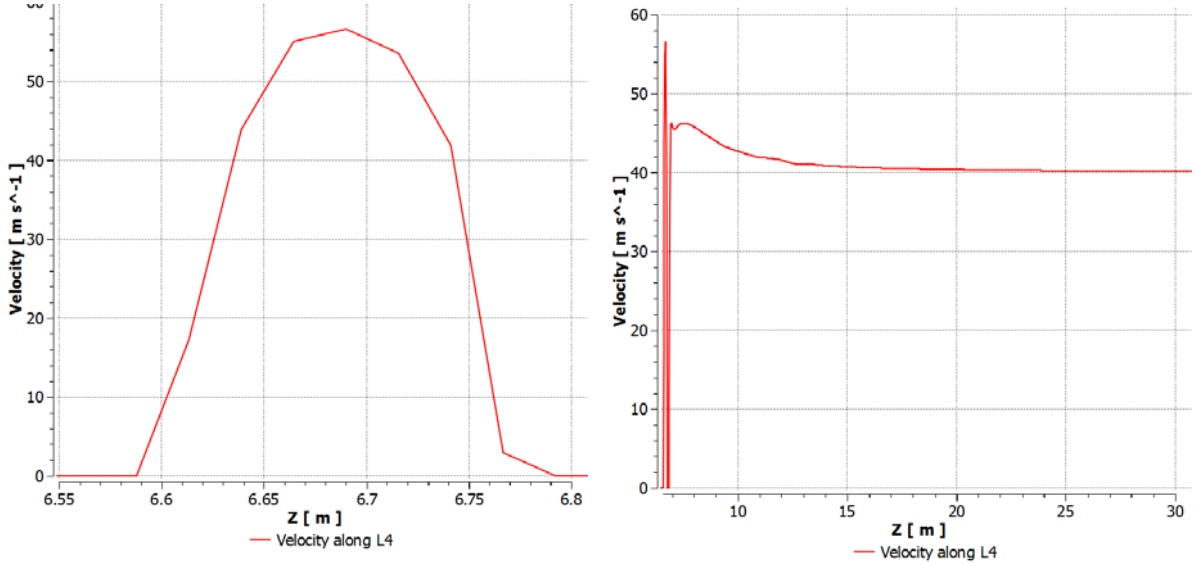


Fig. 5. 54. Wind velocity profile in the cavity and above roof along Line 4

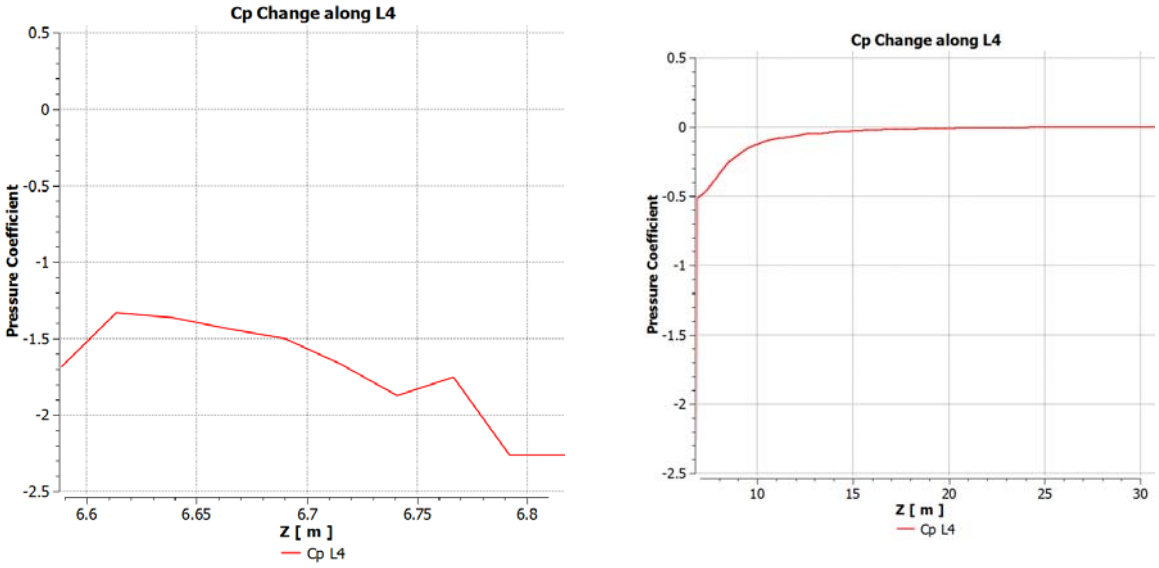


Fig. 5. 55. Pressure coefficient variation in the cavity and above the panels along Line 4

For the middle point of the roof, along Line 5, Fig. 5.56 depicts the velocity profile in the roof-panels cavity, where the velocity increased from 0 on the roof surface to a peak of 62.30 m/s, at 3” (0.075m) into the gap, then it decreased gradually to 56 m/s in the middle of the space, and to 0 m/s at the bottom surface of the panels. Moreover, the velocity on top of the solar panel surface

increased sharply to 49.50 m/s at 8” above the panels, then it decreased to 40 m/s at 23.50 m above the roof surface.

Figure 5.57 shows that the pressure coefficient in the cavity was -1.70 at the roof surface and then decreased slightly to – 1.60 at the bottom surface of the panels, which means that a nearly uniform pressure coefficient distribution was registered in the gap. On top of the panels, the pressure coefficient was lower, -0.46 on top of the panels, then increased slightly to -0.60 at 18” (0.45m) above the panel surface, gradually decreased to 0 above the panels at 23.50m above the roof surface.

Thus, for the middle of the roof, the wind velocity was very high, however the pressure in the wind field domain was not significantly affected, because no vortex core formation was in the proximity of line 5.

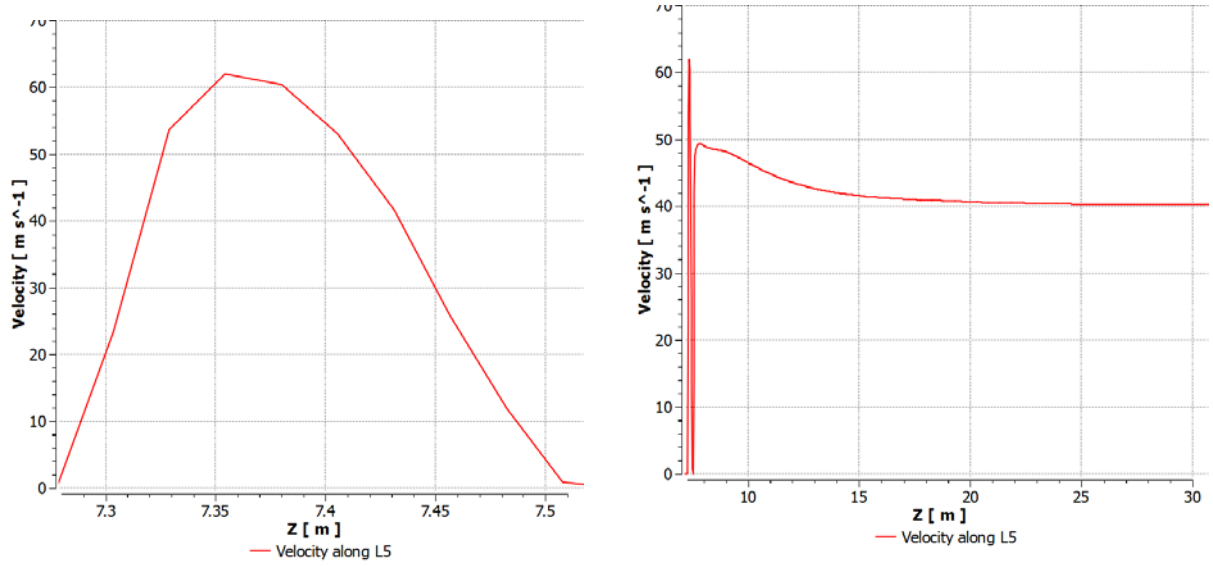


Fig. 5. 56. Wind velocity profile in the cavity and above roof along Line 5

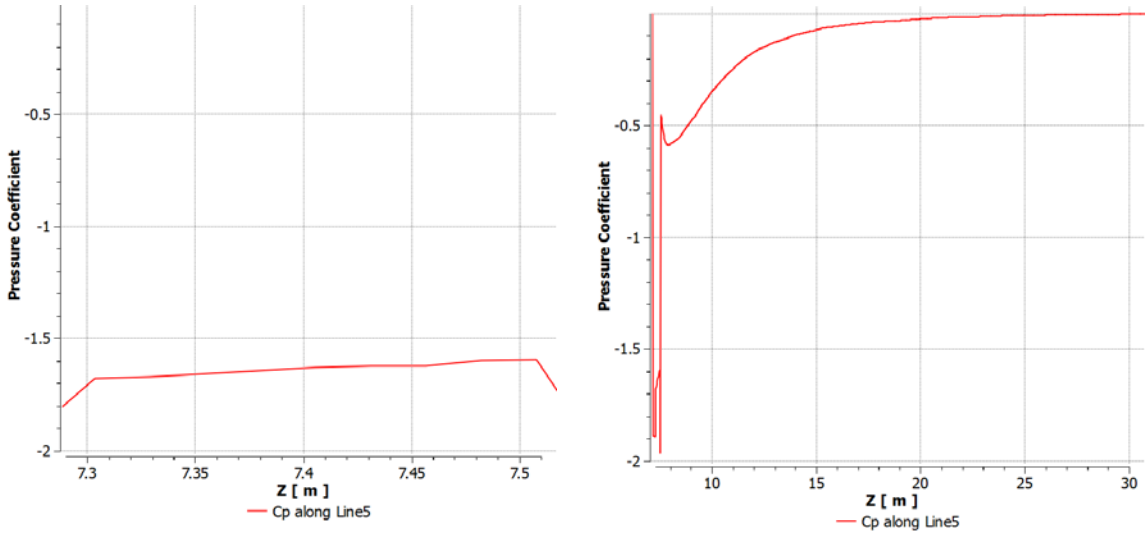


Fig. 5. 57. Pressure coefficient variation in the cavity and above the panels along Line 5

For the middle of the panels edge located near the ridge, along Line 6, the wind velocity in the cavity increased from 0 m/s on the roof surface to a high of 66.30 m/s, at 2” (0.051m) above the roof surface, then decreased gradually to 58 m/s in the middle of the space, and to 0 m/s again, at the bottom surface of the panels (Fig. 5.658). This is the highest wind velocity registered for the roof-panels cavity. However, the velocity on top of the solar panel surfaces increased sharply to 65.0 m/s at 8” above the panels, then decreases to 40 m/s at 23.50 m above the roof surface.

Figure 5.59 depicts the pressure coefficient profile between the roof surface and the bottom surface of the panels, for the same case of 10” (0.254 m) clearance; for line 6, the pressure coefficient in the cavity was very low, of -2.66 at the roof surface, associated with a high suction, then decreased slightly to -2.50 in the middle of the gap, and continues to decrease to – 2.05 at 0.75” under the bottom surface of the panels, where it then increased sharply to -3.40 at the bottom surface of the panels. These negative pressure coefficients were the lowest for the cavity regions investigated, thus the suction was the highest; this can be attributed to the high velocity formed in the gap, but also to the significant vortex core formations detected in the ridge region, as described in the previous subsections. On the top of the panels, the pressure coefficient was -1.60 on top of the panels, then decreased continuously to 0 at 23.50m above the roof surface.

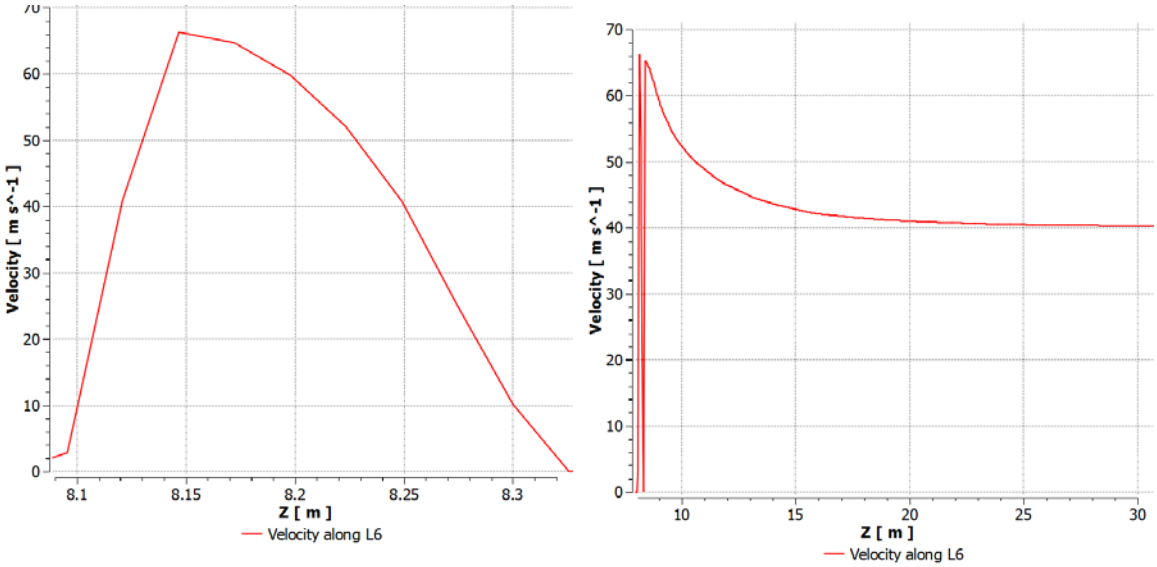


Fig. 5. 58. Wind velocity profile in the cavity and above roof along Line 6

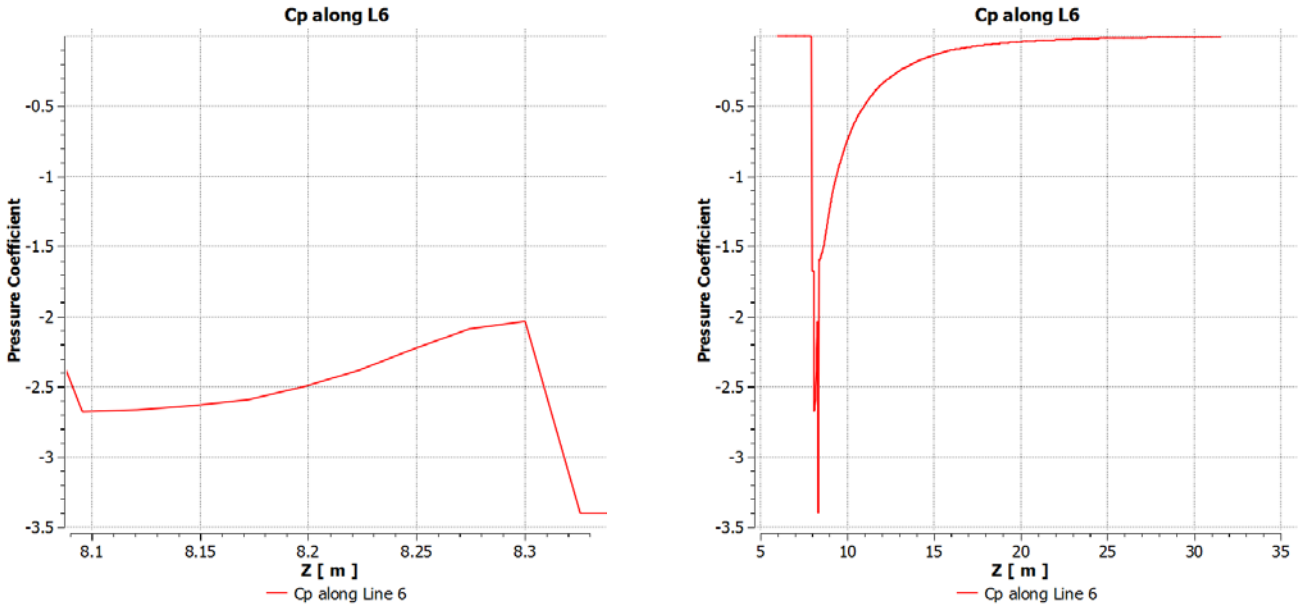


Fig. 5. 59. Pressure coefficient variation in the cavity and above the panels along Line 6

Moreover, the figures above, Figs. 5.58 to 5.59, show that under the solar panels which have a roof clearance of 10”, the wind flow is much faster (46 m/s to 66 m/s) than for a 3” roof clearance (10 m/s to 25 m/s), see 4.2. Thus it can be concluded that the wind velocity in the middle of the 10”

roof clearance in the roof – panels cavity is greater than the incoming velocity of 40 m/s, as detailed below (Fig.5.60). In addition, the maximum wind speed above the panels decreased slightly from the cavity maximum wind speeds to 46 m/s, 46 m/s, 47 m/s, 49 m/s, 56 m/s and 65 m/s for the lines L1, L2, L3, L4, L5 and L6, respectively. Moreover, the pressure coefficients registered for the 10" cavity space (-0.6, -0.9, -1.4, -1.7, -1.9 and -2.7) are lower than those registered for the 3" cavity space (or roof clearance) (0.10, -0.20, -0.60, -0.80, -2.80), for the incoming wind speed of 40 m/s.

The pressure coefficients in the roof-panels cavity, on the bottom surface of the panels, were very different, -0.60 to -1.70 for the two lines L1 and L4 along the same edge A of the panels (Fig. 5.61). Along the middle lines, L2 and L5, the pressure coefficients in the cavity increased to -0.90 to -1.90, while the Cp in the cavity further increased to -1.40 and -2.50 along the two lines L3 and L6, near the ridge of the roof (Fig.5.62). The maximum corresponding velocities were 46, 57, 46, 62, 58 and 66 m/s along lines L1, L4, L2, L5, L3 and L6 respectively (Fig.5.60).

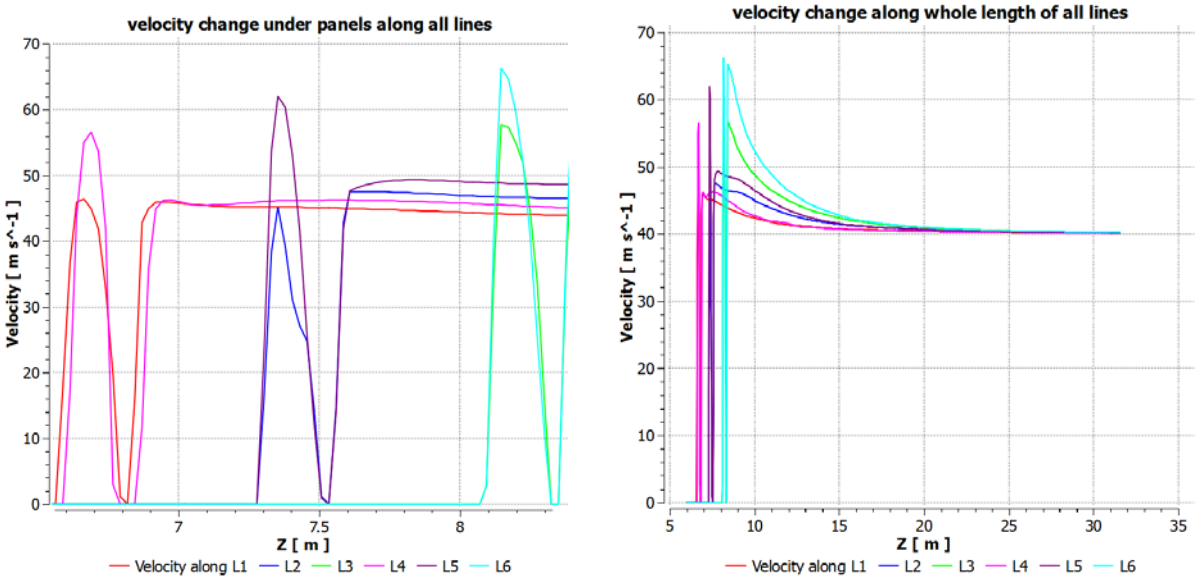


Fig. 5. 60. Wind velocity profile in the cavity and above roof along all 6 lines

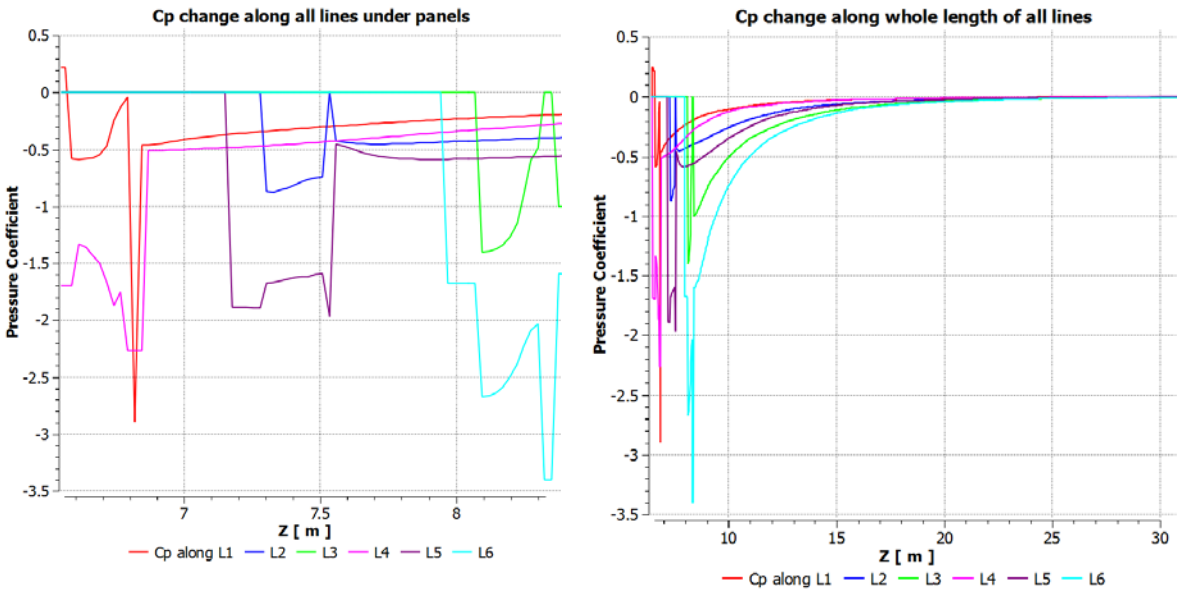


Fig. 5. 61. Pressure coefficient variation in the cavity and above the panels along all 6 lines

5.1.9. Wind flow characteristics and three-dimensional vortex formations for gable roofs without solar panels for wind direction 90º

The pressure coefficients in the roof-panels cavity and on top of the panels are influenced by the high wind velocity around the roof, but also by the three-dimensional vortex formations generated at edges of the solar panels arrays, at the ridge and in between the solar panels rows. However, it is not well understood the role that the solar panel array plays in the generation of these vortices. Therefore, to elucidate this question, a succinct analysis for three-dimensional vortex formations around gable roofs without solar panels arrays installed, was conducted. The same roof slope of 27º was selected for this investigation. Figures 5.62 shows that the pressure coefficient contours on the roof surface without solar panels, had low suction values with negative Cp of -0.05 to -1.41, or small positive pressure, with Cp between 0 and 0.40 on the windward side of the roof; for the leeward side, Fig, 5.63 a higher suction was noticed with Cp between -0.96 and -3.66. However, the lowest pressure coefficients are present near the ridge, mostly on the leeward side of the roof

and on edges A, B, D and F. Narrow areas at the ridge but near the D and F edges on leeward side are subject to the lowest pressure on the roof without solar panels (-4.11 to -4.56).

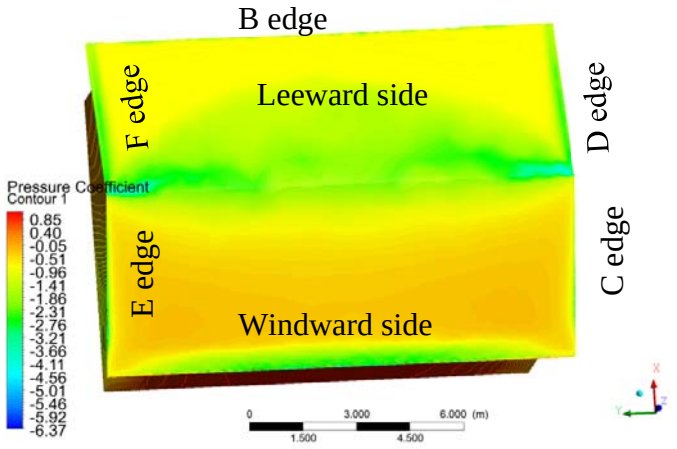


Fig. 5. 62. Pressure coefficient contours top view, windward, slope 27º, wind direction 90º

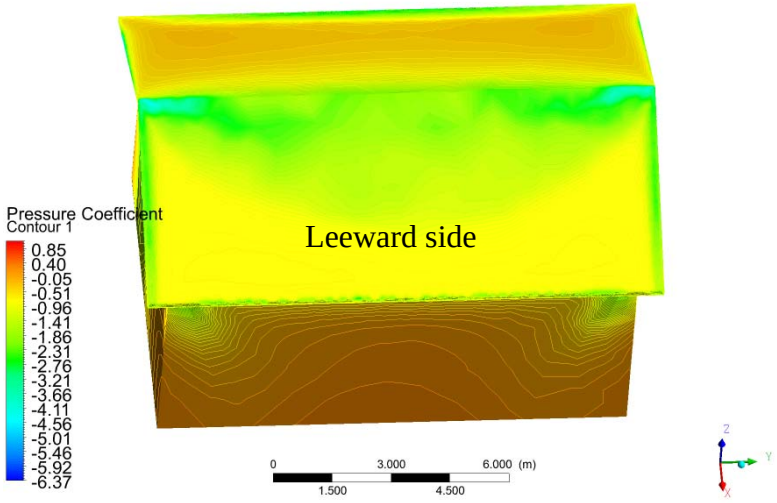


Fig. 5. 63. Pressure coefficient contours top view, leeward, slope 27º, wind direction 90º

Figures 5.62, 5.63, and 5.64 show the vortex cores formations on the roof without solar panels and around the building. The main difference between these and the vortex cores on a similar roof with

solar panels, was that the size of the ridge vortex cores, which is much larger for the roof without solar panels than the building vortex cores displayed in Figs. 5.64 to 5.65.

Moreover, from comparing the flow formations in Figs. 5.64 to 5.65 for the roofs with solar panels, it can be deduced that the vortex cores at edges of the roof without solar panels are comparable in size to the same-edge vortex cores of the roof with solar panels (Figs. 5.36-5.37). Also, there are no middle roof vortex cores on either the windward or leeward surfaces of the roof without solar panels, while middle-roof vortex cores exist between the panel rows, and on top and bottom surface of the panels.

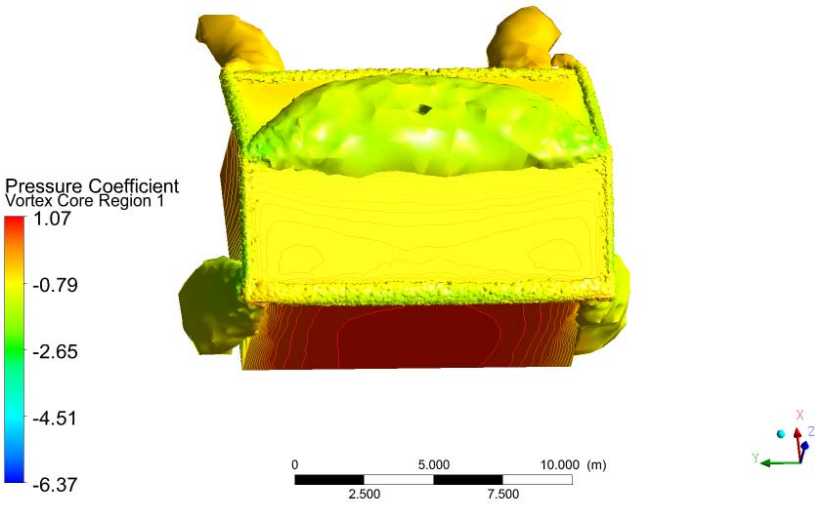


Fig. 5. 64. Vortex core representation for windward side of the roof, slope 27 º, wind direction 90º

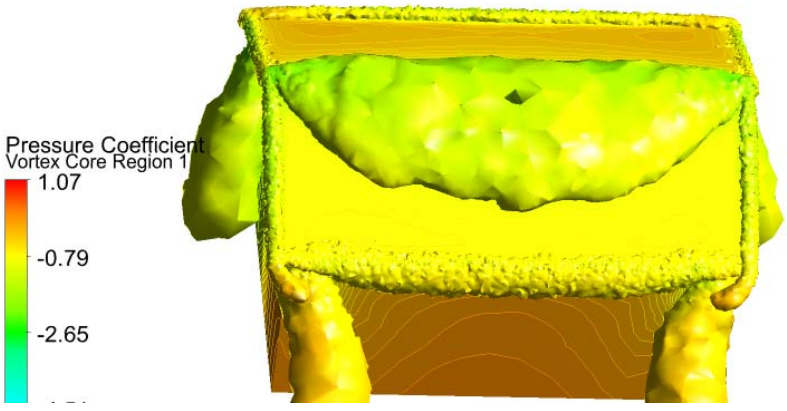


Fig. 5. 65. Vortex core representation for leeward side of the roof, slope 27 º, wind direction 90º

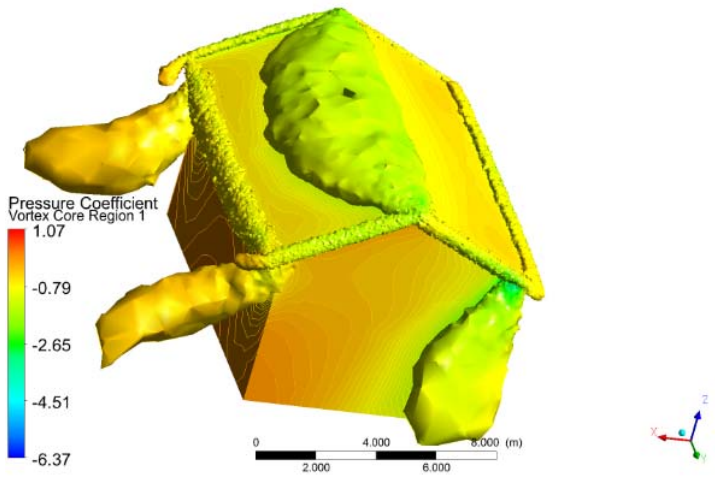
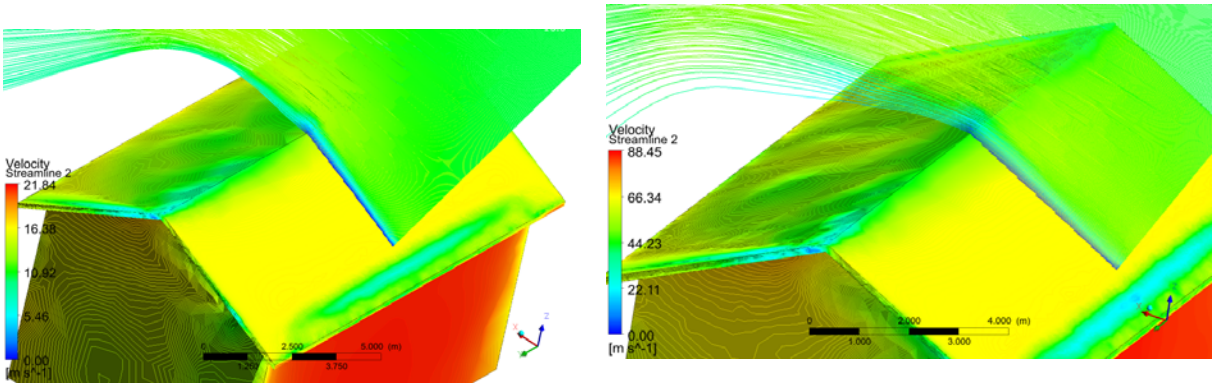


Fig. 5. 66. Vortex core representation, isometric view, slope 27 º, wind direction 90º

Figure 5.67 demonstrates the distribution of wind speed on a perpendicular plane at the middle of the roof without solar panels installed. In comparison with Fig. 5.33, which shows the velocity for lines perpendicular to the roof with solar panels, for the current case, the velocity remains smaller than the incoming free stream for nearly 0.10 m above the panels, then increased rapidly to 46 m/s to 78 m/s beyond 0.10 above the panels; thereafter the velocity decreased to reach the incoming free stream wind speeds at 13.5 to 23.50 m above the roof surface. However, the velocity stays below the incoming free stream velocity value of 40 m/s, for 0.30 m to 1.0 m above the surface of the roof without solar panels on the windward side, and then increased to reach 40 m/s incoming free steam speed. For the leeward side of the roof without panels, the velocity remained below the free stream for 1.00 m to 3.50 m above the leeward surface of roof without panels (Fig. 5.67).

On the other hand, the flow velocity near and above the ridge of the roof with solar panels reaches 78 m/s (Fig. 5.33), which is much faster than the flow speed above the ridge of the roof without solar panels (25 m/s to 30 m/s for 40m/s free stream speed).



a) b)

Fig. 5. 67. Streamlines on middle of roof, Line 4, slope 27 º, wind direction 90º, wind speeds 10 and 40 m/s

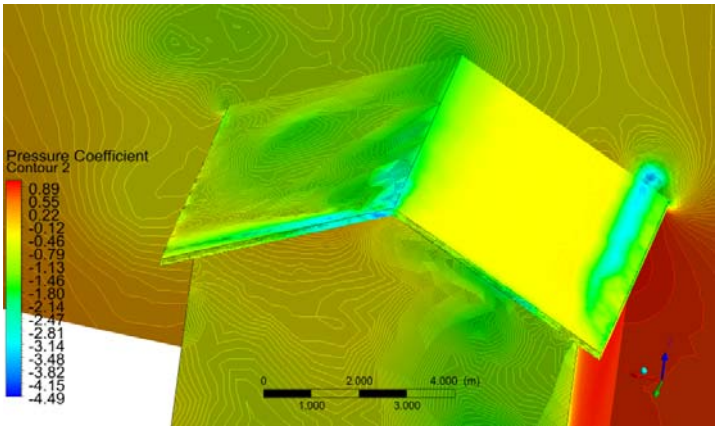


Fig. 5. 68. Pressure coefficients on transverse plane on the middle of the building, slope 27 º, wind direction 90º

Figure 5.68 shows the pressure coefficient distribution on the building roof, which is mainly -0.46 on the windward side away from the south overhang, and -1.13 to -1.60 on the leeward surface of the roof. In comparison with Figs. 5.24, the Cp on top of the panels on the windward side are lower than the Cp on windward side of roof without panels. However, the Cp on top of the panels on leeward side of the roof are lower than the Cp on the leeward side of the roof without panels. Moreover, the Cp on the ridge of the roof with solar panels is -2.36 to -5.61 (Fig. 5.1), which is much higher than the Cp of -1.60 to -3.14 on the ridge of the roof without solar panels (Fig. 5.68) It is obvious that the solar panels array can induce higher suction on the surface of the roof, in the vicinity of the ridge, however these very low pressure areas are located outside the panel array, thus these are not exposed to high suction.

5.1.10. Net pressure coefficients on roof with and without solar panels array for wind directions 90º and 45º, clearance 10” and spacing 2”

The distribution of all polylines on the roof surface without panels, which were set 200 mm apart from each other (Fig. 5.69), was similar to the polylines distribution used for the roof surface with solar panels, such that pressure coefficients comparison between these two cases can be performed. Also for results consistency, the same roof slope of 27º was used. The pressure coefficients were recorded along these polylines, and the values were used in the calculation of the average pressure coefficients for sections of the roof or for entire paneled roof area, for either the windward or leeward surfaces. However, only some polylines (located in the middle and near edges of either the windward or leeward surfaces) are explained in detail in this section while the complete results are provided in Appendix D.

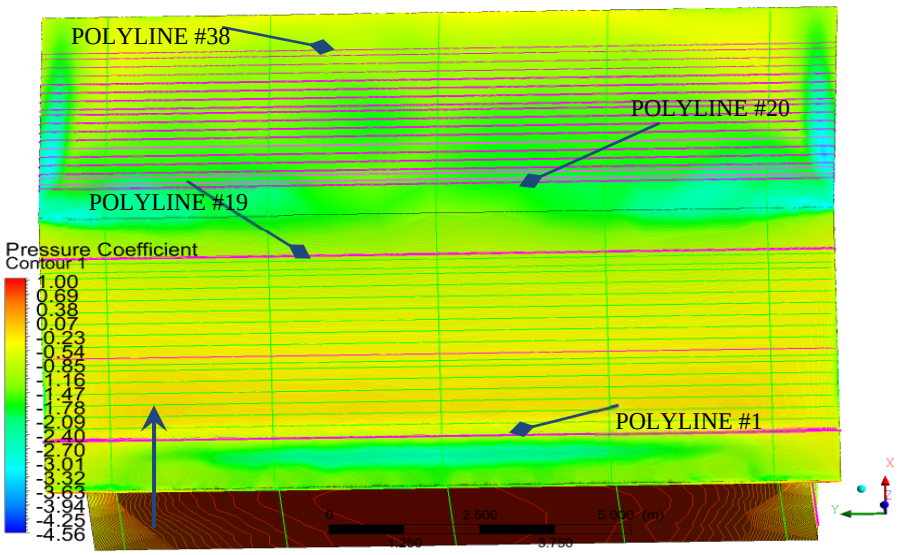
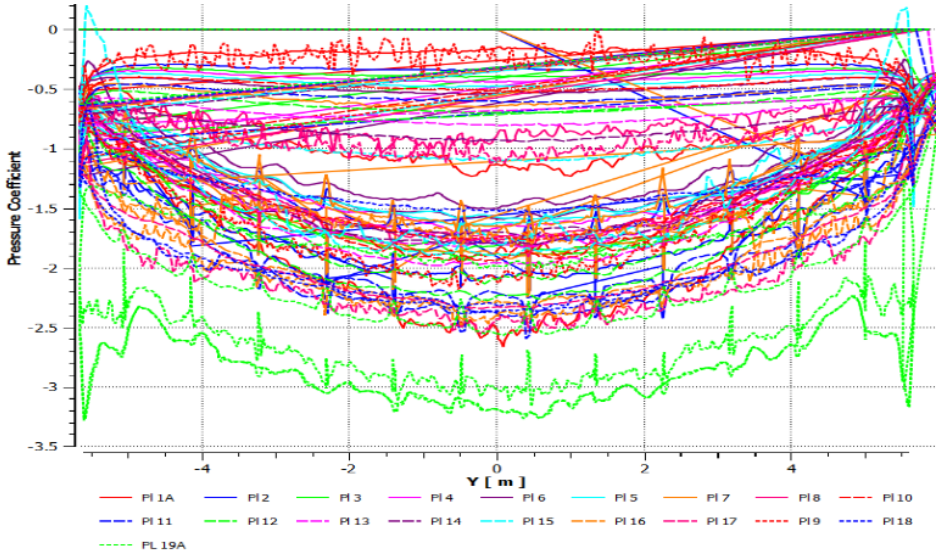


Fig. 5. 69. Roof without solar panels, slope 27 º, wind direction 90º

Figure 5.70 shows the pressure coefficients along the length of the polylines 21 to 38, on the windward and leeward sides of the roof of the building, including at the top of the panels, bottom surface of the panels, and surface of the roof, for wind direction 90º. The polylines show a gradual transition of the pressure coefficients from a smaller suction near the A and B edges of the roof (PL 1 and PL 38) to higher suction near the ridge (PL 19 and PL 20). The effect of the solar panels supports are represented by the regular drops in pressure coefficients, registered only along the polylines crossing the areas in the vicinity of the supports.

Fig. 5.71 depicts the pressure coefficients along the polylines on the windward and leeward sides of the roof without solar panels, for wind direction 90º. The same gradual transition towards higher suction is noticed for the roof without solar panels, with the exception of the first polyline, PL1, near edge A of the roof, which registered the highest suction, as it can also be noticed in Fig. 5.68 representing the pressure coefficients on the roof surface. For the leeward side of the roof, the presence of the ridge vortex core formation was signaled by the lower pressure coefficients registered in the middle region of the roof for polyline 21 to 26. Also it should be noted that the pressure coefficients values were integrated along all the polylines and the average values were considered on each polyline for each of the three surfaces (top and bottom surface of the panels and the surface of the roof) as presented in the tables below.



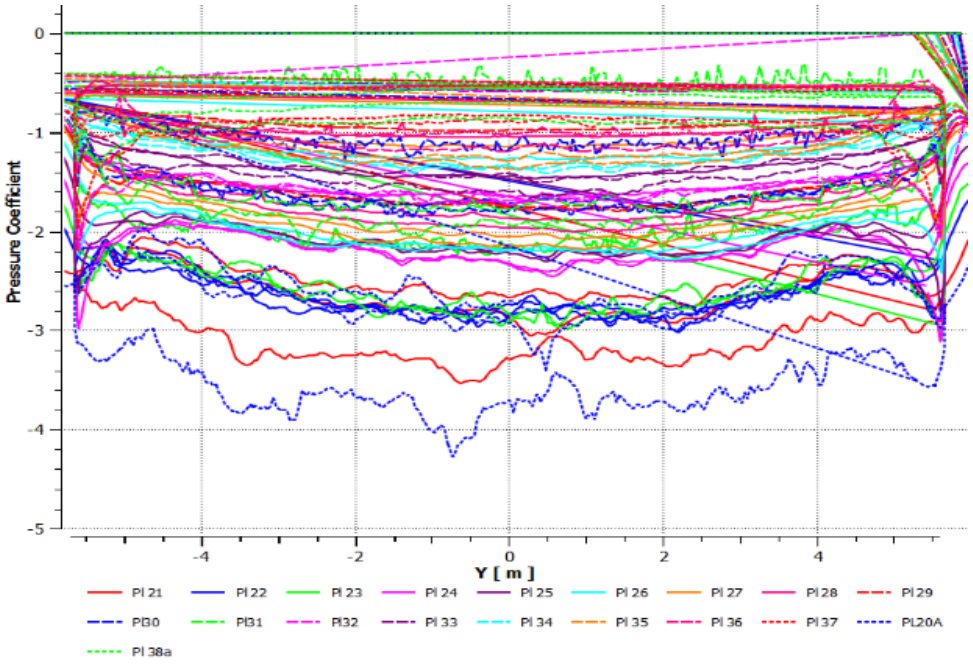
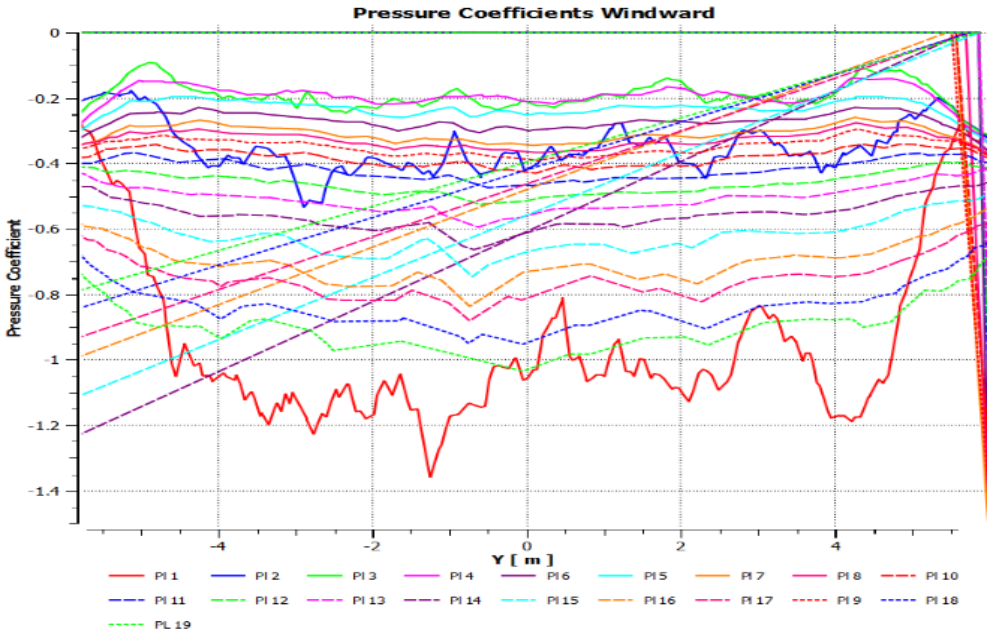


Fig. 5. 70. Pressure coefficients, windward and leeward sides for the roof with solar panels, slope 27 º, wind direction 90º



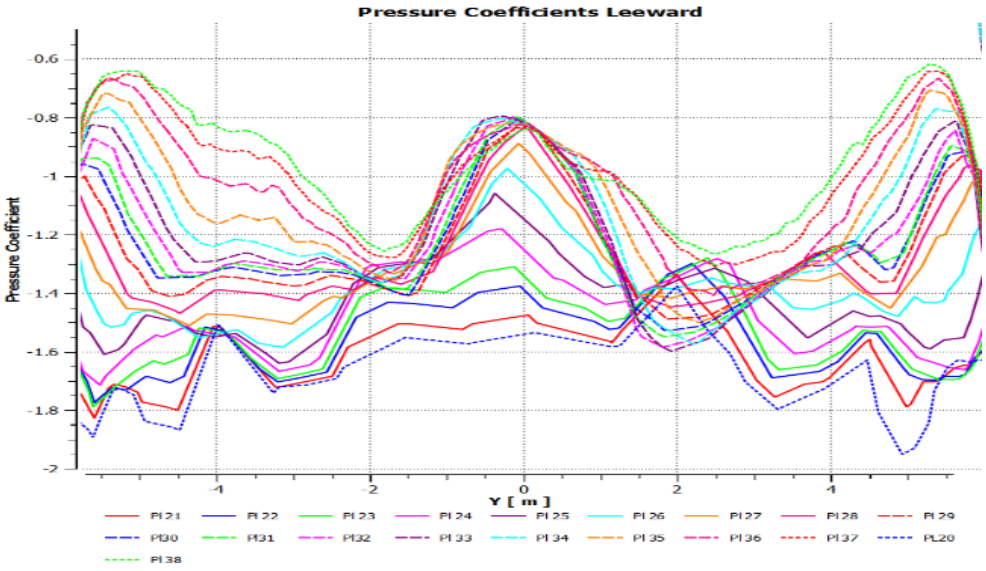


Fig. 5. 71. Pressure coefficients, windward and leeward sides for the roof without solar panels, slope 27 º, wind direction 90º

The following tables, from Table 5.1 to Table 5.5, disclose the integration results of the pressure coefficients along all the investigated polylines, where each polyline crosses 3 planes (roof surface and bottom and top of the panels), which are all parallel to the roof surface; thus three different pressure coefficient polylines were assigned, where each polyline sits on a different surface. The pressure coefficient polylines located on the roof surface without solar panels installed, are integrated for the polylines crossing under the solar array area only, and dismissed the roof areas beyond the peripheries of the solar panel array.

Each polyline, on each surface has 400 points equally distributed along the polyline, either on top of the panels, bottom surface of the panels, or the roof surface under the panels. The average value of the pressure coefficients is taken for each polyline at each surface.

The solar panels array sits on the metal supporting racks, which are able to redistribute wind loads and transfer the loads to the roof structure. The net pressure coefficients, which can be used in the calculation of the design wind loads on the solar panels and then on the racks, are the differences between the pressure coefficients on the top and bottom surface of the panels, and were calculated in separate columns in Tables 5.1 and 5.5.

The net pressure coefficients (top + roof surface – bottom surface of the panels) were calculated in a separate column and then were divided by the pressure coefficients of the roof without solar

panels, which give the ratios of the total pressure coefficients on the roof with solar panels to the coefficients on the corresponding roof without solar panels. The conclusions on the presented results are summarized hereafter.

Table 5. 1. Pressure coefficients for roof without solar panels vs. net pressure coefficients for the roof-panels system, slope 27º, 90º, windward side

Polylines	Cp for roof without panels	CP for bottom surface of the panels	Cp for roof under the panels	Cp on top surface of the panels	Cp difference top –bottom surfaces of the panels	Net Cp for the system roof-panels	Ratio of net Cp on system roof-panels / roof without solar panels
PL1	-0.85	-1.80	-0.92	-0.23	1.57	0.65	-0.76
PL2	-0.37	-1.76	-1.42	-0.33	1.43	0.01	-0.03
PL3	-0.24	-1.52	-1.48	-0.39	1.13	-0.35	1.46
PL4	-0.23	-1.40	-1.34	-0.42	0.98	-0.36	1.57
PL5	-0.25	-0.25	-1.21	-0.45	-0.20	-1.41	5.64
PL6	-0.28	-1.20	-1.19	-0.49	0.71	-0.48	1.71
PL7	-0.32	-1.17	-1.24	-0.58	0.59	-0.65	2.03
PL8	-0.34	-1.40	-1.29	-0.76	0.64	-0.65	1.91
PL9	-0.36	-1.50	-1.26	-0.24	1.26	00	00
PL10	-0.39	-1.53	-1.48	-0.48	1.05	-0.43	1.10
PL11	-0.43	-1.98	-1.80	-0.54	1.44	-0.36	0.84
PL12	-0.48	-1.84	-1.68	-0.6	1.24	-0.44	0.92
PL13	-0.53	-1.56	-1.42	-0.68	0.88	-0.54	1.02
PL14	-0.58	-1.45	-1.40	-0.8	0.65	-0.75	1.29
PL15	-0.66	-1.41	-1.38	-0.95	0.46	-0.92	1.39
PL16	-0.74	-2.02	-1.56	-1.56	0.46	-1.10	1.49
PL17	-0.79	-2.03	-0.91	-0.91	1.12	0.21	-0.27
PL18	-0.87	-2.04	-1.96	-1.33	0.71	-1.25	1.44
PL19	-0.92	-1.60	-2.06	-1.63	-0.03	-2.09	2.27
Ave	-0.51	-1.55	-1.42	-0.70	0.85	-0.57	1.13
STD	0.23	0.42	0.30	0.41	0.48	0.62	1.33
COV	0.46	0.27	0.21	0.59	0.56	-1.08	-0.02

Table 5. 2. Pressure coefficients for roof without solar panels vs. net pressure coefficients for the roof-panels system, slope 27º, wind direction 90º, leeward side

Polylines	Cp for roof without panels	CP for bottom surface of the panels	Cp for roof under the panels	Cp on top surface of the panels	Cp difference top –bottom surfaces of the panels	Net Cp for the system roof-panels	Ratio of net Cp on system roof-panels / roof without solar panels
Pl20	-1.8	-2.87	-2.6	-3.8	-0.93	-3.53	1.96
Pl21	-1.78	-3.11	-2.58	-2.82	0.29	-2.29	1.29
Pl22	-1.74	-2.31	-2.62	-2.49	-0.18	-2.80	1.61
Pl23	-1.7	-2.26	-2.61	-1.99	0.27	-2.34	1.38
Pl24	-1.66	-2.18	-2.17	-1.54	0.64	-1.53	0.92
Pl25	-1.63	-2.25	-2.11	-1.34	0.91	-1.20	0.74
Pl26	-1.6	-2.15	-2.09	-1.16	0.99	-1.10	0.69
Pl27	-1.56	-1.96	-1.89	-1.03	0.93	-0.96	0.62
Pl28	-1.53	-1.76	-1.70	-0.94	0.82	-0.88	0.58
Pl29	-1.5	-1.63	-1.61	-0.87	0.76	-0.85	0.57
Pl30	-1.46	-1.62	-1.61	-0.65	0.97	-0.64	0.44
Pl31	-1.42	-1.80	-1.74	-0.54	1.26	-0.48	0.34
Pl32	-1.35	-1.58	-1.54	-0.56	1.02	-0.52	0.39
Pl33	-1.33	-1.46	-1.41	-0.56	0.90	-0.51	0.38
Pl34	-1.31	-1.28	-1.26	-0.56	0.72	-0.54	0.41
Pl35	-1.14	-1.21	-1.22	-0.56	0.65	-0.57	0.50
Pl36	-1.08	-1.05	-1.01	-0.56	0.49	-0.52	0.48
Pl37	-1.01	-0.99	-0.90	-0.59	0.40	-0.50	0.50
Pl38	-0.97	-0.96	-0.80	-0.58	0.38	-0.42	0.43
Ave	-1.45	-1.81	-1.76	-1.22	0.59	-1.17	0.80
STD	0.26	0.61	0.59	0.93	0.50	0.91	0.47
COV	-0.18	-0.33	-0.33	-0.76	0.85	-0.78	0.58

Table 5. 3. Pressure coefficients for roof without solar panels vs. net pressure coefficients for the roof-panels system, slope 27º, wind direction º45, windward side

Polylines	Cp for roof without panels	CP for bottom surface of the panels	Cp for roof under the panels	Cp on top surface of the panels	Cp difference top – bottom surfaces of the panels	Net Cp for the system roof-panels	Ratio of net Cp on system roof-panels / roof without solar panels
Pl1	-0.36	-0.60	-0.43	-0.41	0.19	-0.24	0.67

Pl2	-0.36	-0.12	-0.52	-0.41	-0.29	-0.81	2.25
Pl3	-0.37	-1.13	-1.00	-0.41	0.72	-0.28	0.76
Pl4	-0.38	-0.62	-0.80	-0.41	0.21	-0.59	1.55
Pl5	-0.4	-0.54	-0.59	-0.41	0.13	-0.46	1.15
Pl6	-0.42	-0.36	-0.54	-0.44	-0.08	-0.62	1.48
Pl7	-0.43	-0.80	-0.60	-0.47	0.33	-0.27	0.63
Pl8	-0.45	-1.20	-1.05	-0.6	0.60	-0.45	1.00
Pl9	-0.45	-0.95	-0.99	-0.29	0.66	-0.33	0.73
Pl10	-0.46	-0.70	-0.95	-0.47	0.23	-0.72	1.57
Pl11	-0.48	-1.29	-1.19	-0.46	0.83	-0.36	0.75
Pl12	-0.49	-0.92	-1.10	-0.5	0.42	-0.68	1.39
Pl13	-0.51	-0.79	-0.87	-0.55	0.24	-0.63	1.24
Pl14	-0.57	-0.71	-0.79	-0.62	0.09	-0.70	1.23
Pl15	-0.65	-0.48	-0.83	-0.71	-0.23	-1.06	1.63
Pl16	-0.69	-1.56	-1.36	-0.98	0.58	-0.78	1.13
Pl17	-0.77	-1.32	-1.37	-0.66	0.66	-0.71	0.92
Pl18	-0.85	-1.10	-1.33	-0.97	0.13	-1.20	1.41
Pl19	-0.9	-1.50	-1.30	-1.14	0.36	-0.94	1.04
Ave	-0.53	-0.88	-0.93	-0.57	0.30	-0.62	1.19
STD	0.17	0.39	0.30	0.23	0.32	0.27	0.41
COV	-0.32	-0.45	-0.33	-0.40	0.104	-0.43	0.35

Table 5. 4. Pressure coefficients for roof without solar panels vs. net pressure coefficients for the roof-panels system, slope 27º, wind direction 45º, leeward

Polylines	Cp for roof without panels	CP for bottom surface of the panels	Cp for roof under the panels	Cp on top surface of the panels	Cp difference top –bottom surfaces of the panels	Net Cp for the system roof-panels	Ratio of net Cp on system roof-panels / roof without solar panels
Pl20	-1.33	-2.38	-1.84	-1.64	0.74	-1.10	0.83
Pl21	-1.31	-2.38	-1.79	-1.49	0.89	-0.90	0.69
Pl22	-1.23	-1.74	-1.54	-1.44	0.30	-1.24	1.01
Pl23	-1.17	-1.41	-1.47	-1.05	0.36	-1.11	0.95
Pl24	-1.08	-1.70	-1.65	-0.9	0.80	-0.85	0.79

Pl25	-1.04	-1.72	-1.44	-0.83	0.89	-0.55	0.53
Pl26	-0.98	-1.21	-1.17	-0.77	0.44	-0.73	0.74
Pl27	-0.94	-1.10	-1.07	-0.74	0.36	-0.71	0.76
Pl28	-0.90	-0.95	-1.10	-0.72	0.23	-0.87	0.97
Pl29	-0.87	-1.38	-1.29	-0.72	0.66	-0.63	0.72
Pl30	-0.84	-1.20	-1.10	-0.8	0.40	-0.70	0.83
Pl31	-0.83	-1.03	-1.10	-0.68	0.35	-0.75	0.90
Pl32	-0.80	-1.35	-1.27	-0.68	0.67	-0.60	0.75
Pl33	-0.76	-1.27	-1.05	-0.68	0.59	-0.46	0.61
Pl34	-0.72	-0.95	-0.93	-0.68	0.27	-0.66	0.92
Pl35	-0.69	-0.88	-0.88	-0.68	0.20	-0.68	0.99
Pl36	-0.67	-0.78	-0.93	-0.69	0.09	-0.84	1.25
Pl37	-0.65	-1.34	-1.16	-0.71	0.63	-0.53	0.82
Pl38	-0.65	-0.96	-0.83	-0.75	0.21	-0.62	0.95
Ave	-0.92	-1.35	-1.24	-0.88	0.48	-0.76	0.83
STD	0.22	0.46	0.30	0.30	0.25	0.21	0.16
COV	-0.24	-0.34	-0.24	-0.35	0.52	-0.27	0.20

Table 5. 5. Pressure coefficients for roof without solar panels vs. net pressure coefficients for the roof-panels system, slope 27º, wind direction 0º

Polylines	Cp for roof without panels	CP for bottom surface of the panels	Cp for roof under the panels	Cp on top surface of the panels	Cp difference top –bottom surfaces of the panels	Net Cp for the system roof-panels	Ratio of net Cp on system roof-panels / roof without solar panels
Pl1	-0.33	-0.38	-0.41	-0.4	0.02	-0.39	1.18
Pl2	-0.33	-0.38	-0.43	-0.42	0.04	-0.39	1.18
Pl3	-0.33	-0.39	-0.49	-0.48	0.09	-0.4	1.21
Pl4	-0.36	-0.39	-0.5	-0.49	0.10	-0.4	1.11
Pl5	-0.36	-0.39	-0.5	-0.49	0.10	-0.4	1.11

Pl6	-0.36	-0.39	-0.5	-0.49	0.10	-0.4	1.11
Pl7	-0.36	-0.38	-0.48	-0.47	0.09	-0.39	1.08
Pl8	-0.35	-0.39	-0.47	-0.46	0.07	-0.4	1.14
Pl9	-0.35	-0.38	-0.47	-0.46	0.08	-0.39	1.11
Pl10	-0.35	-0.38	-0.48	-0.47	0.09	-0.39	1.11
Pl11	-0.35	-0.38	-0.52	-0.52	0.14	-0.38	1.09
Pl12	-0.35	-0.38	-0.52	-0.52	0.14	-0.38	1.09
Pl13	-0.34	-0.38	-0.52	-0.52	0.14	-0.38	1.12
Pl14	-0.34	-0.38	-0.52	-0.51	0.13	-0.39	1.15
Pl15	-0.34	-0.38	-0.46	-0.45	0.07	-0.39	1.15
Pl16	-0.34	-0.4	-0.44	-0.43	0.03	-0.41	1.21
Pl17	-0.34	-0.4	-0.43	-0.41	0.01	-0.42	1.24
Pl18	-0.34	-0.38	-0.43	-0.43	0.05	-0.38	1.12
Pl19	-0.33	-0.38	-0.43	-0.43	0.05	-0.38	1.15
Ave	-0.34	-0.38	-0.47	-0.47	0.08	-0.39	1.14
STD	0.01	0.01	0.04	0.04	0.04	0.01	0.04
COV	-0.03	-0.02	-0.08	-0.08	0.50	-0.03	0.04

When comparing the ratios of net Cp obtained for the three surfaces of the roof-panels system to the roof surface without solar panels (Net Cp_system / Cp_roof), for the windward and leeward sides of the roof (the last column in the tables 5.1 to 5.5 above), it was noticed that, for both wind directions, 45º and 90º, the windward side registered highly fluctuating differences from one polyline to the other, while the ratios for the leeward side were more consistent. Also for the windward side, except for the first three polylines for 90º, and except for the polyline 38 for 45º, the ratios Net Cp_system / Cp_roof were smaller than unity which means that the net pressure coefficient for roof with solar panels was smaller than the pressure coefficients registered for the roof without solar panels (Tables 5.3 and 5.4). However for the windward side of the roof, the ratios net Cp_system / Cp_roof were smaller than 1.0 for polylines 1, 2, 9 11, 12 and 17, and were between 1.00 and 1.5 for polylines 10, 13, 14, 15 and 18 and were higher than 1.5 for polylines 3, 4, 5, 6, 7, 8 and 19, when 90º wind direction is considered (Table 5.1). For 45º wind direction, the windward side of the roof registered ratios NetCp_system / Cp_roof smaller than 1.0 for 1, 3, 7, 9, 11 and 17, between 1.0 and 1.5 for polylines 4, 5, 6, 8, 12 to 17 and 18 and above 1.5 only for polylines 2, 4, 10 and 15 (Table 5.3). Therefore a clear pattern cannot be deduced, however it can

be considered that the net pressure on the roof with solar panels was higher than the pressure on the roof without panels near the A edge of the roof and near the ridge, while for the middle section of the roof, these were more balanced or the net pressure on roof surface without panels was lower than for the case when panels are installed.

It is interesting to note that for the 0º wind direction (Table 5.5) the ratios Net Cp system / Cp roof were in between 1.09 to 1.24, thus the pressure on the roof was slightly higher when the panels were installed, however the distribution was more consistent than for the previous cases of 90º and 45º. Also, the windward and leeward sides are not presented because the flow runs parallel with edges A and B of the roof, thus these are symmetric in regard to wind direction.

5.2. Effects of roof clearance 3” and array spacing 2” on roof mounted solar panels, inclined roof 27º, wind direction 90º, 45º and 0º

The previous cases were discussed for the cavity clearance between the roof and the panels of 10”, however in order to determine the effect of this height, a smaller clearance of 3” was investigated in the current section. All results, descriptions and explanations for the current case which employs cavity clearance 3” and array spacing 2” are similar to the Section 5.1; moreover part of the results can be found in Chapter 4, Section 4.1, and will not be duplicated herein. Similarly, the relevant tabulated results of integration of pressure coefficients on the three surfaces of the roof-panels system, in comparison with the roof without solar panels, are presented in Chapter 4. Table 4.6 to Table 4.10, present the integration results of the pressure coefficients along all polylines for wind directions 90º, 45º and 0º. The pressure coefficient for the polylines located on the roof surface were integrated under the solar array area, while the roof areas beyond the peripheries of the solar panel array were dismissed. Thereafter the average value of the pressure coefficients was considered for each polyline crossing each of the surfaces investigated. The differences between the pressure coefficients on the top and bottom surface of the panels were calculated in separate columns in Tables 4.6 and 4.10. The total pressure coefficients (top + roof surface – bottom surface of the panels) were also determined in a separate column and then divided by the pressure coefficients on the roof without solar panels for obtaining the ratio NetCp_system / Cp_roof. The main conclusions and the comparison with the case of 10” clearance were presented below.

5.3. Conclusions

From the cases presented above it is concluded that:

- For the slope 27º, 2” spacing, and clearances 3” and 10”, the solar panels mounted on the gable roof result in the redistribution of pressure on the roof with solar panels in comparison with the roof without solar panels, on both sides of the roof. Due to this redistribution, the suction on the windward side increased while decreasing on the leeward side of the roof with solar panels was observed.
- The redistribution of pressure also results in a reduction of the largest suction coefficients to 79% and 80% of that on roof without panels, for the spacing/clearance cases 2”/3” and 2”/10” respectively (Tables 4.7, and 5.2), which are all on the leeward side of the roofs. These reductions are for same wind direction 90º for which the highest suction on roofs with and without solar panels was registered.
- As the clearance between the solar panels and the roof surface increased from 3” to 10”, the total suction (negative pressure coefficients) on the leeward side of the roof increased slightly for 90º and 0º wind directions. However, the total suction on the leeward side of the roof decreased slightly for 45º wind direction.

- When clearance /spacing is 3”/2”, the pressure on the roof under the panels are almost equal to the pressure on the bottom surface of the panels. As a result, the pressure coefficients on the roof with solar panels can be approximated by the pressure coefficients for the top of the solar panels. The error in this approximation is less than 1% for wind direction 90º and leeward side of the wind direction 45º case; this error increased to 6 % for windward side for the wind direction 45º, Tables (4.6-4.10).

- Both clearances 3” and 10” cause a redistribution of pressure, towards more consistent pressure coefficients values on windward and leeward sides of the roof, where these coefficients become closer to the ones registered for the roof without solar panels. Consequently, the roof – panels system is subject to much lower wind-induced pressure as a summation of the horizontal pressures projection in the wind direction, on both roof sides,

windward and leeward. However, when clearance increased from 3” to 10”, the corresponding horizontal pressure, projected on the wind direction increased for wind direction 90º, while slightly decreases for wind direction 45º.

- The net pressure on solar panels for clearance /spacing is 3”/2”, is directed towards the roof, where highest net pressure is for wind direction 90º and lowest is for wind direction 0º. However, when clearance increased from 3” to 10”, the net pressure on the solar panels, increased considerably, where the highest increase is for wind direction 90º, and lowest is for wind direction 0º.

5.4. Effects of roof clearance 3” and array spacing 8” on roof mounted solar panels, inclined roof 27º, wind directions 90º, 45º, and 0º

5.4.1. Pressure contour distributions, wind direction 90º

The effects of panel row spacing are examined hereafter for 8” spacing, 3” roof clearance, and 90º wind direction, for roof slope 27º, where this array configuration will be compared with 2” row spacing and 3” roof clearance of the same roof slope of 27º. However, the results of the pressure coefficient integrations will be presented in tables to allow for a complete comparison with the other wind direction cases. The first configuration is presented in detail, while the latter was already presented in Section 4.1 in Chapter 4.

Figure 5.72 shows the pressure coefficient contours for , slope 27º and wind direction 90º, for roof surfaces with solar panels mounted with clearance 3” and row spacing 8”, while Fig. 5.73 shows the configuration of the polylines used to record the pressure coefficients. In addition, Fig. 5.73 shows the polylines PL1, PL9 and PL16 on the windward side of the roof.

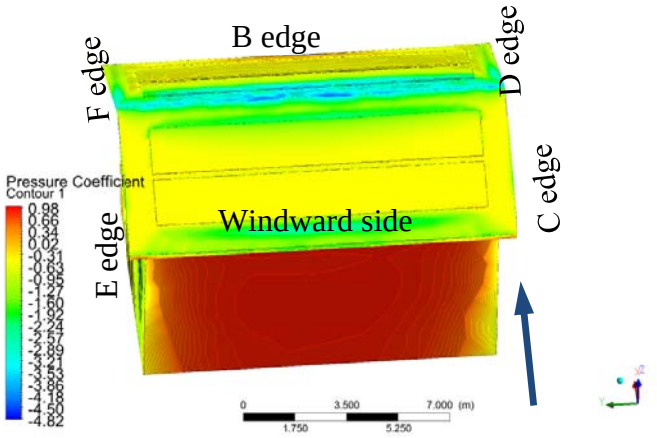


Fig. 5.72, Pressure coefficient contours of roof with solar panels, slope 27º, windward, wind direction 90º

Figure 5.74 a) depicts the pressure coefficient distribution on the bottom surface of the solar panels on the windward side of the roof, for wind direction 90º. Fig. 5.74 a) reveals a significant similarity with Fig. 5.75, which illustrates the pressure coefficient distributions on the roof under the solar panels on the windward side and for the same wind direction of 90º. As shown, the Cp changed from 0.31 to -2.89 on both the bottom surface of the panels and on the roof surface under the panels. The similarity between the Cp distributions and values on the two surfaces is high.

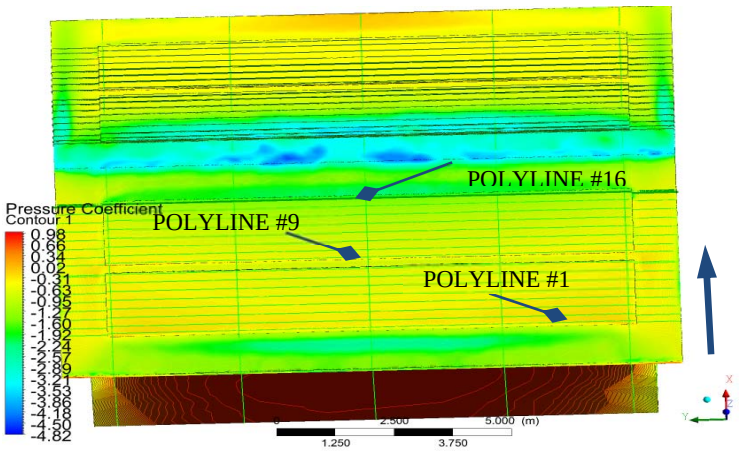


Fig. 5. 73. Pressure coefficients on top of solar panels with Plines, slope 27º, windward, wind direction 90º

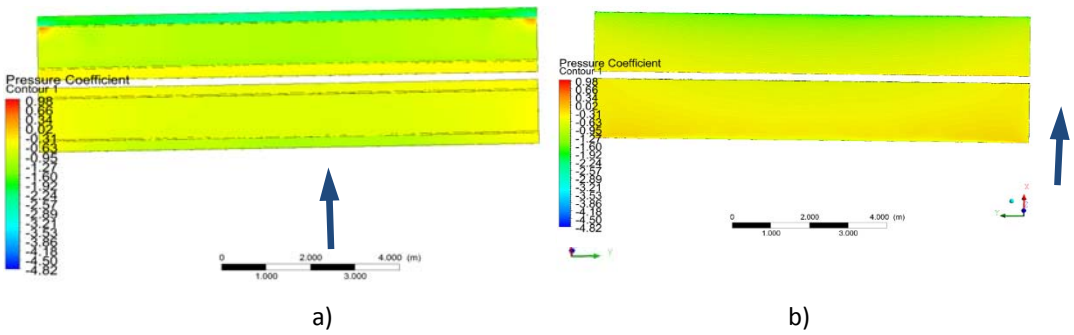


Fig. 5. 74. Pressure coefficients on a) Bottom surface of the solar panels, b) Top surface of the solar panels for slope 27º wind direction 90º, windward side

However, the pressure coefficient distribution on top of the solar panels mounted on the windward surface which is displayed in Fig. 5.74 b), points out lower pressure coefficients, in the range of -0.31 to -2.24, than those for either the bottom surface of the panels or the roof surface under the panels.

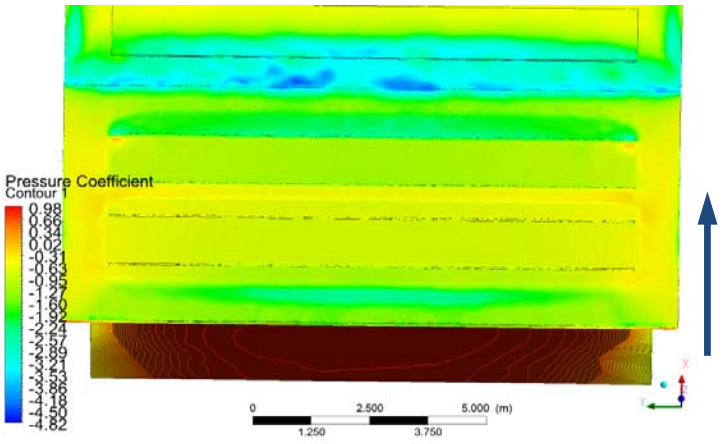


Fig. 5. 75. Pressure coefficients on roof under solar panels, slope 27º, windward, wind direction 90º

In the same manner, the pressure coefficients on the roof under the solar panels for the leeward side of the roof, are very similar to those for the bottom surface of the solar panels, as portrayed in Figs. 5.876 and 5.77 a) respectively. In addition, the pressure coefficient distributions on top surface of the solar panels mounted on the leeward side, are illustrated in Fig. 5.77 b), which shows a slightly lower pressure coefficient distribution than either the bottom surface of the panels or the roof surface under the panels.

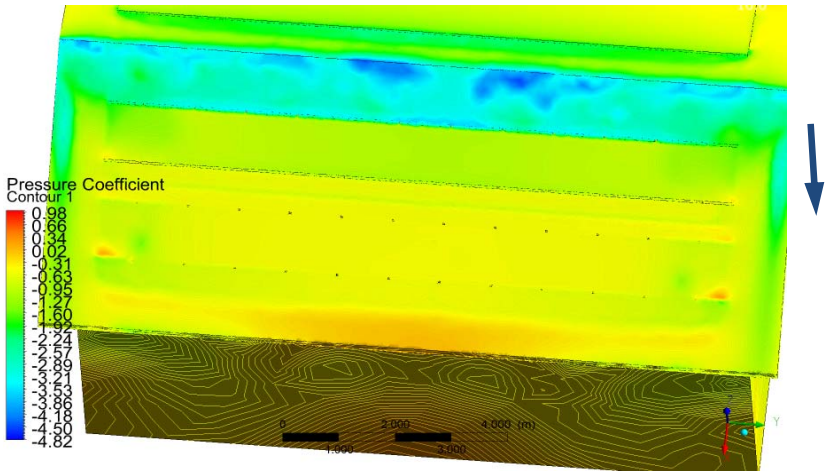


Fig. 5. 76. Pressure coefficients on roof under solar panels, slope 27º, leeward, wind direction 90º

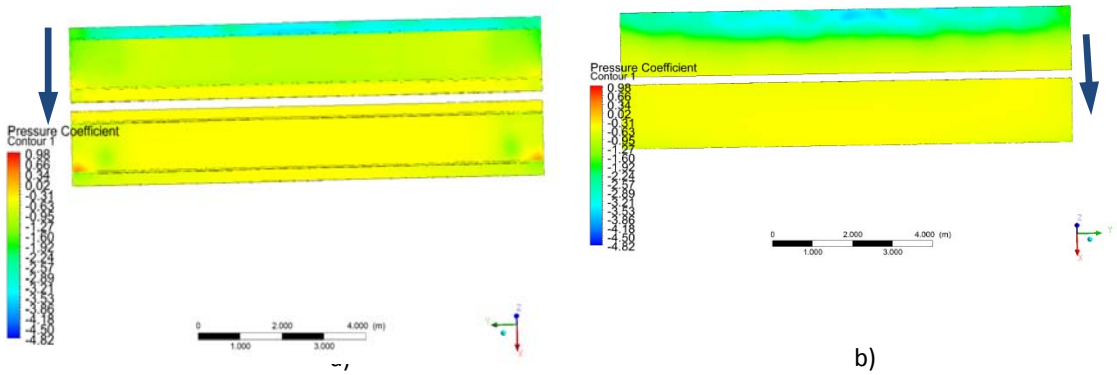


Fig. 5. 77. Pressure coefficients a) Bottom surface of the solar panels, b) Top surface of the solar panels, slope 27º, leeward side, wind direction 90^{o}

5.4.2. Pressure coefficient distributions for roof mounted solar panels and roof without solar panels for windward side of the roof

The effects the solar panels installed on the roof have on the wind-induced pressure on the roof of the building can be understood by analyzing the wind-induced pressure on the four surfaces, i.e., the roof surface under the solar panels, the bottom and top surfaces of the solar panels, and the roof surface without solar panels.

The total pressure is calculated by averaging the pressure coefficients along 17 longitudinal lines along the top and bottom surfaces of the solar panels, along the roof surface under the solar panels, and on same roof surface when no panels are installed.

It is assumed that the pressure coefficient at any point on the roof surface under the panels is a direct summation of the Cp of the corresponding 3 relevant points located on the three surfaces (bottom and top of the panels and the roof surface under the panels), and are located on lines perpendicular to each of those surfaces. Each set of three relevant points is located on one line perpendicular to the roof.

5.4.2.1. Pressure coefficients on bottom surface of the solar panels vs. roof surface under solar panels

Wind direction 0º will not be described in details in this section; however the integration results will be presented in the Table 5.10 below. Figure 5.78 depicts the wind pressure coefficients for the roof under the solar panels versus the Cp on the bottom surface of the solar panels, for wind direction 90º. Figure 5.78 shows that the differences between the Cp are very small (0 to 0.15) between the corresponding points on the lines PL1, PL9 and PL16. However, for most of the length of PL1, the Cp for both surfaces are very close to each other, while for the line PL16, the difference is slightly larger (0-0.08). Nonetheless, on line PL9, the Cp registered on the roof under the panels was about 0.10 lower than that on the Cp on the bottom surface of the panels.

Representation of the wind pressure coefficients recorded on the top and bottom surfaces of the solar panels and on the roof surface under the solar panels, for wind directions 90º and 45º, are shown in Figs. 5.78 to Fig 5.85.

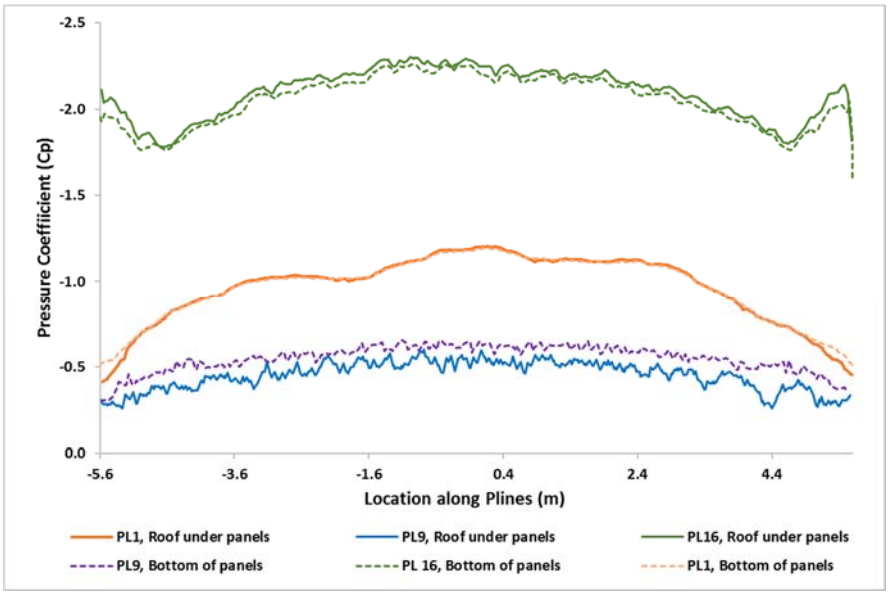


Fig. 5. 78. Pressure coefficients on bottom surface of solar panels vs. on roof under the panels, slope 27º, windward, wind direction 90º

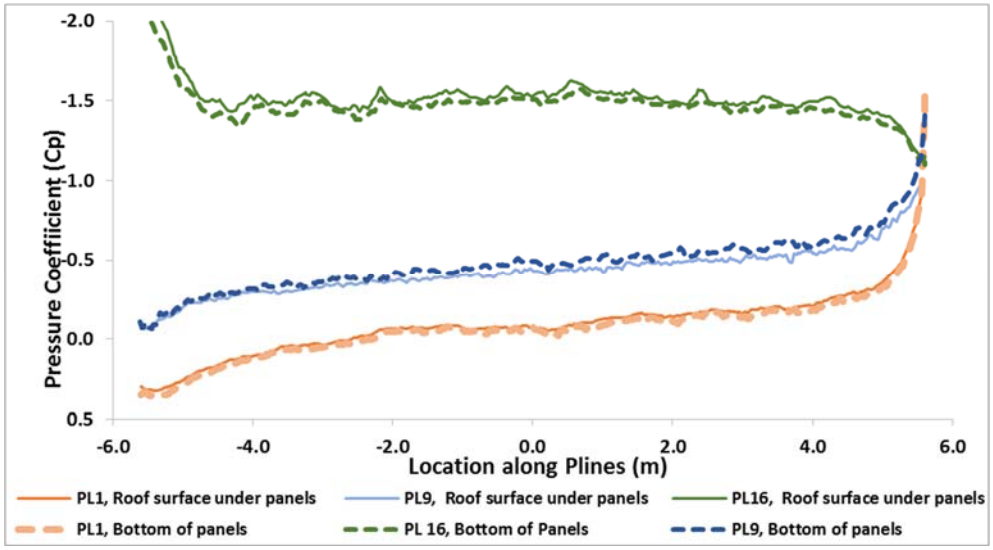


Fig. 5. 79. Pressure coefficients on bottom surface of solar panels vs. on roof under the panels, slope 27º, windward, wind direction 45º

For the 45° wind direction (Fig. 5.79), the Cp along the three lines PL1, PL9 and PL16 on the roof under the panels and on the bottom surface of the panels, demonstrated high similarity in trends and values, throughout their entire length. The differences in values between the corresponding lines range from 0 along most of the PL1, to 0.05 along the other two lines, PL9 and PL16. In

contrast to wind direction 90º, the pressure coefficients along PL1 and PL9 increased moderately from the C edge, to the highest values near the D edge. Nonetheless, the Cp for PL16 remain nearly constant for almost whole of the line.

5.4.2.2. Pressure coefficients on roof surface without solar panels vs. roof surface under solar panels

Wind-induced pressure coefficients registered on the roof surface under the solar panels and on the roof surface without solar panels for wind directions 90º and 45º, are shown in Figs. 5.80 and Fig 5.81 respectively. For wind direction 90°, the Cp along lines PL1 and PL 9 on the roof under panels are slightly higher than the Cp on the roof surface without panels. However, the pressure coefficients on PL16 located on the roof surface under the panels is much higher than the Cp on PL16 located on the roof surface without panels. This indicates different effects of the solar panels on the Cp on the roof surface, depending on the location on the roof. On the other hand, the Cp along all lines on the roof surface under the panels and on the roof without panels are symmetric. Although the Cp on the roof without panels along the three lines seems nearly constant, at approximately -0.41 along PL9, however, the Cp along the corresponding line PL9 on the roof under panels increased from -0.28 near edges to -0.55 in the middle. Nonetheless, the Cp on PL1 on the roof without solar panels increased from -0.46 near edges to -0.99 at the middle, and the Cp on the corresponding PL1 on the roof with solar panels changed similarly from -0.46 near edges to -1.20 at the middle.

Moreover, while the Cp on PL16 on the roof without panels changed from -0.80 near edges to -1.01 near the middle of the line, the Cp on PL16 located on the roof under panels changed from -2.0 near edges to -2.28 at the middle of the line, which is much higher than the Cp on the corresponding line located on the roof with no panels.

For wind direction 45°, the Cp along PL16 on the roof under the panels were much lower than the Cp on the corresponding lines on the roof without panels. However, the Cp along PL1 on the roof surface under the panels is moderately higher than the Cp on the corresponding line PL1, on the roof without panels. Nonetheless, the Cp along PL9 on the roof surface under the panels is nearly equal to the Cp on the corresponding line on the roof without panels. To further elaborate, the pressure coefficients along PL16 on the roof without panels remained nearly constant at -1.0, while

the Cp along PL16 on the roof under the solar panels was nearly constant at around -1.50 along most of the line. The pressure coefficients along PL9 on the roof without panels increased from -0.23 on the C edge to -0.90 on the E edge of the solar array, while the Cp along PL9 on the roof under the solar panels increases from -0.07 on the C edge to -1.0 on the E edge, and was very similar to the Cp on the corresponding line for the roof without panels.

Similarly, the pressure coefficients along PL1 on the roof without panels increased moderately from -0.02 on the C edge to -0.92 on the E edge of the solar array. However, the Cp along PL1 for the roof under the solar panels increased considerably, from 0.30 on the C edge to -0.99 on the E edge, while remaining moderately lower than the corresponding line on the roof without panels.

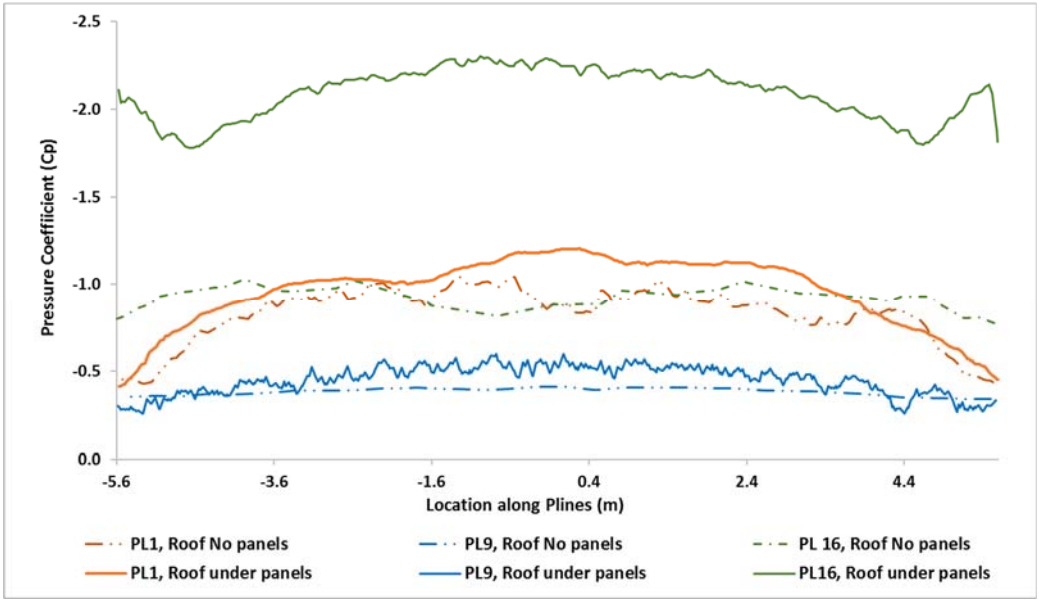


Fig. 5. 80. Pressure coefficients on roof without solar panels vs. on roof under the panels, slope 27º, windward, wind direction 90º

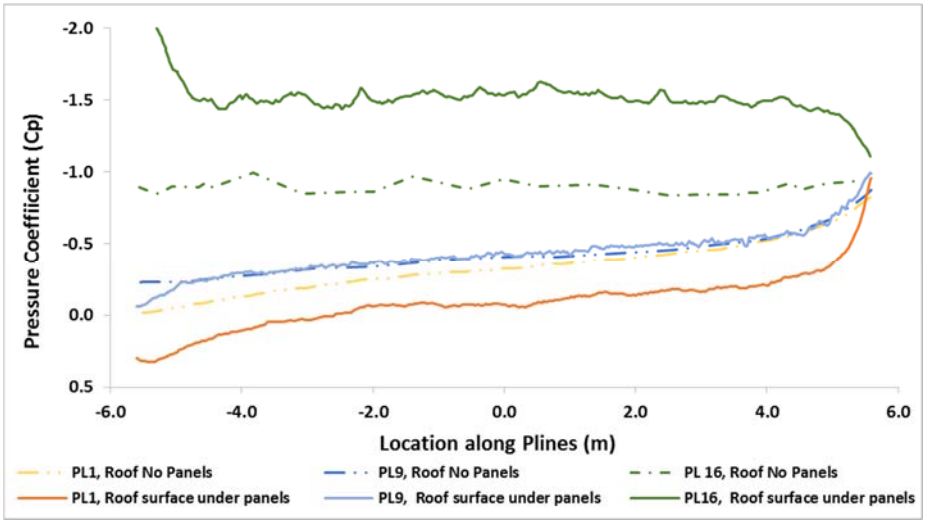


Fig. 5. 81. Pressure coefficients on roof without solar panels vs. on roof under the panels, slope 27º, windward, wind direction 45º

5.4.2.3. Pressure coefficients on bottom surface of the solar panels vs. roof surface without solar panels

The wind pressure coefficients registered on the bottom surface of the solar panels and on the roof surface without solar panels, for wind directions 90º and 45º, are shown in Figs. 5.82 and Fig 5.83 respectively. When the wind direction is 90°, the Cp along lines PL1 and PL 9 on the bottom surface of the panels are slightly lower than the Cp on the roof surface with no panels. However, the pressure coefficients on PL16 located on the bottom surface of the panels are much lower than the Cp on PL16 located on the roof surface without panels. On the other hand, the Cp along all the lines on bottom surface of the panels and on the roof without panels are symmetric. In addition, although the Cp on the roof without panels along the three lines seem nearly constant, around the value of -0.38 along PL9, however, the Cp along the corresponding line PL9 on the bottom surface of panels increased from -0.28 near the C and E edges to -0.63 in the middle of the line. For the line PL1, the Cp on the roof without solar panels increased from -0.46 near edges to -0.99 at the middle of the line, and the Cp on the bottom surface of the panels changed from -0.52 near edges to -1.19 at the middle of the line. Also, for the line PL16, the Cp on the roof surface without panels changed from -0.78 near the C and E edges, to -1.01 near middle of the line, while the Cp on the bottom surface of the panels changed from -2.0 near the C and E edges to -2.25 at the middle

of the line; thus the Cp on the roof surface under the panels is much lower than the Cp on the corresponding line located on the roof without panels, indicating a higher wind-induced suction.

For the 45° wind direction (Fig.5.83), the Cp along PL 16 on the bottom surface of the panels is much lower than the Cp on the corresponding line on the roof without panels. However, the Cp along PL1 on the bottom surface of the panels is moderately (in comparison with the other 2 lines) higher than the Cp on the corresponding line PL1on the roof without panels, while the Cp along PL9 on the bottom surface of the panels is very close to the Cp on the corresponding line on the roof without panels. On the other hand, the pressure coefficients along PL16 on the roof without panels remained nearly constant at -0.85, while the Cp along PL16 on the bottom surface of solar panels remains constant at nearly -1.52 along most of the line. However, the pressure coefficients along PL9 on the roof without panels increased from -0.23 on the C edge to -0.83 on the E edge of the solar panels array, while the Cp along the PL9 line on the bottom surface of the solar panels increased from -0.07 on the C edge to -1.12 on the E edge.

Similarly, along PL1, the pressure coefficients on the roof surface without panels increased from -0.02 on the C edge to -0.83 on the E edge of the solar panel array. However, the Cp along PL1 on the bottom surface of the solar panels increased considerably from 0.35 on the C edge to -1.53 on the E edge, while remaining moderately lower than the pressure coefficients on the roof without panels for the corresponding line.

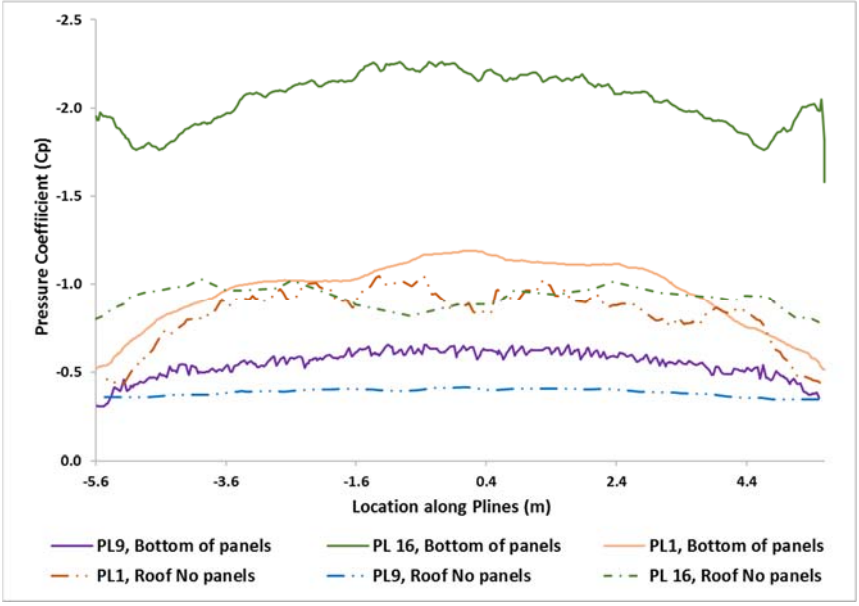


Fig. 5. 82. Pressure coefficients on bottom surface of solar panels vs. on roof without solar panels, slope 27º, windward, wind direction 90º

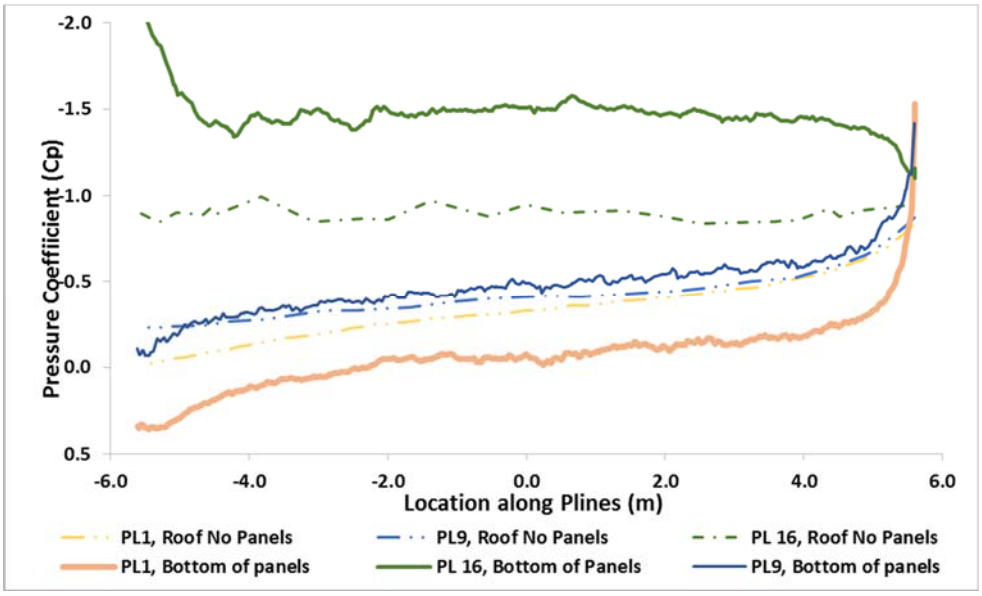


Fig. 5. 83. Pressure coefficients on bottom surface of solar panels vs. on roof without solar panels, slope 27º, windward, wind direction 45º

5.4.2.4. Pressure coefficients on top surface of the solar panels vs. roof without solar panels

The pressure coefficients recorded on top of the solar panels and on the roof surface without solar panels for wind directions 90º and 45º are shown in Figs. 5.84 and Fig 5.85 respectively.

For wind direction 90°, the Cp along line PL 9 on top of the panels are slightly lower than the Cp on the roof surface with no panels. However, the pressure coefficients on PL16 located on the top surface of the panels is much lower than the Cp on PL16 located on the roof surface without panels. Nonetheless, the Cp along line PL1 on top of the panels were moderately (in comparison with the other 2 lines) lower than the Cp on the roof surface with no panels. On the other hand, the Cp along all lines on top of the panels and on the roof without panels were symmetric. Although the Cp on the roof without panels along the three lines seem nearly constant, and is nearly -0.41 along PL9; however, the Cp along the corresponding line PL9 on the top of the panels increased from -0.42 near edges to -0.59 in the middle. The Cp on PL1 on the roof without solar panels increased from -0.44 near edges to -1.03 at the middle of the line, and the Cp on the corresponding PL1 line on top of the panels changes from -0.37 near edges to -0.44 at the middle. For the roof without panels the Cp on PL16 changed from -0.80 near edges, to -1.01 near the middle of the line, while the Cp on PL16 on top surface of the panels changed from -1.33 near edges to -1.80 at the middle of the line, which is much lower than the Cp for the corresponding line located on the roof without panels.

For the 45° wind direction, the Cp along PL1 and PL 16 on top of the panels were moderately lower than the Cp of the corresponding lines on the roof without panels. However, the Cp along PL9 on top of the panels was slightly lower than the Cp for the corresponding line on the roof without panels. The pressure coefficients along PL16 on the roof without panels remained nearly constant at -0.85, while the Cp along PL16 on top of the solar panels remained constant at nearly -1.17 along most of the line. The pressure coefficients along PL9 on the roof without panels increased from -0.23 on the C edge to -0.83 on the E edge of the solar array, while the Cp along PL9 on top of the solar panels increases from -0.48 on the C edge to -1.22 on the E edge, while remaining lower than the Cp on the roof without panels. Similarly, the pressure coefficient along PL1 on the roof without panels increased moderately from -0.02 on the C edge to -0.82 on the E edge of the solar array. However, the Cp along PL1 on top of the panels increased considerably from -016 on the C edge to -1.61 on the E edge, while remaining moderately lower than the Cp on the corresponding line of the roof without panels for most of the line length, registering however much fluctuation.

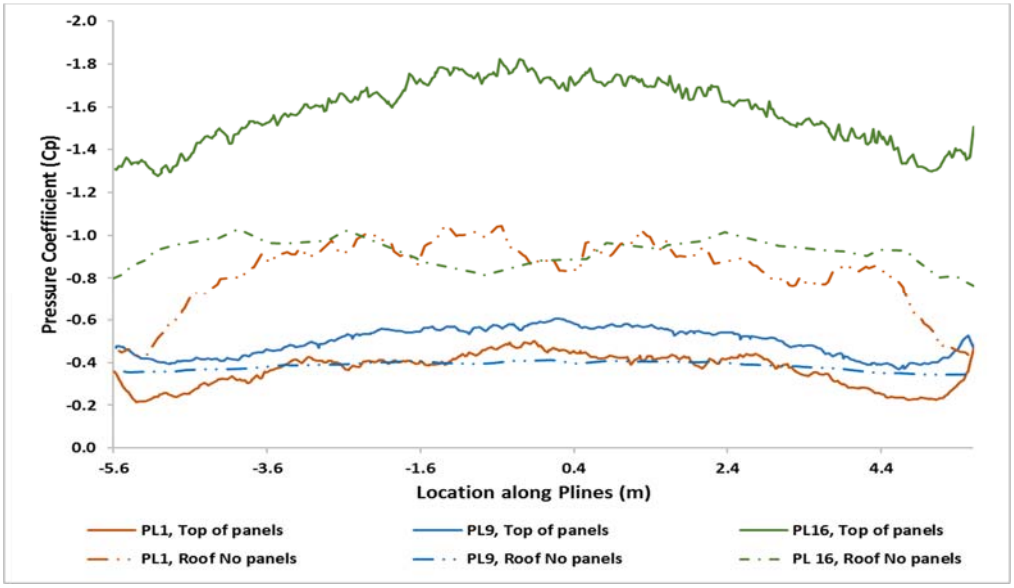


Fig. 5. 84. Pressure coefficients of roof without solar panels vs. top of solar panels, slope 27º, windward, wind direction 90º

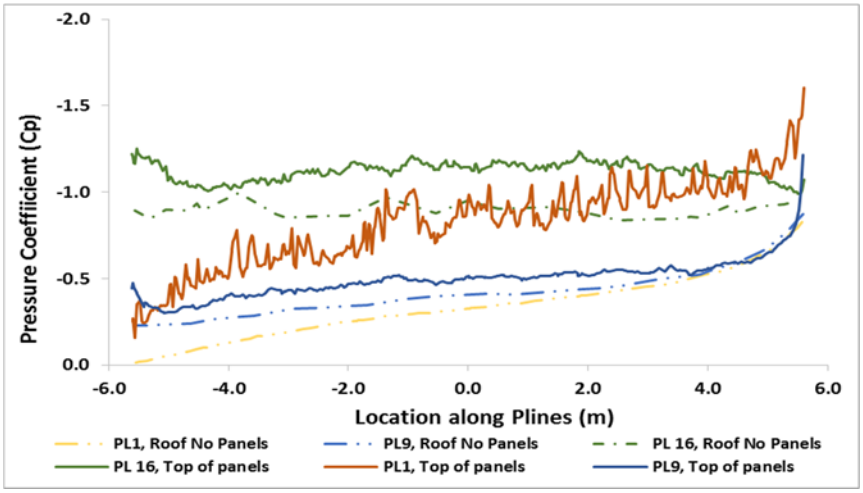


Fig. 5. 85. Pressure coefficients of roof without solar panels vs. top of solar panels, slope 27º, windward, wind direction 45º

5.4.3. Pressure coefficient distributions for roof mounted solar panels and for roof without panels for the leeward side of the roof

For the case of roof slope 27º, clearance 3”, spacing 8”and wind directions 90º, 45º and 0º, the wind-induced pressure on the building roof is analyzed on four surfaces: the roof surface under the solar panels, the bottom and top surfaces of the panels, and the roof surface without solar panels. Total pressure is calculated by the integration of pressure coefficients sampled along 19 longitudinal lines along the top and bottom surfaces of the solar panels and on the roof surface under the panels. However, it is assumed that the pressure coefficients at any point on the roof are obtained by the algebraic summation of the corresponding three relevant points located on the three surfaces of the roof-panels system (bottom, top surfaces of the panels, and the roof surface under the panels), and on lines perpendicular to each of those surfaces.

The following figures represent the pressure coefficients only for the wind directions 90º and 45º, because the case of 0º wind direction generates much lower pressure coefficients than the other two directions. The results of the integrations in the 0 wind direction are included in Table 5.10 below.

5.4.3.1. Pressure coefficients on bottom surface of the solar panels vs. roof surface under solar panels

Figure 5.86 depicts the wind pressure coefficients for the roof surface under the solar panels versus the Cp on the bottom surface of the solar panels, for which very small differences were noticed, from 0.20 to 0, between the corresponding points on lines PL20, PL 29 and PL 38. Wind pressure coefficients registered on the top and bottom surfaces of the solar panels, and on the roof surface under the solar panels mounted on the leeward side of the roof, and on the roof without solar panels for wind directions 90º and 45º are shown in Figs. 5.86 to Fig 5.93.

Figure 5.86 depicts the case of wind direction 90°, for which the Cp along lines PL20, PL28 and PL 38, on the roof under the panels and on the bottom surface of the panels. The Cp for PL28 showed a slightly lower Cp on the roof surface under the panels, than the Cp on the bottom surface of the panels, where the Cp along the roof surface changed from -0.74 near edges D and F, to -0.71 in the middle, and the Cp on the bottom surface of the panels varied from -0.74 near the D

and F edges, to -0.73 in the middle of the line. In addition, the Cp on PL35 on the roof surface under the panels was -1.05 near edges and it decreased to -0.58 in the middle of the line, while the Cp on the corresponding line on the bottom surface of the panels is slightly lower, -0.76 near edges and -0.54 in the middle of the line.

However, the Cp along the PL 20 line on the bottom surface of the panel and on the roof surface under the panels, fluctuated from -2.41 near the D and F edges of the array to -3.54 in the middle of the lines.

For wind direction 45°, the Cp along all the three lines PL20, PL28 and PL35 on the roof under panels and on bottom surface of the panels were very close to each other, and this similarity holds along most of the length of the three lines, Fig. 5.87.

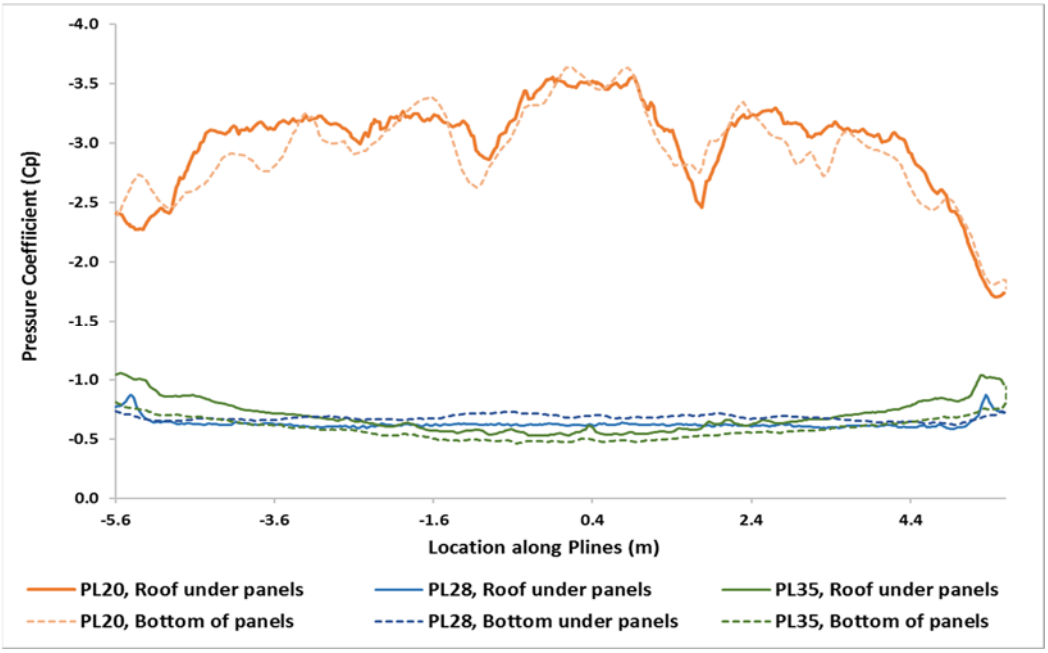


Fig. 5. 86. Pressure coefficients on bottom surface of solar panels vs. on roof under the panels, slope 27º, leeward, wind direction 90º

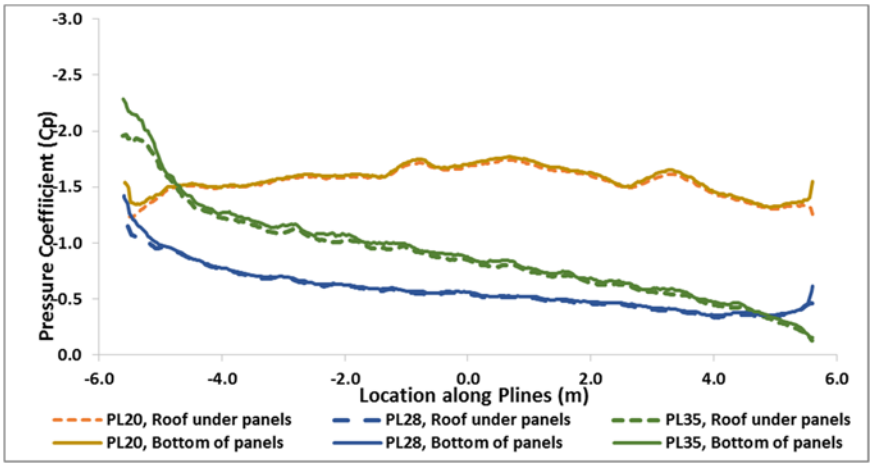


Fig. 5. 87. Pressure coefficients on bottom surface of solar panels vs. on roof under the panels, slope 27º, leeward, wind direction 45º

5.4.3.2. Pressure coefficients on roof surface without solar panels vs. roof surface under solar panels

The wind pressure coefficients registered on the roof surface under the solar panels and on the roof surface without panels, for wind directions 90º and 45º are shown in Figs. 5.88 and Fig 5.89.

For wind direction 90°, where the wind direction is perpendicular to the ridge of the roof, the Cp along lines PL20 on the roof under the panels is much lower than the Cp on the roof surface without panels. However, the pressure coefficients on both PL28 and PL35 located in the middle of roof surface under panels and near the B edge of the leeward array, are moderately lower than the Cp on the corresponding lines on the roof surface without panels. The differences between the effects of solar panels on Cp distribution on the roof surface underneath the panels depend on the location on the roof, where the Cp increases the most near the D edge of the leeward array from the Cp on the roof surface without panels. It was also noticed that the distribution of the Cp along the lines on the roof surface under the panels and on the roof without panels, are symmetric. The Cp on the roof without panels along the three lines varied between -1.05 near the D and F edges and up to -1.72 at the middle of the line for PL 29, and between -0.62 near D and F edges and up to -1.19 on the middle of the line for P38. The Cp coefficients changed between -2.20 near the D and F edges to -1.61 in the middle of PL20. Similarly, the Cp along the three corresponding lines on the roof under the panels, changed from -1.03 near the D and F edges, to -0.54, in the middle of PL35, and

from -0.76 near the same edges to -0.63 in the middle of PL28, while for the PL 20 line, the Cp changed between -2.48 near edges to -3.49 near the middle of the line.

Figure 5.89 shows the Cp on the roof under panels versus the roof without solar panels for the 45° wind direction. The Cp along the two lines PL20 and PL35 on the roof under panels are lower than the Cp on the corresponding lines on the roof without panels. Moreover, the Cp along line PL28 on the roof under the panels is lower than those registered for the corresponding line PL28 on the roof surface without panels. For PL20, the pressure coefficients along on the roof without panels decreased from -1.59 on the D edge, to -1.19 in the middle of the line, while the Cp along PL20 on the roof under the solar panels increased from -1.20 on the D edge to -1.74 on the middle of the array, and remained much lower than the corresponding line on the roof without panels for most of the line. The pressure coefficients along PL28 on the roof without panels decreased from -1.26 on the D edge to -0.61 on the F edge of the solar array, while the Cp along PL28 on the roof under solar panels decreased from -1.29 on the D edge to -0.46 on the F edge. Similarly, the pressure coefficients along PL35 on the roof without panels decreased from -1.30 on the D edge to -0.19 on the F edge of the solar array, while the pressure coefficients along PL35 on the roof under the solar panels decreased considerably, from -1.96 on the D edge to -0.13 on the F edge, while remaining lower than the corresponding line on the roof without panels for the entire length of the line.

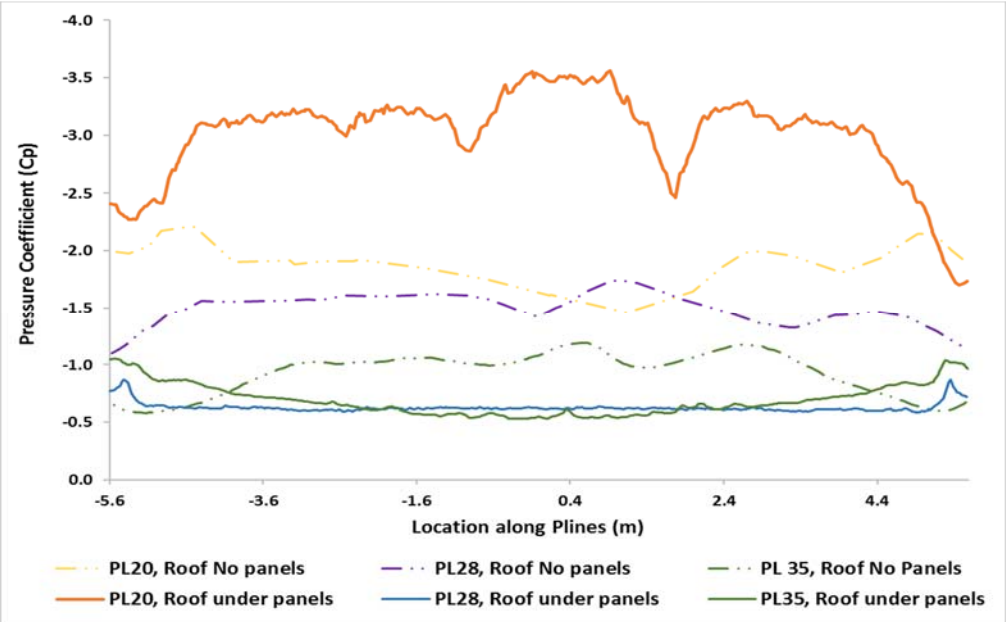


Fig. 5. 88. Pressure coefficients on roof without solar panels vs. on roof under the panels, slope 27º, leeward, wind direction 90º

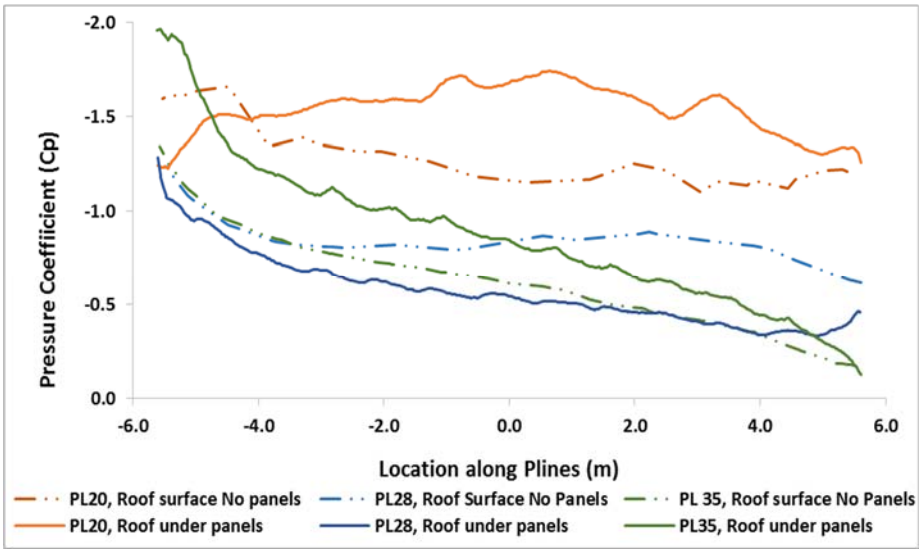


Fig. 5. 89. Pressure coefficients on roof without solar panels vs. on roof under the panels, slope 27º, leeward, wind direction 45º

5.4.3.3. Pressure coefficients on bottom surface of the solar panels vs. roof surface without solar panels

Figures 5.90 and 5.91 show the pressure coefficients recorded on the bottom surface of the solar panels and on the roof surface without solar panels for wind directions 90º and 45º. For wind direction 90°, the Cp along line PL20 on the bottom surface of the panels was much lower than the Cp on the roof surface with no panels. However, the pressure coefficients on PL28 and PL35 located in the middle of bottom panels and near the B edge of the leeward array, respectively, were moderately lower than the Cp on the corresponding lines located on the roof surface without panels, in comparison with the PL20 line. Furthermore, the Cp along the three lines on the bottom surface of the panels and on the roof without panels were symmetric. The Cp on the roof without panels along the three lines changed slightly throughout the lines, where the Cp varied between -1.05 near the D and F edges and up to a high of -1.72 for PL 29, and between -0.62 near D and F edges to up to -1.19 along the P38 line; also this changed from -2.00 near the D and F edges to -1.61 in the middle of PL20. For the bottom surface of the panels the Cp along the three corresponding lines changed from -0.80 near the D and F edges to -0.48 in the middle of PL35, and from -0.77 near the D and F edges to -0.70 in the middle of PL28, while for PL20 it changed between -2.39 near the D and F edges to -3.60 near the middle of the line.

Figure 5.91 shows the Cp on the bottom surface of the panels versus the roof without solar panels for the 45° wind direction. The Cp along the lines PL20 and PL35 on the bottom surface of the panels were lower than the Cp on the corresponding lines on the roof without panels. However, the Cp along line PL28 on the bottom surface of the panels was lower than on the corresponding line on the roof surface without panels. For the top area near the ridge, the pressure coefficients along PL20 on the roof without panels decreased from -1.60 on the D edge to -1.15 on middle of the line, while the Cp along PL20 on the bottom surface of solar panels decreased from -1.54 near the D and F edges, to -1.25 in the middle of the line, and remains much lower than the corresponding line on the roof without panels for most of the line length.

However, the pressure coefficients along PL28 on the roof without panels decreased from -1.34 on the D edge to -0.61 on the F edge of the solar array, while the Cp along PL28 on the bottom surface of solar panels decreased from -1.46 on the D edge to -0.61 on the F edge.

Similarly, the pressure coefficients along PL35 on the roof without panels decrease from -1.34 on the A edge to -0.19 on the B edge of the solar array. However, the Cp along PL35 on the bottom surface of solar panels decreased considerably from -2.22 on the A edge to -0.18 on the B edge, while remaining lower than the corresponding line on the roof without panels for most of the line length.

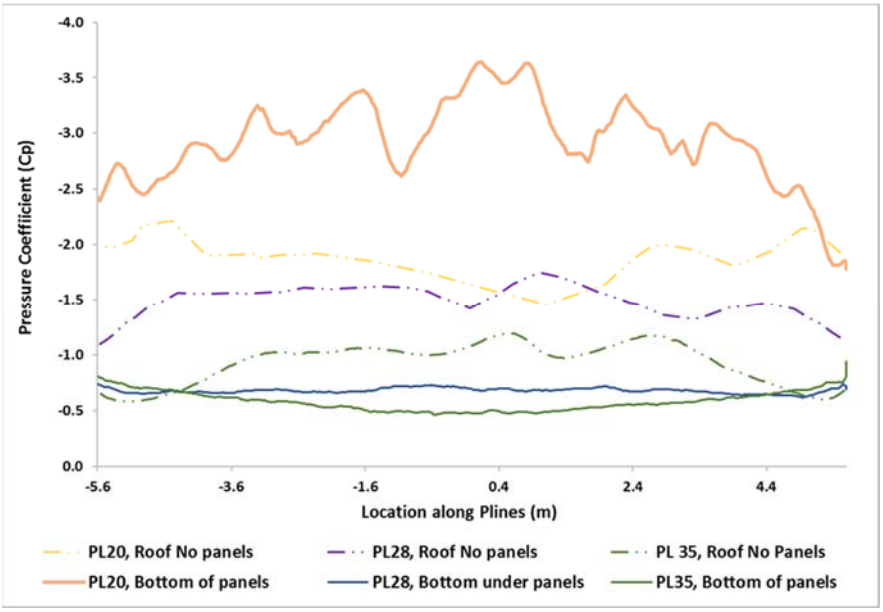


Fig. 5. 90. Pressure coefficients on bottom surface of solar panels vs. on roof without solar panels, slope 27º, leeward, wind direction 90º

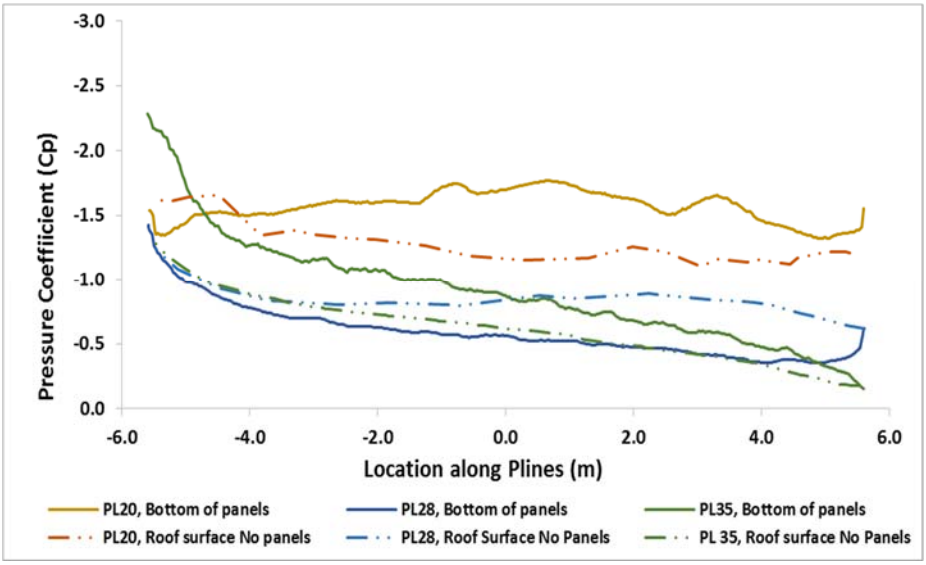


Fig. 5. 91. Pressure coefficients on bottom surface of solar panels vs. on roof without solar panels, slope 27º, leeward, wind direction 45º

5.4.3.4. Pressure coefficients on top surface of the solar panels vs. roof surface without solar panels

Figures 5.92 and 5.93 illustrate the wind pressure coefficients registered on top of the solar panels and on the roof surface without solar panels for wind directions 90º and 45º. When the wind direction is 90°, the Cp along the line PL20 on top of the panels is much lower than the Cp on the roof surface with no panels. However, the pressure coefficients on PL28 and PL35 (located in the middle of the solar panel array and near the B edge of the leeward array), are moderately lower than the Cp on the corresponding lines on the roof surface without panels, in comparison with the other Pl20 line. The Cp along the three lines on top panels and on the roof without panels are symmetric. Moreover, the Cp on the roof without panels changed between -1.05 near the D and F edges and up to -1.72 along PL 29, and between -0.62 near the D and F edges and up to -1.19 along P38; for line PL20 the changes were between -2.00 near the D and F edges to -1.61 in the middle of the line. The Cp along the three corresponding lines on top of the panels changed from -1.10 near the D and F edges to -0.54 in the middle of PL35 line, and from -0.84 near the D and F edges to -0.61 in the middle of PL28; the changes for PL20 line were lower than those registered for the previous case, namely these were between -2.27 near the D and F edges to -3.45 near the middle of PL20.

Figure 5.93 shows the Cp on top of the panels versus roof without solar panels for the 45° wind direction. The pressure coefficients along PL20 and PL35 on top of the panels were lower than the Cp on the corresponding lines on the roof without panels. However, the Cp along the line PL28 on top of the panels was lower than on the corresponding PL28 on the roof surface without panels. For the PL 20 line, the pressure coefficients on the roof without panels decreased from -1.60 on the D edge to -1.15 in the middle of the line, while the Cp on top of the solar panels increased from -1.30 on the D edge to -1.59 in the middle of the line, and remained lower than that on the corresponding line on the roof without panels for most of the length of the line. Likewise, the pressure coefficients on PL35 on the roof without panels decreased from -1.34 on the D edge to -0.19 on the F edge of the solar array. The Cp along PL35 on top of the solar panels decreased considerably from -1.93 on the D edge to -0.18 on the F edge; also this was lower than the corresponding line on the roof without panels. The pressure coefficients along PL28 on the roof without panels decreased from -1.34 on the D edge to -0.61 on the F edge of the solar array, while the Cp along PL28 on top of the solar panels decreased from -1.43 on the D edge to -0.61 on the F edge.

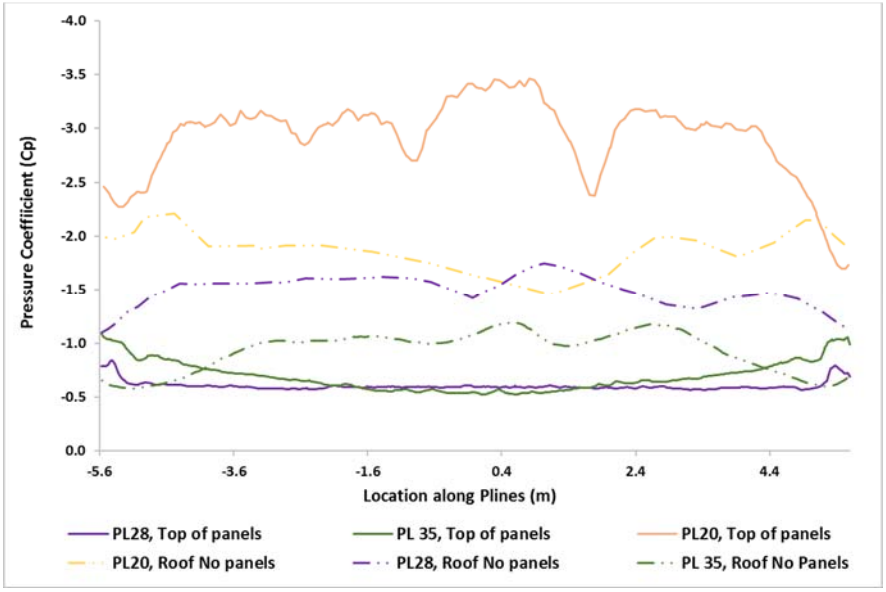


Fig. 5. 92. Pressure coefficients on roof without solar panels vs. top of solar panels, slope 27º, leeward, wind direction 90º

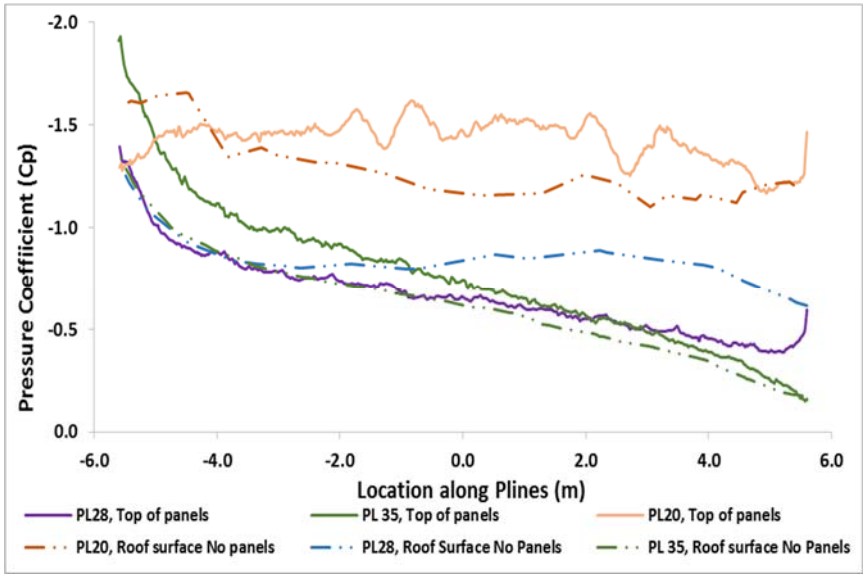
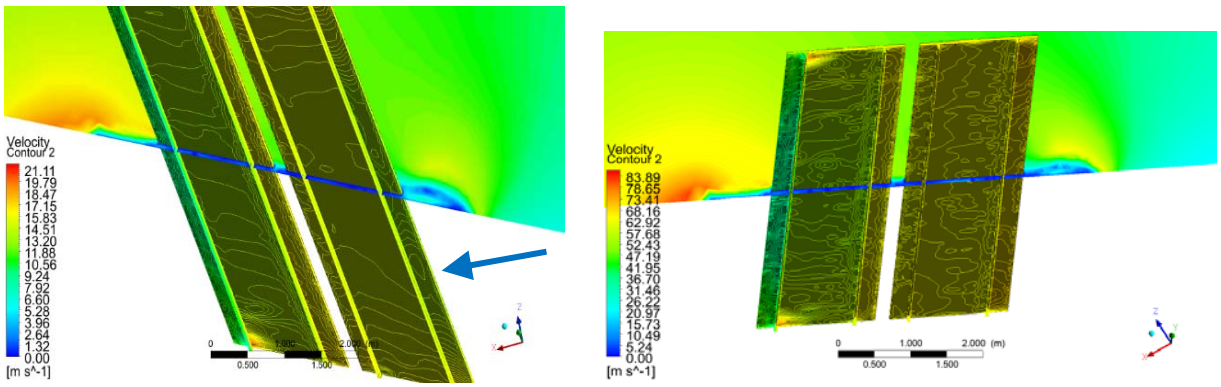


Fig. 5. 93. Pressure coefficients on roof without solar panels vs. top of solar panels, slope 27º, leeward, wind direction 45º

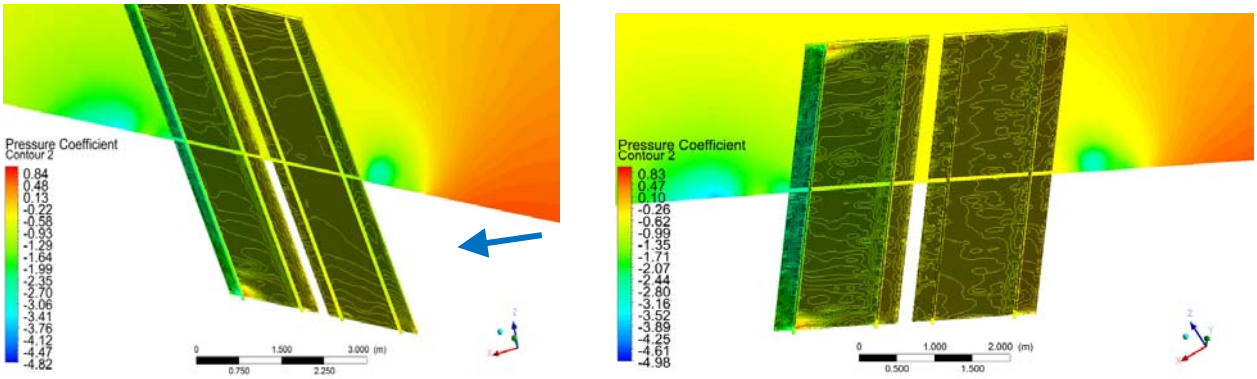
5.4.4. Wind flow characteristics for gable roofs with solar panels for 90º wind direction

Figure 5.94 shows the velocity distribution in the gap under the bottom surface of the windward panel array on a plane perpendicular to the roof, for wind speeds 10 m/s and 40 m/s. The velocity magnitude in the 3" gap is 1.32 to 3.96 m/s, or 5.24 to 20.97m/s, which are much lower than the corresponding free stream speeds of 10 m/s and 40 m/s, respectively. In addition, Figure 5.95 shows the pressure coefficient distributions on the bottom surface of the panels and along a perpendicular plane crossing through the cavity under the panels. In general, the pressure coefficients in the cavity ranged from -0.26 to -3.89. The pressure coefficients were the same for the 10 m/s and 40 m/s wind speeds.



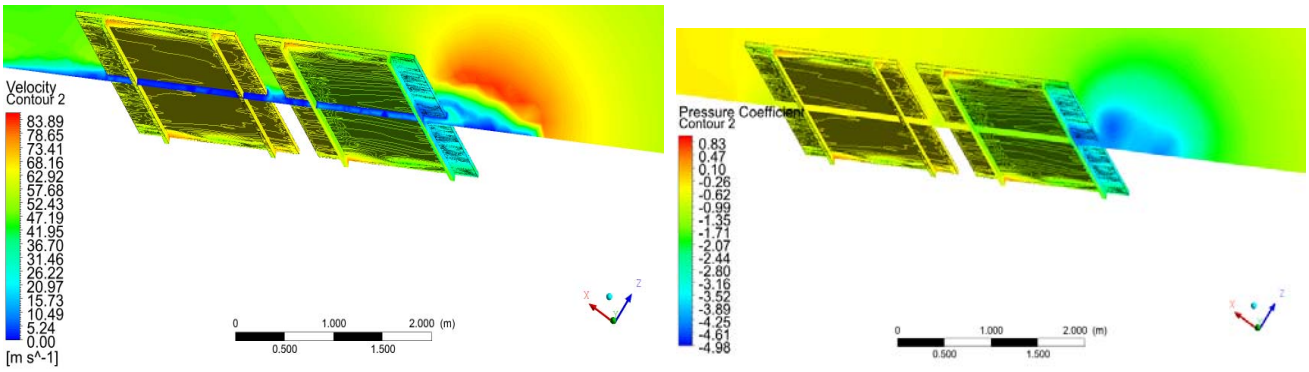
a) b)

Fig. 5. 94. Velocity on a perpendicular plane under panels, wind speeds a) 10 m/s and b) 40 m/s, windward, wind direction 90º



a) b)

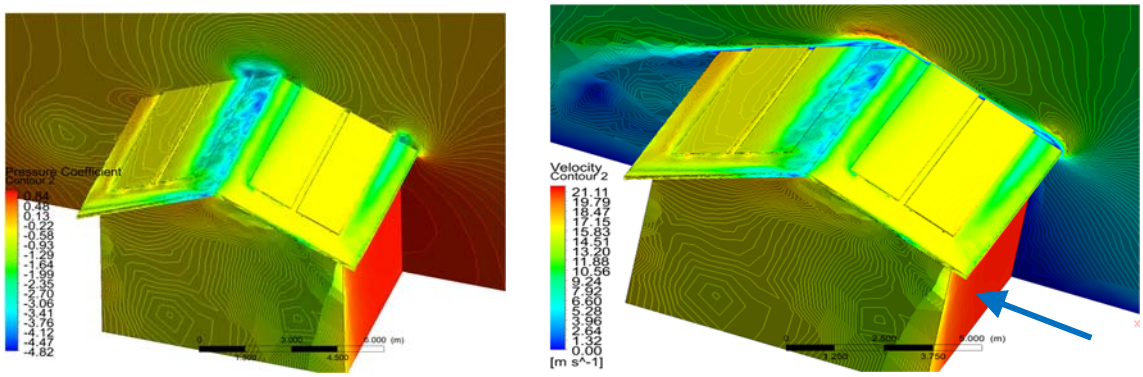
Fig. 5. 95. Pressure coefficients on a perpendicular plane under panels, wind speeds a) 10 m/s and b) 40 m/s, windward, wind direction 90º



a) b)

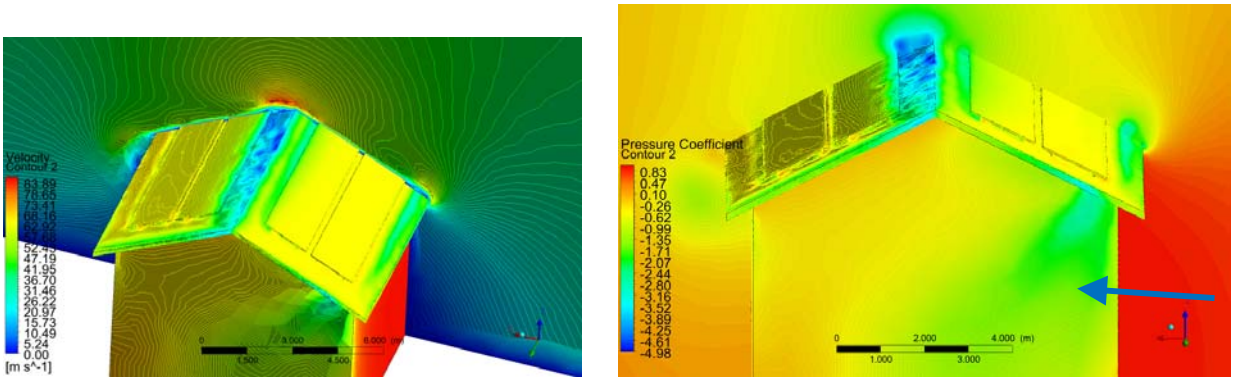
Fig. 5. 96. Pressure coefficients and velocity on a perpendicular plane under panels, leeward, wind direction 90º, wind speed 40 m/s

Similarly, the flow speed in the gap under the panels on the leeward sider for wind speed 40 m/s was 5.24 to 20.97 m/s, which is much lower than the free stream speed. This low speed continues for about 1.0 m on both sides of the panels at the level of the array. However, the flow speed increased sharply above the ridge to 83 m/s at nearly 24" (0.61m) above the roof surface. In addition, the highest flow speed was registered on the leeward side of the ridge (Figs. 5.94, 5.96 and 5.97). The largest reductions in pressure coefficients on the bottom surface of the panels and in the cavity under the panels were located under the D edge of the leeward array near the building ridge. Nonetheless, with the increased distance from the ridge, the Cp increased on both the bottom surface of panels and in the cavity. Thus, Cp decreased gradually towards the front of the windward array (Fig. 5.95) and towards the B edge of the leeward array at the back of the building (Fig.5.97 and Fig. 5.98).



a) b)

Fig. 5. 97. a) Pressure coefficients and b) velocity distribution on a perpendicular plane, wind speed 10m/s, wind direction 90º



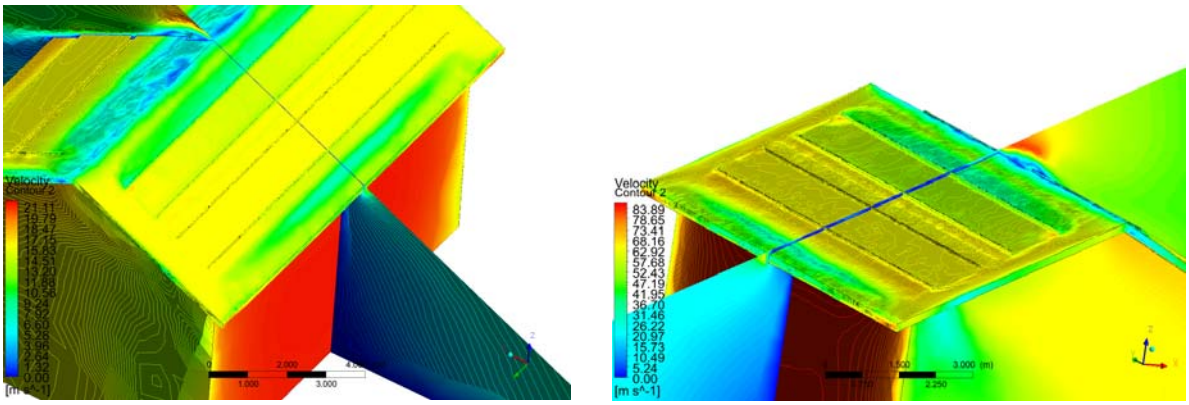
a) b)

Fig. 5. 98. a) Velocity and b) pressure coefficients on perpendicular planes, wind speed 40 m/s, wind direction 90º

Figures 5.97 and 5.98 show the distribution of pressure coefficients and the velocities on a plane perpendicular to the middle of the model, for wind speeds 10 m/s and 40 m/s, respectively.

The pressure coefficient representation in Figs. 5.97 and 5.98 seem identical, although they are for different free stream flows of 10 m/s and 40 m/s, respectively. Both Figs. 5.97 and 5.98 show that the Cp on top of the panels near the ridge on the leeward side was much lower (-2.35 to -0.93) than the CP on the top of the panels on the windward side near the ridge (-0.58 to -1.29). In addition, the Cp decreased with the distance from the Cp epicenter (near the ridge on the leeward side), as shown in the concentric Cp contours in Fig. 5.97 and Fig. 5.98. In other words, the lowest pressure coefficient contours were on the leeward side of the roof near the ridge. After the ridge, on the leeward side, the pressure coefficients increased gradually towards the A and B edges of the leeward and windward arrays, except near the D edge overhang, where the pressure coefficients significantly increased again. However, the low pressure near the A edge overhang is located on the roof outside the windward array, and is much lower than the highest pressure coefficients near the ridge. Moreover, the lowest pressure coefficient areas correspond to the highest flow speeds, as displayed in Fig. 5.97 and 5.98, where over the ridge the flow reached 83 m/s or 21 m/s corresponding to 40 m/s and 10 m/s respectively. On the other hand, it is noted that the wind flow under the overhang level was much slower than the free stream speed (dark blue color). The slow flow velocity extended to a distance similar to the overhang height on the front and back of the building when the flow is 40 m/s, while the slower flow extends further on the back of the building when the flow was 10 m/s.

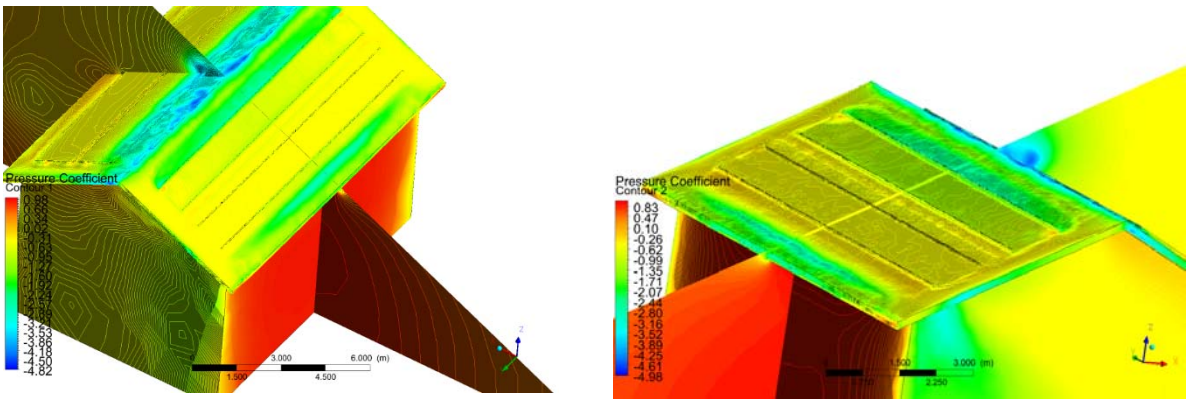
Velocity distributions under the panels along the perpendicular plane are presented in Fig. 5.99 for wind speeds 10 m/s and 40 m/s. The flow speed in the gap under the panels varied between 0- 3.96 m/s and 0 -16 m/s for 10 m/s and 40 m/s respectively, and those wind speeds are much smaller than the wind speed of the free stream.



a) b)

Fig. 5. 99. Velocity on a perpendicular plane under the solar panels, wind speeds a) 10 m/s and b) 40 m/s, wind direction 90º

The two graphs in Fig. 5.100 expose the pressure coefficients on the roof surface under the windward array for different free stream flows of 10 m/s and 40 m/s. Both graphs show that the Cp on the roof under the panels increased from 0.10 near the A edge of the windward array to -2.07 at the B edge side of the array. In addition, the Cp in the cavity matches the Cp on the roof surface. However, the lowest pressure coefficients on the windward side of the roof, -2.44 to -4.61, were located either on the A edge overhang or near the ridge on the roof outside the windward arrays.



a) b)

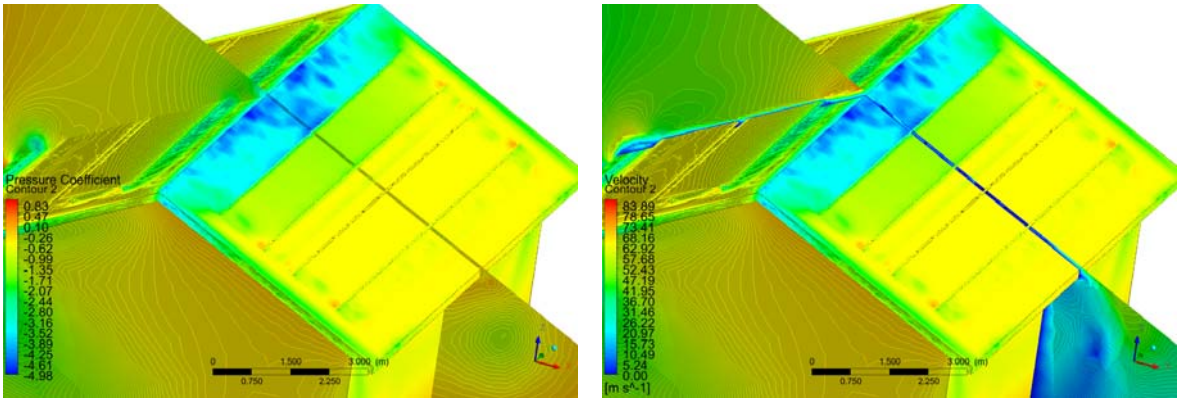
Fig. 5. 100. Pressure coefficients on a perpendicular plane under the solar panels, windward, wind speeds a) 10 m/s and b) 40 m/s, wind direction 90º

For the leeward side of the roof, the two graphs in Figs. 5.101 exhibit the pressure coefficients and velocities on the roof surface under the leeward array for the free stream flow of 40 m/s.

The pressure coefficients on the roof under the panels increased from -0.62 near the B edge of the leeward array to -3.16 at the A edge side of the array near the ridge. In addition, the Cp in the gap is close to the Cp on the roof surface. However, the lowest pressure on the leeward side of the roof, -3.52 to -4.98, covers a narrow strip of 12" (0.30m) width beyond the railing support of the panels near the ridge (Figs. 5.101 and 5.102) on the roof surface under the panels. Nonetheless, this very low pressure continues to cover the entire area on the roof surface on the leeward side until the ridge. The area near the ridge however is located outside the leeward array.

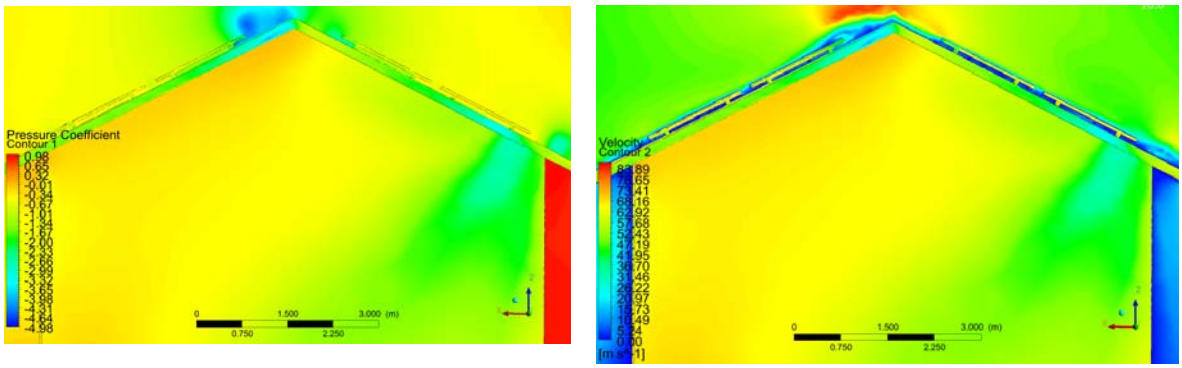
On the other hand, the wind flow speed (5.24 to 21.97 m/s) in the cavity between the roof surface and the bottom surface of the panels was much slower than the free stream speed (40m/s).

Other views of the Cp and velocity profiles across the plane perpendicular to the roof are displayed in Fig. 5102 below. From Fig. 5.102 it can be noted that the flow speed above the panels is higher than the free stream, while under the panels this is lower than the free stream.



\+ a) b)

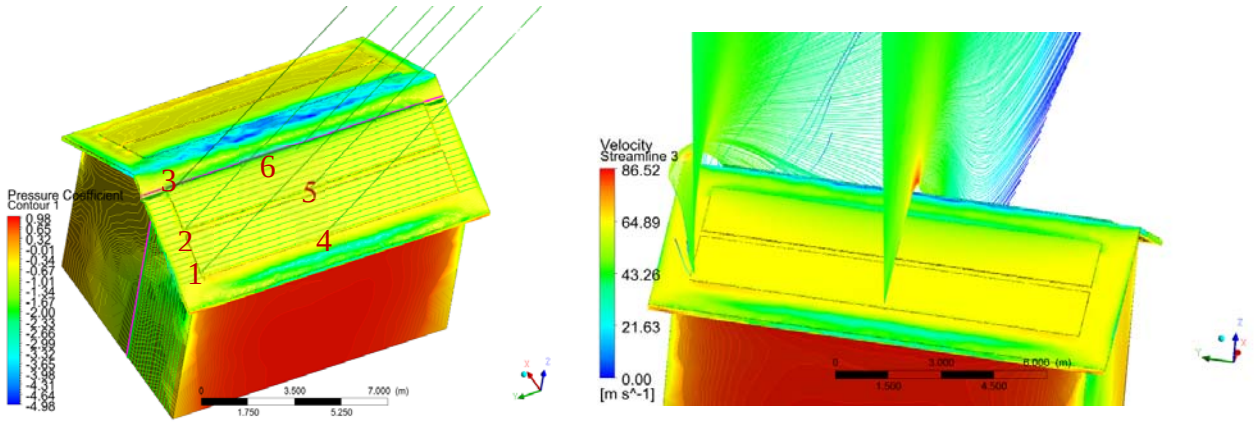
Fig. 5. 101. Pressure coefficients and velocity on a perpendicular plane under the solar panels, leeward, wind speed 40m/s, wind direction 90°



a) b)

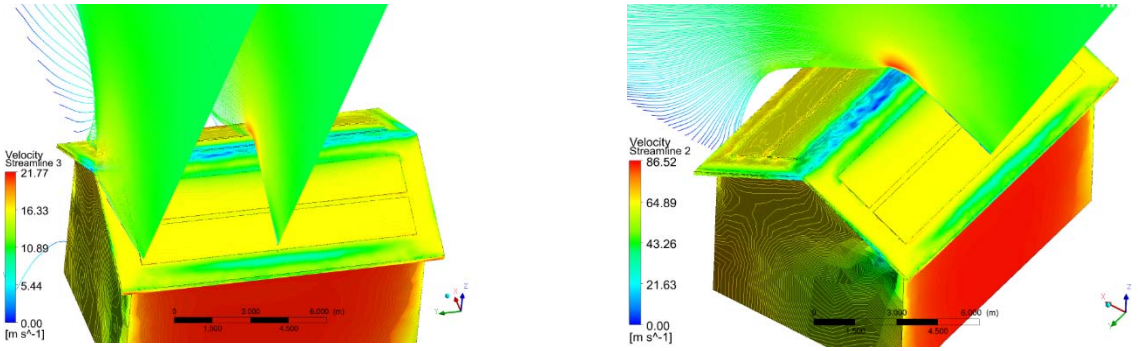
Fig. 5. 102. Velocity and pressure coefficients on a perpendicular plane under the solar panels, wind speed 40m/s wind direction 90º

Figure 5.103 shows the six lines perpendicular on the roof which were used to track the velocity and the pressure variation. Three lines are located near the E edge of the solar panels and the other 3 lines are near the middle cross-section.



a) b)

Fig. 5. 103. a) Lines for the cavity velocity and b) streamlines, windward, wind direction 90º, wind speed 40 m/s



a) b)

Fig. 5. 104. Velocity stream lines at middle and west cross-section planes, wind speeds a) 10 m/s and b) 40 m/s, windward, wind direction 90º

Figure 5.103. b shows the velocity streamlines along the Lines 1 and 4. The flow along Line 4 is laminar with straight profile for the middle region, while the other streamlines along Line 1 were redirected under a curved trajectory towards the outside of the panel array or outside the entire roof. Figure 5.104 presents the streamline flows for 10 m/s and 40 m/s streams above the roof for both windward and leeward sides of the roof. Both streamlines showed the same velocity changes relative to the free stream speed, wherein the flows accelerate more near the roof surfaces than the free stream speeds. However, the flows accelerate the most (21.77 m/s and 86.52 m/s for 10 m/s and 40 m/s freestream speeds respectively) in the region above the ridge, while they return to freestream speed at 13.50 to 23.50m above the roof surfaces.

5.4.5. Wind flow characteristics and three-dimensional vortex formations for gable roofs without solar panels for wind direction 90º

Figures 5.105 and 5.106 illustrate the building and roof vortex cores shown from the windward side on top of the panels and on the roof underneath the panels respectively. The sizes of the building vortex cores are an order of magnitude larger than the sizes of the roof vortices generated by the panels. The overall vortex cores on the entire building are shown on Fig. 5.105 from the windward side, where the largest vortex cores were located on the leeward and on the sides of the building. Smaller flow vortices are located on the roof at the ridge and at the windward front edge. Further, smaller vortex cores are located around edges of the solar panels, and the next-smallest

vortex cores are located on the surface of the solar panels, while the smallest vortex cores are on the roof surface under the panels (Fig. 5.106).

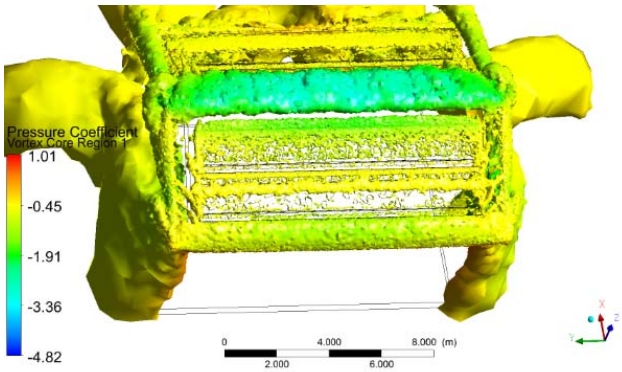


Fig. 5. 105. Vortex core distribution on roof with panels installed and around the structure; no building is shown

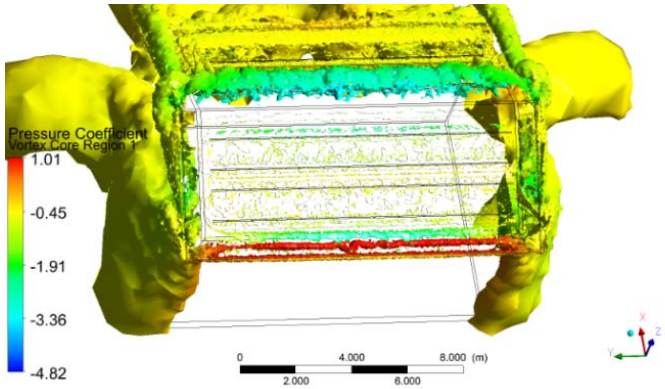


Fig. 5. 106. Vortex core distribution on roof under panels and around the structure, windward, wind direction 90º

In comparison with the distribution of vortex cores on top of the panels (Fig. 5.107) and the bottom surface of the panels (Fig. 5.108) with those on roof surface under the panels (Fig.5.106), the roof surface exhibits slightly smaller vortex cores on the windward side than the corresponding areas on the top and bottom surface of the panels. Figure 5.107 illustrates the vortex cores on top of the panels and around the roof on the windward side, where the size of those vortex cores is the largest at the ridge and near the A edge of the roof. Moderate-size vortex cores are shown in the spacing between rows, while the smallest vortex cores are shown on the panels. Similarly, Fig. 5.108 illustrates the vortex cores on the bottom surface of the panels, and around the roof for the windward side, where the size of those vortex cores was greatest at the ridge and near the A edge of the roof. Moderate-size vortex cores are shown in the spacing between the rows, while the

smallest vortex cores are shown on the panels. In general, smaller vortex cores are present on the bottom surface of the panels than on the corresponding areas on top of the panels.

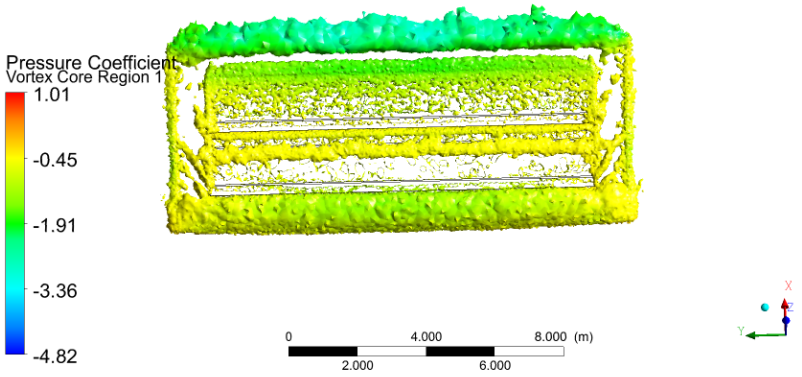


Fig. 5. 107. Vortex core distribution on top of the panels, windward

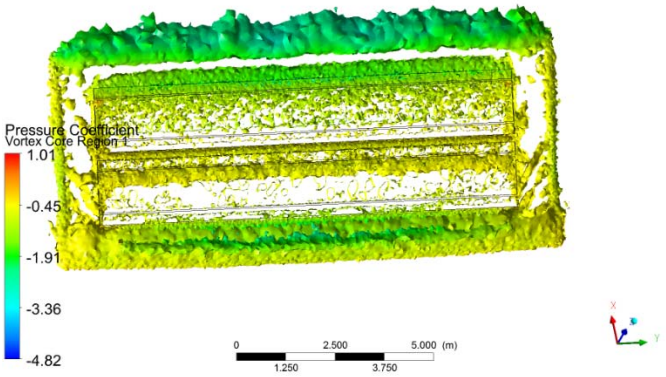


Fig. 5. 108. Vortex core distribution on bottom surface of the panels, windward

Figure 5.109 illustrates the vortex cores on top of the panels and around the roof on the leeward side, where the size of the ridge vortex cores is slightly smaller than those on the back side of the building. The ridge vortex cores are much greater than those at the B edge of the leeward array. However, much smaller vortex cores than those on the ridge and on the B edge are shown in the spacing between rows, while the smallest vortex cores are shown on the surfaces of the panels. Similarly, Figure 5.110 illustrates the vortex cores on the bottom surface of the panels and on the roof in the leeward direction, where the size of the vortex cores at the ridge was much bigger than those at the B edge of the leeward array. However, moderate-size vortex cores are shown in the spacing between rows, while the smallest vortex cores generated on the panels. The distribution of the vortex cores seems very similar between the top and the bottom surface of the panels.

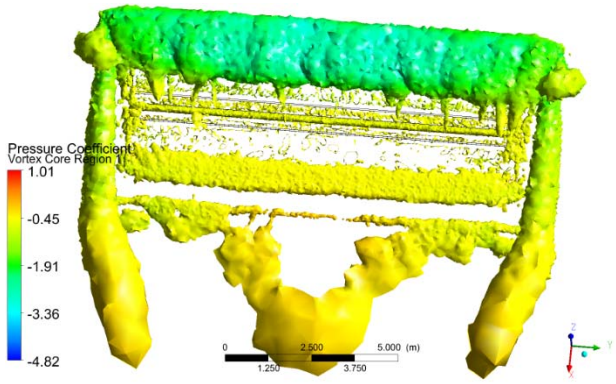


Fig. 5. 109. Vortex core distribution on top of the panels, leeward

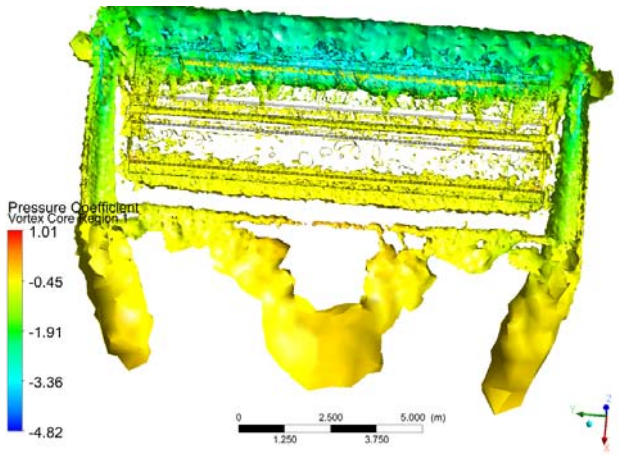


Fig. 5. 110. Vortex core distribution on bottom surface of the panels, leeward

5.4.6. Wind flow characteristics for gable roofs with solar panels for 45º wind direction, windward side of the roof

For wind direction 45º, the velocity distribution under the panels on the windward side is shown in Fig. 5.111, and it remains lower than the free stream speed for most of the path under the panels. However, the wind speed in the gap becomes slightly higher than the free stream speed between the two rows of the panels.

The distribution of flow velocities under the leeward panel array is shown in Fig. 5.112, where the distribution is similar to the flow velocity distribution under the windward array. However, the velocities under the windward and leeward arrays are much higher than the flow velocities when the panels are subject to a 90º wind direction flow.

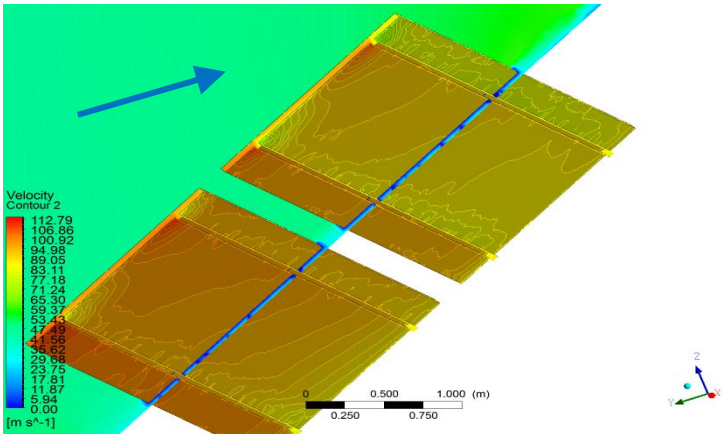


Fig. 5. 111. Velocity on a perpendicular plane under panels, low wind speed, windward, wind direction 45º

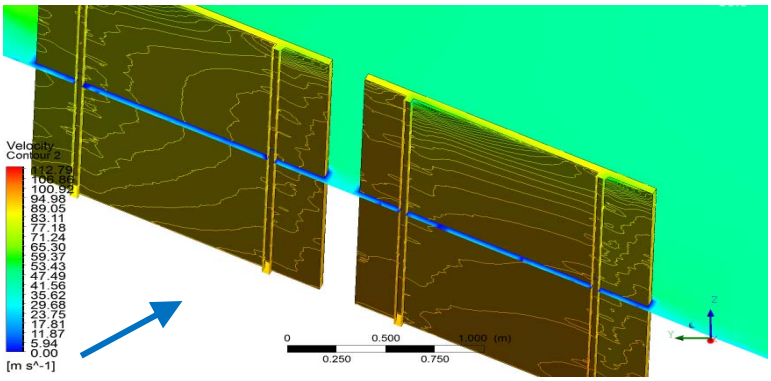


Fig. 5. 112. Velocity on a perpendicular plane under panels, low wind speed, leeward, wind direction 45º

The distribution of flow velocities on top of the windward panel array is shown in Fig. 5.113, while that on top of the leeward panel array is illustrated in Fig. 5.114.

Both distributions indicate higher flow speeds on top of the panels than free streams, which is similar to the observation with the 90º flow.

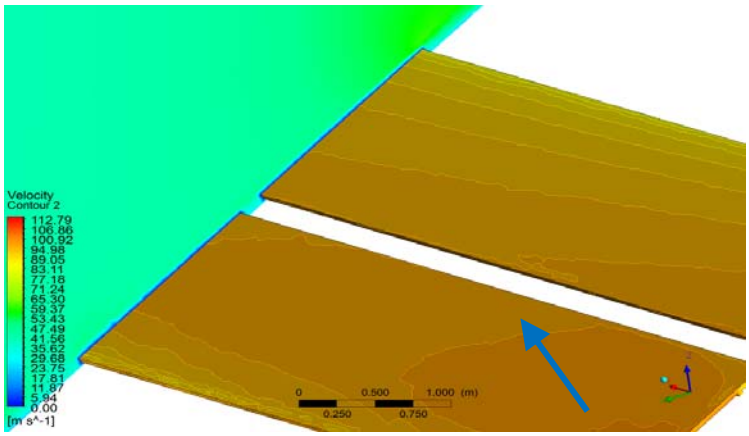


Fig. 5. 113. Velocity on a perpendicular plane above panels, low wind speed, windward, wind direction 45º

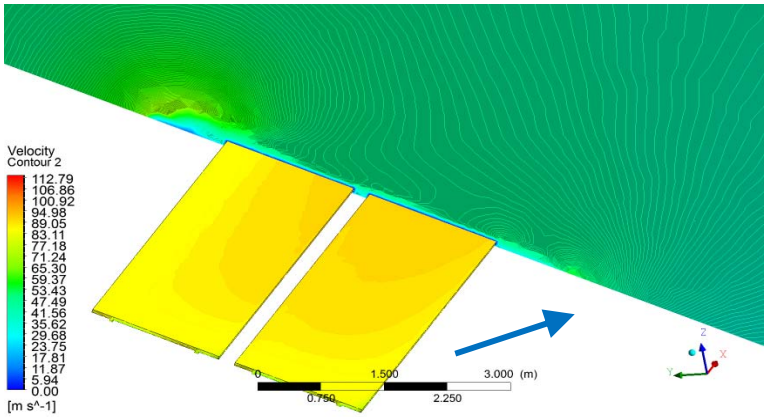


Fig. 5. 114. Velocity on a perpendicular plane above panels, low wind speed, leeward, wind direction 45º

The pressure coefficients on top of the panels on the leeward and windward sides are depicted in Fig. 5.115 and Figs. 5.117 to 5.123.

The lowest pressure coefficients are located near the building ridge on the leeward surface but outside the windward array boundaries (Fig. 5.115). The pressure coefficients decrease gradually to -1.98 to -0.24 towards the front of the windward array, and increase to 0.33 to -1.40 towards the end of the leeward array at the back of the building,

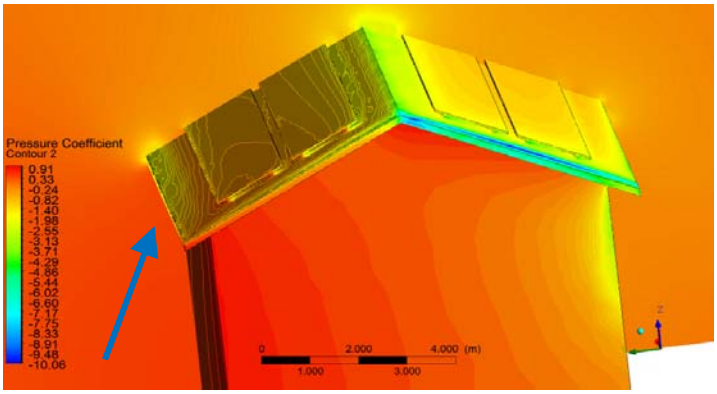


Fig. 5. 115. Pressure coefficients on a perpendicular plane, wind direction 45º

Fig. 5.116 exhibits the velocity distribution on a perpendicular plane to the middle of the building. The highest wind speed registered for this plane was 71.24 m/s near the ridge, and a smaller wind flow speed of 65.30 m/s was shown at the windward and leeward overhangs. Moreover, at the surface of the building model the velocity was 0 m/s and it increased with the distance from the building surface, and finally reaching the free stream velocity magnitude.

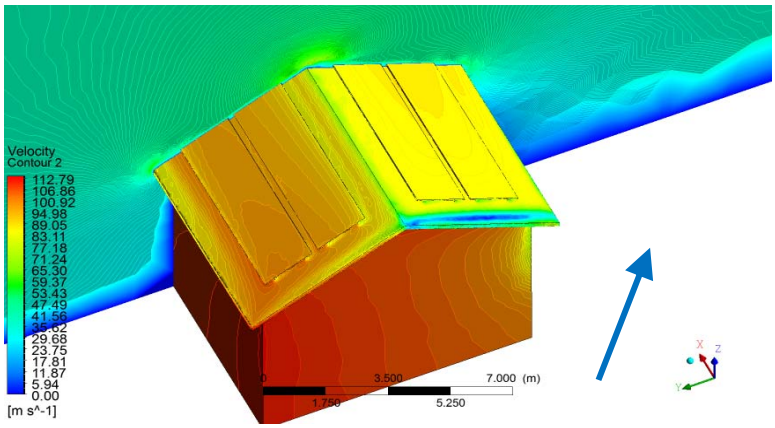


Fig. 5. 116. Velocity on perpendicular plane, wind direction 45º

The overall pressure coefficients distribution on the building with solar panels is depicted in Fig. 5.117, which shows the highest pressure coefficients (-7.49 to -3.83) at the B edge of the roof, and then lower coefficients -3.31 to -1.73 at the ridge . However, no solar panels are installed on these very low-pressure regions, because the panels are mounted beyond 1.0 m from edges of the roof, primarily to avoid the high-suction zones of the roof, as per the NBCC 2015 recommendations.

Moreover, Fig. 5.118 depicts the Cp on the roof viewed from the leeward side, and clearly shows the lower Cp at the ridge area on the leeward side of the roof, also Fig. 5.118 portrays a gradual change of Cp on the leeward array from the lowest Cp near the C edge and the highest near the E edge of the roof.

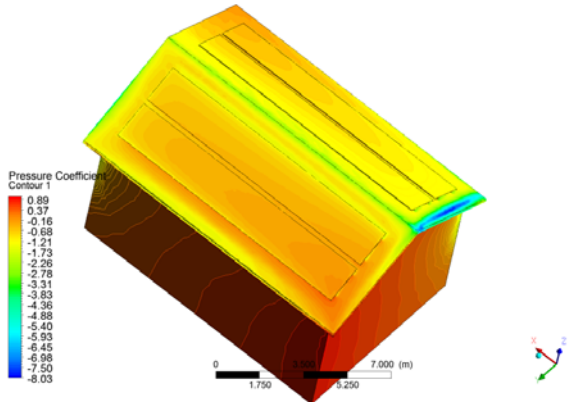


Fig. 5. 117. Pressure coefficients on whole building, roof with solar panels, slope 27º, windward, wind direction 45º

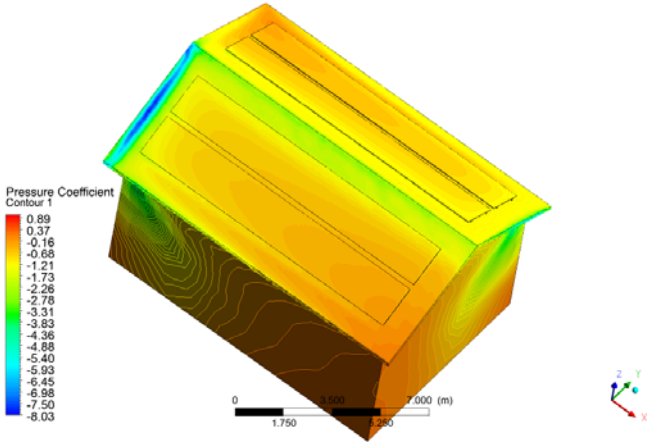
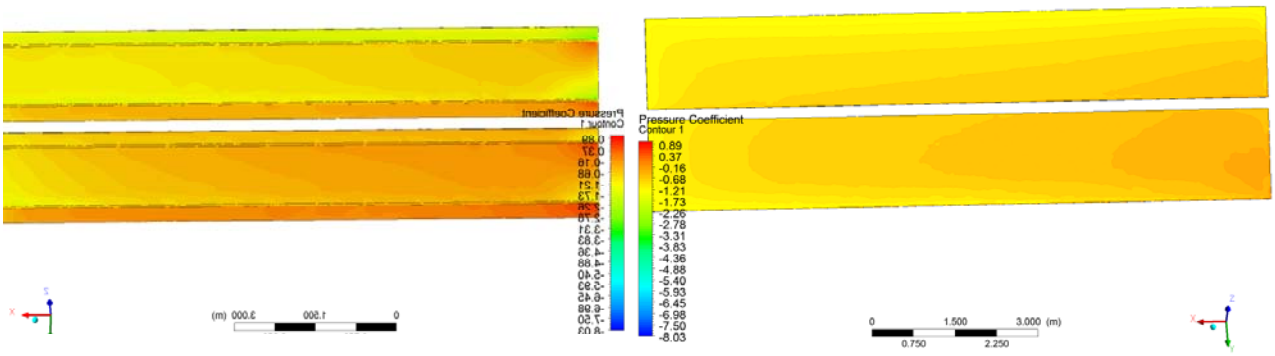


Fig. 5. 118. Pressure coefficients on whole building, roof with solar panels, slope 27º, leeward, wind direction 45º

Detailed distributions of the pressure coefficients on the top and bottom surface of the panels and the roof surface under the panels are represented in Figs. 5.119 to Fig.5.122.

Figure 5.119 shows the pressure coefficients on the bottom (a) and top (b) of the windward panel array under the 45º wind direction. On the bottom surface of the panels, the Cp ranges from 0.37 to -2.26, which is different from the distribution on top of the panels (-0.16 to -1.21). However,

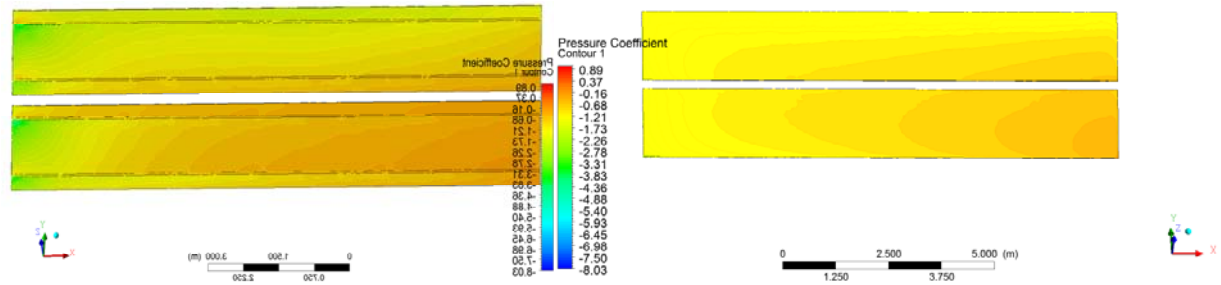
there is high similarity between the Cp on the roof surface under the panels (Fig.5.121) and the Cp on the bottom surface of the panels (Fig. 5.119) in both the Cp distributions and their values.



(a) (b)

Fig. 5. 119. Pressure coefficients on: a) bottom surface of the panels, b) top of the panels, slope 27º, windward, wind direction 45º

Similarly, Fig. 5.120 shows the pressure coefficients on the bottom (a) and top (b) of the leeward panel array under the 45º wind direction. On the bottom surface of the panels, the Cp ranges from -0.16 to -3.38, which is different from the distribution on top of the panels (-0.16 to -1.21). However, the Cp on the roof surface under the panels (Fig.5.122) and on the bottom surface of the panels (Fig. 5.120) have very similar distributions and magnitudes.



(a) (b)`

Fig. 5. 120. Pressure coefficients on: a) bottom surface of the panels, b) top of the panels, slope 27º, leeward, wind direction 45º

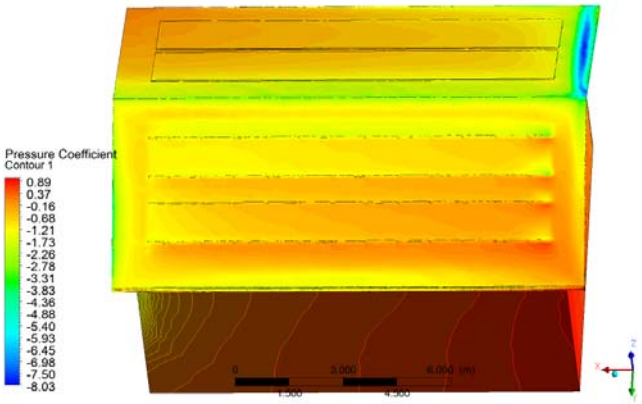


Fig. 5. 121. Pressure coefficients on roof surface under the panels, slope 27º, windward, wind direction 45º

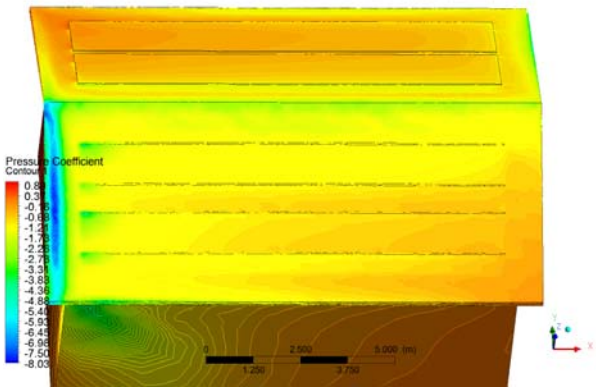


Fig. 5. 122. Pressure coefficients on roof surface under the panels, slope 27º, leeward, wind direction 45º

Figure 5.123 shows the building model with all 38 polylines used for the integration of the Cp coefficient on the 6 surfaces (3 surfaces on the windward side of the roof and 3 surfaces on leeward side). Each set of 3 surfaces includes the top and bottom surface of the panels and the roof surface under the arrays.

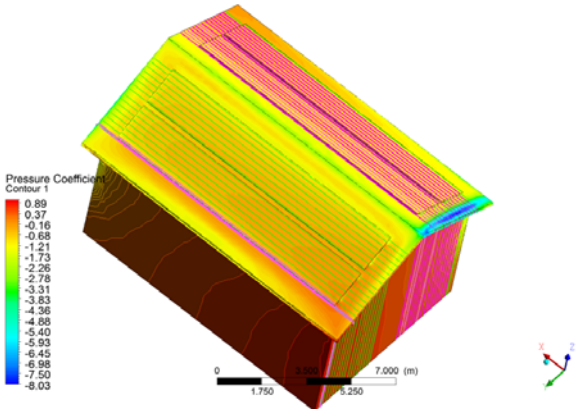


Fig. 5. 123. Pressure coefficients on roof surface along with distribution of the polylines used to calculate the pressure coefficients along the 3 surfaces, slope 27º, leeward, wind direction 45º

5.4.7. Detailed distribution of vortex cores on roof with solar panels

Figures 5.124 to Fig. 5.129 illustrate both the building and roof vortex cores shown from windward, leeward, and on the roof surface under the panels respectively, wherein the size of the building vortex cores (Figs 5.126 to 5.129) is much larger than the sizes of the vortices generated by edges of the roof and by edges of the panels.

On the other hand, the vortex cores on roof surface (Figs. 5.128 and 5.129) are much smaller than those on the top or bottom surface of the panels (Figs. 5.124 and 5.125).

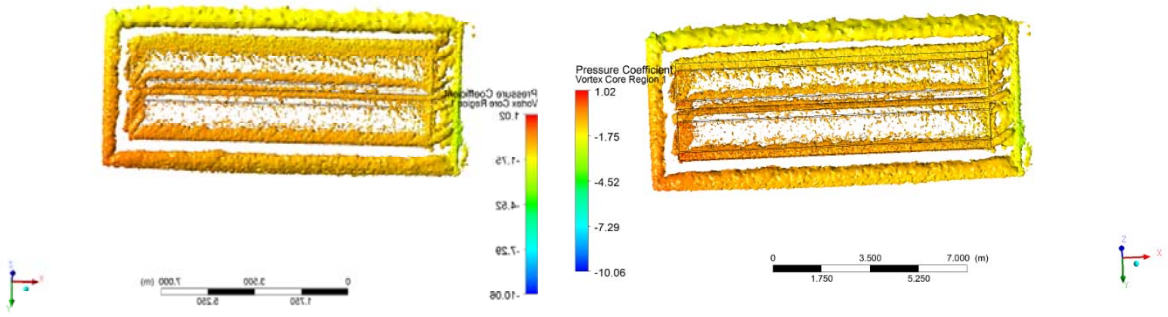


Fig. 5. 124. Vortex core distributions on: a) top of the panels, b) bottom surface of the panels, slope 27º, windward, wind direction 45º

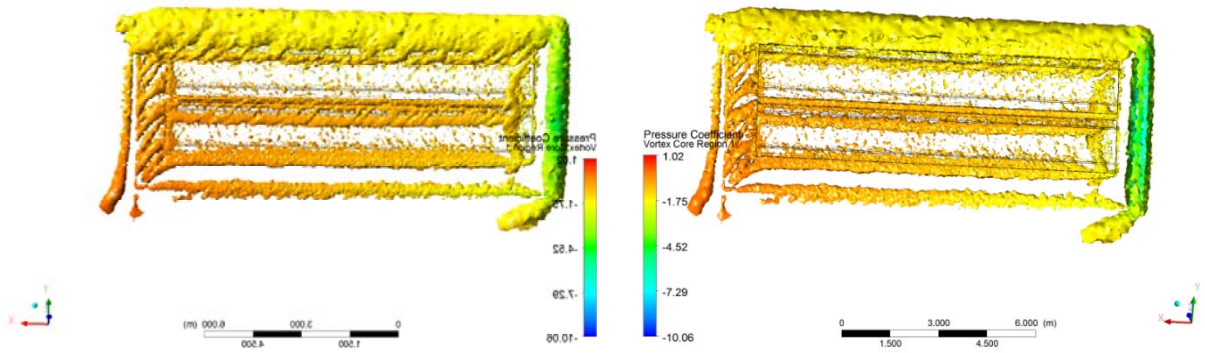


Fig. 5. 125. Vortex core distributions on: a) top of the panels, b) bottom surface of the panels, slope 27º, leeward, wind direction 45º

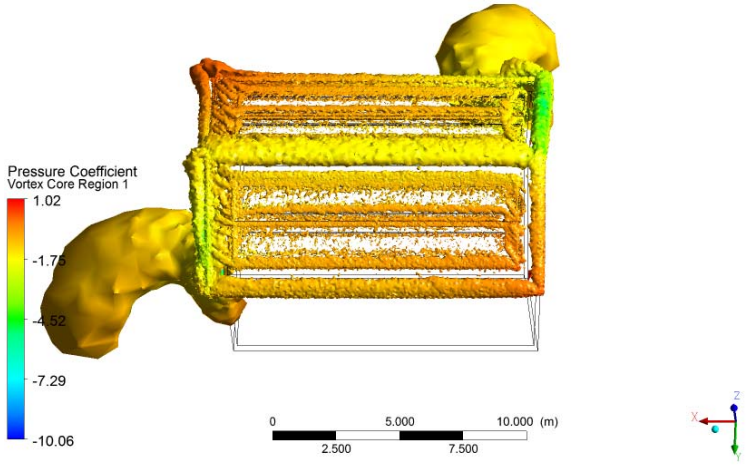


Fig. 5. 126. Vortex core distributions on roof with panels, slope 27º, windward, wind direction 45º

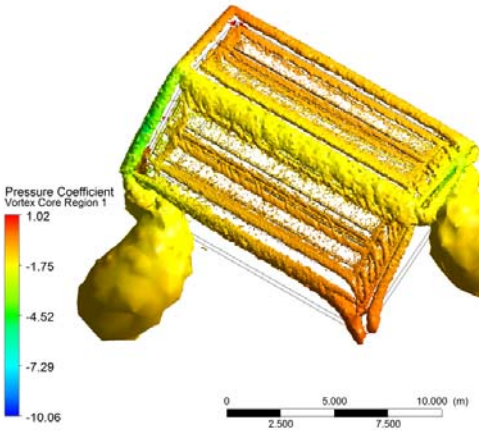


Fig. 5. 127. Vortex core distributions on roof with panels, slope 27º, leeward, wind direction 45º

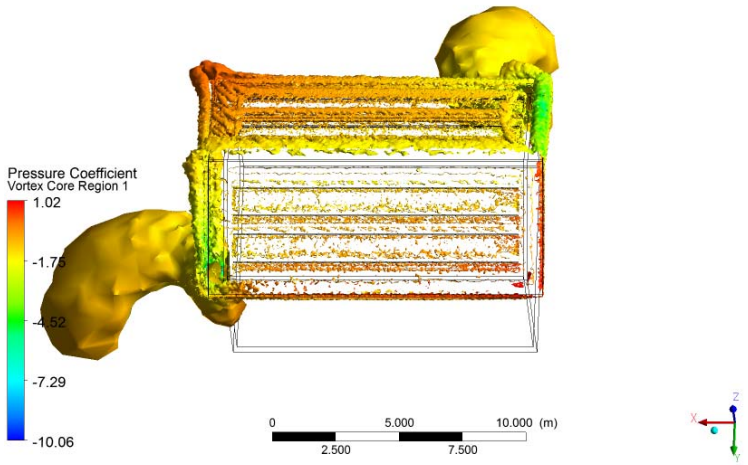


Fig. 5. 128. Vortex core distributions on roof under panels, slope 27º, windward, wind direction 45º

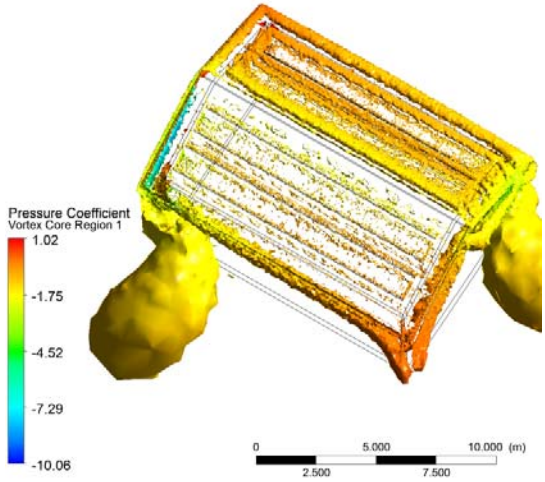


Fig. 5. 129. Vortex core distributions on roof under panels, slope 27º, leeward, wind direction 45º

5.4.8. Wind pressure coefficient and flow distributions along 6 lines perpendicular to panels under and above the panels, windward

The distribution of velocities and of the pressure coefficients along Lines 1 to 6 are represented in Figures 5.130 to 5.141, for the 90° wind direction and 40 m/s incoming wind speed. For each line, two figures and four graphs are presented. The first graph is for the wind speed inside the cavity between the roof surface and the bottom surface of the solar panels, and the second one is for the roof surface to the upper surface of the solar panels and up to 15-30 m above their surfaces.

Near the corner of the solar panel array along Line 1, the distribution velocity profile in the space between the roof surface and bottom surface of the panels for the 3” (0.076 m) clearance height is shown in Fig. 5.130, wherein the velocity changes from 0 on the surface of the roof to 18 m/s slightly beyond the middle of the cavity between the panels and the roof, and then returns back to 0 at the top of this space on the bottom surface of the panel.

Also, along Line 1 and above the solar panel surfaces, the velocity increased to 45 m/s in the first 4” (0.102m) above the top of the panels, then slightly falls to 44.8 m/s, and then increased back to 46 m/s at nearly 30” (0.76 m) above the roof surface, returning to the ambient speed (40m/s) at 13.50 m above the roof surface.

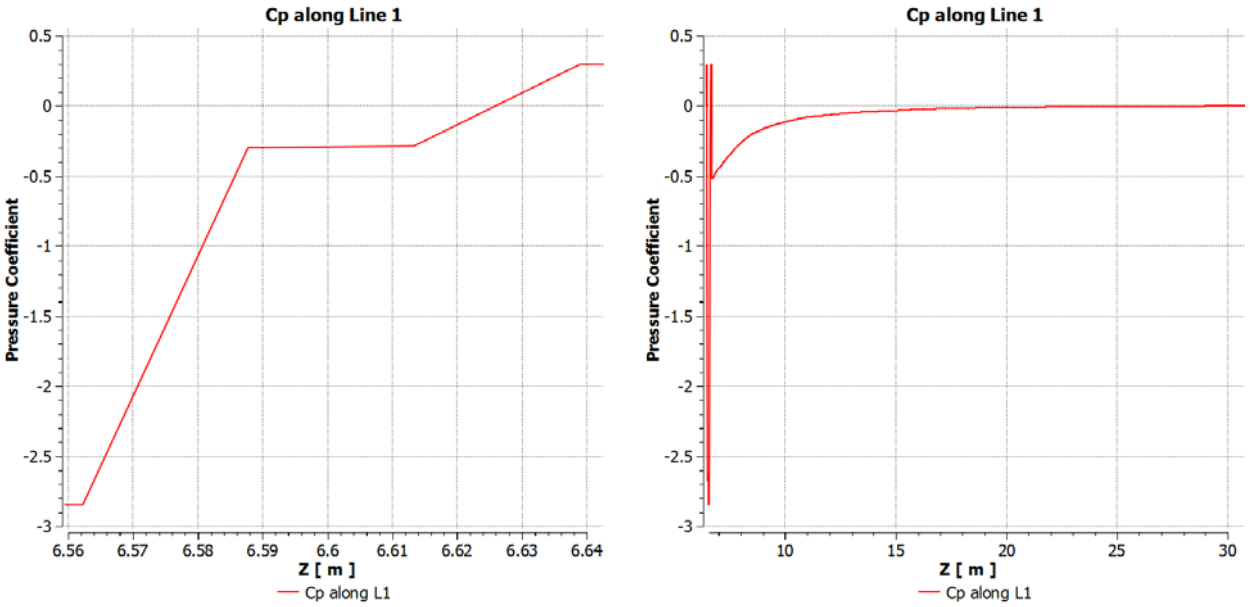


Fig. 5. 130. Pressure coefficient variation in the cavity and above the panels along Line 1

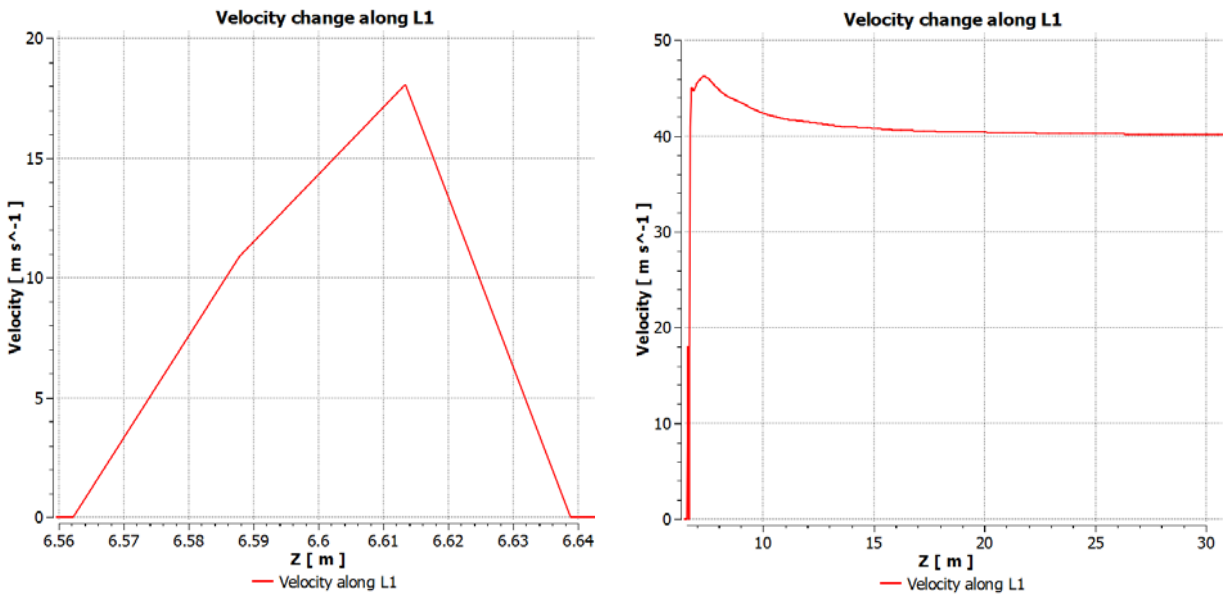


Fig. 5. 131. Wind velocity profile in the cavity and above roof along Line 1

The pressure coefficient profiles between the roof surface and the bottom surface of the panels for the 3" (0.076 m) space height, wherein the pressure coefficient decreased from -2.84 to -0.30 in the first 1" (0.025m) above the roof surface, then remains constant for another 1", and then decreased again to 0.3 at the bottom surface of the panels, Fig. 5.131.

However, the Cp decreased sharply to -0.50 on top surface of the panels and then afterwards decreased gradually to 0 at 13.5 m above the roof surface.

Along the Line 2 located in the middle of the D edge of the panel array, Fig. 5.132 shows the velocity profile between the roof surface and bottom surface of the panels for the 3" (0.076m) space height, wherein the velocity increased from 0 m/s on the roof surface to 1.45 m/s at 1" (0.254) above the roof surface, then drops to 0.75 m/s in the middle of the cavity. Afterwards, the flow speeds peaks at 2.9 m/s nearly 0.75" below the bottom surface of the panels, then it decreased gradually to 0 m/s at the bottom surface of the panels.

Above the solar panel surfaces, the velocity increased to 47.8 m/s at 4" (0.102m) above the roof surface, then it decreased to 47 m/s at 20" (0.50m) above the top of the panels and remained constant until 50" (1.25 m) above the panels. Above this height the velocity decreased to 40 m/s at 23.5 m above the roof surface.

Figure 5.133 shows the pressure coefficient profile between the roof surface and the bottom surface of the panels for the 3” (0.076 m) space height, wherein the pressure coefficient decreased from -0.97 at the surface under the panels to -0.49 at 0.40” (0.01m) above the roof surface, then remains constant for most of the cavity until 0.40” (0.01m) below the bottom surface of the panels, where it decreased to -0.30 at the bottom surface of the panels.

On top of the panels, the Cp decreased to -0.47 on the panel surface at 4” (0.10m) above the panels, and afterwards decreased gradually to 0 at 30m above the ground (23.5 m above the roof surface).

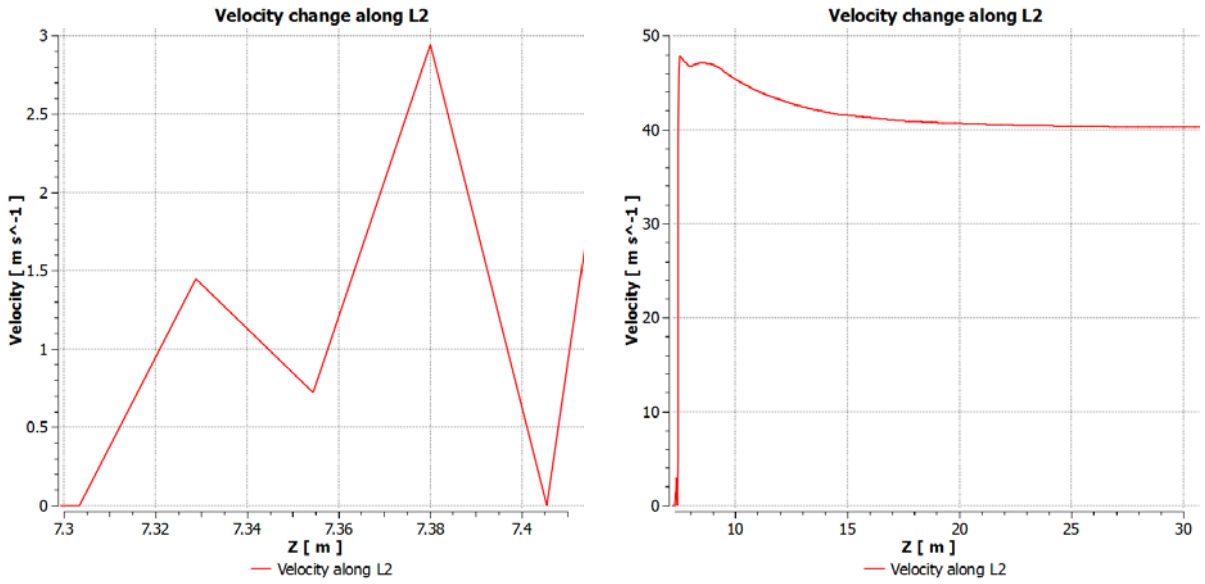


Fig. 5. 132. Wind velocity profile in the cavity and above roof along Line 2

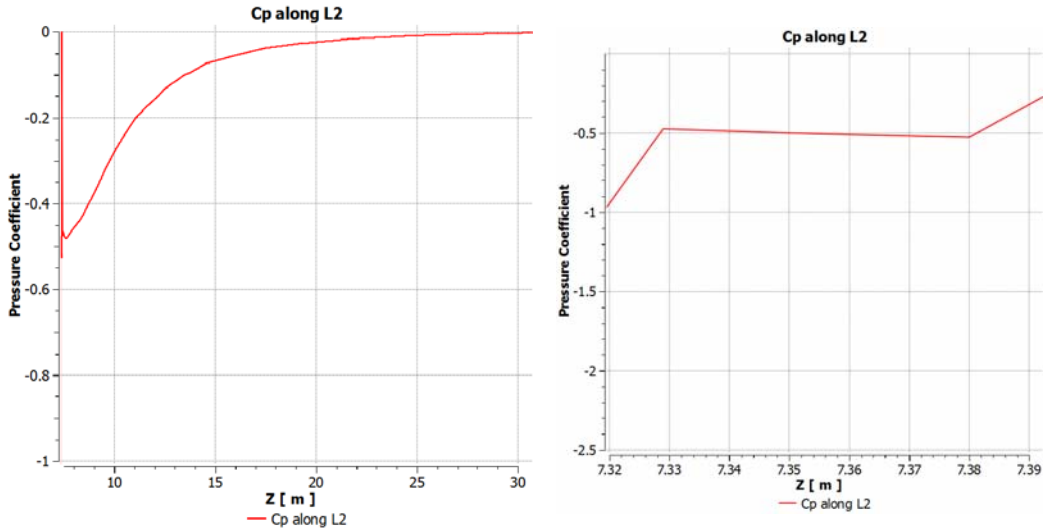


Fig. 5. 133. Pressure coefficient variation in the cavity and above the panels along Line 2

On the E edge side of the panels, along Line 3, Figure 5.134 shows the velocity profile between the roof surface and bottom surface of the panels for the 3" (0.076m) clearance, wherein the velocity increased from 0 on the surface to 8.40 m/s near the middle of the gap, then decreases again to 0 at the bottom surface of the panels.

Above the solar panel surfaces the velocity increased sharply to 55.8.0 m/s at 4" above the top surface of the panel, then decreased to 40 m/s at 30 m above the ground, or 23.50 m above the panels.

Figure 5.135 illustrates the pressure coefficient profile between the roof surface and the bottom surface of the panels for 3" (0.076) clearance, wherein the pressure coefficient is -1.32 at the roof surface, then it increased to -2.10 at 1" (0.025m) above the roof surface and remains constant for one more inch (0.025m), and then increased to 0.23 at the bottom surface of the panel.

On top of the panels, the pressure coefficient starts at -1.0 near the top surface of the panels, then increased gradually above the panels' surface to 0 at 23.5 m above the roof.

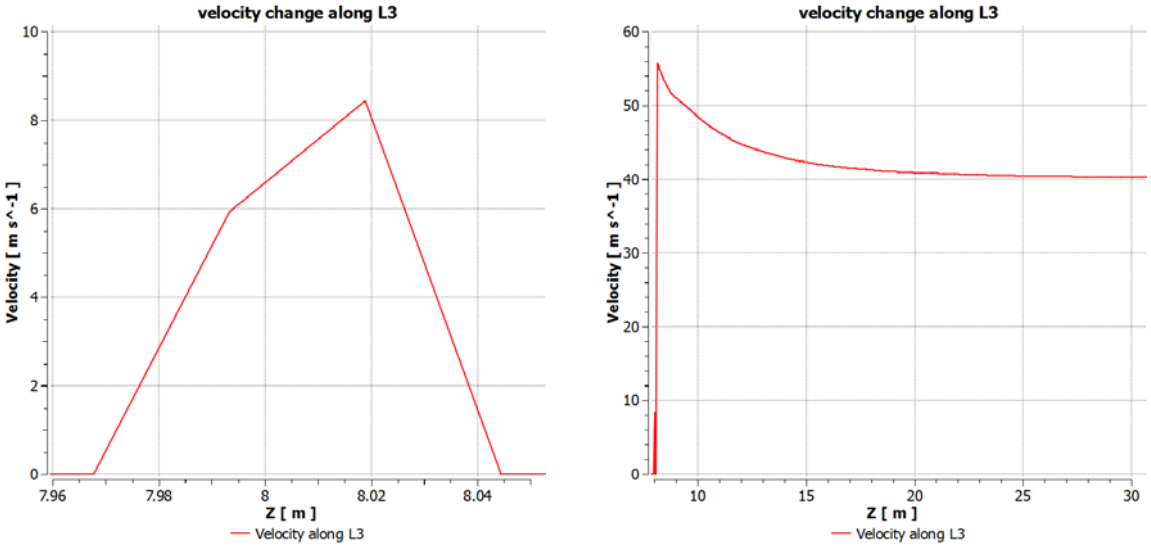


Fig. 5. 134. Wind velocity profile in the cavity and above roof along Line 3

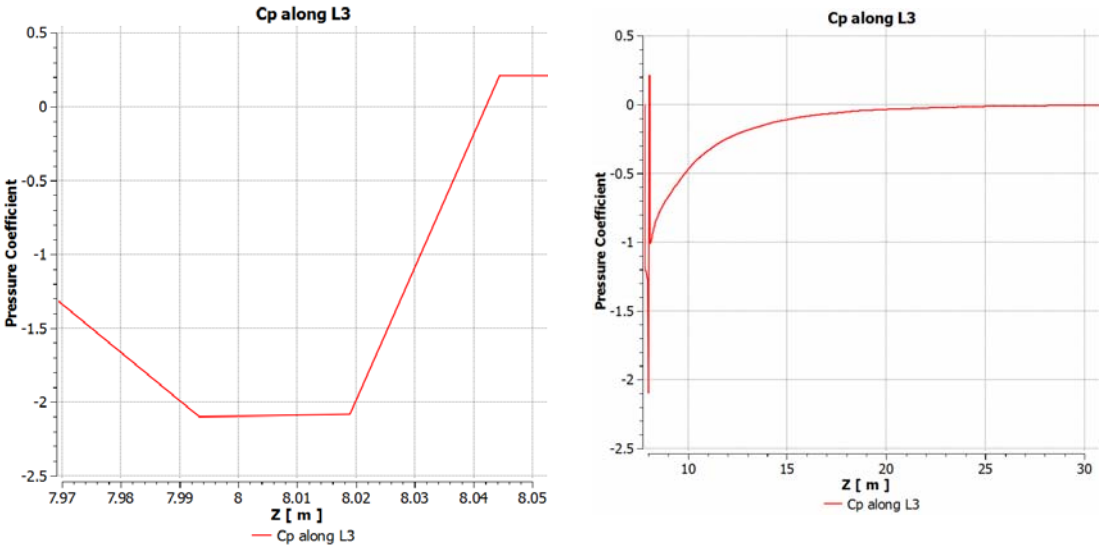


Fig. 5. 135. Pressure coefficient variation in the cavity and above the panels along Line 3

In the middle of the A edge side of the panels, along Line 4, Fig. 5.136 shows the velocity profile between the roof surface and the bottom surface of the panels for 3" (0.076m) clearance, wherein the velocity increased from 0 on the surface to 5 m/s in the middle of the space, then decreases again to 0 at the bottom surface of the panels.

Above the solar panel surfaces, the velocity increased sharply from 0 at the top of the panels to 48 m/s at 40" (1.0m) above the surface, then decreases gradually to 40 m/s at 20 m above the ground, coinciding with 13.5m above the roof.

Figure 5.137 shows the pressure coefficient profile between the roof surface and the bottom surface of the panels for 3" (0.0.76 m) clearance, wherein the pressure coefficient is -0.46 at the roof surface under the panels and then decreases slightly to -0.44 in the middle of the gap, and then the Cp decreases slightly to -0.43 at the bottom surface of the panels.

On top of the panels, the pressure coefficient is lower than under the panels, where it starts at -0.63 at top of the panels and then decreased gradually above the panels' surface to 0 at 13.5m above the roof surface.

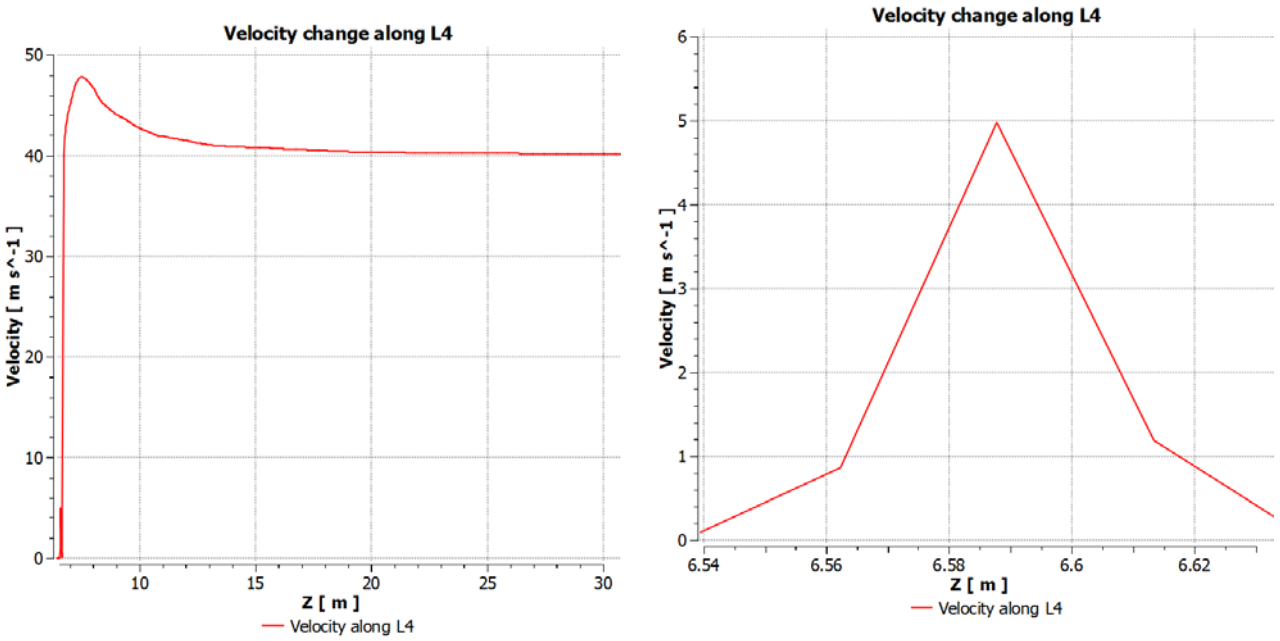


Fig. 5. 136. Wind velocity profile in the cavity and above roof along Line 4

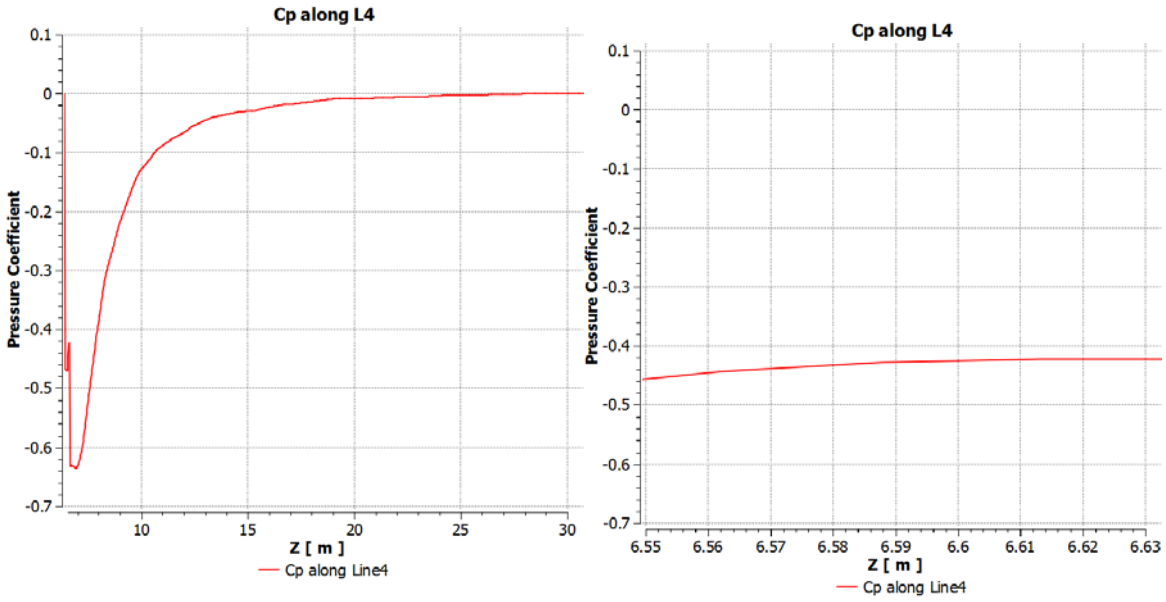


Fig. 5. 137. Pressure coefficient variation in the cavity and above the panels along Line 4

In the middle of the roof, along Line 5, Fig. 5.138 shows the velocity profile between the roof surface and the bottom surface of the panels for 3" clearance and 8" spacing, wherein the velocity increased from 0 on the roof surface to 2.25 m/s in the middle of the space, and then returns to 0

at bottom surface of the panels. However, the wind speed in the middle of the 3” gap is an order of magnitude less than the velocity in the middle of space for 10” clearance and 2” spacing, (62m/s), as shown in Fig. 5.54.

The velocity near top of the solar panel surfaces increased to 51 m/s and then decreases slightly to 49 m/s at 20” (0.51m) above the panels, remain nearly constant for another 20” and then decreases to 40 m/s at 30 m above the ground.

Figure 5.139 shows the pressure coefficient profile between the roof surface and the bottom surface of the panels for 3” clearance and 8” spacing. The pressure coefficient is -0.585 at the roof surface, then increases slightly to -0.61 in the middle of the gap, and then further increases slightly to –0.62 at the bottom surface of the panels.

On top of the panels, the pressure coefficient is slightly higher (-0.738) at the top of the panels, then decreased sharply to -0.67 at 4” above the panels, and after that it gradually decreased above the solar panels’ surface to 0 at 30 m above the ground.

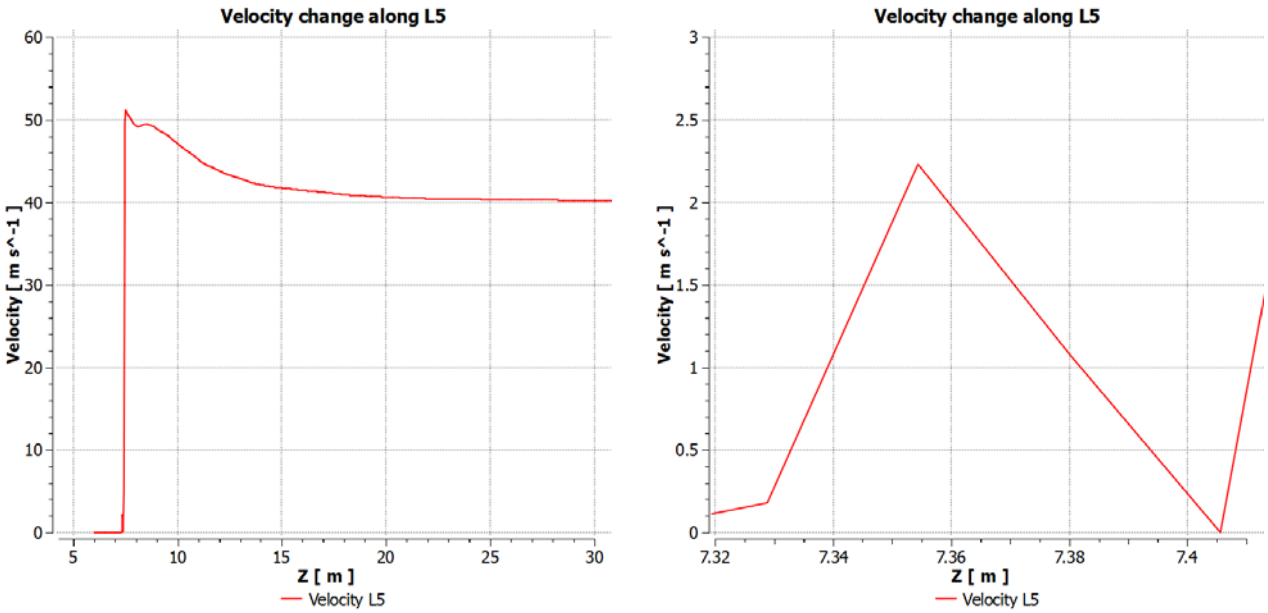


Fig. 5. 138. Wind velocity profile in the cavity and above roof along Line 5

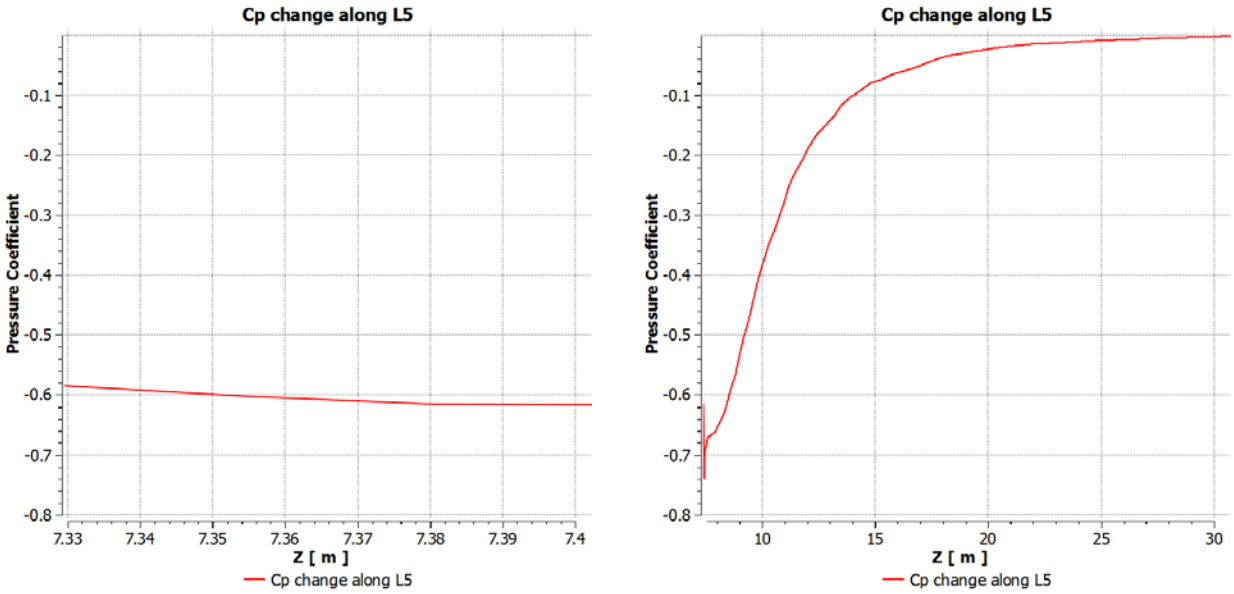


Fig. 5. 139. Pressure coefficient variation in the cavity and above the panels along Line 5

In the middle of the B edge, along Line 6, Figure 5.140 shows the velocity profile between the roof surface and the bottom surface of the panels for 3" clearance and 8" spacing, wherein the velocity increased from 0 on the surface to 5.1 m/s in the middle of the space, then decreases again to 0 at the bottom surface of the panels. The wind speed in the space between the roof and panels is an order of magnitude less than the wind speed for the corresponding line at clearance 10" and 2" spacing (66 m/s), as shown in Fig. 5.56.

The flow velocity near the solar panel top surfaces increased sharply to 63 m/s, then decreases to 40 m/s at 30 m above the ground.

Figure 5.141 shows the pressure coefficient profile between the roof surface and the bottom surface of the panels for 3" clearance and 8" spacing, wherein the pressure coefficient is -2.40, which increases slightly to -2.50 at ¾" (0.02m) above the roof surface, then remains constant until the bottom surface of the panels.

On top of the panels, the pressure coefficient decreases to -0.40 at the top of the panels, then increases sharply to -2.50 at nearly 8" (0.20m) above the panels, then decreased greatly to -1.54 at 10" (0.25m) above the top of the solar panels, then gradually decreased above the solar panels surface to 0 at 30 m above the ground.

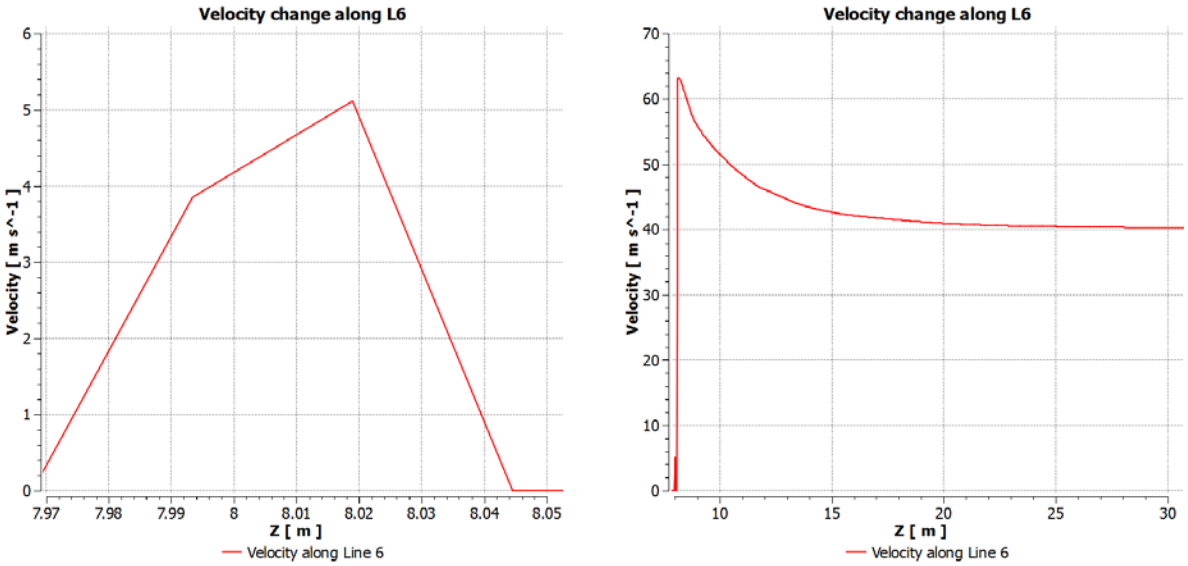


Fig. 5. 140. Wind velocity profile in the cavity and above roof along Line 6

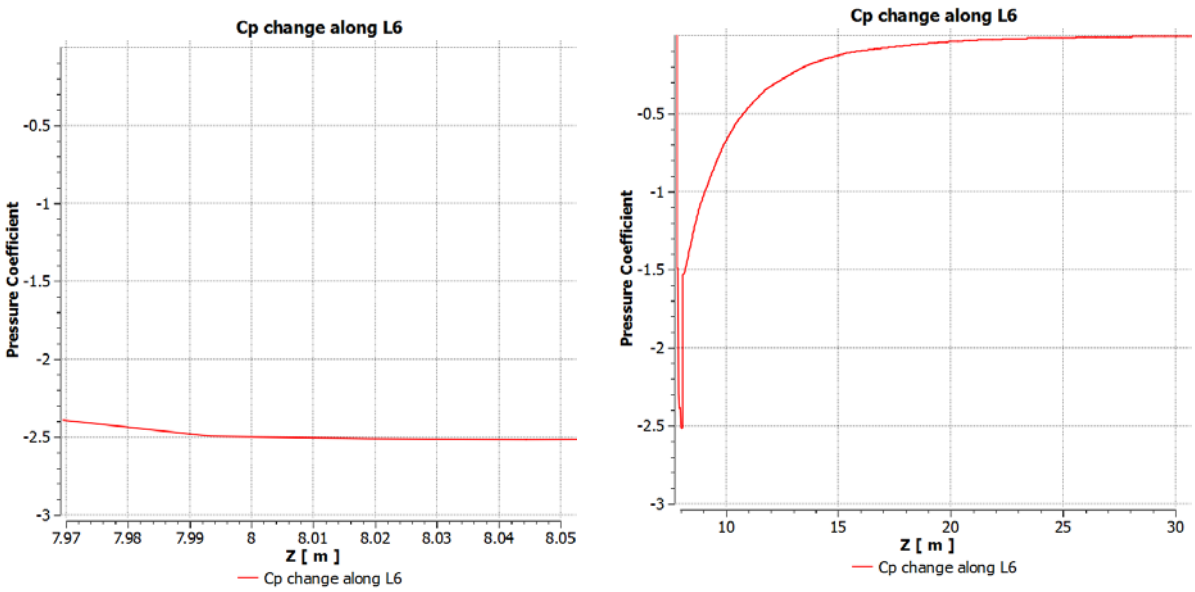


Fig. 5. 141. Pressure coefficient variation in the cavity and above the panels along Line 6

Fig. 5.142 shows the wind flow under and above the panels for all the 6 lines. The wind flow under the solar panels with a roof clearance of 3” is 3 m/s to 18 m/s. However, the wind flow for the 10” clearance is much faster (46m/s to 66 m/s) than for the 3” roof clearance. That is, the wind velocity in the middle of the 10” roof clearance is larger than the ambient wind speed, while for the 3” roof

clearance the flow speed in the gap is much less than the free stream wind speed, as detailed below in the graphs in Figs. 5.130 to 5.141.

However, the pressure coefficients in the 10” space (-0.6, -0.9, -1.4, -1.7, -1.9 and -2.7) are lower in most of the space between the roof and panels than those in the 3” space (0.20, -0.60, -0.65, -1.90, -2.10 and -2.50), where those Cp correspond to L1, L4, L2, L5, L3 and L6 respectively.

In addition, the wind speed above the panels increased greatly from the cavity wind speeds to 46 m/s, 47 m/s, 48 m/s, 51 m/s, 56 m/s and 63 m/s for the same order of lines respectively.

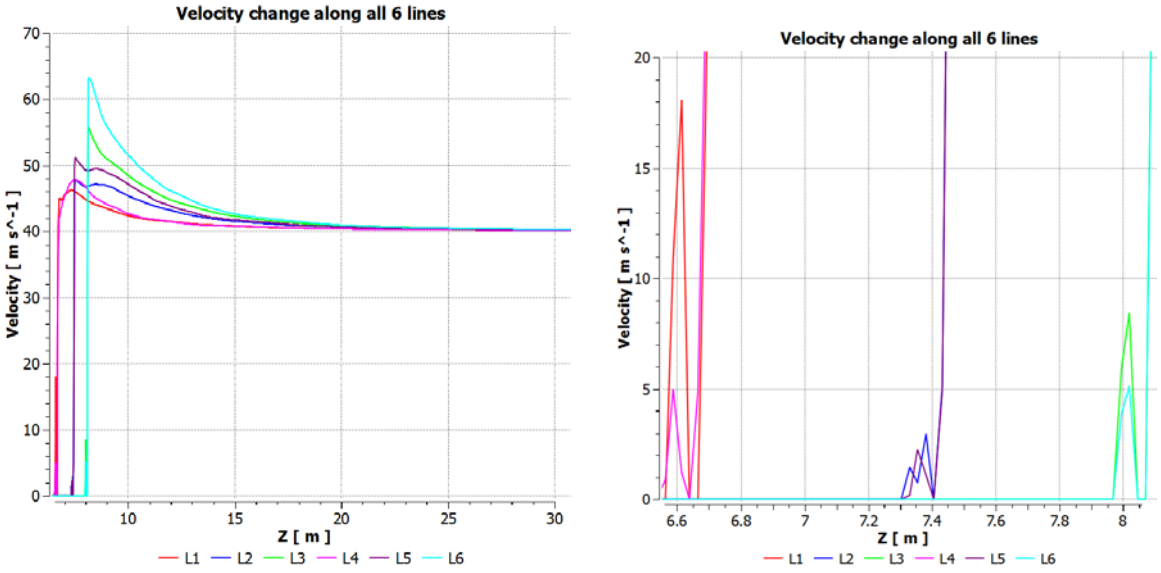


Fig. 5. 142. Wind velocity profile in the cavity and above roof along all 6 lines

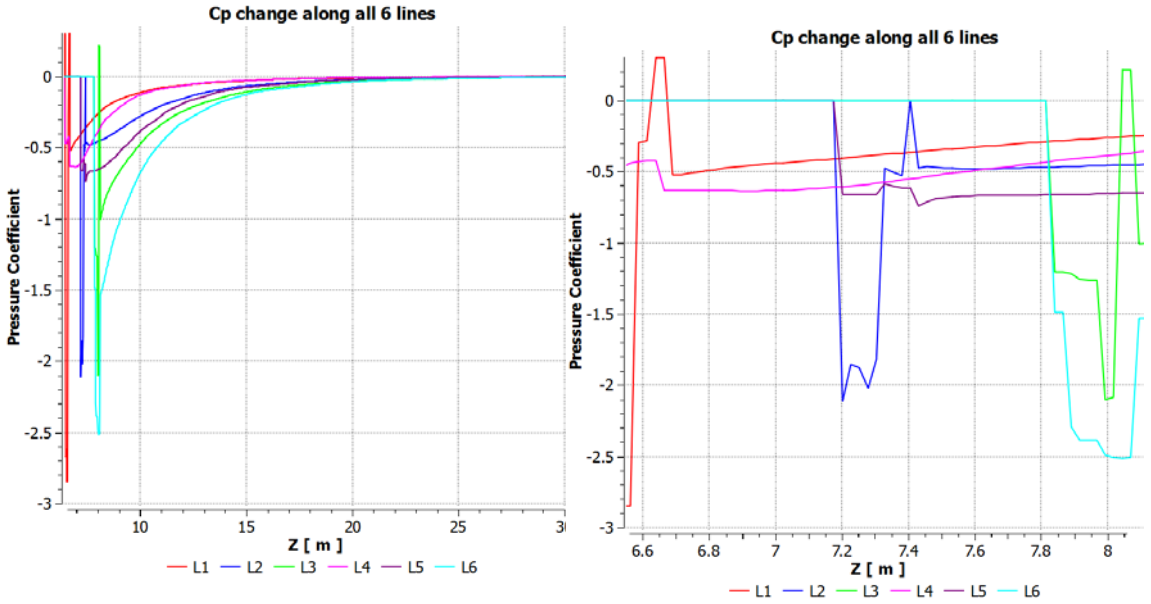


Fig. 5. 143. Pressure coefficient variation in the cavity and above the panels along all 6 lines

Figure 5.144 shows the pressure coefficients along all polylines on the windward side of the building, including at the top of the panels, bottom surface of the panels, and surface of the roof, under wind direction 90º.

Similarly, for wind direction 45º, Figure 5.145 shows the pressure coefficients along the whole length of all polylines on the leeward side of the roof, including at the top of the panels, bottom surface of the panels, and surface of the roof.

It should be noted that the pressure coefficients values were integrated along all the polylines and the polylines in the 0º wind direction as well. Then, average values were taken for each line on the corresponding surface (i.e., top or bottom surface of panels or surface of the roof).

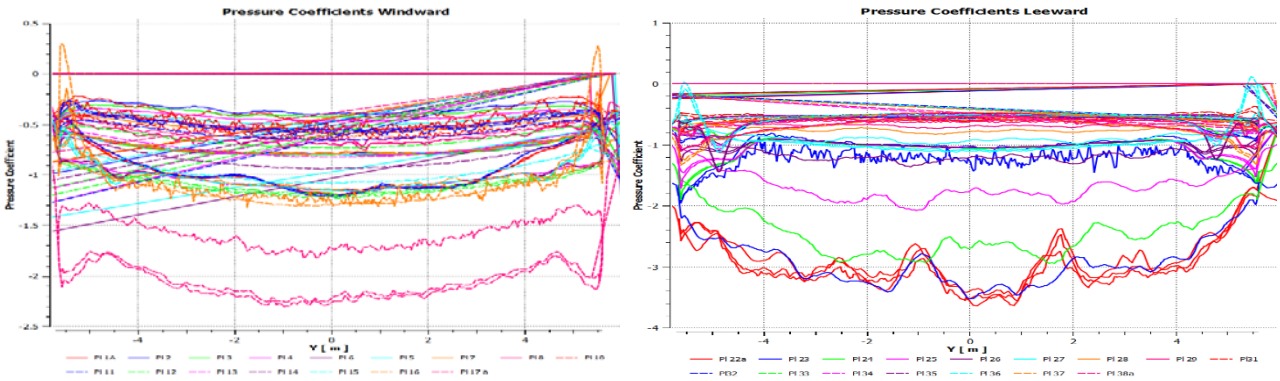


Fig. 5. 144. Pressure coefficients, windward and leeward, slope 27º, wind direction 90º

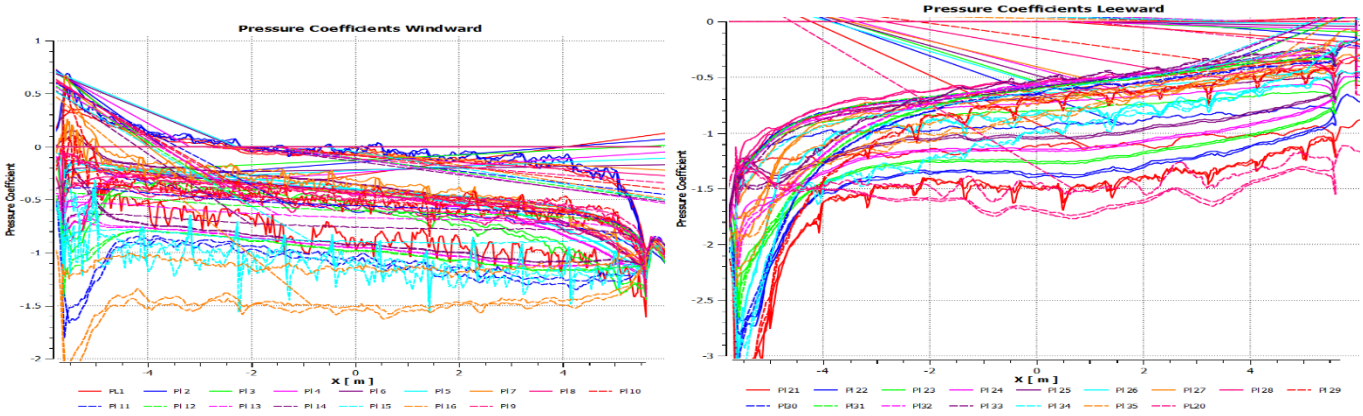


Fig. 5. 145. Pressure coefficients, windward and leeward, slope 27º, leeward Direction 45º

5.4.9. Integration of pressure coefficients on surfaces of roof mounted solar panels in comparison with roof without solar panels, slope 27º, wind directions 90º and 45º, clearance 3”, spacing 8”

The following tables, Table 5.6 to Table 5.10, disclose the integration results of the pressure coefficients along all polylines, where each polyline crosses 3 planes (roof surface, bottom and top of the panels) which are all parallel to the roof surface, making 3 different pressure coefficient polylines where each polyline sits on a different parallel surface. The pressure coefficient polylines located on the roof surface are integrated only under the solar array area, and are neglected on the roof areas beyond the peripheries of the array.

The pressure coefficients on the corresponding roof without solar panels are shown in a column in Tables 5.1 to 5.5, and are used to calculate the ratios of the pressure coefficients on top on the

panels to the pressure coefficients on the roof without solar panels. The coefficients for the roof without panels are not repeated in the Tables 5.6 to 5.10 because they would be identical.

The total pressure coefficients, which are the results of the pressure coefficients for 3 corresponding strips 0.20 m wide, where each strip is located on one of the 3 parallel surfaces, are summed and averaged in a separate column. Then, the average pressure coefficients along each strip / polyline are divided by the pressure coefficients for the roof without solar panels, which gives the ratios of the pressure coefficients of the roof with solar panels to the coefficients of the corresponding roof without solar panels. Those ratios are reported in the last columns of Tables 5.6 and 5.10. Conclusions on presented results are summarized thereafter.

Table 5. 6. Pressure coefficients for roof without solar panels vs. total pressure coefficients, slope 27º, wind direction 90º, windward

Polylines	CP for bottom surface of the panels	Cp for roof under the panels	Cp on top surface of the panels	Cp difference top –bottom surfaces of the panels	Net Cp for the system roof-panels	Ratio of net Cp on system roof-panels / roof without solar panels
Pl1	-0.94	-0.94	-0.38	0.56	-0.38	0.45
Pl2	-0.93	-0.93	-0.37	0.56	-0.37	1.00
Pl3	-0.7	-0.7	-0.39	0.31	-0.39	1.63
Pl4	-0.7	-0.7	-0.42	0.28	-0.42	1.83
Pl5	-0.70	-0.70	-0.45	0.25	-0.45	1.80
Pl6	-0.70	-0.70	-0.49	0.21	-0.49	1.75
Pl7	-0.71	-0.71	-0.51	0.20	-0.51	1.59
Pl8	-0.70	-0.70	-0.55	0.15	-0.55	1.62
P9	-0.54	-0.45	-0.53	0.01	-0.44	1.13
Pl10	-0.50	-0.48	-0.55	-0.05	-0.53	1.23
Pl11	-1.04	-1.01	-0.67	0.37	-0.64	1.33
Pl12	-0.95	-0.95	-0.75	0.20	-0.75	1.15
Pl13	-0.95	-0.95	-0.85	0.10	-0.85	1.15
Pl14	-0.97	-0.97	-0.97	00	-0.97	1.23
Pl15	-1.05	-0.97	-1.15	-0.10	-1.07	1.23
Pl16	-2.10	-2.06	-1.6	0.50	-1.56	1.70

Ave	-0.89	-0.87	-0.66	0.22	-0.65	1.36
STD	0.37	0.36	0.34	0.21	0.32	0.37
COV	-0.41	-0.42	-0.51	0.93	-0.50	0.27

Table 5. 7. Pressure coefficients for roof without solar panels vs. total pressure coefficients, slope 27º, wind direction 90º, leeward

Polylines	CP for bottom surface of the panels	Cp for roof under the panels	Cp on top surface of the panels	Cp difference top –bottom surfaces of the panels	Net Cp for the system roof-panels	Ratio of net Cp on system roof-panels / roof without solar panels
Pl20	-2.99	-2.89	-2.91	0.08	-2.81	1.60
Pl21	-1.13	-1.04	-2.92	-1.79	-2.83	1.65
Pl22	-1.05	-1.05	-2.42	-1.37	-2.42	1.45
Pl23	-1.02	-1.02	-1.84	-0.82	-1.84	1.13
Pl24	-0.99	-0.99	-1.28	-0.29	-1.28	0.80
Pl25	-0.98	-0.98	-0.88	0.10	-0.88	0.56
Pl26	-0.60	-0.60	-0.72	-0.12	-0.72	0.47
Pl27	-0.62	-0.62	-0.63	-0.01	-0.63	0.42
Pl28	-0.56	-0.55	-0.54	0.02	-0.53	0.36
Pl29	-0.60	-0.60	-0.52	0.08	-0.52	0.38
Pl30	-0.57	-0.57	-0.51	0.06	-0.51	0.38
Pl31	-0.57	-0.57	-0.51	0.06	-0.51	0.39
Pl32	-0.59	-0.59	-0.52	0.07	-0.52	0.40
Pl33	-0.56	-0.56	-0.53	0.03	-0.53	0.50
Pl34	-0.74	-0.74	-0.56	0.18	-0.56	0.56
Pl35	-0.73	-0.73	-0.7	0.03	-0.70	0.74
Ave	-0.89	-0.88	-1.12	-0.23	-1.11	0.77
STD	0.60	0.57	0.89	0.58	0.86	0.46
COV	-0.67	-0.65	-0.79	-2.52	-0.77	0.62

Table 5. 8. Pressure coefficients for roof without solar panels vs. total pressure coefficients, slope 27º, wind direction 45º, windward

Polylines	Cp for roof without panels	CP for bottom surface of the panels	Cp for roof under the panels	Cp on top surface of the panels	Cp difference top – bottom surfaces of the panels	Net Cp for the system roof-panels	Ratio of net Cp on system roof-panels / roof without solar panels
Pl1	-0.36	-0.09	-0.10	-0.82	-0.73	-0.83	2.31
Pl2	-0.36	-0.08	-0.09	-0.55	-0.47	-0.56	1.56
Pl3	-0.37	-0.61	-0.64	-0.45	0.16	-0.48	1.30
Pl4	-0.39	-0.52	-0.52	-0.43	0.09	-0.43	1.13
Pl5	-0.42	-0.48	0.48	-0.43	0.05	-0.53	1.33
Pl6	-0.43	-0.43	-0.43	-0.43	00	-0.43	1.02
Pl7	-0.45	-0.40	-0.43	-0.45	-0.05	-0.48	1.12
Pl8	-0.45	-0.58	-0.61	-0.48	0.10	-0.51	1.13
Pl9	-0.47	-0.45	-0.48	-0.51	-0.06	-0.54	1.20
Pl10	-0.49	-0.47	-0.51	-0.51	-0.04	-0.55	1.20
Pl11	-0.51	-1.09	-1.12	-0.55	0.54	-0.58	1.21
Pl12	-0.59	-1.02	-1.02	-0.52	0.50	-0.52	1.06
Pl13	-0.67	-0.95	-0.95	-0.59	0.36	-0.59	1.16
Pl14	-0.73	-0.92	0.92	-0.67	0.25	-1.17	2.05
Pl15	-0.83	-1.06	-1.10	-0.84	0.22	-0.88	1.35
Pl16	-0.90	-1.50	-1.53	-1.11	0.39	-1.14	1.65
Ave	-0.53	-0.67	-0.51	-0.58	0.08	-0.64	1.36
STD	0.17	0.39	0.61	0.19	0.33	0.24	0.36
COV	-0.32	-0.58	-1.21	-0.33	4.03	-0.37	0.27

Table 5. 9. Pressure coefficients for roof without solar panels vs. total pressure coefficients, slope 27º, wind direction 45º, leeward

Polylines	Cp for roof without panels	CP for bottom surface of the panels	Cp for roof under the panels	Cp on top surface of the panels	Cp difference top –bottom surfaces of the panels	Net Cp for the system roof-panels	Ratio of net Cp on system roof-panels / roof without solar panels
Pl20	-1.33	-1.55	-1.56	-1.45	0.10	-1.46	1.10
Pl21	-1.29	-1.51	-1.52	-1.15	0.36	-1.16	0.90
Pl22	-1.20	-1.42	-1.43	-0.93	0.49	-0.94	0.78
Pl23	-1.12	-1.33	-1.34	-0.83	0.50	-0.84	0.75
Pl24	-1.05	-1.24	-1.35	-0.76	0.48	-0.87	0.83
Pl25	-0.98	-1.20	-1.21	-0.73	0.47	-0.74	0.76

Pl26	-0.93	-0.92	-0.93	-0.69	0.23	-0.7	0.75
Pl27	-0.89	-0.74	-0.76	-0.69	0.05	-0.71	0.80
Pl28	-0.85	-0.61	-0.61	-0.69	-0.08	-0.69	0.81
Pl29	-0.83	-0.92	-0.93	-0.65	0.27	-0.66	0.80
Pl30	-0.80	-0.85	-0.85	-0.64	0.21	-0.64	0.80
Pl31	-0.75	-0.82	-0.82	-0.63	0.19	-0.63	0.84
Pl32	-0.71	-0.73	-0.73	-0.62	0.11	-0.62	0.87
Pl33	-0.68	-0.69	-0.69	-0.64	0.05	-0.64	0.94
Pl34	-0.66	-1.05	-1.06	-0.68	0.37	-0.69	1.05
Pl35	-0.65	-0.89	-0.90	-0.79	0.10	-0.80	1.23
Ave	-0.92	-1.03	-1.04	-0.79	0.33	-0.80	0.88
STD	0.58	0.31	0.31	0.22	0.34	0.23	0.14
COV	-0.77	-0.30	-0.30	-0.28	1.04	-0.28	0.16

Table 5. 10. Pressure coefficients for roof without solar panels vs. total pressure coefficients, slope 27º, wind direction 0º

Polylines	Cp for roof without panels	CP for bottom surface of the panels	Cp for roof under the panels	Cp on top surface of the panels	Cp difference top –bottom surfaces of the panels	Net Cp for the system roof-panels	Ratio of net Cp on system roof-panels / roof without solar panels
Pl1	-0.33	-0.32	-0.35	-0.36	0.04	-0.31	0.94
Pl2	-0.33	-0.32	-0.36	-0.37	0.05	-0.31	0.94
Pl3	-0.33	-0.32	-0.42	-0.42	0.10	-0.32	0.97
Pl4	-0.36	-0.32	-0.42	-0.42	0.10	-0.32	0.89
Pl5	-0.36	-0.32	-0.42	-0.42	0.10	-0.32	0.89
Pl6	-0.36	-0.32	-0.42	-0.42	0.10	-0.32	0.89
Pl7	-0.36	-0.32	-0.42	-0.42	0.10	-0.32	0.89
Pl8	-0.35	-0.32	-0.38	-0.39	0.07	-0.31	0.89
Pl9	-0.35	-0.32	-0.38	-0.39	0.07	-0.31	0.89
Pl10	-0.35	-0.32	-0.39	-0.4	0.08	-0.31	0.89
Pl11	-0.35	-0.33	-0.42	-0.42	0.09	-0.33	0.94
Pl12	-0.35	-0.33	-0.42	-0.42	0.09	-0.33	0.94
Pl13	-0.34	-0.33	-0.42	-0.42	0.09	-0.33	0.97
Pl14	-0.34	-0.33	-0.42	-0.42	0.09	-0.33	0.97
Pl15	-0.34	-0.33	-0.42	-0.42	0.09	-0.33	0.97
Pl16	-0.34	-0.3	-0.33	-0.33	0.03	-0.3	0.88

Ave	-0.35	-0.32	-0.40	-0.40	0.08	-0.32	0.92
STD	0.09	0.01	0.03	0.03	0.02	0.01	0.04
COV	-0.26	-0.02	-0.08	-0.07	0.28	-0.03	0.04

5.4.10. CONCLUSIONS

- The installed solar panels on roof with spacing/clearances 2"/ 3", 2"/10", and 8"/3", result in the redistribution of pressure on both sides of the roof with solar panels in comparison with the roof without solar panels. In this redistribution, the suction on the windward side increased while decreasing on the leeward side of the roof with solar panels. The redistribution of pressure results in reduction of the largest suction coefficients (wind direction 90º) on the leeward sides to 77%, 79% and 80% correspond to 8"/3", 2"/3", and 2"/10" spacing /clearance respectively in comparison with suction of roof without panel, (Tables 5.7, 4.7, and 5.2).

  Different for the leeward, ,Installing solar panels on roof with spacing,/clearances 2"/ 3", 2"/10", and 8"/3", increased the suction (for wind direction 90º) by 27%, 84% and 12% corresponding to 8"/3", 2"/3", and 2"/10" spacing /clearance respectively in comparison with suction of roof without panels, (Tables 5.6, 4.6, and 5.1).

- On the other hand, for wind direction 45º, the installed solar panels on roof with spacing,/clearances 2"/ 3", 2"/10", and 8"/3", the solar panels mounted on the gable roof, result that the suction on the windward side for wind direction 90º, increased by 21%, 26% and 17% correspond to 8"/3", 2"/3", and 2"/10" spacing /clearance respectively in comparison with suction of roof without panels, (Tables 5.6, 4.6, and 5.1).

- Increasing the spacing from 2" to 8" slightly reduces the largest total suction coefficients on leeward of solar panels, for wind direction 90º, while increased slightly the total suction coefficients on same side of the roof when wind direction changes to 45º.

- For all the 3 configurations of spacing / clearance stated herein, (8”/3”, 2”/3” and 2”/10”) the pressure on the roof under the panels is almost equal to the pressure on the bottom surface of the panels. As a result, the pressure coefficients for the roof with solar panels can be approximated by the pressure coefficients of the top of the solar panels. The error in this approximation is nearly 1% for wind direction 90º and leeward in wind direction 45º while increased to 6 % for windward in wind direction 45º, Tables (4.6-4.10).

- On the other hand, all the 3 configurations of spacing / clearance stated herein cause a redistribution of the pressure coefficients, towards balancing of pressure coefficients on windward and leeward, where those coefficients become closer than on the roof without solar panels. Consequently, the roof structure with solar panels is subject to much less horizontal pressure as a summation of the horizontal forces on both sides, windward and leeward. However, when spacing increased from 2” to 8”, the corresponding horizontal forces increase for wind direction 90º, while remain constant for wind direction 45º.

- When the spacing increased from 2” to 8”, the net pressure coefficients on the solar panels, for wind direction 90º is directed toward the roof surface for both spacings, while the net pressure coefficients changed from pressure to suction on the leeward side.

- However, when spacing increased from 2” to 8”, the net pressure on the solar panels, for wind direction 45º, increased considerably on the leeward, while remained nearly constant on the windward side.

CHAPTER 6

Discussion and results

6.1. Summary of the research

A comprehensive database of pressure coefficients on roof mounted solar panels was developed under the current research project, with different installation parameters, subjected to various wind speeds. Wind effects on solar panels mounted on gable roofs inclined at 15º, 27º and 35º were numerically investigated by using CFD simulations, with the panels arranged at 2" and 8" spacing between solar panel rows, and clearances between the solar panels and roof surface of 3" and 10". Three different wind directions 0º, 45º and 90º with roof ridges and two wind speeds, 10 m/s and 40 m/s, were analysed for each configuration.

A total of 97 simulation cases, including 36 cases of roof-mounted solar panels, subjected to 10 m/s wind speed, which were compared to 9 cases of sloped roofs without solar panels were conducted. In addition, 18 cases of roof-mounted solar panels subjected to 40 m/s wind speed, which were compared to 9 cases of roof without solar panels, were performed. For carrying out a comprehensive results comparison, 25 cases were conducted simulating existing full-scale and wind tunnel experiments reported in the literature.

6.2. Contribution and novelty of the current research

To the knowledge of the author, no studies have explored in detail the effects of wind on gable-roof-mounted solar panels. The following gaps in the literature were identified:

- Investigation of variation of wind-induced pressure coefficients on gable roof surfaces versus the bottom and/or top surfaces of solar panels, due to changes in roof slopes and wind direction, and how these compare with the pressure coefficients on gable roofs without solar panels.

- Investigation of variation of wind pressure coefficients on the following three surfaces: roof surface under the solar panels and on the bottom and top surfaces of solar panels, due to changes in the spacing between the solar panel arrays and/or clearance between the roof surface and the panels, and how these compare with pressure coefficients of roofs without solar panels.
-

The current thesis aims at filling these gaps identified in previous research and intends to clarify the wind effects on the three surfaces: i.e., the roof surface underneath the solar panels and the top and bottom surfaces of the panels, for different wind directions, roof slopes, spacing between arrays of panels, and clearance between the roof and the bottom surface of the solar panels.

Moreover, this dissertation compares the pressure coefficients recorded for the roof-panels system consisting in the three mentioned surfaces, with those obtained for roofs without any solar panels mounted. To investigate the effects of wind on the three surfaces due to changes in wind direction, roof slope, clearance or/and spacing between panel arrays, this study analyzed 45 cases, including 36 cases for gable-roof-mounted solar panels and 9 cases for corresponding roofs without solar panels, all subjected to 10 m/s wind speed. Part of these analyses were repeated partially for a wind speed of 40 m/s, to verify any changes in pressure coefficients due to change in wind speed. The wind-induced pressure coefficients for residential roofs have been investigated for lower wind speeds (around 10 m/s) which are induce a steady effect at roof level of low rise residential building (Oh, 2014); however the current research investigated higher wind speeds of 40 m/s which are applicable for windstorm prone regions.

The analyses conducted using 10 m/s wind speed investigated the effects of three roof slopes, 15º, 27º and 35º, and three wind directions, 0º, 45º and 90 º, on panels spaced 2" apart and with 3" clearance from the roof. Based on the pressure coefficients obtained for all the investigated cases, the roof slopes and wind directions for which the wind had the worse effect on the pressure induced on the roof-panels system, were determined. The effects of clearance and spacing were investigated for 2" and 8" spacing and 3" and 10" clearance for the combination of critical roof slopes and wind directions cases; the same cases were repeated for 40 m/s for verification of the changes in pressure coefficients.

The investigations encompass monitoring pressure coefficients and velocity changes on all surfaces (roof, bottom and top of the panels) and inside the cavity between the panels and the roof. In addition, integrations of pressure coefficients on all surfaces were performed using 20 polylines on each of the surfaces, and the average pressure coefficients on the entire surface of the panels were calculated. Thereafter, the net pressure coefficients on the roof – panels system were calculated.

6.3. Correlation between pressure coefficients on the roof, panel surfaces, and roof without solar panels

The correlation between the pressure coefficients on two different surfaces reflects the extent of pressure equalization between those surfaces. The equation used for the correlation coefficient is:

$$Correl\ (X,Y) = \frac{\sum(x-\bar{x})(y-\bar{y})\sum(x-\bar{x})(y-\bar{y})}{\sqrt{\sum(x-\bar{x})\sum(x-\bar{x})^2\sum(y-\bar{y})\sum(y-\bar{y})^2}}$$

where $\bar{x}$ and $\bar{y}$ are the sample mean or average for array 1 and array 2, respectively.

6.3.1. Correlation between pressure coefficients on top and bottom surfaces of roof tiles/pavers

It is noteworthy to mention that no studies of correlations between solar panels surfaces mounted on flat roofs were reported in the available literature (Kopp et al., 2015; Stenabaugh, 2015). As such, there are no existing data in the literature to compare with the correlation values and graphs obtained in this dissertation. Therefore, a brief discussion of the wind flow around pavers is noted here since maintain similar properties of double-layer roof system.

In the current study the mean values of pressure coefficients were calculated on each polyline and for each of the 3 surfaces of the roof with panels and for roof surface without solar panels (nearly ten thousand points on each surface). Correlations between all the means were determined so that one point, in the correlation graphs below, represents correlation of the means of 2 surface in one

case (Fig. 6.3 and 6.9). Habtea et al. (2017) studied the effects of wind on the ridge, hip and perimeter roof tiles installed with a cavity underneath. The wind effects on tiles E1 and E2 installed on the long side of the half-cut hip roof (which resemble the gable roof) are shown in Figure 6.1. In Fig, 6.1, wind direction 315º corresponds to 45º in the current study, and wind direction 270º and 360º correspond to 90º and 0º, respectively.

The correlation charts are derived in Fig. 6.2, and tabulated in Table 6.1, based on the data presented in Fig. 6.1. The results show that there is high correlation in wind directions 270º and 315º while there is no correlation in the wind directions 0º. This trend is derived directly from full-scale experimental results, and the evolution of the correlation between the upper surface and the cavity pressures resemble the correlation between the corresponding surfaces on top and bottom of the solar panels in this thesis, with minor discrepancies.

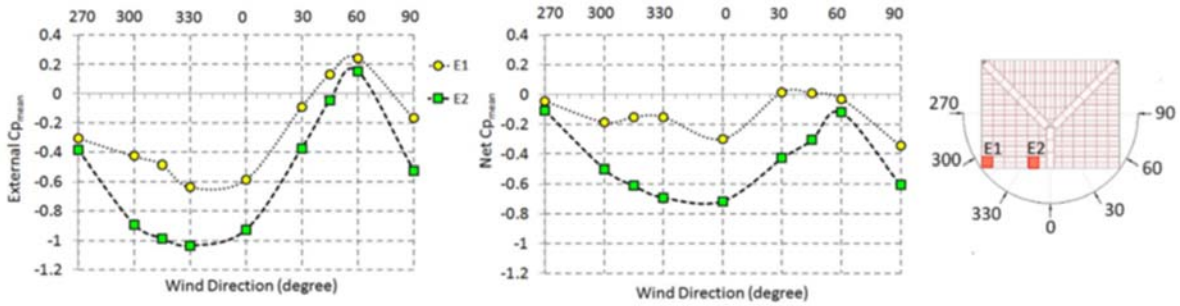


Fig.6. 1. External and net C_{pmean} on the tiles on the long side of a half-cut hip roof (Habte et al., 2017)

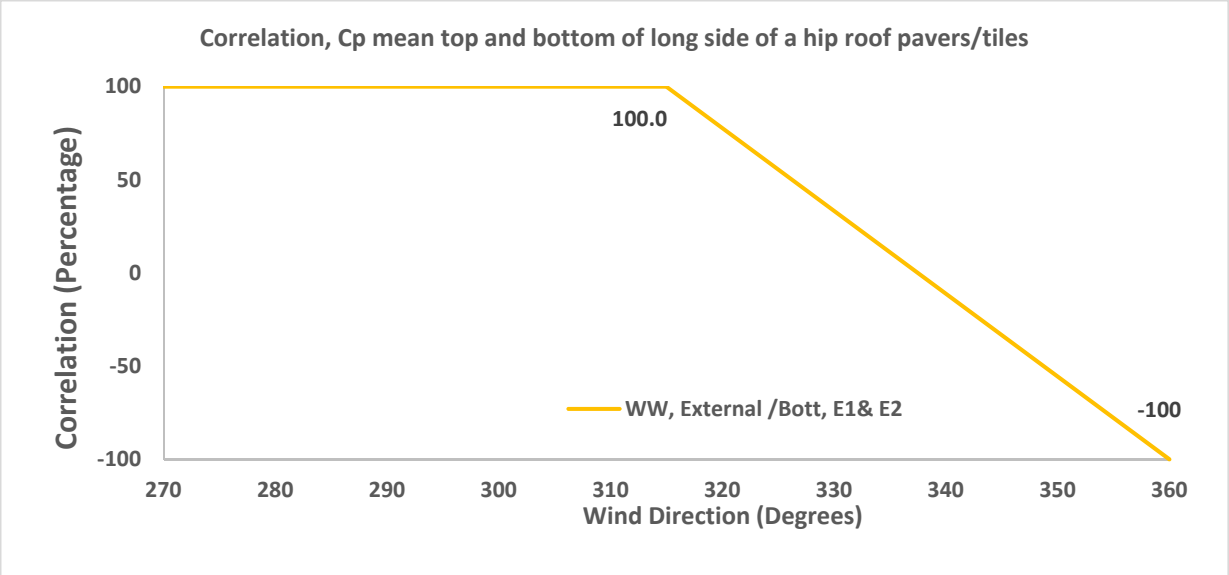


Fig.6. 2. Correlation between Cp on top surface of the tiles and in the cavity Cp under tiles of a half-cut hip roof, for roof slope 18.5º (Drawn based on Habte et al., 2017)

The derived values from Fig. 6.1. of Habte et al. (2017) are based on the equation:

$$external\ Cp - Bottom\ Cp = Net\ pressure\ on\ tile$$

Table 6. 1. Derived Cp values from Fig. 1.6 of Habte et al. (2017)

Wind speed direction (degrees)	Half-cut hip tile's designation	Top surface Cp	Net pressure Cp	Cavity Cp
270	E1	-0.32	-0.05	-0.27
270	E2	-0.39	-0.1	-0.29
315	E1	-0.48	-0.17	-0.31
315	E2	-0.98	-0.6	-0.38
360	E1	-0.6	-0.31	-0.29
360	E2	-0.94	-0.72	-0.22

Figure 6.2 shows that the correlation between the top and bottom surfaces of the tiles is extremely high for wind direction 135º (corresponding to 45º in the current study). However, there is no correlation in both wind directions 90º and 180º which correspond to 90º and 0º for T1 and T2, while correspond to 0º and 90º for T3 and T4, Fig.6.2, in the current study.

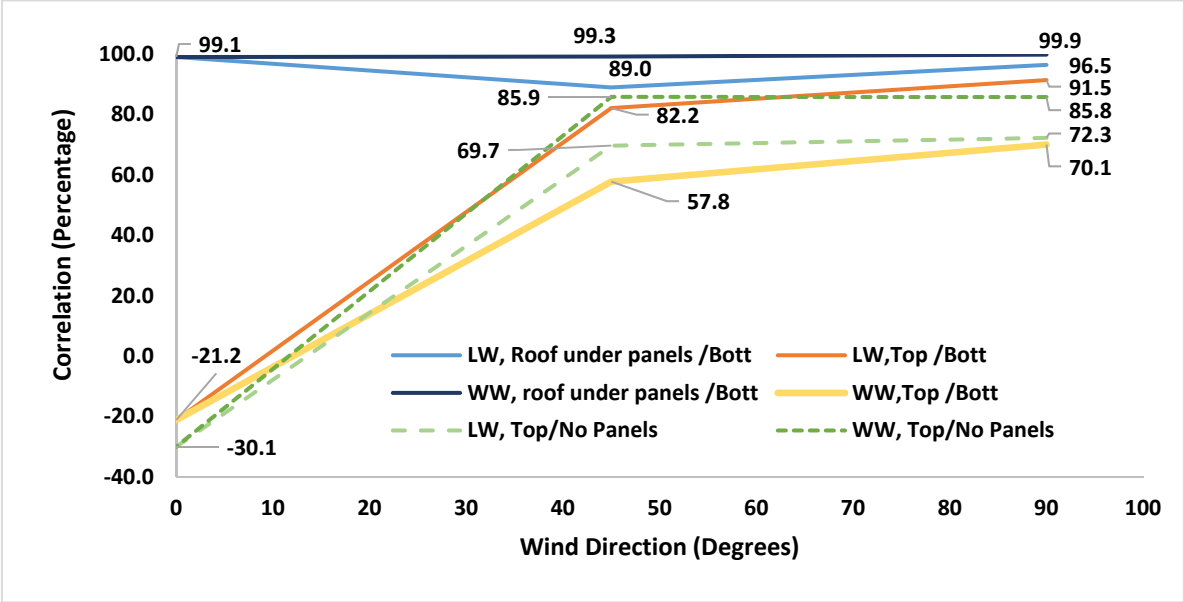
6.3.2. Correlations between pressure coefficients on top, bottom of the panels, roof surface, 2" spacing, 3" clearance, 35º roof slope and roof without solar panels

The correlations between the pressure coefficients on three pairs of surfaces, for the cases investigated in the current study, are presented in Figures 6.3, for roof slope 35º, spacing 2" and clearance 3". The three pairs of surfaces considered for determining the pressure coefficients correlation were:

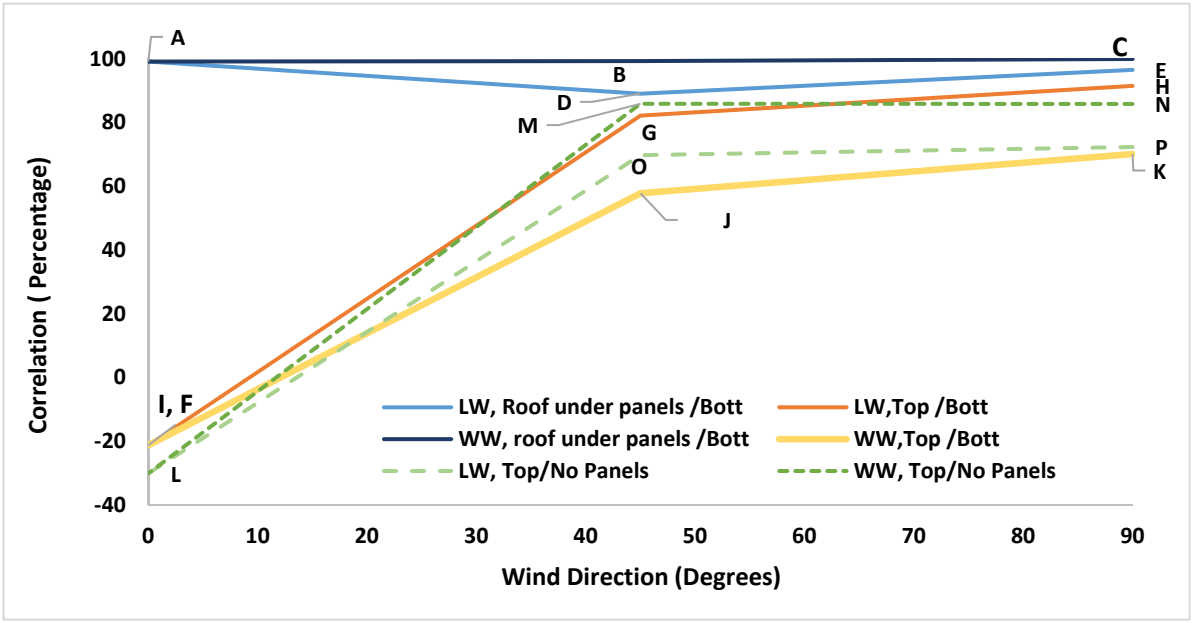
- Bottom of the panels and roof surface
- Bottom of the panels and top of the panels
- Top of the panels and the corresponding roof without solar panels

The first pair of surfaces, which are the surfaces of the cavity, depict the highest correlations, above 0.99, for wind directions 45º and 90º as it can be seen in Fig. 6.3.a). Similarly, for the windward side, the correlation is very high 0.99 at 0º, decreases slightly to 0.89 for 45º, and increases thereafter again to 0.97 for 90º wind direction (Fig. 6.3 a).

The top and bottom of the panels show much smaller correlations, where the highest correlation for the leeward surfaces of the panels is 0.92 for the 90º wind direction. This value decreases to 0.82 for 45º, and then drops suddenly to -0.21 for 0º. The correlation for the windward side of the roof is lower than for the leeward side, for all wind directions, where the highest correlation is 0.7 for the 90º wind direction, then it reduces gradually to 0.58 for 45º and then decreases sharply to -0.21 for 0º (Fig 6.3a).



(a)



(b)

Fig.6. 3. Correlation between pressure coefficients for the three pairs of surfaces, for leeward and windward sides, S2"C 3" and roof slope 35º a) Correlation values b) Location of correlation coefficients

The pair of surfaces depicting the top of the panels and roof without solar panels show the highest correlation between surfaces. On the windward side the correlation is 0.86 for the 90º wind

direction. The value remains constant for the 45º wind direction but drops sharply to -0.30 for the 0º wind direction. The correlations between the leeward pairs of surfaces are less than those for the corresponding windward surfaces for all wind directions with 0.72 being the highest correlation, for the 90º wind direction, reducing slightly to 0.70 for 45º and decreasing sharply thereafter to -0.30 for the 0º wind direction. For an easier reference to the correlation values above, letters were assigned to the location each correlation coefficient was determined (Fig. 6.3. b)), and these were used for clarifying the details presented in the figures below. Also, the pressure coefficients for the four different surfaces, which are used in the calculation of the correlation coefficient, were presented in Tables 4.1 to 4.5., in the Chapter 4.

Every data point in Fig 6.3 represents pressure coefficients series for a given pair of the four surfaces: top and bottom surfaces of the panels, roof surface under panels, and roof surface without solar panels installed. Detailed graphic representations of each series are shown in Figures 6.4 to 6.8, which illustrate the distributions of Cp values for each correlated pair of surfaces as Cp of one surface is a function of Cp on the other surface of the pair.

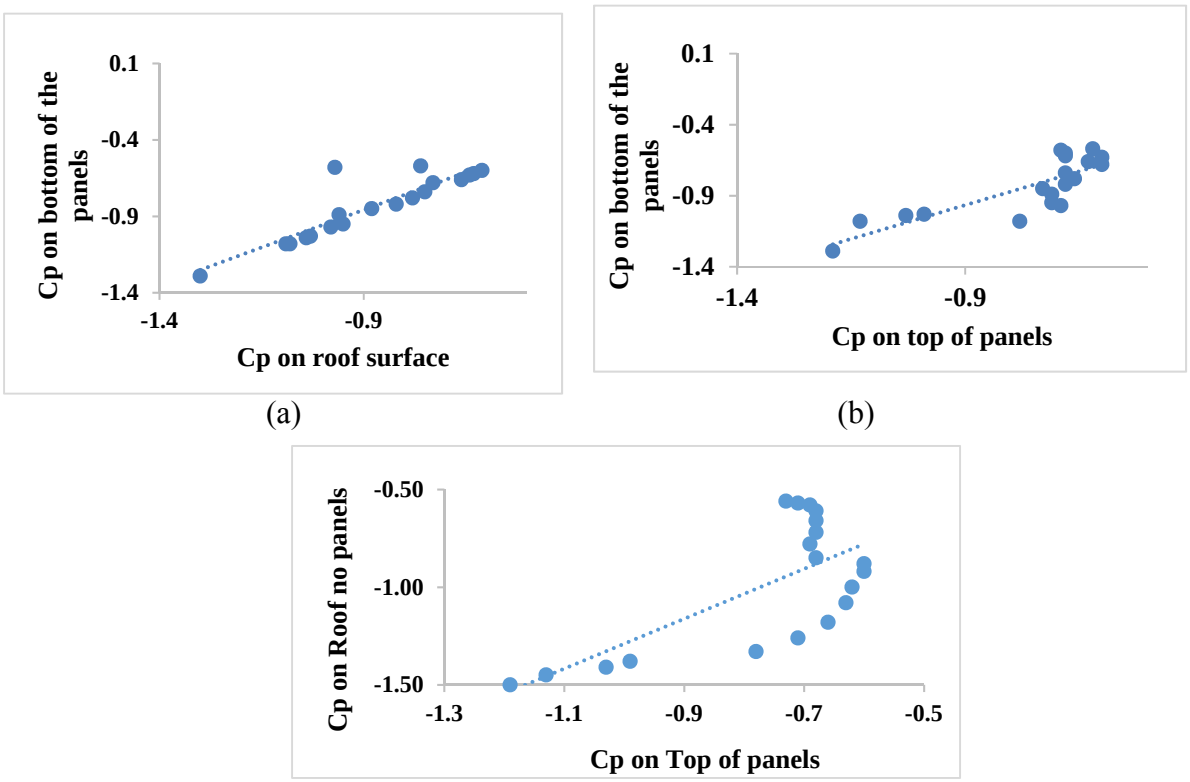


Fig.6. 4. Cp as a function of one surface Cp of the other, 2" spacing, 3" clearance, slope 35º, wind direction 45º, leeward side a) Bottom of panels Vs roof surface under the panels, b) Bottom of panels Vs top of the panels c) Roof without panels Vs top of the panels

As shown in Fig. 6.4 a) and b), the Cp data points on the bottom surface of the panels and on the roof surface, for the leeward side of the roof, are distributed very close to a straight line, which is illustrated by a very high correlation factor, 0.96 (Fig. 6.3 a), while the Cp points of the top and bottom of the panels, on the same leeward side, are distributed farther from the straight line, with a correlation factor of 0.82 (Fig. 6.3 a).

Fig. 6.4 c) shows the Cp points of top surface of the panels and on the roof surface without solar panels installed, for the leeward side of the roof. The points are distributed much farther from the straight line than the other two surface pairs represented in Fig. 6.4 a) and b). This is reflected in a much lower correlation factor of 0.70 (Fig. 6.3a). A high correlation coefficient between the

pressures recorded on two surfaces represents relatively small differences or higher pressure equalization and means that one depends on the other.

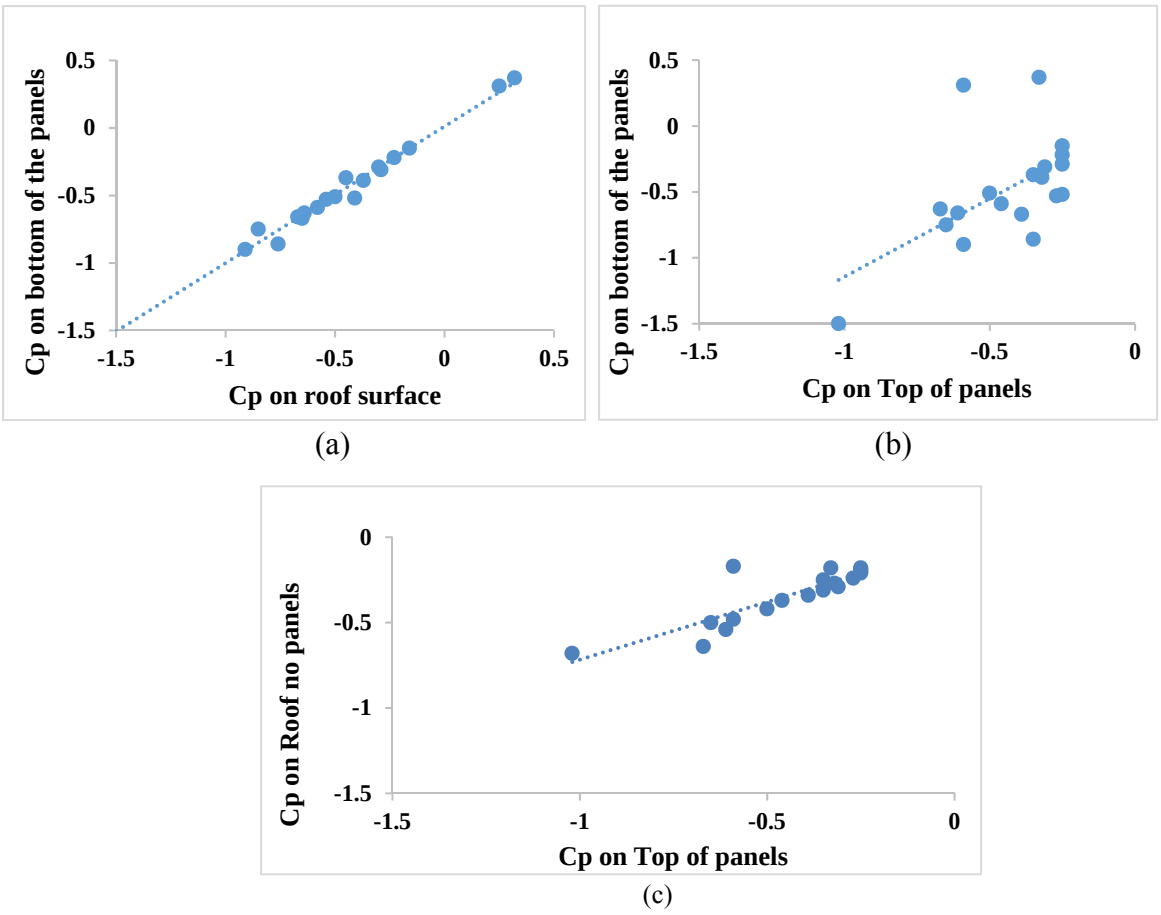


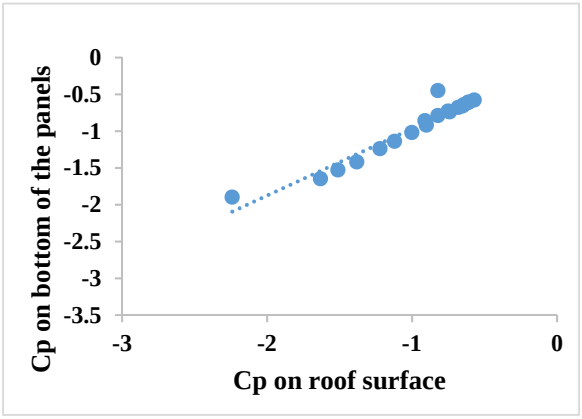
Fig.6. 5. Cp as a function of one surface Cp of the other, 2" spacing, 3" clearance, slope 35º, wind direction 45º, windward a) Point B, Bottom of panels Vs roof surface under the panels b) Point I, Bottom Vs top of the panels c) Point M, Roof without panels Vs top of the panels

This dependence is clearer in the cavity surfaces, Fig. 6.4.a, where higher pressure in the cavities means higher pressures on both cavity surfaces with some small differences because of spacing effects.

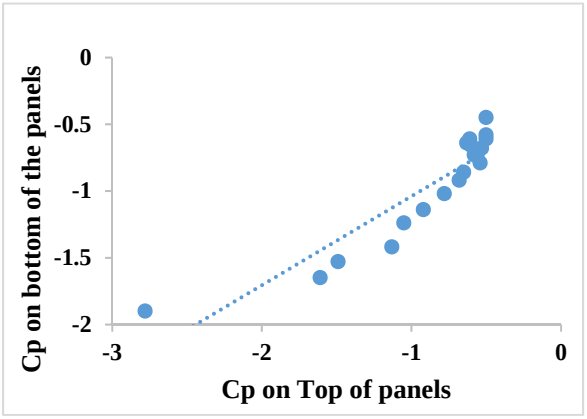
In Figure 6.5 a), the Cp points for the cavity surfaces (bottom of panels and roof surfaces) on the windward side of the roof are distributed close to a straight line corresponding to a 0.99 correlation factor (Fig. 6.3a). However, distribution of the Cp points of the top and bottom surfaces of the panel on the windward side is more scattered (0.58 correlation, Fig. 6.3a), as shown in Fig. 6.5 b).

Fig. 6.5 c) shows that the Cp points on the top surface of the panels and on the roof without solar panels, for the windward side of the roof, are slightly scattered (0.86 correlation factor, Fig. 6.3a).

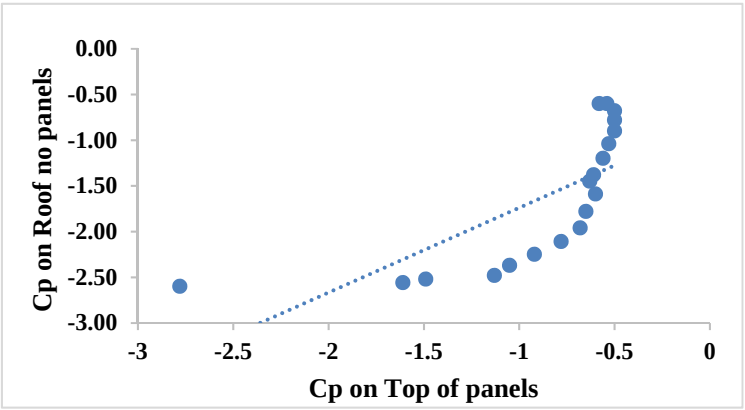
For the 90º wind direction, Fig. 6.6 a) illustrates the Cp points on the bottom surface of the panels and on the roof surface under the panels, on the leeward side, which are distributed very close to a straight line (correlation 0.97, Fig. 6.3a), while the Cp points located on the top and bottom surfaces of the panels (Fig. 6.6 b), on the same leeward side are more scattered (correlation 0.92 (Fig. 6.3a)). A smaller correlation factor is 0.70 (Fig. 6.3a) was noticed in Fig. 6.6 c), for the distribution of the Cp points on the top surface of the panels and roof surface without solar panels, on the leeward side of the roof. The Cp points are more scattered when compared with the other two pairs of surfaces represented in Figs. 6.6 a) and b).



(a)



(b)



(C)

Fig.6.6. Cp as a function of one surface Cp of the other, 2" spacing, 3" clearance, slope 35º, wind direction 90º, leeward side a) Point E, Bottom Vs Roof surface under the panels b) Point H, Bottom Vs Top of the panels c) Point P, Roof without panels Vs Top of the panels

Figure 6.7 a) represents the distribution of Cp points on the bottom surface of the panels and the roof surface on the windward side of the roof, which indicates a very high correlation factor (0.99). This might be a result of identical pressures at the bottom of the panels and the roof surfaces. However, the distribution of Cp points on the top and bottom of the panel surfaces on the windward side is more scattered (0.70 correlation, Fig. 6.3a), as shown in the second graph of Fig. 6.7 b). Fig. 6.7 c) shows the distribution of Cp points of the top of the panels and roof without solar panels on the windward side of the roof. The last two series of points are very close to a straight line, which indicates a high correlation factor, 0.86 (Fig. 6.3a). The last correlation factor infers less scatter than the points of the top and bottom of the panels, but more scatter than for the pressure in the cavity.

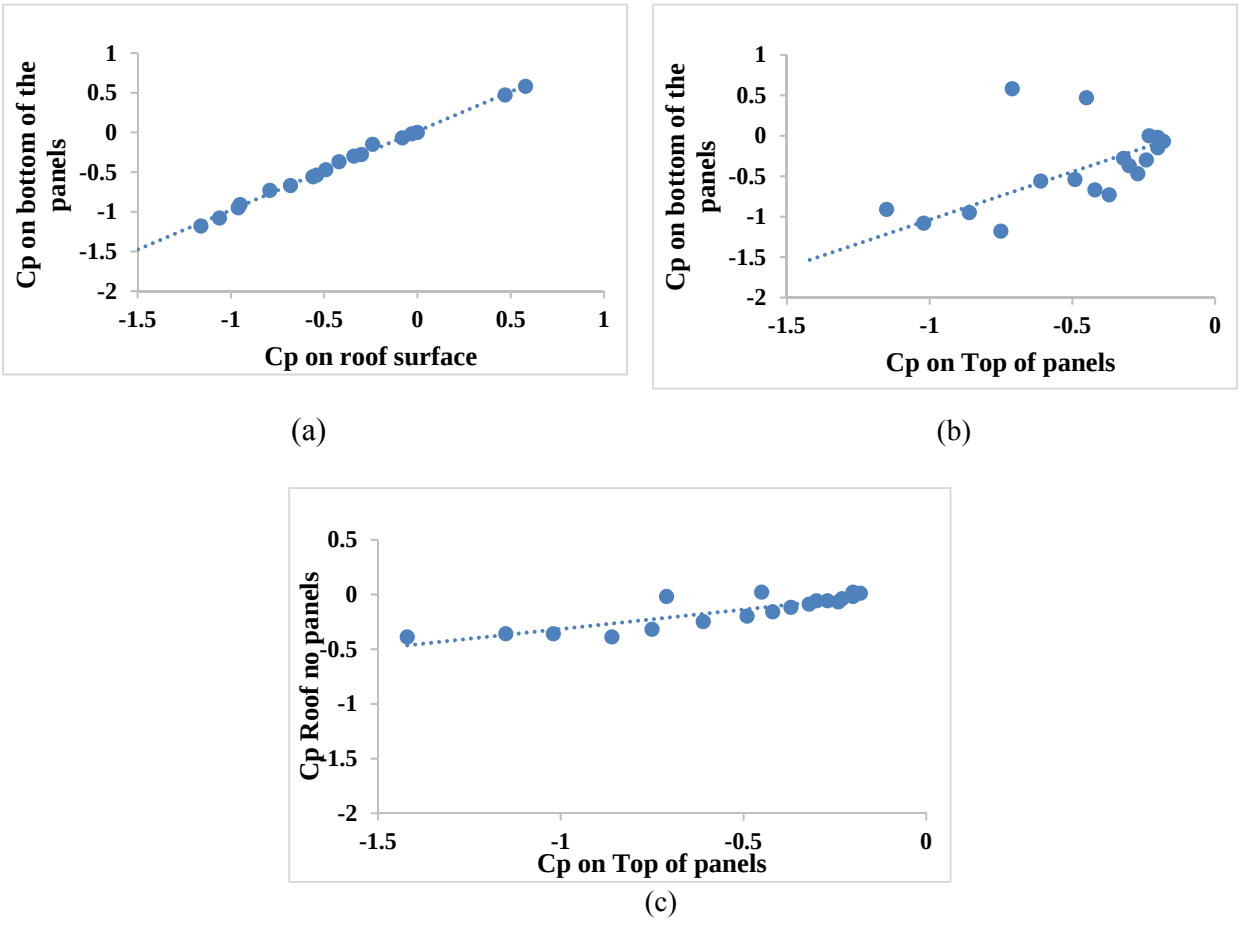
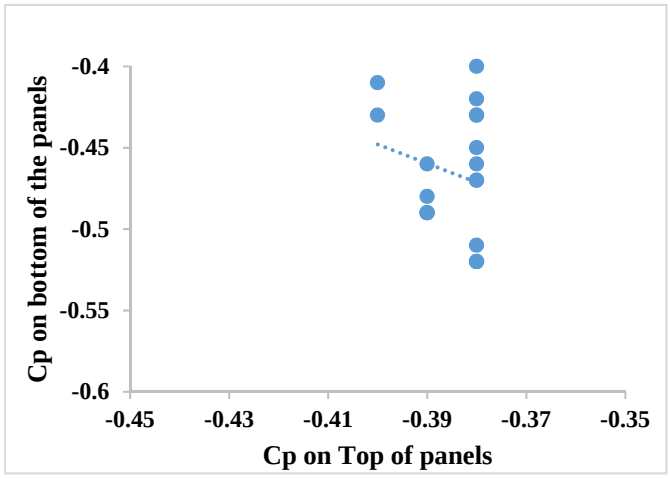
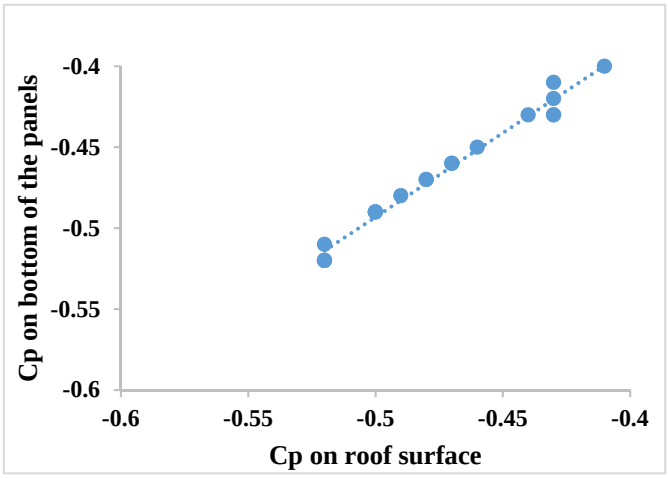


Fig.6. 7. Cp as a function of one surface Cp of the other, 2" spacing, 3" clearance, slope 35º, wind direction 90º, windward a) Point C, Bottom of panels Vs roof surface under the panels b) Point K, bottom Vs top of the panels c) Point N, Roof without panels Vs top of the panels

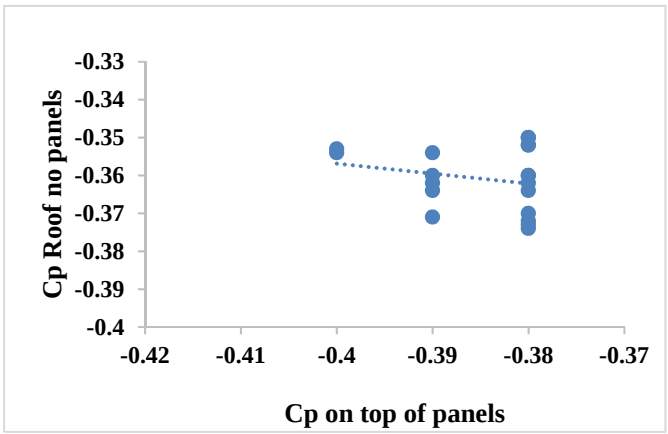
The distribution of Cp data for the bottom of the panels and roof surfaces on the windward side of the roof, represented in Figure 6.8 b) for the 0º wind direction is very close to a straight line with a very high correlation factor of 0.99 (Fig. 6.3a). In contrast, the distribution of Cp points on the top and bottom of the panel surfaces on the windward side is quite scattered, or negatively related (-0.21 correlation Fig. 6.3a), as shown in Fig. 6.8 a). Determining negative correlation factors means that there are no common proportional relationship between the two variables. Similarly, Fig. 6.8 c), shows a very scattered distribution (-0.30 correlation, Fig. 6.3a) of the Cp points of the top of the panels and the roof without solar panels surface.



(a)



(b)

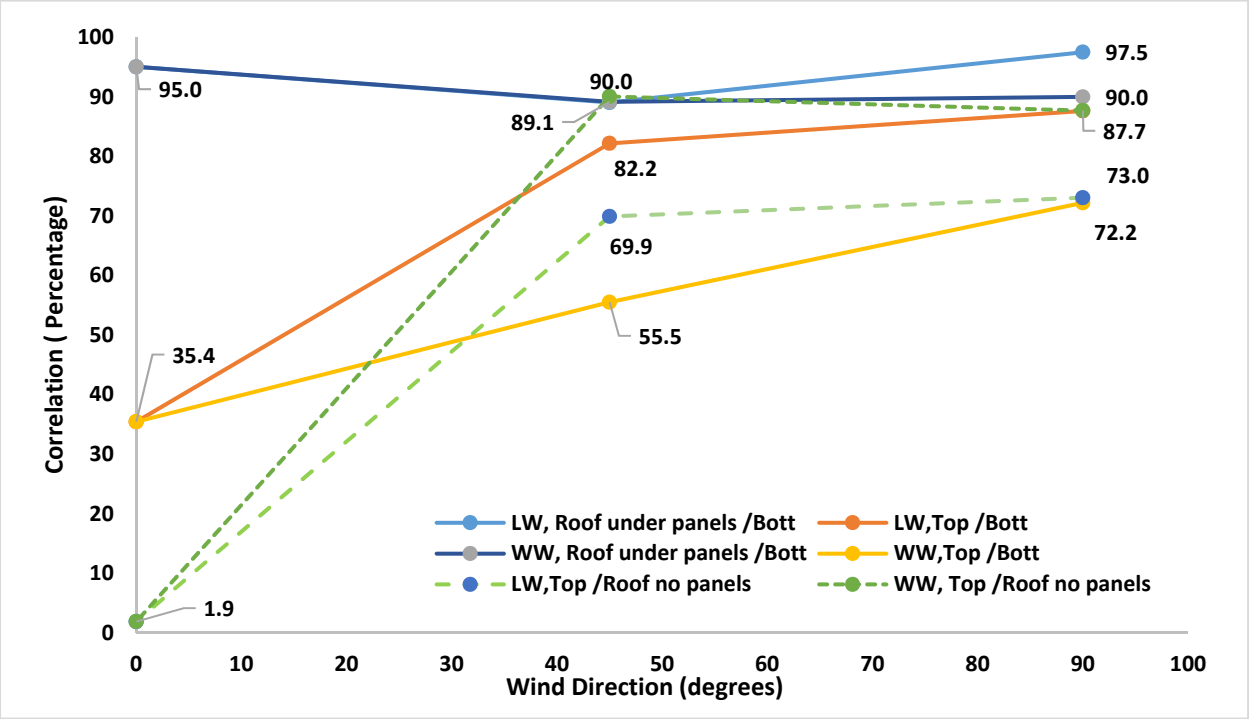


(c)

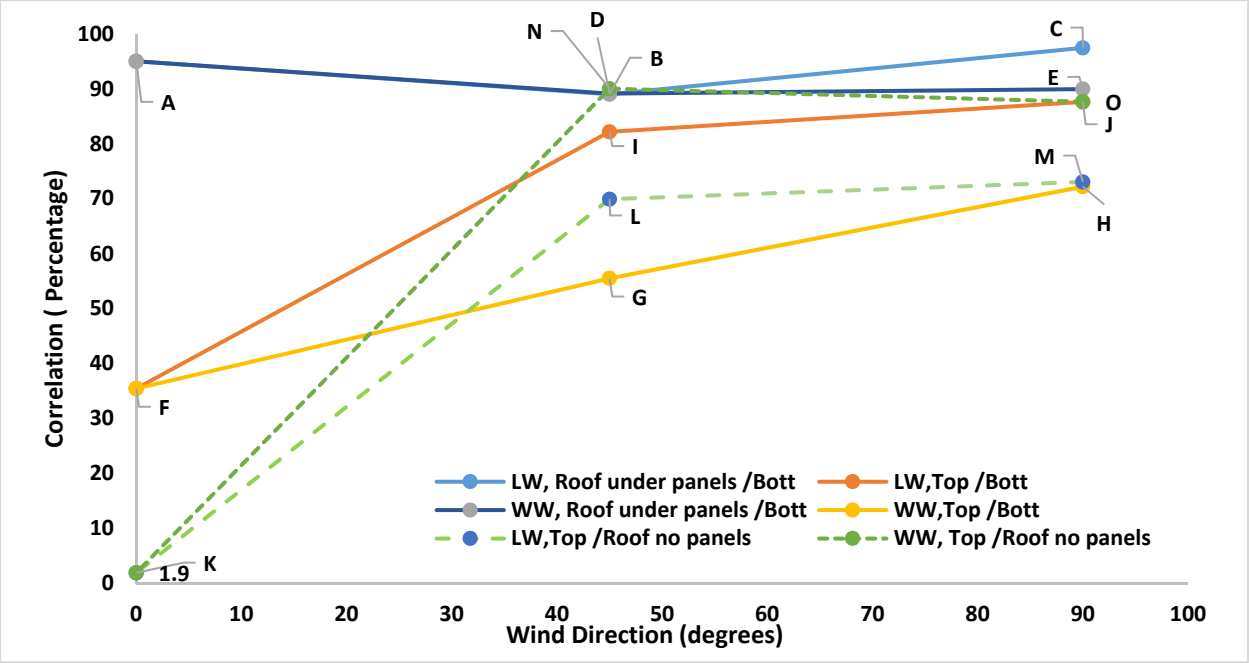
Fig.6. 8. Cp as a function of one surface Cp of the other, 2" spacing, 3" clearance, slope 35º, wind direction 0º a) Point F, bottom Vs top of the panels, b) Point A, bottom Vs roof surface under the panels, c) Point L, Roof without panels Vs top of the panels.

6.3.3. Correlations between pressure coefficients on top, bottom of the panels and roof surface, 2” spacing, 10” clearance, 35º roof slope and roof without solar panels

Figure 6.9 below presents the correlations of the top and bottom of panels, top of panels and roof without panels and the bottom of the panels and roof under the panels (cavity). The surfaces of cavity, depict highest correlations, for wind directions 0º and 90º (0.95 and 97.5, respectively), while they have slightly less correlation, 0.89 than top of panels and roof without panels on windward, 0.90, for wind direction 45º, Fig. 6.9.a. Similar trends are noticed for the other surfaces, with the 2” spacing , 3” clearance, for wind directions 45º and 90º. However, for wind direction 0º, the other 2 pairs show higher correlations for 2” spacing and 10” clearance than the 2” spacing and 10” clearance.



(a)



(b)

Fig.6. 9. Correlation between pressure coefficients of the surfaces, 2" spacing, 10" clearance, slope 35º , a) Correlation values b) Location of correlation coefficients

Detailed pressure coefficients of the four different surfaces, which are used in the calculation of the correlation coefficient, are presented in Table C1, C3, C5, C7 and C9. The detailed presentation of each series are shown in Appendix G, where the Figures illustrate the distributions of Cp values for each correlated surface of a pair as a function of the other surface Cp of the same pair.

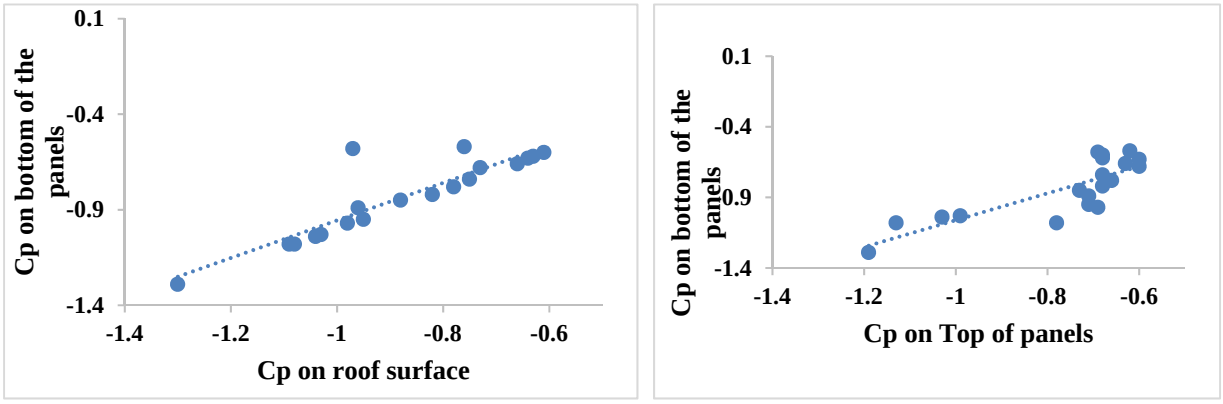
Table 6. 2. Cp on top and bottom surfaces of solar panels, and on the roof surface under the panels, for clearance 10", spacing 2"

Leeward 90º wind direction				Windward 90º wind direction			
Polylines	Cp Top of panels	Cp roof under panels	Cp Bottom of panels	Polylines	Cp Top of panels	Cp roof under panels	Cp Bottom of panels
Pl17	-1.6	-2.68	-3.11	Pl1A	-0.1	-0.15	-0.33
Pl18	-2.29	-2.60	-3.04	Pl2	-0.08	-0.27	-0.02
Pl19	-1.23	-2.36	-2.49	Pl3	-0.1	-1.06	-0.97
Pl20	-0.98	-2.24	-2.29	Pl4	-0.12	-0.82	-0.52
Pl21	-0.88	-1.93	-2.22	Pl5	-0.15	-0.47	-0.24
Pl22	-0.78	-1.65	-1.82	Pl6	-0.23	-0.3	0.11
Pl23	-0.71	-1.52	-1.54	Pl7	-0.55	-0.73	-1.24
Pl24	-0.69	-1.62	-1.76	Pl8	-0.14	-1.01	-0.97
Pl25	-0.85	-1.54	-1.74	Pl9	-0.26	-0.92	-0.76
Pl26	-0.64	-1.56	-1.52	Pl10	-0.34	-1.15	-1.07
Pl27	-0.48	-1.38	-1.56	Pl11	-0.42	-1.00	-0.79
Pl28	-0.48	-1.01	-1.36	Pl12	-0.52	-0.83	-0.64
Pl29	-0.48	-0.75	-0.92	Pl13	-0.66	-0.65	-0.45
Pl30	-0.48	-0.66	-0.64	Pl14	-1.4	-1.39	-1.62
Pl31	-0.5	-1.00	-1.25	Pl15	-1.03	-1.47	-1.47
Pl32	-0.68	-0.65	-1.11	Pl16	-1.23	-1.50	-1.36

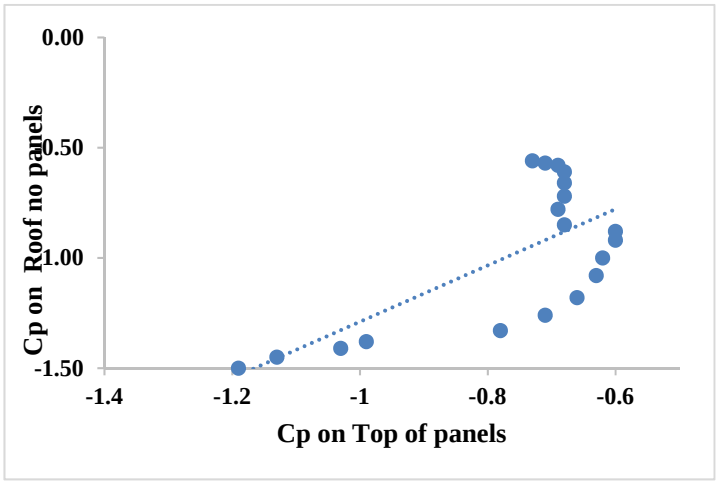
Leeward 45º wind direction				Wind ward 45º wind direction				0º wind direction			
Polylines	Cp Top	Cp roof under panels	Cp bottom of panels	Polylines	Cp Top	Cp roof under panels	Cp bottom of panels	Polylines	Cp Top	Cp roof under panels	Cp bottom of panels
Pl20a	-1.19	-1.3	-1.29	Pl1A	-0.3	-0.15	-0.29	Pl1A	-0.35	-0.36	-0.37
Pl21	-1.13	-1.09	-1.08	Pl2	-0.17	-0.21	0.07	Pl2	-0.34	-0.36	-0.38
Pl22	-1.03	-1.04	-1.04	Pl3	-0.29	-0.65	-0.59	Pl3	-0.34	-0.39	-0.41
Pl23	-0.99	-1.03	-1.03	Pl4	-0.18	-0.49	-0.31	Pl4	-0.34	-0.41	-0.41
Pl24	-0.78	-1.08	-1.08	Pl5	-0.2	-0.33	-0.24	Pl5	-0.34	-0.41	-0.41
Pl25	-0.71	-0.95	-0.95	Pl6	-0.21	-0.33	-0.06	Pl6	-0.34	-0.42	-0.42
Pl26	-0.66	-0.78	-0.78	Pl7	-0.23	-0.34	0.15	Pl7	-0.36	-0.43	-0.43
Pl27	-0.63	-0.66	-0.66	Pl8	-0.45	-0.65	-0.56	Pl8	-0.38	-0.43	-0.43
Pl28	-0.62	-0.76	-0.57	Pl9	-0.15	-0.68	-0.72	Pl9	-0.38	-0.43	-0.43
Pl29	-0.6	-0.73	-0.68	Pl10	-0.25	-0.61	-0.40	Pl10	-0.35	-0.43	-0.43
Pl30	-0.6	-0.64	-0.63	Pl11	-0.29	-0.97	-0.88	Pl11	-0.35	-0.43	-0.43
Pl31	-0.68	-0.61	-0.60	Pl12	-0.33	-0.75	-0.55	Pl12	-0.35	-0.44	-0.44
Pl32	-0.69	-0.98	-0.97	Pl13	-0.39	-0.55	-0.48	Pl13	-0.35	-0.44	-0.44
Pl33	-0.68	-0.82	-0.82	Pl14	-0.46	-0.48	-0.36	Pl14	-0.35	-0.44	-0.44
Pl34	-0.68	-0.75	-0.74	Pl15	-0.52	-0.50	-0.23	Pl15	-0.35	-0.42	-0.42
Pl35	-0.68	-0.63	-0.62	Pl16	-0.79	-0.89	-0.98	Pl16	-0.36	-0.42	-0.42
Pl36	-0.69	-0.97	-0.58	Pl17	-0.52	-1.00	-0.91	Pl17	-0.37	-0.39	-0.42
Pl37	-0.71	-0.96	-0.89	Pl18	-0.72	-0.92	-0.68	Pl18	-0.35	-0.40	-0.41
Pl38~~a~~	-0.73	-0.88	-0.85	Pl19a	-0.84	-0.92	-0.70	Pl19a	-0.35	-0.39	-0.40

Every correlation coefficient data point in Fig 6.9 represents a correlation value of a pair of pressure coefficient series corresponding to the Cp on two surfaces. Each of those series of points is illustrated in one of the following figures (Fig. 6.10 to Fig. 6.14), which depict one Cp series as function of the other Cp series for the selected pair of surfaces. A linear trend line is added to the points for comparison. Pressure coefficients for the case with 35º inclined roof without solar panels, subjected to 90º, 45º, and 0º wind directions are listed in Table 6.2.

As shown in Fig. 6.10 a), the Cp data points for the bottom of the panels and roof surfaces on the leeward side of the roof, aligns well along a straight line, which is reflected by the high correlation factor of 0.89 (Fig. 6.9 a). This observation is consisted with what was reported in the previous case. The Cp data for the top and bottom surfaces of the panels on the same leeward side, include points which are distributed close to a straight line (correlation 0.82, Fig. 6.9 a) as it can be noticed in Fig. 6.10 b), but are not as close along the line as the Cp data reported for the surfaces encompassing the cavity.



(a) (b)



(c)

Fig.6. 10. Cp as a function of one surface Cp on the other, 2" spacing, 10" clearance, slope 35º, wind direction 45º, leeward a) Point B, Bottom of the panels Vs roof surface b) Point B, Bottom Vs top of the panels c)Point L, Top of the panels Vs Roof without panels

Fig. 6.10 c) shows that the Cp points for the top of the panels and roof without solar panels surfaces, on the leeward side of the roof, are distributed much farther from a straight line than the other two surface pairs represented in Figs. 6.10 a) and b). Some points in Fig. 6.10 c) align with a line nearly perpendicular to the trend line, which is reflected in a correlation factor of 0.70 (Fig. 6.9 a), much lower than the other two surface pairs in Figs. 6.10 a) and b).

In Figure 6.11 a), the Cp points for the bottom of the panels and the roof surfaces on windward side of the roof are distributed close to a straight line, which is reflected by the high correlation factor of 0.89.

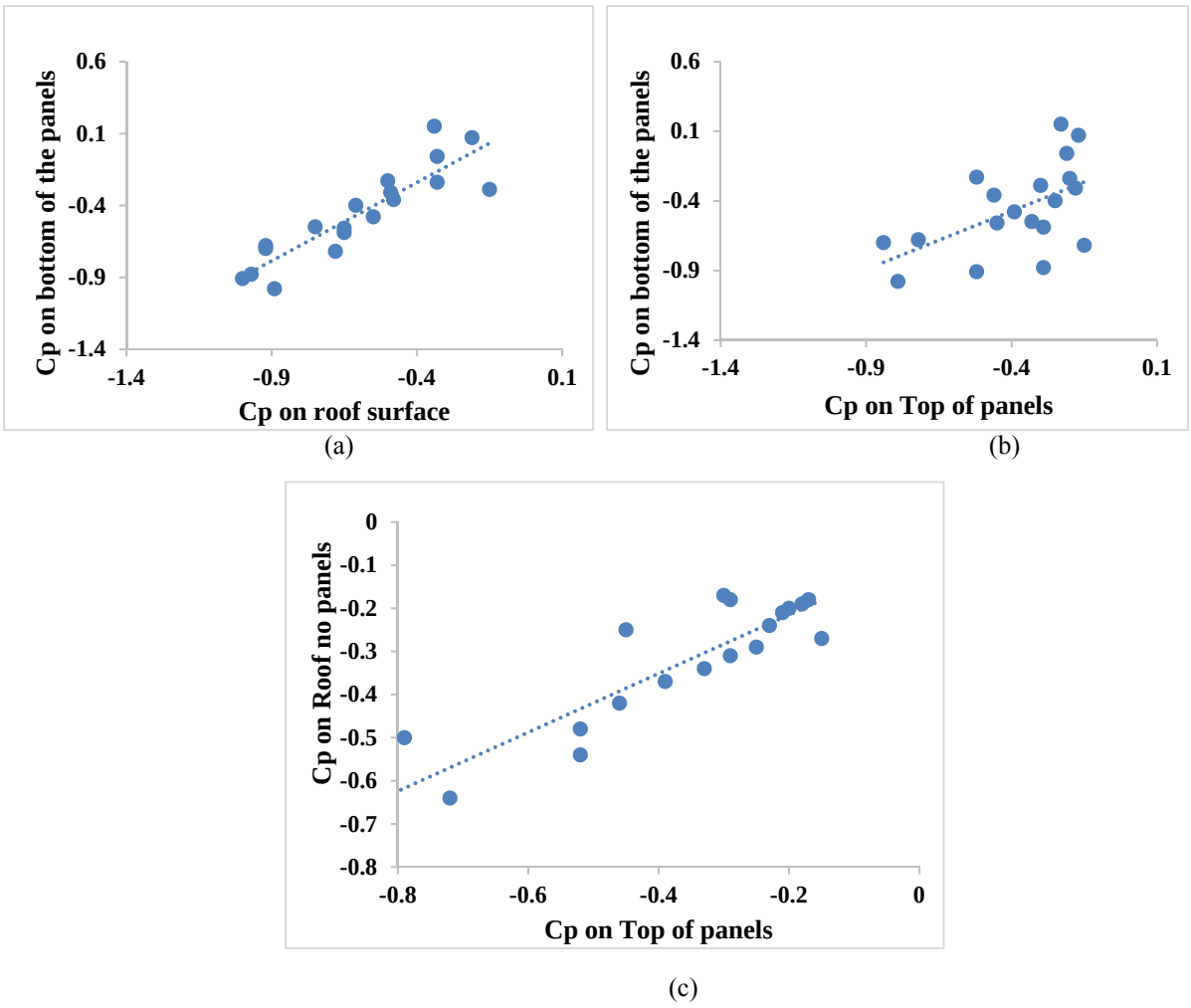


Fig.6. 11. Cp as a function of one surface Cp on the other, 2" spacing, 10" clearance, slope 35º, wind direction 45º, windward a) Point D, Bottom of the panels Vs roof surface b) Point G, Bottom Vs Top of the panels (45º,WW) c) Point N, Top of the panels Vs Roof without panels

Similarly, Fig. 6.11 c, which represents the Cp points on top of the panels and roof without solar panels surfaces on the windward side of the roof, shows that those points are distributed close to a straight line. However, the distribution of Cp points for the top and bottom surfaces of the panel surfaces on the windward side (Fig. 6.11, b), shows lower correlation factor, i.e., 0.56 (Fig. 6.9 a).

For the 90º wind direction on the leeward side of the roof, similar with the other investigated cases, the best correlation was found for the Cp data points registered on the bottom surface of the panels and on the roof surface, as it can be noticed in Fig. 6.12 a), where a correlation of 0.98 is observed (Fig. 6.9 a).

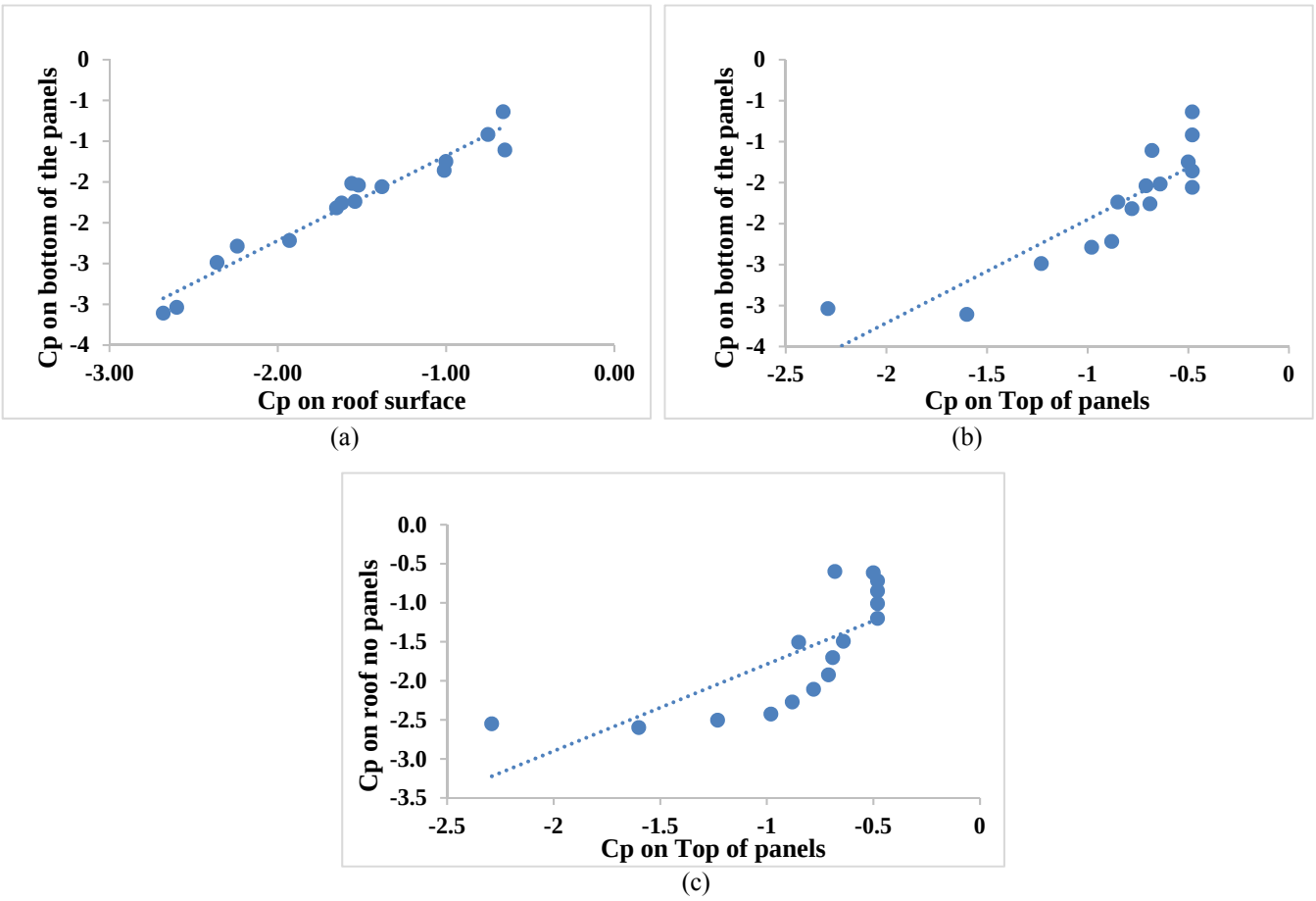


Fig.6. 12. Cp as a function of one surface Cp on the other, 2" spacing, 10" clearance, slope 35º, wind direction 90º, leeward a) Point C Bottom of panel Vs roof surface b) Point J Bottom Vs Top of the panels c) Point M, Top of the panels Vs Roof without panels

The Cp data points located on the top and bottom of the panels, on the same leeward side of the roof (Fig. 6.12 b), are distributed slightly farther from the straight line (correlation of 0.88 in Fig. 6.9 a). Moreover Fig. 6.12 c) shows the distribution of the Cp points on the top of the panels and on the roof surface without solar panels, for the leeward side of the roof, for which the pressure coefficient data was found to be scattered with a lower correlation coefficient of 0.73 (Fig. 6.9 a) than the other two surfaces pairs in Figs. 6.12 a) and b).

On the windward side of the roof, for the same wind direction of 90º, the distribution of the Cp points on the bottom of the panels and on the roof surfaces is still distributed along the line, however it is more scattered than that for the leeward side of the roof, also registering a lower correlation factor of (0.90 in Fig. 6.9 a)) than for the leeward side of the roof.

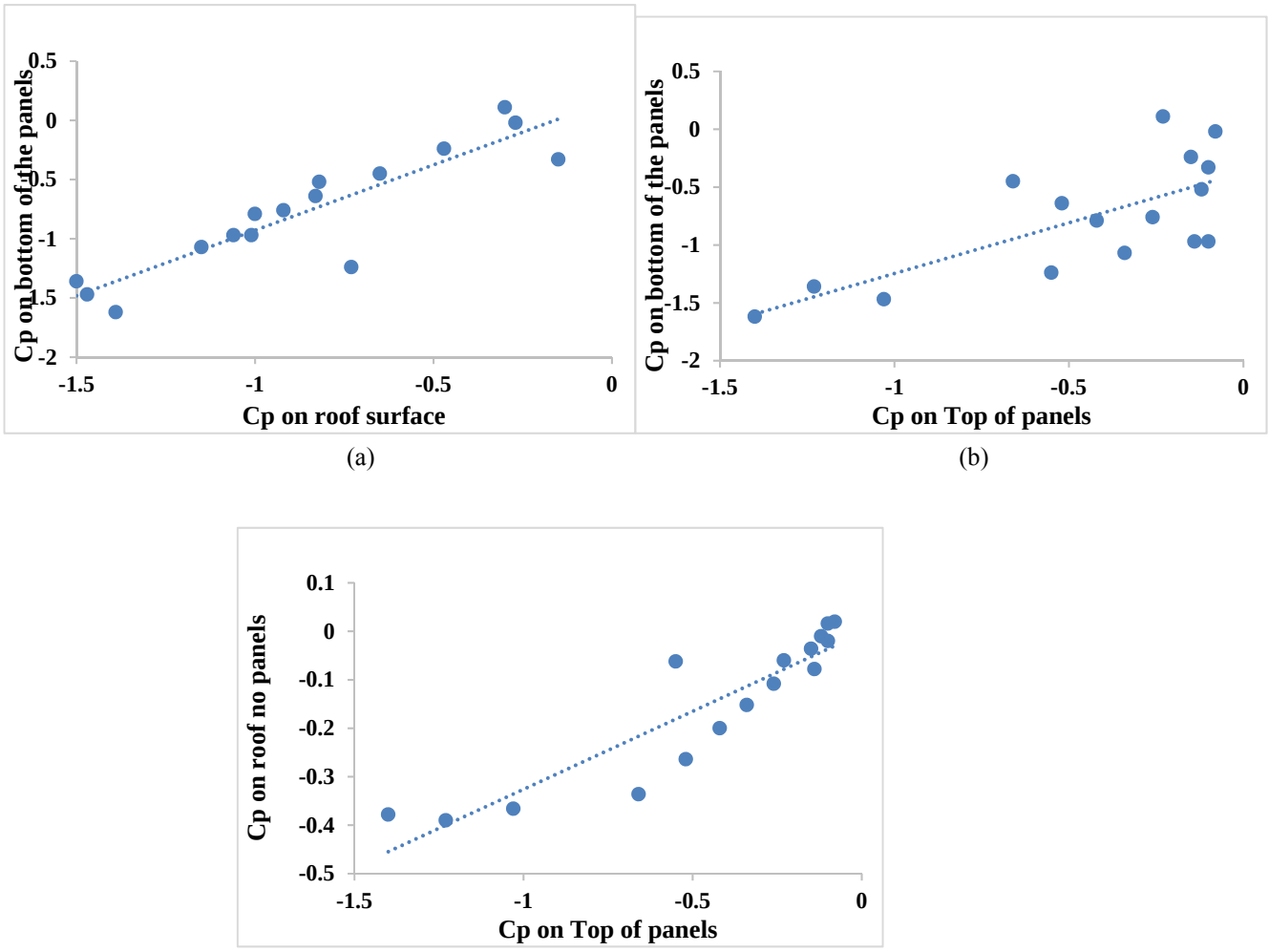
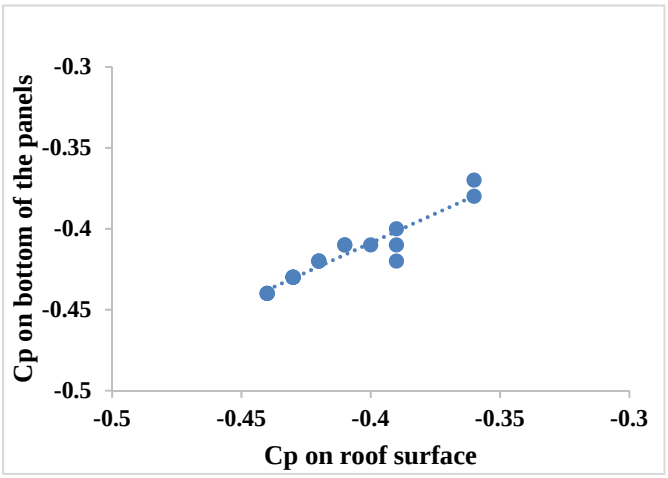


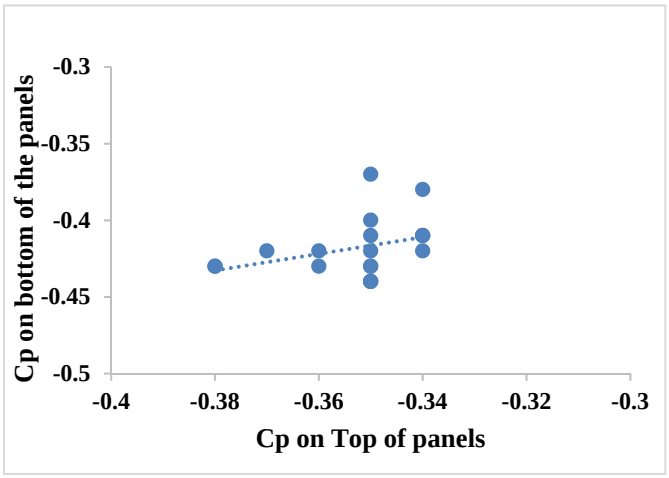
Fig.6. 13. Cp as a function of one surface Cp of the other, 2" spacing, 10" clearance, slope 35º, wind direction 90º, windward a) point E, Bottom of panel Vs roof surface b) Point H, Bottom Vs Top of the panels c) Point O Top of the panels Vs Roof Without panels

For 0º wind direction, Figure 6.14 a) shows that the distribution of the Cp data points for the bottom of the panels and the roof surface is very close to a straight line, with correlation factor of 0.95 (Fig. 6.9 a). However, the distribution of the Cp points for the top and bottom panel surfaces is very scattered, as it can be noticed in Fig. 6.14 b) with a correlation factor of 0.35 (Fig. 6.9 a). As well, the Cp data points for the top of the panels and the roof surface without solar panels are much

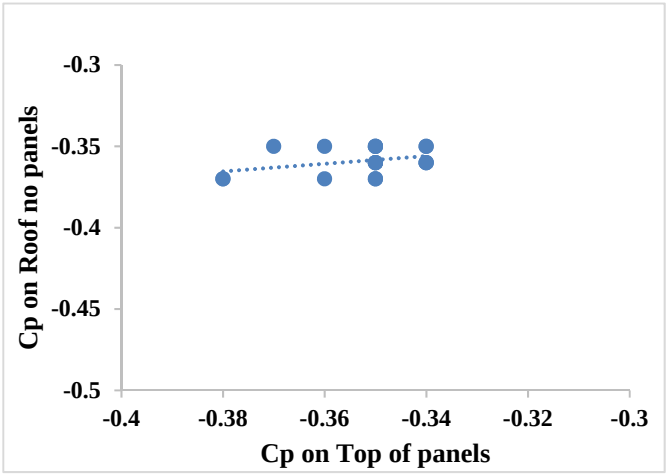
more scattered, and all points are distributed nearly perpendicular to the straight trend line (Fig. 6.12 c), which determines the lowest correlation factor of 0.02, as noticed in Fig. 6.9 a.



(a)



(b)



(c)

Fig.6. 14. Cp as a function of one surface Cp on the other, 2" spacing, 10" clearance, slope 35º, wind direction 0.0º a) Point A, Bottom of panel Vs roof surface b) Point K, Top of the panels Vs Without panels Roof c) Point F Roof without panels Vs Top of the panels

6.4. Pressure coefficients correlations summary

The only correlation coefficients determined for double layer systems available in the literature were derived for the roof paver full-scale experimental results, (Habte et al. (2017)), thus this study was used for comparing with the currently obtained correlation coefficients between top and bottom surfaces of the panels. As reported in Habte et al. (2017), there is no correlation for 360º (0º for the current investigation) wind direction, however very high correlations for the 315º (45º for the current investigation) and 270º (90º for the current investigation) wind directions were signaled; these findings are similar to the observations found in this study for the top and bottom surfaces of the panels, for the windward side of the roof.

Slight differences were also found between the results from the current study and those reported by Habte et al. (2017) due to the fact that the study by Habte et al. (2017) used only two points for determining the pressure correlations based on the experiment on a long side of a half-cut hip roof; this configuration is not very similar to the gable roof; also a second reason could be the fact that the roof pitch used in the full-scale experiments had 18.4º inclination which is different from the 35º roof inclination used in this study.

For the current study, two main patterns were determined from the graphs representing 12 cases.

1- The first pattern applies to all the cases for top and bottom of panels, and for top of the panels and roof without panels, (F to P), and applies on the cavity surfaces when the panels have large gaps, 8” spacing and 10” clearance. This pattern shows no correlations or very small correlations for 0º (F and L) wind direction, while depicts high correlations for 90º (H, N, P, K) and 45º (G, I, M, O) wind directions.
2- The second pattern applies for cavity surfaces (A, B, C, D, E) when one the gaps is small, or on the cases with combinations of S2”C3”, S2”C10” and S8”C3”. This pattern represents extremely high correlations, 0.89 for the 3 wind directions and 2 sides of the roof.

For the second pattern, cavity surfaces in the windward side shows highest correlations for the S2”C3” and S2”C10” panel arrangements, while both windward and leeward show same correlations for S8”C3” panels arrangement.

However, for the first pattern, top and bottom of the panels, the leeward side presents higher correlations than windward side, where differences are large for S2”C3”, S2”C10” and S8”C3” while those differences become much smaller for S8”C10”.

On the other hand, However, for the first pattern, top of the panels and roof without panels, windward side presents higher correlations than windward side, where differences are large for S2”C3”, S2”C10” and S8”C3” while those differences become much smaller for S8”C10”.

In addition, for S8”C10” and S8”C3” the correlation increases highly for wind direction 0º, (L) to nearly 0.45 to 0.47.

Moreover, for S2”C3”, S2”C10” and S8”C3” the wind direction 90º (C,E, H, N, P, K) has the largest correlation factors, for S8”C10” the wind direction 45º(B, D, G, I, M, O) has slightly higher correlations than the 90º.

Based on the above analysis the pressure equalization is identified in graphs, in different surfaces for specific cases. For quantifications of the pressure equalizations between top and bottom of the panels, or for cavity pressures, the integration tables to be used.

6.5. Pressure equalization classification on solar panels and in the roof-panel cavity

Initially the current research focused on determining the wind induced pressures on the solar panels installed flush on inclined roofs, however in order to estimate the net pressure coefficient which acts on the roof and solar panels system, the pressure equalization phenomena on double layers roof systems, as defined by Koop et al. (2015) and Kopp et al. (2012), was investigated. The double layers roof system used by Kopp et al 2012 was represented by the flat roof-inclined solar panels systems, while the one analyzed by Kopp et al. (2015) included the inclined roof and flush mounted solar panels, thus more similar to the current research. The roof slope, gap between panels and the panel height above the roof used by Kopp et al. (2015) were 30º, 0 cm - 12 cm and 0 cm – 20 cm, respectively. The current study considered roof slopes of 35º, 27º and 15º. Gap between panels of 2” and 8”and panel heights above the roof of 3” and 10” as per the installation instructions provided by solar panels manufacturers guidelines (UNIRAC, 2014).

The pressure equalization occurs when the external pressure on the wind panel partially equalizes the internal pressure measured in the cavity between the roof and the solar panel, as per the studies available in the literature (Kopp et al (2012 and 2015), Oh, 2014).

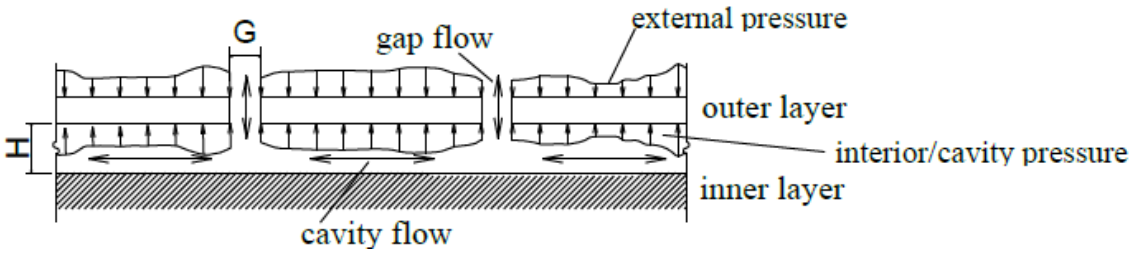


Fig.6. 15. Section view of double-layer system and sketch of pressure equalization (Oh, PhD thesis, 2014).

The convention employed in the current research for investigating pressure equalization is slightly different by defining two processes for balancing the pressure. The first one is similar to the one used by Oh, (2014), namely the external pressure registered on the upper surface of the solar panel partially balances the pressure in the cavity registered on the bottom surface of the panel (Fig. 6.16 a). A second convention system was used for determining the equalization of pressure between the pressures registered in the cavity, on the bottom surface of the panel and the surface of the roof (Fig. 6.16 b).

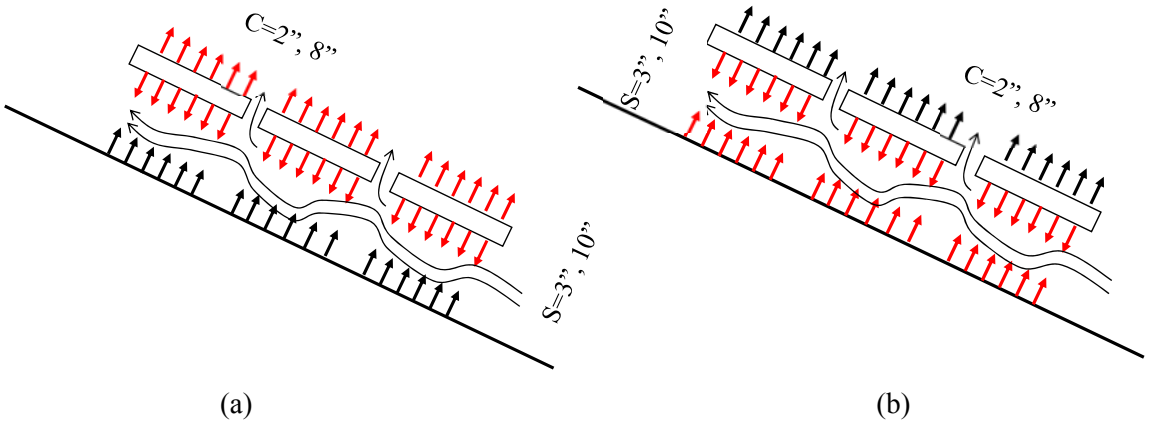


Fig.6. 16. Schematics of pressure equalization mechanism a) Pressure equalization on the panels, b) Pressure equalization in the cavity

Moreover, if the difference between the two pressure coefficients is lower than 5%, then the pressure equalization is considered to occur. When the pressure difference between the two is higher than 5% but lower than 50%, the pressure equalization is considered as partial. When the difference between the two pressure coefficients is higher than 50%, it is considered that there is no pressure equalization between the two pressure coefficients. A large number of cases were identified for the pressure difference range 5% to 50% and were not reported in the classification below. The cases with partial and extreme pressure equalization on the panels, are all the cases except the four cases reported in 3) below. Following this convention several cases were identified to qualify for extreme pressure equalization as follows:

1) Pressure equalization on the panels (Fig. 6.16 a)
   - Slope 15º, wind direction 45º, leeward, S2"C3"
   - Slope 35º, wind direction 45º, windward, S8"C3"
   - Slope 15º, wind direction 90º, windward S8"C3"

2) Pressure equalization in the cavity (Fig. 6.16 b)
   - Slope 27º, wind direction 90º, leeward and windward, S2"C3"

- Slope 27º, wind direction 45º, leeward and windward, S2”C3”
- Slope 27º, wind direction 0º, S2”C3”
- Slope 15º, wind direction 90º, leeward and windward, S2”C3”
- Slope 15º, wind direction 45º, leeward and windward, S2”C3”
- Slope 15º, wind direction 0º, S2”C3”
- Slope 35º, wind direction 90º, leeward and windward, S2”C3”
- Slope 35º, wind direction 45º, leeward and windward, S2”C3”.
- Slope 35º, wind direction 0º, S2”C3”
- Slope 27º, wind direction 90º, leeward S2”C10”
- Slope 27º, wind direction 45º, windward S2”C10”
- Slope 27º, wind direction 0º, S2”C10”

- Slope 27º, wind direction 90º, leeward and windward, S8”C3”.
- Slope 27º, wind direction 45º, leeward S8”C3”
- Slope 27º, wind direction 0º, S8”C3”
- Slope 35º, wind direction 90º, leeward S2”C10”
- Slope 35º, wind direction 0º, S2”C10”
- Slope 35º, wind direction 90º, leeward and windward, S8”C3”
- Slope 35º, wind direction 45º, leeward and windward, S8”C3”.
- Slope 35º, wind direction 0º, S8”C3”
- Slope 35º, wind direction 45º, leeward, S8”C10”
- Slope 27º, wind direction 90º, leeward and windward , S8”C10”
- Slope 27º, wind direction 45º, windward and leeward , S8”C10”.
- Slope 27º, wind direction 0º, S8”C10”.
- Slope 15º, wind direction 90º, windward, S2”C10”.
- Slope 15º, wind direction 0º, S2”C10”.
- Slope 15º, wind direction 45º, leeward, S8”C3”.
- Slope 15º, wind direction 90º, leeward and windward , S8”C3”
- Slope 15º, wind direction 0º, S8”C3”
- Slope 15º, wind direction 45º, leeward, S8”C10”
- Slope 15º, wind direction 90º, leeward and windward , S8”C10”
- Slope 15º, wind direction 0º, S8”C10”

3) No pressure equalization on panels:
   - Slope 27º, wind direction 90º, leeward and windward, S2”C10”
   - Slope 35º, wind direction 90º, leeward and windward, S2”C10”
   - Slope 27º, wind direction 90º, windward , S8”C10”
   - Slope 15º, wind direction 90º, leeward, S2”C10”

Therefore, it was noticed that most of the cases (all, except 4 cases) investigated have more than 50 % pressure equalization on the panels (Fig. 6.16 a). However, all the investigated cases have more than 50% pressure equalization threshold in the cavity formed between the solar panel and the roof surface, (Fig. 6.16 b). For roof inclinations of 15º and 35º, for the space between the panels of S = 8” and clearance above the roof of C = 3”, the pressure equalization occurs between the upper and lower surfaces of the solar panel, for 45º and 90º wind speed directions. For most of the cases with space between panels of S = 2” and clearance above roof of C = 3” the pressure equalization took place between the roof surface and the lower surface of the panel. The same was noticed for the cases with S = 8” and C = 10”. This finding is novel as most of the studies (Bienkiewicz and Sun (1992), Choi et. al. (1998), Kopp et al., (2012), Geurts et al, (2013), Stenabaugh (2015), Oh (2014), Kopp et al., (2015)) have looked only at the pressures on the solar panel, when discussing the pressure equalization, and did not report the pressures on the roof surface underneath the panels. The net pressure coefficients are affected by these two types of pressure equalization, because the sum between the pressures on the three elements of the system is considered: the roof surface, the lower surface of the panel and the upper surface of the panel.

6.6. Implication on the design code

The results of the analyses performed in the current study provide extensive information for the development of new guidelines for solar panel installation on gable roofs.

6.6.1. Comparison with NBC 2010 for gable roofs with no panels

The following findings provide guidance for new provisions for construction codes for gable-roof-mounted solar panels.

This study found that the solar panels installed on gable roofs, generally, are subjected to net suction pressure coefficients less than the corresponding roof surface without solar panels. That is true for 27º and 35º roof slopes but not for 15º roof slope. .

- The total suction registered on either side of the gable roofs due to the installation of solar arrays decreased in comparison with the suction of corresponding roof without solar panels. For example, the maximum suction is -1.14 corresponding to an area of 10 m^2 of solar array installed on 27º gable roof, which represents 56% of the maximum suction on without panels gable roofs, as per NBC 2010, Fig. 20 and Fig. 21.

- Pressure equalization in the cavities is well-developed, where the Cp on the bottom surface of the panels and the roof surface are nearly equal for many of the roof slopes, wind directions and panel configurations, as detailed in the above section.

6.6.2. Comparison with SEAOC PV2 2012 and common practice

The SEACO PV2-2012 defines Normalized Wind Area using a magnification factor of Cp for small wind-exposed areas/roofs ≤ 1000ft (~ 93 m^3). Those factors are calculated for the roof used in this research as 2.76, 3.16, and 3.67 for 35º, 27º and 15º respectively.

The normalized area as defined by SEACO PV2-2012 is $A_n = \left[\frac{1000}{(\max(a_{pv}, 15ft))^2}\right] A$

where:

A_n = Normalized area, sf

A = Effective wind area for structural element being designed, in sf

$a_{pv} = 0.5\sqrt{hW_L}$, but need not exceed h, in ft.

h = Roof height above ground, ft

W_L = Length of the building, ft

The Effective Wind Area, which is used to evaluate the G Cp on wind-exposed surfaces according to ASCE 7-10 and to evaluate Cp Cg according to NBC 2010, corresponds to the tributary area of the force component being considered or the areas which contribute to the force affecting that member. For example, the effective wind area for a fastener is the area secured by that fastener. Another example is a slab, where the tributary area is defined as the area supported by the member bounded by the lines of support (NBC 2010, Structural Commentaries, Part 4 of Division B).

Nonetheless, for narrow and long areas such as roof trusses which are spaced closely together, the width of the effective wind area used to evaluate CpCg need not be taken as less than one-third the length of the area. In other members of indirect support, this area is bounded by the lines of support of the member and the lines of zero shear in the members supported, assuming that a uniformly distributed load is acting on the structure. This definition, which requires a structural analysis to determine the locations of zero shear, should be followed when determining the forces that members carry (NBC 2010, Commentary F, Live Load, 12).

The current study shows some consistency with the total Cp on the flat roof supporting the solar panels, (or net pressure on the solar panels) as per SEAOC PV2-2012 guidelines. These guidelines provide for panels inclined 15º, 27º and 35º and mounted on a flat roof, 1.18, 0.63 and 0.47 for 10, 100 and 306 sf (nearly 1, 10 and 28.5 m^2) effective areas respectively, which are 118%, 73% and 55% of the Cp magnitude on roof without solar panels, as defined in ASCE 7-10, 1.0, 0.86, and 0.86 respectively. The effective areas should be transferred to normalized areas as defined by the SEAOC PV2-2012, (Fig. 17 below, and ASCE 7-10 figures in appendix G).

On the other hand, this thesis gives very similar comparative values, where it calculated the maximum total pressure coefficients on the solar panels mounted on the gable roofs, 15º, 27º and 35º, to be -1.82, and -1.14 for 1 m2 and (10 m2 to 28.5m2) which constitute 75% and 58% of the corresponding CP for a roof without solar panels according to NBC (2010). Those values of Cp corresponding to 27º inclined roof, Fig. 6.20 and Fig.6.21.

This study found smaller magnitudes for the net pressure coefficients on solar panels, 57% (-1.15), 22% (-0.45), and 14% (-0.28) of the pressure coefficient magnitudes for a roof without solar

panels, which correspond to 1.0 m2, 10 m2 and 28.5m2 effective areas respectively, Fig. 6.18 and Fig.6.20. Those net pressure magnitudes correspond to 15º inclined roofs, which coincide with the largest net pressures on the solar panels. That means the other slopes, 27º and 35º, result in smaller magnitudes of net pressure on mounted solar panels (Fig. 6.18).

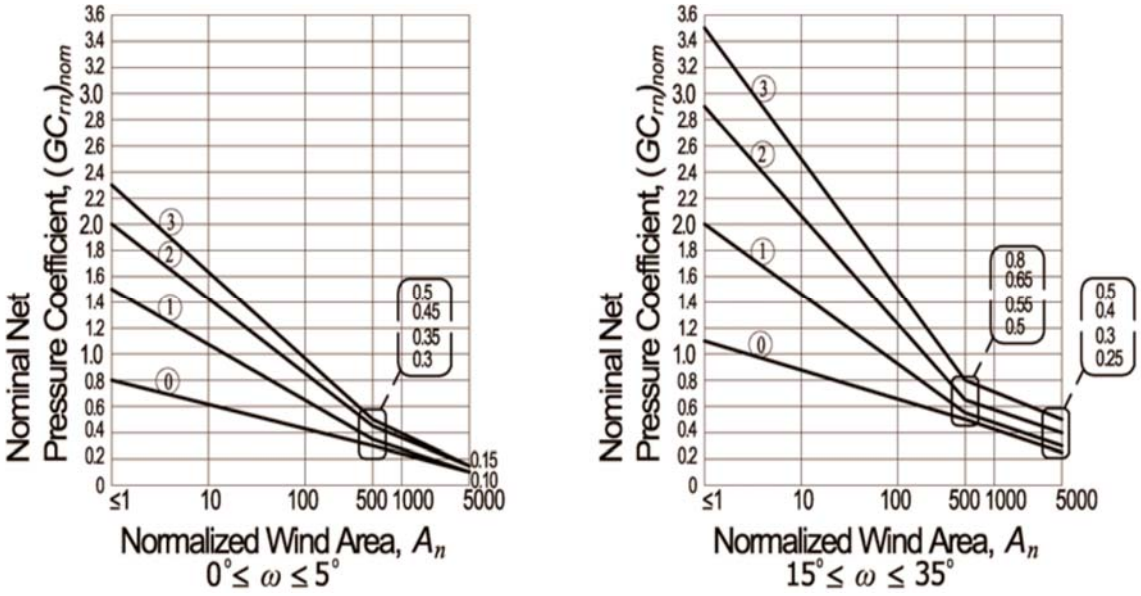


Fig.6. 17. Nominal Net Pressure Coefficients, for Low-Profile Solar Photovoltaic Arrays on Flat Roofs (SEAOC PV2-2012)

Other notes on the differences and similarities between the findings in this study and the existing code SEAOC PV2-2012 and practice are explained in the following.

- SEACO 2012 requires a minimum gap of 0.5” around each solar module or 1” between rows of panels to allow pressure equalization above and below the panels. That is in line with findings in this study, where the spacing between panel rows are 2” or 8”. However, The SEACO PV2-2012 does not stipulate the gap between the roof and solar panel, where according to this study, the pressure equalization does not happen (<50%) for S2” C 10” for all 3 slopes and for 90º wind direction, and for S8” C10” for 27º slope and 90º wind direction of the windward side. In all the other cases, this study found that pressure equalization happens partially (>50%) or completely (>95%), between the top and bottom of the panels.
- On the other hand, if the panels are parallel to the flat roof and the clearance between the bottom of panels and the roof surface is 10”, with minimum gaps as stated above,

SEACO 2012 allows the component and cladding procedure as per ASCE 7-10 30.4 (ASCE 7-10 6.5.12.4) to be used for wind loads. However, this research finds that when a 10" clearance exists under the panels, there is a significant reduction in net wind pressure on the solar panels, to ~ 14% to 47% of the wind loads on roof without solar panels as defined by NBC 2010. In addition, the total wind loads on the roof are reduced to ~55% to 74% of the wind loads on roof without solar panels as defined by NBC 2010. The smaller ratios correspond to large areas (≥ 10m^2), while larger ratios correspond to 1m areas, which are slightly less than the area of a single-module solar panel.

- SEACO 2012 requires the solar panels to be installed at least $2(h_2 - h_{pt})$ or 4 feet, whichever is greater from the edge of the roof, where $h_2$is solar panel height above roof at raised edge, and h_{pt} is mean parapet height above adjacent roof surface. This requirement is in line with the assumption of the current research, which assumes a minimum distance complying with the definition of a minimum end zone width of ~1 m (3.3ft) in the NBC 2010. A similar zone has a width of ~ 0.9 m (3ft) in ASCE 7-10.
- SEACO 2012 stipulates that a roof covered with solar arrays need not to be simultaneously exposed to wind loads on the solar panels and on the roof structure. The roof should be exposed to the wind loads separately, i.e., assuming that no solar panels exist on the roof. This requirement implies that solar panels do not increase the pressure on flat roofs. The current study confirms this assumption for gable roofs.

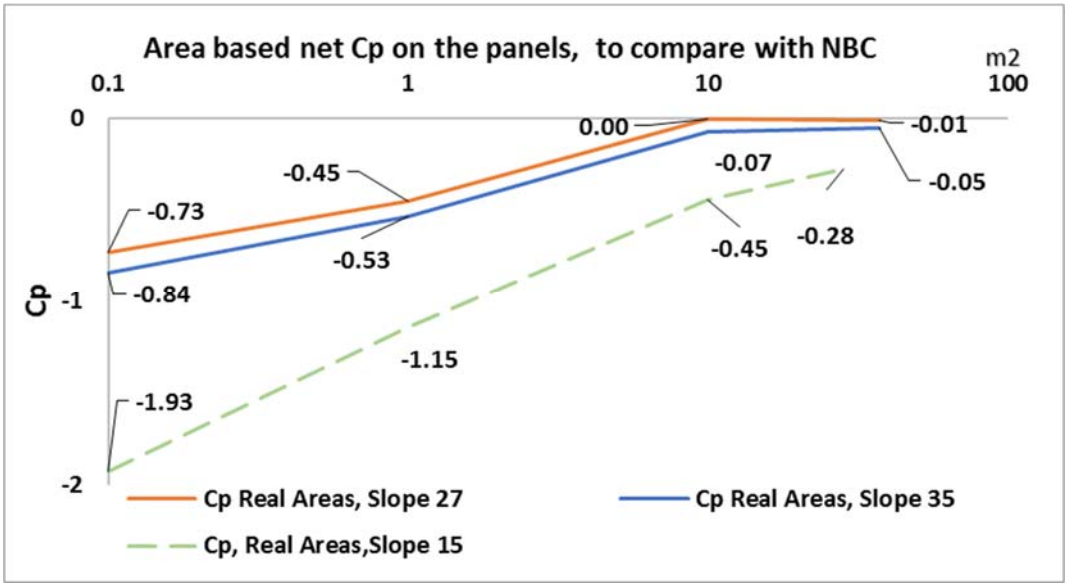


Fig.6. 18. Area based Net Cp on solar panels, this research, spacing 2", clearance 3"

- However, this study notes reduction in total Cp on gable roof surfaces with solar panels installed, where it is shown that the maximum total pressure magnitude on the gable roofs, due installation of solar panels, is 74% and 55% of Cp on roof without solar panels for areas $1m^2$ and $\geq 10m^2$ respectively. Those ratios correspond to a 27º inclined gable roof with solar panels, while the other studied gable roofs with solar panels are exposed to lower total Cp magnitudes.

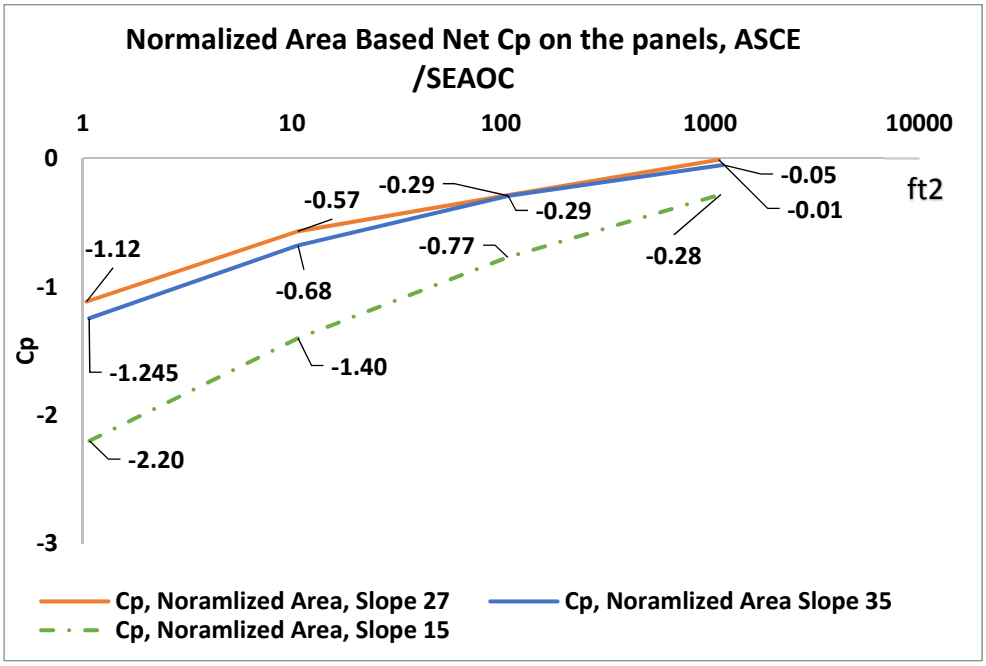


Fig.6. 19. Normalized Area based Net Cp on solar panels, this research, spacing 2", clearance 3"

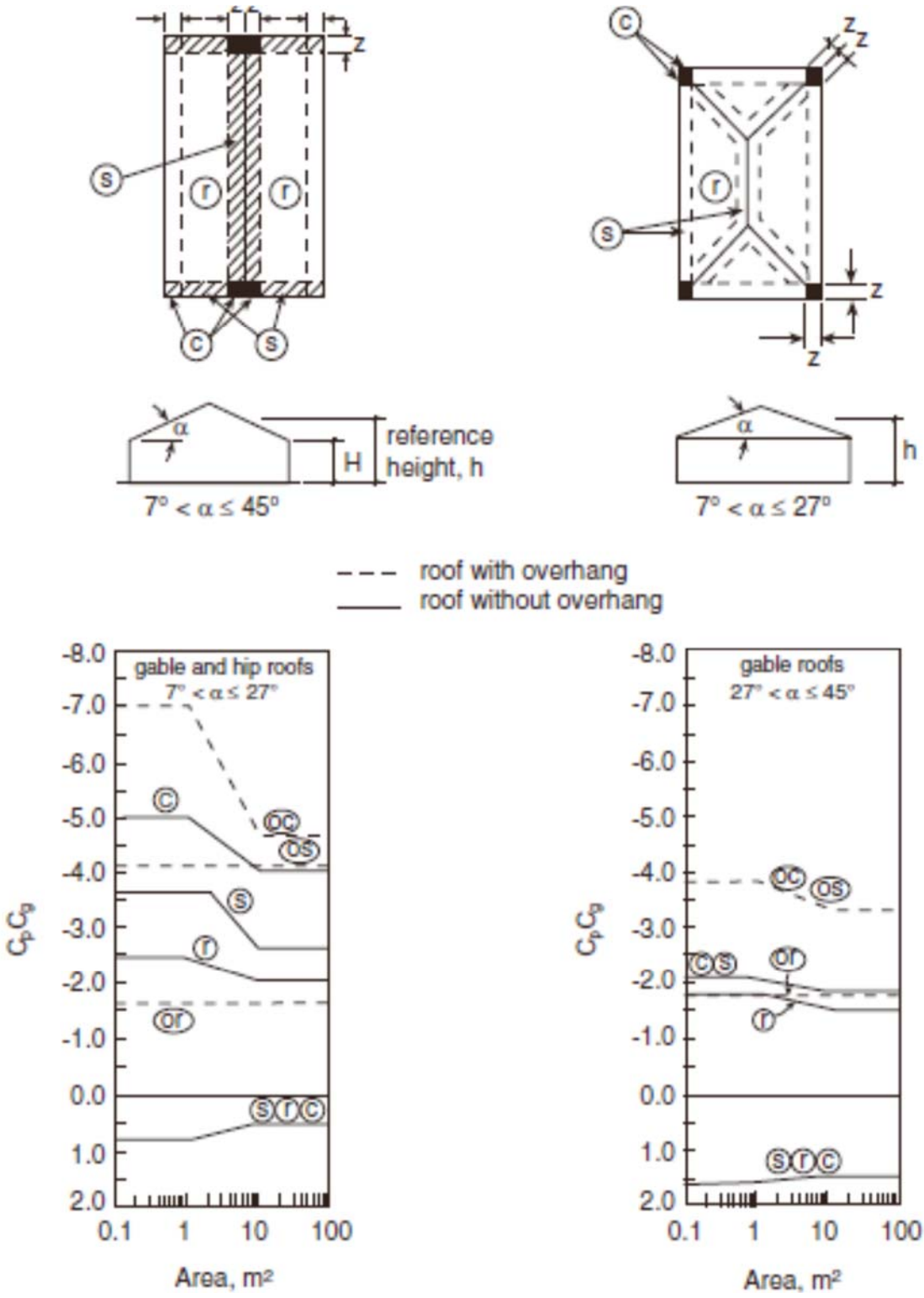


Fig.6. 20. External peak composite pressure-gust coefficients, CpCg, on single-span gabled and hipped roofs, slope of 7° or greater for the design of structural components and cladding (NBC Structural Commentaries, 2015, Part 4 of Division B).

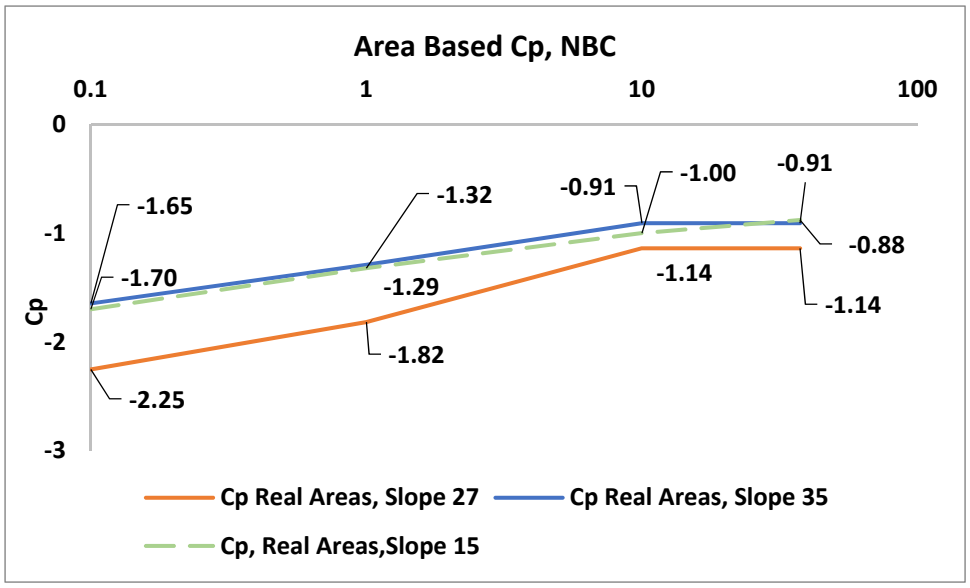


Fig.6. 21. Area based total Cp, this research, spacing 2", C 3"

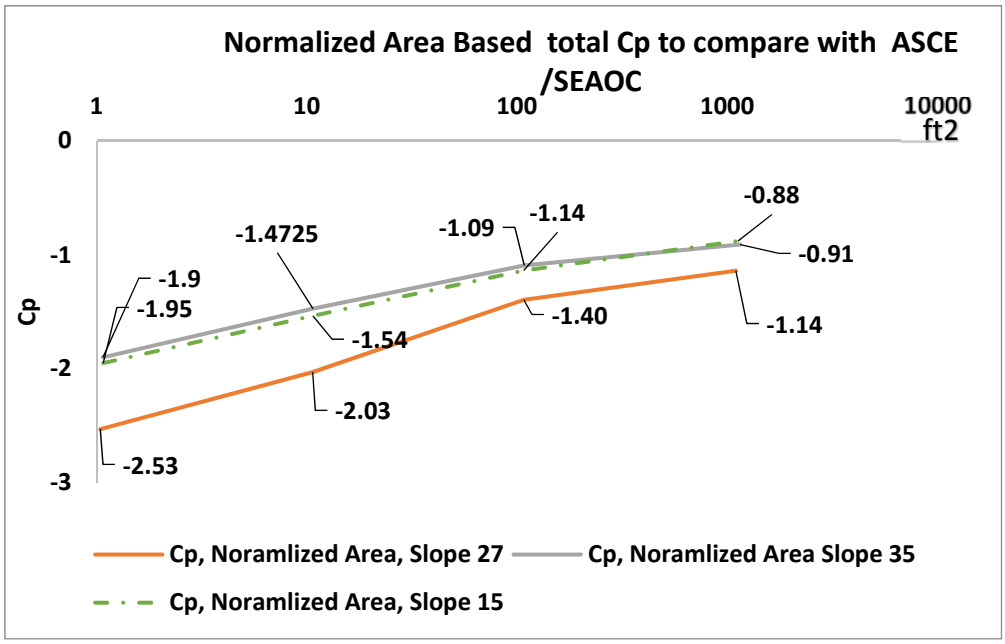


Fig.6. 22. Total Cp, Normalized area, (m^2) based, this research, spacing 2", clearance 3"

6.7. **Conclusions**

- Current design practice for solar panels on gable roofs assumes that solar panels mounted on gable roofs are subjected to pressure coefficients similar to those on roof without solar panels. In addition, wind load effects of installed solar panels on gable roofs are ignored or considered too low to affect the roof design. However, according to the current research, this common practice seems to be too conservative for solar panels installed in internal areas (as designated by NBCC 2015 or ASCE 07) of the gable roofs. This finding is applicable to all roof slopes. That is because of reduction in pressure on top of the panels, the partial pressure equalization between top and bottom of the solar panels and higher cavity pressure than the top of the panels. This partial pressure equalization results in net pressure directed towards the roof surface for nearly all configurations of panels mounted on gable roof inclined at 35º and 27º, except for 8" spacing and 3" clearance solar panels mounted on a 27º inclined roof.

- The wind effects on gable roofs inclined 15º with solar panels create much higher net suction, nearly 22 % more than the largest average suction on roof without solar panels. That means higher anchorage requirements for roofs inclined at 15º, however, lower anchorage requirements for roofs inclined 35º and 27º. Nonetheless, 15º inclined roofs are optimum for solar panels in countries near the tropics such as India, Mexico, Korea, middle Brazil, and most of Australia, while the 35º and 27º inclined roofs are mostly applicable and used in Canada, China, USA and Europe.

- The results of this study are in line with the SEAOC PV2-2012 guidelines set for solar panels mounted on roofs inclined at less than 7º. That because the SEAOC PV2-2012 gives relative total net Cp suctions on solar panels to those on the without panels roof according to ASCE 07, which are very similar to the corresponding values concluded in this study when compared to without panels roof according to NBC (2010).

- The SEAOC PV2-2012 requires designing the panels and their supporting components based on the pressure coefficients determined from the ASCE 7-10 for roofs, not for panels and their parts; thus, it requires double checking by application of the ASCE 7-10 on the entire roof without solar panels installed, in a separate case (SEAOC PV2-2012, 3.2.3.6).

- Nonetheless this study found smaller magnitudes for the maximum net pressure coefficients on solar panels as than Cp magnitudes of roof without solar panels, for all areas and all slopes 15º, 27º and 35º. Those net Cp correspond to 15º inclined roofs, which means that the other slopes, 27º and 35º, result in smaller net Cp on the mounted solar panels (Fig. 6.18).

- There is significant reduction in the total pressure coefficient on roof after installation of the solar panels, where total Cp after installation of the solar panels become 60%-82% of the pressure coefficients on gable roofs without panels, inclined 35º and 27 º respectively. Although the total pressure on 15º inclined roofs increases by 22% from roof without solar panel, however, the total CP after the increase still very close the total Cp on 35º with solar panels, (or 60% of Cp on 35º without panels), Fig. 6.21.

- The reduction in total Cp for the whole area of the roof array on windward or leeward, requires that the supporting rails of the solar panels can redistribute the wind loads to the roof, and then the railing should be continuous.

CHAPTER 7

Conclusions

7.1 Summary

This dissertation is written based on extensive numerical analysis using CFD simulation to investigate the effects of wind on solar panels mounted of gable roofs. The analyses include effects of spaces between solar panel arrays, effects of roof clearance between the solar panels and roof surface. Moreover, this research analyses the effects of wind directions and wind speed for different roof slopes. A comprehensive database of pressure coefficients for solar panels with the different installation parameters, were developed. The CFD analyses encompassed nearly 140 simulation cases among which 35 cases simulated existing full-scale and wind tunnel experiments in the literature, for validating the currently CFD proposed model. Detailed description of the wind pressure coefficients on the three parallel surfaces, namely top and bottom of the panels and the roof surface, were presented and discussed. The results are also compared with the case of roof with no solar panels installed. The outcome of this research project will contribute to the debate on how solar panels on sloped roof can be analyzed and designed for wind pressures.

7.2 Limitations of the research

The current study does not address the following aspect:

- The effects of tilting solar panels and rotation of the panels about the horizontal axis parallel to the roof surface. The main reason for this omission is that such configurations are not common in the construction industry for solar panel installed on the gable roofs.
- The study does not address several intermediate values spacings between panel arrays and clearances between roof surfaces and bottom of the panels. The assumption is that the pressure coefficients results for the intermediate spacings and clearances can be interpolated between the analyzed parameters.
- The study also does not cover the case of flat roof mounted solar panels which are widely addressed in the literature.

- Moreover, the study is limited to 0º, 45º and 90º wind directions with roof ridge, which are similar to those covered in the existing design codes (NBCC 2010, and ASCE 2007). For other dominating wind directions, the wind pressure coefficients might be interpolated between the results of the analyzed wind directions in this study.

7.3 General findings

Several general conclusions are formulated in this section, while more detailed remarks determined for the investigated cases will be presented in the following sections.

- It was found that the installation of solar panels arrays on gable roofs affects the pressure on both sides of the roof, increasing the pressure on leeward side and decreasing it on the windward side, for roof slopes 27 º and 35 º slopes. This pressure redistribution also decreases the pressure magnitudes on solar panels mounted on gable roofs, in comparison with roofs with no solar panels installed. However, this trend is observed to be different for roofs inclined at 15 º. This finding differs from what has been established in common practise for solar panels installation on gable roofs, where it is assumed that the pressure on solar panels would be the same as that on roofs without panels.

- The average wind pressure on roof surface under the panels is nearly equal to the wind pressure on the bottom surface of the panels, which implies the occurrence of the pressure equalization in the cavities between the bottom surface of the solar panels and the roof surface. That is true for all array configurations.

- Due to the pressure equalization between the roof surface and bottom surface of the panels, the total pressure coefficients on roofs with solar panels can be approximated with the pressure coefficients applied on top of the solar panels mounted on 27º, 35º and 15º inclined roofs. This approximation shows an error of 1-5 % for all cases, except for the solar panels arrays with small spacing (2”) and large clearance (10”), where this estimation is conservative and differs by nearly 23 %.

7.4 Wind effects on roof mounted solar panels, due changes in wind directions or /and roof slopes

- It was found that wind direction 90º generates higher pressure coefficient magnitudes than those generated for the 45º and 0º directions, for the gable roof mounted solar panels.

- A reduction in the resultant pressure coefficient magnitudes on the gable roofs with solar panels is observed when compared to the case of gable roofs with no panels, that is due to the installation of solar panels, for all the investigated array configurations. An exception to this is the increase in resultant pressure coefficient magnitudes for the 15º inclined gable roofs.

- The net pressure coefficients on solar panels mounted on gable roofs has positive values, indicating that the overall wind-induced pressures act downwards on the roof-panel system for the roof slopes 27º and 35º; this is due to strong cavity effect under the arrays, which leads to the pressure equalization between the roof and the panel. Also, this explains why there is a reduction in the magnitudes of total pressure coefficients on these inclined roofs. However, there is net suction increase for the 15º inclined roofs with solar panels, representing nearly 29% of the suction corresponding to the roofs with no panels.

7.5 Wind effects on roof mounted solar panels due to change in roof clearance

- When roof clearance increases, the total pressure coefficient on gable roofs decreases significantly on the windward side, while these magnitudes only decrease slightly on the leeward side of the roof That is true for slopes 27º and 35º while opposed trend is observed for 15º slope.

- When roof clearance increases, the cavity pressures increase significantly on both windward and leeward sides of the roof, while the pressure coefficient on top of the panels increases slightly leeward and decreases more on windward. On the other hand, the net pressure coefficient on the solar panels becomes directed towards the roof, in both leeward and windward surfaces after the increase in clearance. That is true for all the slopes.

7.6 Wind effects on roof mounted solar panels due to change in array spacing

When panel array spacing increases, the total suction coefficients on the roof decreases significantly on the windward side , while the suction decreases slightly on the leeward side of the roof. This implies higher wind-induced pressures acting on the roof structure as a whole. That applies to slopes 27º and 35º while opposed trend is observed for 15º slope.

- When panel array spacing increases, cavity suction slightly increases on the windward and decreases on the leeward of the roof. That leads the net pressure on the panels becomes slight suction of the leeward and pressure on the windward panels. . That applies to slopes 27º and 35º while opposed trend is observed for 15º slope.

7.7 Implication on the design codes

In general, the results of the analyses performed in this study show some differences when compared with the current solar panel installation practices and show good consistency with existing SEAOC PV2-2012 solar panel installation code provisions.

- Current practice for solar panel installation on gable roofs assumes that solar panels mounted on gable roofs are subjected to similar pressure coefficients to those on roofs with no solar panels. In addition, the effects of the installed solar panels on the gable roofs are ignored or are considered too low to be employed in the verification of the roof structural designs. However, according to this research, this common practice seems to be too conservative. That result applies to all roof slopes. That because pressures distributed on top and bottom of the solar panels, result in net pressure directed towards the roof surface for gable roof inclined at 35º, and result in slight suction for gable roofs inclined at 27º. However, these wind-induced effects result in higher net suction for gable roofs inclined at 15º. After the installation of solar panels, the roof is subjected to nearly 60%-82% of the pressure coefficients on gable roofs with no panels inclined at 35º and 27º respectively. However, the total wind pressure coefficients on gable roofs inclined at 15º with solar panels installed, are nearly 29 % higher suction than the roofs with no panels, which might need to be considered in the design of the gable roofs for solar panels.

- Those results are very much in line with the SEAOC PV2-2012 guidelines which are set for solar panels mounted on roofs inclined less than 7º with solar panels inclined between 15º to 35º, where both give higher pressure magnitudes than the ASCE without panels. The SEAOC PV2-2012 provides suction values in the interior roof areas designated # 1 in ASCE 07. However, these provisions are specified for similar roof size and height of the building model as those used in the current study, but for a flat roof, considering the corresponding inclined solar panels installed on roof areas as defined in the ASCE 07.

- Installation of solar panels on gable roof, does not increase the maximum amplitude of pressure coefficients above those prescribed for the gable roofs with no panels, and if the solar panels or roof surface underneath are designed using the pressure coefficients values already stipulated for the roof without panels, the design would be conservative.

7.8 Main contributions and conclusions

The pressure coefficients on gable roof mounted solar panels were calculated on the three surfaces, including top and bottom of panels as well as the roof under the panels. In addition, pressure coefficients on corresponding roofs without solar panels were determined. The pressure coefficients were then integrated over 19 polylines on both roof surfaces. The conclusions arising from the current research study are summarized below. It should be noted that conclusion items 2, 3, 4 and 6 can be considered original contribution to the scientific knowledge in this area, while conclusion items 1 and 5 primarily substantiate and confirm existing knowledge.

1. Installation of solar panel arrays on gable roofs with proper gaps (e.g. S2” C 3”, S2” C 10”) reduces the maximum total suction on the roofs with slopes of 27º and 35º, while for 15º slope, an increase of total suction is observed. For the 15º slope, the solar panels caused an increase in total pressure coefficients, on both windward and leeward surfaces, with the largest increase being observed on the leeward surface.

2. Solar panels on gable roofs are found to be subjected to a net pressure or net suction that is significantly lower than that for roofs with no solar panels, for all investigated cases. For example, the minimum reduction is when net pressure recued to 40% of that on corresponding roof without solar panels, while for all other cases, the net pressure reduces to less than 40% of the that on roof without solar panels.

3. Solar panels on gable roofs are found cause moderate reduction of the total suction on the roof surface for slopes of 27º and 35º Where it reduces to at least 80 % of the that on bare roofs. However, the solar panels on gable roofs cause increase in total suction for 15° slope gable roofs.

4. Installation of solar panel arrays on gable roofs with appropriate gaps (e.g. S 2" C 3", S2" C10"), reduces the total suction on the leeward surface and increases the total suction on the windward surfaces of the roof. That reduces the total resultant pressure along the wind direction, on the entire roof surface.

5. An increase in clearance with the roof surface or spacing between arrays of solar panels, moderately increases the net pressure/suction on the panels and may reverses the net pressure direction, particularly for the 90° wind direction. An increase in clearance leads to decreases in the net suction and increases in the net pressure on the panels for all slopes and wind directions.

6. An increase in spacing or clearance beyond 2" and 3", respectively, additionally decreases the total pressure on roof surface for the windward side while decreases slightly the total suction on the leeward side for roof slopes of 27º and 35º. However, for 15º slope, total suction on both sides of the roof increases slightly.

7.8 Further researches on wind effects on gable roof mounted solar panels

- This study covers CFD calculations of wind effects on solar panels mounted on gable roofs and explored new areas in clarifying the wind-induced effects. However, this study did not perform experimental work. Consequently, it is recommended that some or all the cases analyzed in this study can be tested in full-scale and/or in wind tunnel facilities, to set a strong base for developing new provisions for design codes.

REFERENCES

1. Alrawashdeh, Hatem; Stathopoulos, Ted (2016) "Roof-mounted solar panels under wind action", 8th International Colloquium on Bluff Body Aerodynamics Northeastern University, Boston, Massachusetts, USA.
2. Aly M. A. (2016), "On the evaluation of wind loads on solar panels: The scale issue", Solar Energy 135 (2016) 423–434.
3. Aly Mousaad Aly and Girma Bitsuamlak, (2013), "Aerodynamics of ground-mounted solar panels: Test model scale effects", Journal of Wind Engineering and Industrial Aerodynamics, Elsevier, 7, Aug., 2013, 123(2013) P 250–260.
4. ANSYS, 2015, "Large Eddy Simulation Theory in the CFX-Solver Theory Guide".
5. Apperley L., Surry D., Stathopoulos T. and Davenport A.G.; (1979), "Comparative Measurements of Wind Pressure on a Model of The Full-Scale Experimental Building at Aylesbury, England"; Journal of Industrial Aerodynamics, 4 (1979) 207—228.
6. ASCE/SEI 7-10, (2010), "Minimum Design Loads for Roofs and Other Structures", American Society of Civil Engineers, ASCE, and Structural Engineering Institute.
7. Banks, David (2013) "The role of corner vortices in dictating peak wind loads on tilted flat solar panels mounted on large, flat roofs" Journal of Wind Engineering and Industrial Aerodynamics, 123 (2013) P192–201.
8. Bienkiewicz, B., & Sun, Y. (1992). "Wind-tunnel study of wind loading on loose-laid roofing systems". Journal of Wind Engineering and Industrial Aerodynamics, 41-44: 1817-1828.
9. Bienkiewicz B.; Sun Y; (1997) "Wind loading and resistance of loose-laid roof paver systems" Journal of Wind Engineering and Industrial Aerodynamics 72(1):401-410, 1997.
10. Bienkiewicz B.; Endo M.; Main J.A. and Fritz W.P., (2009). "Comparative Inter-laboratory Study of Wind Loading on Low-rise Industrial Buildings". ASCE/SEI Structural Congress, American Society of Civil Engineers, Austin, Texas, April–May.
11. Bistuamlak G.T. and Aly M.A., 2014, "Wind pressures on solar panels mounted on residential homes", J. Archit. Eng., 2014, 20(1): 04013003.
12. Bistuamlak G.T. and Dagnew A. K., 2013, "Computational evaluation of wind loads on buildings: A review", Wind and structures an international journal, June 2013.

13. Bistuamlak G.T. Dagnew A. K., Erwin J., 2010, “Evaluation of wind loads on solar panel modules using CFD”, The Fifth International Symposium on Computational Wind Engineering (CWE2010), Chapel Hill, North Carolina, USA May 23-27, 2010.
14. Blackmore, P. A., & Geurts, C. P. (2008). “Wind loads on roof mounted PV modules”, Paper presented at the WES Conference. Guildford, UK.
15. Bronkhorst, A. J., Geurts, C. P., Bentum, C. V., & Grepinet, F. (2010). “Wind tunnel and CFD modelling of wind pressures on solar energy systems on flat roofs”. 5th International Symposium on Computational Wind Engineering, Chapel Hill, North Carolina, USA.
16. Browne Matthew T.L. Gibbons Michael P. M., Gamble Scott, Galsworthy Jon, (2013) “Wind loading on tilted roof-top solar arrays: The parapet effect”, Journal of Wind Engineering and Industrial Aerodynamics, 123 (2013) P 202-213.
17. Cao, Jinxin; Yoshida, Akihito; Saha, Proshit Kumar ; Tamura, Yukio (2013) “Wind loading characteristics of solar arrays mounted on flat roofs”, Journal of Wind Engineering and Industrial Aerodynamics,123 (2013) 214 – 225.
18. Chakrabarti, S. K. , Hernández, S., Brebbia, C. A , (2005), “Fluid Structure Interaction and Moving Boundary Problems”, WIT Press.
19. Choi ECC, Wang Z. “Pressure-equalization of curtain wall systems”. Journal of Wind Engineering and Industrial Aerodynamics 1998;73:251-66
20. Chowdhury J. M., and Hangan H., (2016), “A numerical approach to the investigation of wind loading on an array of ground mounted solar photovoltaic (PV) panels”, Journal of Wind Engineering and Industrial Aerodynamics 153 (2016) 60-70.
21. Chung, Kung-Ming, Chang, Keh-Chin, Chou, Chin-Cheng, “Wind loads on residential and large-scale solar collector models” , Journal of Wind Engineering and Industrial Aerodynamics, 99 (2011) 59–64
22. CWE2010, p. 8.
23. Dagnew A. K. 2012, “Computational evaluation of wind loads on low and high-rise buildings”, PHD Florida International University.
24. Doudak, G. (2005) “Field determination and modeling of load paths in wood structures. PhD Thesis, McGill University, Montreal, QC, Canada.

25. Doudak, Ghasan; Zisis, Ioannis; Smith, Ian; Stathopoulos, Ted; August (2011) " Cladding pressures and primary structural system forces of a wood building exposed to strong winds", Can. J. Civ. Eng. 38: 974–983 (2011).
26. Fritz W.P.; Bienkiewicz, B.; Cui B.; Flamand; O.; Ho T.C.E.; Kikitsu H.; Letchford C.; W. and Simiu, E., (2008). "International comparison of wind tunnel estimates of wind effects on low-rise buildings: *test-related uncertainties"*. Journal of Structural Engineering ASCE 134, N12, Dec 2008, pp. 1887-1890.
27. Gerhardt, H.J.; Janser, F.; 1994"Wind loads on wind permeable facades". Journal of Wind Engineering and Industrial Aerodynamics 53, 37–48.
28. Geurts C., Bronkhorst A., Franke J., Grepinet F., Van Bentum C., 2010, "Wind tunnel and CFD modelling of wind pressures on solar energy systems on flat roofs" The fifth international symposium on computational wind engineering (CWE2010)
29. Geurts, C., & Steenbergen, R. (2009). "Full scale measurements of wind loads on stand-off photovoltaic systems". In C. Borri (Ed.), 5th European and African conference on wind engineering, EACWE, Florence, Italy, (pp. 1-12).
30. Geurts, C.P.W., Van Bentum, C.A., (2007). "Wind loads on solar energy roofs", Heron 52 (3), 201–222.
31. Geurts, C.; and Blackmore, P. (2013). "Wind loads on stand-off photovoltaic systems on pitched roofs". Journal of Wind Engineering and Industrial Aerodynamics, 123: 239-249.
32. Habte F. et al, (2017), "Wind loading on ridge, hip and perimeter roof tiles: A full-scale experimental study", Journal of Wind Engineering and Industrial Aerodynamics, J. Wind Eng. Ind. Aerodynamics, Elsevier, 166 (2017), P 90-105.
33. Höffer R., Galffy Mozes, Niemann H. J., (2007), "Wind-induced random vibrations of structures", Institute for Structural Engineering, Faculty of Civil Engineering, Ruhr-University Bochum, Germany. CISM International Centre for Mechanical Sciences, Wind Effects on Roofs and Design of Wind-Sensitive Structures, Vol. 493, PP 105-136.
34. Holmes J. D, (2001), reprinted 2003, "Wind loading of structures", Spon Press, 29West 35th Street, New York, NY 10001, P 366.

35. Holmes J.D. and Best R.J., (1977) "Wind tunnel measurements of mean pressure on building models and comparison with full-scale data", 6th Australian Hydraulics and Fluid Mechanics Conference, Adelaide, Australia, 1977.
36. Holmes, J. D. (1973) 'Wind pressure fluctuations on a large roof', Ph.D. thesis, Monash University, Australia.
37. IEA,International Energy Agency, (2014), "Performance and Reliability of Photovoltaic Systems,Subtask 3.2: Review of Failures of Photovoltaic Modules", External final report IEA-PVPS March 2014, ISBN 978-3-906042-16-9.
38. Irtaza H., Agarwal A., (2018), "CFD Simulation of Turbulent Wind Effect on an Array of Ground-Mounted Solar PV Panels", J. Inst. Eng. India Ser. A (June 2018) 99(2):205–218
39. Kopp, Gregory A; Pratt, R. Nicolas, "Velocity measurements around low-profile, tilted, solar arrays mounted on large flat-roofs, for wall normal wind directions", University of Western Ontario, Boundary Layer Wind Tunnel Laboratory, Faculty of Engineering, London, Ontario, Canada N6A5B9, Journal of Wind Engineering and Industrial Aerodynamics, J. Wind Eng. Ind. Aerodynamics, Elsevier, 123 (2013), 226-238.
40. Kopp G. A. and Pratt R. N., (2013), "Velocity measurements around low-profile, tilted, solar arrays mounted on large flat-roofs, for wall normal wind directions", Journal of wind engineering and industrial aerodynamics, 123 (2013) 226–238.
41. Kopp, Gregory A; Gavanski, Eri; Kordi, Bahareh; Vickery, Peter J; "Wind loads on roof sheathing of houses", Journal of Wind Engineering and Industrial Aerodynamics, J. Wind Eng. Ind. Aerodynamics, Elsevier, 114 (2013) 106–121.
42. Kopp, Gregory A, "Guest Editorial for SI: Solar array and wind loads", University of Western Ontario, Boundary Layer Wind Tunnel Laboratory, Faculty of Engineering, London, Ontario, Canada N6A5B9, Journal of Wind Engineering and Industrial Aerodynamics, J. Wind Eng. Ind. Aerodynamics, Elsevier, 123 (2013), P 191.
43. Kopp, Gregory A; Farquhar, Steve ; Morrison, Murray J.; "Aerodynamic mechanisms for wind loads on tilted, roof-mounted, solar arrays" Journal of Wind Engineering and Industrial Aerodynamics, 111 (2012) 40–52.
44. Kopp, Gregory A; Oh, Jeong Hee "An experimental study of pressure distributions within an air-permeable, double-layer roof system in regions of separated flow", Journal of Wind Engineering and Industrial Aerodynamics, 138 (2015) 1-12.

45. Kumar, K. (2000). Pressure equalization of rain screen walls: a critical review. Building and Environment, 35: 161-179.
46. Mendis P. et al, (2007), "Wind Loading on Tall Buildings" EJSE Special Issue.
47. National Building Code of Canada 2010, Structural Commentaries.
48. NBCC, National Building Code of Canada, 2010.
49. O'Brien, C., Neff, D., Bienkiewicz, B., & Dinwoodie, T. (2004). Optimization of wind resistance of photo voltaic roofing systems. Structures 2001 (pp. 2578-2587). Reston, VA: American Society of Civil Engineers.
50. Oh, Jeong Hee (2014) "Wind-Induced Pressures in Air Permeable, Double-Layer Roof Systems in Regions of Separated Flow", PHD thesis, The University of Western Ontario.
51. Optimum Tilt of Solar Panels, (2016), http://www.solarpaneltilt.com/.
52. Pratt, R. Nicolas; Kopp, Gregory A., (2013) "Velocity measurements around low-profile, tilted, solar arrays mounted on large flat-roofs, for wall normal wind directions", Journal of Wind Engineering and Industrial Aerodynamics, 123 (2013) P 226-238.
53. Quick Mount PV. Mounting Solutions, (2016), www.quickmountpv.com, 2700 Mitchell Dr., Bldg 2 | Walnut Creek, CA 94598.
54. Radu, A; Axinte, E.; Theohari, C.; 1986. "Steady wind pressures on solar collectors on flat-roofed buildings". Journal of Wind Engineering and Industrial Aerodynamics 23, 249–258.
55. Reina G.P., De Stefano G., 2017, "Computational evaluation of wind loads on sun-tracking ground-mounted photovoltaic panel array", Journal of Wind Engineering and Industrial Aerodynamics 170 (2017) 283-293.
56. Reynolds A. J., (1974) "Tubulent Flows in Engineering", Department of Mechanical Engineering, Brunel University, London, PP. 462.
57. Richardson, G.M. et al. (1991), "Comparisons of wind-tunnel and full-scale surface pressure measurements on low-rise pitched-roof buildings" Journal of Wind Engineering and Industrial Aerodynamics, Elsevier Science Publishers B.V., Amsterdam, Netherlands. 38 (1991) 249-256.
58. Robertson, A.P., Hoxey, R., Moran, P., (1985). "A full-scale study of wind loads on agricultural ridged canopy roof structures and proposals for design". J. Wind Eng. Ind. Aerodyn. 21, 167–205.

59. Samani, Zeinab; Thesis 2016 “Wind Loading on Full-scale Solar Panels”, The University of Western Ontario Graduate Program in Civil and Environmental Engineering, Supervisors Horia Hangan, Girma Bitsuamlak.
60. Schellenberg, Andreas; Maffeib, Joe; Telleen, Karl and Wardc, Rob; (2013), “Structural analysis and application of wind loads to solar arrays”, Journal of Wind Engineering and Industrial Aerodynamics, 2, Elsevier, 2 Aug., 2013, 123, P 261-27.
61. SEAOC, Solar Photovoltaic Systems Committee, (2012) “Wind Design For Low-Profile Solar Photovoltaic Arrays On Flat Roofs”, Report SEAOC PV2-2012, August 2012.
62. Shademan M., Hangan H., (2009), “Wind loading on solar panels at different inclination angles”, 11th American conference on Wind Engineering- San Juan, Puerto Rico, June 22-26, 2009.
63. Solar America for Codes and Standards, “Wind Loads Calculations for PV Arrays, June 2010.
64. Solar Energy Industries Association (SEIA), (2015) “Solar Energy Facts: Q2 2015, Solar Leading The Way With 40% Of All 2015 Electric Capacity”. http://www.seia.org/research-resources/solar-industry-data.
65. Solar Pro, “Pitched roof PV mounting”, Issue 3.2 Feb/March 2010,
66. Solar Vision 2025 Canadian Solar Industries Association, (CANSIA, 2010), Beyond Market Competitiveness, December 2010.
67. Stathopoulos T and Zhou Y.S, 1995, “Numerical evaluation of wind pressures on flat roofs with the k-ε model”, Pergamon (Elsevier later).
68. Stathopoulos, Ted. (1979) Turbulent Wind Action on Low Rise Buildings, Ph. D. Thesis, The University of Western Ontario.
69. Stathopoulos, Ted et al, (1983), “Scale Effects in Wind Tunnel Testing of Low Buildings” Journal of Wind Engineering and Industrial Aerodynamics, 13 (1983) P313–326.
70. Stathopoulos, Ted; Xypnitou, Eleni; Zisis, Ioannis; “Local and overall wind pressure and force coefficients for solar panels” Journal of Wind Engineering and Industrial Aerodynamics, 125 (2014) P195-206.
71. Stathopoulos, Ted; Xypnitou, Eleni; Zisis, Ioannis; “Wind Loads on Rooftop Solar Panel Systems: A Contribution to NBCC 2015”, The International Association for Wind Engineering (IAWE) 2015
72. Unirac Code- Compliant Installation Manual, (2014).

73. Unirac Installation Manual, (2009) April.
74. Wang, Kai; Thesis (1998), " wind pressure coefficients for gable roofs of intermediate slopes", Concordia University, Montreal, Quebec, Canada, October 1998
75. Wind records are published on 3/19/2012 by Colorado State University, USA, from real measurements taken at Pingree Park, Site #4050, ALP 81 - CSU Pingree Park Campus, Larimer County, CO. http://projects-web.engr.colostate.edu/ALP/ALP_81_Pingree_Park.htm.
76. Wood, G.; Denoon, R.; Kwok, K. (2001). "Wind loads on industrial solar panel arrays and supporting roof structure". Wind and Structures, 4(6): 481-494.
77. Xypnitou, Eleni; "Wind Loads On Solar Panel Systems Attached To Building Roofs" A thesis in the department of building, civil and environmental engineering, Concordia University Montreal, Quebec, Canada. Supervisor, T. Stathopoulos.
78. Zisis, I., (2006), "Structural monitoring and wind tunnel studies of a low wooden building". MASc Thesis, Concordia University, Montreal, QC, Canada. 2006.
79. Zisis, Ioannis G., (2011) "Wind Load Paths on Wood Buildings", PhD thesis, Concordia University, Montreal, QC, Canada.

Appendix A

Chapters 1-3

A-I- Turbulence intensities

The root mean square (RMS) data extracted from the wind speed measurements measure gustiness in a turbulence and is defined as per Eq. (6), (Holmes J.D.2001):

$$\sigma_u = \frac{1}{T}\left(\int_0^T \left[U_t - \overline{U}\right]^2\right)^{\frac{1}{2}} \tag{6}$$

Where: Ut is velocity total component in direction of mean wind and $U_t = \overline{U} + u(t)$

u(t) is turbulence velocity component along longitudinal axis u. Similarly, other standard deviations can be calculated in the other two coordinate directions. (Holmes J.D.2001)

Another parameter characterizing the gustiness in wind flow is the turbulence intensity which is defined as the ratio of the standard deviation of the wind speed to the mean value of the wind speed for a certain direction:

$$I_u = \frac{\sigma_u}{\overline{U}} \tag{7}$$

Iu is known as the longitudinal wind speed deviation and $\overline{U}$ is the mean velocity in the longitudinal direction. Similarly, the Lateral and Vertical deviations can be determined. [Holmes J.D.2001]

Measurements of gales near ground have found that the standard deviation of longitudinal wind speed, σ_u is equal to 2.5 u^* *where* u^* is the friction velocity in Eq. (2). Then the turbulence intensity, *Iu*, is given by:

$$I_u = \frac{\sigma_u}{U_z} = \frac{2.5u^*}{\frac{u^*}{k}\log(\frac{Z}{Z_0})} = \frac{2.5u^*}{\frac{u^*}{0.4}\log(\frac{Z}{Z_0})} = \frac{1}{\log(\frac{Z}{Z_0})} \tag{8}$$

where u^* *is friction velocity*

Eq. 8 shows that the turbulence intensity is related to roughness length, *zo*.
Table 2 shows that the turbulence intensity decreases with the height above the ground for rural terrain, for a roughness length of 0.04 m. [Holmes J.D.2001]

Table A. 1 Longitudinal Turbulence Intensity in Rural Terrain.

Z (m)	2	5	10	20	50	100	200	500	600
I_u	0.26	0.21	0.18	0.16	0.14	0.13	0.12	0.11	0.10

Similarly, the lateral turbulence intensity is [Holmes J.D.2001]:

$$I_u = \frac{\sigma_v}{U_z} = \frac{2.2u^*}{\frac{u^*}{k}\log(\frac{Z}{Z_0})} == \frac{0.88}{\log(\frac{Z}{Z_0})} \tag{9}$$

and the vertical intensity is [Holmes J.D.2001]:

$$I_u = \frac{\sigma_w}{U_z} = \frac{1.4u^*}{\frac{u^*}{k}\log(\frac{Z}{Z_0})} == \frac{1.40}{\log(\frac{Z}{Z_0})} \tag{10}$$

Fig. 7 compares the measured turbulence intensity profiles along a 325 m height tower in China with the calculated profiles according to the ASCE (1999) and AIJ-RLB-1996 [Holmes J.D.2001]. Fig. 7 shows that the ASCE (1999) and AIJ-RLB-1996 codes give unconservative values at the levels 47 m and 120 m above the ground, but they are in good agreement at 280 m height. As a result, the wind- resistant designs of solar panels according to the mentioned codes will be unconservative as the design wind loads are relevant to the turbulence longitudinal profile values. [Holmes J.D.2001]

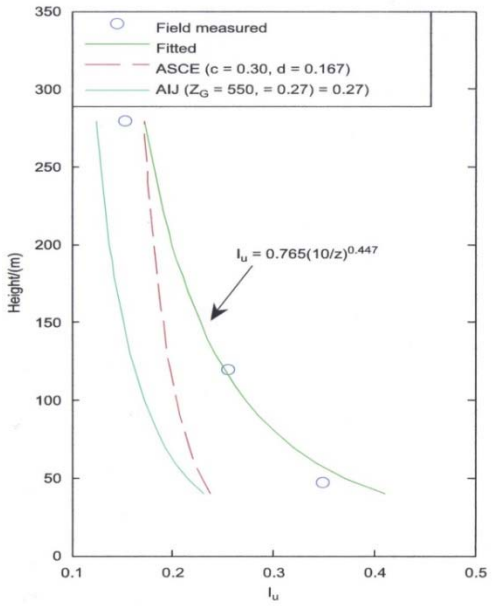


Fig. A. 1. Longitudinal Turbulence Intensity Profiles [See Li Q. S. et al, 2010].

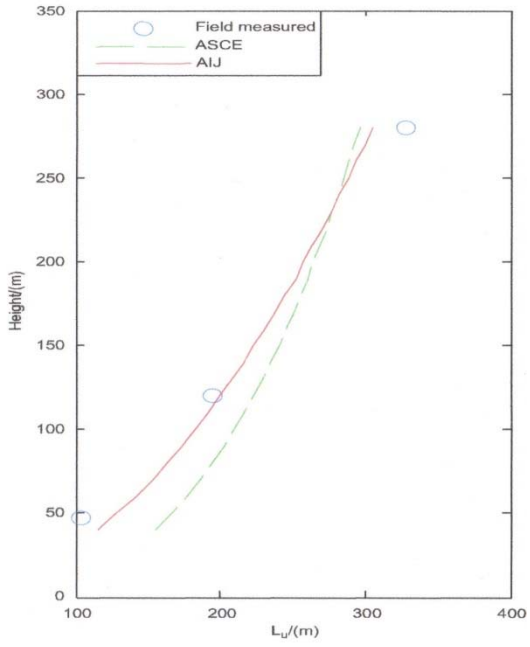


Fig.1-Turbulence longitudinal integral length scale profiles.

Fig. A. 2. "Boundary layer wind structure from observations on a 325 m tower" (See Li Q. S. et al, 2010)

A-II- Integral Scale of Turbulence

Integral scale of turbulence is a measure of the average size of turbulence eddy. The length of eddy development in the longitudinal direction can be estimated from the following equation [Li Q. S. et al, 2010]:

$$L_u^x = \frac{1}{\overline{U}^2}\int_0^\infty Ru_1u_2(x)dx \tag{11}$$

Where, $Ru_1u_2(x)$ is the cross-covariance of the longitudinal velocity components $u_1=u(x_1,y_1, z_1, t)$ and $u_2=u(x+x_1, y_1, z_1, t)$, for which similar velocity components in the three coordinates x, y, z exist for the longitudinal, cross-wind and vertical directions The AIJ-RLB-(1996) and ASCE (1999) design codes estimate the longitudinal turbulence integral length scaled as :

$$L_u^x = 100(\frac{z}{30})^{0.5} \qquad AIJ-RIB-1996$$

$$L_u^x = l(\frac{z}{10})^{\varepsilon'} \qquad ASCE-1999 \tag{12}$$

Where l and ε' are constants depending on terrain. In the previous study (Li Q. S. et al, 2010) was selected as 97.536 m and $\varepsilon'=\frac{1}{3}$ for urban terrain, (Li Q. S. et al, 2010).

A-III- Power Spectral Density of Velocity

Spectral density describes the energy distribution of the wind velocities, and can be estimated from (von Karman, 1948; Panofsky and McCormik, 1959; Davenport, 1961; Kaimal et al., 1972) as follows,

$$\frac{nS_u(n)}{\sigma_u^2} = \frac{4L_u^x n/U}{\left[1+70.8(L_u^x n/U)^2\right]^{5/6}} \qquad \text{Von Karman (Longitudinal)}$$

$$\frac{nS_i(n)}{\sigma_i^2} = \frac{4L_i^x n/U\left[1+755.2(L_i^x n/U)^2\right]}{\left[1+283.2(L_i^x n/U)^2\right]^{11/6}} \quad \text{Where: i=v, w, Von Karman (Lateral and Vertical)}$$

$$\frac{nS_u(n)}{U_0^{*2}} = \frac{4x^2}{\left[1+x^2\right]^{4/3}} \quad Where: x = \frac{1200n}{U(10)} \quad Davenport(Longitudinal) \tag{13}$$

$$\frac{nS_v(n)}{U_0^{*2}} = \frac{15f}{\left[1+9.5f\right]^{5/3}} \quad Where: f = \frac{zn}{U} \quad Kaimal(Lateral)$$

$$\frac{nS_w(n)}{U_0^{*2}} = \frac{6f}{\left[1+4f\right]^{2}} \quad Where: f = \frac{zn}{U} \quad Panofsky(Vertical)$$

Where n is the frequency, z is the anemometer height, U (10) is mean end speed at 10 m height and U_0^* is friction velocity explained elsewhere herein,

Where

f is normalized velocity,

S_u is spectral density in longitudinal direction, S_v. S_w are spectral density in lateral directions.

L_u is a longitudinal turbulence length scale,

L_v, L_w are lateral turbulence length scales,

Fig. 9 shows the averages of the power spectral density functions of the three wind speeds components (longitudinal, lateral and vertical) at different heights of 47, 120 and 280 m (See Li Q. S. et al, 2010). Fig. 10 compares the empirical spectral models with the measured spectral at height 120m. (See Li Q. S. et al, 2010).

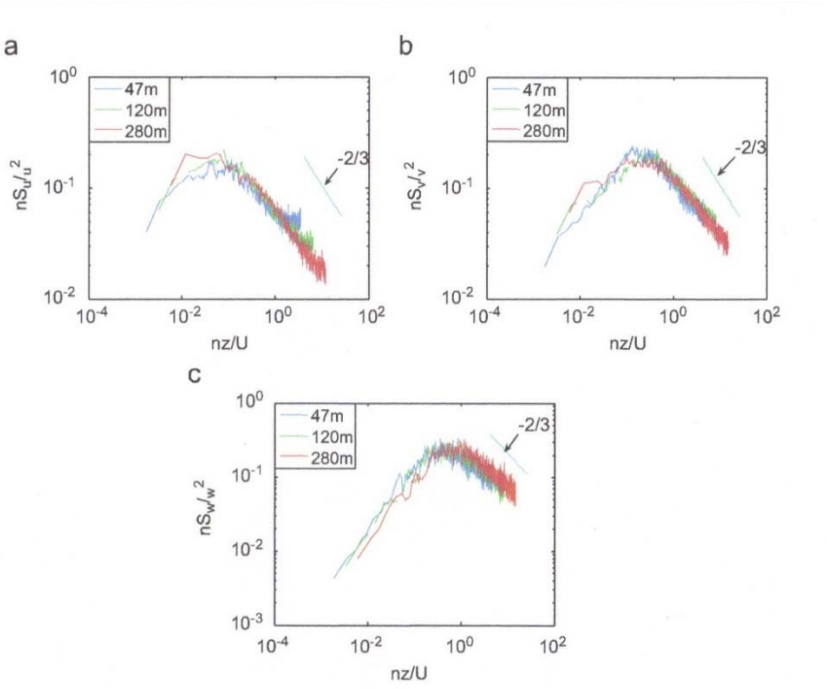


Fig. A. 3. Averages power spectral density functions at 47, 120 and 280 m

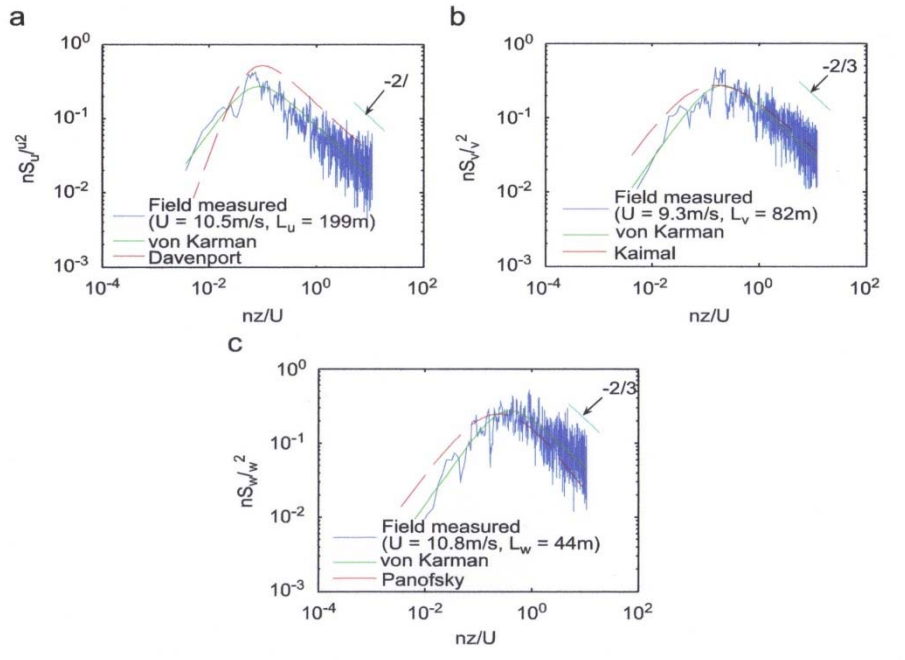


Fig. A. 4. Comparison of empirical spectral models with measured spectral at 120m.

A-IV- Validation case 4: residential building modeled with CFD and LES algorithm

For expanding the CFD simulations for building structures with roof slopes higher than 19.5°, validation using LES algorithm was performed by comparing the pressure results, with the measurements records reported for a full-scale building of dimensions 13.5 m × 7.0 m × 5.73 m (length × width × height which has a roof slope of 22.5° (Apperley et al, 1979). A 1:500 model of the building was also tested, and pressure coefficients measured on the surface of the roof thorough 114 pressure taps located at 203 mm apart to avoid the interference effect. The test wind speed was 15 m/s, while the full-scale measurements were recorded for 30 m/s. The positive pressure peaks and the negative pressure peaks were separately analysed, herewith the negative pressure coefficients peaks described.

As it can be noticed in Figs.3.13 a) and b) the peak negative pressure coefficients were reported in the wind tunnel test were slightly higher than the values reported from the full-scale tests, however for the windward edge of the roof these were in the range of -1.7 to -2.63 and -1.64 to -2.03 for the wind tunnel experiment and the full-scale measurements respectively. Peak pressure coefficients of -2.12 to -0.93 and -1.95 to -0.62 for wind tunnel experiment and the full-scale measurements respectively, were registered for the middle cross-section of the roof.

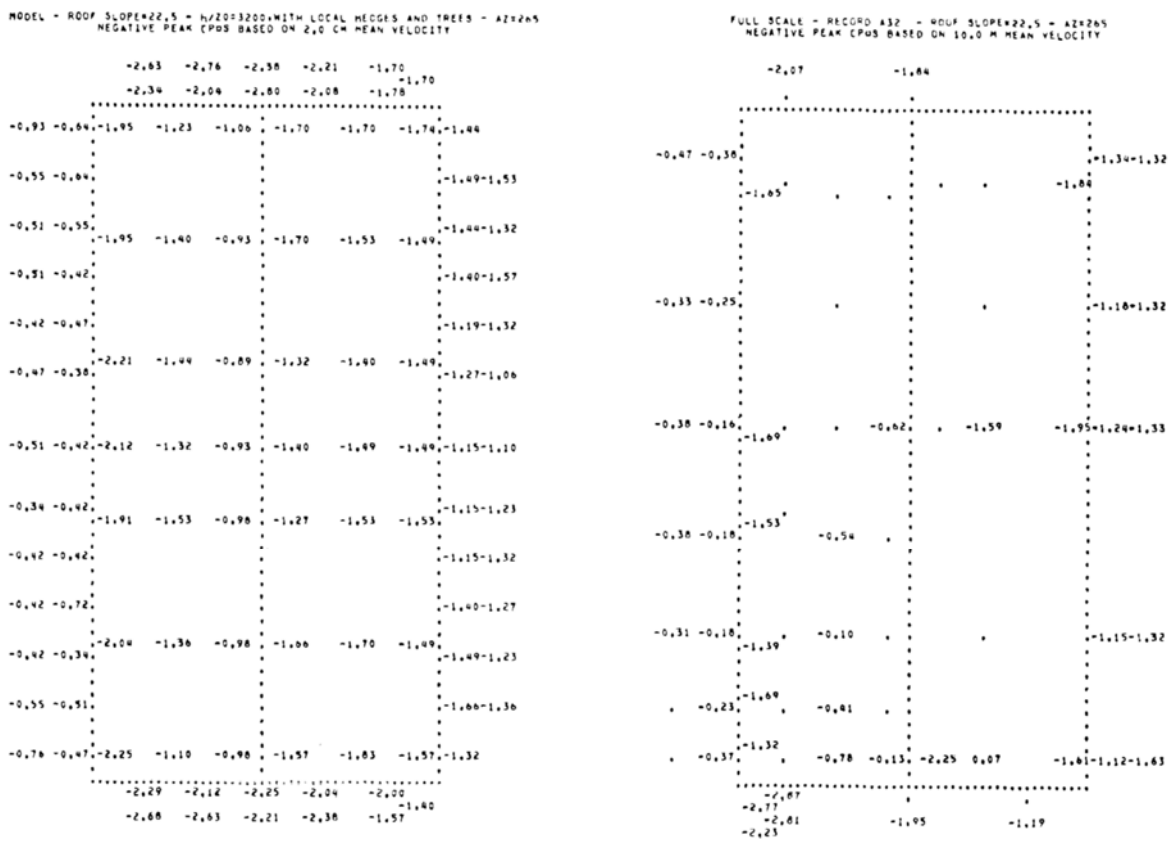


Fig. A. 5. Negative peak pressure coefficients for roof slope 22.5° for a) Wind tunnel model (1:500) and b) Full-scale measurements (Apperley et al, 1979)

The CFD simulations were performed for a building model of the same geometrical sizes and same roof slope as the full-scale building instrumented by Apperley et al, (1979), and pressure coefficients results were compared with the wind tunnel model and the full-scale measurements they reported. Peak negative pressure coefficients of -0.95 to -2.6 were predicted on the windward edge of the roof, and these were in the same range with both the wind tunnel and full-scale pressure coefficients reported by Apperley et al, (1979). However, the pressure coefficients increase towards the interior of the roof perimeter, especially along the ridge, where values of up to -4.7 were obtained, values which were not captured by Apperley et al, (1979) because no pressure taps were installed in that region. Along the middle cross-section of the roof, the peak negative pressure coefficients were in the range of -1.35 to -0.37, results which were in closer agreement with the full-scale measurements than the wind tunnel experiments reported by Apperley et al, (1979).

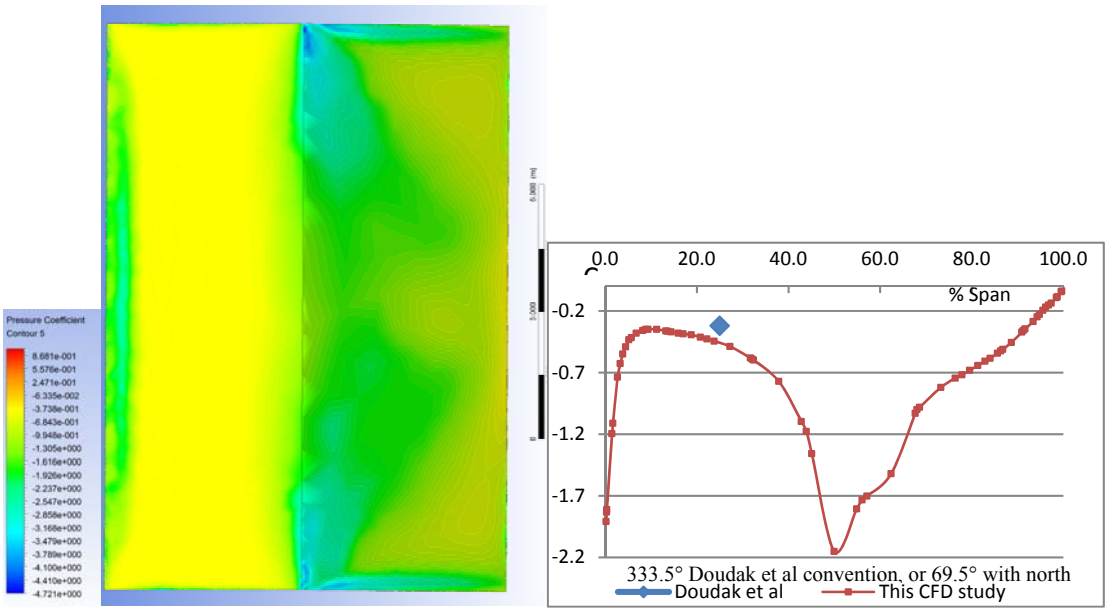


Fig. A. 6. CFD Peak negative pressure coefficients for the residential building roof sloped at 22.5°

A-V- Demonstration of Wind effects on singular solar panels mounted on open bases,

Figs. 3.62 and 3.64 illustrate 4 single panels front and back views, while Figs. 3.63 and 3.65 illustrate 4 double panels with 3" between the pairs. All panels are mounted on open bases ~ 1 m high above ground. The inclinations, from left to right, are 0 º, 15 º, 35 º and -15 º. In comparison, single and pair of solar panels subject to similar pressure coefficients on top and back surfaces.

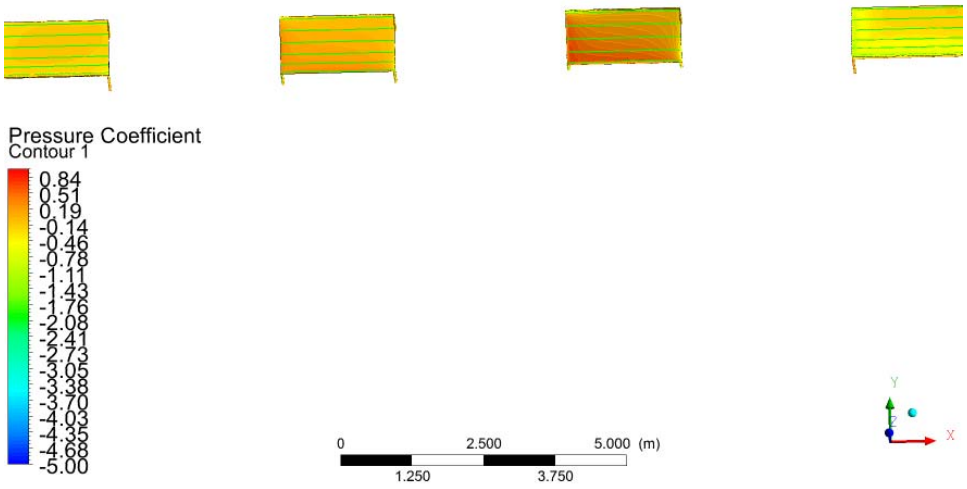


Fig. A. 7. Single panels above open spaces, Top of panels

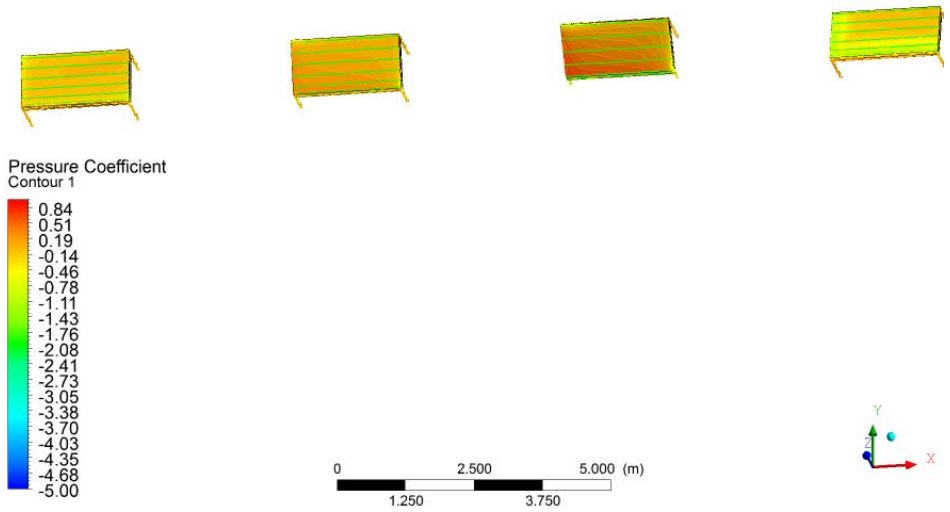


Fig. A. 8. Pairs of Panels with 3” gaps between, mounted of 4 legs and open bases, Top of **panels**

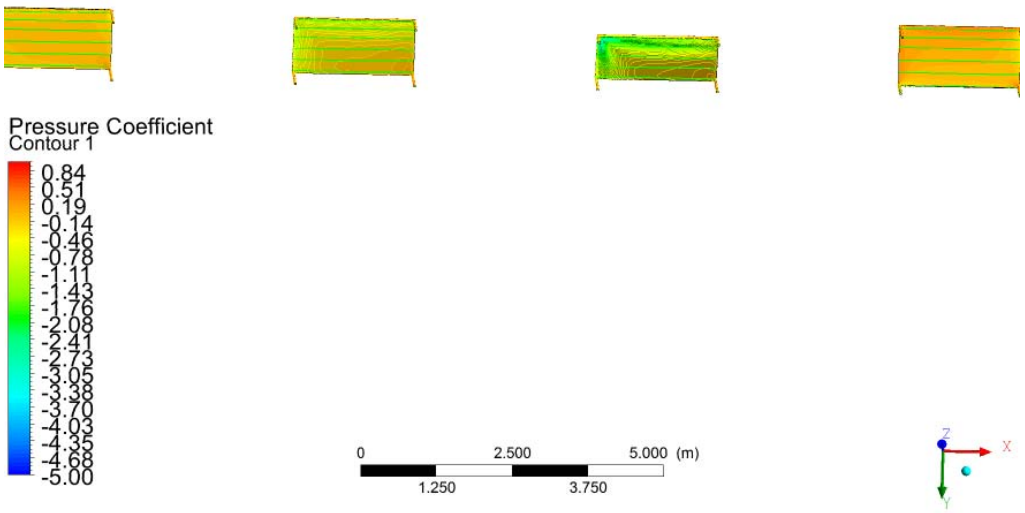


Fig. A. 9. Single panels above open spaces, Bottom of panels

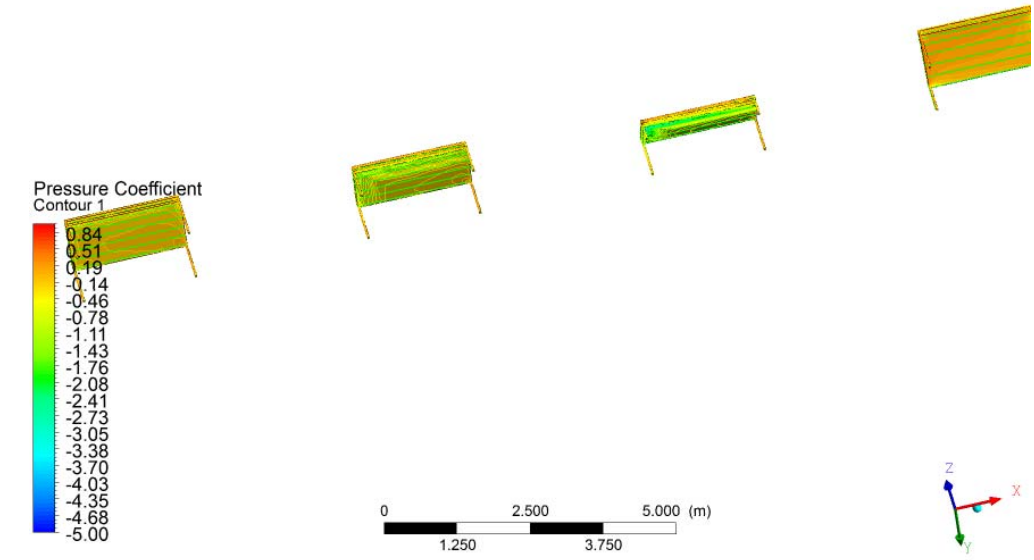


Fig. A. 10. Pairs of panels with 3" gasp above open spaces, bottom of panels

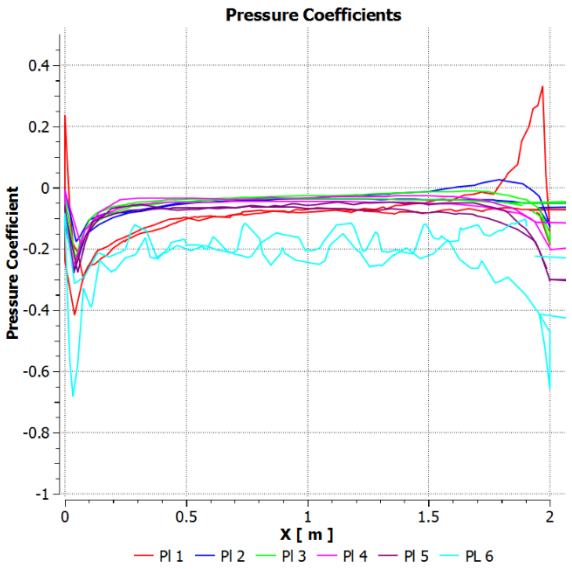


Fig. A. 11. Single Panel, open base, 0 º S, 45WD

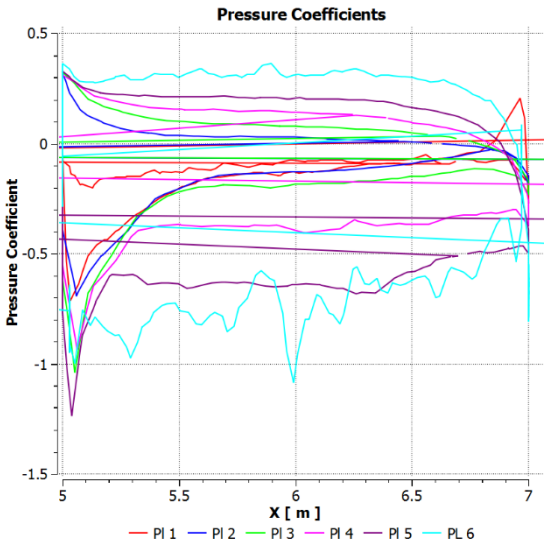


Fig. A. 12. Single Panel, 15 º S, open base, 45 º WD

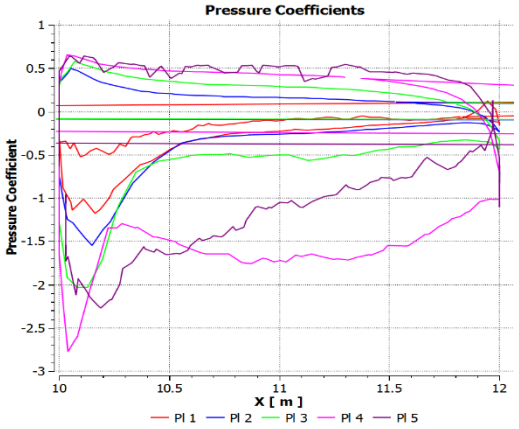


Fig. A. 13. Single Panel, open base, 35 º S, 45WD,

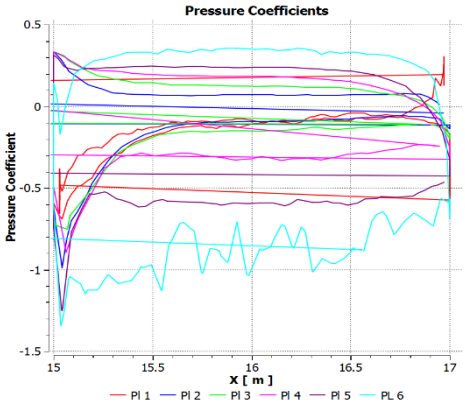


Fig. A. 14. Single Panel, -15 º S, open base, 45 º **WD**

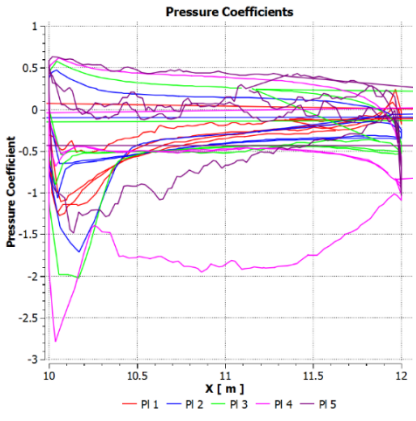


Fig. A. 15. Double Panel 3” gap, open base, 35º S, 45WD

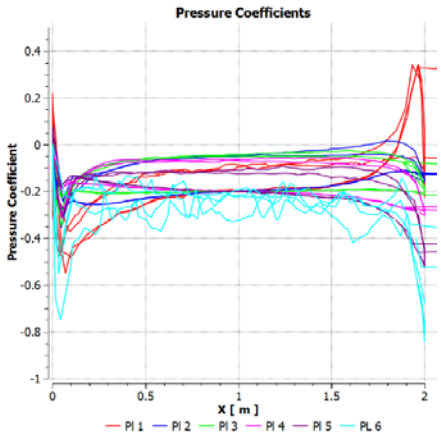


Fig. A. 16. Double Panel 3” gap, open base, 0º S, 45WD

APPENDIX B

Chapter 4

B-I- Pressure coefficients for slope 27º, wind direction 45º, spacing 2", clearance 3"

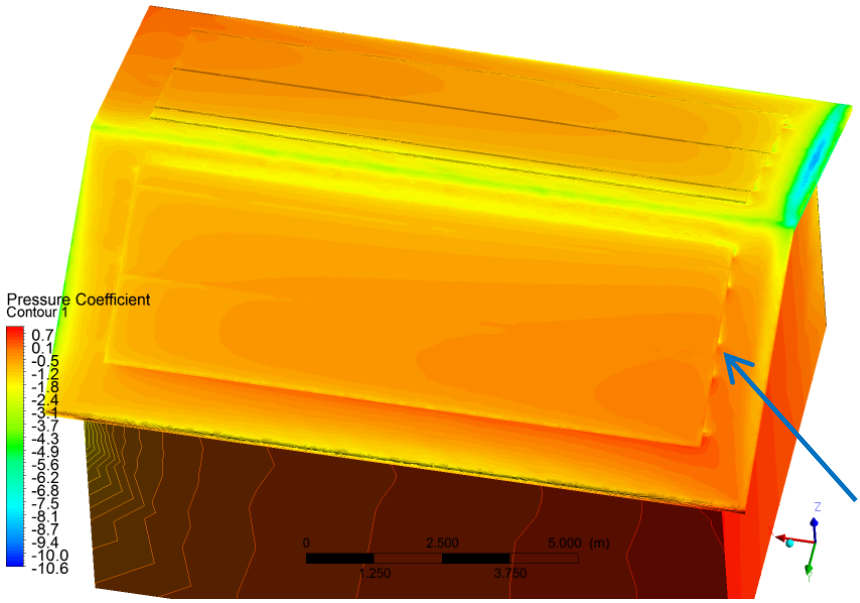


Fig.B. 1, Cp of whole building , WW, WD 45º,

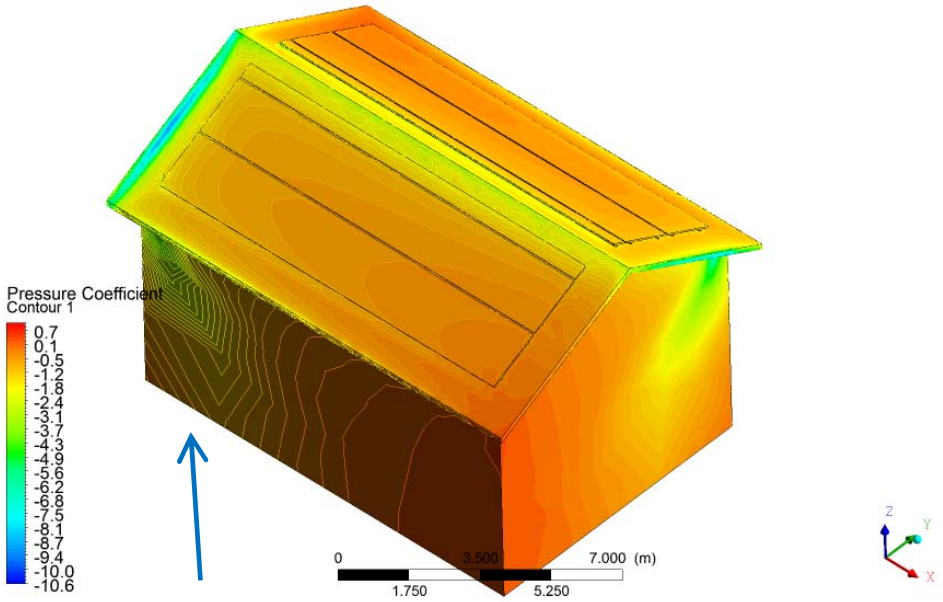


Fig.B. 2, Cp whole building, LW, WD 45º,

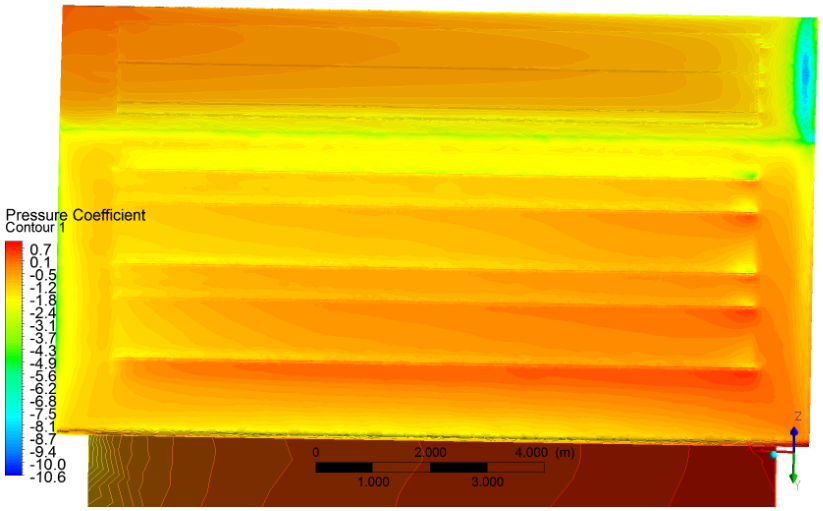


Fig. B. 3. Cp Roof under panels, WW, WD 45º,

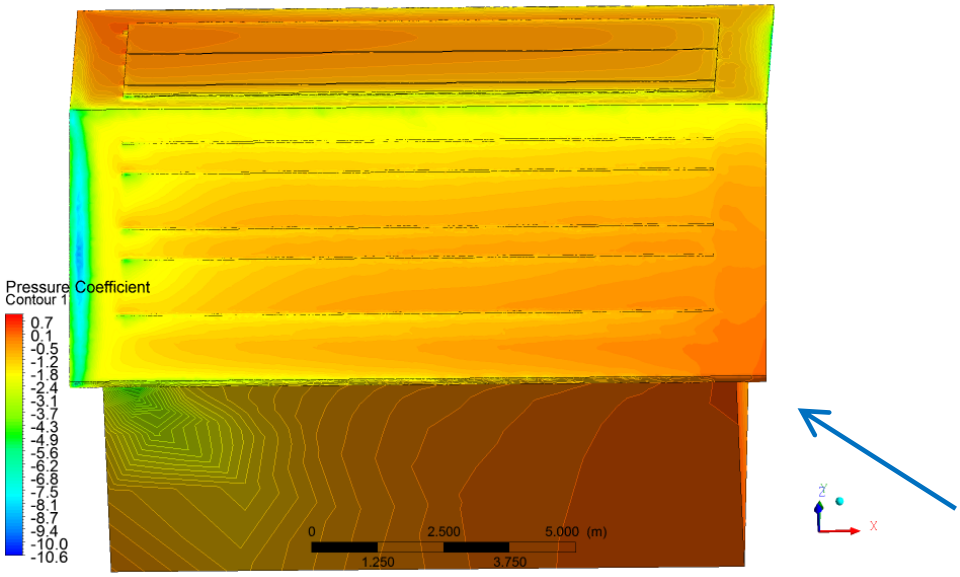


Fig.B. 4. Cp Roof under panels, LW, WD 45º

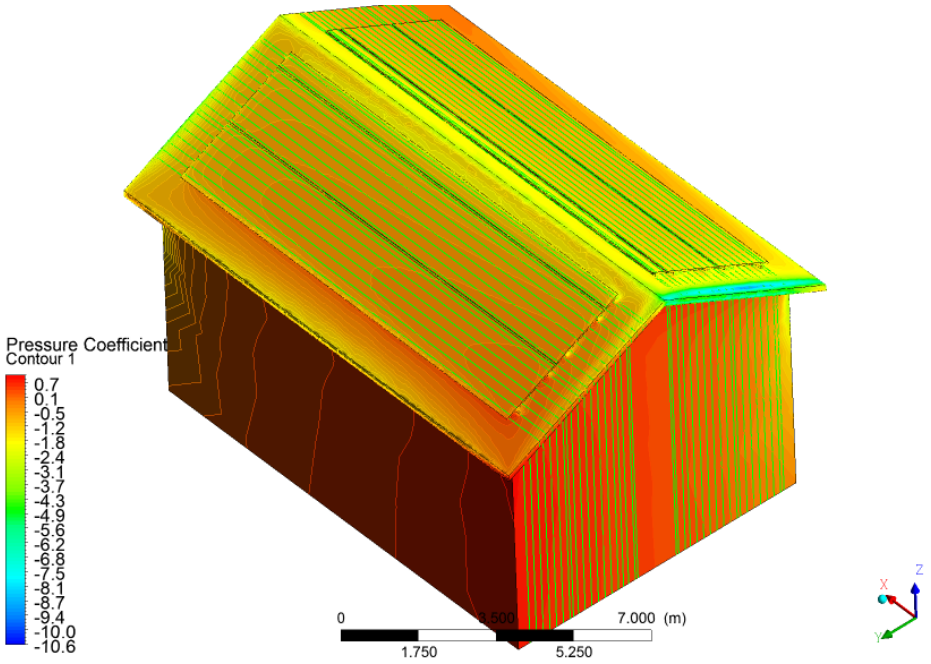


Fig.B. 5, Cp Whole building Plines, WW, WD 45º,

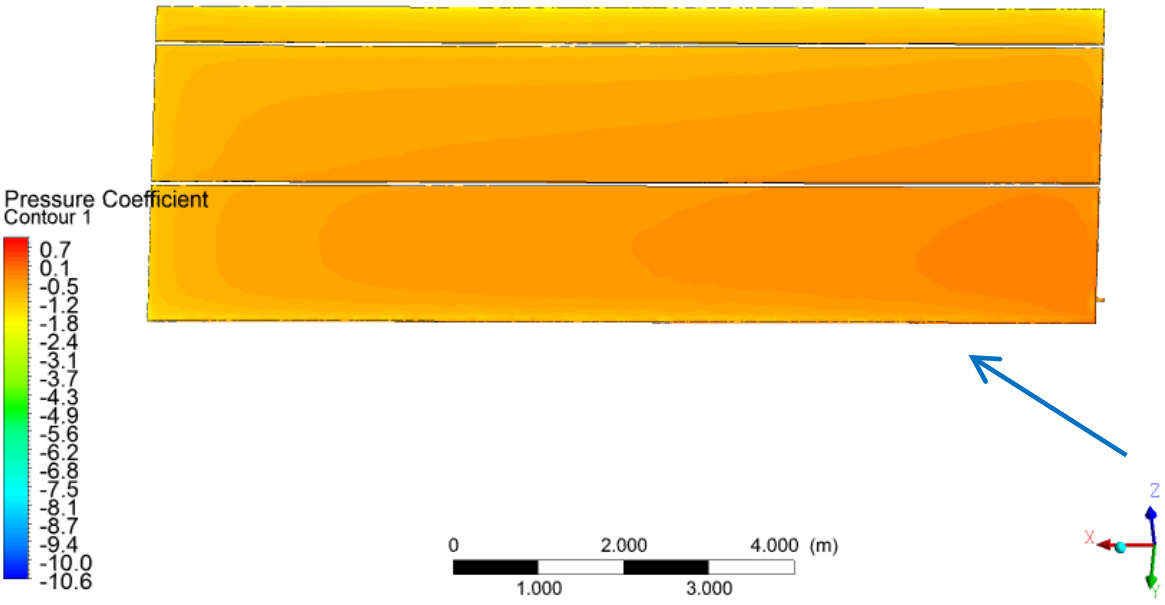


Fig.B. 6, Cp Whole building, Top of panels, WW, WD 45º

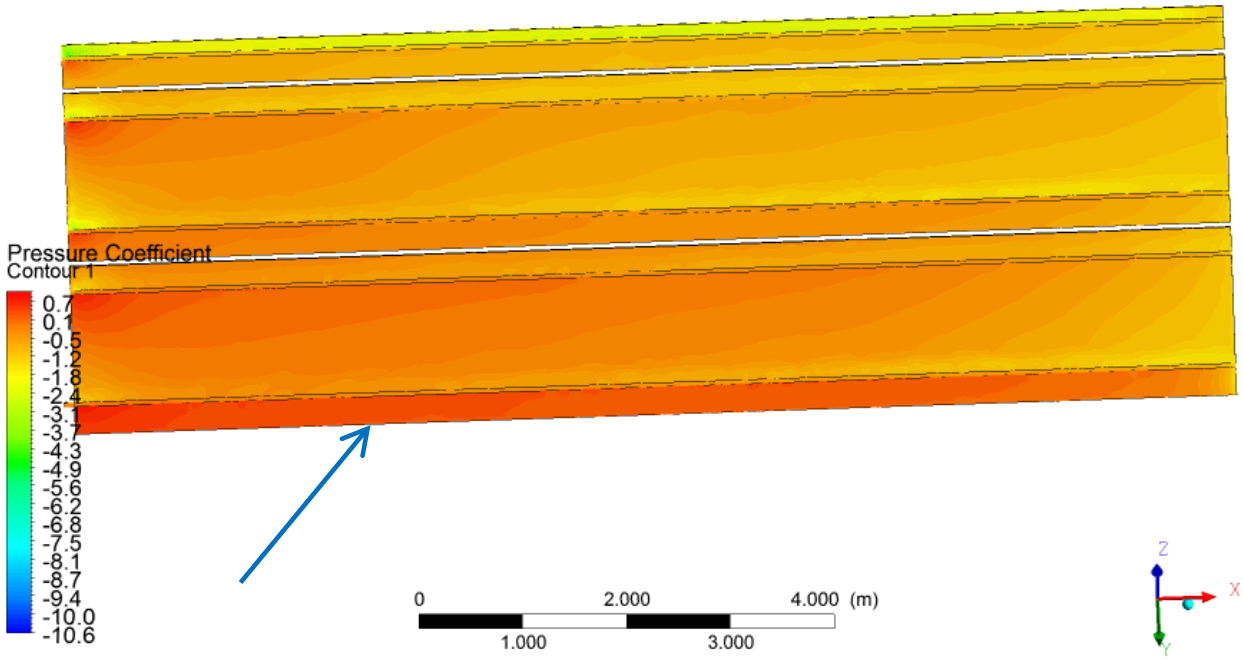


Fig.B. 7, Cp Bottom of panels, WW, WD 45º,

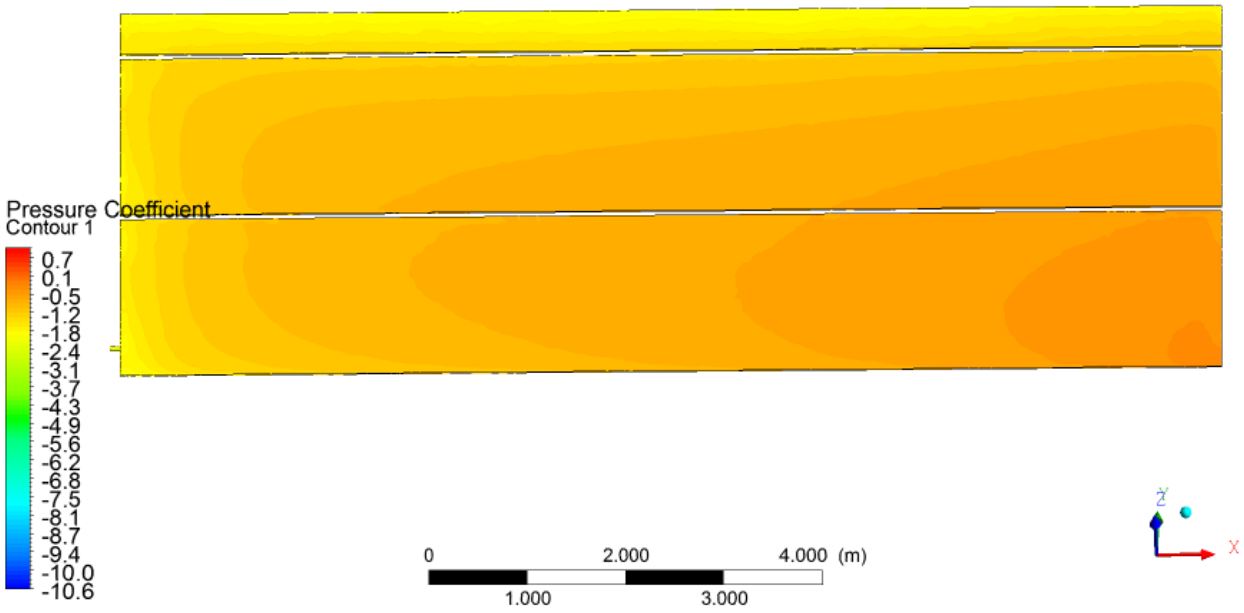


Fig.B. 8, Cp top of panels, LW, WD 45º,

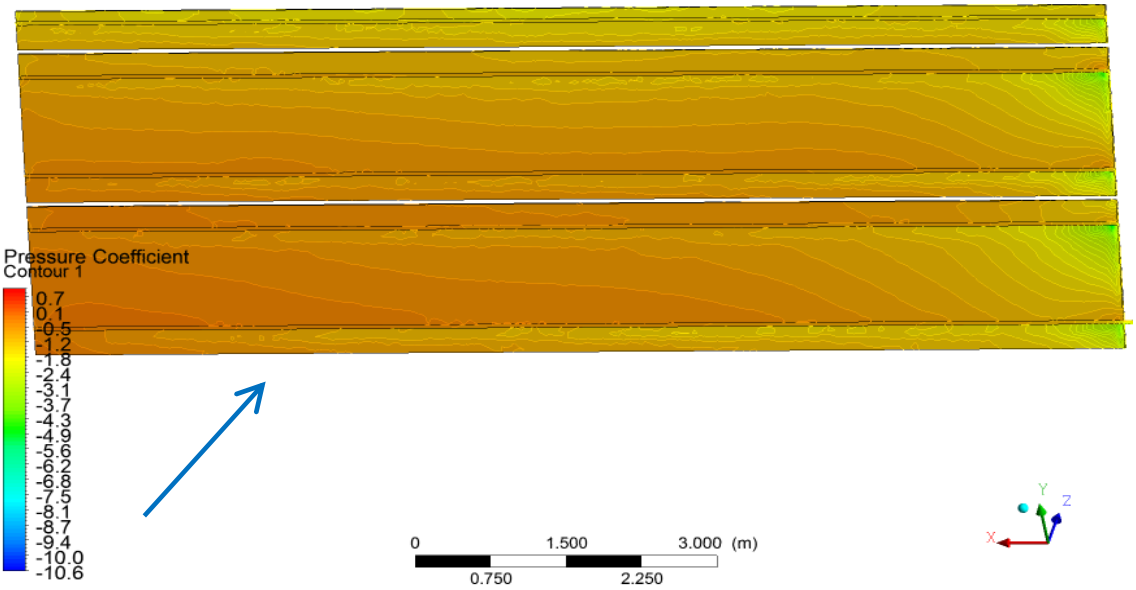


Fig.B. 9, Cp Bottom of the panels, LW, WD 45º,

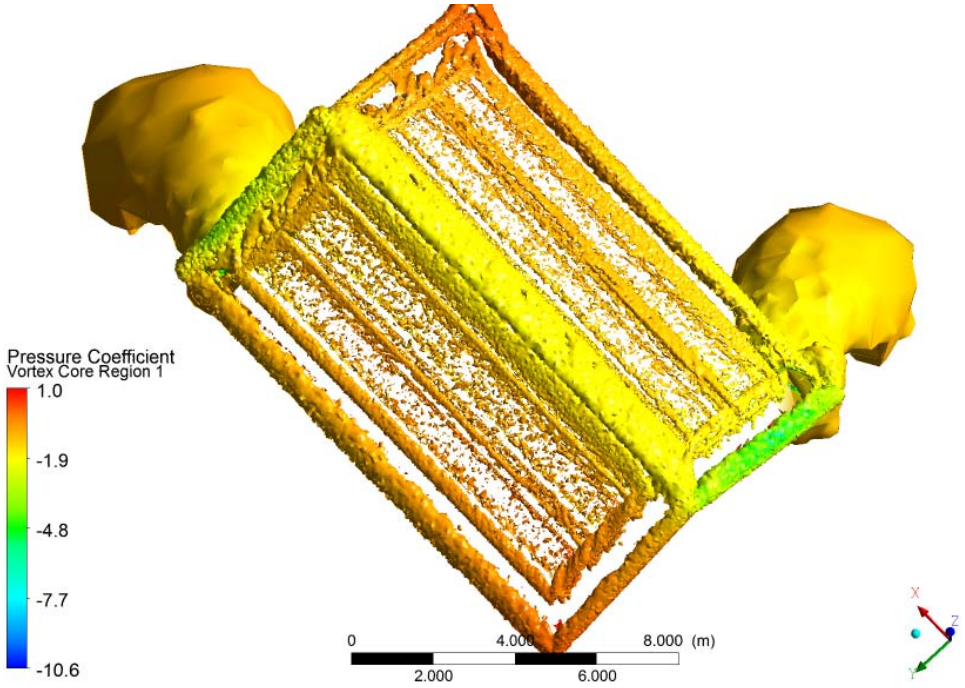


Fig.B. 10, Vortices, top view, WW, WD 45º,

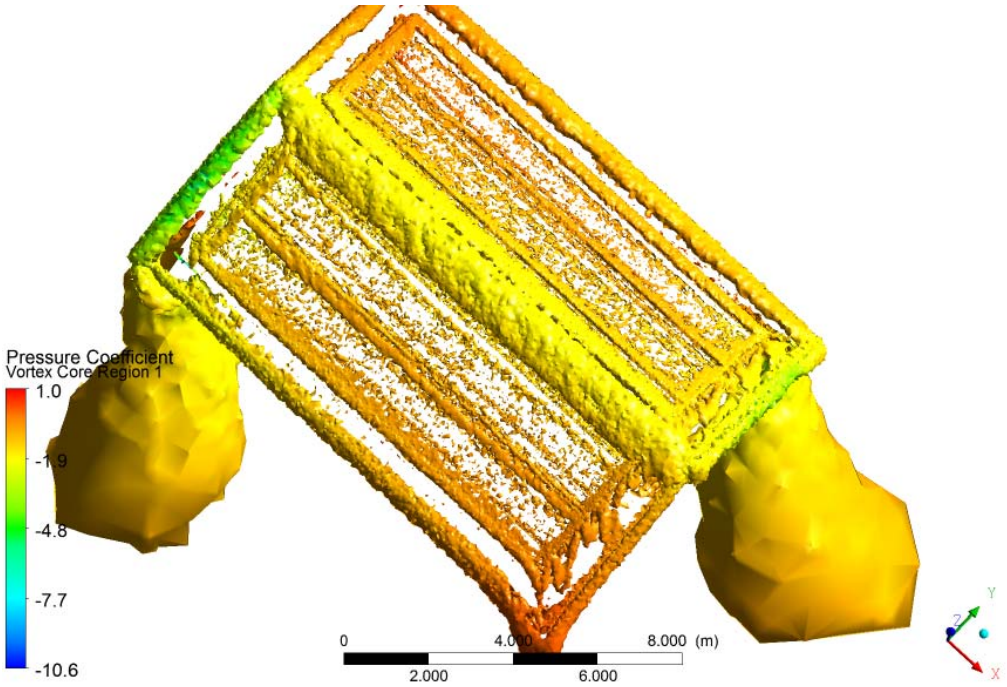


Fig.B. 11, Vortices, LW, WD 45º,

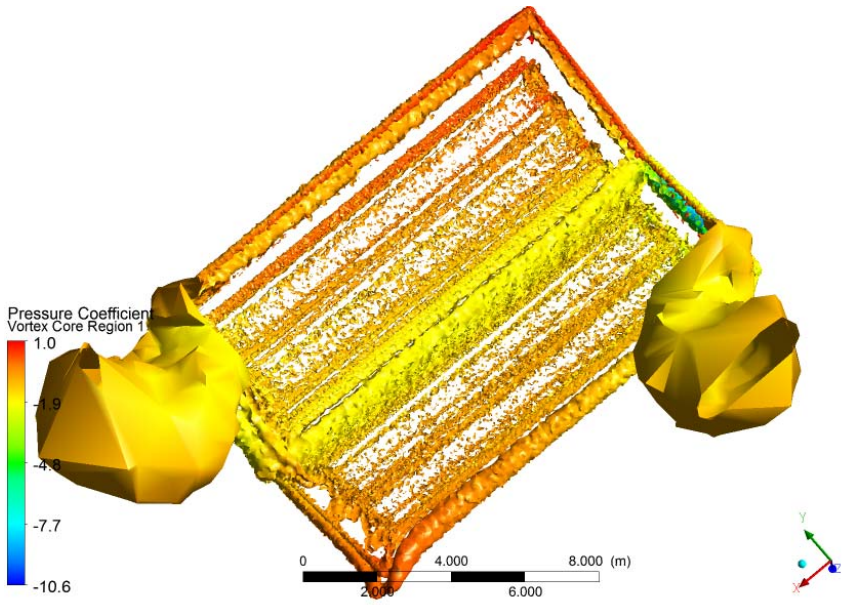


Fig.B. 12, Vortices, under the panels, WD 45º,

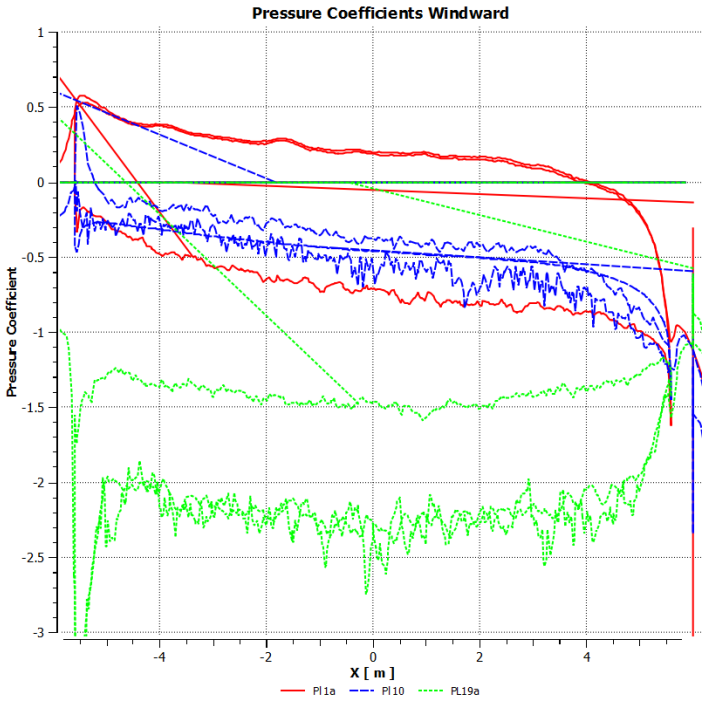


Fig.B. 13, Cp along 3 main polylines, WW, WD 45º,

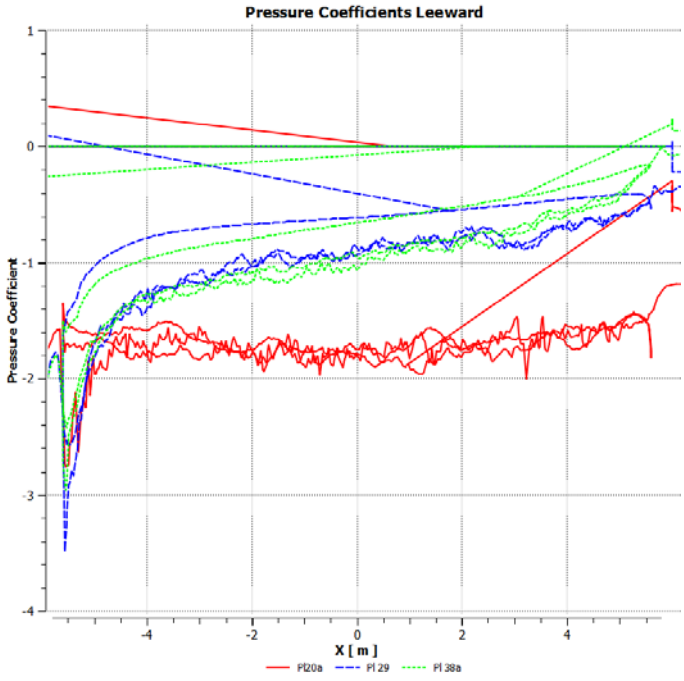


Fig.B. 14, Cp along 3 main polylines, LW, WD 45º,

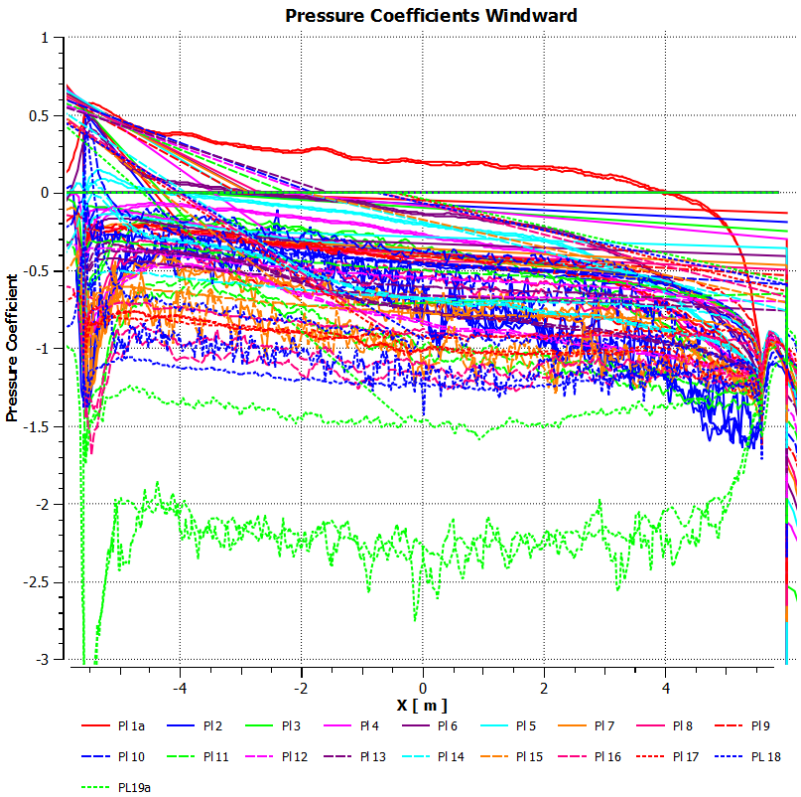


Fig.B. 15, Cp along all the polylines, LW, WD 45º,

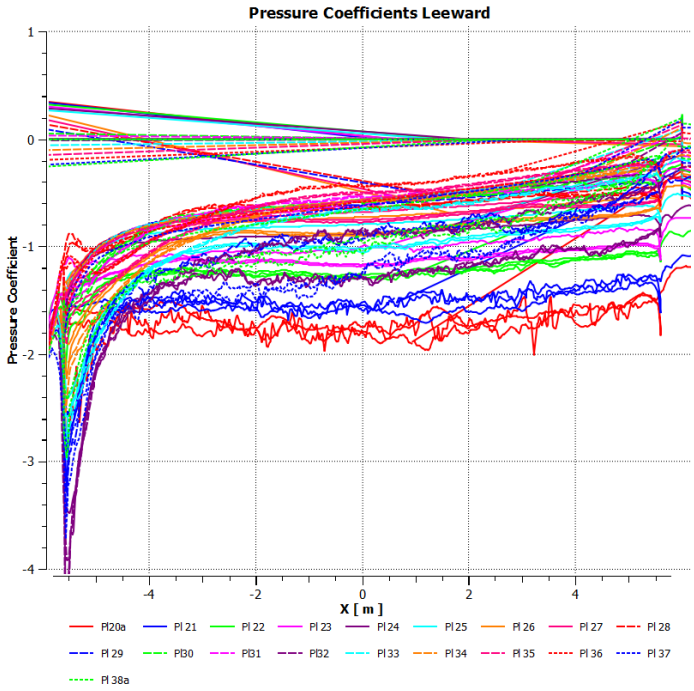


Fig.B. 16, Cp along all the polylines, LW, WD 45º,

B-II- Pressure coefficients for slope 27º, wind direction 0.0º, spacing 2", clearance 3"

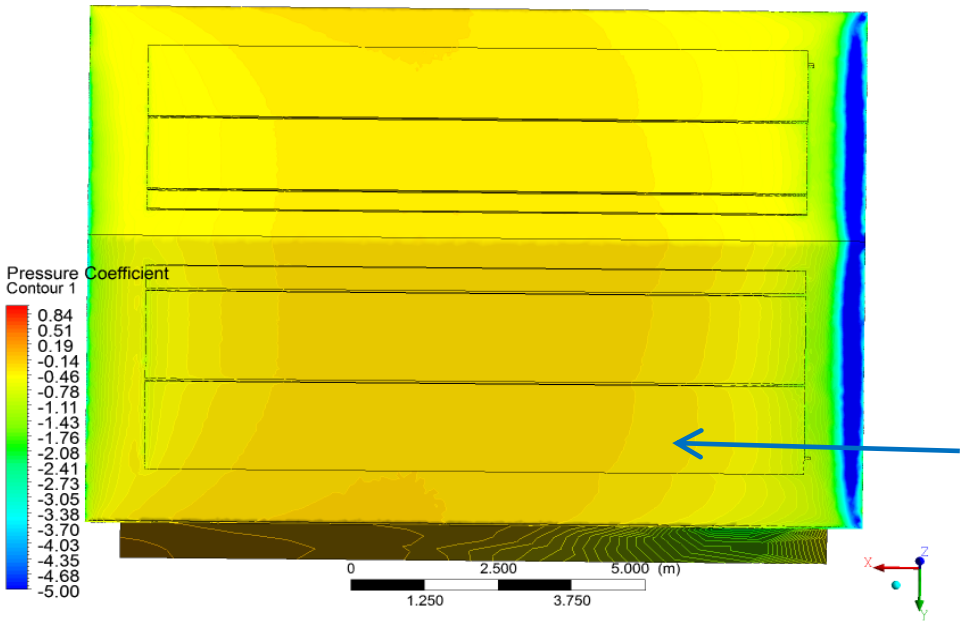


Fig.B. 17, Cp of whole building, Top view, WD 0.0º,

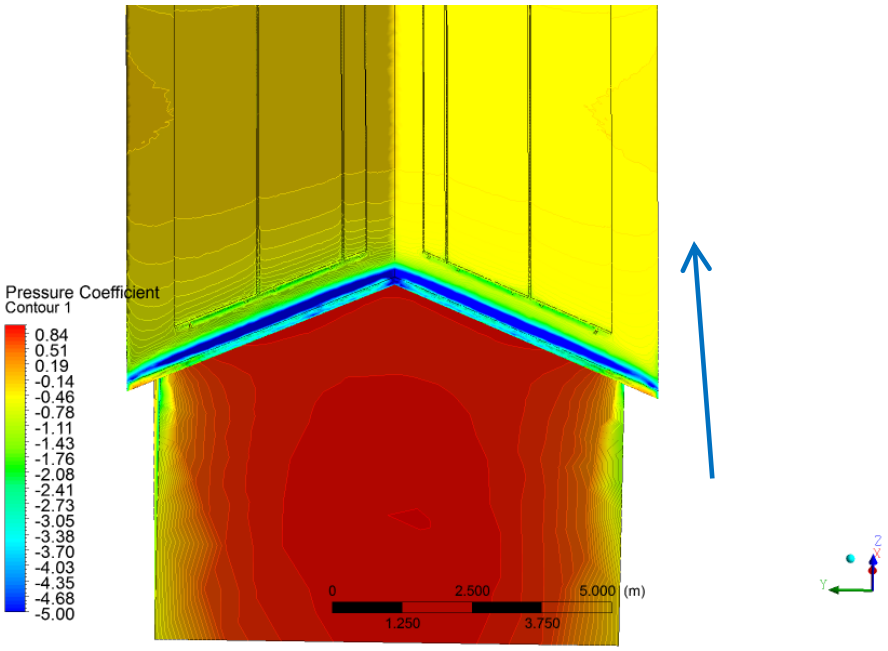


Fig.B. 18, Cp whole building, WW, WD 0.0º

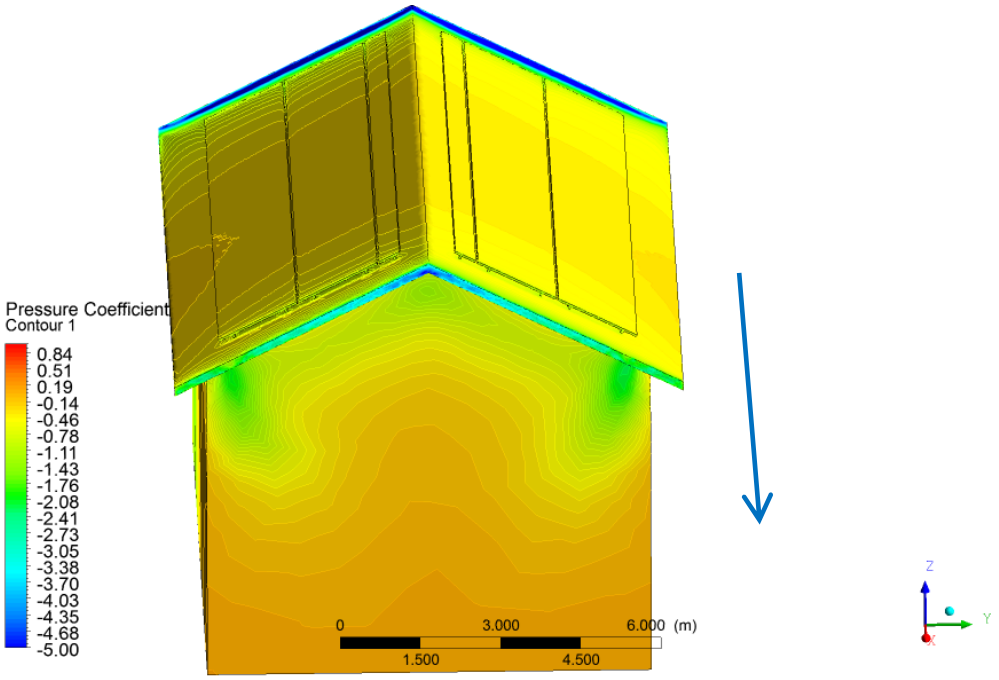


Fig.B. 19, Cp whole building, LW, WD 0.0º

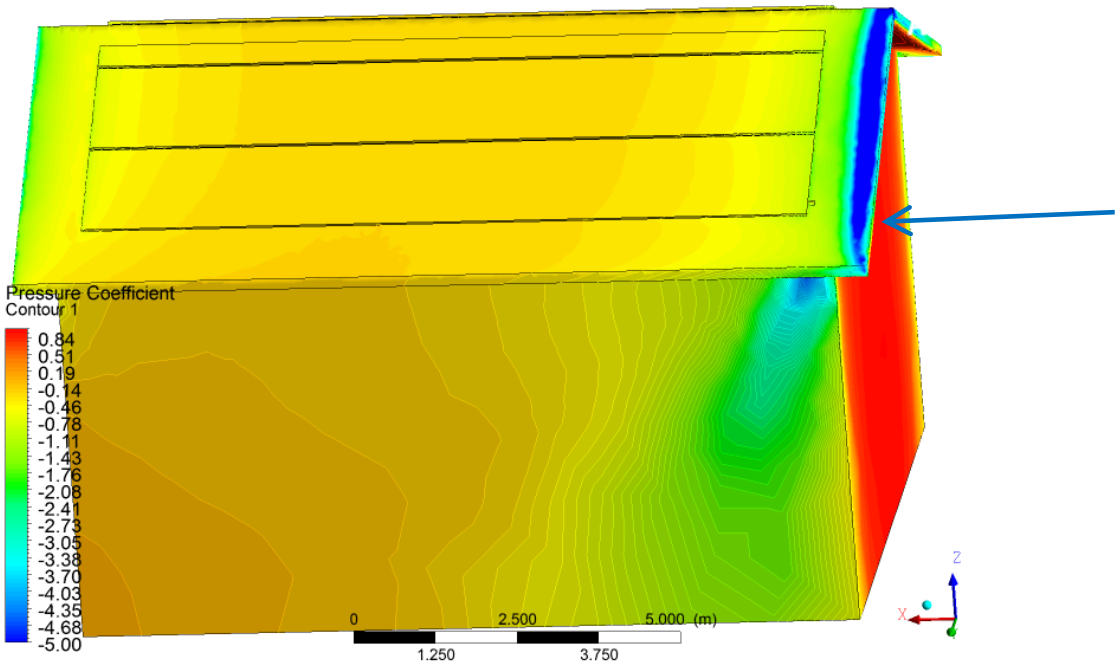


Fig.B. 20, Cp side of the building, WD 0.0º

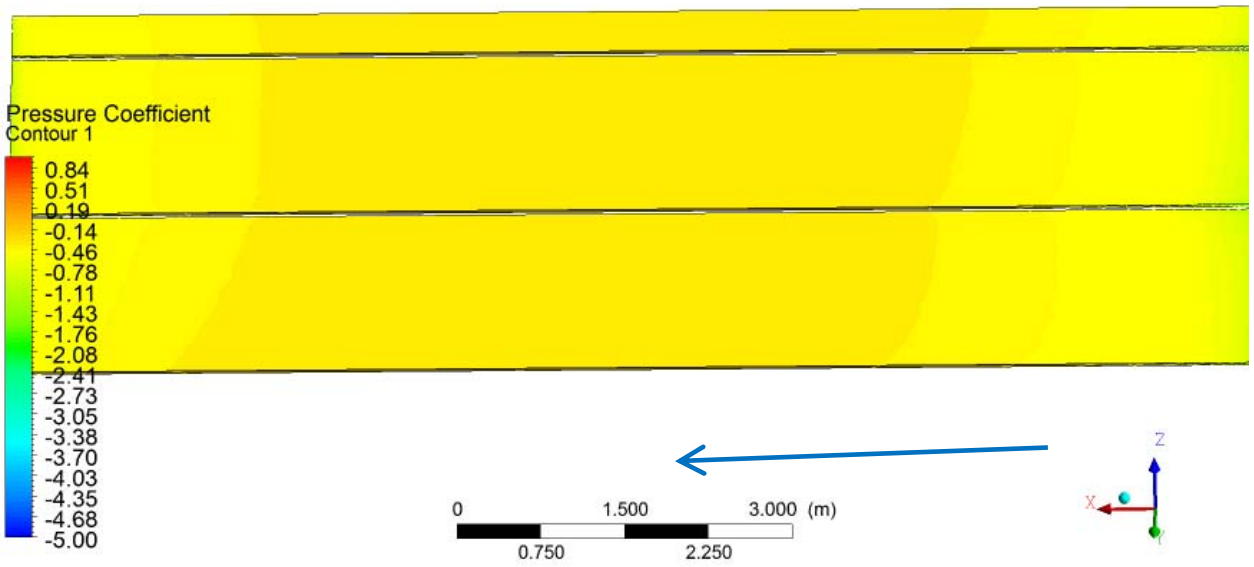


Fig.B. 21, Cp Top of the panels, WD 0.0º

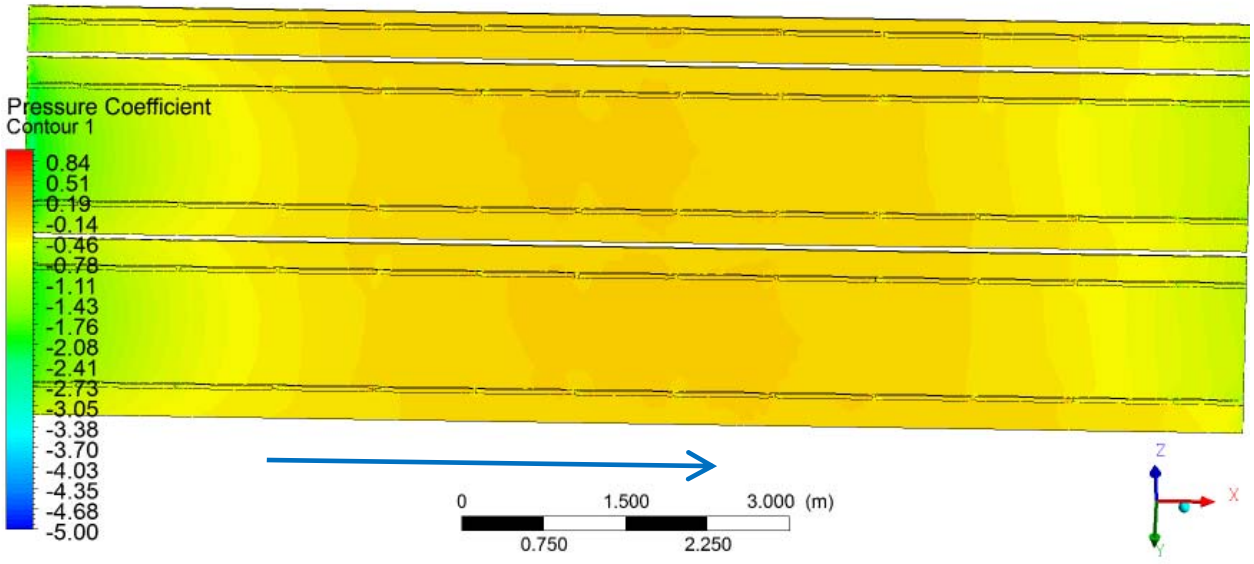


Fig.B. 22, Cp Bottom of the panels, WD 0.0º,

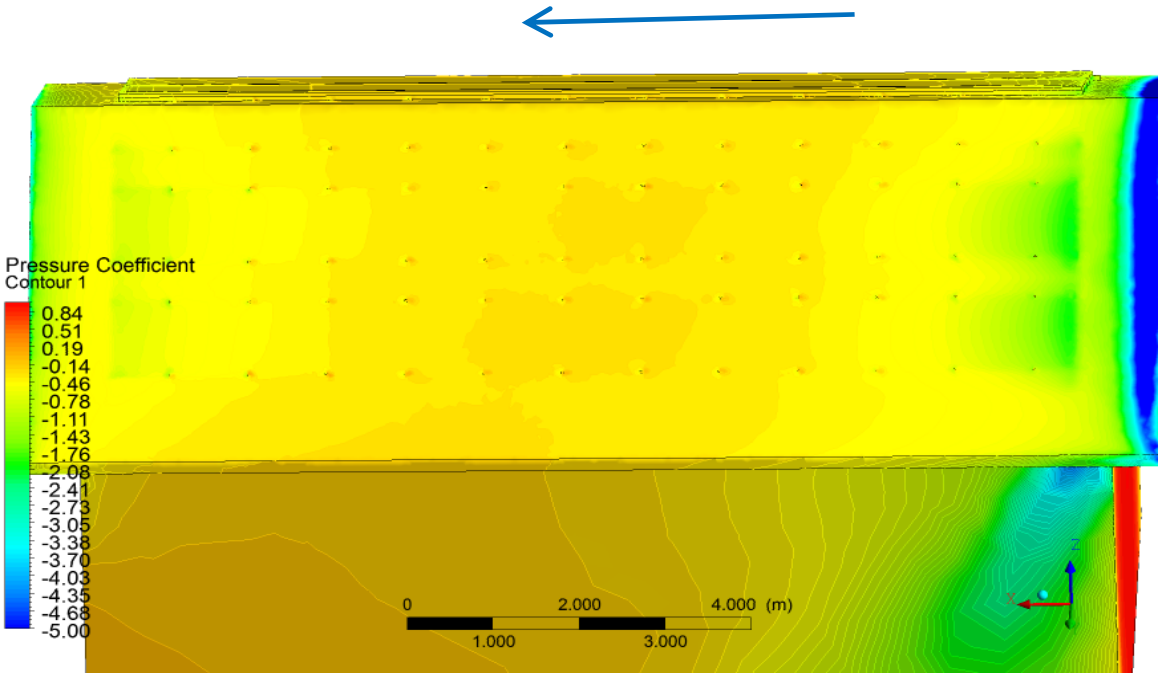


Fig.B. 23, Cp Roof surface under the panels, WD 0.0º,

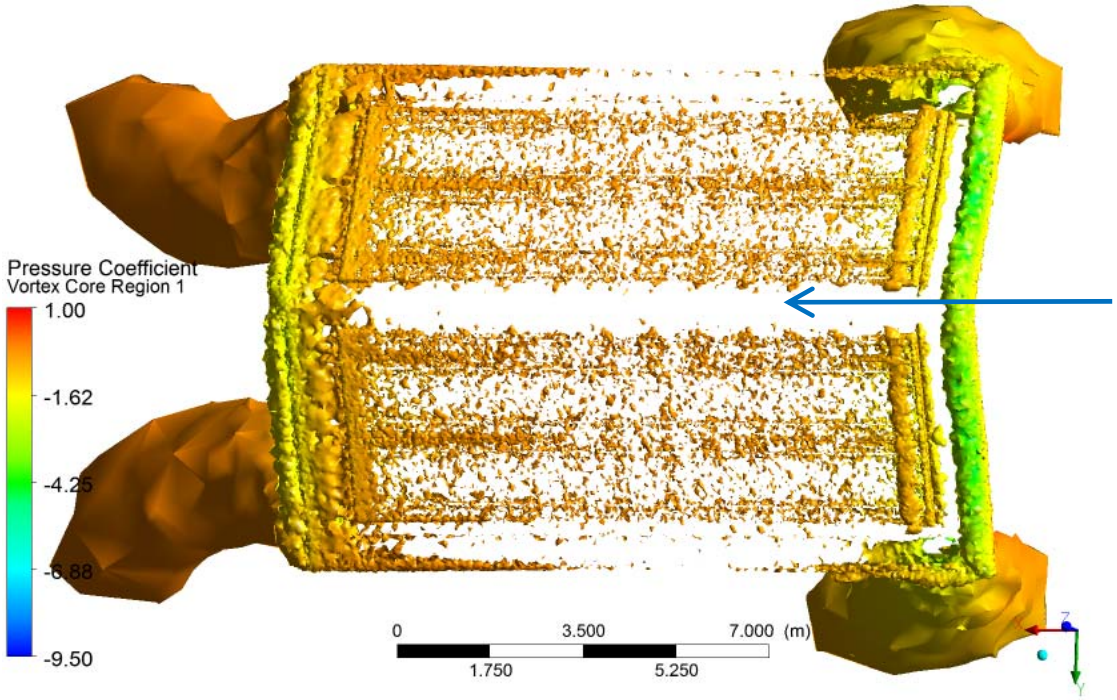


Fig.B. 24, Vortices, Top of the building, WD 0.0º,

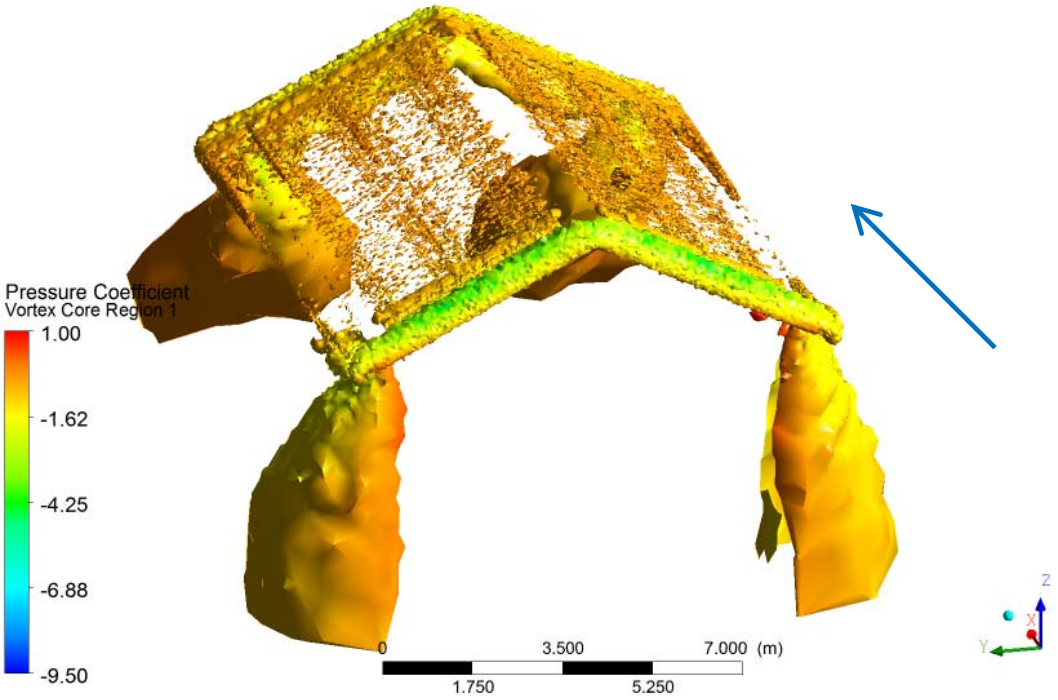


Fig.B. 25.1, Vortices whole building, WW, WD 0.0º

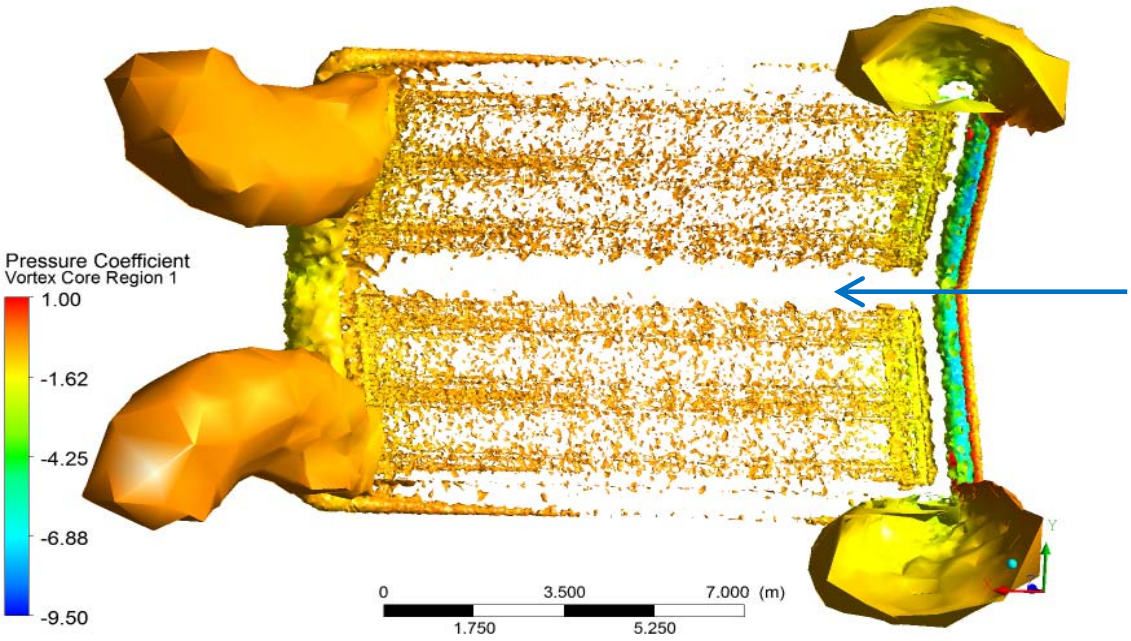


Fig.B. 26.2, Vortices whole building, WW, WD 0.0º

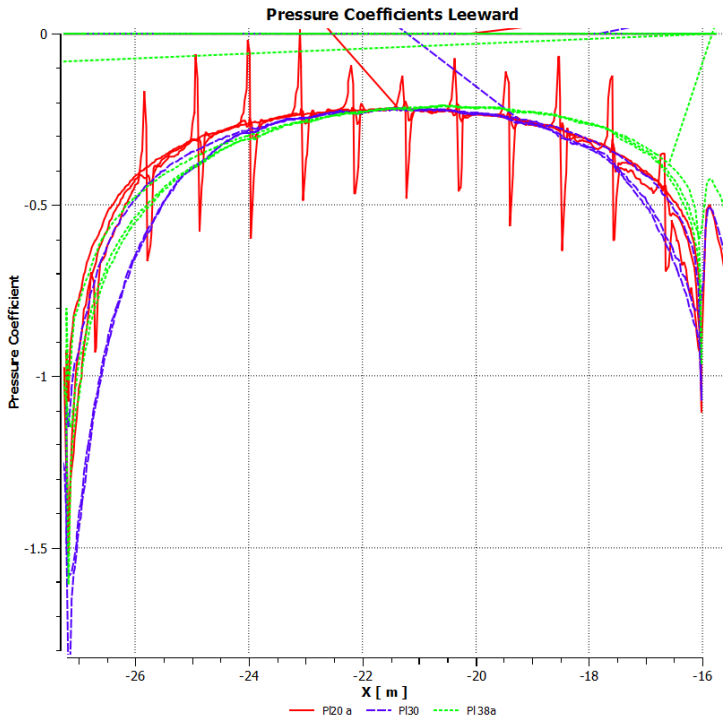


Fig.B. 27, Vortices Bottom of the building, WD 0.0º,

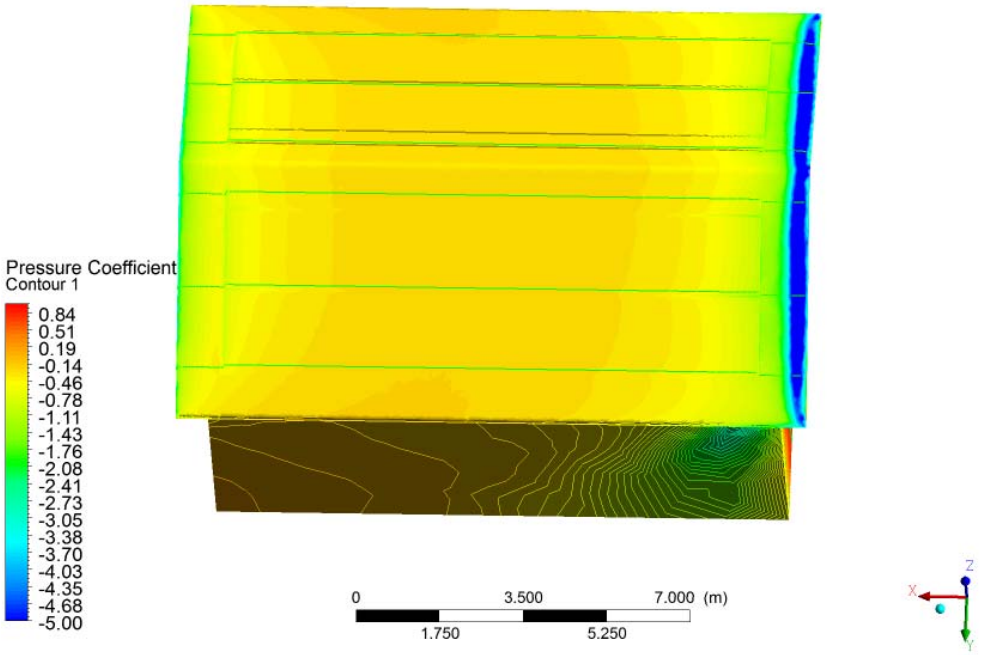


Fig.B. 28, Cp along the main plines on one side of the building, WD 0.0º,

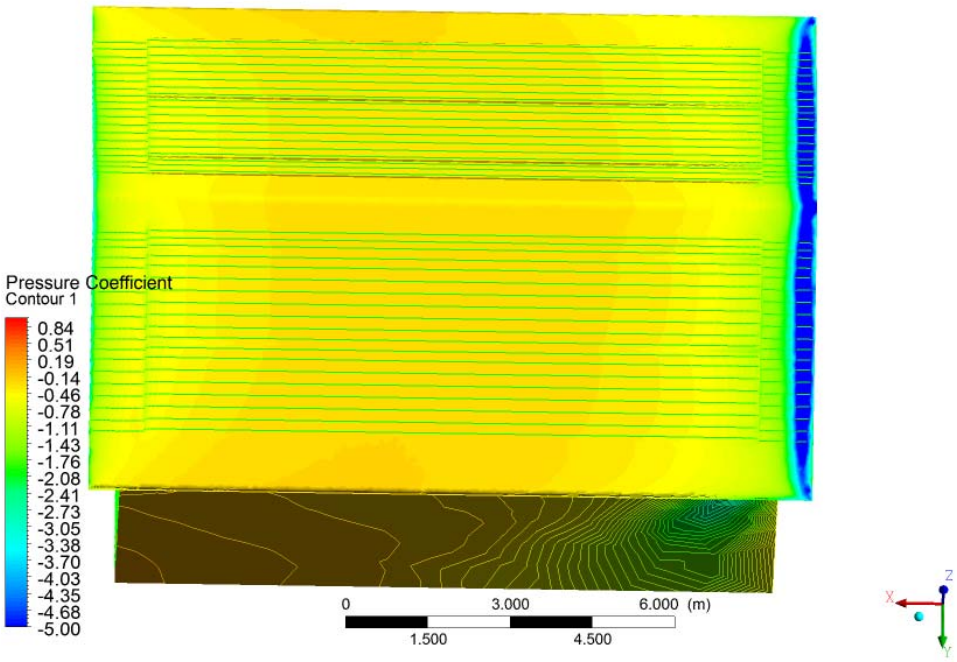


Fig.B. 29, Cp with all polylines of the whole roof, WD 0.0º,

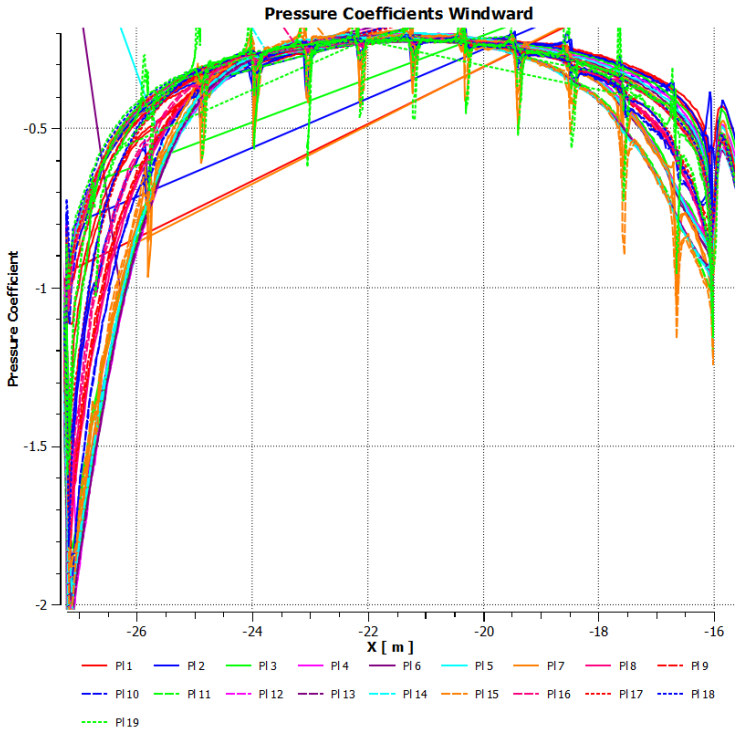


Fig.B. 30, Cp along all polylines, on one side of the building, WD 0.0º

B-III- Wind Pressure Coefficient and Flow Distributions under and above the solar panels, Windward side, 90º Wind Direction, 2" Spacing, 3" Roof Clearance, Slope 35º

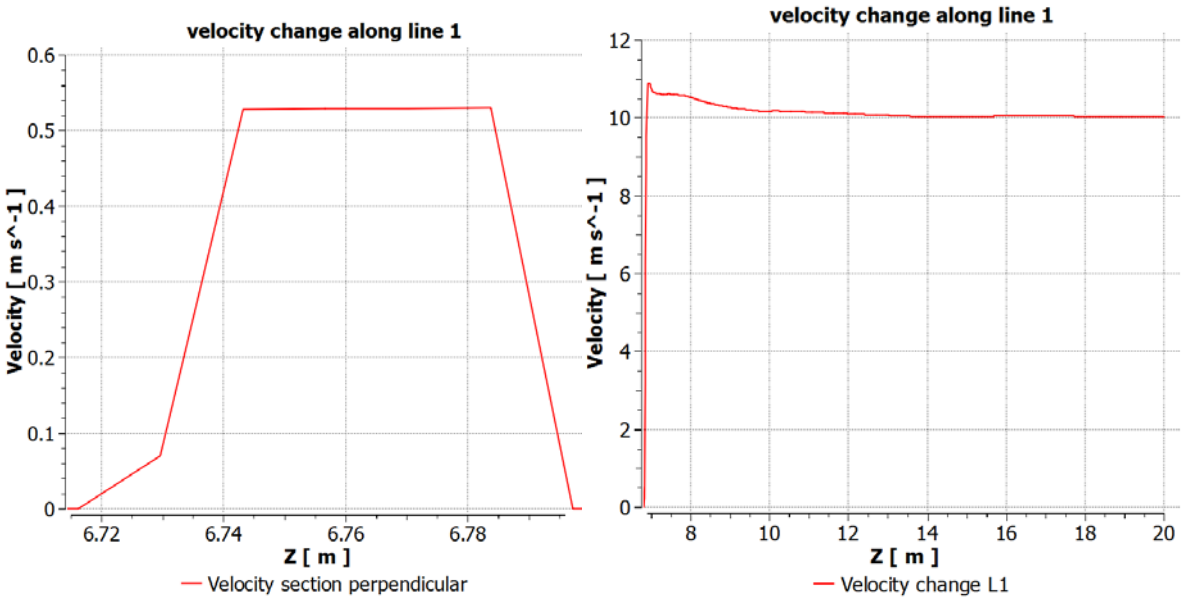


Fig.B. 31,Velocity changes between panels, and above roof, Line 1, 10 m/sec

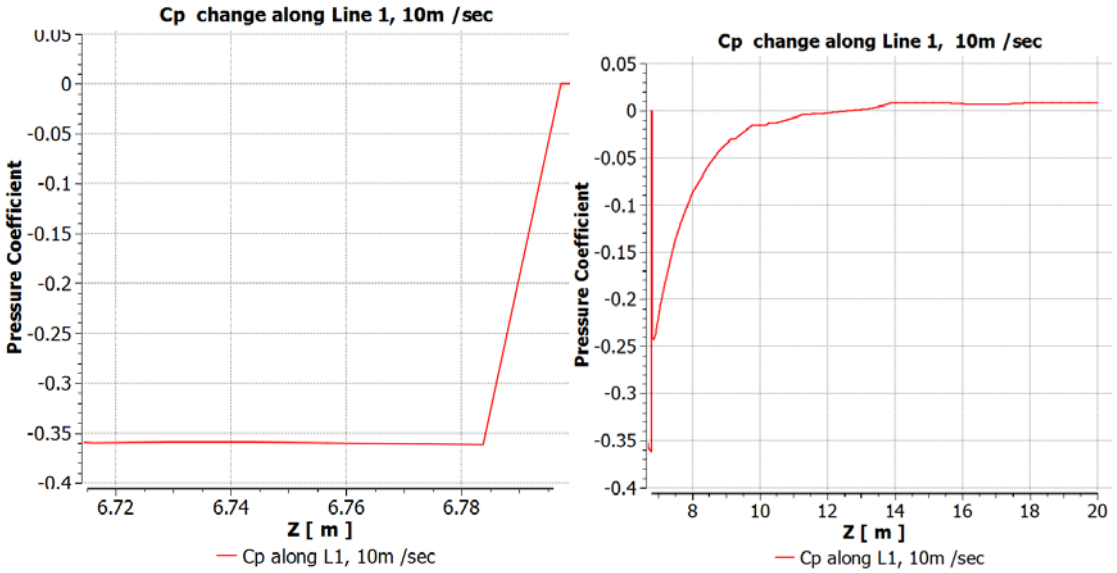


Fig.B. 32, Pressure changes between panels, and above roof, Line 1, 10m/sec

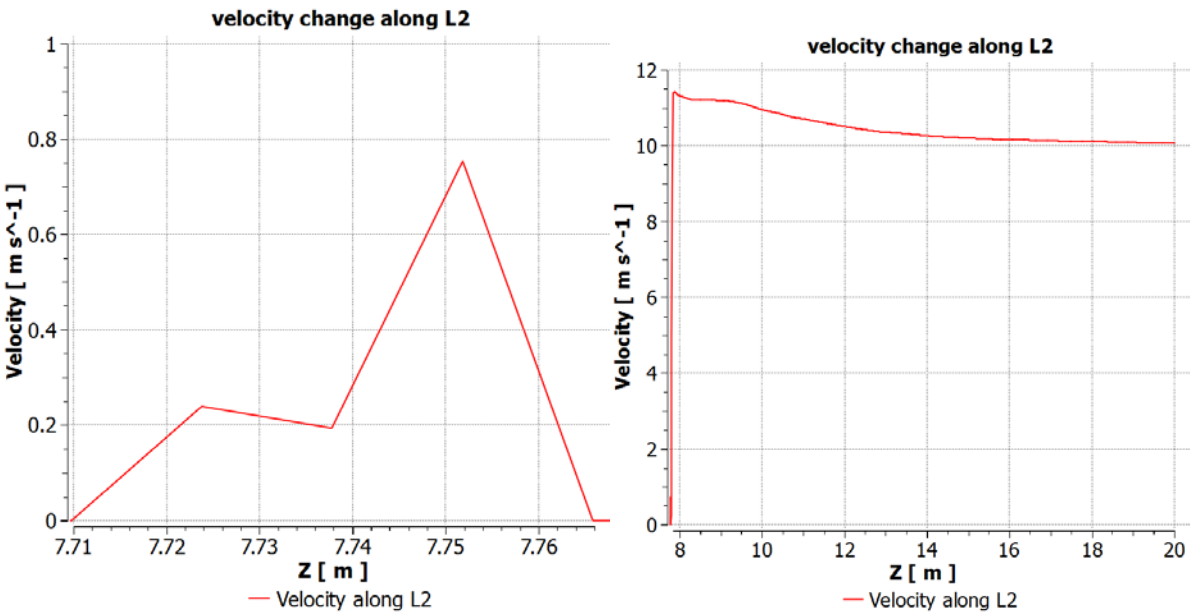


Fig.B. 33, Velocity changes between panels, and above roof, Line 2, 10m/sec

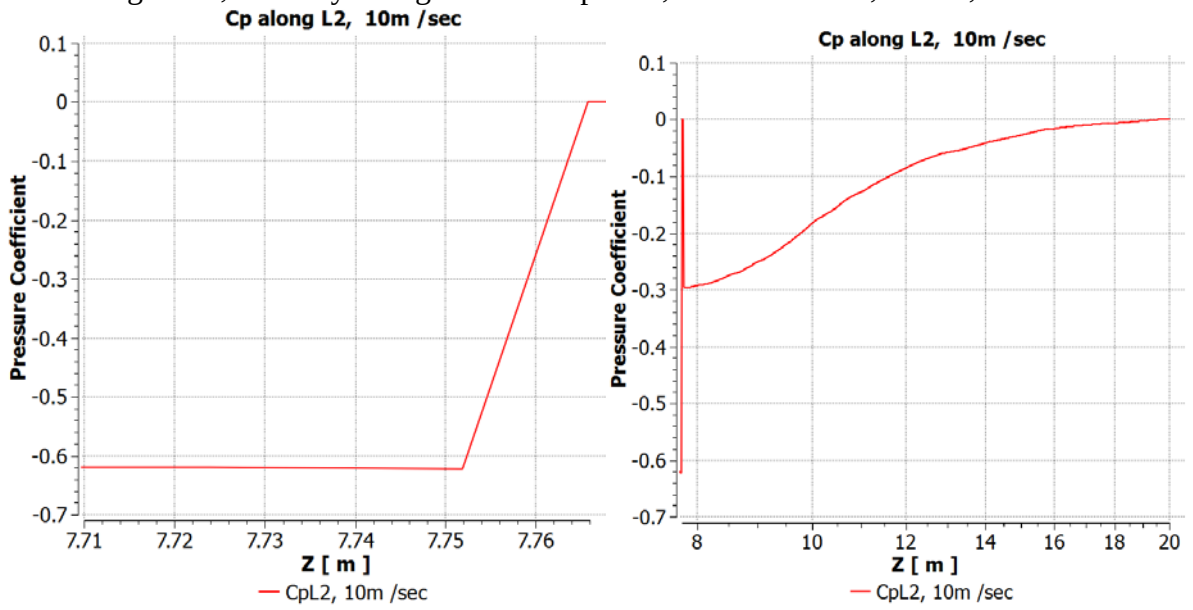


Fig.B. 34, Cp changes between panels, and above roof, Line 2, 10m/sec

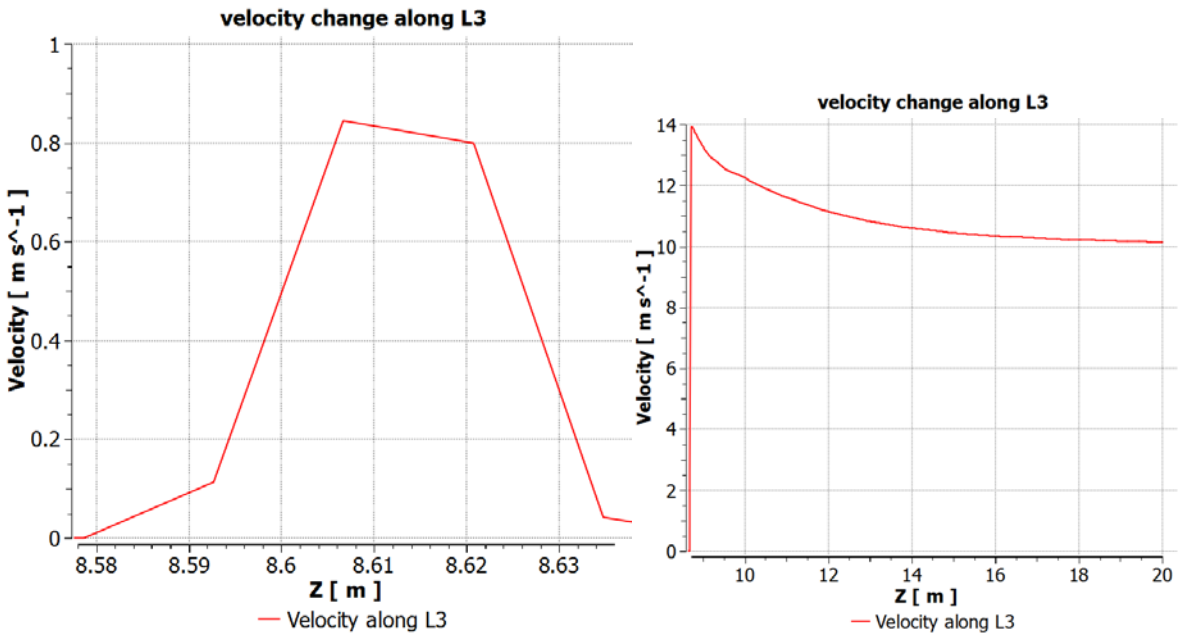


Fig.B. 35Velocity changes between panels, and above roof, Line 3, 10 m/sec

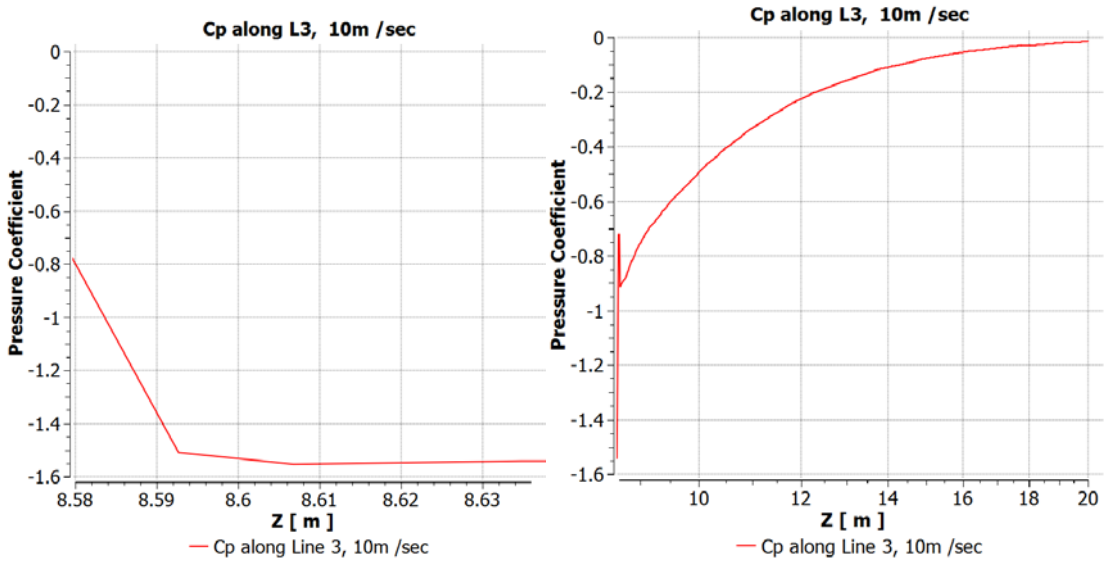


Fig.B. 36, Cp changes between panels, and above roof, Line 3, 10m/sec

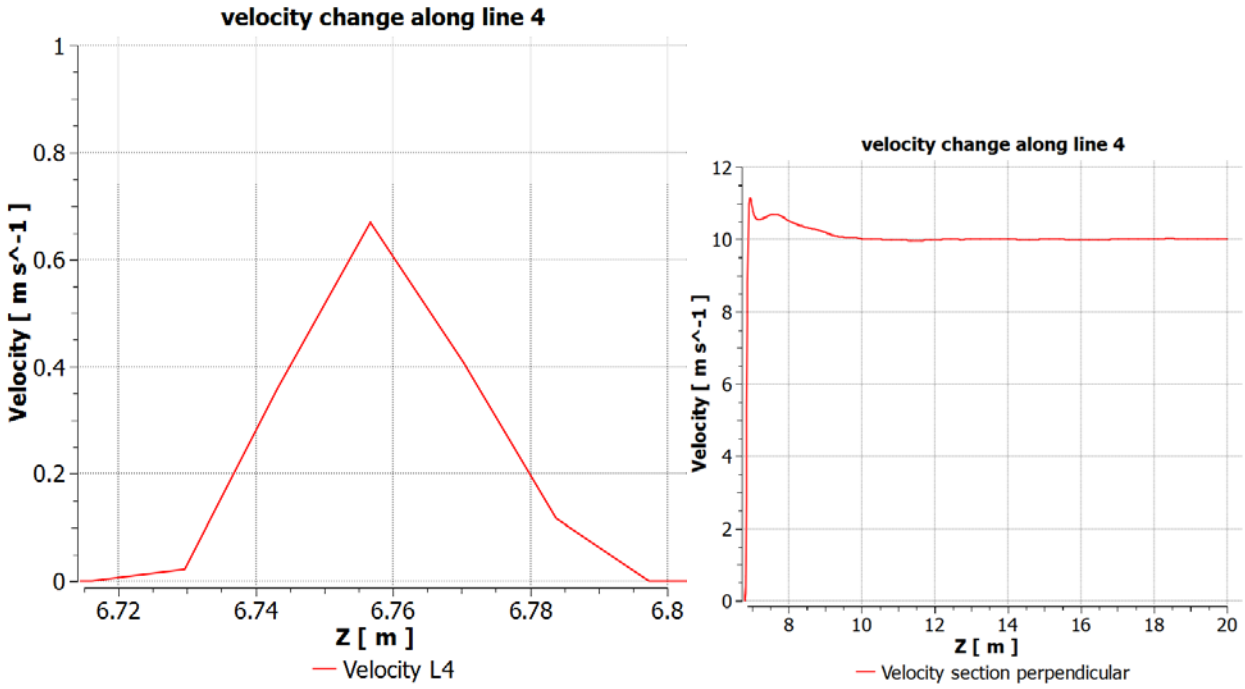


Fig.B. 37, Velocity changes between panels, and above roof, Line 4, 10m/sec

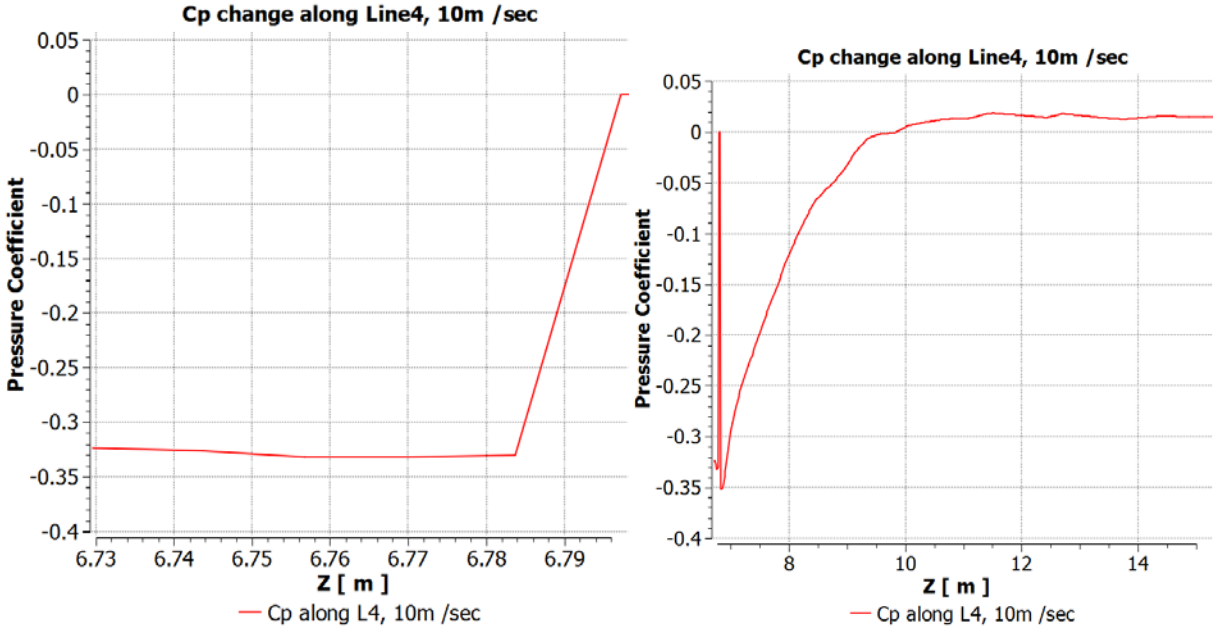


Fig.B. 38, Cp changes between panels, and above roof, Line 4, 10m/sec

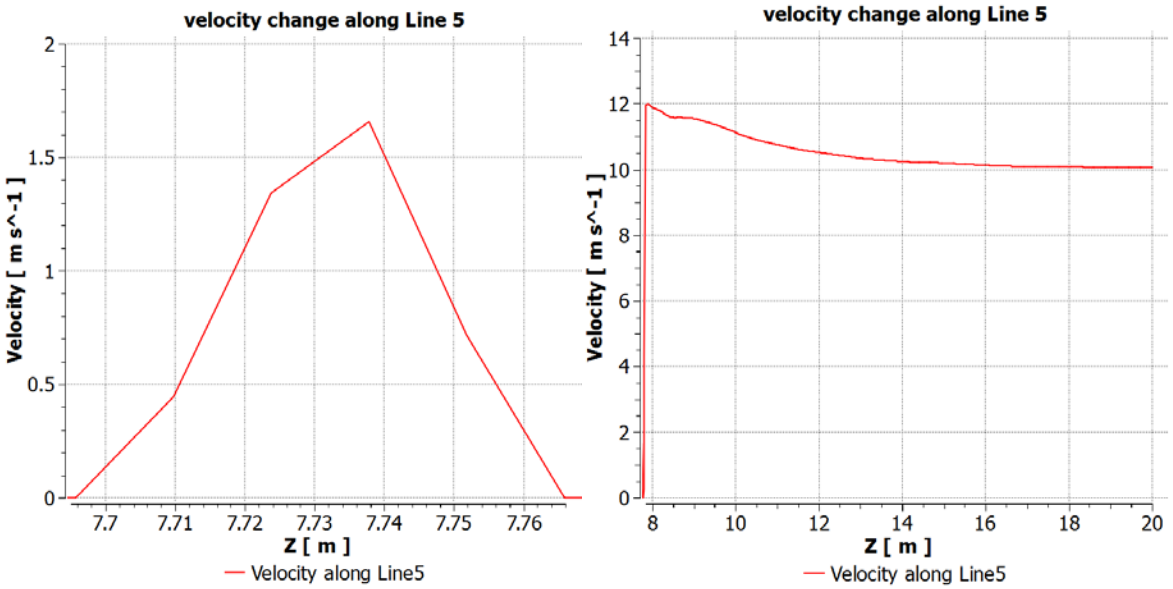


Fig.B. 39, Velocity changes between panels, and above roof, Line 5, 10m/sec

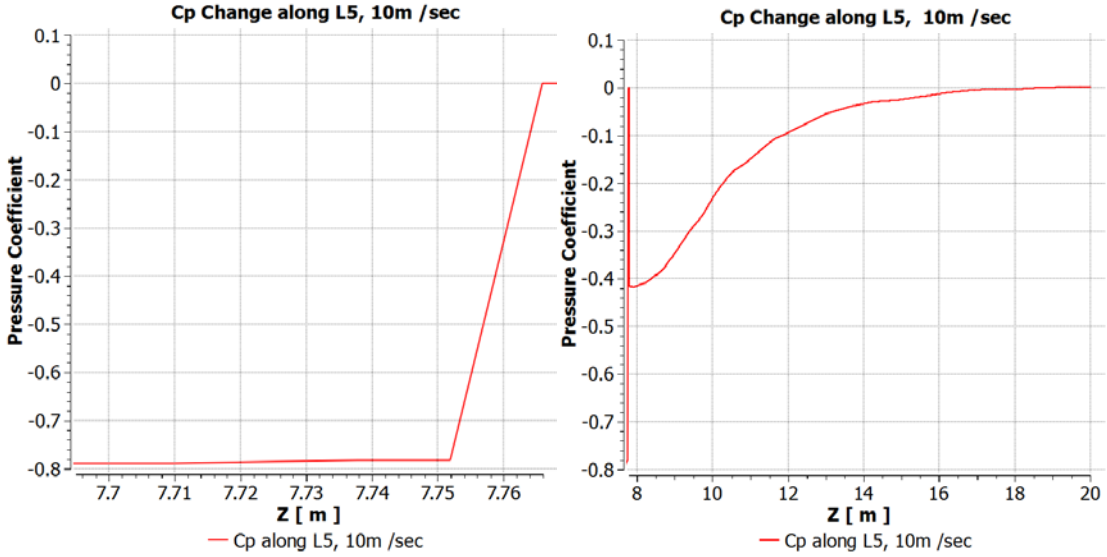


Fig.B. 40, Cp changes between panels, and above roof, Line 5, 10m/sec

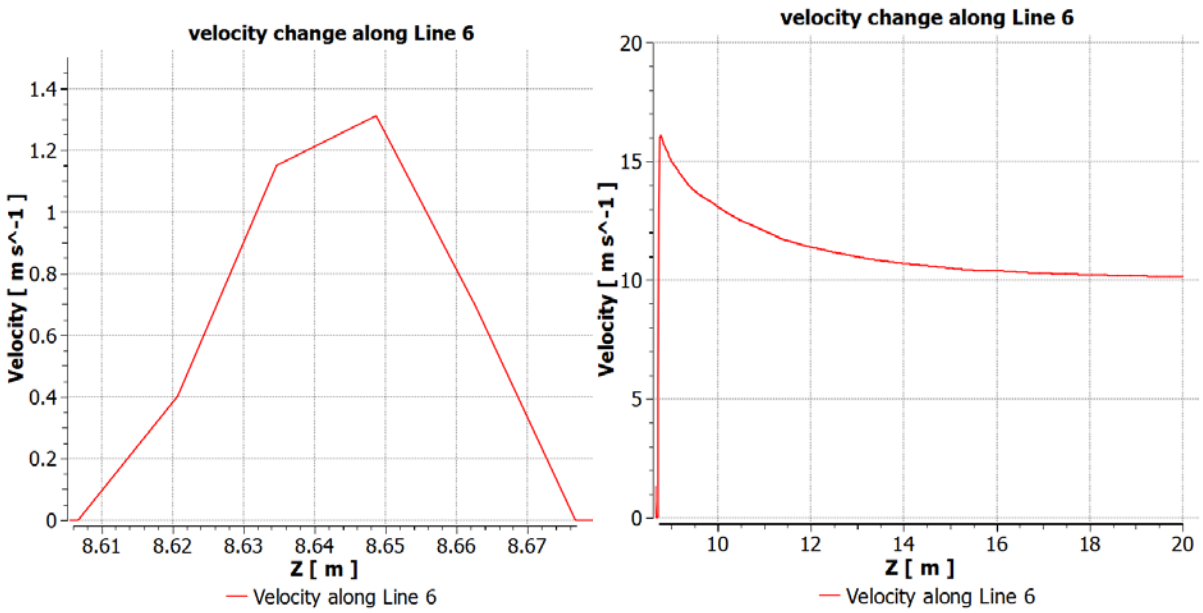


Fig.B. 41, Velocity changes between panels, and above roof, Line 6, 10m/sec

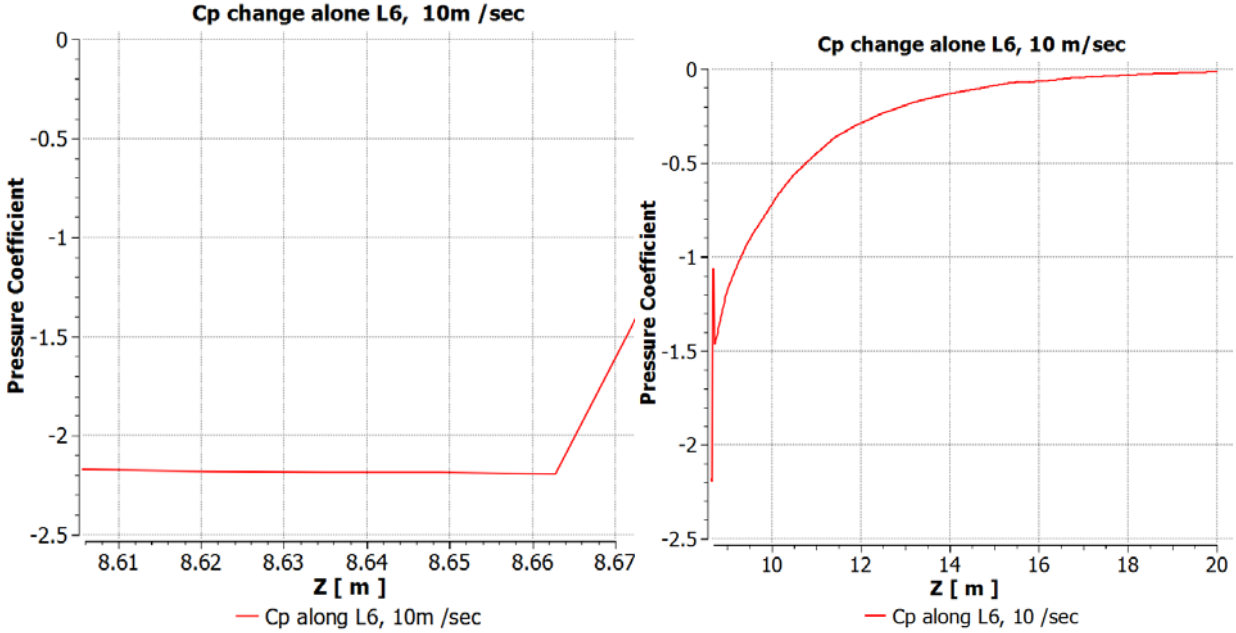


Fig.B. 42, Cp changes between panels, and above roof, Line 6, 10 m/sec

B-IV- Wind Pressure Coefficient and Flow Distributions under and above the solar panels, Windward side, 90º Wind Direction, 2” Spacing, 3” Roof Clearance, Slope 27º

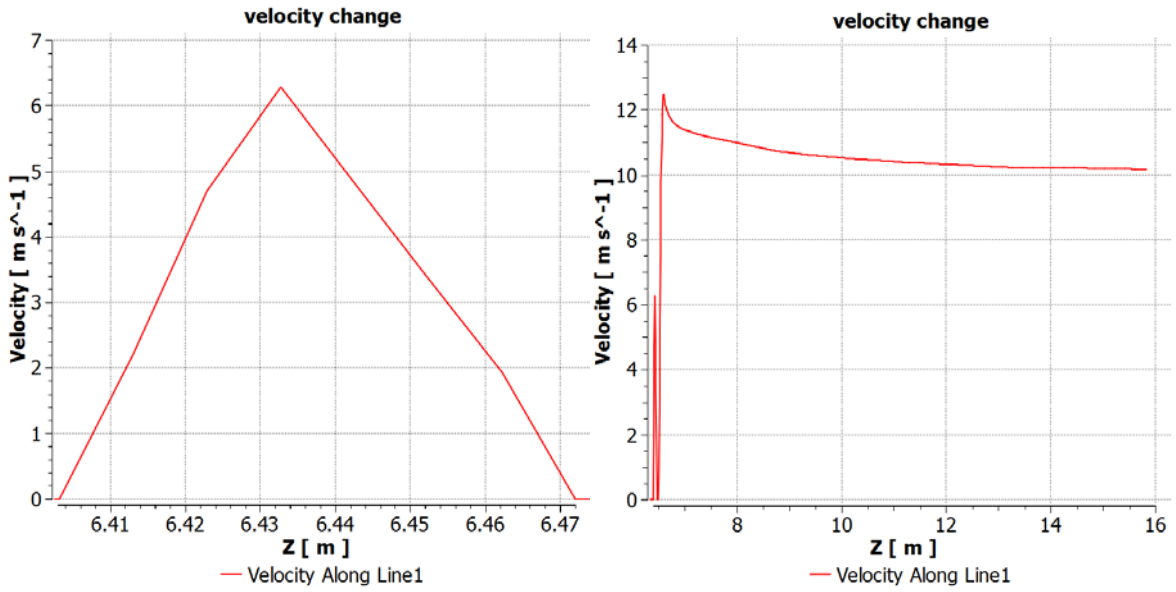


Fig.B. 43. Velocity changes between panels, and above roof, Line 1, 10m/sec

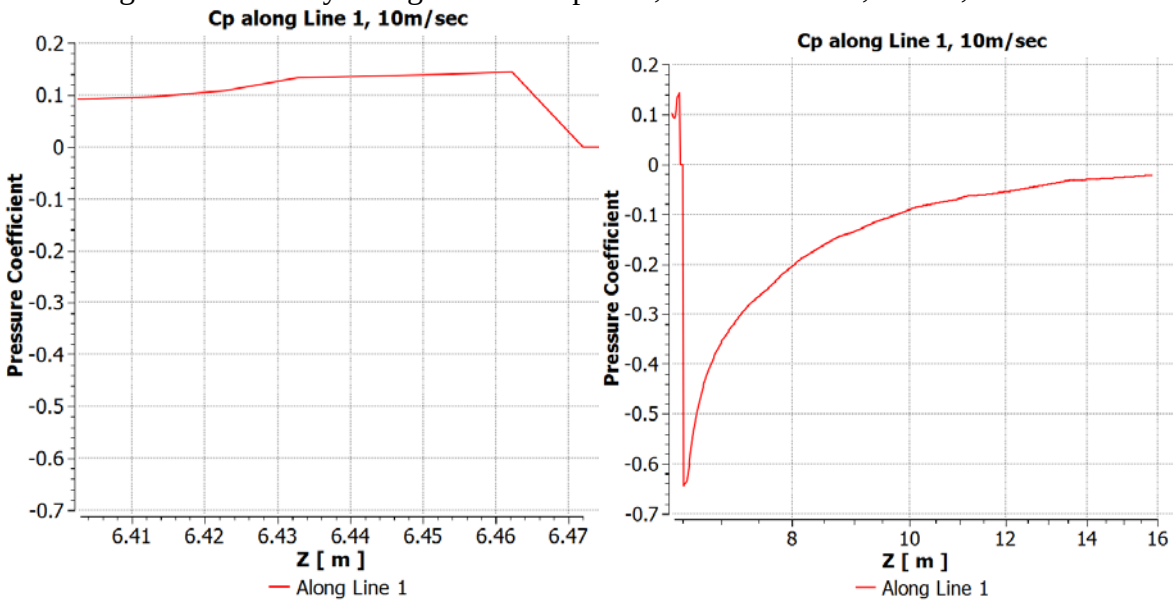


Fig.B. 44. Pressure changes between panels, and above roof, Line 1, 10m/sec

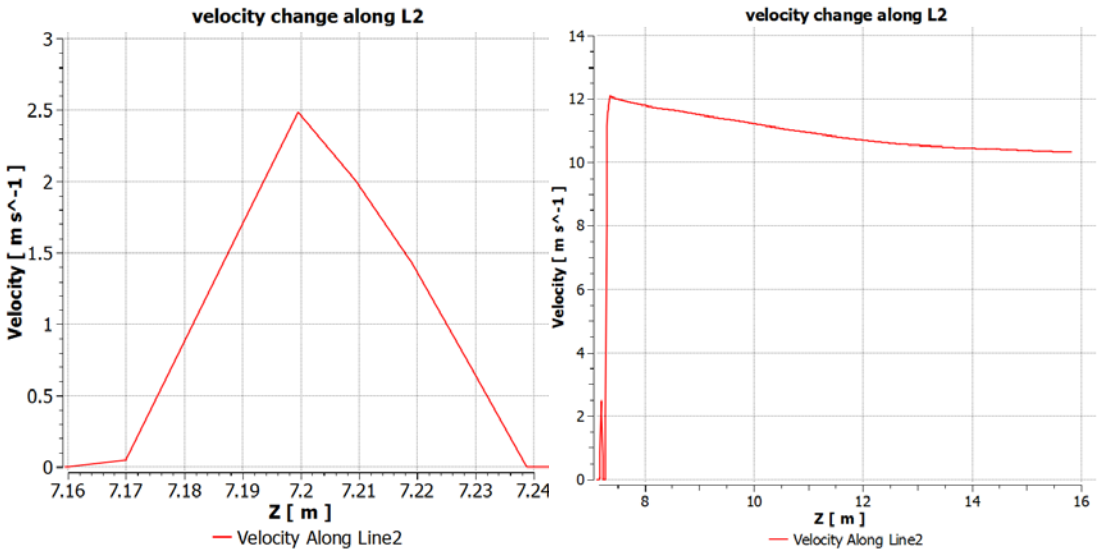


Fig.B. 45. Velocity changes between panels, and above roof, Line 2, 10m/sec

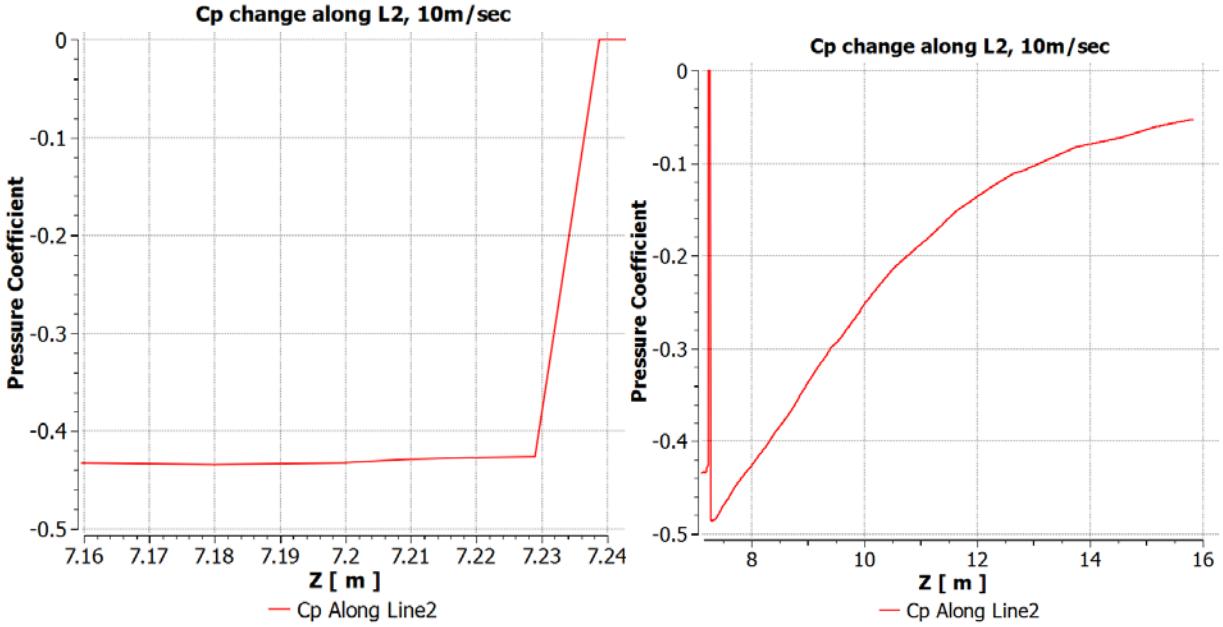


Fig.B. 46, Cp changes between panels, and above roof, Line 2, 10m/sec

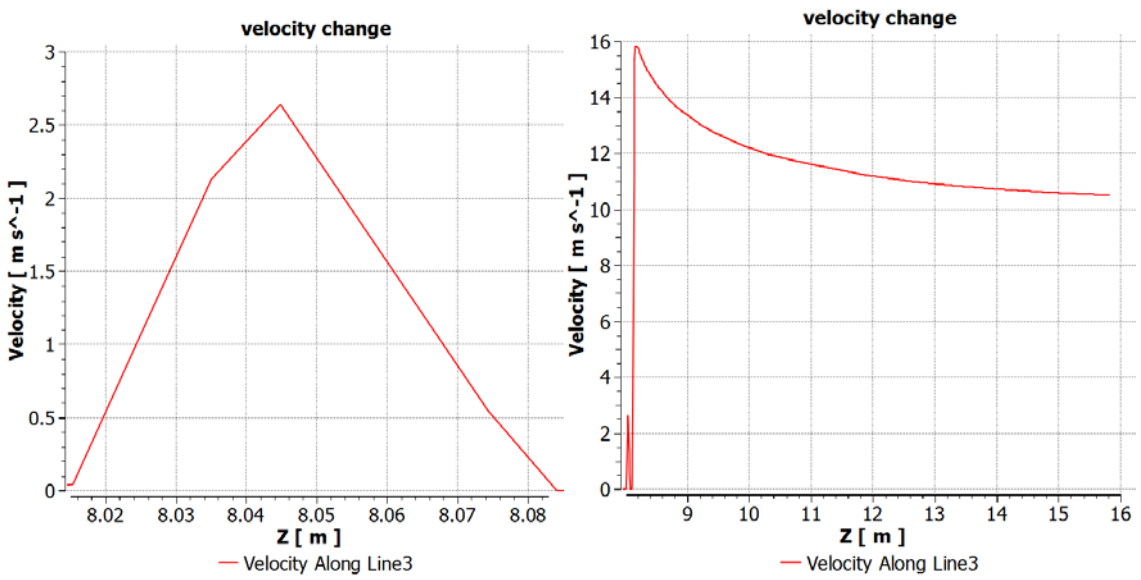


Fig.B. 47,Velocity changes between panels, and above roof, Line 3, 10m/sec

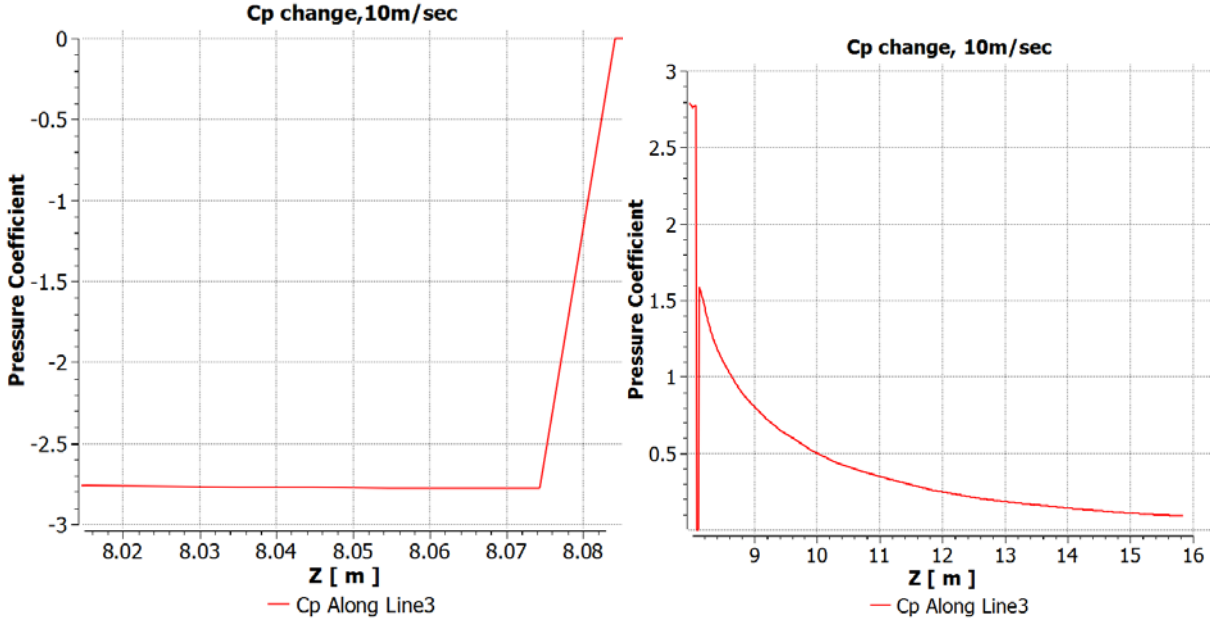


Fig.B. 48, Cp changes between panels, and above roof, Line 3, 10 m/sec

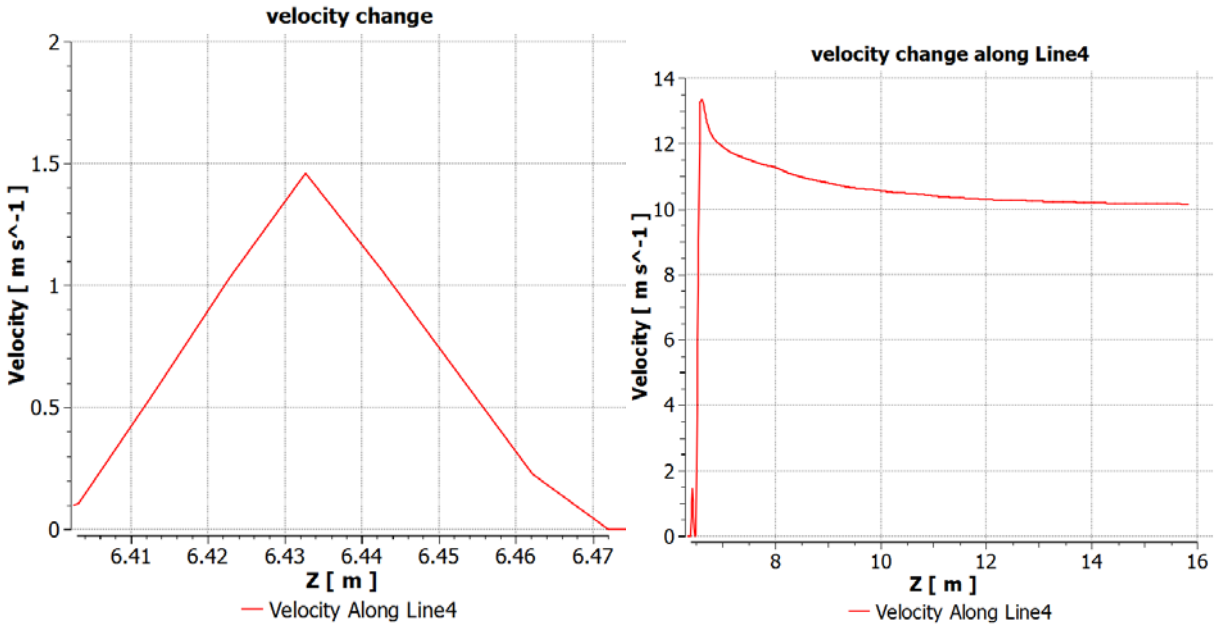


Fig.B. 49, Velocity changes between panels, and above roof, Line 4, 10 m/sec

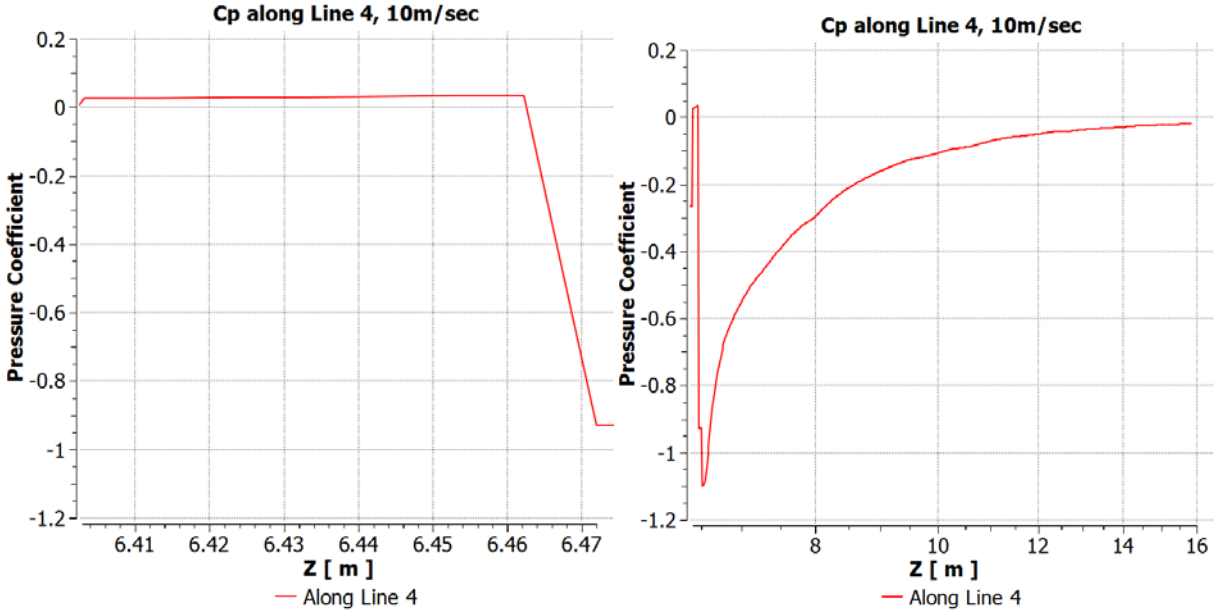


Fig.B. 50, Cp changes between panels, and above roof, Line 4, 10m/sec

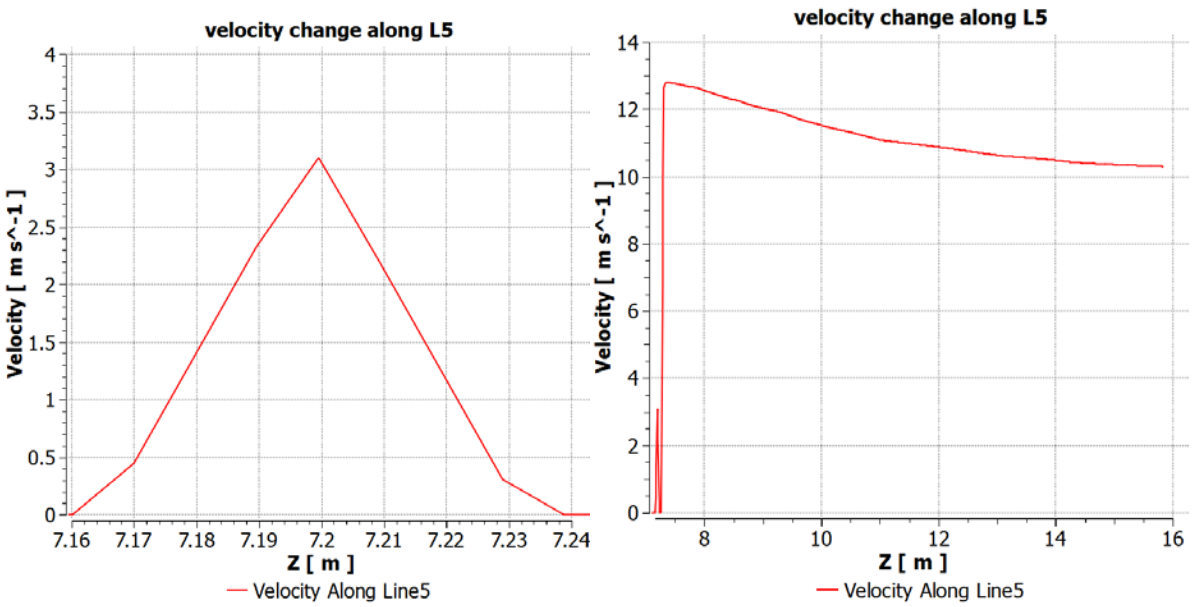


Fig.B. 51, Velocity changes between panels, and above roof, Line 5, 10m/sec

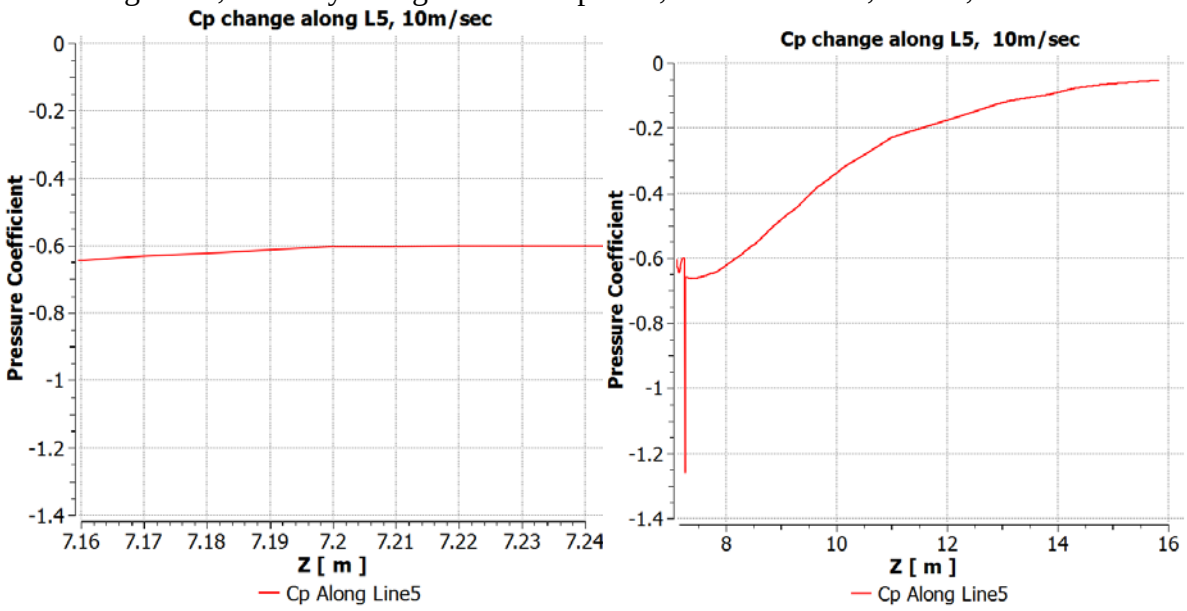


Fig.B. 52, Cp changes between panels, and above roof, Line 5, 10m/sec

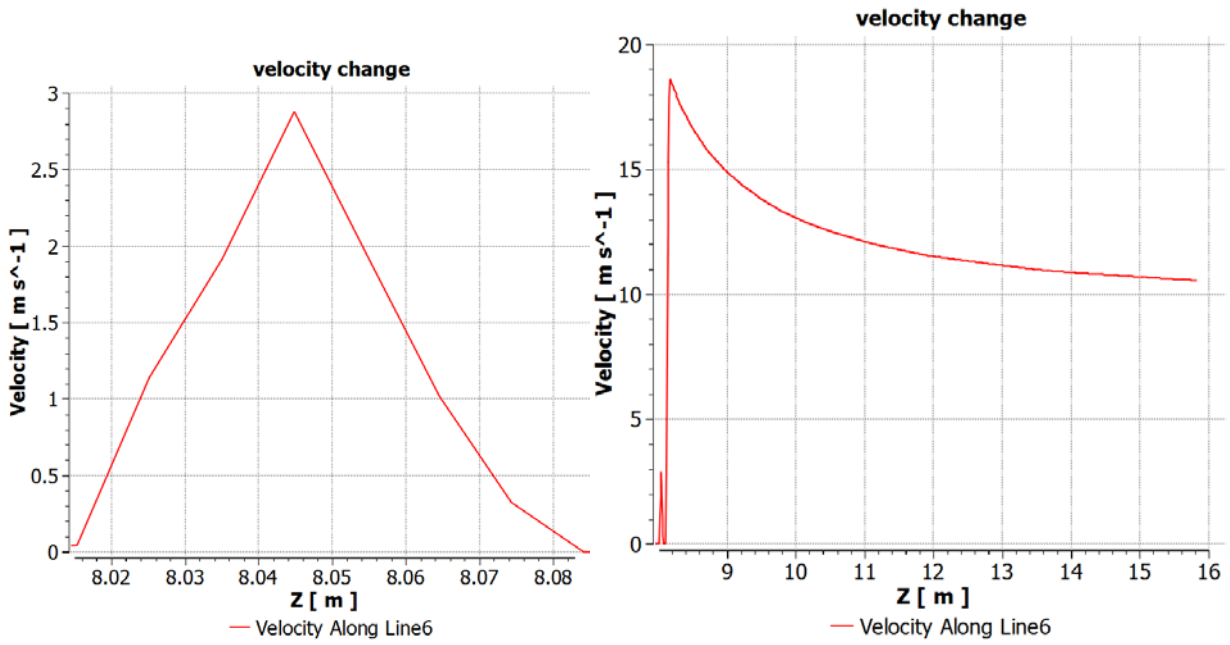


Fig.B. 53, Velocity changes between panels, and above roof, Line 6, 10m/sec

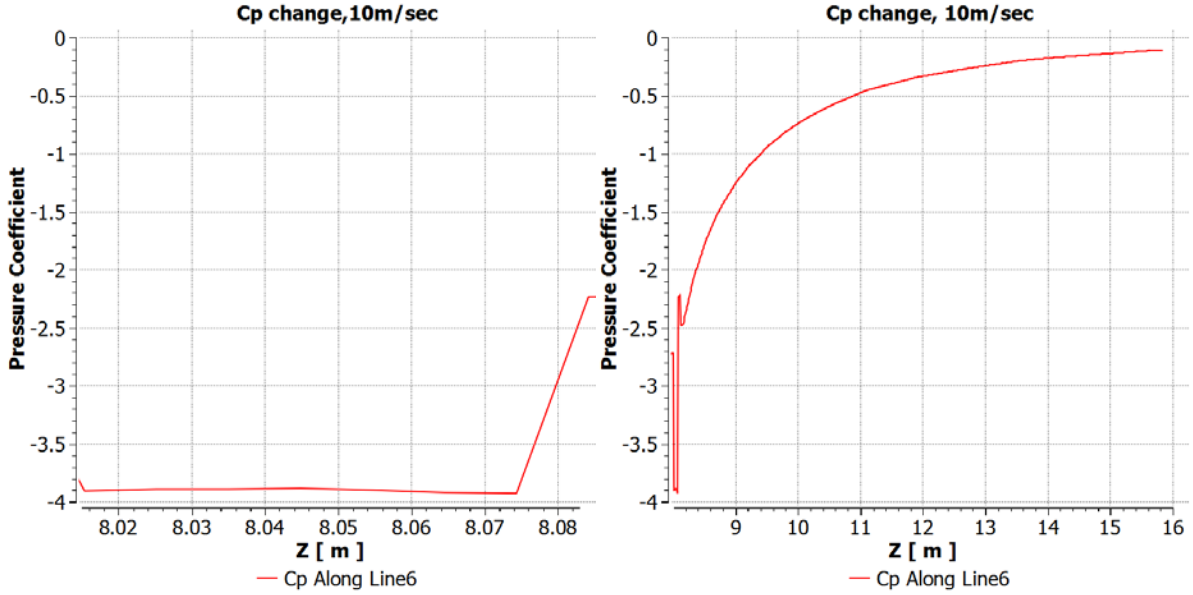


Fig.B. 54, Cp changes between panels, and above roof, Line 6, 10m/sec

B-V- Wind Pressure Coefficient and Flow Distributions, along same 6 Perpendicular Lines, Windwards, Bare Roof, Wind Direction 90º

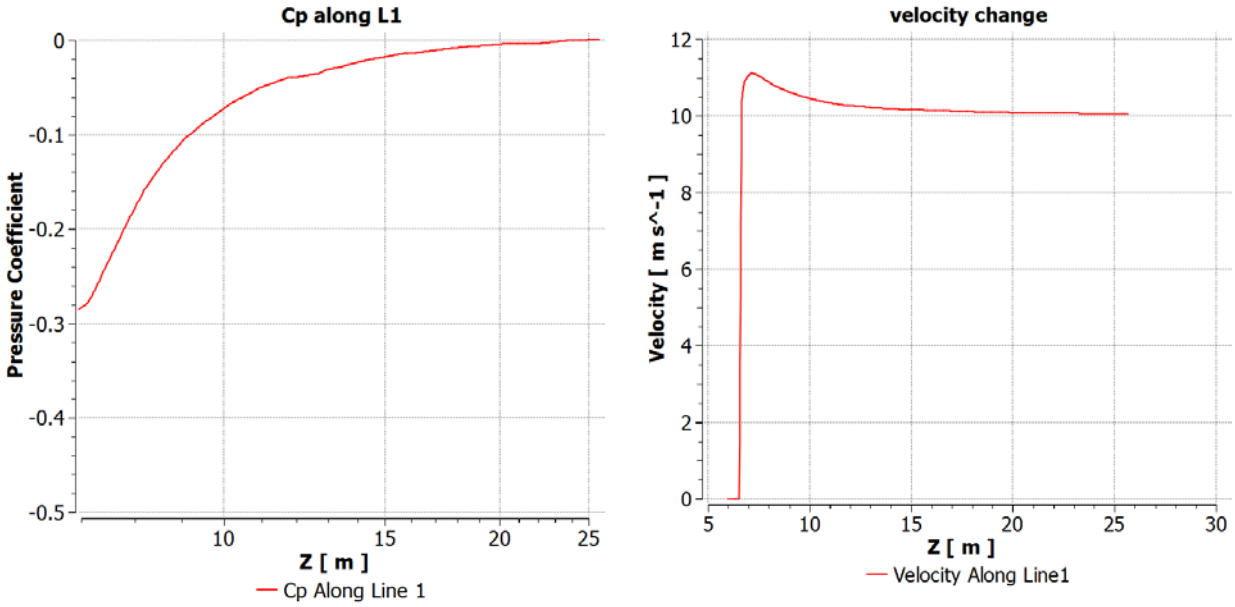


Fig.B. 55, CP and Velocity change along Line1, wind direction 90º, 10m/sec

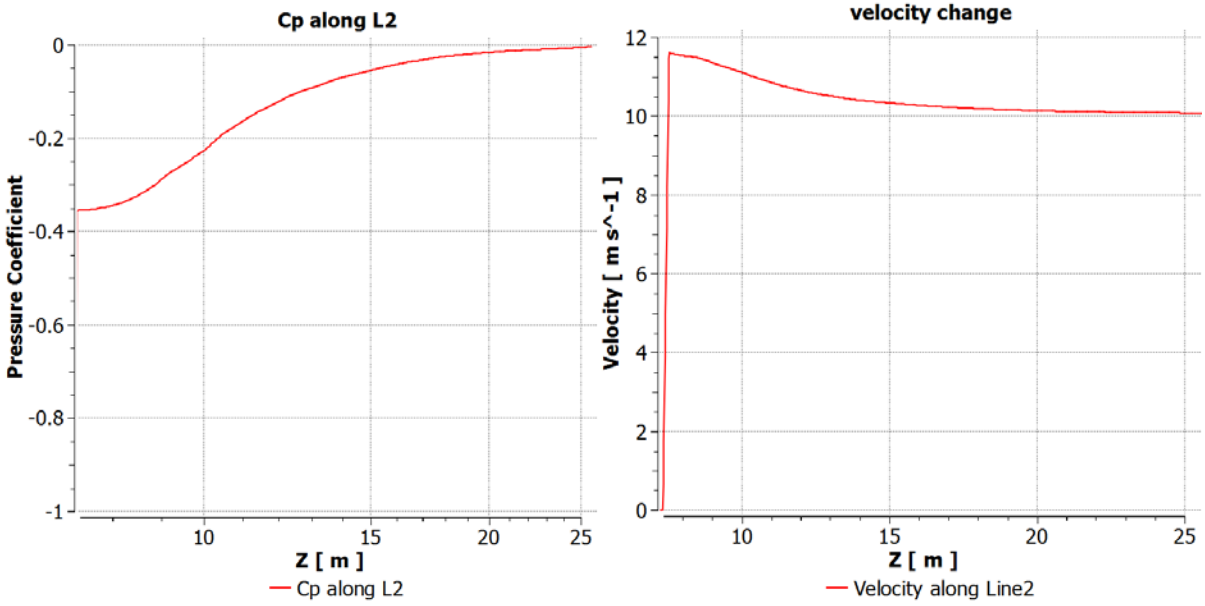


Fig.B. 56, CP and Velocity change along Line2, wind direction 90º, 10m/sec

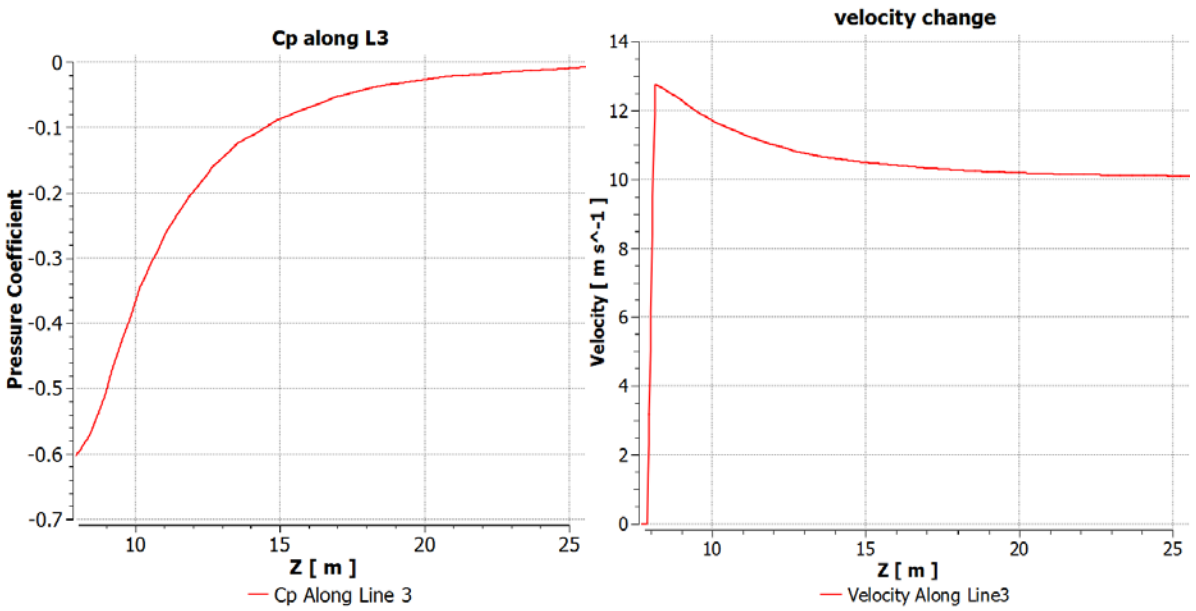


Fig.B. 57, CP and Velocity change along Line3, wind direction 90º, 10m/sec

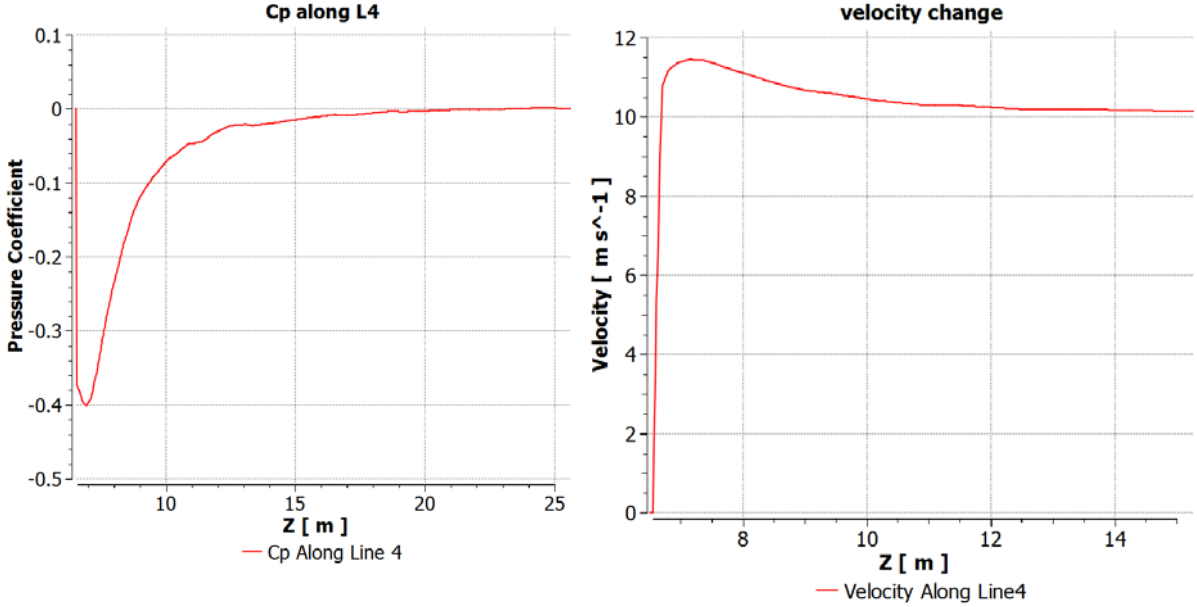


Fig.B. 58, CP and Velocity change along Line4, wind direction 90º, 10m/sec

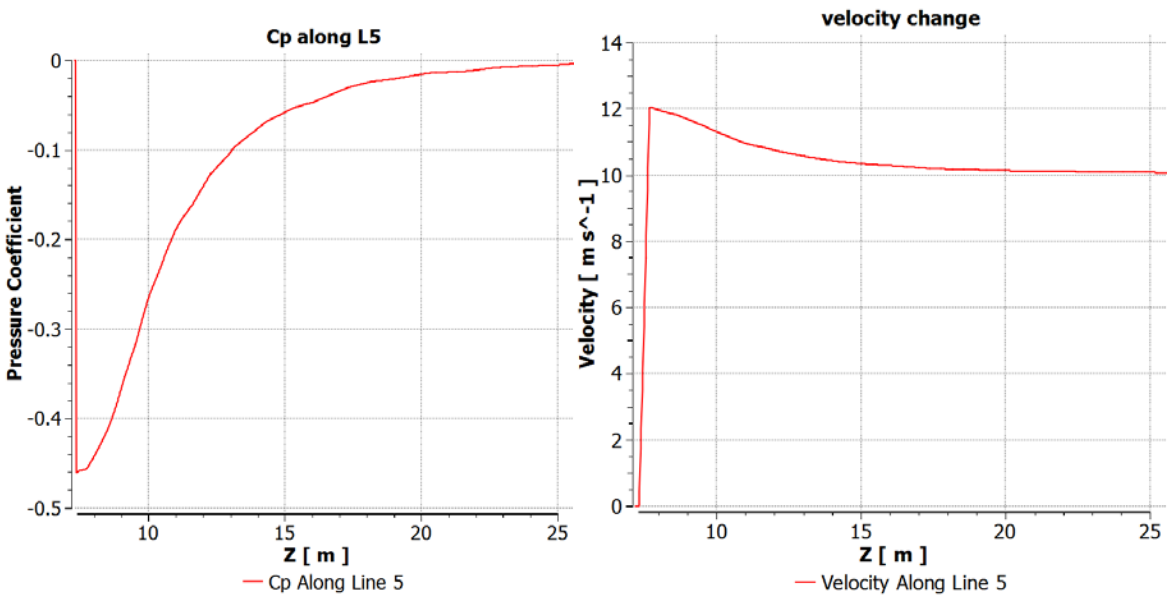


Fig.B. 59, CP and Velocity change along Line5, wind direction 90º, 10m/sec

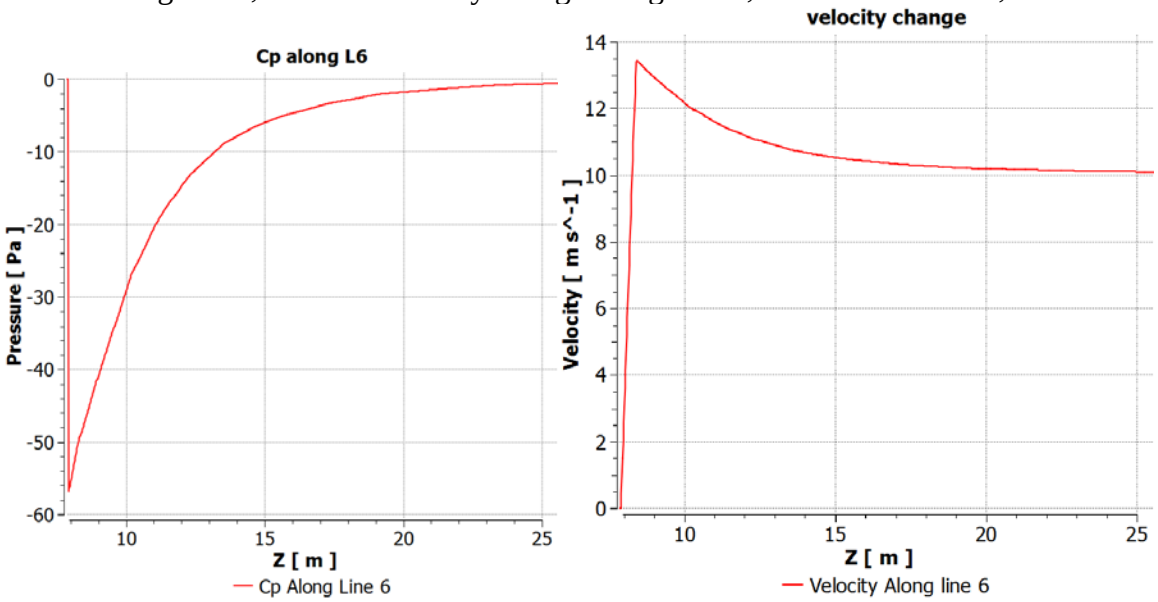


Fig.B. 60, CP and Velocity change along Line6, wind direction 90º, 10m/sec

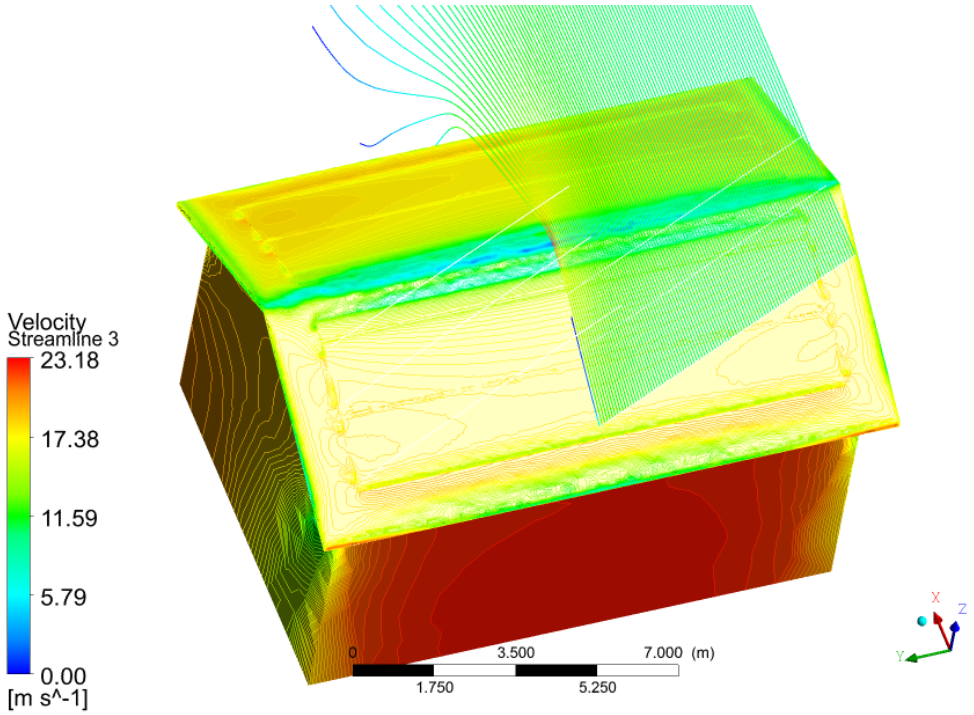


Fig.B. 61, Velocity stream lines above the roof with panels, wind direction 90º, 10m/sec

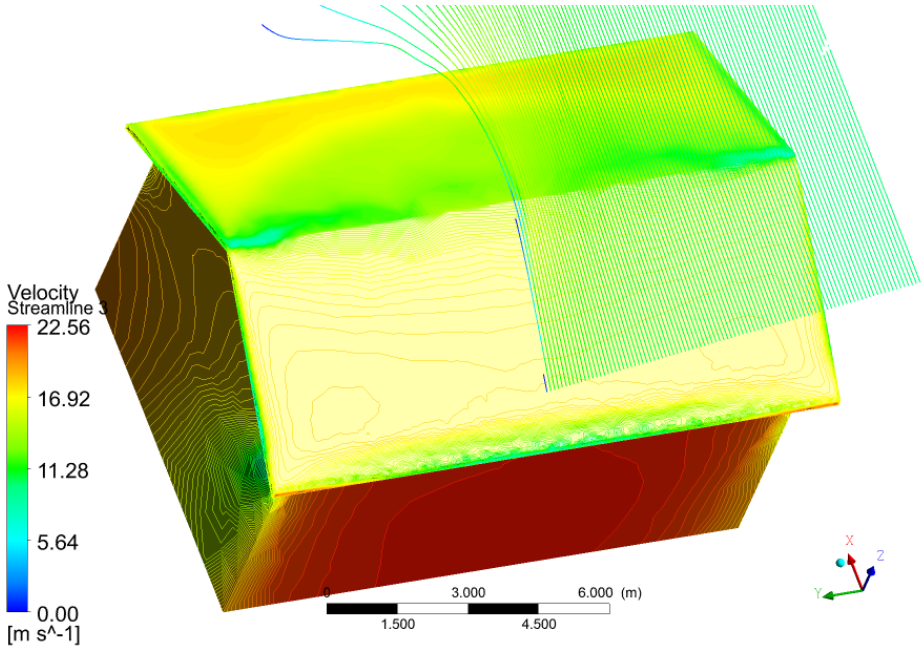


Fig.B. 62, Velocity stream lines above the roof without panels, wind direction 90º, 10m/sec

B-VI- Wind Pressure Coefficient and Flow Distributions under and above the solar panels, Windward side, 90º Wind Direction, 2” Spacing, 3” Roof Clearance, Slope 15º

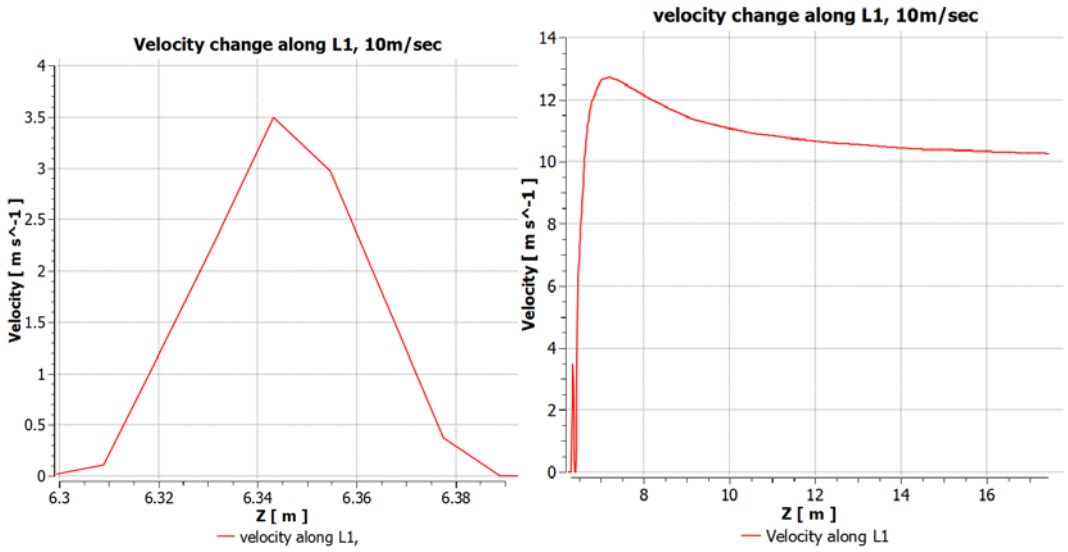


Fig.B. 63. Velocity changes between panels, and above roof, Line 1, 10m/sec

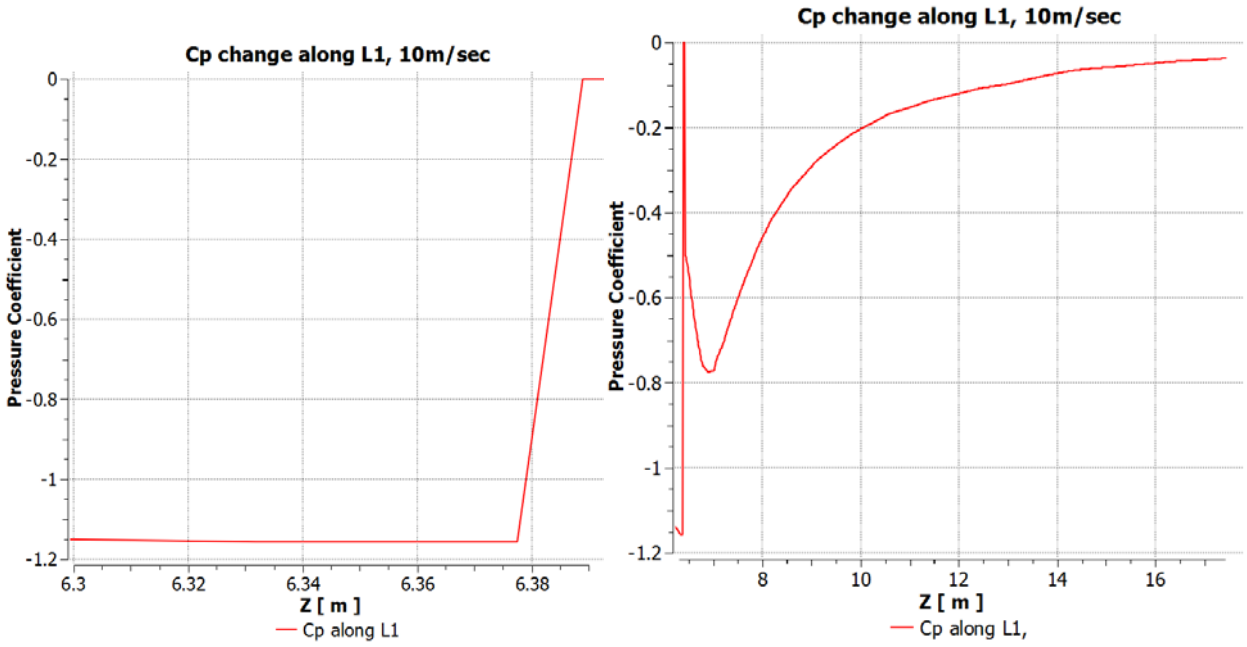


Fig.B. 64. Pressure changes between panels, and above roof, Line 1, 10m/sec

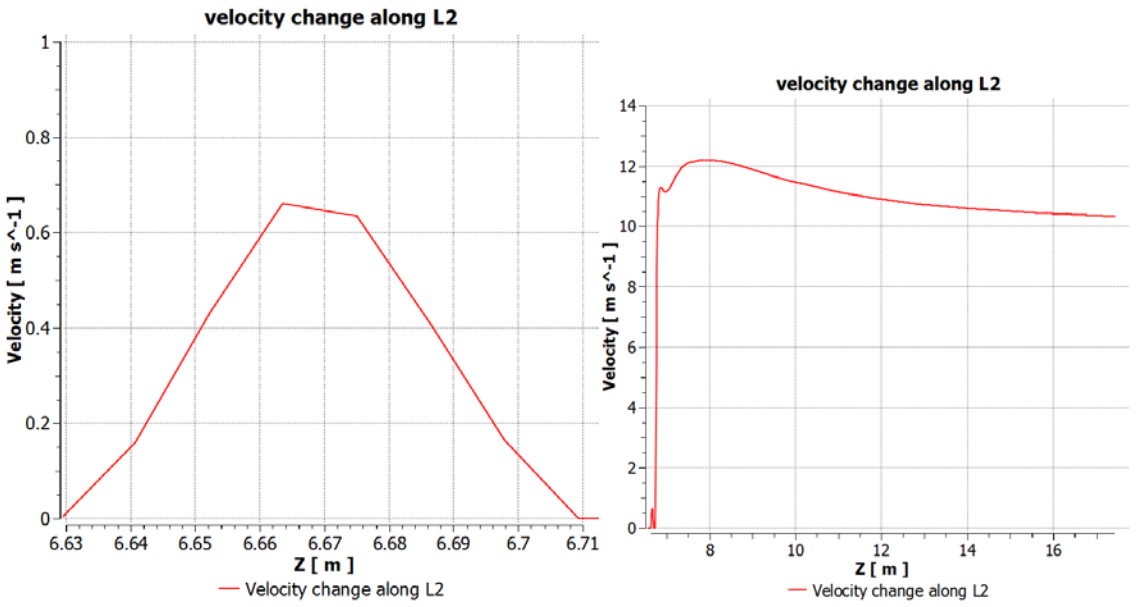


Fig.B. 65, Velocity changes between panels, and above roof, Line 2, 10m/sec

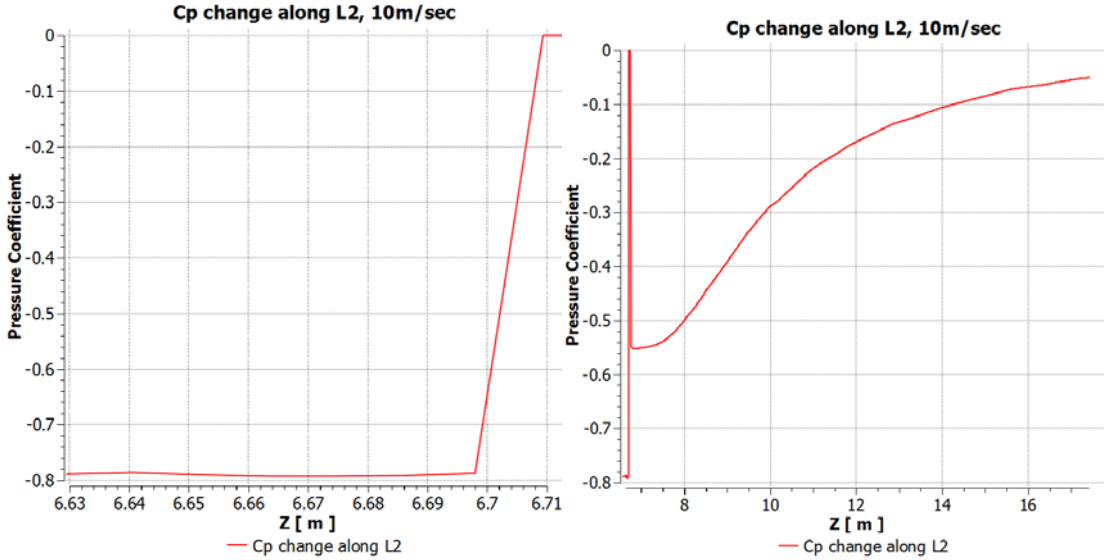


Fig.B. 66, Cp changes between panels, and above roof, Line 2, 10m/sec

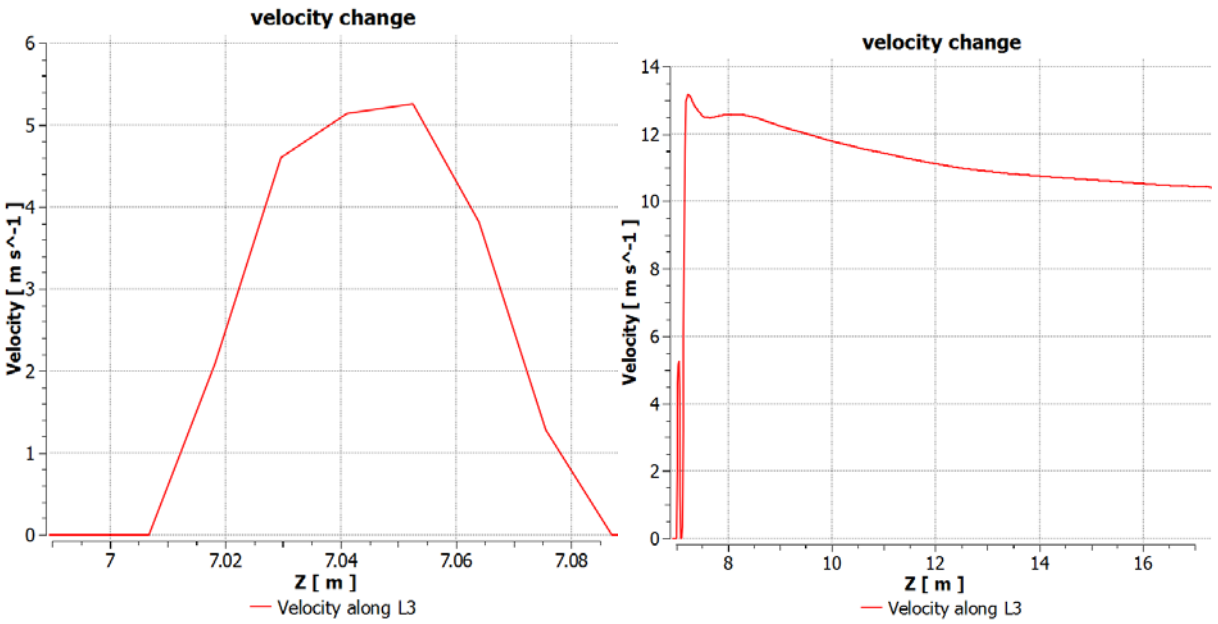


Fig.B. 67, Velocity changes between panels, and above roof, Line 3, 10m/sec

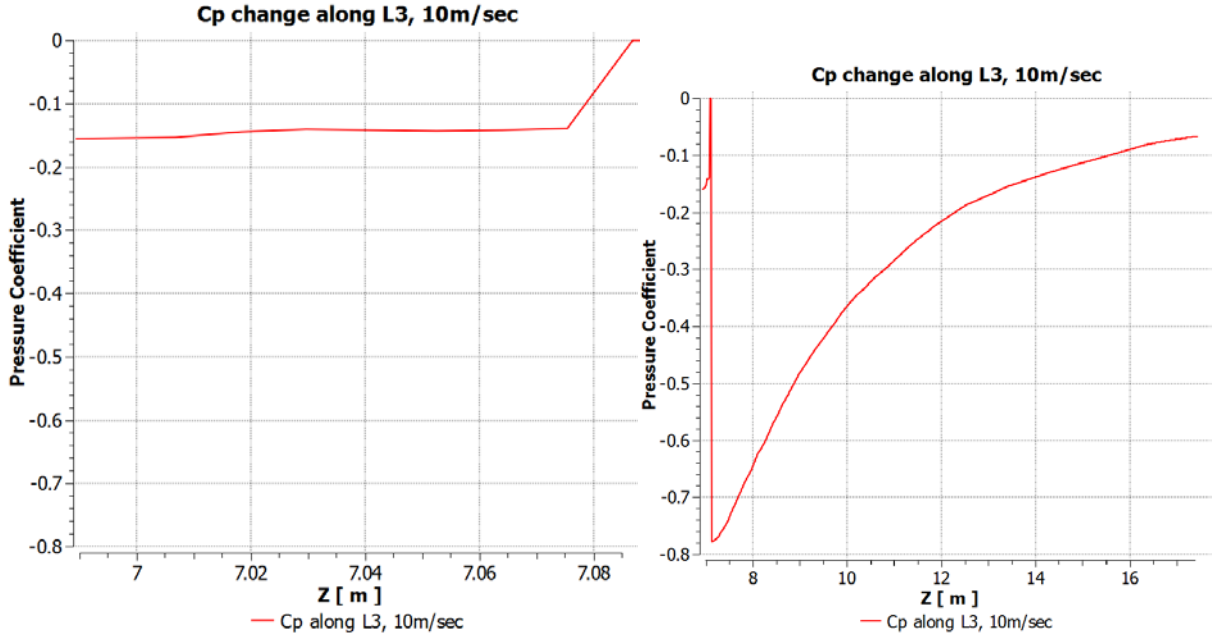


Fig.B. 68, Cp changes between panels, and above roof, Line3, 10m/sec

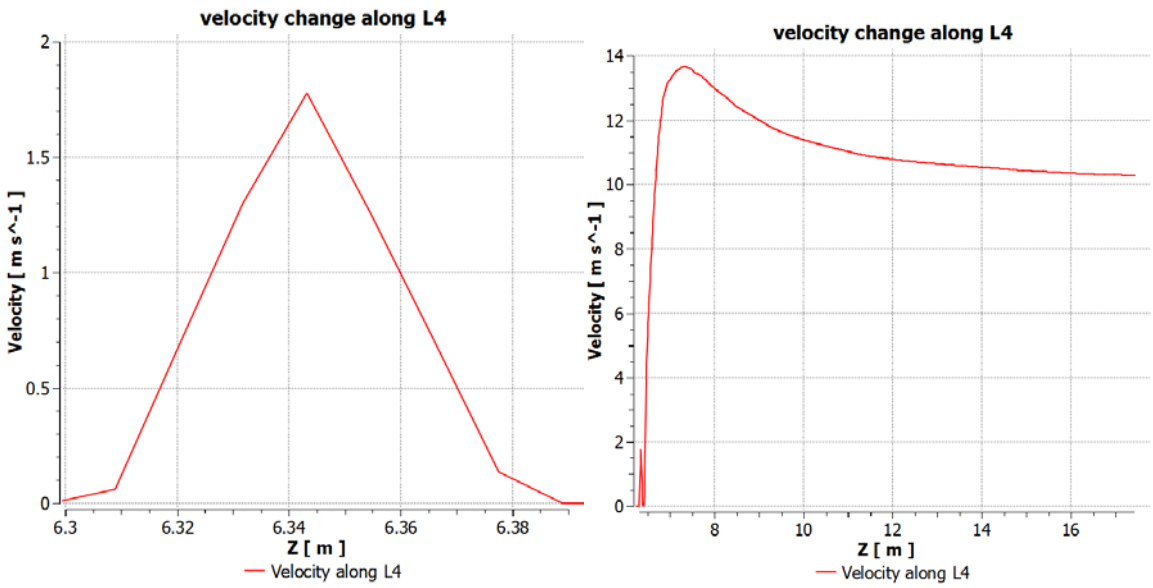


Fig.B. 69, Velocity changes between panels, and above roof, Line 4, 10m/sec

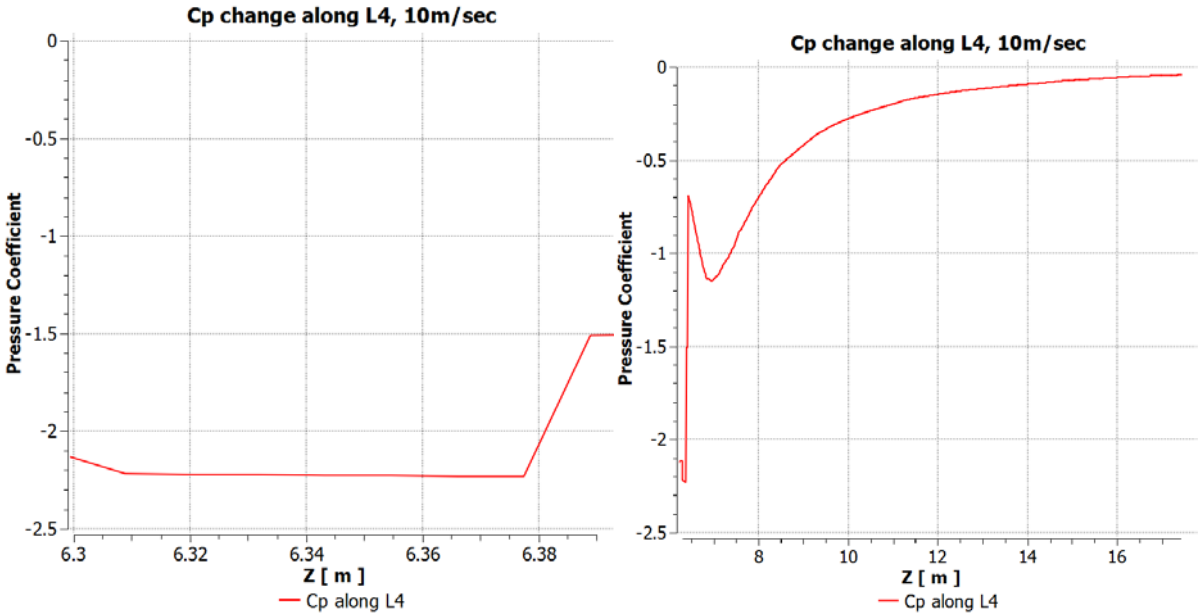


Fig.B. 70, Cp changes between panels, and above roof, Line 4, 10m/sec

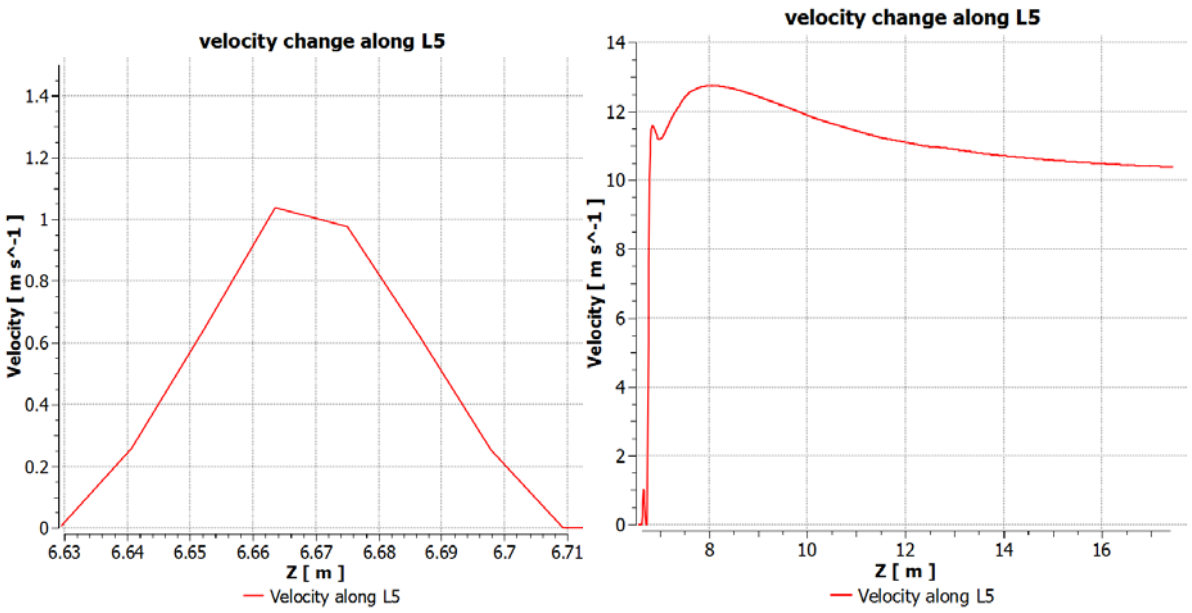


Fig.B. 71, Velocity changes between panels, and above roof, Line 5, 10m/sec

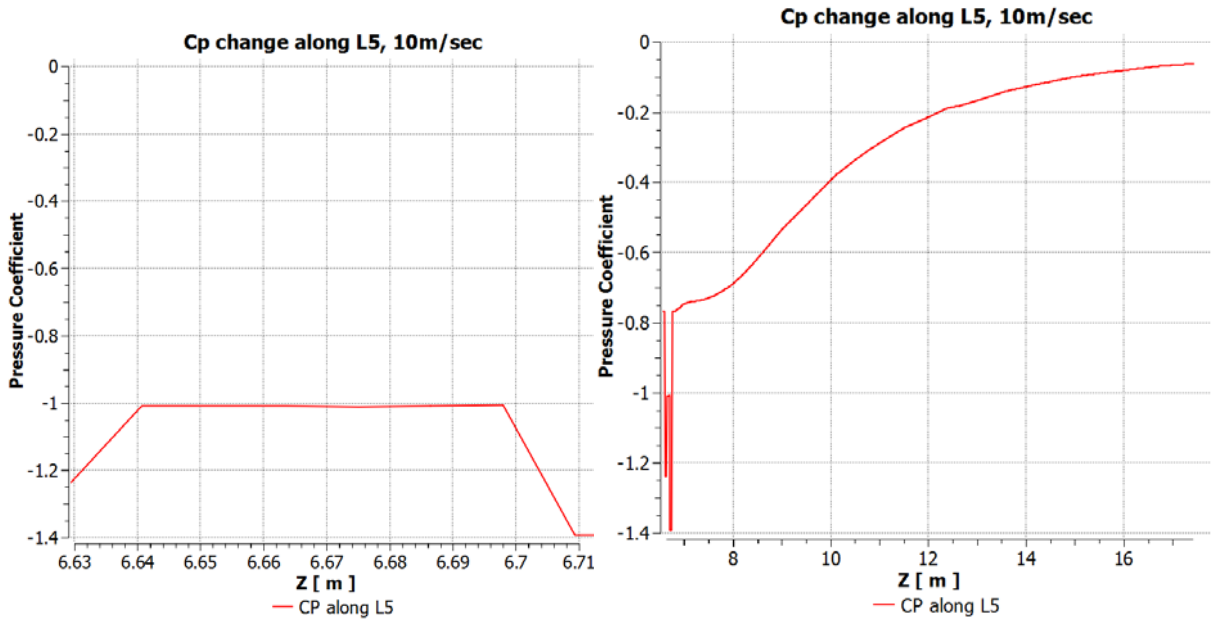


Fig.B. 72, Cp changes between panels, and above roof, Line 5, 10m/sec

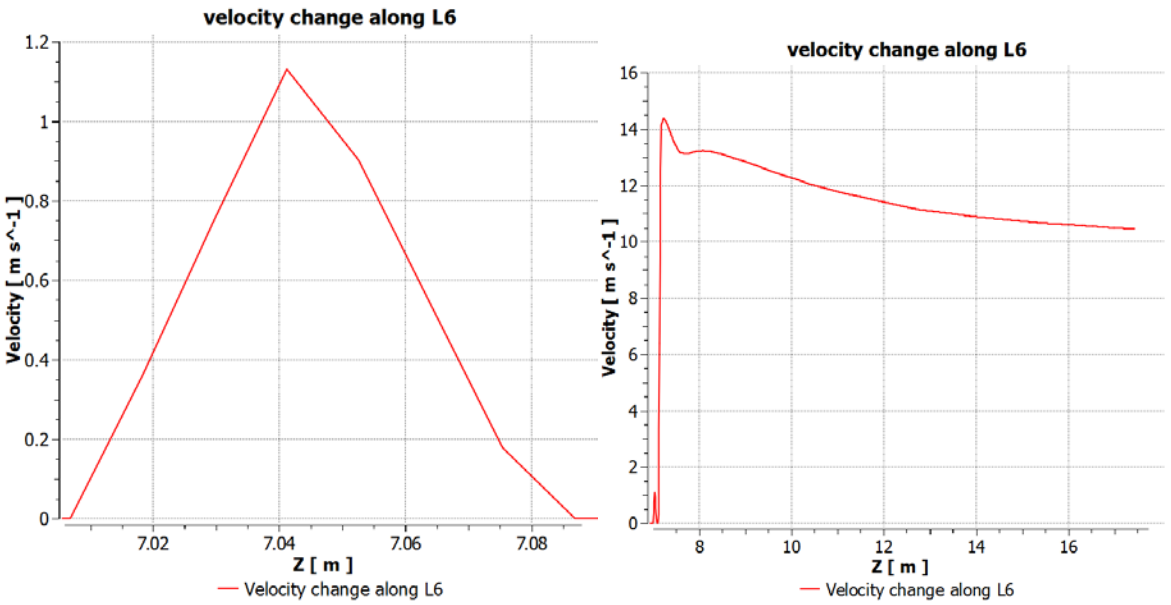


Fig.B. 73, Velocity changes between panels, and above roof, Line 6, 10m/sec

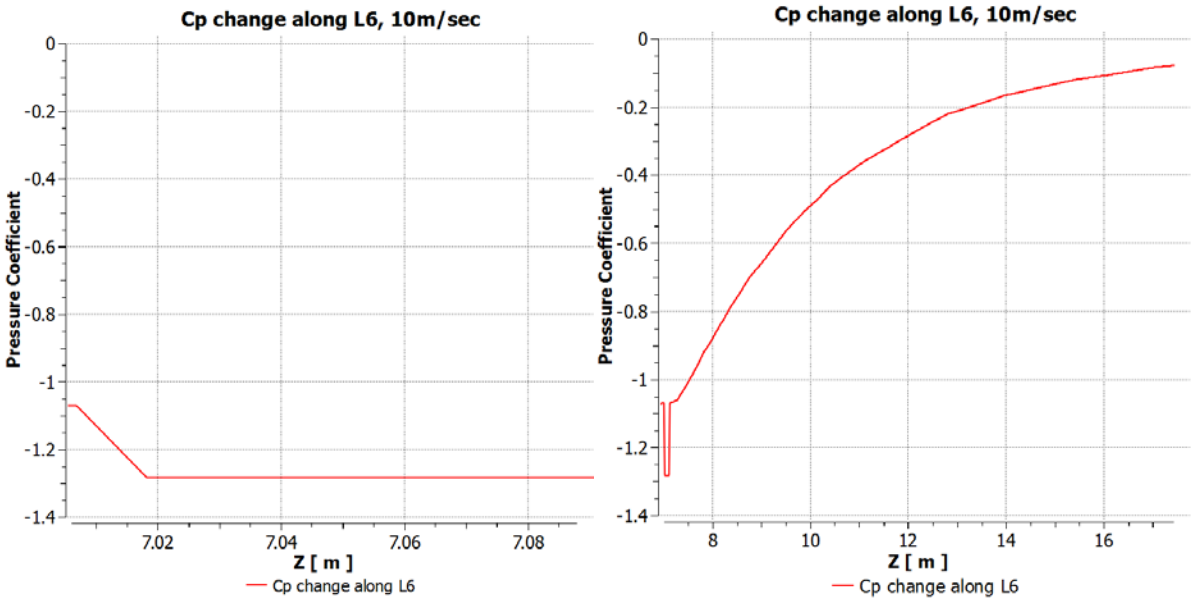
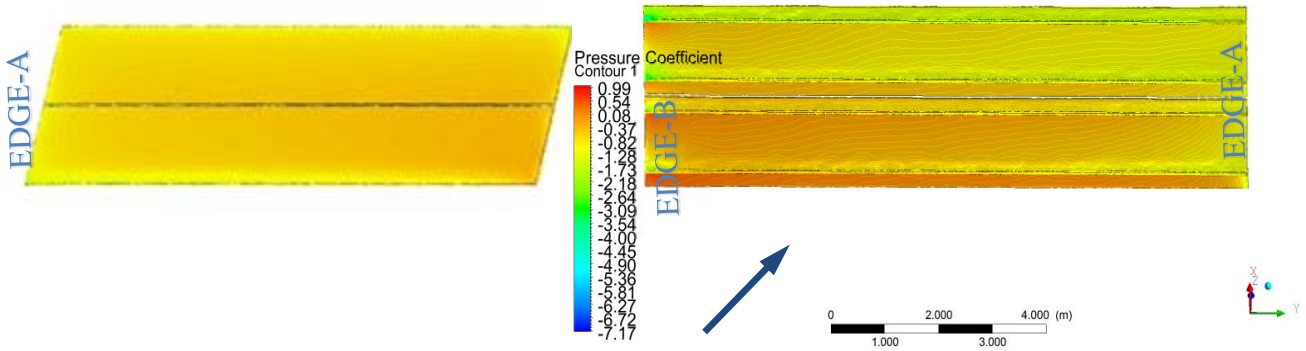


Fig.B. 74, Cp changes between panels, and above roof, Line 6, 10m/sec

B-VII- Pressure contours for solar panels on 15º inclined roofs for wind direction 45º

Flow details presented in Fig.B. 74, show pressure coefficients on top and bottom of solar panels mounted on windward side of a gable roof surface subject to wind in direction 45º.



(a) (b)

Fig.B. 75, Pressure coefficients on top (a) and bottom (b) of the solar panels, windward, slope 15º, wind direction 45º

When comparing the three figures, Fig.B. 74 (a) and Fig.B. 74 (b) it is noticed that distribution of pressure coefficients recorded on bottom of the panels, 0.99 to -4.90 are different from those recorded on top of the panel, 0.08 to -1.28, However, the distribution and values of recorded Cp on bottom of the panels and those corresponding records on roof under the panels, Fig.B. 75 are very similar.

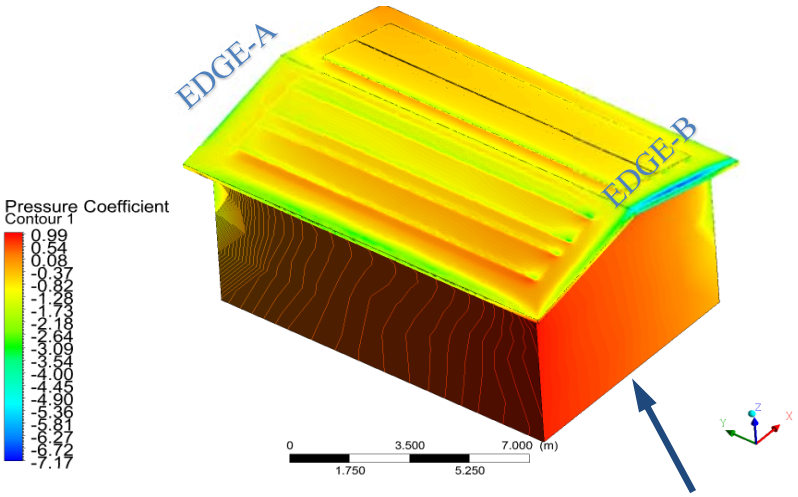


Fig.B. 76, A cut off shows pressure coefficients on roof under solar panels, windward, slope 15º, wind direction 45º

The overall distribution of pressure coefficients on the house, depicted in Fig.B. 76 reveals that the lowest Cp on the roof is concentrated along the edge B on the leeward side of the roof, and second lowest pressure areas are on south and edges A and B on the windward side. However, none of the panels are exist in those very low-pressure areas. In addition, it can be noticed from this figure, that Cp on top of the panels on the leeward, are lightly lower than Cp on top of the panels on the windwards.

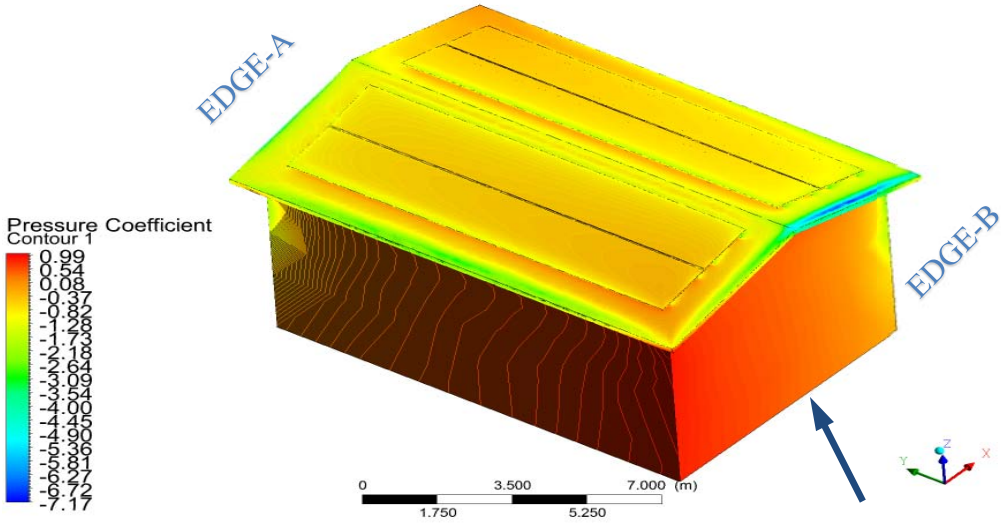


Fig.B. 77, Pressure coefficient on top surface of the solar panels in both windward and leeward, slope 15º, wind direction 45º

B-VIII-0.0º Pressure contours for solar panels mounted on 15º inclined roofs for wind direction

When comparing the pressure coefficients records on top Fig. B.78. (b) and bottom, Fig. B.78 (a) it can be noticed that distribution of pressure coefficients on bottom of the panels is lower the than the Cp of top of the panels, near the wind ward and leeward edges. However, pressure coefficients, on roof surface under the panels, Fig. B.74 are like those, on top of the panels.

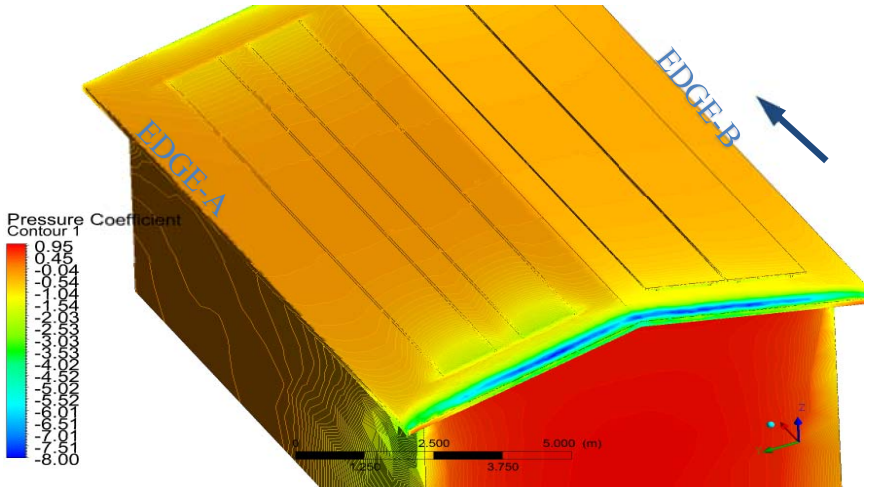
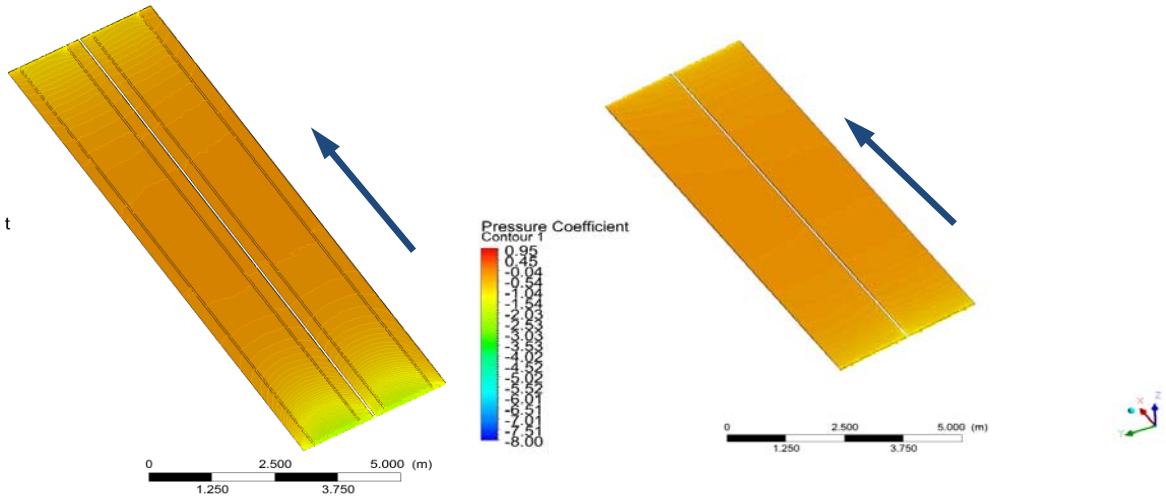


Fig.B. 78, Cp on roof under solar panels, Slope 35, windward, wind direction 0.0



(a) (b)

Fig.B. 79, Pressure coefficients on bottom (a) and top (b) of solar panels, windward, slope 15º, wind direction 0.0º

The overall distribution of pressure coefficients on the house, depicted in Fig. B.79 shows that the lowest Cp on the roof is concentrated along front windward edges of the roof, and second lowest pressure areas are the edges A and B and back leeward edges. However, none of the panels are exist in those very low-pressure areas. In addition, it can be noticed from those figures, that either sides of the gable roof are subject to same exact pressure coefficient distribution, which is expected for symmetrical geometry and flow.

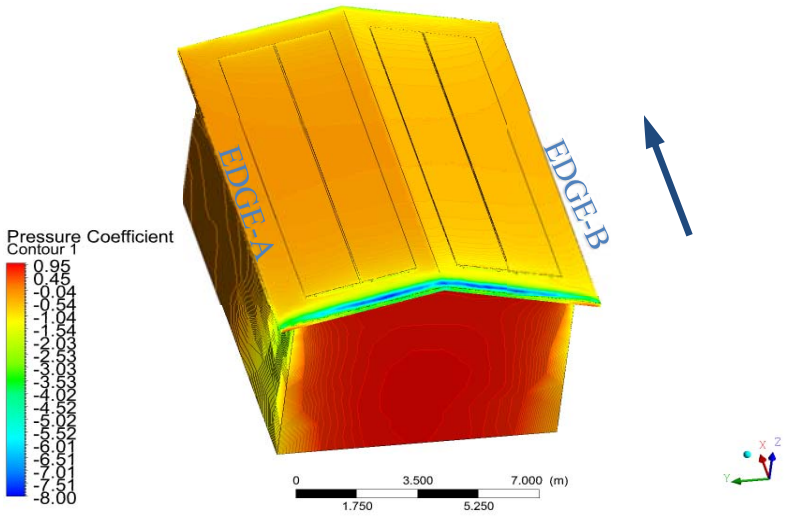


Fig.B. 80, Pressure coefficients on Roof mounted solar panels and around the building, windward, slope 15º, wind direction 0.0º

B-IX- Comparison of pressure coefficient distribution on roof mounted solar panels and on roof without solar panels, slope 15º

To reflect the wind effects on the roof surfaces with panels, the distribution of pressure coefficients on specific three polylines is monitored on the three surfaces hereafter.

B-IX-i Pressure coefficients on bottom surface of the solar panels Vs. roof surface under solar panels, for 15º inclined roofs and 90º, 45º and 0º wind directions, windward

On the windward surface, the monitored Cp on roof surface under panels and on bottom surface of the panel, is illustrated on Fig. B.80 for 90°, when the wind direction is perpendicular to the

ridge. In this figure Cp along lines PL1, PL9 and PL17 on roof under panels and on bottom of the panels, depict very high similarity throughout the whole length of the lines, which is much higher than those on roofs with panels installed on 27º and 35º inclined roofs. However, Cp along PL9 reveals slight differences in the range of 0.03, where Cp on roof under panels is nearly -1.06 to -1.50 in average Vs – 1.0 to -1.50 for Cp on bottom of the panels. Moreover, pressure coefficients on either surface on all lines PL1, PL9 and PL17 demonstrate much lower pressure coefficients in the middle of the lines, -2.3, -0.95 and -2.1 respectively, than on edges of the panel arrays, -1.0, -0.5 and -1.5 respectively, Fig. B.80.

When observing the pressure coefficient changes in wind flow at 45°, Fig. B.81, Cp along all the three lines PL1, PL 9 and PL17 on roof under panels and on bottom of the panels, demonstrates extremely similar values along whole lengths of the lines, which are way closer than Cp on corresponding surfaces in the other slopes reported above, 27º and 35º. However, Cp on PL17 depicts slight differences nearly 0.02 in average along the length of the line PL17. It is noticed as well that the pressure coefficients on both PL1 and PL9 decrease slightly, from 0.3, -0.35 at the windward ends to -1.5, -1.0 towards the leeward ends of the lines PL1 and PL9 respectively. However, Cp remains constant on PL17 at -1.5 for most of the length while decreases sharply to -2.25 near windward edge. Fig. B.81.

On the other hand, the pressure coefficients for wind direction 0º, along PL1, PL9 and PL17 on both roof surface under panels and on bottom surface of the panels, are extremely similar, which might be considered as Cp on one surface mirrors the other. However, Cp along the 3 lines on either surface, reduces highly from -0.2 in the middle of the array to, -1.4 to -1.8 in the windward side, and to -0.7 to -1.0 on the leeward side, while they change slightly in the middle parts along8.0 m long of those lines. Nonetheless, wind direction 0.0 does not govern the wind design pressure coefficients on gable roofs, either with or without panels, Fig. B.82.

In addition, high similarity of Cp on the three lines in the last case, might be attributed to symmetrical geometry and flow in that case, and because the flow is parallel to surfaces where much less turbulences happen.

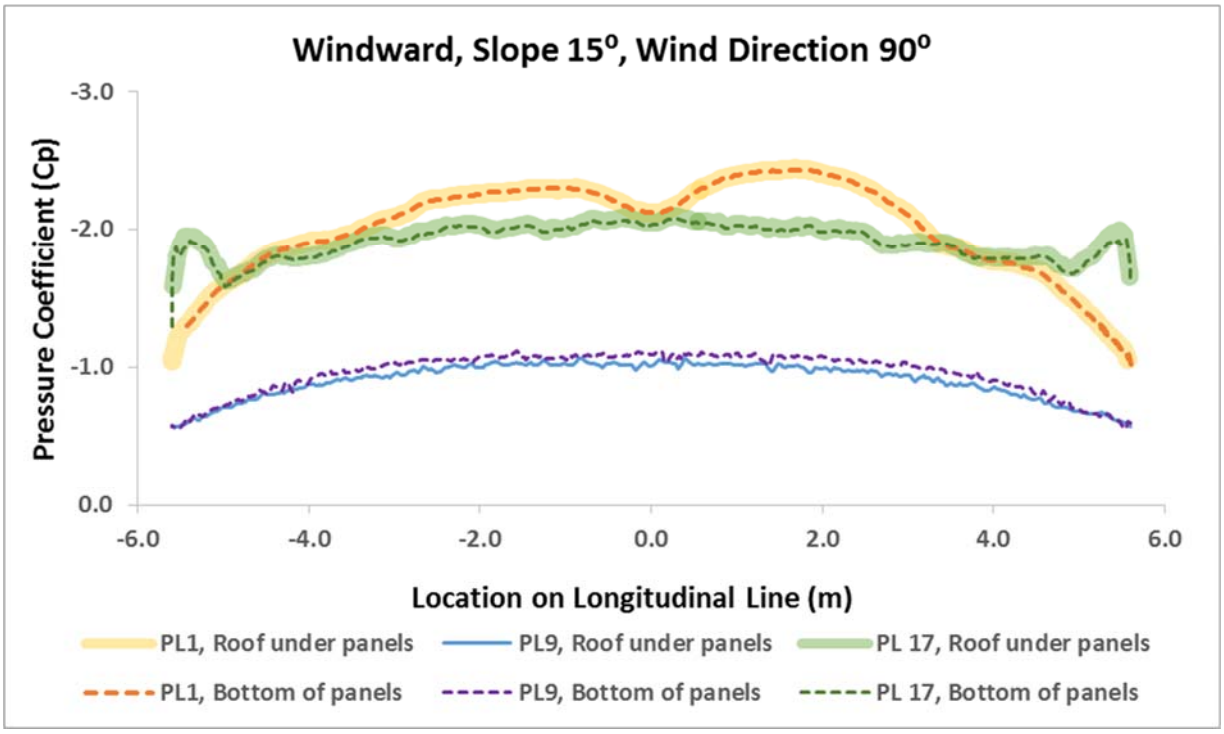


Fig.B. 81, Pressure coefficient distribution on the bottom surface of the solar panels and on the roof surface under the panels, for roof slope 15º, and wind direction 90º, windward side

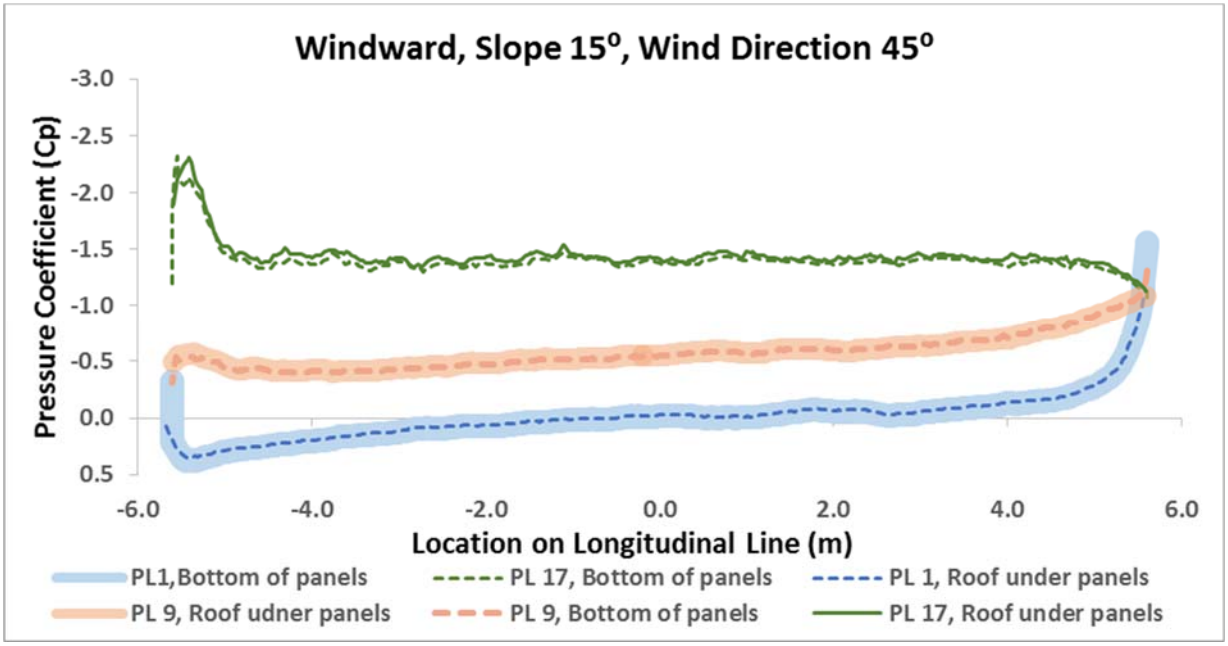


Fig.B. 82, Pressure coefficient distribution on the bottom surface of the solar panels and on the roof surface under the panels, for roof slope 15º, and wind direction 45º, windward side

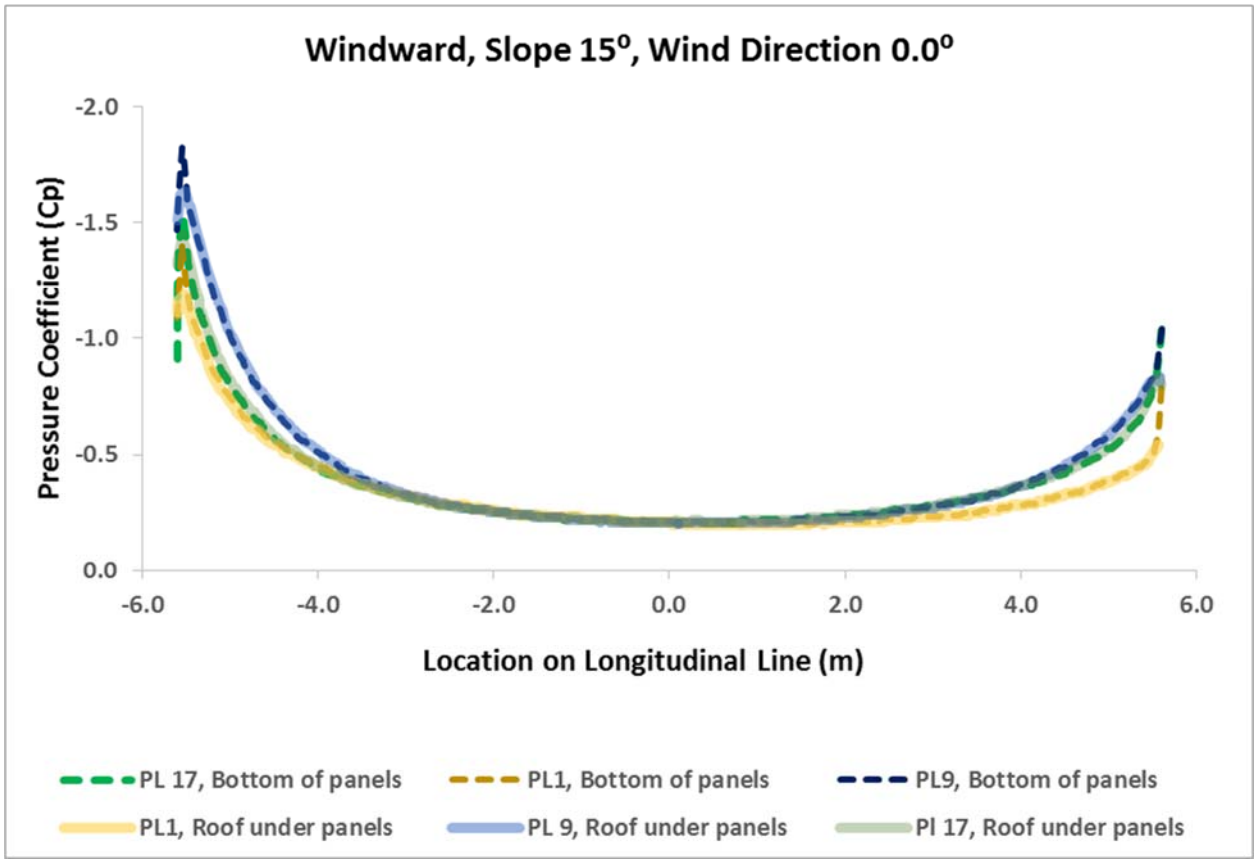


Fig.B. 83, Pressure coefficient distribution on the bottom surface of the solar panels and on the roof surface under the panels, for roof slope 15º, and wind direction 0.0º, windward side

B-IX-ii- Pressure coefficient on roof under panels vs. roof without panels, for 15º inclined roofs and 90º, 45º and 0º wind directions, windward

Presentation of the wind-induced pressure coefficients on the roof without solar panels surface and on the roof surface under the solar panels, for wind direction 90º, 45º, and 0º, are shown in Figs. B.83, B.84 and B.85 respectively.

When wind flow makes, 90°, with the ridge of the roof, Cp along PL1 on roof surface under panels shows pressure coefficients, -1.0 to -2.3, which are much lower than Cp on the corresponding line on roof without panels, -0.8 to -1.50. Similarly, PL17 shows suction, -1.6 to -2.1, which is much lower than Cp on the corresponding line on roof without panels, -0.80 to -0.90. However, pressure coefficients on PL9 on roof under panels, near middle of the array, are -0.5 to -0.90, which are moderately lower than the pressure coefficients along PL9 on the roof without panels, -0.50 to -0.60. On the other hand, Cp on all the lines are symmetrical around the

middle of the roof, that for both roof surfaces under the panels and roof surface without solar panels, Fig. B.83.

When wind flows at 45° wind direction (Fig. B.84) it is noticed that pressure coefficients on roof under the panels and on the roof surface without solar panels have similar trends. For example, pressure coefficients on PL1 located near the windward edge of the solar array, is 0.35 to -1.10 which is much higher than corresponding line on the roof with no panels, 0.3 to -0.75. Nonetheless, PL17 located nearest to the ridge , pressure coefficients on roof under panels, -1.1 to -2.25 are much lower than Cp on the corresponding lines on the roof with no panels, which is nearly constant about -0.75. On contrary, Cp on the middle line PL 9, ranges from -0.6 to -1.10 is slightly lower than the corresponding line on the roof without panels, -0.60 to -0.75. In addition, pressure coefficients along PL1 and PL9 on both surfaces decrease towards the windward edge of the roof.

On contrary, for wind direction 0º, pressure coefficients along all the polylines PL1, PL9 and PL17 on roof surface under panels are slightly different from those on roof without panels. In addition, Cp along all the three lines reduces highly from -0.23 in middle of array to -0.75 to -1.65 in the windward side, and to -0.50 to -0.75 on the leeward side, while remains nearly constant in the middle parts of those lines, Fig. B.85.

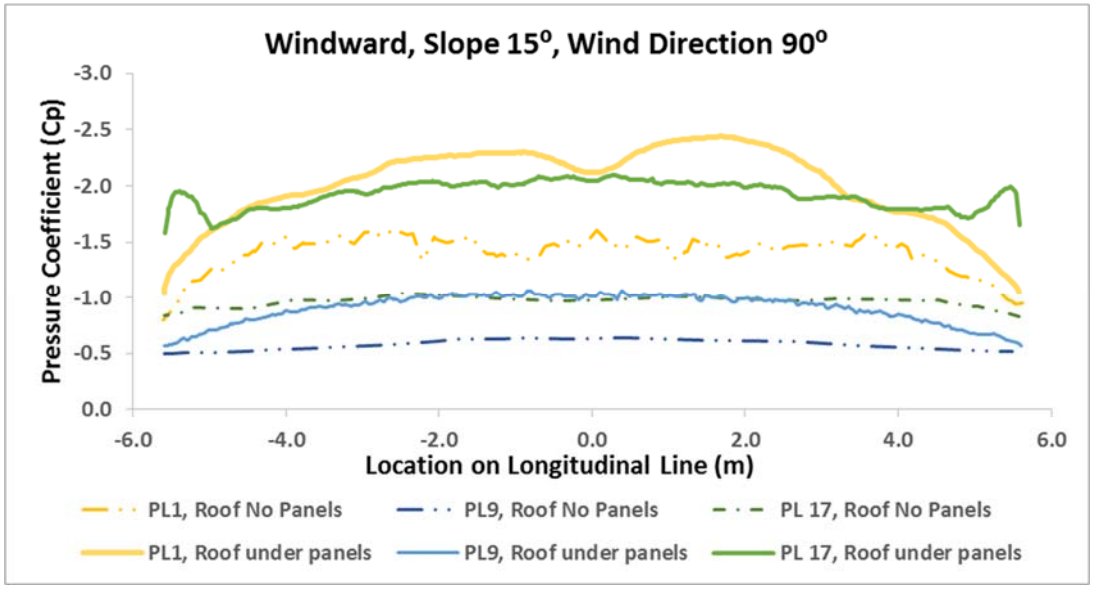


Fig.B. 84, Pressure coefficient distribution on roof without solar panels and on the roof surface under the panels, for roof slope 15º, and wind direction 90º, windward side

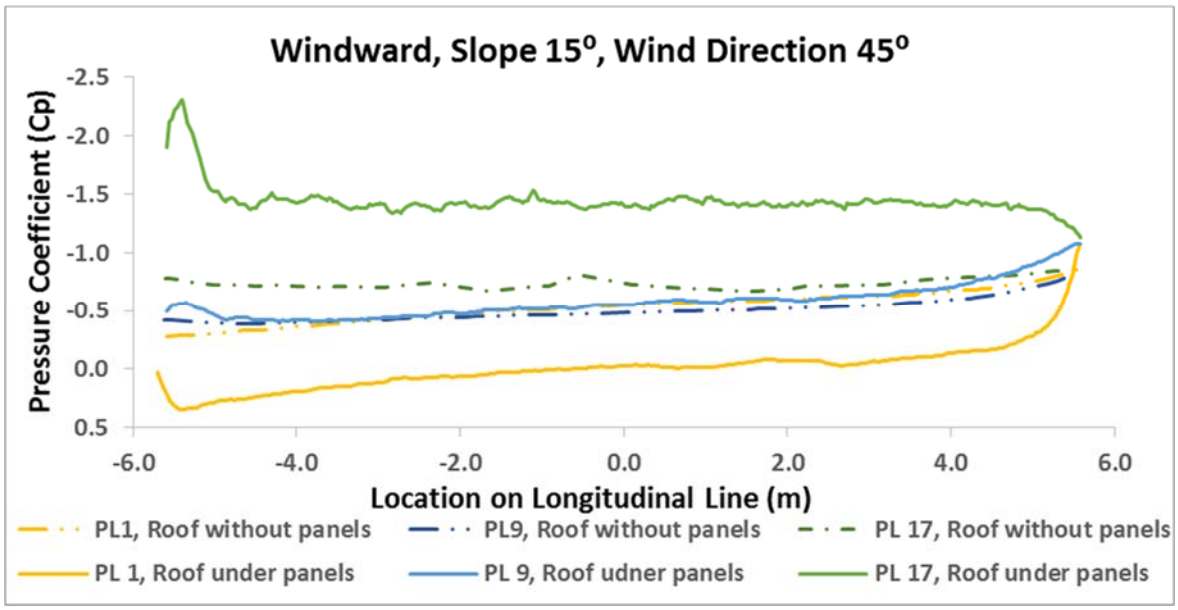


Fig.B. 85, Pressure coefficient distribution on roof without solar panels and on the roof surface under the panels, for roof slope 15º, and wind direction 45º, windward side

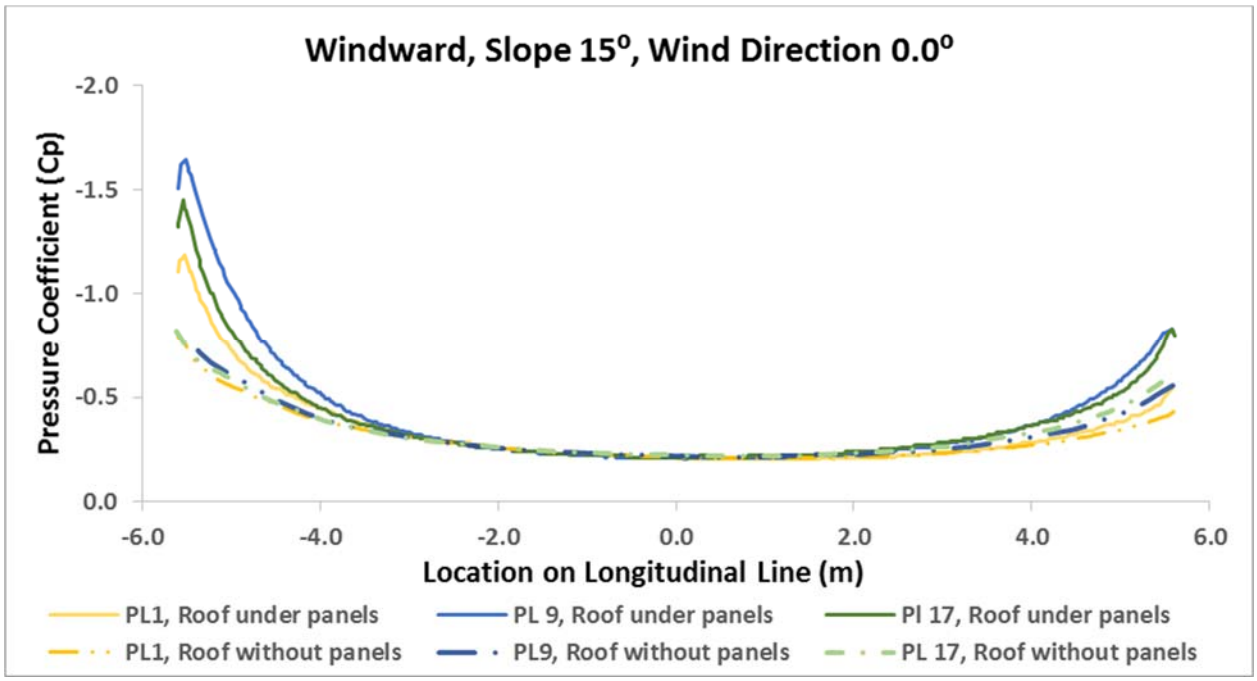


Fig.B. 86, Pressure coefficient distribution on roof without solar panels and on the roof surface under the panels, for roof slope 15º, and wind direction 0.0º, windward side

B-IX-iii Pressure coefficients on bottom surface of the solar panels Vs. roof without panels, for 15º inclined roofs and 90º, 45º and 0º wind directions, windward

Wind-induced pressure coefficients on the roof surface without solar panels and on bottom surface of the solar panels, for wind direction 45º, 90º and 0º, are shown in Figs. B.86, B.87, and B.88 respectively.

As wind flows at 90° wind direction Cp along PL1 on bottom surface of panels recorded -1.30 to -2.40, much lower than Cp on the corresponding line on roof without panels, -0.80 to -1.50. Similarly, PL17 shows suction, -1.3 to -2.1, which is much lower than Cp on the corresponding line on roof without panels, -0.80 to -1.00. However, pressure coefficients on PL9 on roof under panels, near middle of the array, recorded -0.5 to -1.0, which are moderately lower than the pressure coefficients along PL9 on the roof without panels, -0.50 to -0.60, Fig. B.86.

Like the other cases in same wind direction, Cp on all the lines are symmetrical around the middle of the roof, that for both bottom surface of panels and roof surface without solar panels.

In case of wind flows at 45° it is noticed that pressure coefficients on PL1is 0.30 to -1.70 which is much higher than corresponding line on the roof with no panels, -0.30 to -0.75. Nonetheless, PL17 located nearest to the ridge, pressure coefficients on bottom of panels -1.2 to -2.30 are much lower than Cp on the corresponding line on the roof with no panels, which is nearly constant about -0.70 to -0.80. On contrary, Cp on the middle line PL 9, is -0.60 to -1.25 is slightly lower than the corresponding line on the roof without panels, -0.45 to -0.70. In addition, there is decrease in pressure coefficients along PL1 and PL9 towards the leeward edge of the roof, Fig. B.87

Differently, for wind direction 0º, pressure coefficients along PL1 and PL17 on bottom of panels are slightly lower, (0.03) than those on roof without panels. However, pressure coefficients along PL 9 on roof under panels are slightly lower than that on roof without panels, nearly 0.06, Fig. 4.147. In addition, Cp along all the three lines reduces highly from -0.23 in middle of array to -0.80 to -1.80 in the windward side, and to -0.45 to -0.75 on the leeward side, while remains nearly constant in the middle parts of those lines, Fig. B.88

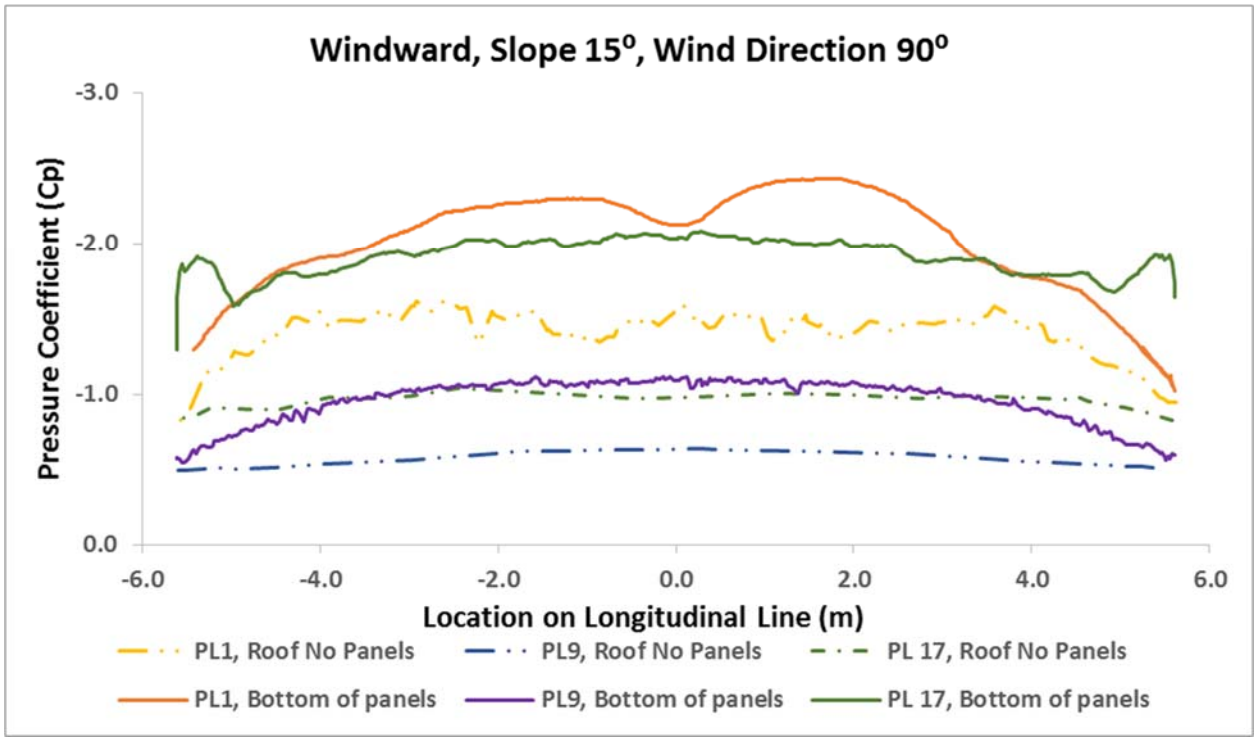


Fig.B. 87, Pressure coefficient distribution on roof without solar panels and on bottom of the panels, for roof slope 15º, and wind direction 90º, windward side

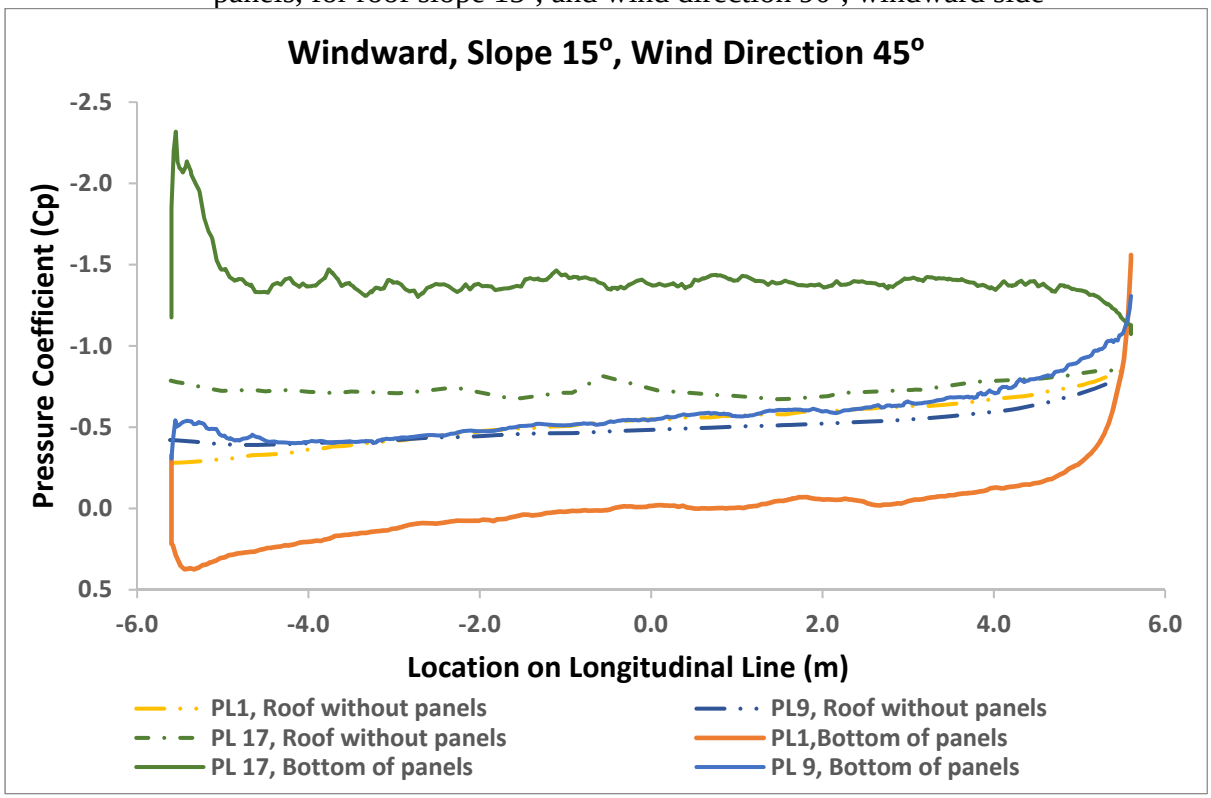


Fig.B. 88, Pressure coefficient distribution on roof without solar panels and on bottom of the panels, for roof slope 15º, and wind direction 45º, windward side

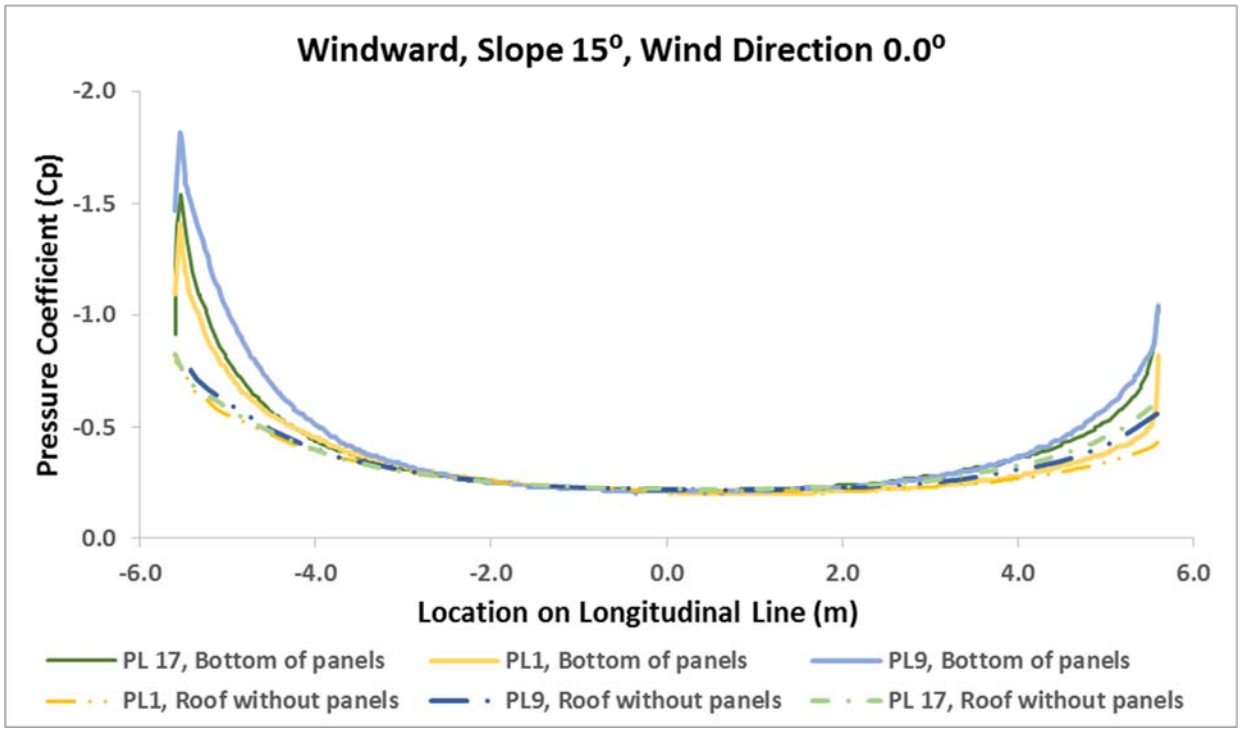


Fig.B. 89, Pressure coefficient distribution on roof without solar panels and on bottom of the panels, for roof slope 15º, and wind direction 0.0º, windward side

B-IX-iv Pressure coefficients on top surface of the solar panels vs. roof without panels, for 15º inclined roofs and 90º, 45º and 0º wind directions, windward

The following Figs. B.89, B.90 and B.91, illustrate the pressure coefficients on the roof without solar panels surface and on top surface of the solar panels, for wind direction 90, 45º and 0º.

When wind blows in the 90° wind direction, the pressure coefficients on top of the panels along PL1 on top surface of panels records pressure coefficients, -0.60 to -0.90, which is much higher than Cp on the corresponding line on roof without panels, -0.75 to -1.60. However, Cp on PL17 shows suction, -1.25 to -1.60, which is much lower than Cp on the corresponding line on roof without panels, -0.80 to -0.90. Nonetheless, pressure coefficients on PL9 on the top of the panels, near middle of the array, are -0.5 to -0.60 are very close to the Cp on PL9 on the roof without panels, -0.50 to -0.60. Very good symmetry is observed in the Cp on all the 3 lines in this wind direction, Fig. B.89.

For 45° wind direction (Fig. B.90) it is noticed that pressure coefficients of the top surface of solar panels on PL1 located near the windward edge of the top of solar array, is -0.30 to -1.50 which is much lower than corresponding line on the roof with no panels, -0.25 to -0.75. Similarly, PL17 located nearest to the ridge, pressure coefficients on top of panels -0.90 to -1.40 are much lower than Cp on the corresponding line on the roof with no panels, which is nearly constant, -0.70 to -0.80. On contrary, Cp on the middle line PL 9, is -0.60 to -1.25 is very close to the Cp on the corresponding line on the roof without panels. In addition, pressure coefficients along PL1 and PL9 on both surfaces decrease towards the leeward edge of the roof.

On contrary, for wind direction 0º, pressure coefficients along PL1, PL9 and PL17 on top of panels are slightly lower, (0.01) than those on roof without panels, Fig. 4.150. In addition, Cp along all the three lines reduces highly from -0.23 in middle of array to -1.0 to -1.30 in the windward side, and to -0.35 to -1.20 in the leeward side, while remains nearly constant in the middle parts of those lines, Fig. B.91.

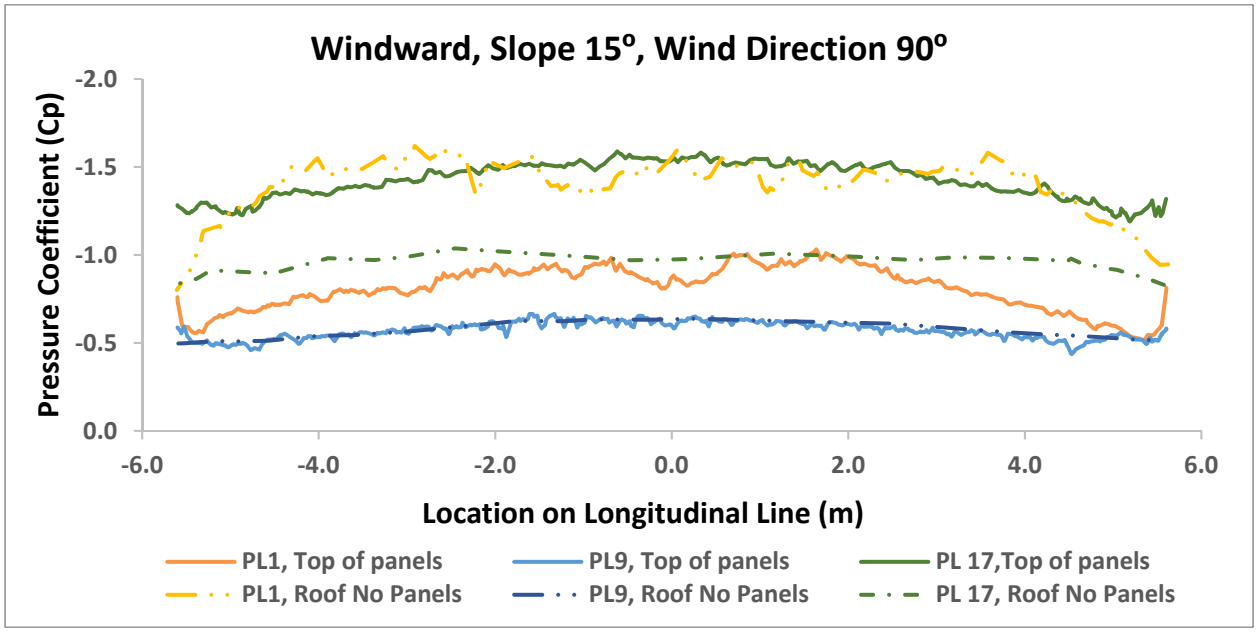


Fig.B. 90, Pressure coefficient distribution on roof without solar panels and on Top of the panels, for roof slope 15º, and wind direction 90º, windward side

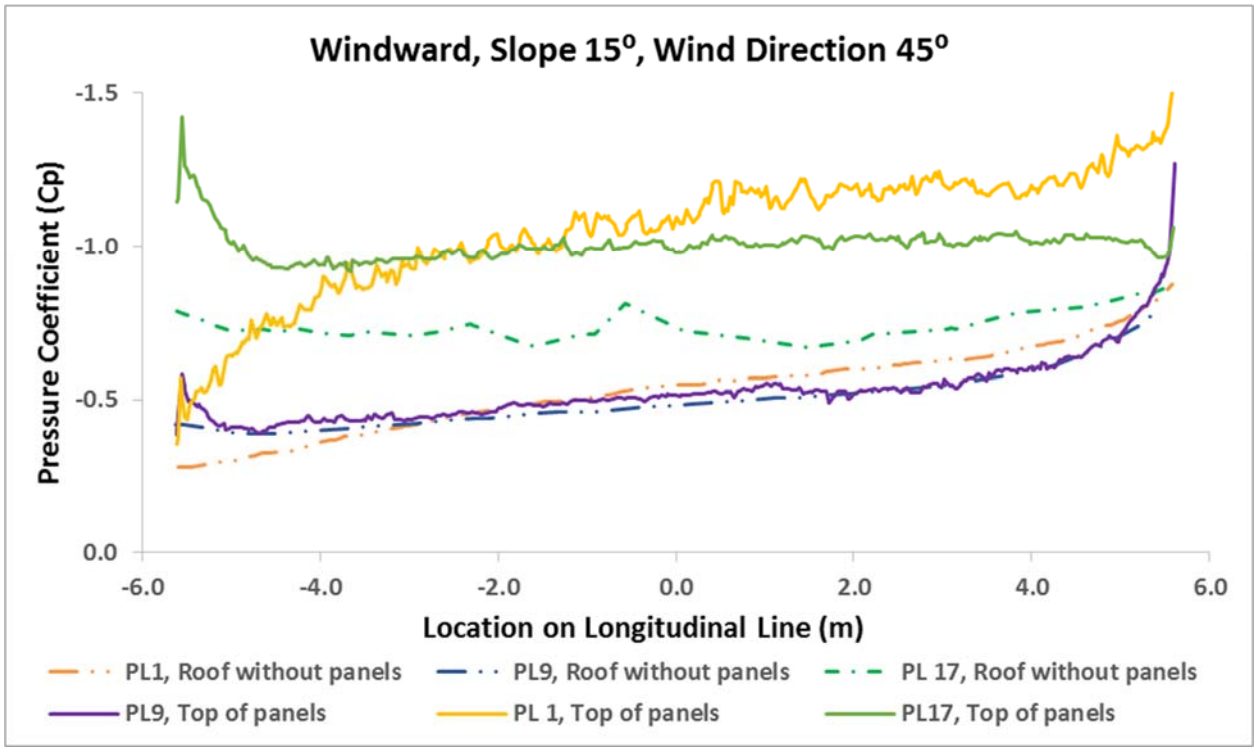


Fig.B. 91, Pressure coefficient distribution on roof without solar panels and on Top of the panels, for roof slope 15º, and wind direction 45º, windward side

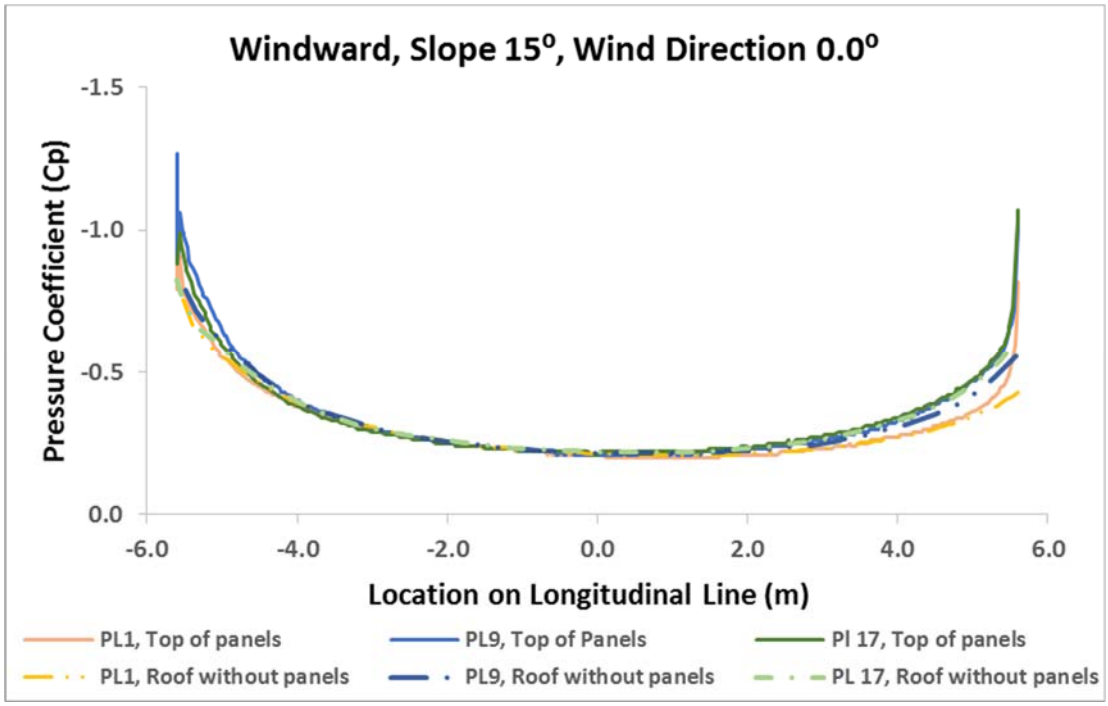


Fig.B. 92, Pressure coefficient distribution on roof without solar panels and on Top of the panels, for roof slope 15º, and wind direction 0.0º, windward side

B-X- Flow-structure interaction for the roof mounted solar panels for wind direction 90º and slope 15º

Figure B.92 illustrates pressure coefficients on bottom of the solar panels and their rail supports, in wind direction 90º, windward side. The lowest pressure coefficients under the panels, -3.50, is shown at south and north edges of the windward array, while higher Cp, -0.98 to -1.70, prevails in the remaining areas. However, there are small spots of much higher Cp, -0.26 to 0.82, are located near edges of rails.

Distribution of wind pressure coefficients on central vertical plane, is shown in Fig. B.93 that helps to appreciate the distribution of Cp around the roof. The vertical plane shows lowest Cp, -4.94 to -3.50, concentrated at the front edge of the windward side of the roof, and second lowest Cp, -2.42 to -1.70, is located near the ridge in either windward and leeward sides.

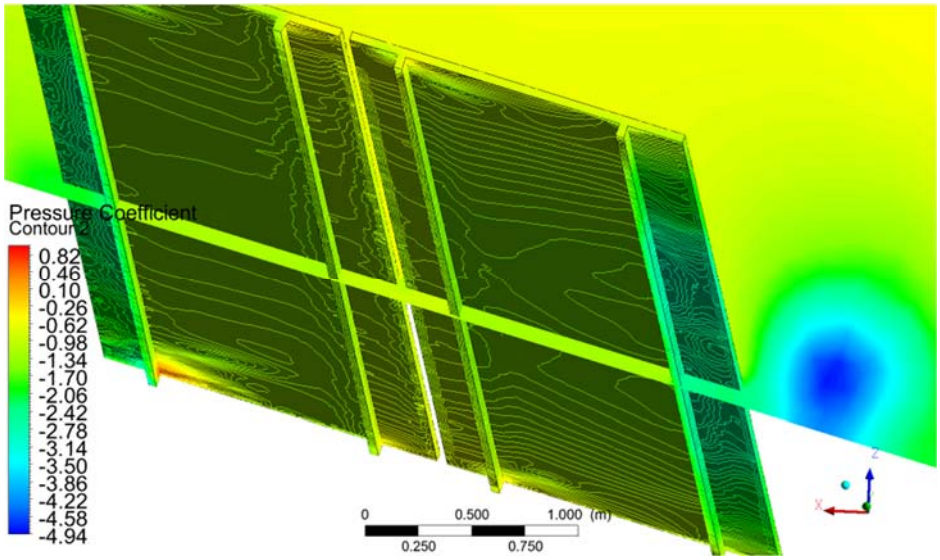


Fig.B. 93, Pressure coefficients on a perpendicular plane under panels, windward, slope 15º, wind direction 90º,

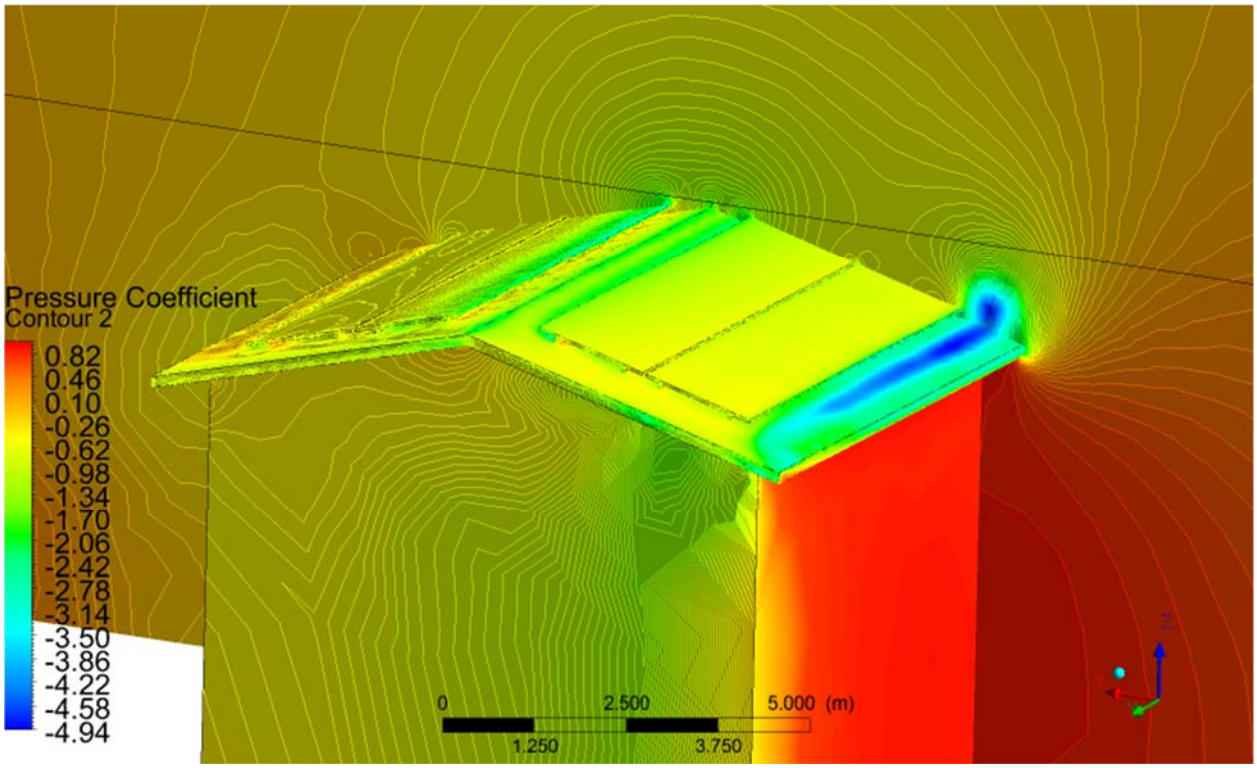


Fig.B. 94, Pressure coefficients on a perpendicular plane with the house, windward, slope 15º, wind direction 90º,

Figures B.94 and B.95 show flow velocity changes across the perpendicular plane, above the roof from two perspective, windward and leeward sides, respectively, by illustrating velocity stream lines at a central vertical plane. As can be noticed from Fig. B.94, the flow starts at 0.0 m/s near roof surface at the windward side, then increases as the distance from panels increases, where it reaches nearly 50 m/sat 4" (0.10 m) above the panel surface and near the front edge of the panel array on the windward side.

However, the velocity of flow increases as the flow approaches the ridge, where it reaches nearly 60 m/s at the back edge of windward panel array, at 4" (0.10 m) distance above the panels. Nonetheless, the flow speed increases higher to 77m/s near the ridge in the area with no panels, and that on both sides of the ridge. In the same manner, flow speed increases as distancing from panel surface, and as approaching the back edges of the leeward side.

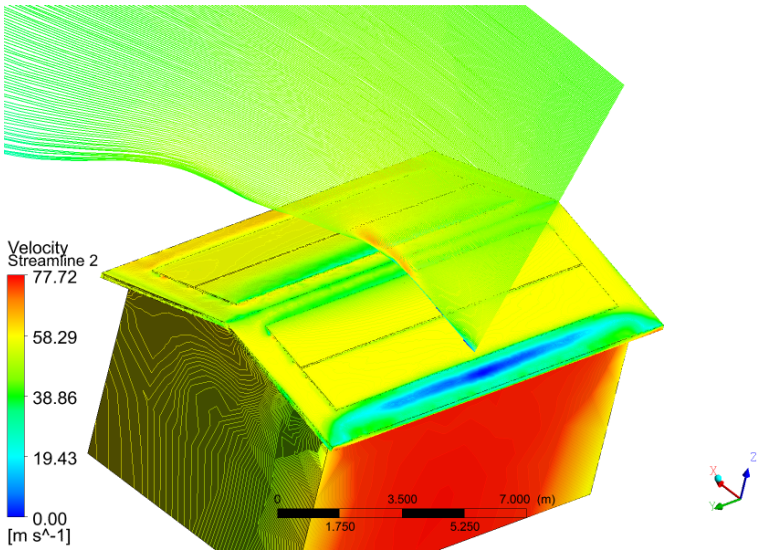


Fig.B. 95, velocity stream lines at middle cross section plane, windward, slope 15º, wind direction 90º,

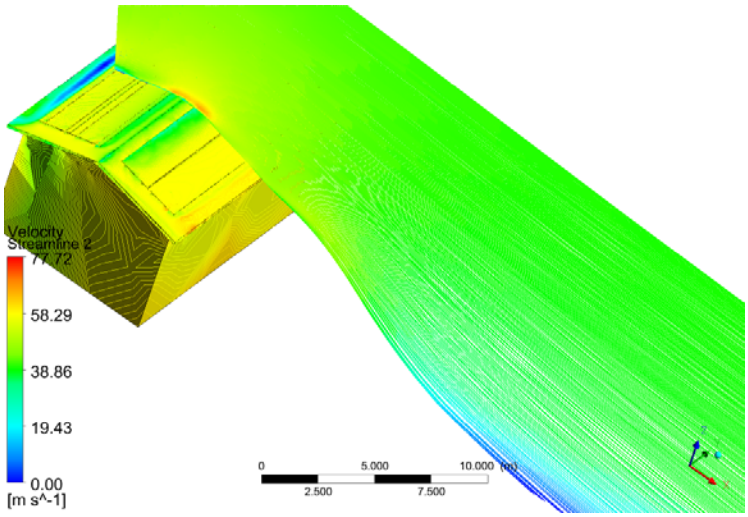


Fig.B. 96, velocity stream lines at middle cross section plane, Leeward, slope 15º, wind direction 90º,

However, difference from the windward, the high flow speed, reaches 77 m/sabove the south edge of leeward side of the panel array, Figure B.95, at height 6" (0.150 m) above the panels. In addition, the high flow speed above the panel array, 77m/sec., extends to nearly middle of the leeward array.

On the other hand, flow speed decreases from 40 m/s to 0.0m/sec, as the flow approaching the ground after passing the building leeward side, beyond the building, Fig. B.95.

The whole distribution of Cp on the top of the roof and solar panels is illustrated in Fig. B.96. The panel array in the windward side is subjected to -0.26 to -1.18, at the south edge of windward side, which is higher than -2.41 to -0.26, on the leeward side. On the other hand, the largest suction of the roof, -2.71to -4.55, is spread along the front edge of the windward side of the roof.

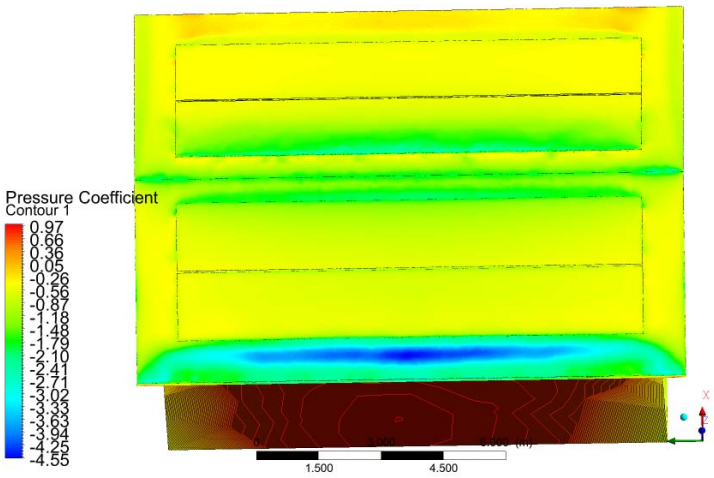


Fig.B. 97, Pressure coefficients contour, whole roof, windward, slope 15º, wind direction 90º,

In Fig. B.97 the vortex core formations are distributed in small sizes around the panels and large sizes around the building, where the largest vortex cores are located at the corners of the building on the leeward side, and on sides of the building. The corner vortices are longitudinal and developed from detachment of flow from the sharp edges and corners of the building. However, the transversal vortex cores which are smaller, are noticed near the ridge on the leeward side. Further smaller transversal vortex cores are located around the edges of the solar panels. Nonetheless, the smallest vortex cores are located on the surface of the roof under solar panels and on surfaces of the solar panels, Figs. B.97 to B.98.

Figures B.98 and B.99 illustrate vortex cores under and on top the solar panels, windward side. Those figures point out the sizes of the vortex cores under the panels are smaller than on top of

panels. However, the pressure coefficients under the panels is much lower on bottom of panels, -4.94 to -1.97, than on top of the panels -1.97 to -4.94.

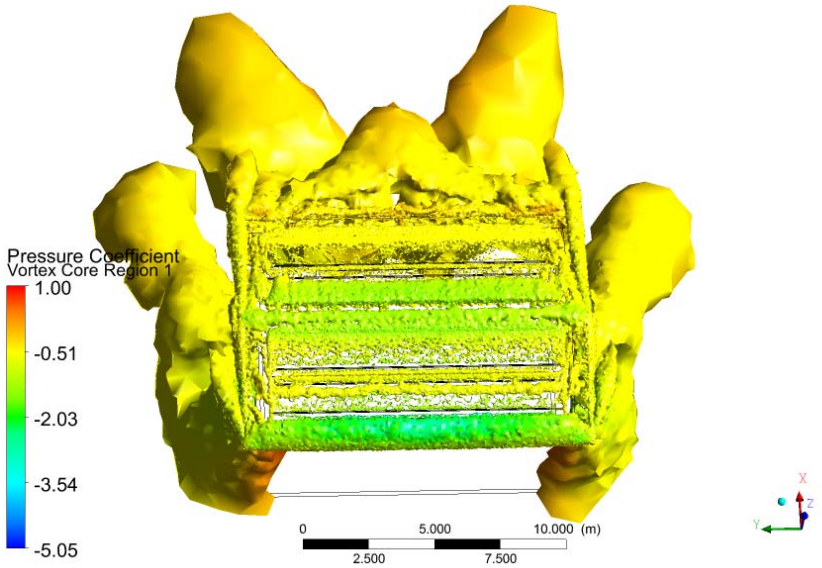


Fig.B. 98, Vortex core distribution on roof and on the building structure, windward, slope 15º, wind direction 90º,

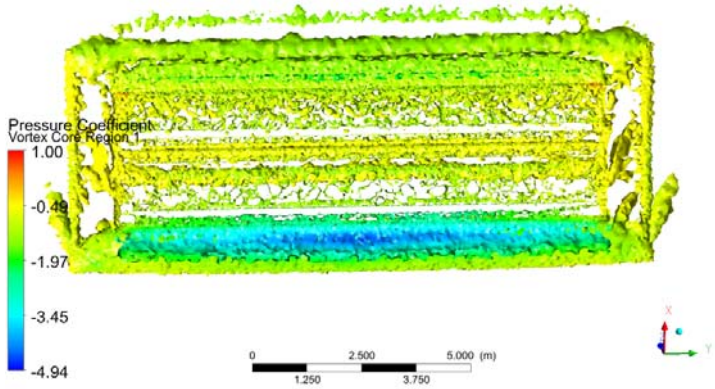


Fig.B. 99, Vortex core distribution, on bottom of the panels, windward, slope 15º, wind direction 90º,

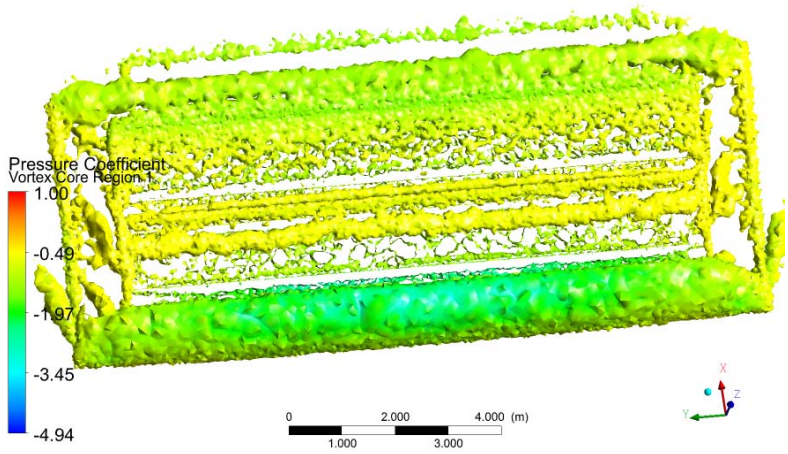


Fig.B. 100, Vortex core distribution, on top of the panels, windward, slope 15º, wind direction 90º,

Figures B.100 and B.101 illustrate vortex cores on bottom and top of the solar panels, respectively, leeward side, without contour background. Those 2 figures point up that there is close similarity in sizes of the vortex cores and pressure coefficients distribution, on bottom and top of the panels, in the leeward side.

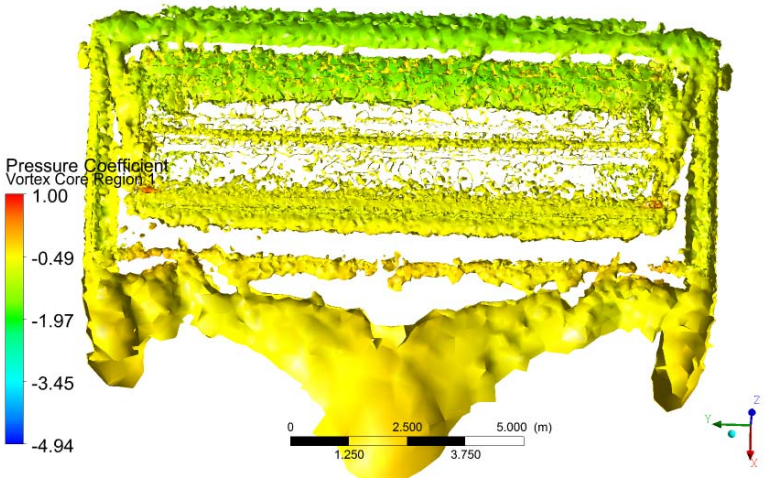


Fig.B. 101, Vortex core distribution, on bottom of the panels, Leeward, slope 15º, wind direction 90º,

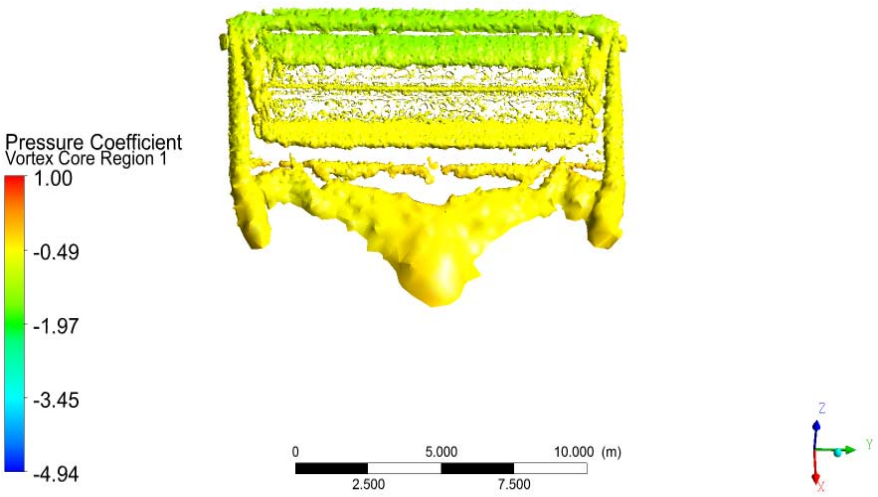


Fig.B. 102, Vortex core distribution, on top of the panels, Leeward, slope 15º, wind direction 90º,

Figures B.102 illustrates vortex cores and Cp distribution on roof under the panels, windward side, along with vortex cores above the panels on the leeward side and around the building. This figure points out vortex cores on top of the panels are way larger in order of magnitude than those in the flow on roof under the solar panels. Similarly, Fig. B.103 shows very small vortex cores on roof under panels in the leeward side of the roof which are much smaller in order of magnitude than those developed on top of the windward array.

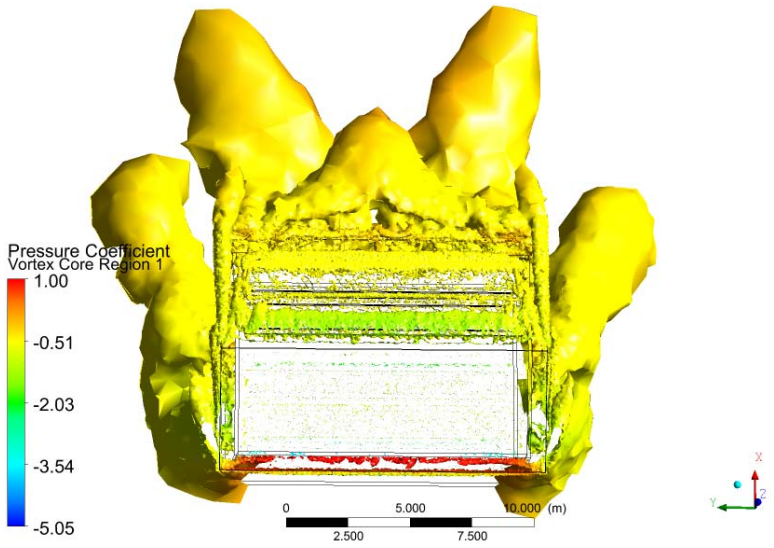


Fig.B. 103, Vortex core distribution, on roof under panels and around the house (turbulent), windward, slope 15º, wind direction 90º,

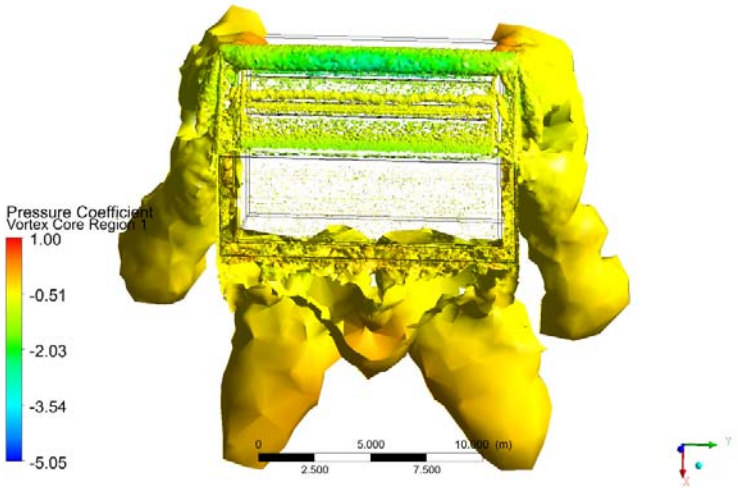
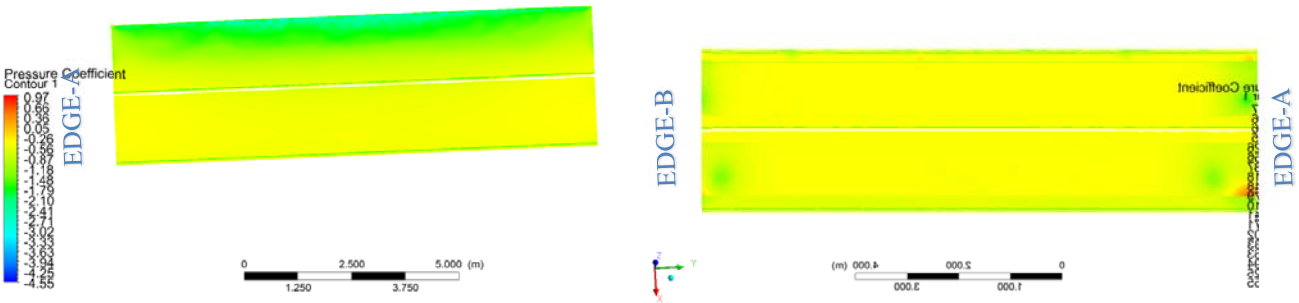


Fig.B. 104,Vortex core distribution, on roof under panels and around the house (turbulent), leeward, slope 15º, wind direction 90º.

Figure B.104 presents distribution of pressure coefficients on top and bottom of the solar panels in the leeward side. The Cp in Fig. B.104 on top and bottom of the panels differ from each other greatly, where Fig. B.104 (a) shows Cp changes from -0.87 to -3.02, while Fig. B.104 (b) points out nearly constant Cp on most of the bottom of the panels, -0.56 to -0.87. However, Fig. B.104 (b) shows 4 spots of lower Cp than the rest of the surface, -1.48 to -2.10, and two small spots of high Cp 0.36 to 0.97 near the corners at the north edge of the leeward array.

On the other hand, Cp presented on Fig. B.104(b) which shows Cp on bottom surface of the panels, leeward side, and Cp presented on Fig. B.105 are very similar, to the degree that they look one mirrors the other. That applies to the nearly constant pressure on most the surfaces, spots of lower Cp and spots of higher Cp.



(a) (b)

Fig.B. 105, Pressure coefficient distribution on (a) Top of panels, (b) Bottom of the panels, Leeward, slope 15º, wind direction 90º,

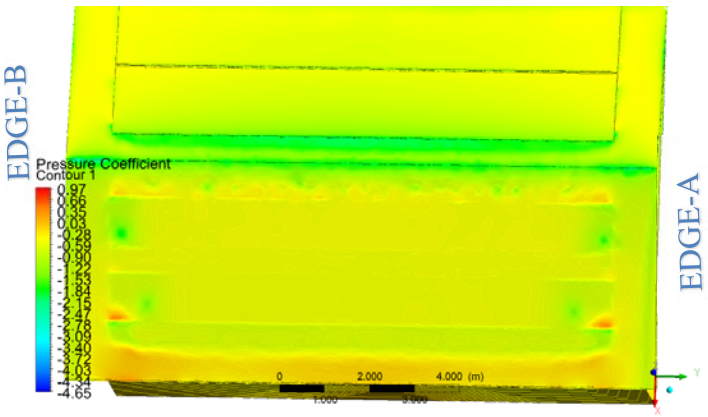


Fig.B. 106, Pressure coefficient distribution on roof under panels Leeward, slope 15º, wind direction 90º,

B-XI- ºWind pressure coefficient and flow distributions along 6 lines perpendicular to panels under and above the panels, windward side, slope 15º, wind direction 90º, wind speeds 40m/s and 10m/s

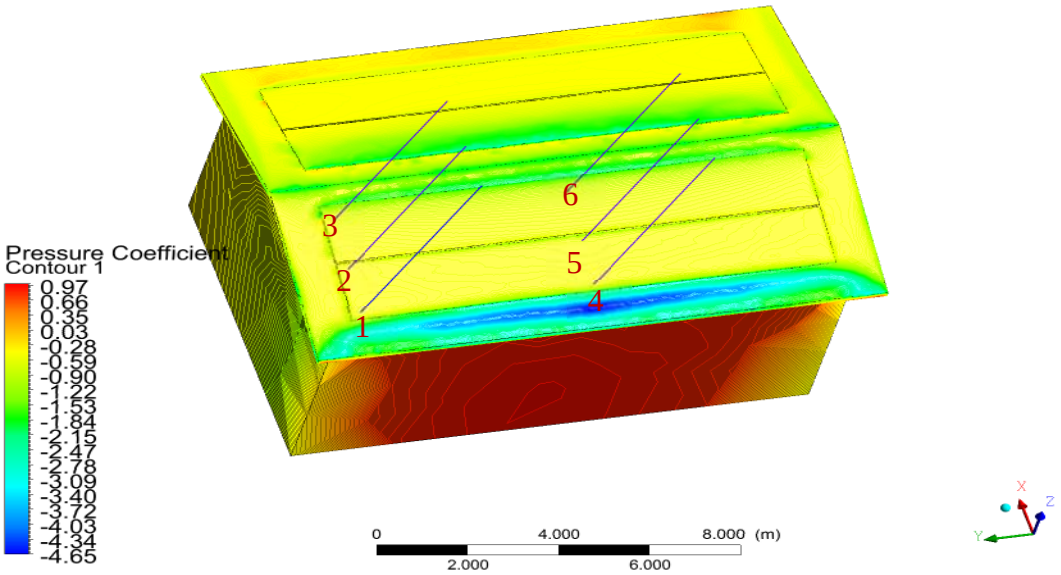


Fig.B. 107, Lines used to draw velocity and pressure changes, windward, slope 15º, wind direction 90º,

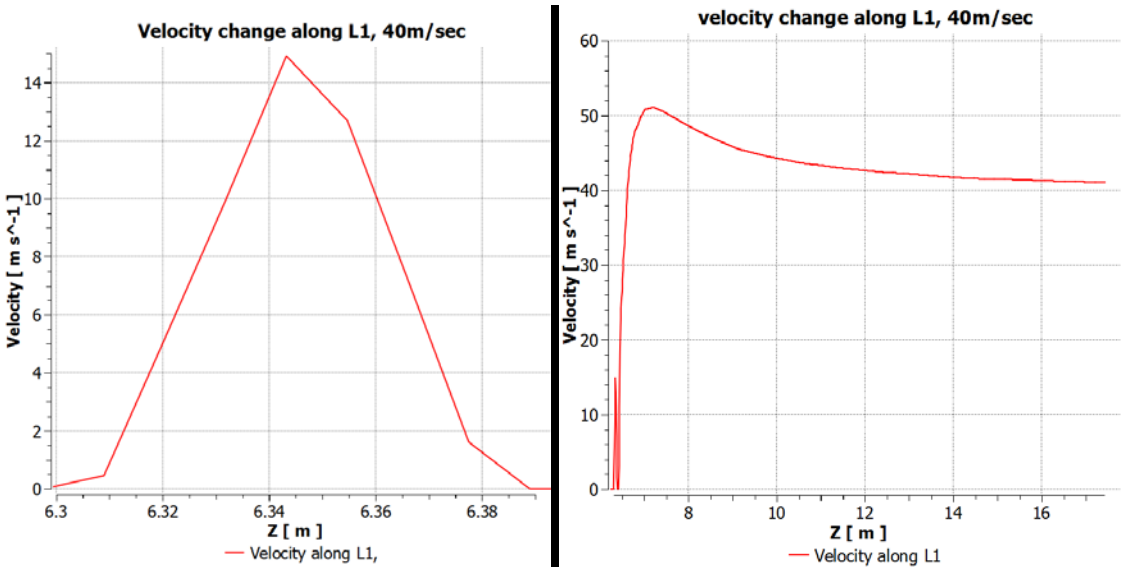
Figure B.106 shows the perpendicular lines on roof which are used to track velocity and pressure coefficient changes in the space between the roof surface under panels and bottom of the panels, then above the panels up to nearly 20m above ground or 12m above the panels until free steam.

The lines are placed on 6 different points distributed near west edge of the solar panel array and near middle cross section of the array.

Figures B.107 to B.108 show distribution of velocities and pressure coefficients, Cp, along the lines 1to 6 for 90° wind direction and 40 m/s incoming wind speed.

For each line, there are two sets of graphs presented where the first set of 2 graphs is for the wind speeds and pressure coefficients inside space between the roof surface and the bottom surface of solar panels, and the second set of 2 graphs is for monitor these variables above the panels up to 15-20 m above their surfaces. Fig. 1.66 represents the distribution of velocity and Cp profiles in the space between the roof surface and bottom of the panels, for 3" (0.075 m) along Line 1 close to edge A. Velocity changes from 0 on surface of the roof to 14.80 m/s near middle of the cavity, then decreases gradually to 0.0 at the bottom surface of the panel.

In addition, above the solar panel surfaces velocity increases to 50.50 m/s at 50" (1.26m) above the panels, then reduces gradually to 40 m/sat 20m and greater, above the ground surfaces, which corresponds to 13.5 m above the roof surface.



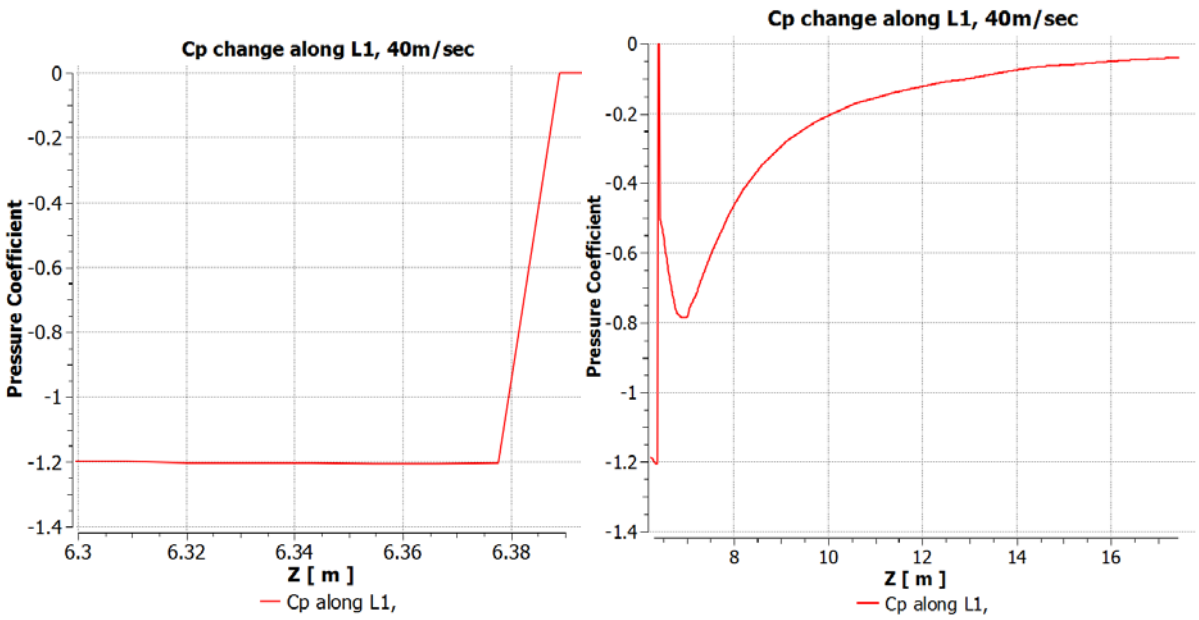


Fig.B. 108, velocity and Cp changes between panels, and above roof, Line 1, 40m/s, windward, wind direction 90º

Figure B.107 shows pressure coefficients remains constant at -1.20 along the whole height of the space between roof surface under panels and bottom of the panels. Then the pressure coefficient increases to -0.52 at the top of the panel surface, where it then decreases again to -0.79 at 50" (1.25mm) above the solar panels, then increases afterwards gradually to 0.0 at nearly 20 m above ground (13.5 m above the roof surface).

At Line 2 located near middle of edge A, Fig. B.108, of the velocity changes from 0 on surface of the roof to 2.75 m/s near middle of the cavity, then decreases gradually to 0.0 at the bottom surface of the panel.

In addition, along Line 2, and above the solar panel surfaces velocity increases to 45 m/sin the first 4" (0.102m) above top of the panels surface, then decreases slightly to 44.50 m/sat 8" (0.204m) then increases again to 49m/s at 50" (1.25m) above the panels, then reduces gradually to 40 m/sat 20m and greater, above the ground surfaces, which corresponds to 13.5 m above the roof surface.

The pressure coefficients along line 2 remains constant at -0.79 along the whole height of the space between roof surface under panels and bottom of the panels. Then the pressure coefficient

increases to -0.55 at the top of the panel surface, where it increases afterwards gradually to 0.0 at nearly 30 m above ground (23.5 m above the roof surface).

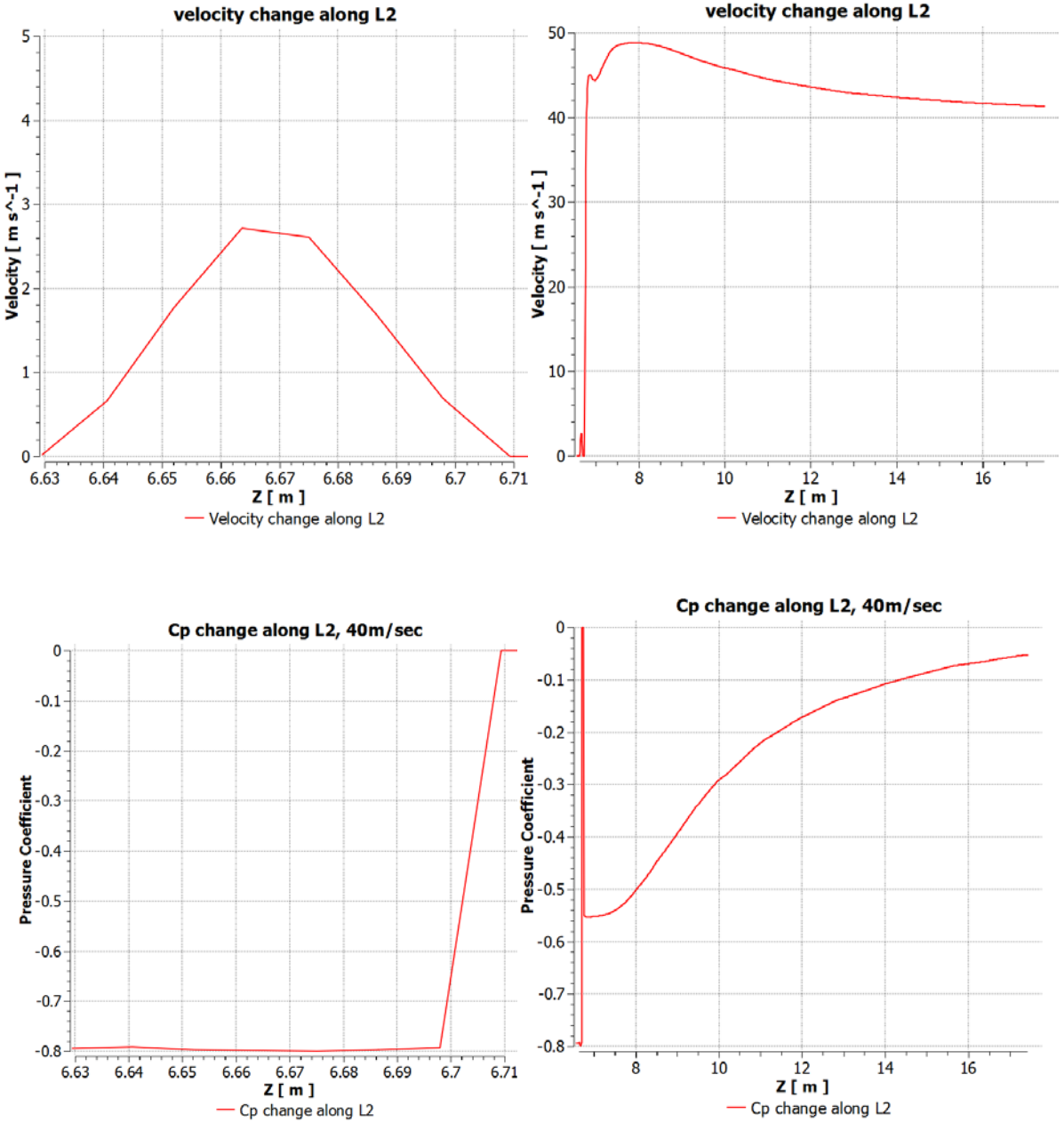


Fig.B. 109, Pressure coefficients and velocity changes between panels, and above roof, Line 2, 40m/s, windward, wind direction 90º

Along Line 3 near edge A and close to ridge, velocity changes from 0 on surface of the roof to 21m/smear middle of the cavity, then decreases gradually to 0.0 at the bottom surface of the panel, Fig. B.109.

In addition, along Line 3, and above the solar panel surfaces velocity increases to 52.60 m/s in the first 4” (0.102m) above top of the panels surface, then decreases slightly to 50.0 m/s at 20” (0.508 m) then increases very slightly again to 50.20 m/sat 28” (0.71m) above the panels, and remain constant until 48” (1.42m) above the panels, then reduces gradually to 40 m/sat 35m and greater, above the ground surfaces, which corresponds to 28.5 m above the roof surface.

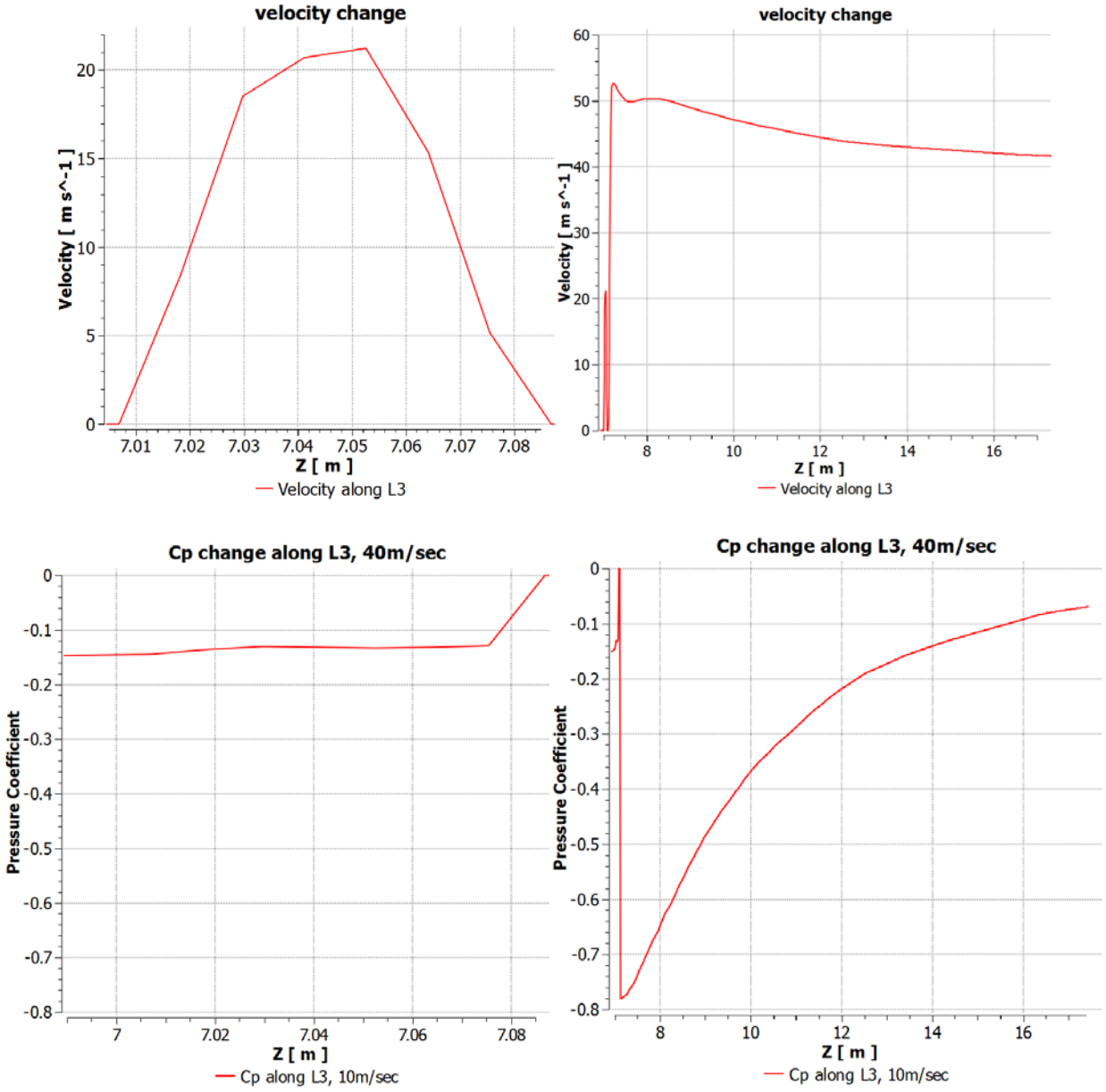
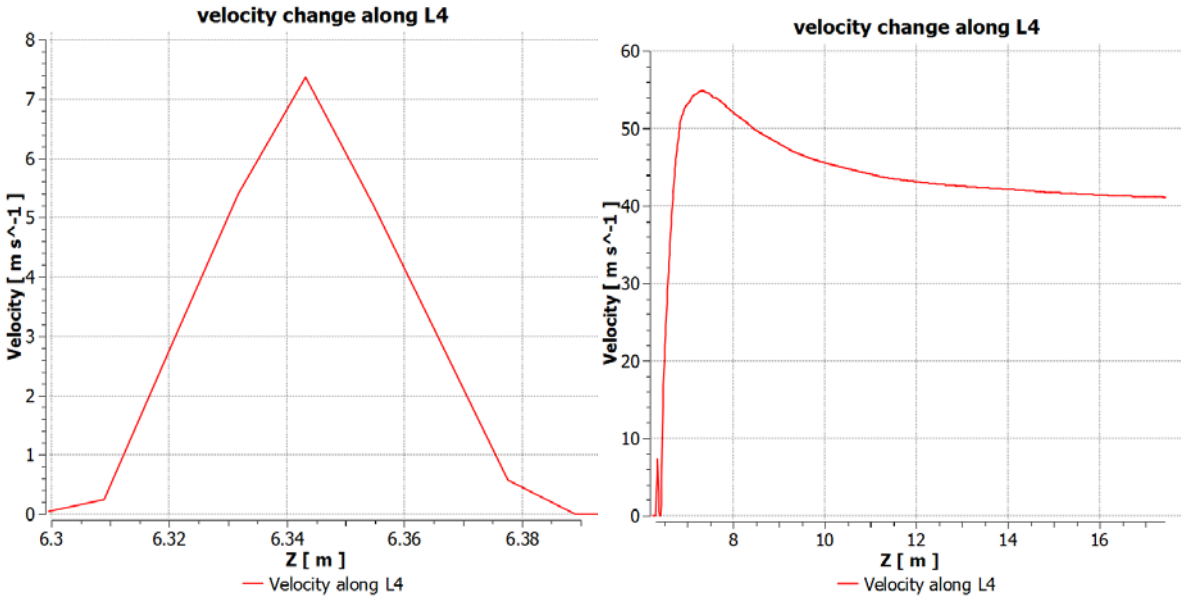


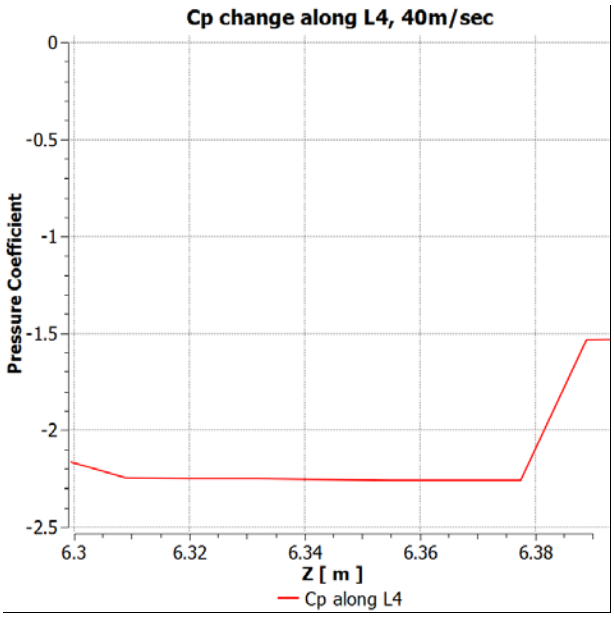
Fig.B. 110, Pressure coefficients and velocity changes between panels, and above roof, Line3, 40m/s, windward, wind direction 90º

Moreover, pressure coefficients along Line 3, Fig. B.110 remains nearly constant at -0.14 along the whole height of the space between roof surface under panels and bottom of the panels. Then the pressure coefficient decreases to -0.78 at the top of the panel surface, where it then increases afterwards gradually to 0.0 at nearly 35 m above ground (28.5 m above the roof surface).

The velocity and pressure coefficients profiles generated along the Line 4 (Fig. B.110) which located near the middle of front edge of the windward array, changes from 0 on surface of the roof to 7.30 m/s near middle of the cavity, then decreases gradually to 0.0 at the bottom surface of the panel.

In addition, along Line 4, and above the solar panel surfaces, velocity increases to 55 m/s at 32" (0.813 m) above the panels, then reduces gradually to 40 m/s at 20m and greater, above the ground surfaces, which corresponds to 13.5 m above the roof surface.





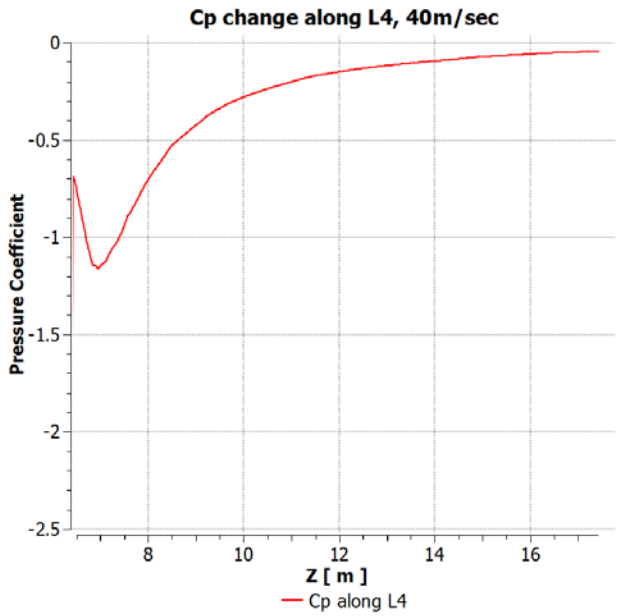


Fig.B. 111, velocity and Cp changes between panels, and above roof, Line 4, 40m/s, windward, wind direction 90^{o}

In the same manner, pressure coefficients, Fig. B.110, between the roof surface and bottom of the panels remains constant at -2.25 along the whole height of the space between roof surface under panels and bottom of the panels. Then the pressure coefficient increases to -0.70 at the top of the panel surface, where it then decreases further to -1.15 at 20” (0.50m) above the panel, where it increases afterwards gradually to 0.0 at nearly 20 m above ground (13.5 m above the roof surface).

Then along Line 5, Fig. B.111, located in the middle of the panels surface, the velocity profile in the space between the roof surface and bottom of the panels changes from 0 on surface of the roof to 4.50 m/s near middle of the cavity, then decreases gradually to 0.0 at the bottom surface of the panel.

In addition, along Line 5, and above the solar panel surfaces velocity increases to 46 m/sin the first 4” (0.102m) above top of the panels surface, then decreases slightly to 44.50 m/sat 8” (0.204m) then increases again to 51 m/s at 50” (1.25 m) above the panels, then reduces afterwards gradually to 40 m/s at 30m and greater, above the ground surfaces, which corresponds to 23.5 m above the roof surface.

The pressure coefficients, created along Line 5, remains constant at -1.00 along the whole height of the space between roof surface under panels and bottom of the panels. Then the pressure coefficient increases to -0.77 at the top of the panel surface, where it then increases afterwards gradually to 0.0 at nearly 30 m above ground (23.5 m above the roof surface), Fig. B.111.

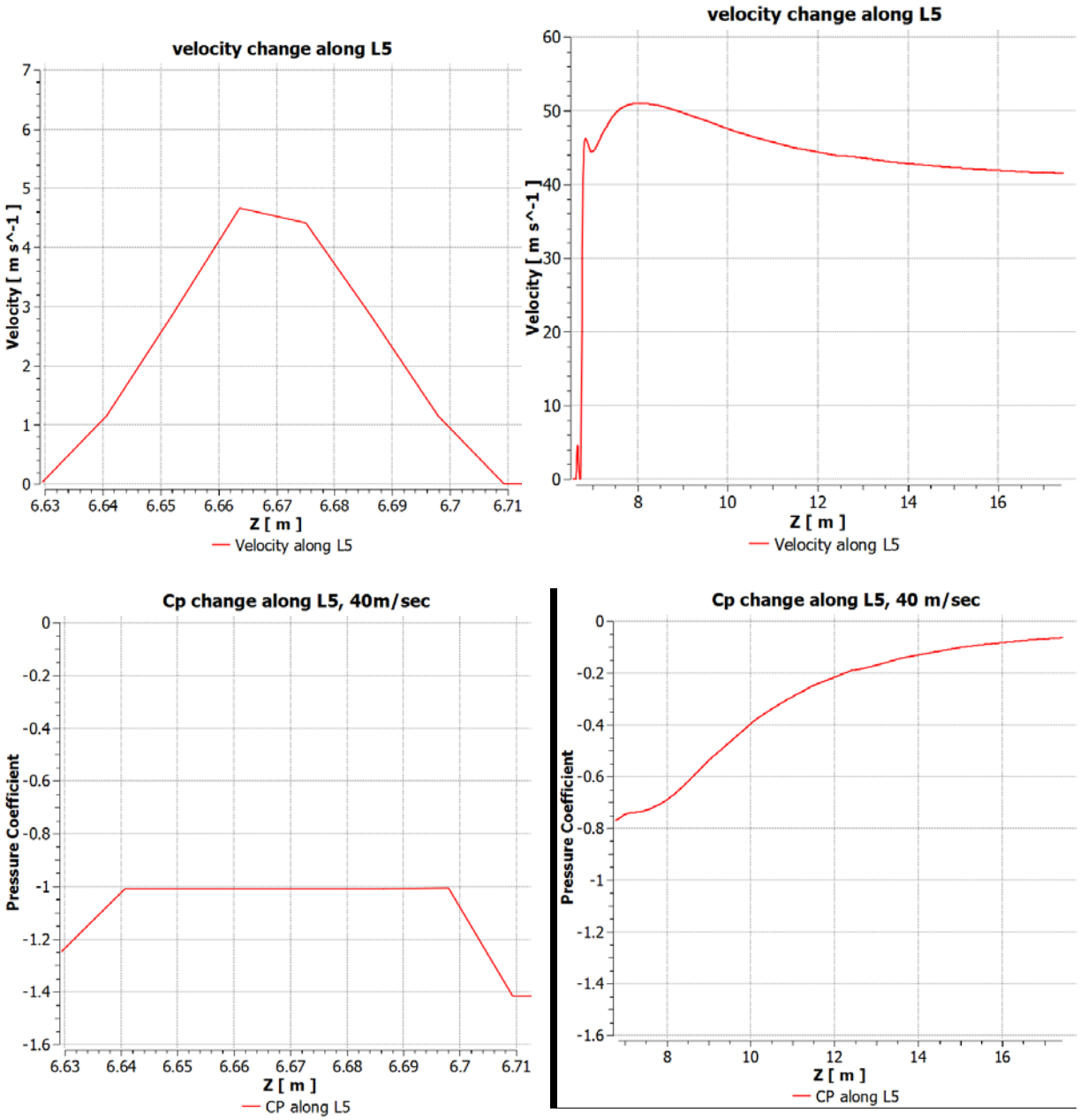
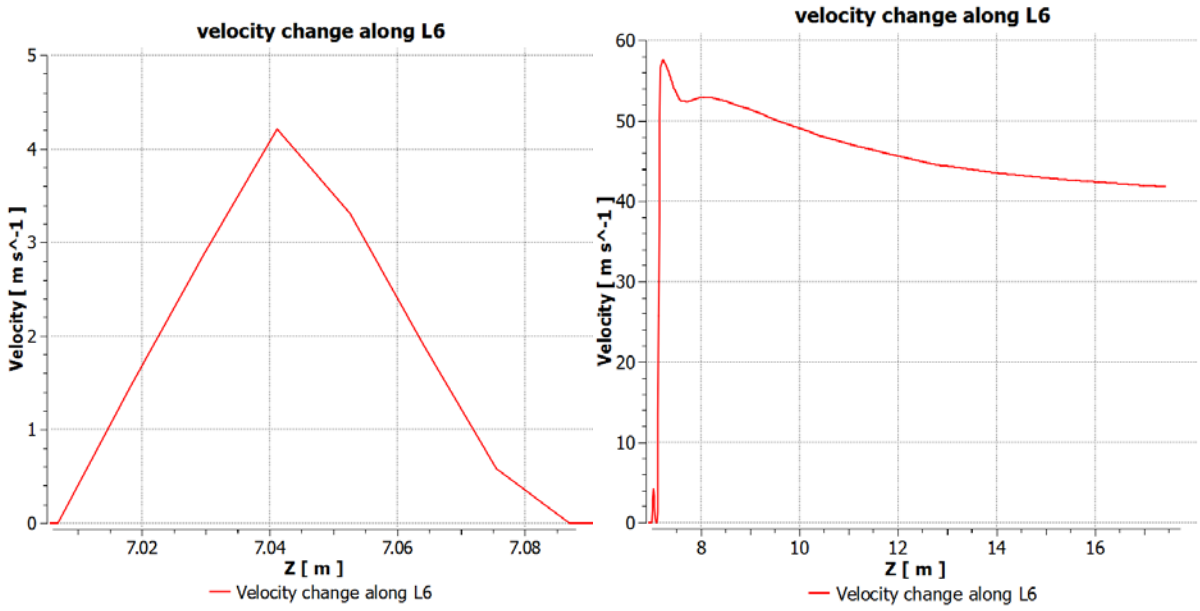


Fig.B. 112, Pressure coefficients and velocity changes between panels, and above roof, Line 5, 40m/s, windward, wind direction 90º

Near the ridge, along Line 6, Fig. B.112, the velocity in the space under the panels, changes from 0 on surface of the roof to 4.20 m/s near middle of the cavity, then decreases gradually to 0.0 at the bottom surface of the panel.

In addition, along Line 6, and above the solar panel surfaces, velocity increases to 57.8 m/sin the first 4” (0.102m) above top of the panels surface, then decreases moderately to 52.30 m/sat 20” (0.501m) then increases very slightly to 53 m/sat 40” (1.02 m) above the panels, then reduces gradually to 40 m/sat 35m and greater, above the ground surfaces, which corresponds to 28.5 m above the roof surface.



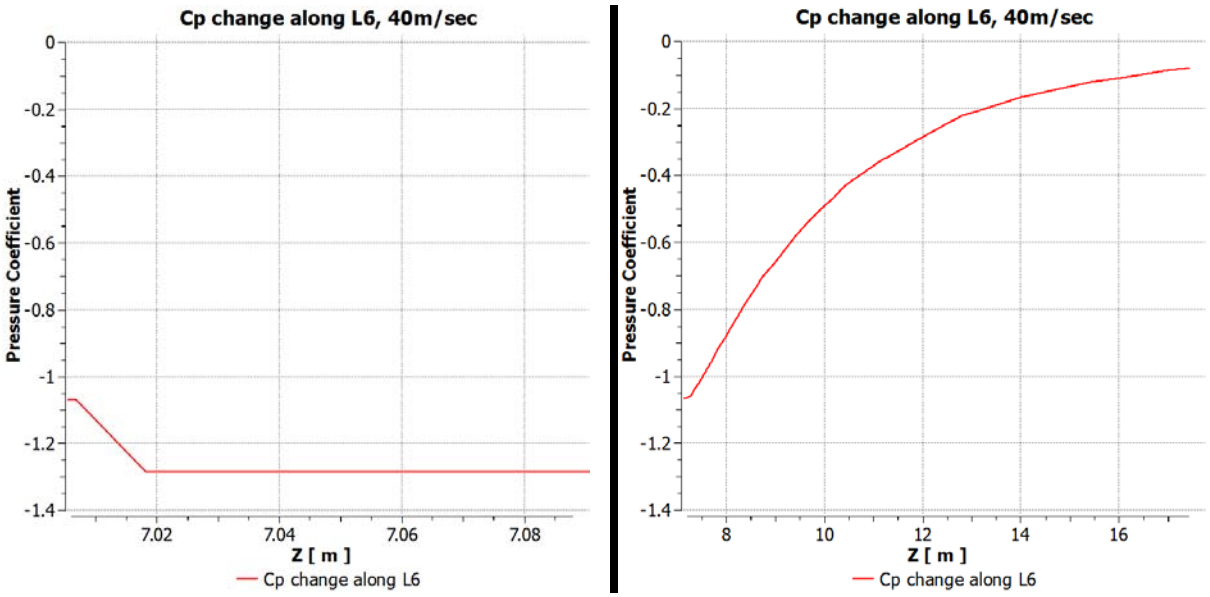


Fig.B. 113, Pressure coefficients and velocity changes between panels, and above roof, Line 6, 40m/s, windward, wind direction 90º

On the other hand, pressure coefficients along L5 remain constant at -1.27 along the whole height of the space between roof surface under panels and bottom of the panels. Then the pressure coefficient increases to -1.07at the top of the panel surface, where it then increases afterwards gradually to 0.0 at nearly 35 m above ground (28.5 m above the roof surface).

The pressure coefficients and velocity along the whole length of the 6 lines perpendicular to the roof and panels due to 10m/sec m/s and 40m/s wind flows are presented in the Figs. B.113 and B.114 respectively. While B.115 and B.116 show pressure coefficients and velocity in the space between panels and roof, along the corresponding length of the 6 lines perpendicular to the roof and panels, due to 10 m/sand 40 m/swine flows respectively.
From those collective figures depict the pressure coefficients for 10 m/s and 40 m/s seem to be replicas, as illustrated in both gap, Figs. B.113 and B.114 and overall line graphs in Figs. B.115 and B.116.

It is noticed that the pressure coefficients are nearly identical for both the 10 m/sand 40 m/sec. In addition, the pressure coefficients decrease from edge A towards the middle of the array, except for L3. That because, on L1 under panels the Cp is -1.20 which decreases to -2.25 at L4 under

panels. Similarly, Cp is -0.79 at L2 reduces to -1.0 at L5 under panels, while Cp is -0.74 along L3 which decreases to -1.07 along L6 under the panels.
However, Cp increases under panels along the flow, at the edge, from front edge to ridge, where Cp on L1, -1.20 increases to -0.74 on L3, and Cp on L4, -2.25 increases to -1.07 on L6.
Similar trends are observed above the panels, where Cp decreases from -0.79 at L1, to -1.15 at L4. In addition, Cp reduces from -0.55 on L2 above panels, to -0.77 on L5 above panels.
Similarly, Cp on L3 is -0.78 which decreases on L6 to -1.27 at the top of the panels.
Another note is that, for all the lines, Cp increases above the panels from the Cp under panels. For example, Cp increases on L2 from -0.79 under the panels to -0.55 on top of the panels.

Although, pressure coefficients values recorded at 40 m/s and 10 m/s wind flows are nearly replicas to each other; however, wind speeds under and above the panels, are proportional to the free stream flow, where it is noticed that all velocities recorded under and on top of the panels for 40 m/s flow are scaled by 4 from those corresponding velocities under 10m/s wind flow.
For example, velocities under panels along L1 and L4 recorded under the panels 14.80 and 7.30 m/sec, and 50.50 and 55.0 m/s above the panels respectively, which correspond to 3.50 m/s and 1.80 m/s respectively under the panels and 12.60 and 13.25 m/s above the panels respectively under 10m/s flow.
Similarly, velocities under panels along L3 and L6 recorded 21.0m/s and 4.25 m/s under the panels, while recorded 52 m/sand 57.80 m/s above the panels respectively for 40 m/s flow, which correspond to 5.20 m/sand 1.06 m/s under panels and 13.0 m/s and 14.45 m/s above panels respectively under 10m/s flow.

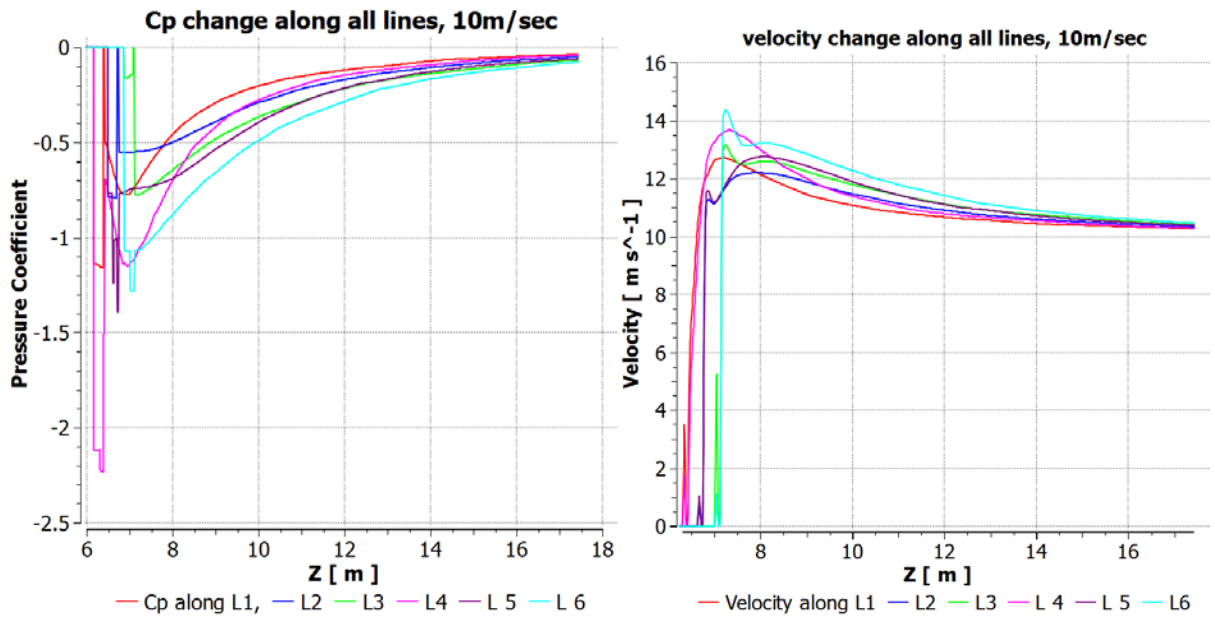


Fig.B. 114, Pressure coefficients and velocity changes between panels and roof, and above the panels, Lines 1-6, 10 m/s, windward, wind direction 90º

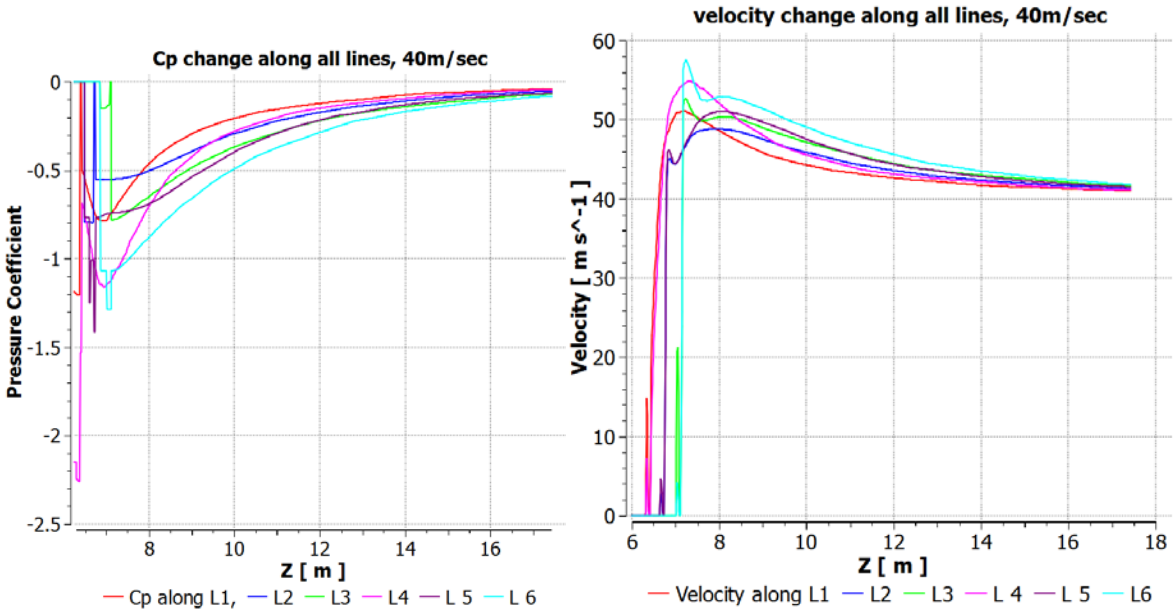


Fig.B. 115, Pressure coefficients and velocity changes between panels and roof, and above the panels, Lines 1-6, 40 m/s, windward, wind direction 90º

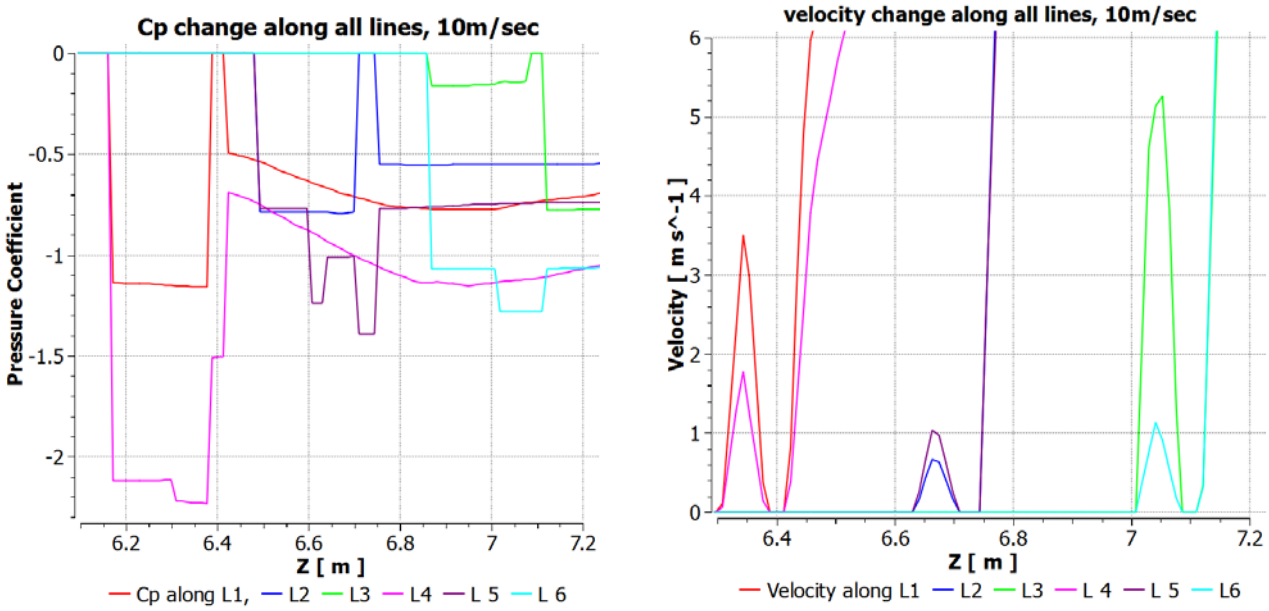


Fig.B. 116, Pressure coefficients and velocity changes between panels and roof, and above the panels, Lines 1-6, 10 m/s, windward, wind direction 90º, Zoom into space between panels and roof

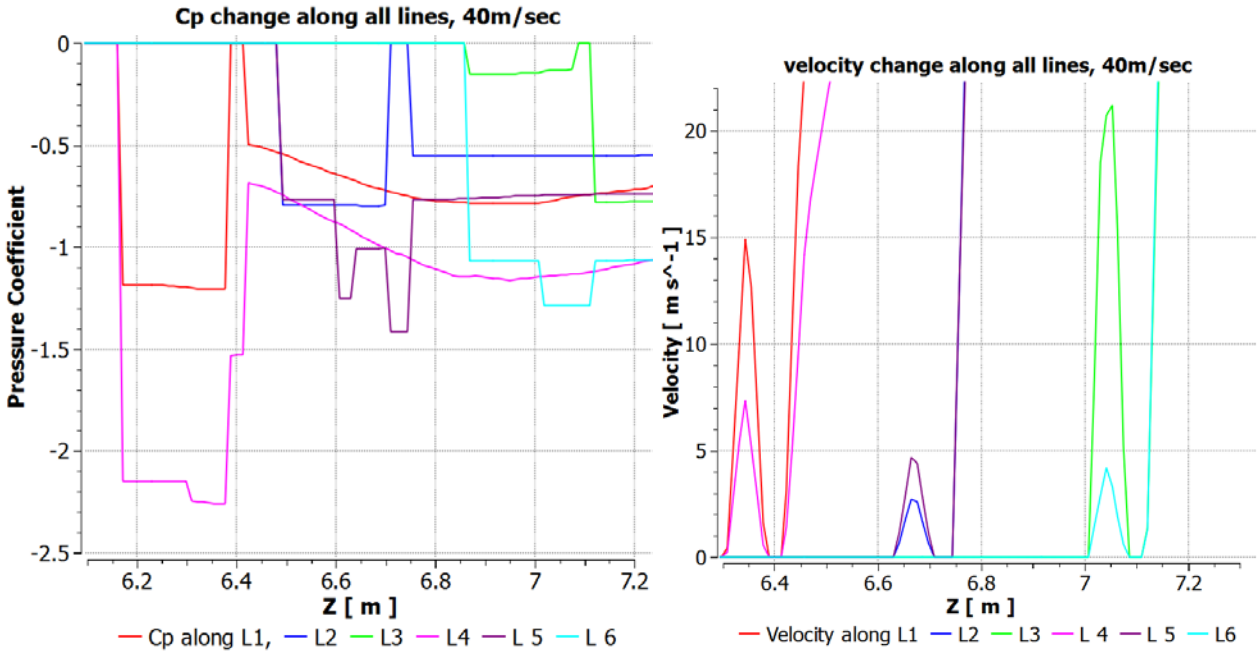


Fig.B. 117, Pressure coefficients and velocity changes between panels and roof, and above the panels, Lines 1-6, 40 m/s, windward, wind direction 90º, Zoom into space between panels and roof.

B-XII- Detailed distribution of wind pressure on roof mounted solar panels in comparison with roof without solar panels, leeward

B-XII-i Pressure coefficient on bottom surface of the solar panels Vs. roof surface under solar panels, for 15º inclined roofs and 90º, 45º and 0º wind directions, leeward

The following Fig. B.117 represents registered Cp on bottom surface of panels and on roof surface under the panels, under the effects of wind direction 90°, when the wind direction being perpendicular to the ridge of the roof. Pressure coefficients along the three lines PL37, PL28, and PL20 on roof under panels, seem to replicate Cp on the corresponding lines on bottom of the panels, where differences between Cp on corresponding lines are nearly zero. The reason for that is may be because the slope in close to flat surface where Conduit effects are strong, which is different from the other higher slopes studied herein. On the other hand, the pressure coefficients along PL37 is nearly constant, -0.70, along 10 m of the array length, while they reduce moderately near both edges to -0.90. Similarly, the pressure coefficients on PL28 are nearly constant, -0.55, along 10 m of the array length, while they reduce slightly near both edges to -0.65.
However, Cp on lines PL20 on the 2 surfaces show moderate fluctuation (-0.3 to -1.0) about average -0.55.

Similarly, when wind flows at 45° wind direction Cp along all the three lines PL20, PL28 and PL37 on roof under panels seem to replicate the Cp on the corresponding lines on bottom of the panels, where differences between each couple of corresponding lines is nearly zero. Different from symmetrical Cp graphs in the wind direction 90º, the pressure coefficients on both PL28 and PL37 decrease moderately for most of the lines lengths and sharply near the windward edge of the array. However, Cp remains nearly constant on PL20 at – 0.25 while decreases sharply near both edges to -0.6 to -1.6, Fig. B.118.

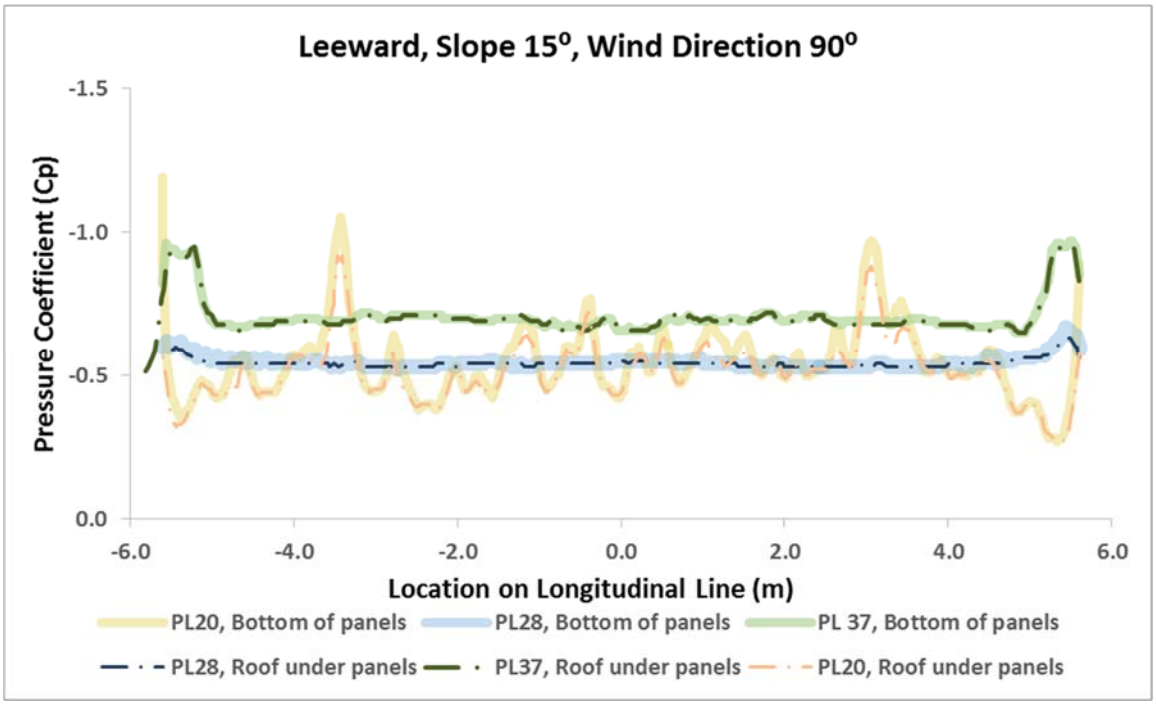


Fig.B. 118. Pressure coefficient distribution on bottom of the panels and on roof under the panels, for roof slope 15º, and wind direction 90º, leeward side

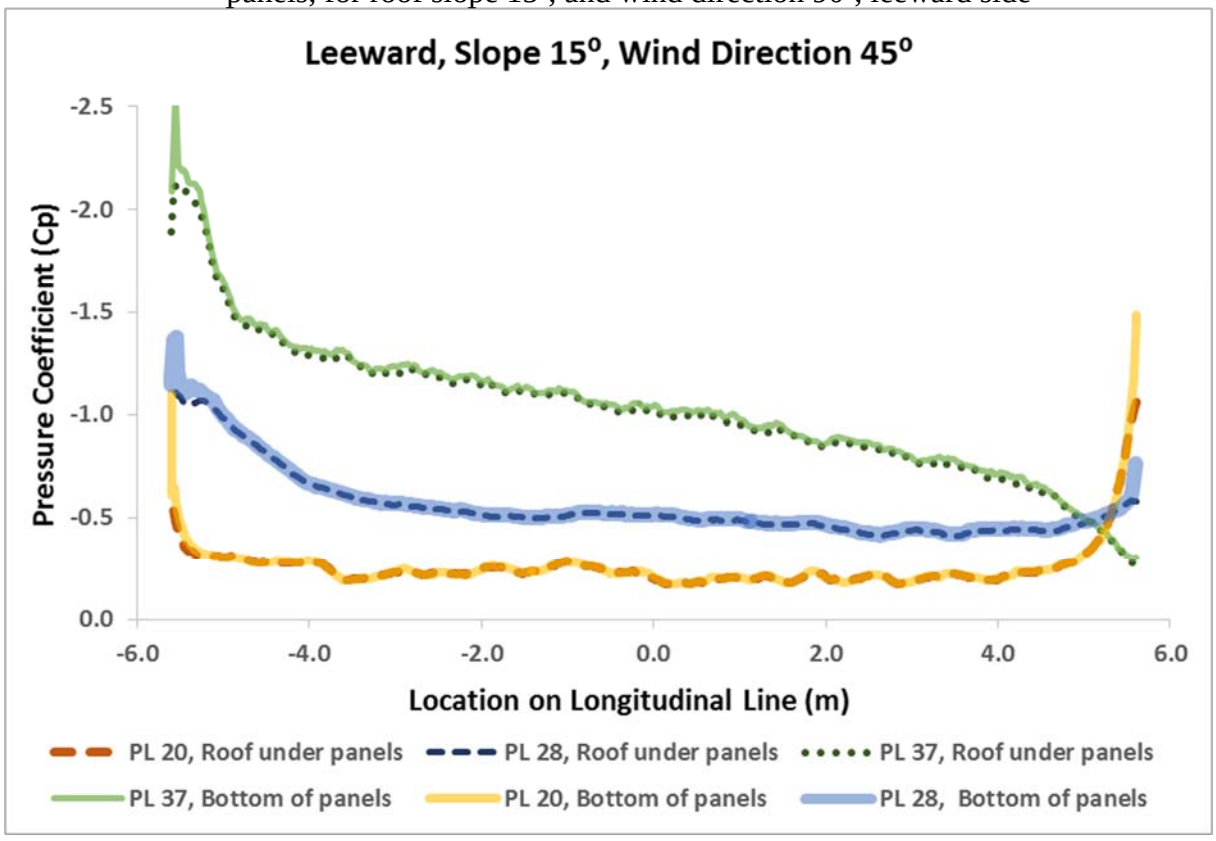


Fig.B. 119, Pressure coefficient distribution on bottom of the panels and on roof under the panels, for roof slope 15º, and wind direction 45º, leeward side

B-XII- ii Pressure coefficient on roof without panels Vs. roof surface under solar panels, for 15º inclined roofs and 90º, 45º and 0º wind directions, leeward

Figure B.119 represents wind pressure coefficients registered on the roof surface without solar panels and on the roof surface under the solar panels in the wind direction 90°, Pressure coefficients along the line PL20 on roof under panels, fluctuates about average nearly -0.5 is much higher than Cp on the corresponding line on roof without panels, -1.10. However, Cp along PL28 on roof under panels, -0.55, is moderately higher than the corresponding PL28 on roof without panels, -0.65. Nonetheless, Cp on PL37 on roof under panels, nearly -0.75 average, is moderately lower than Cp on PL37 on roof without panels, -0.50. On the other hand, the pressure coefficients on PL37 is nearly constant, -0.70, along 10 m of the array length, while it reduces moderately near both edges to -0.90. Similarly, the pressure coefficients on PL28 is nearly constant, -0.55, along 10 m of the array length, while it reduces very slightly near both edges to -0.60. However, Cp on lines PL20 on the roof surface under the panels shows moderate fluctuation (-0.3 to -1.0) about average -0.55.

The pressure coefficients, on the roof under panels and corresponding roof without solar panels, under wind flows at 45° wind direction, are presented in Fig. B.120 below. The Fig. B.120 shows, Cp on PL20, -0.20 to -0.1.15, on roof under the panels, are much higher than corresponding Cp on roof without panels, -1.0 to -1.15.

However, Cp along PL 28 on roof under the panels is slightly higher, by 0.1 than corresponding line on roof without panels, while Cp on PL 37 on roof under the panels, -0.35 to -2.15 is much lower, than Cp on corresponding line on roof without panels, -0.35 to -1.15.

In addition, the pressure coefficients on both PL28 and PL37 decrease moderately towards the windward side of the array near the ridge, for most of the lines lengths. However, Cp remains nearly constant on PL20 at – 0.25 while decreases sharply near both edges to -0.6 to -1.6, Fig. B.120.

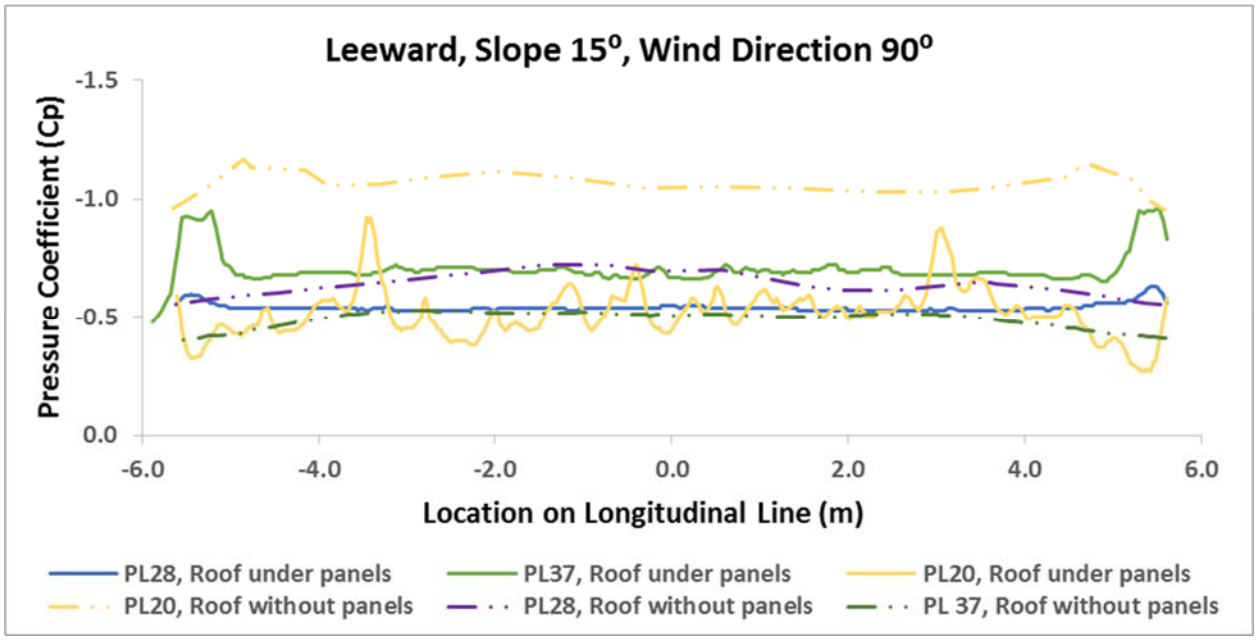


Fig.B. 120. Pressure coefficient distribution on roof without solar panels and on roof under the panels, for roof slope 15º, and wind direction 90º, leeward side

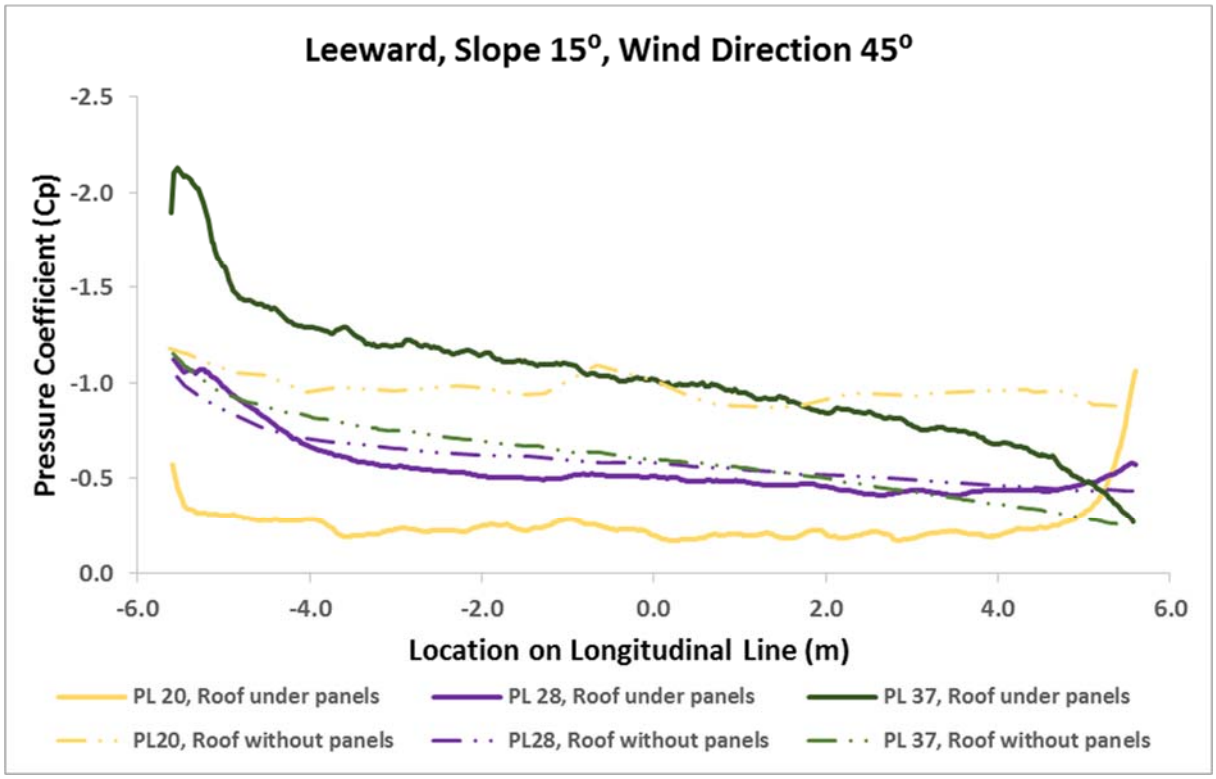


Fig.B. 121. Pressure coefficient distribution on roof without solar panels and on roof under the panels, for roof slope 15º, and wind direction 45º, leeward side

B-XII-iii Pressure coefficient on roof without panels vs. bottom of the panels surface, for 15º inclined roofs and 90º, 45º and 0º wind directions, Leeward

Figure B.121 presents wind pressure coefficients registered on the roof surface without solar panels and on the bottom surface of solar panels in the wind direction 90°, where pressure coefficients along line PL20 on bottom of the panels, fluctuates about an average nearly -0.55 which is much higher than Cp on the corresponding line on roof without panels, -1.10. Nonetheless, Cp along PL28 on bottom surface of the panels, -0.55, is moderately higher than the corresponding PL28 on roof without panels, -0.65. Nonetheless, Cp on PL37 on bottom surface of the panels, nearly -0.70 for most of the length, which is moderately lower than Cp on PL37 on roof without panels, -0.50. On the other hand, the pressure coefficients on PL37 on bottom of the panels is nearly constant, -0.70, along 10 m of the array length, while it reduces abruptly near both edges to -0.90. Likewise, the pressure coefficients on PL28 is nearly constant, -0.55, along 10 m of the array length, while it reduces slightly near both edges to -0.60. However, Cp on lines PL20 on the bottom surface of the panels displays moderate fluctuation (-0.3 to -1.0) about average -0.55.

The graph illustrated in Fig. B.122 demonstrates pressure coefficients on bottom of panels and roof without solar panels, for the case of 45° Pressure coefficients, on PL37 on bottom surface of the panels, -0.35 to -2.5 is much lower than Cp on corresponding PL 37 on roof without panels, -0.35 to -1.10. However, Cp on PL 20 on bottom surface of the panels, -0.20 to -1.50 is much higher than Cp on the corresponding line on roof without panels, -1.0 to -1.10. Nonetheless, the Cp along PL 28 on bottom of the panels, -0.45 to -1.40 is slightly higher than Cp of corresponding line on roof without panels, -0.45 to -1.05.

In addition, the pressure coefficients on both PL28 and PL37 decrease moderately toward the windward edge of the array near the ridge. However, Cp remains nearly constant on PL20 at – 0.25 while decreases sharply near both edges to -0.6 to -1.6, Fig. B.122.

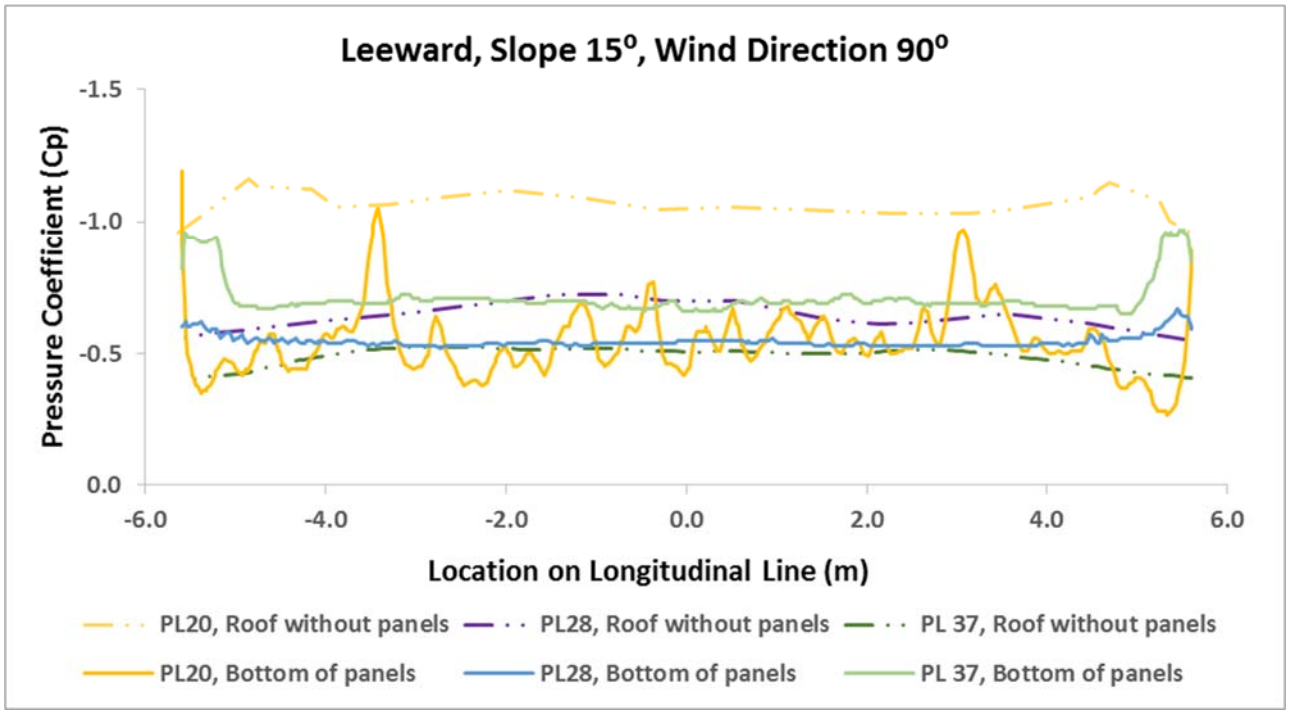


Fig.B. 122. Pressure coefficient distribution on roof without solar panels and on Bottom of the panels, for roof slope 15º, and wind direction 90º, leeward side

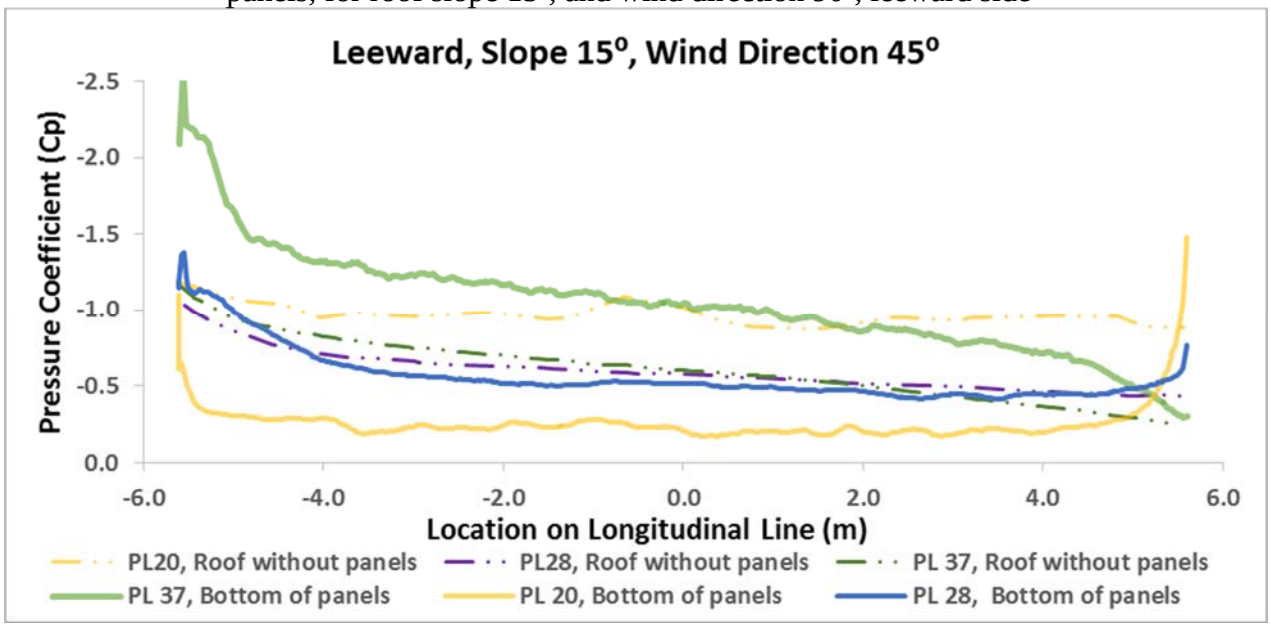


Fig.B. 123. Pressure coefficient distribution on roof without solar panels and on Bottom of the panels, for roof slope 15º, and wind direction 45º, leeward side

B-XII-iv Pressure coefficient on roof without panels vs. top of the panels surface, for 15º inclined roofs and 90º, 45º and 0º wind directions, leeward

The graphs of wind pressure coefficients registered on the top surface of the solar panels and on the roof surface without solar panels, for wind directions 90º and 45º angles with ridge, are shown in Figs. B.123 and B.124 respectively.

The pressure coefficients recorded for wind direction 90°, w along the line PL20 on top surface of the panels, fluctuates along the whole length of the PL20 and ranges from -1.20 to -2.70 which is much lower than Cp on the corresponding line on roof without panels, -1.10 which remains nearly constant along the whole length of the line. However, Cp along PL28 on top surface of the panels, -0.55 is slightly lower than corresponding line on roof without panels, -0.60. Nonetheless, Cp along PL37 on top surface of the panels, -0.50 is slightly higher than corresponding line on roof without panels, -0.45.

Monitoring the pressure coefficients recorded on top of the panels and roof without panels, for 45° wind direction with the shows that Cp along all the three lines PL20, PL28 and PL37 on top surface of the panels are to be lower than Cp on the corresponding lines on top surface of the panels. That where Cp on PL20 on top of the panels, -1.50 to -1.90, is much lower than the Cp on the corresponding line on roof surface without panels, -1.0. In addition, Cp on PL37 on top surface of the panels, -0325 to -1.60, is moderately lower than Cp on the corresponding line on roof without panels, -0.35 to -1.20. However, Cp on PL28 on top surface of the panels, -0.50 to -1.30, is slightly lower than Cp on the corresponding line on roof without panels, -0.50 to -1.10.
On the other hand, the pressure coefficients on both PL28 and PL37 decrease toward the windward side of the array near the ridge.

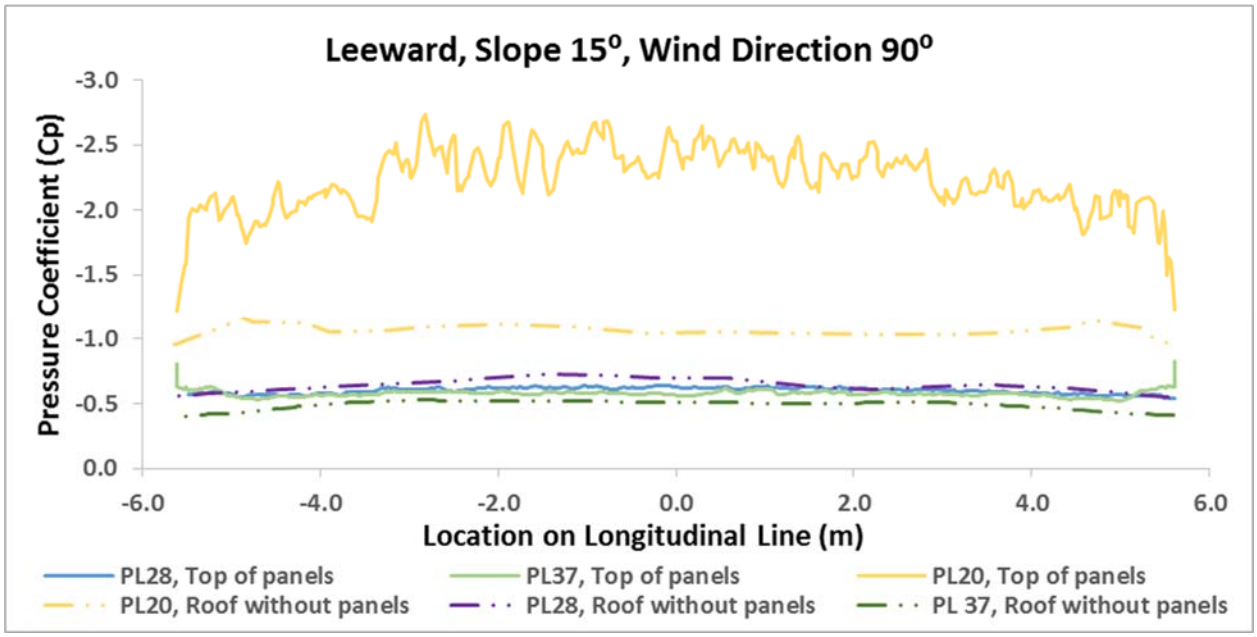


Fig.B. 124, Pressure coefficient distribution on roof without solar panels and on Top of the panels, for roof slope 15º, and wind direction 90º, leeward side

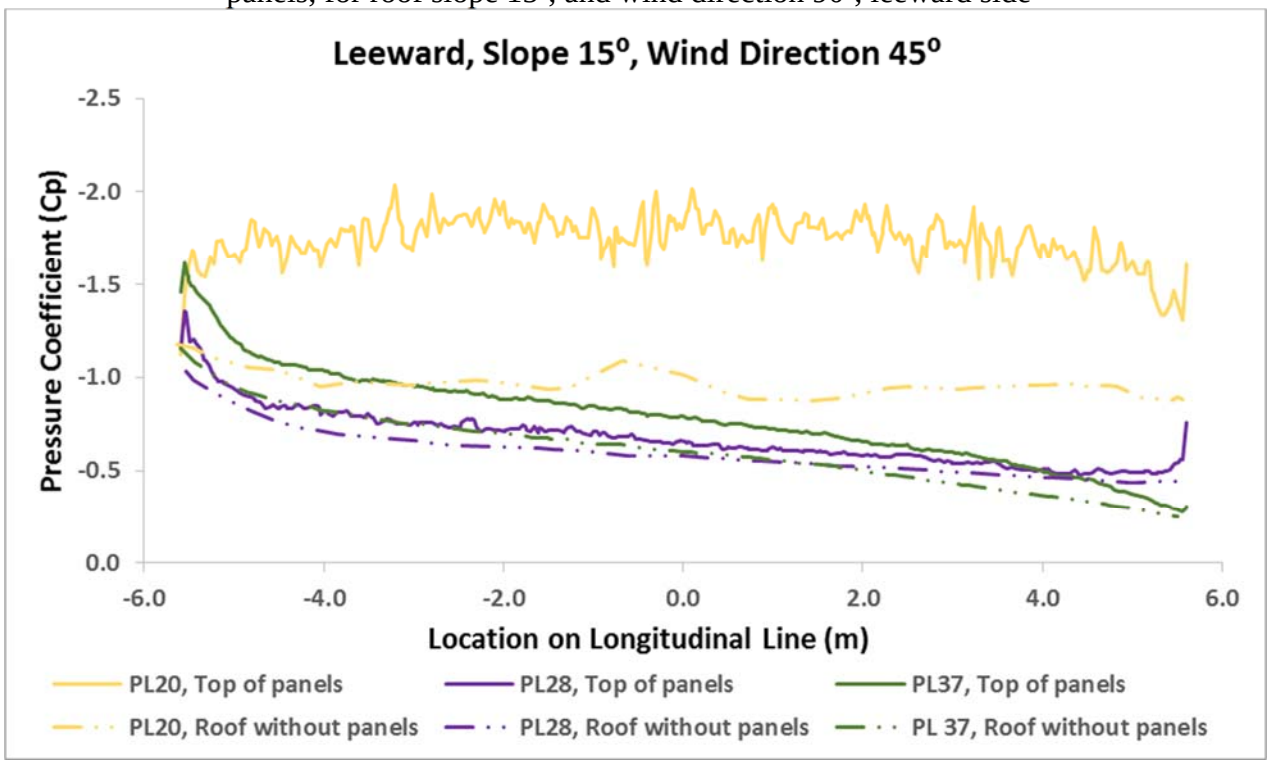


Fig.B. 125. Pressure coefficient distribution on roof without solar panels and on Top of the panels, for roof slope 15º, and wind direction 45º, leeward side

B-XIV- Pressure coefficient distribution on roof mounted solar panels and on roofs with no panels, for wind directions 90º, 45º and 0º wind, windward surface

XIV.1. Pressure coefficients on bottom surface of solar panels vs. roofs without solar panels, roof slope 35º

For wind direction 90° (Fig. B.126) the Cp values along the PL1 line are higher (Cp = 0.5-0.6) than the corresponding line on the roof without panels (Cp = 0.02). The ridge line, PL19 shows higher suction (Cp = -0.5 to -1.2) than the corresponding line on the roof without panels (Cp = -0.3 to -0.7). The suction coefficients on PL10 on the roof surface under the panels, near the middle of the array, are slightly higher (Cp = -0.25 to -0.35) than the pressure coefficients along PL10 on the roof without panels (Cp = -0.05 to -0.15). Considering the wind direction which is perpendicular to the ridge of the roof, the Cp values on all the lines are symmetric around the middle of the roof, for both roof surfaces under the panels and roof surface without solar panels (Fig. B.126).

For the case of 45° wind direction (Fig. B.127), it can be observed that the pressure coefficients have very similar trends for the bottom surface of the solar panels when compared with the roof surface without solar panels, especially for the inner region of the roof. However, for line PL1, located near the windward A edge of the solar array (Fig. 4.6), the pressure coefficients are higher (Cp = 0.55 to -0.6) than those obtained on the corresponding line on the roof with no panels (Cp = 0.2 to -0.6). The middle line (PL 10) on the bottom surface of the solar panels shows slightly different pressure coefficients from the corresponding line on the roof without panels. In addition, pressure coefficients along PL1 and PL10 decrease towards the leeward edge of the roof to Cp=-1.25 on the roof under the panels and to Cp=-0.6 on the roof without panels (Fig B.127).

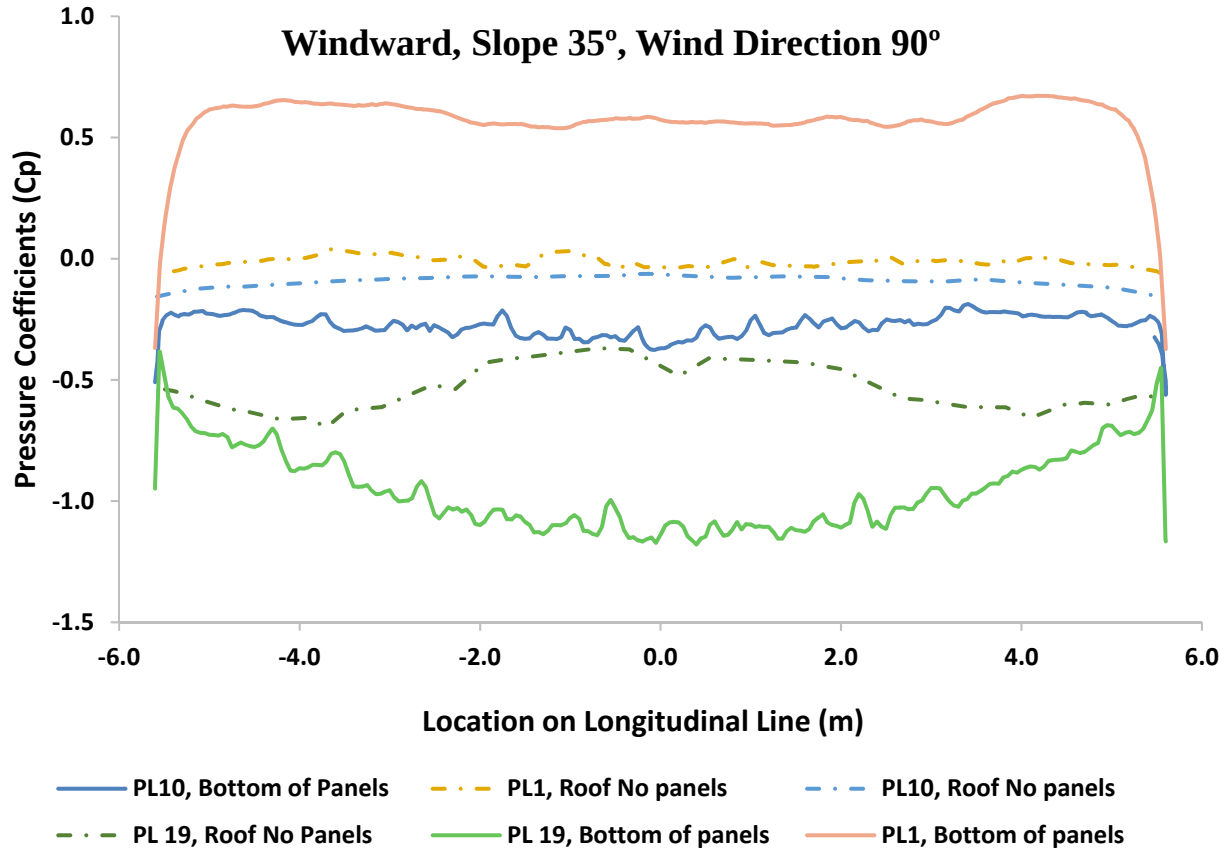


Fig.B. 126. Pressure coefficient distribution on the bottom of the panels and on roof surface without mounted panels, slope 35º, and wind direction 90º, windward side

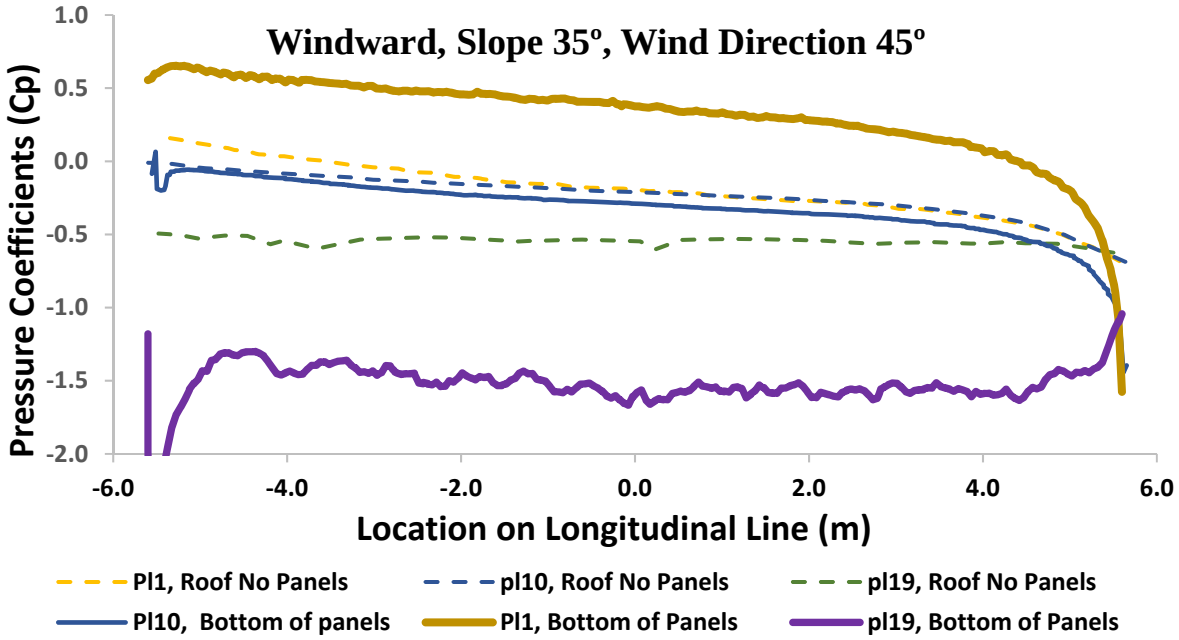


Fig.B. 127. Pressure coefficient distribution on the bottom of the panels and on roof surface without mounted panels, slope 35º, and wind direction 45º, windward side

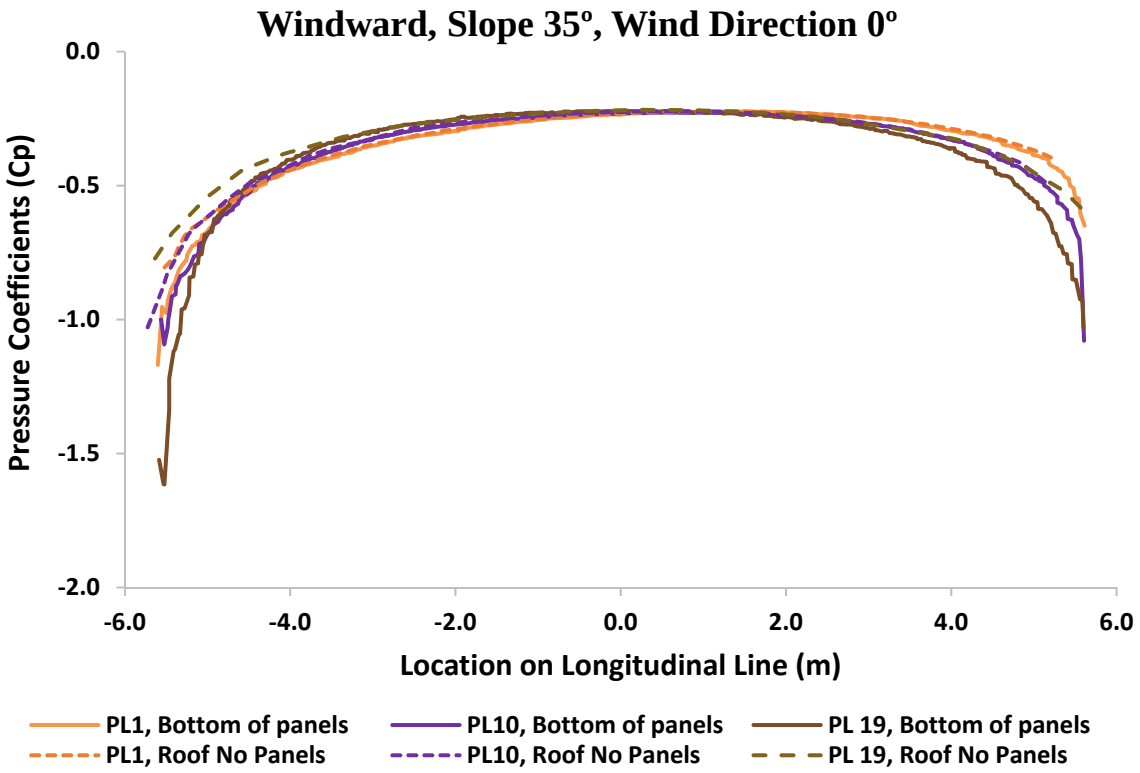


Fig.B. 128. Pressure coefficient distribution on the bottom of the panels and on roof surface without mounted panels, slope 35º, and wind direction 0º

For wind direction 0º, the pressure coefficients along PL1 and PL10 on bottom surface of solar panels are slightly lower than those on the roof without panels. Moreover, the pressure coefficients along PL 19 on roof under the panels are slightly lower than those on the roof without panels (Fig. B.128). The Cp values along all three lines reduce sharply from Cp=-0.25 in the middle of the array to Cp=-0.8 to -1.6 on the windward edge, and to Cp=-0.5 to -1.2 on the leeward edge of the roof, while it remains nearly constant in the middle section of these lines.

XIV.2. Pressure coefficient on bottom surface of solar panels vs. roofs without solar panels, roof slope 35º

Wind pressure coefficients on roof surface without solar panels and on the bottom surface of the solar panels, for wind directions 90º, 45º and 0º angles with ridge, are presented in Fig. B.129, Fig. B.130 and Fig. B.128, respectively.

For wind direction 90°, Cp along the line PL20 shows lower pressure coefficients, Cp = -1.1 to -2.1 for the bottom surface of the panels, than the corresponding line on the roof surface without panels, which registered values from Cp= -2.0 to Cp= -3.5. Similarly, PL29 shows much lower suction for the bottom surface of the panels, with pressure coefficients between Cp=-0.7 to -1.2, than the corresponding line on the roof without panels, where pressure coefficients are -1.0 to -2.0. However, pressure coefficients for most length of the line PL38 on the bottom surface of the panels, are slightly lower, by nearly 0.1, than the pressure coefficients along PL38 on the roof without panels. Cp along line PL38, on the bottom surface of the panels becomes slightly higher, by 0.1 near A and B edges of the roof, than the corresponding lines on the roof without panels. On the other hand, Cp coefficients for all three lines are symmetrical around the middle of the roof, for both bottom surface of the panels and the roof surface without solar panels, (Fig. B.129).

In the case of 45° wind direction (Fig. B.130) it is noticed that the pressure coefficients have similar trends for the bottom surface of the solar panels and the roof surface without solar panels. However, for line PL20 located at the edge of the solar panels array nearest to the ridge, on the leeward side, pressure coefficients are lower for most of the line length, with up to 0.25 than the corresponding line on the roof with no panels. Similarly, for PL38 located near the lower roof edge pressure coefficients are lower, on the bottom surface of the panels with up to Cp= -1.5 than the corresponding line on the roof with no panels, (Cp=-0.2 to -1.3), where most of the differences are located near the ridge side. On contrary, PL29 located in middle of the array (Fig.6), pressure coefficients are higher for most of the bottom surface of the panels, (Cp=-0.25 to -3.0) than the corresponding line on the roof with no panels, (Cp= -0.75 to -1.2), where most of the differences are located near the leeward edge A. However, the Cp on PL29 on bottom of the panels, becomes lower (0 to 1.7) than on the corresponding line on roof without panels, near the ridge part of that line. In addition, suction pressure coefficients on PL29 and PL38 on the bottom surface of the panels, increase sharply from Cp=0 and Cp=-0.25 at the leeward edge B, to Cp=-2.9 to -3.0 towards the windward edge A of the roof for the roof under the panels. However, suction Cp along PL20 increases slightly from Cp=-1.3 at the windward edge A of the roof to Cp=-1.75 at the leeward edge B for lines under the panels and on roof without solar panels respectively.

Due to the flow symmetry and structure, for wind direction 0º, Cp is the same on both sides of the gable roof surfaces. Consequently, the graphs and description are as I presented in Fig. B.128 and section B.XIV.1 above.

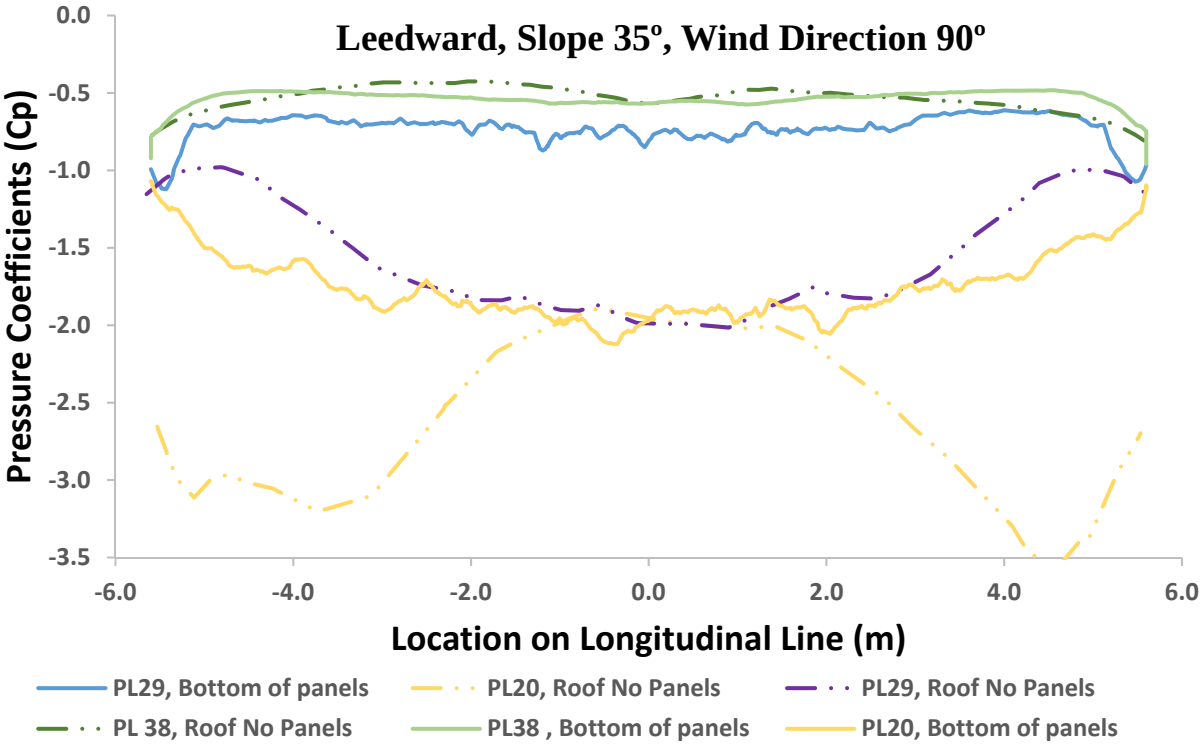


Fig.B. 129. Pressure coefficient distribution on the bottom surface of the solar panels and on the roof surface without panels, for roof slope 35º, and wind direction 90º, leeward side

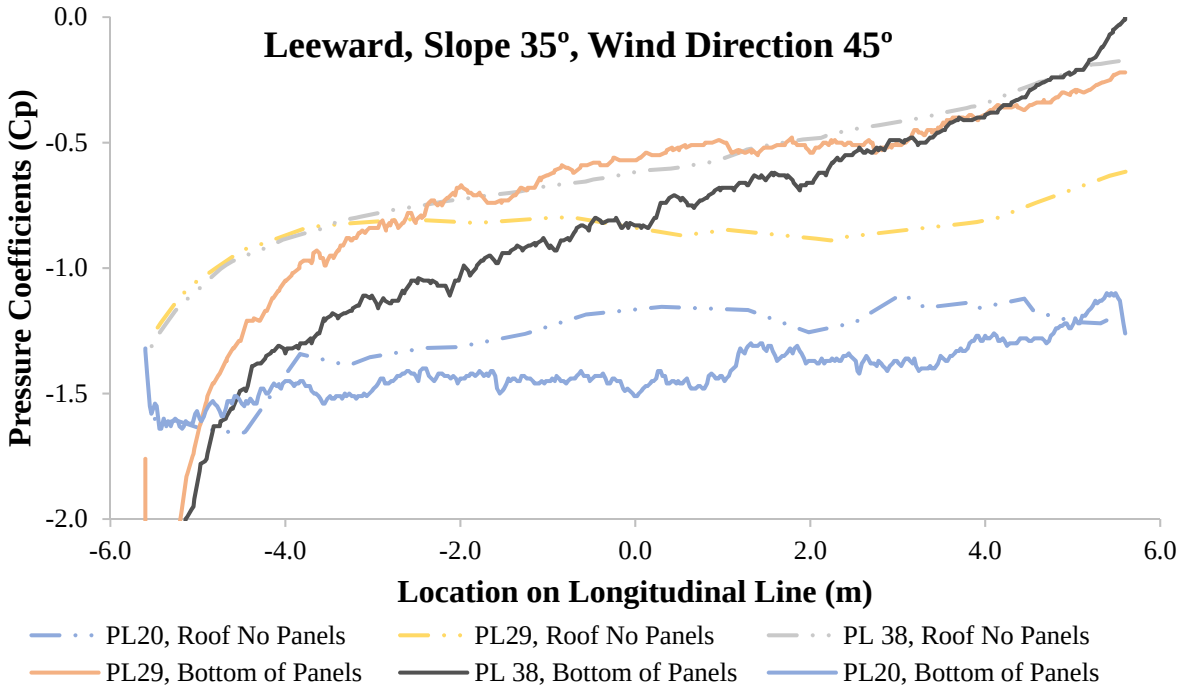


Fig.B. 130. Pressure coefficient distribution on the bottom surface of the solar panels and on the roof surface without panels, for roof slope 35º, and wind direction 45º, leeward side

XIV.3. Pressure coefficients on the bottom surface of the solar panels vs. roofs without solar panels, roof slope 27º

Details on the pressure coefficients obtained for the roof surface without solar panels and on the bottom surface of the solar panels are provided to elucidate the effect of the gap on the wind-induced pressure. Explicit comparisons of the wind-induced pressure coefficients on the roof surface with no panels installed and on the bottom surface of the solar panels, for wind direction 45º, 90º and 0º, are shown in Figs. B.131, B.132 and B.133, respectively.

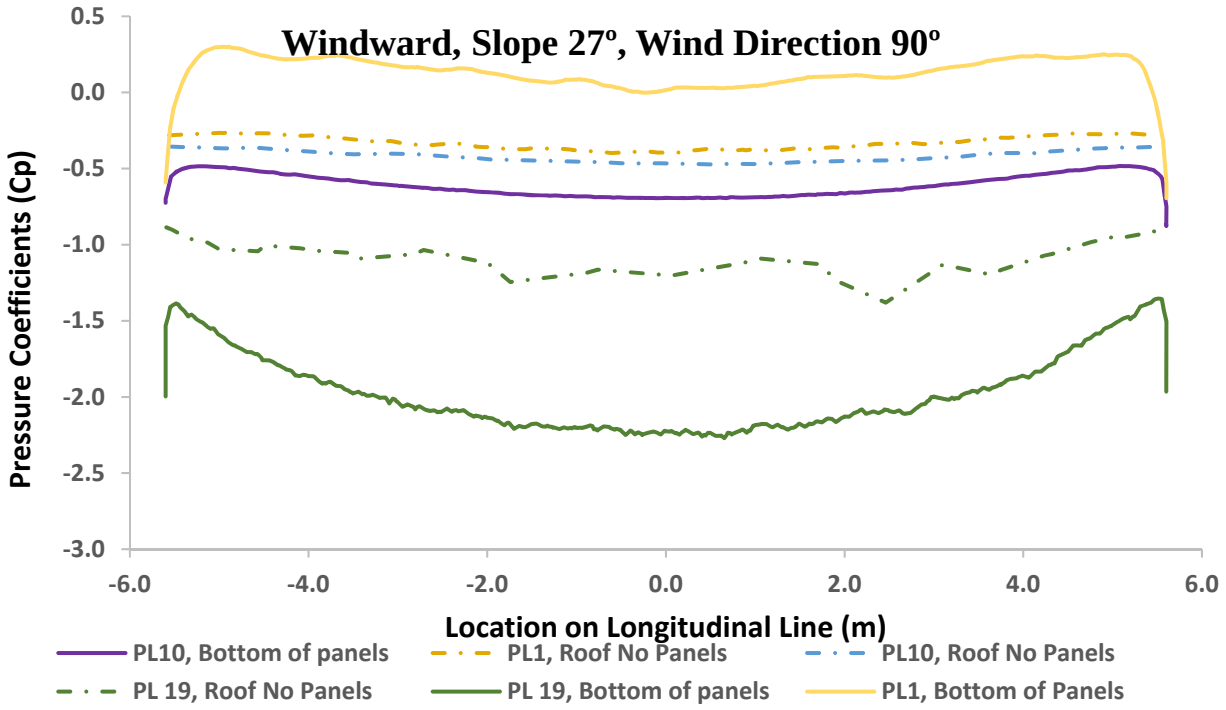


Fig.B. 131. Pressure coefficient distribution on bottom surface of the solar panels and on the roof surface without mounted solar panels, for roof slope 27º, and wind direction 90º, windward side

When wind direction is 90°, which is perpendicular to the ridge of the roof, Cp along line PL1 on the bottom surface of the panels, shows positive pressure (Cp =0 to 0.3) in most of the lines, while Cp on the corresponding line on the roof surface without panels shows suction in the range between (Cp=-0.3 to -0.4). Line PL19 shows much higher suction, with pressure coefficients of (Cp=-1.4 to -2.25), than the corresponding line on the roof without panels, for which Cp are in the range of (Cp=-0.9 to -1.25). The pressure coefficients on PL10 are higher, -0.5 to -0.70, than the pressure coefficients along PL10, (Cp=-0.40. Cp on all the lines are symmetrical around the middle of the roof for both bottom surface of the panels and the roof surface without solar panels (Fig. B.131). Considering wind direction 45° (Fig. B.132) it can be observed that for line PL1 located near the edge C of the solar array (Fig. 4. 57), the pressure coefficients are much higher, (Cp=0.50 to -1.0) than the pressure coefficients on the corresponding line on the roof with no panels, (Cp=0 to -0.75). For line PL19, the pressure coefficients are much higher on the bottom surface of the panels, (Cp=-1.5 to -3.0) than the coefficients on the corresponding line on the roof with no panels, which is nearly constant about (Cp=-1.0). In contrast, the middle line PL 10 shows slightly lower pressure coefficients at first half of the line on the windward side, and then slightly higher in the second half of the line on the leeward side, (Cp=0.5 to -1.2) for the bottom surface of the panel, than the

corresponding line on the roof without panels, (Cp=-0.25 to -0.75). In addition, pressure coefficients along PL1 and PL10 on both surfaces decrease towards the leeward edge of the roof, while pressure coefficients on line PL19 are relatively constant.

For wind direction 0º, the pressure coefficients along PL1, PL10 and PL19 on bottom surface of the panels are slightly different than those on roof without panels, where the average difference is close to zero (Fig. B.133). Moreover, Cp along all the three lines reduces highly from (Cp=-0.25) in the middle of the array to (Cp=-0.75 to -1.20) in the windward edge A, and to (Cp=-0.50 to -0.90) on the leeward edge B, while it remains nearly constant in the middle parts of those lines.

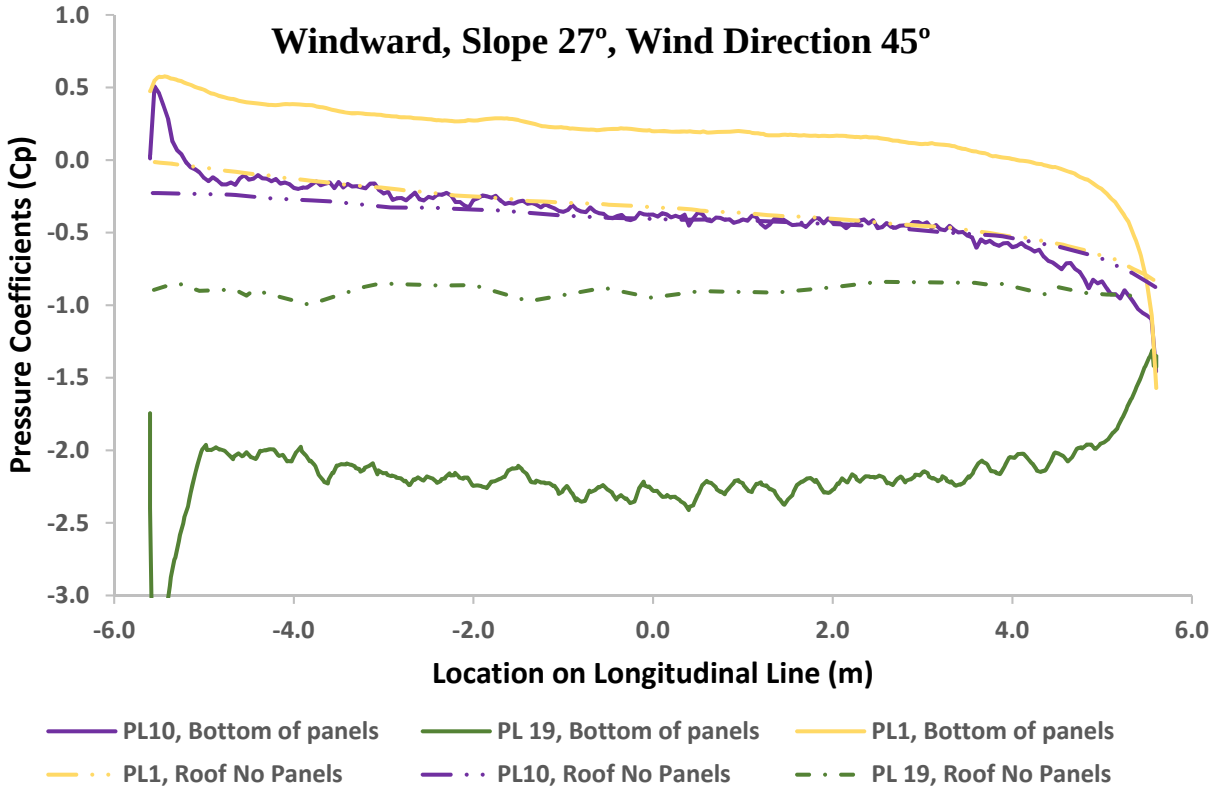


Fig.B. 132. Pressure coefficient distribution on bottom surface of the solar panels and on the roof surface without mounted solar panels, for roof slope 27º, and wind direction 45º, windward side

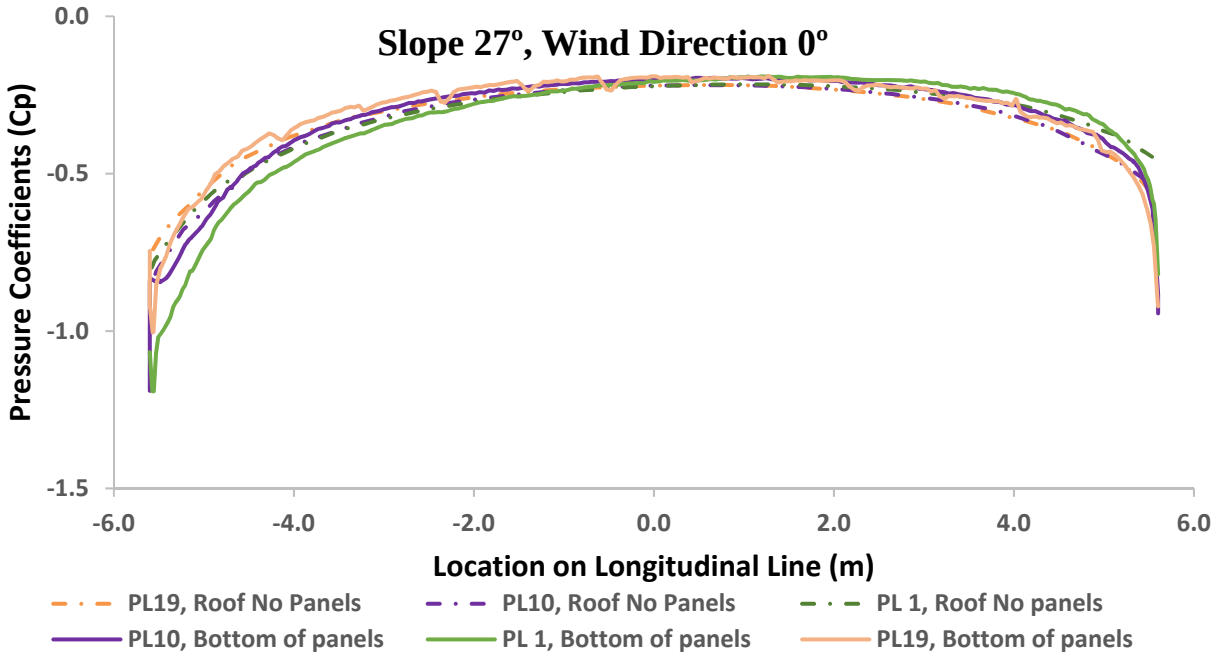


Fig.B. 133. Pressure coefficient distribution on bottom surface of the solar panels and on the roof surface without mounted solar panels, for roof slope 27º, and wind direction 0º

XIV.4. Pressure coefficients on bottom of solar panels vs. roofs without solar panels, roof slope 27º

The following Figs. Fig. B.134, Fig. B.135 and Fig. B.133 show change in pressure coefficients along the main lines, PL20, PL29 and PL38 on the bottom of solar panels mounted on the leeward surface of the roof, compared with those on roof surface without solar panels.

For 90°, the wind direction perpendicular to the ridge, Cp along PL29 on bottom of the panels shows much higher-pressure coefficients by nearly (Cp=0 to 0.8) than Cp on the corresponding line on roof without panels which recorded (Cp=-0.9 to -1.65). However, Cp on PL38 bottom of the panels shows slightly higher suction, (Cp=-0.65 to -0.75), than the Cp on corresponding line on roof without panels, (-0.6 to -0.75). However, Cp on PL20 on bottom of the panels, is (0 to 0.7) lower for 3.5 m near edge A and 3.5 m near edge B of the array, while it is slightly (0-0.2) higher than Cp on the corresponding PL 20 in 5 m in middle part of the array. On the other hand, Cp on all the lines are symmetrical around the middle of the roof, that for both bottom of the panels and roof surface without solar panels. Fig. Fig. B.134.

When discussing the 45° wind direction (Fig. Fig. B.135) it is noticed that pressure coefficients have similar trends, for bottom of the panels solar panels installed and roof without solar panels. However, on line PL20 located near the ridge, (Fig. 6), along bottom of the panels, the pressure coefficients are much higher by 0 to 0.7 than corresponding line on the roof with no panels which range from (Cp=-1.3 to -1.6). In addition, Cp on middle line PL 29, on roof under panels, starts at (Cp=-3.0) at windward side, which is higher by about 1.7 than the than Cp on the corresponding line on the roof without panels, and then increases gradually, until 4 m from the leeward edge of the array, B, where it becomes higher afterwards by nearly average 0 to 0.1 until the end of the array at the leeward side. In addition, all Cp along the lines PL29 and PL38 on both surfaces increase towards the leeward edge of the roof starting at much higher pressure coefficient at the windward side.

Effects of wind flow at direction 0º, are exactly like the case section 4.3.2.3 above, and illustrated in Fig. Fig. B.133, because of symmetrical flow and geometry in 0º wind direction.

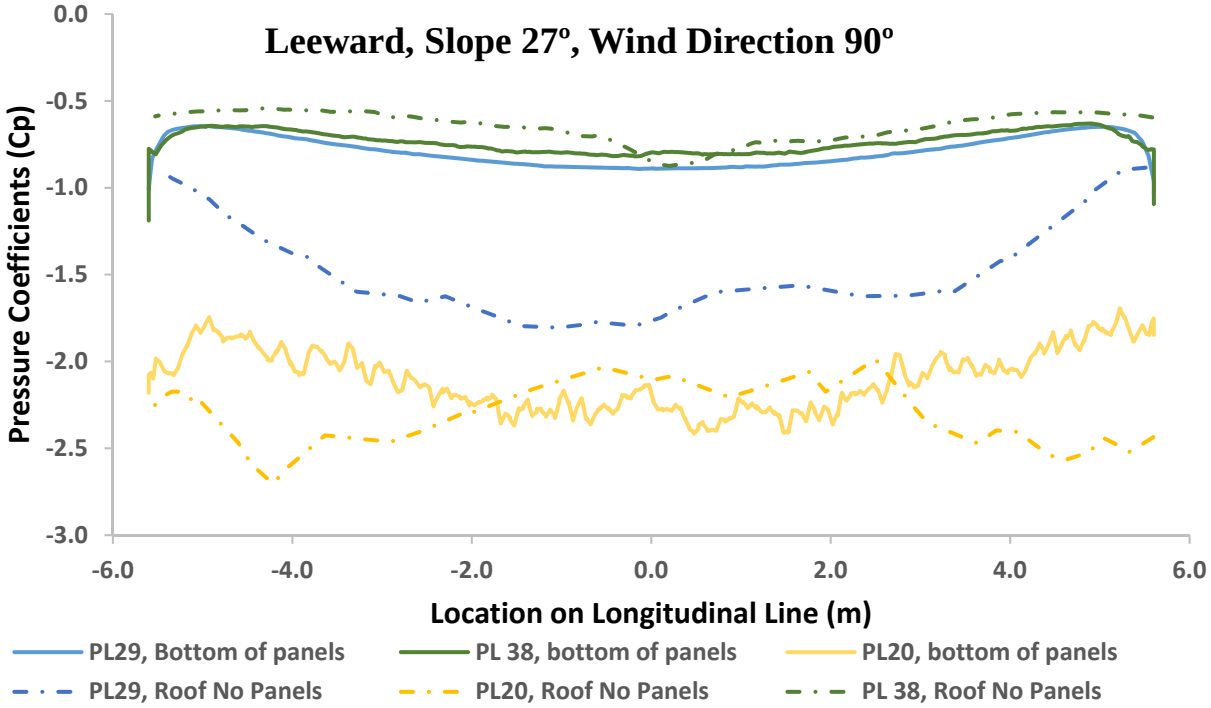


Fig.B. 134. Pressure coefficient distribution on bottom surface of the solar panels and on the roof without mounted solar panels, for roof slope 27º, and wind direction 90º, leeward side

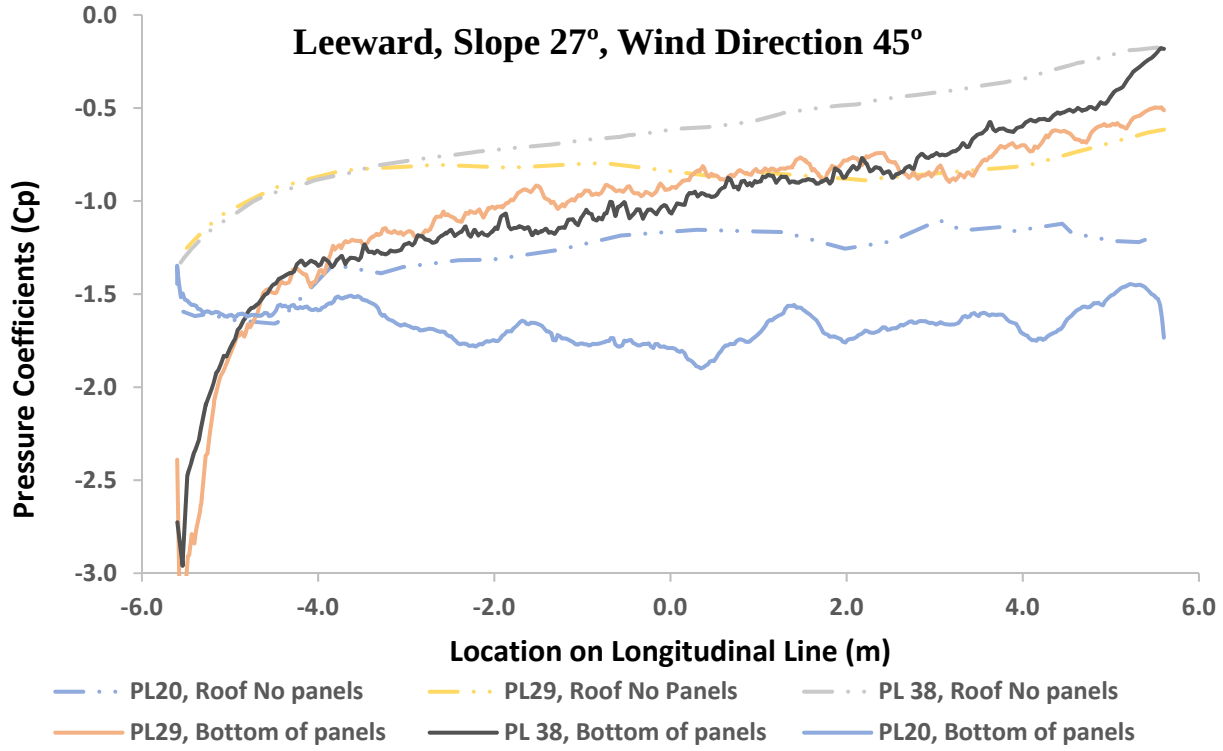


Fig.B. 135. Pressure coefficient distribution on bottom surface of the solar panels and on the roof without mounted solar panels, for roof slope 27º, and wind direction 45º, leeward side

APPENDIX (C)

Chapter 5, Remaining cases Slope 35º

C.1 Slope 35º,

1.1. 2” Spacing, 10” Clearance

1.1.1. Wind direction 45º,

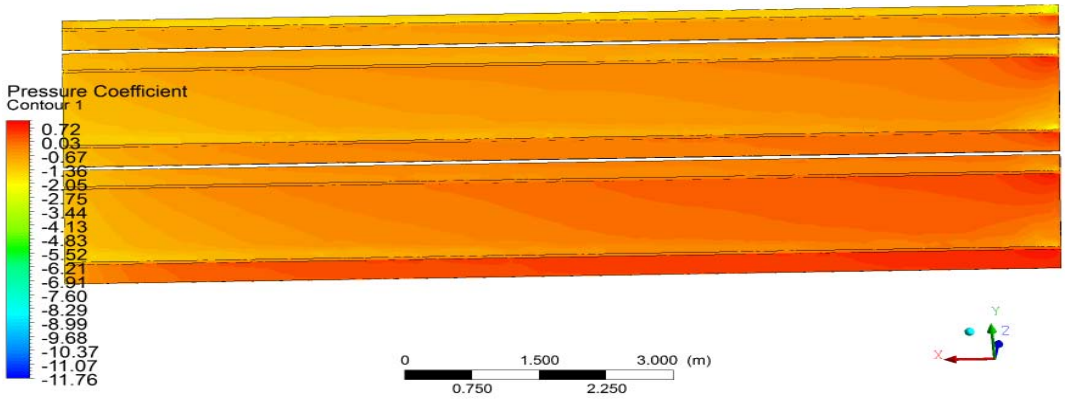


Fig. C. 1. Cp on bottom of the solar panels,

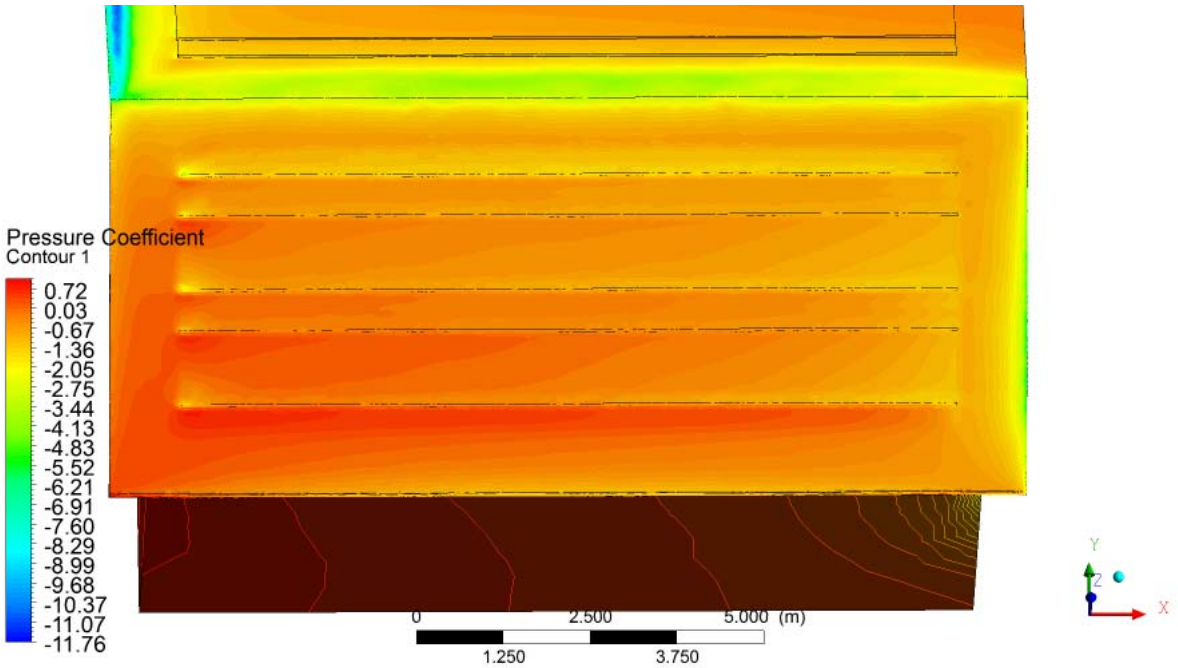


Fig. C. 2. Cp on Roof under the solar panels, cut off solar panels

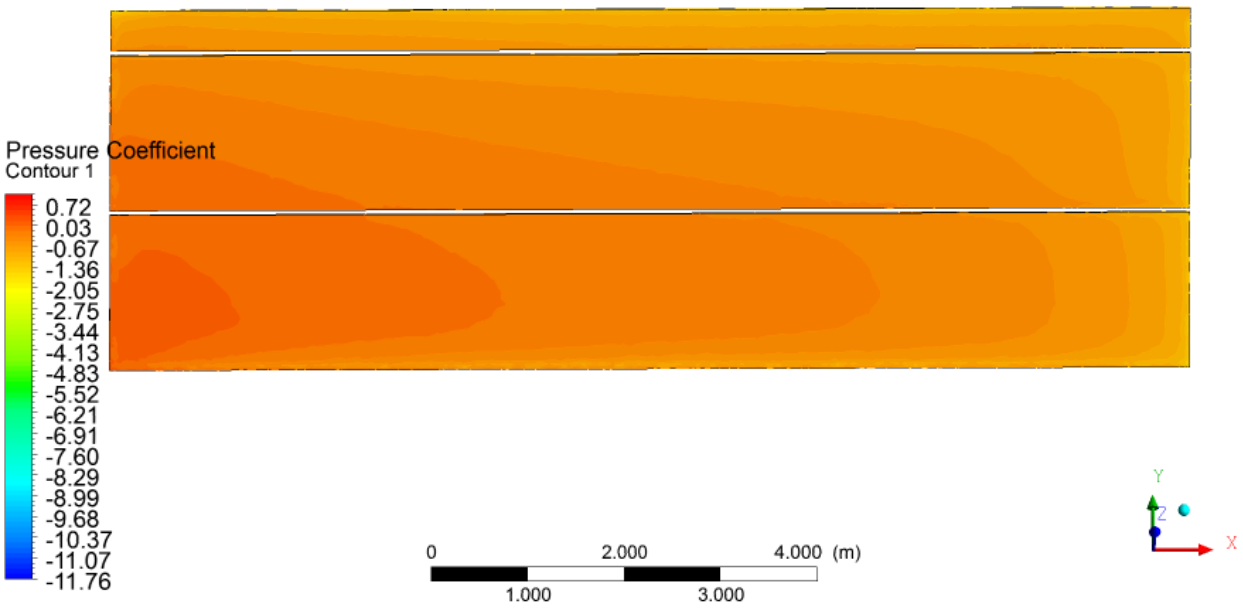


Fig. C. 3. Cp on top of the solar panel

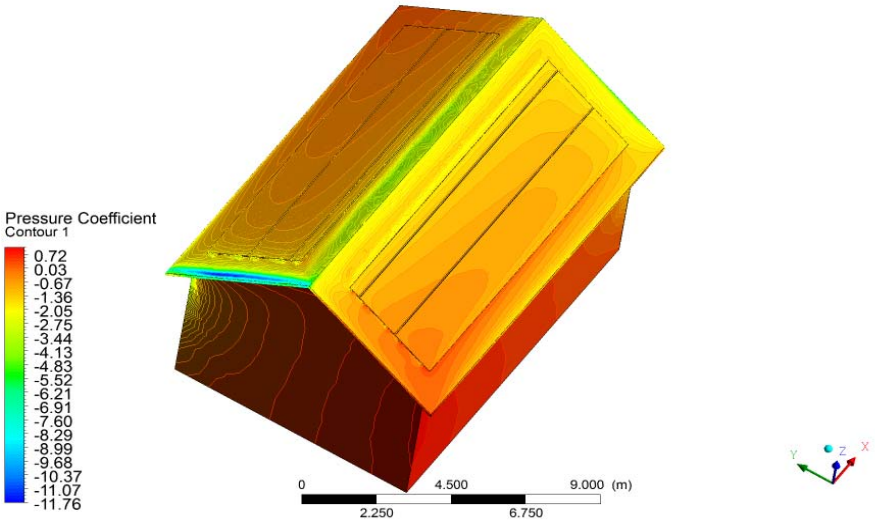


Fig. C. 4. Pressure coefficient on top surface of the solar panels WD 45º.

1.1.2. WIND DIRECTION 90º

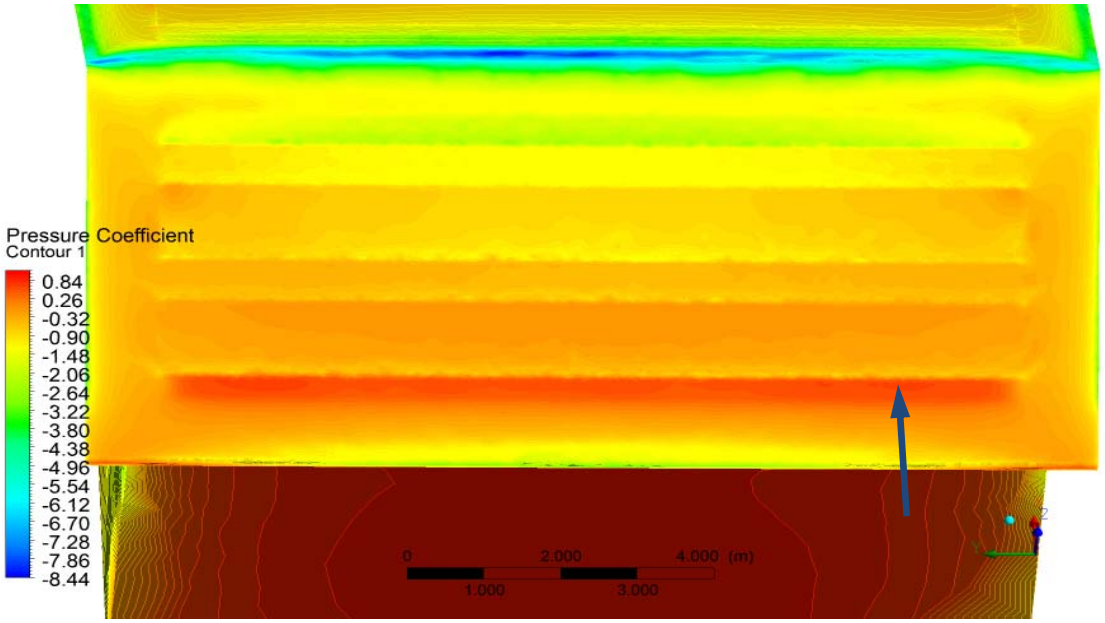


Fig. C. 5. CP on roof under solar panels, S 35º, WW, WD 90º

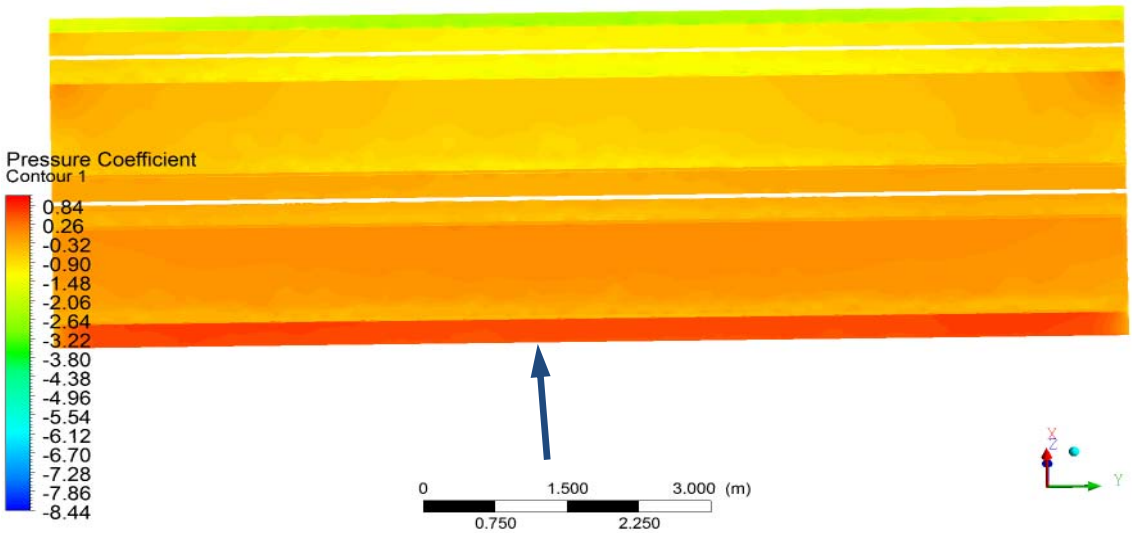


Fig. C. 6. Cp on bottom of solar panels, S 35º, WW, WD 90º

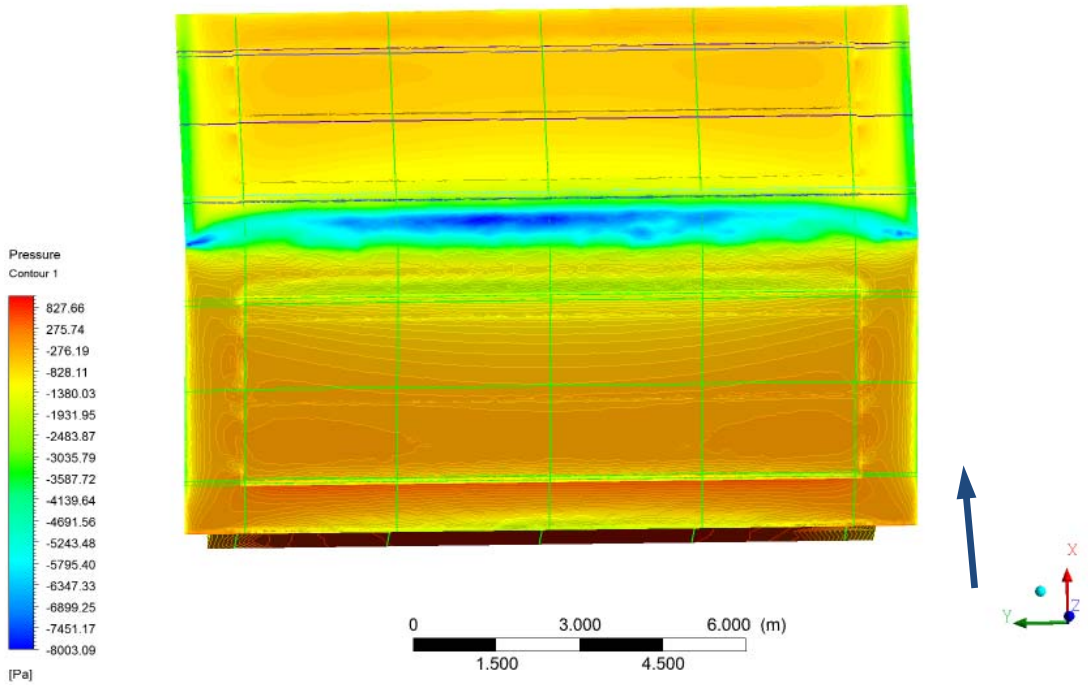


Fig. C. 7. Cp on top of solar panels with plines, S 35º, WW, WD 90º

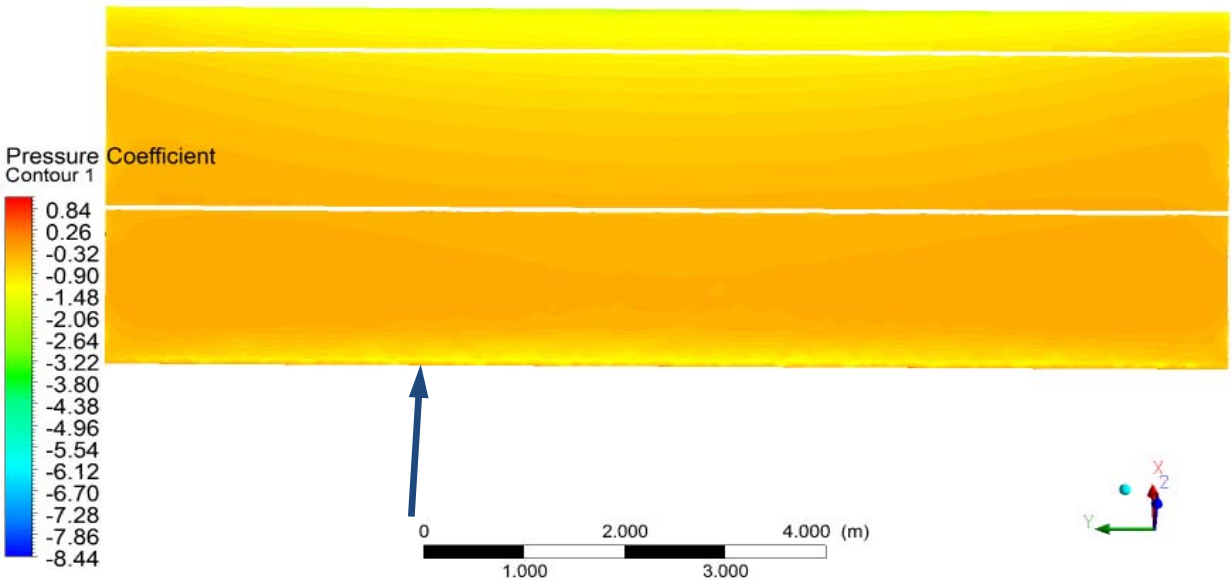


Fig. C. 8. Cp on top of solar panels, S 35º, WW, WD 90º

1.1.3. WIND DIRECTION 0.0º

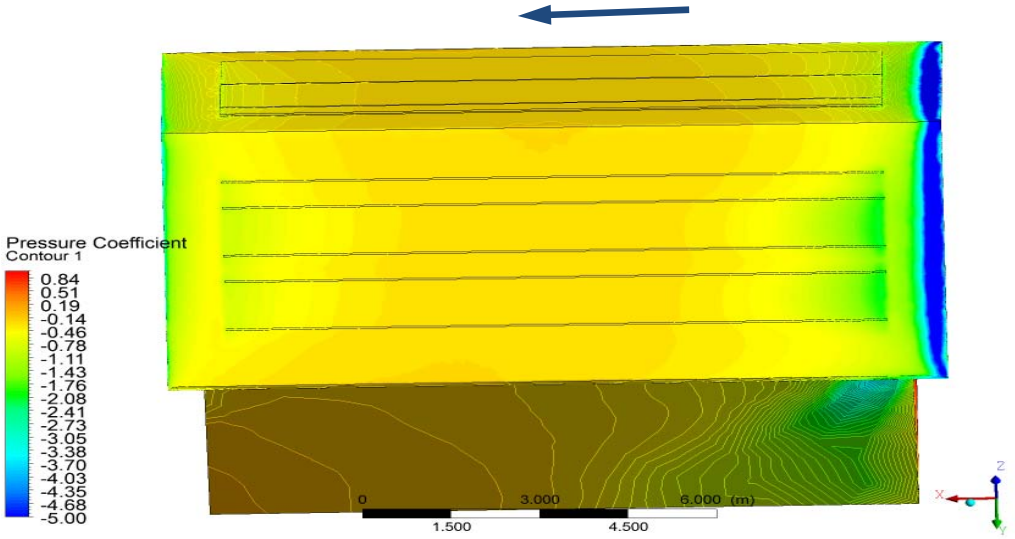


Fig. C. 9. Cp on roof under solar panels with Plines S 35º, WW, WD 0.0º

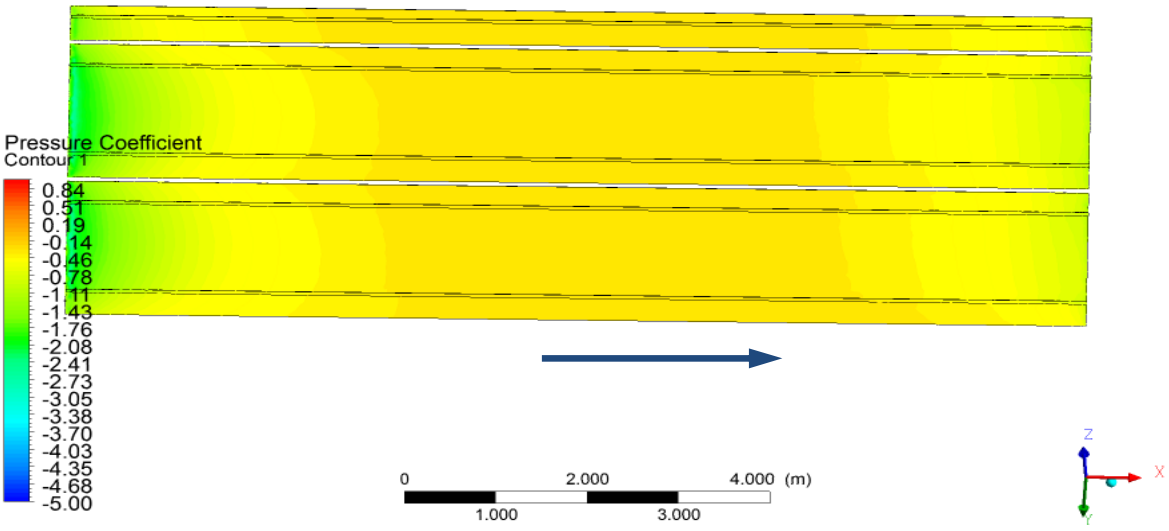


Fig. C. 10. Cp, on bottom of solar panels, S 35º, WW, WD 0.0º

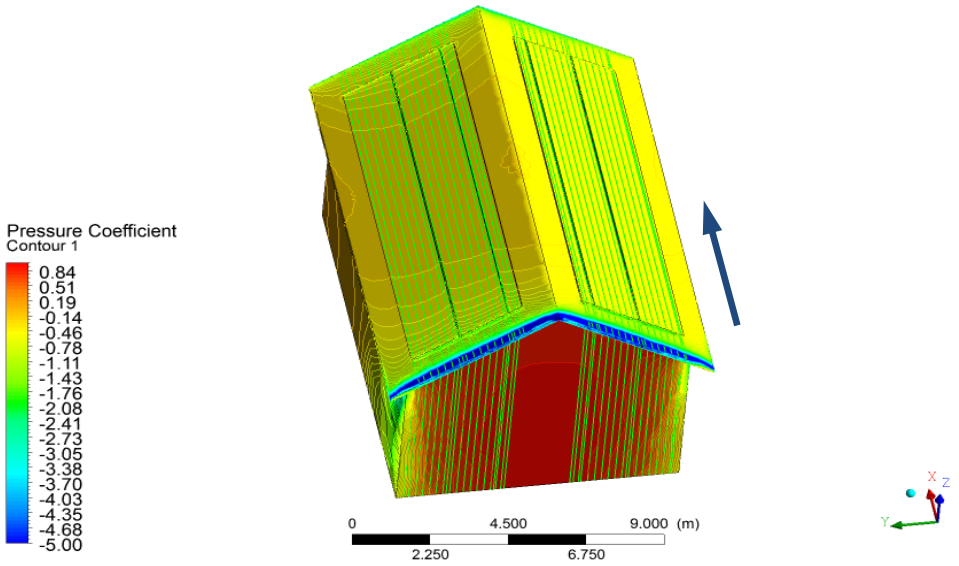


Fig. C. 11. Cp on top of solar panels and roof with Plines, S 35º, WW, WD 0º

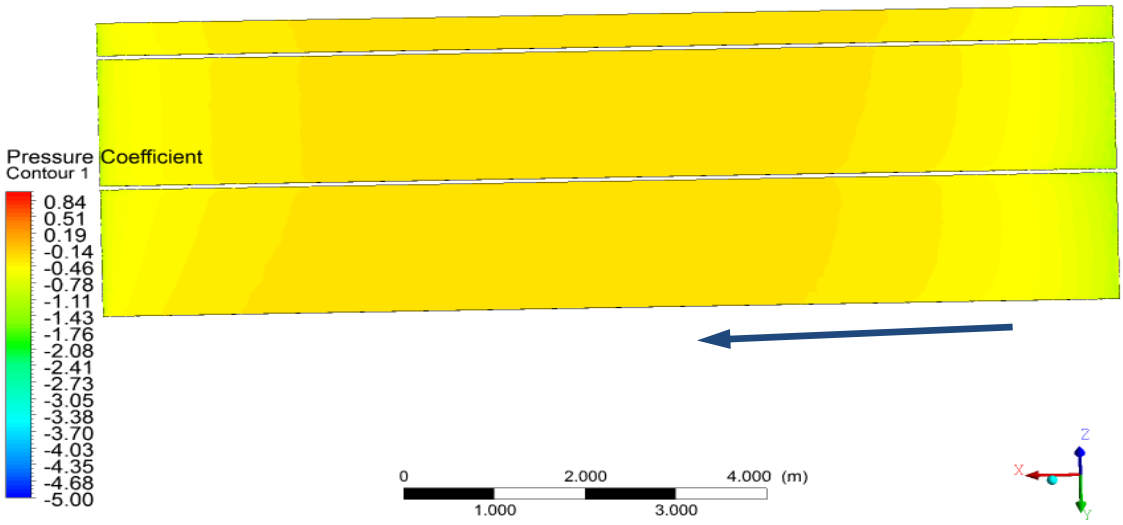


Fig. C. 12. Cp on top of solar panels, S 35º, WW, WD 0º

1.1.4. Detailed Distribution of Wind Pressure on roof mounted solar panels in comparison with bare roofs, Windward, 2" apart, 10" roof space

A. Bottom of solar panels vs. roof under solar panels,

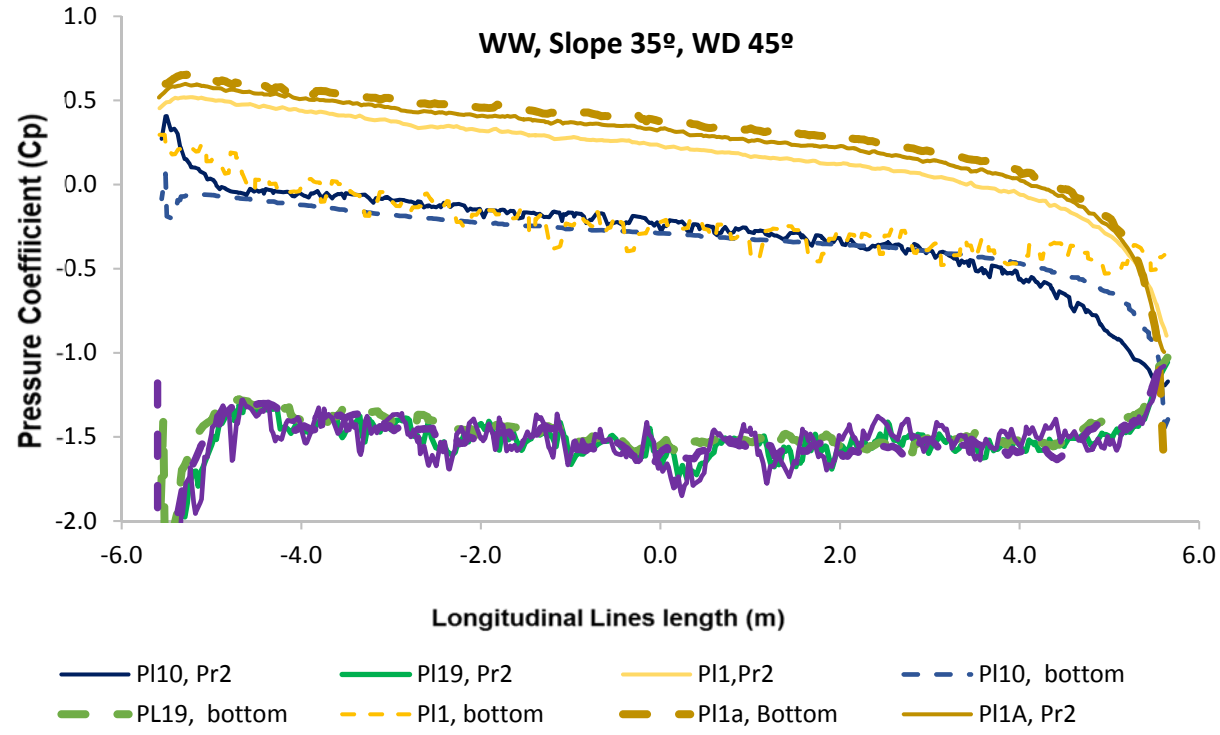


Fig. C. 13. Cp on bottom of solar panels vs. on roof under the panels, Pr2, S 35º, WW, WD 45º

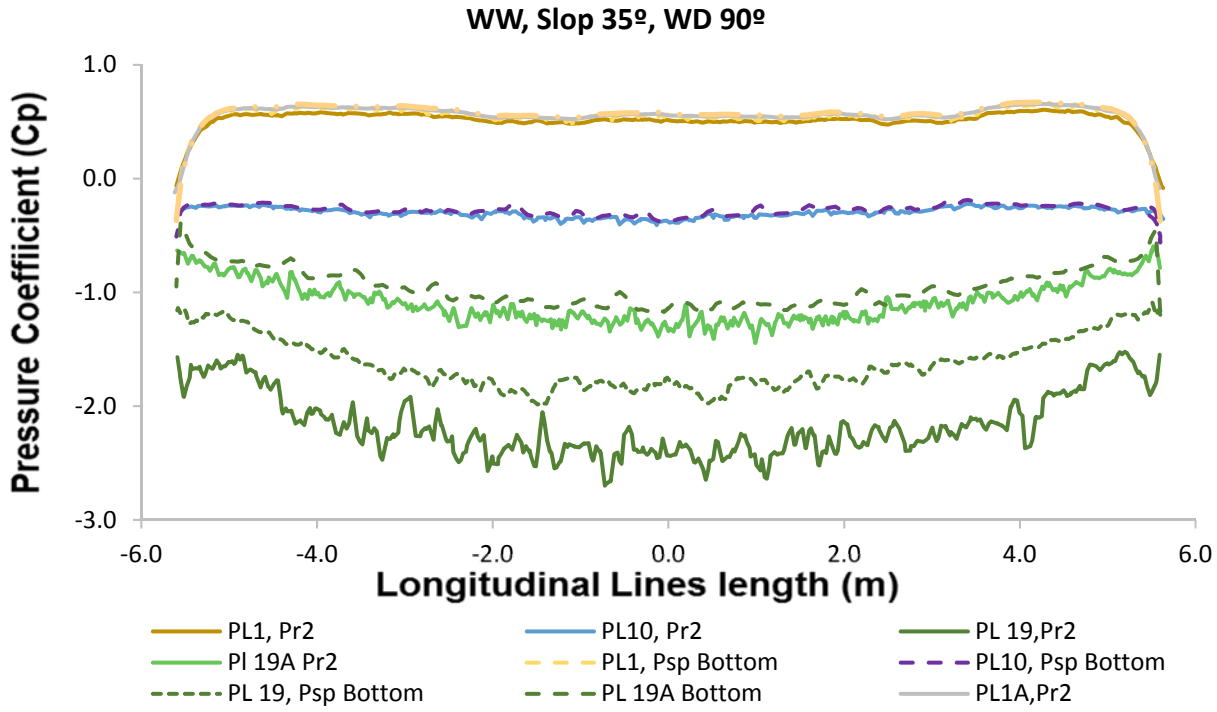


Fig. C. 14. Cp on bottom of solar panels vs. on roof under the panels, Pr2, S 35 º, WW, WD 90 º

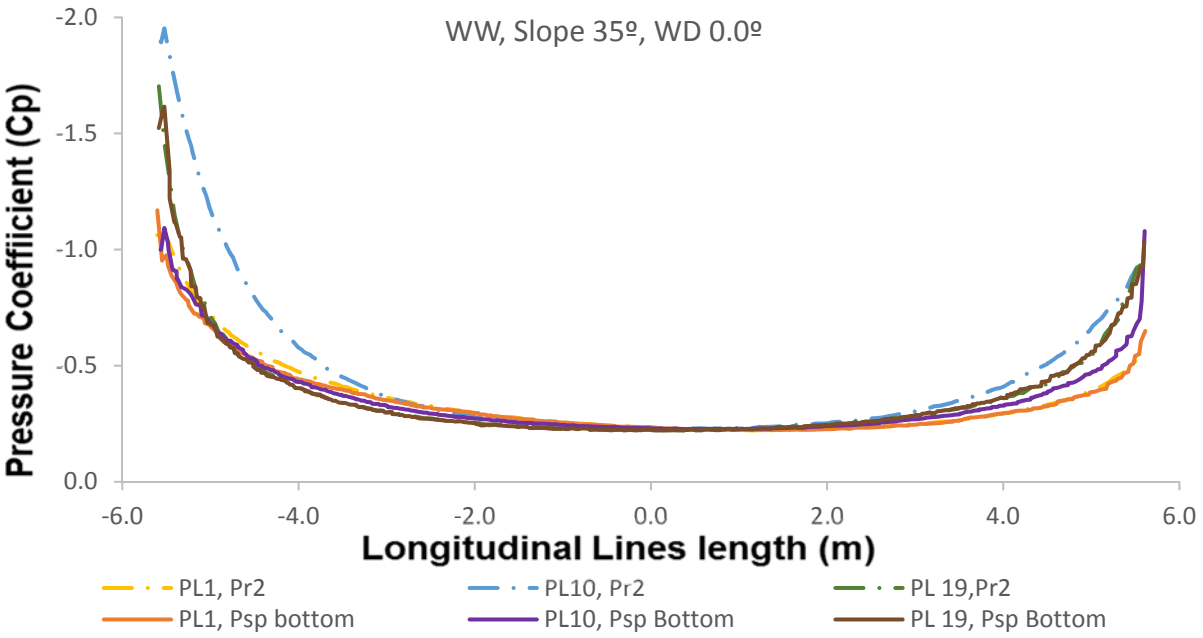


Fig. C. 15. Cp on bottom of solar panels vs. on roof under the panels, Pr2, S 35 º, WW, WD 0.0º

B. Roof under solar panels vs. bare roofs,

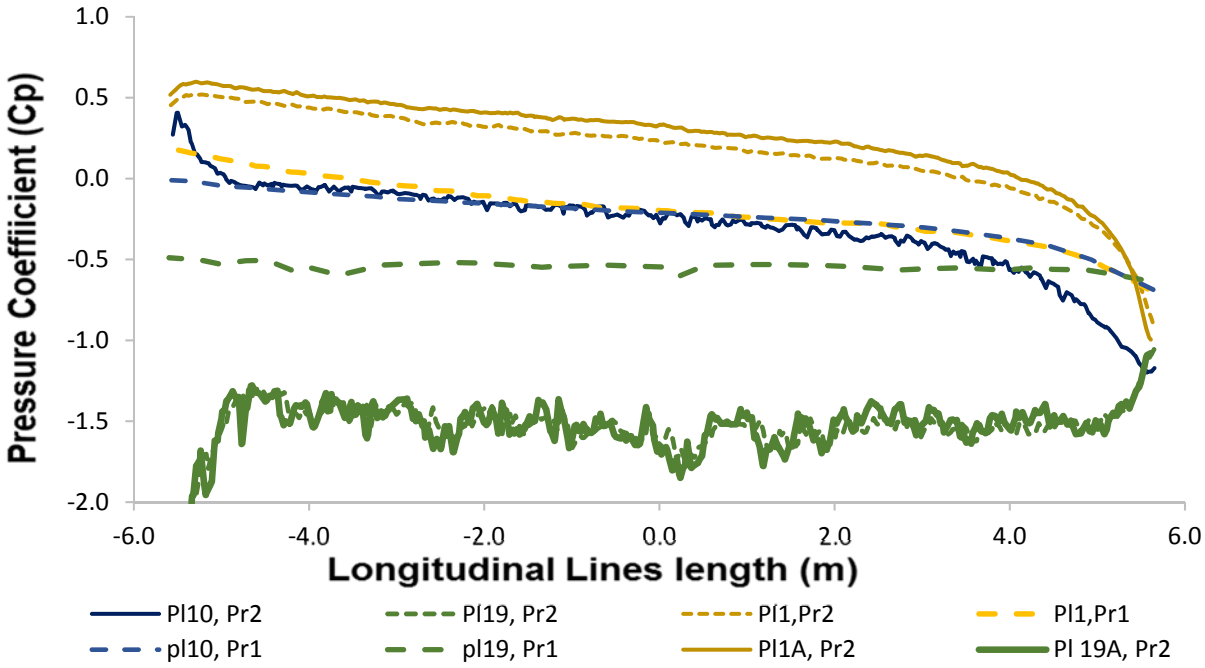


Fig. C. 16. Cp on bare roof Pr1 vs. on roof under the panels, Pr2, S 35º, WW, WD 45º

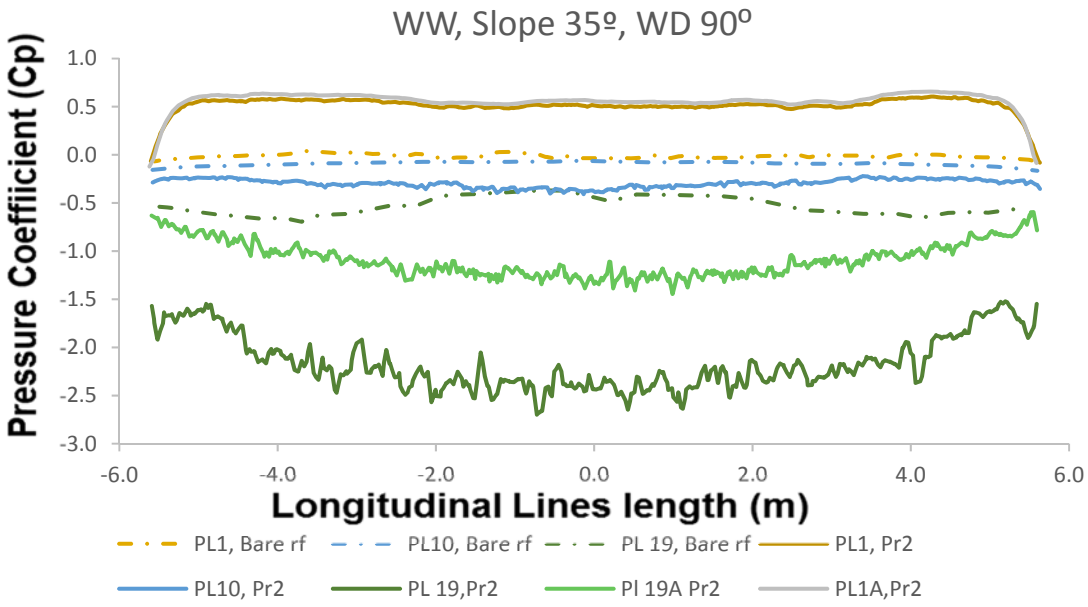


Fig. C. 17. Cp on bare roof Pr1 vs. on roof under the panels, Pr2, S 35º, WW, WD 90º

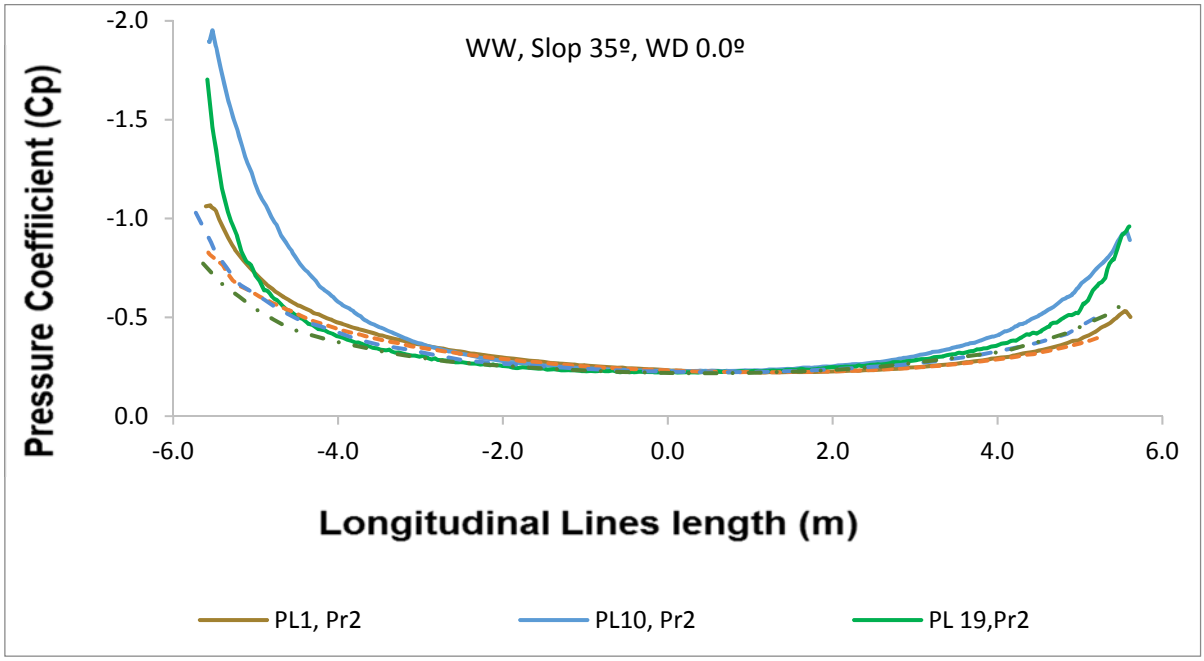


Fig. C. 18. Cp on bare roof Pr1 vs. on roof under the panels, Pr2, S 35º, WW, WD 0.0º

C. Bottom of the solar panels vs. bare roofs,

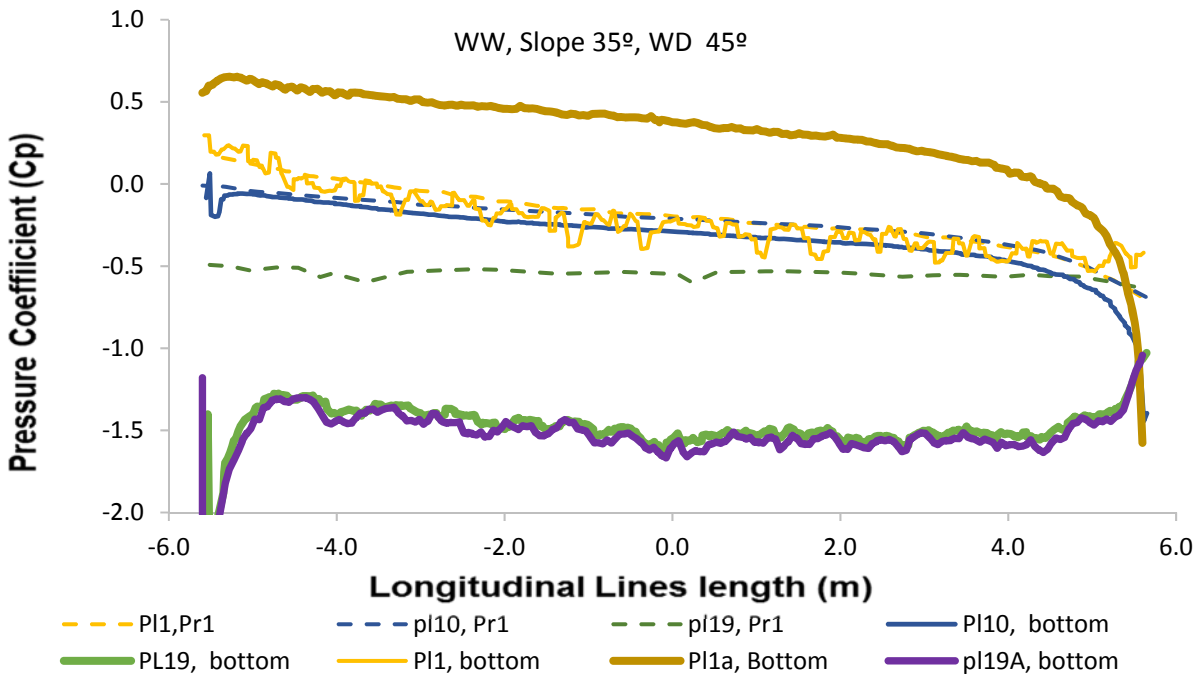


Fig. C. 19. Cp on bottom of solar panels Psp vs. on bare roof, Pr1, S 35 º, WW, WD 45 º

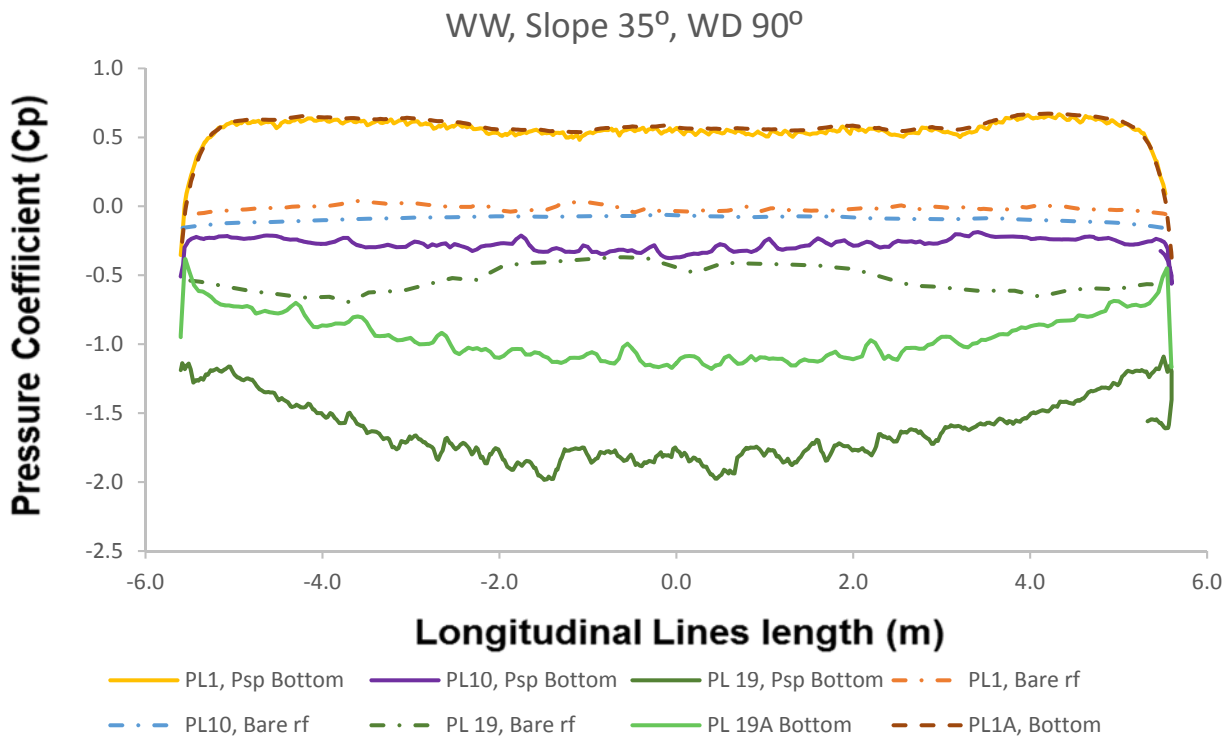


Fig. C. 20. Cp on bottom of solar panels Psp vs. on bare roof, Pr1, S 35 º, WW, WD 90 º

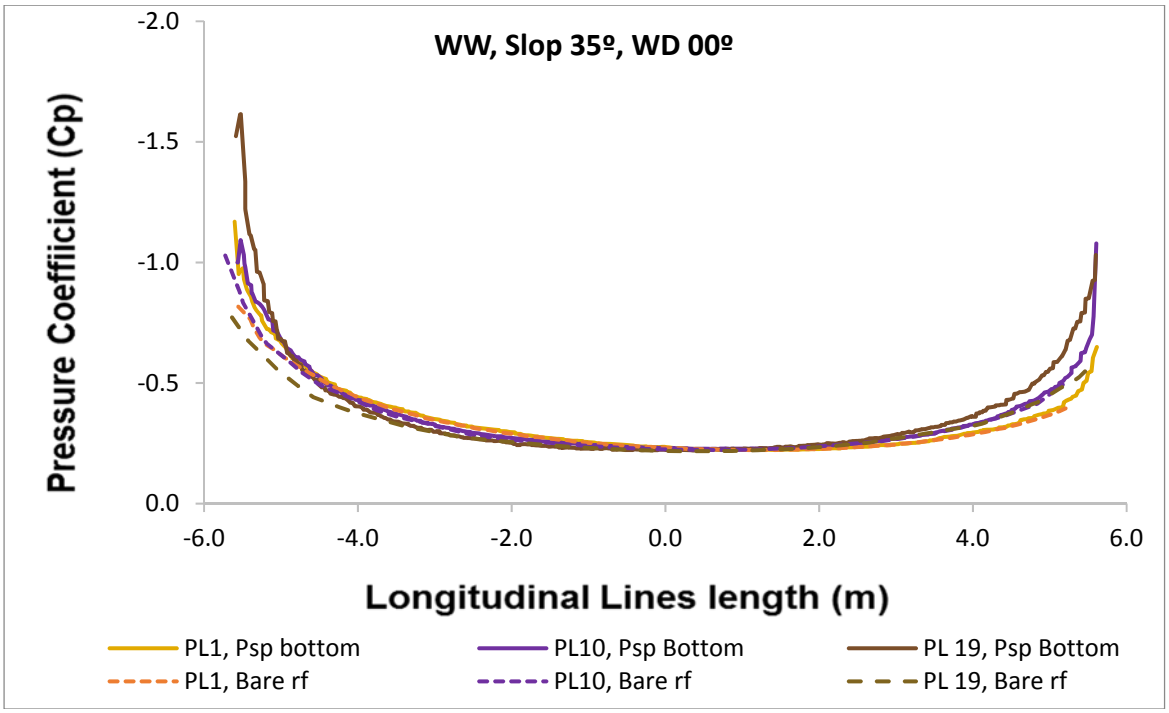


Fig. C. 21. Cp on bottom of solar panels Psp vs. on bare roof, Pr1, S 35 º, WW, WD 0.0 º

D. Bare roofs Pr1 Vs resultant Pr2 +Psp,

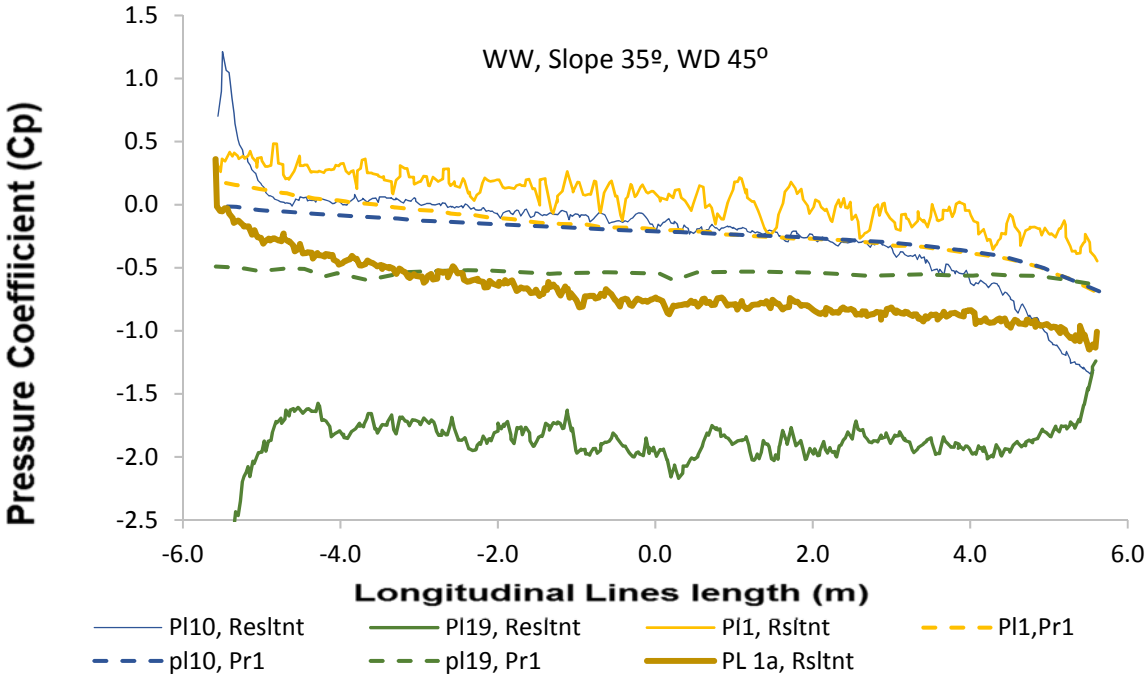


Fig. C. 22. Cp of bare roofs Pr1 Vs resultant Pr2 + Psp, S 35 º, WW, WD 45 º

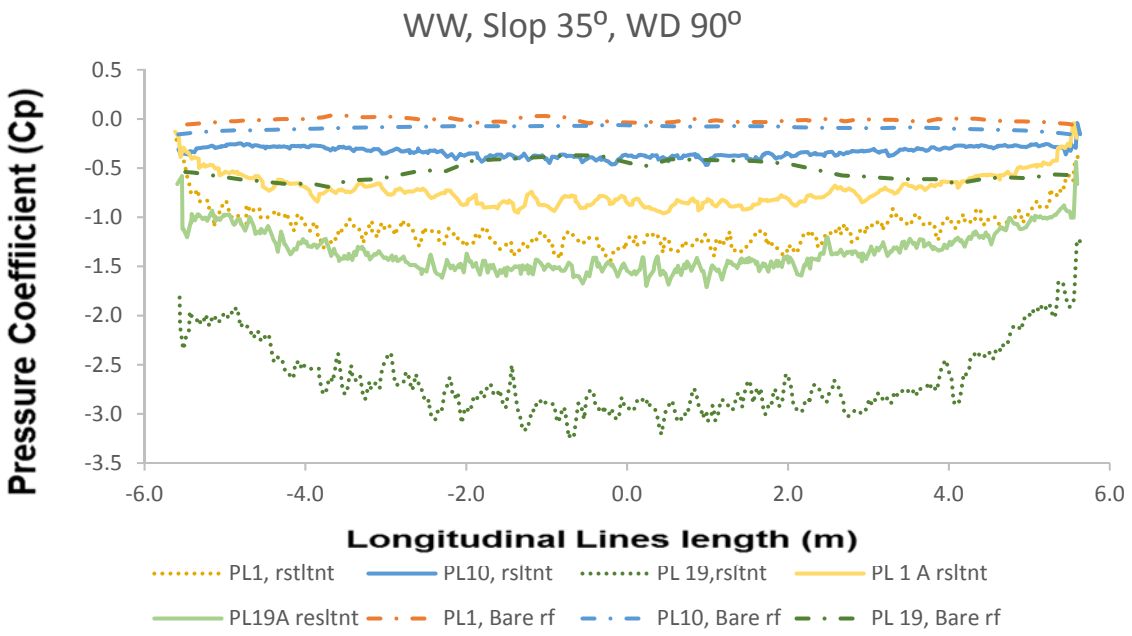


Fig. C. 23. Cp of bare roofs Pr1 Vs resultant Pr2 + Psp, S 35 º, WW, WD 90 º

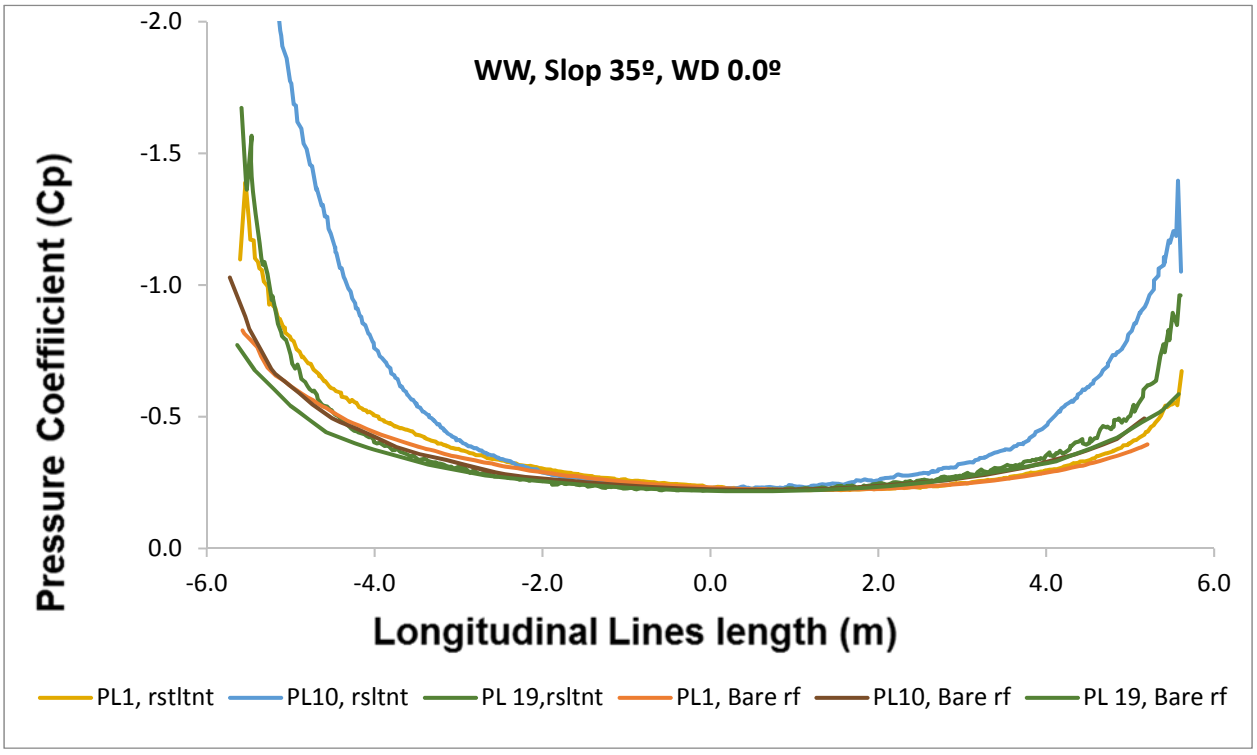


Fig. C. 24. Cp of bare roofs Pr1 Vs resultant Pr2 + Psp, S 35 º, WW, WD 0.0 º

E. Bare roofs Pr1 Vs top of the panels,

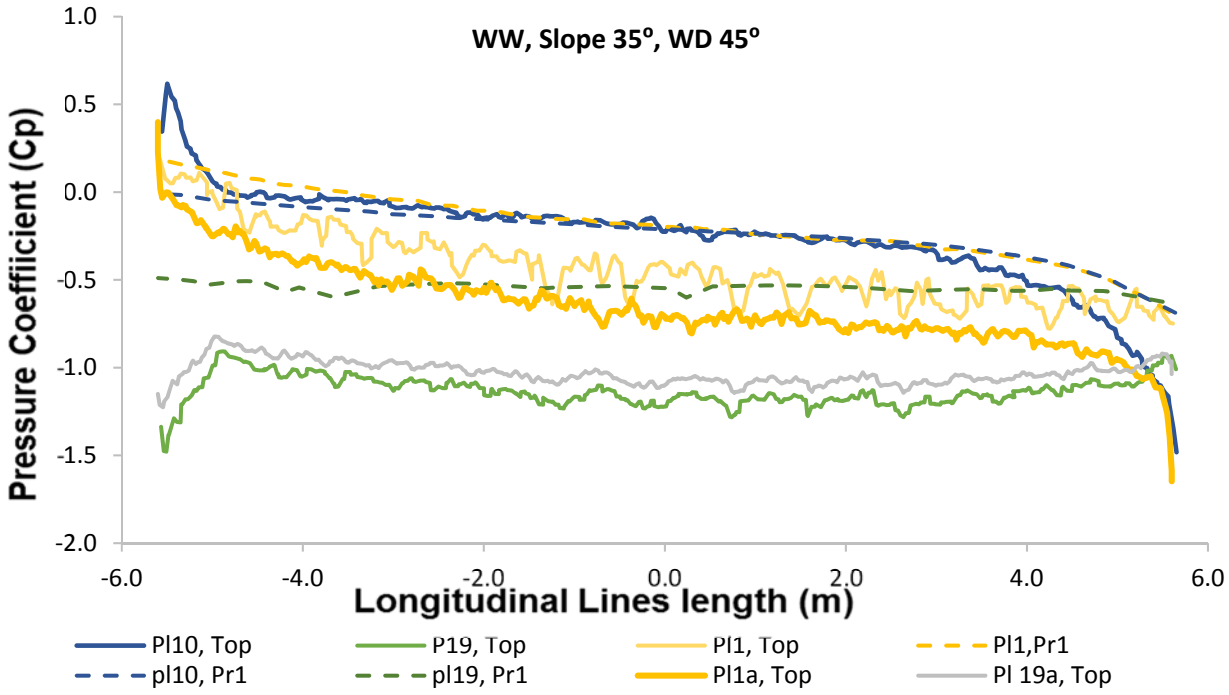


Fig. C. 25. Cp of bare roofs Pr1 Vs top of panels, S 35º, WW, WD 45 º

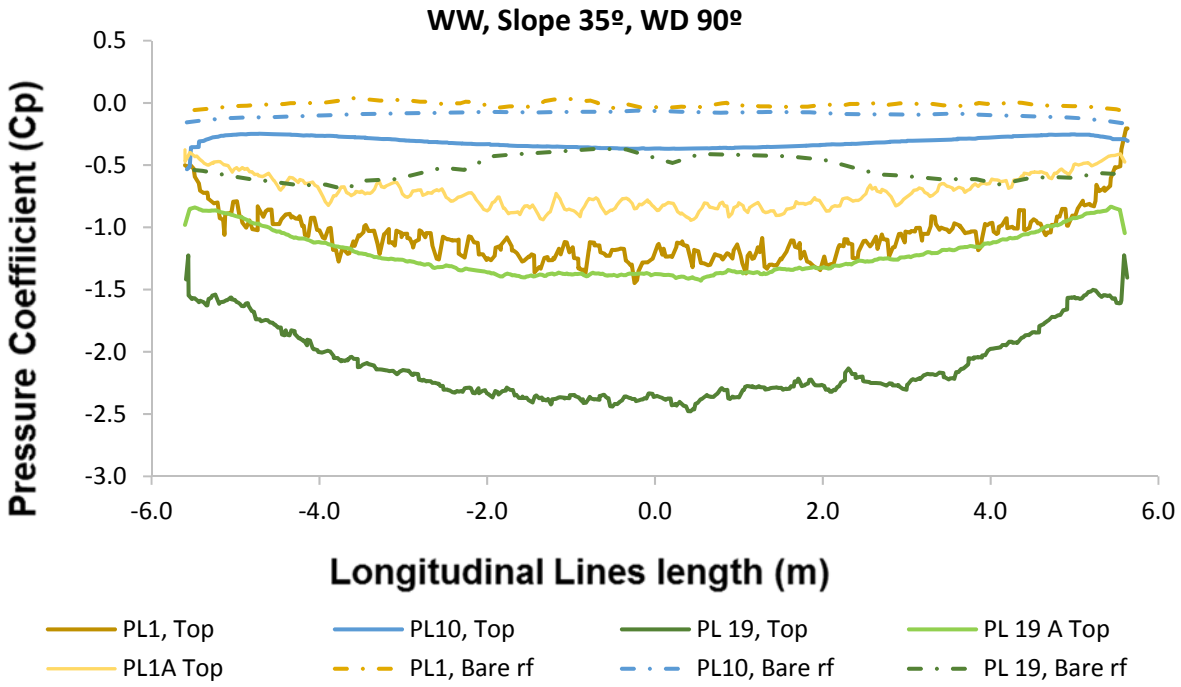


Fig. C. 26. Cp of bare roofs Pr1 Vs top of panels, S 35º, WW, WD 90 º

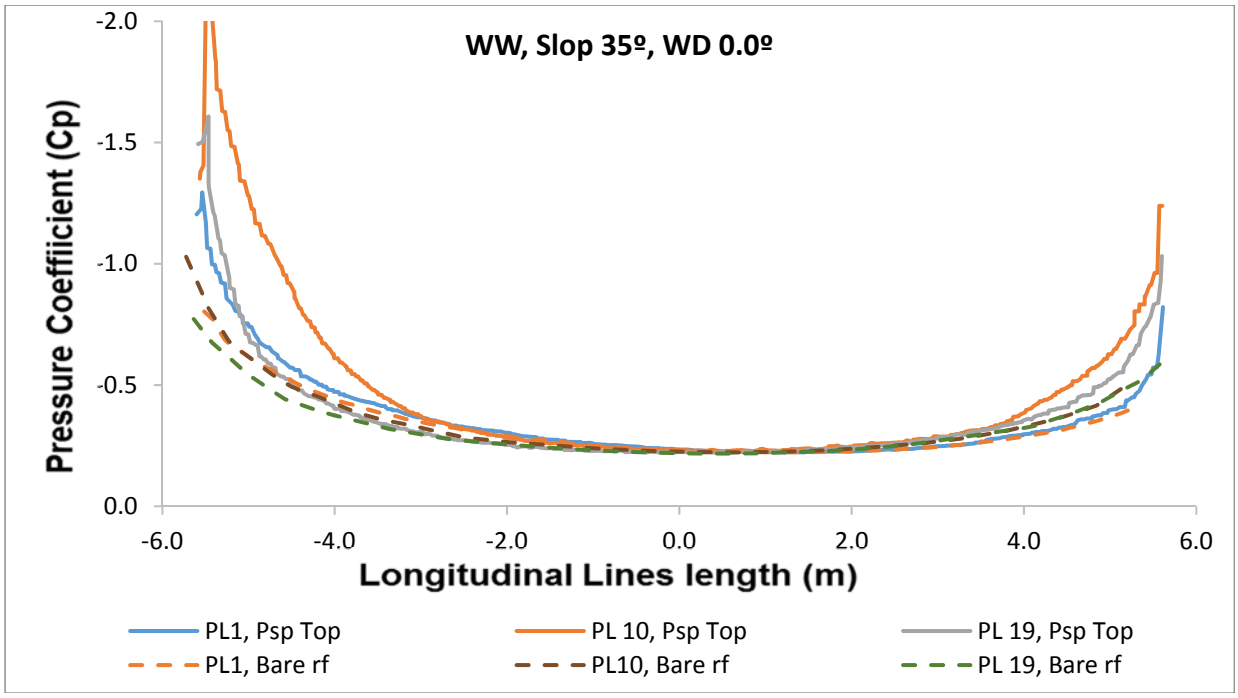


Fig. C. 27. Cp of bare roofs Pr1 Vs top of panels, S 35º, WW, WD 0.0 º

1.1.5. Detailed Distribution of Wind Pressure on roof mounted solar panels in comparison with roof under panels and bare roofs, Leeward, 2" spacing , 10" roof clearance

A. Bottom of solar panels vs. roof under solar panels,

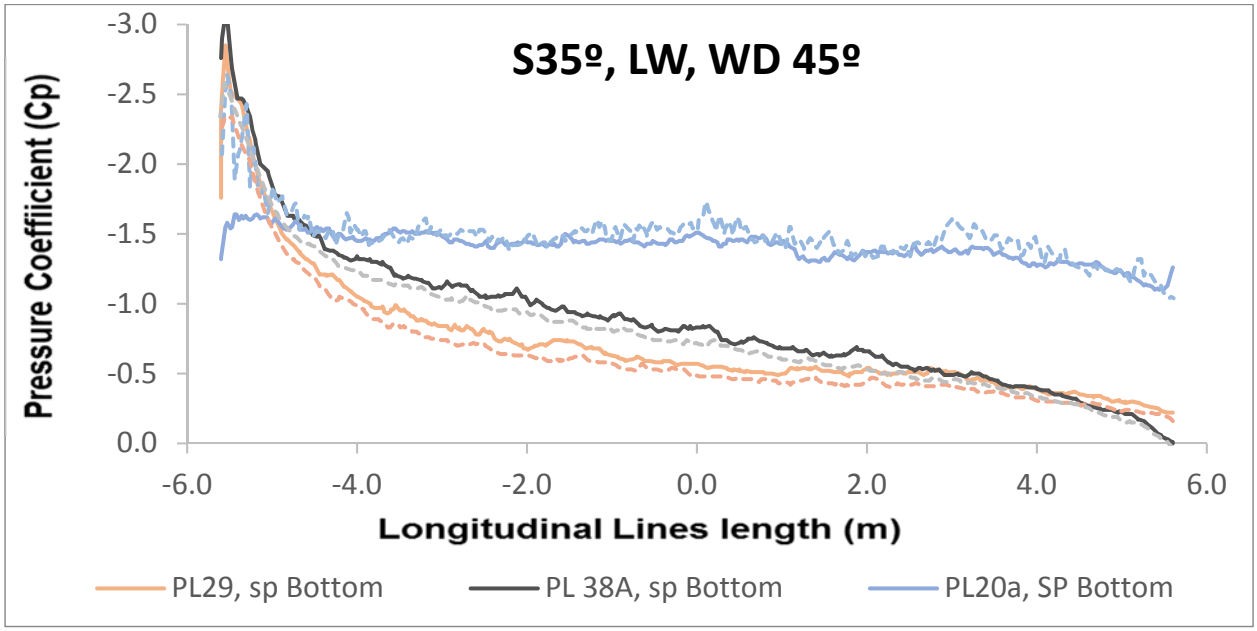


Fig. C. 28. Cp on bottom of solar panels Psp vs. on roof under the panels, Pr2, S 35º, WD 45º

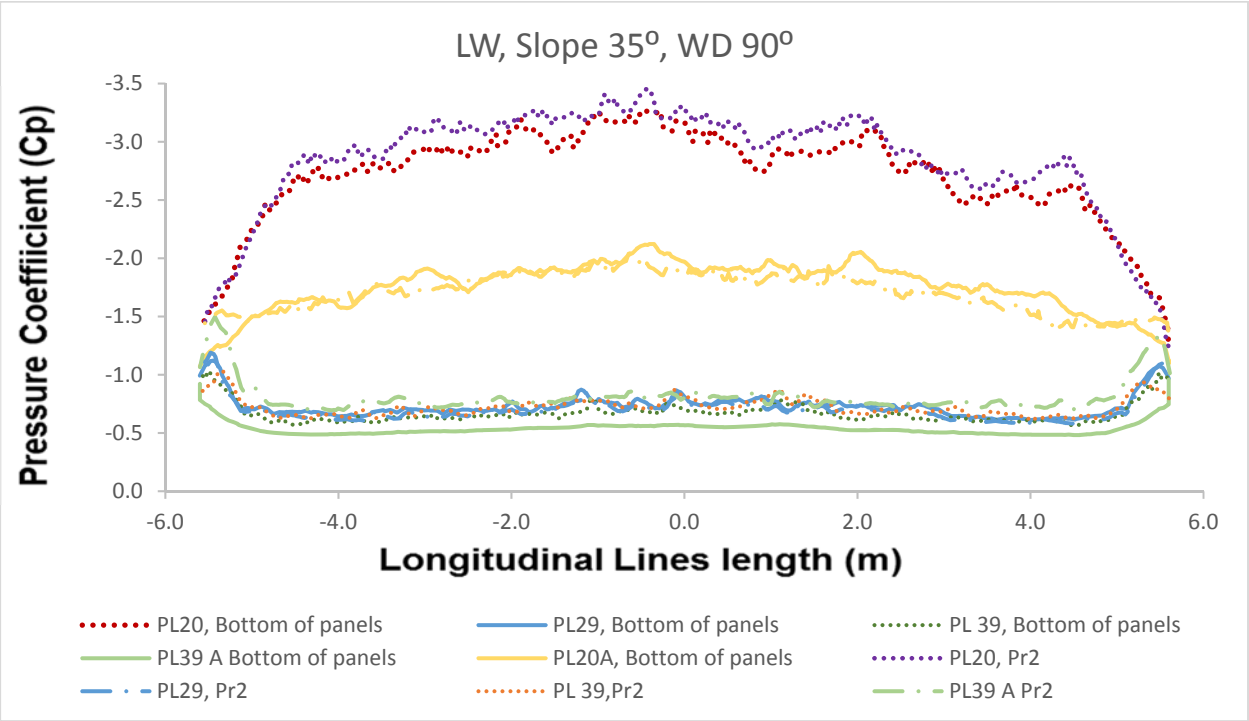


Fig. C. 29. Cp on bottom of solar panels Psp vs. on roof under the panels, Pr2, S 35º, LW, WD 90º

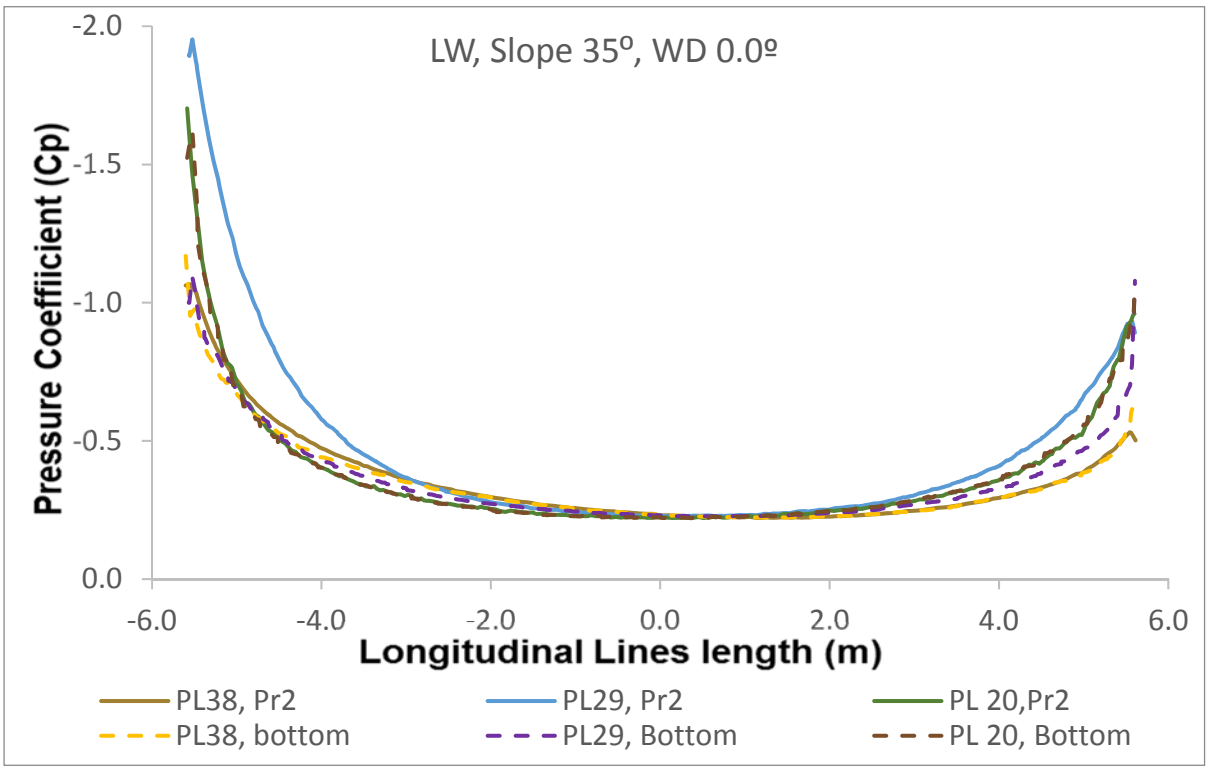


Fig. C. 30. Cp on bottom of solar panels Psp vs. on roof under the panels, Pr2, S 35 º, LW, WD 0.0º

B. Roof under solar panels vs. bare roofs,

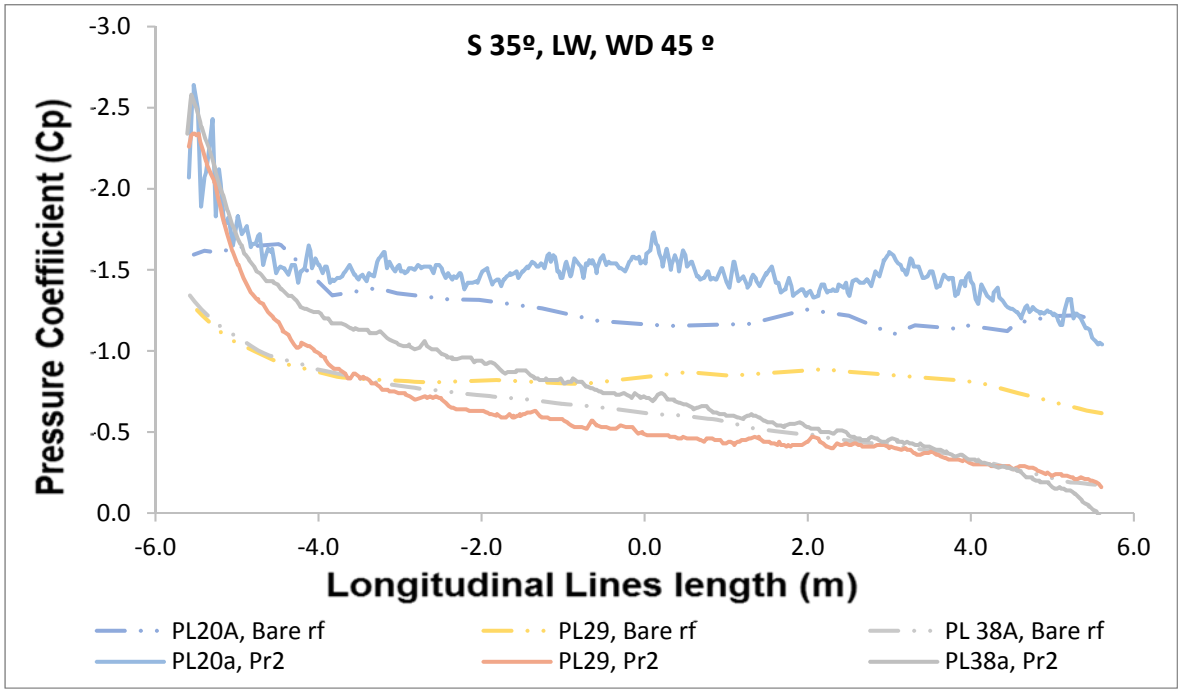


Fig. C. 31. Cp on bare roof Pr1 vs. on roof under the panels, Pr2, S 35º, LW, WD 45º

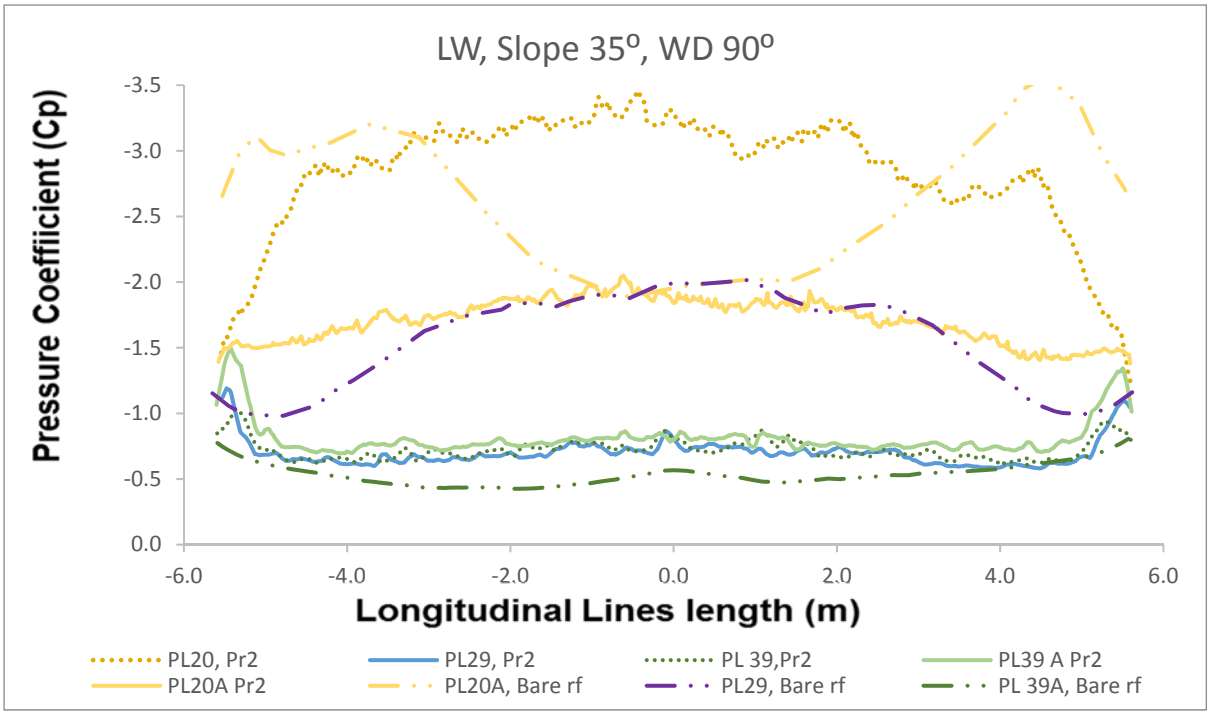


Fig. C. 32. Cp on bare roof Pr1 vs. on roof under the panels, Pr2, S 35º, LW, WD 90º

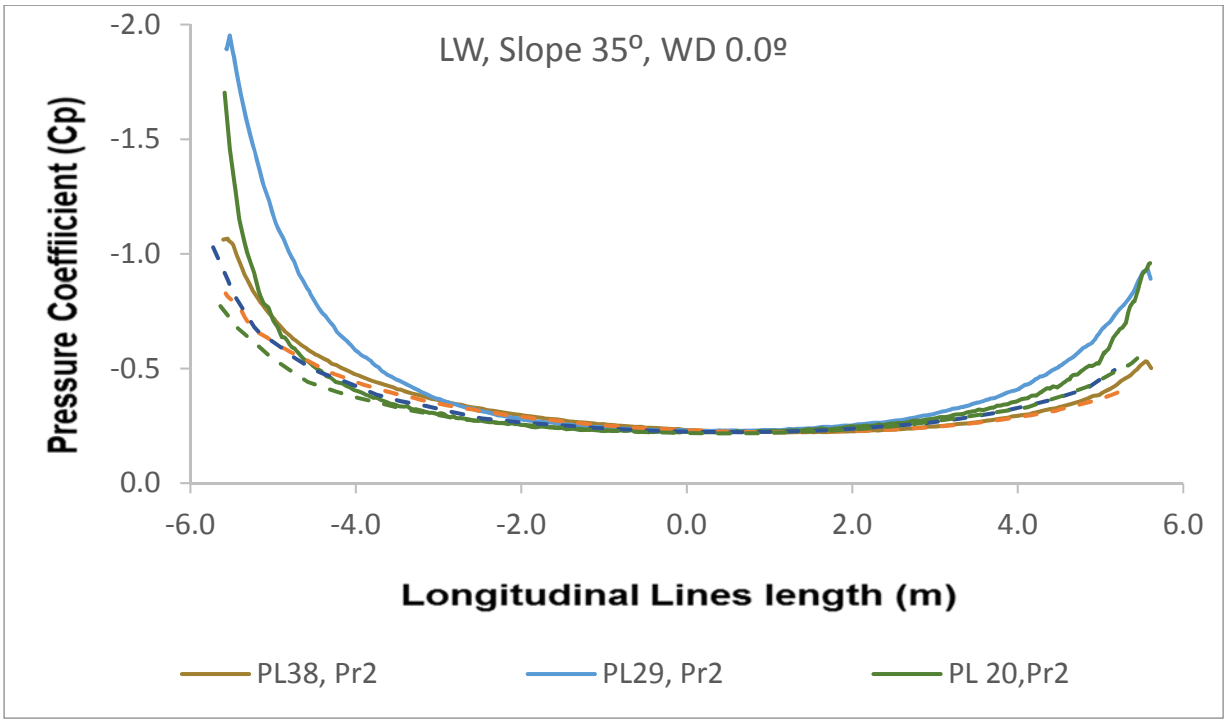


Fig. C. 33. Cp on bare roof Pr1 vs. on roof under the panels, Pr2, S 35º, WD 0.0º

C. Bottom of the solar panels vs. bare roofs,

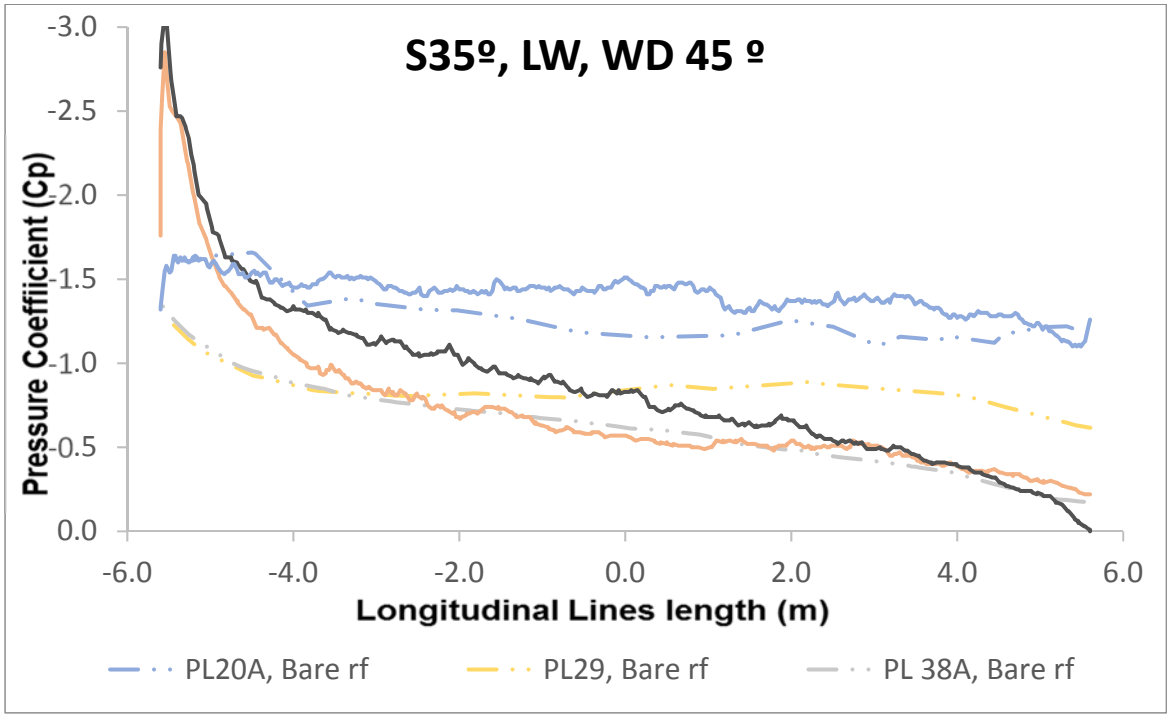


Fig. C. 34. Cp on bottom of solar panels Psp vs. on bare roof, Pr1, S 35º, LW, WD 45º

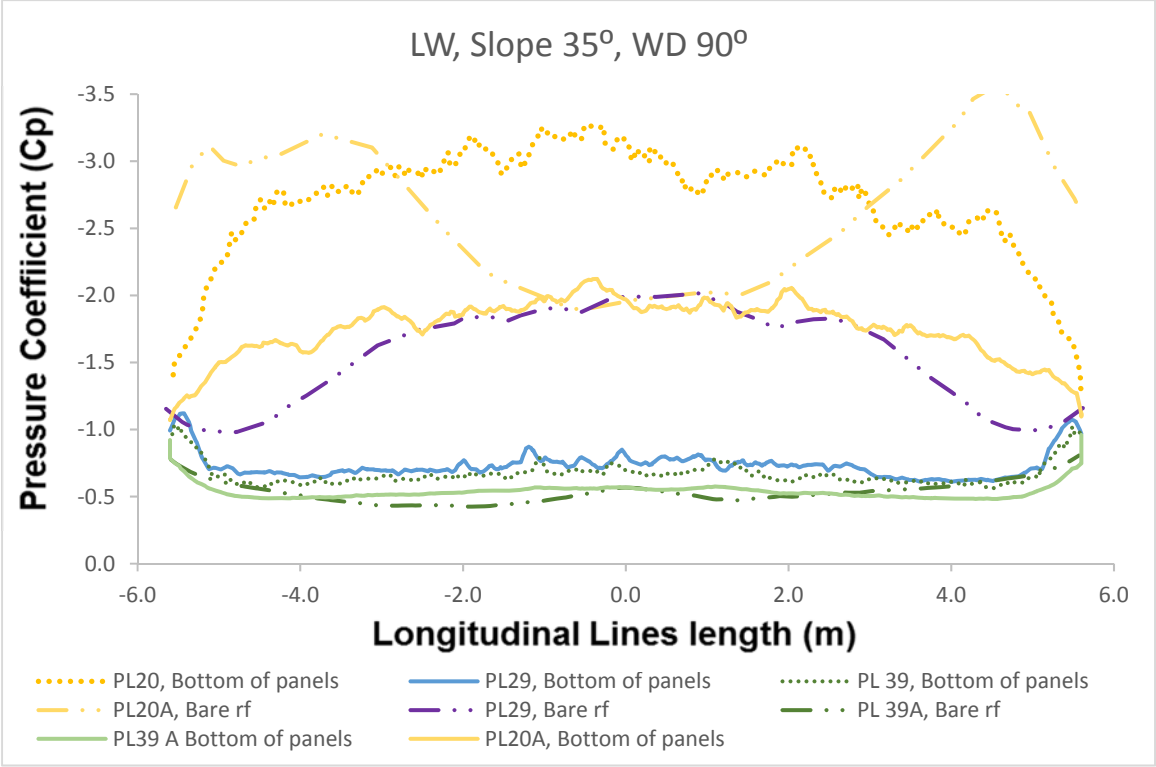


Fig. C. 35. Cp on bottom of solar panels Psp vs. on bare roof, Pr1, S 35º, LW, WD 90º

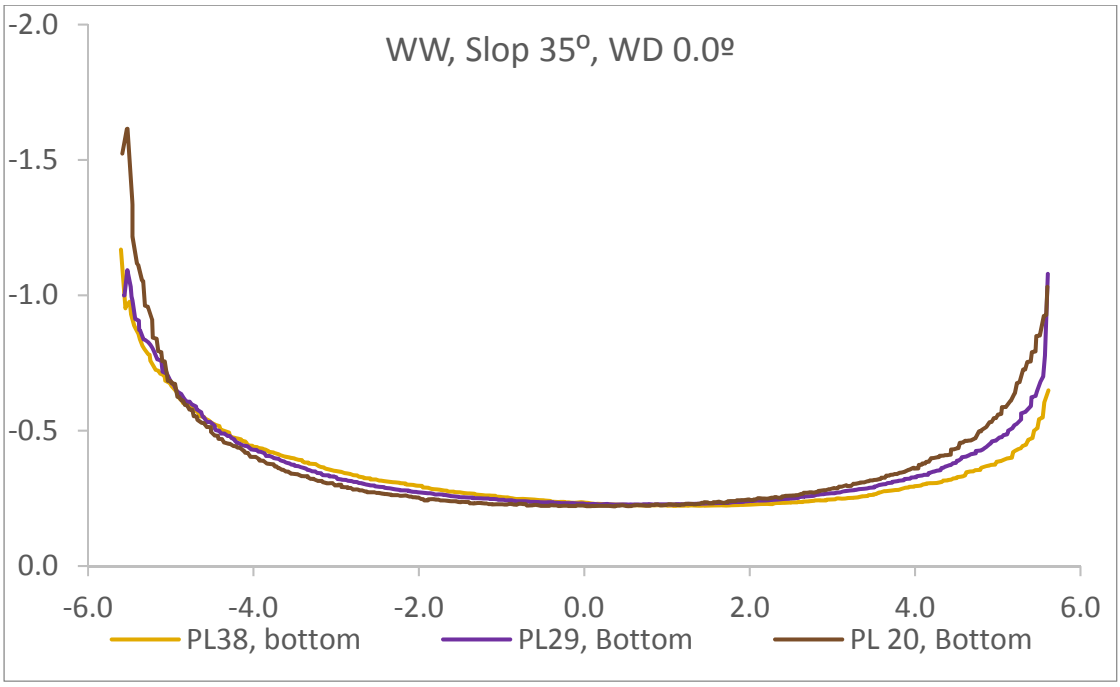


Fig. C. 36. Cp on bottom of solar panels Psp vs. on bare roof, Pr1, S 35º, WD 0.0º

D. Bare roofs Pr1 Vs top of the panels,

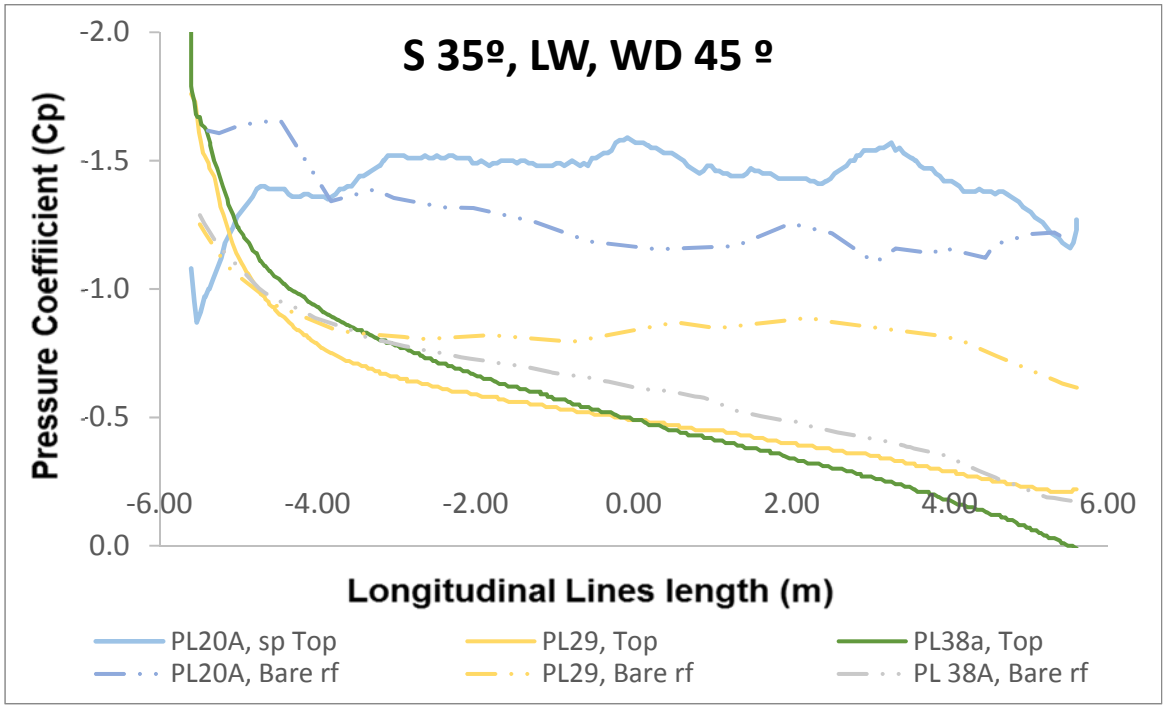


Fig. C. 37. Cp of bare roofs Pr1 Vs top of panels, S 35º, LW, WD 45º

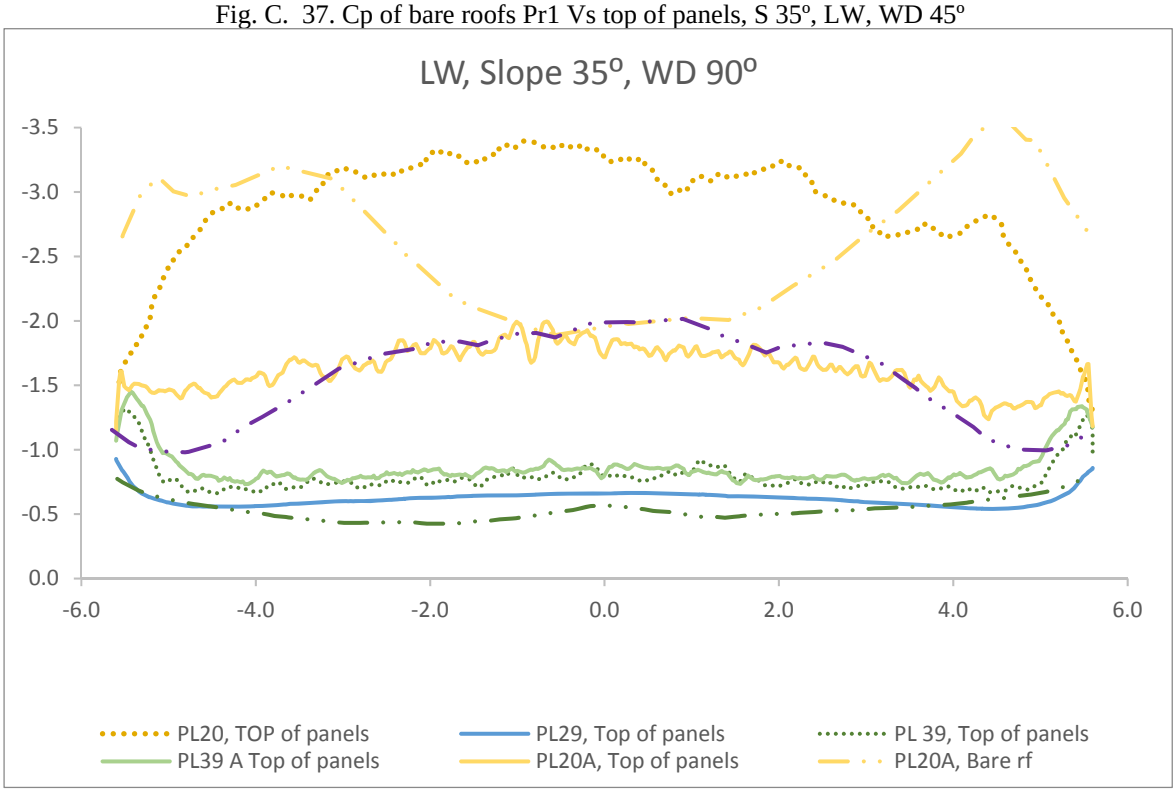


Fig. C. 38. Cp of bare roofs Pr1 Vs top of panels, S 35º, LW, WD 90º

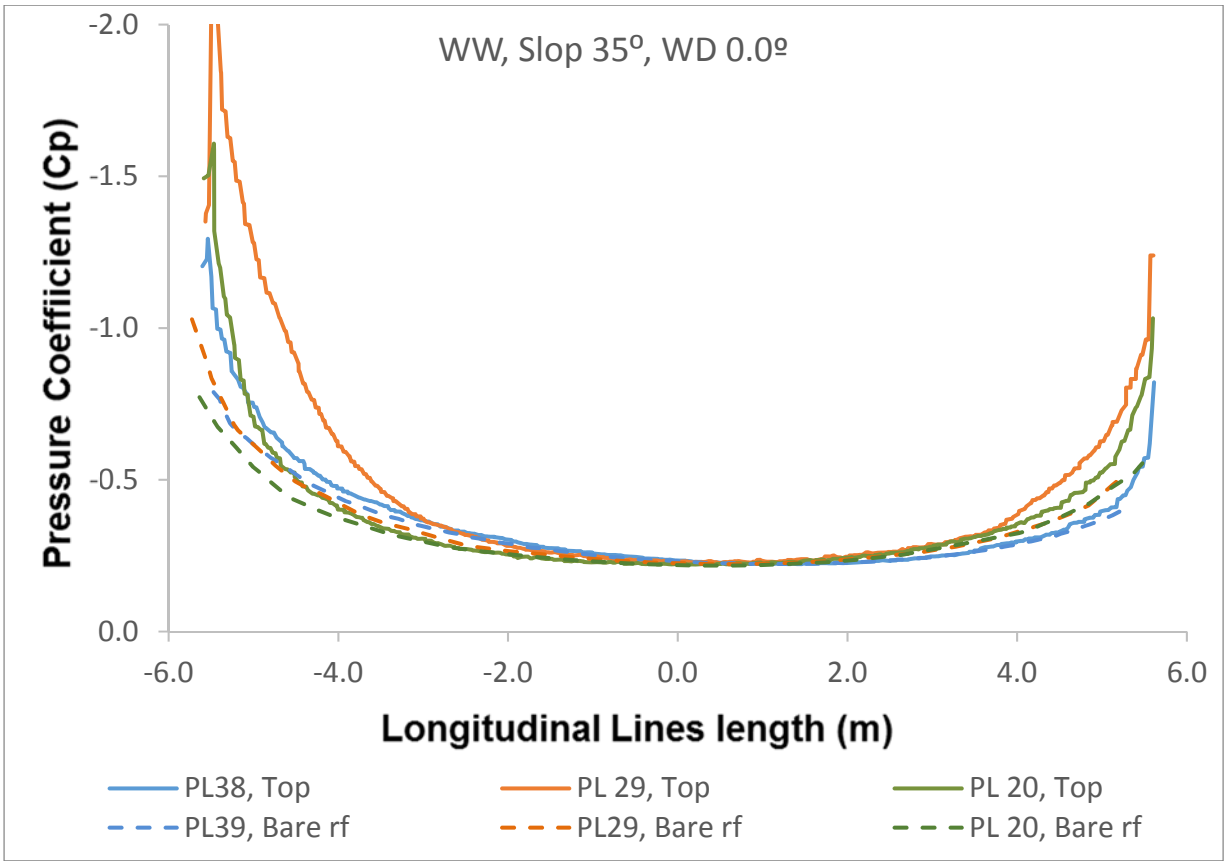


Fig. C. 39. Cp of bare roofs Pr1 Vs top of panels, S 35º, WD 0º

E. Bare roofs Pr1 Vs resultant,

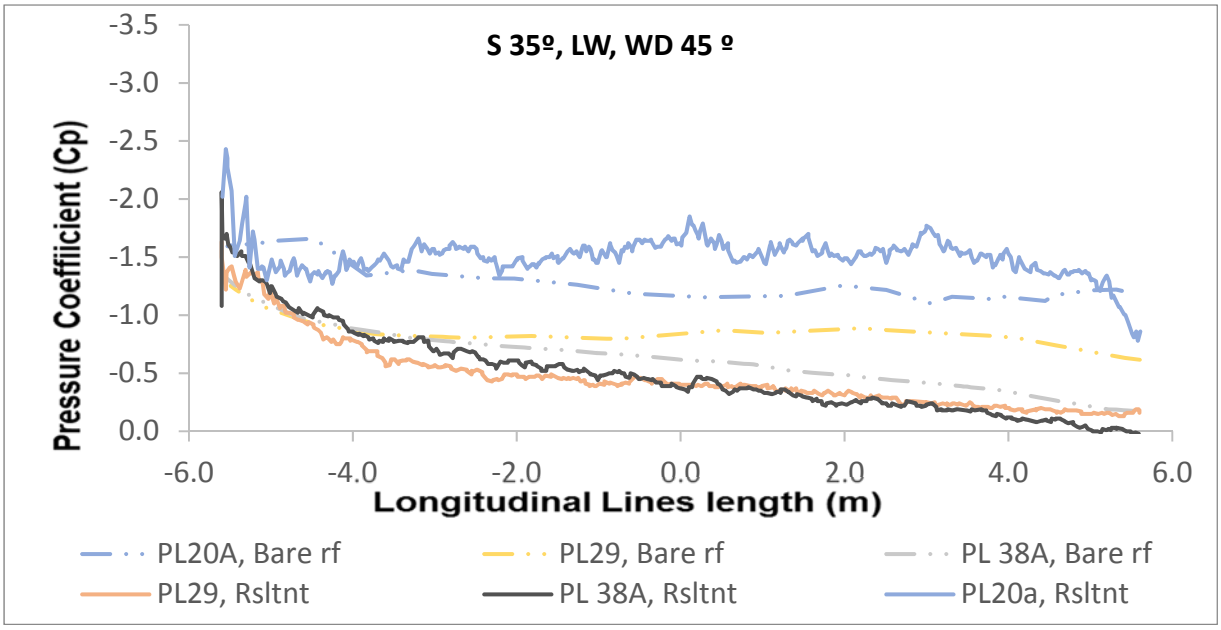


Fig. C. 40. Cp of bare roofs Pr1 Vs resultant, S 35 º, LW, WD 45 º

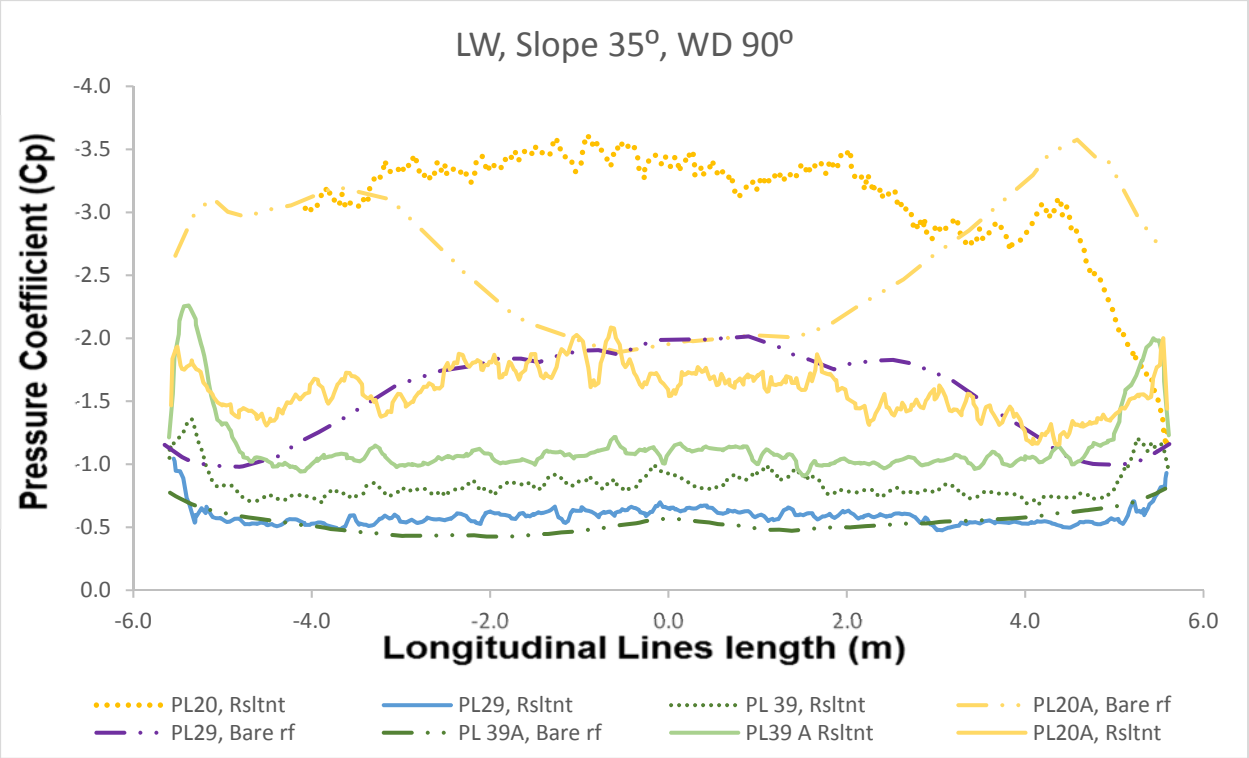


Fig. C. 41. Cp of bare roofs Pr1 Vs resultant, S 35 º, LW, WD 45 º

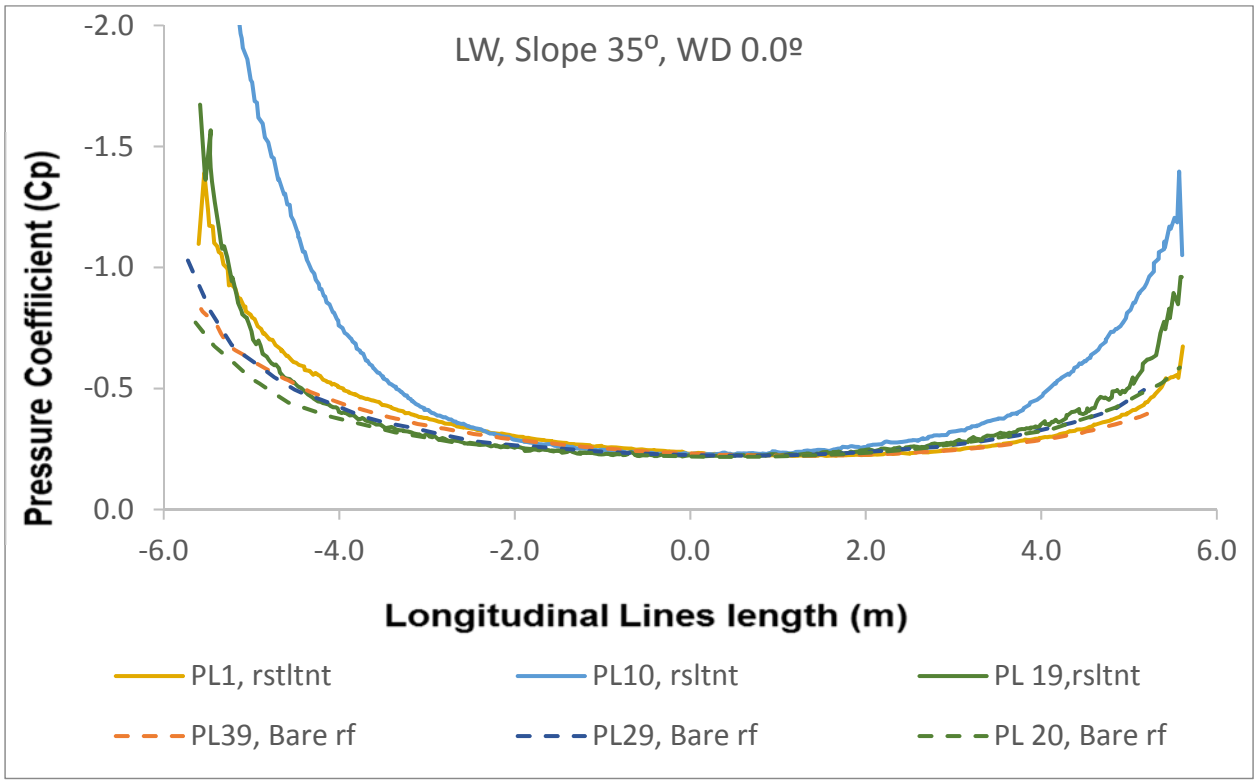


Fig. C. 42. Cp of bare roofs Pr1 Vs resultant, S 35 º, LW, WD 0.0 º

1.1.6. Detailed Distribution of Wind Pressure, and flow on roof mounted solar panels, 2” apart, 10” roof space,

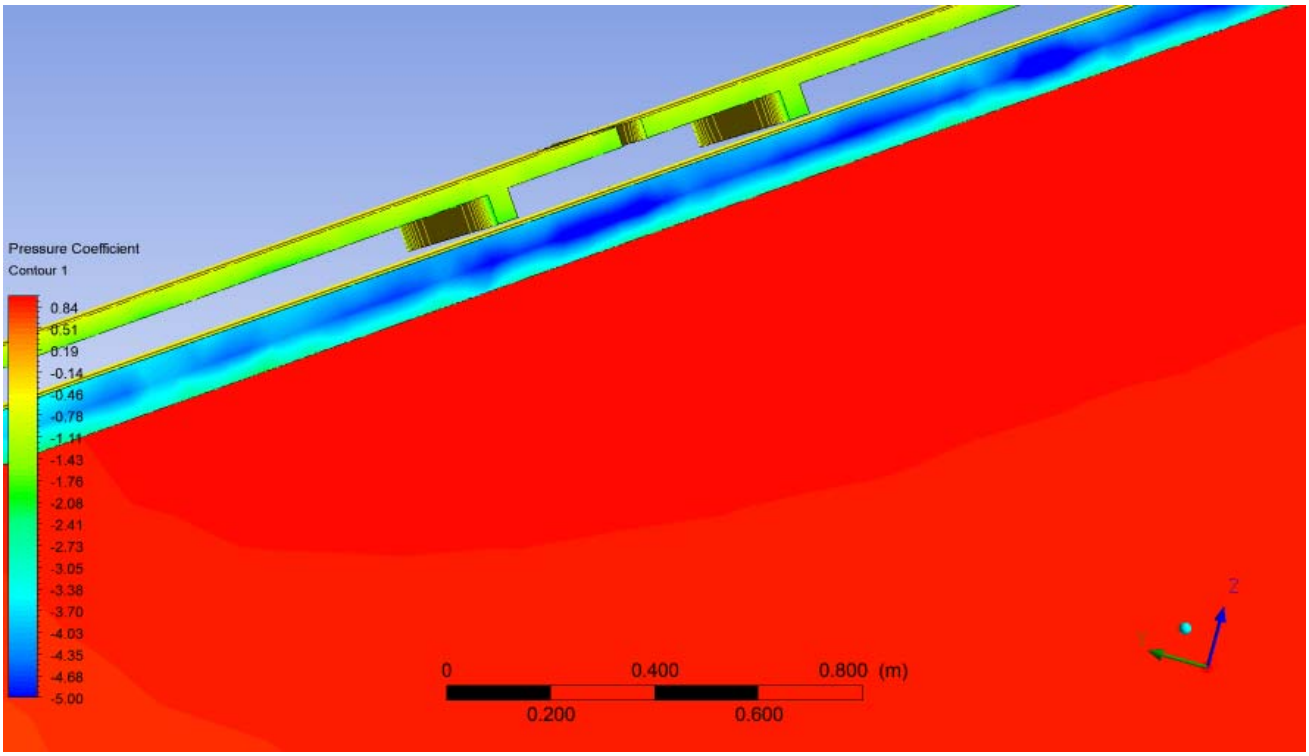


Fig. C. 43. Close view shows separation of solar panels from roof structure, WD 0º.

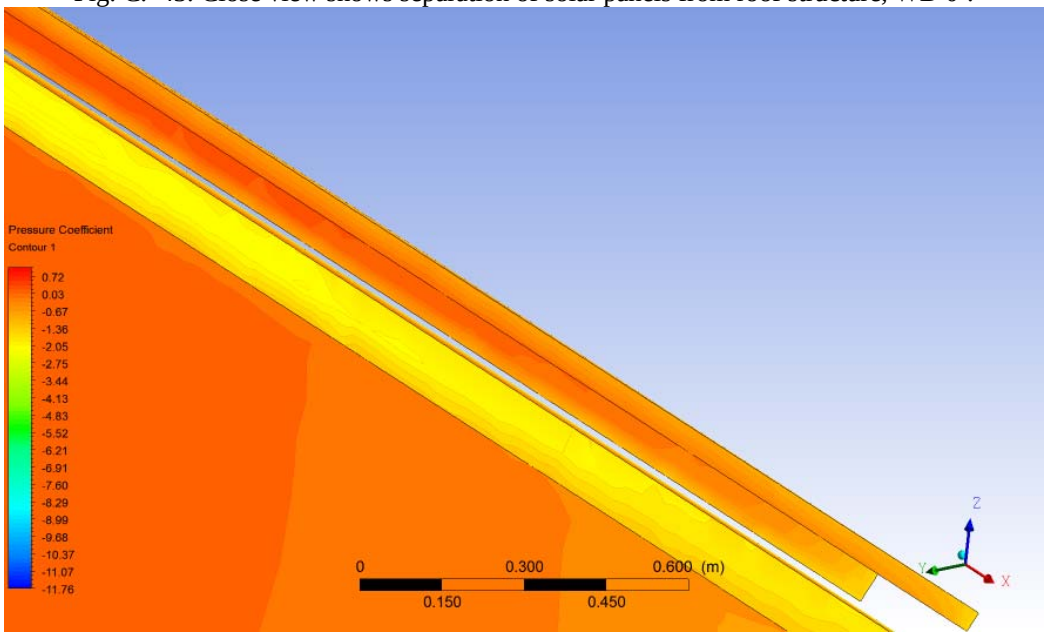


Fig. C. 44. Close view shows separation of solar panels from roof structure, WD 45º

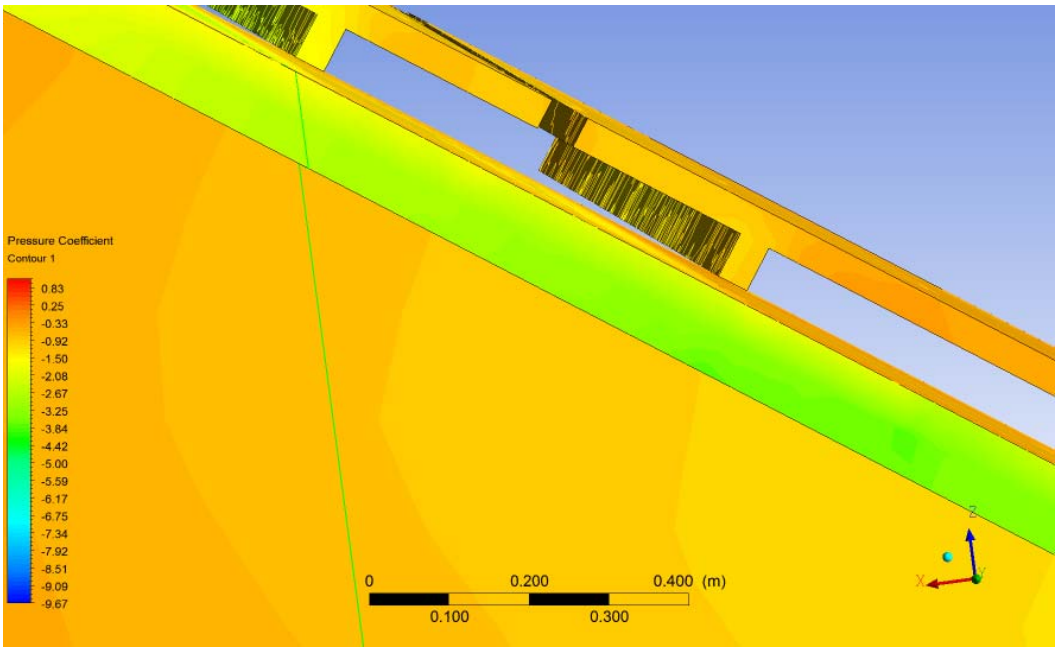


Fig. C. 45. Close view shows separation of solar panels from roof structure, WD 90º

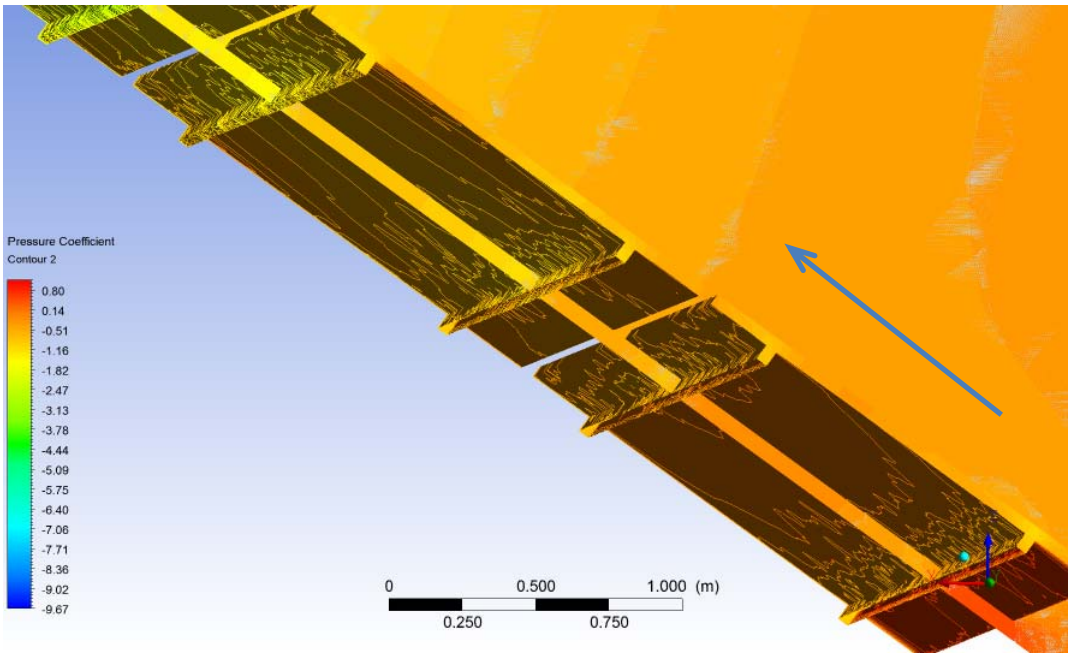


Fig. C. 46. Cp on a perpendicular plane under panels, Close up WD 90º

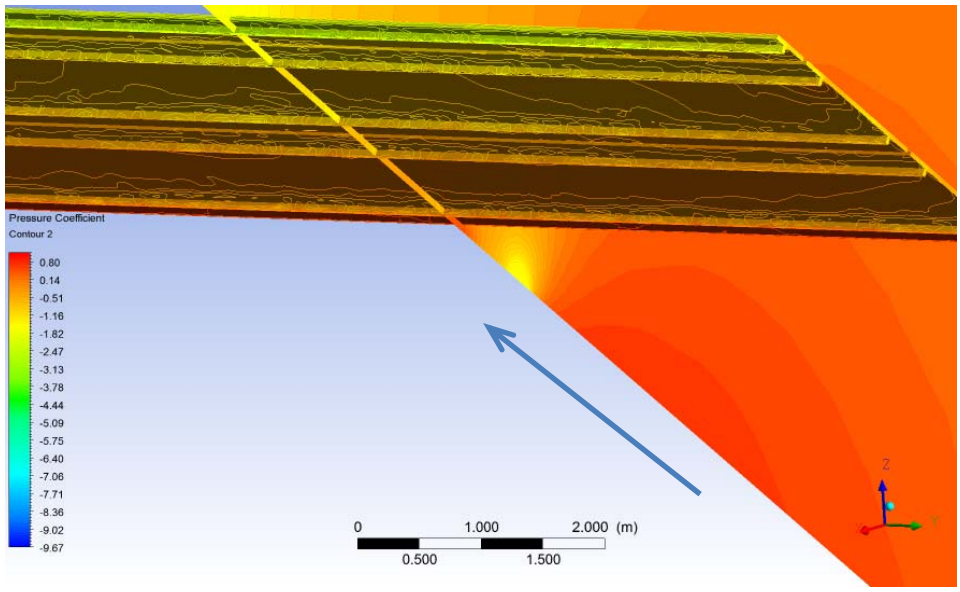


Fig. C. 47. Cp on a perpendicular plane under panels, WD 90º

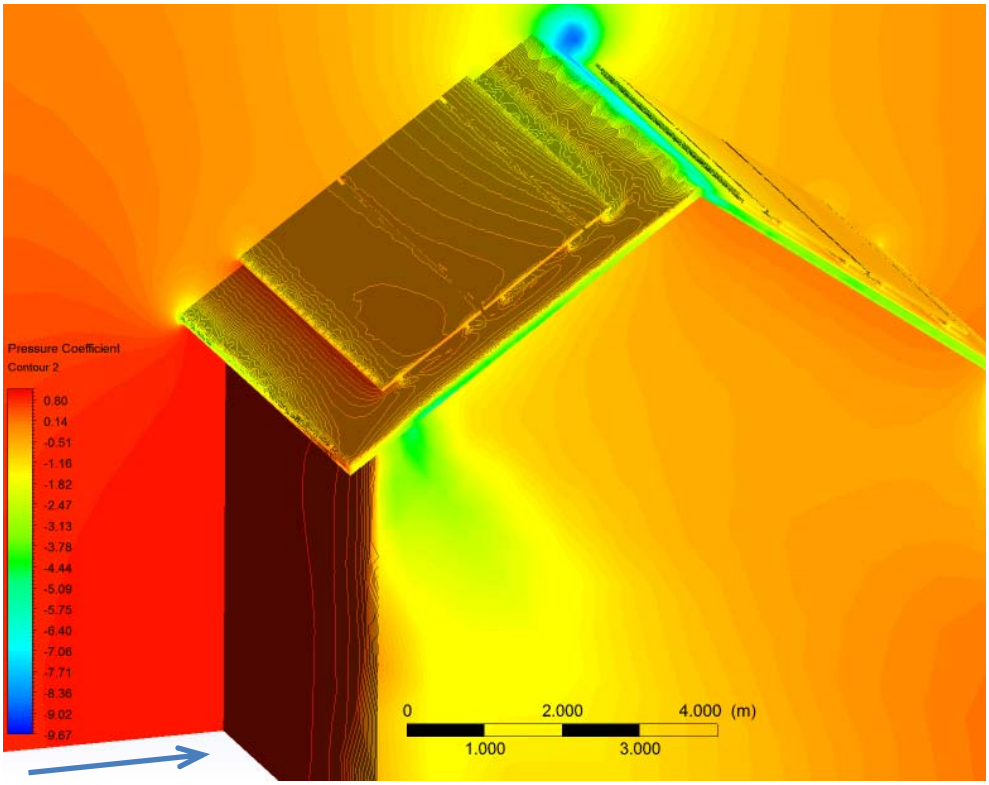


Fig. C. 48. Cp on a perpendicular plane with the house, WD 90º

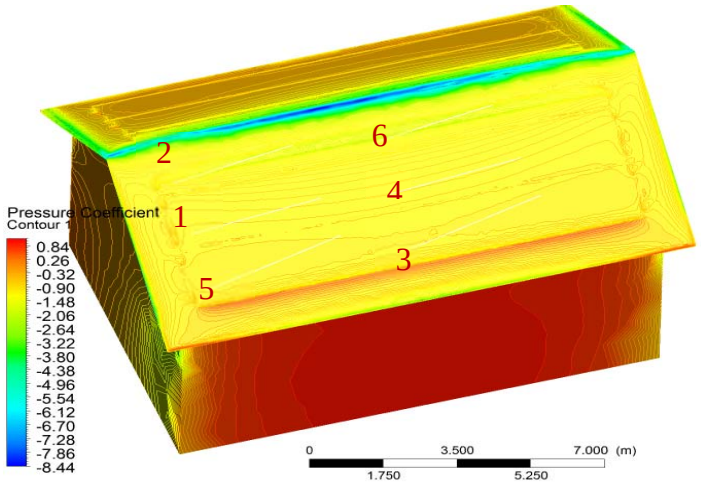


Fig. C. 49. Lines used to draw velocity and pressure changes, WD 90º

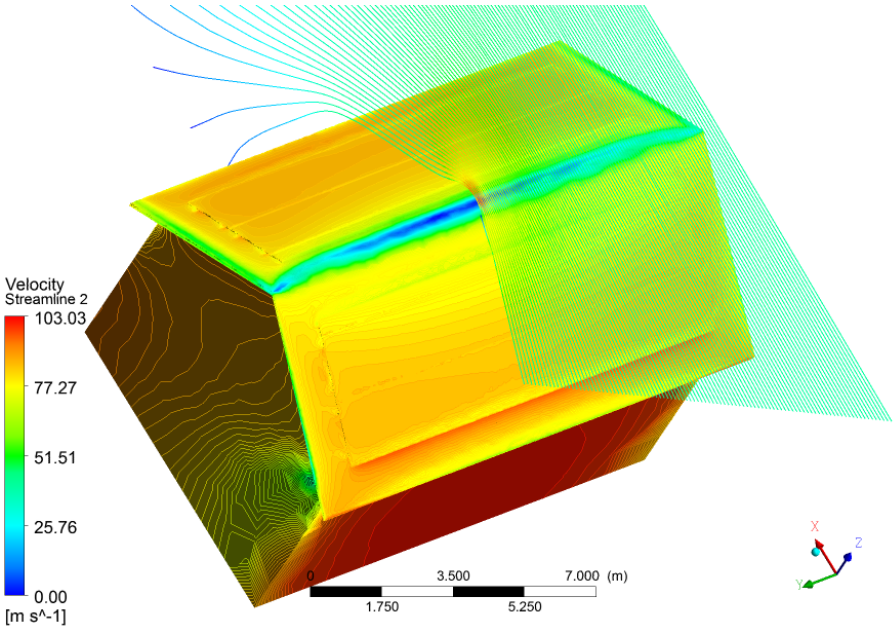


Fig. C. 50. Velocity stream lines at middle cross section plane , WD 90º

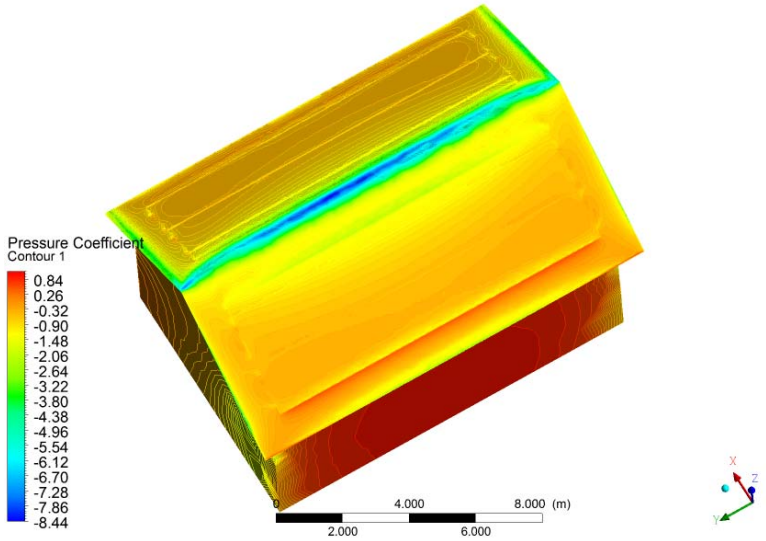


Fig. C. 51. Cp contour, whole roof, WD 90º

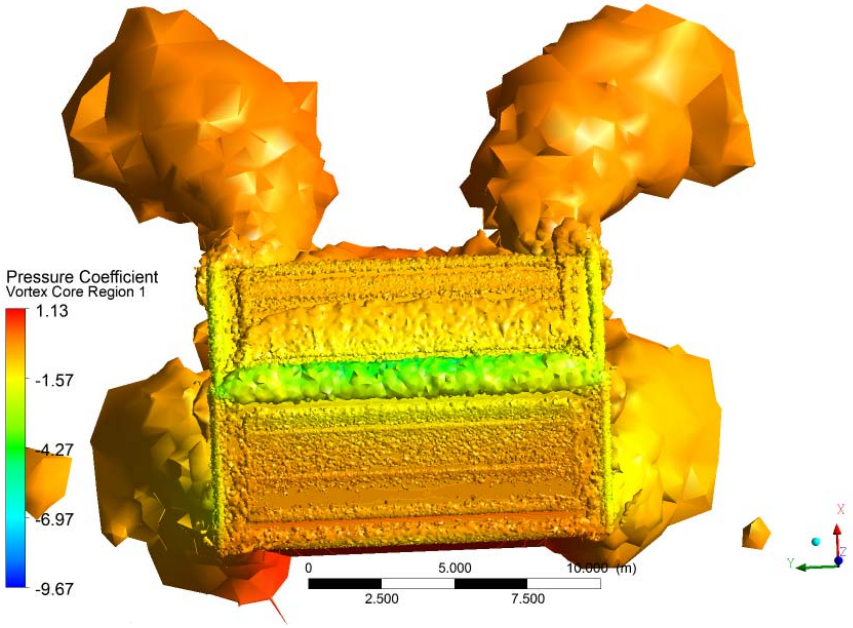


Fig. C. 52. Turbulence distribution on roof and on the building structure, WD 90º

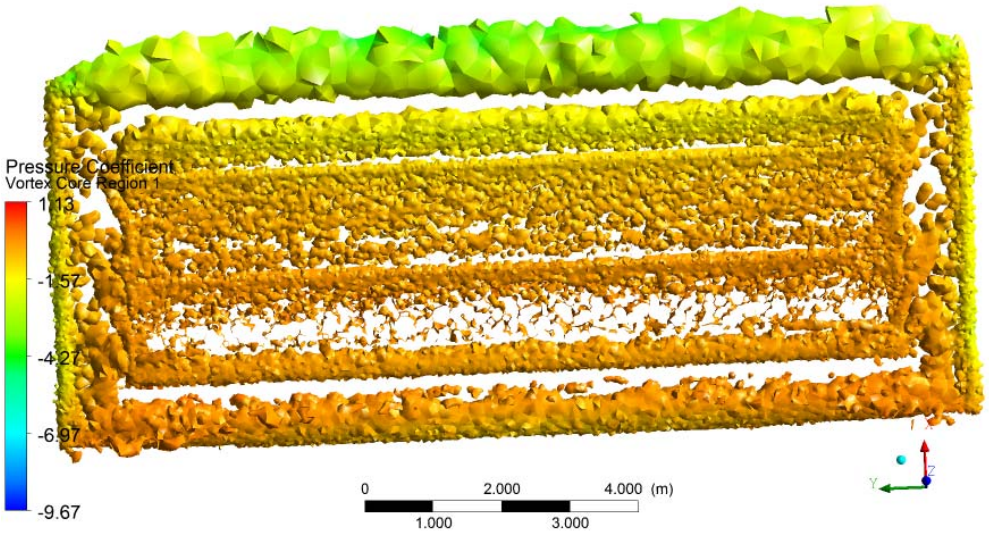


Fig. C. 53. Turbulence distribution, on top of the panels, No contours shown, WD 90º

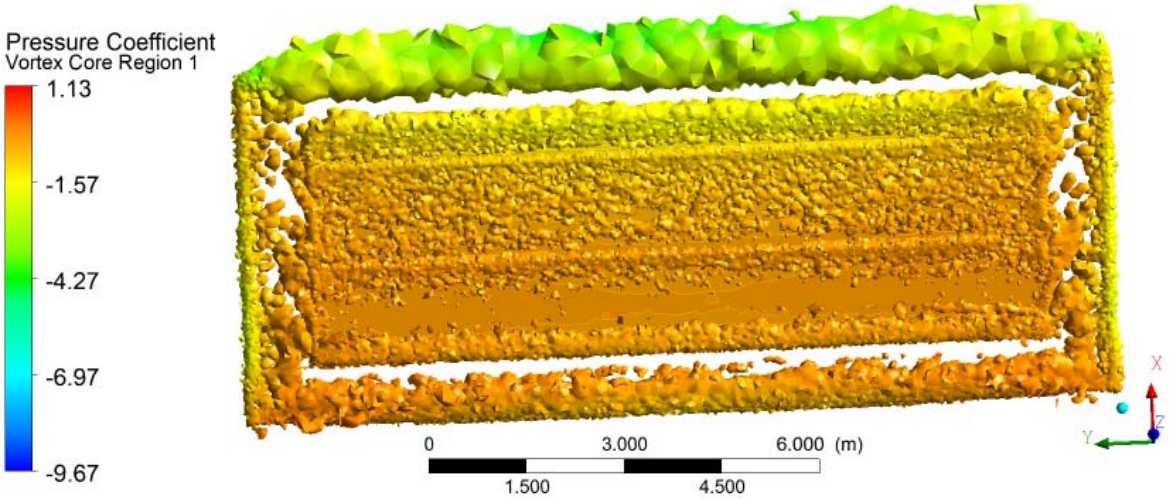


Fig C 1, Turbulence distribution, on top of the panels contours shown, WD 90º

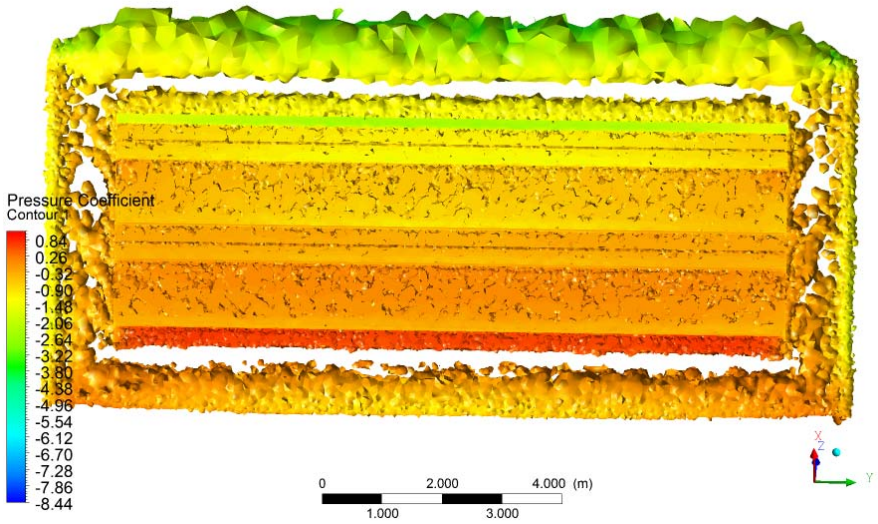


Fig. C. 54. Turbulence distribution, on bottom of the panels, contours shown, WD 90º

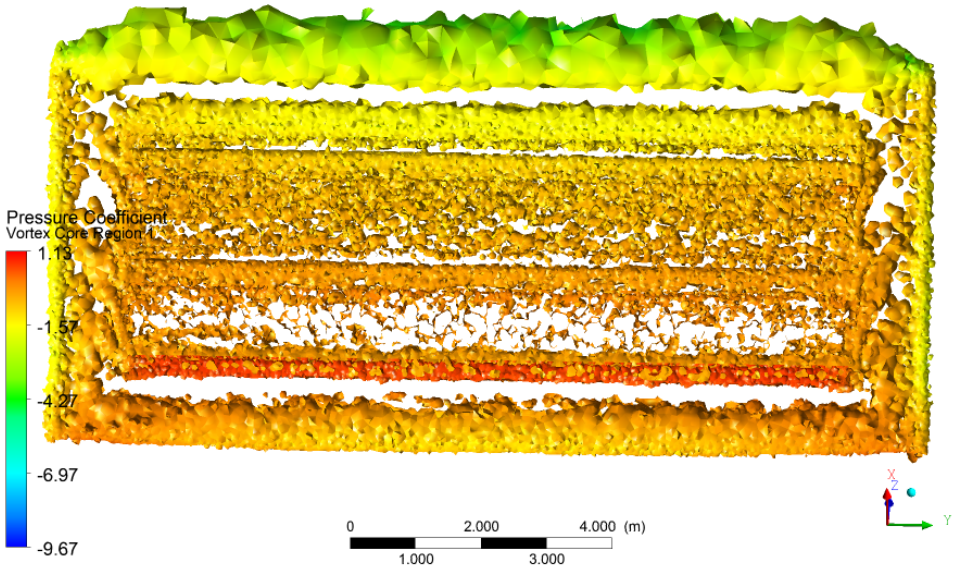


Fig. C. 55. Turbulence distribution, on bottom of the panels, No contours shown, WD 90º

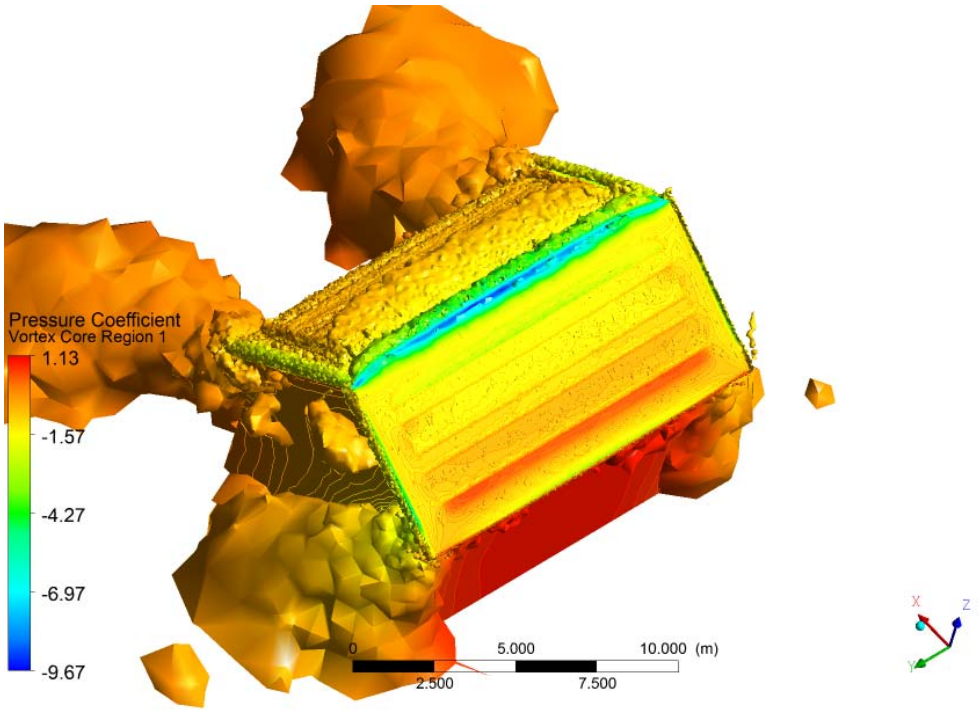


Fig. C. 56. Turbulence distribution, on roof under panels (laminar flow) and around the house (turbulent)

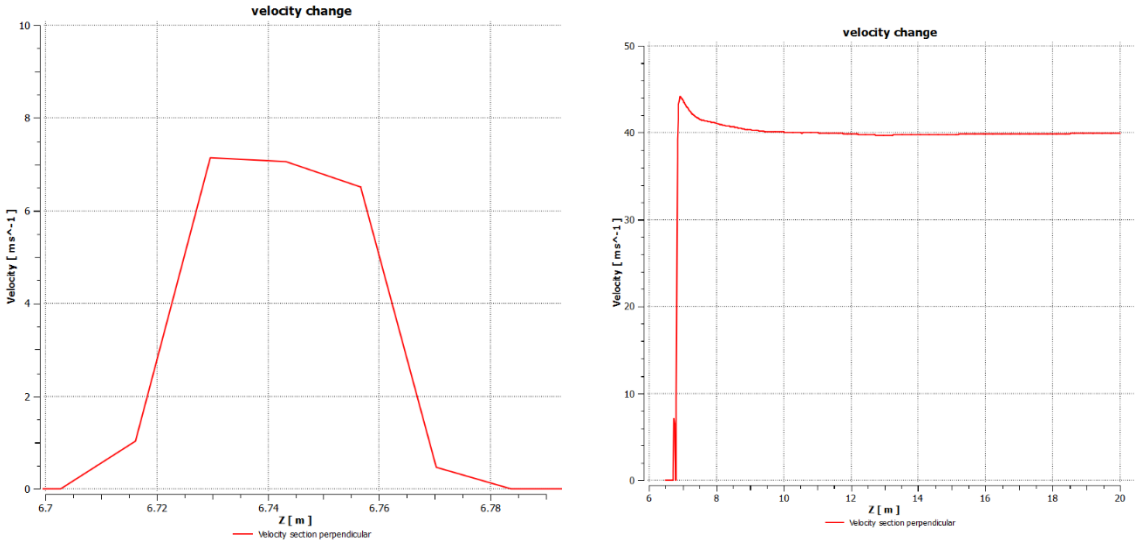


Fig. C. 57. Velocity changes between panels, and above roof, Line 5, SW corner.

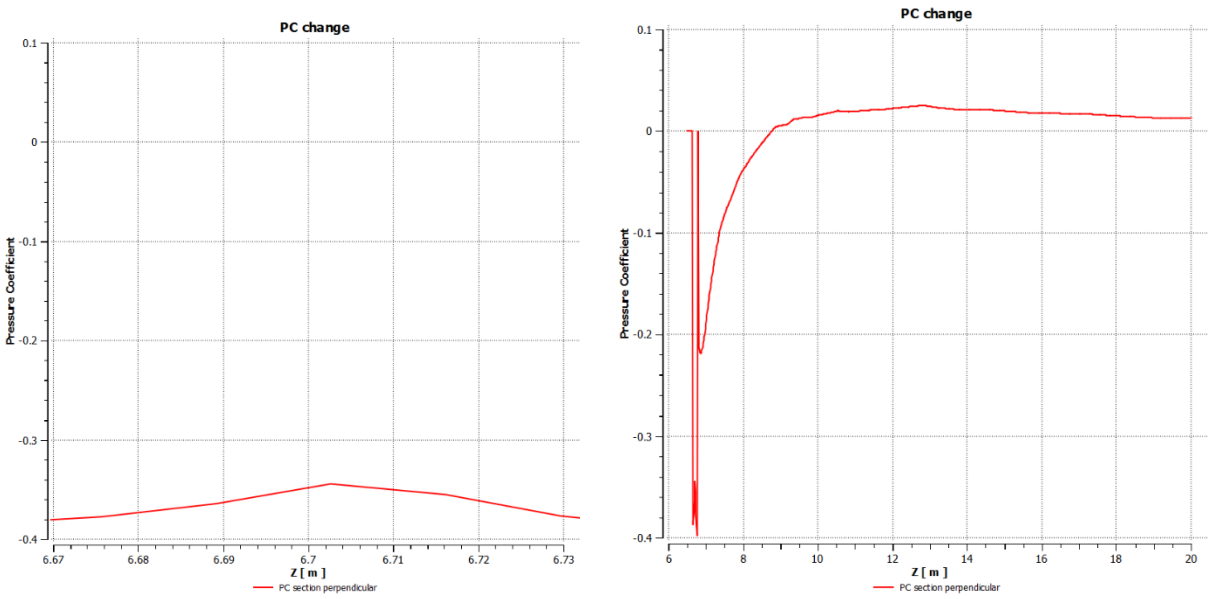


Fig. C. 58. Pressure changes between panels, and above roof, Line 5, SW corner.

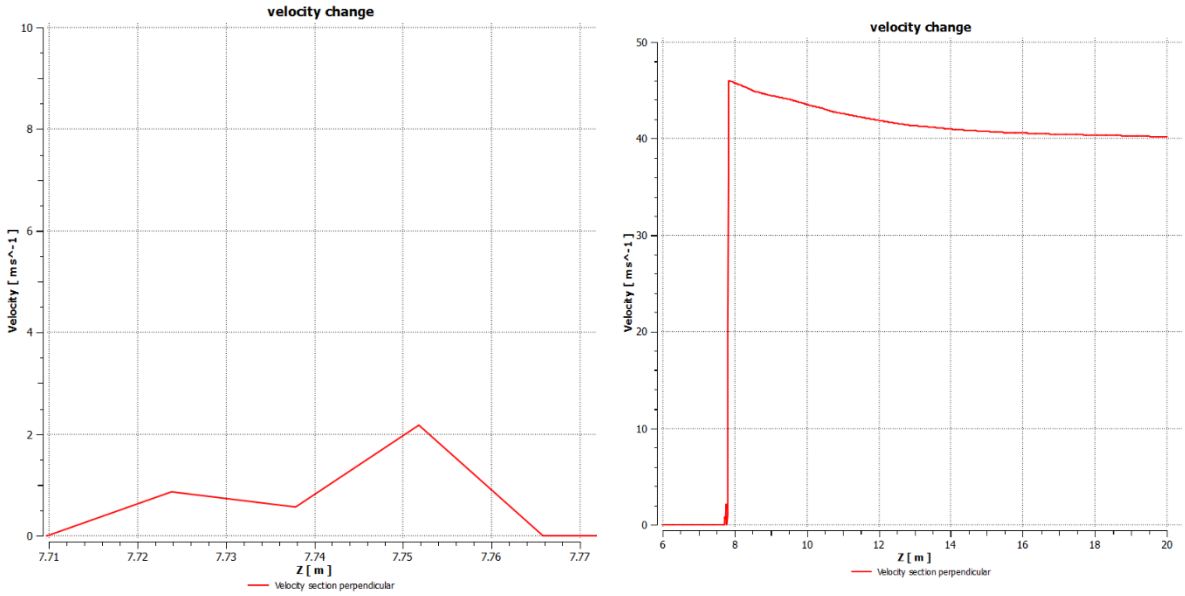


Fig. C. 59. Velocity changes between panels, and above roof, Line 1, W middle .

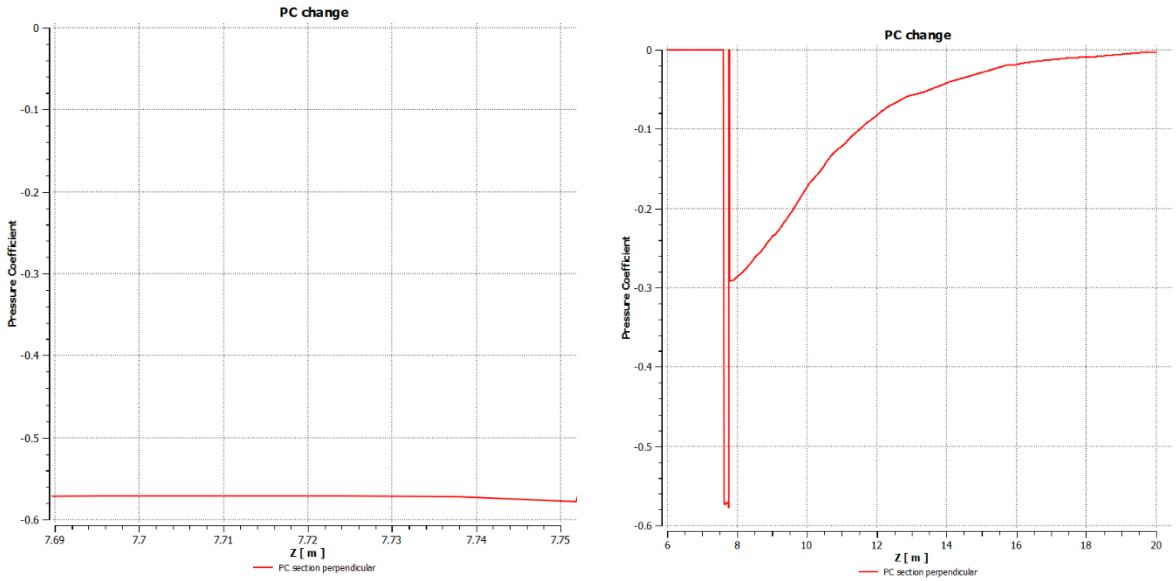


Fig. C. 60. Cp changes between panels, and above roof, Line 1, W middle.

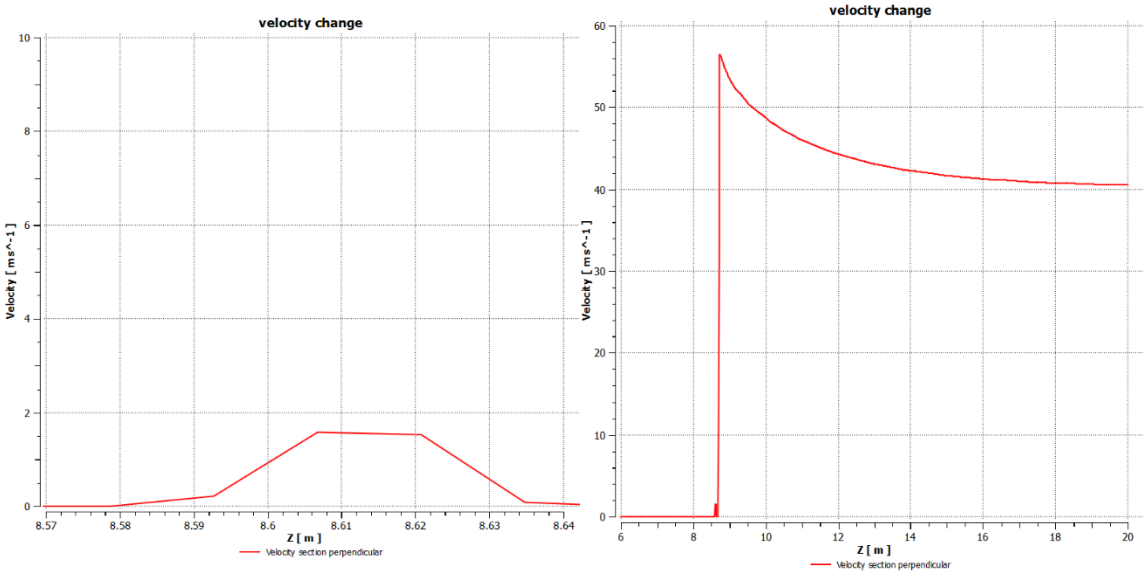


Fig. C. 61. Velocity changes between panels, and above roof, Line 2, NW.

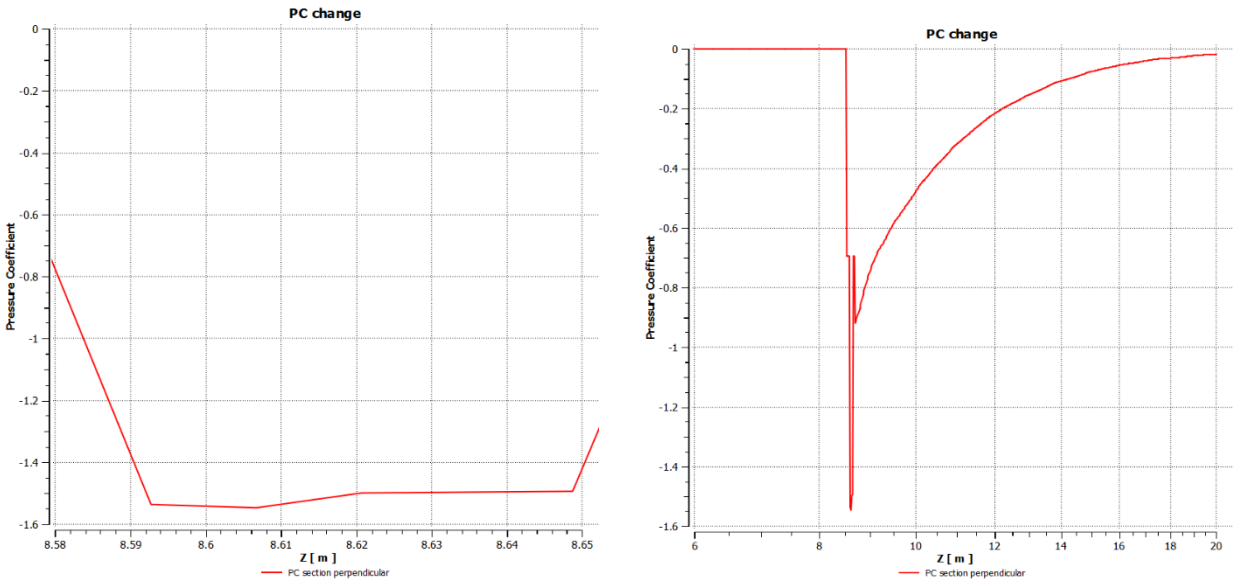


Fig. C. 62. Cp changes between panels, and above roof, Line 2, NW.

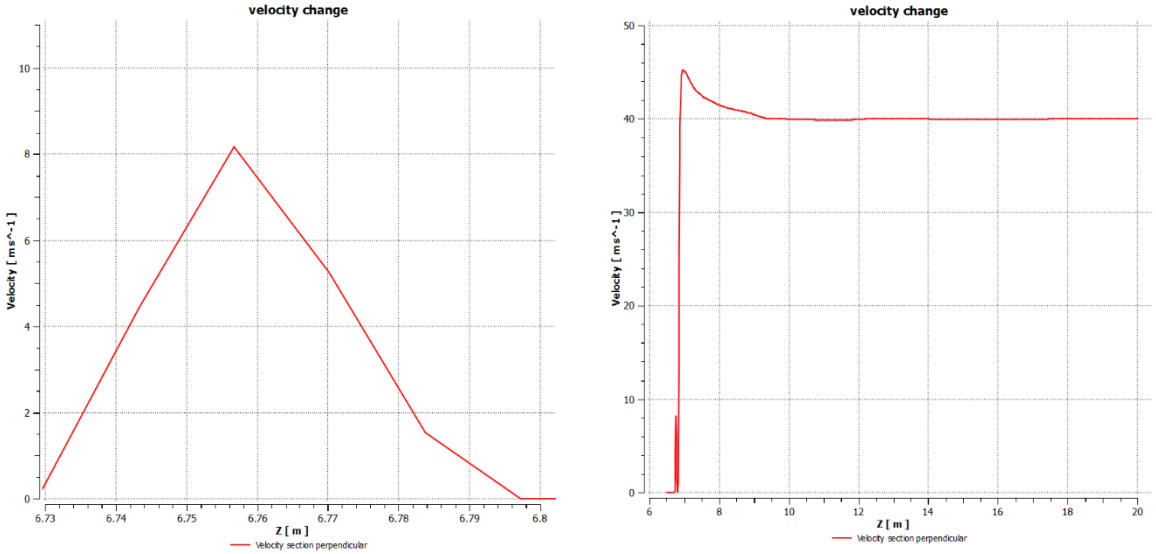


Fig. C. 63. Velocity changes between panels, and above roof, Line 3, S middle.

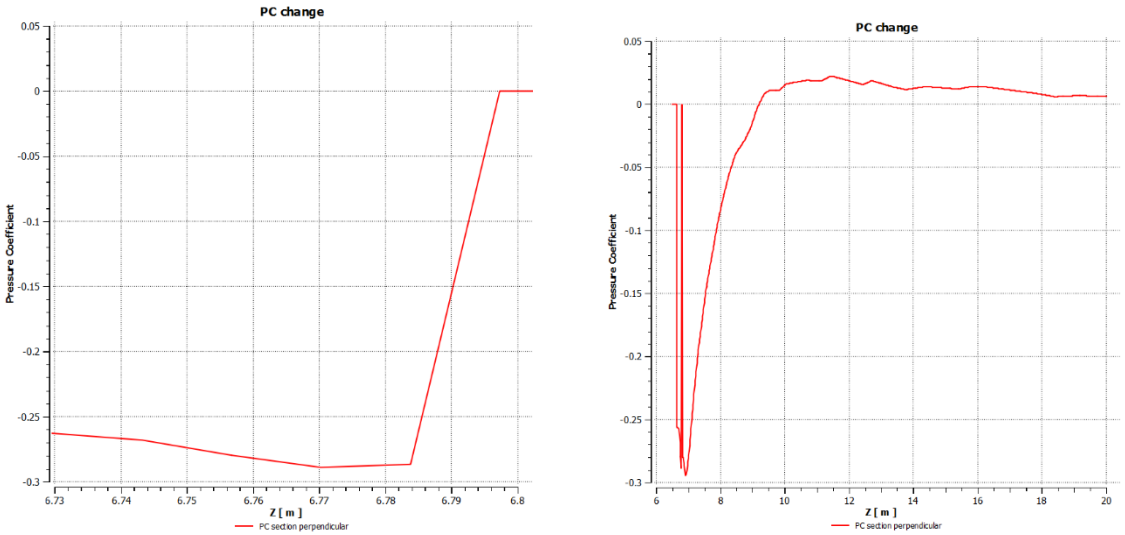


Fig. C. 64. Cp changes between panels, and above roof, Line 3, S middle.

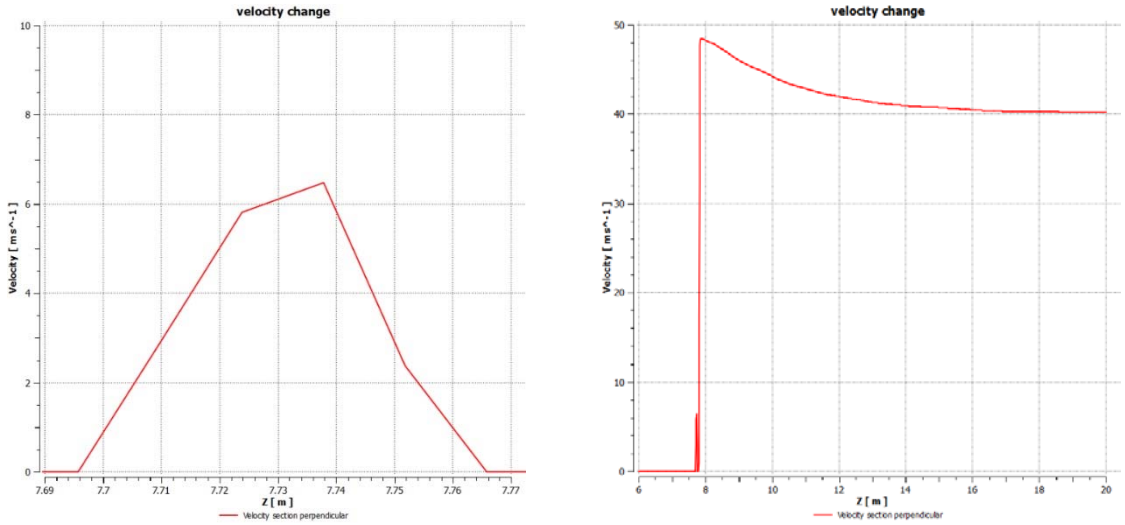


Fig. C. 65. Velocity changes between panels, and above roof, Line 4, M middle.

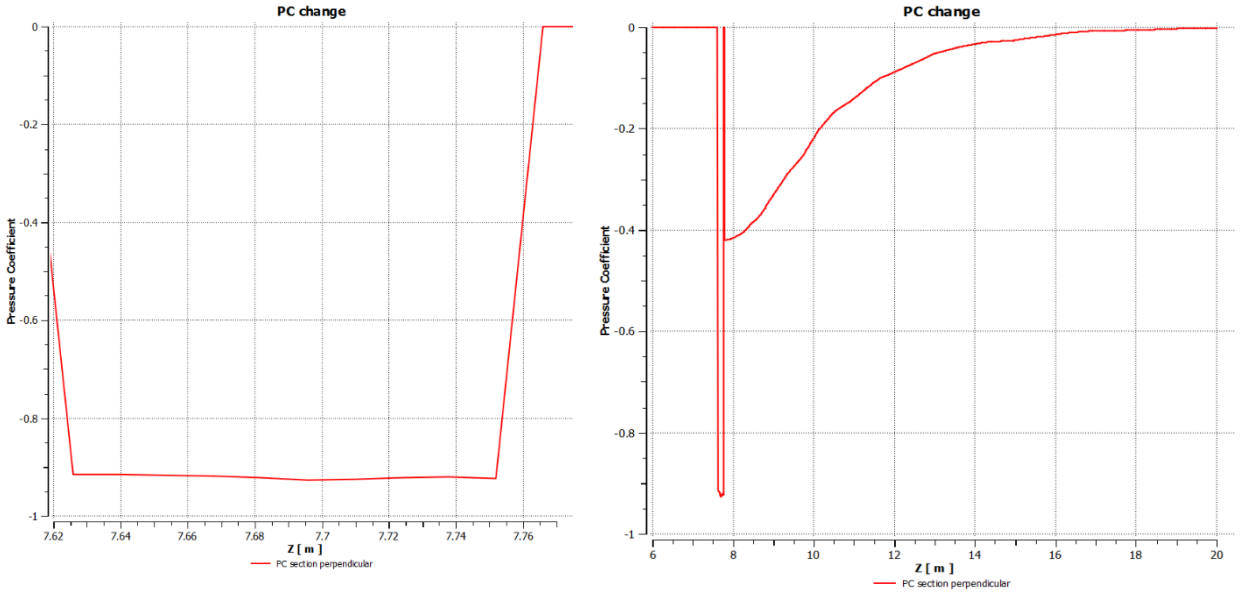


Fig. C. 66. Cp changes between panels, and above roof, Line 4, M middle.

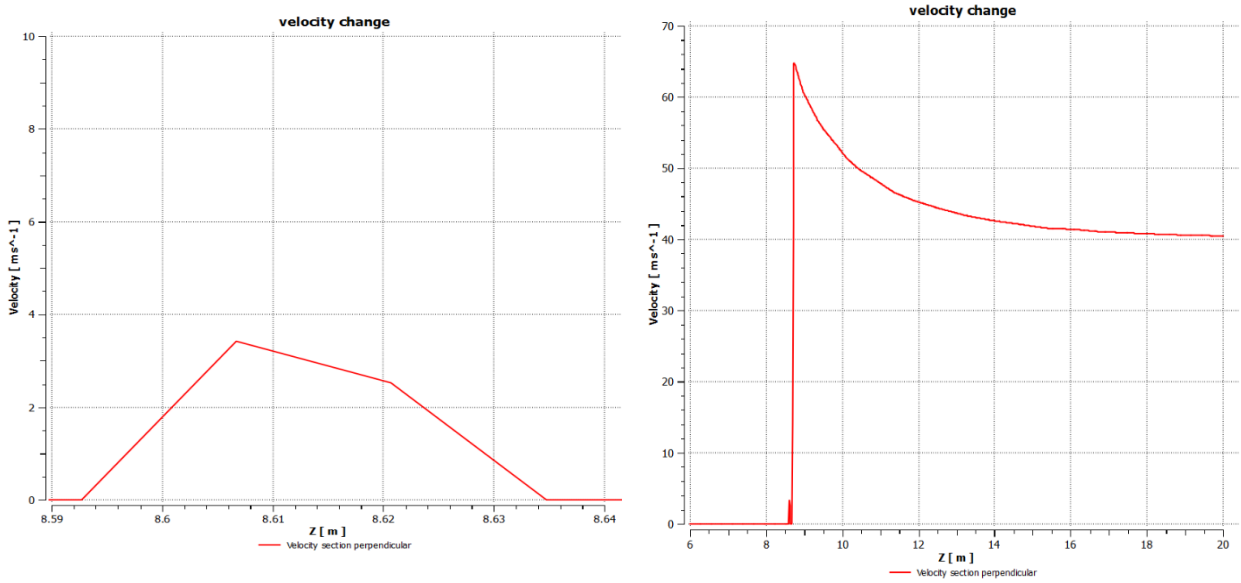


Fig. C. 67. Velocity changes between panels, and above roof, Line 6, N middle.

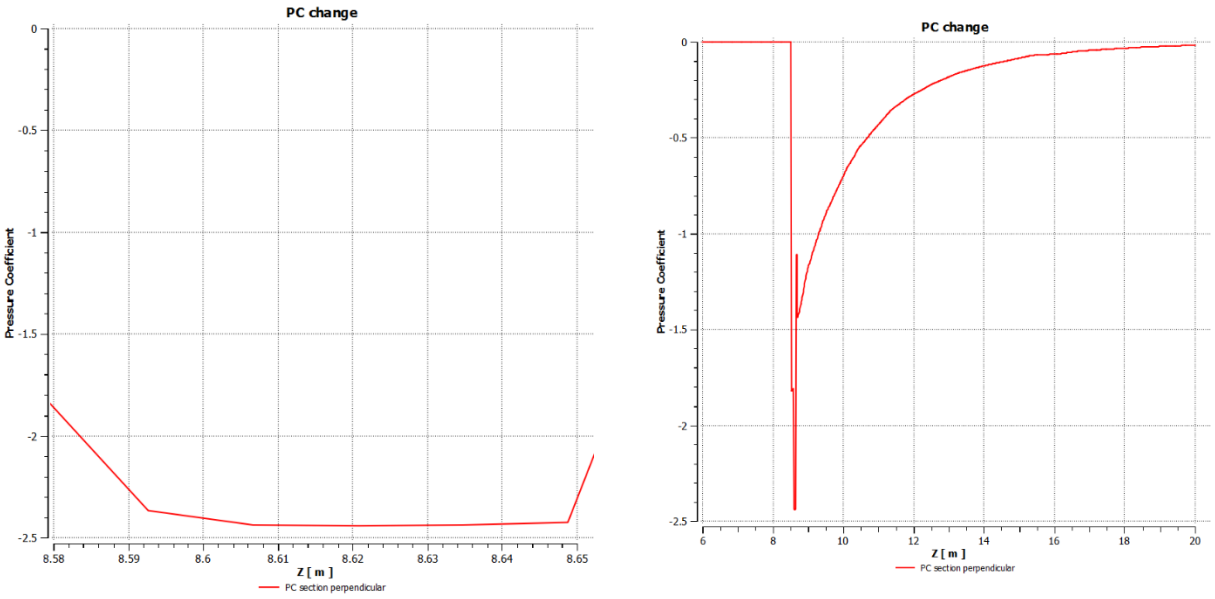


Fig. C. 68. Cp changes between panels, and above roof, Line 6, N middle.

1.1.7. Calculation of resultant Cp of the three surfaces of roof mounted solar panels in comparison with bare roofs, Leeward, 2" apart, 10" roof space

Tabulated results of the integration,

Table C. 1. Cp on bare roofs vs. roof under solar panels, Slope 35º, 45º, windward

	Cp Bare roof	Cp (SP)	Cp (SP/BRf)
Pl1A	-0.23	-0.36	1.57
Pl2	-0.20	-0.30	1.50
Pl3	-0.19	-0.26	1.36
Pl4	-0.19	-0.25	1.30
Pl5	-0.19	-0.25	1.32
Pl6	-0.20	-0.26	1.32
Pl7	-0.21	-0.28	1.39
Pl8	-0.21	-0.29	1.36
Pl9	-0.21	-0.29	1.35
Pl10	-0.23	-0.30	1.29
Pl11	-0.25	-0.33	1.33
Pl12	-0.28	-0.37	1.32
Pl13	-0.31	-0.42	1.35
Pl14	-0.34	-0.48	1.40
Pl15	-0.38	-0.56	1.47

Pl16	-0.41	-0.75	1.82
Pl17	-0.43	-0.75	1.73
Pl18	-0.51	-0.79	1.55
Pl19 A	-0.56	-1.11	1.99
Ave	-0.29	-0.44	1.52

Table C. 2. Cp bare roofs vs. roof under solar panels, Slope 35º, wind direction 45º, Leeward

Polylines	Cp Bare roof	Cp (SP)	Cp (SP/BRf)
Pl20A	-1.55	-1.94	1.32
Pl21	-1.49	-1.24	0.84
Pl22	-1.47	-1.23	0.87
Pl23	-1.43	-1.11	1.09
Pl24	-1.38	-1.11	0.86
Pl25	-1.30	-0.77	0.60
Pl26	-1.19	-0.71	0.61
Pl27	-1.09	-0.75	0.69
Pl28	-0.98	-0.64	0.67
Pl29	-0.89	-0.63	0.73
Pl30	-0.81	-0.86	1.11
Pl31	-0.79	-0.77	1.13
Pl32	-0.72	-0.54	0.86
Pl33	-0.63	-0.54	0.86
Pl34	-0.58	-0.56	1.00
Pl35	-0.56	-0.56	1.00
Pl36	-0.56	-0.55	1.03
Pl37	-0.53	-0.61	1.19
Pl38A	-0.53	-0.75	1.64
Cp	-0.97	-0.84	0.87

Table C. 3. Cp on bare roofs vs. roof under solar panels, Slope 35º, 90º, windward

Polylines	Cp Bare roof	Cp (SP)	Pr2	Cp Bott	Diff	Ttl Cp	Ttl/Brf
Pl1A	-0.02	-0.71	0.58	0.58	-1.29	-0.71	35.50
Pl2	0.02	-0.45	0.47	0.47	-0.92	-0.45	-22.50
Pl3	0.02	-0.2	-0.24	-0.15	-0.05	-0.29	-14.50

Pl4	0.01	-0.18	-0.08	-0.07	-0.11	-0.19	-19.00
Pl5	-0.02	-0.2	-0.03	-0.02	-0.18	-0.21	10.50
Pl6	-0.04	-0.23	0	0	-0.23	-0.23	5.75
Pl7	-0.06	-0.27	-0.49	-0.47	0.20	-0.29	4.83
Pl8	-0.06	-0.3	-0.42	-0.37	0.07	-0.35	5.83
Pl9	-0.07	-0.24	-0.34	-0.30	0.06	-0.28	4.00
Pl10	-0.09	-0.32	-0.30	-0.28	-0.04	-0.34	3.78
Pl11	-0.12	-0.37	-0.79	-0.73	0.36	-0.43	3.58
Pl12	-0.16	-0.42	-0.68	-0.67	0.25	-0.43	2.69
Pl13	-0.20	-0.49	-0.54	-0.54	0.05	-0.49	2.45
Pl14	-0.25	-0.61	-0.56	-0.56	-0.05	-0.61	2.44
Pl15	-0.32	-0.75	-1.16	-1.18	0.43	-0.73	2.28
Pl16	-0.36	-1.02	-1.06	-1.08	0.06	-1.0	4.00
Pl17	-0.39	-0.86	-0.96	-0.95	0.09	-0.87	2.72
Pl18	-0.36	-1.15	-0.95	-0.91	-0.24	-1.19	3.31
Pl19a	-0.39	-1.42	-2.09	-2.05	0.63	-1.46	3.74
Cp	-0.15	-0.54	-0.51	-0.49	-0.05	-0.56	3.69
SDT	0.15	0.36	0.61	0.61	0.44	0.36	11.94
Cov	0.99	0.67	1.20	1.25	9.16	0.64	3.24

Table C. 4. Cp bare roofs vs. roof under solar panels, Slope 35º, wind direction 90º, Leeward

Polylines	Bare Roof	Cp (SP)	Pr2	Cp Bott	Diff	Ttl Cp	Ttl/Brf
Pl20a	-2.60	-2.78	-2.24	-1.9	-0.88	-3.12	1.20
Pl21	-2.56	-1.61	-1.63	-1.65	0.04	-1.59	0.62
Pl22	-2.52	-1.49	-1.51	-1.53	0.04	-1.47	0.58
Pl23	-2.48	-1.13	-1.38	-1.42	0.29	-1.09	0.44
Pl24	-2.37	-1.05	-1.22	-1.24	0.19	-1.03	0.43
Pl25	-2.25	-0.92	-1.12	-1.14	0.22	-0.9	0.40
Pl26	-2.11	-0.78	-1.00	-1.02	0.24	-0.76	0.36
Pl27	-1.96	-0.68	-0.90	-0.92	0.24	-0.66	0.34
Pl28	-1.78	-0.65	-0.91	-0.86	0.21	-0.7	0.39
Pl29	-1.59	-0.6	-0.65	-0.66	0.06	-0.59	0.37
Pl30	-1.45	-0.63	-0.64	-0.64	0.01	-0.63	0.43
Pl31	-1.38	-0.61	-0.61	-0.61	0.00	-0.61	0.44
Pl32	-1.20	-0.56	-0.74	-0.74	0.18	-0.56	0.47
Pl33	-1.04	-0.53	-0.68	-0.68	0.15	-0.53	0.51
Pl34	-0.90	-0.5	-0.61	-0.61	0.11	-0.5	0.56

Pl35	-0.78	-0.5	-0.57	-0.58	0.08	-0.49	0.63
Pl36	-0.68	-0.5	-0.82	-0.45	-0.05	-0.87	1.28
Pl37	-0.60	-0.54	-0.82	-0.79	0.25	-0.57	0.95
Pl38a	-0.60	-0.58	-0.75	-0.73	0.15	-0.6	1.00
Cp	-1.62	-0.88	-0.99	-0.96	0.08	-0.91	0.60
SDT	0.73	0.57	0.44	0.41	0.25	0.62	0.29
Cov	0.45	0.65	0.44	0.43	3.13	0.68	0.48

Table C. 5. Cp on bare roofs vs. roof under solar panels, Slope 35º, 0.0º

	Cp Bare roof	Cp (SP)	Cp (SP/BRf)
Pl1A	-0.37	-0.36	0.97
Pl2	-0.37	-0.36	0.97
Pl3	-0.37	-0.36	0.97
Pl4	-0.37	-0.37	1.00
Pl5	-0.37	-0.37	1.00
Pl6	-0.38	-0.37	0.97
Pl7	-0.38	-0.37	0.97
Pl8	-0.38	-0.39	1.03
Pl9	-0.38	-0.38	1.00
Pl10	-0.38	-0.38	1.00
Pl11	-0.38	-0.38	1.00
Pl12	-0.38	-0.37	0.97
Pl13	-0.37	-0.37	1.00
Pl14	-0.37	-0.37	1.00
Pl15	-0.37	-0.37	1.00
Pl16	-0.37	-0.38	1.03
Pl17	-0.37	-0.39	1.05
Pl18	-0.37	-0.37	1.00
Pl19 A	-0.37	-0.37	1.00
Cp	-0.37	-0.37	1.00

1.2. 8” Spacing, 3” Clearance

1.2.1. Wind direction 45º,

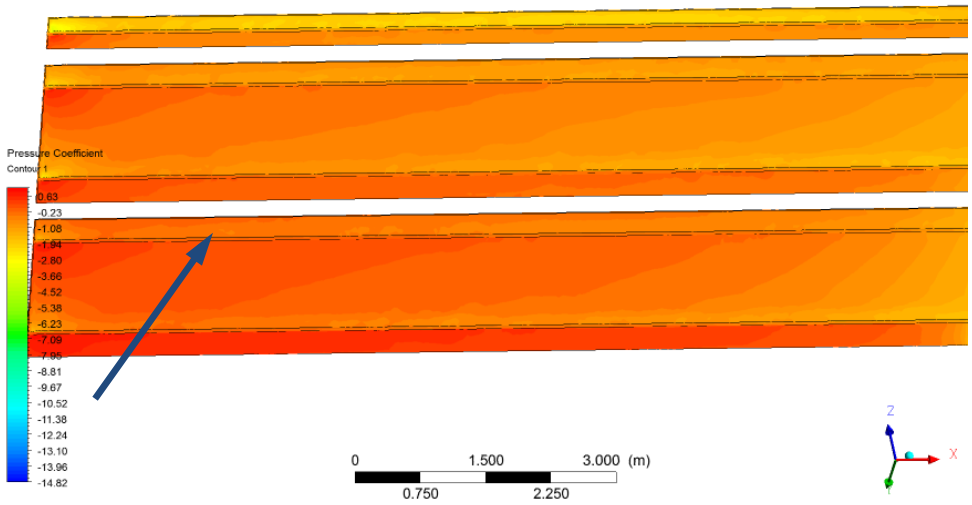


Fig. C. 69. Cp on bottom of the solar panels, WW, WD 45º

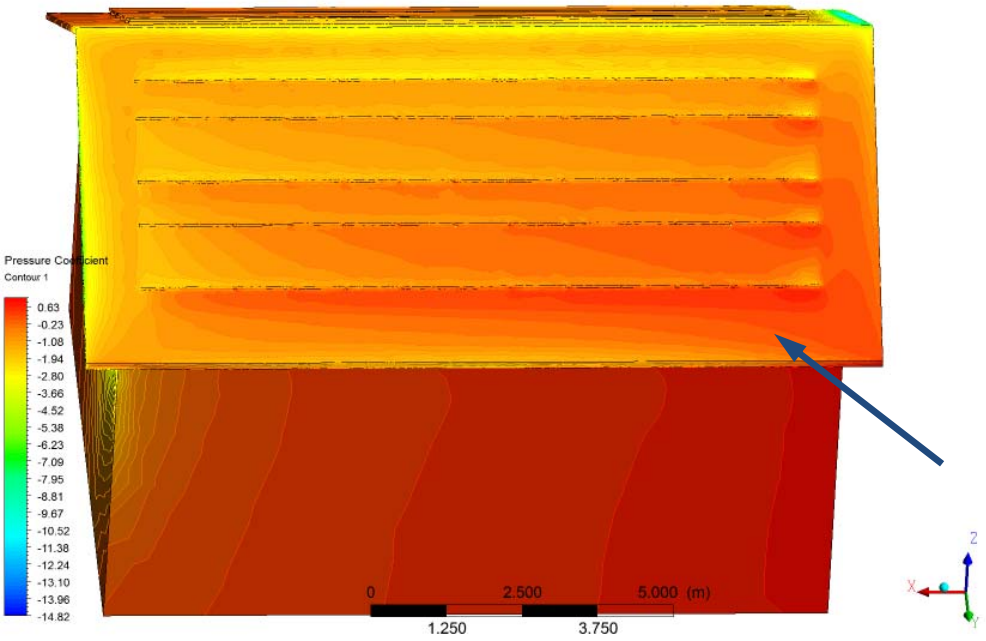


Fig. C. 70. Cp on Roof under the solar panels, solar panels cut off, WW, WD 45º

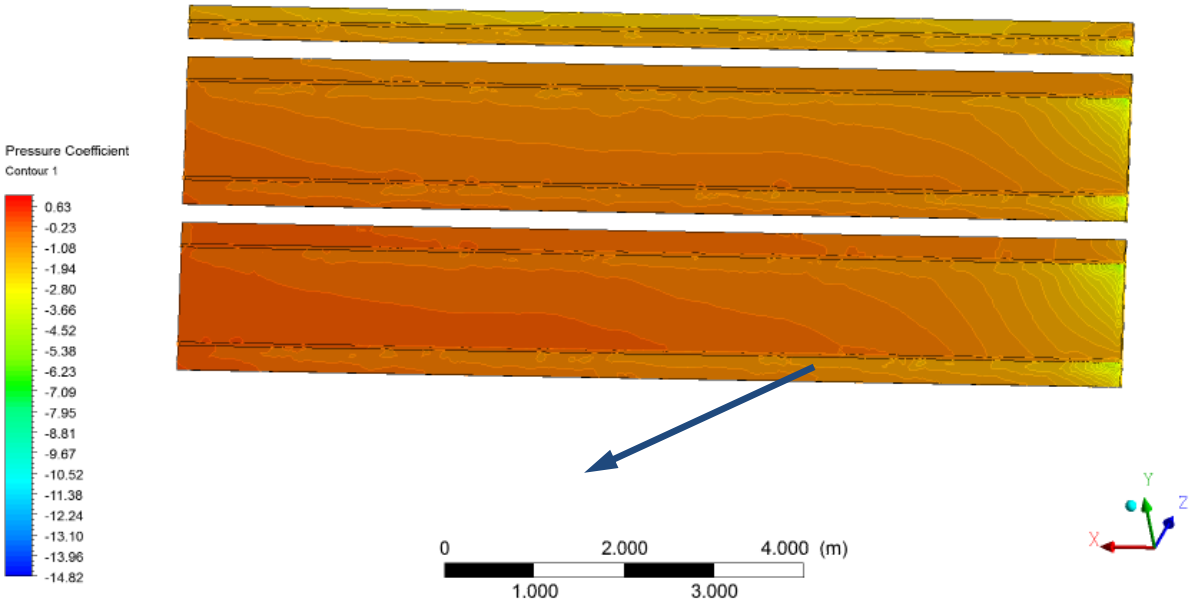


Fig. C. 71. Cp on bottom of the solar panels, LW, WD 45º

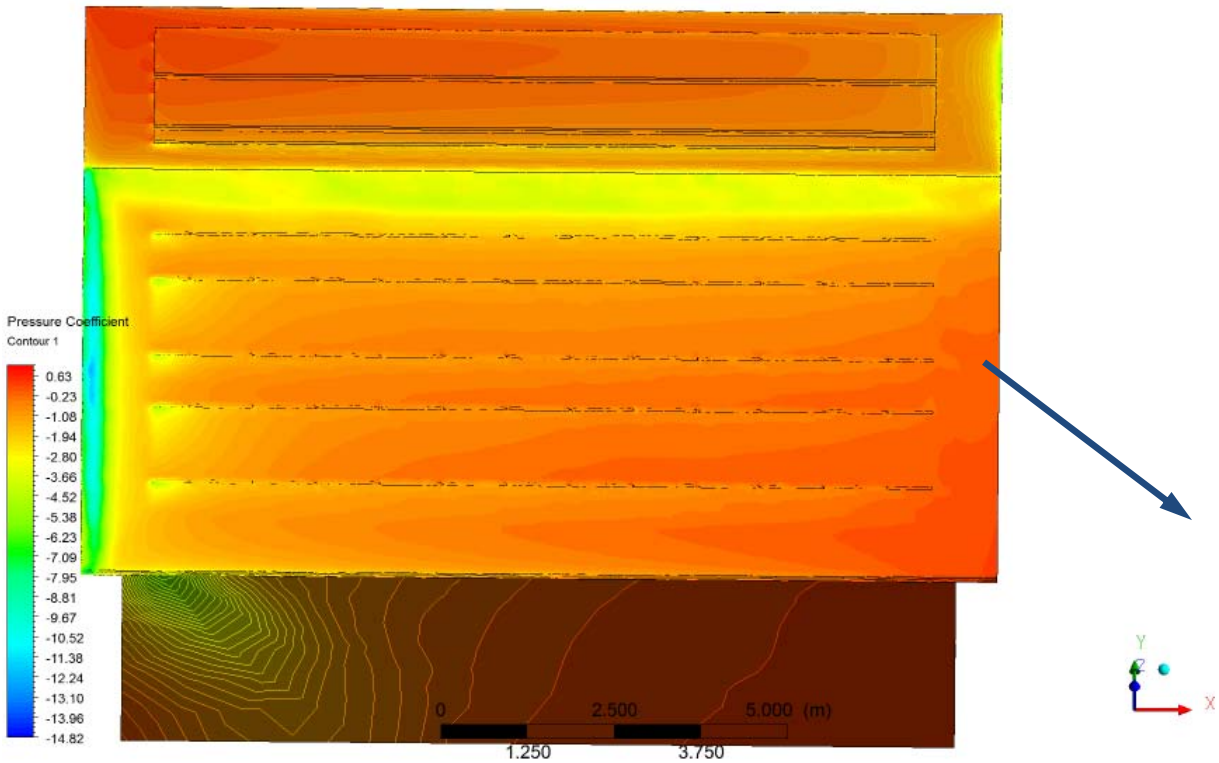


Fig. C. 72. Cp on Roof under the solar panels, solar panels cut off, LW, WD 45º

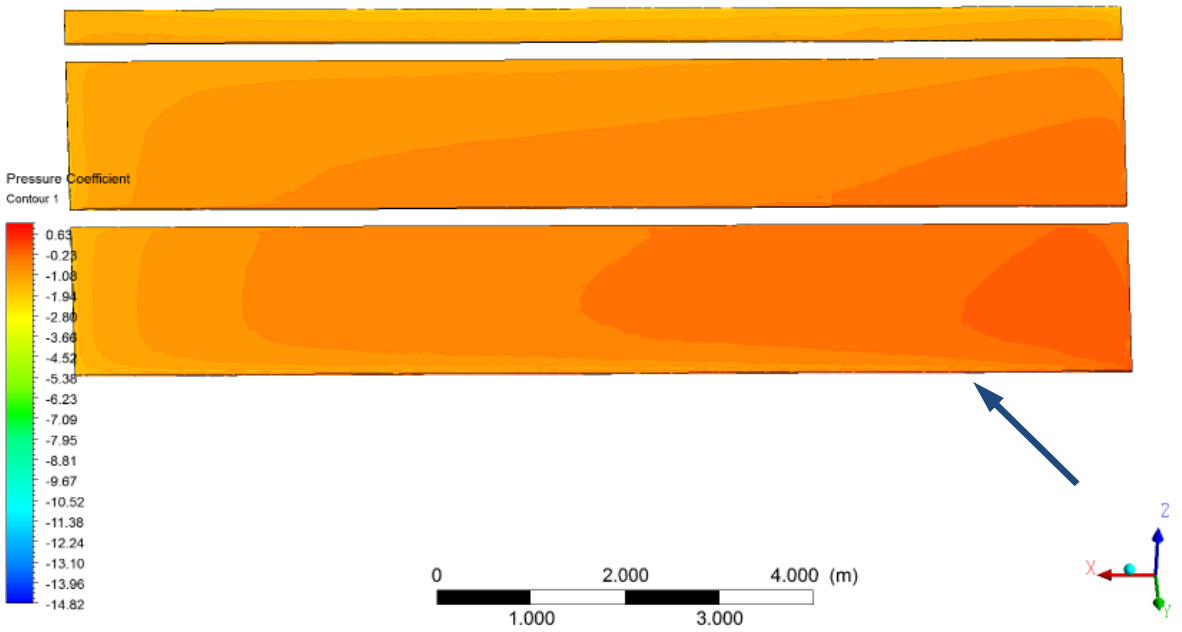


Fig. C. 73. Cp on top of the solar panel, WW, WD 45º

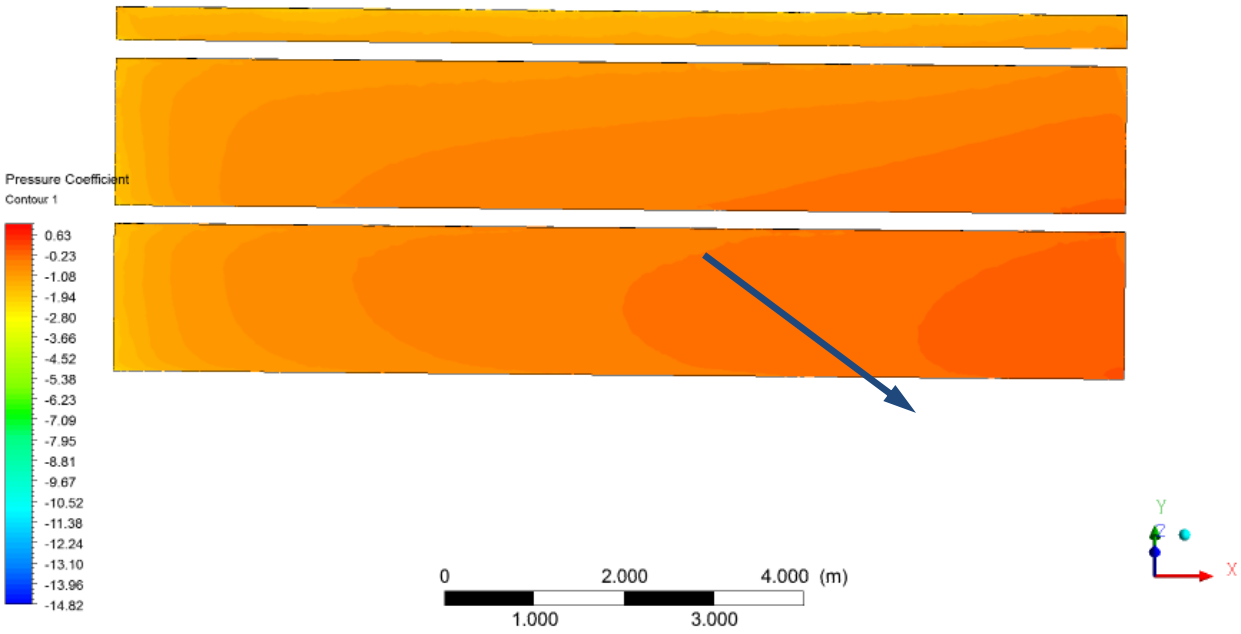


Fig. C. 74. Cp on top of the solar panel, LW, WD 45º

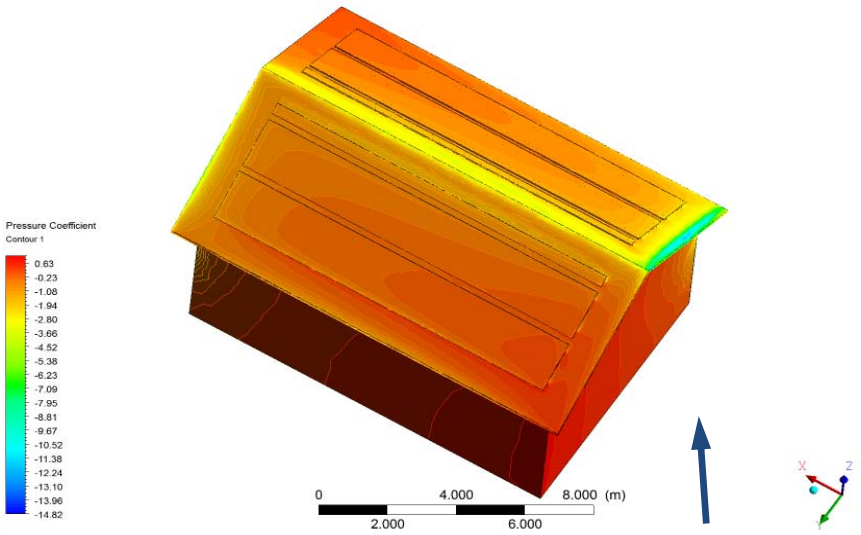


Fig. C. 75. Pressure coefficient on top surface of the solar panels WD 45º, WW, WD 45º

1.2.2. WIND DIRECTION 90º

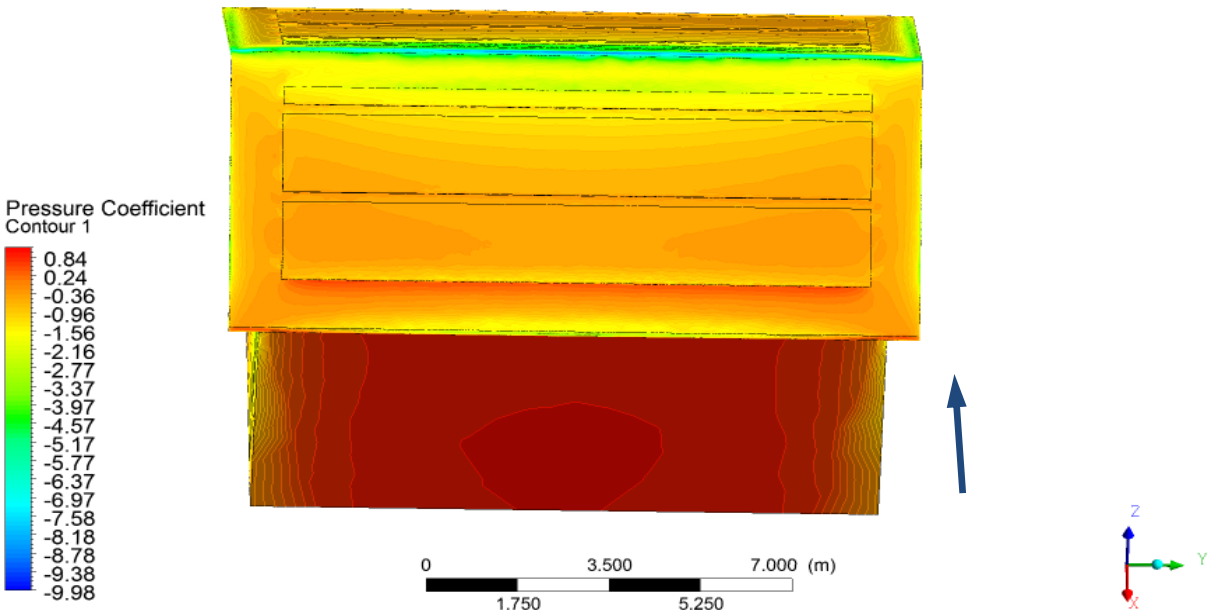


Fig. C. 76. CP on whole building and solar panels, S 35º, WW, WD 90º

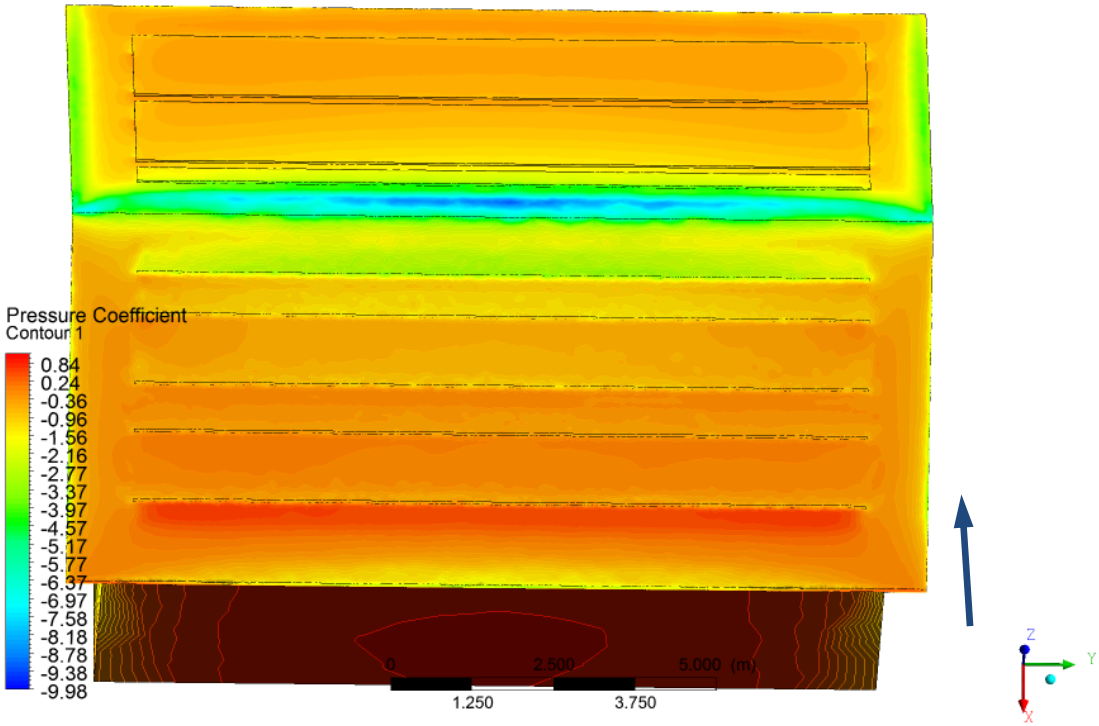


Fig. C. 77. CP on roof under solar panels, S 35º, WW, WD 90º

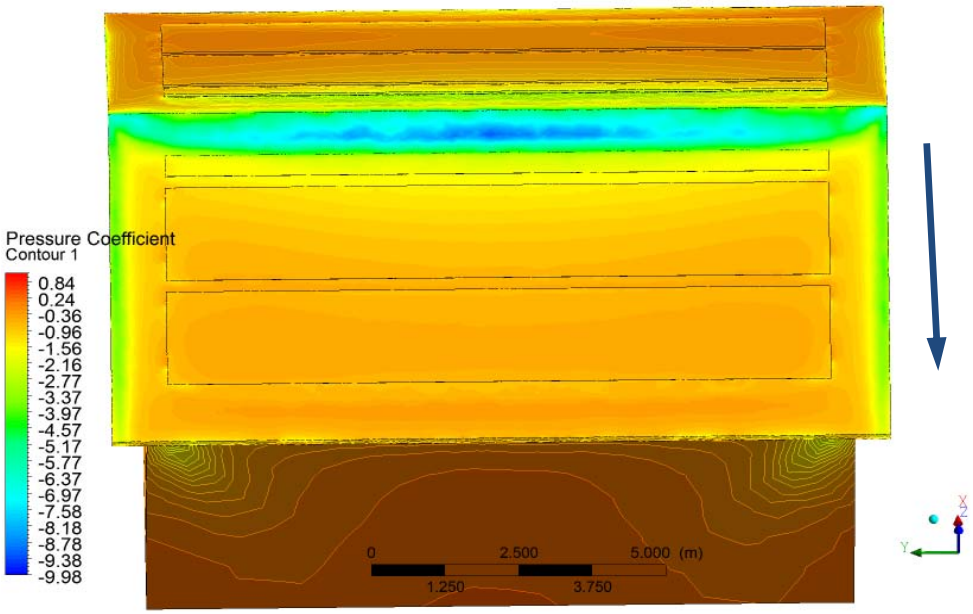


Fig. C. 78. CP on whole building and solar panels, S 35º, LW, WD 90º

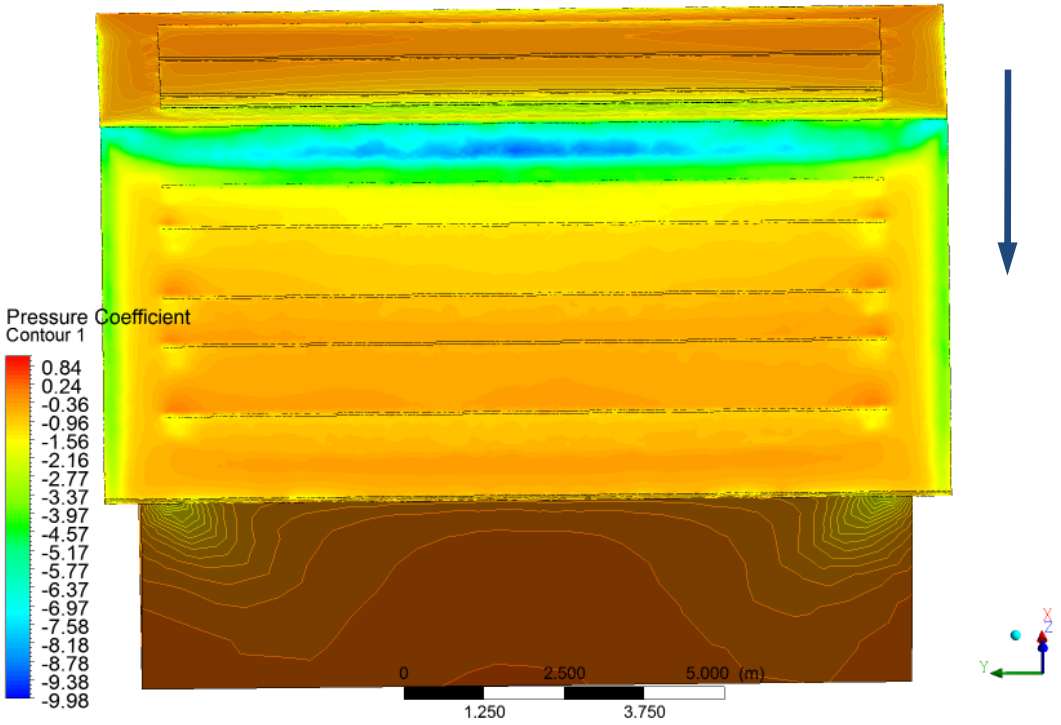


Fig. C. 79. CP on roof under solar panels, S 35º, LW, WD 90º

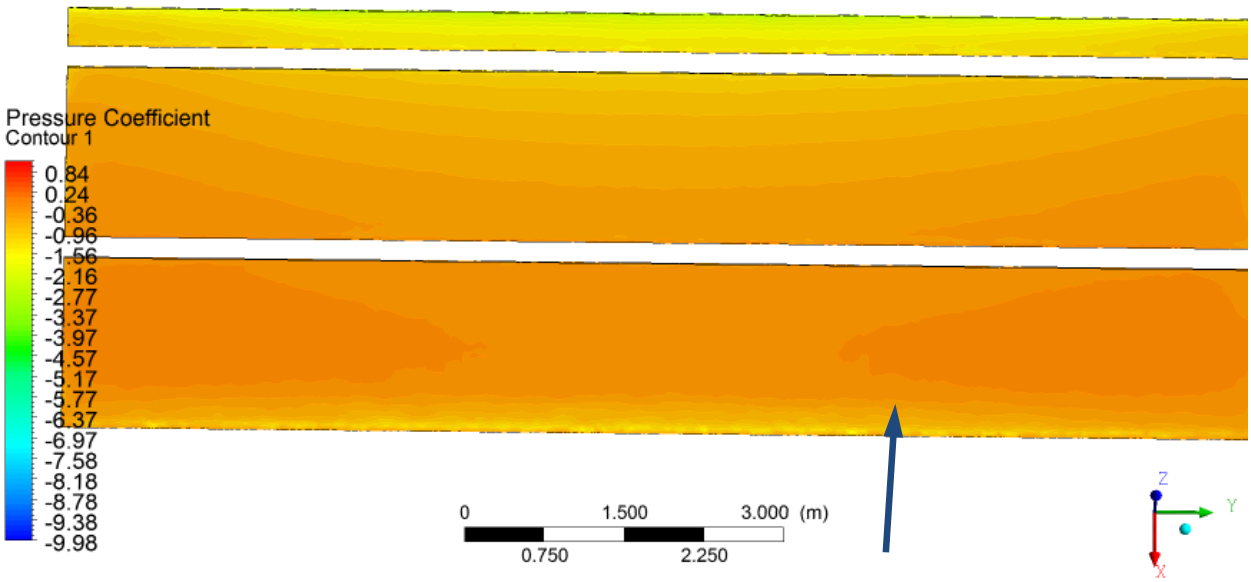


Fig. C. 80. CP on top of solar panels, S 35º, WW, WD 90º

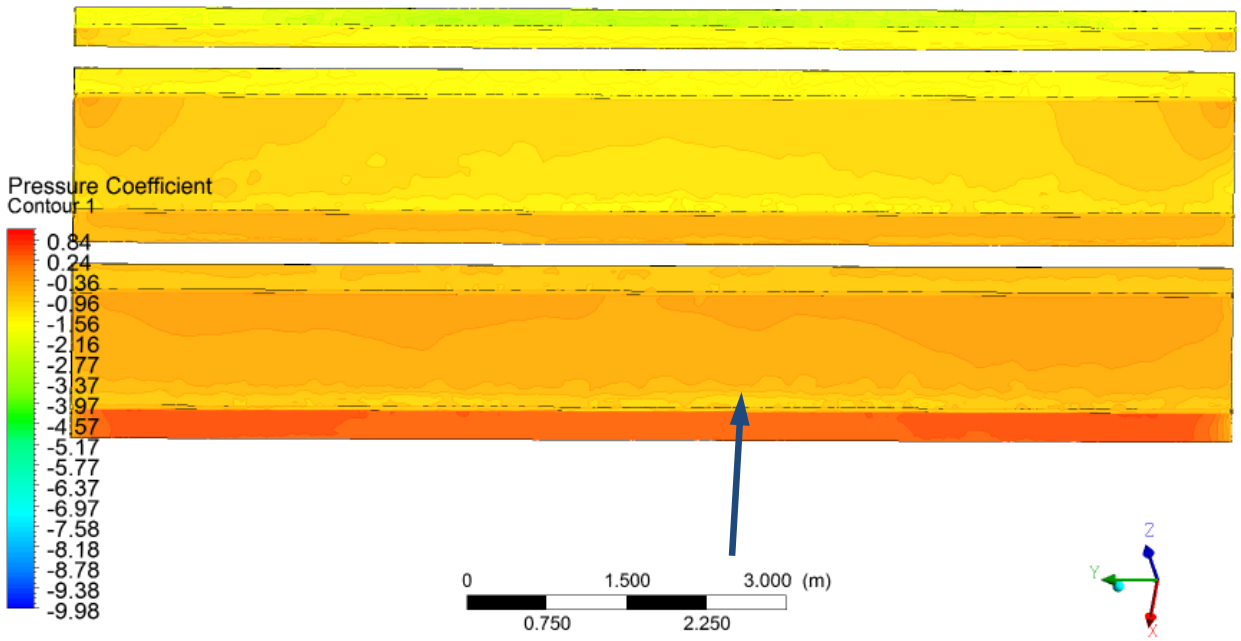


Fig. C. 81. CP on bottom of solar panels, S 35º, WW, WD 90º

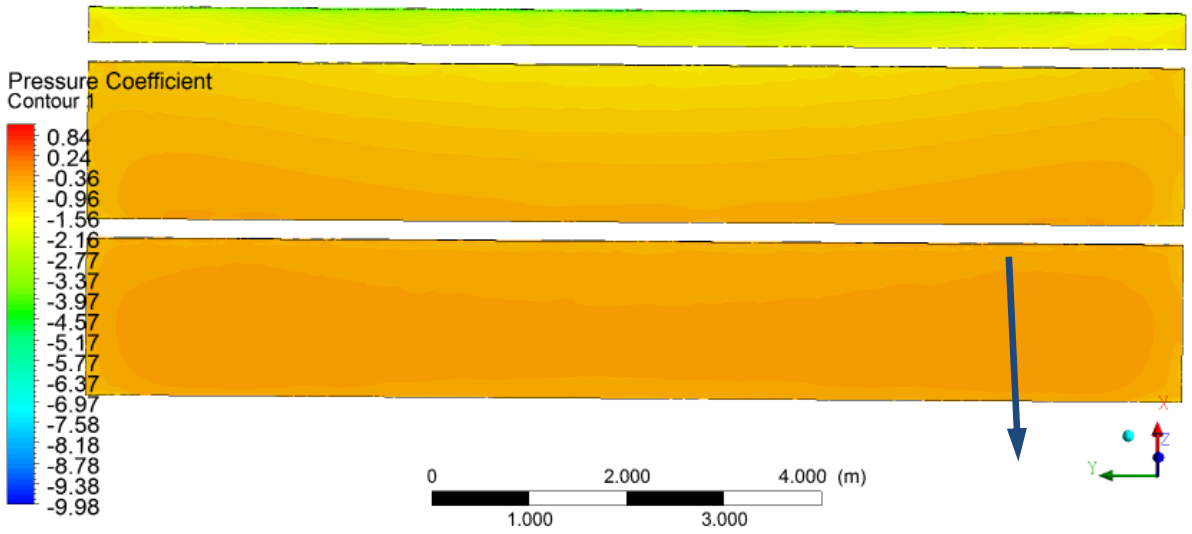


Fig. C. 82. CP on top of solar panels, S 35º, LW, WD 90º

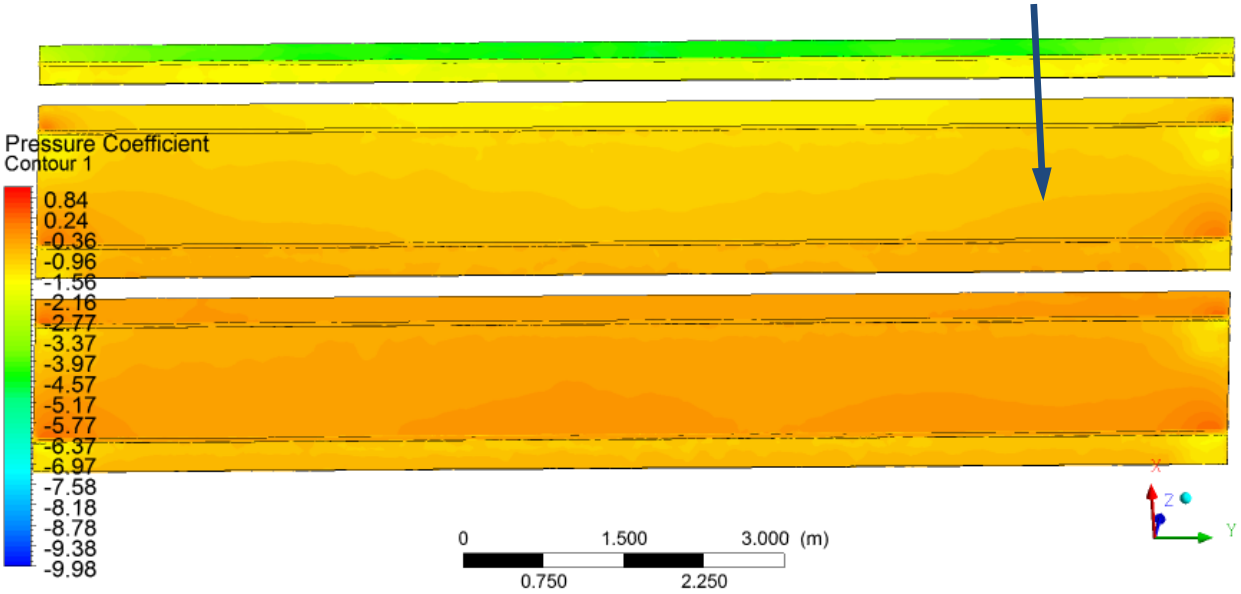


Fig. C. 83. CP on bottom of solar panels, S 35º, LW, WD 90º

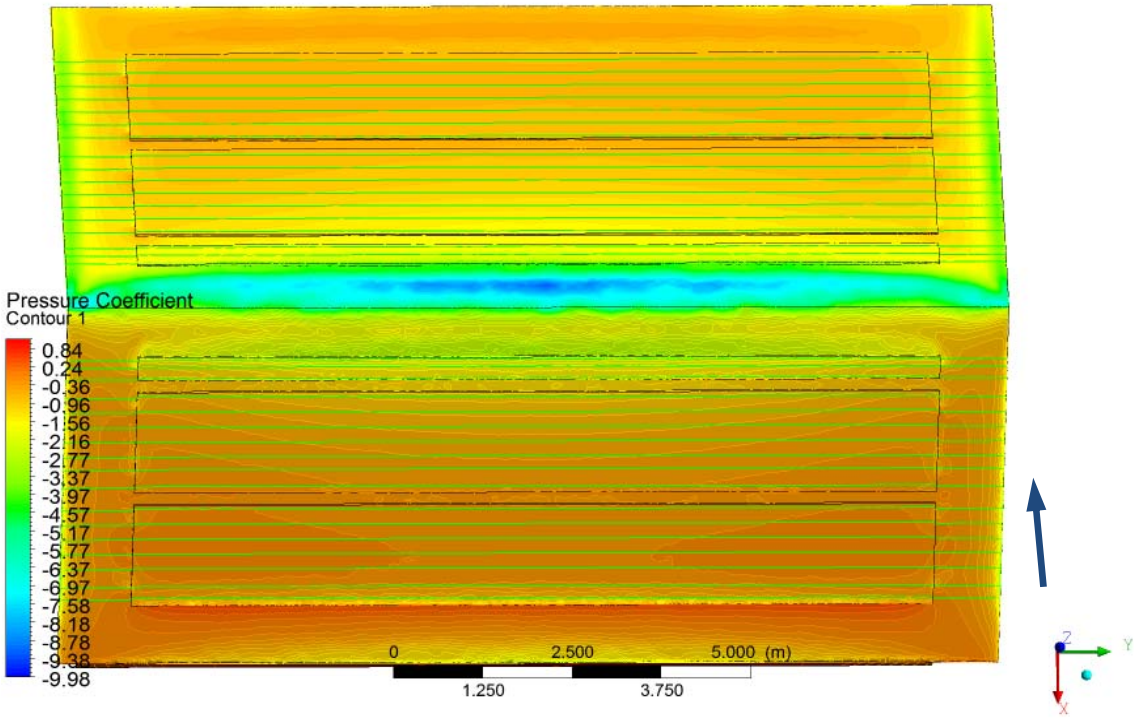


Fig. C. 84. Cp on top of solar panels with plines, S 35º, WW, WD 90º

1.2.3. WIND DIRECTION 0.0º

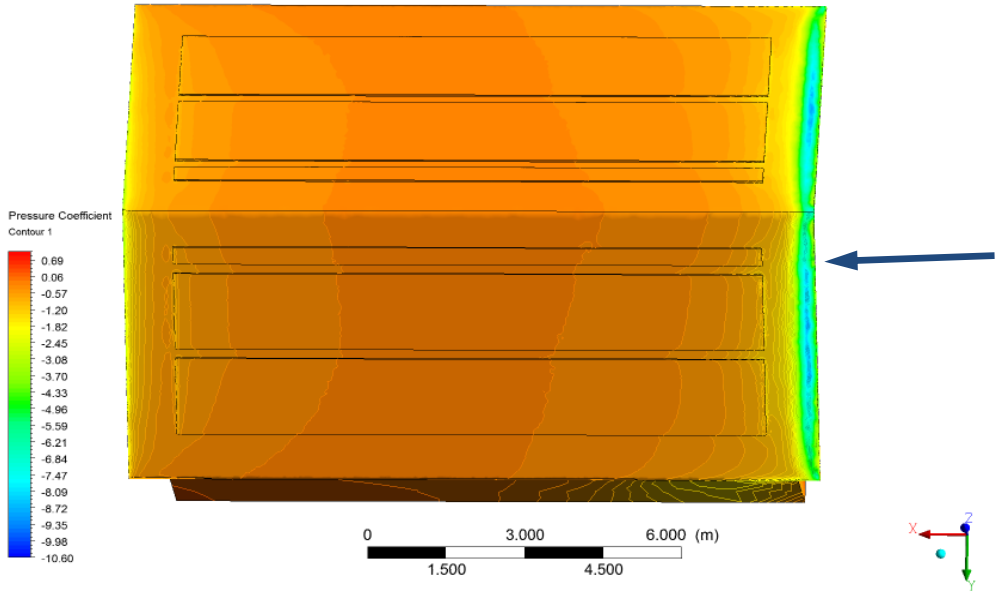


Fig. C. 85. Cp on roof with solar panels, S 35º, WD 0.0º

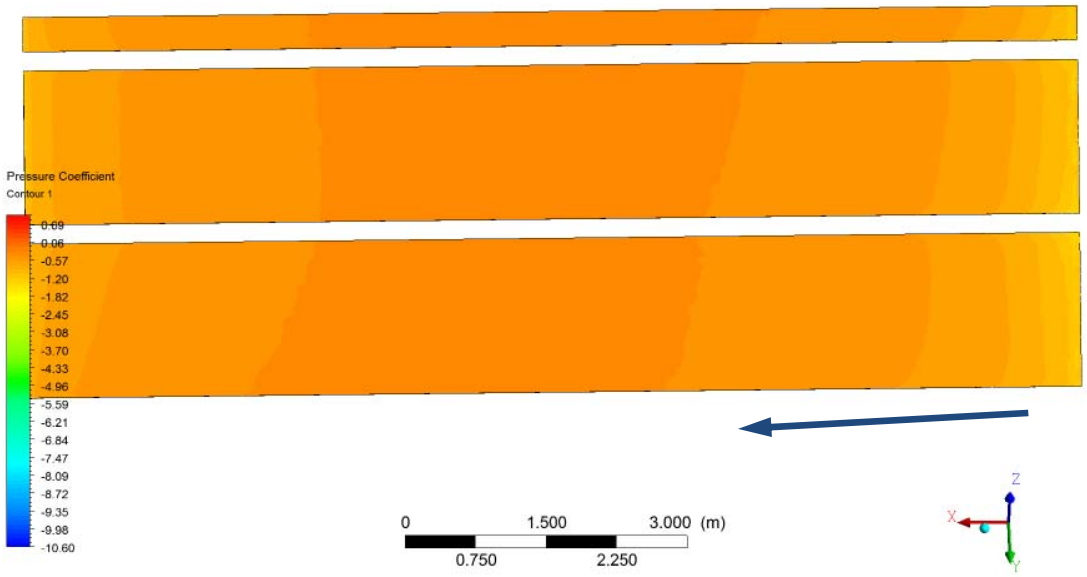


Fig. C. 86. Cp on top of solar panels, S 35º, WD 0.0º

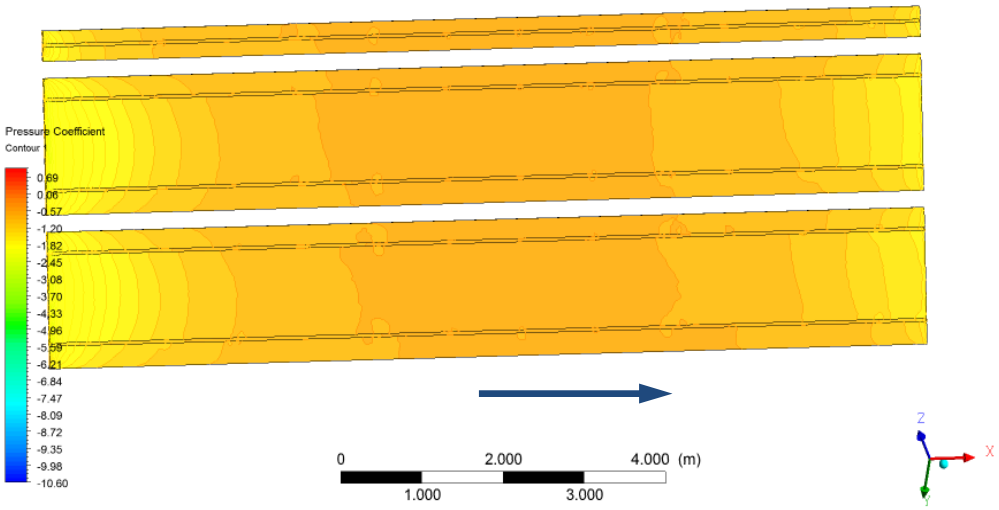


Fig. C. 87. Cp on bottom of solar panels, S 35º, WW, WD 0.0º

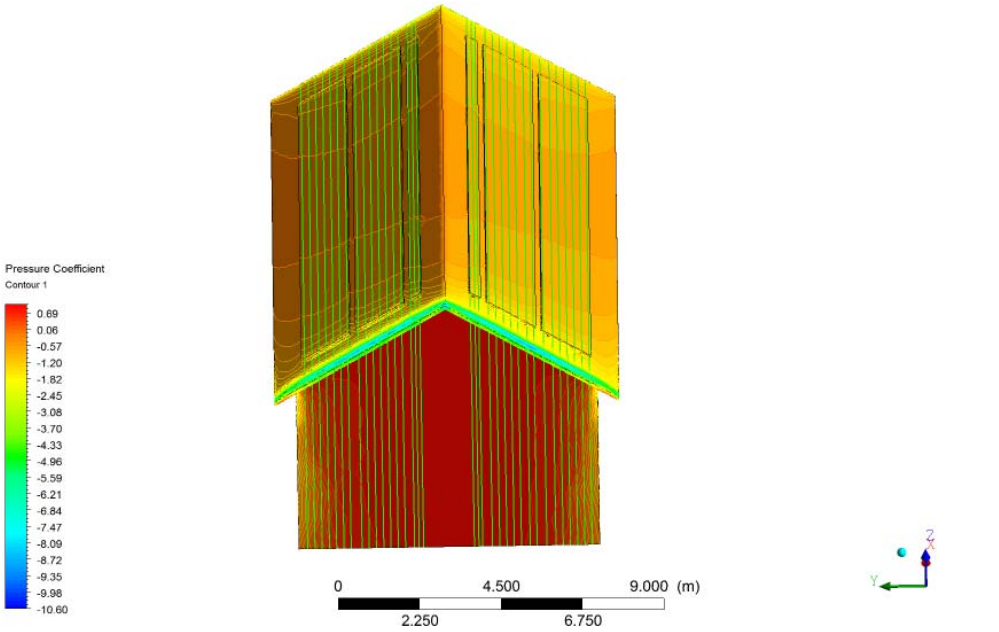


Fig. C. 88. Cp on top of solar panels and roof with Plines, S 35º, WW, WD 0º

1.2.4. Detailed Distribution of Wind Pressure on roof mounted solar panels in comparison with bare roofs, Windward, 2” apart, 10” roof space

A. Bottom of solar panels vs. roof under solar panels,

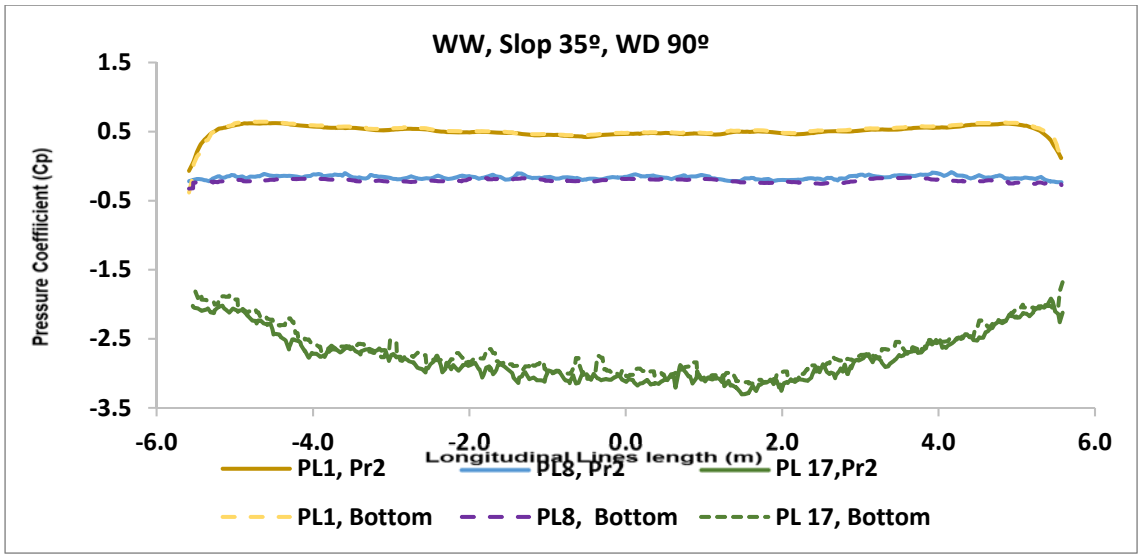


Fig. C. 89. Cp on bottom of solar panels vs. on roof under the panels, Pr2, S 35 º, WW, WD 90 º

B. Roof under solar panels vs. bare roofs,

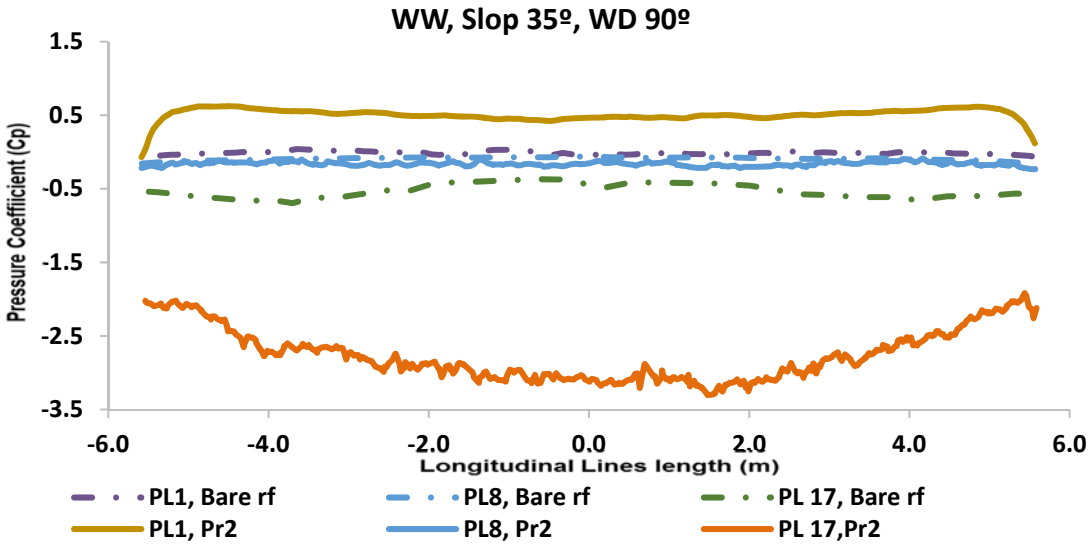


Fig. C. 90. Cp on bare roof Pr1 vs. on roof under the panels, Pr2, S 35º, WW, WD 90º

C. Bottom of the solar panels vs. bare roofs,

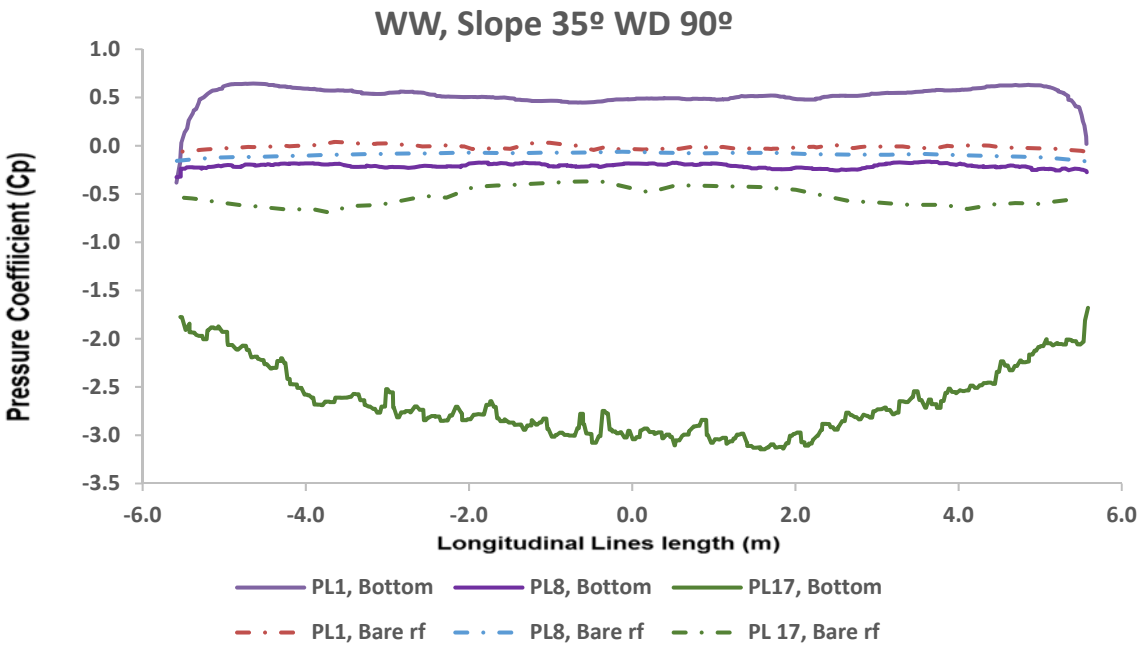


Fig. C. 91. Cp on bottom of solar panels Psp vs. on bare roof, Pr1, S 35 º, WW, WD 90 º

D. Bare roofs Pr1 Vs resultant Pr2 +Psp,

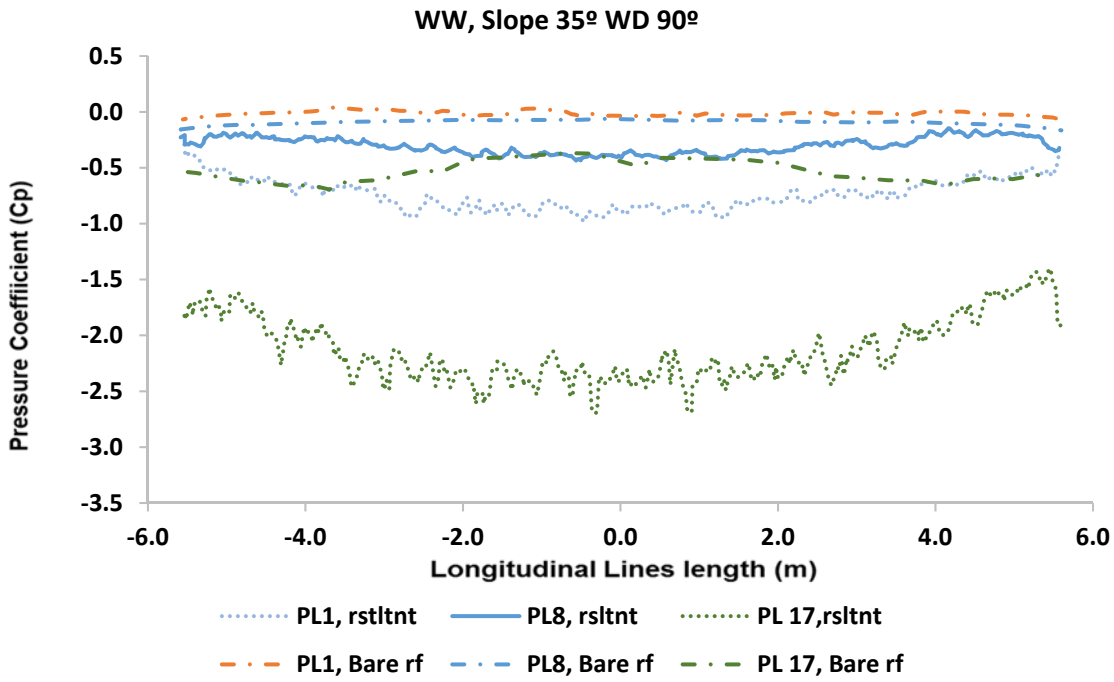


Fig. C. 92. Cp of bare roofs Pr1 Vs resultant Pr2 + Psp, S 35 º, WW, WD 90 º

E. Bare roofs Pr1 Vs top of the panels,

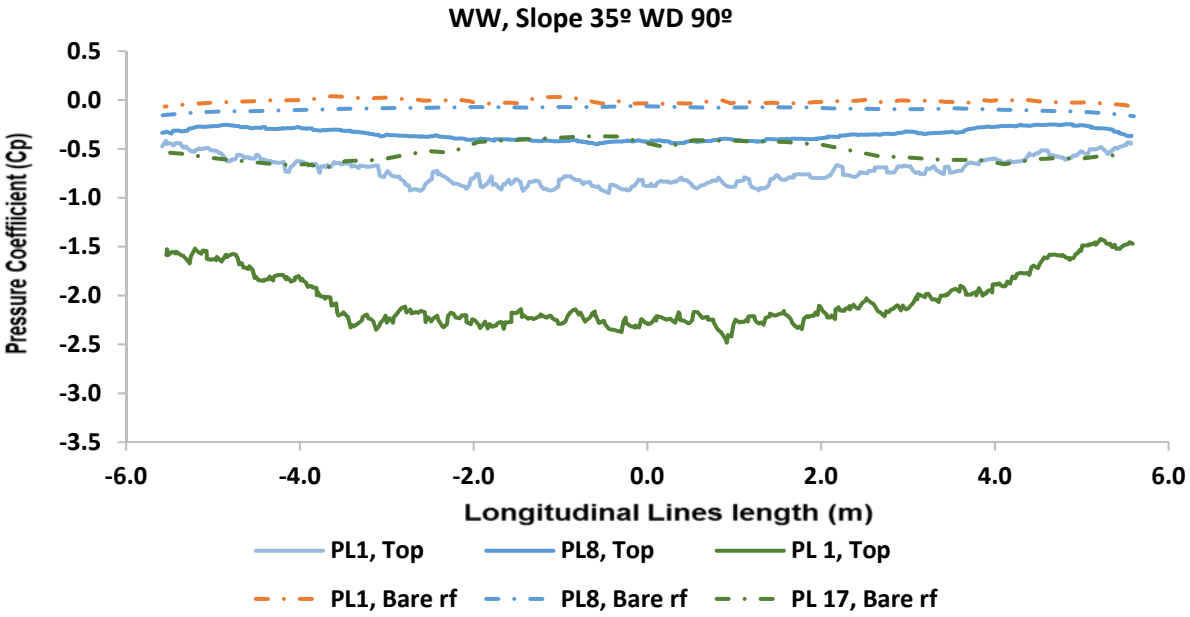


Fig. C. 93. Cp of bare roofs Pr1 Vs top of panels, S 35º, WW, WD 90 º

1.2.5. Detailed Distribution of Wind Pressure on roof mounted solar panels in comparison with roof under panels and bare roofs, Leeward, 2" spacing , 10" roof clearance

A. Bottom of solar panels vs. roof under solar panels,

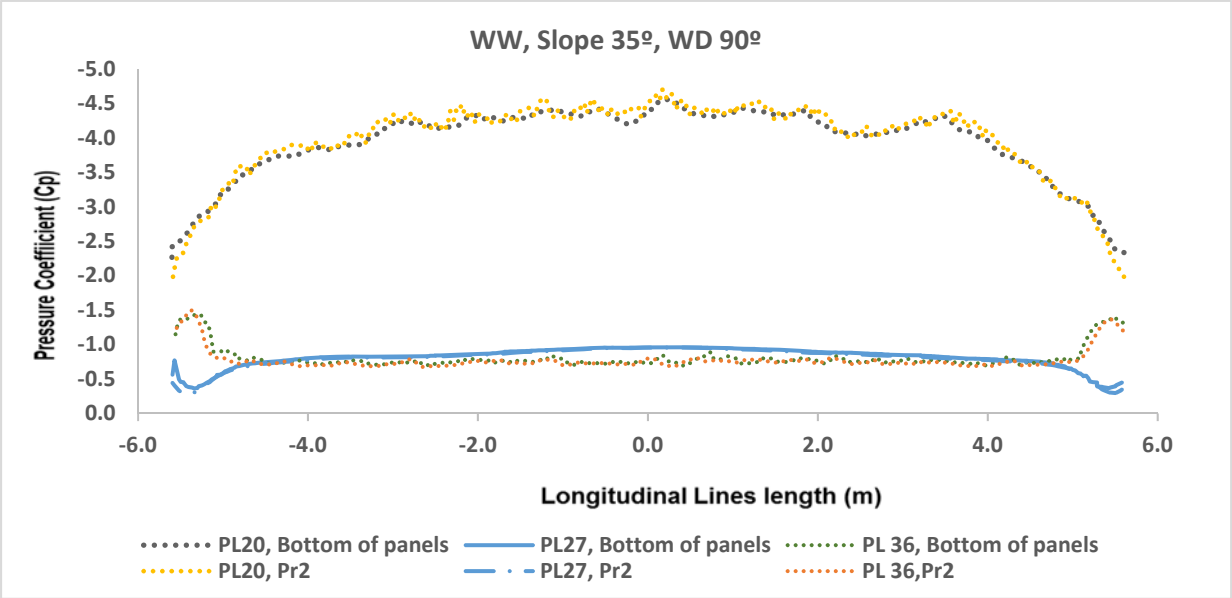


Fig. C. 94. Cp on bottom of solar panels Psp vs. on roof under the panels, Pr2, S 35º, LW, WD 90º

B. Roof under solar panels vs. bare roofs,

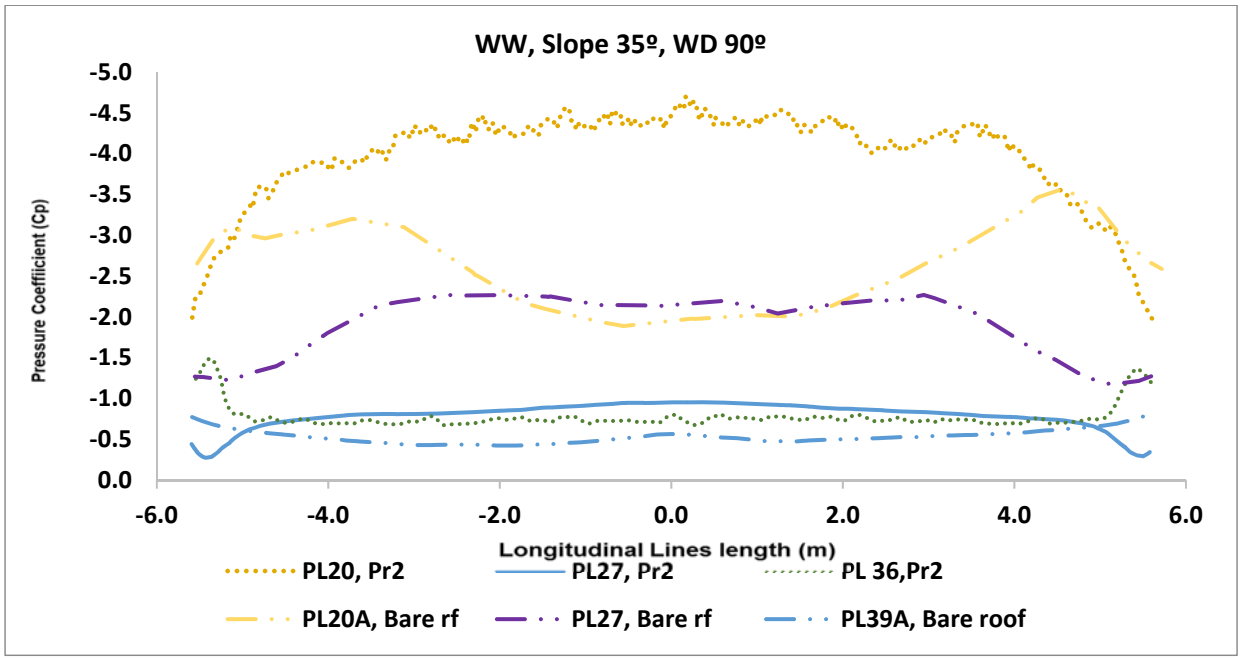


Fig. C. 95. Cp on bare roof Pr1 vs. on roof under the panels, Pr2, S 35º, LW, WD 90º

C. Bottom of the solar panels vs. bare roofs,

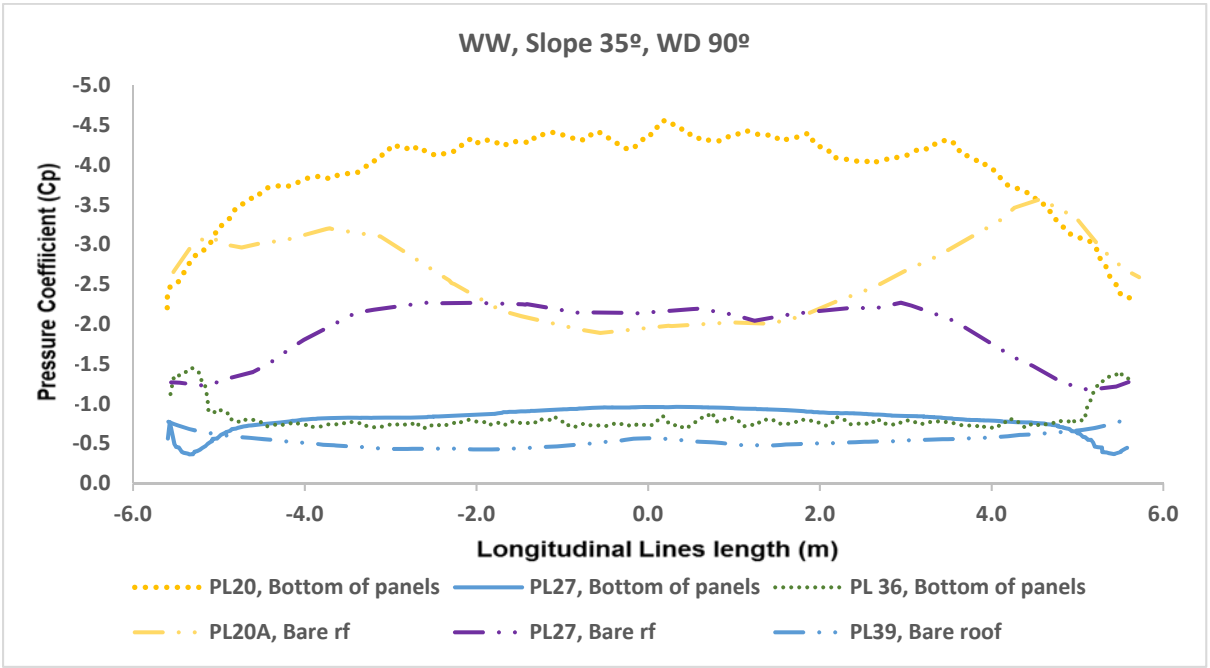


Fig. C. 96. Cp on bottom of solar panels Psp vs. on bare roof, Pr1, S 35º, LW, WD 90º

D. Bare roofs Pr1 Vs top of the panels,

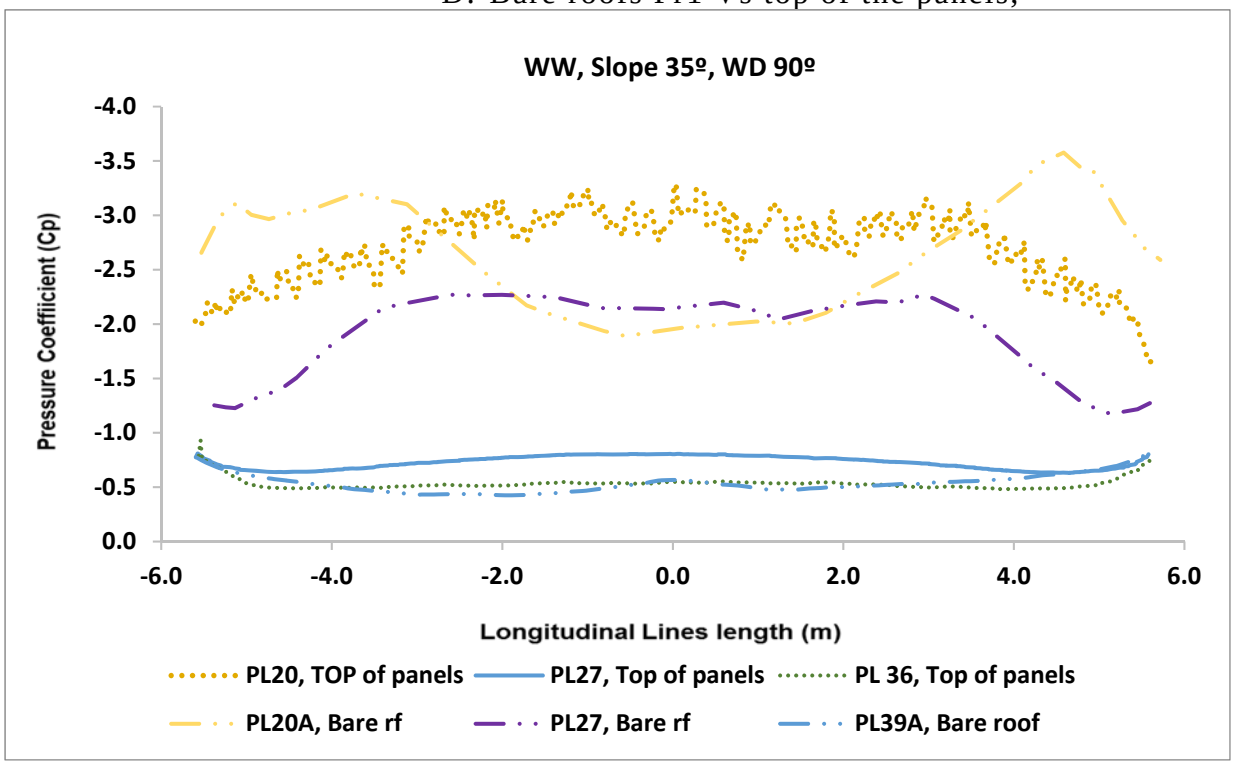


Fig. C. 97. Cp of bare roofs Pr1 Vs top of panels, S 35º, LW, WD 90º

E. Bare roofs Pr1 Vs resultant

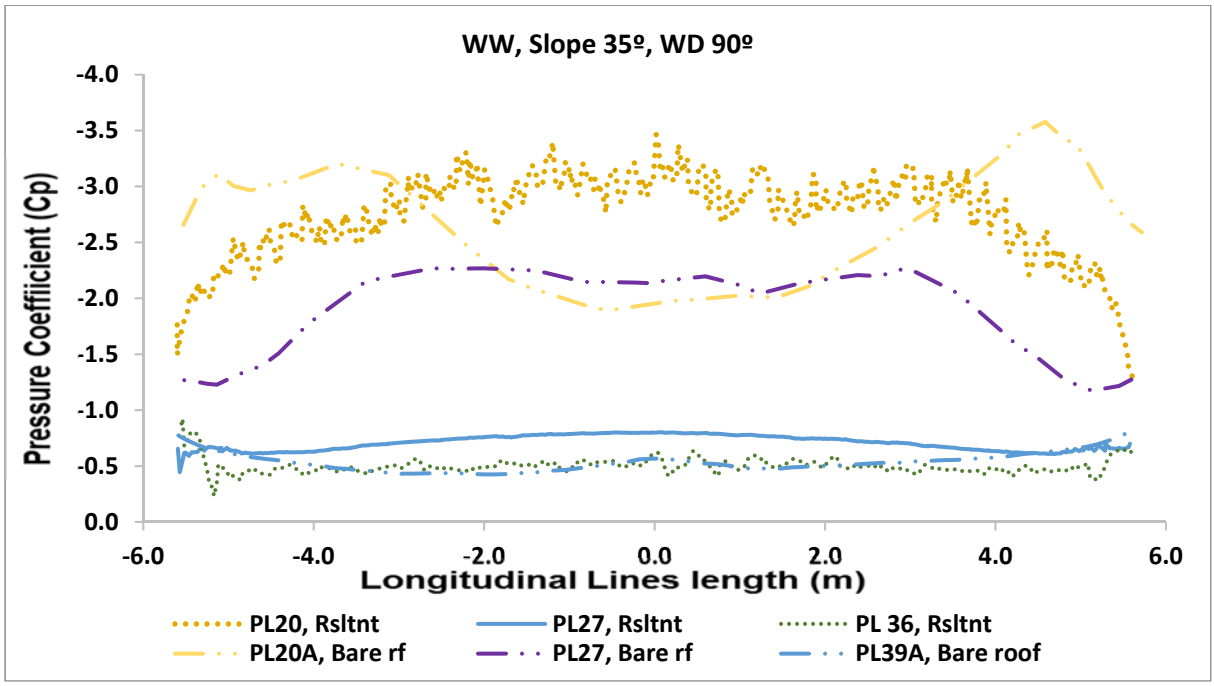


Fig. C. 98. Cp of bare roofs Pr1 Vs resultant, S 35 º, LW, WD 90 º

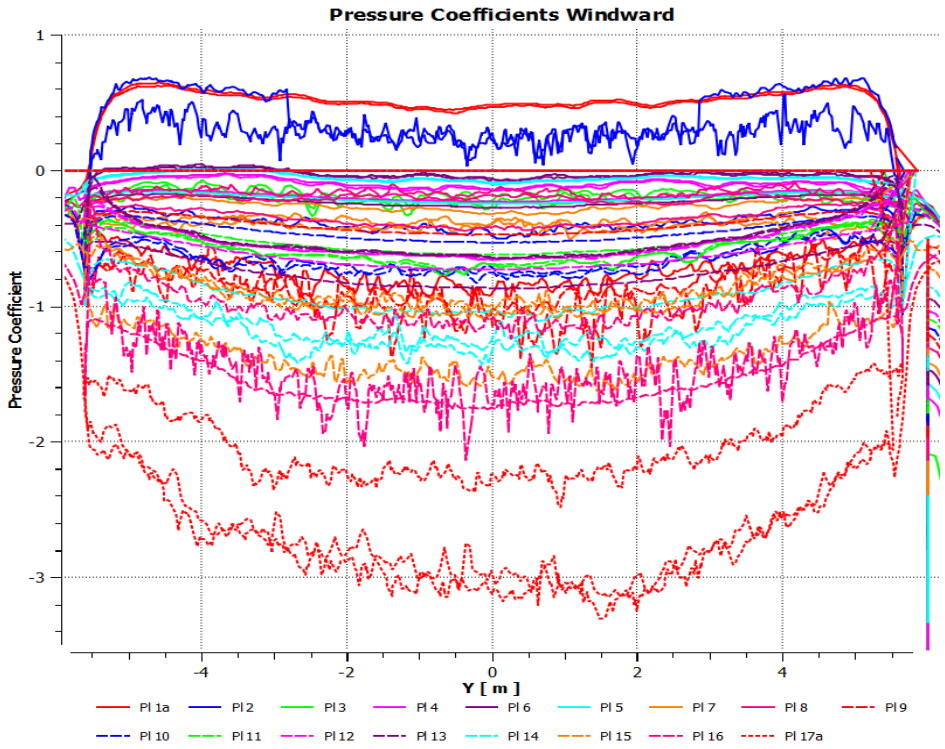


Fig. C. 99. Cp, All polylines, S 35 º, WW, WD 90 º

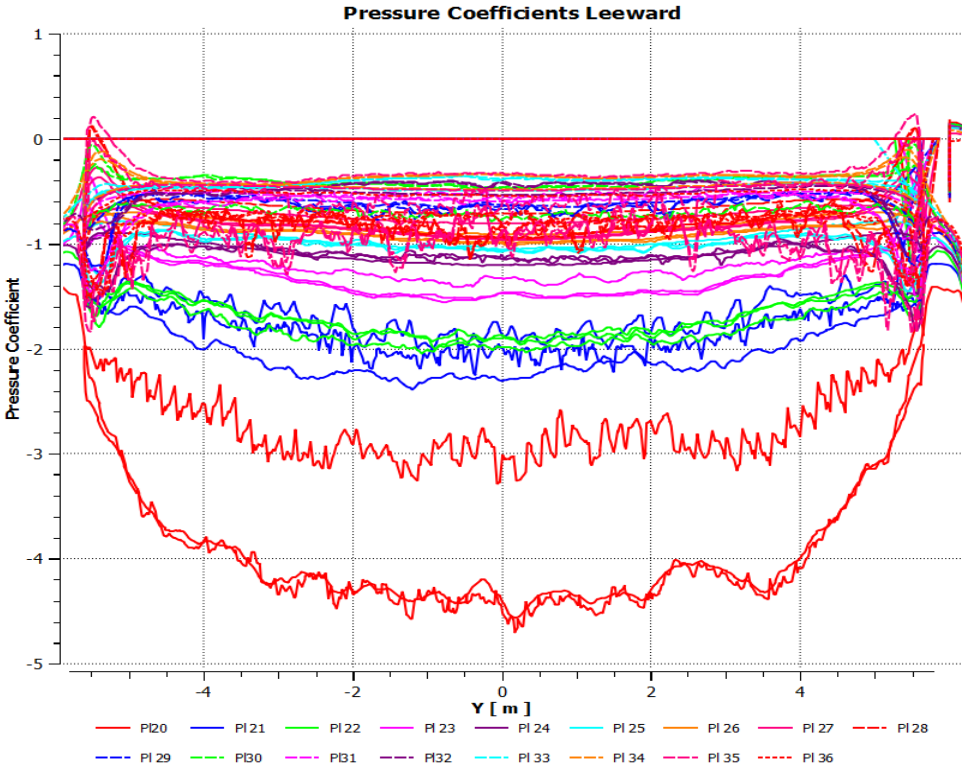


Fig. C. 100. Cp, All polylines, S 35 º, LW, WD 90 º

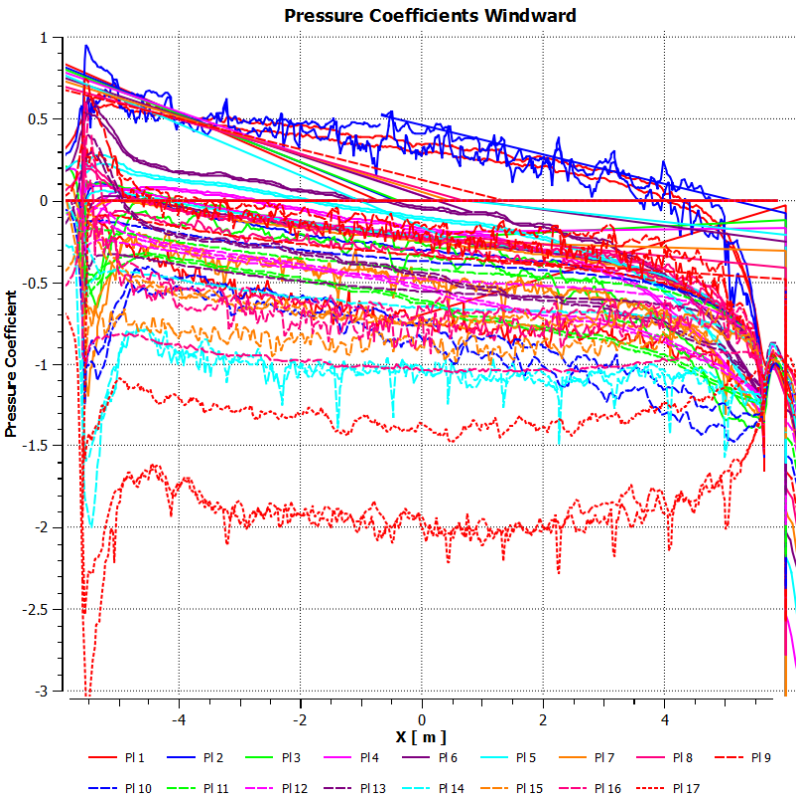


Fig. C. 101. Cp, All polylines, S 35 º, WW, WD 45 º

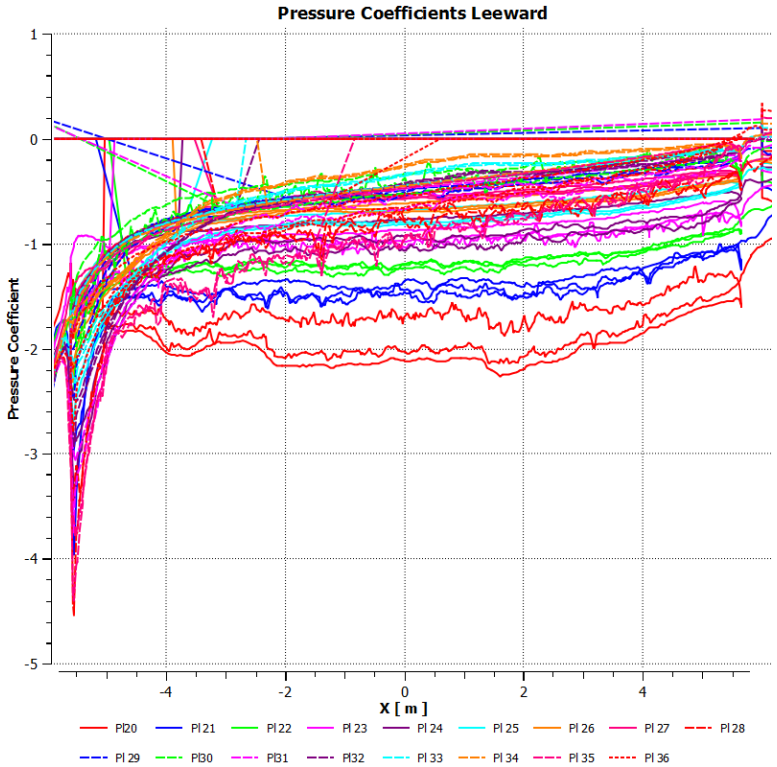


Fig. C. 102. Cp, All polylines, S 35 º, LW, WD 45 º

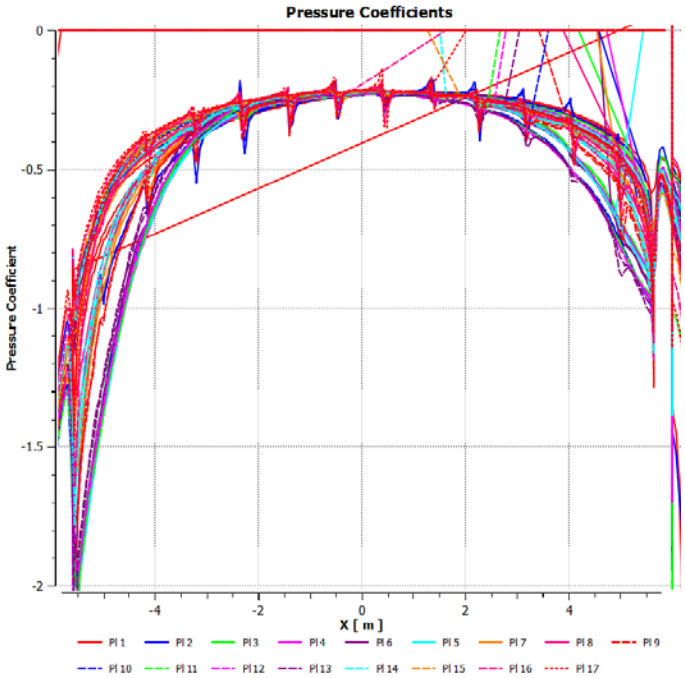


Fig. C. 103. Cp, All polylines, S 35 º, WD 0.0 º

1.2.6. Detailed Distribution of Wind Pressure, and flow on roof mounted solar panels, 2" apart, 10" roof space,

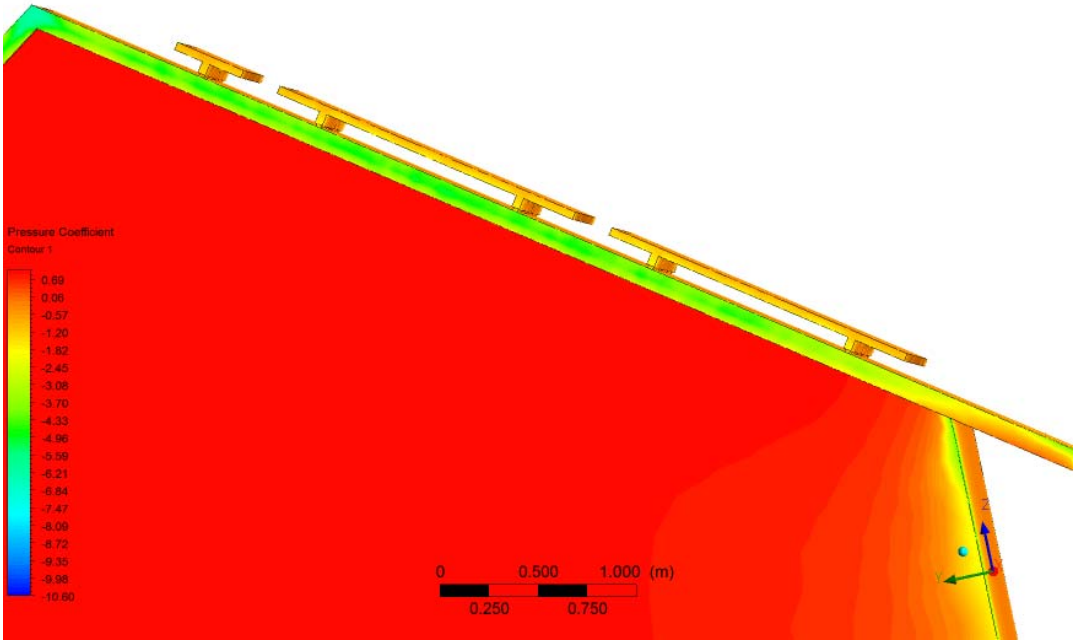


Fig. C. 104. Close view shows separation of solar panels from roof structure, WD 0º.

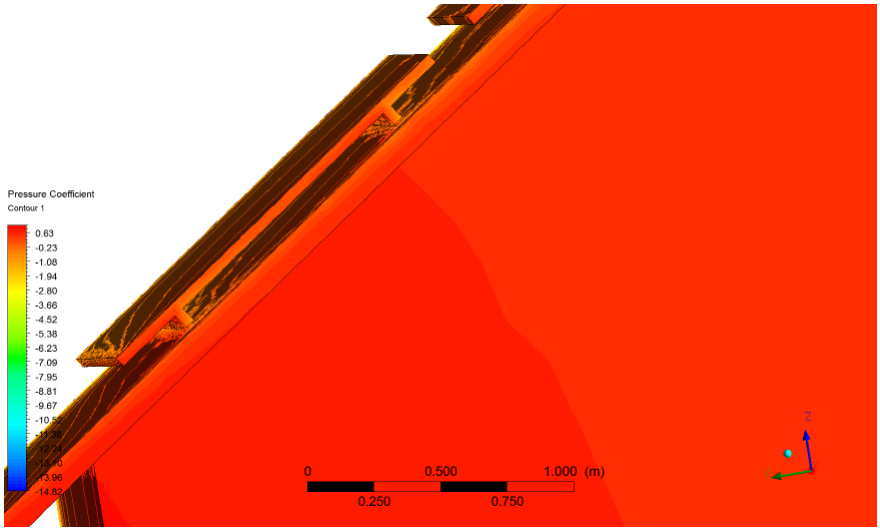


Fig. C. 105. Close view shows panels on rails and spaces, WD 45º

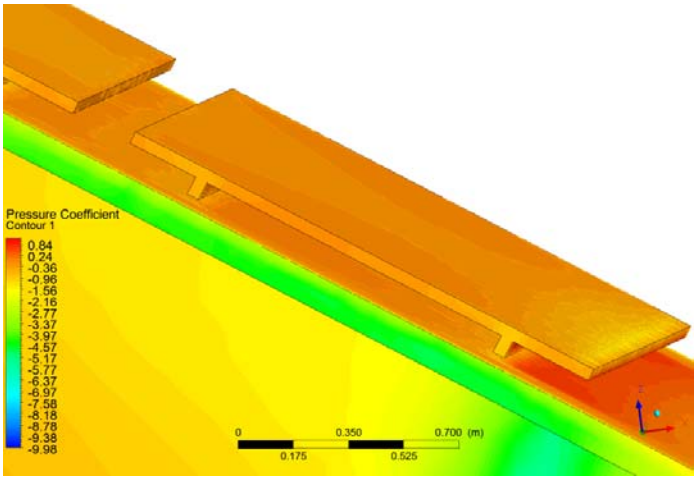


Fig. C. 106. Close view shows separation of solar panels from roof structure, WW, WD 90º

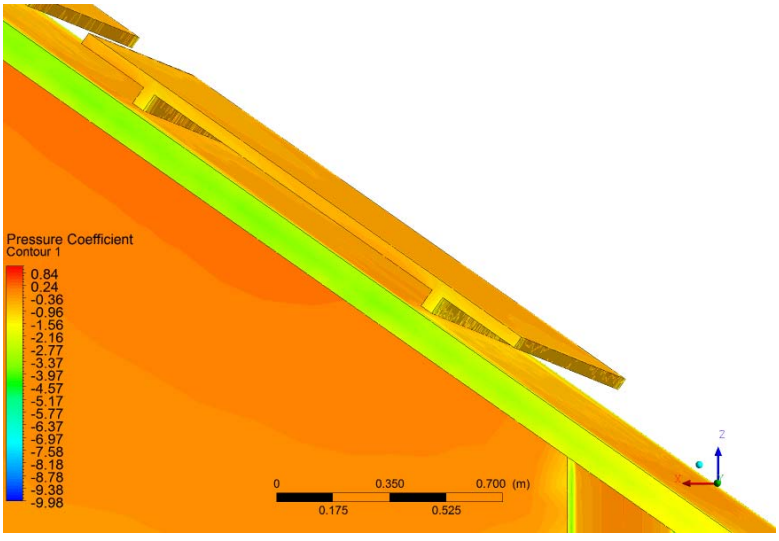


Fig. C. 107. Close view shows separation of solar panels from roof structure, LW, WD 90º

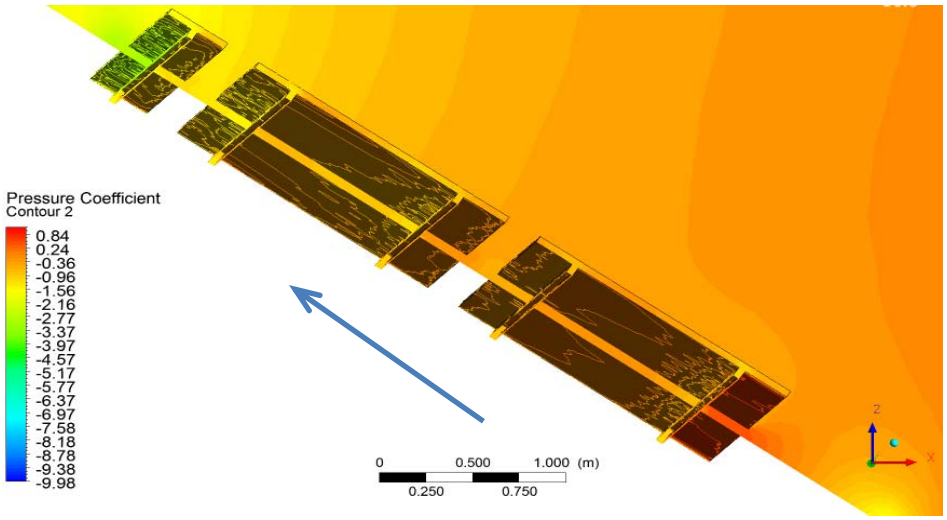


Fig. C. 108. Cp on a perpendicular plane under panels, Close up WD 90º, WW

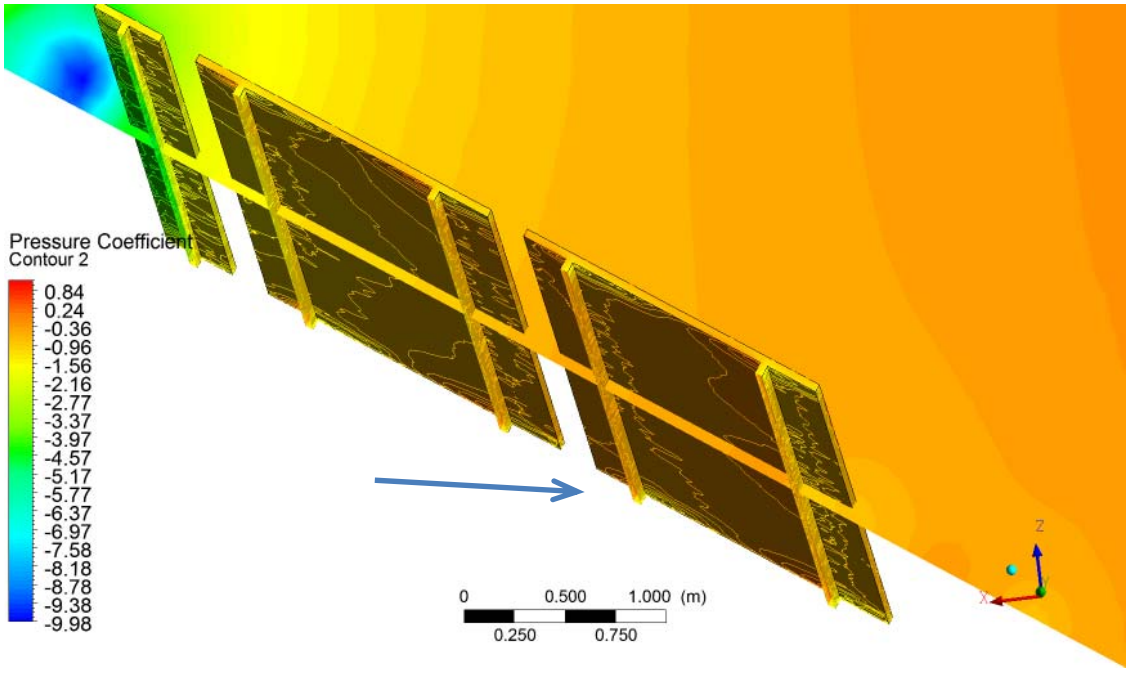


Fig. C. 109. Cp on a perpendicular plane under panels, WD 90º, LW

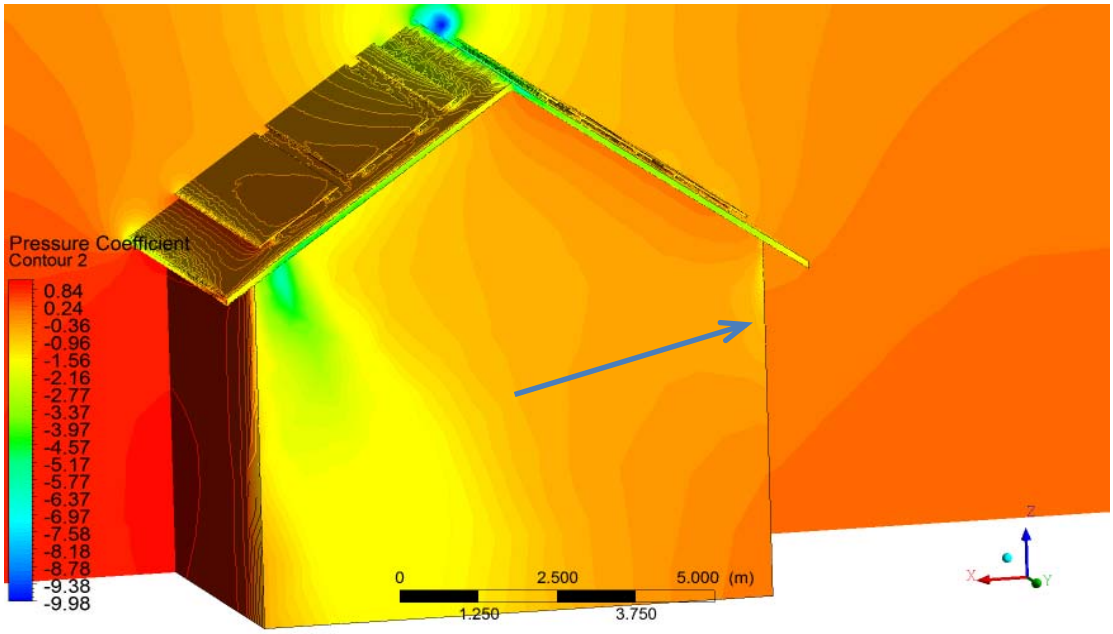


Fig. C. 110. Cp on a perpendicular plane with the house, WD 90º

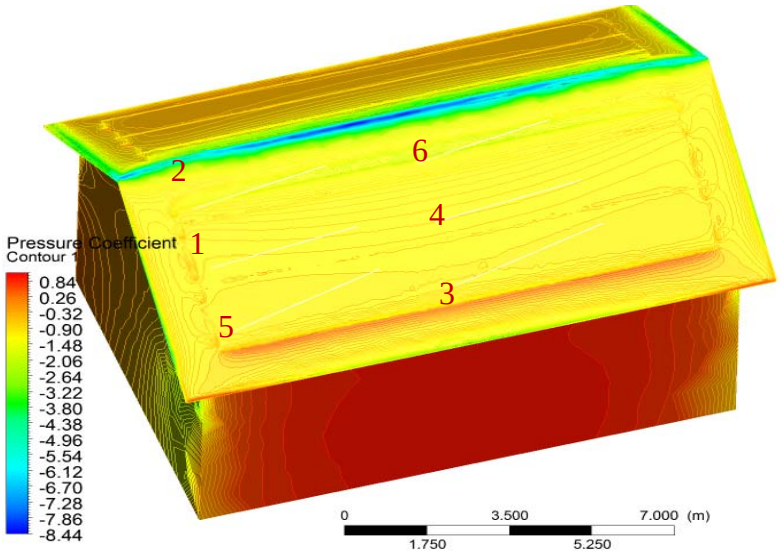


Fig. C. 111. Lines used to draw velocity and pressure changes, WD 90º.

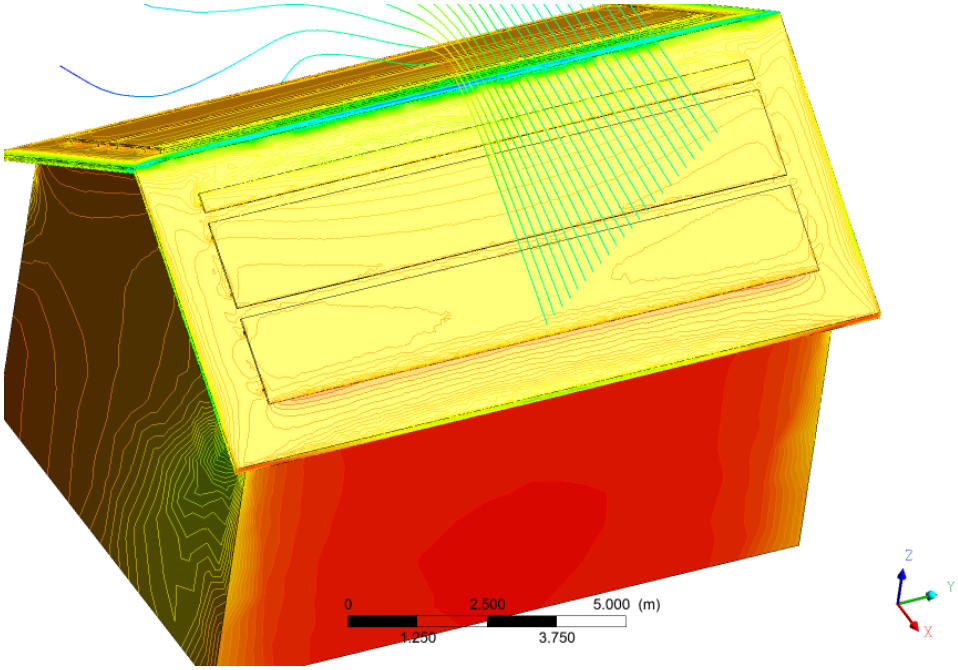


Fig. C. 112. Velocity stream lines at middle cross section plane , WD 90º

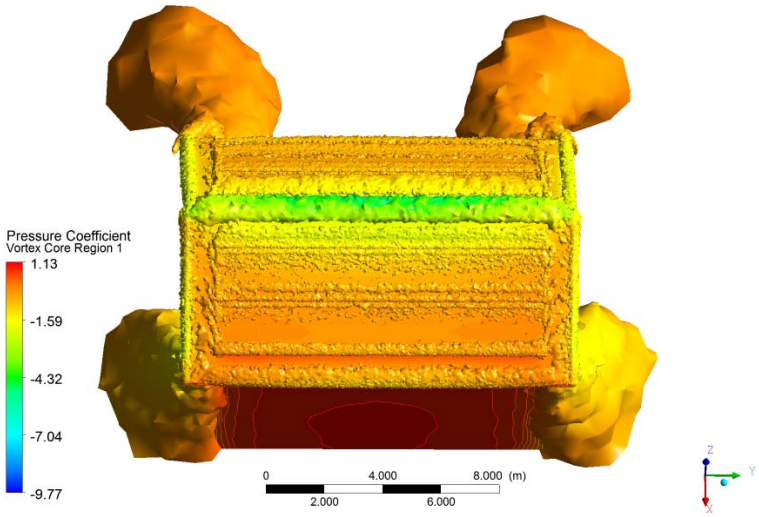


Fig. C. 113. Turbulence distribution on roof and on the building structure, WD 90º , WW

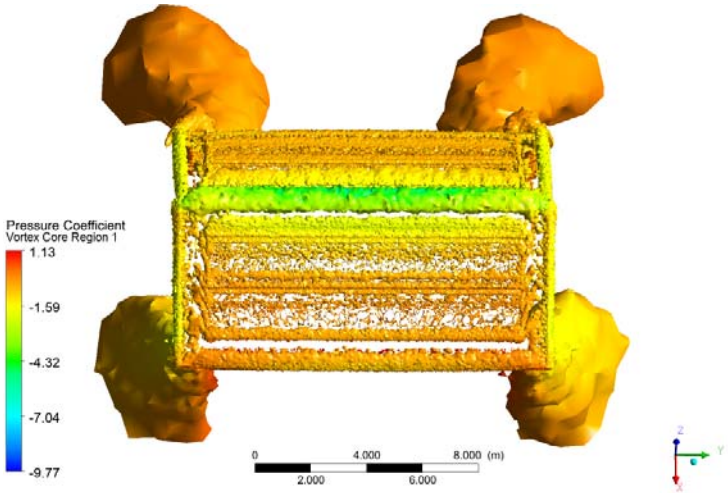


Fig. C. 114. Turbulence distribution on roof without building contour structure, WD 90º , WW

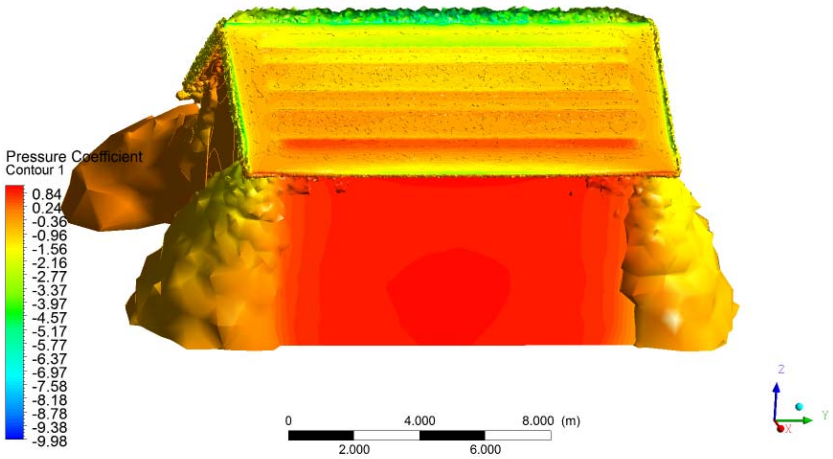


Fig. C. 115. Turbulence distribution on roof under panels, WD 90º , WW

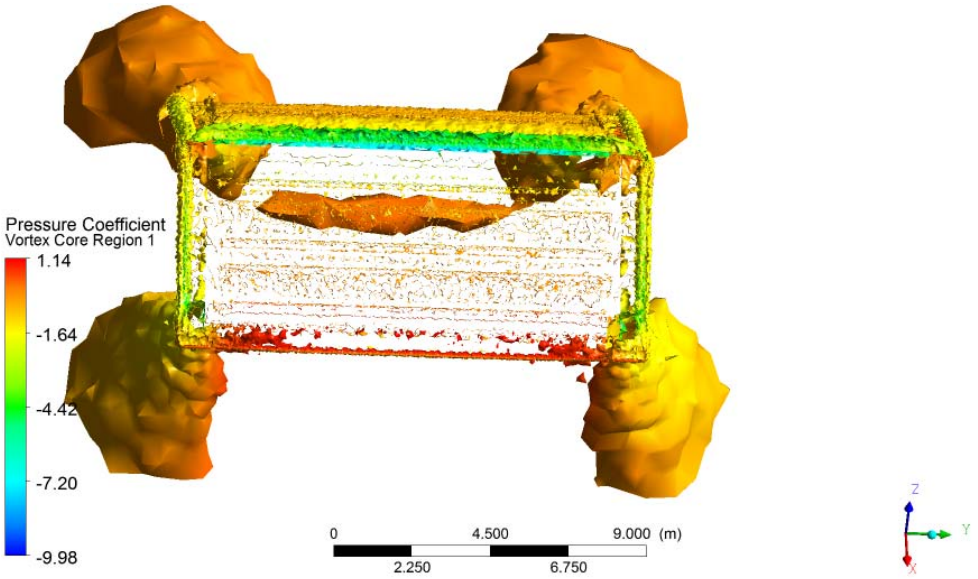


Fig. C. 116. Turbulence distribution on roof under panels, without building contour structure, WD 90º , WW

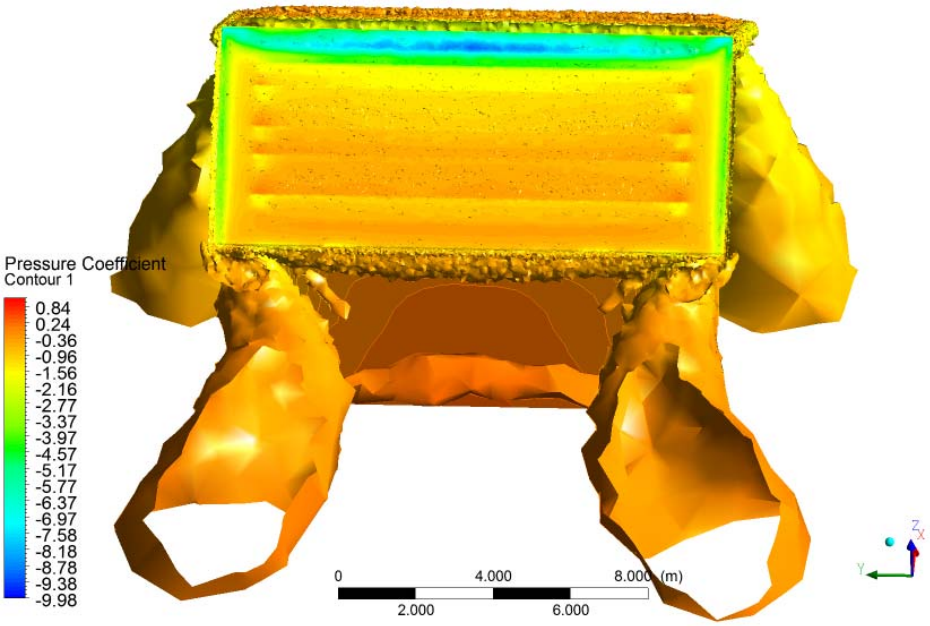


Fig. C. 117. Turbulence distribution on roof under panels, WD 90º , LW

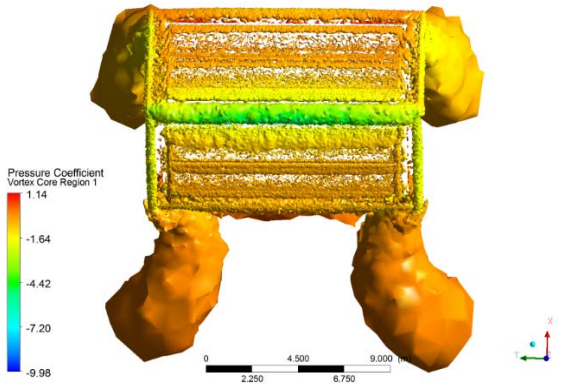


Fig. C. 118. Turbulence distribution on roof without building contour structure, WD 90º , LW

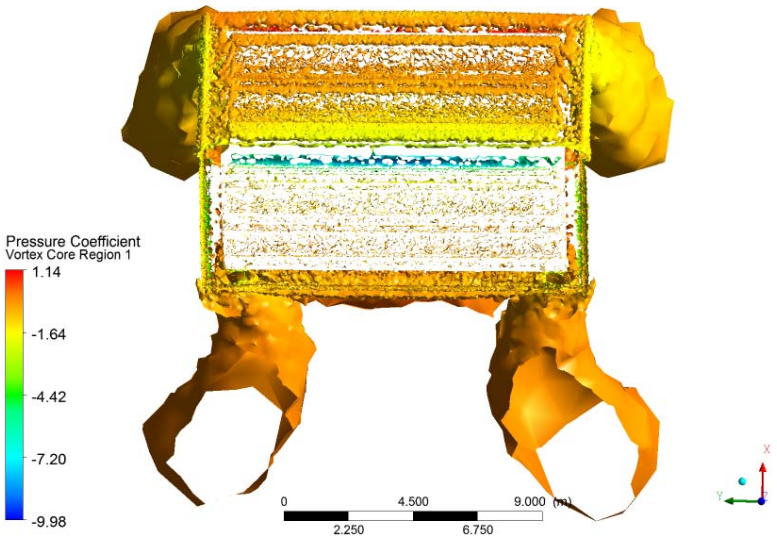


Fig. C. 119. Turbulence distribution on roof under panels, without building contour structure, WD 90º , LW

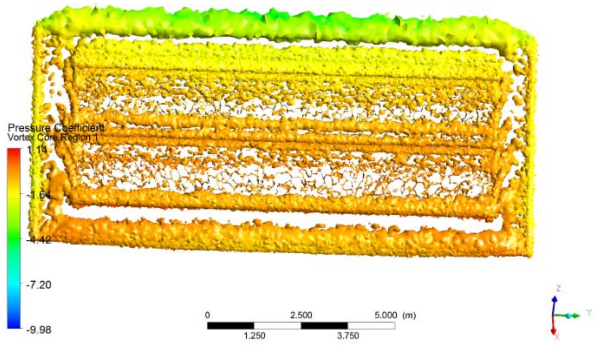


Fig. C. 120. Turbulence distribution, on top of the panels, No Building contours shown, WD 90º, WW

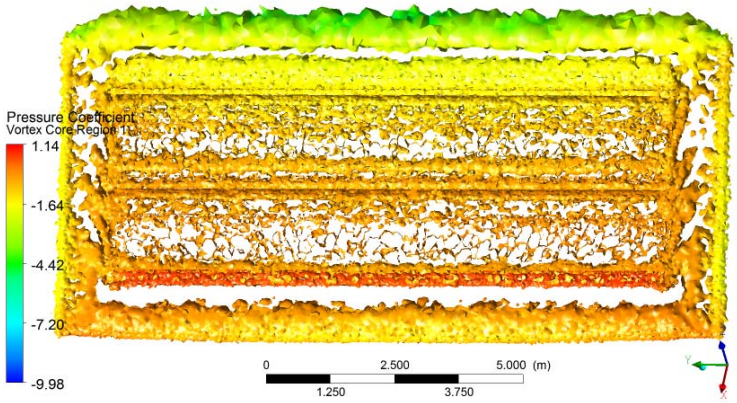


Fig. C. 121. Turbulence distribution, on bottom of the panels, No Building contours shown, WD 90º, WW

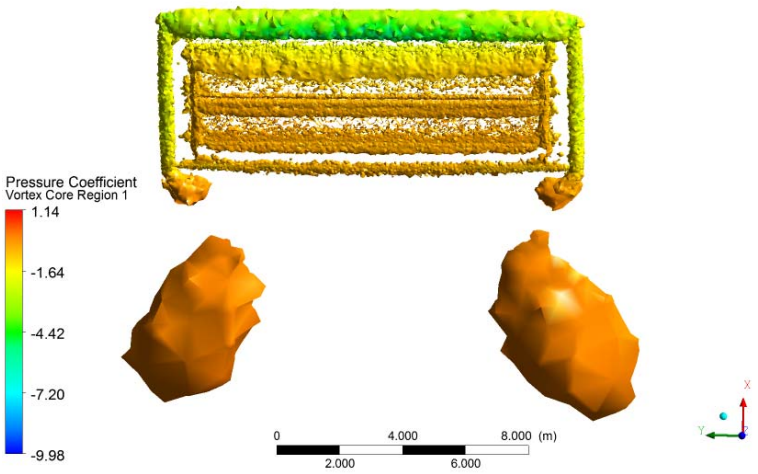


Fig. C. 122. Turbulence distribution, on top of the panels, No Building contours shown, WD 90º, LW

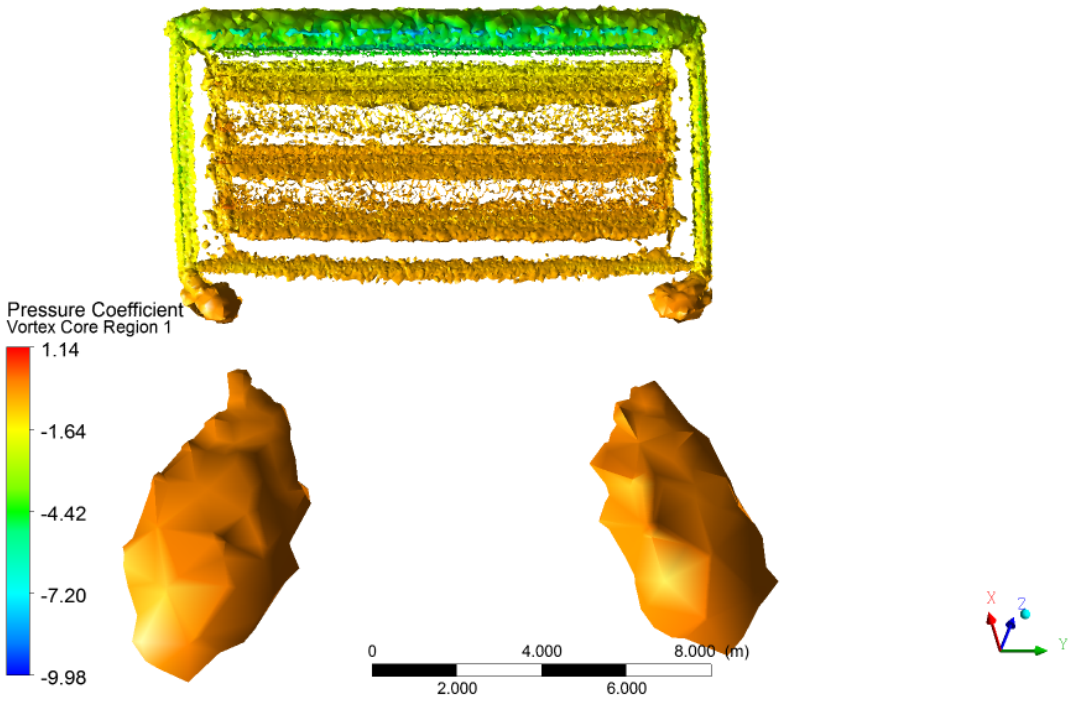


Fig. C. 123. Turbulence distribution, on bottom of the panels, No Building contours shown, WD 90º, LW

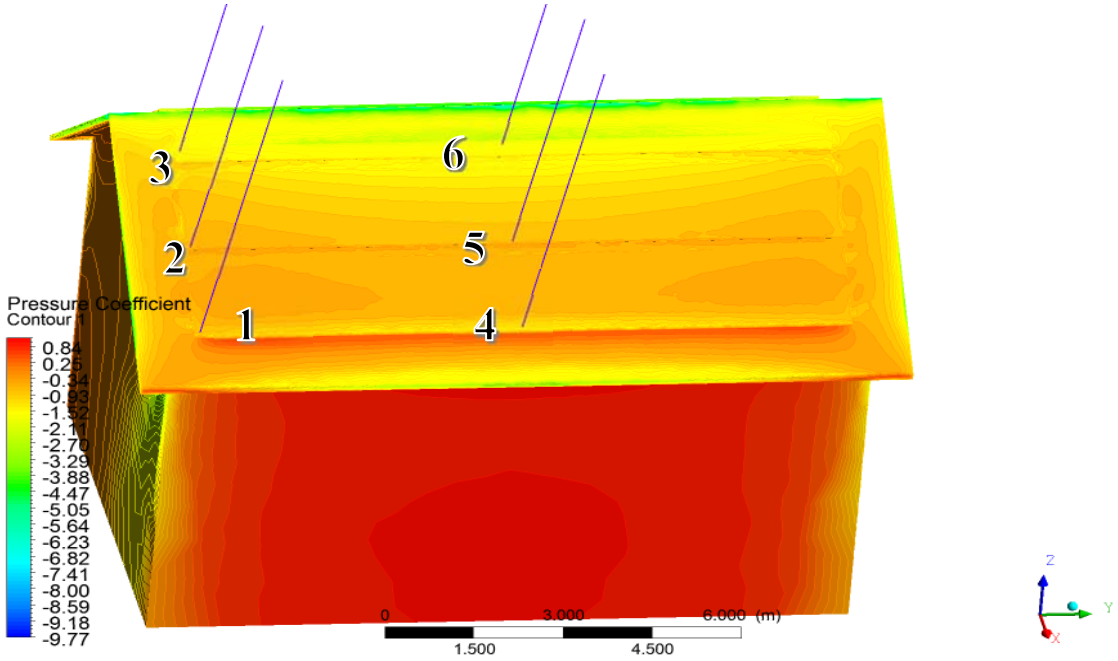


Fig. C. 124. The 6 lines used in detecting velocity and Cp changes along, WW

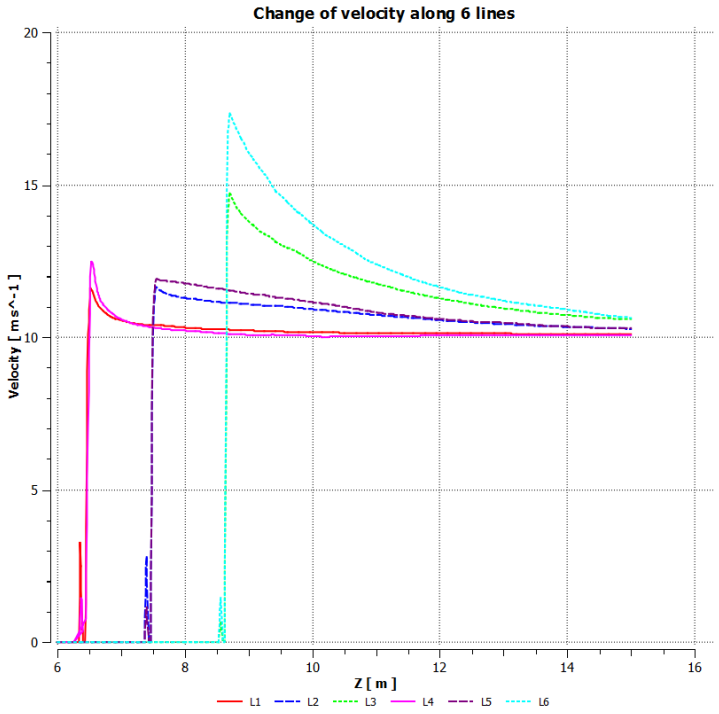


Fig. C. 125. Velocity changes between panels, and above roof, all 6 lines, WW

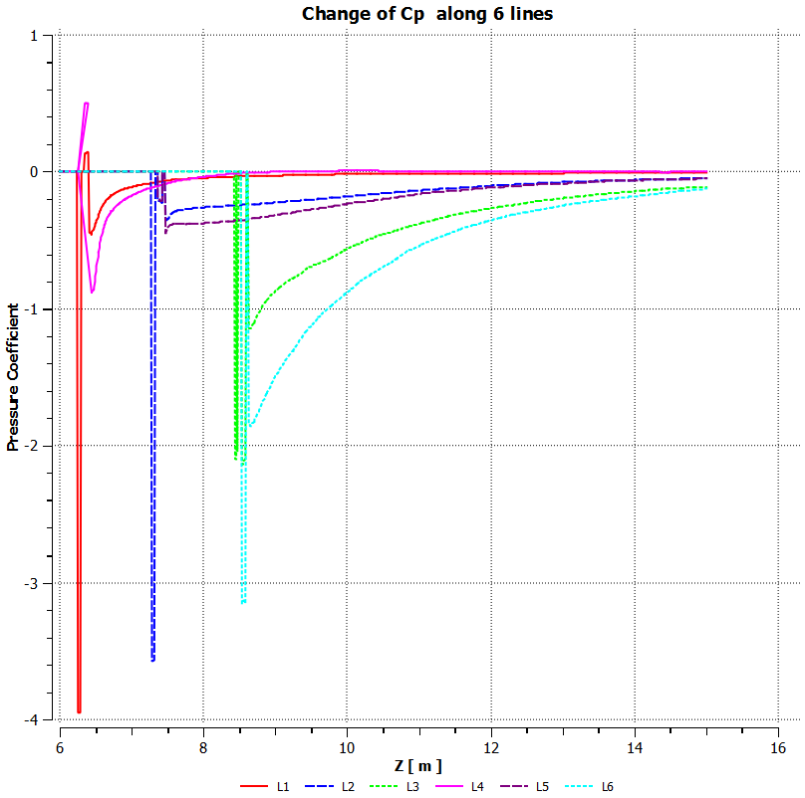
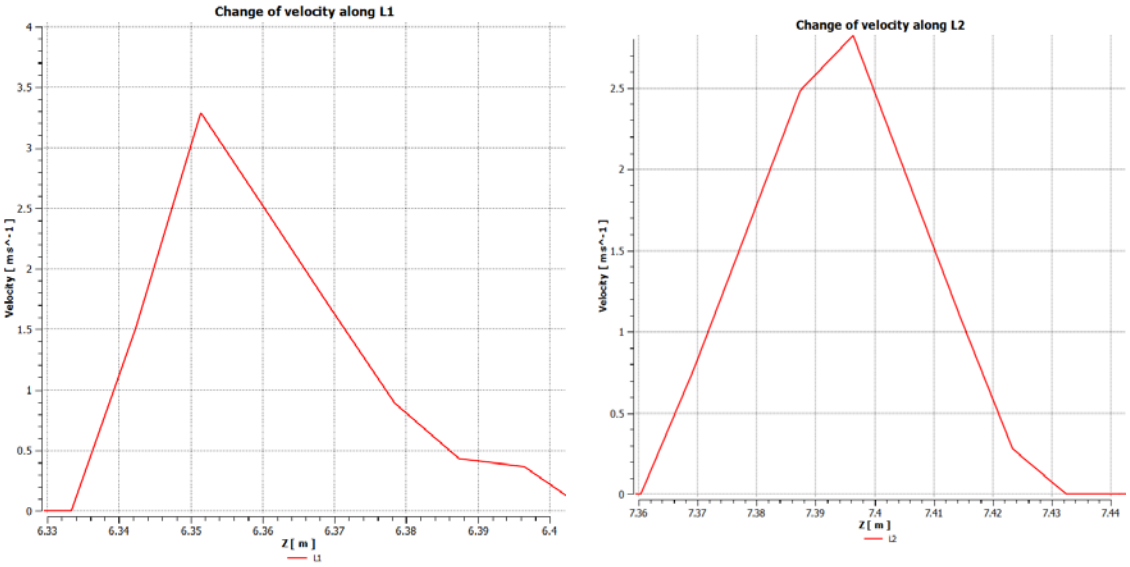


Fig. C. 126. Pressure changes between panels, and above roof, all 6 lines, WW



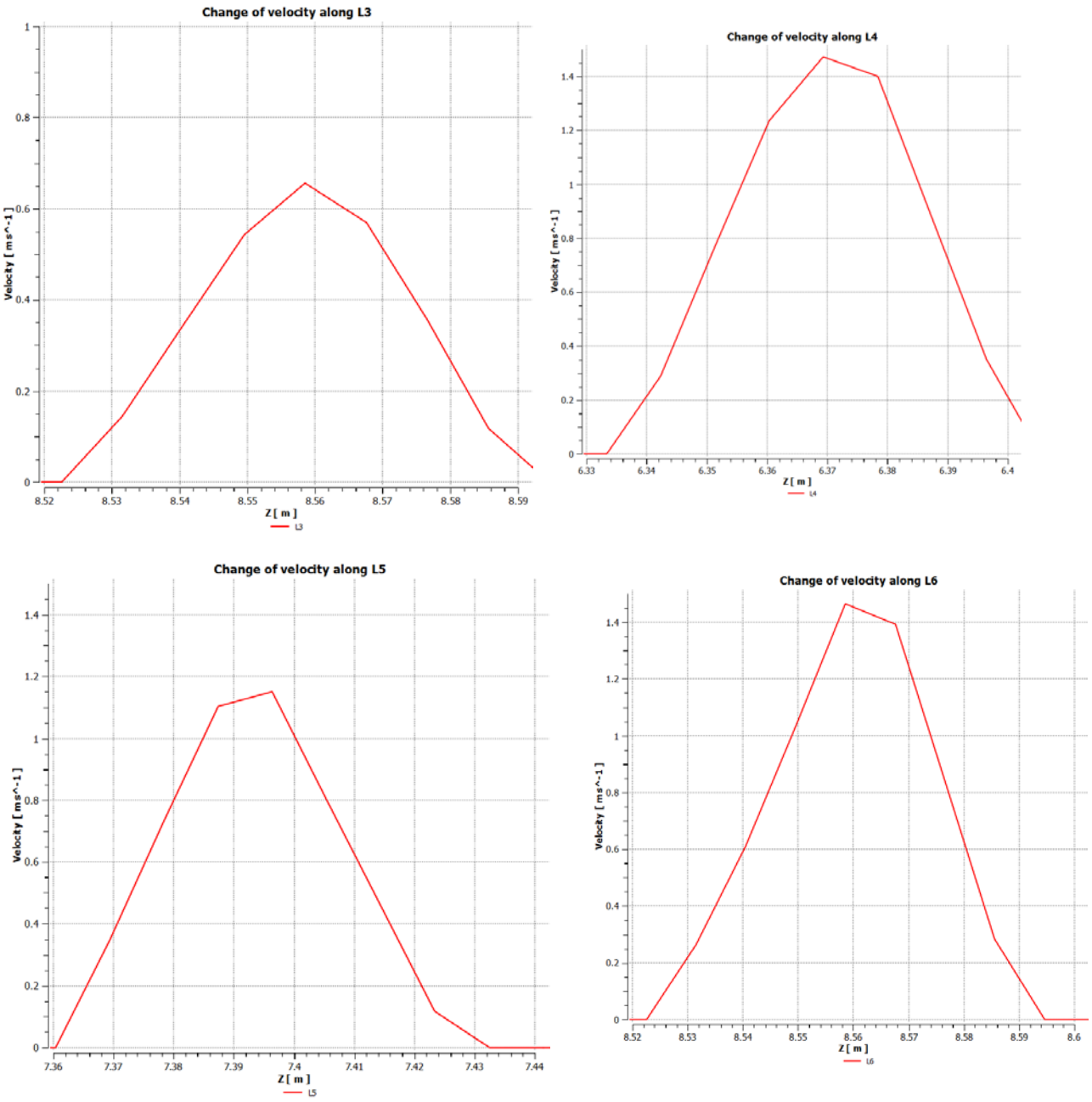
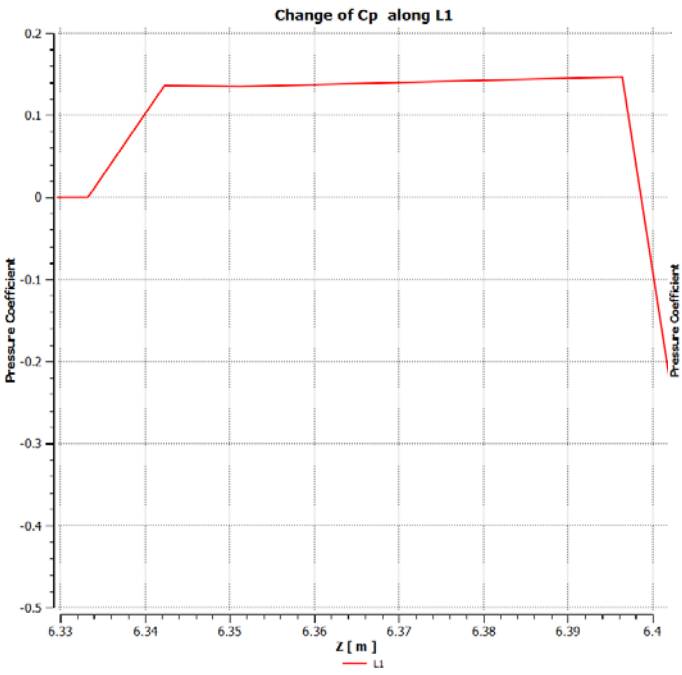
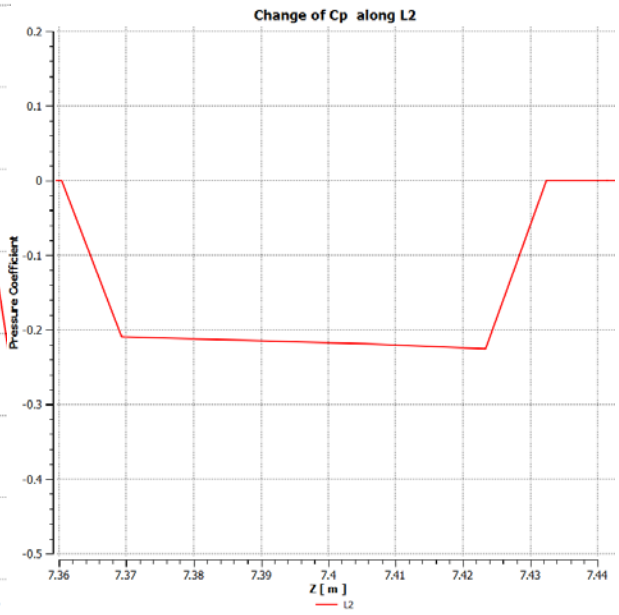
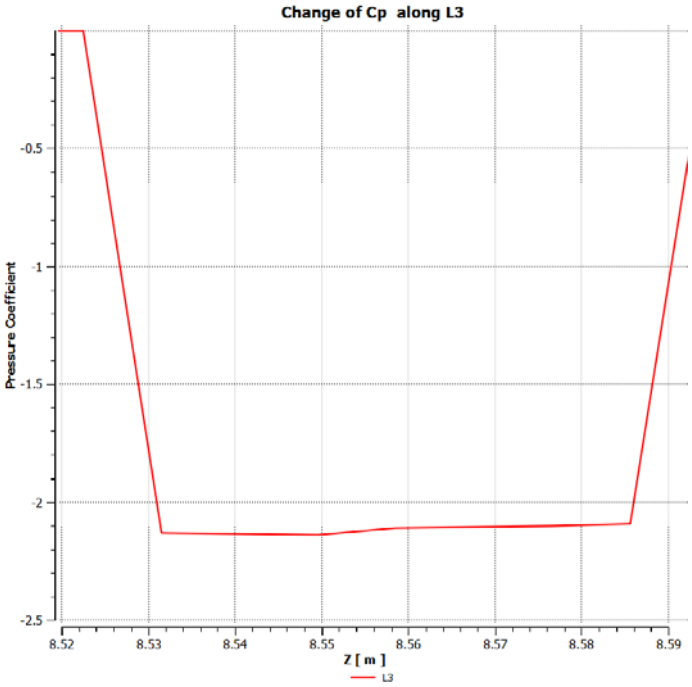
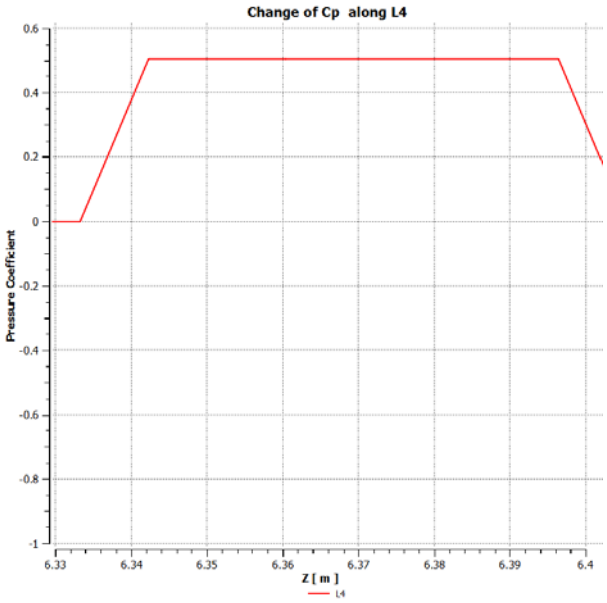


Fig. C. 127. Velocity changes between panels, each of the 6 lines, WW


Change of Cp along L1
Pressure Coefficient
Z [m]
L1


Change of Cp along L2
Pressure Coefficient
Z [m]
L2


Change of Cp along L3
Pressure Coefficient
Z [m]
L3


Change of Cp along L4
Pressure Coefficient
Z [m]
L4

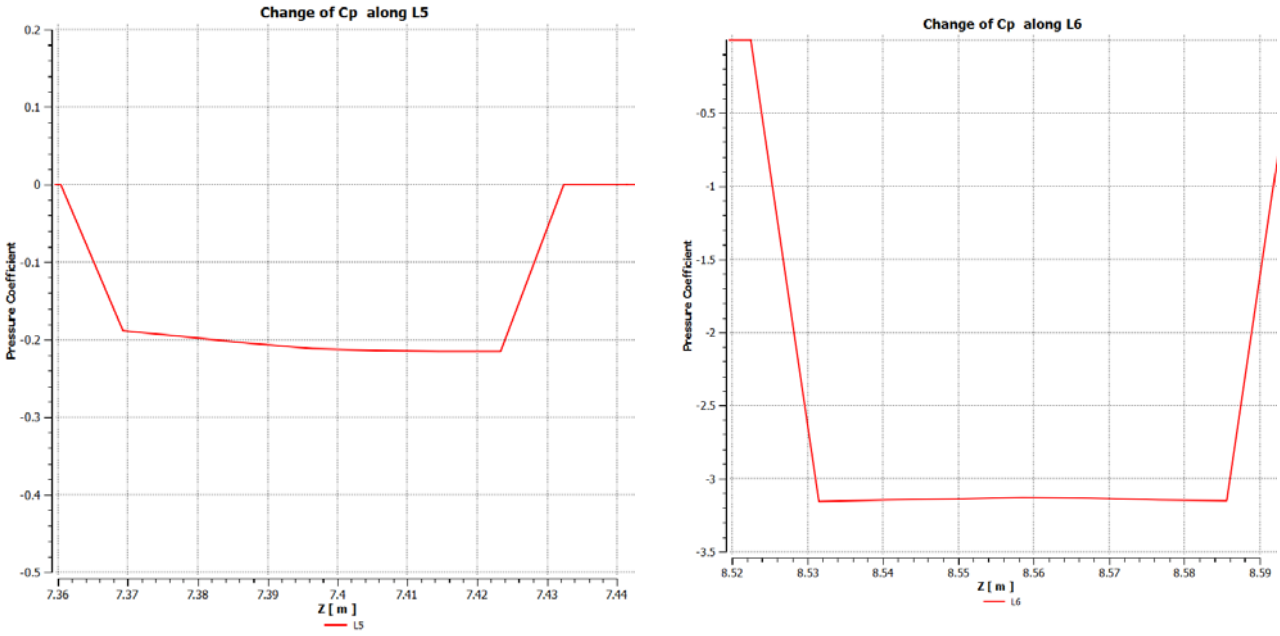


Fig. C. 128. Cp changes between panels, each of the 6 lines, WW

1.2.7. Calculation of resultant Cp of the three surfaces of roof mounted solar panels in comparison with bare roofs, Leeward, 2" apart, 10" roof space

Tabulated results of the integration,

Table C. 6. Cp on bare roofs vs. roof under solar panels, Slope 35º, 45º, windward

Polylines	Cp (SP)	Pr2	Cp Bott	Diff	Ttl Cp	Ttl/Brf
Pl1A	-0.65	0.2	0.23	-0.88	-0.68	4.00
Pl2	-0.28	0.22	0.24	-0.52	-0.3	1.67
Pl3	-0.24	-0.31	-0.28	0.04	-0.27	1.50
Pl4	-0.24	-0.26	-0.26	0.02	-0.24	1.26
Pl5	-0.25	-0.31	-0.31	0.06	-0.25	1.25
Pl6	-0.25	-0.36	-0.36	0.11	-0.25	1.19
Pl7	-0.26	-0.49	-0.49	0.23	-0.26	1.08
Pl8	-0.32	-0.25	-0.25	-0.07	-0.32	1.28
Pl9	-0.34	-0.22	-0.17	-0.17	-0.39	1.44
Pl10	-0.36	-0.94	-0.82	0.46	-0.48	1.66
Pl11	-0.4	-0.70	-0.69	0.29	-0.41	1.28
Pl12	-0.45	-0.61	-0.60	0.15	-0.46	1.28
Pl13	-0.54	-0.55	-0.54	0.00	-0.55	1.41
Pl14	-0.63	-1.07	-1.06	0.43	-0.64	1.36
Pl15	-0.85	-0.68	-0.65	-0.20	-0.88	1.76
Pl16	-0.98	-0.67	-0.62	-0.36	-1.03	2.19
Pl17a	-1.28	-1.95	-1.93	0.65	-1.3	2.60
Cp	-0.49	-0.53	-0.50	0.01	-0.51	1.60

SDT	0.30	0.50	0.50	0.37	0.31	0.72
Cov	0.62	0.95	0.99	26.51	0.60	0.45

Table C. 7. Cp bare roofs vs. roof under solar panels, Slope 35º, wind direction 45º, Leeward

Polylines	Cp (SP)	Pr2	Cp Bott	Diff	Ttl Cp	Ttl/Brf
Pl20a	-1.64	-1.86	-1.76	0.12	-1.74	1.16
Pl21	-1.37	-1.45	-1.44	0.07	-1.38	0.95
Pl22	-1.23	-1.18	-1.18	-0.05	-1.23	0.87
Pl23	-0.83	-0.97	-0.92	0.09	-0.88	0.63
Pl24	-0.76	-0.96	-1.06	0.30	-0.66	0.50
Pl25	-0.7	-0.87	-0.86	0.16	-0.71	0.56
Pl26	-0.66	-0.77	-0.76	0.10	-0.67	0.57
Pl27	-0.63	-0.64	-0.64	0.01	-0.63	0.58
Pl28	-0.58	-0.87	-0.89	0.31	-0.56	0.56
Pl29	-0.54	-0.56	-0.58	0.04	-0.52	0.57
Pl30	-0.45	-0.64	-0.58	0.13	-0.51	0.58
Pl31	-0.6	-0.73	-0.80	0.20	-0.53	0.62
Pl32	-0.6	-0.68	-0.68	0.08	-0.6	0.77
Pl33	-0.6	-0.60	-0.60	0.00	-0.6	0.83
Pl34	-0.6	-0.48	-0.48	-0.12	-0.6	0.91
Pl35	-0.61	-1.08	-1.09	0.48	-0.6	0.98
Pl36a	-0.68	-0.77	-0.80	0.12	-0.65	1.12
Cp	-0.77	-0.89	-0.89	0.12	-0.77	0.75
SDT	0.33	0.35	0.34	0.14	0.35	0.21
Cov	0.42	0.39	0.38	1.20	0.45	0.29

Table C. 8. Cp on bare roofs vs. roof under solar panels, Slope 35º, 90º, windward

Polylines	Cp (SP)	Pr2	Cp Bott	Diff	Ttl Cp	Ttl/Brf
Pl1A	-0.62	0.55	0.55	-1.17	-0.62	31.00
Pl2	-0.39	0.25	0.39	-0.78	-0.53	-26.50
Pl3	-0.2	-0.21	-0.19	-0.01	-0.22	-13.75
Pl4	-0.2	-0.11	-0.11	-0.09	-0.2	40.00
Pl5	-0.21	-0.07	-0.07	-0.14	-0.21	7.00
Pl6	-0.24	-0.04	-0.04	-0.20	-0.24	4.44
Pl7	-0.26	-0.42	-0.38	0.12	-0.3	5.00
Pl8	-0.36	-0.21	-0.17	-0.19	-0.4	5.80
Pl9	-0.39	-0.80	-0.78	0.39	-0.41	4.41
Pl10	-0.45	-0.68	-0.66	0.21	-0.47	3.73
Pl11	-0.55	-0.62	-0.62	0.07	-0.55	3.20
Pl12	-0.65	-0.57	-0.57	-0.08	-0.65	2.95
Pl13	-0.74	-0.56	-0.56	-0.18	-0.74	2.69
Pl14	-0.88	-1.20	-1.15	0.27	-0.93	2.66
Pl15	-1.37	-0.88	-0.84	-0.53	-1.41	3.71
Pl16	-1.44	-1.00	-0.89	-0.55	-1.55	5.64
Pl17a	-2.05	-2.75	-2.69	0.64	-2.11	6.03
Cp	-0.65	-0.55	-0.52	-0.13	-0.68	4.49
SDT	0.52	0.73	0.72	0.44	0.54	14.30

Cov	0.81	1.32	1.39	3.38	0.79	3.19

Table C. 9. Cp bare roofs vs. roof under solar panels, Slope 35º, wind direction 90º, Leeward

Polylines	Cp (SP)	Pr2	Cp Bott	Diff	Ttl Cp	Ttl/Brf
Pl20	-2.79	-3.97	-3.94	1.15	-2.82	1.08
Pl21	-2.06	-1.84	-1.74	-0.32	-2.16	0.85
Pl22	-1.8	-1.70	-1.69	-0.11	-1.81	0.72
Pl23	-1.2	-1.29	-1.27	0.07	-1.22	0.50
Pl24	-1.08	-1.12	-1.11	0.03	-1.09	0.47
Pl25	-0.96	-1.02	-1.01	0.05	-0.97	0.45
Pl26	-0.84	-0.91	-0.9	0.06	-0.85	0.43
Pl27	-0.75	-0.8	-0.79	0.04	-0.76	0.43
Pl28	-0.66	-0.77	-0.77	0.11	-0.66	0.42
Pl29	-0.58	-0.66	-0.65	0.07	-0.59	0.41
Pl30	-0.69	-0.40	-0.39	-0.30	-0.7	0.53
Pl31	-0.55	-0.61	-0.60	0.05	-0.56	0.49
Pl32	-0.5	-0.50	-0.49	-0.01	-0.51	0.53
Pl33	-0.47	-0.43	-0.43	-0.04	-0.47	0.57
Pl34	-0.47	-0.38	-0.37	-0.10	-0.48	0.69
Pl35	-0.48	-0.98	-0.99	0.51	-0.47	0.77
Pl36a	-0.53	-0.76	-0.75	0.22	-0.54	0.90
Cp	-0.70	-0.76	-0.75	0.05	-0.71	0.54
SDT	0.24	0.28	0.28	0.18	0.24	0.15
Cov	0.34	0.37	0.37	3.24	0.35	0.27

Table C. 10. Cp on bare roofs vs. roof under solar panels, Slope 35º, 0.0º

Polylines	Cp (SP)	Pr2	Cp Bott	Diff	Ttl Cp	Ttl/Brf
Pl1A	-0.36	-0.34	-0.34	-0.02	-0.36	1.03
Pl2	-0.36	-0.35	-0.35	-0.01	-0.36	1.03
Pl3	-0.36	-0.43	-0.43	0.07	-0.36	1.03
Pl4	-0.36	-0.43	-0.43	0.07	-0.36	1.03
Pl5	-0.36	-0.43	-0.43	0.07	-0.36	1.03
Pl6	-0.36	-0.43	-0.43	0.07	-0.36	1.00
Pl7	-0.37	-0.46	-0.46	0.09	-0.37	1.03
Pl8	-0.35	-0.5	-0.5	0.15	-0.35	0.97
Pl9	-0.36	-0.48	-0.48	0.12	-0.36	1.03
Pl10	-0.35	-0.58	-0.57	0.22	-0.36	1.03
Pl11	-0.35	-0.58	-0.57	0.22	-0.36	1.03
Pl12	-0.35	-0.58	-0.57	0.22	-0.36	1.03
Pl13	-0.35	-0.57	-0.57	0.22	-0.35	1.00
Pl14	-0.35	-0.42	-0.42	0.07	-0.35	1.00
Pl15	-0.35	-0.37	-0.37	0.02	-0.35	1.00
Pl16	-0.35	-0.37	-0.37	0.02	-0.35	1.03
Pl17a	-0.35	-0.37	-0.37	0.02	-0.35	1.03
Cp	-0.36	-0.45	-0.45	0.10	-0.36	1.02
SDT	0.01	0.08	0.08	0.08	0.01	0.02
Cov	0.02	0.19	0.18	0.87	0.02	0.02

1.3. 8” Spacing, 10” Clearance

1.3.1. Wind direction 45º,

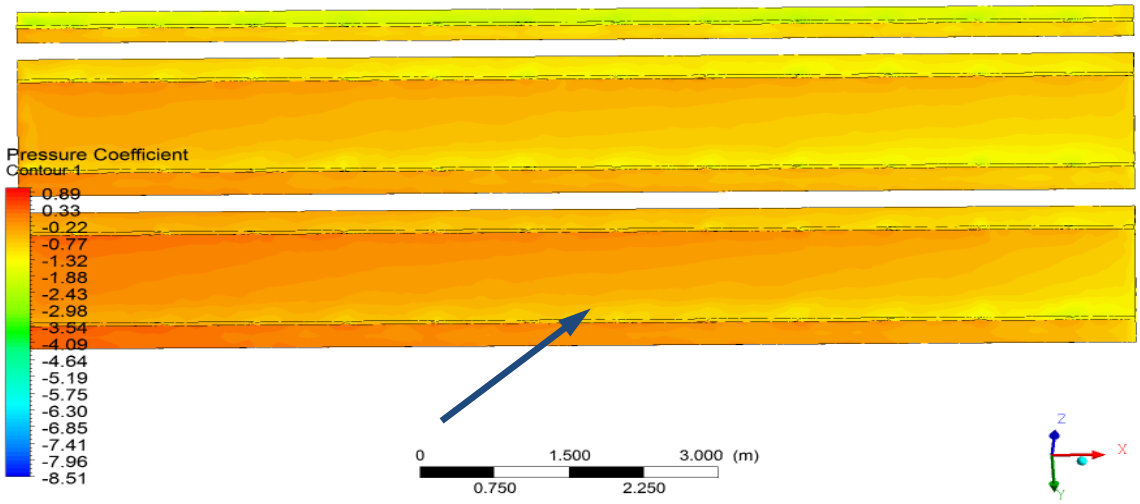


Fig. C. 129. Cp on bottom of the solar panels, WW, WD 45º

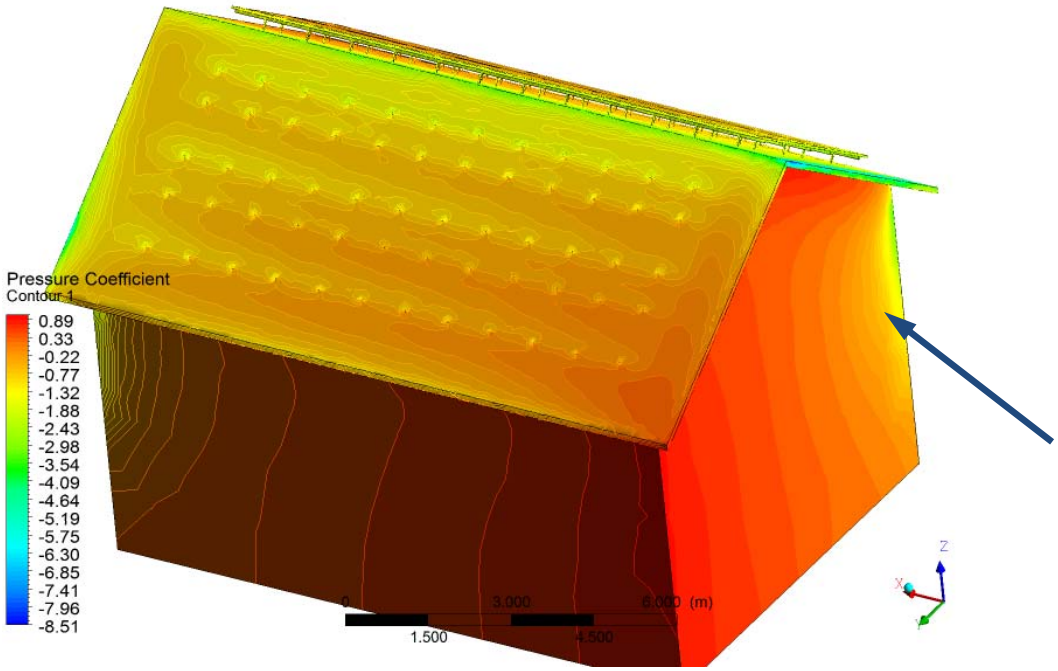


Fig. C. 130. Cp on Roof under the solar panels, solar panels cut off, WW, WD 45º

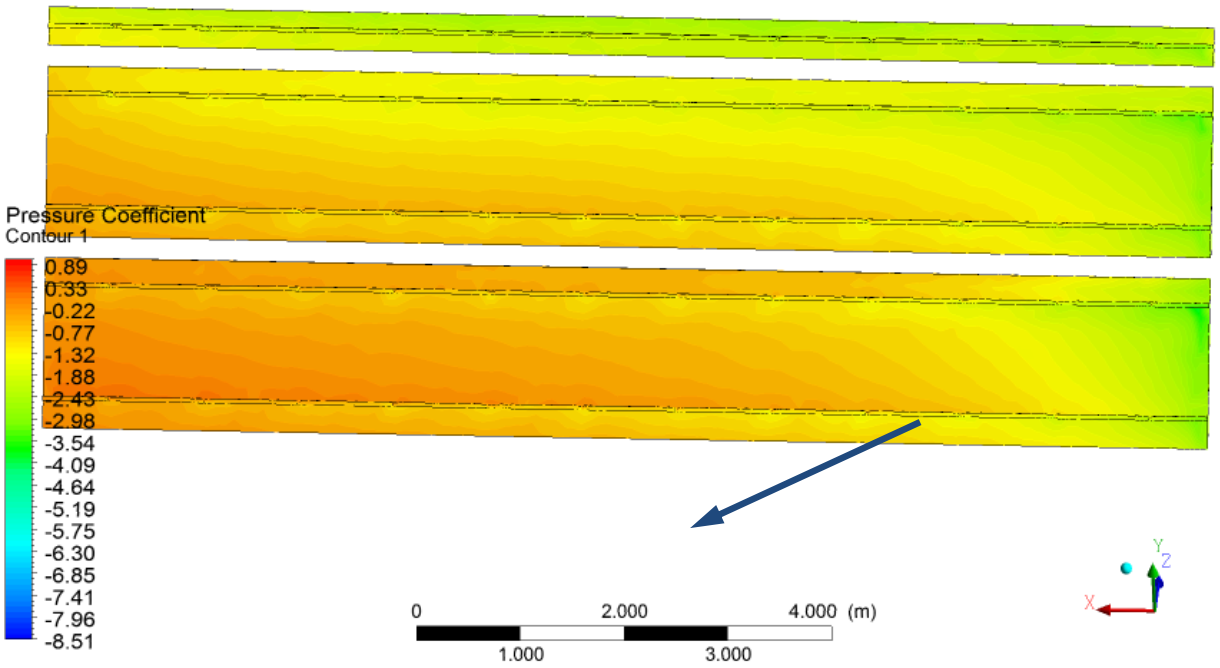


Fig. C. 131. Cp on bottom of the solar panels, LW, WD 45º

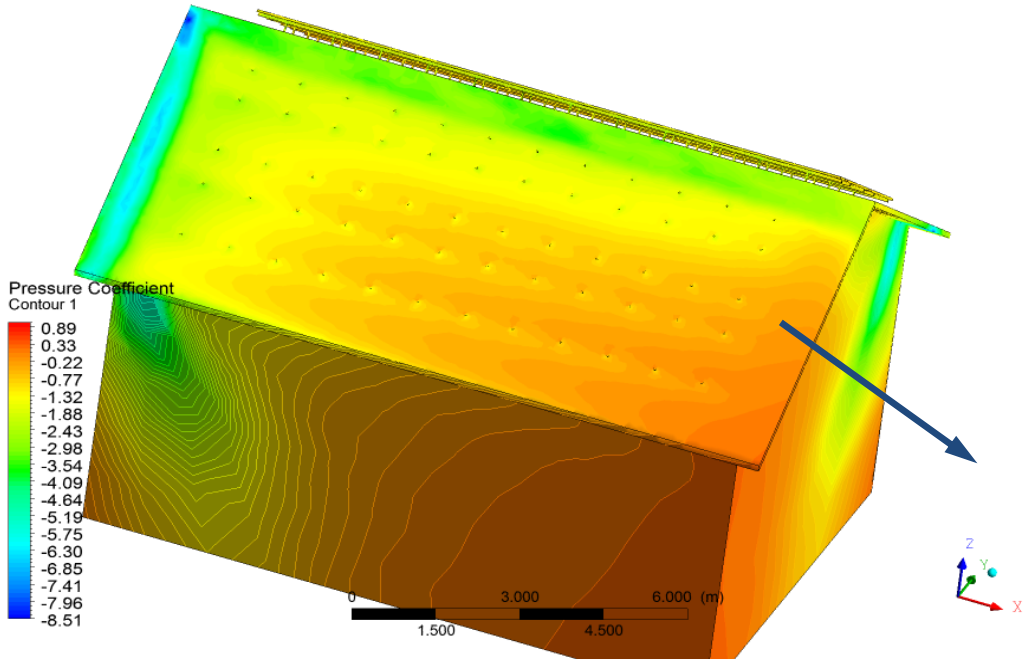


Fig. C. 132. Cp on Roof under the solar panels, solar panels cut off, LW, WD 45º

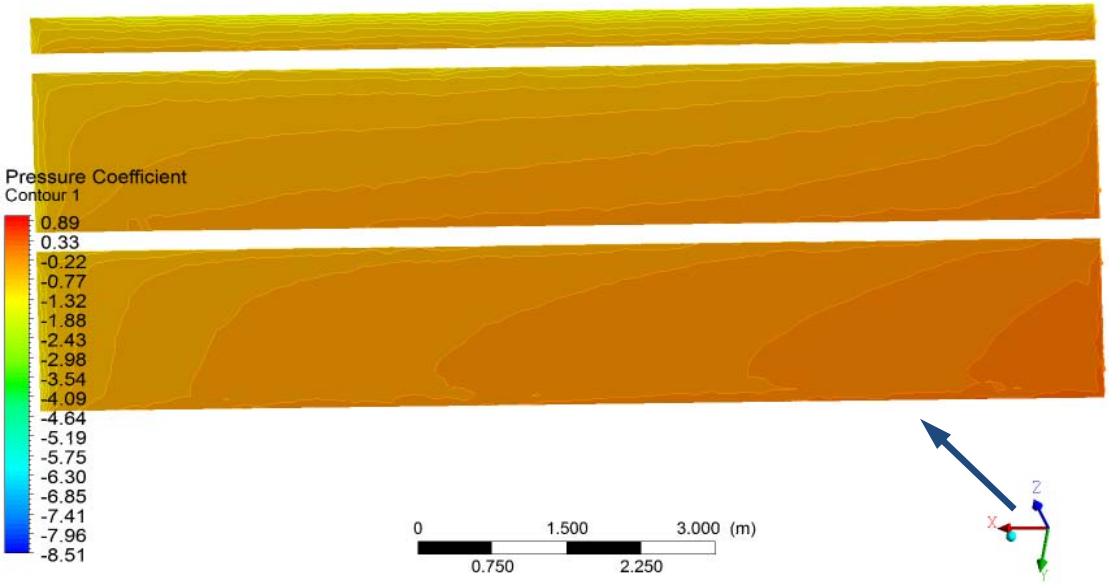


Fig. C. 133. Cp on top of the solar panel, WW, WD 45º

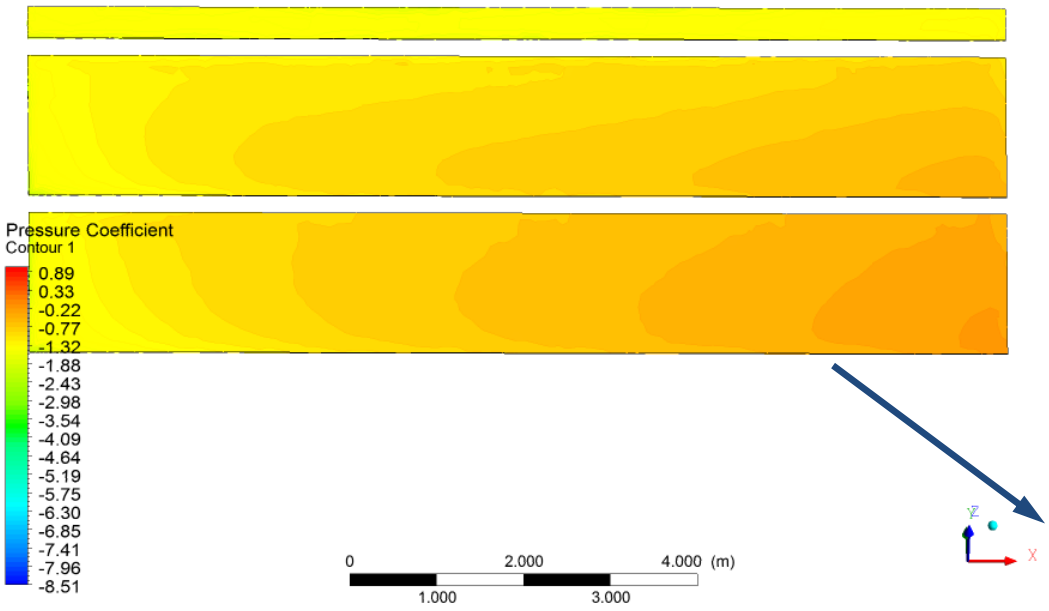


Fig. C. 134. Cp on top of the solar panel, LW, WD 45º

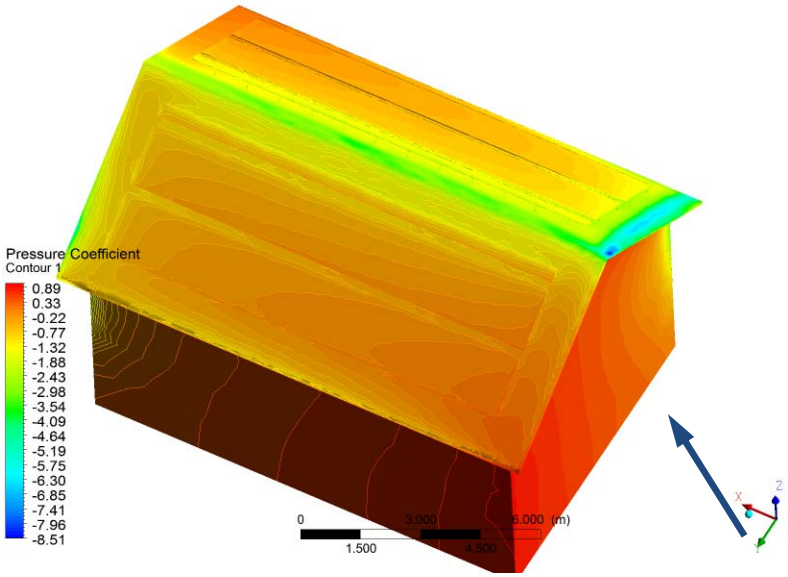


Fig. C. 135. Pressure coefficient on top surface of the solar panels WD 45º, WW, WD 45º

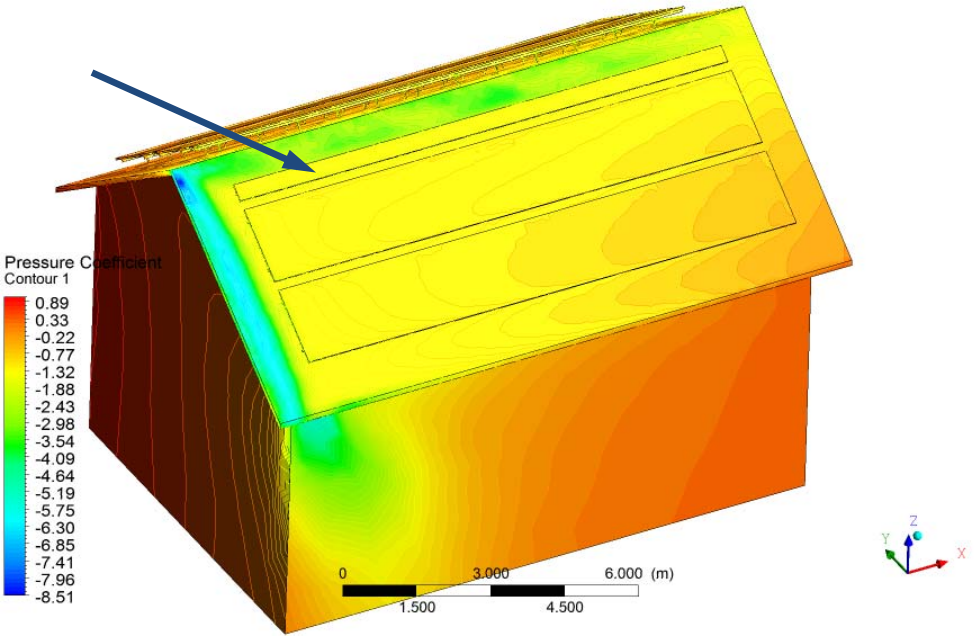


Fig. C. 136. Pressure coefficient on top surface of the solar panels WD 45º, LW, WD 45º

1.3.2. WIND DIRECTION 90º

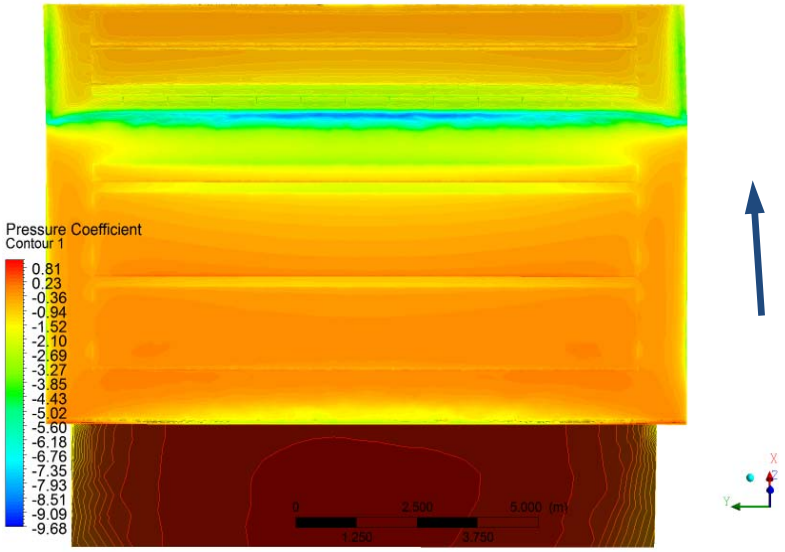


Fig. C. 137. CP on whole building and solar panels, S 35º, WW, WD 90º

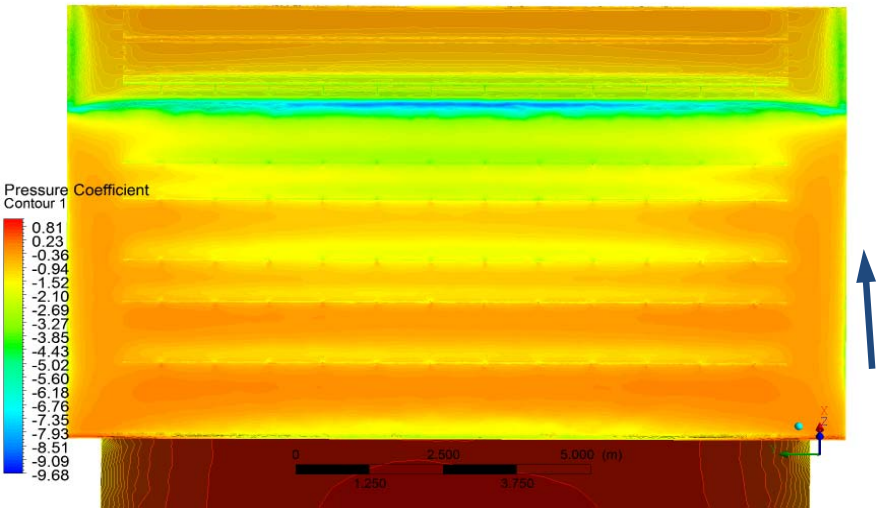


Fig. C. 138. CP on roof under solar panels, S 35º, WW, WD 90º

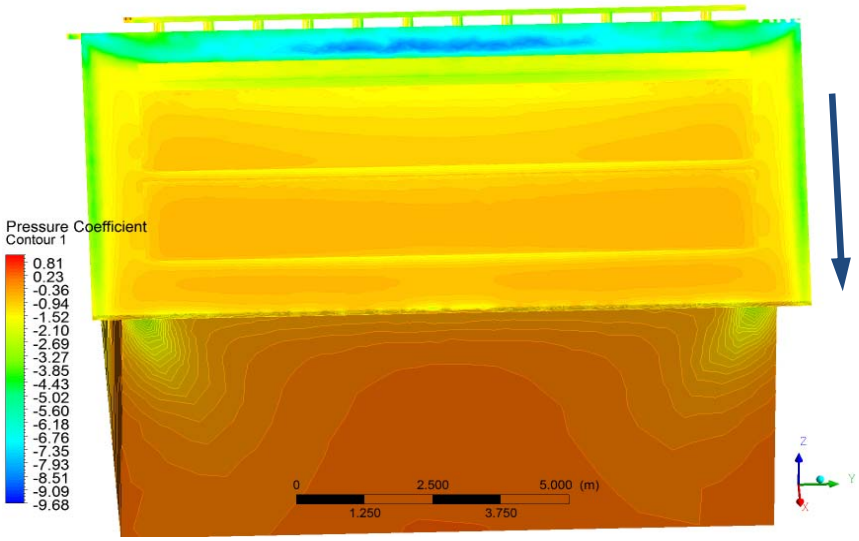


Fig. C. 139. CP on whole building and solar panels, S 35º, LW, WD 90º

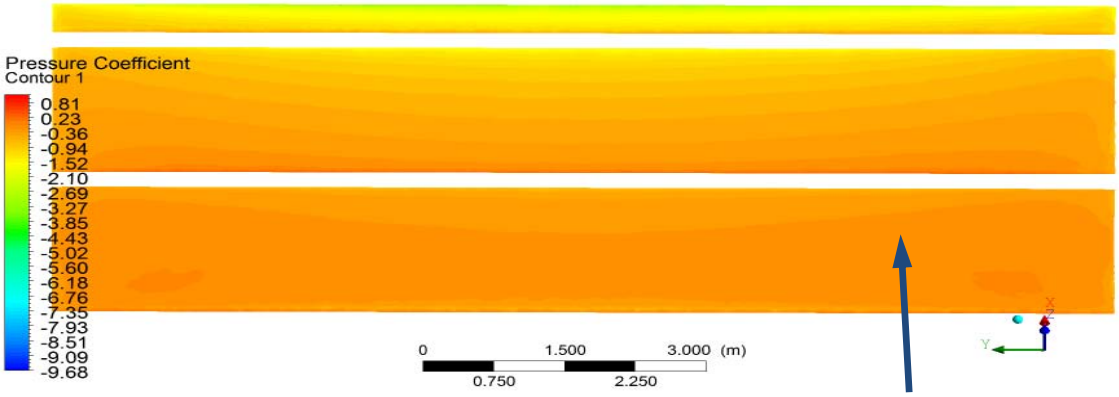


Fig. C. 140. CP on top of solar panels, S 35º, WW, WD 90º

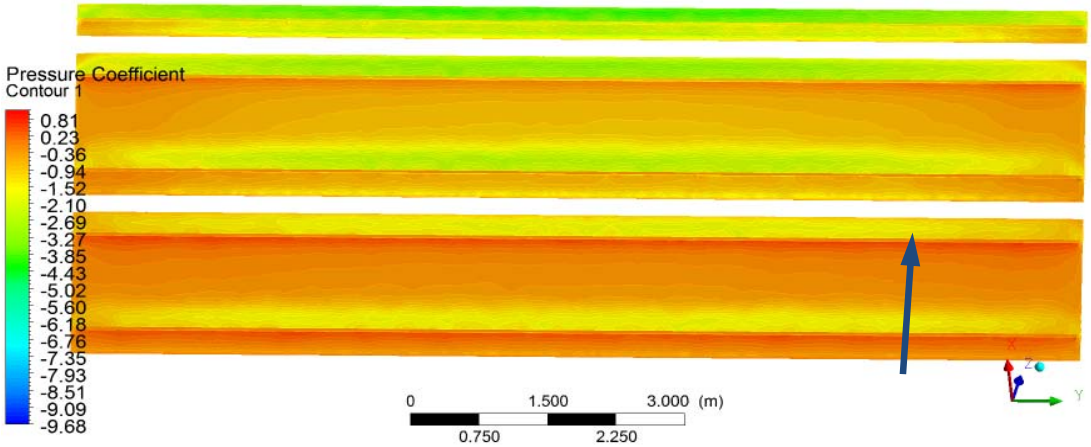


Fig. C. 141. CP on bottom of solar panels, S 35º, WW, WD 90º

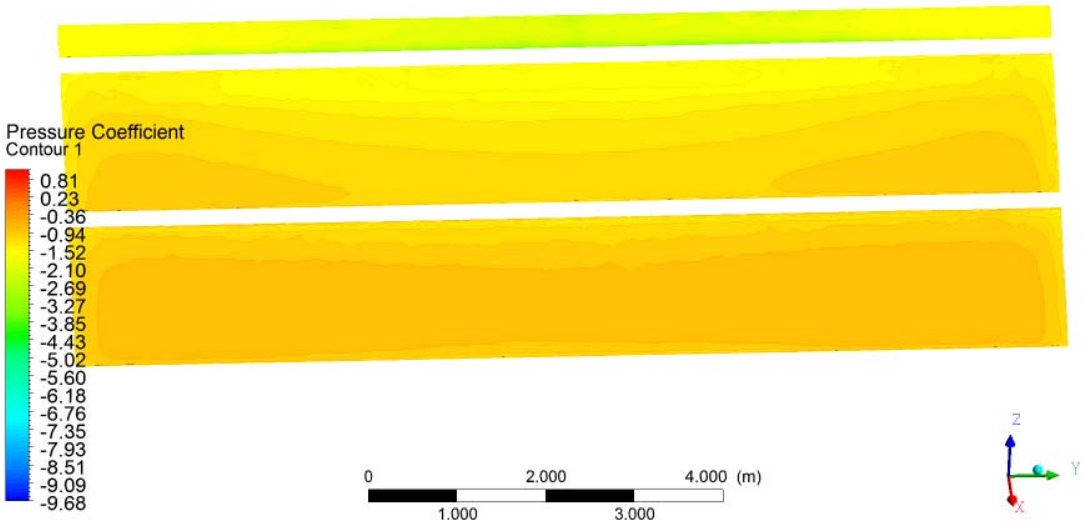


Fig. C. 142. CP on top of solar panels, S 35º, LW, WD 90º

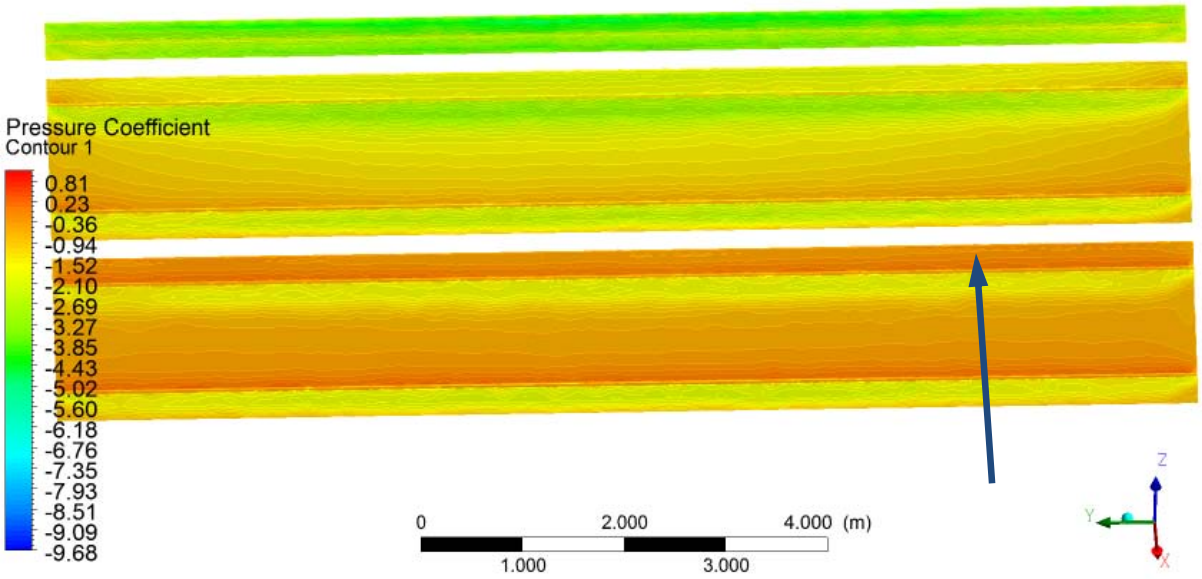


Fig. C. 143. CP on bottom of solar panels, S 35º, LW, WD 90º

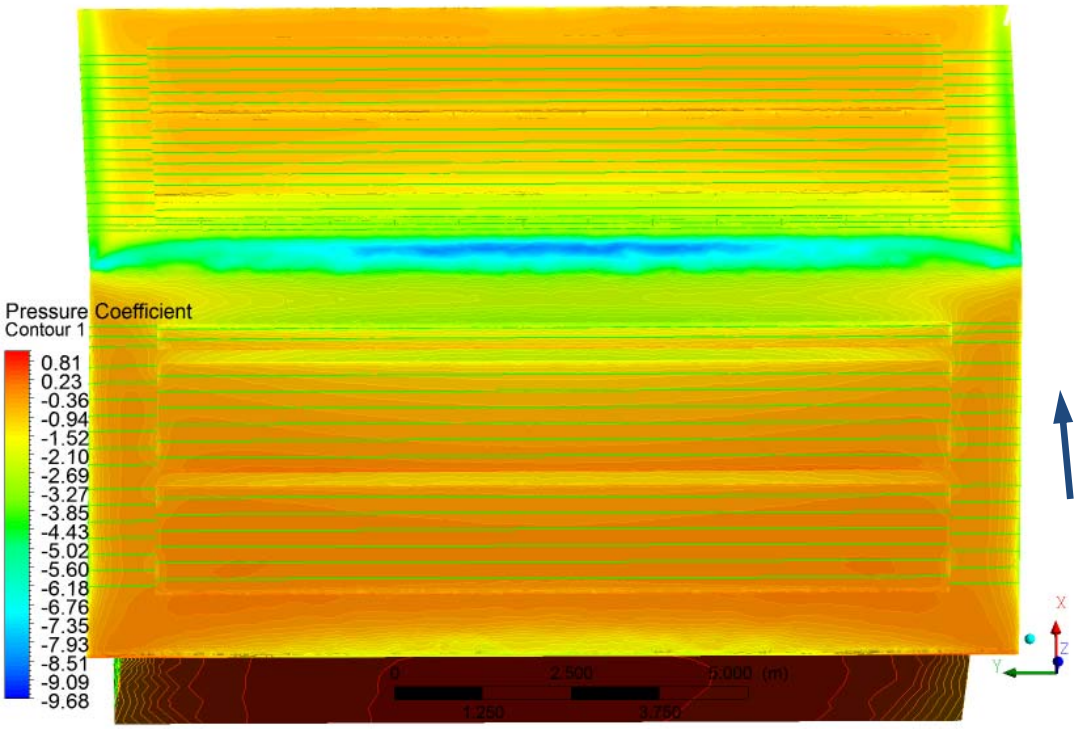


Fig. C. 144. Cp on top of solar panels with plines, S 35º, WW, WD 90º

1.3.3. WIND DIRECTION 0.0º



Fig. C. 145. Cp on roof with solar panels, S 35º, WD 0.0º

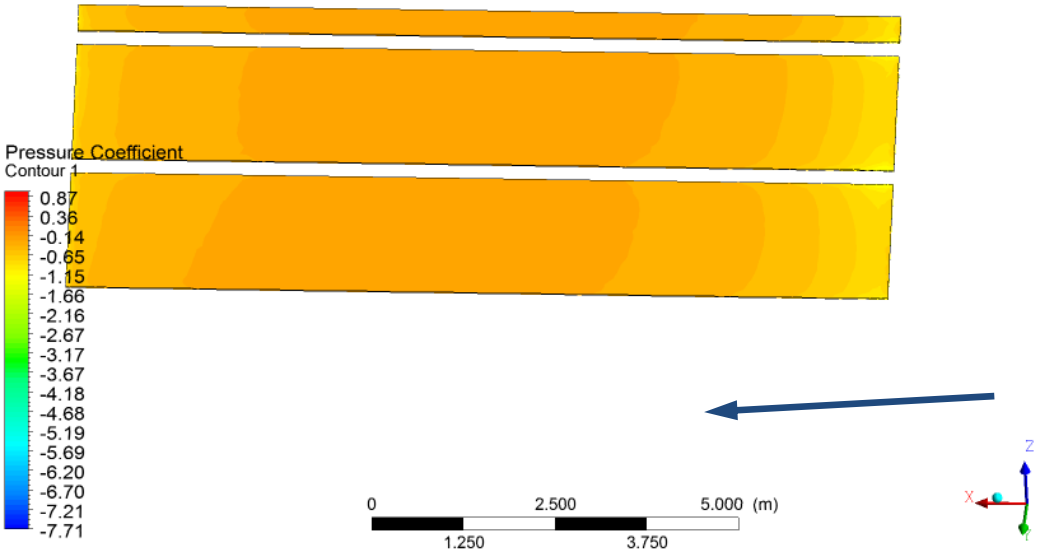


Fig. C. 146. Cp on top of solar panels, S 35º, WD 0.0º

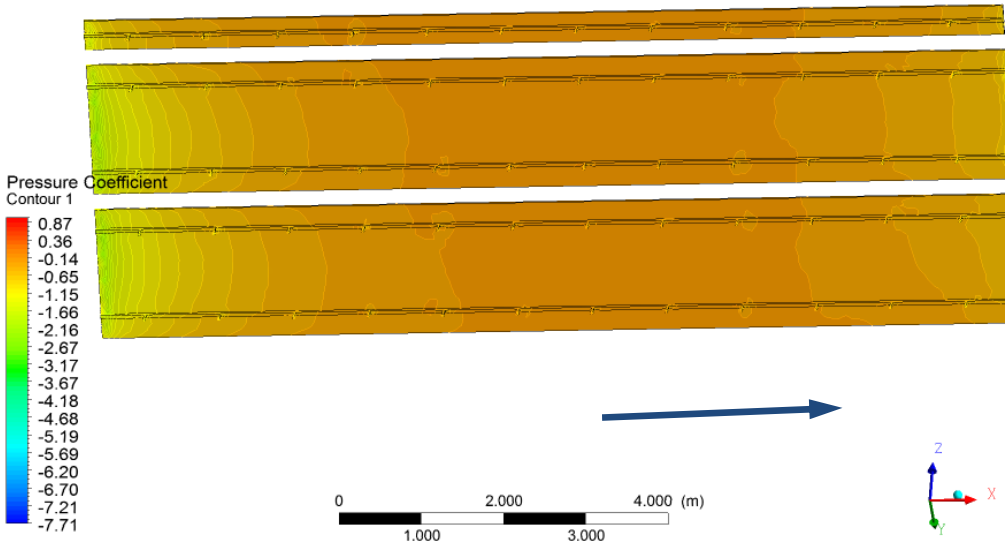


Fig. C. 147. Cp on bottom of solar panels, S 35º, WW, WD 0.0º

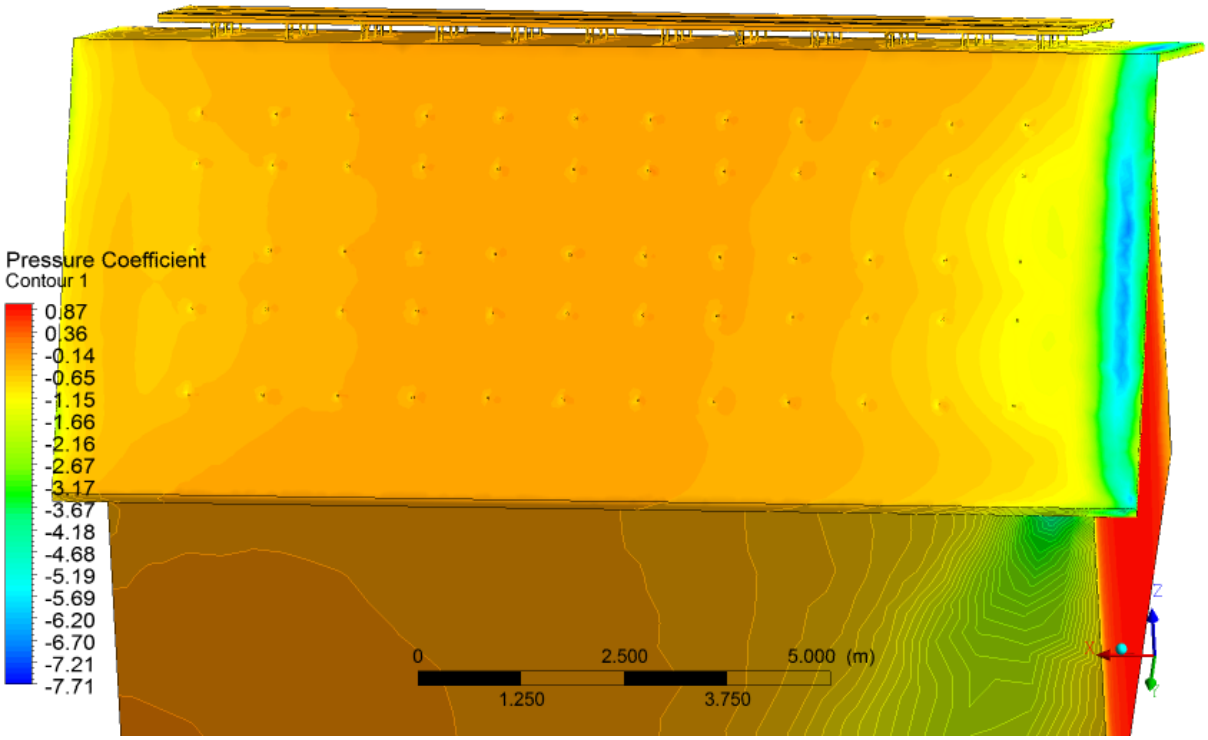


Fig. C. 148. Cp on roof under the solar panels, S 35º, WW, WD 0.0º

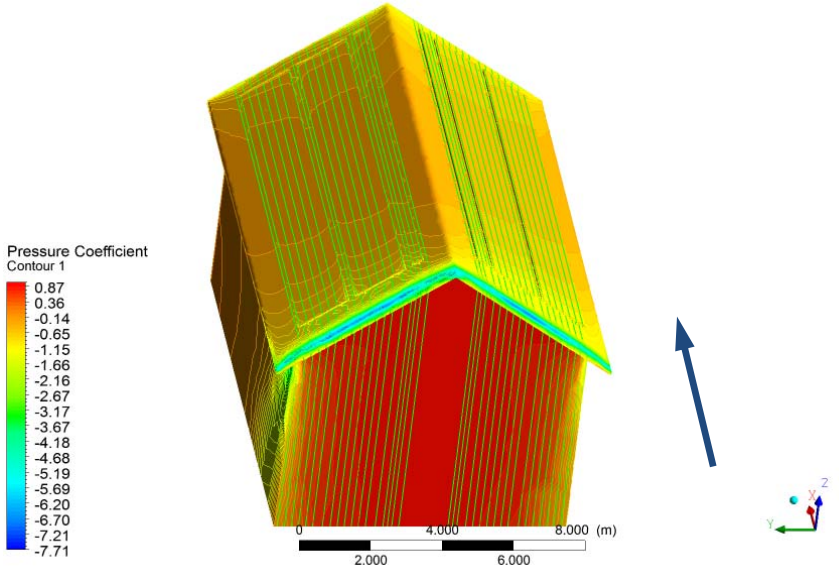


Fig. C. 149. Cp on top of solar panels and roof with Plines, S 35º, WW, WD 0º

1.3.4. Detailed Distribution of Wind Pressure on roof mounted solar panels in comparison with bare roofs, Windward, S8" , C10"

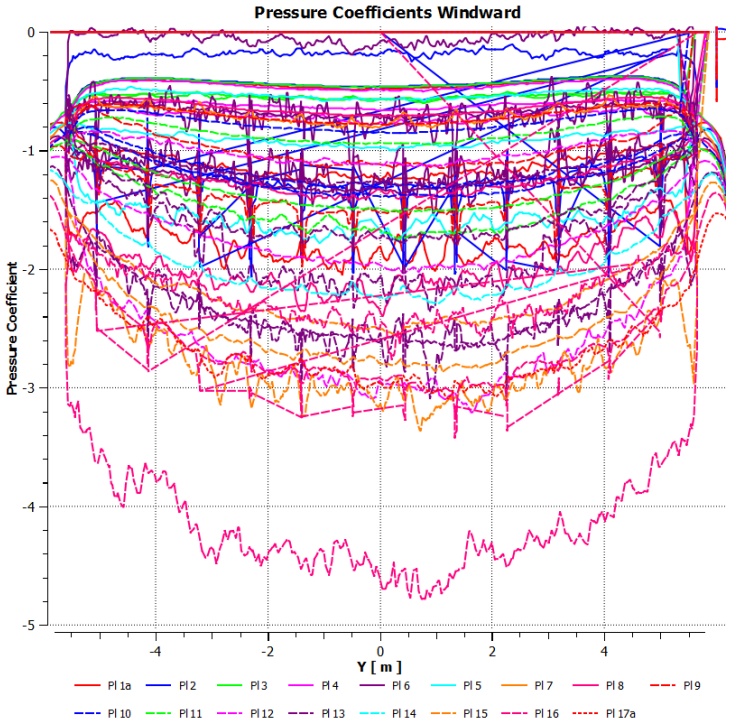


Fig. C. 150. Cp, All polylines, S 35 º, WW, WD 90 º

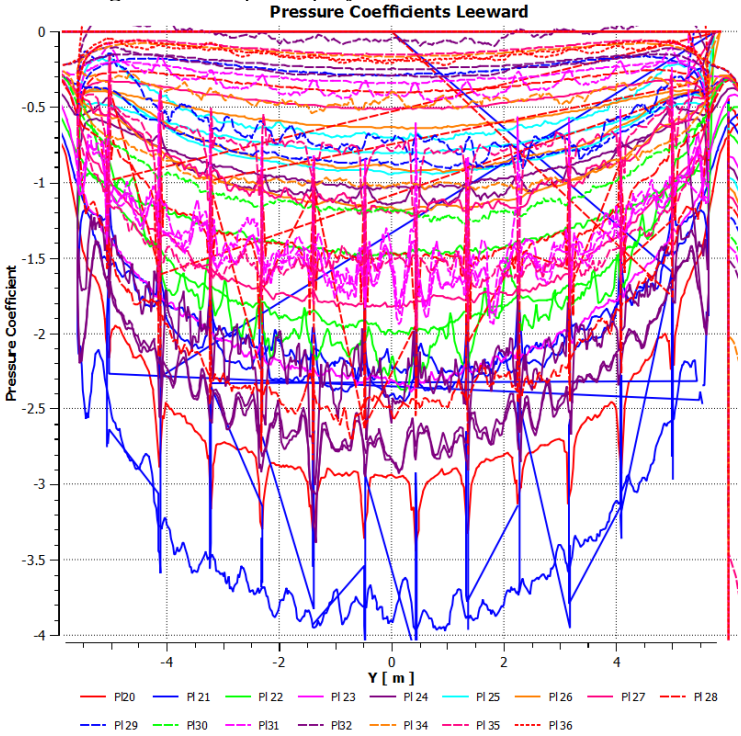


Fig. C. 151. Cp, All polylines, S 35 º, LW, WD 90 º

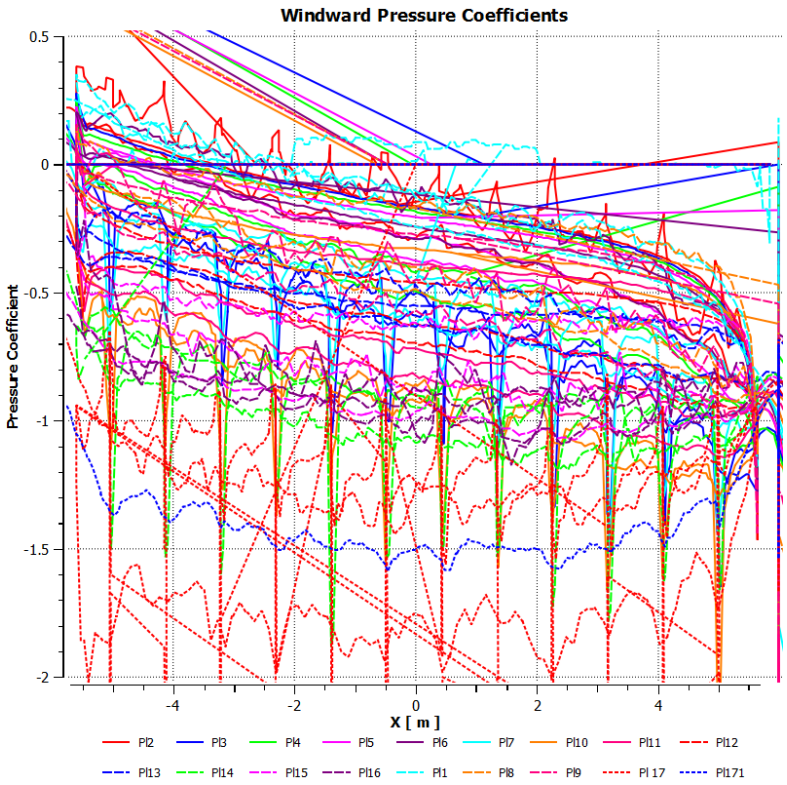


Fig. C. 152. Cp, All polylines, S 35 º, WW, WD 45 º

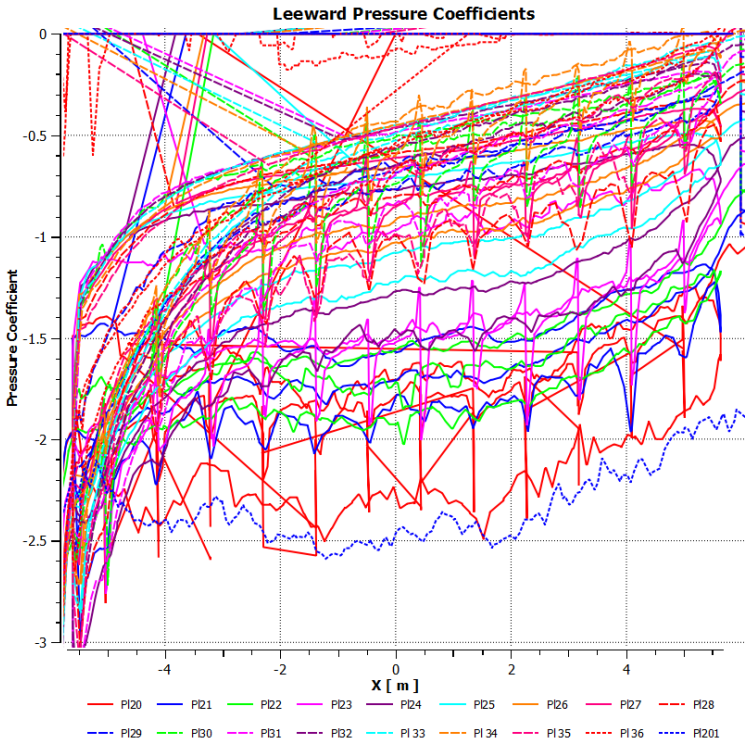


Fig. C. 153. Cp, All polylines, S 35 º, LW, WD 45 º

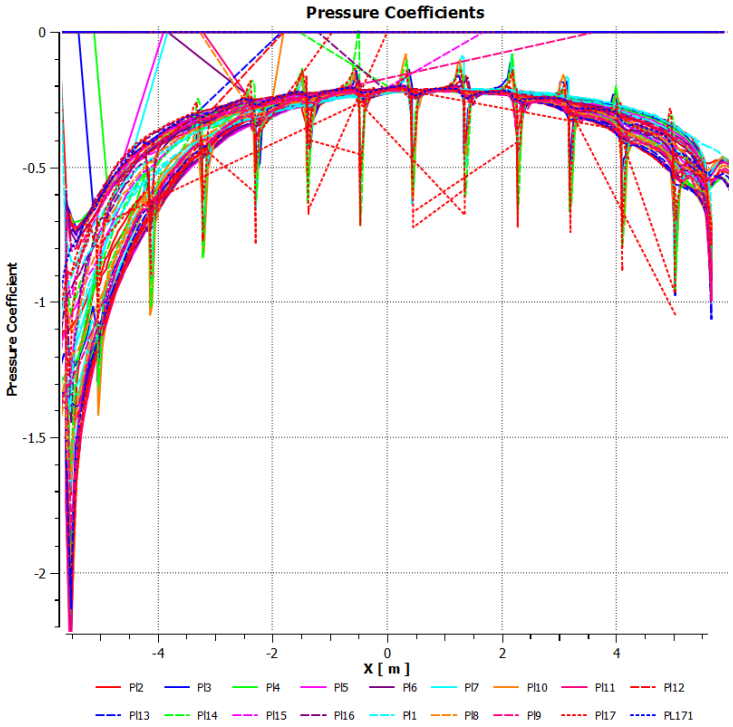


Fig. C. 154. All polylines, S 35 º, LW, WD 0.0 º

1.3.5. Detailed Distribution of Wind Pressure, and flow on roof mounted solar panels, S 8", C10"

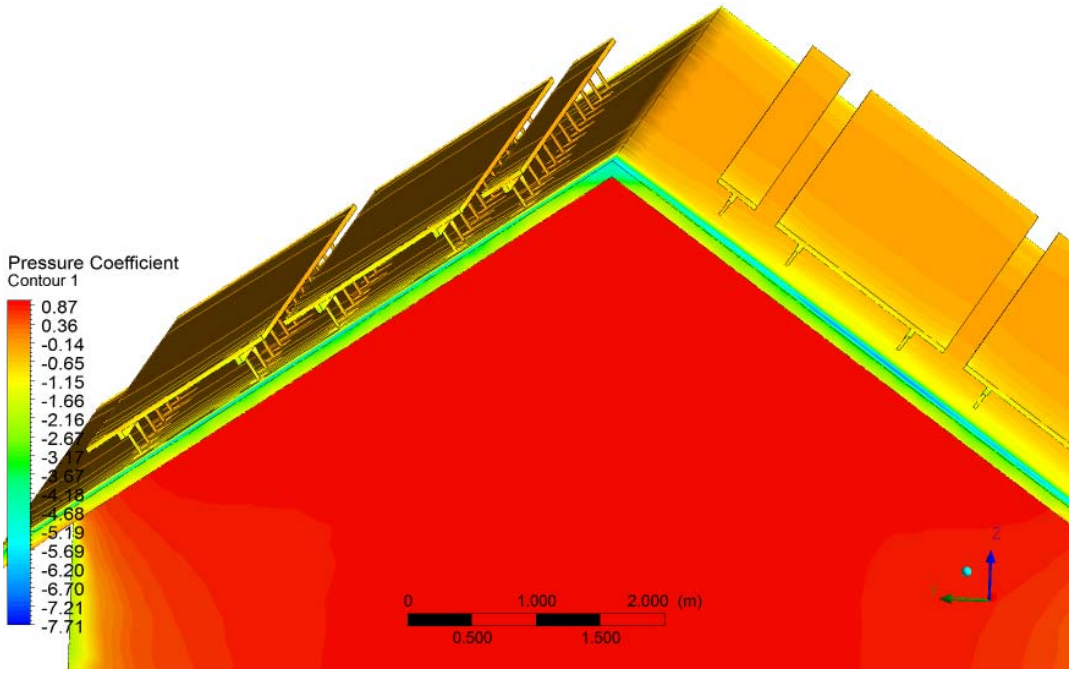


Fig. C. 155. Close view shows separation of solar panels from roof structure, WD 0º.

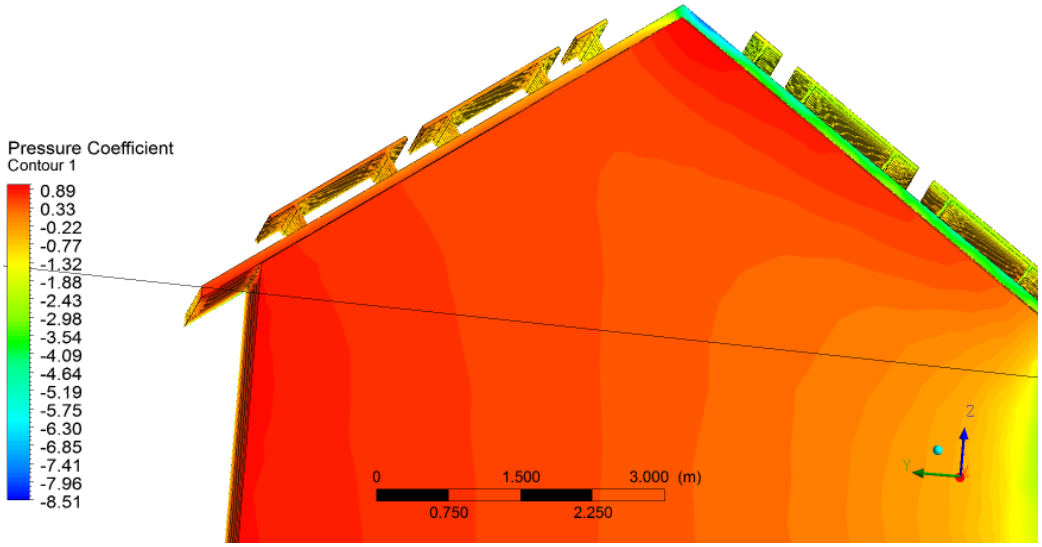


Fig. C. 156. Close view shows panels on rails and spaces, WD 45º

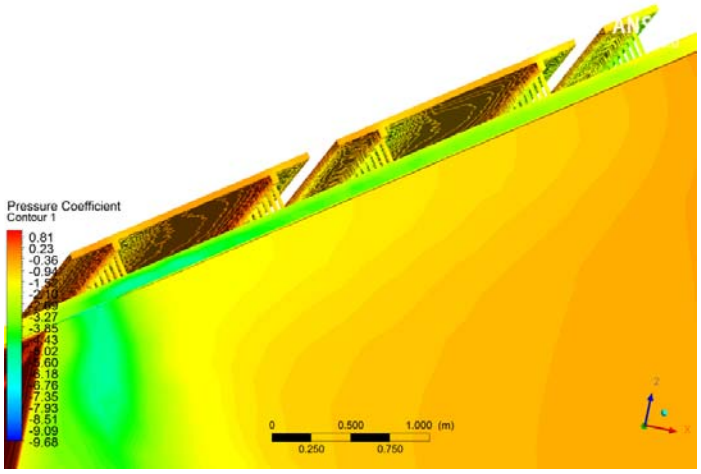


Fig. C. 157. Close view shows separation of solar panels from roof structure, WW, WD 90º

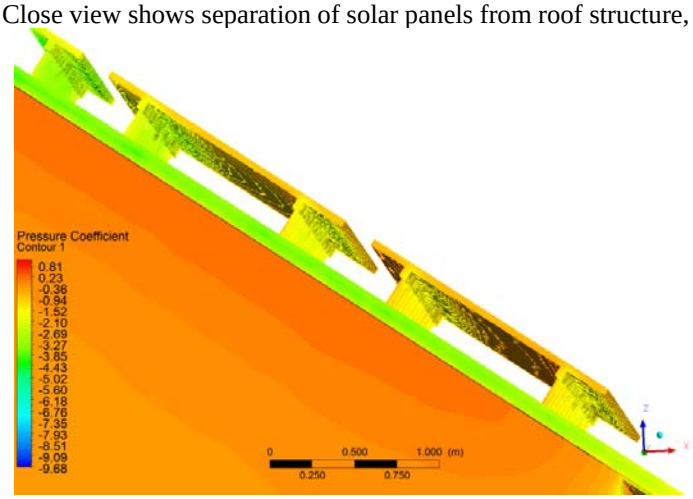


Fig. C. 158. Close view shows separation of solar panels from roof structure, LW, WD 90º

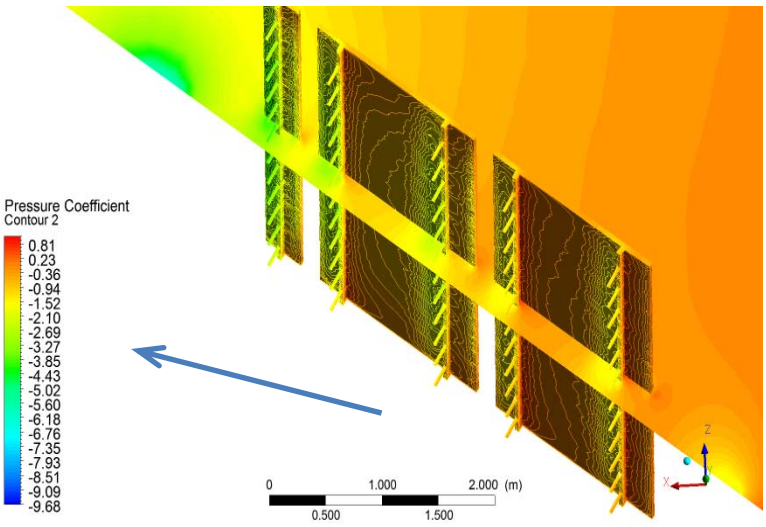


Fig. C. 159. Cp on a perpendicular plane under panels, Close up WD 90º, WW

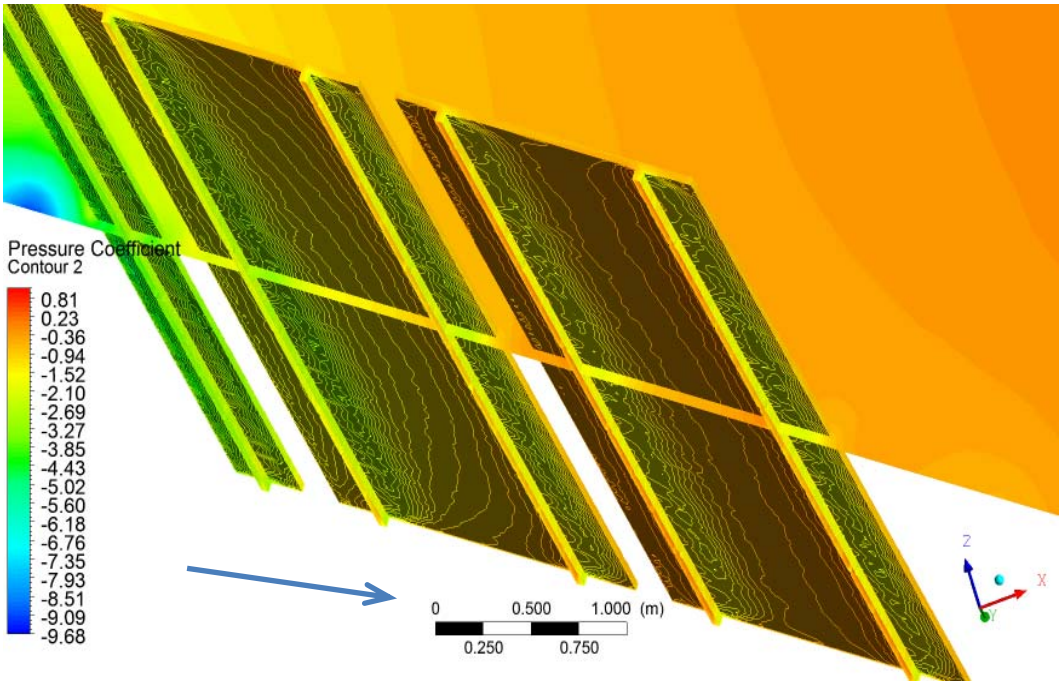


Fig. C. 160. Cp on a perpendicular plane under panels, WD 90º, LW

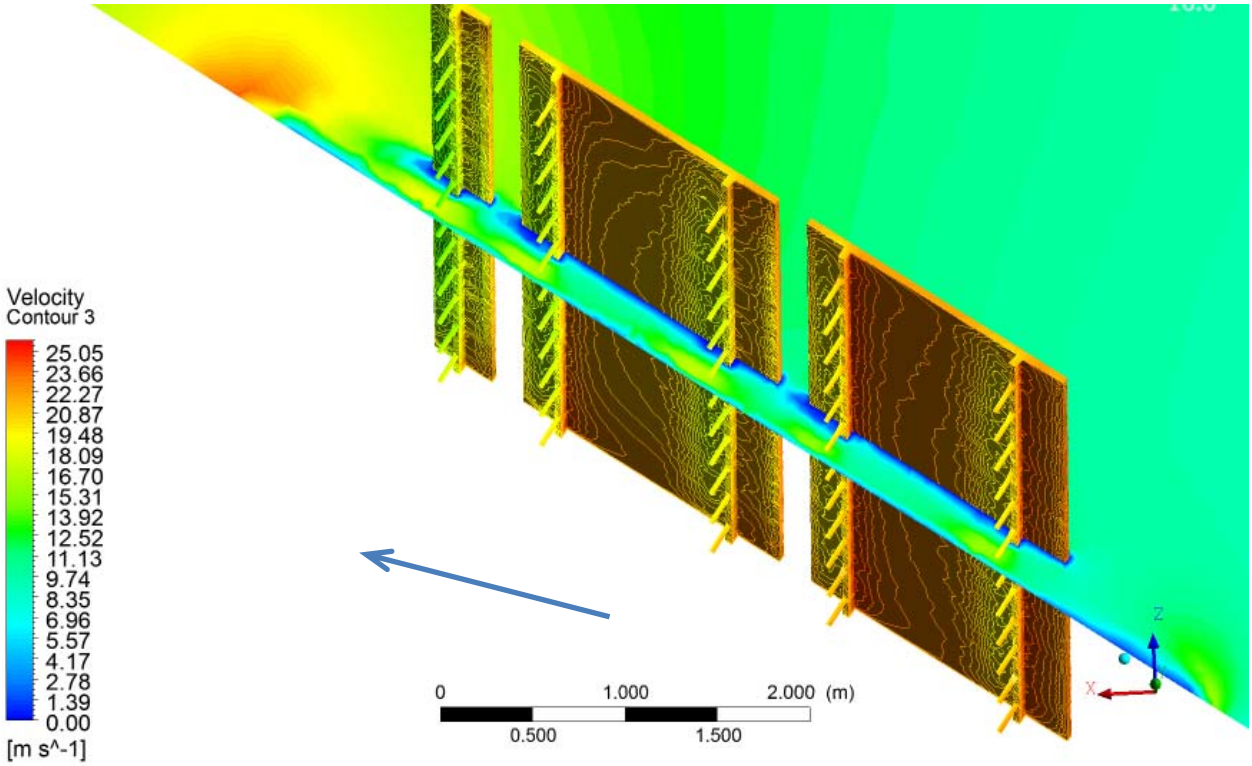


Fig. C. 161. Velocity distribution on a perpendicular plane under panels, Close up WD 90º, WW

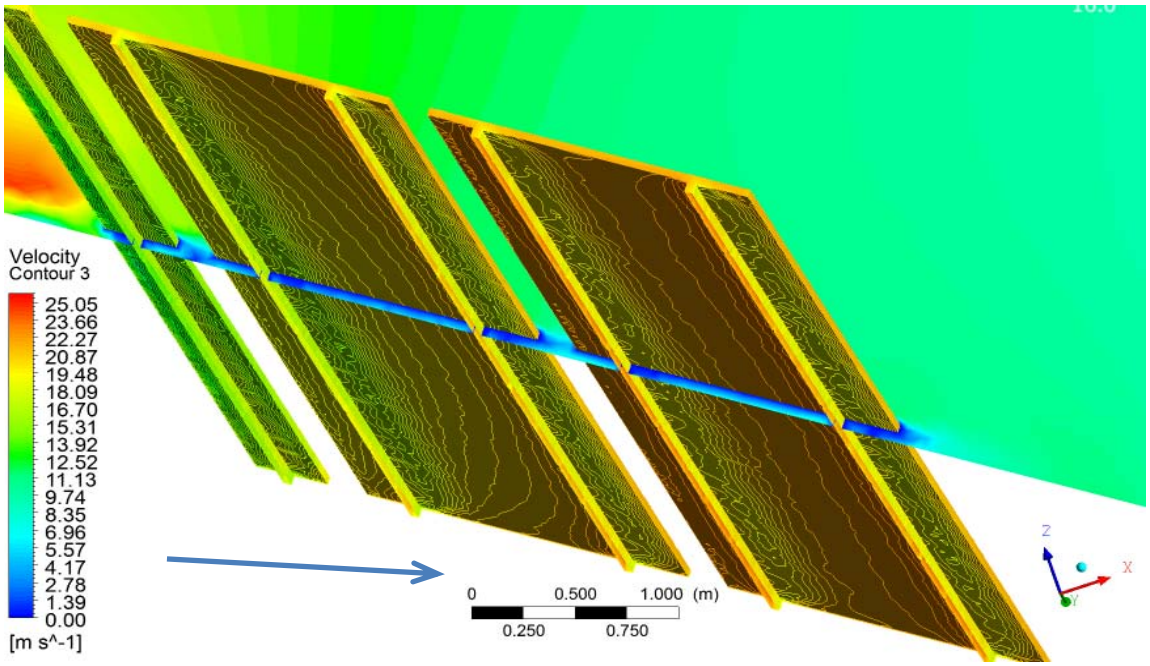


Fig. C. 162. Velocity distribution on a perpendicular plane under panels, Close up WD 90º, LW

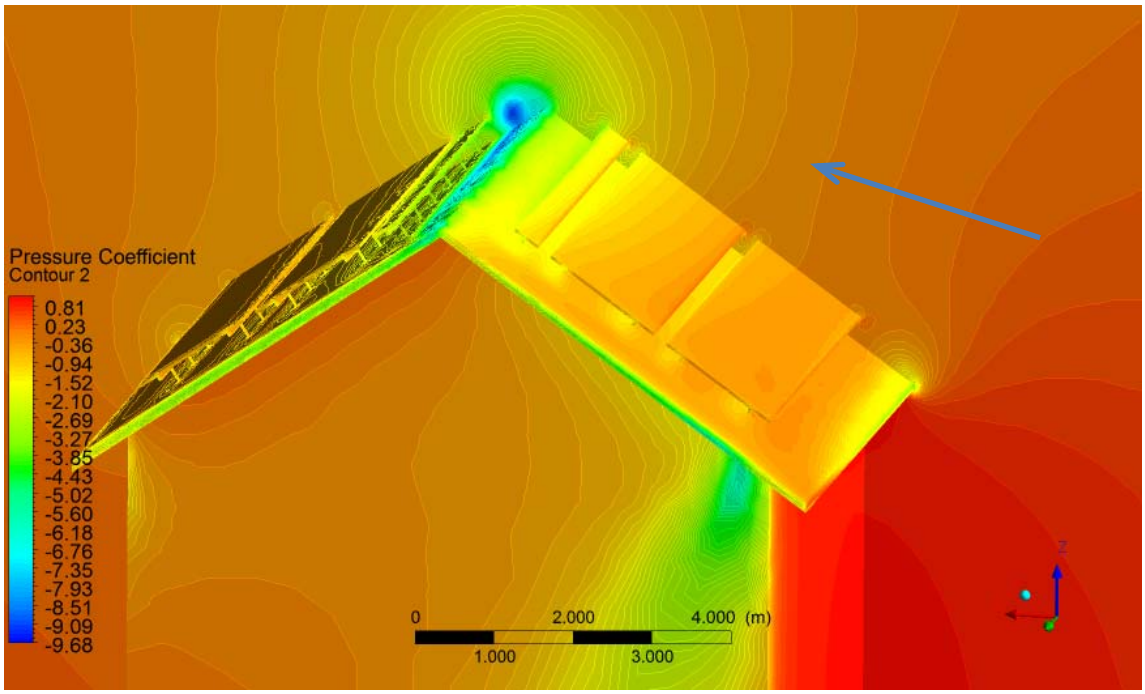


Fig. C. 163. Cp on a perpendicular plane with the ridge of the house, WD 90º

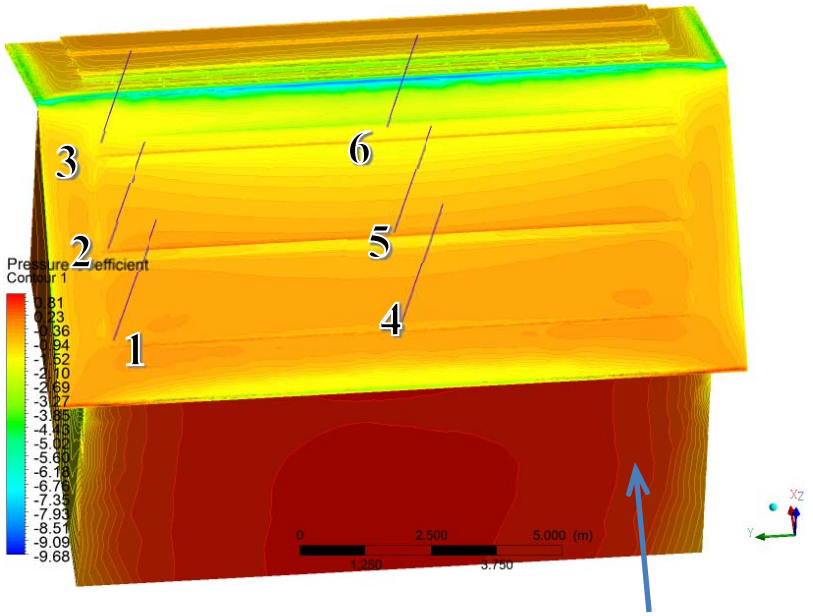


Fig. C. 164. Lines used to draw velocity and pressure changes, WD 90º

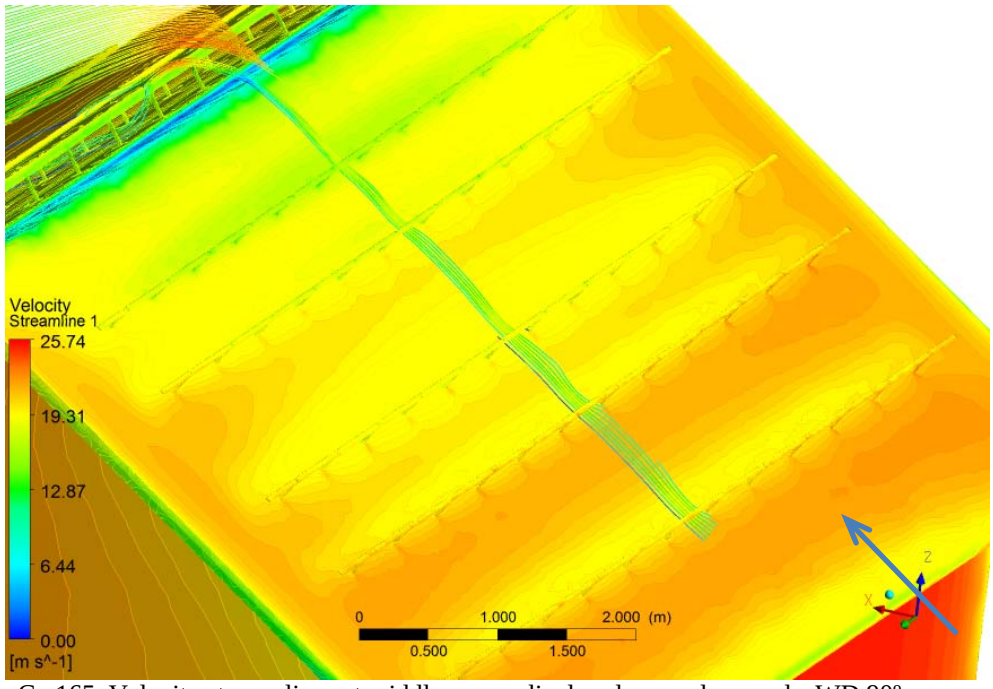


Fig. C. 165. Velocity stream lines at middle perpendicular plane under panels, WD 90º

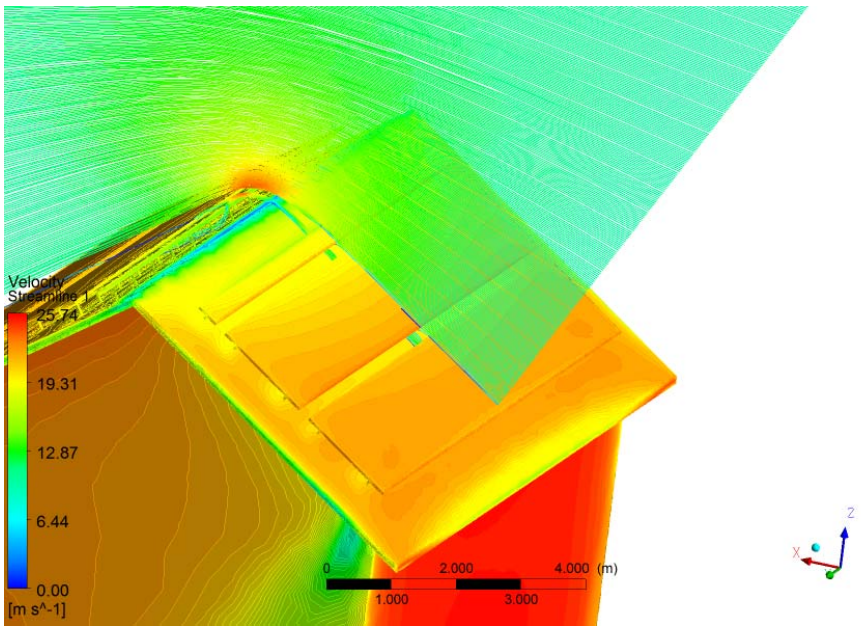


Fig. C. 166. Velocity stream lines at middle perpendicular plane above panels, WD 90º

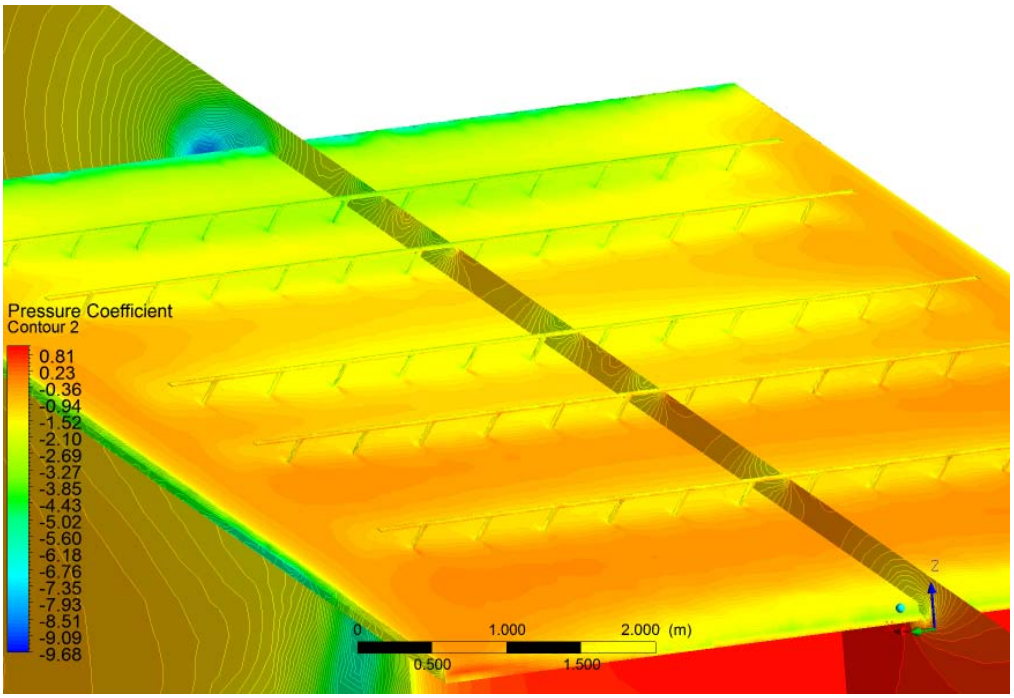


Fig. C. 167. Cp distribution on a perpendicular plane under panels, top view, WD 90º, WW

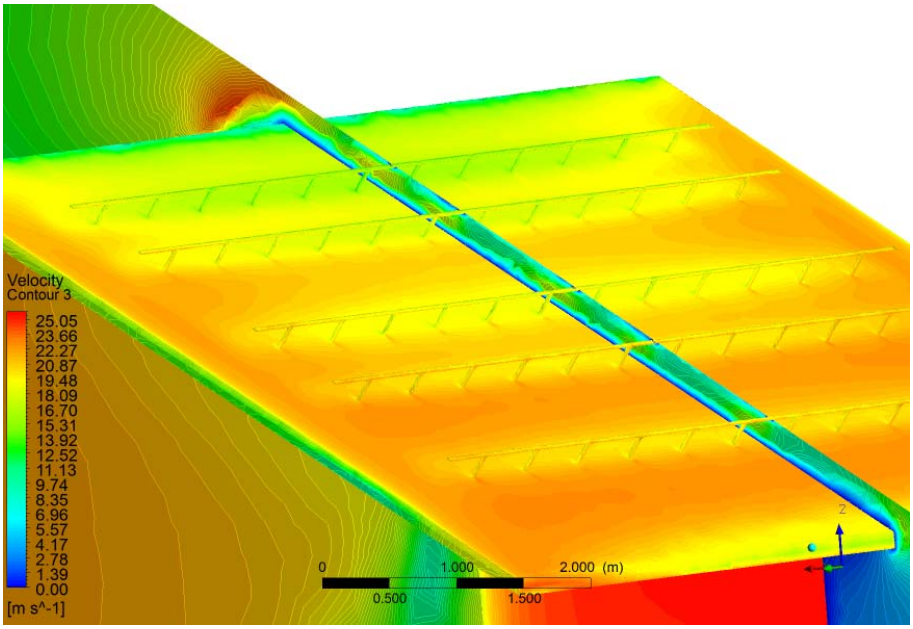


Fig. C. 168. Velocity distribution on a perpendicular plane under panels, top view, WD 90º, WW

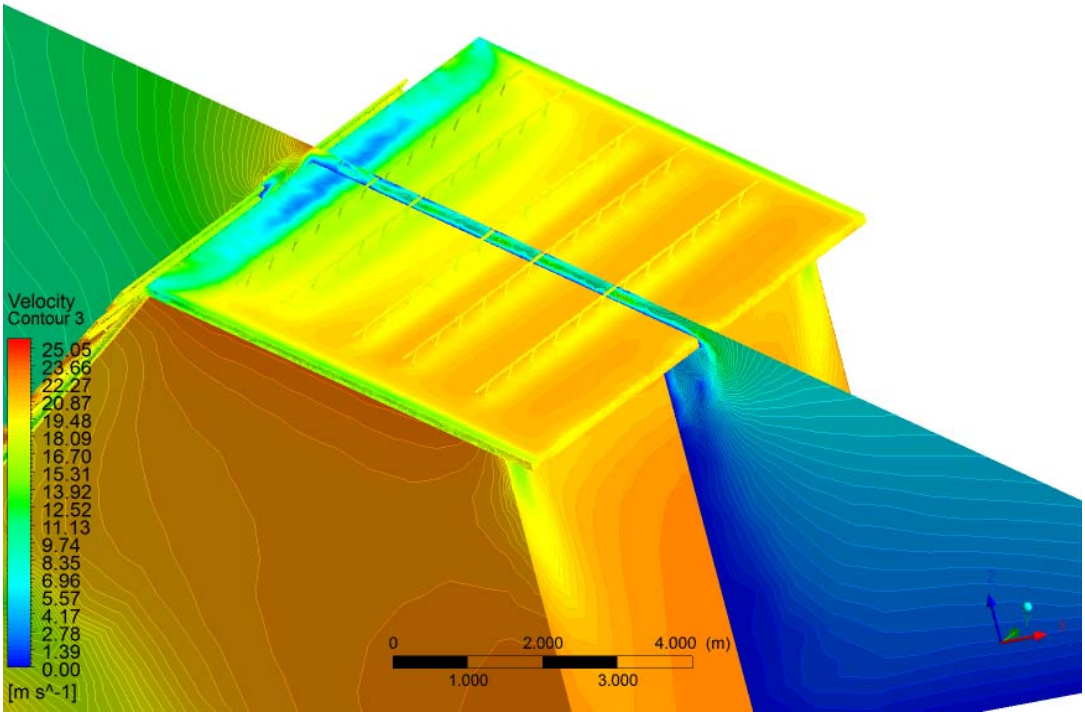


Fig. C. 169. Velocity distribution on a perpendicular plane under panels, top view, WD 90º, LW

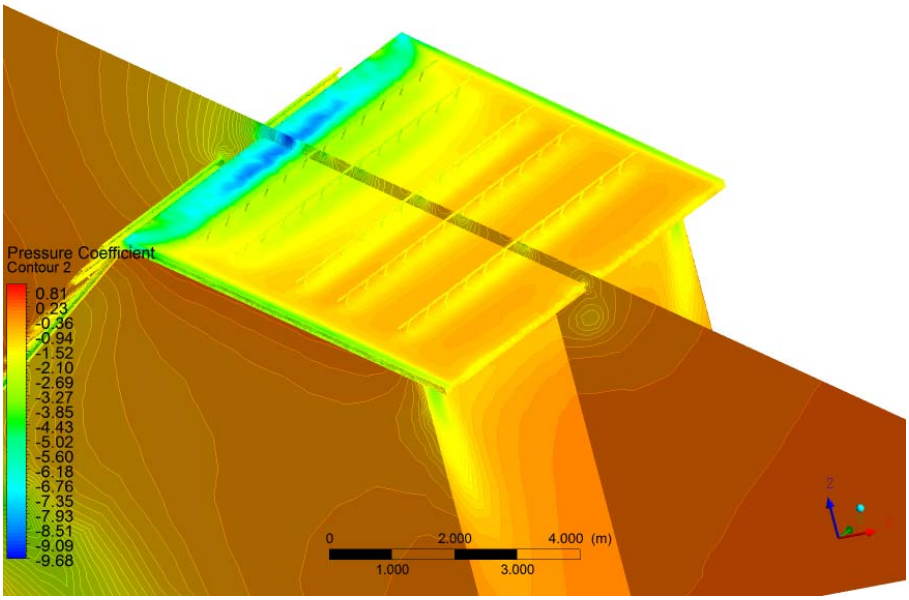


Fig. C. 170. Cp distribution on a perpendicular plane under panels, top view, WD 90º, LW

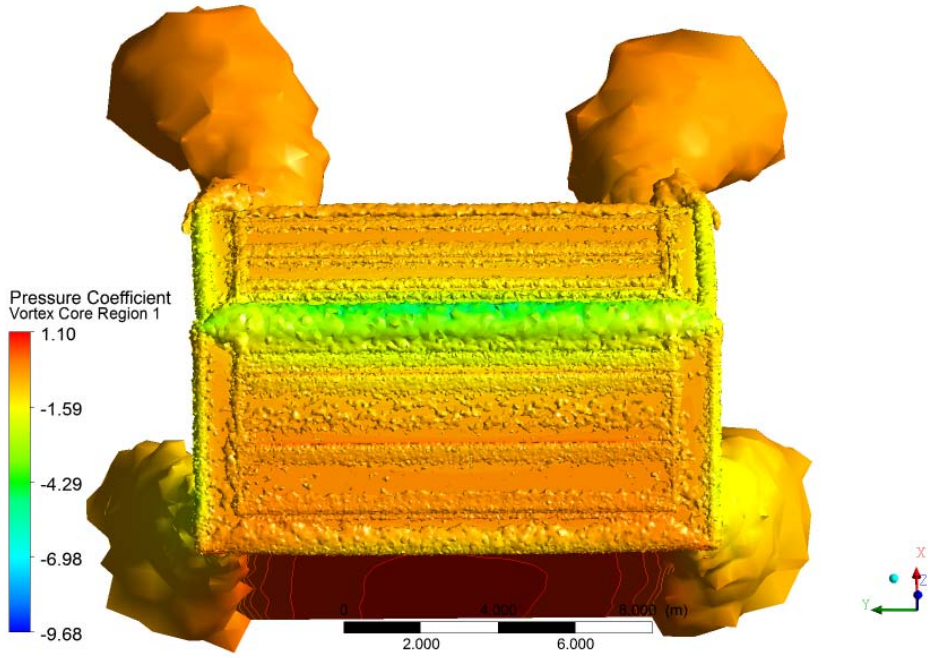


Fig. C. 171. Turbulence distribution on roof and on the building structure, WD 90º , WW

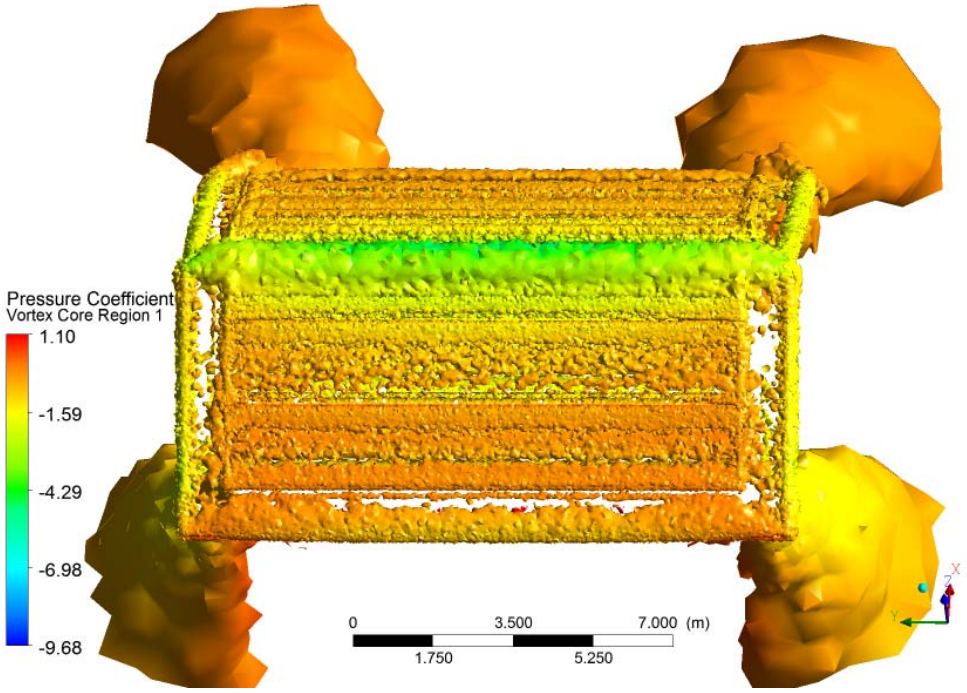


Fig. C. 172. Turbulence distribution on roof without building contour structure, WD 90º , WW

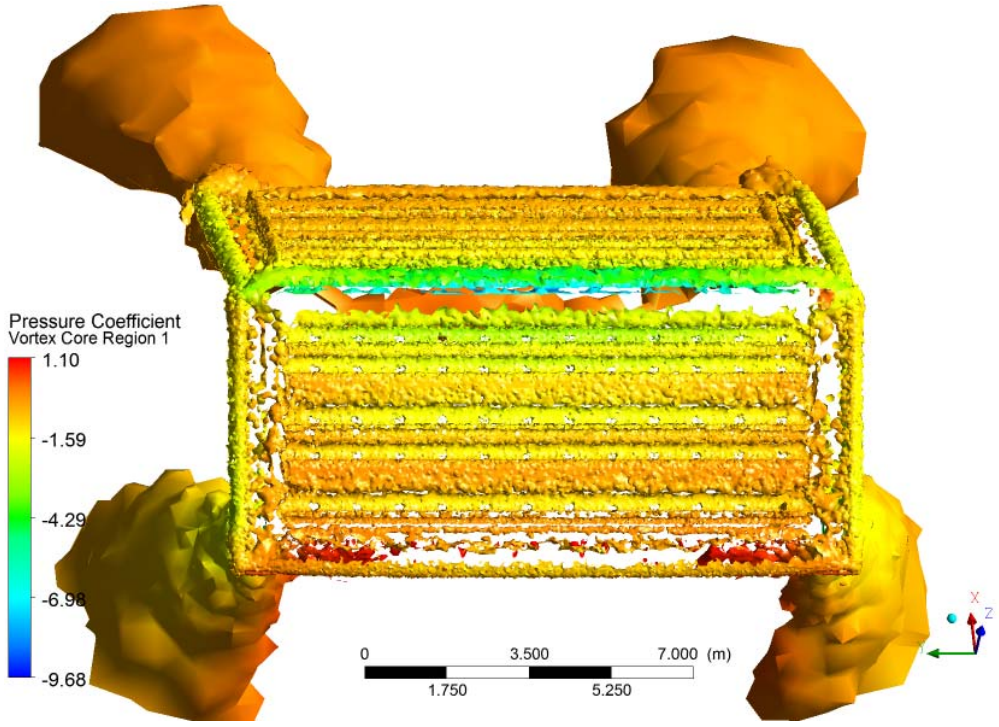


Fig. C. 173. Turbulence distribution on roof under panels, WD 90º , WW

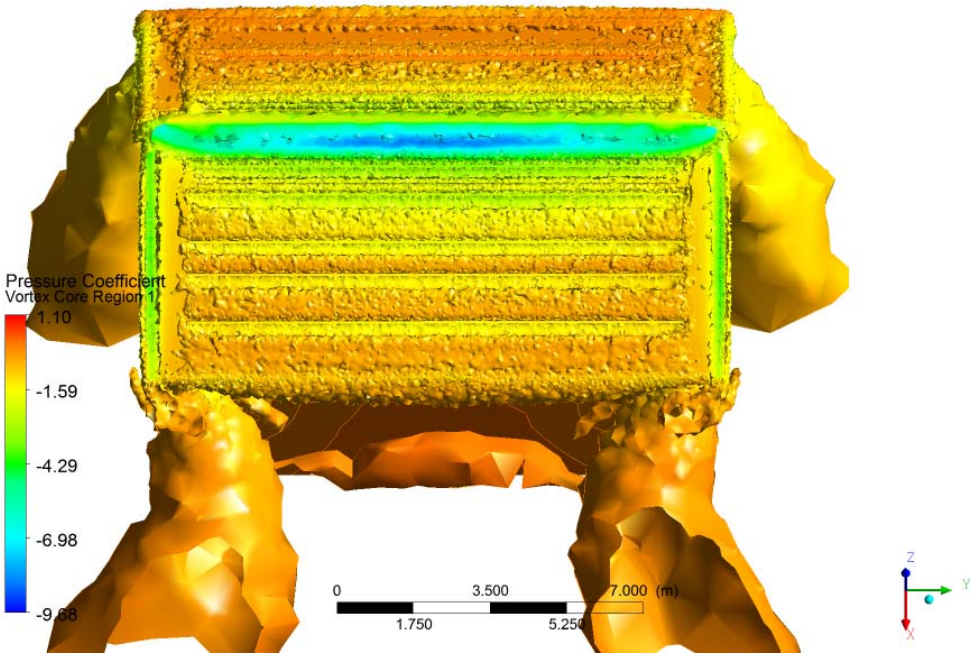


Fig. C. 174. Turbulence distribution on roof under panels, building contour showed, WD 90º , LW

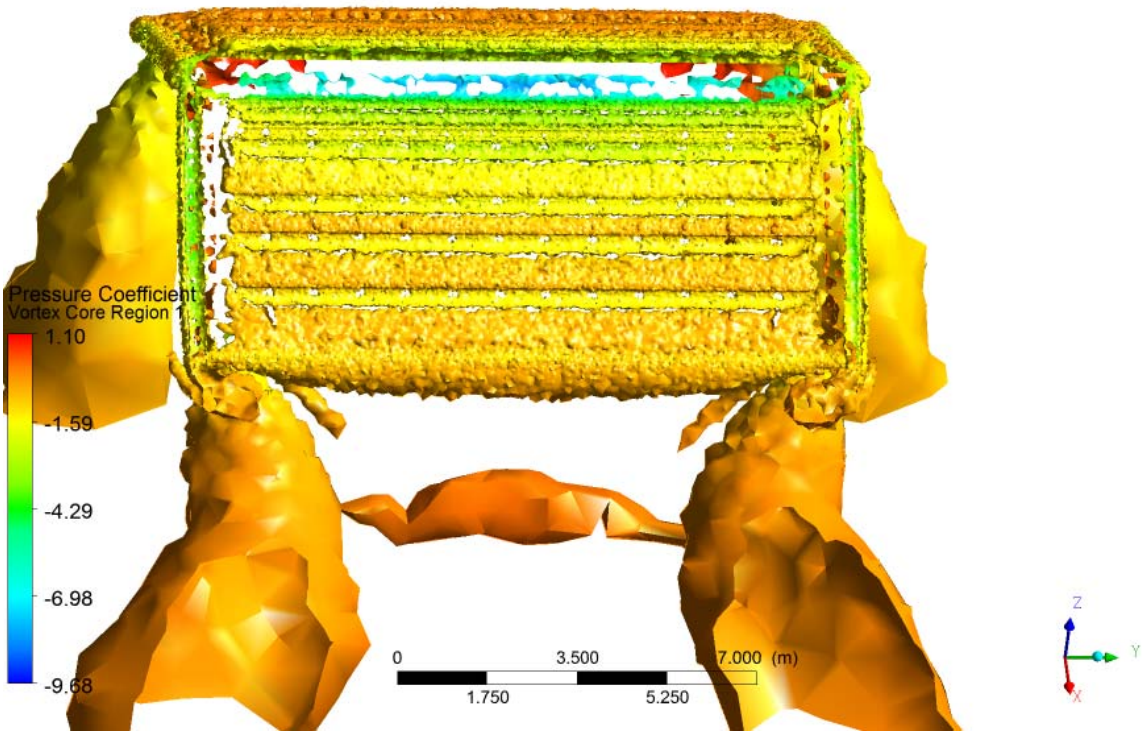


Fig. C. 175. Turbulence distribution on roof under panels, No building contour showed, WD 90º , LW

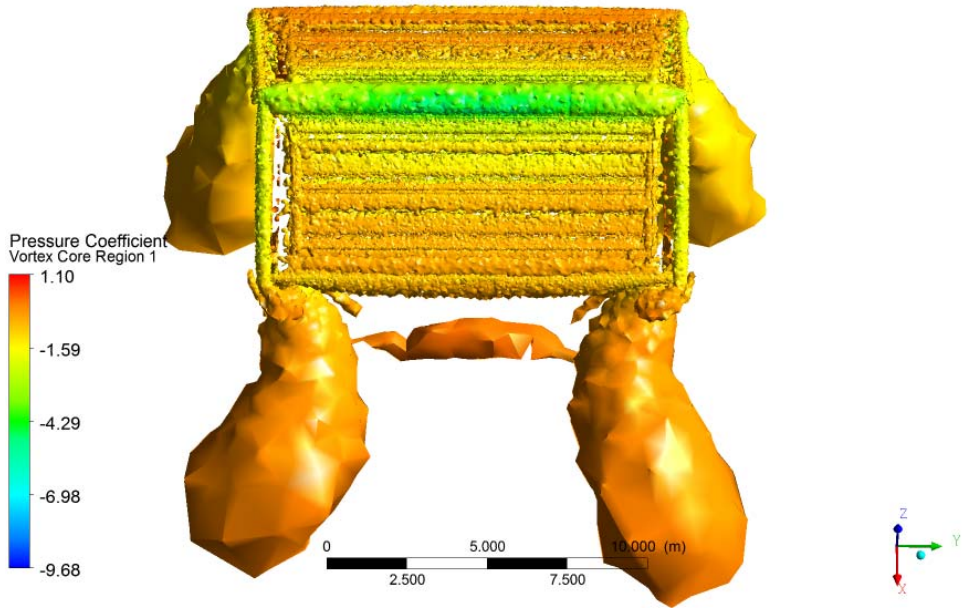


Fig. C. 176. Turbulence distribution, No building contour showed, WD 90º , LW

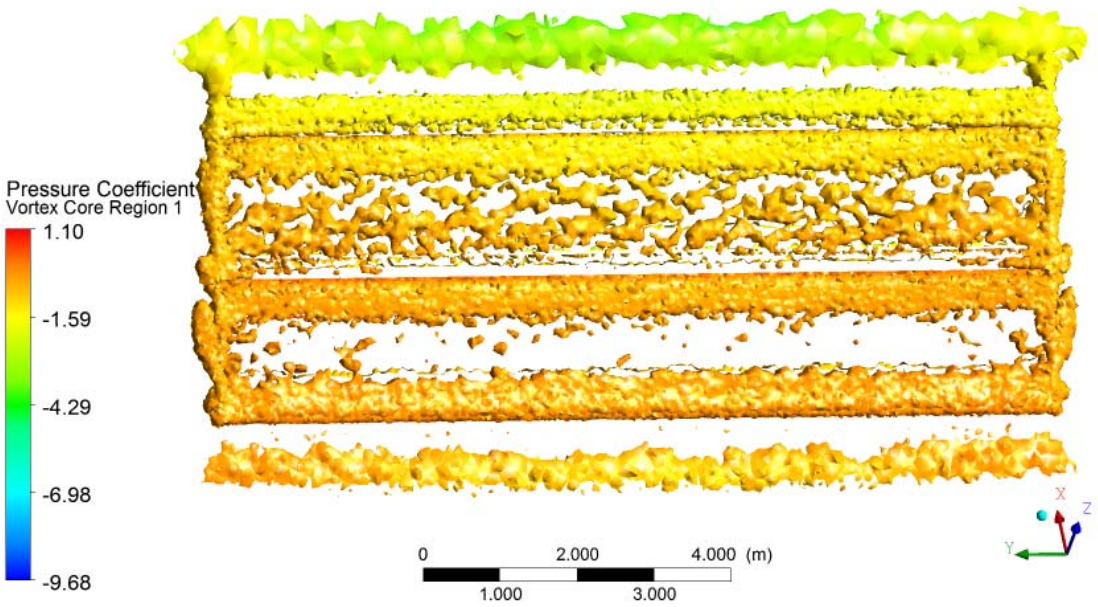


Fig. C. 177. Turbulence distribution, on top of the panels, No Building contours shown, WD 90º, WW

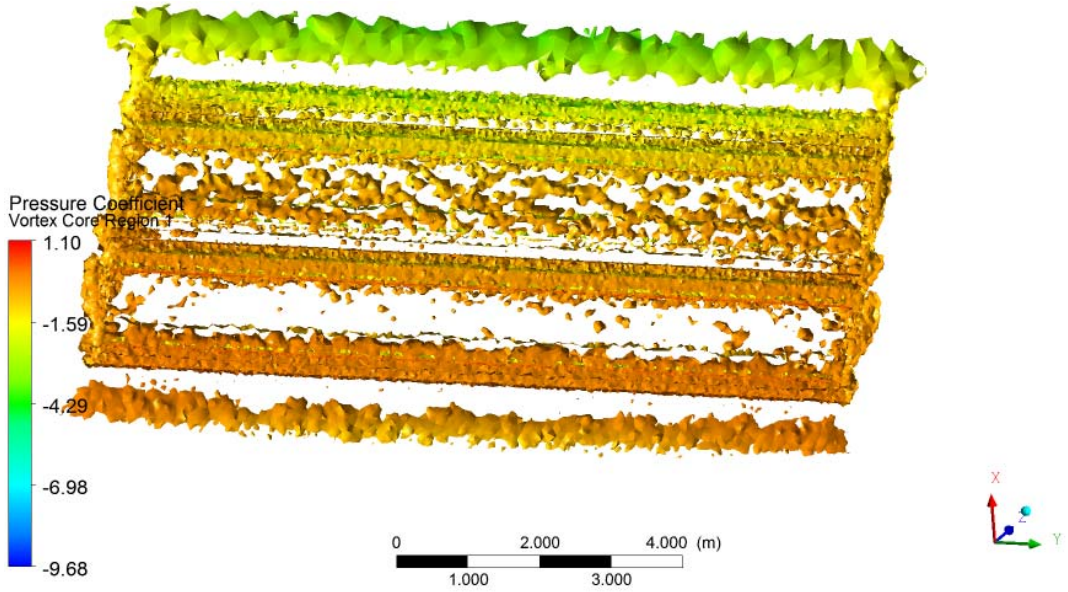


Fig. C. 178. Turbulence distribution, on bottom of the panels, No Building contours shown, WD 90º, WW

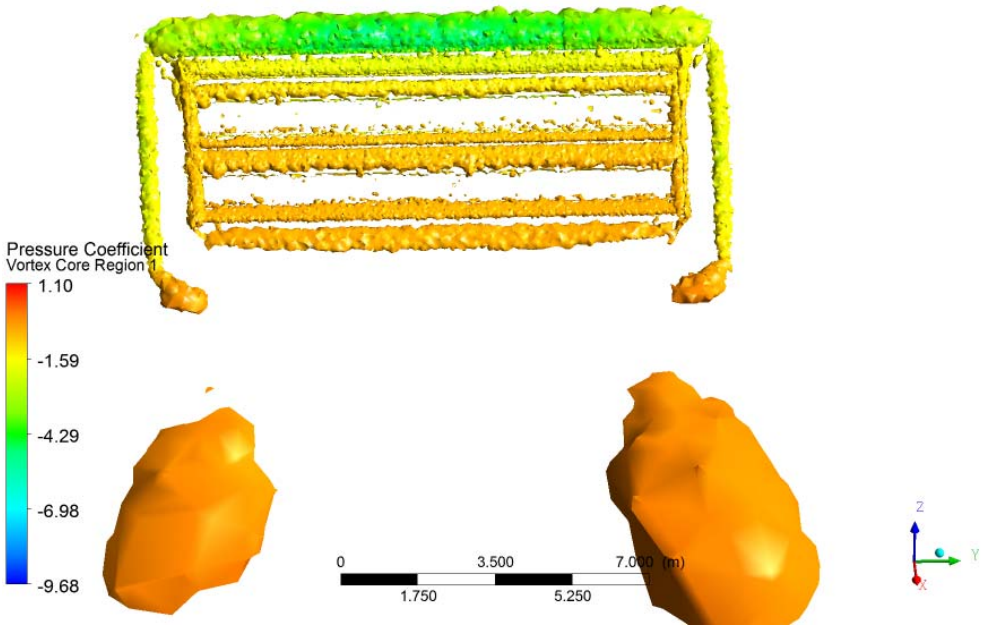


Fig. C. 179. Turbulence distribution, on top of the panels, No Building contours shown, WD 90º, LW

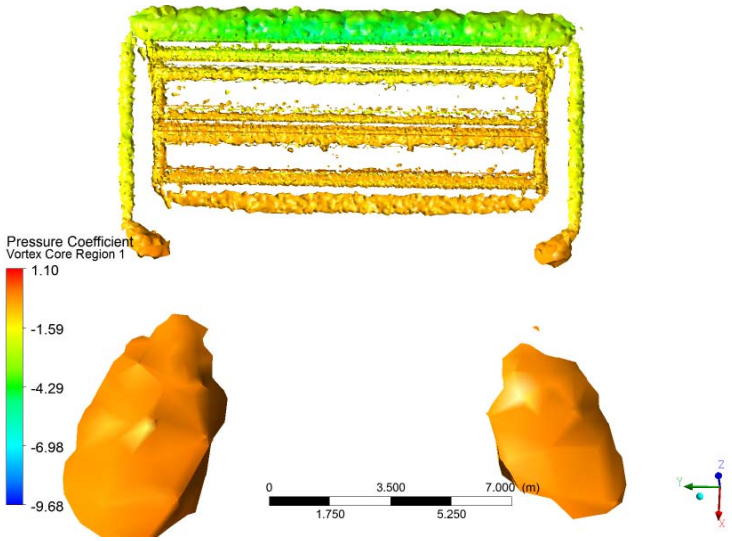


Fig. C. 180. Turbulence distribution, on bottom of the panels, No Building contours shown, WD 90º, LW

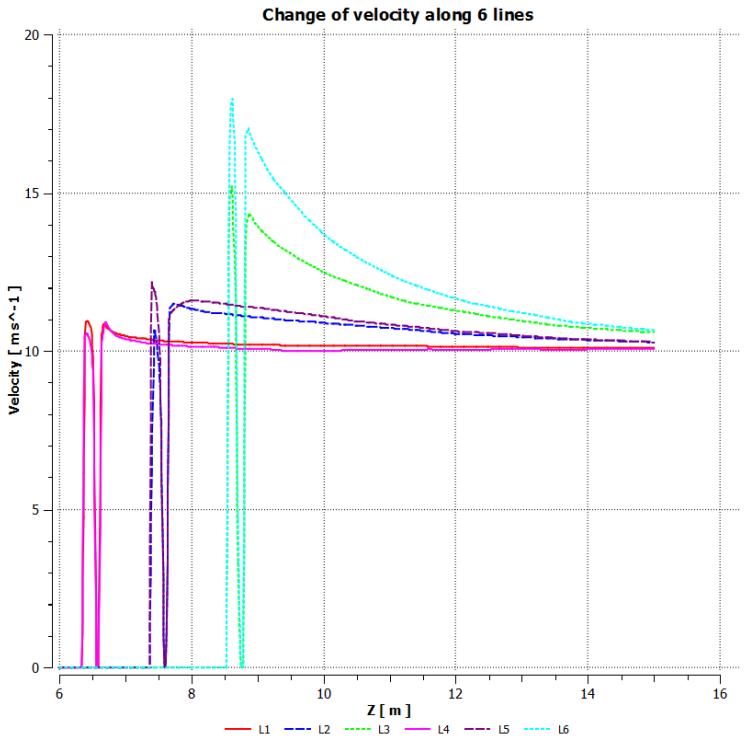


Fig. C. 181. Velocity changes between panels, and above roof, all 6 lines, WW

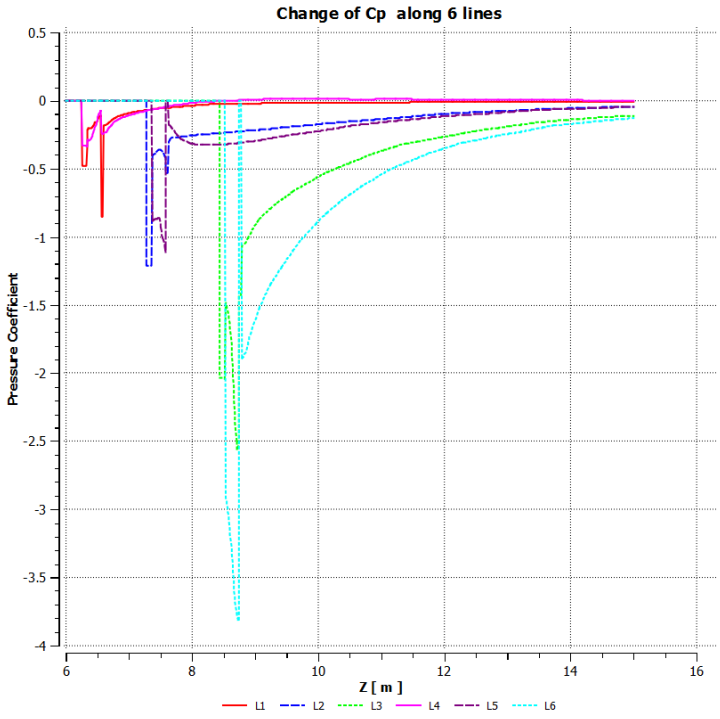
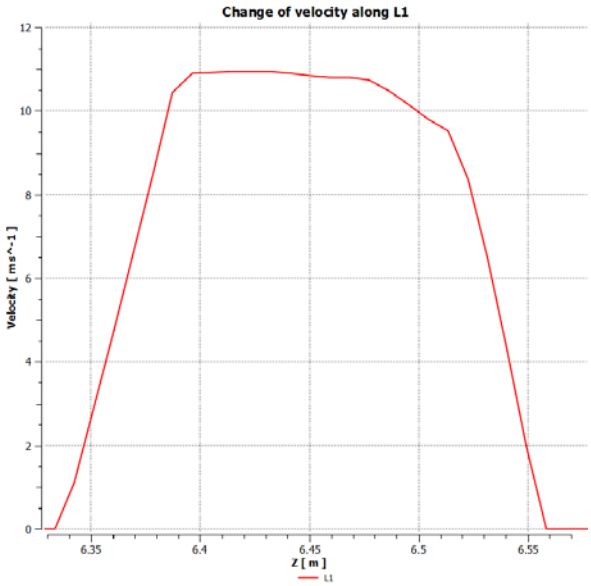
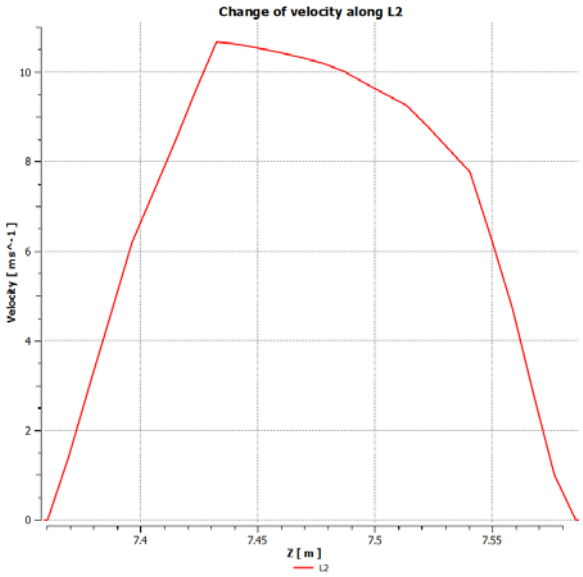
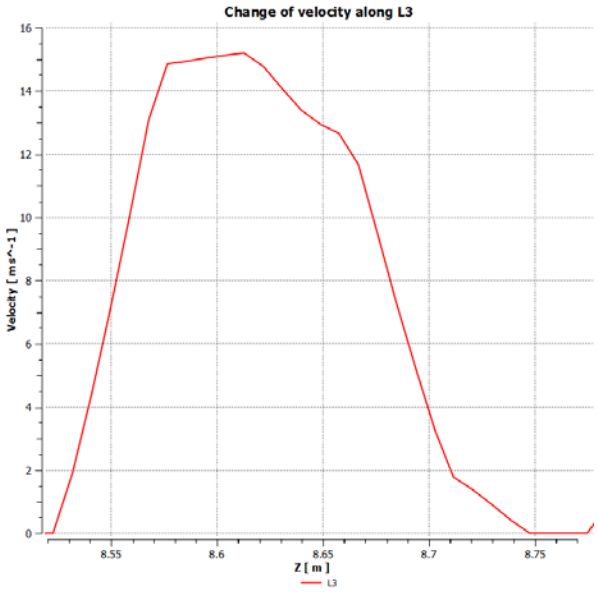
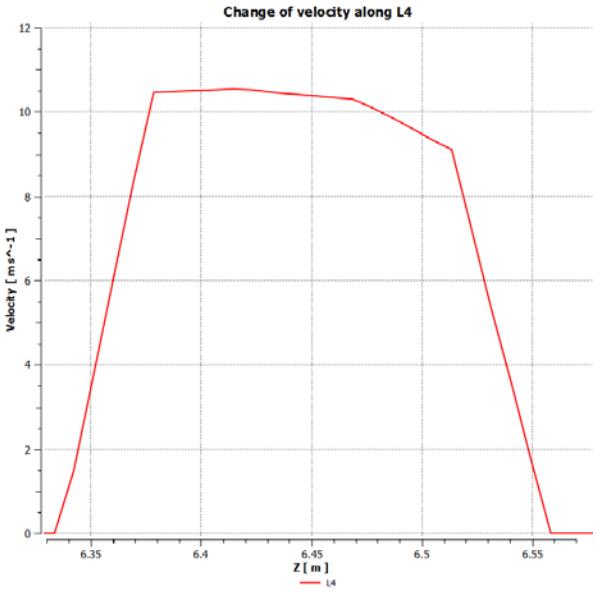


Fig. C. 182. Pressure changes between panels, and above roof, all 6 lines, WW


Change of velocity along L1
Velocity [ms^-1]
Z [m]
L1


Change of velocity along L2
Velocity [ms^-1]
Z [m]
L2


Change of velocity along L3
Velocity [ms^-1]
Z [m]
L3


Change of velocity along L4
Velocity [ms^-1]
Z [m]
L4

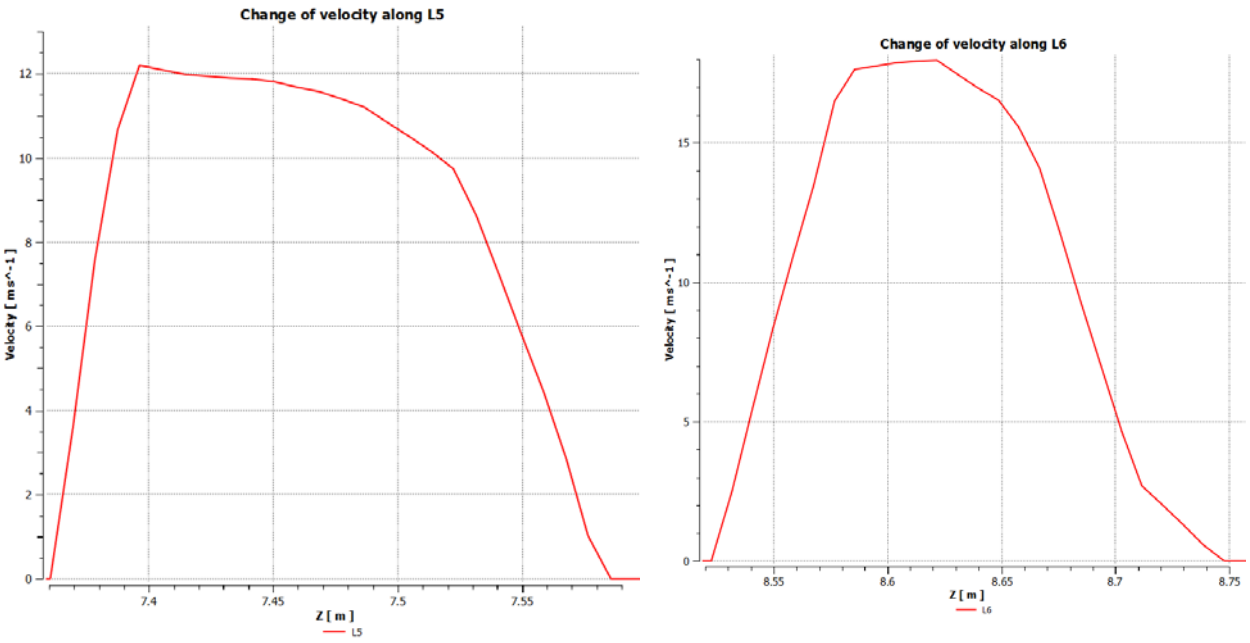
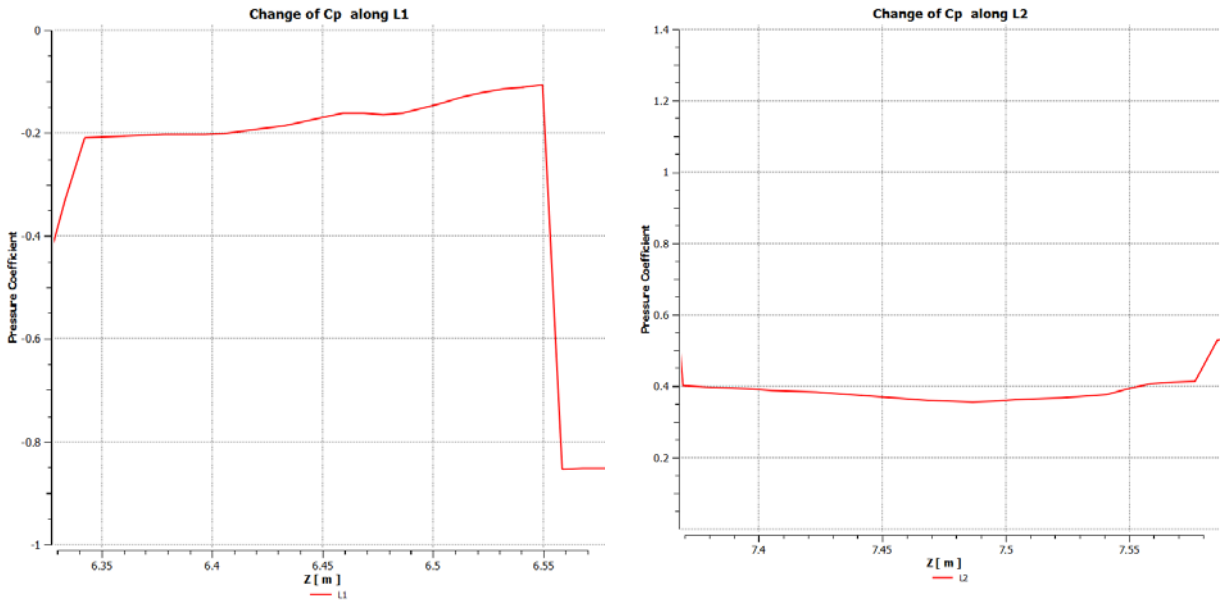


Fig. C. 183. Velocity changes between panels, each of the 6 lines, WW



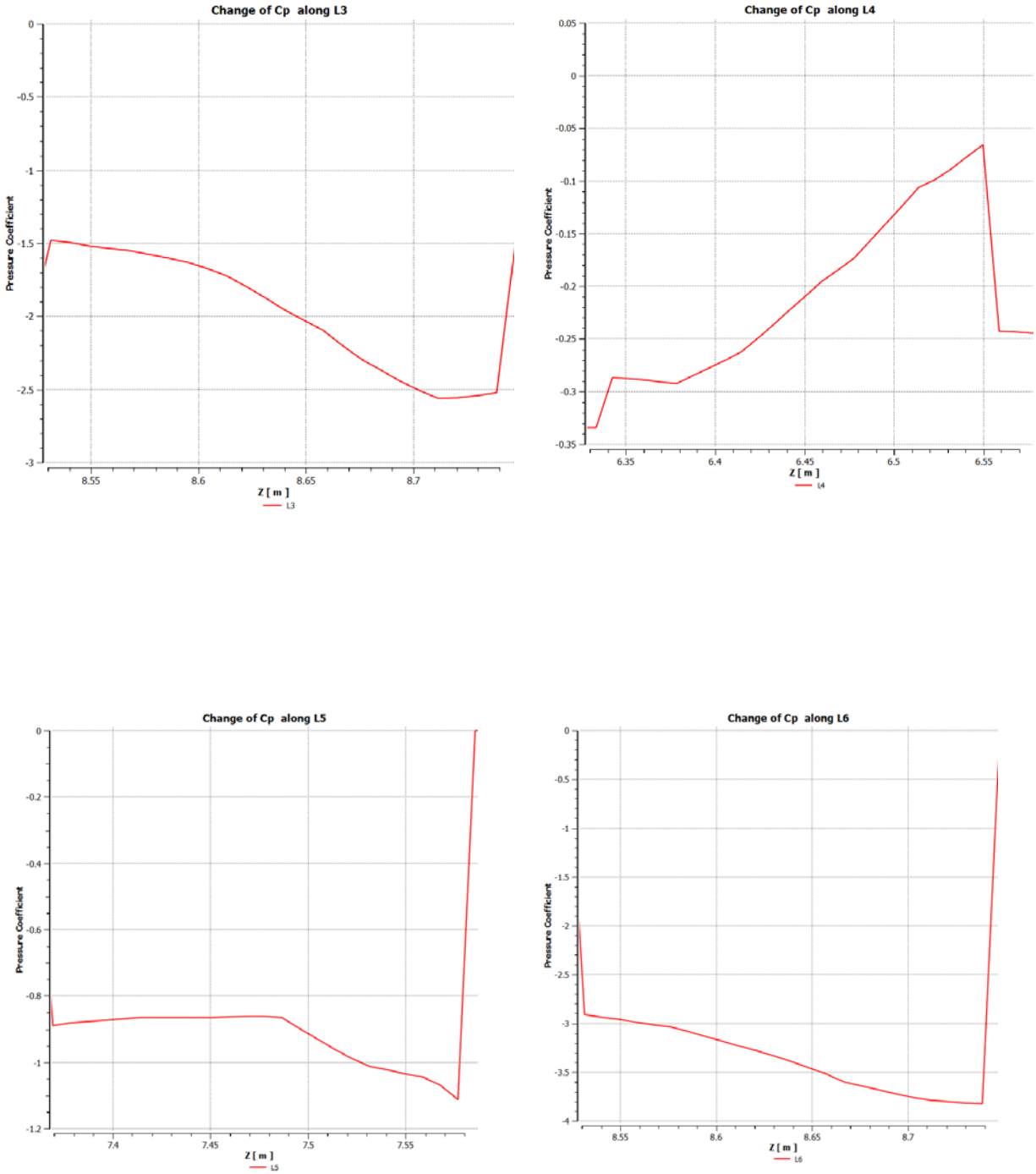


Fig. C. 184. Cp changes between panels, each of the 6 lines, WW

1.3.6. Calculation of resultant Cp of the three surfaces of roof mounted solar panels in comparison with bare roofs, Leeward, 2” apart, 10” roof space

Tabulated results of the integration,

Table C. 11. Cp on bare roofs vs. roof under solar panels, Slope 35º, 45º, windward

Polylines	Cp (SP)	Pr2	Cp Bott	Diff	Ttl Cp	Ttl/Brf
Pl1A	-0.17	-0.27	-0.23	0.06	-0.21	1.24
Pl2	-0.2	-0.52	-0.18	-0.02	-0.54	3.00
Pl3	-0.2	-0.46	-0.51	0.31	-0.15	0.81
Pl4	-0.2	-0.36	-0.37	0.17	-0.19	0.95
Pl5	-0.21	-0.29	-0.29	0.08	-0.21	-1.02
Pl6	-0.23	-0.5	-0.15	-0.08	-0.58	2.58
Pl7	-0.39	-0.53	-0.57	0.18	-0.35	1.40
Pl8	-0.16	-0.59	-0.38	0.22	-0.37	1.37
Pl9	-0.26	-0.90	-0.38	0.12	-0.78	2.69
Pl10	-0.32	-0.80	-0.88	0.56	-0.24	0.77
Pl11	-0.38	-0.70	-0.71	0.33	-0.37	1.07
Pl12	-0.45	-0.62	-0.62	0.17	-0.45	1.15
Pl13	-0.54	-0.98	-0.48	-0.06	-1.04	2.31
Pl14	-0.9	-0.98	-1.02	0.12	-0.86	1.76
Pl15	-0.58	-0.97	-0.84	0.26	-0.71	1.34
Pl16	-0.89	-1.15	-0.87	-0.02	-1.17	2.39
Pl17	-1.2	-1.43	-1.70	0.50	-0.93	1.75
Cp	-0.43	-0.71	-0.60	0.17	-0.54	1.69
SDT	0.31	0.32	0.39	0.18	0.32	0.95
Cov	0.71	0.45	0.65	1.07	0.60	0.56

Table C. 12. Cp bare roofs vs. roof under solar panels, Slope 35º, wind direction 45º, Leeward

Polylines	Cp (SP)	Pr2	Cp Bott	Diff	Ttl Cp	Ttl/Brf
Pl20a	-1.6	-2.33	-2.28	0.68	-1.65	1.10
Pl21	-1.48	-1.78	-1.8	0.32	-1.46	1.01
Pl22	-1.53	-1.7	-1.8	0.27	-1.43	1.02
Pl23	-0.97	-1.73	-1.68	0.71	-1.02	0.75
Pl24	-0.75	-1.62	-1.65	0.90	-0.72	0.56
Pl25	-0.73	-1.38	-1.34	0.61	-0.77	0.64
Pl26	-0.69	-1.19	-1.15	0.46	-0.73	0.66
Pl27	-0.66	-1.04	-0.98	0.32	-0.72	0.71
Pl28	-0.66	-1.00	-1.15	0.49	-0.51	0.55
Pl29	-0.77	-0.87	-0.82	0.05	-0.82	0.94
Pl30	-0.52	-0.84	-0.70	0.18	-0.66	0.80
Pl31	-0.51	-0.86	-1.08	0.57	-0.29	0.39
Pl32	-0.51	-0.86	-0.84	0.33	-0.53	0.77
Pl33	-0.5	-0.79	-0.78	0.28	-0.51	0.81
Pl34	-0.5	-0.76	-0.74	0.24	-0.52	0.88
Pl35	-0.51	-0.78	-1.09	0.58	-0.2	0.35
Pl36	-0.5	-0.81	-0.63	0.13	-0.68	1.21
Cp	-0.79	-1.20	-1.21	0.42	-0.78	0.77
SDT	0.38	0.47	0.48	0.23	0.40	0.24
Cov	0.48	0.40	0.40	0.55	0.52	0.31

Table C. 13. Cp on bare roofs vs. roof under solar panels, Slope 35º, 90º, windward

Polylines	Cp (SP)	Pr2	Cp Bott	Diff	Ttl Cp	Ttl/Brf
Pl1A	-0.12	-0.23	-0.23	0.11	-0.12	6.00
Pl2	-0.09	-0.86	0.04	-0.13	-0.99	-49.50
Pl3	-0.11	-0.73	-0.85	0.74	0.01	0.67
Pl4	-0.14	-0.32	-0.35	0.21	-0.11	22.00
Pl5	-0.18	-0.18	-0.14	-0.04	-0.22	6.29
Pl6	-0.23	-0.57	0.15	-0.38	-0.95	15.83
Pl7	-0.54	-0.57	-1.04	0.50	-0.07	1.08
Pl8	-0.18	-0.62	-0.61	0.43	-0.19	2.38
Pl9	-0.25	-1.22	-0.79	0.54	-0.68	5.91
Pl10	-0.36	-1.11	-1.23	0.87	-0.24	1.60
Pl11	-0.47	-0.75	-0.75	0.28	-0.47	2.35
Pl12	-0.6	-0.59	-0.55	-0.05	-0.64	2.37
Pl13	-0.78	-1.12	-0.18	-0.60	-1.72	5.06
Pl14	-1.11	-1.45	-2.04	0.93	-0.52	1.39
Pl15	-0.98	-1.82	-1.10	0.12	-1.7	4.64
Pl16A	-2.15	-2.23	-2.70	0.55	-1.68	4.48
Cp	-0.52	-0.90	-0.77	0.26	-0.64	4.22
SDT	0.54	0.57	0.75	0.43	0.60	14.88
Cov	1.04	0.63	0.98	1.70	0.94	3.52

Table C. 14. Cp bare roofs vs. roof under solar panels, Slope 35º, wind direction 90º, Leeward

Polylines	Cp (SP)	Pr2	Cp Bott	Diff	Ttl Cp	Ttl/Brf
Pl17a	-2.53	-3.6	-3.7	1.17	-2.43	0.93
Pl18	-2.5	-2.43	-2.94	0.44	-1.99	0.78
Pl19	-1.29	-2.4	-2.38	1.09	-1.31	0.52
Pl20	-1.05	-2.33	-2.32	1.27	-1.06	0.44
Pl21	-0.97	-2.29	-2.27	1.30	-0.99	0.43
Pl22	-0.85	-1.63	-1.45	0.60	-1.03	0.49
Pl23	-0.78	-1.19	-1.09	0.31	-0.88	0.46
Pl24	-0.74	-1.05	-1.30	0.56	-0.49	0.29
Pl25	-0.84	-1.19	-1.28	0.44	-0.75	0.49
Pl26	-0.52	-0.83	-0.48	-0.04	-0.87	0.62
Pl27	-0.52	-0.79	-1.20	0.68	-0.11	0.09
Pl28	-0.48	-0.91	-0.90	0.42	-0.49	0.48
Pl29	-0.45	-0.58	-0.50	0.05	-0.53	0.63
Pl30	-0.42	-0.38	-0.30	-0.12	-0.5	0.68
Pl31	-0.42	-0.41	-1.22	0.80	0.39	-0.63
Pl32	-0.58	-0.87	-0.95	0.37	-0.5	0.83
Cp	-0.93	-1.43	-1.52	0.58	-0.85	0.52
SDT	0.67	0.92	0.95	0.45	0.67	0.36
Cov	0.71	0.64	0.63	0.77	0.80	0.69

Table C. 15. Cp on bare roofs vs. roof under solar panels, Slope 35º, 0.0º

Polylines	Cp (SP)	Pr2	Cp Bott	Diff	Ttl Cp	Ttl/Brf
Pl1A	-0.34	-0.43	-0.36	0.02	-0.41	1.17
Pl2	-0.31	-0.43	-0.43	0.12	-0.31	0.89

Pl3	-0.31	-0.43	-0.43	0.12	-0.31	0.88
Pl4	-0.31	-0.43	-0.43	0.12	-0.31	0.86
Pl5	-0.31	-0.43	-0.43	0.12	-0.31	0.86
Pl6	-0.32	0.40	-0.43	0.11	0.51	-1.40
Pl7	-0.36	-0.40	-0.40	0.04	-0.36	0.97
Pl8	-0.36	-0.41	-0.40	0.04	-0.37	1.00
Pl9	-0.33	-0.43	-0.41	0.08	-0.35	0.95
Pl10	-0.31	-0.41	-0.41	0.10	-0.31	0.84
Pl11	-0.3	-0.43	-0.41	0.11	-0.32	0.89
Pl12	-0.31	-0.43	-0.43	0.12	-0.31	0.86
Pl13	-0.31	-0.33	-0.43	0.12	-0.21	0.58
Pl14	-0.32	-0.32	-0.34	0.02	-0.3	0.85
Pl15	-0.31	-0.33	-0.33	0.02	-0.31	0.89
Pl16	-0.31	-0.33	-0.33	0.02	-0.31	0.89
Pl17a	-0.31	-0.31	-0.31	0.00	-0.31	0.89
Cp	-0.32	-0.35	-0.39	0.08	-0.27	0.75
SDT	0.02	0.20	0.04	0.05	0.21	0.57
Cov	0.06	0.57	0.11	0.62	0.76	0.75

APPENDIX D

Chapter 5, Remaining cases Slope 27º

D.1. Slope 27º,

1.1. 8” Spacing, 10” Clearance

1.1.1. Wind direction 45º,

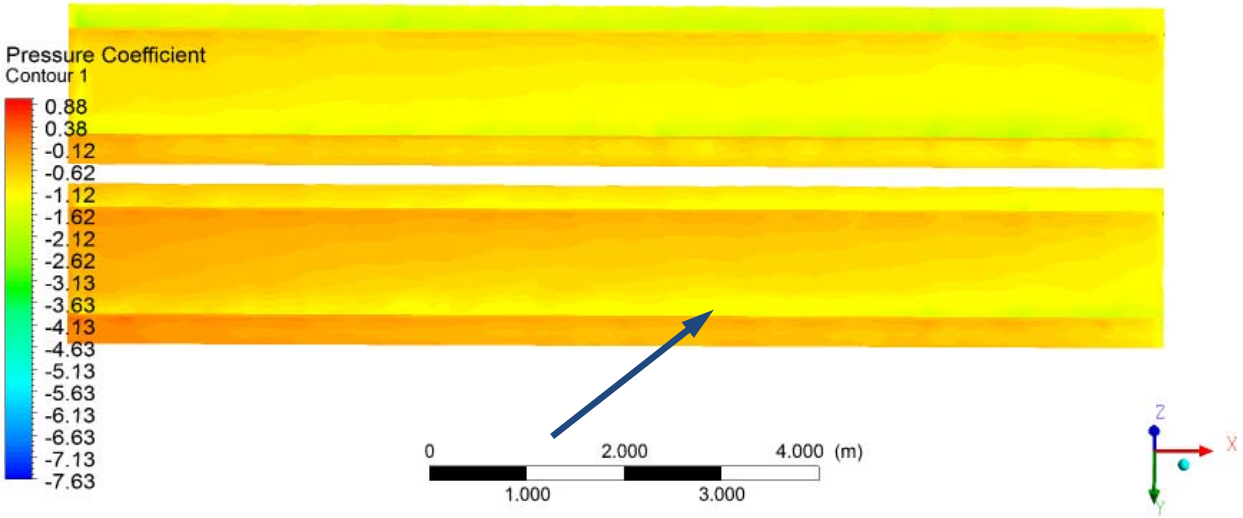


Fig. D. 1. Cp on bottom of the solar panels, WW, WD 45º

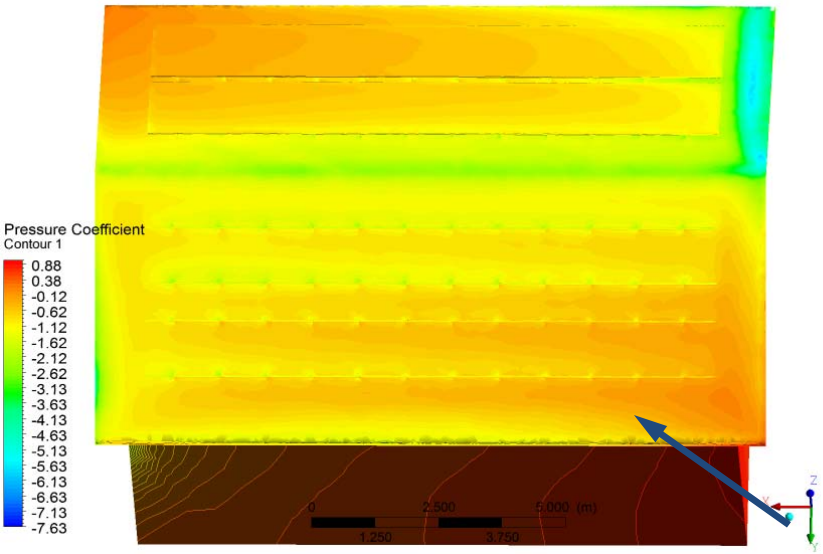


Fig. D. 2. Cp on Roof under the solar panels, solar panels cut off, WW, WD 45º

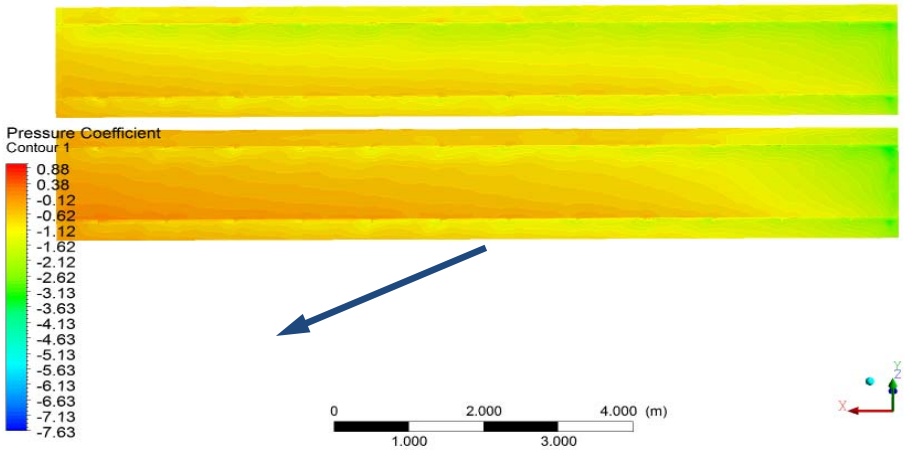


Fig. D. 3. Cp on bottom of the solar panels, LW, WD 45º

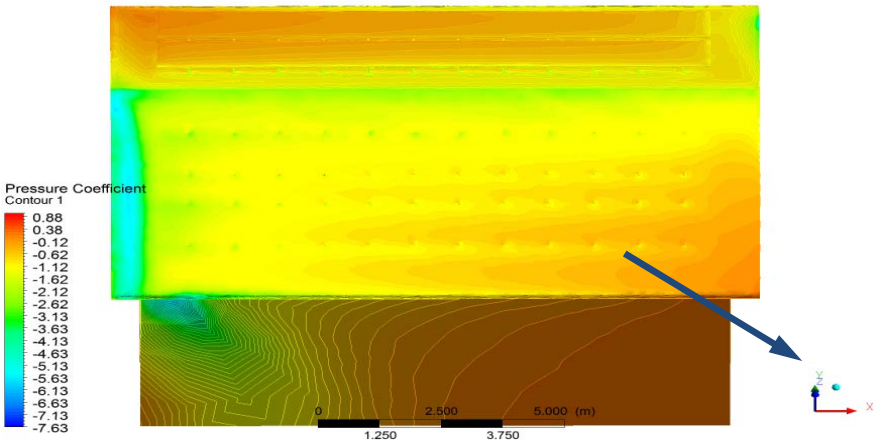


Fig. D. 4. Cp on Roof under the solar panels, solar panels cut off, LW, WD 45º

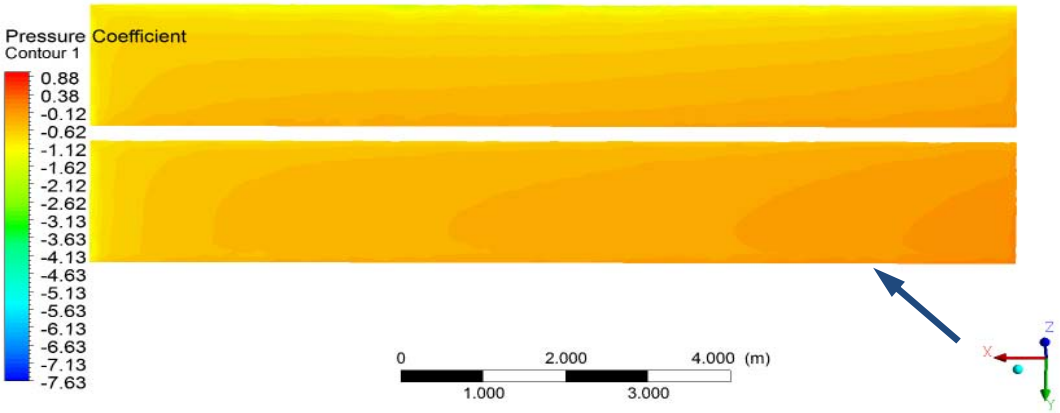


Fig. D. 5. Cp on top of the solar panel, WW, WD 45º

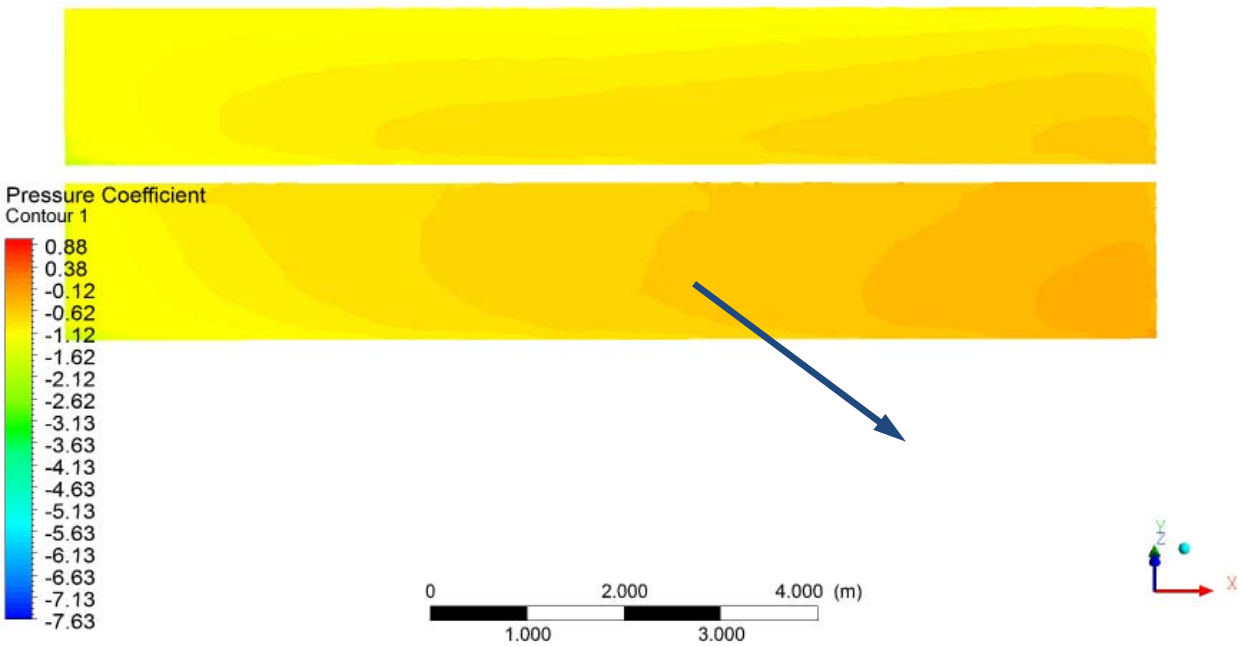


Fig. D. 6. Cp on top of the solar panel, LW, WD 45º

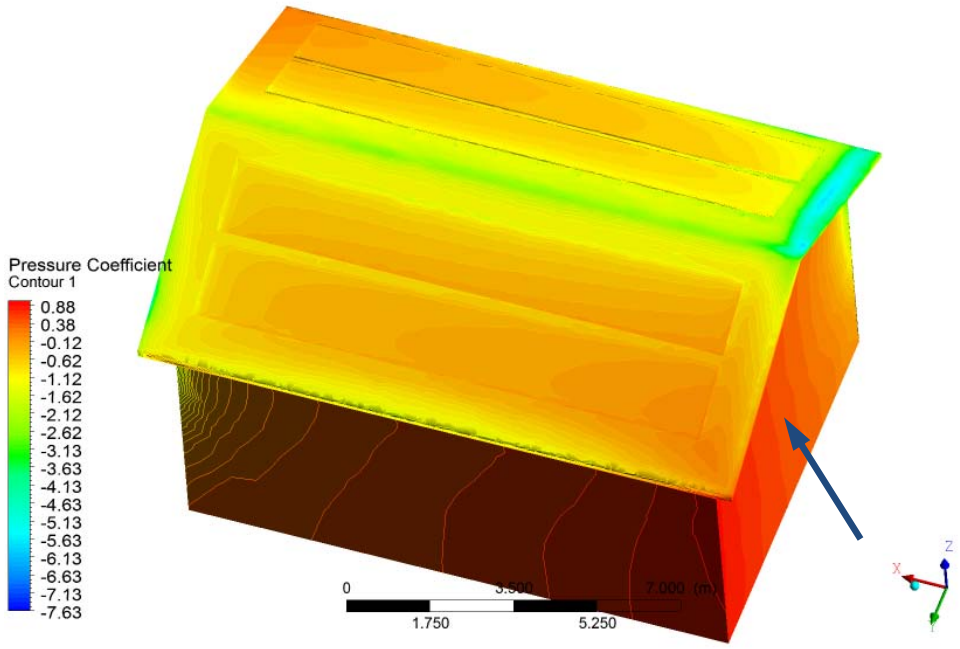


Fig. D. 7. Cp on top surface of the solar panels, WW, WD 45º

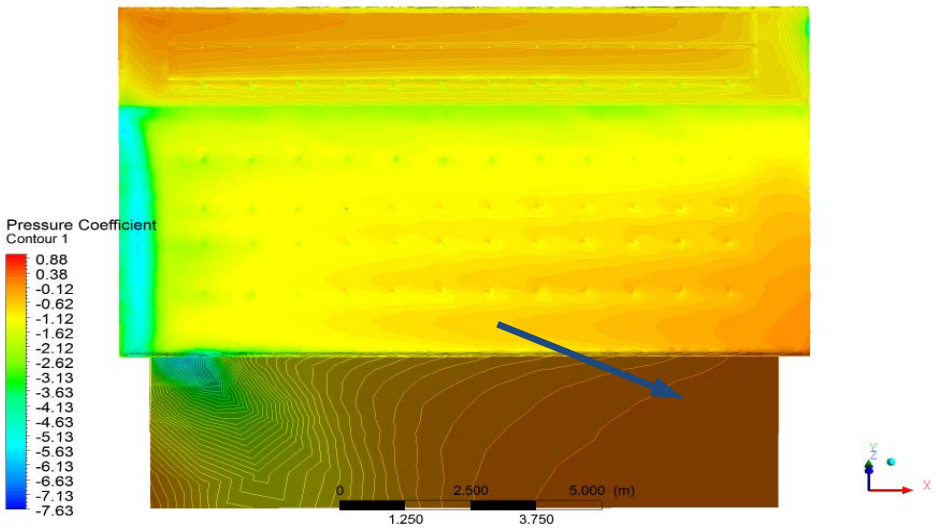


Fig. D. 8. Cp on top surface of the solar panels, LW, WD 45º

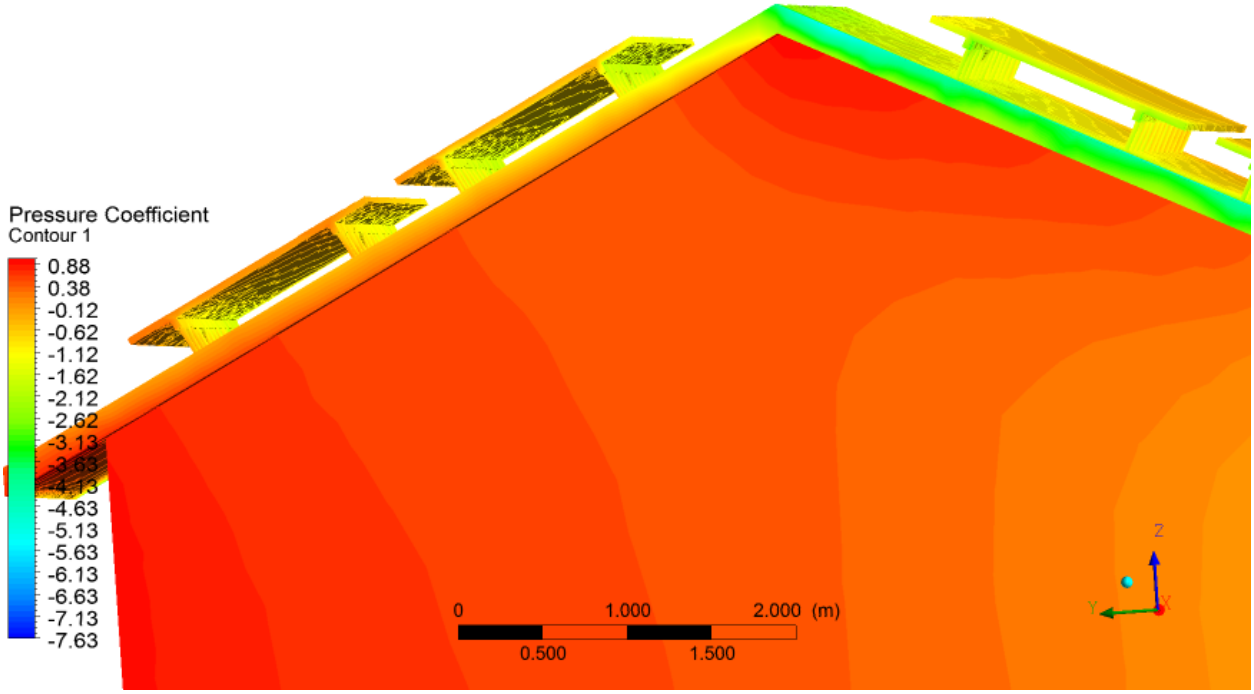


Fig. D. 9. Cp, Close view panel support to roof, WW, WD 45º

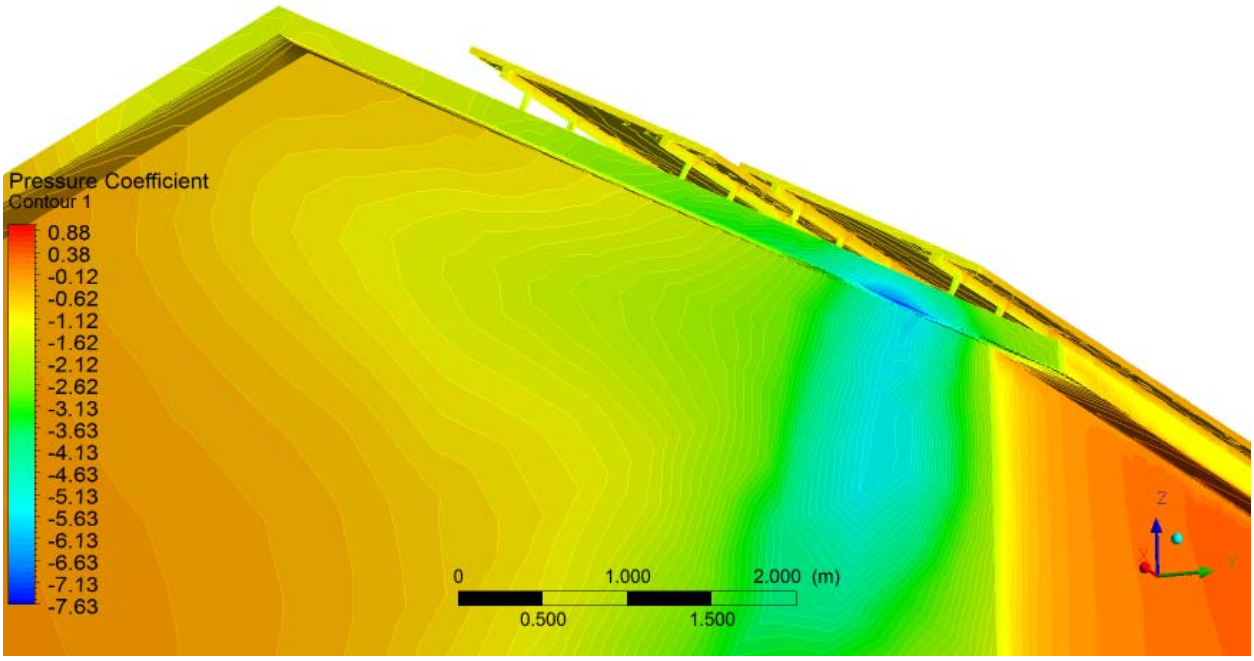


Fig. D. 10. Cp, Close view panel support to roof, LW, WD 45º

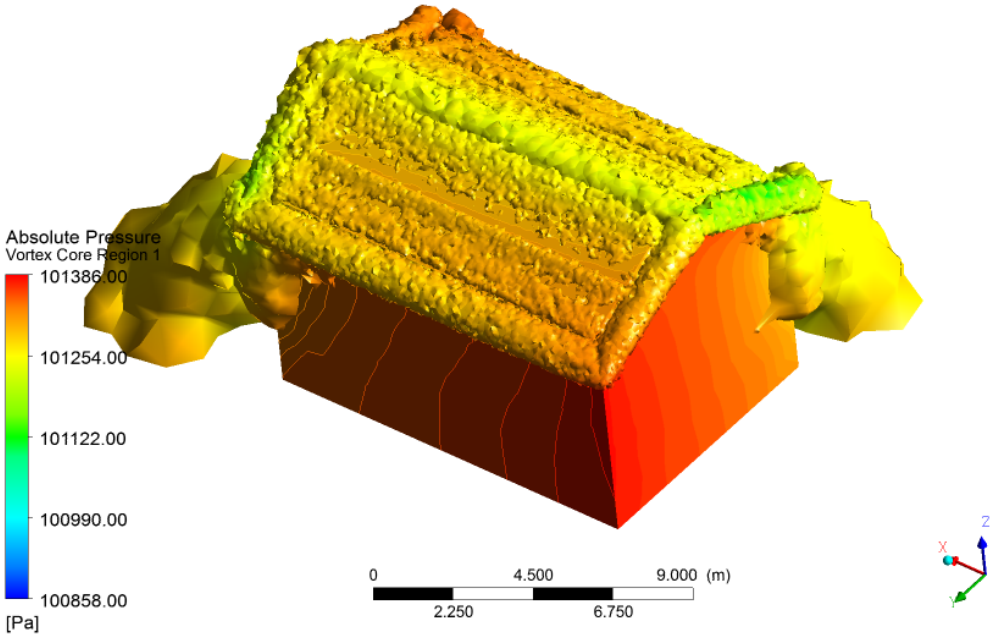


Fig. D. 11. Turbulences, WD 45º, WW

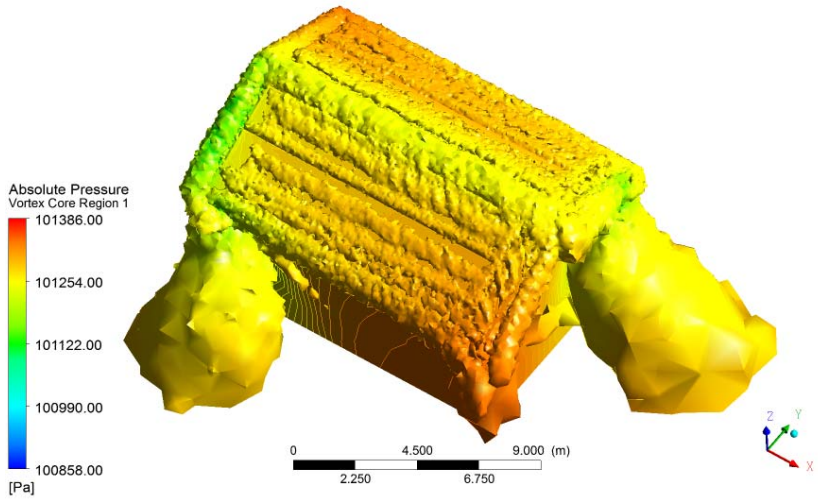


Fig. D. 12. Turbulences, WD 45º, LW

1.1.2. WIND DIRECTION 90º

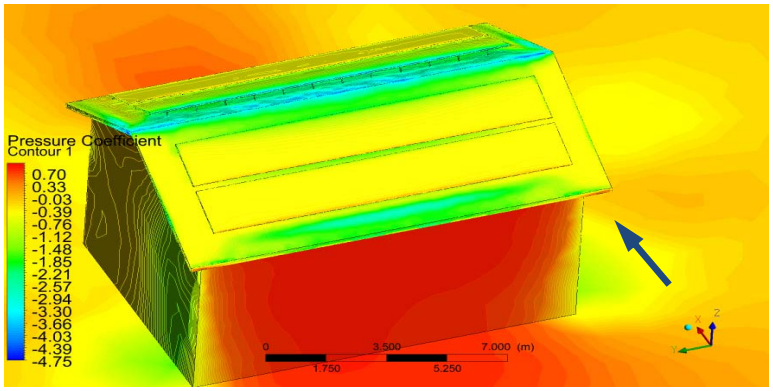


Fig. D. 13. CP on whole building and solar panels, S 27º, WW, WD 90º

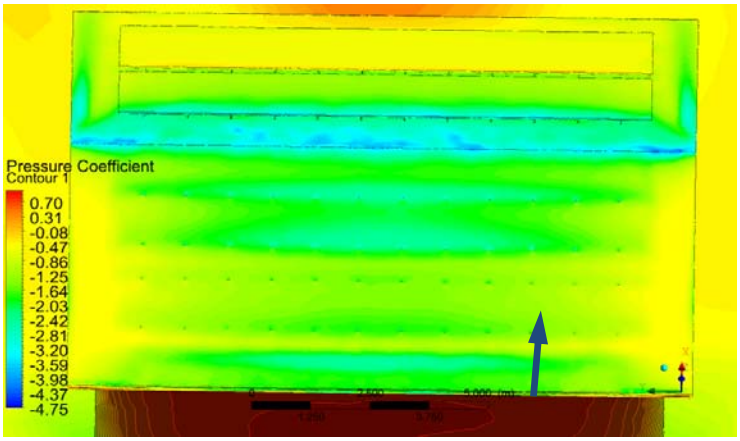


Fig. D. 14. CP on roof under solar panels, S 27º, WW, WD 90º

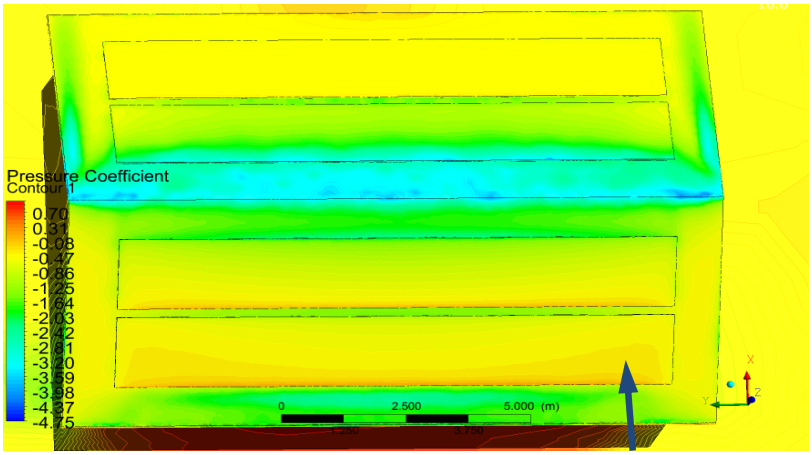


Fig. D. 15. CP on roof, S 27º, WW, WD 90º

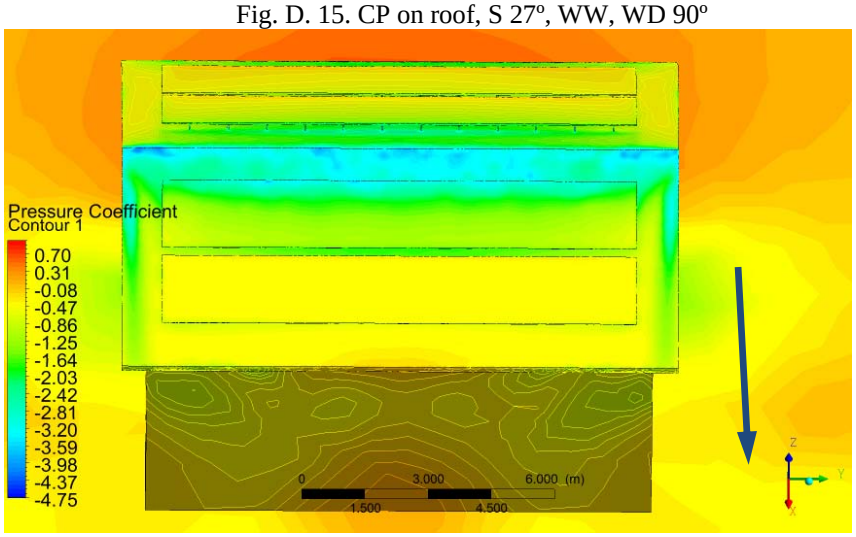


Fig. D. 16. CP on whole building and solar panels, S 27º, LW, WD 90º

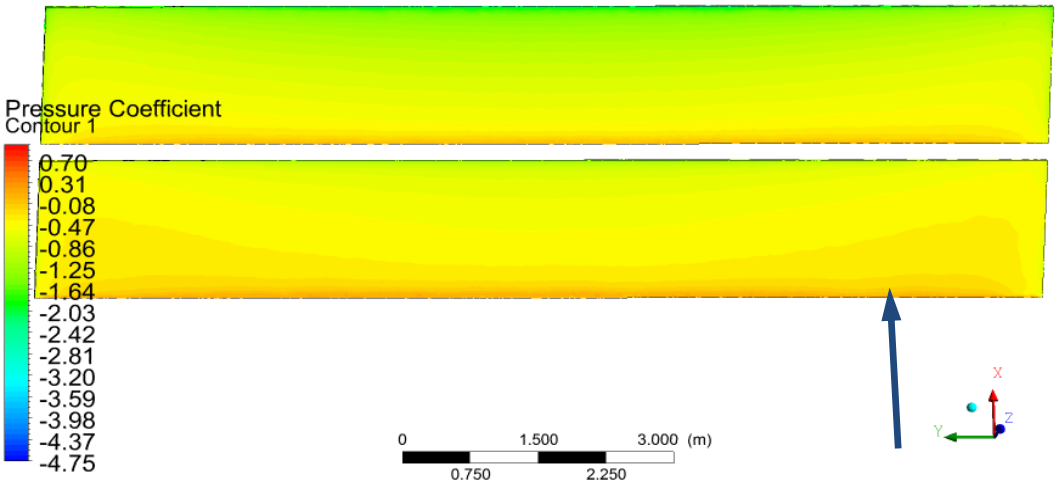


Fig. D. 17. CP on top of solar panels, S 27º, WW, WD 90º

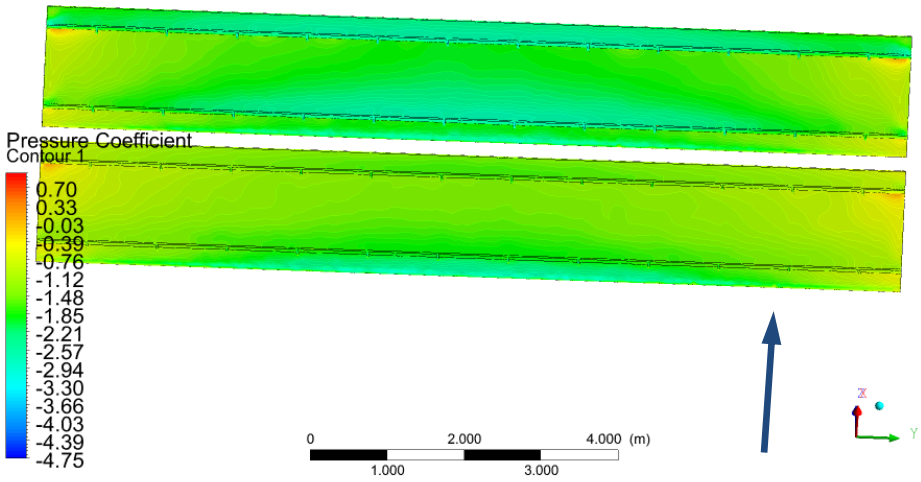


Fig. D. 18. CP on bottom of solar panels, S 27º, WW, WD 90º

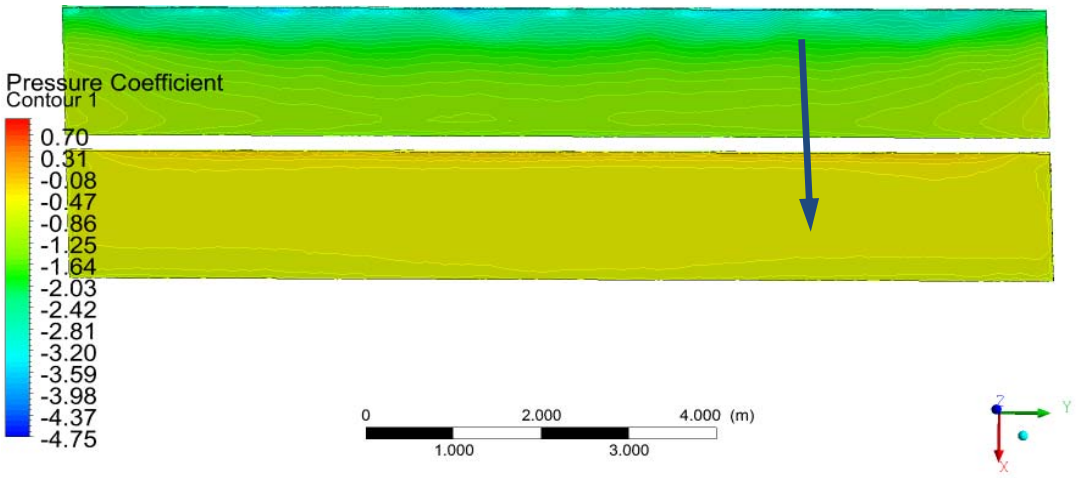


Fig. D. 19. CP on top of solar panels, S 27º, LW, WD 90º

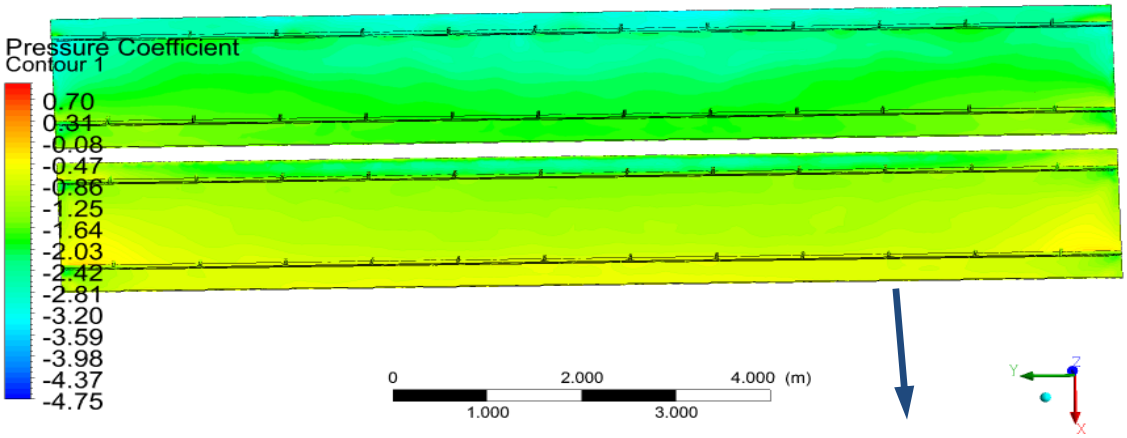


Fig. D. 20. CP on bottom of solar panels, S 27º, LW, WD 90º

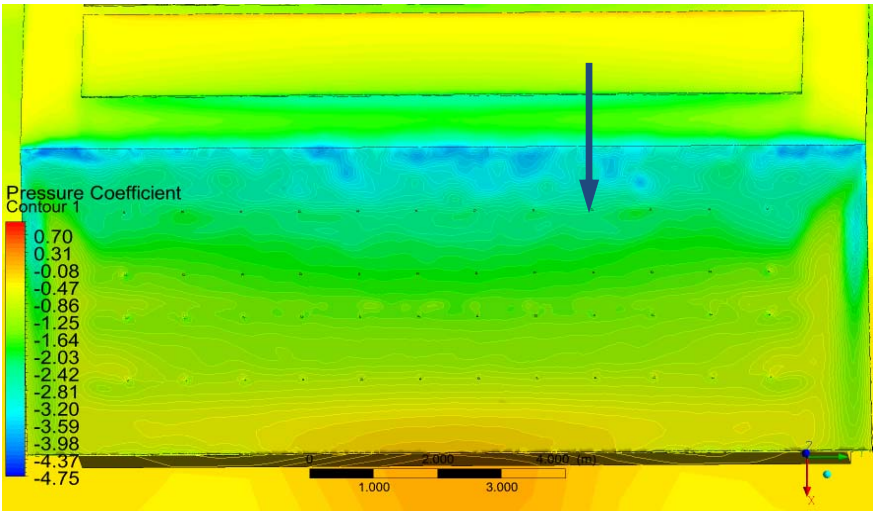


Fig. D. 21. CP on roof under solar panels, S 27º, LW, WD 90º

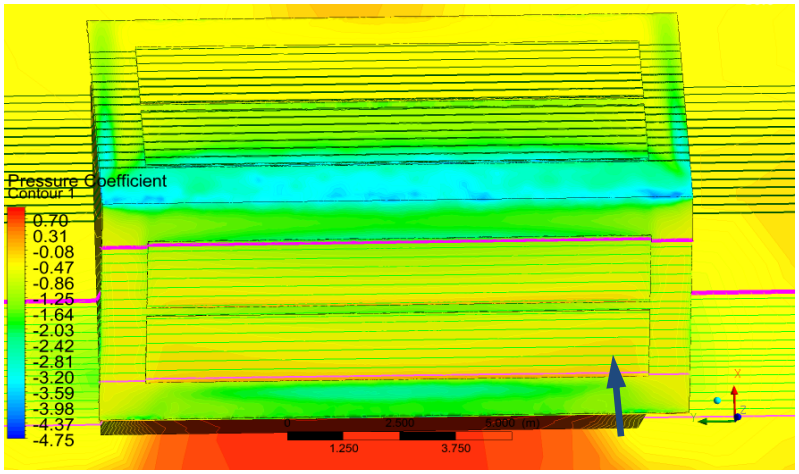


Fig. D. 22. Cp on top of solar panels with plines, S 27º, WW, WD 90º

1.1.3. WIND DIRECTION 0º

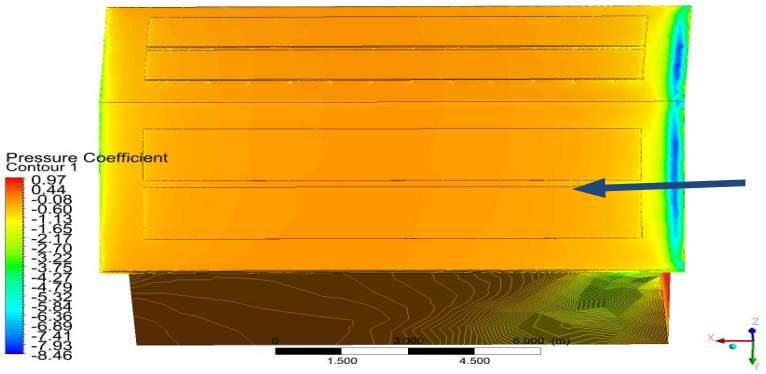


Fig. D. 23. Cp on roof with solar panels, S 27º, WD 0.0º

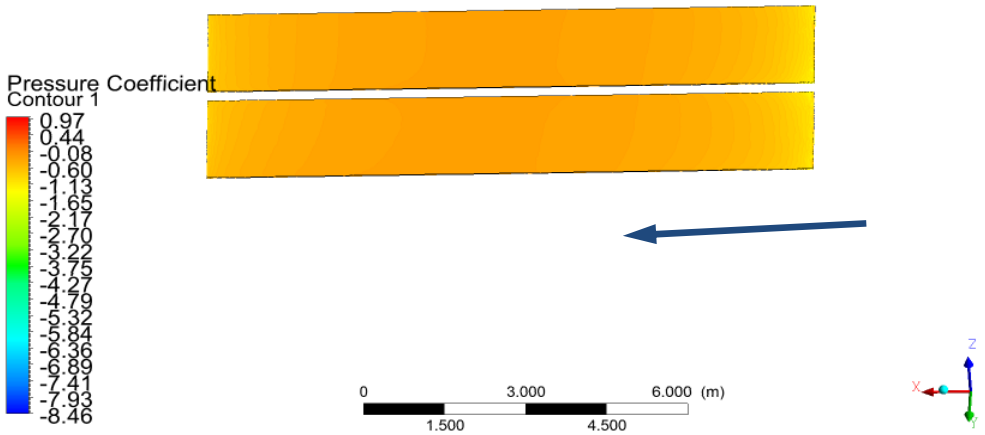


Fig. D. 24. Cp on top of solar panels, S 27º, WD 0º

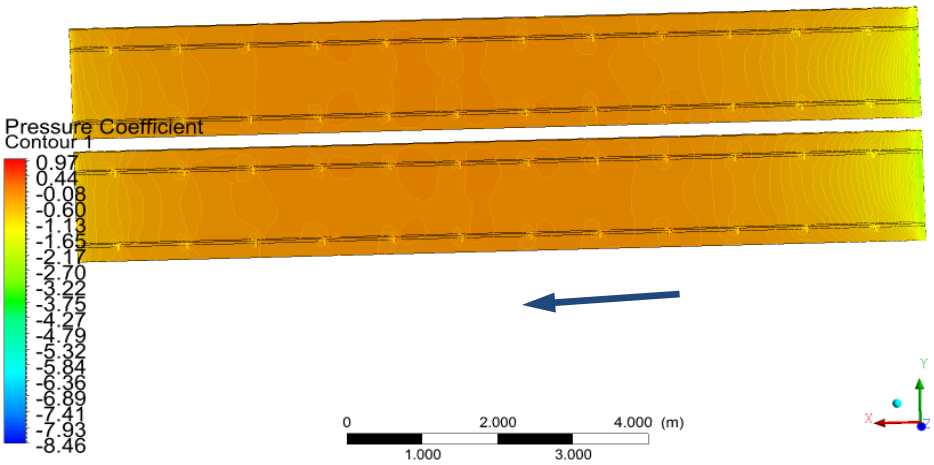


Fig. D. 25. Cp on bottom of solar panels, S 27º, WW, WD 0º

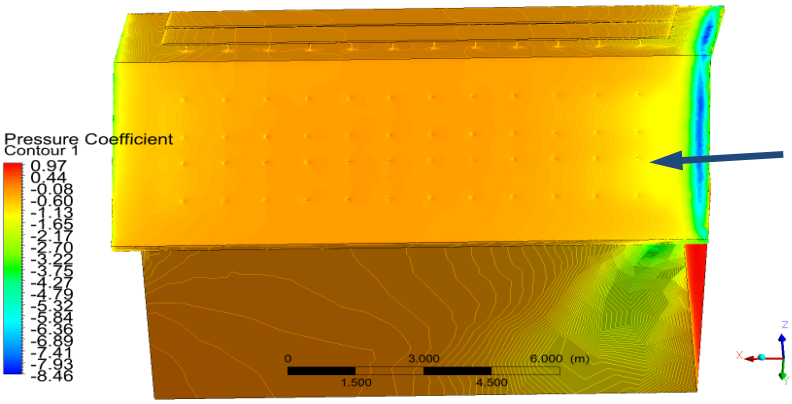


Fig. D. 26. Cp on roof under the solar panels, S 27º, WW, WD 0º

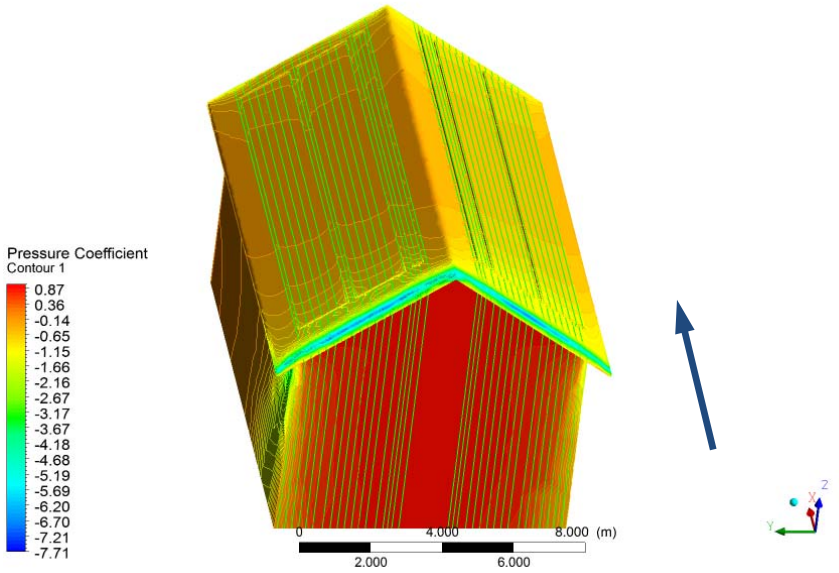


Fig. D. 27. Polylines distributions on the roofs, S 27º, WW, WD 0º

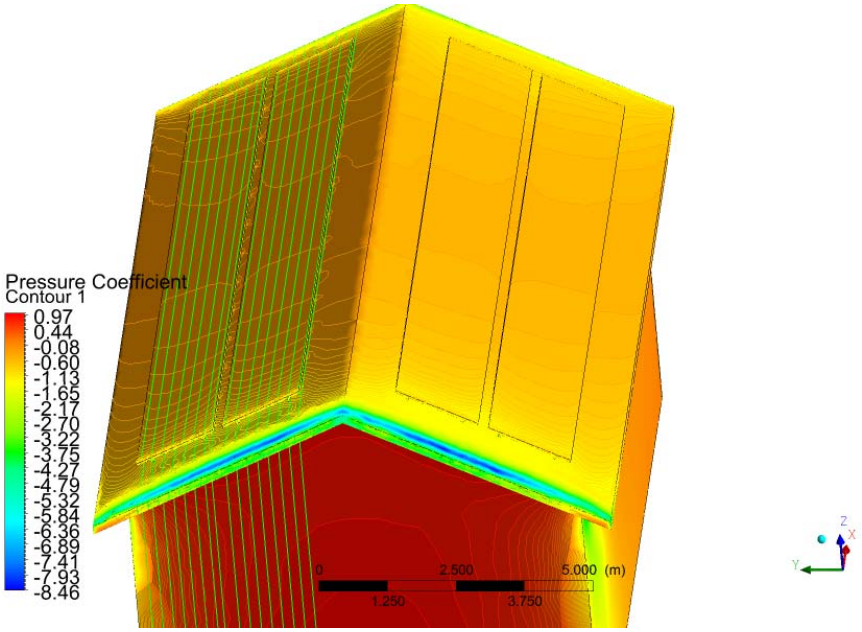


Fig. D. 28. Cp on top of solar panels and roof with Plines, S 27º, WW, WD 0º

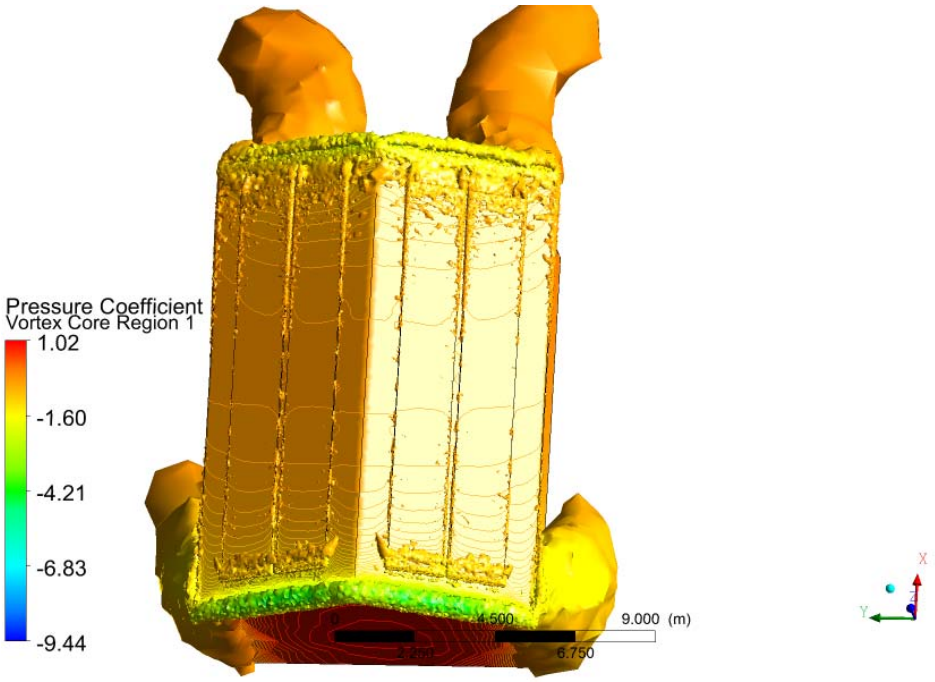


Fig. D. 29.Turbulences and Cp, S 27º, WW, WD 0º

1.1.4. Detailed Distribution of Wind Pressure and Wind Speed on Roof Mounted Solar Panels In Comparison with Bare Roofs, Windward, S8" , C10"

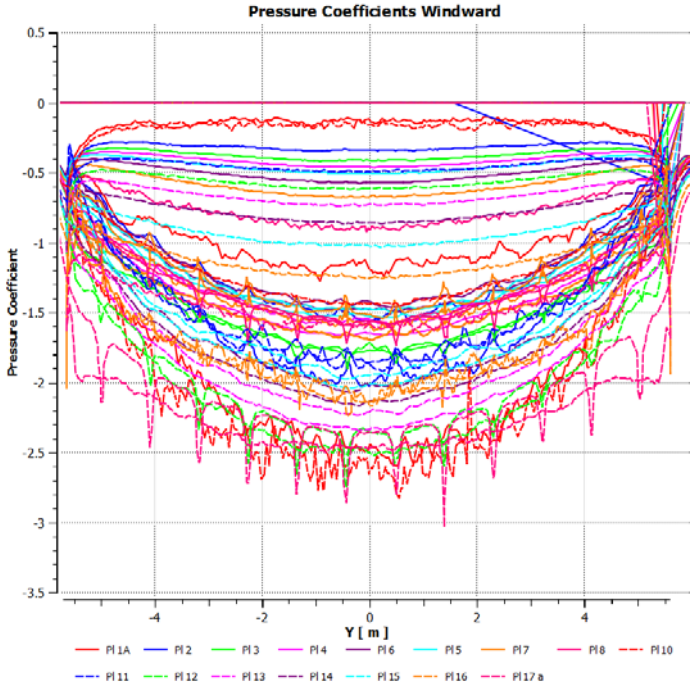


Fig. D. 30. Cp, All polylines, S 27 º, WW, WD 90 º

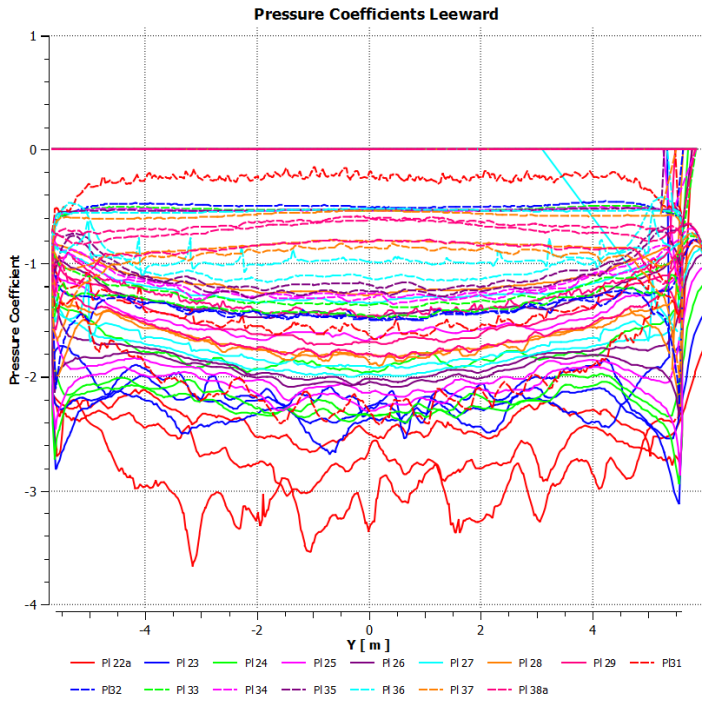


Fig. D. 31. Cp, All polylines, S 27 º, LW, WD 90 º

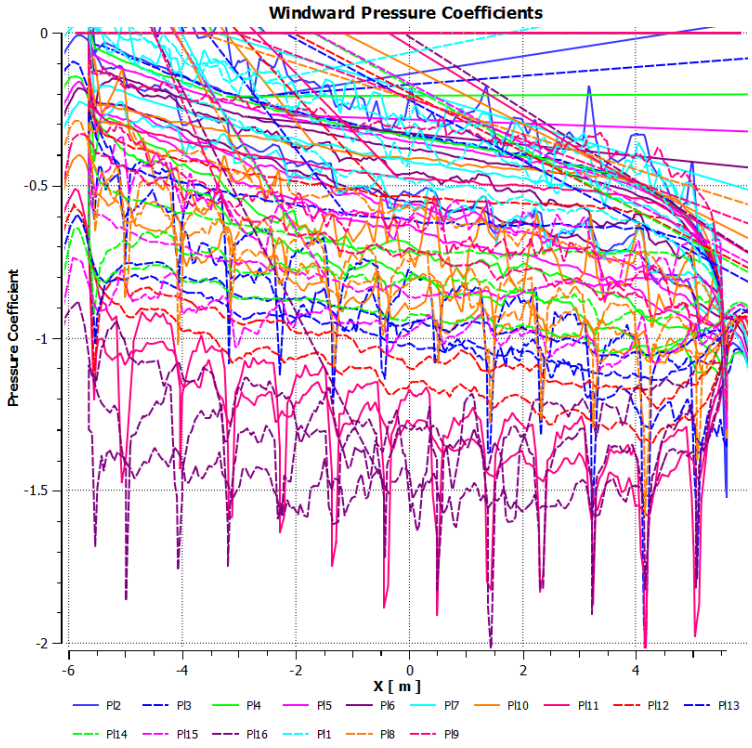


Fig. D. 32.Cp, All polylines, S 27 º, WW, WD 45 º

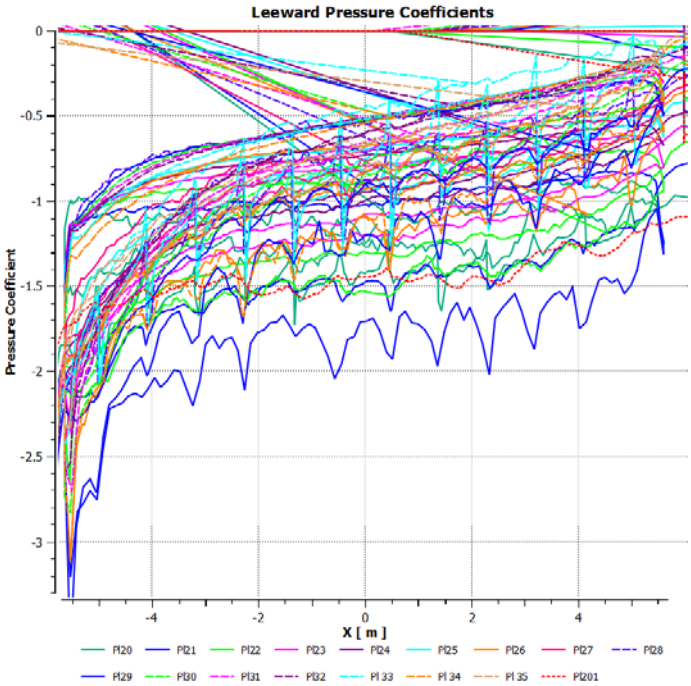


Fig. D. 33 Cp, All polylines, S 27 º, LW, WD 45 º

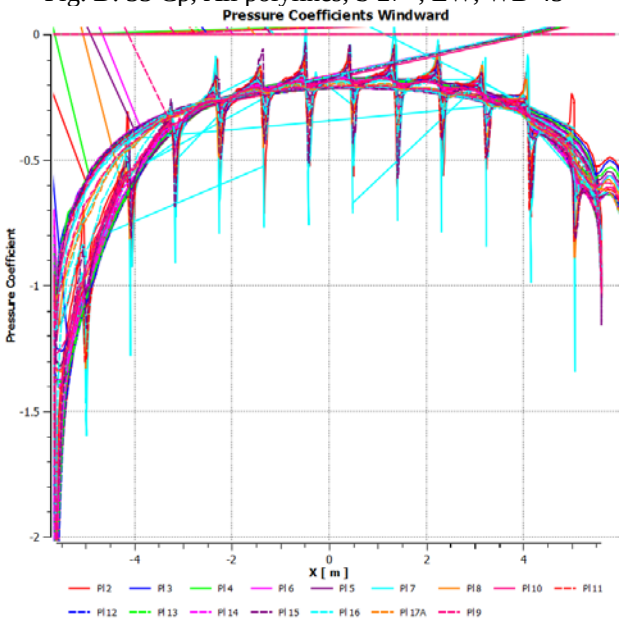


Fig. D. 34 Cp, All polylines, S 27 º, LW, WD 0.0 º

1.1.5. Detailed Distribution Of Wind Pressure and Speed, and Flow on Roof Mounted Solar Panels, S 8", C10"

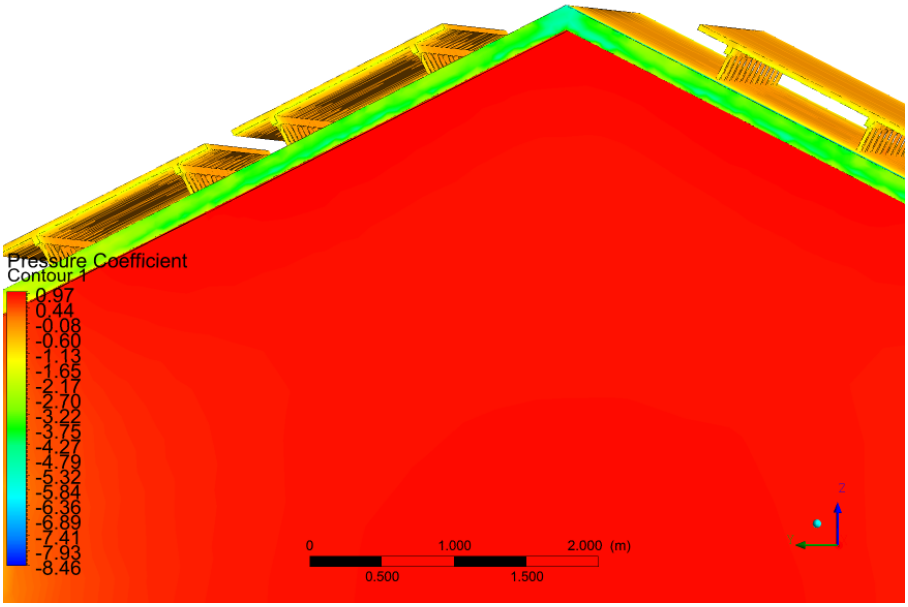


Fig. D. 35. Close view shows panel supports to roof, WD 0º.

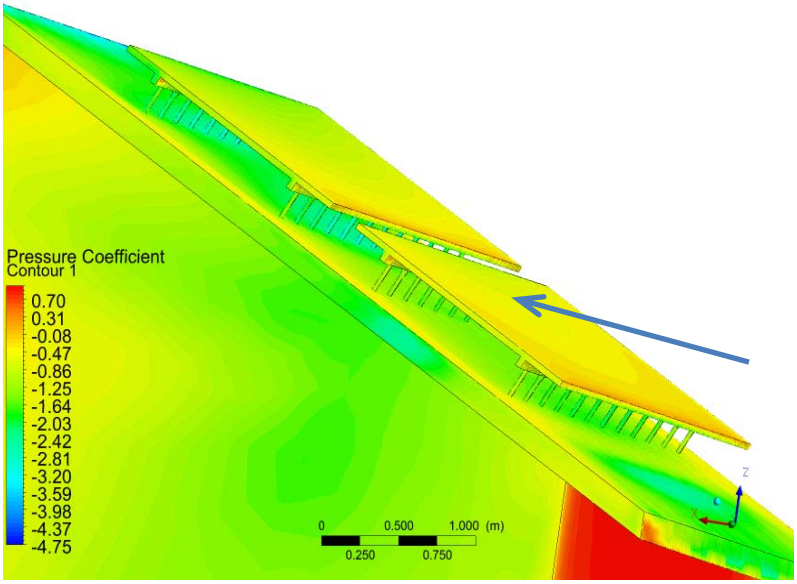


Fig. D. 36. Close view shows panel support to roof, WW, WD 90º

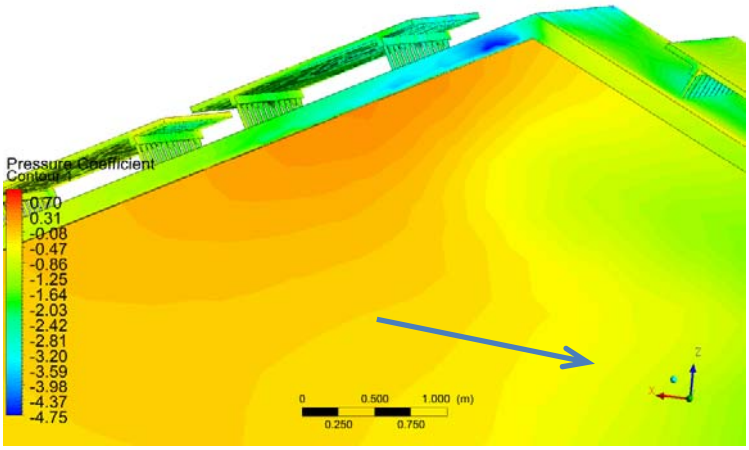


Fig. D. 37. Close view shows panel support to roof, LW, WD 90º

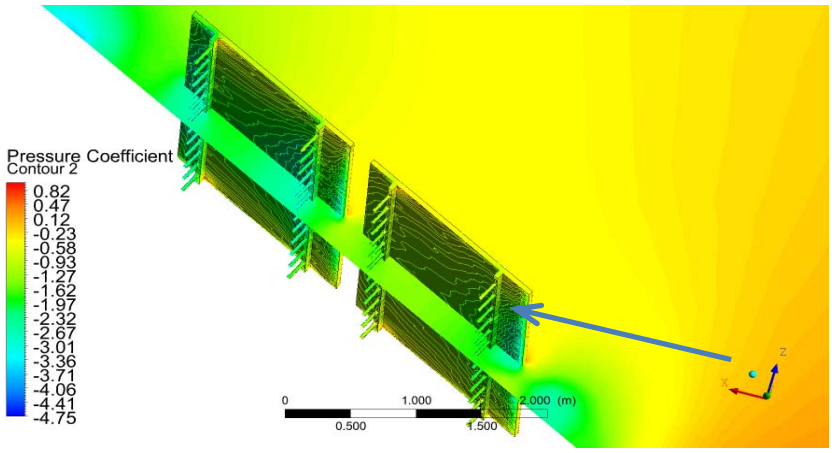


Fig. D. 38. Cp on a perpendicular plane under panels, Close up WD 90º, WW

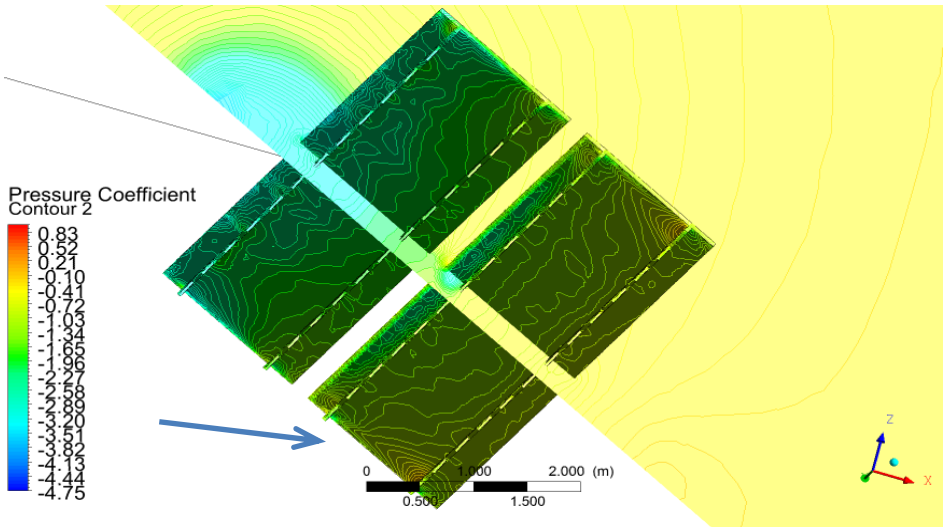


Fig. D. 39. Cp on a perpendicular plane under panels, WD 90º, LW

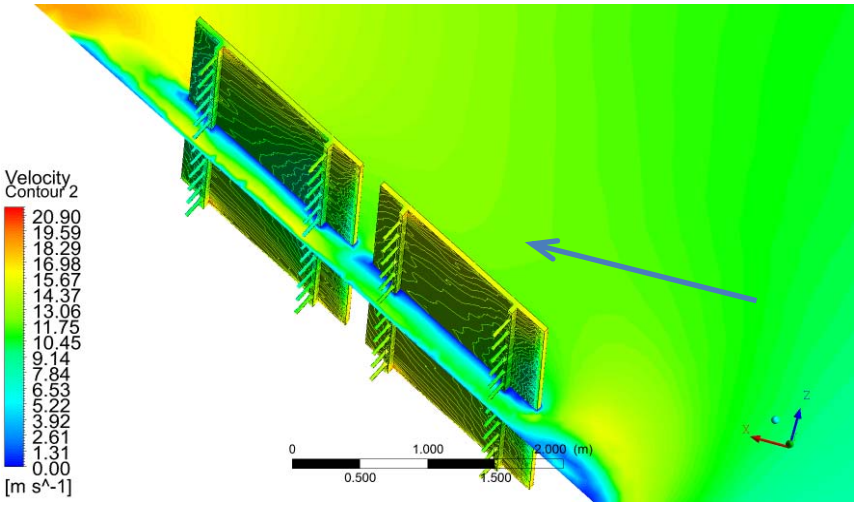


Fig. D. 40. Velocity distribution on a perpendicular plane under panels, Close up WD 90º, WW

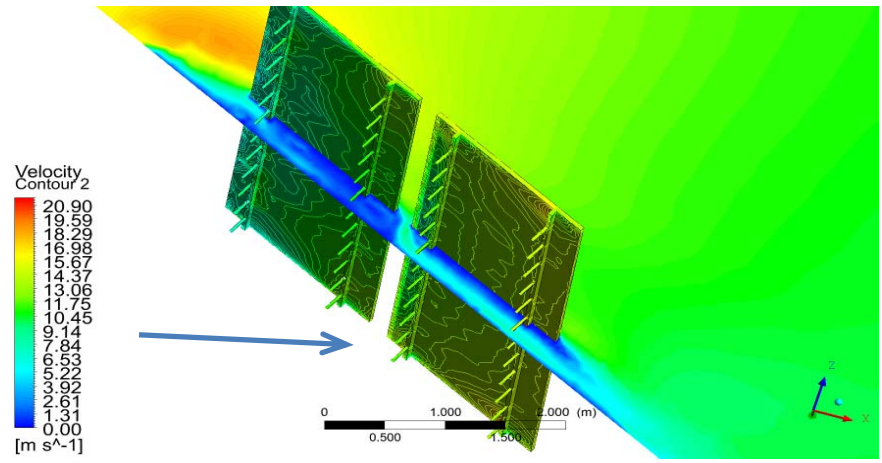


Fig. D. 41. Velocity distribution on a perpendicular plane under panels, Close up WD 90º, LW

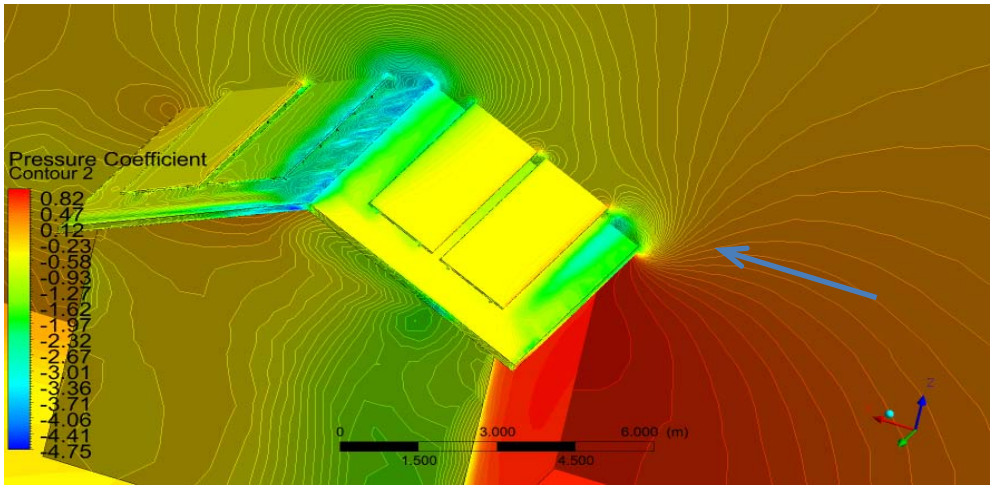


Fig. D. 42. Cp on a perpendicular plane with the ridge of the house, WD 90º

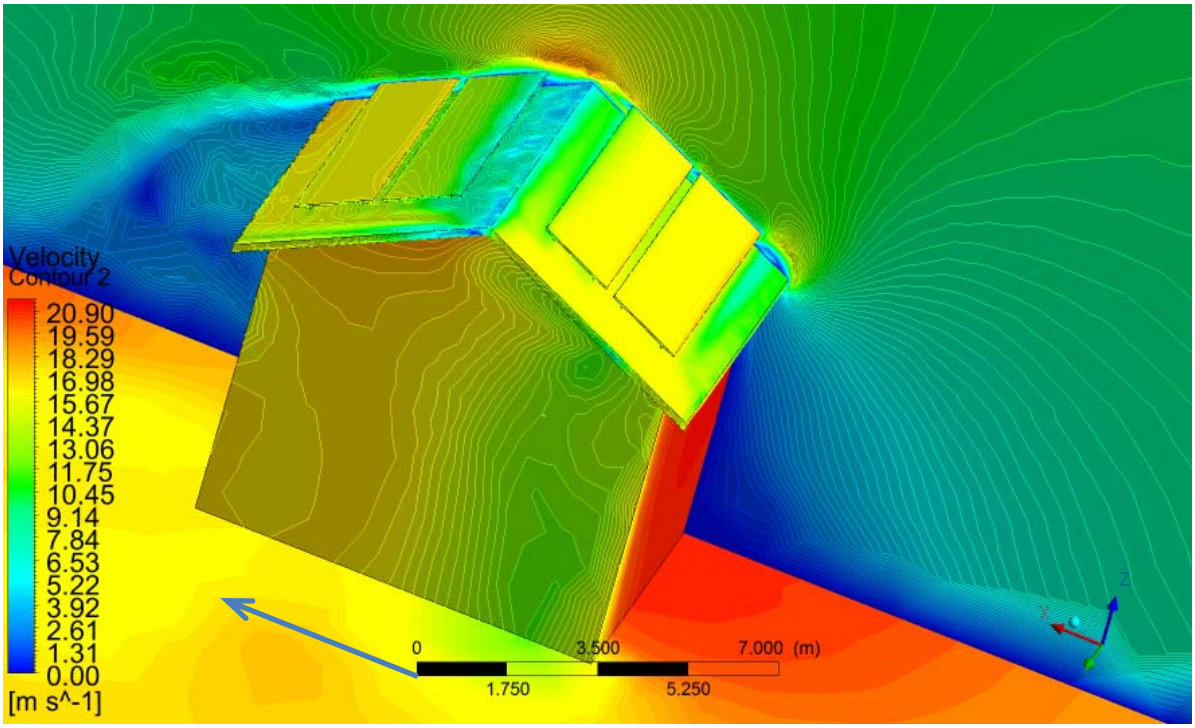


Fig. D. 43. Wind velocity on a perpendicular plane with the ridge of the house, WD 90º

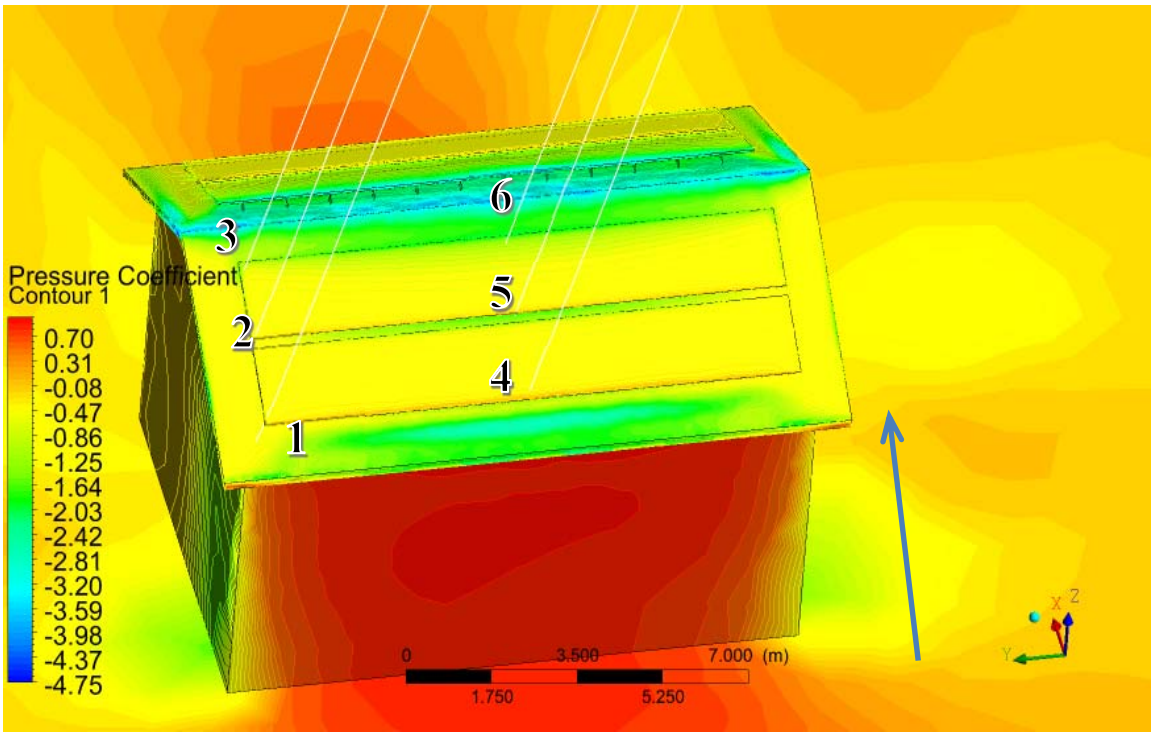


Fig. D. 44. Lines used to draw velocity and pressure changes, WD 90º

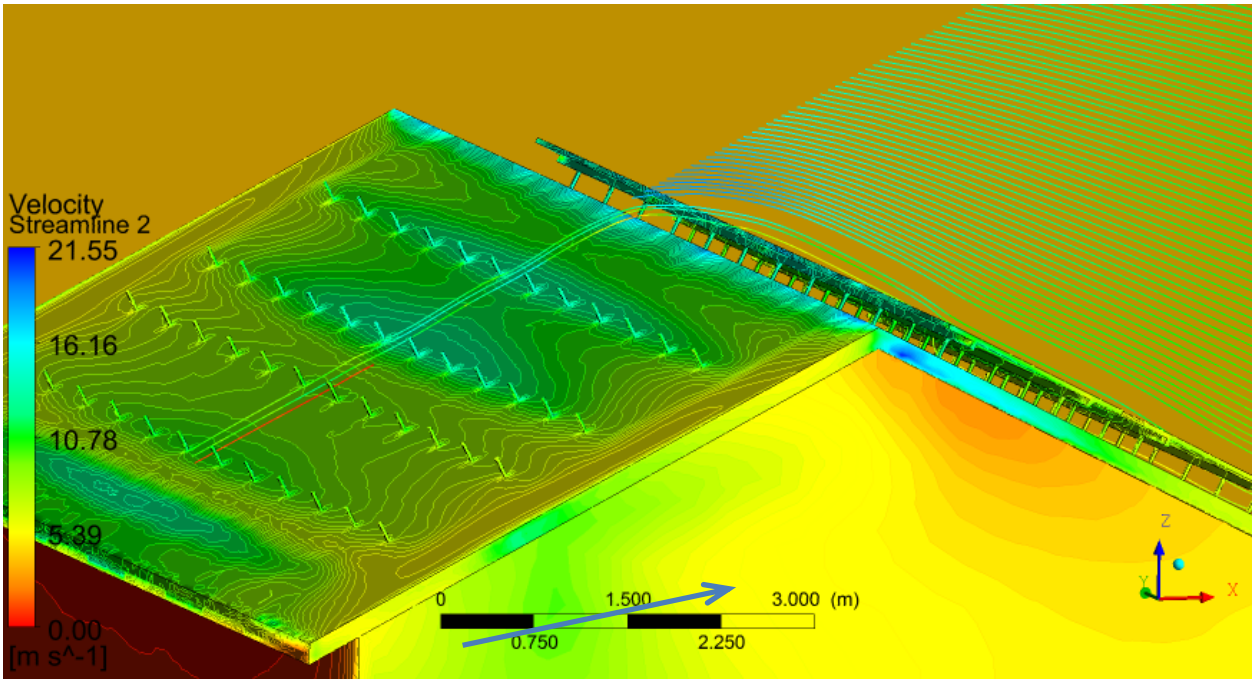


Fig. D. 45. Velocity stream lines at middle perpendicular plane under panels, WD 90º

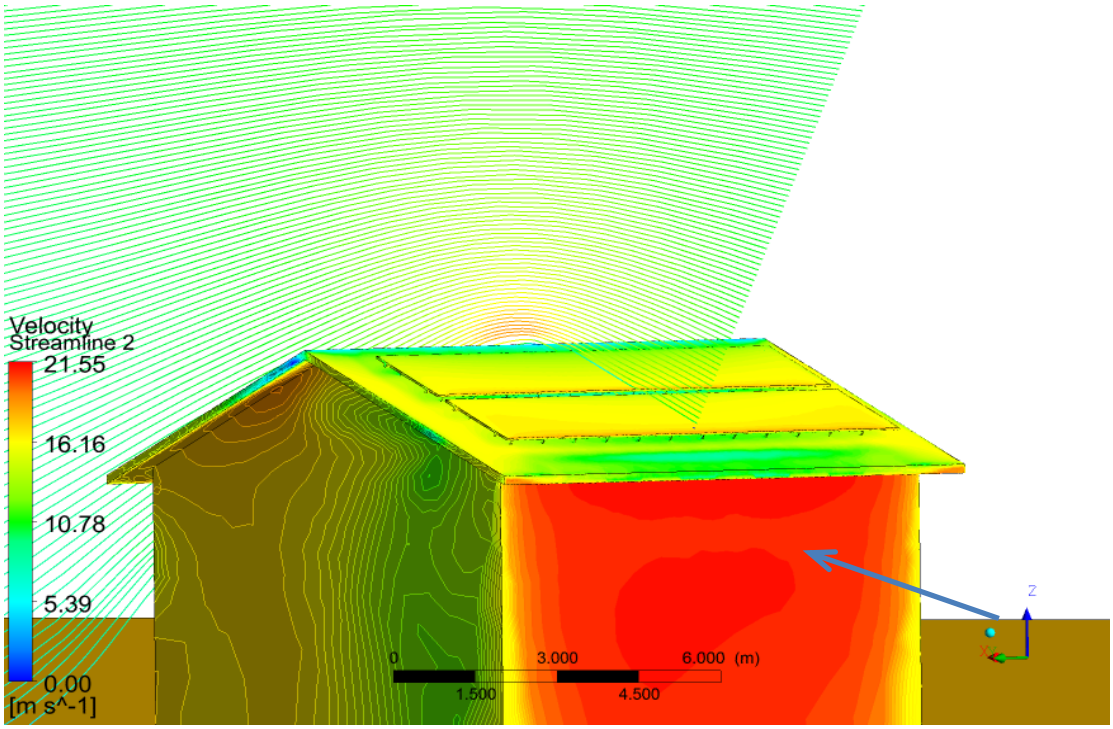


Fig. D. 46. Velocity stream lines at middle perpendicular plane above panels, WD 90º

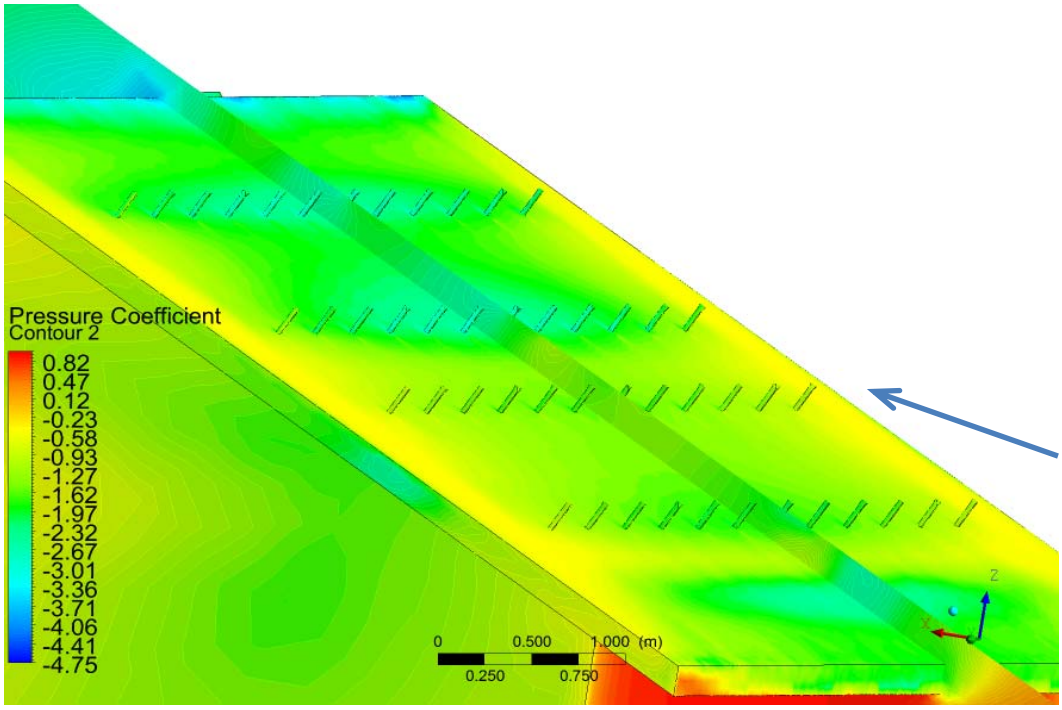


Fig. D. 47. Cp distribution on a perpendicular plane under panels, top view, WD 90º, WW

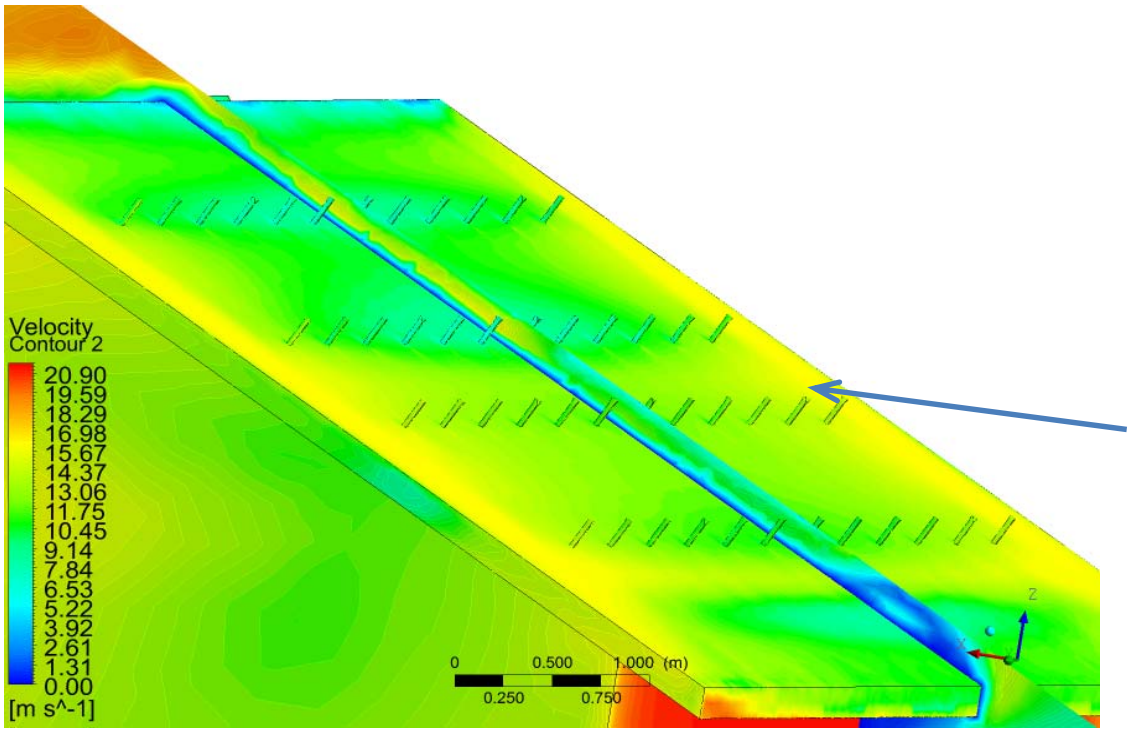


Fig. D. 48. Velocity distribution on a perpendicular plane under panels, top view, WD 90º, WW

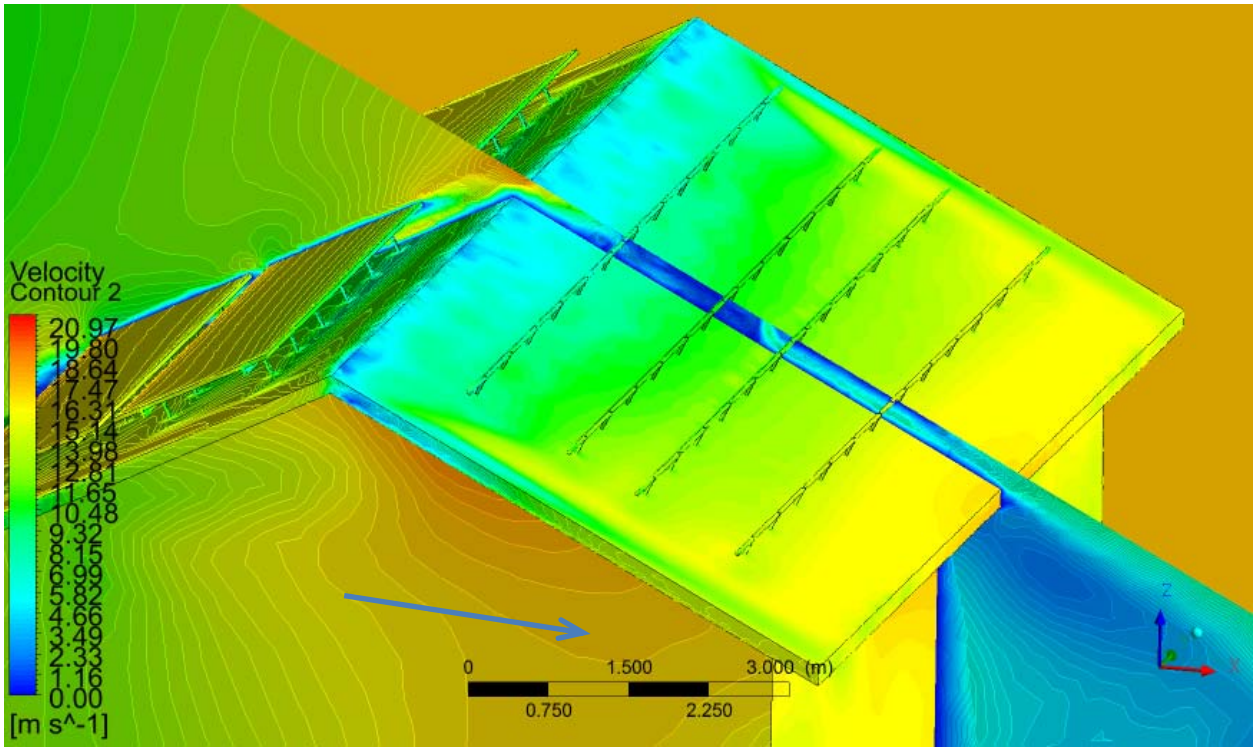


Fig. D. 49. Velocity distribution on a perpendicular plane under panels, top view, WD 90º, LW

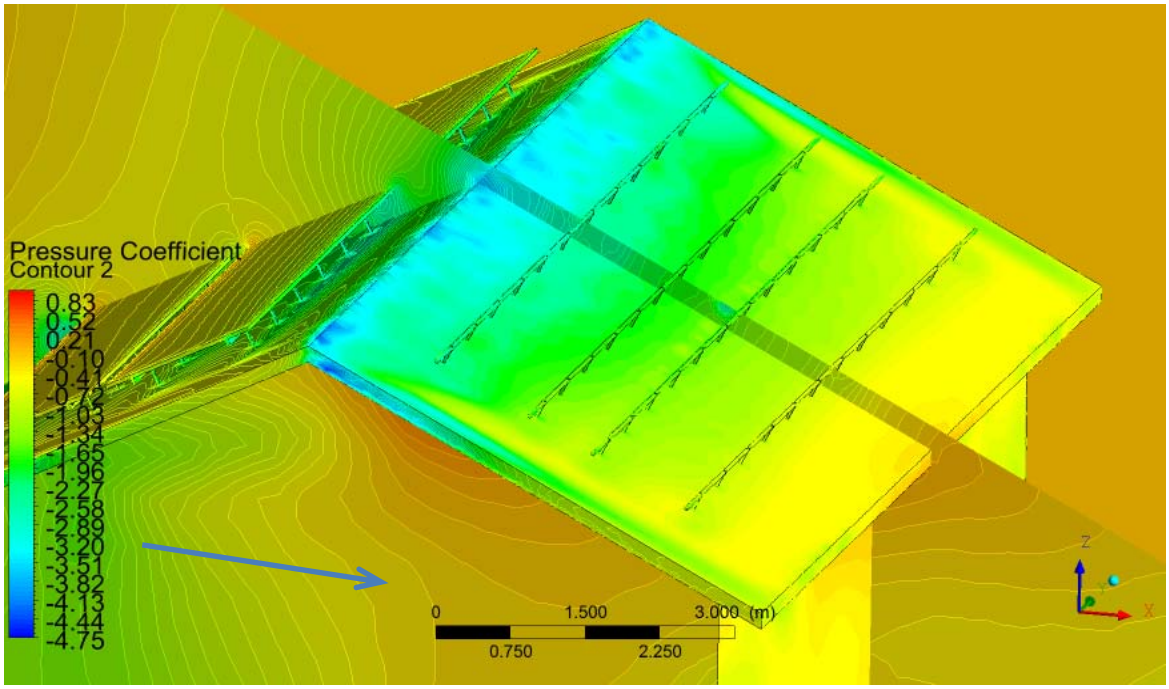


Fig. D. 50. Cp distribution on a perpendicular plane under panels, top view, WD 90º, LW

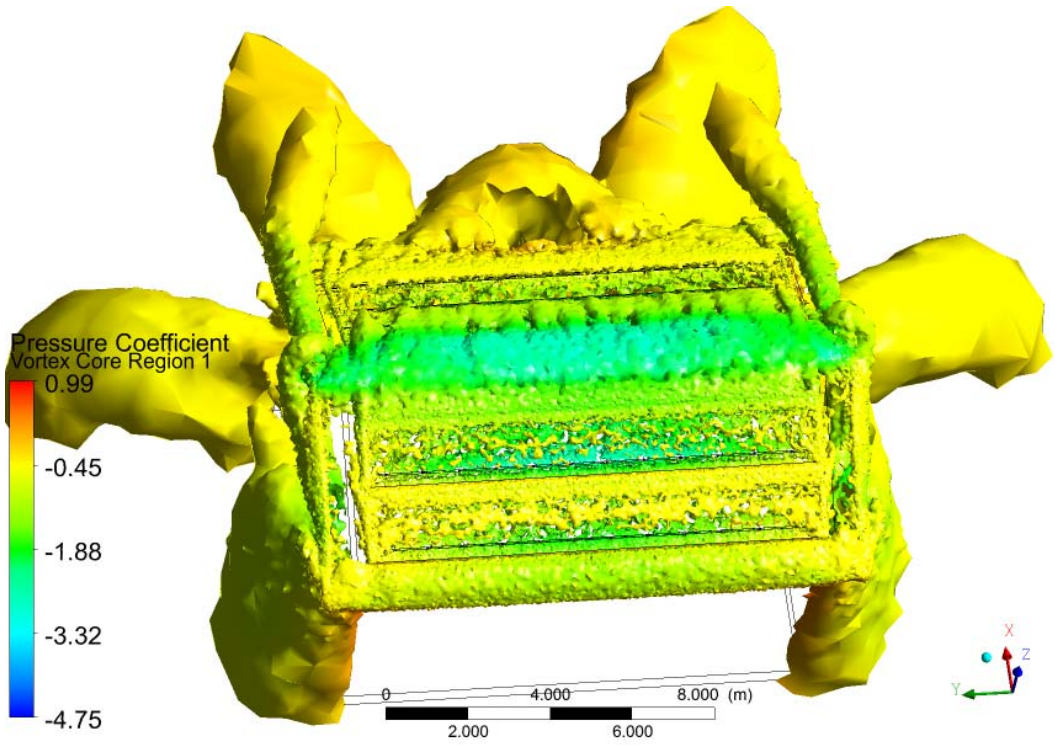


Fig. D. 51. Turbulence distribution on roof without building contour, WD 90º , WW

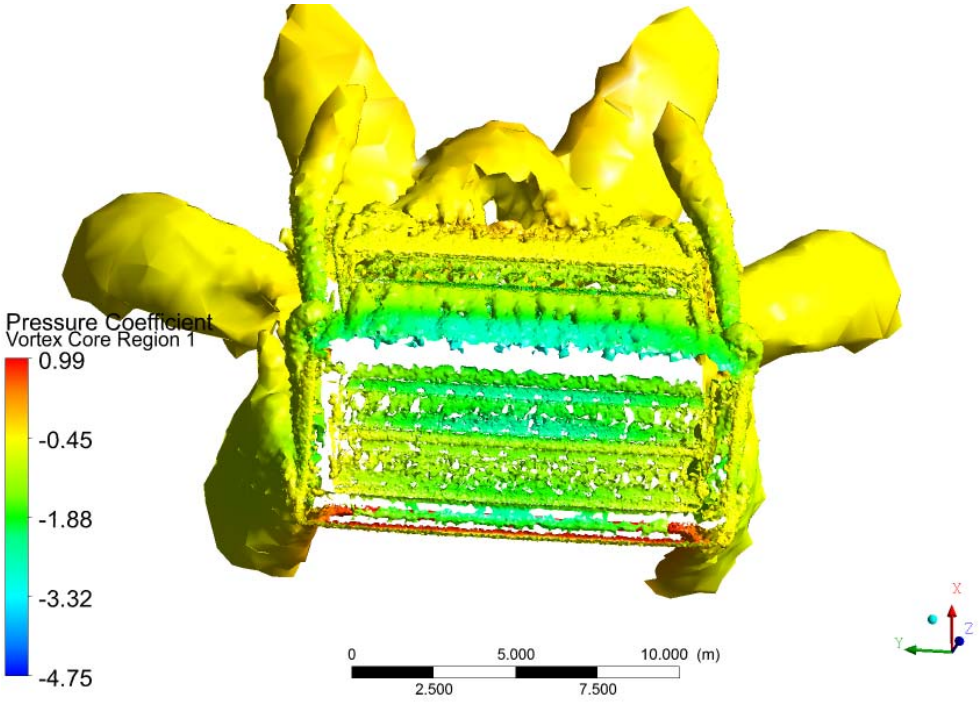


Fig. D. 52. Turbulence distribution on roof under panels, WD 90º , WW

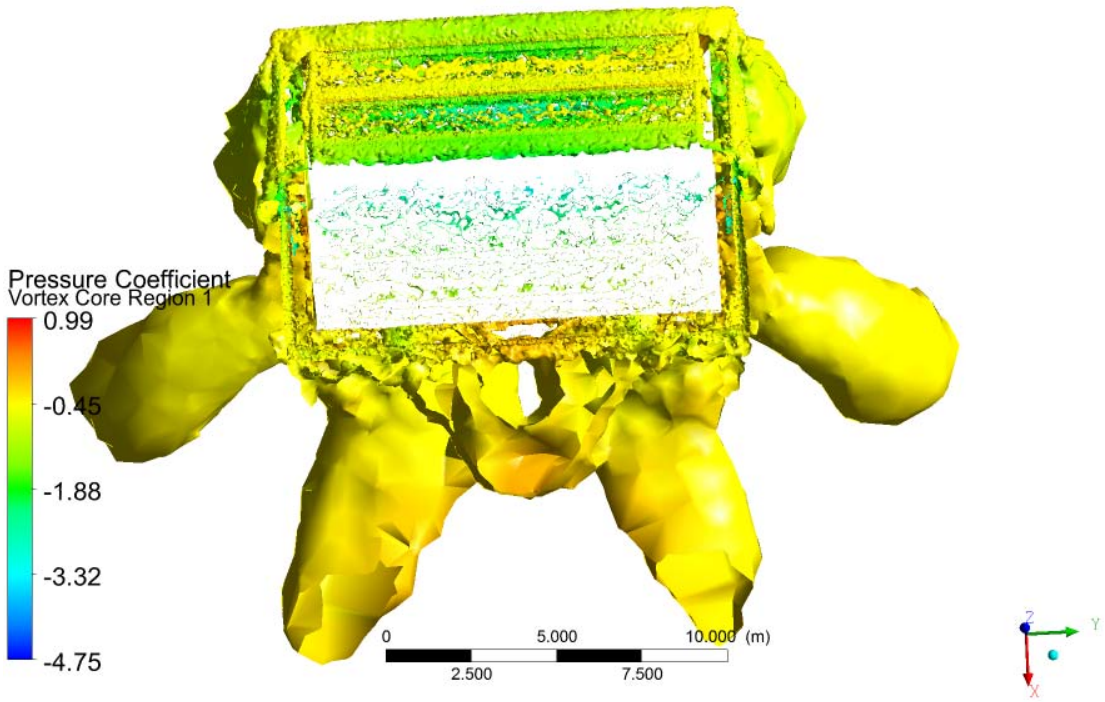


Fig. D. 53. Turbulence distribution on roof under panels, No building contour showed, WD 90º , LW

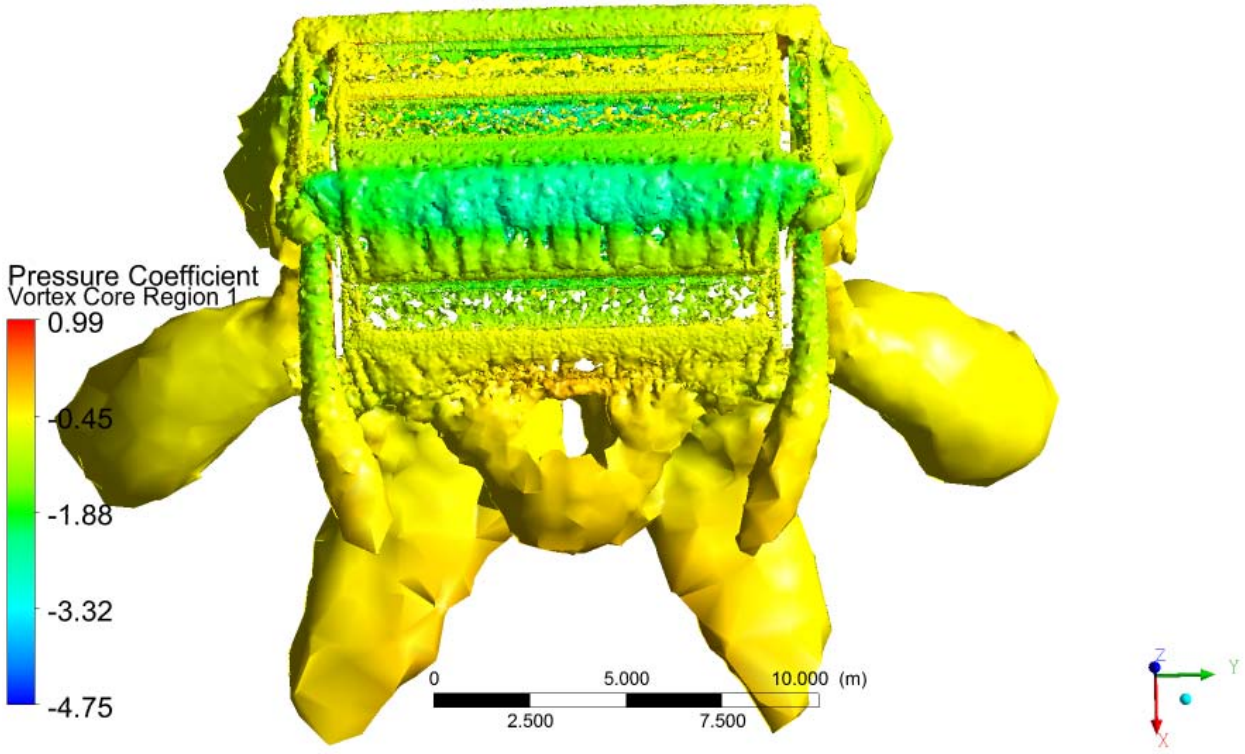


Fig. D. 54. Turbulence distribution, No building contour showed, WD 90º , LW

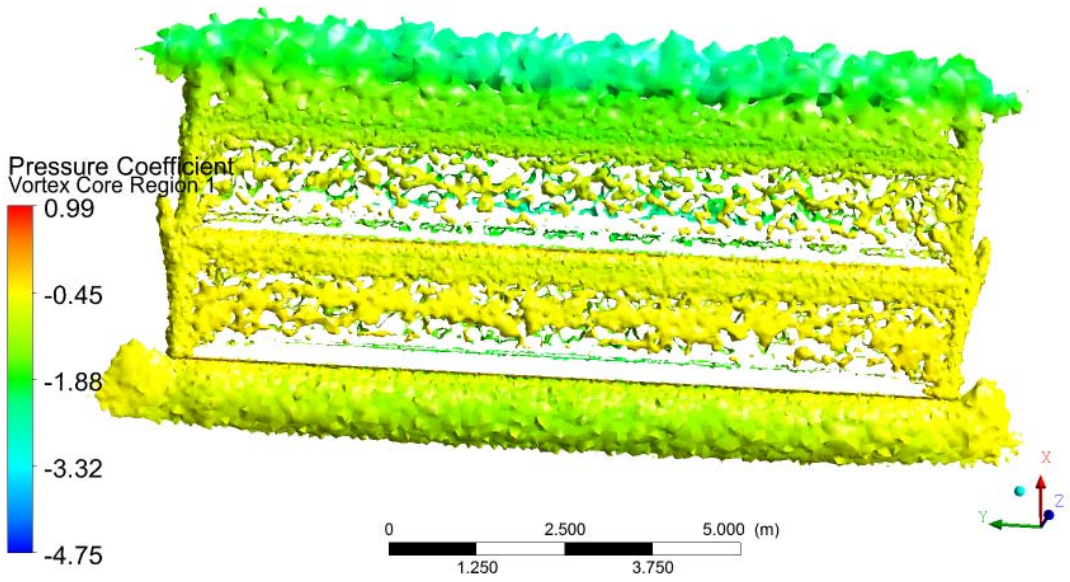


Fig. D. 55. Turbulence distribution, on top of the panels, No Building contours shown, WD 90º, WW

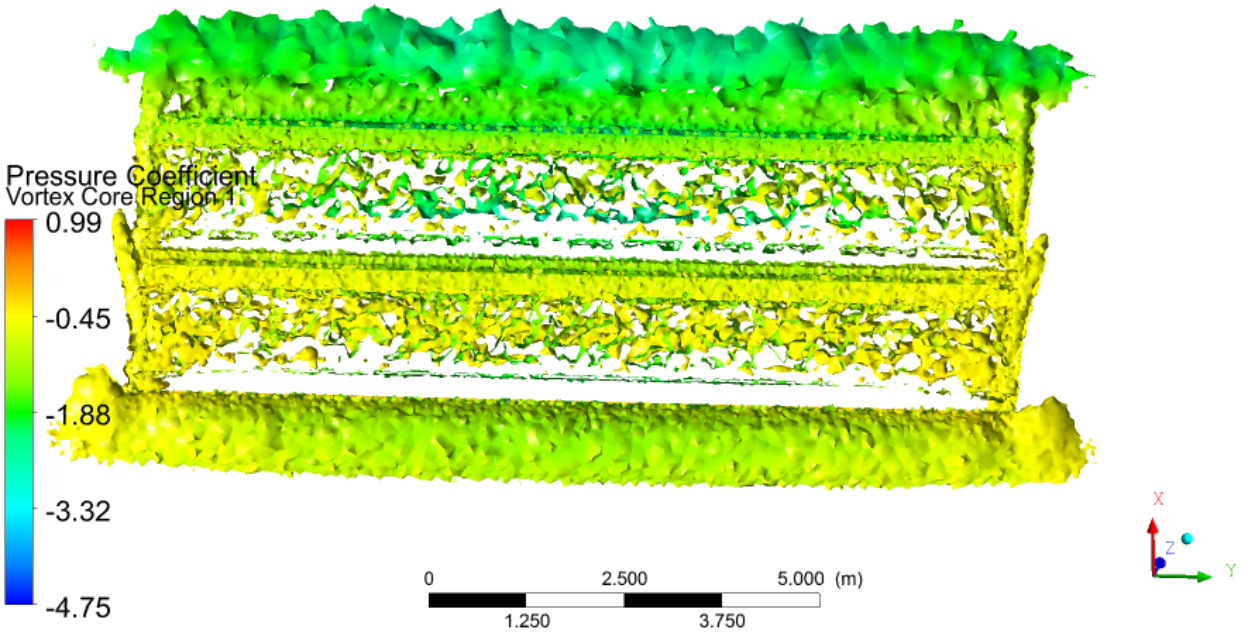


Fig. D. 56. Turbulence distribution, on bottom of the panels, No Building contours shown, WD 90º, WW

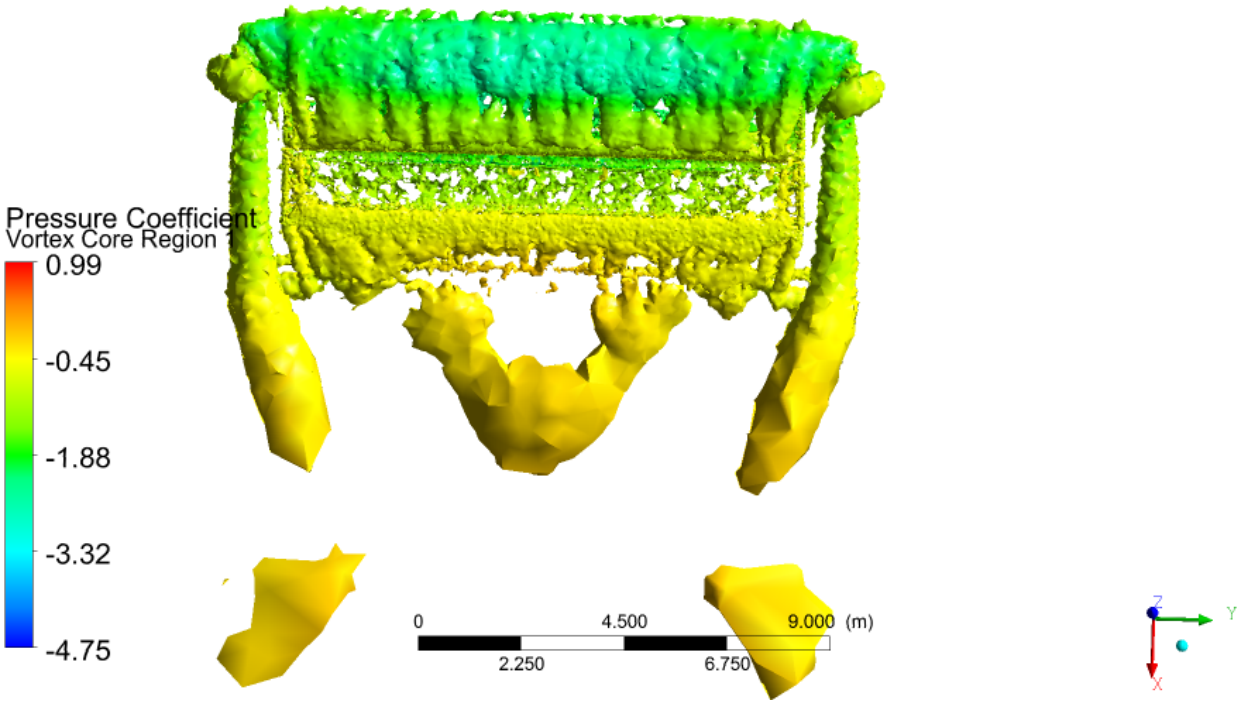


Fig. D. 57. Turbulence distribution, on top of the panels, No Building contours shown, WD 90º, LW

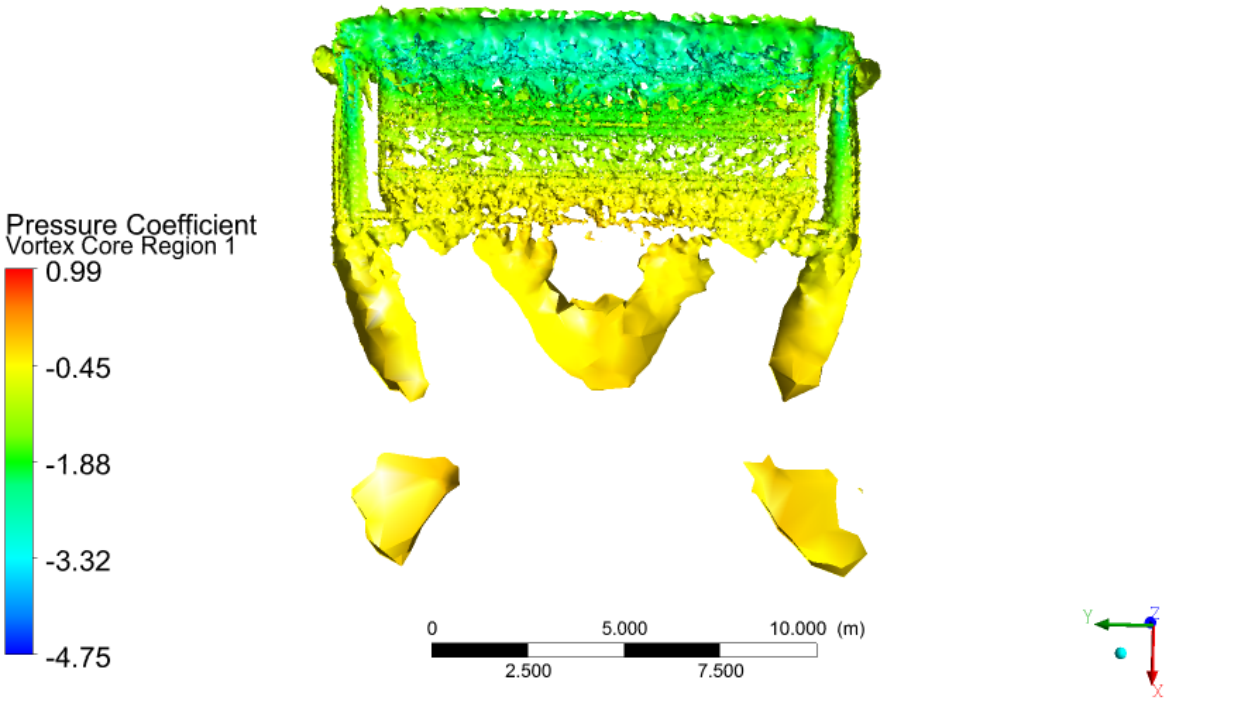


Fig. D. 58. Turbulence distribution, on bottom of the panels, No Building contours shown, WD 90º, LW

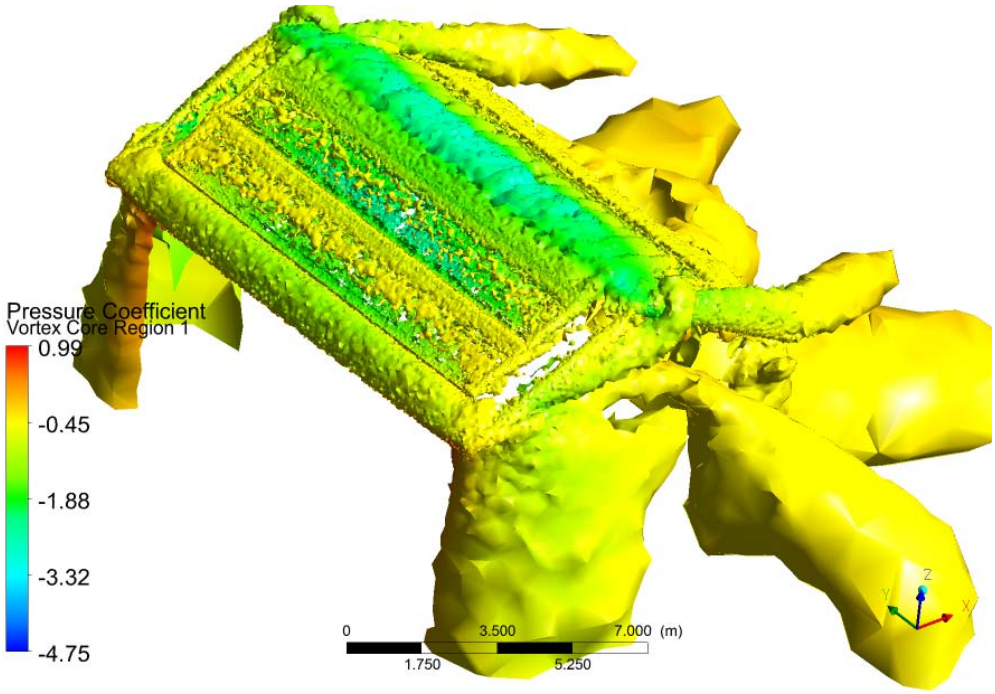


Fig. D. 59. Turbulence distribution, on the building with panels, No Building contours shown, WD 90º, LW

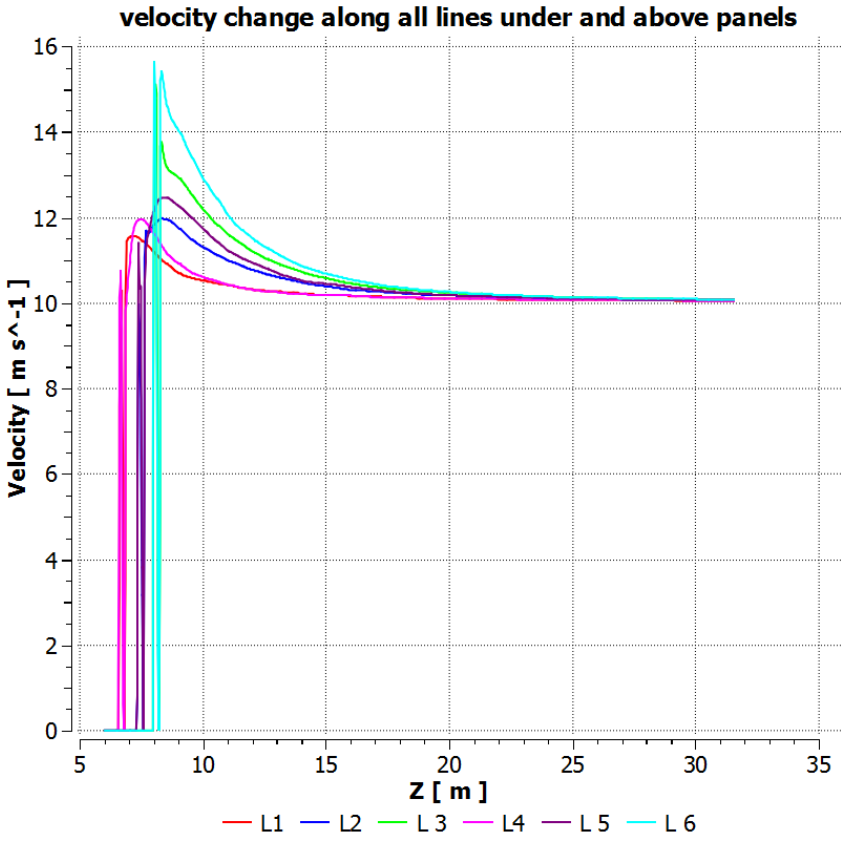


Fig. D. 60. Velocity changes between panels, and above roof, all 6 lines, WW

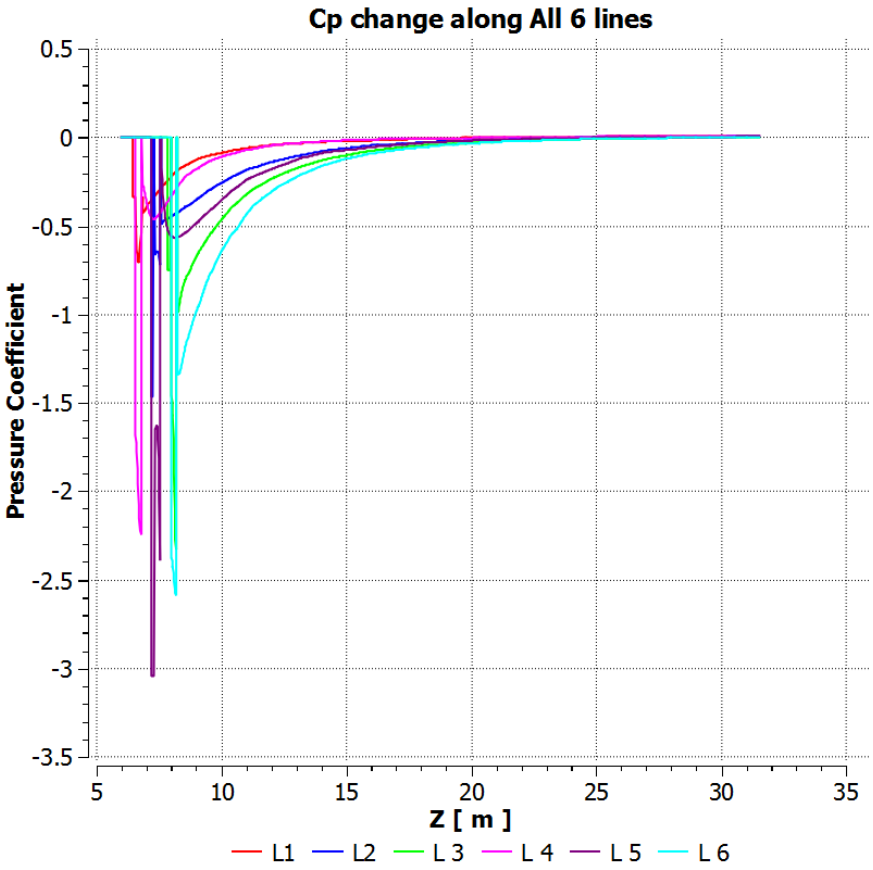
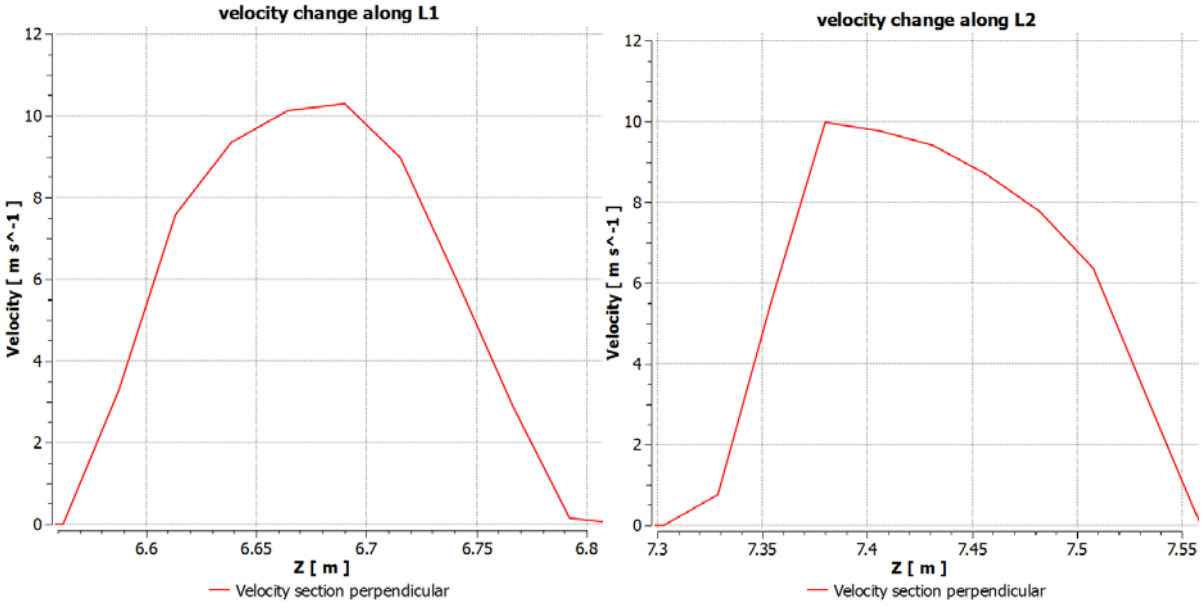


Fig. D. 61. Pressure changes between panels, and above roof, all 6 lines, WW



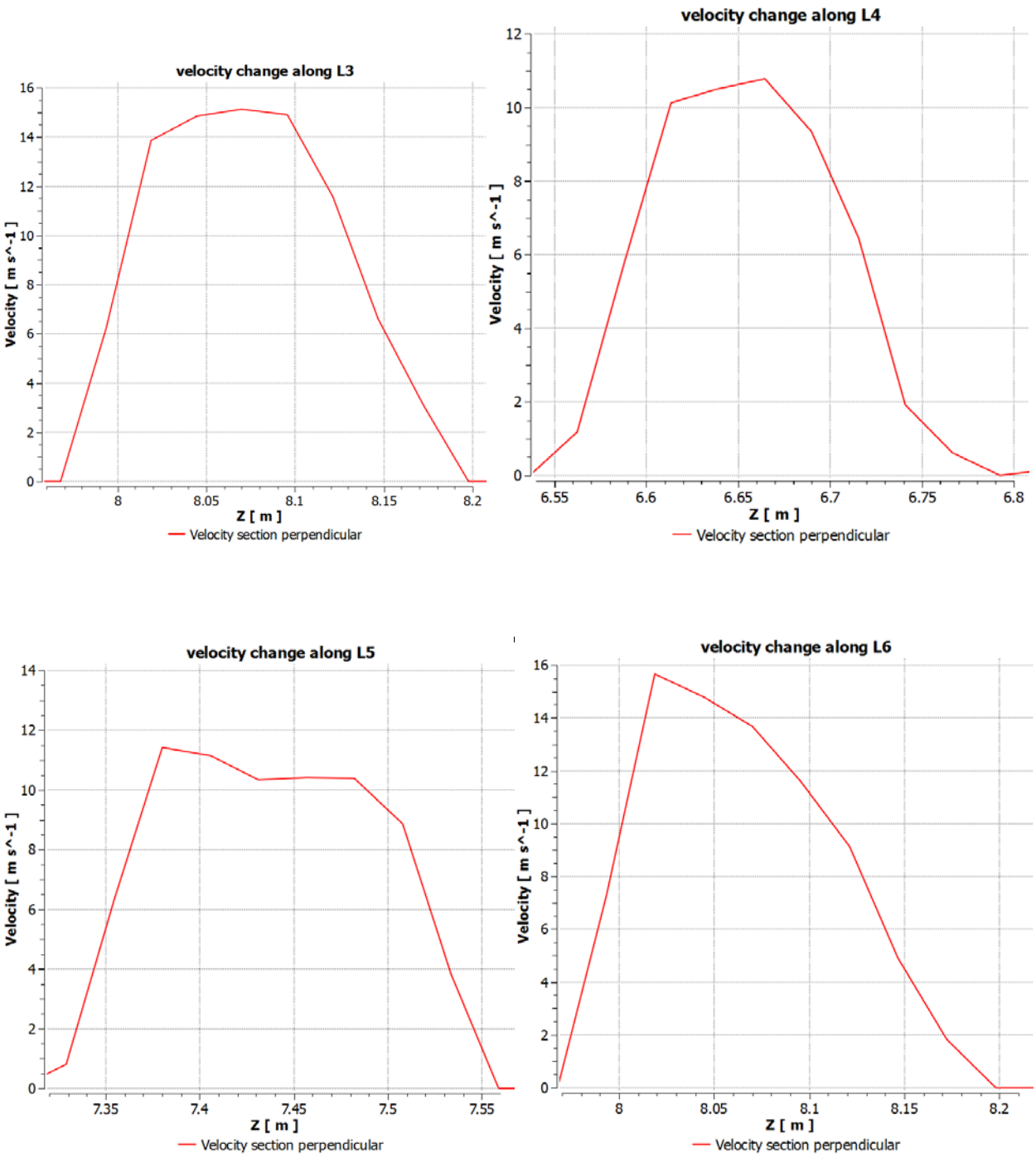
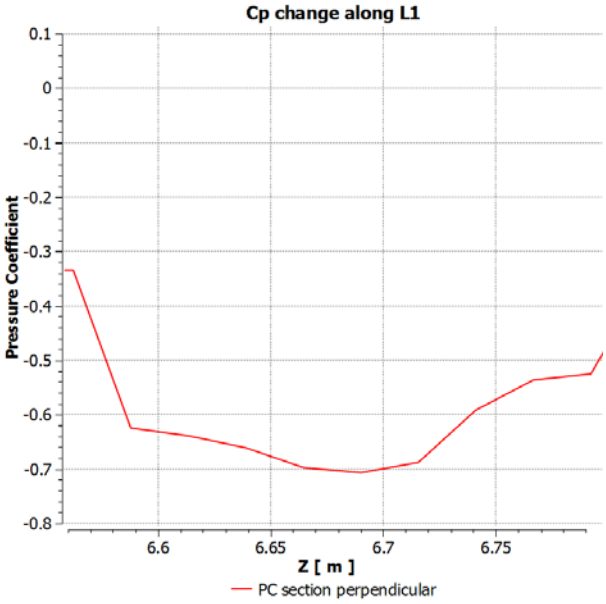
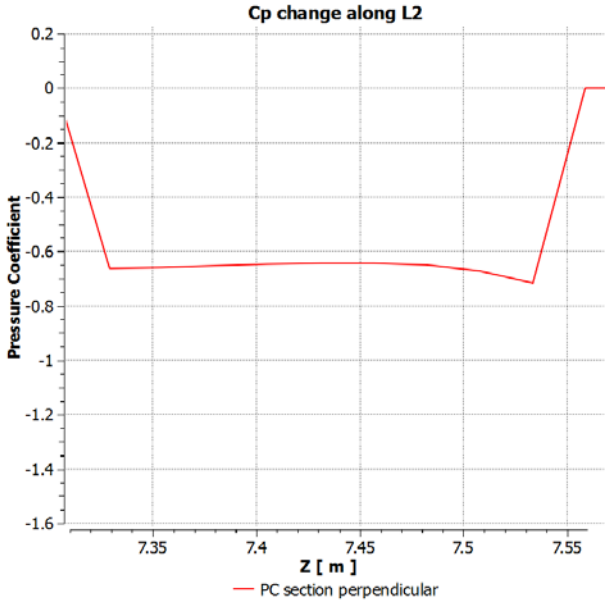
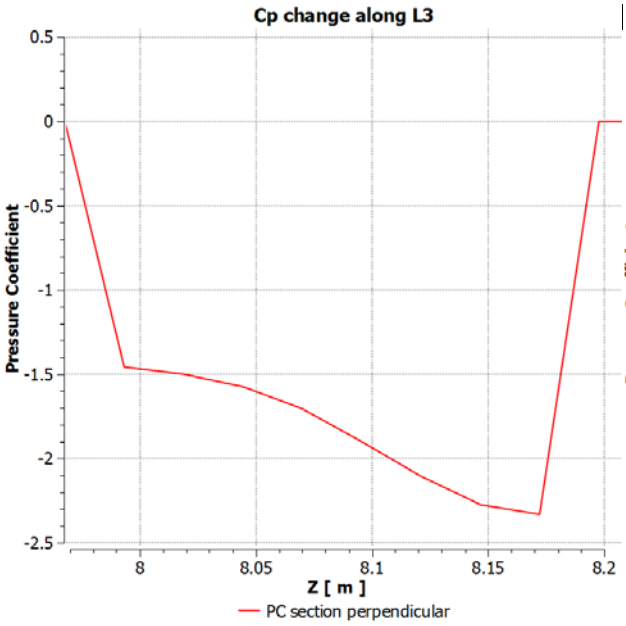
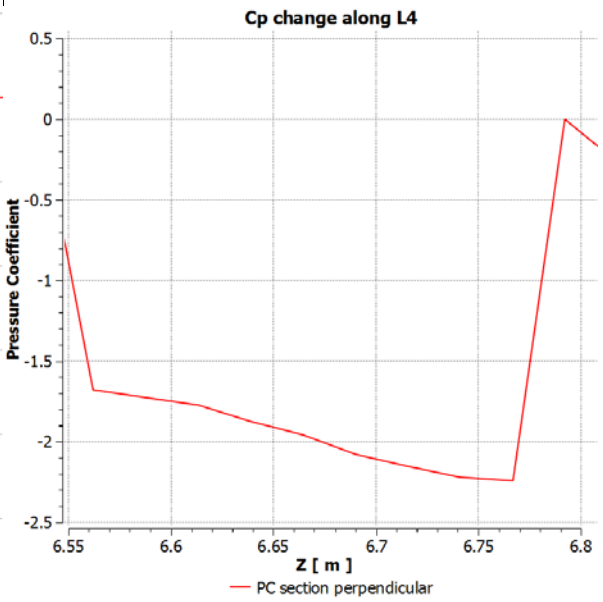


Fig. D. 62. Velocity changes between panels, each of the 6 lines, WW


Cp change along L1
Pressure Coefficient
0.1
0
-0.1
-0.2
-0.3
-0.4
-0.5
-0.6
-0.7
-0.8
6.6
6.65
6.7
6.75
Z [m]
PC section perpendicular


Cp change along L2
Pressure Coefficient
0.2
0
-0.2
-0.4
-0.6
-0.8
-1
-1.2
-1.4
-1.6
7.35
7.4
7.45
7.5
7.55
Z [m]
PC section perpendicular


Cp change along L3
Pressure Coefficient
0.5
0
-0.5
-1
-1.5
-2
-2.5
8
8.05
8.1
8.15
8.2
Z [m]
PC section perpendicular


Cp change along L4
Pressure Coefficient
0.5
0
-0.5
-1
-1.5
-2
-2.5
6.55
6.6
6.65
6.7
6.75
6.8
Z [m]
PC section perpendicular

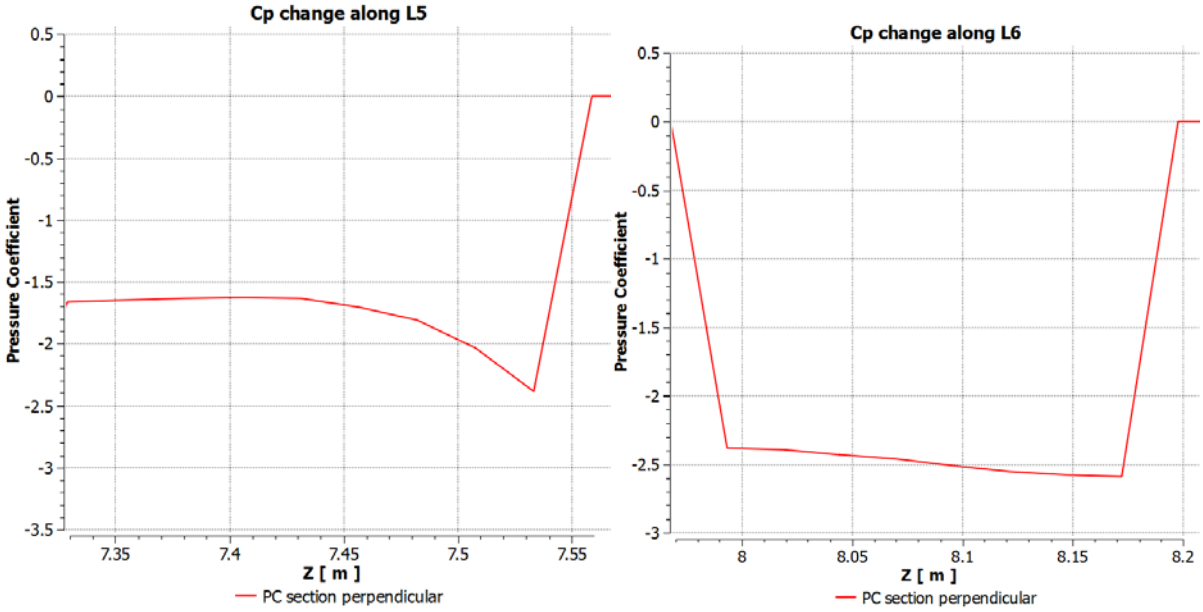


Fig. D. 63. Cp changes between panels, each of the 6 lines, WW

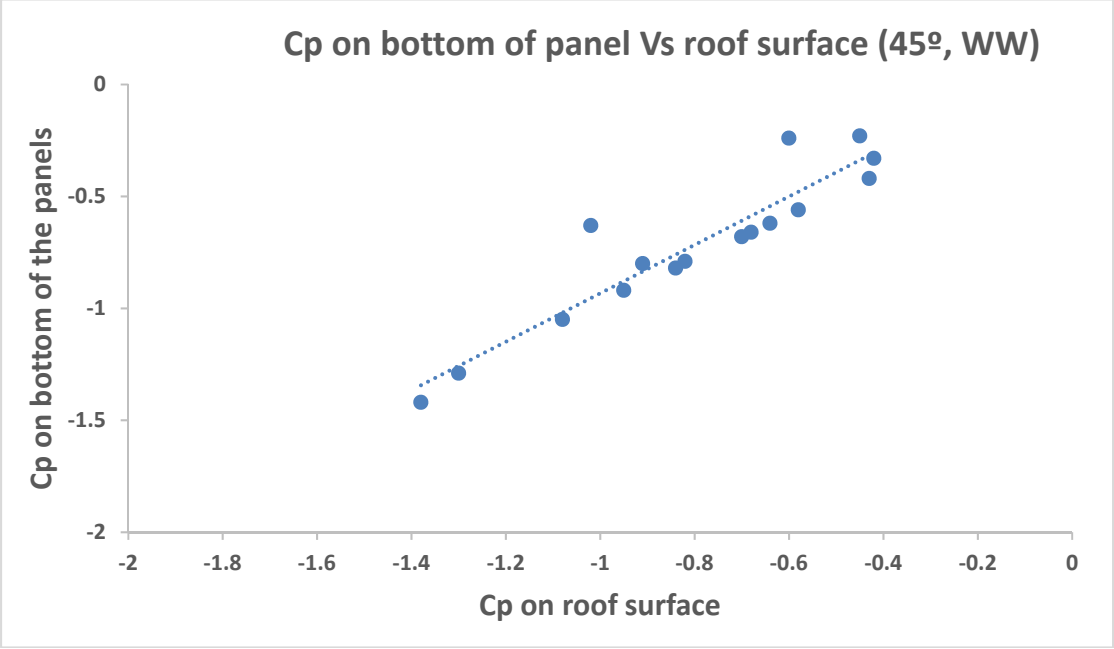


Fig. D. 64. Correlation between Cp on Top Vs Roof Surface, WD 45º, WW, S 27º, S8" C10"

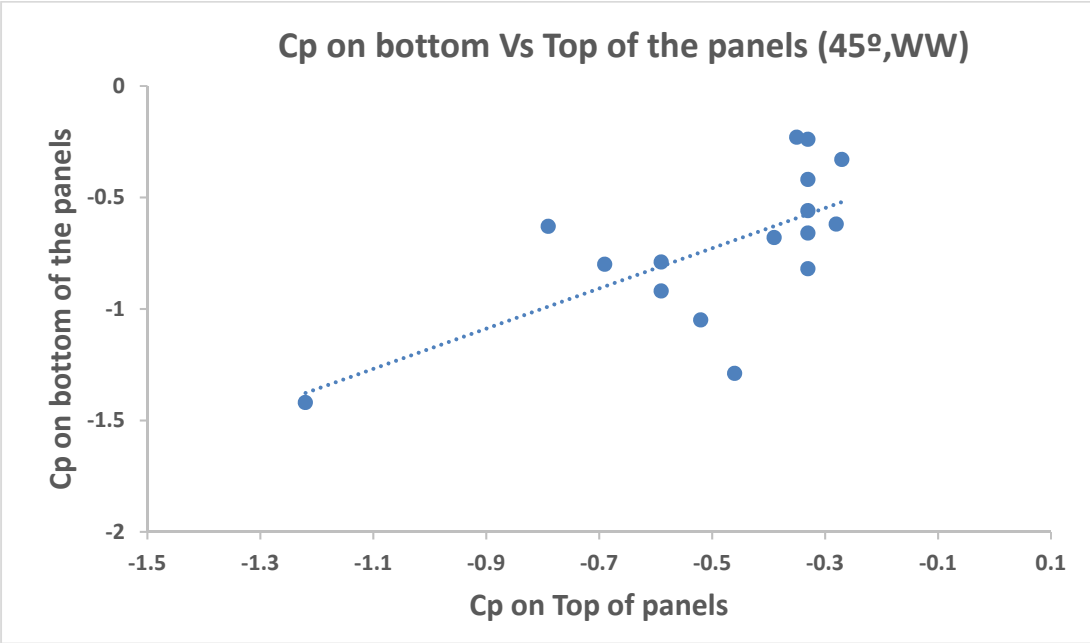


Fig. D. 65. Correlation between Cp on Top Vs Bottom of panels, WD 45º, WW, S 27º, S8" C10"

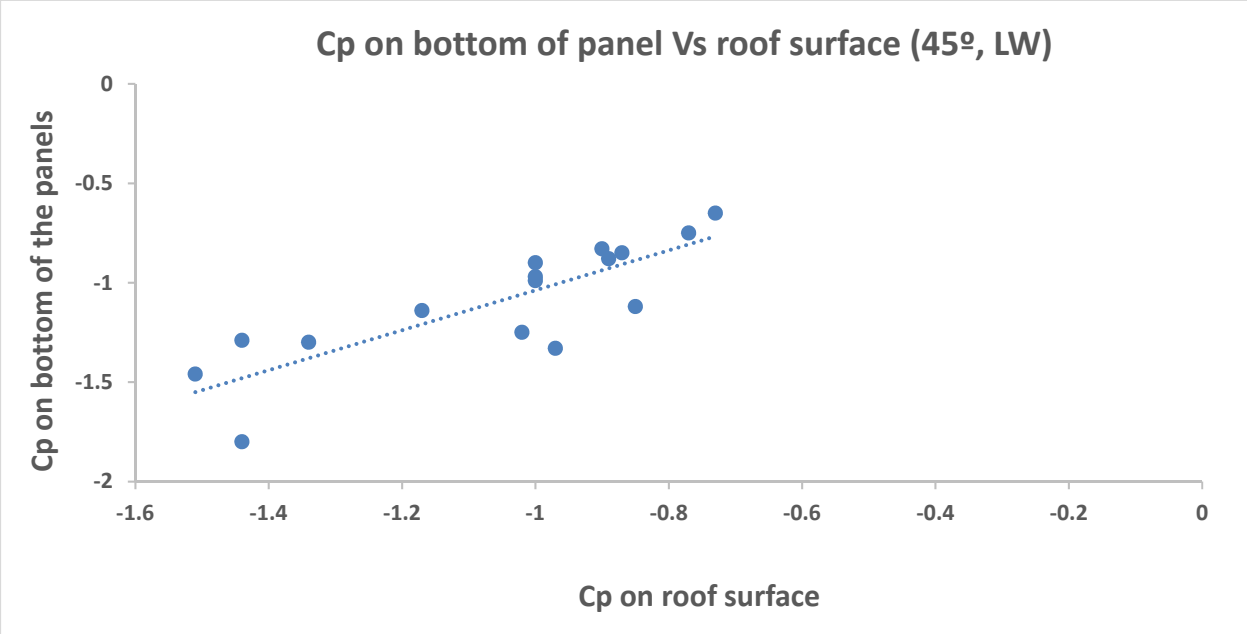


Fig. D. 66. Correlation between Cp on Top Vs Roof Surface, WD 45º, LW, S 27º, S8" C10"

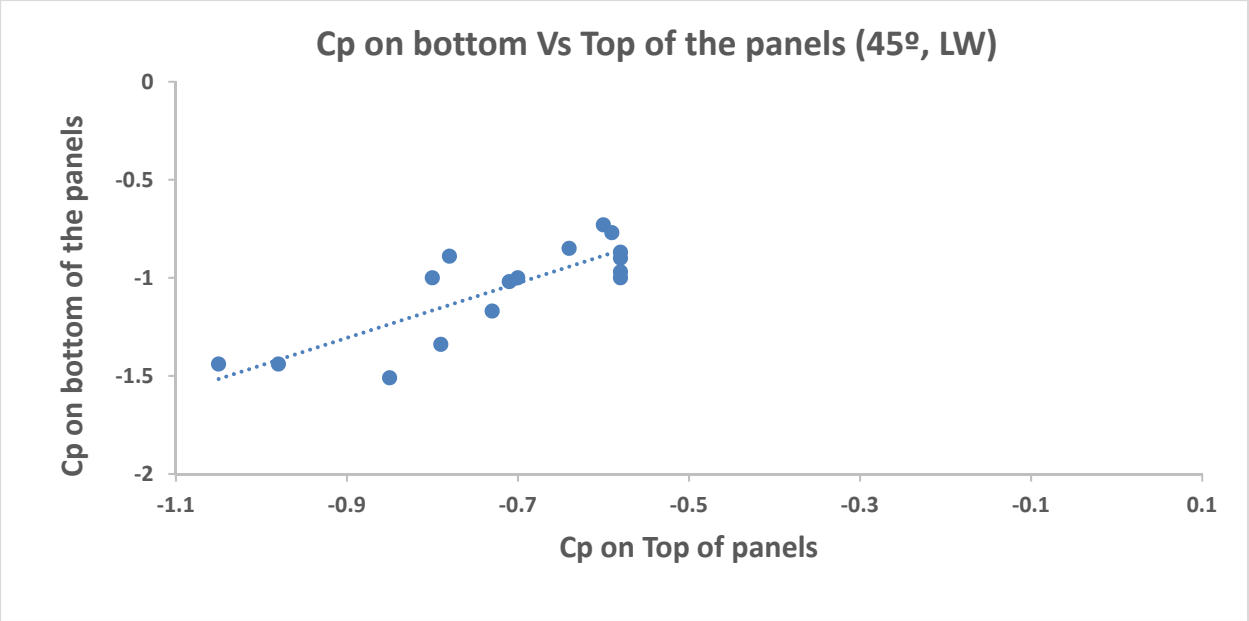


Fig. D. 67. Correlation between Cp on Top Vs Bottom of panels, WD 45º, LW, S 27º, S8" C10"

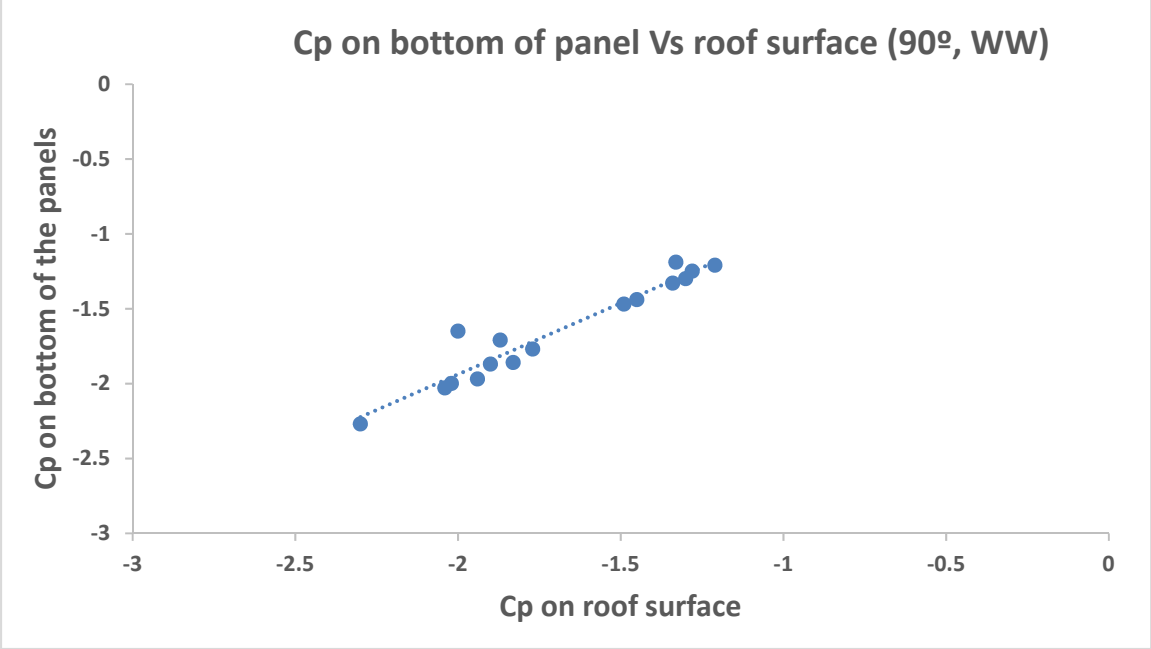


Fig. D. 68. Correlation between Cp on Top Vs Roof Surface, WD 90º, WW, S 27º, S8" C10"

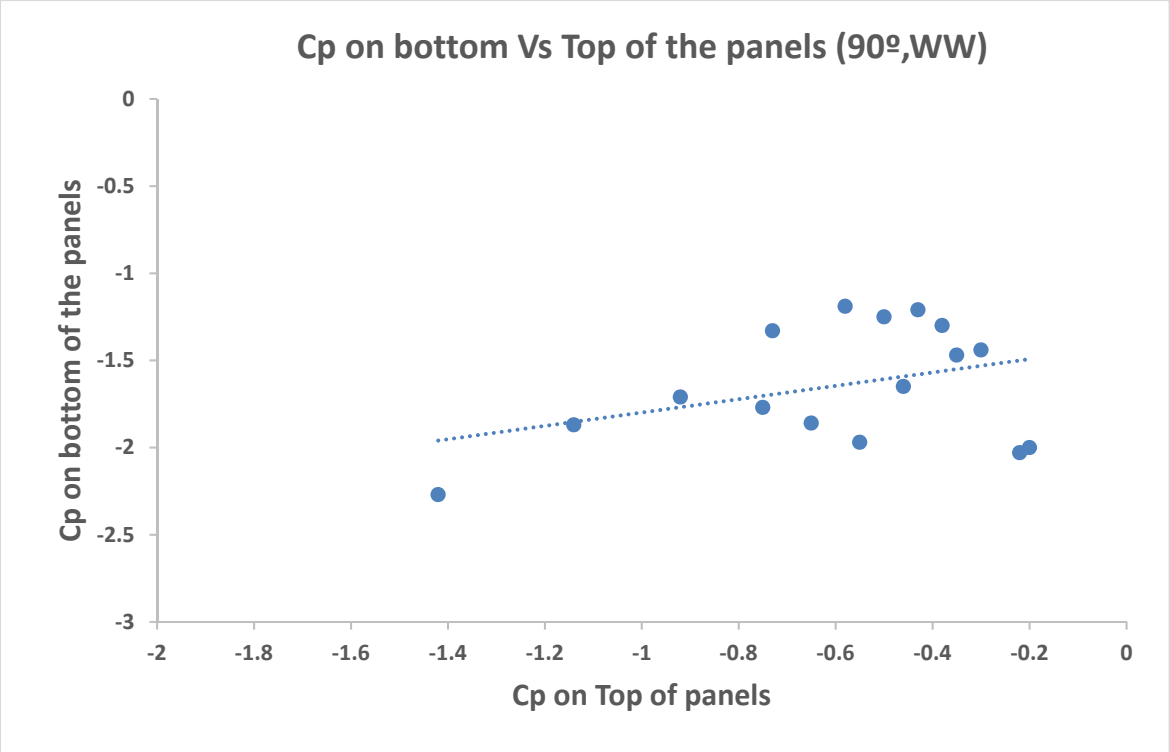


Fig. D. 69. Correlation between Cp on Top Vs Bottom of panels, WD 90º, WW, S 27º, S8" C10"

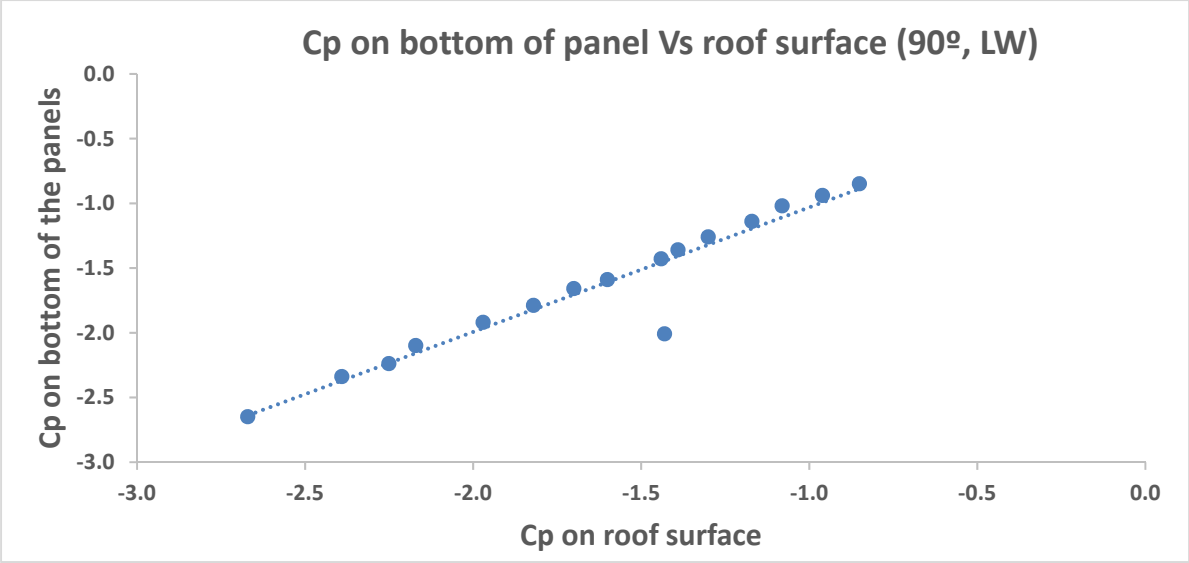


Fig. D. 70. Correlation between Cp on Top Vs Roof Surface, WD 90º, LW, S 27º, S8" C10"

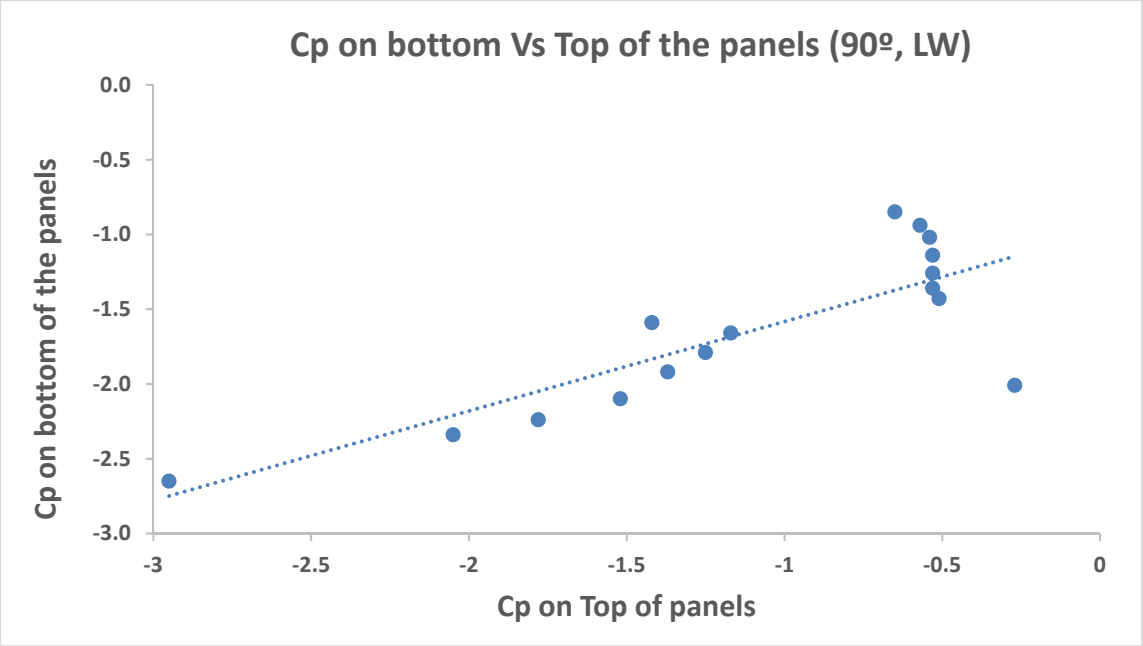


Fig. D. 71. Correlation between Cp on Top Vs Bottom of panels, WD 90º, LW, S 27º, S8" C10"

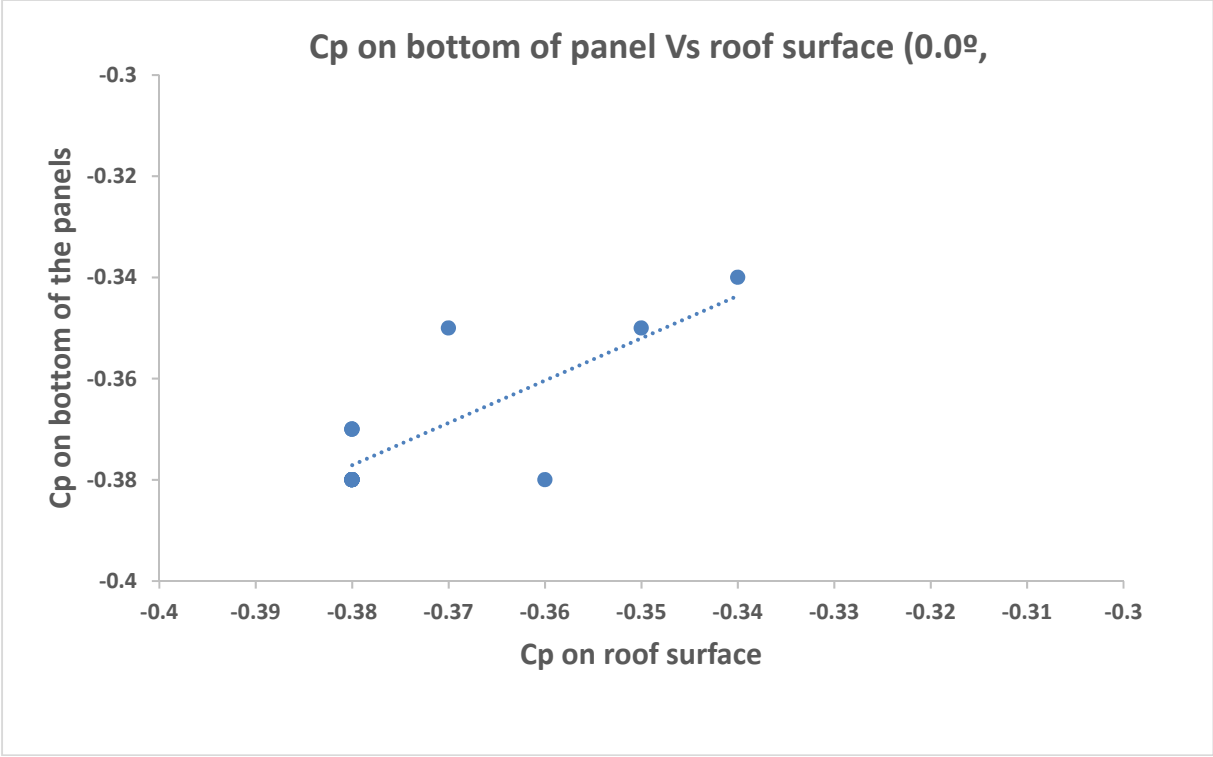


Fig. D. 72. Correlation between Cp on Top Vs Bottom of panels, WD 0.0º, S 27º, S8" C10"

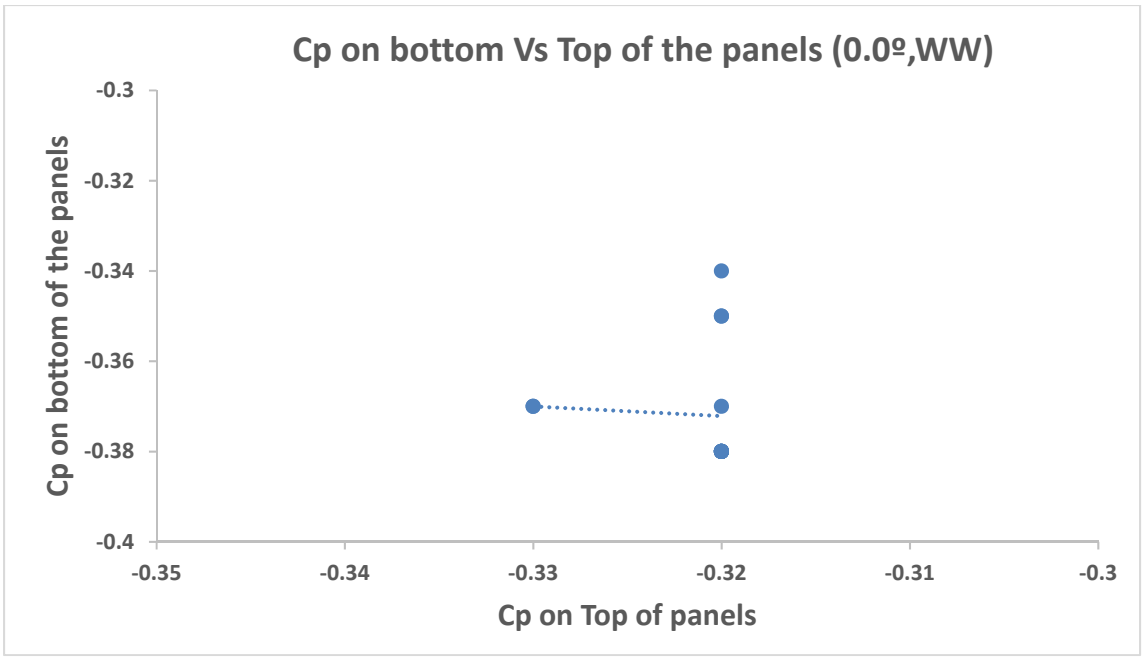


Fig. D. 73. Correlation between Cp on Top Vs Roof Surface, WD 0.0º, S 27º, S8" C10"



Fig. D. 74. Correlation factors between pressure coefficients on the three surfaces with wind directions, S8" C10"

1.1.6. Integration of Cp on the three surfaces and Cp resultant of roof mounted solar panels in comparison with bare roofs, S8" C 10"

Tabulated results of the integration,

Table D. 1. Cp on bare roof Vs. roof under solar panels and solar panels surfaces, Slope 27º, 45º, WW

Polylines	Cp (SP)	Pr2	Cp Bott	Diff	Ttl Cp	Ttl/Brf
Pl1A	-0.27	-0.42	-0.33	0.06	-0.36	2.12
Pl2	-0.33	-0.6	-0.24	-0.09	-0.69	3.83
Pl3	-0.33	-0.84	-0.82	0.49	-0.35	1.90
Pl4	-0.33	-0.68	-0.66	0.33	-0.35	1.79
Pl5	-0.33	-0.58	-0.56	0.23	-0.35	1.68
Pl6	-0.33	-0.43	-0.42	0.09	-0.34	1.42
Pl7	-0.35	-0.45	-0.23	-0.12	-0.57	2.36
Pl8	-0.59	-0.82	-0.79	0.20	-0.62	2.23
Pl9	-0.28	-0.64	-0.62	0.34	-0.3	1.01
Pl10	-0.39	-0.70	-0.68	0.29	-0.41	1.23
Pl11	-0.46	-1.30	-1.29	0.83	-0.47	1.27
Pl12	-0.52	-1.08	-1.05	0.53	-0.55	1.27
Pl13	-0.59	-0.95	-0.92	0.33	-0.62	1.27
Pl14	-0.69	-0.91	-0.80	0.11	-0.8	1.53
Pl15	-0.79	-1.02	-0.63	-0.16	-1.18	2.42
Pl16	-1.22	-1.38	-1.42	0.20	-1.18	2.25
Cp	-0.49	-0.80	-0.72	0.23	-0.57	1.68
SDT	0.25	0.29	0.34	0.26	0.28	0.70
Cov	0.51	0.37	0.48	1.13	0.49	0.42

Table D. 2. Cp on bare roofs Vs. Top of the Panels, Slope 27º, WD 45º, WW

Polylines	Cp Bare roof	Cp (SP)	Cp (SP/BRf)
Pl1A	-0.17	-0.27	1.59
Pl2	-0.18	-0.33	1.83
Pl3	-0.184	-0.33	1.79
Pl4	-0.196	-0.33	1.68
Pl5	-0.208	-0.33	1.59
Pl6	-0.24	-0.33	1.38
Pl7	-0.242	-0.35	1.45
Pl8	-0.278	-0.59	2.12
Pl9	-0.30	-0.28	0.95
Pl10	-0.33	-0.39	1.17
Pl11	-0.37	-0.46	1.24
Pl12	-0.43	-0.52	1.20
Pl13	-0.488	-0.59	1.21
Pl14	-0.52	-0.69	1.32

Pl15	-0.62	-0.79	1.27
Pl16	-0.68	-1.22	1.79
Cp	-0.34	-0.49	1.43
SDT	0.16	0.25	0.31
Cov	0.48	0.51	0.22

Table D. 3. Cp on bare roof Vs. roof under solar panels and solar panels surfaces, Slope 27º, WD 45º, LW

Polylines	Cp (SP)	Pr2	Cp Bott	Diff	Ttl Cp	Ttl/Brf
Pl20a	-1.05	-1.44	-1.29	0.24	-1.2	0.80
Pl21	-0.98	-1.44	-1.8	0.82	-0.62	0.43
Pl22	-0.85	-1.51	-1.46	0.61	-0.9	0.64
Pl23	-0.79	-1.34	-1.3	0.51	-0.83	0.61
Pl24	-0.73	-1.17	-1.14	0.41	-0.76	0.60
Pl25	-0.7	-1	-0.9	0.20	-0.8	0.68
Pl26	-0.71	-1.02	-1.25	0.54	-0.48	0.45
Pl27	-0.8	-1.00	-0.99	0.19	-0.81	0.84
Pl28	-0.58	-0.90	-0.83	0.25	-0.65	0.73
Pl29	-0.58	-0.97	-1.33	0.75	-0.22	0.26
Pl30	-0.58	-1.00	-0.97	0.39	-0.61	0.78
Pl31	-0.58	-0.87	-0.85	0.27	-0.6	0.85
Pl32	-0.59	-0.77	-0.75	0.16	-0.61	0.95
Pl33	-0.6	-0.73	-0.65	0.05	-0.68	1.15
Pl34	-0.64	-0.85	-1.12	0.48	-0.37	0.65
Pl35	-0.78	-0.89	-0.88	0.10	-0.79	1.41
Cp	-0.72	-1.06	-1.09	0.37	-0.68	0.74
SDT	0.15	0.25	0.30	0.23	0.22	0.28
Cov	0.20	0.24	0.27	0.61	0.33	0.38

Table D. 4. Cp on bare roofs Vs. Top of the Panels, Slope 27º, WD 45º, LW

Polylines	Bare Roof	Cp (SP)	Cp (SP/BRf)
Pl20A	-1.50	-1.05	0.70
Pl21	-1.44	-0.98	0.68
Pl22	-1.40	-0.85	0.61
Pl23	-1.36	-0.79	0.58
Pl24	-1.27	-0.73	0.57
Pl25	-1.18	-0.7	0.59
Pl26	-1.06	-0.71	0.67
Pl27	-0.97	-0.8	0.83
Pl28	-0.90	-0.58	0.65
Pl29	-0.86	-0.58	0.68
Pl30	-0.78	-0.58	0.74
Pl31	-0.71	-0.58	0.82
Pl32	-0.64	-0.59	0.92
Pl33	-0.59	-0.6	1.01
Pl34	-0.57	-0.64	1.12

Pl35	-0.56	-0.78	1.39
Cp	-0.99	-0.72	0.79
SDT	0.33	0.15	0.23
Cov	0.34	0.20	0.29

Table D. 5. Cp on bare roof Vs. roof under solar panels and solar panels surfaces, Slope 27º, WD 90º, WW

Polylines	Cp (SP)	Pr2	Cp Bott	Diff	Ttl Cp	Ttl/Brf
Pl1A	-0.2	-2.02	-2	1.80	-0.22	11.00
Pl2	-0.3	-1.45	-1.44	1.14	-0.31	-15.50
Pl3	-0.35	-1.49	-1.47	1.12	-0.37	-23.13
Pl4	-0.38	-1.3	-1.3	0.92	-0.38	38.00
Pl5	-0.43	-1.21	-1.21	0.78	-0.43	11.94
Pl6	-0.5	-1.28	-1.25	0.75	-0.53	8.83
Pl7	-0.58	-1.33	-1.19	0.61	-0.72	11.61
Pl8	-0.73	-1.34	-1.33	0.60	-0.74	9.49
Pl10	-0.22	-2.04	-2.03	1.81	-0.23	2.13
Pl11	-0.46	-2.00	-1.65	-2.00	-4	26.32
Pl12	-0.55	-1.94	-1.97	1.42	-0.52	2.60
Pl13	-0.65	-1.83	-1.86	1.21	-0.62	2.35
Pl14	-0.75	-1.77	-1.77	1.02	-0.75	2.23
Pl15	-0.92	-1.87	-1.71	0.79	-1.08	2.86
Pl16	-1.14	-1.90	-1.87	0.73	-1.17	3.48
Pl17	-1.42	-2.30	-2.27	0.85	-1.45	3.84
Cp	-0.60	-1.69	-1.65	0.85	-0.85	5.58
SDT	0.33	0.34	0.34	0.85	0.91	13.99
Cov	0.56	0.20	0.21	1.00	1.08	2.51

Table D. 6. Cp on bare roofs Vs. Top of the Panels, Slope 27º, WD 90º, WW

Polylines	Cp Bare roof	Cp (SP)	Cp (SP/BRf)
Pl1A	-0.02	-0.2	10.00
Pl2	0.02	-0.3	-15.00
Pl3	0.016	-0.35	-21.88
Pl4	-0.01	-0.38	38.00
Pl5	-0.036	-0.43	11.94
Pl6	-0.06	-0.5	8.33
Pl7	-0.062	-0.58	9.35
Pl8	-0.078	-0.73	9.36
Pl10	-0.11	-0.22	2.04
Pl11	-0.15	-0.46	3.03
Pl12	-0.20	-0.55	2.75
Pl13	-0.26	-0.65	2.46
Pl14	-0.336	-0.75	2.23
Pl15	-0.38	-0.92	2.43

Pl16	-0.37	-1.14	3.11
Pl17	-0.39	-1.42	3.64
Cp	-0.15	-0.60	3.95
SDT	0.15	0.33	12.58
Cov	0.99	0.56	3.18

Table D. 7. Cp on bare roof Vs. roof under solar panels and solar panels surfaces, Slope 27º, WD 90º, LW

Polylines	Cp (SP)	Pr2	Cp Bott	Diff	Ttl Cp	Ttl/Brf
Pl22	-2.95	-2.67	-2.65	-0.30	-2.97	1.14
Pl23	-2.05	-2.39	-2.34	0.29	-2.1	0.82
Pl24	-1.78	-2.25	-2.24	0.46	-1.79	0.72
Pl25	-1.52	-2.17	-2.1	0.58	-1.59	0.66
Pl26	-1.37	-1.97	-1.92	0.55	-1.42	0.62
Pl27	-1.25	-1.82	-1.79	0.54	-1.28	0.61
Pl28	-1.17	-1.70	-1.66	0.49	-1.21	0.63
Pl29	-1.42	-1.60	-1.59	0.17	-1.43	0.84
Pl31	-0.27	-1.43	-2.01	1.74	0.31	-0.21
Pl32	-0.51	-1.44	-1.43	0.92	-0.52	0.37
Pl33	-0.53	-1.39	-1.36	0.83	-0.56	0.47
Pl34	-0.53	-1.30	-1.26	0.73	-0.57	0.56
Pl35	-0.53	-1.17	-1.14	0.61	-0.56	0.66
Pl36	-0.54	-1.08	-1.02	0.48	-0.6	0.83
Pl37	-0.57	-0.96	-0.94	0.37	-0.59	0.95
Pl38a	-0.65	-0.85	-0.85	0.20	-0.65	1.08
Cp	-1.10	-1.64	-1.64	0.54	-1.10	0.67
SDT	0.73	0.54	0.54	0.43	0.79	0.31
Cov	0.66	0.33	0.33	0.79	0.72	0.46

Table D. 8. Cp on bare roofs Vs. Top of the Panels, Slope 27º, WD 90º, LW

Polylines	Bare Roof	Cp (SP)	Cp (SP/BRf)
Pl22	-2.60	-2.95	1.13
Pl23	-2.55	-2.05	0.80
Pl24	-2.50	-1.78	0.71
Pl25	-2.41	-1.52	0.63
Pl26	-2.28	-1.37	0.60
Pl27	-2.11	-1.25	0.59
Pl28	-1.92	-1.17	0.61
Pl29	-1.70	-1.42	0.84
Pl31	-1.51	-0.27	0.18
Pl32	-1.40	-0.51	0.36
Pl33	-1.20	-0.53	0.44
Pl34	-1.01	-0.53	0.52
Pl35	-0.85	-0.53	0.62

Pl36	-0.72	-0.54	0.75
Pl37	-0.62	-0.57	0.92
Pl38	-0.60	-0.65	1.08
Cp	-1.62	-1.10	0.68
SDT	0.73	0.73	0.25
Cov	0.45	0.66	0.37

Table D. 9. Cp on bare roof Vs. roof under solar panels and solar panels surfaces, Slope 27º, WD 0.0º

Polylines	Cp (SP)	Pr2	Cp Bott	Diff	Ttl Cp	Ttl/Brf
Pl1A	-0.32	-0.35	-0.35	0.03	-0.32	0.91
Pl2	-0.32	-0.37	-0.35	0.03	-0.34	0.97
Pl3	-0.32	-0.38	-0.38	0.06	-0.32	0.90
Pl4	-0.32	-0.38	-0.38	0.06	-0.32	0.89
Pl5	-0.32	-0.38	-0.38	0.06	-0.32	0.89
Pl6	-0.32	-0.38	-0.38	0.06	-0.32	0.86
Pl7	-0.32	-0.36	-0.38	0.06	-0.3	0.81
Pl8	-0.33	-0.38	-0.37	0.04	-0.34	0.92
Pl9	-0.33	-0.38	-0.37	0.04	-0.34	0.92
Pl10	-0.32	-0.38	-0.38	0.06	-0.32	0.88
Pl11	-0.32	-0.38	-0.38	0.06	-0.32	0.89
Pl12	-0.32	-0.38	-0.38	0.06	-0.32	0.89
Pl13	-0.32	-0.38	-0.38	0.06	-0.32	0.90
Pl14	-0.32	-0.38	-0.38	0.06	-0.32	0.91
Pl15	-0.32	-0.38	-0.37	0.05	-0.33	0.94
Pl16	-0.32	-0.34	-0.34	0.02	-0.32	0.91
Cp	-0.32	-0.37	-0.37	0.05	-0.32	0.90
SDT	0.00	0.01	0.01	0.01	0.01	0.03
Cov	0.01	0.03	0.04	0.27	0.03	0.04

Table D. 10. Cp on bare roofs Vs. Top of the Panels, Slope 27º, WD 0.0º

Polylines	Cp Bare roof	Cp (SP)	Cp (SP/BRf)
Pl1A	-0.35	-0.32	0.91
Pl2	-0.35	-0.32	0.91
Pl3	-0.354	-0.32	0.90
Pl4	-0.36	-0.32	0.89
Pl5	-0.36	-0.32	0.89
Pl6	-0.37	-0.32	0.86
Pl7	-0.37	-0.32	0.86
Pl8	-0.37	-0.33	0.89
Pl9	-0.37	-0.33	0.89
Pl10	-0.362	-0.32	0.88
Pl11	-0.36	-0.32	0.89
Pl12	-0.36	-0.32	0.89

Pl13	-0.356	-0.32	0.90
Pl14	-0.35	-0.32	0.91
Pl15	-0.35	-0.32	0.91
Pl16	-0.35	-0.32	0.91
Cp	-0.36	-0.32	0.90
SDT	0.01	0.00	0.02
Cov	0.02	0.01	0.02

APPENDIX E

Chapter 5, Remaining cases Slope 15º

E.1. Slope 15º,

1.1. 2” Spacing, 10” Clearance

1.1.1. Wind direction 45º,

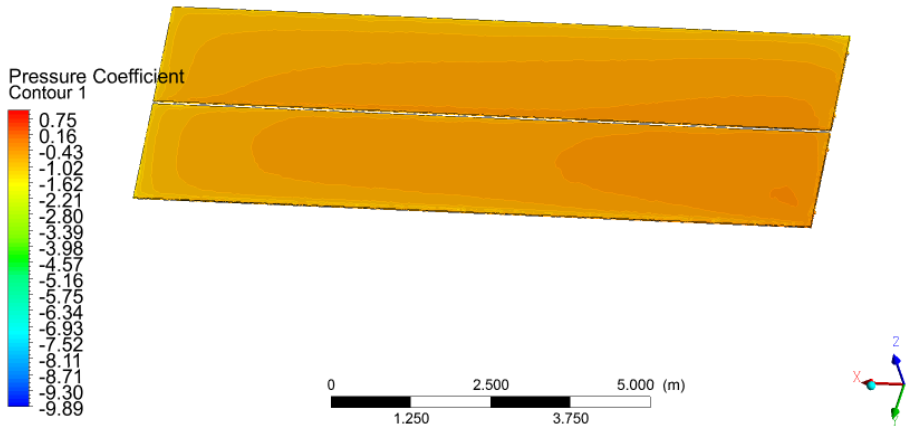


Fig. E. 1. Cp on top of the solar panels, WW

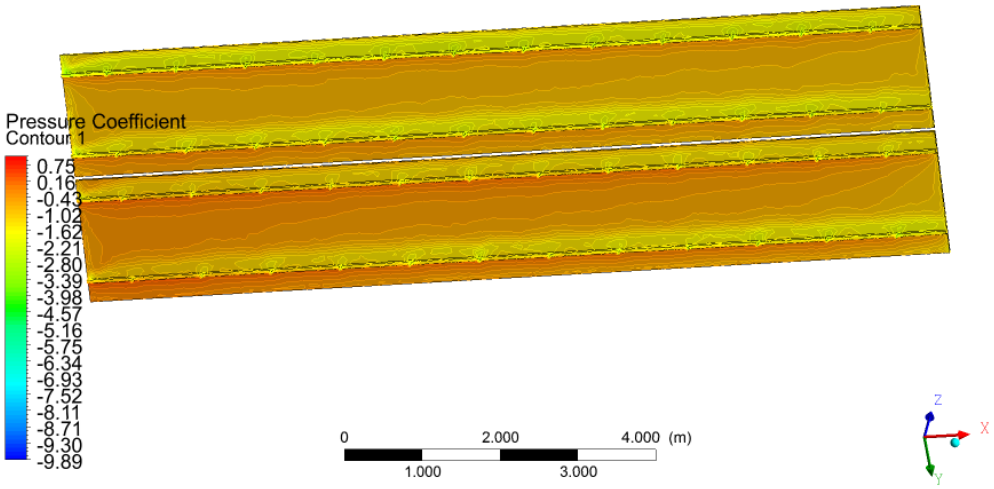


Fig. E. 2. Cp on bottom of the solar panels, WW

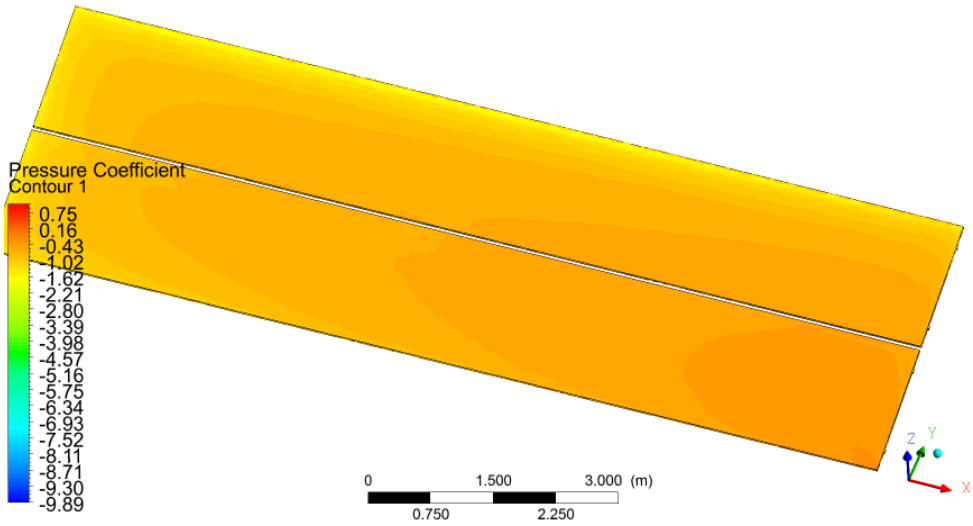


Fig. E. 3. Cp on top of the solar panels, LW

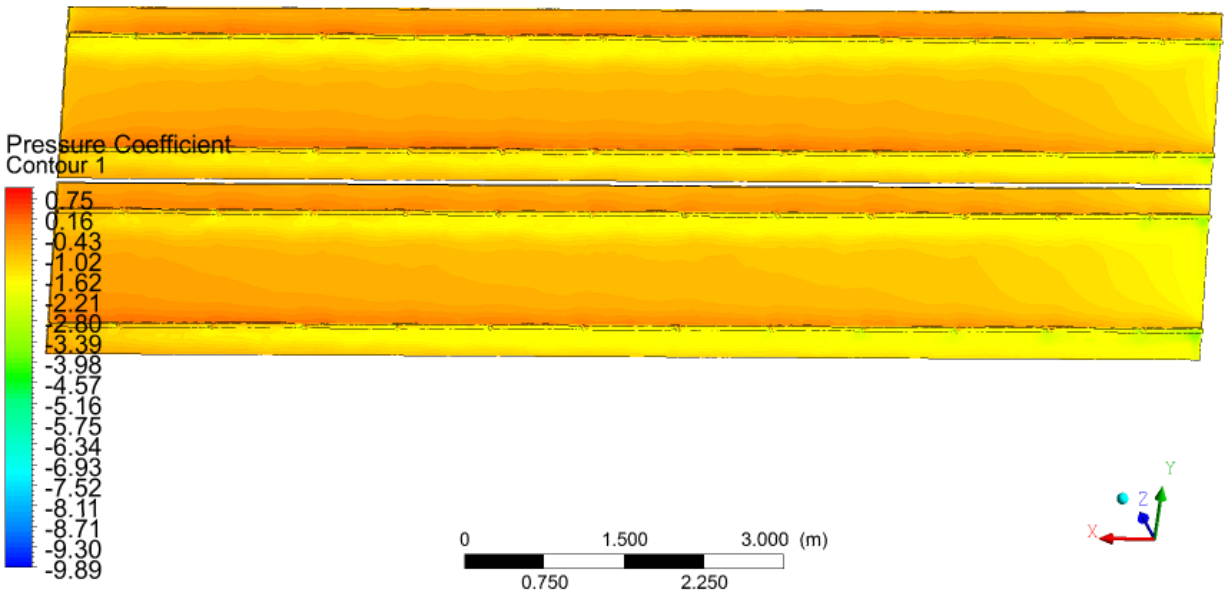


Fig. E. 4. Cp on bottom of the solar panels, LW

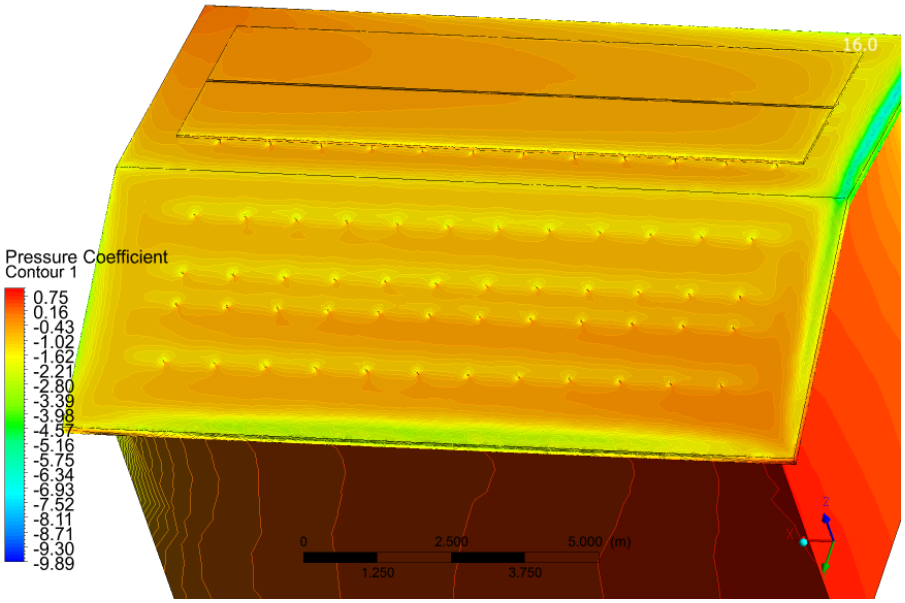


Fig. E. 5. Cp on Roof under the solar panels, cut off solar panels, WW

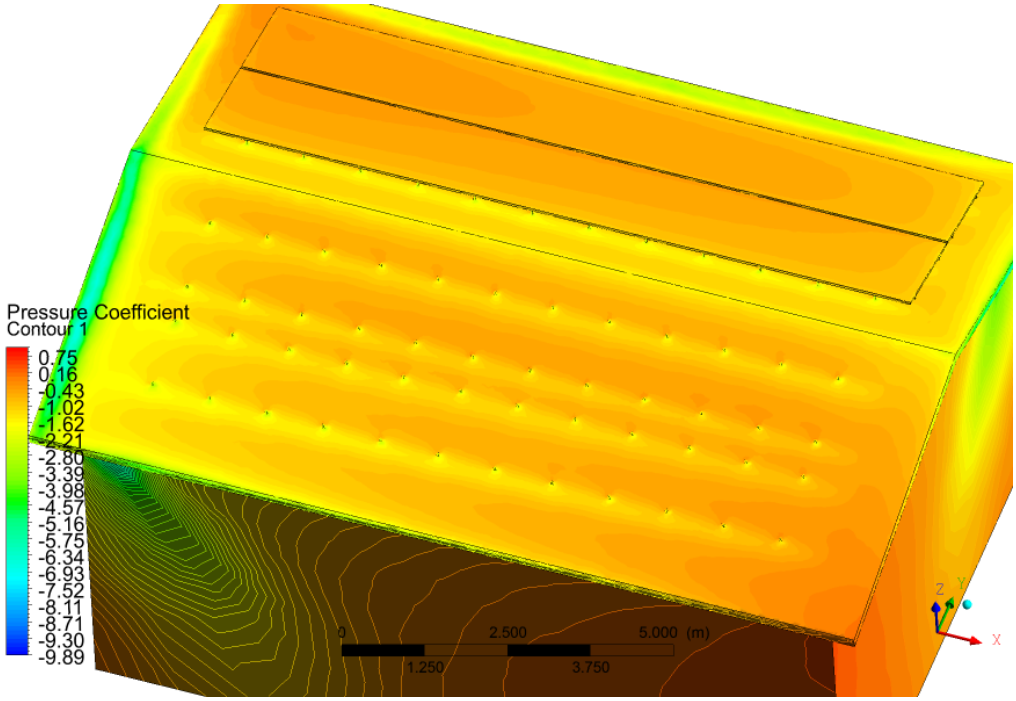


Fig. E. 6. Cp on Roof under the solar panels, cut off solar panels, LW

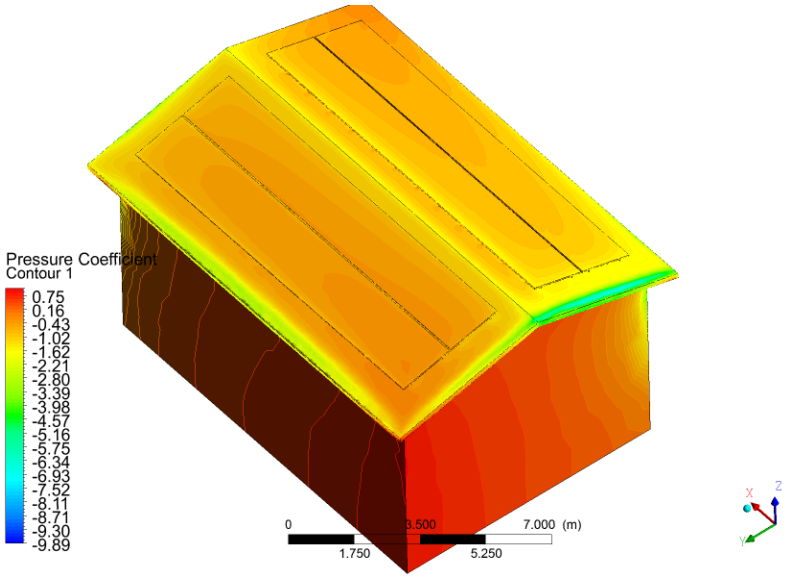


Fig. E. 7. Pressure coefficient on building surfaces with solar panels, WD 45º, WW

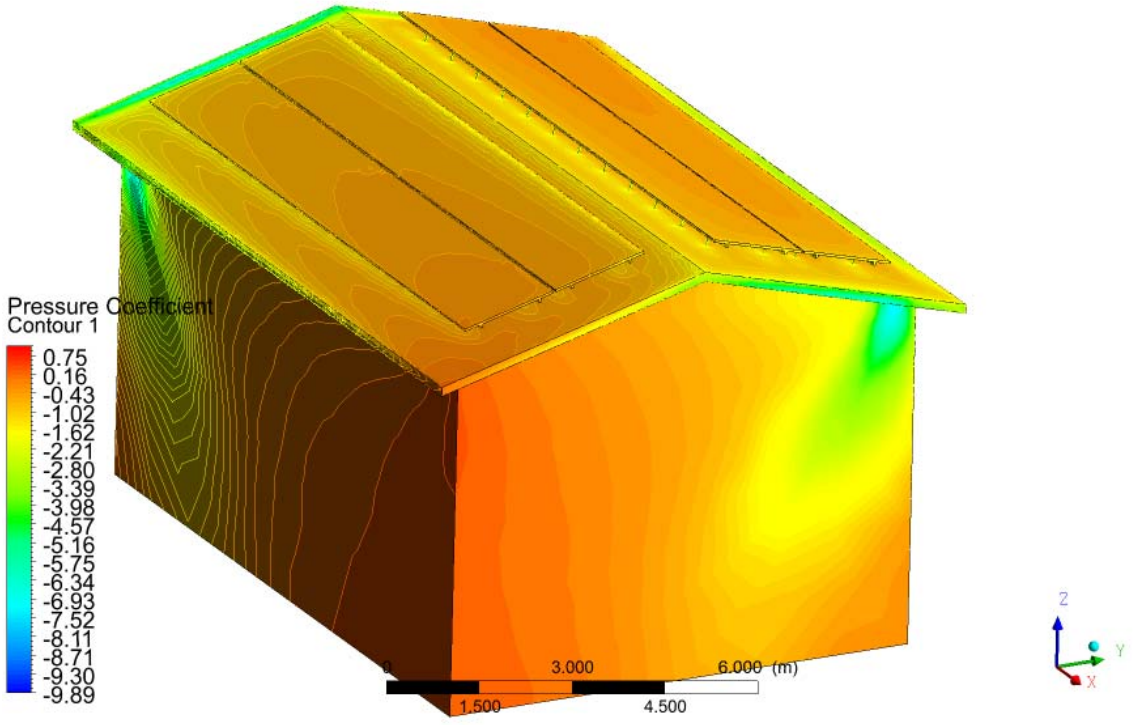


Fig. E. 8. Pressure coefficient on building surfaces with solar panels, WD 45º, LW

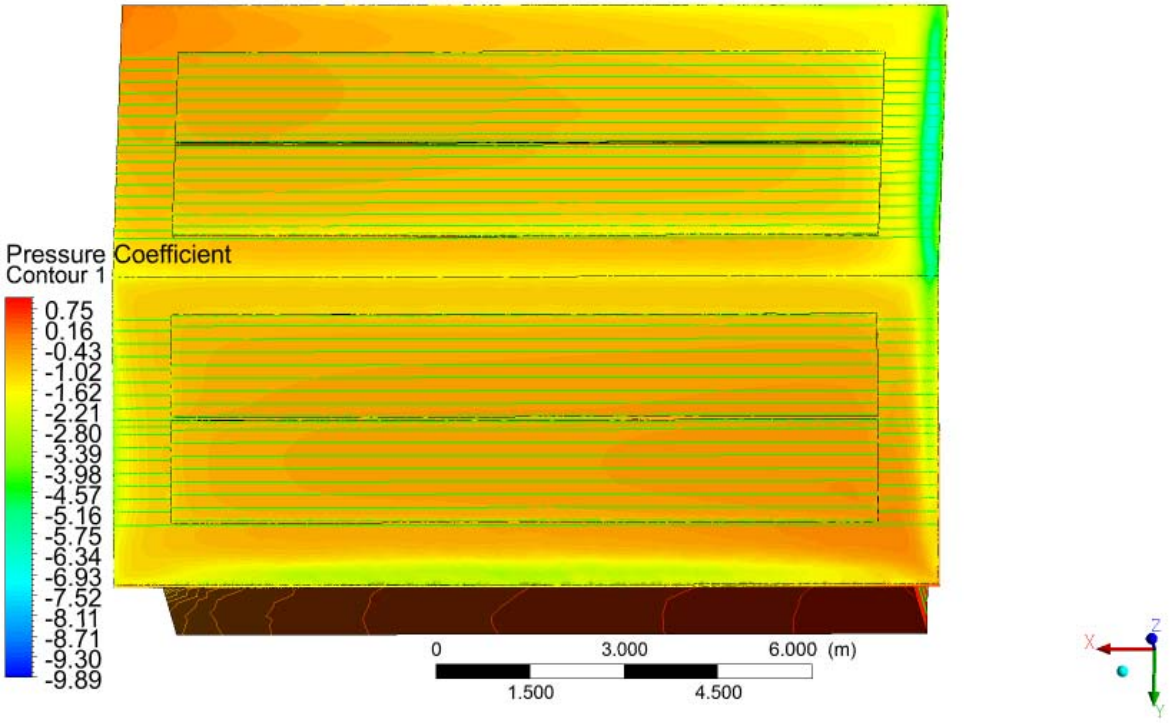


Fig. E. 9. Pressure coefficient on roof, plines,

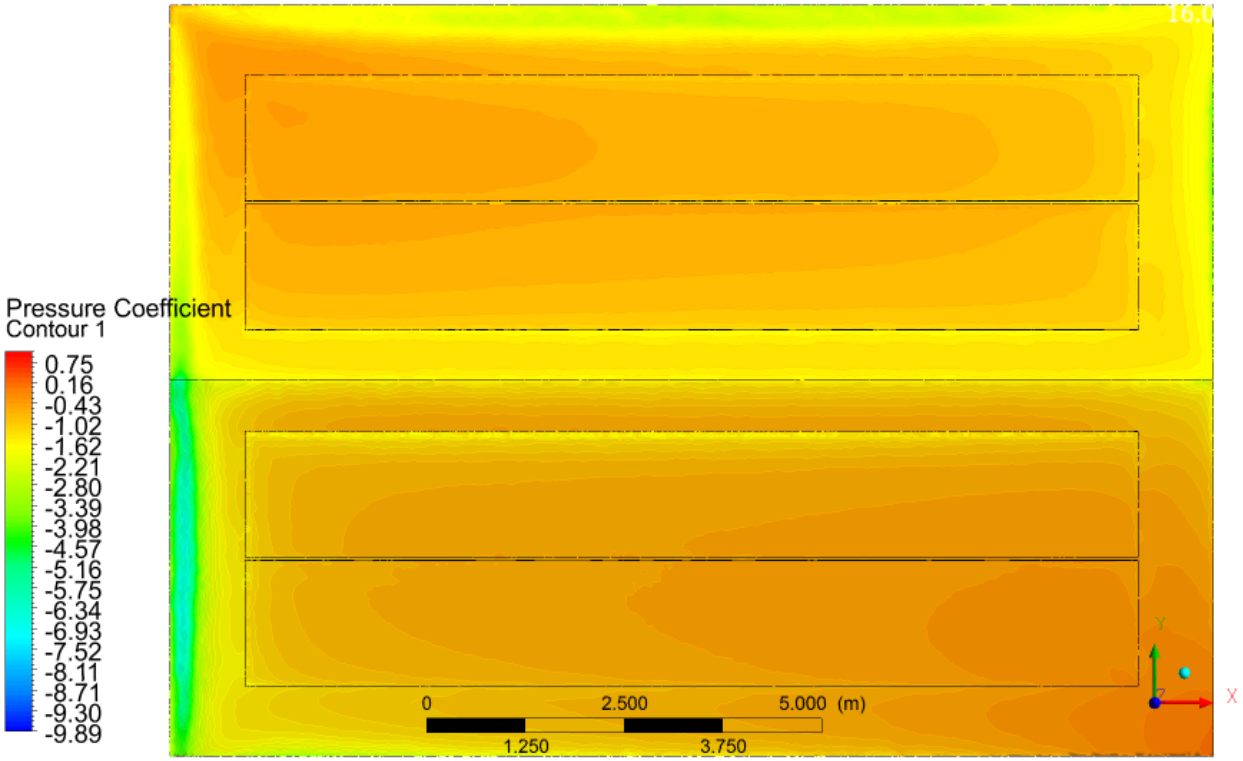


Fig. E. 10. Pressure coefficient on roof, top view,

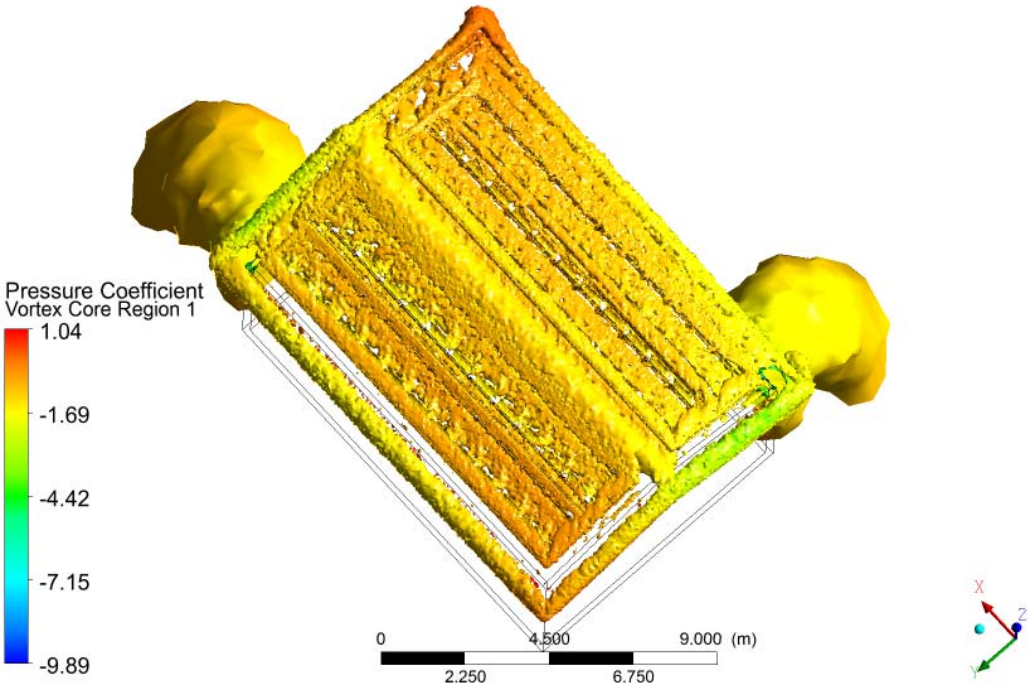


Fig. E. 11. Turbulence distribution with Cp, WW,

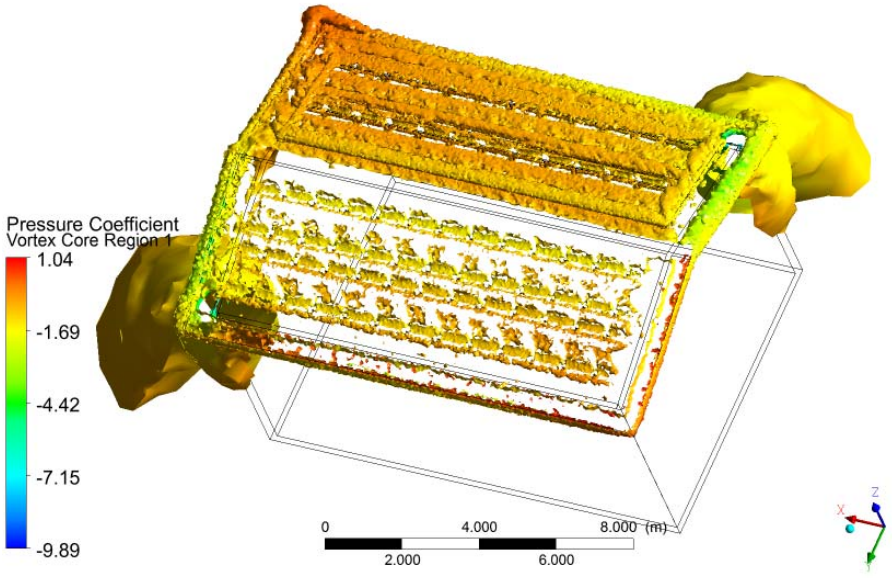


Fig. E. 12. Turbulence distribution and Cp on roof under panels, WW, and LW on panels

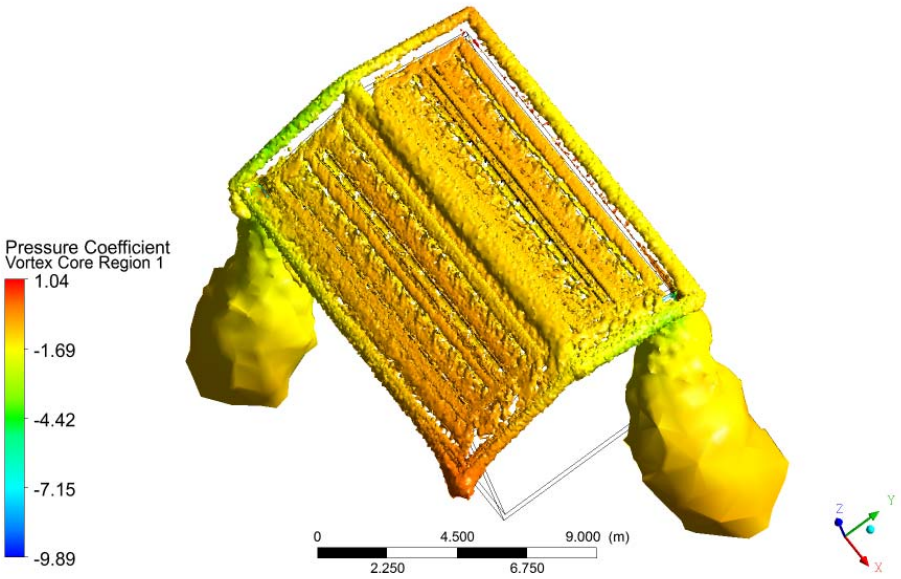


Fig. E. 13. Turbulence distribution, with CP on roof and top of panels, LW,

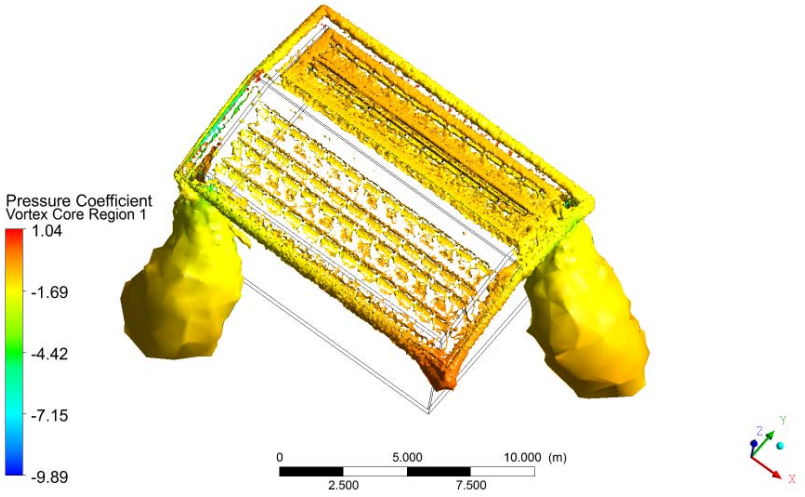


Fig. E. 14. Turbulence distribution, with CP on roof under panels LW and WW with panels

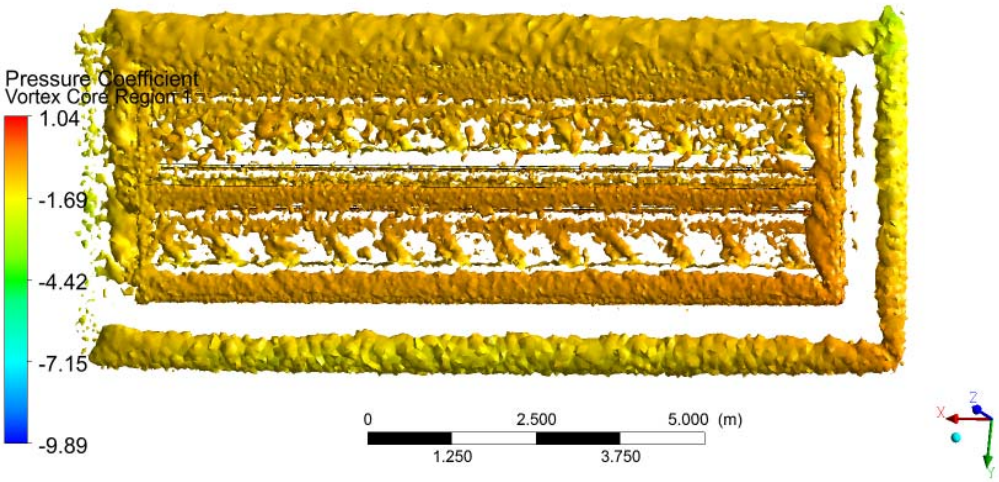


Fig. E. 15. Turbulence distribution, with CP on top of panels, WW,

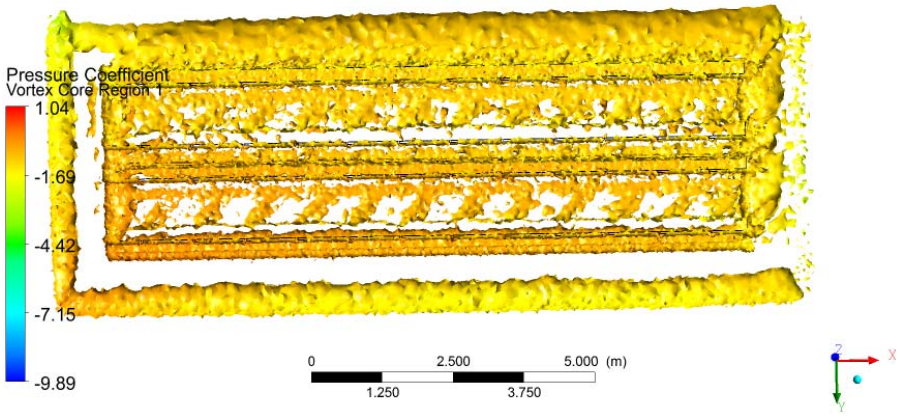


Fig. E. 16. Turbulence distribution, with CP on bottom of panels, WW,

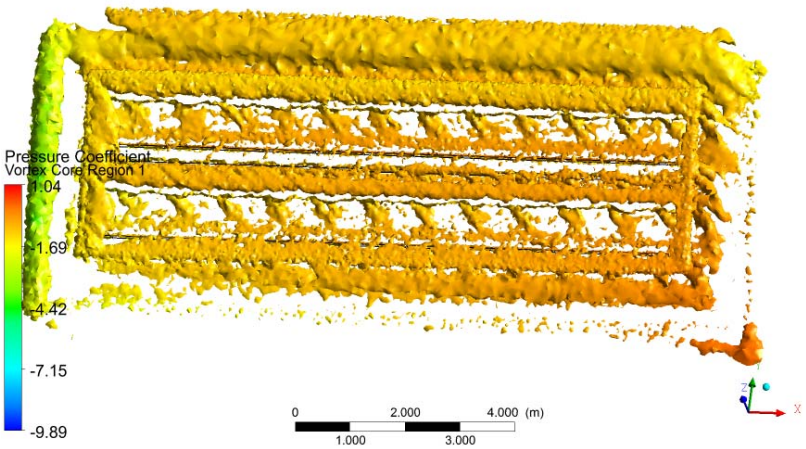


Fig. E. 17. Turbulence distribution, with CP on top of panels, LW,

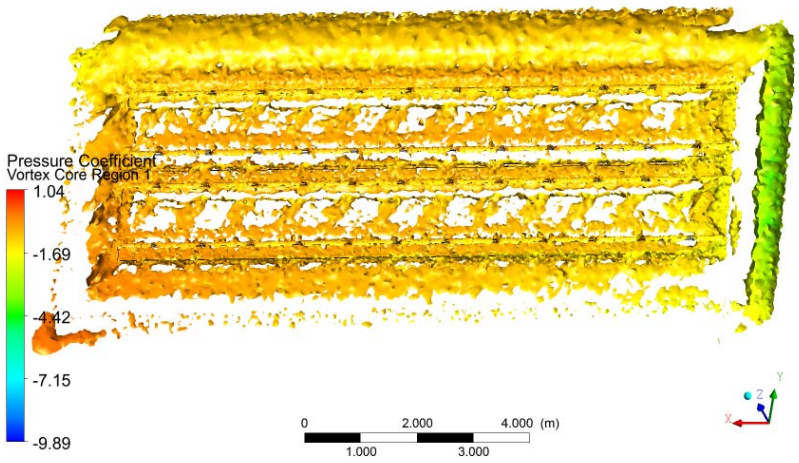


Fig. E. 18. Turbulence distribution, with CP on bottom of panels, LW,

1.1.2. WIND DIRECTION 90º

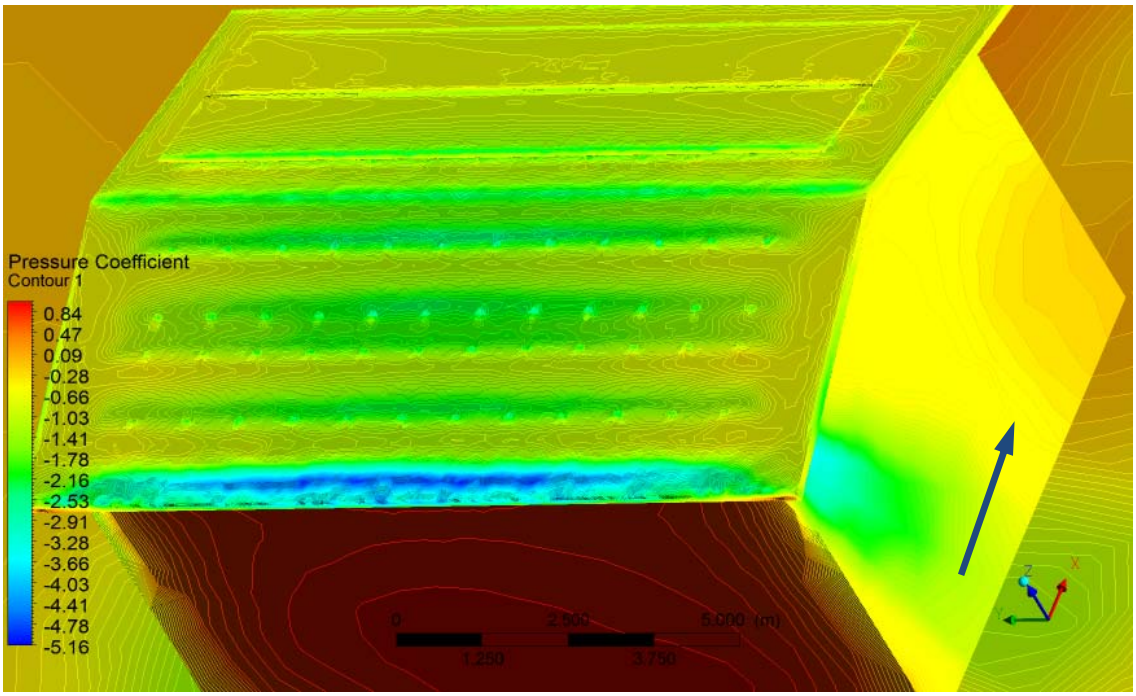


Fig. E. 19. CP on roof under solar panels, S 15º, WW, WD 90º

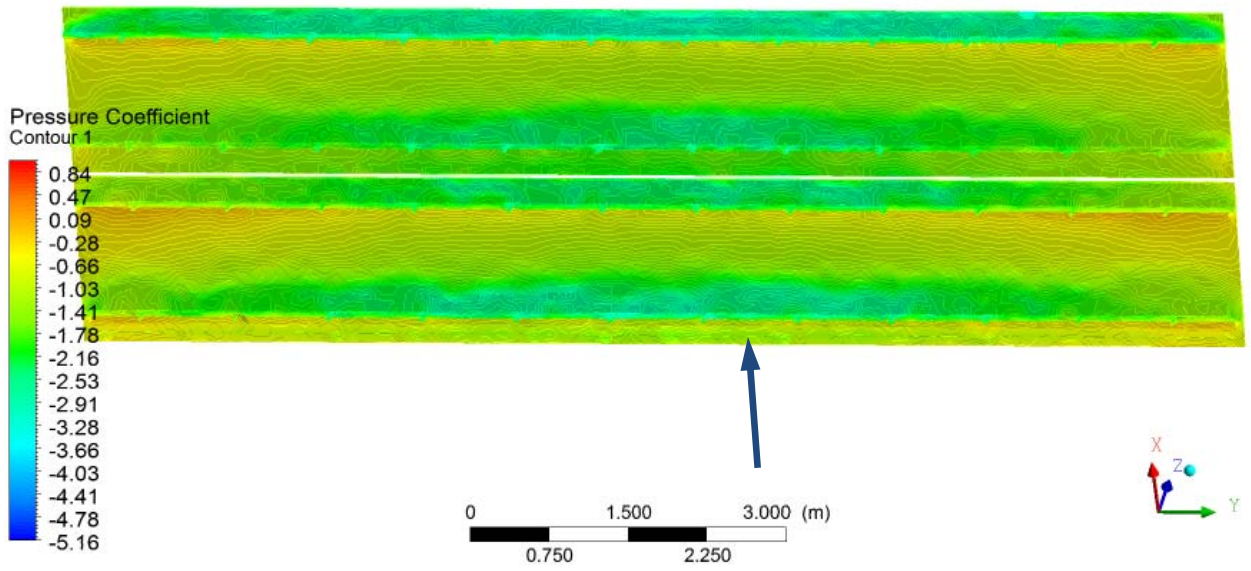


Fig. E. 20. C P on bottom of solar panels, S 15º, WW, WD 90º

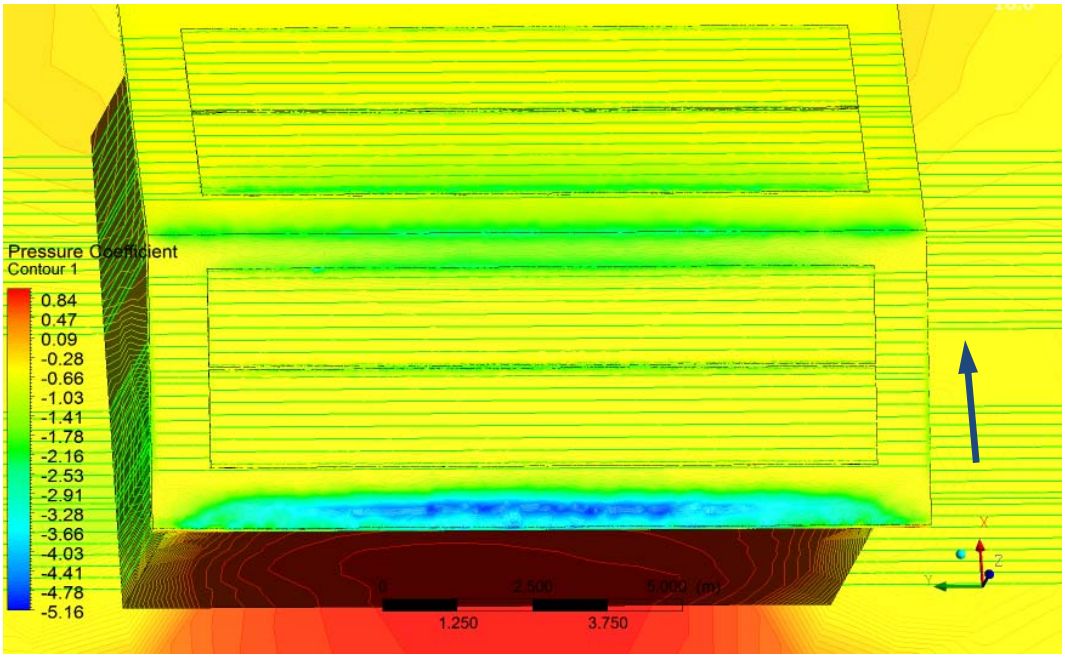


Fig. E. 21. Cp on top of solar panels with plines, S 15º, WW, WD 90º

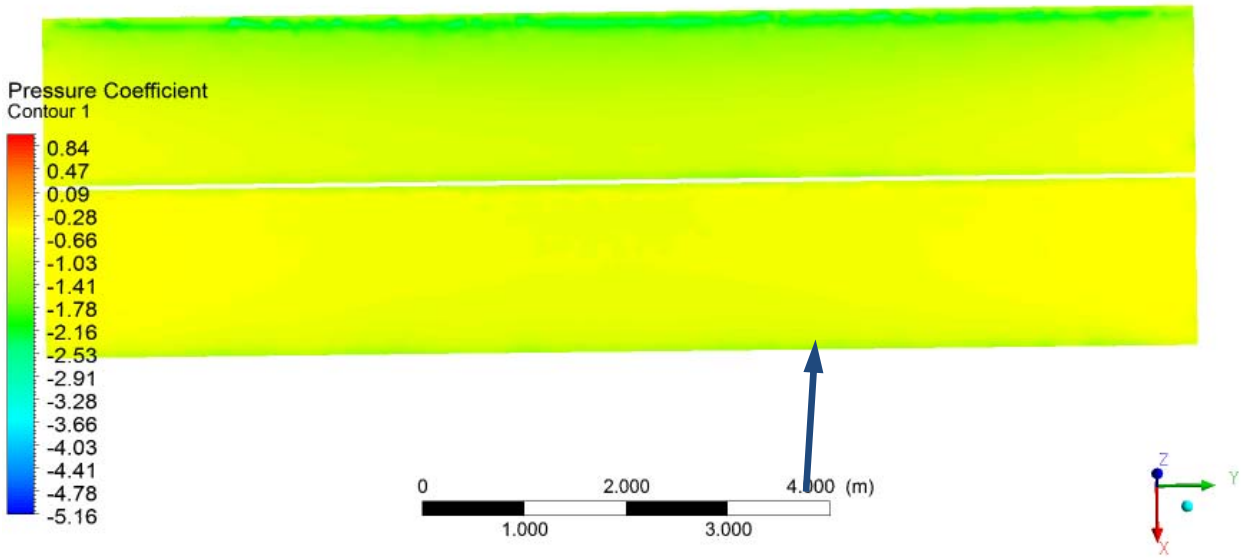


Fig. E. 22. Cp on top of solar panels, S 15º, WW, WD 90º

1.1.3. WIND DIRECTION 0º

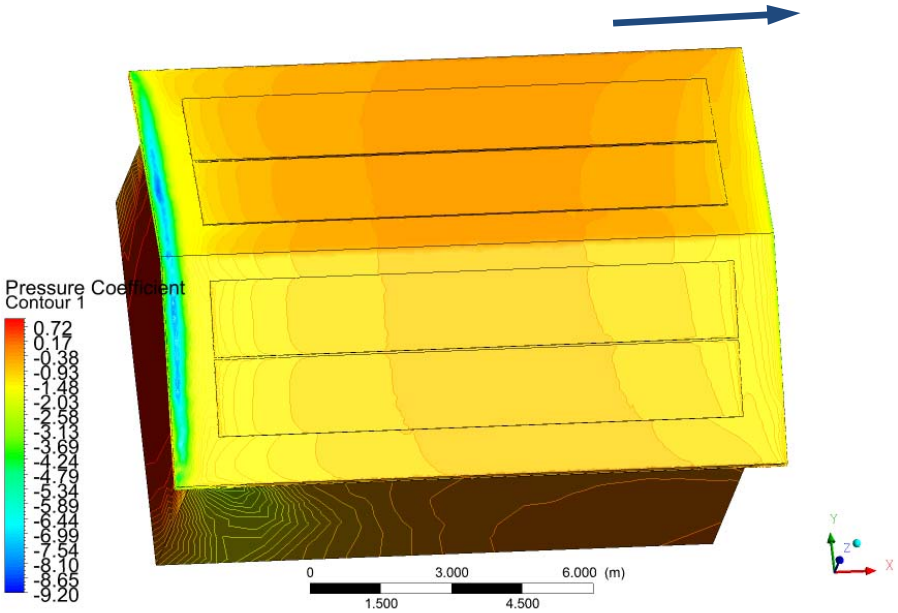


Fig. E. 23. Cp on roof with solar panels, top view, S 15º, WD 0º

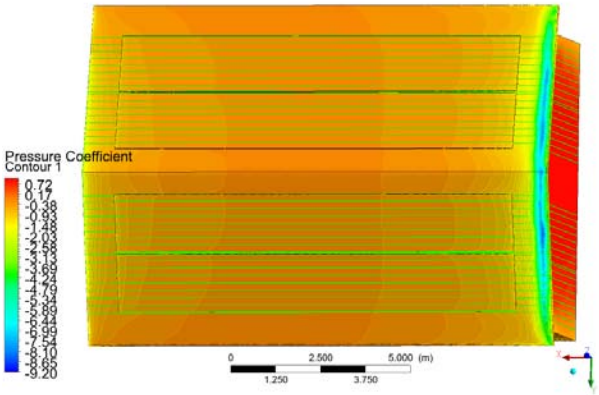


Fig. E. 24. Cp on roof with solar panels and Plines S 15º, WD 0º

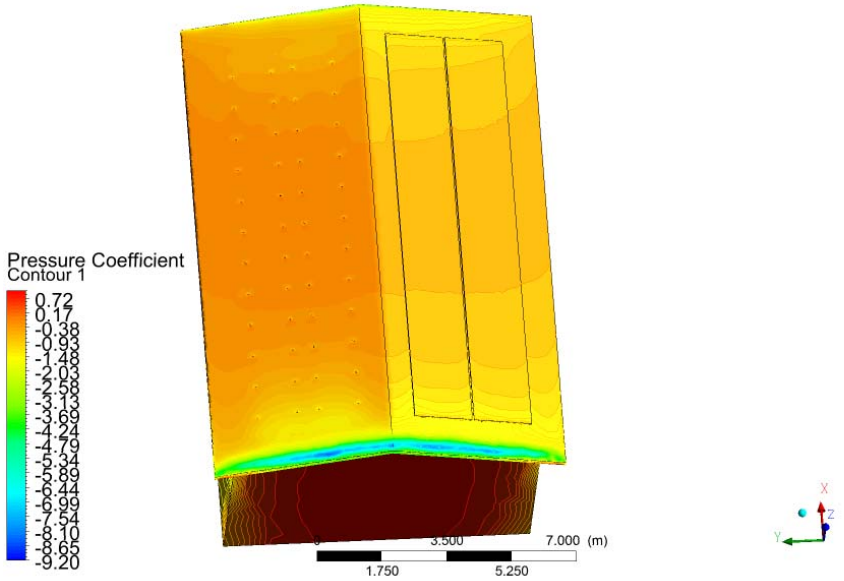


Fig. E. 25. Cp on roof under solar panels on one side and on solar panels on the other side, S 15º, WD 0º

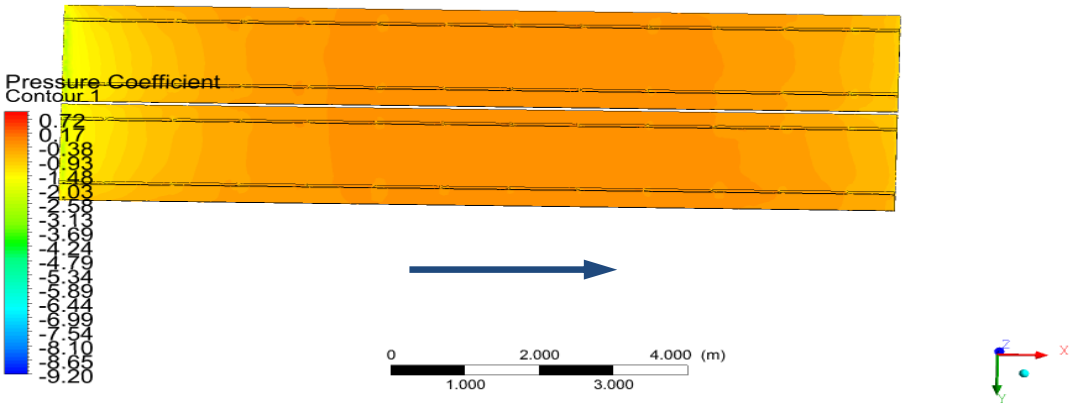


Fig. E. 26. Cp, on bottom of solar panels, S 15º, WD 0º

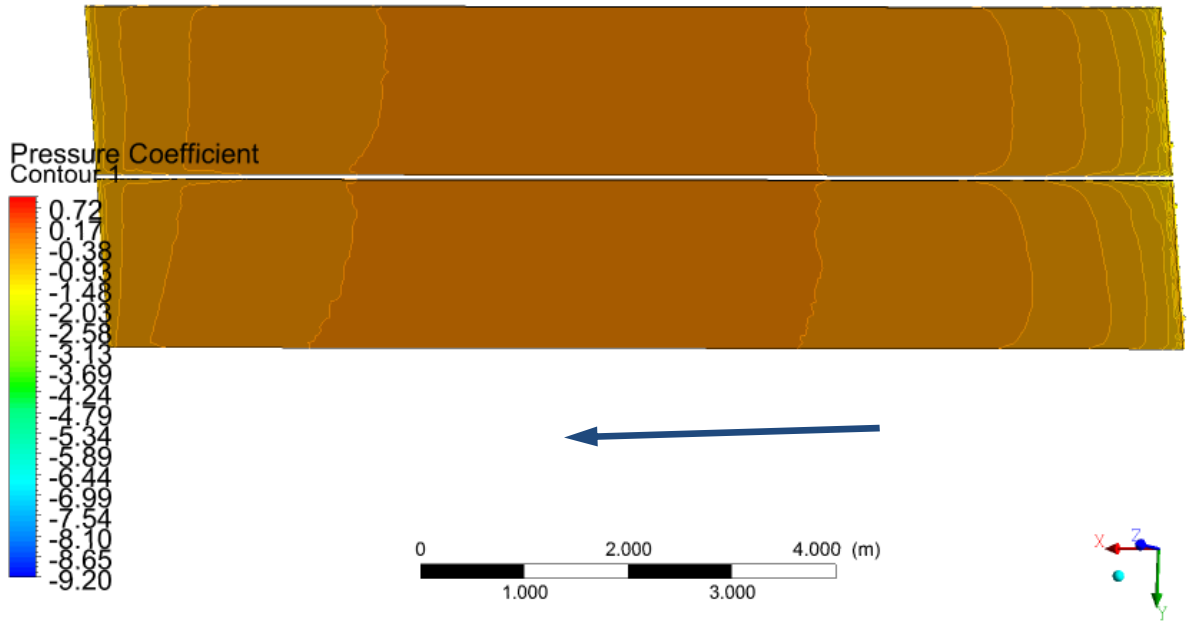


Fig. E. 27. Cp on top of solar panels, S 15º, WD 0º

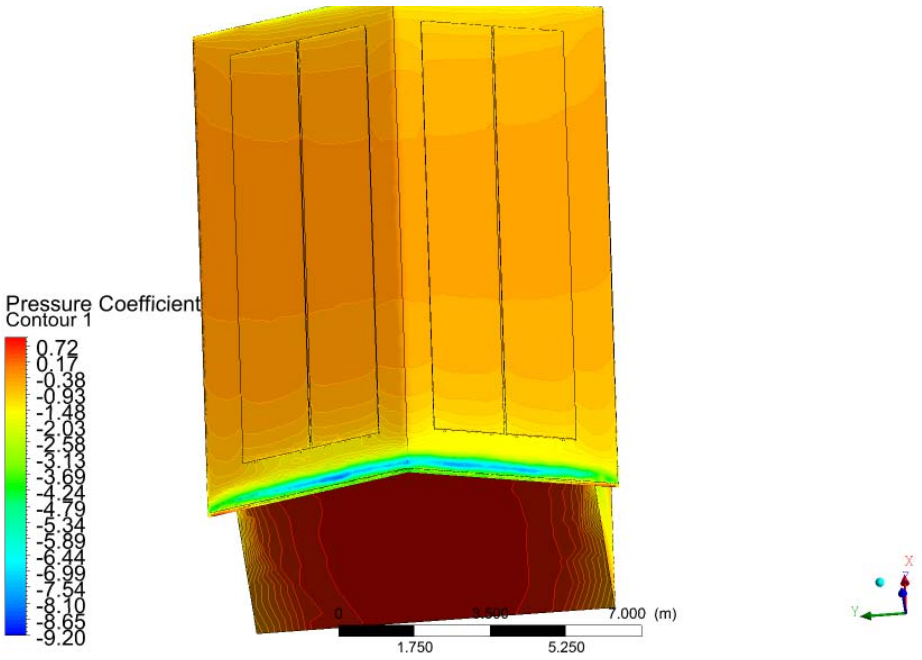


Fig. E. 28. Cp on building with the solar panels, S 15º, WD 0º, WW

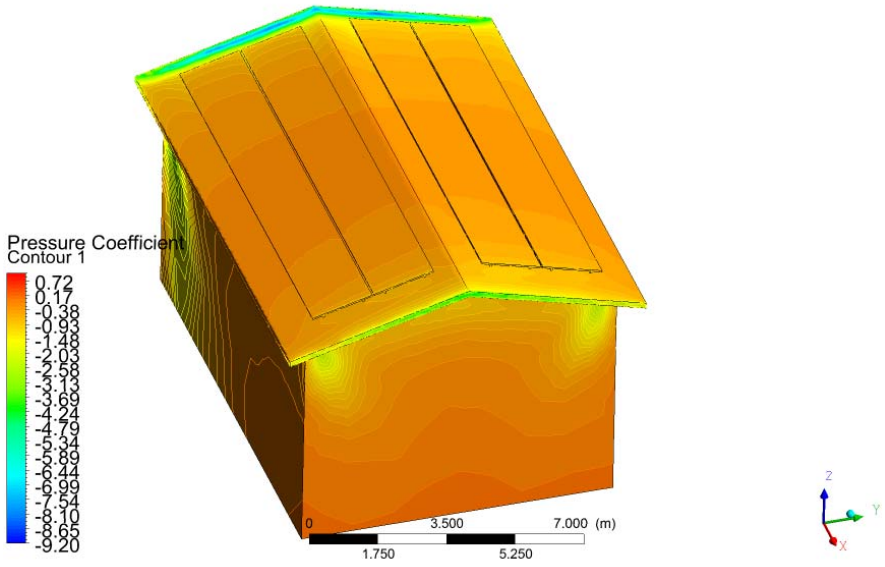


Fig. E. 29. Cp on building with the solar panels, S 15º, WD 0º, LW

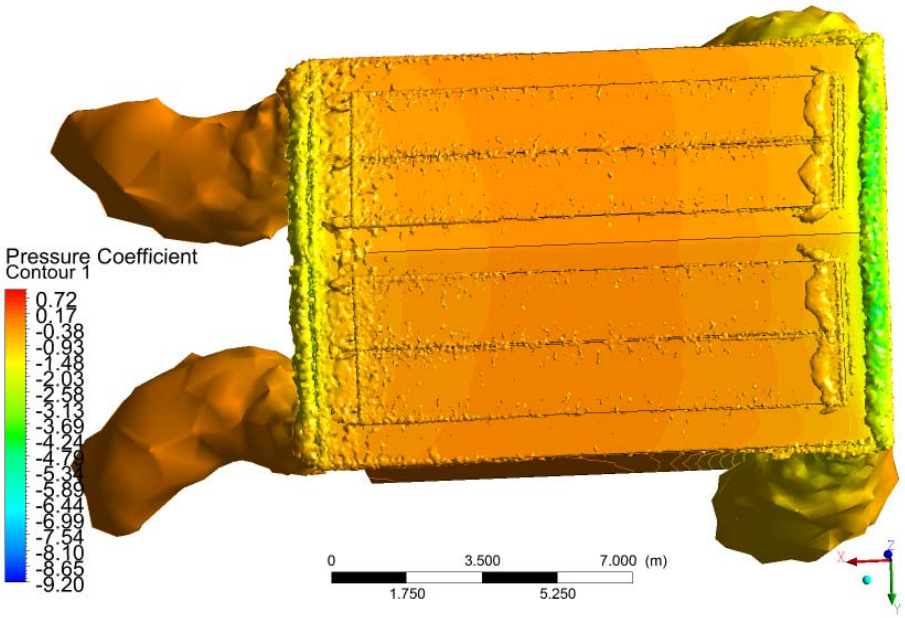


Fig. E. 30. Cp on building with turbulences, top view, S 15º, WD 0º

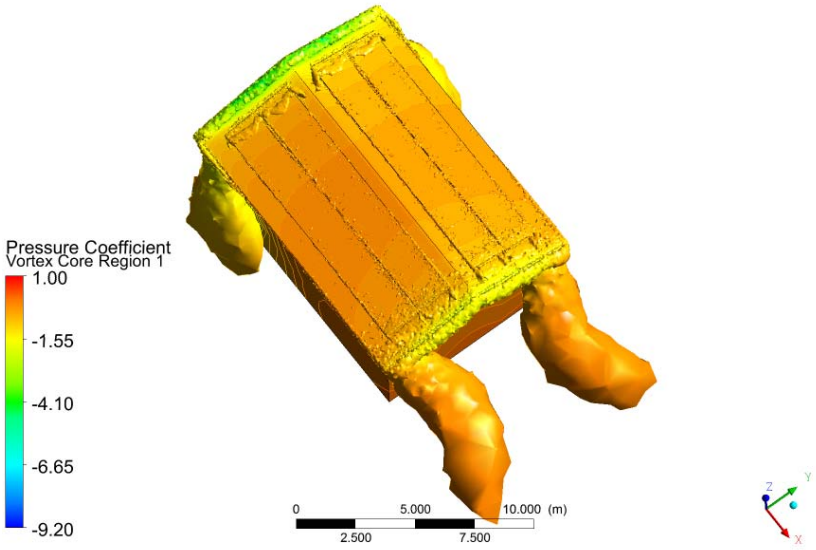


Fig. E. 31. Cp on building with turbulences, LW view, S 15º, WD 0º

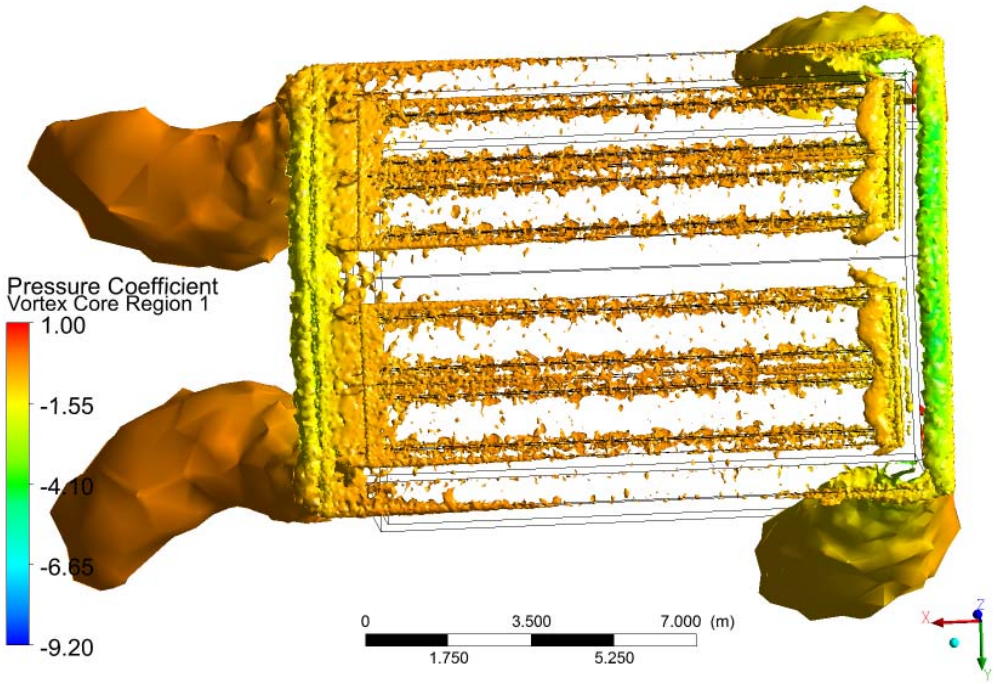


Fig. E. 32. Cp on building with turbulences, top view no building contours are shown, S 15º, WD 0º

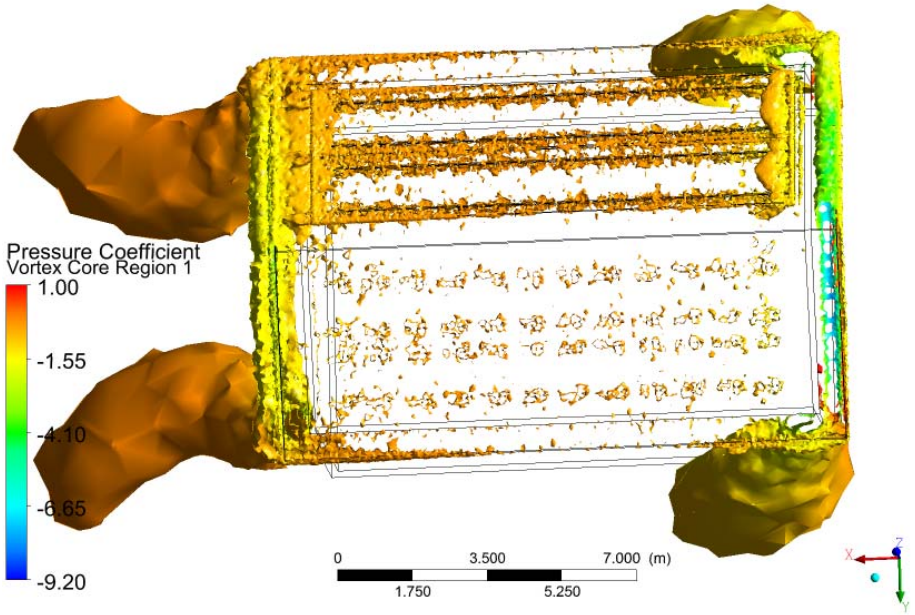


Fig. E. 33. Cp on turbulences above solar panels on one side and on roof under solar panels on the other side, top view no building contours are shown, S 15º, WD 0º

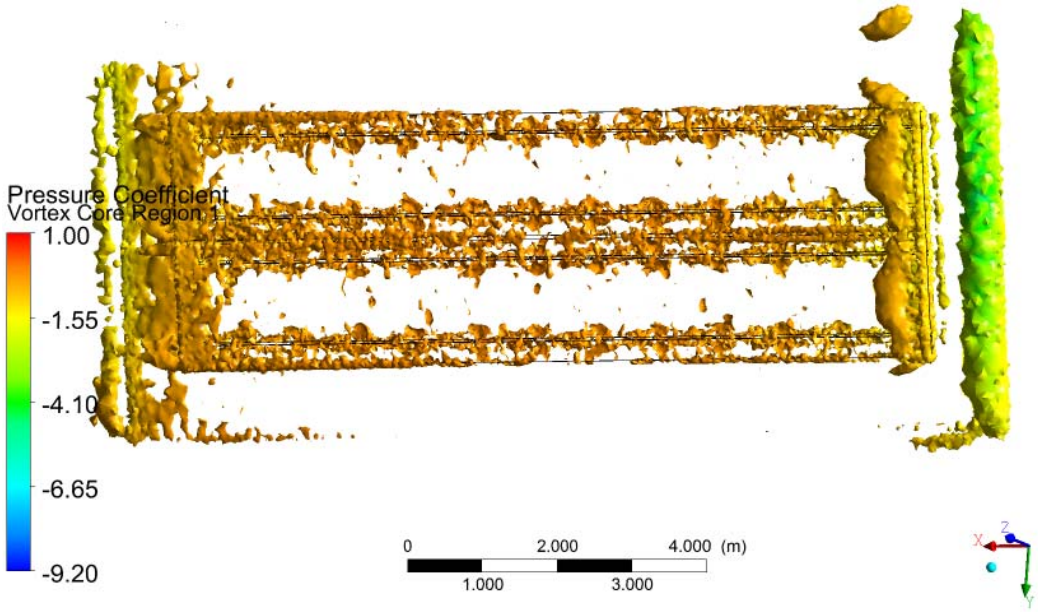


Fig. E. 34. Cp on turbulences above solar panels on one side of the roof, no building contours, S 15º, WD 0º

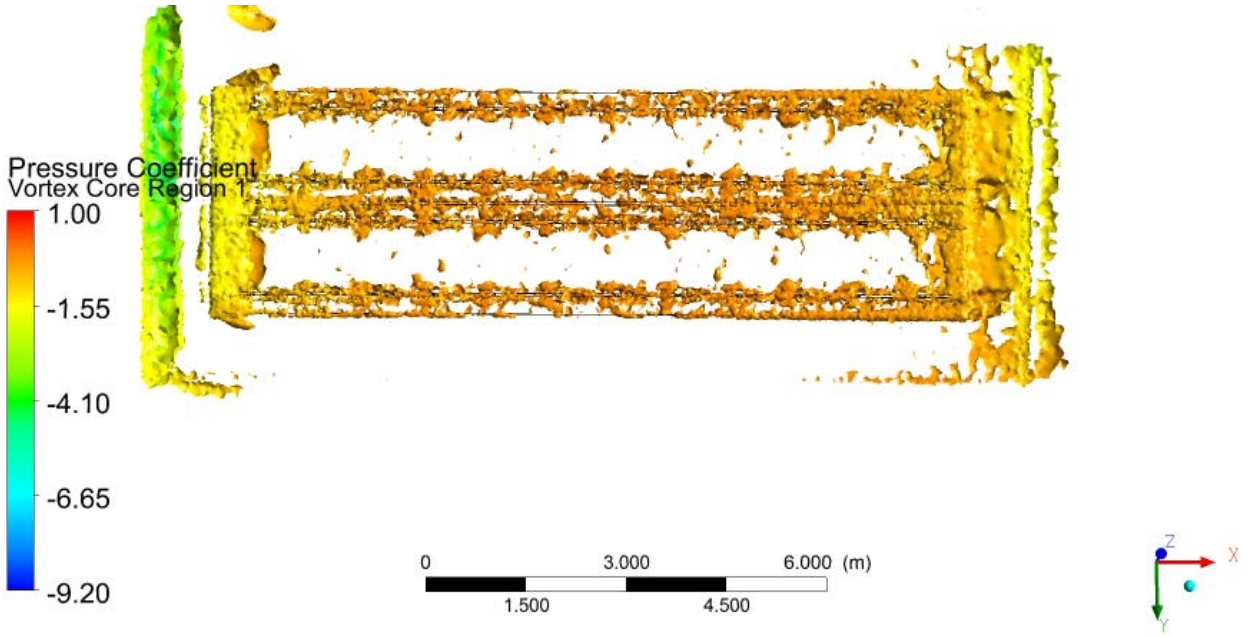


Fig. E. 35. Cp on turbulences above solar panels on one side of the roof, no building contours, S 15º, WD 0º

1.1.4. Detailed Distribution of Wind Pressure and Speed on Roof Mounted Solar Panels, S2"C10"

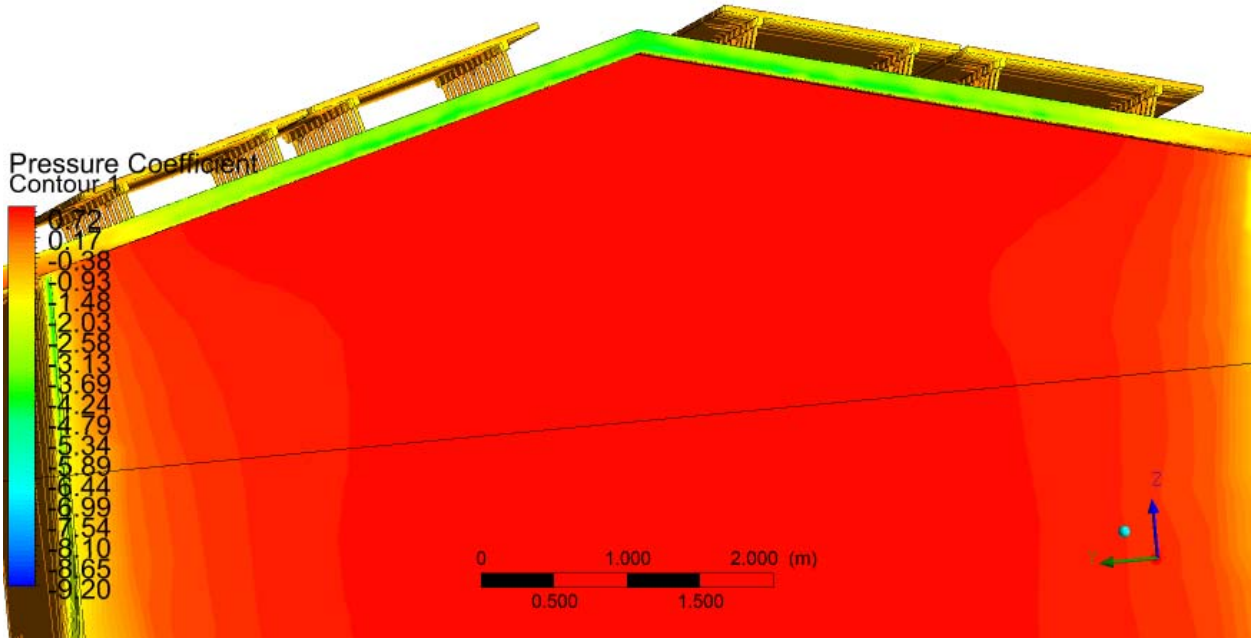


Fig. E. 36. Close view shows space under solar panels and support of the solar panels, WD 0º, WW.

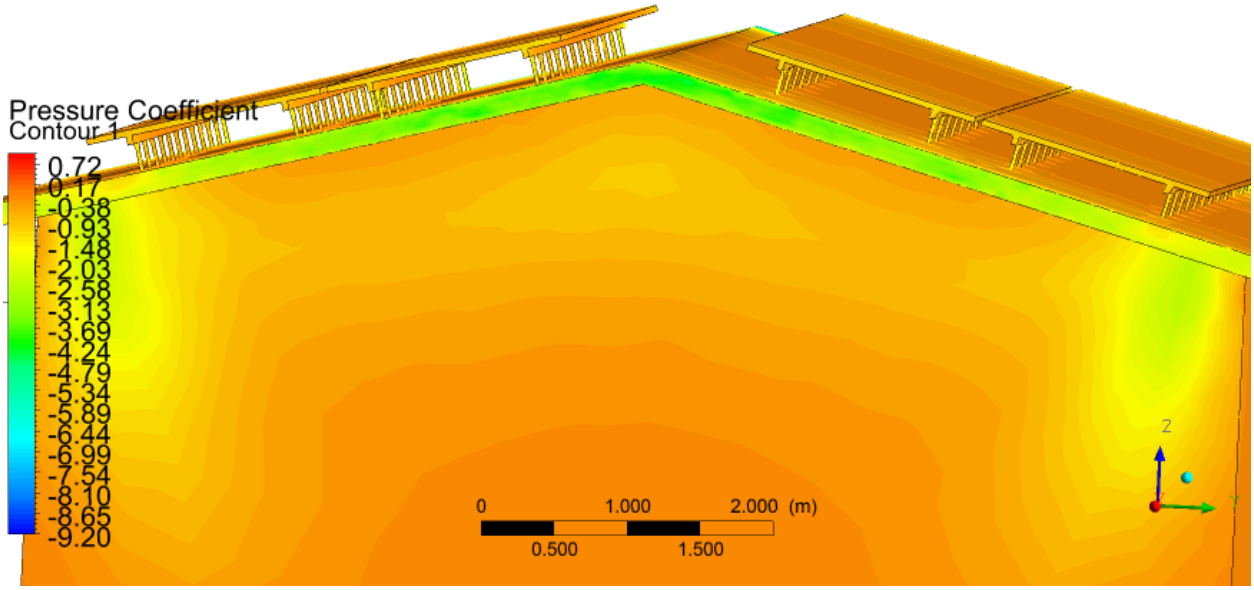


Fig. E. 37. Close view shows space under solar panels and support of the solar panels, WD 0º, LW.

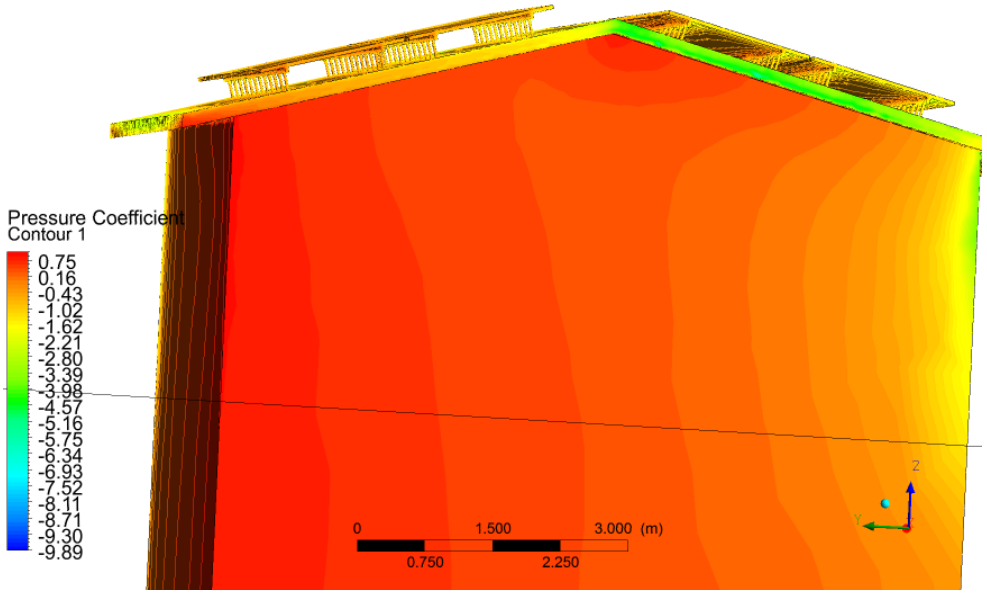


Fig. E. 38. Close view shows space under solar panels and solar panel support, WD 45º, WW

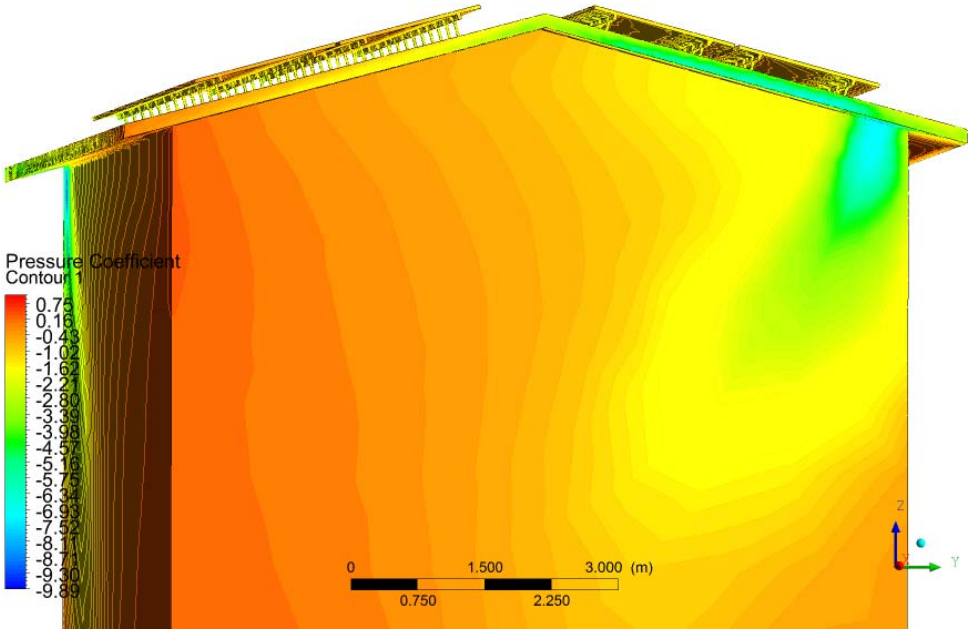


Fig. E. 39. Close view shows space under solar panels and solar panel support, WD 45º, LW

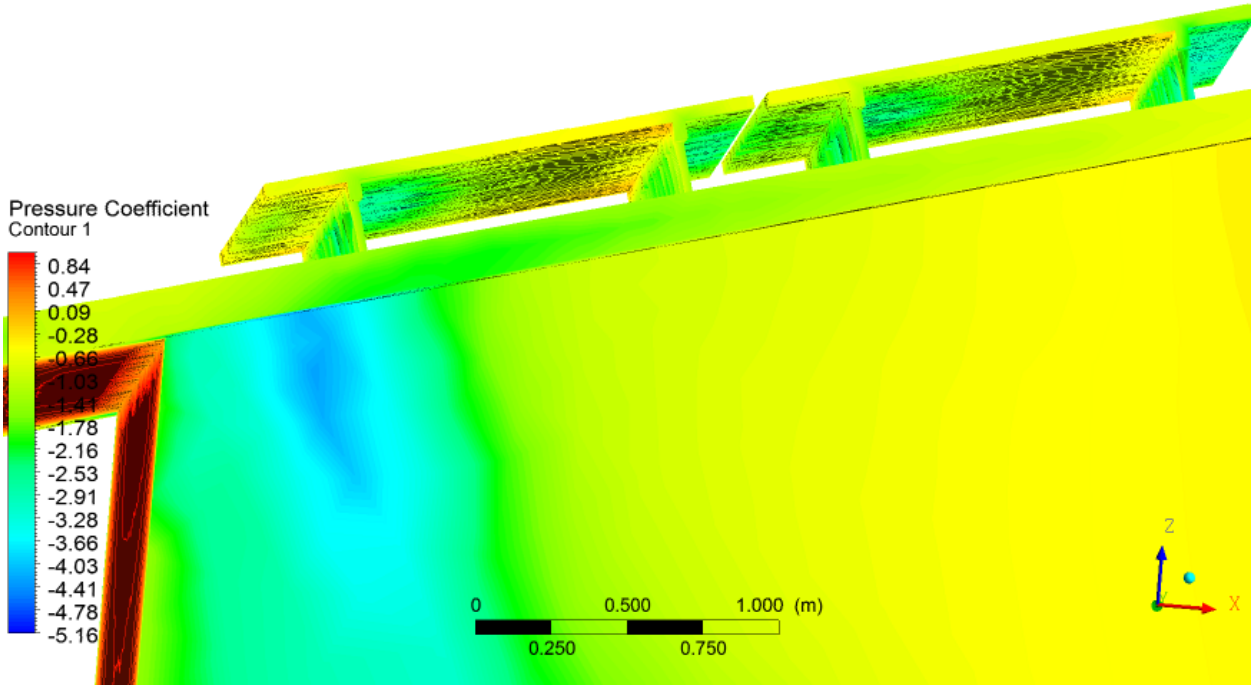


Fig. E. 40. Close view shows space under solar panels and solar panel support, WD 90º, LW

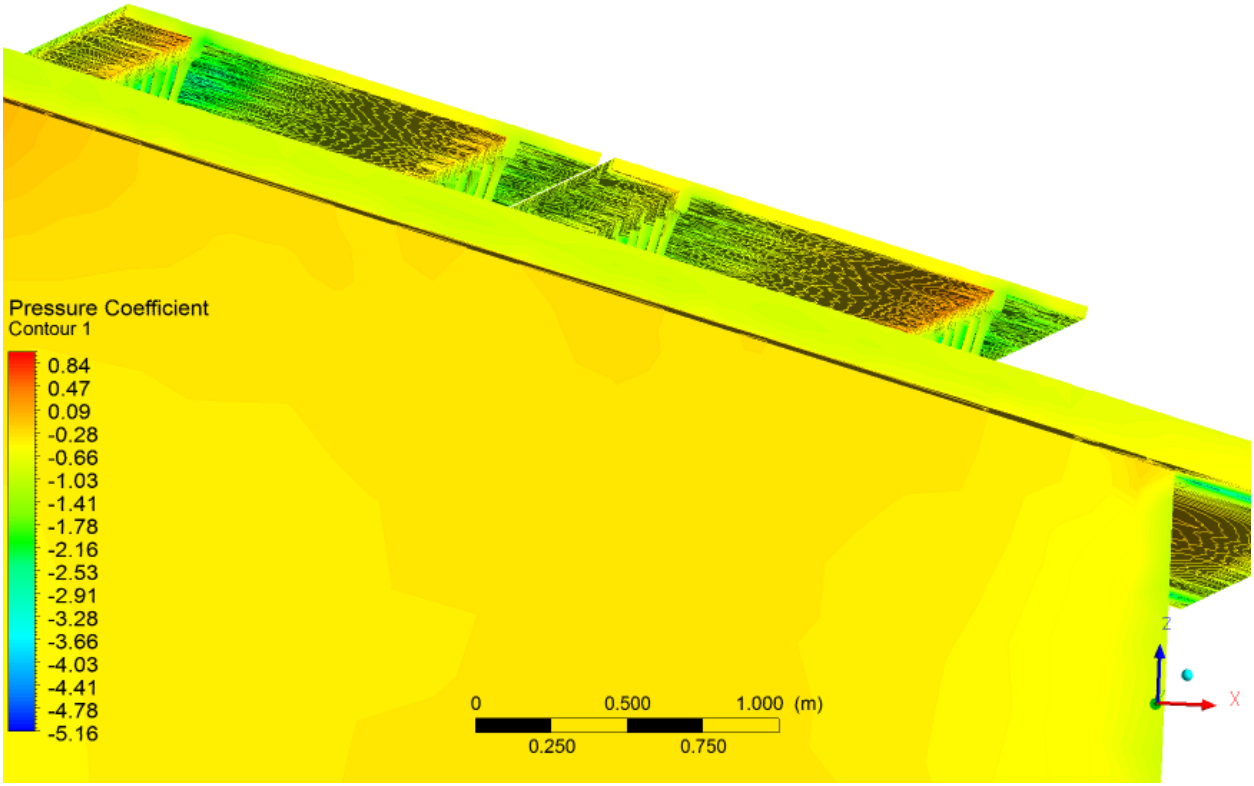


Fig. E. 41. Close view shows space under solar panels and solar panel support, WD 90º, LW

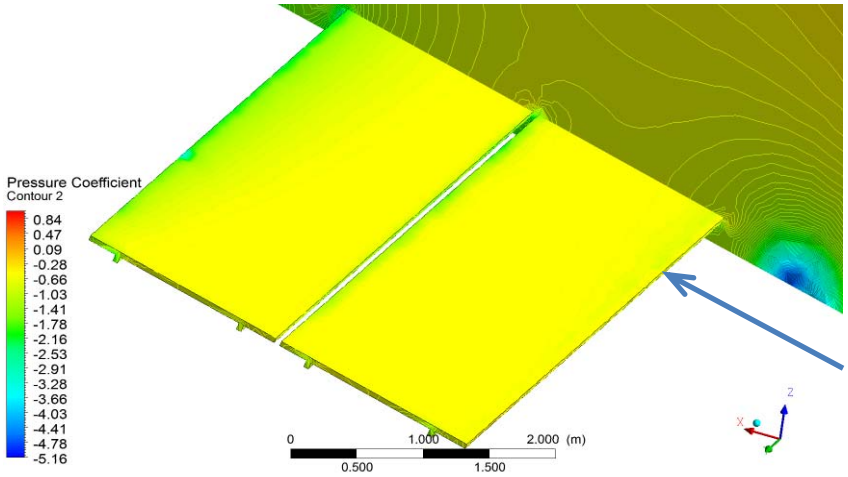


Fig. E. 42. Cp on a perpendicular plan on top of panels, Close up WD 90º, WW

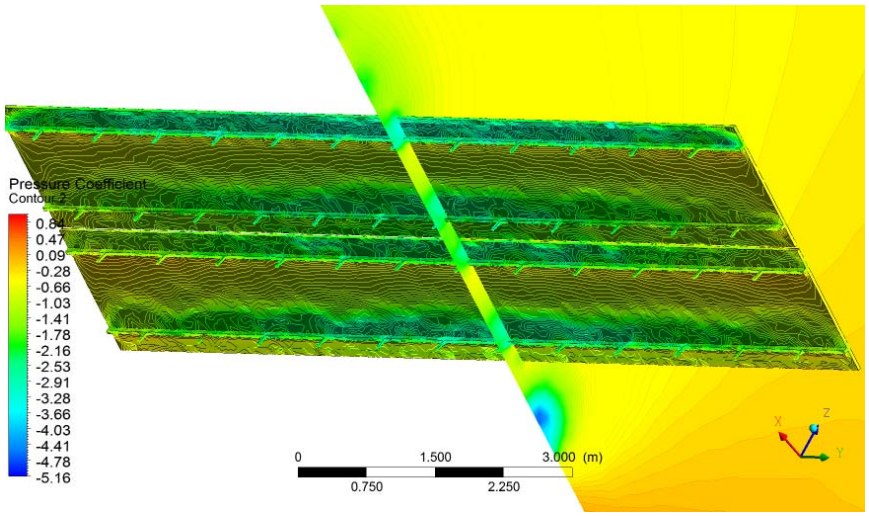


Fig. E. 43. Cp on a perpendicular plan on bottom of panels, Close up WD 90º, WW

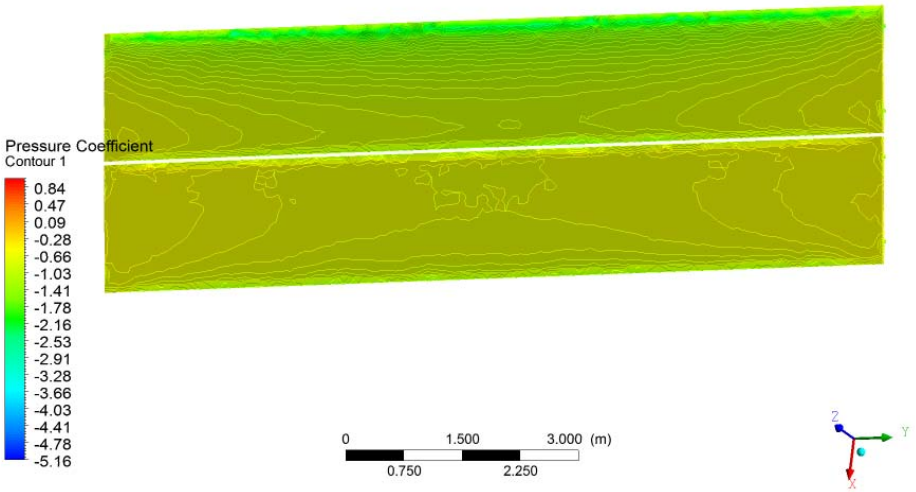


Fig. E. 44. Cp on top of panels, WD 90º, LW

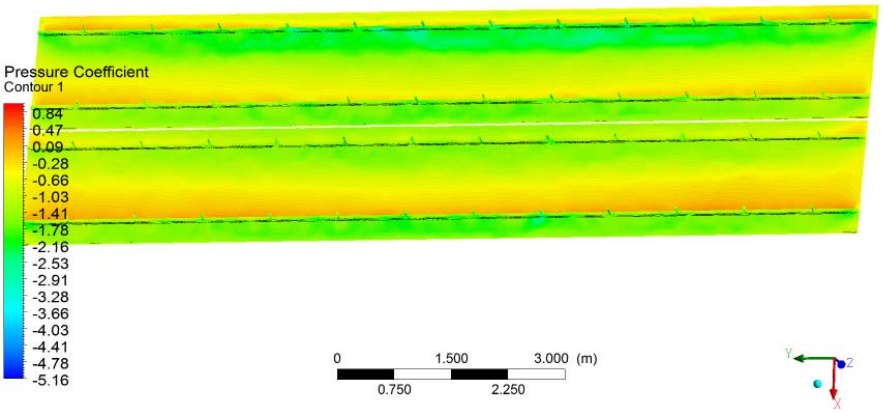


Fig. E. 45. Cp on bottom of panels, WD 90º, LW

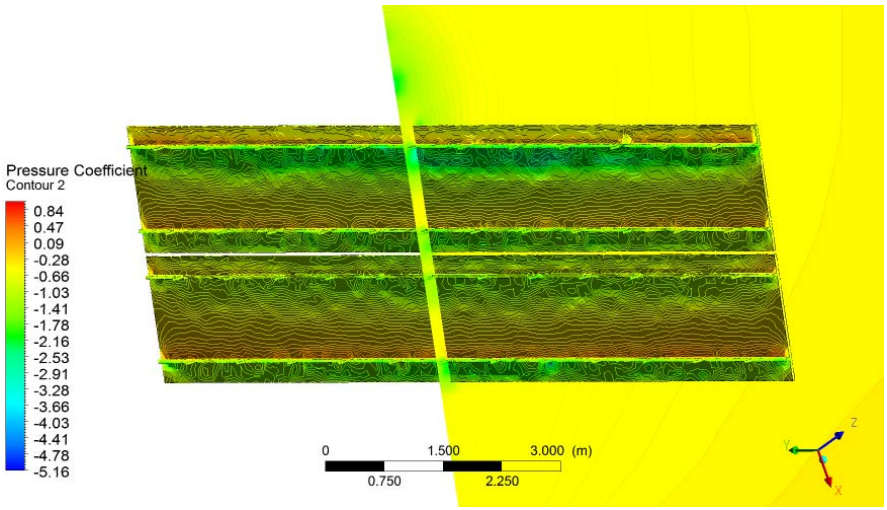


Fig. E. 46. Cp on a perpendicular plane under panels, WD 90º, LW

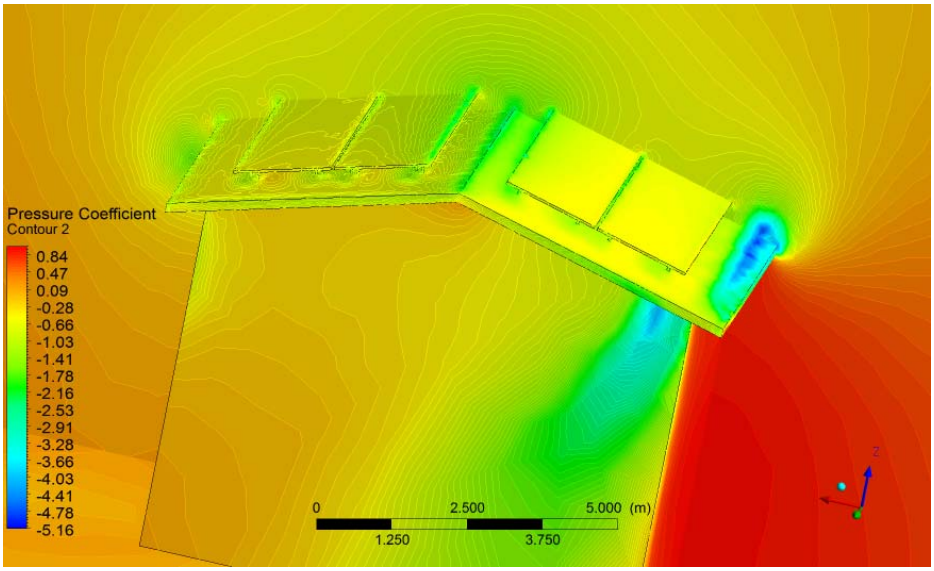


Fig. E. 47. Cp on a perpendicular plane with the house, WD 90º

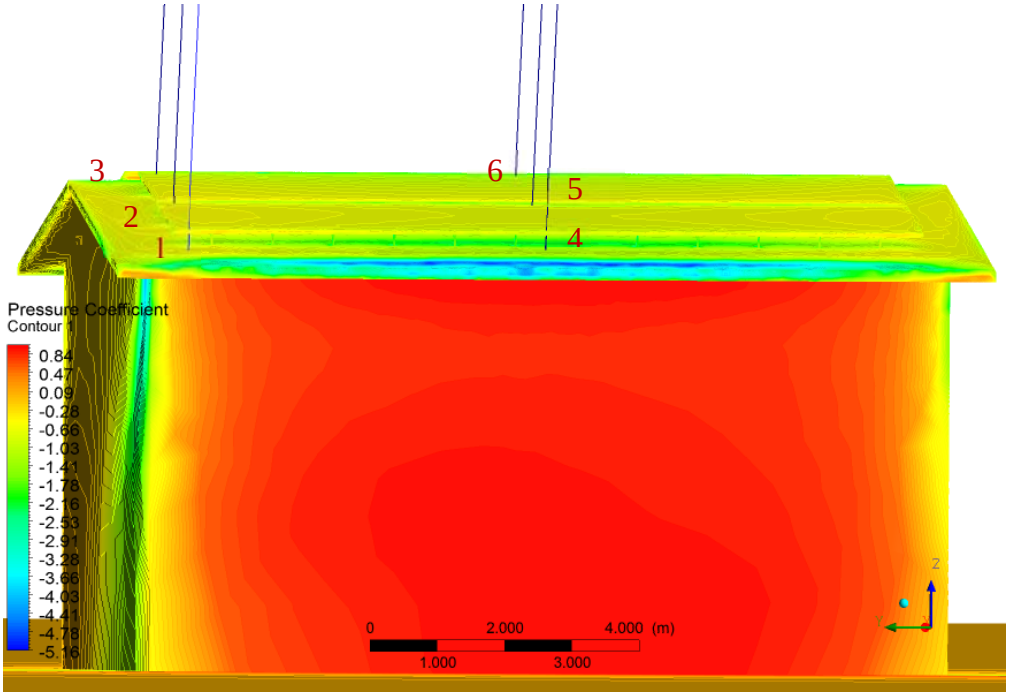


Fig. E. 48. Lines used to draw velocity and pressure changes, WD 90º

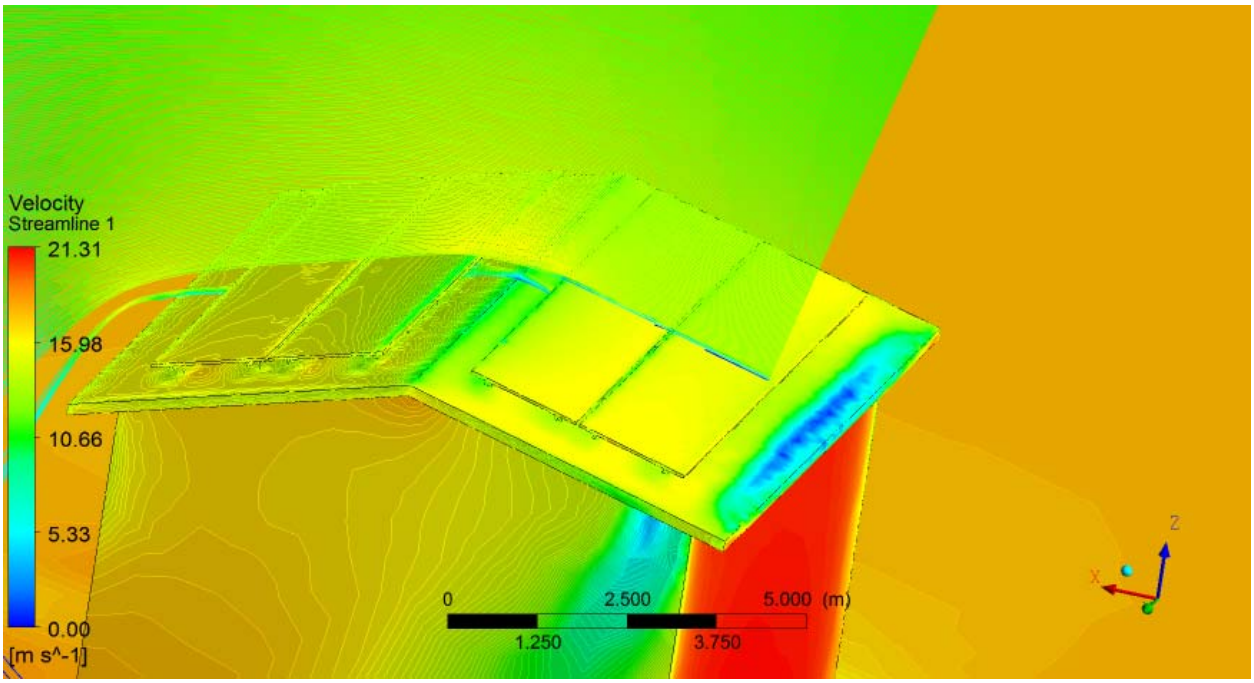


Fig. E. 49. Velocity stream lines at middle cross section plane , WD 90º

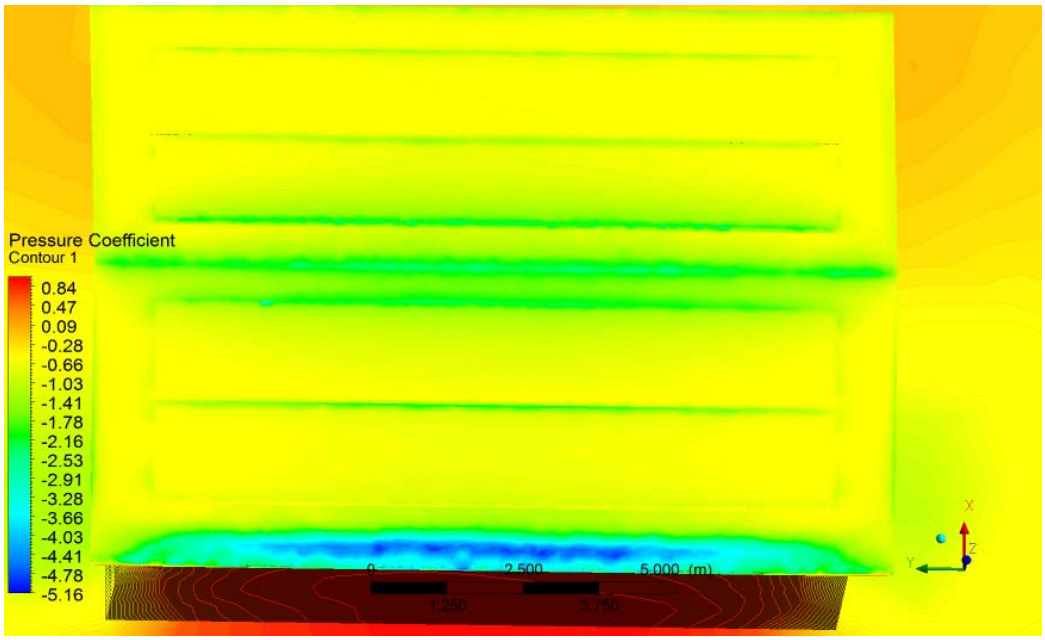


Fig. E. 50. Cp contour, whole roof, WD 90º

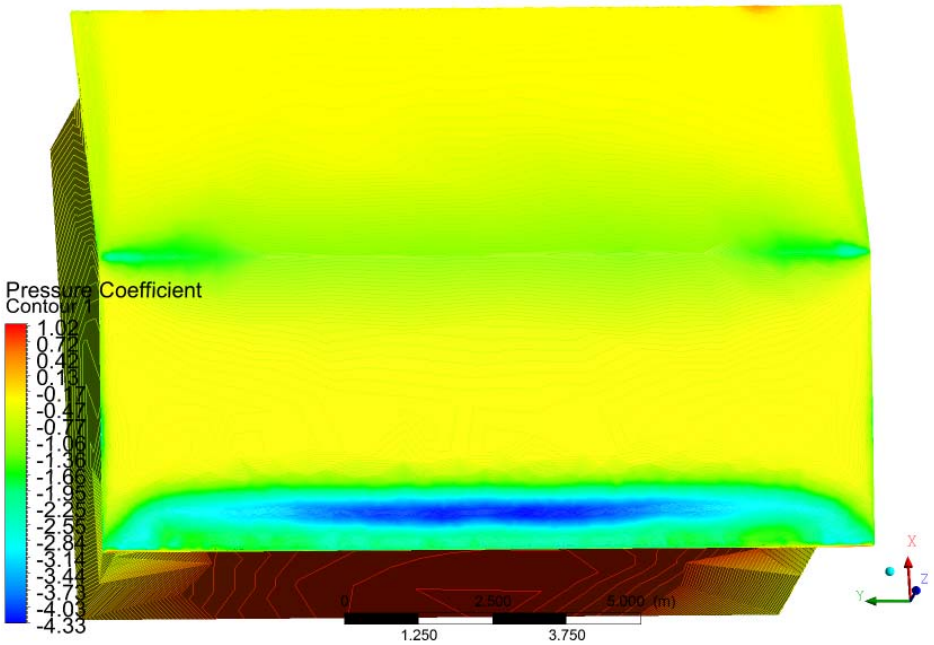


Fig. E. 51. Cp contour, whole roof, Bare roof, WD 90º,

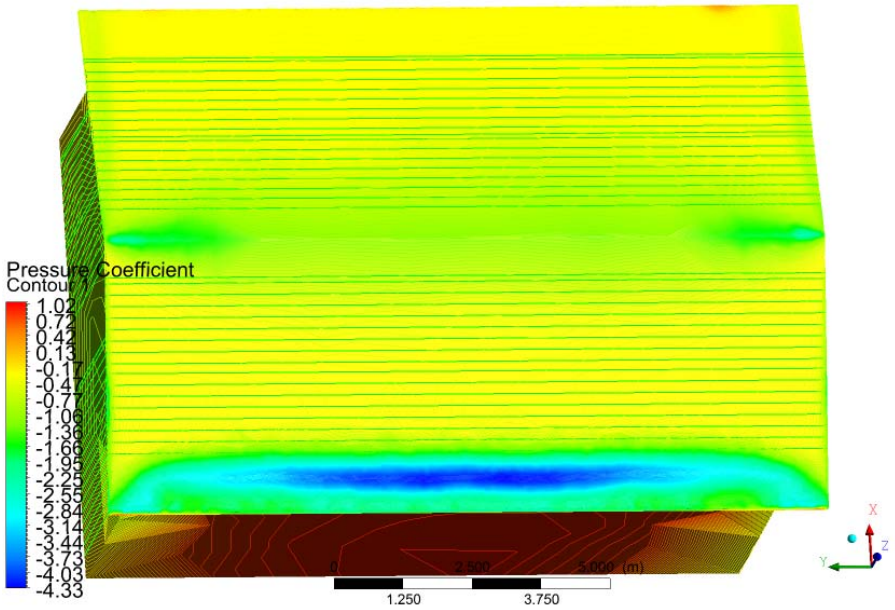


Fig. E. 52. Cp contour, whole roof, Bare roof with plines, WD 90º,

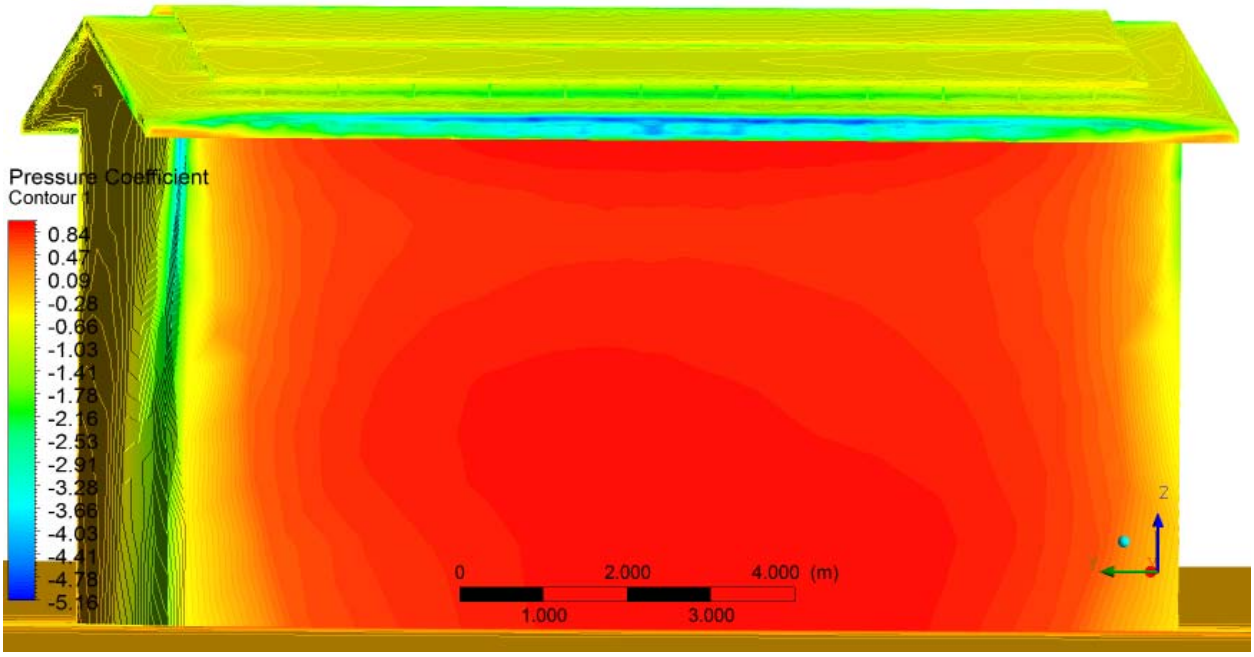


Fig. E. 53. Cp contour whole building, WD 90º, WW

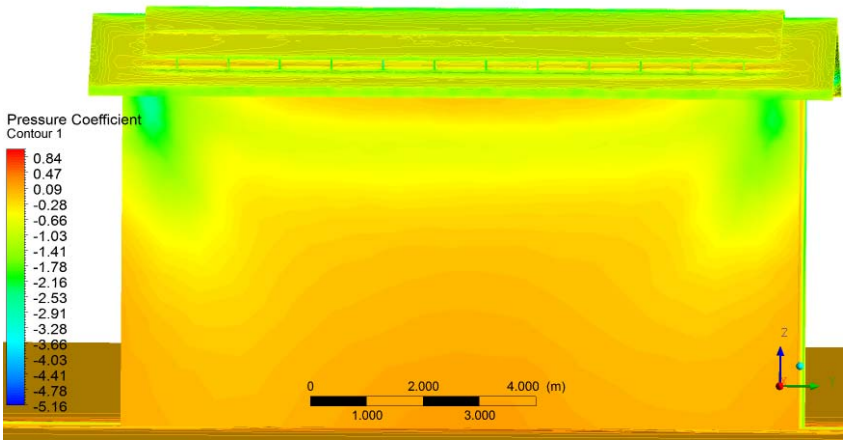


Fig. E. 54. Cp contour whole building, WD 90º, LW

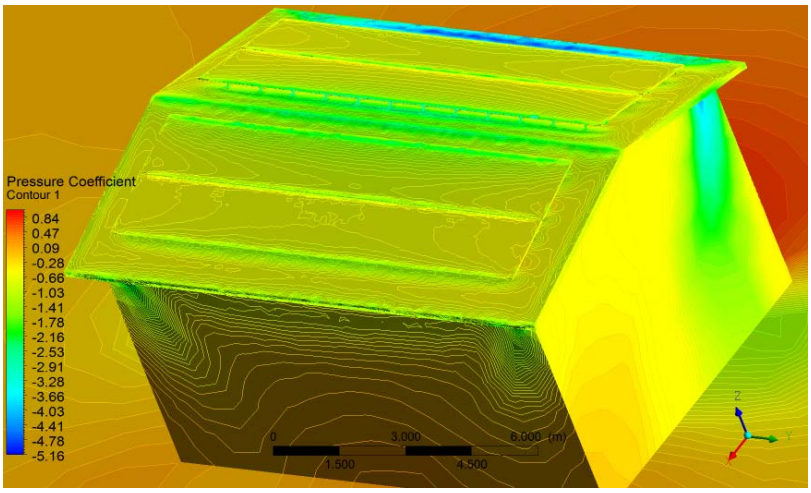


Fig. E. 55. Cp contour whole building, perspective view, WD 90º, LW

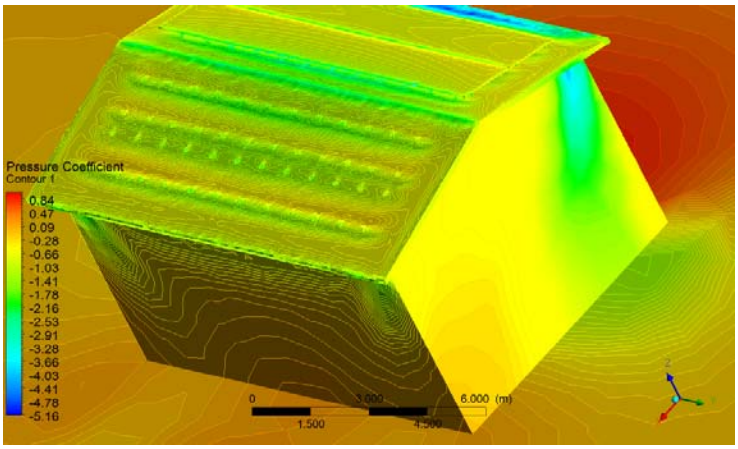


Fig. E. 56. Cp contour whole building, perspective view, roof under panels, WD 90º, LW

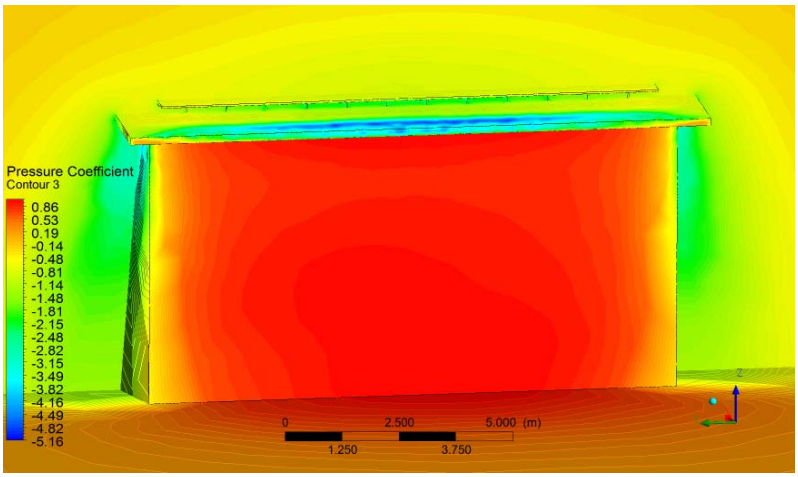


Fig. E. 57. Cp on a perpendicular longitudinal plane with the house, WD 90º, WW

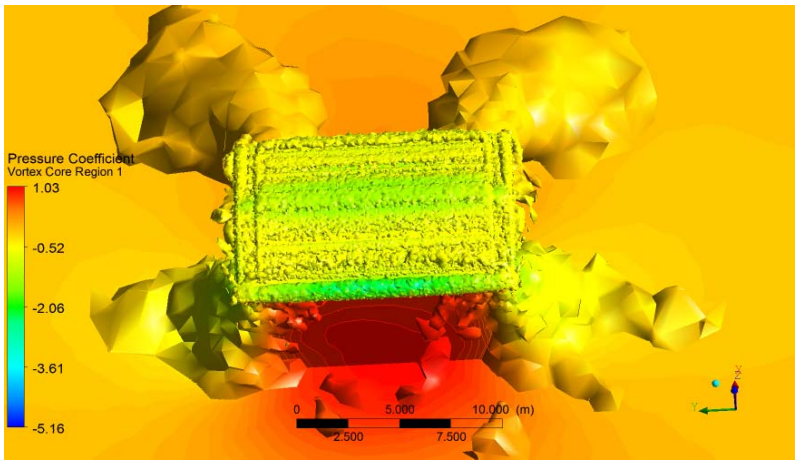


Fig. E. 58. Turbulence distribution on roof and on the building structure, with building contours, WD 90º, WW

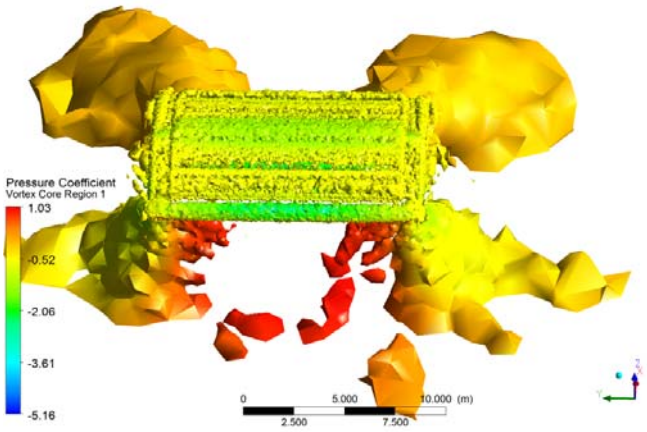


Fig. E. 59. Turbulence distribution on roof and building structure, with No building contours, WD 90º , WW

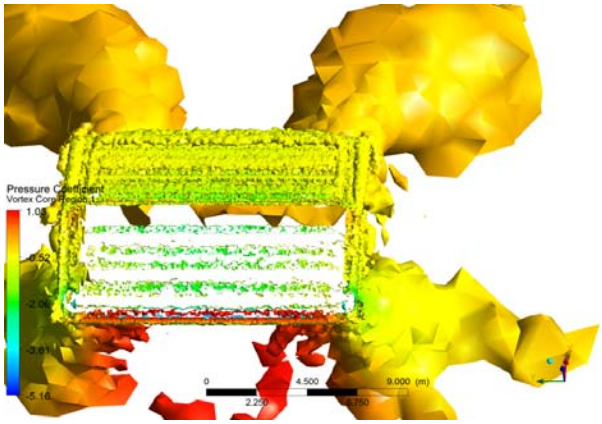


Fig. E. 60. Turbulence distribution on roof under panels and building structure, with No building contours, WW

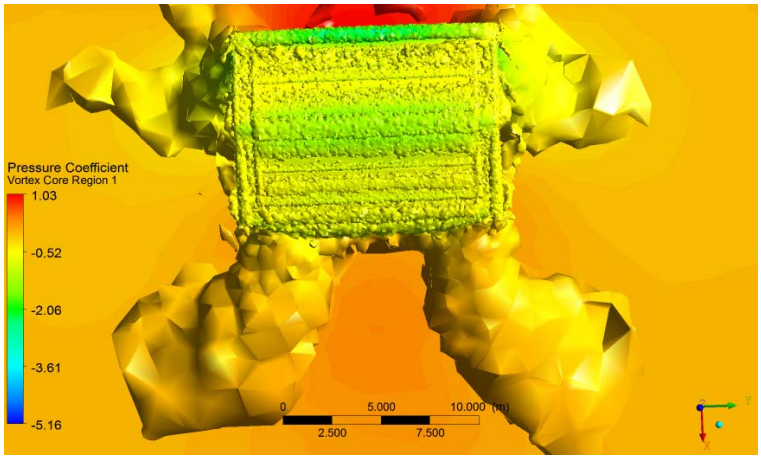


Fig. E. 61. Turbulence distribution on roof and on the building structure, with building contours, WD 90º, LW

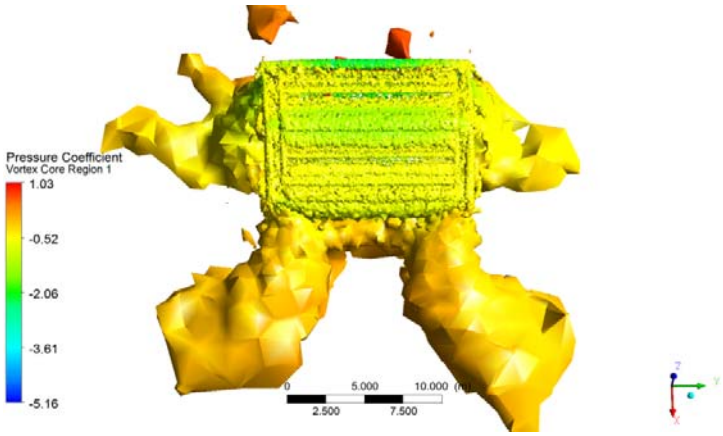


Fig. E. 62. Turbulence distribution on roof and building structure, with No building contours, WD 90º , LW

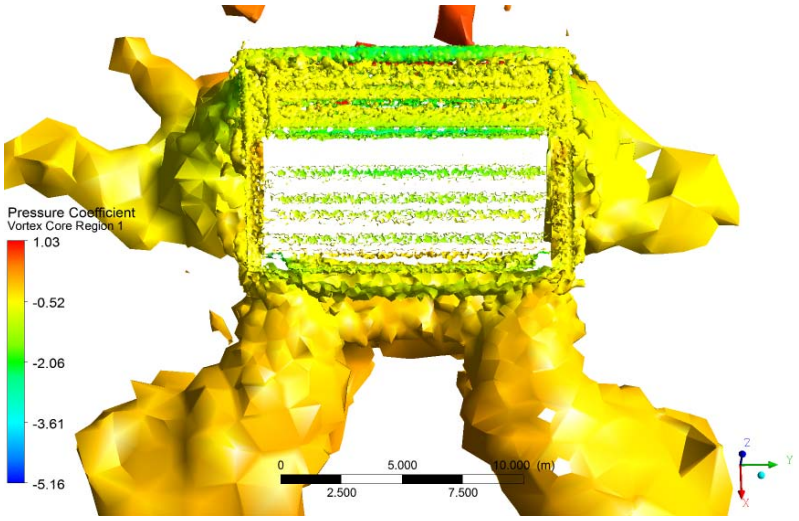


Fig. E. 63. Turbulence distribution on roof under panels and building structure, with No building contours, LW

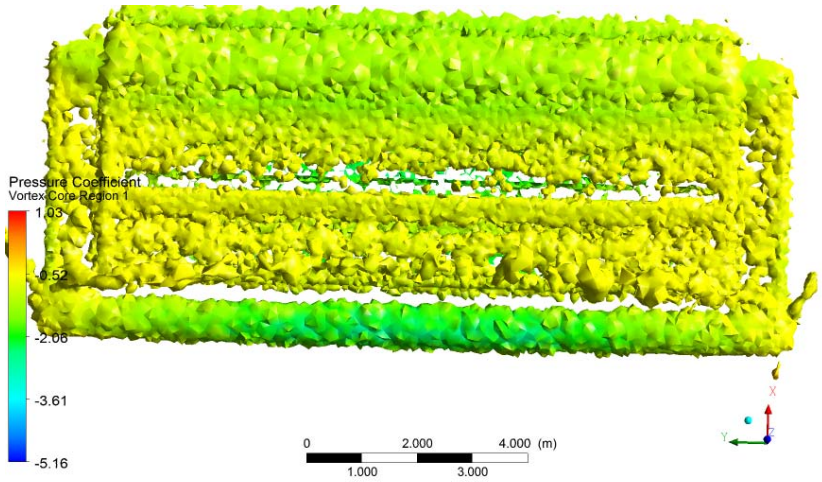


Fig. E. 64. Turbulence distribution, on top of the panels, No contours shown, WD 90º, WW

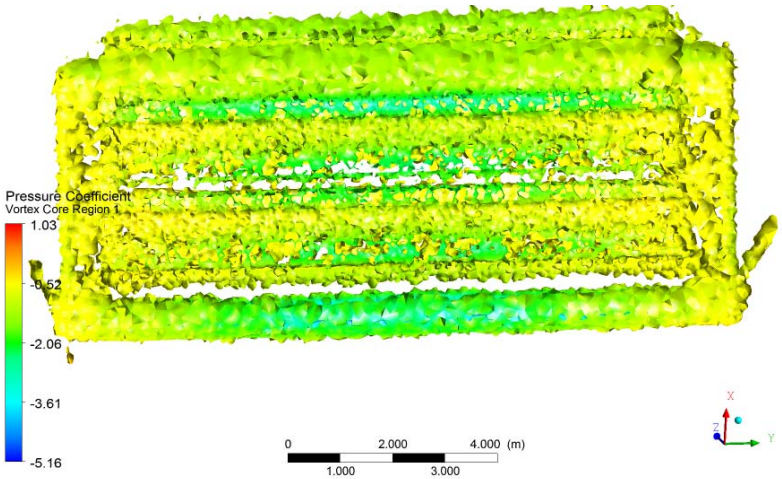


Fig. E. 65. Turbulence distribution, on bottom of the panels, No contours shown, WD 90º, WW

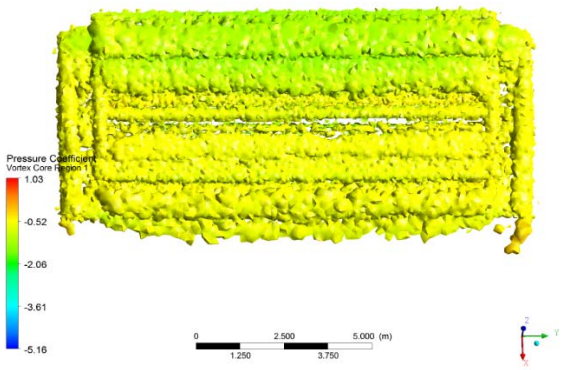


Fig. E. 66. Turbulence distribution, on top of the panels, No contours shown, WD 90º, LW

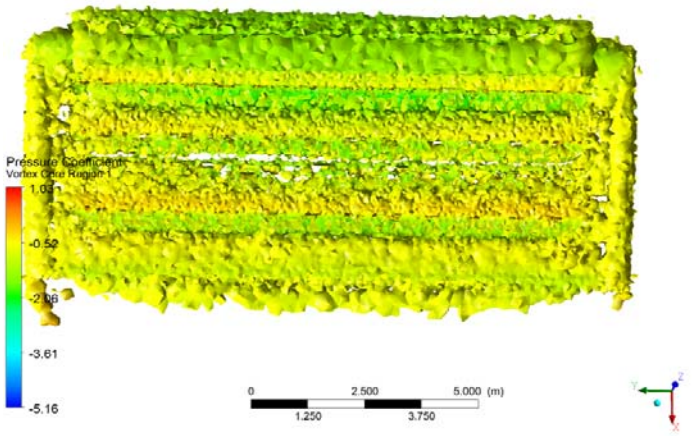


Fig. E. 67. Turbulence distribution, on bottom of the panels, No contours shown, WD 90º, LW

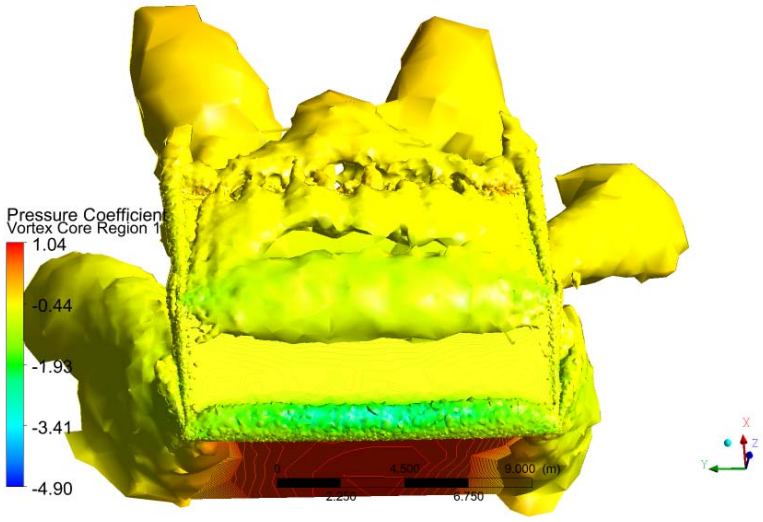


Fig. E. 68. Turbulence distribution, on top of bare roof, WD 90º, WW, S15º

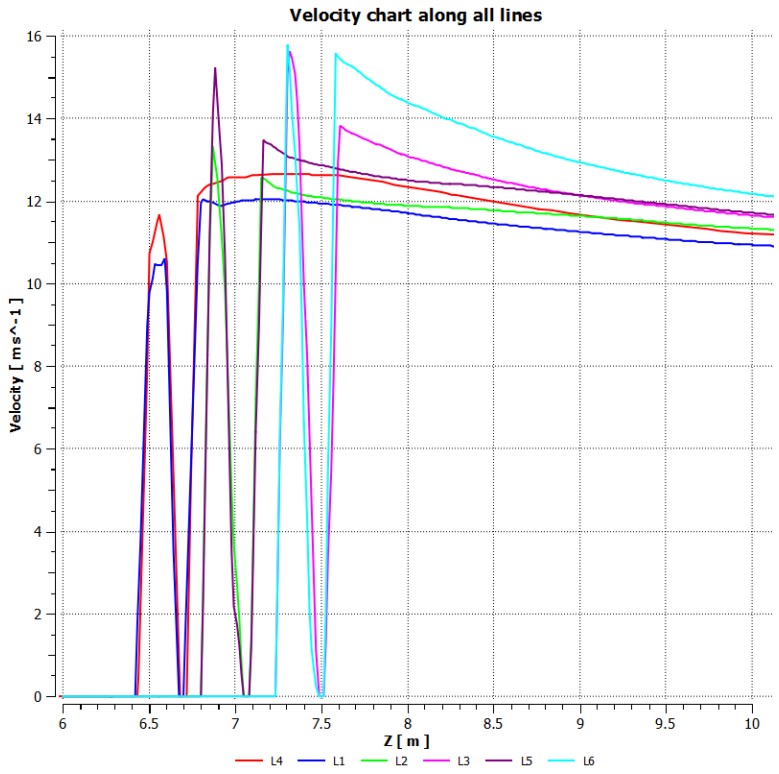


Fig. E. 69. Velocity changes between panels, and above roof, all lines.

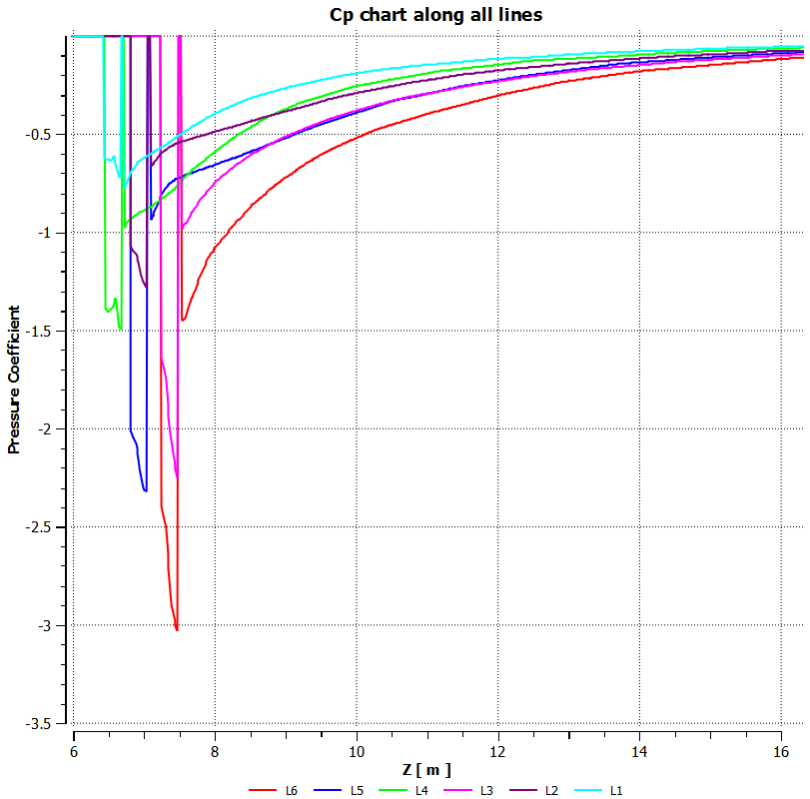


Fig. E. 70. Cp changes between panels, and above roof, all lines.

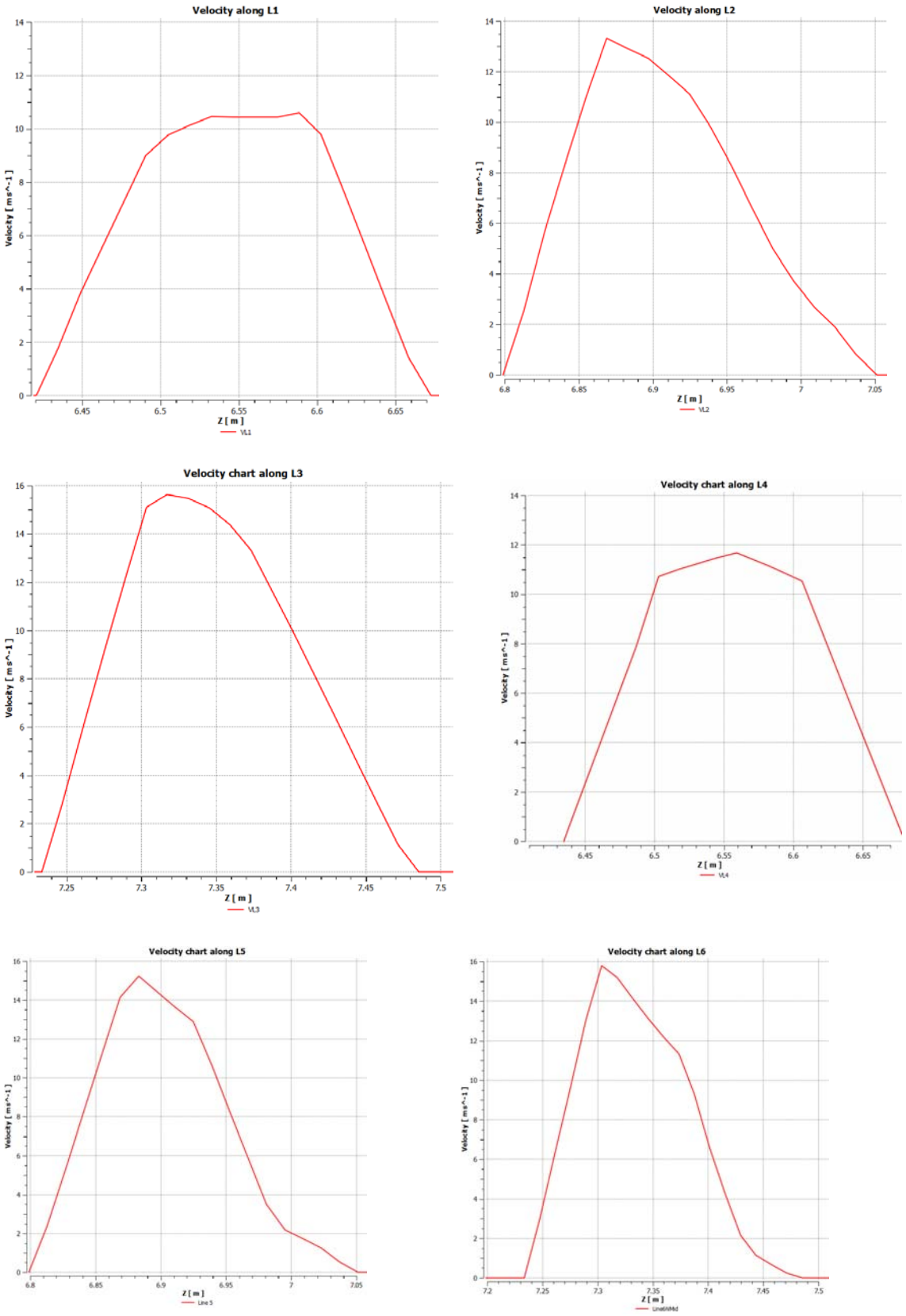


Fig. E. 71. Velocity changes between panels, all lines separated.

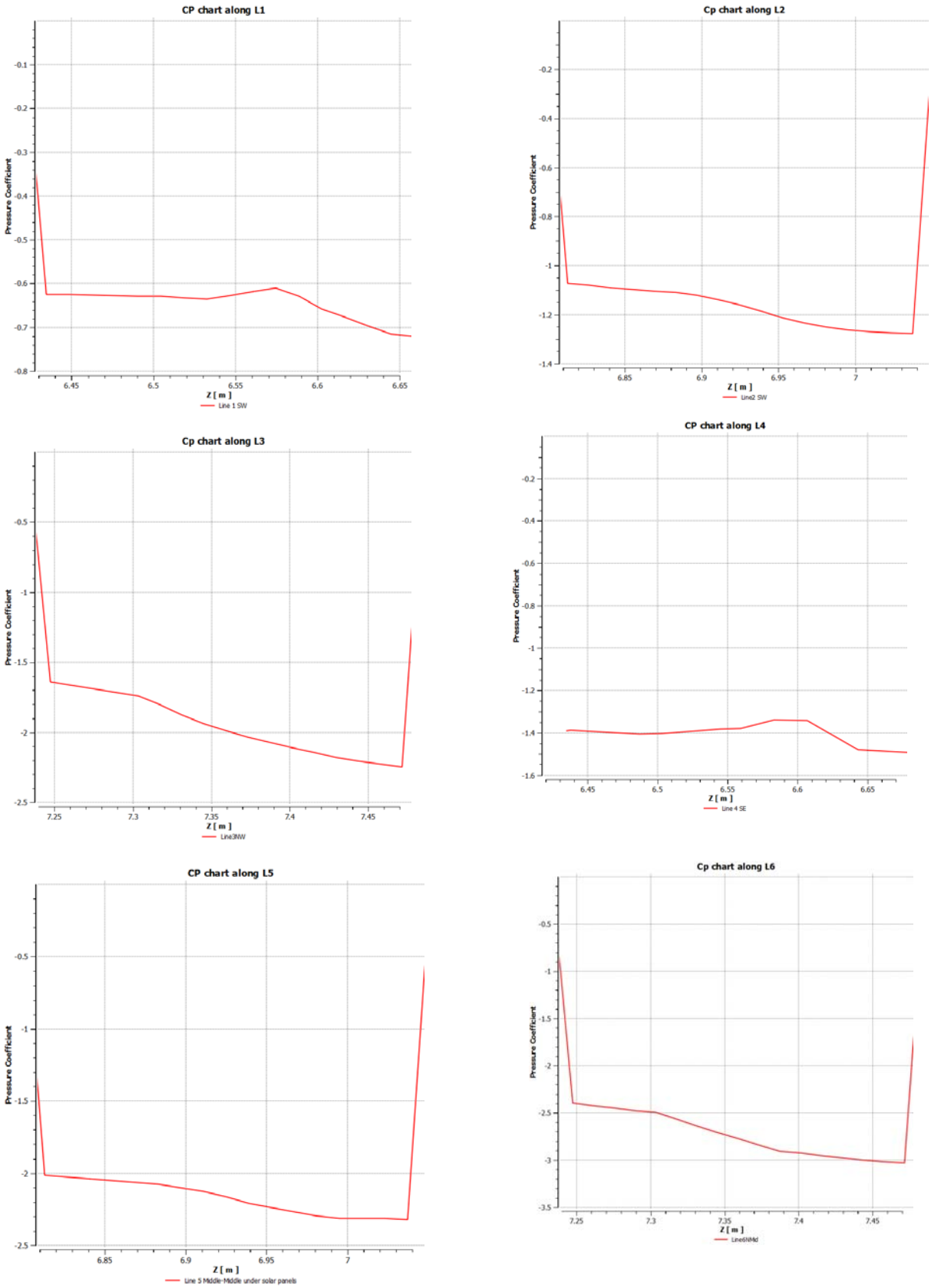


Fig. E. 72. Cp changes between panels, all lines separated.

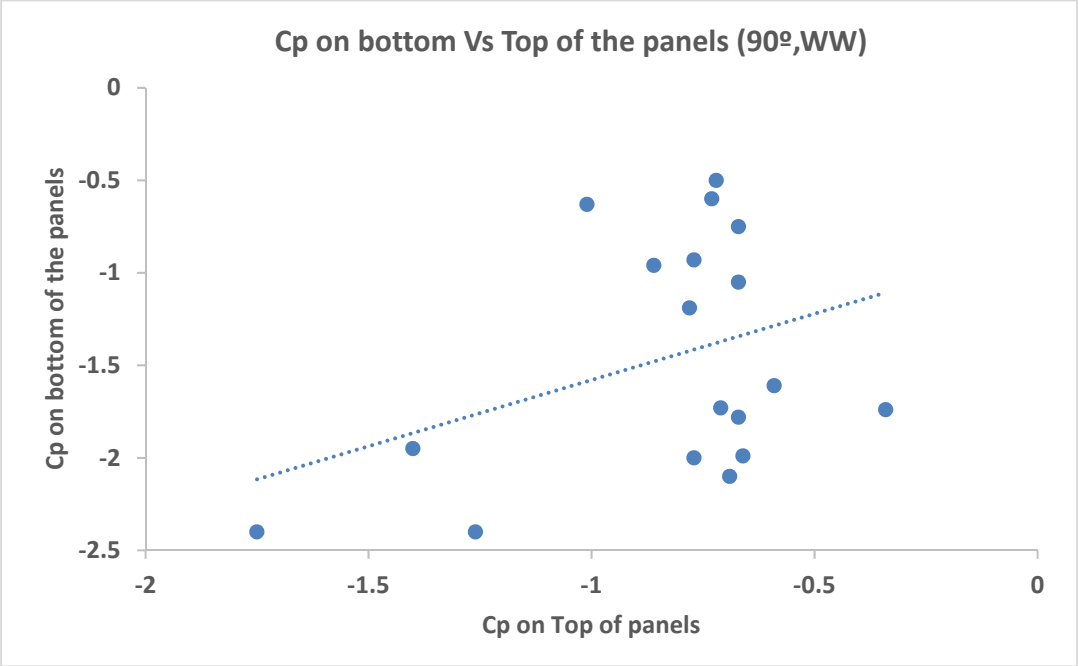


Fig. E. 73. Correlation between Cp on top and bottom of panels surfaces, WW, WD 90º

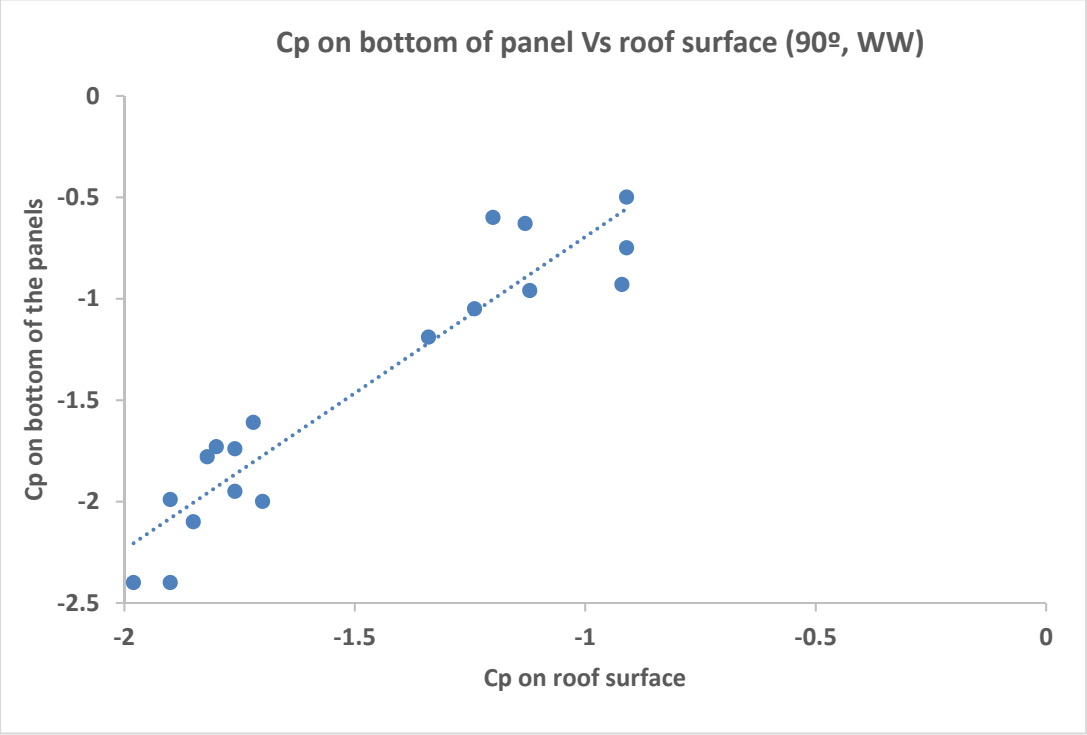


Fig. E. 74. Correlation between Cp on bottom of panels and roof surfaces, WW, WD 90º

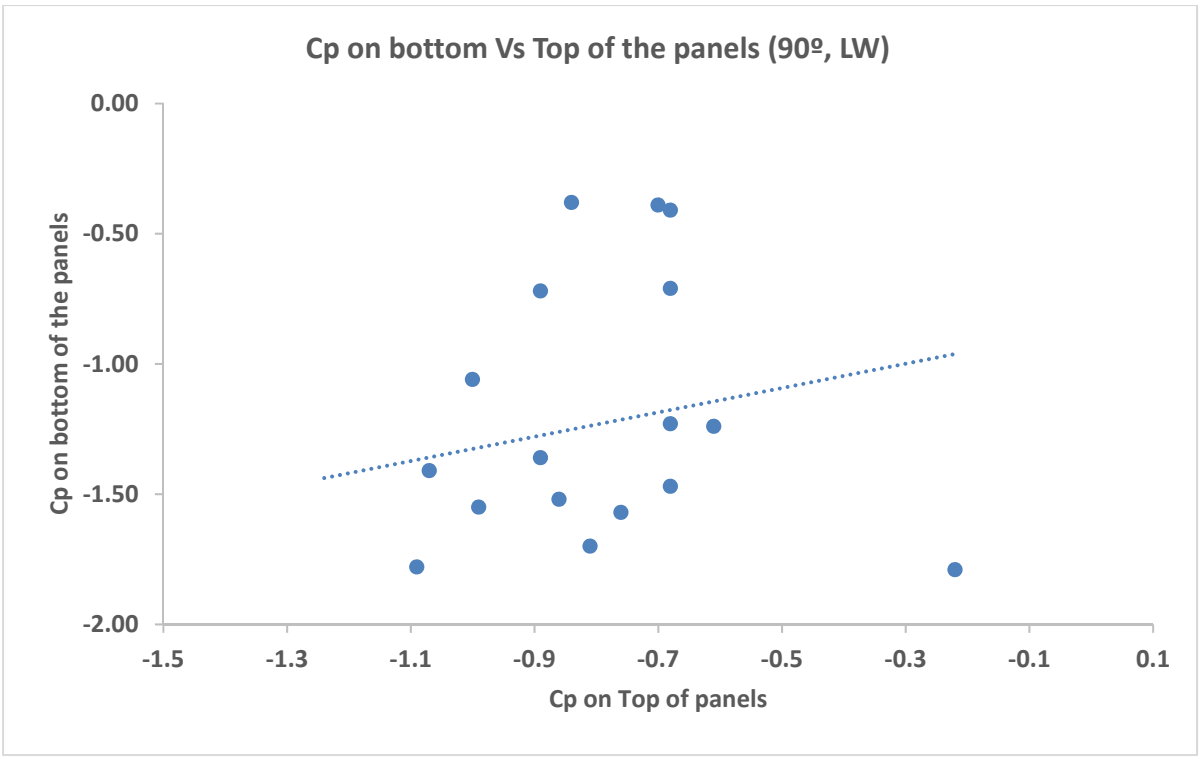


Fig. E. 75. Correlation between Cp on top and bottom of panels surfaces, LW, WD 90º

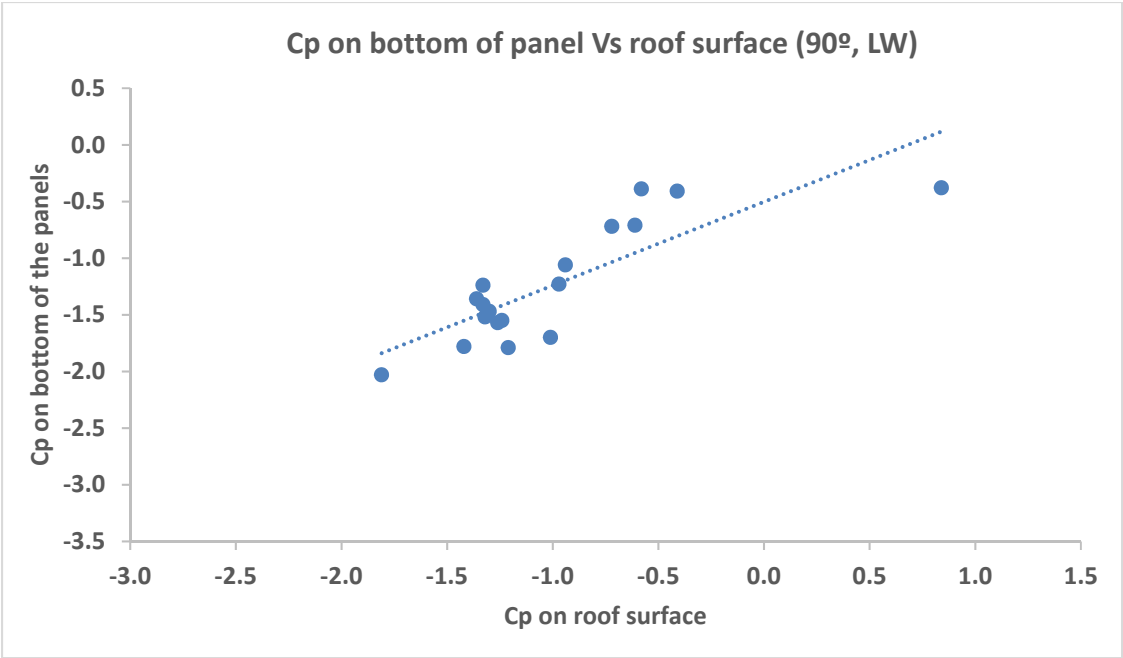


Fig. E. 76. Correlation between Cp on bottom of panels and roof surfaces, LW, WD 90º

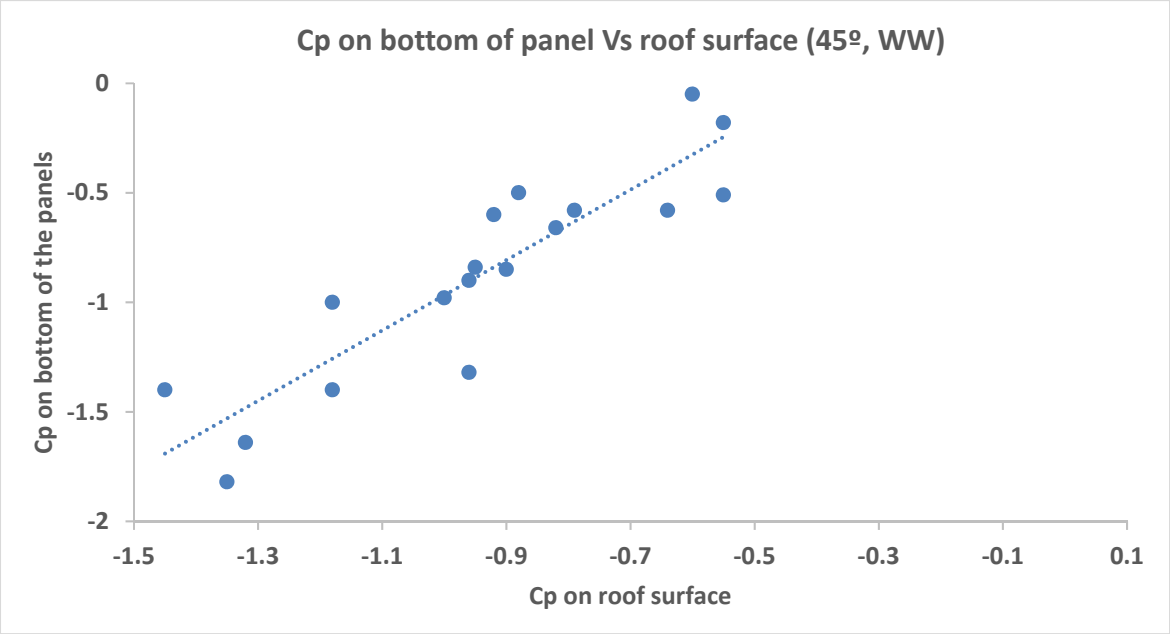


Fig. E. 77. Correlation between Cp on bottom of panels and roof surfaces, WW, WD 45º

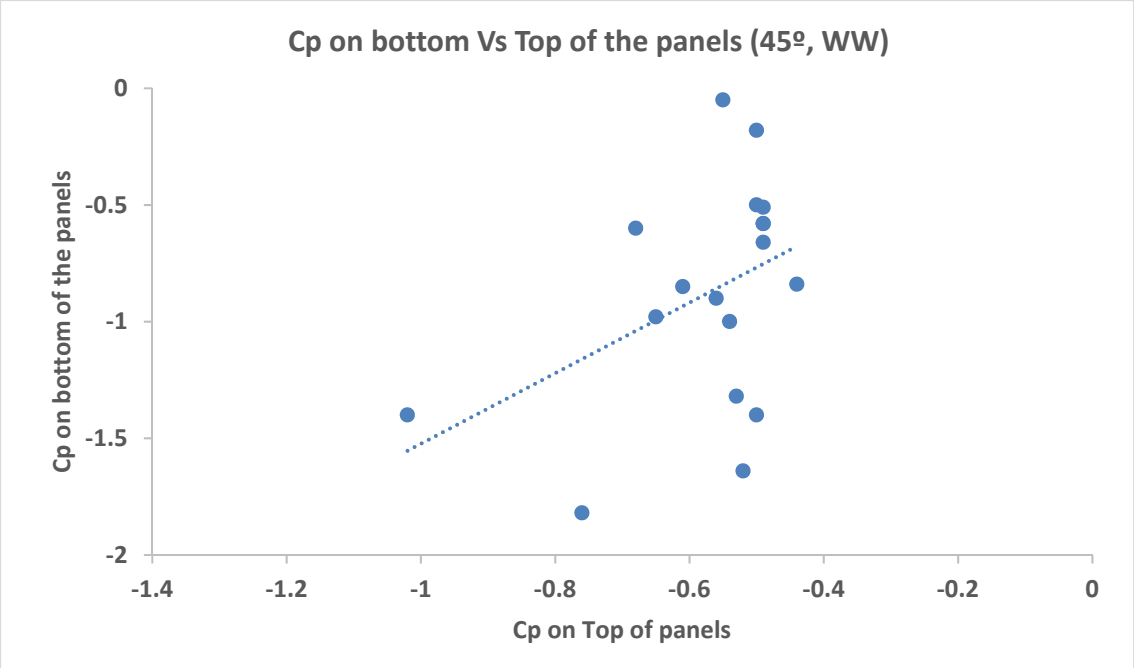


Fig. E. 78. Correlation between Cp on top and bottom of panels surfaces, WW, WD 45º

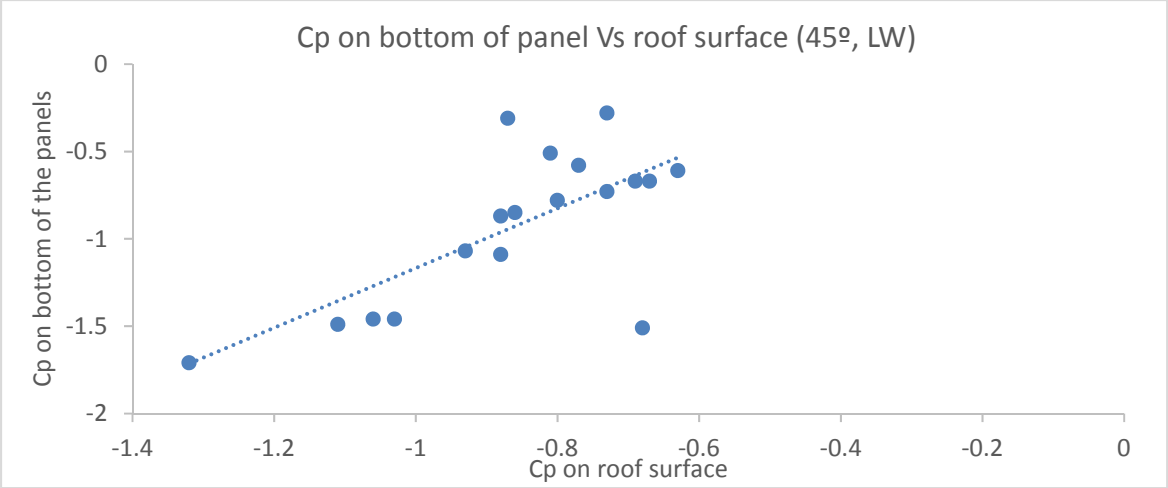


Fig. E. 79. Correlation between Cp on bottom of panels and roof surfaces, LW, WD 45º

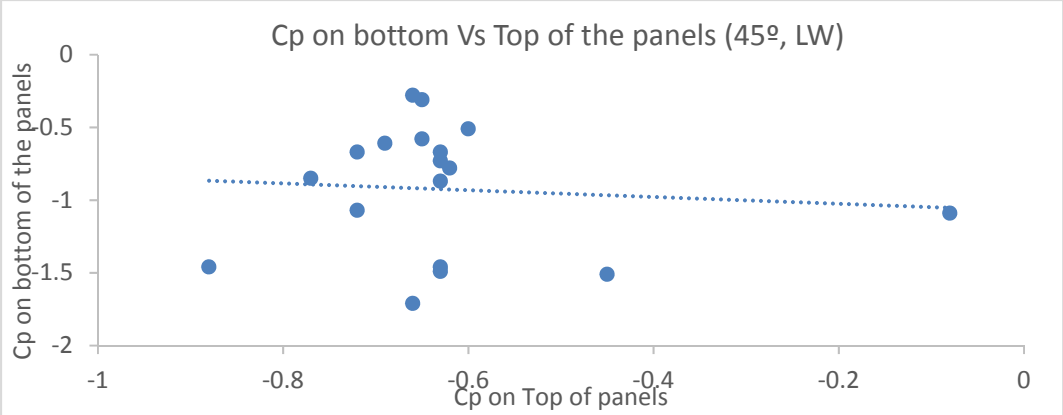


Fig. E. 80. Correlation between Cp on top and bottom of panels surfaces, LW, WD 45º

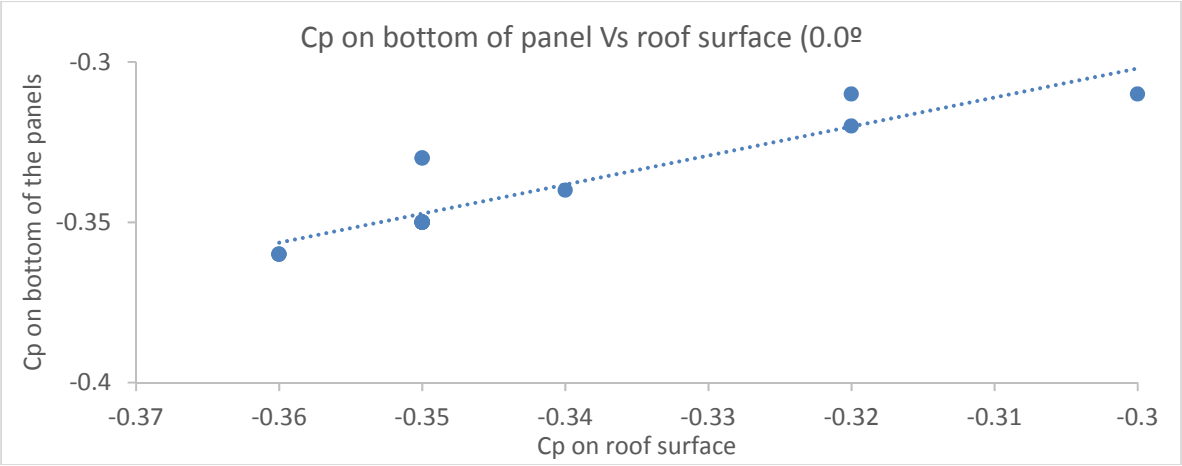


Fig. E. 81. Correlation between Cp on bottom of panels and roof surfaces, WD 0º

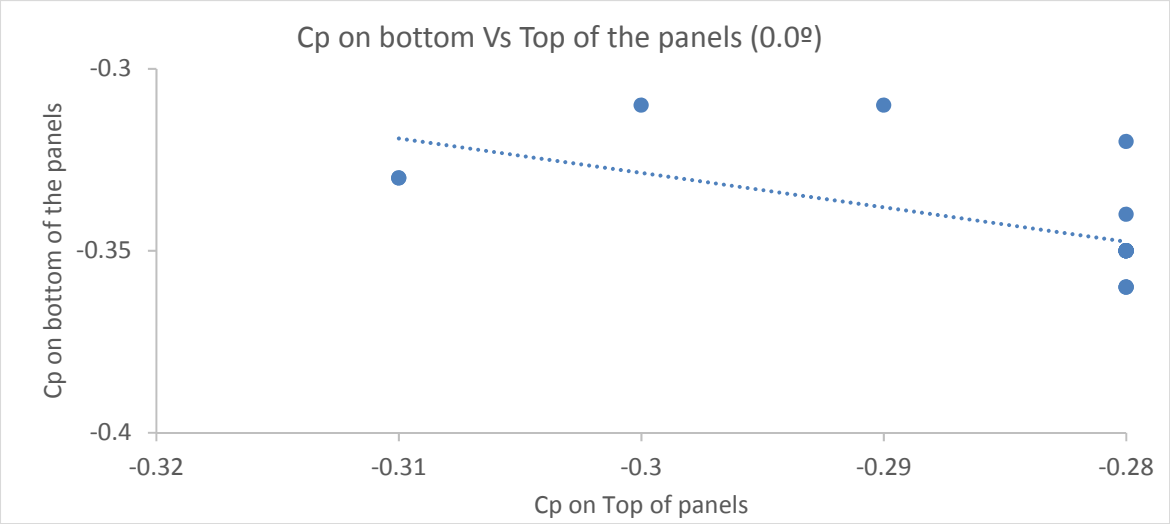


Fig. E. 82. Correlation between Cp on top and bottom of panels surfaces, WD 0º

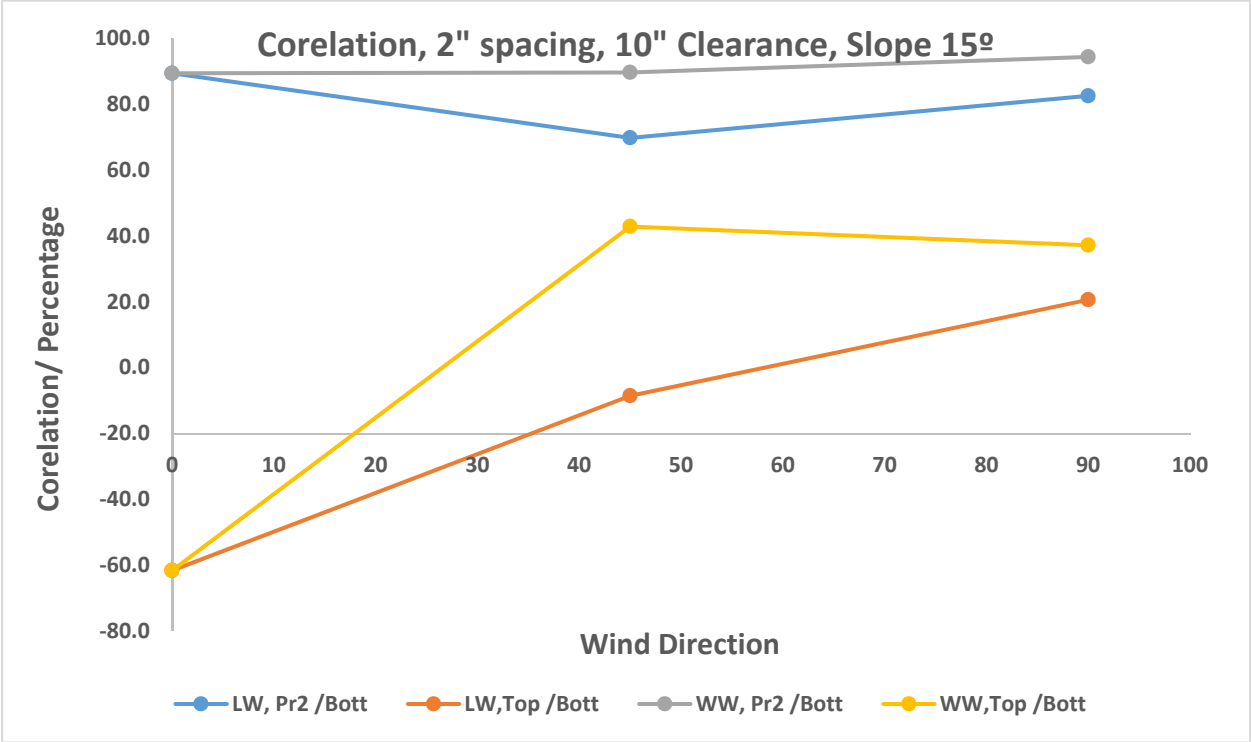


Fig. E. 83. Correlation between Cp on top, bottom of panels and roof surface, with wind directions.

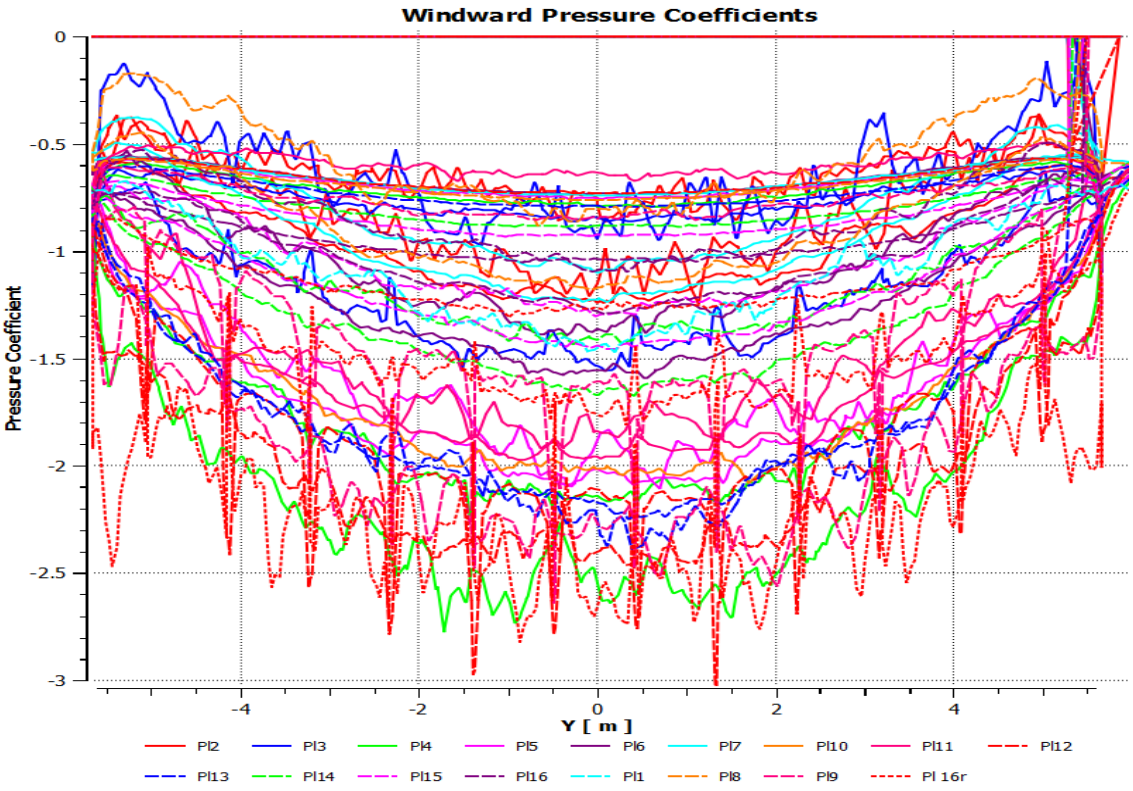


Fig. E. 84. All Cp charts, WW, WD 90º

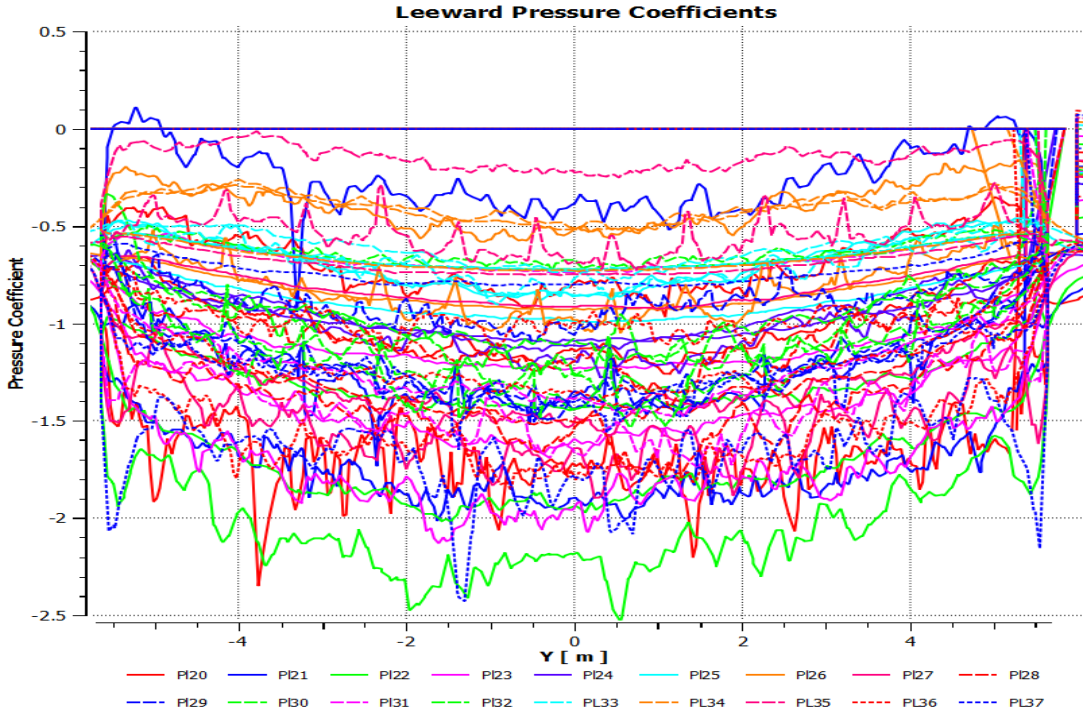


Fig. E. 85. All Cp charts, LW, WD 90º

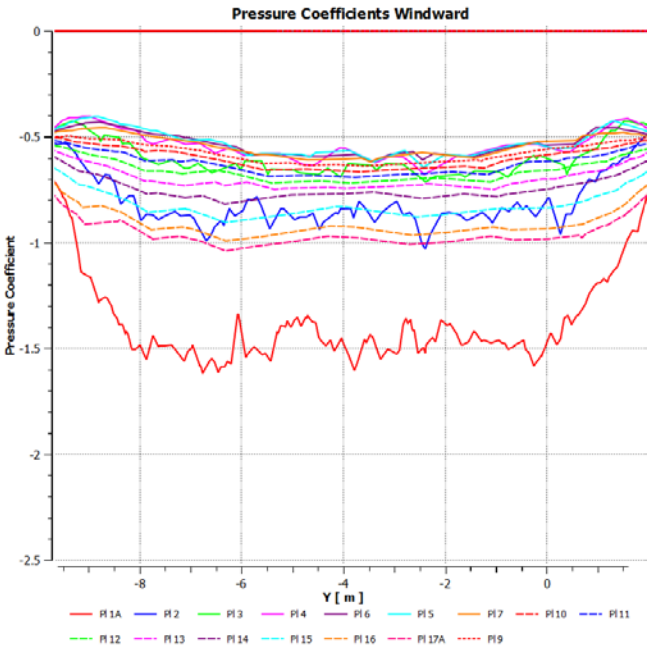


Fig. E. 86. All Cp charts, WW, WD 90º Bare Roof, S15º

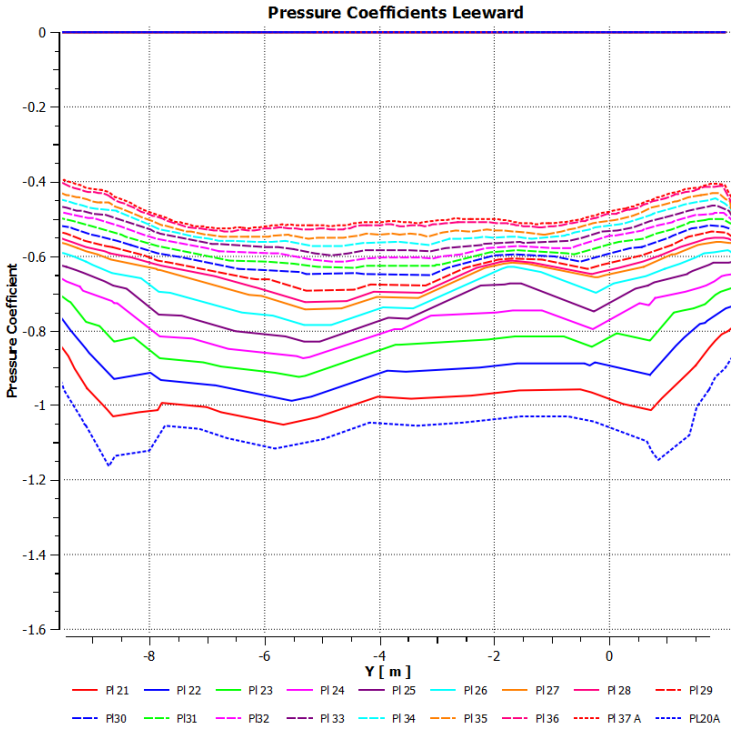


Fig. E. 87. All Cp charts, LW, WD 90º Bare Roof, S15º

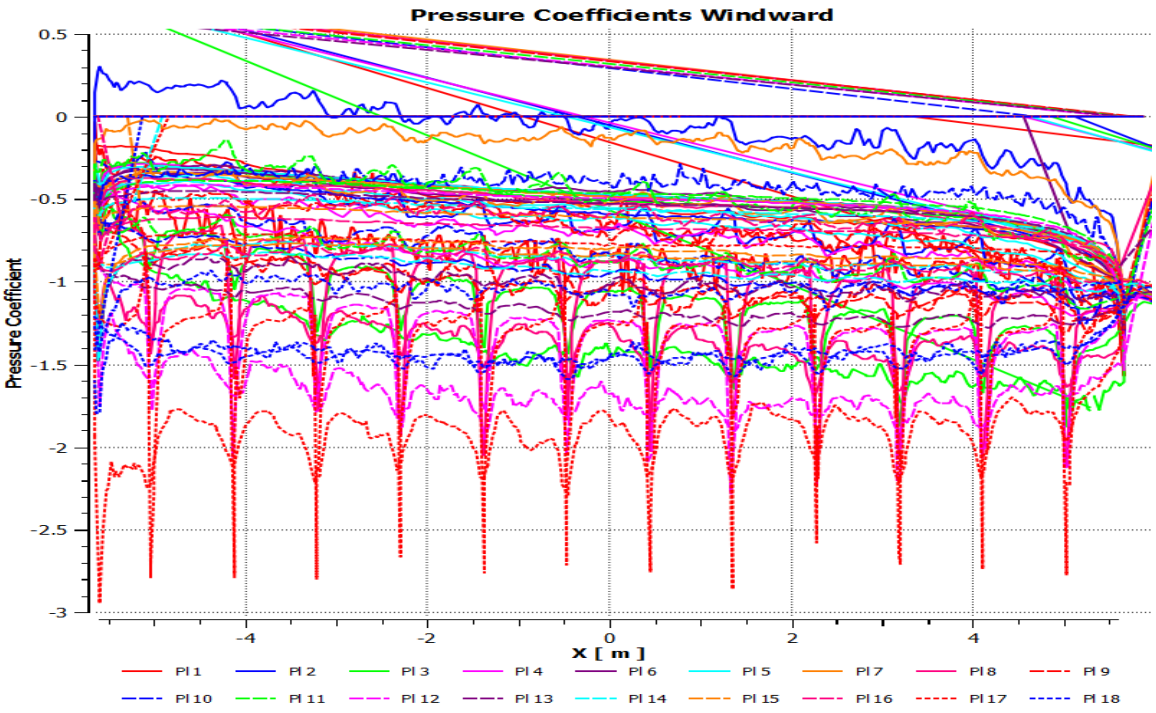


Fig. E. 88. All Cp charts, WW, WD 45º

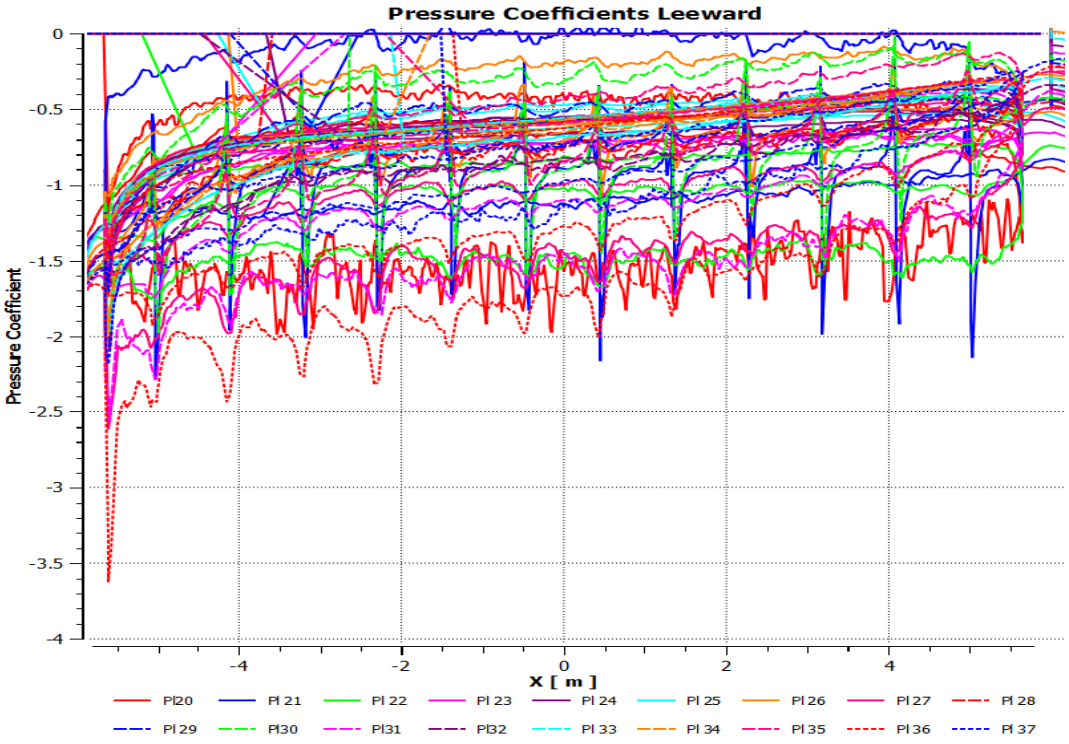


Fig. E. 89. All Cp charts, LW, WD 45º

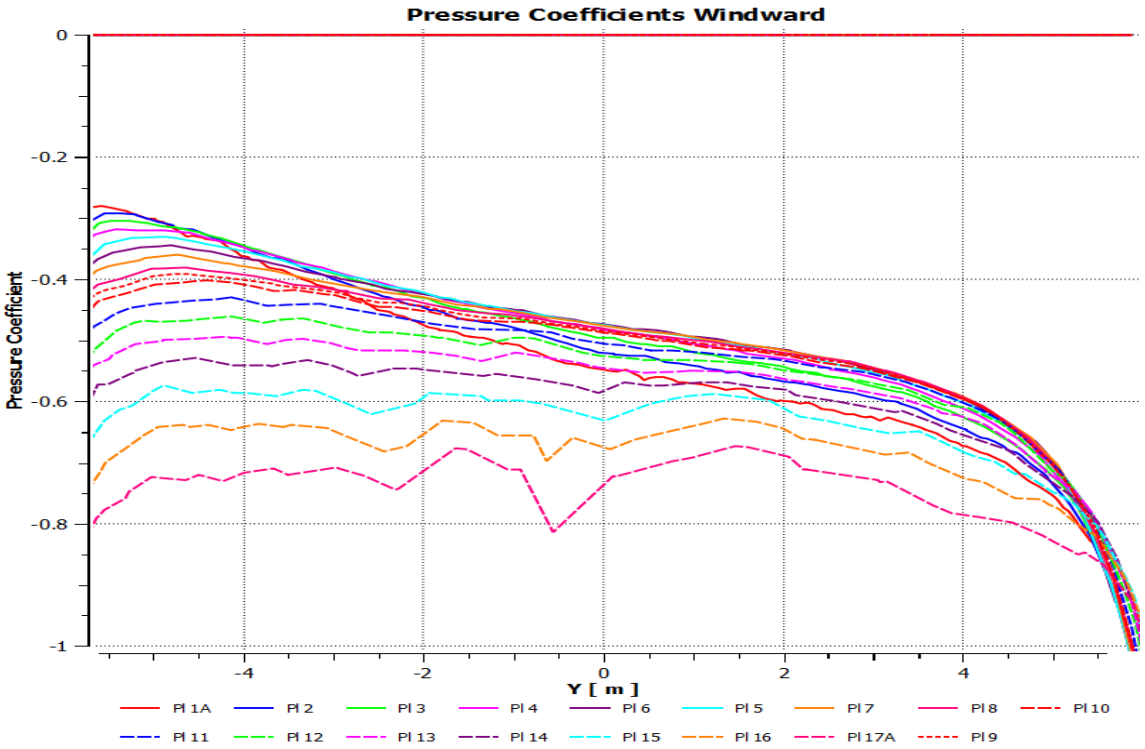


Fig. E. 90. All Cp charts, WW, WD 45º Bare Roof, S15º

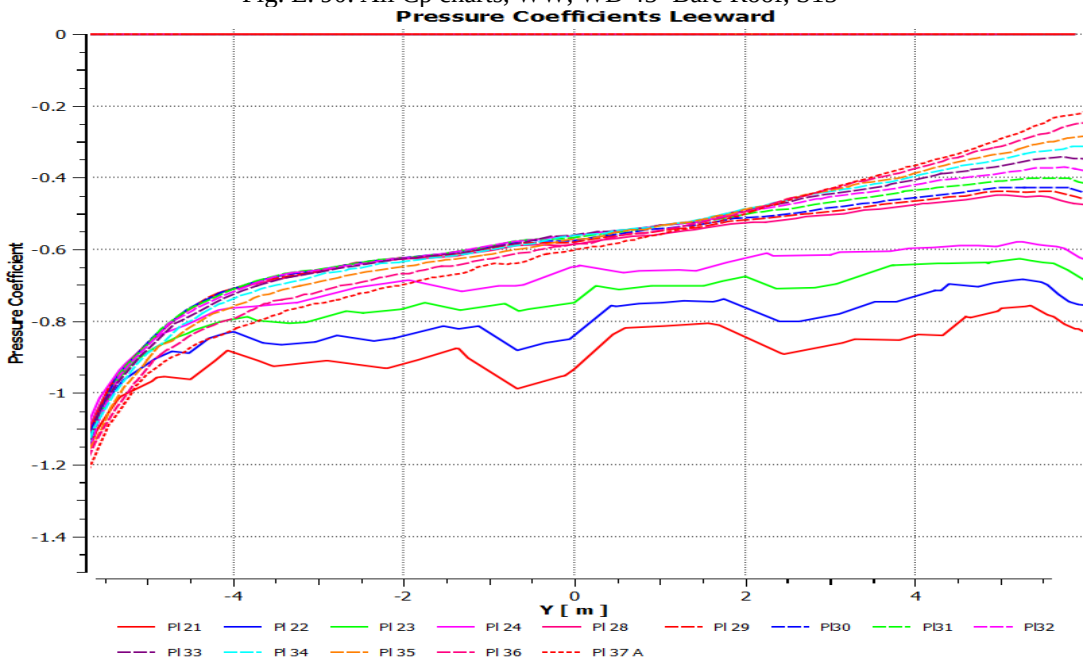


Fig. E. 91. All Cp charts, LW, WD 45º Bare Roof, S15º

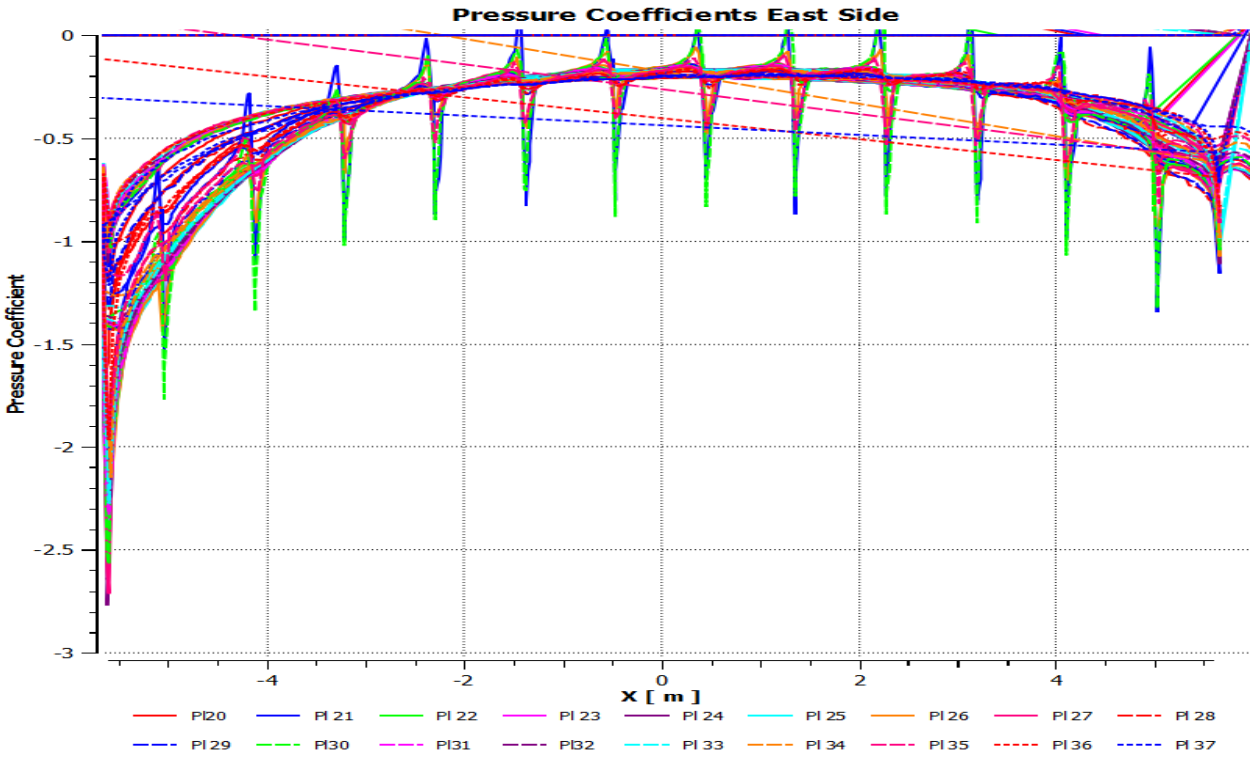


Fig. E. 92. All Cp charts, WD 0º

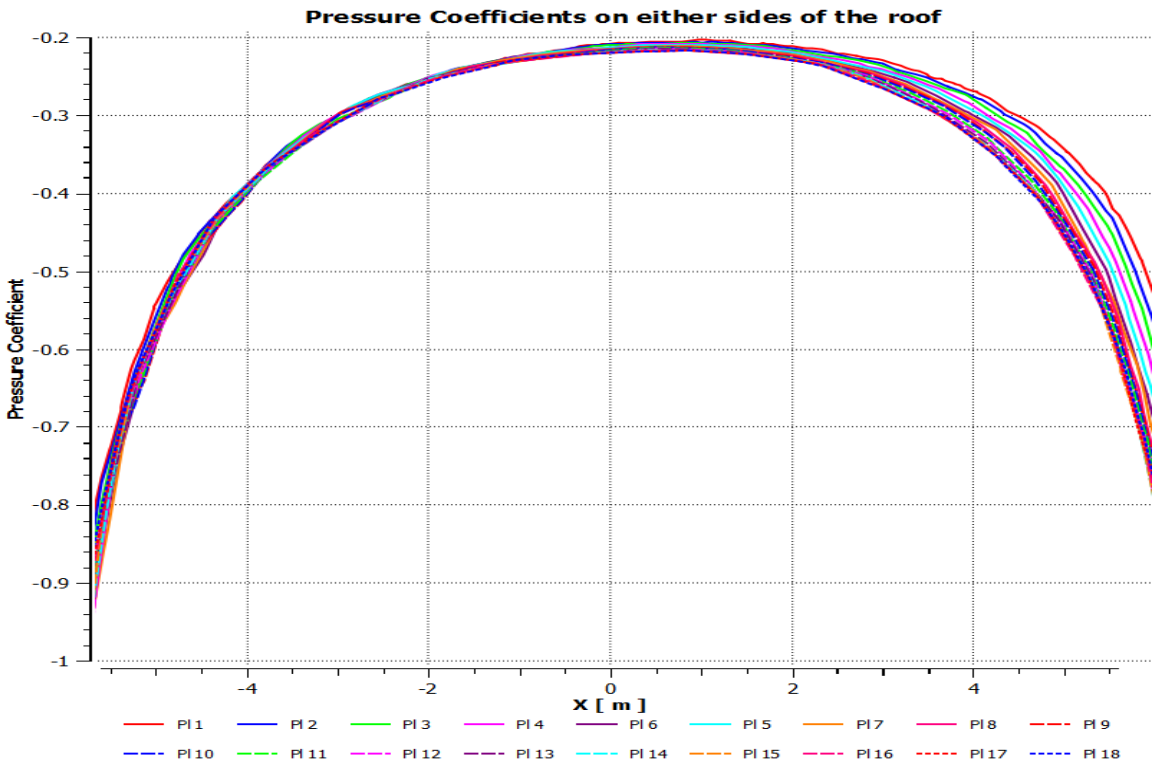


Fig. E. 93. All Cp charts, WD 0º Bare Roof, S15º

1.1.5. Integration of Cp on The Three Surfaces and the Resultant of CP on Roof Mounted Solar Panels in Comparison with Bare Roof, S2"C10"

Tabulated results of the integration,

Table E. 1. Cp on bare roof Vs. roof under solar panels and solar panel surfaces, Slope 15º, 45º, windward

Polylines	Cp (SP)	Pr2	Cp Bott	Diff	Ttl Cp	Ttl/Brf
Pl1A	-0.49	-0.79	-0.58	0.09	-0.7	1.32
Pl2	-0.55	-0.6	-0.05	-0.50	-1.1	2.16
Pl3	-0.5	-1.18	-1.4	0.90	-0.28	0.55
Pl4	-0.49	-0.82	-0.66	0.17	-0.65	1.27
Pl5	-0.49	-0.64	-0.58	0.09	-0.55	1.08
Pl6	-0.49	-0.55	-0.51	0.02	-0.53	1.06
Pl7	-0.5	-0.55	-0.18	-0.32	-0.87	1.74
Pl8	-0.53	-0.96	-1.32	0.79	-0.17	0.34
Pl9	-0.65	-1.00	-0.98	0.33	-0.67	1.31
Pl10	-0.44	-0.95	-0.84	0.40	-0.55	1.08
Pl11	-0.5	-0.88	-0.50	0.00	-0.88	1.69
Pl12	-0.52	-1.32	-1.64	1.12	-0.2	0.37
Pl13	-0.54	-1.18	-1.00	0.46	-0.72	1.29
Pl14	-0.56	-0.96	-0.90	0.34	-0.62	1.05
Pl15	-0.61	-0.90	-0.85	0.24	-0.66	1.08
Pl16	-0.68	-0.92	-0.60	-0.08	-1	1.54
Pl17	-0.76	-1.35	-1.82	1.06	-0.29	0.41
Pl18	-1.02	-1.45	-1.40	0.38	-1.07	1.43
Cp	-0.57	-0.94	-0.88	0.31	-0.64	1.15
SDT	0.14	0.27	0.48	0.44	0.28	0.50
Cov	0.24	0.29	0.55	1.45	0.44	0.43

Table E. 2. Cp on bare roof Vs Top of Panels, Slope 15º, 45º, WW

Polylines	Cp Bare roof	Cp (SP)	Cp (SP/BRf)
Pl1A	-0.53	-0.49	0.92
Pl2	-0.51	-0.55	1.08
Pl3	-0.51	-0.5	0.98
Pl4	-0.51	-0.49	0.96
Pl5	-0.51	-0.49	0.96
Pl6	-0.5	-0.49	0.98
Pl7	-0.5	-0.5	1.00
Pl8	-0.5	-0.53	1.06
Pl9	-0.51	-0.65	1.27
Pl10	-0.51	-0.44	0.86
Pl11	-0.52	-0.5	0.96
Pl12	-0.54	-0.52	0.96

Pl13	-0.56	-0.54	0.96
Pl14	-0.59	-0.56	0.95
Pl15	-0.61	-0.61	1.00
Pl16	-0.65	-0.68	1.05
Pl17	-0.7	-0.76	1.09
Pl18	-0.75	-1.02	1.36
Cp	-0.56	-0.57	1.03
SDT	0.08	0.14	0.12
Cov	0.13	0.24	0.12

Table E. 3. Cp bare roof Vs. roof under solar panels and solar panel surfaces, Slope 15º, WD 45º, LW

Polylines	Cp (SP)	Pr2	Cp Bott	Diff	Ttl Cp	Ttl/Brf
Pl20a	-0.45	-0.68	-1.51	1.06	0.38	-0.43
Pl21	-0.08	-0.88	-1.09	1.01	0.13	-0.16
Pl22	-0.88	-1.06	-1.46	0.58	-0.48	0.65
Pl23	-0.77	-0.86	-0.85	0.08	-0.78	1.15
Pl24	-0.72	-0.67	-0.67	-0.05	-0.72	1.13
Pl25	-0.69	-0.63	-0.61	-0.08	-0.71	1.15
Pl26	-0.66	-0.73	-0.28	-0.38	-1.11	1.82
Pl27	-0.63	-1.03	-1.46	0.83	-0.2	0.33
Pl28	-0.62	-0.80	-0.78	0.16	-0.64	1.08
Pl29	-0.65	-0.77	-0.58	-0.07	-0.84	1.42
Pl30	-0.65	-0.87	-0.31	-0.34	-1.21	2.07
Pl31	-0.63	-1.11	-1.49	0.86	-0.25	0.43
Pl32	-0.63	-0.88	-0.87	0.24	-0.64	1.11
Pl33	-0.63	-0.73	-0.73	0.10	-0.63	1.11
Pl34	-0.63	-0.69	-0.67	0.04	-0.65	1.16
Pl35	-0.6	-0.81	-0.51	-0.09	-0.9	1.64
Pl36	-0.66	-1.32	-1.71	1.05	-0.27	0.50
Pl37	-0.72	-0.93	-1.07	0.35	-0.58	1.04
Cp	-0.63	-0.86	-0.93	0.30	-0.56	0.95
SDT	0.16	0.18	0.44	0.48	0.40	0.64
Cov	0.26	0.21	0.47	1.62	0.71	0.67

Table E. 4. Cp bare roof Vs. Top of Solar Panels, Slope 15º, WD 45º, LW

Polylines	Bare Roof	Cp (SP)	Cp (SP/BRf)
Pl20	-0.89	-0.45	0.51
Pl21	-0.81	-0.08	0.10
Pl22	-0.74	-0.88	1.19
Pl23	-0.68	-0.77	1.13
Pl24	-0.64	-0.72	1.13
Pl25	-0.62	-0.69	1.11
Pl26	-0.61	-0.66	1.08
Pl27	-0.60	-0.63	1.05
Pl28	-0.60	-0.62	1.04
Pl29	-0.59	-0.65	1.10

Pl30	-0.59	-0.65	1.11
Pl31	-0.58	-0.63	1.09
Pl32	-0.58	-0.63	1.10
Pl33	-0.57	-0.63	1.11
Pl34	-0.56	-0.63	1.13
Pl35	-0.55	-0.6	1.09
Pl36	-0.54	-0.66	1.22
Pl37	-0.56	-0.72	1.29
Cp	-0.63	-0.63	1.00
SDT	0.10	0.16	0.28
Cov	0.15	0.26	0.28

Table E. 5. Cp on bare roof Vs. roof under solar panels and solar panels surfaces , Slope 15º, WD 90º, WW

Polylines	Cp (SP)	Pr2	Cp Bott	Diff	Ttl Cp	Ttl/Brf
Pl1A	-0.77	-0.92	-0.93	0.16	-0.76	0.55
Pl2	-0.73	-1.2	-0.6	-0.13	-1.33	1.62
Pl3	-0.69	-1.85	-2.1	1.41	-0.44	0.72
Pl4	-0.67	-1.82	-1.78	1.11	-0.71	1.31
Pl5	-0.67	-1.24	-1.05	0.38	-0.86	1.62
Pl6	-0.67	-0.91	-0.75	0.08	-0.83	1.57
Pl7	-0.72	-0.91	-0.50	-0.22	-1.13	1.98
Pl8	-0.77	-1.70	-2.00	1.23	-0.47	0.87
Pl9	-1.4	-1.76	-1.95	0.55	-1.21	2.12
Pl10	-0.34	-1.76	-1.74	1.40	-0.36	0.60
Pl11	-0.59	-1.72	-1.61	1.02	-0.7	1.11
Pl12	-0.66	-1.90	-1.99	1.33	-0.57	0.86
Pl13	-0.71	-1.80	-1.73	1.02	-0.78	1.10
Pl14	-0.78	-1.34	-1.19	0.41	-0.93	1.21
Pl15	-0.86	-1.12	-0.96	0.10	-1.02	1.21
Pl16	-1.01	-1.13	-0.63	-0.38	-1.51	2.29
Pl17	-1.26	-1.90	-2.40	1.14	-0.76	0.83
Pl18	-1.75	-1.98	-2.40	0.65	-1.33	1.73
Cp	-0.84	-1.50	-1.46	0.63	-0.87	1.21
SDT	0.33	0.39	0.64	0.60	0.33	0.52
Cov	0.40	0.26	0.44	0.96	0.38	0.43

Table E. 6. Cp on bare roof Vs. Top of Panels, Slope 15º, 90º, WW

Polylines	Cp Bare roof	Cp (SP)	Cp (SP/BRf)
Pl1A	-1.38	-0.77	0.56
Pl2	-0.82	-0.73	0.89

Pl3	-0.61	-0.69	1.13
Pl4	-0.54	-0.67	1.24
Pl5	-0.53	-0.67	1.26
Pl6	-0.53	-0.67	1.26
Pl7	-0.57	-0.72	1.26
Pl8	-0.54	-0.77	1.43
Pl9	-0.57	-1.4	2.46
Pl10	-0.60	-0.34	0.57
Pl11	-0.63	-0.59	0.94
Pl12	-0.66	-0.66	1.00
Pl13	-0.71	-0.71	1.00
Pl14	-0.77	-0.78	1.01
Pl15	-0.84	-0.86	1.02
Pl16	-0.80	-1.01	1.26
Pl17	-0.92	-1.26	1.37
Pl18	-0.96	-1.75	1.82
Cp	-0.72	-0.84	1.16
SDT	0.22	0.33	0.43
Cov	0.30	0.40	0.37

Table E. 7. Cp on bare roof Vs. roof under solar panels and solar panels surfaces, Slope 15º, WD 90º, LW

Polylines	Cp (SP)	Pr2	Cp Bott	Diff	Ttl Cp	Ttl/Brf
Pl20	-0.81	-1.01	-1.70	0.89	-0.12	0.11
Pl21	-0.22	-1.21	-1.79	1.57	0.36	-0.37
Pl22	-1.24	-1.81	-2.03	0.79	-1.02	1.13
Pl23	-1.09	-1.42	-1.78	0.69	-0.73	0.86
Pl24	-1	-0.94	-1.06	0.06	-0.88	1.14
Pl25	-0.89	-0.72	-0.72	-0.17	-0.89	1.24
Pl26	-0.84	0.84	-0.38	-0.46	0.38	-0.56
Pl27	-0.86	-1.32	-1.52	0.66	-0.66	1.00
Pl28	-1.07	-1.33	-1.41	0.34	-0.99	1.55
Pl29	-0.89	-1.36	-1.36	0.47	-0.89	1.44
Pl30	-0.61	-1.33	-1.24	0.63	-0.7	1.15
Pl31	-0.68	-1.30	-1.47	0.79	-0.51	0.88
Pl32	-0.68	-0.97	-1.23	0.55	-0.42	0.75
Pl33	-0.68	-0.61	-0.71	0.03	-0.58	1.05
Pl34	-0.68	-0.41	-0.41	-0.27	-0.68	1.21
Pl27	-0.7	-0.58	-0.39	-0.31	-0.89	1.62
Pl36	-0.99	-1.24	-1.55	0.56	-0.68	1.28
Pl37	-0.76	-1.26	-1.57	0.81	-0.45	0.87
Cp	-0.83	-0.93	-1.12	0.29	-0.64	1.03
SDT	0.16	0.59	0.48	0.44	0.33	0.51
Cov	0.19	0.64	0.43	1.50	0.52	0.49

Table E. 8. Cp bare roof Vs. Top of The Panels, Slope 15º, WD 90º, LW

Polylines	Bare Roof	Cp (SP)	Cp (SP/BRf)
PL20	-1.10	-0.81	0.74
PL21	-0.98	-0.22	0.22
PL22	-0.90	-1.24	1.38
PL23	-0.85	-1.09	1.28
PL24	-0.77	-1	1.30
PL25	-0.72	-0.89	1.24
PL26	-0.68	-0.84	1.24
PL27	-0.66	-0.86	1.30
PL28	-0.64	-1.07	1.67
PL29	-0.62	-0.89	1.44
PL30	-0.61	-0.61	1.00
PL31	-0.58	-0.68	1.17
PL32	-0.56	-0.68	1.21
PL33	-0.55	-0.68	1.24
PL34	-0.53	-0.68	1.28
PL35	-0.52	-0.7	1.35
PL36	-0.49	-0.99	2.02
PL37	-0.48	-0.76	1.58
Cp	-0.68	-0.82	1.29
SDT	0.10	0.16	0.15
Cov	0.14	0.20	0.12

Table E. 9. Cp on bare roof Vs. roof under solar panels and solar panels surfaces, Slope 15º, WD 0º

Polylines	Cp (SP)	Pr2	Cp Bott	Diff	Ttl Cp	Ttl/Brf
Pl1A	-0.29	-0.3	-0.31	0.02	-0.28	0.64
Pl2	-0.28	-0.32	-0.32	0.04	-0.28	0.62
Pl3	-0.28	-0.34	-0.34	0.06	-0.28	0.61
Pl4	-0.28	-0.35	-0.35	0.07	-0.28	0.60
Pl5	-0.28	-0.35	-0.35	0.07	-0.28	0.58
Pl6	-0.28	-0.35	-0.35	0.07	-0.28	0.57
Pl7	-0.28	-0.35	-0.35	0.07	-0.28	0.57
Pl8	-0.28	-0.35	-0.35	0.07	-0.28	0.57
Pl9	-0.31	-0.35	-0.33	0.02	-0.33	0.66
Pl10	-0.31	-0.35	-0.33	0.02	-0.33	0.65
Pl11	-0.28	-0.35	-0.35	0.07	-0.28	0.55
Pl12	-0.28	-0.35	-0.35	0.07	-0.28	0.55
Pl13	-0.28	-0.36	-0.36	0.08	-0.28	0.55
Pl14	-0.28	-0.36	-0.36	0.08	-0.28	0.55

Pl15	-0.28	-0.36	-0.36	0.08	-0.28	0.54
Pl16	-0.28	-0.35	-0.35	0.07	-0.28	0.54
Pl17	-0.28	-0.35	-0.35	0.07	-0.28	0.54
Pl18	-0.3	-0.32	-0.31	0.01	-0.31	0.60
Cp	-0.29	-0.35	-0.34	0.06	-0.29	0.58
SDT	0.01	0.02	0.02	0.02	0.02	0.04
Cov	0.04	0.05	0.05	0.41	0.06	0.07

Table E. 10. Cp bare roof Vs. Top of the Panels, Slope 15º, WD 0º

	Cp Bare roof	Cp (SP)	Cp (SP/BRf)
Pl1A	-0.44	-0.29	0.66
Pl2	-0.45	-0.28	0.62
Pl3	-0.46	-0.28	0.61
Pl4	-0.47	-0.28	0.60
Pl5	-0.48	-0.28	0.58
Pl6	-0.49	-0.28	0.57
Pl7	-0.49	-0.28	0.57
Pl8	-0.49	-0.28	0.57
Pl9	-0.5	-0.31	0.62
Pl10	-0.51	-0.31	0.61
Pl11	-0.51	-0.28	0.55
Pl12	-0.51	-0.28	0.55
Pl13	-0.51	-0.28	0.55
Pl14	-0.51	-0.28	0.55
Pl15	-0.52	-0.28	0.54
Pl16	-0.52	-0.28	0.54
Pl17	-0.52	-0.28	0.54
Pl18	-0.52	-0.3	0.58
Cp	-0.49	-0.29	0.58
SDT	0.03	0.01	0.03

1.2. 8” Spacing, 3” Clearance

1.2.1. Wind direction 45º,

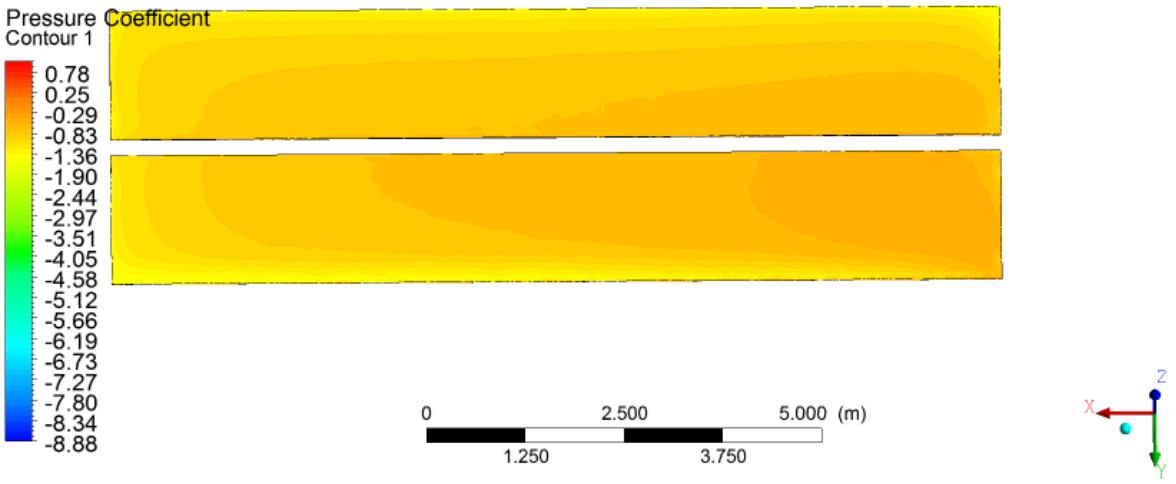


Fig. E. 94. Cp on top of the solar panels, WW, WD 45º

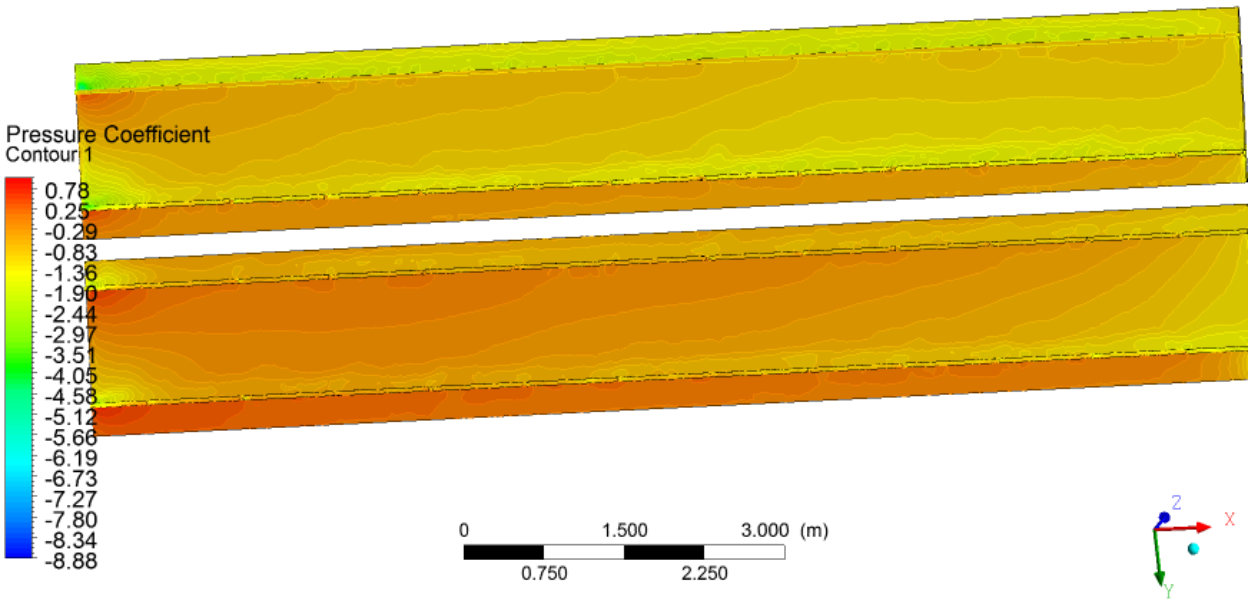


Fig. E. 95. Cp on bottom of the solar panels, WW, WD 45º

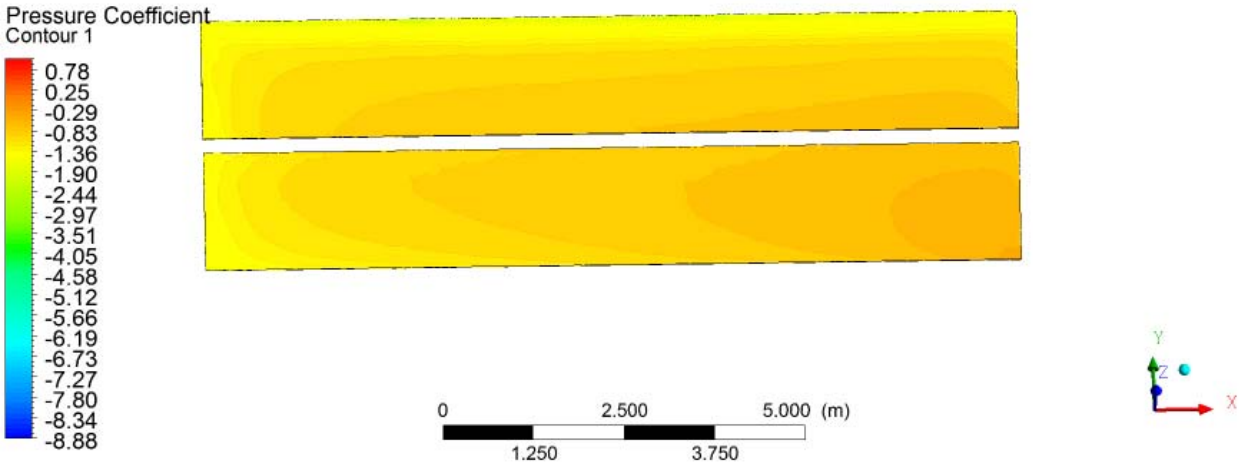


Fig. E. 96. Cp on top of the solar panels, LW, WD 45º

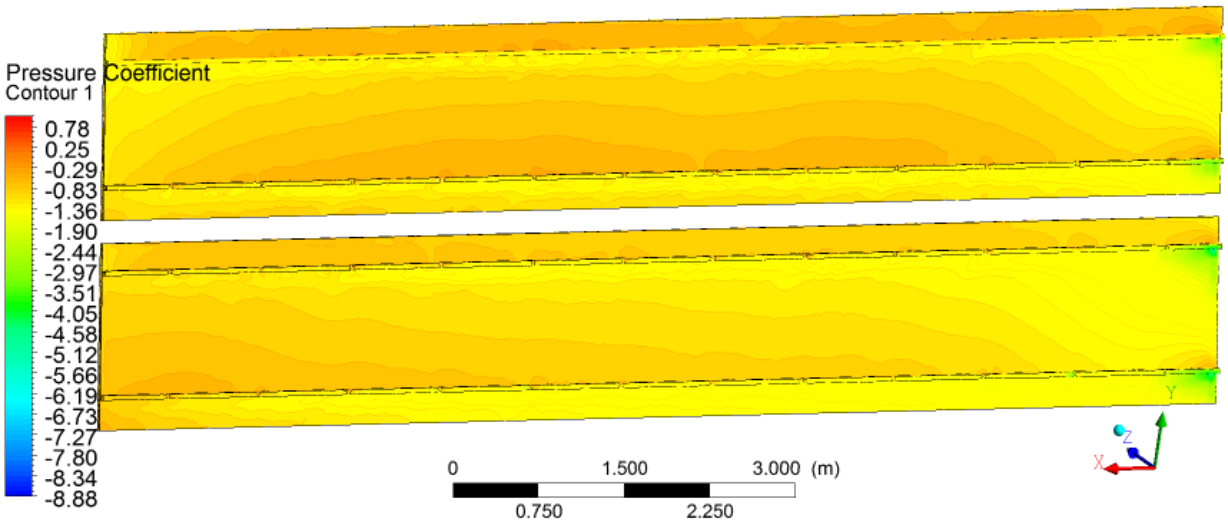


Fig. E. 97. Cp on bottom of the solar panels, LW, WD 45º

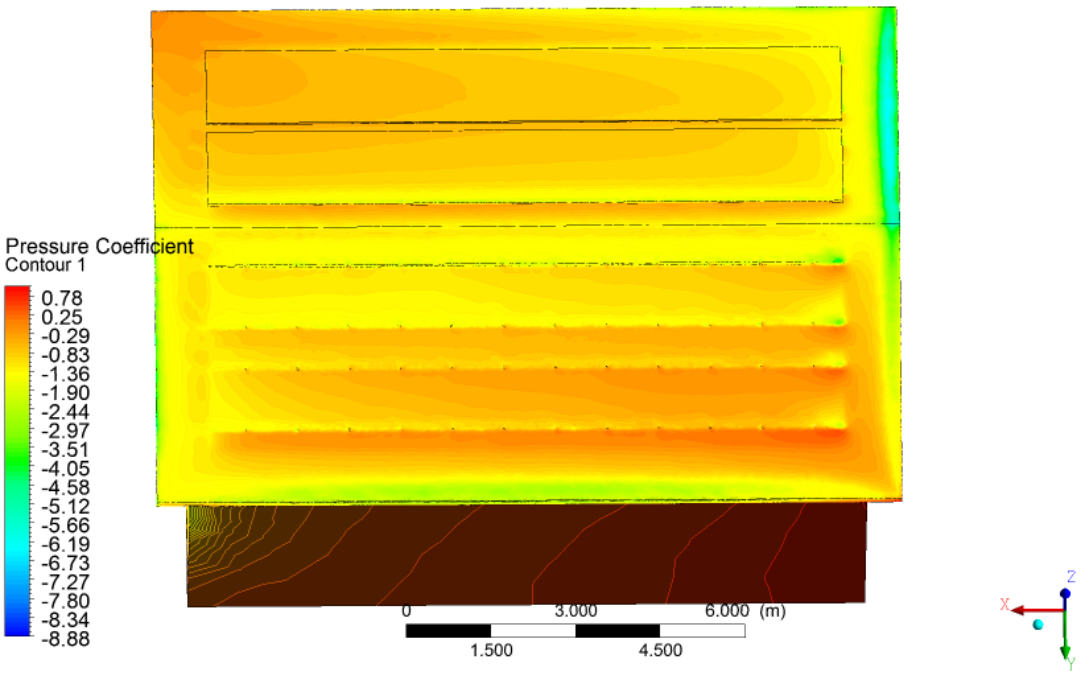


Fig. E. 98. Cp on Roof under the solar panels, cut off solar panels, WW, WD 45º

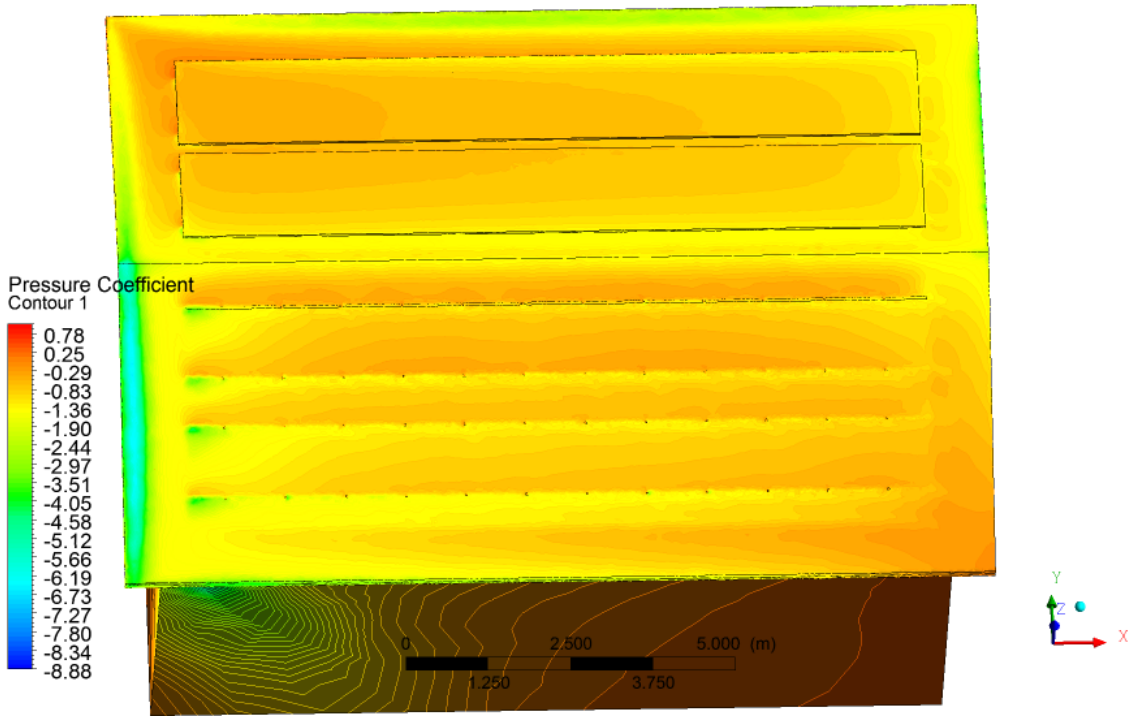


Fig. E. 99. Cp on Roof under the solar panels, cut off solar panels, LW, WD 45º

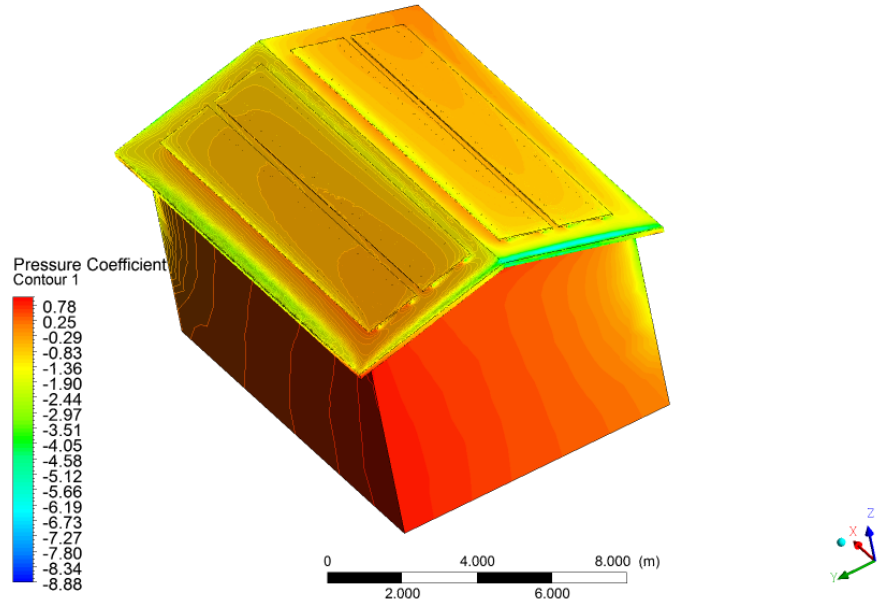


Fig. E. 100. Pressure coefficient on building surfaces with solar panels, WD 45º, WW

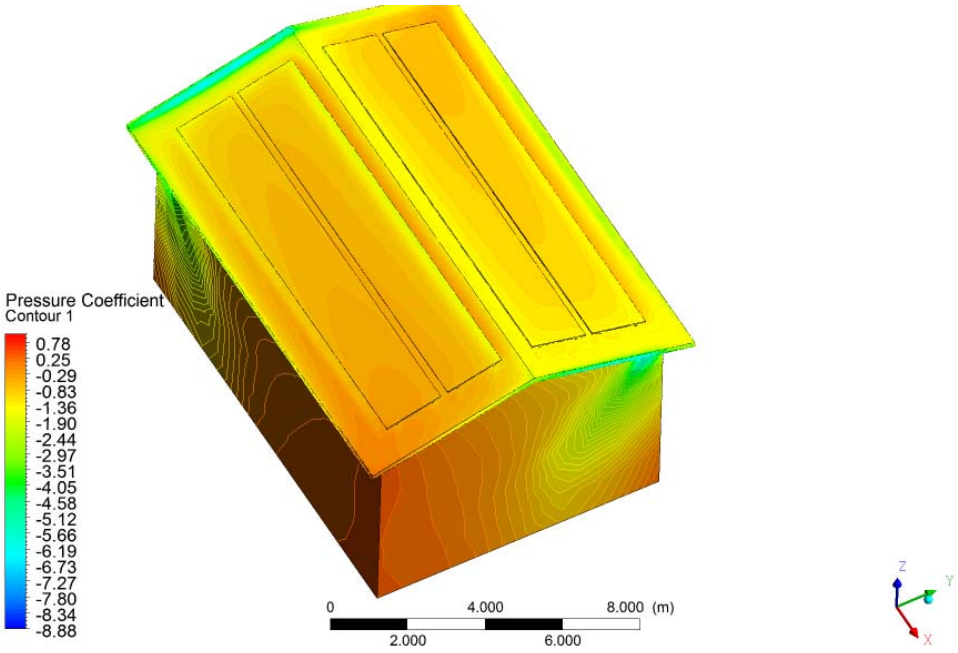


Fig. E. 101. Pressure coefficient on building surfaces with solar panels, WD 45º, LW

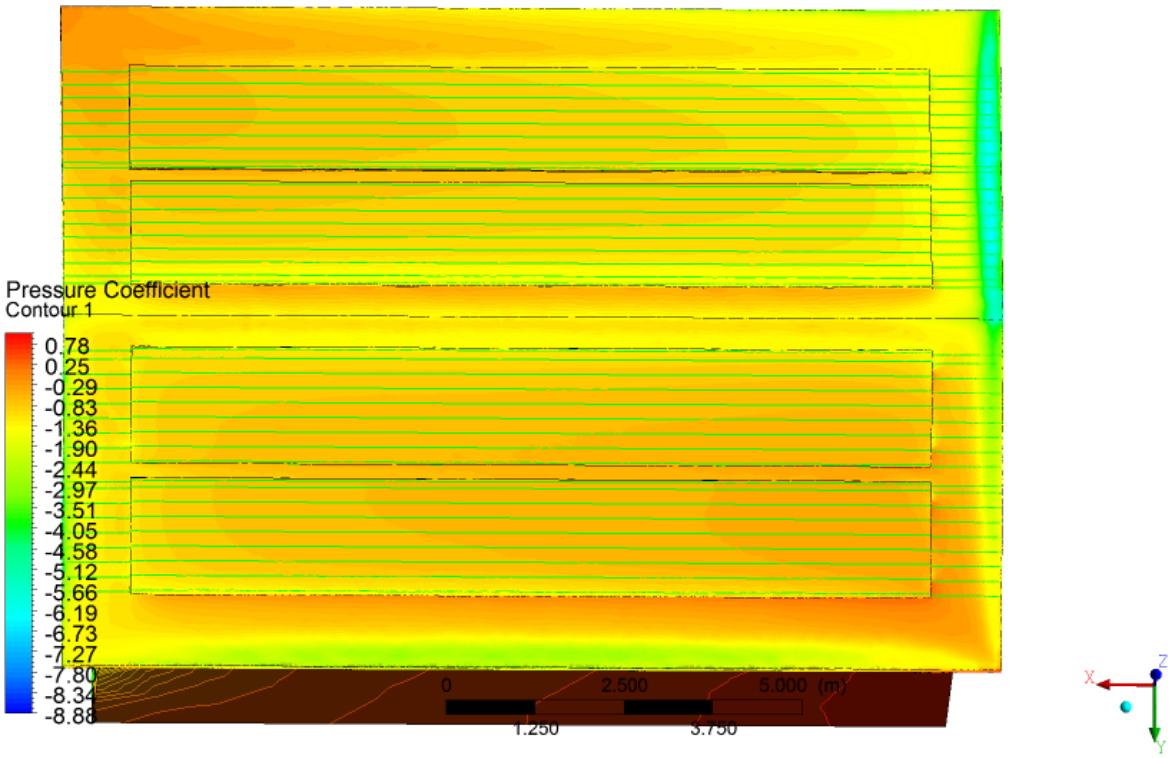


Fig. E. 102. Pressure coefficient on roof, plines, , WD 45º

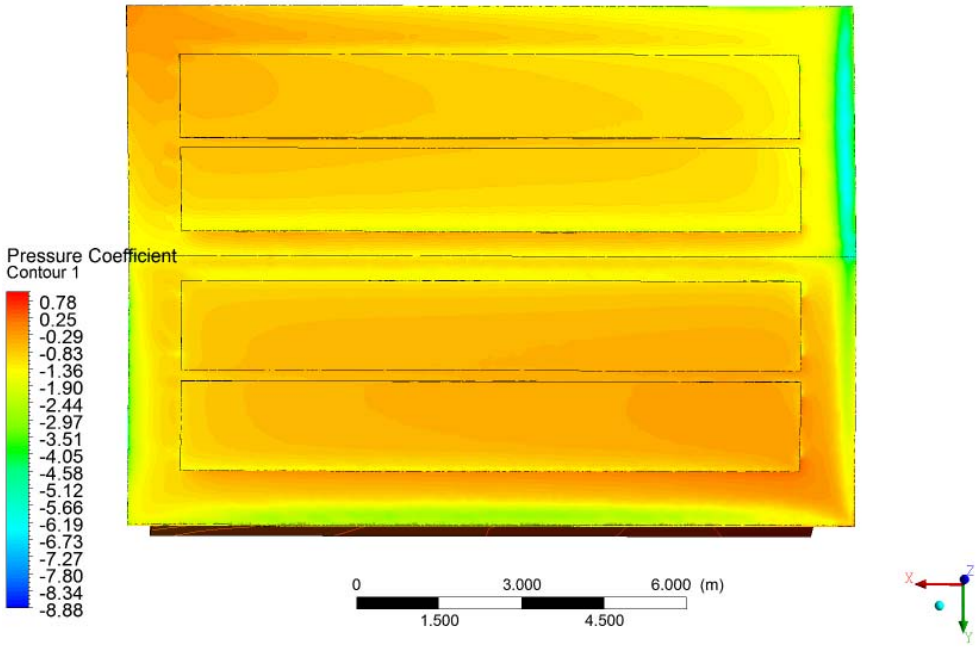


Fig. E. 103. Pressure coefficient on roof, top view, WD 45º

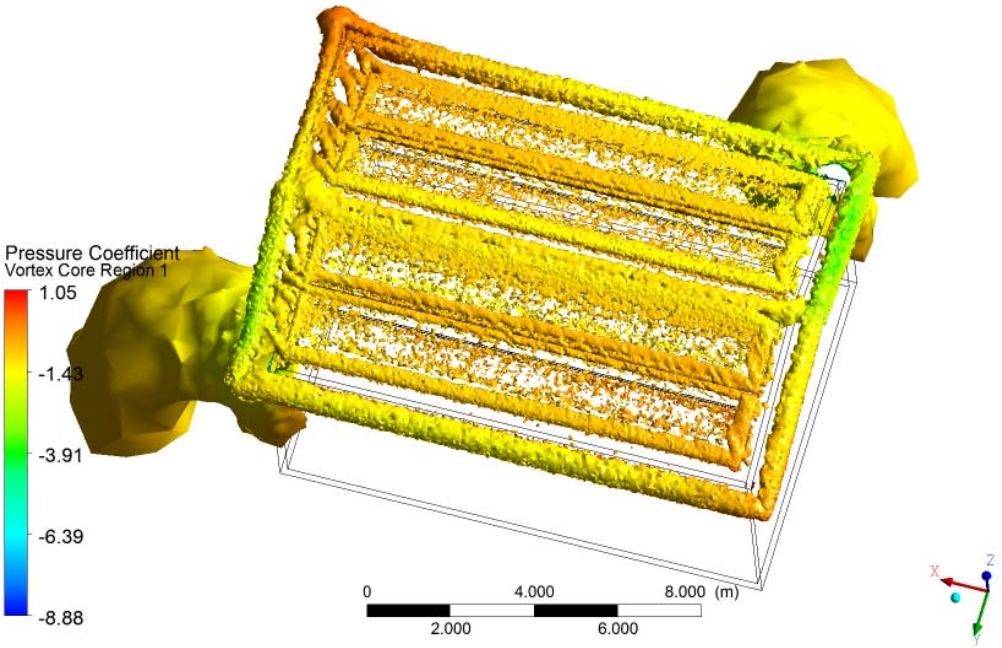


Fig. E. 104. Turbulence distribution, with CP on roof and top of panels, WW, WD 45º

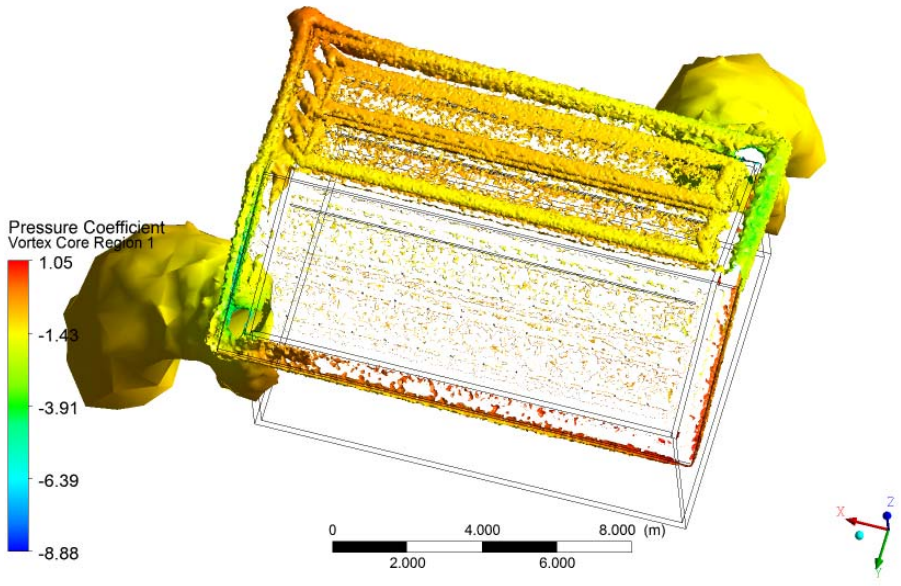


Fig. E. 105. Turbulence distribution, with CP on roof under panels WW and LW with panels

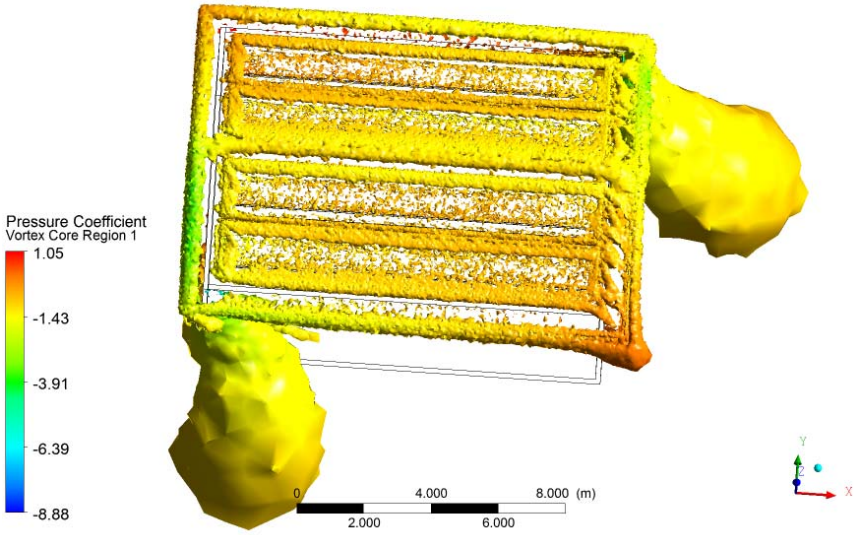


Fig. E. 106. Turbulence distribution, with CP on roof and top of panels, LW, WD 45º

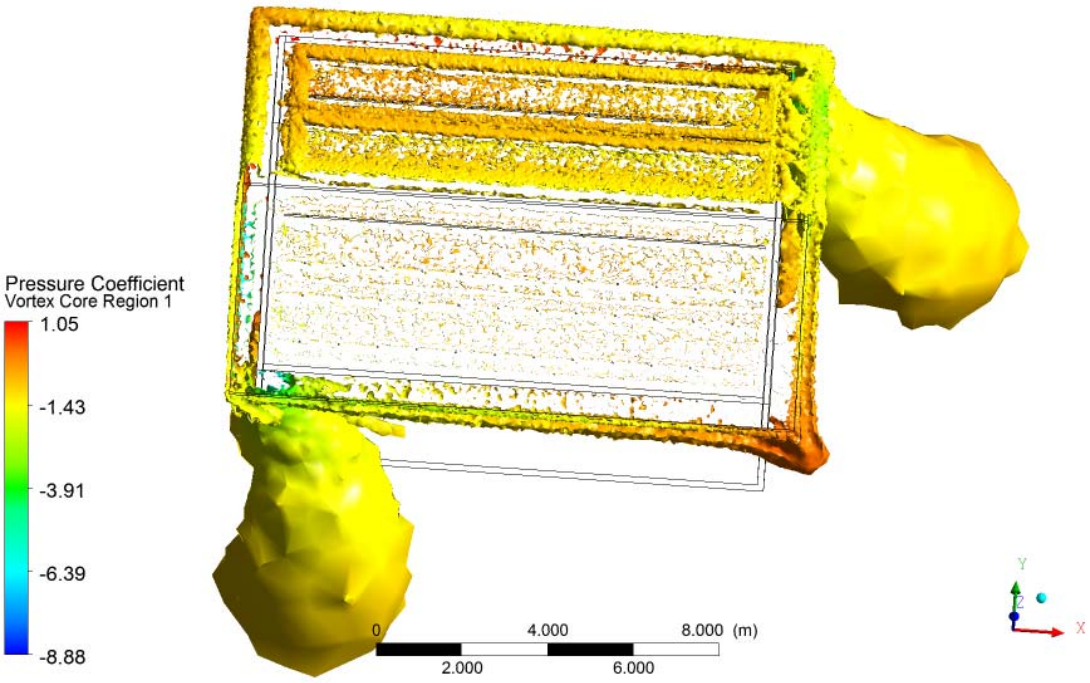


Fig. E. 107. Turbulence distribution, with CP on roof under panels LW and WW with panels,

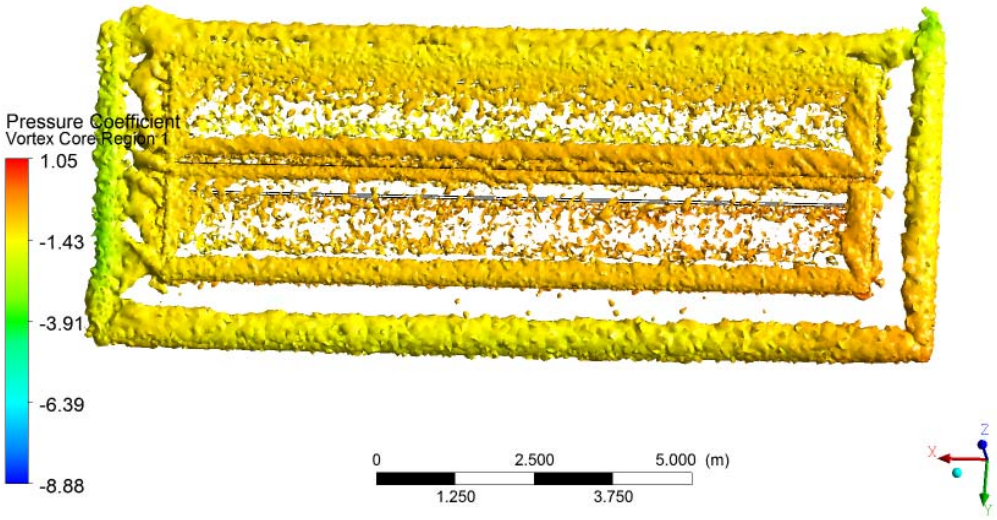


Fig. E. 108. Turbulence distribution, with CP on top of panels, WW, WD 45º

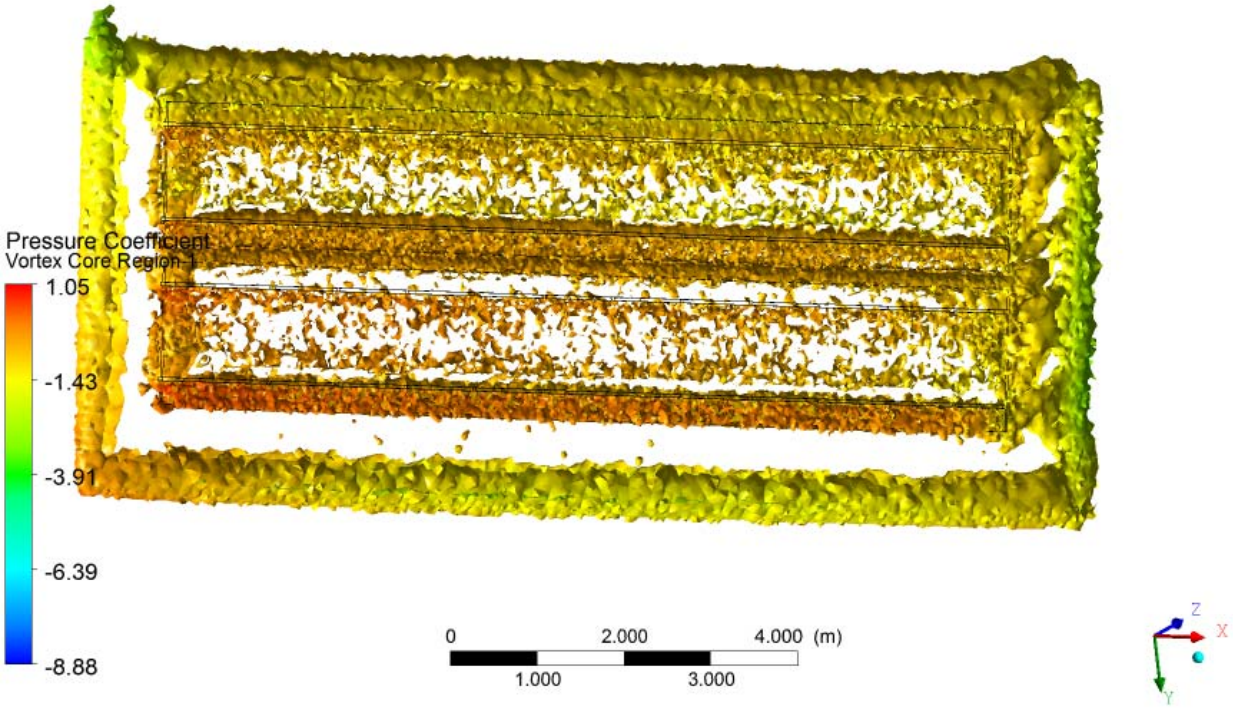


Fig. E. 109. Turbulence distribution, with CP on bottom of panels, WW, WD 45º

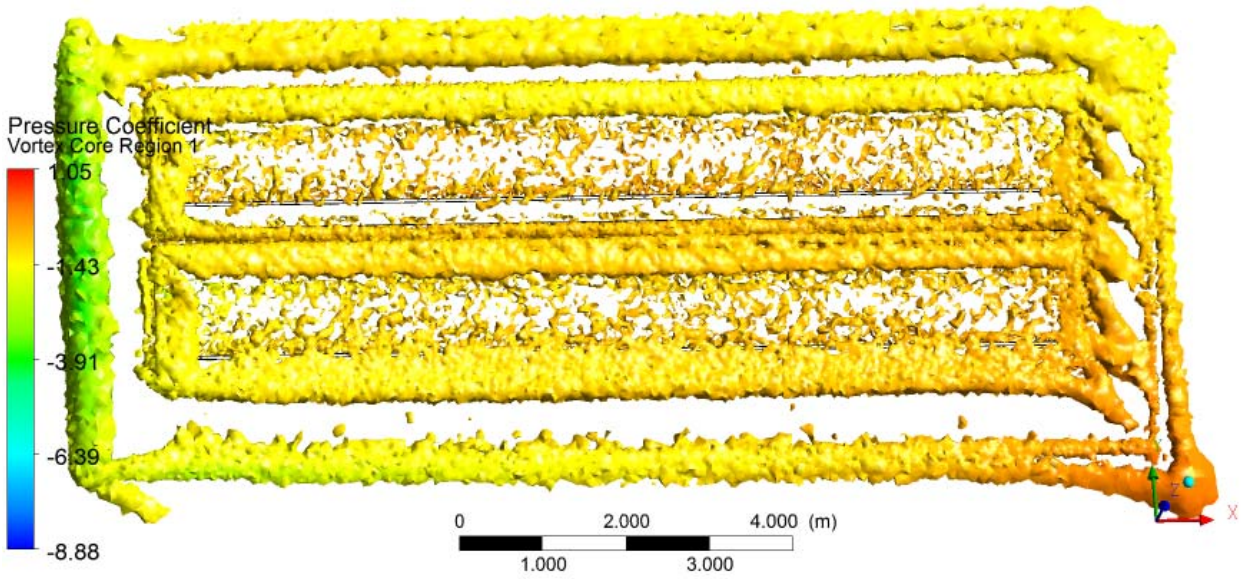


Fig. E. 110. Turbulence distribution, with CP on top of panels, LW, , WD 45º

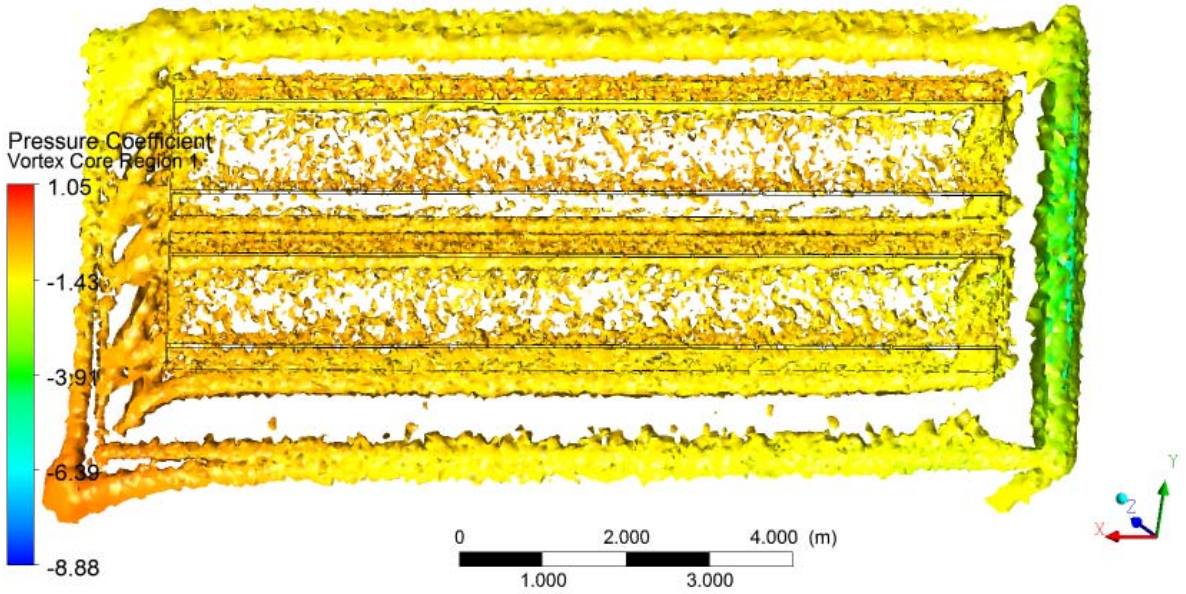


Fig. E. 111. Turbulence distribution, with CP on bottom of panels, LW, WD 45º

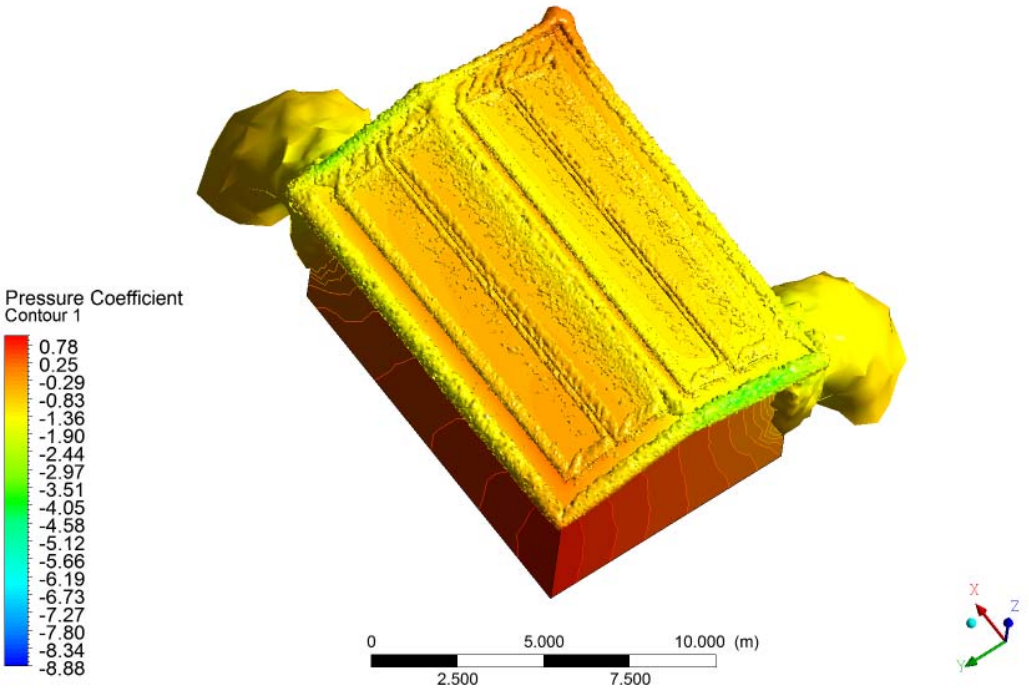


Fig. E. 112. Turbulence distribution, with CP on whole building and panels, WW, WD 45º

1.2.2. WIND DIRECTION 90º

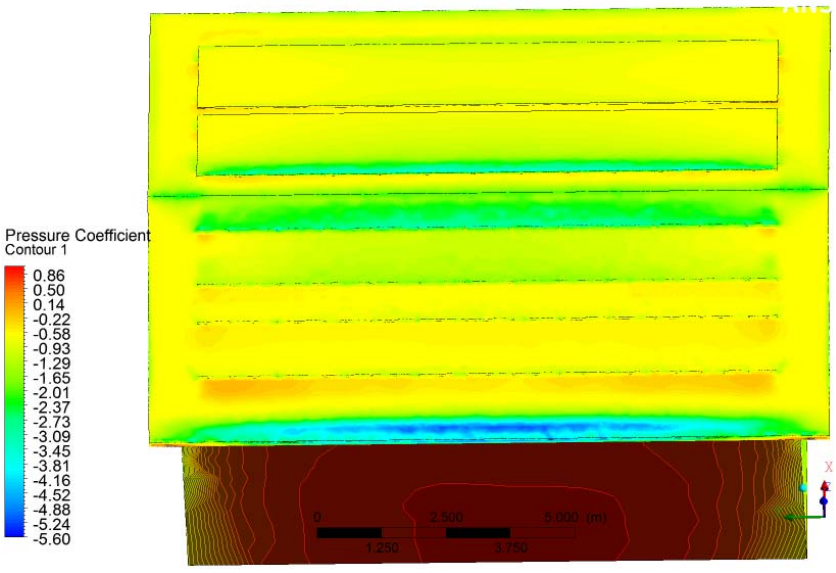


Fig. E. 113. CP on roof under solar panels, S 15º, WW, WD 90º

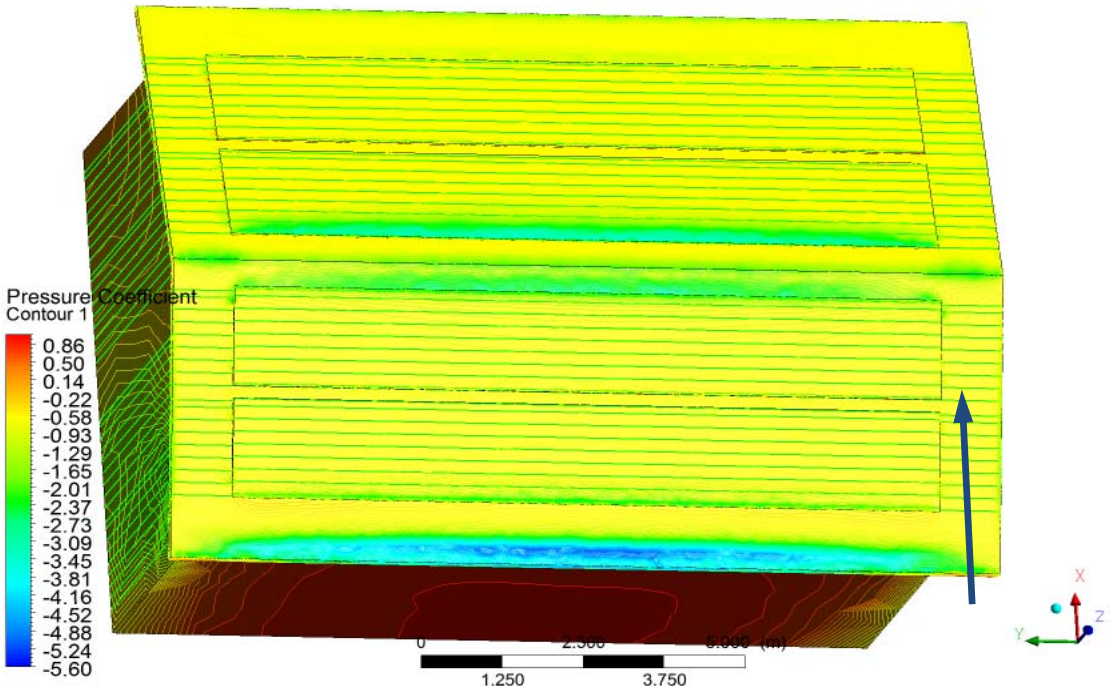


Fig. E. 114. Cp on top of solar panels with plines, S 15º, WW, WD 90º

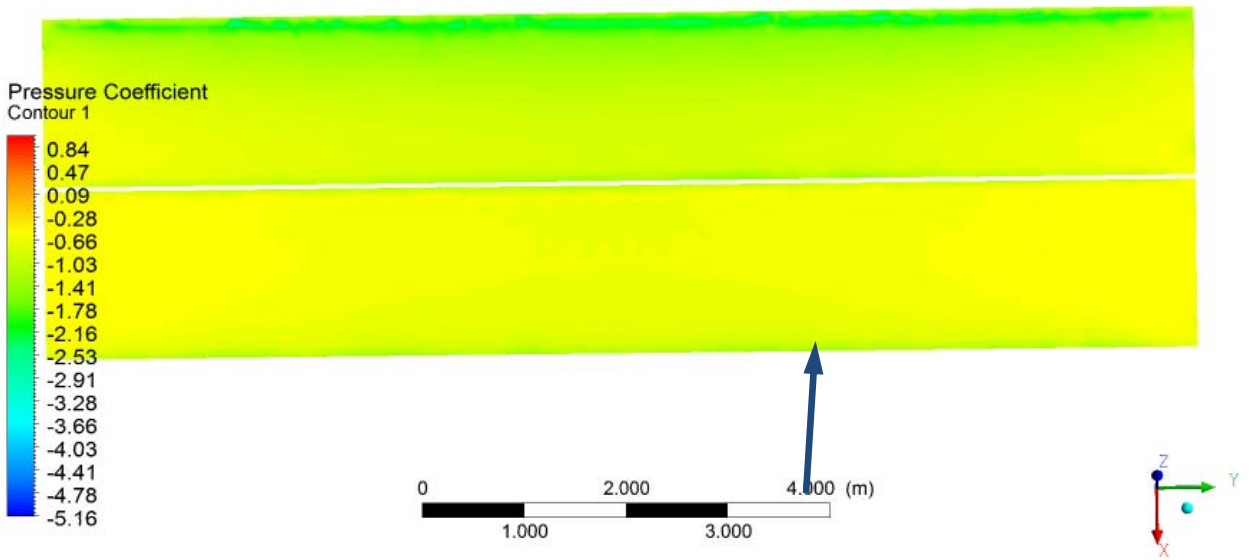


Fig. E. 115. Cp on top of solar panels, S 15º, WW, WD 90º

1.2.3. WIND DIRECTION 0º

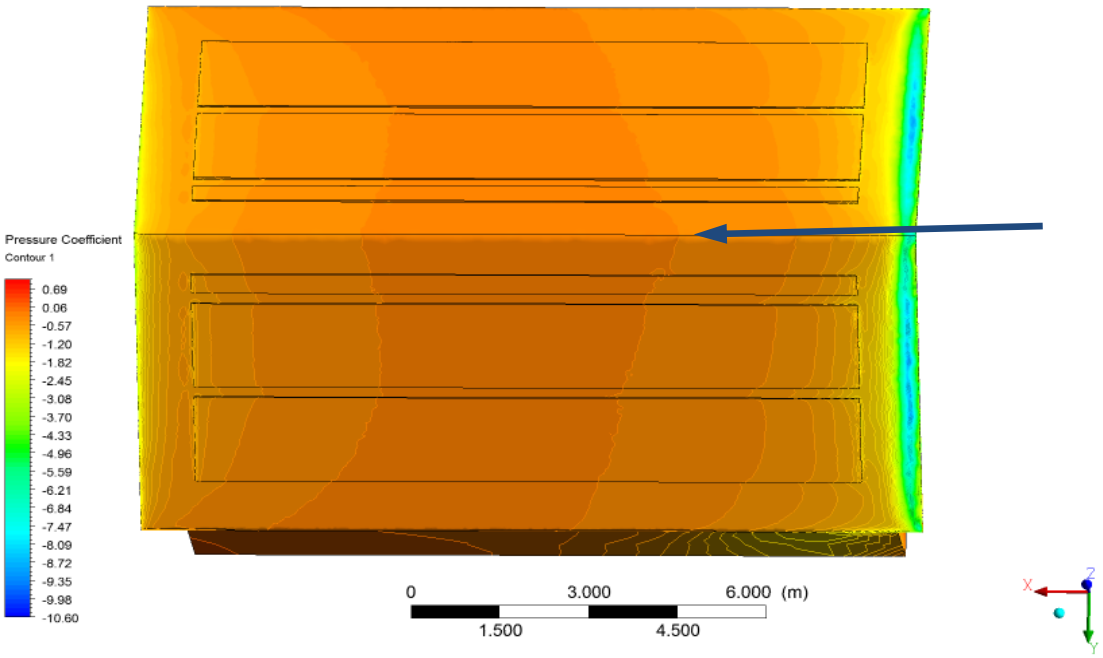


Fig. E. 116. Cp on roof with solar panels, top view, S 15º, WD 0º

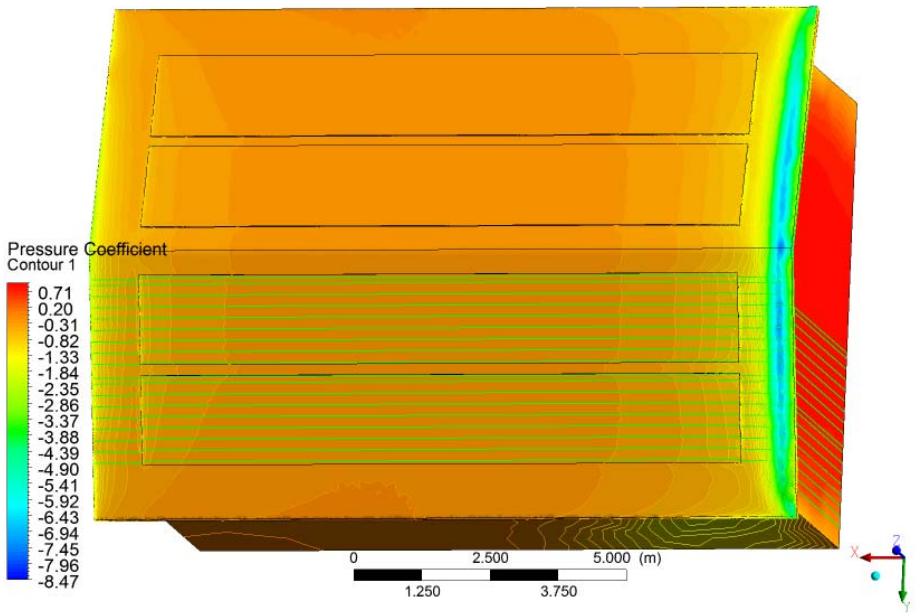


Fig. E. 117. Cp on roof with solar panels and Plines S 15º, WD 0º

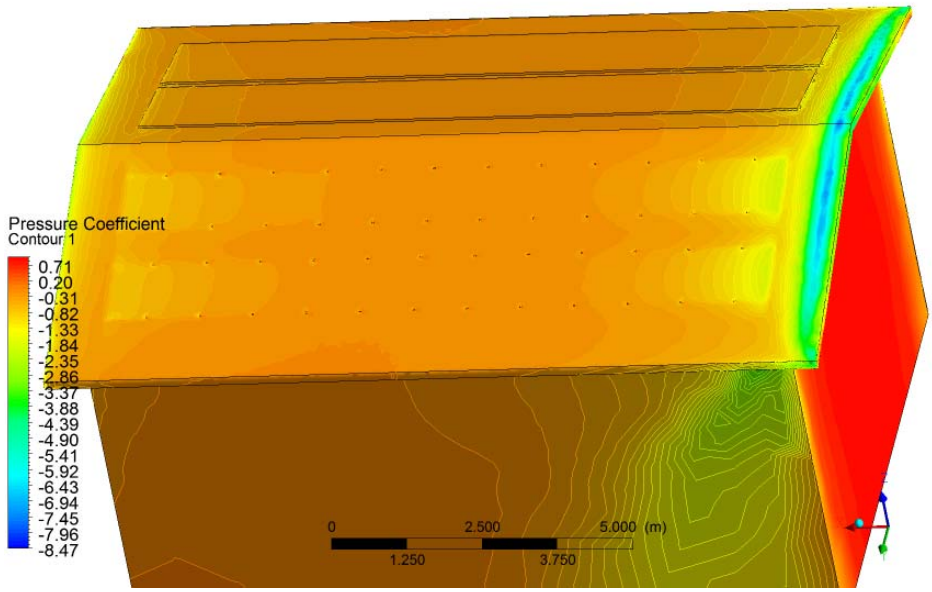


Fig. E. 118. Cp on roof under solar panels on one side and on solar panels on the other side, S 15º, WD 0º

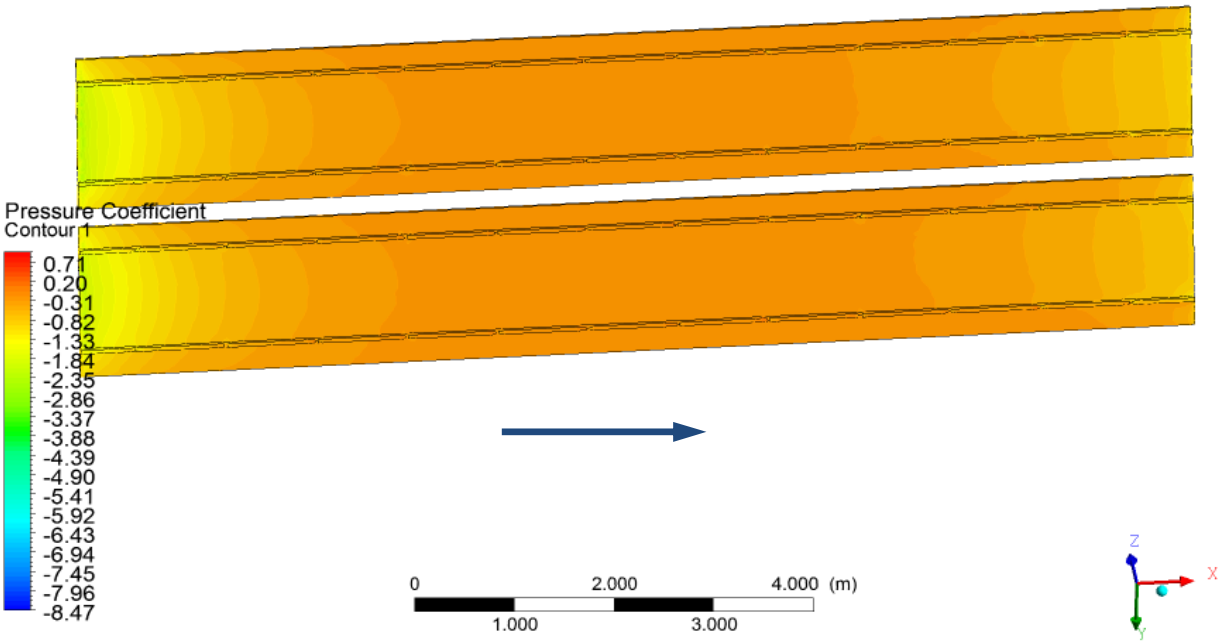


Fig. E. 119. Cp, on bottom of solar panels, S 15º, WD 0º

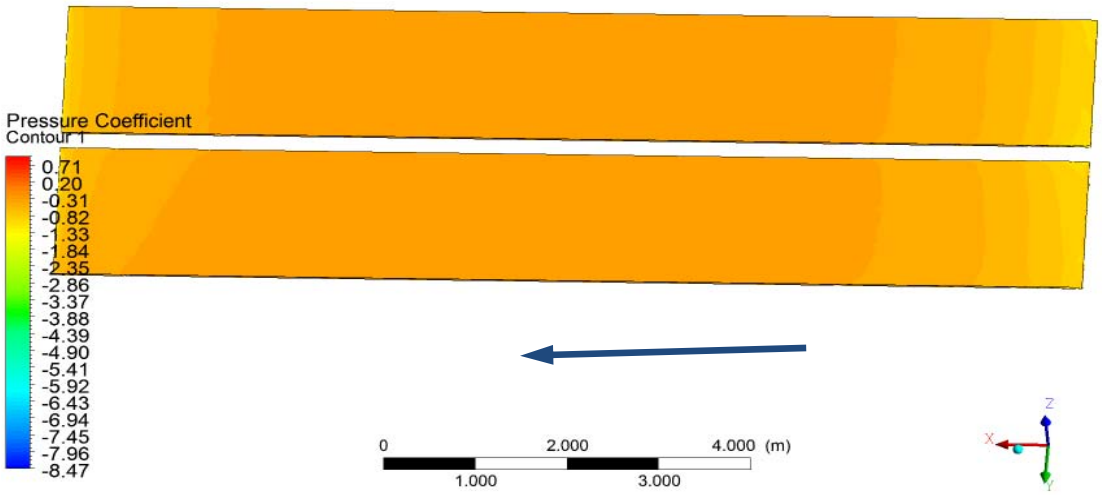


Fig. E. 120. Cp on top of solar panels, S 15º, WD 0º

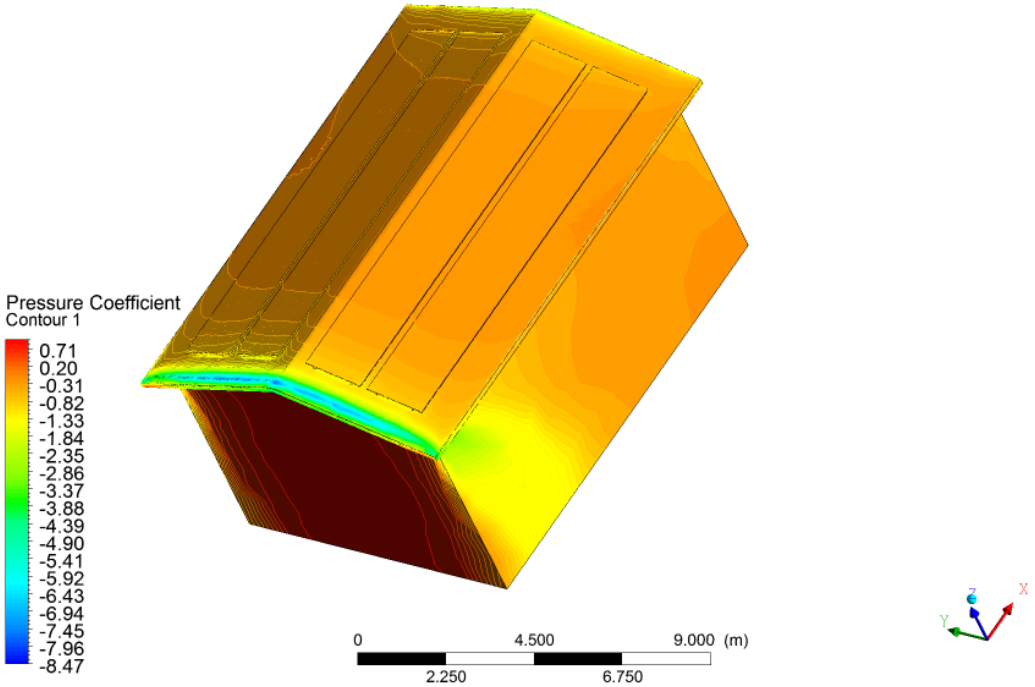


Fig. E. 121. Cp on building with the solar panels, S 15º, WD 0º, WW

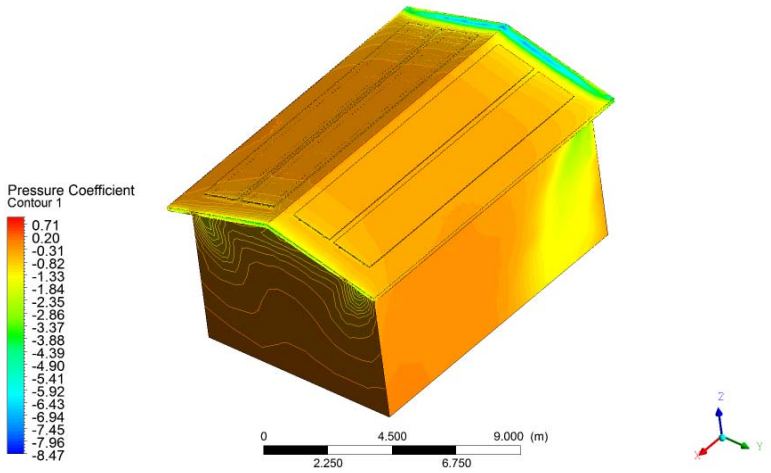


Fig. E. 122. Cp on building with the solar panels, S 15º, WD 0º, LW

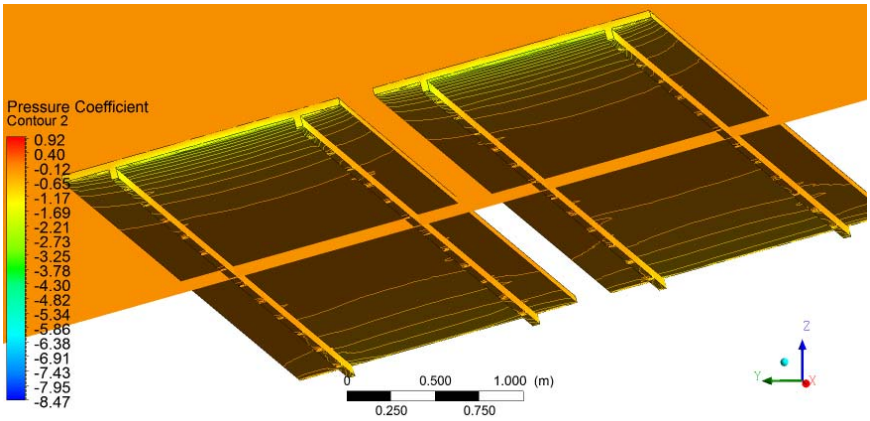


Fig. E. 123. Cp on a perpendicular plan and on bottom of panels, WD 0º, WW

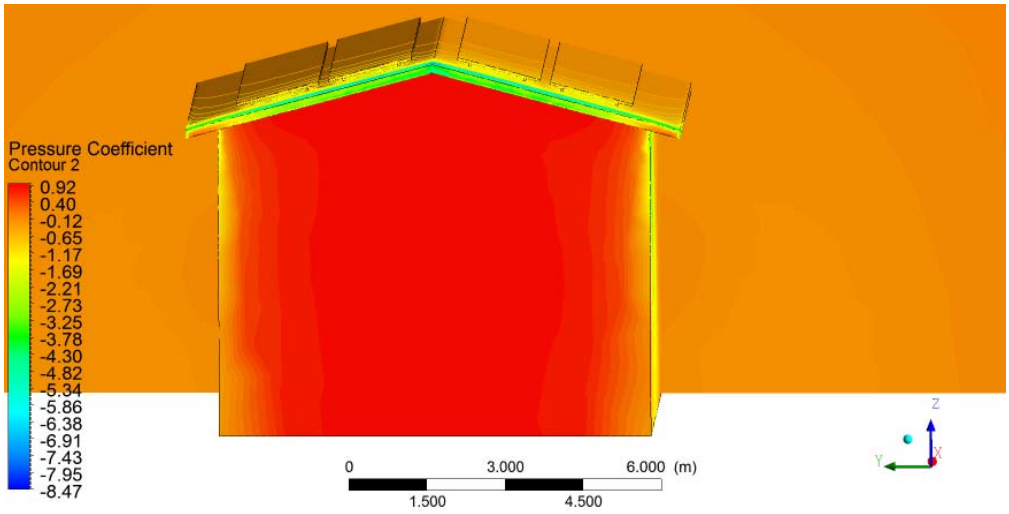


Fig. E. 124. Cp distribution on a perpendicular plan to the ridge of the building, WD 0º, WW

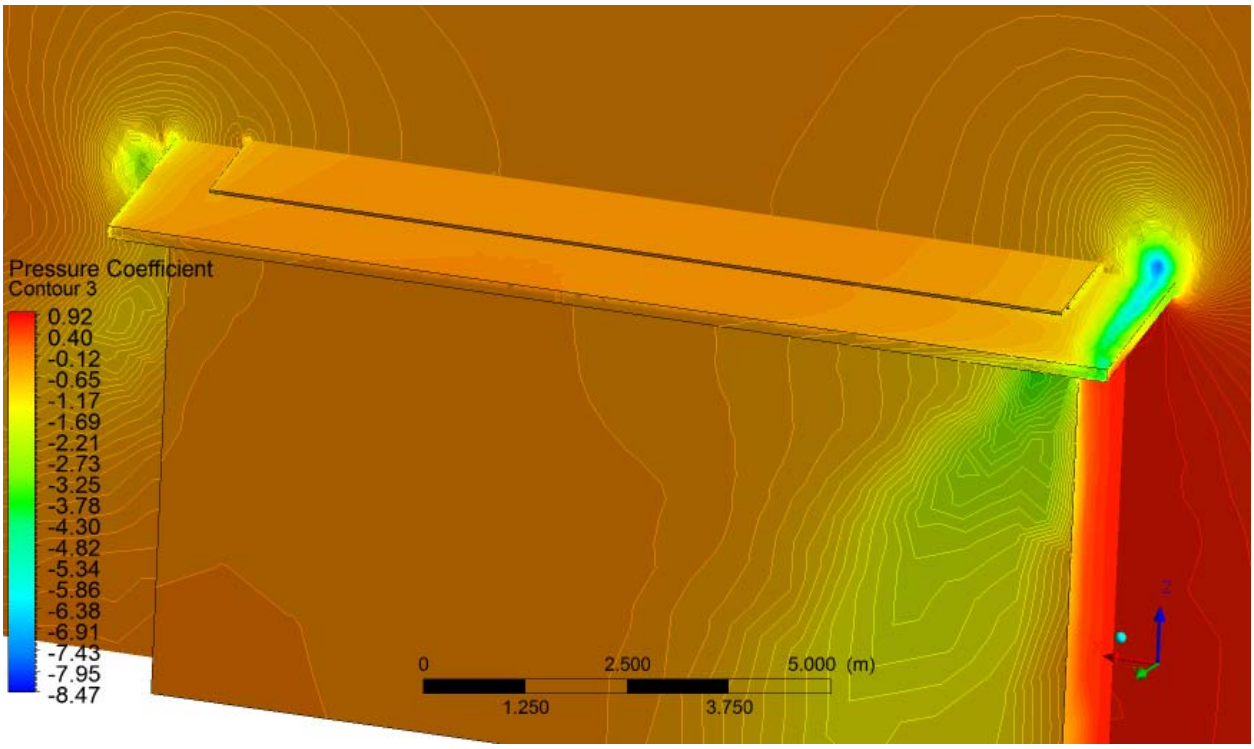


Fig. E. 125. Cp distribution on a plan parallel to the ridge of the building, WD 0º, WW, close view

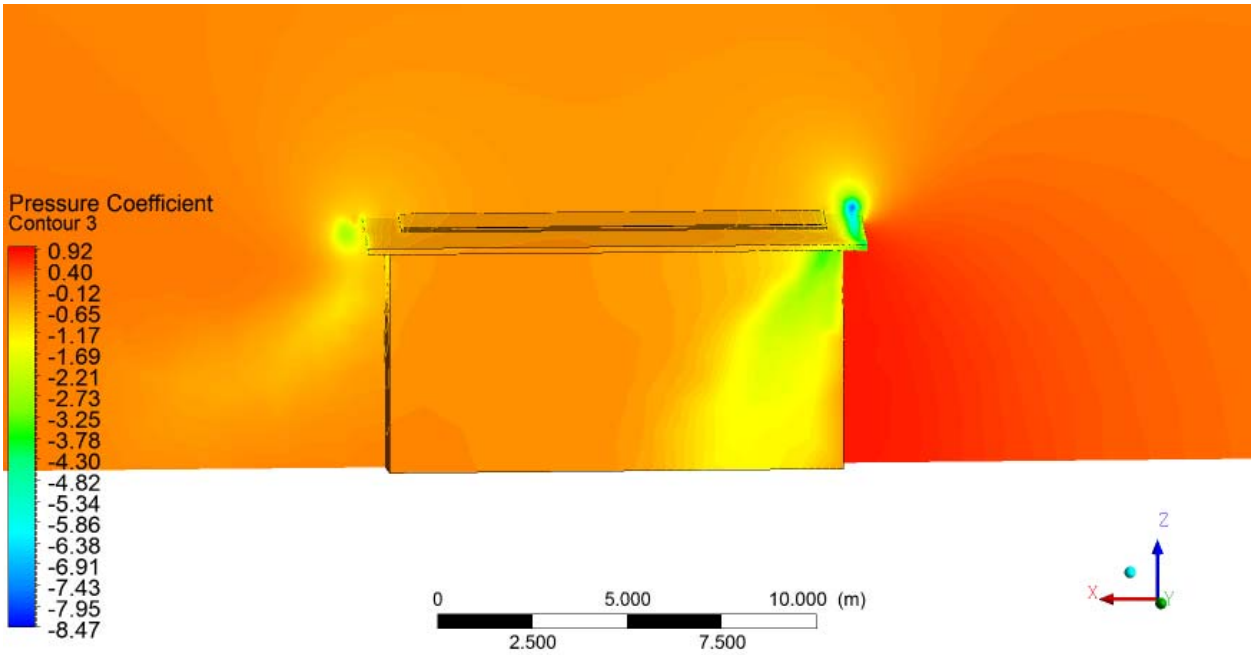


Fig. E. 126. Cp distribution on a plan parallel to the ridge of the building, WD 0º, WW, distant view

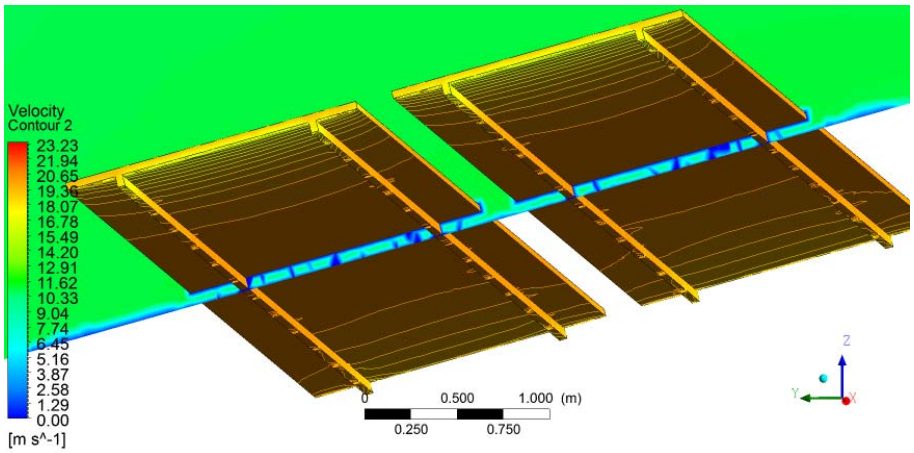


Fig. E. 127. Velocity distribution bottom of panels and a perpendicular plan to the building ridge, WD 0º

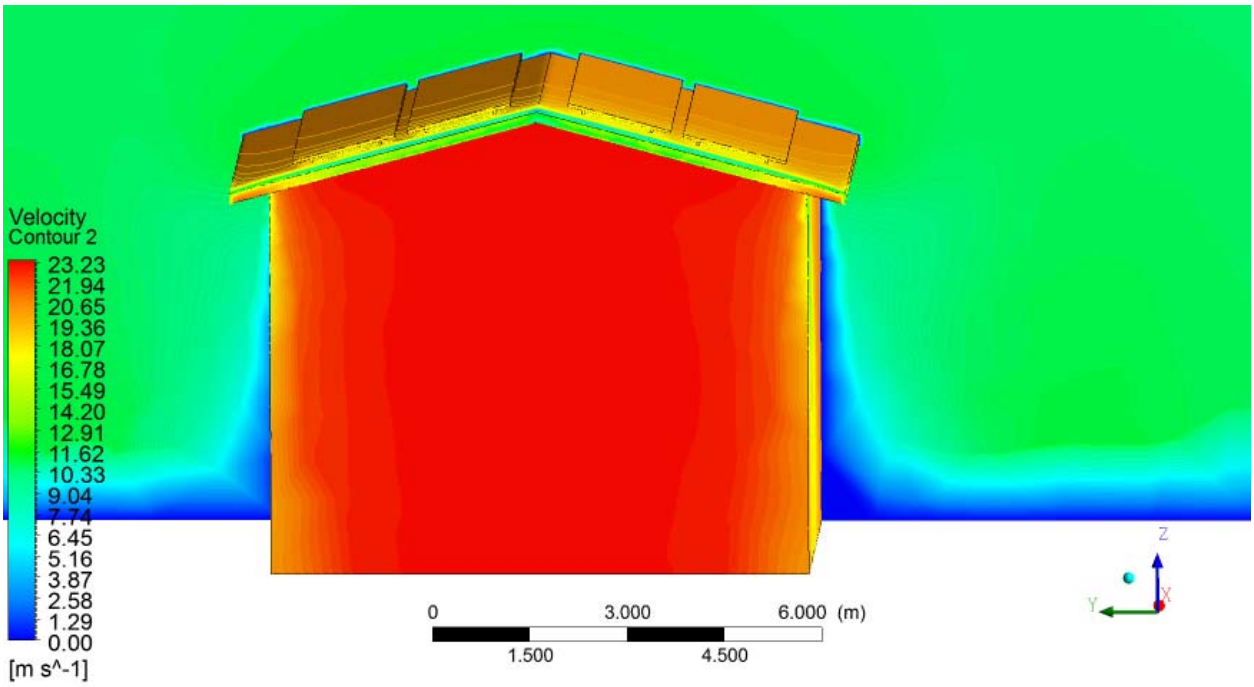


Fig. E. 128. Velocity distribution on a perpendicular plan to the ridge of the building, WD 0º, WW

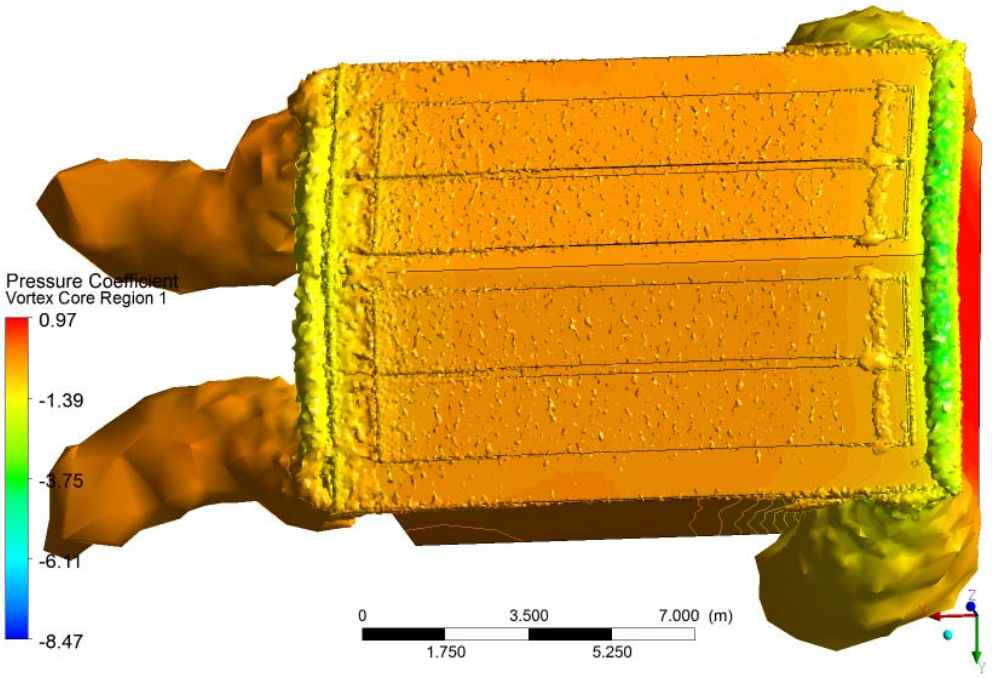


Fig. E. 129. Cp on building with turbulences, top view, S 15º, WD 0º

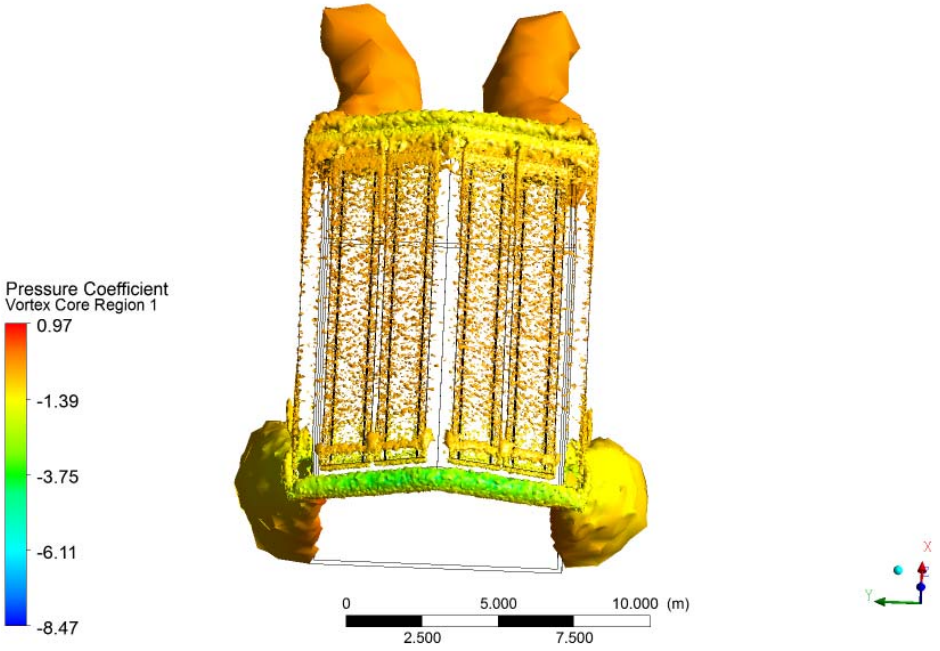


Fig. E. 130. Turbulence distribution, with CP, top view no building contours are shown, WW, S 15º, WD 0º

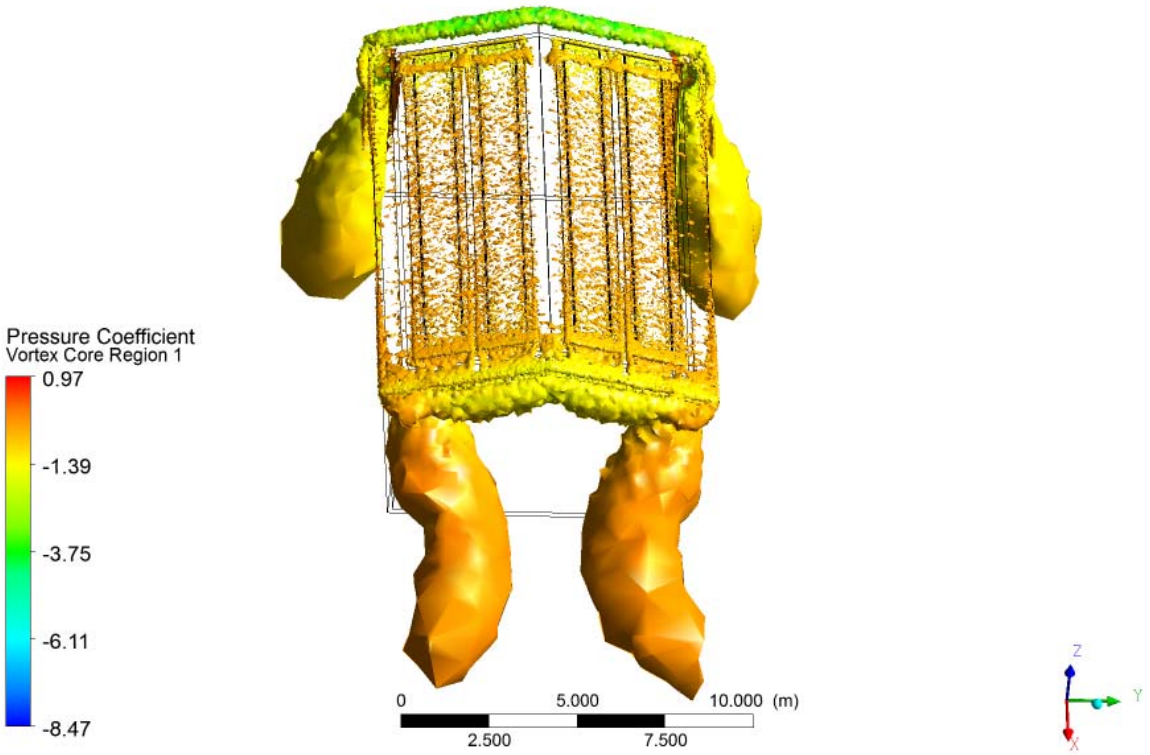


Fig. E. 131. Turbulence distribution, with CP, top view no building contours are shown, LW, S 15º, WD 0º

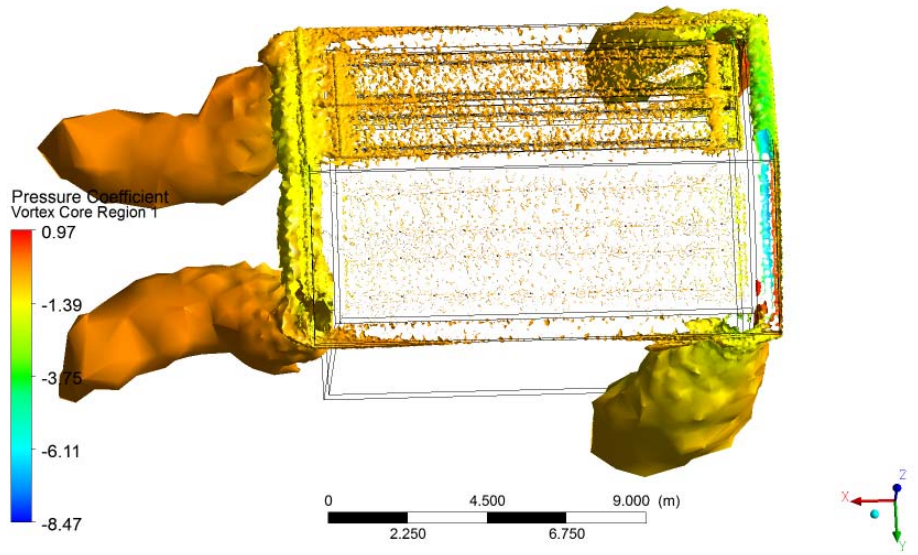


Fig. E. 132. Turbulence distribution, with CP above solar panels on one side and on roof under solar panels on the other side, top view no building contours are shown, S 15º, WD 0º

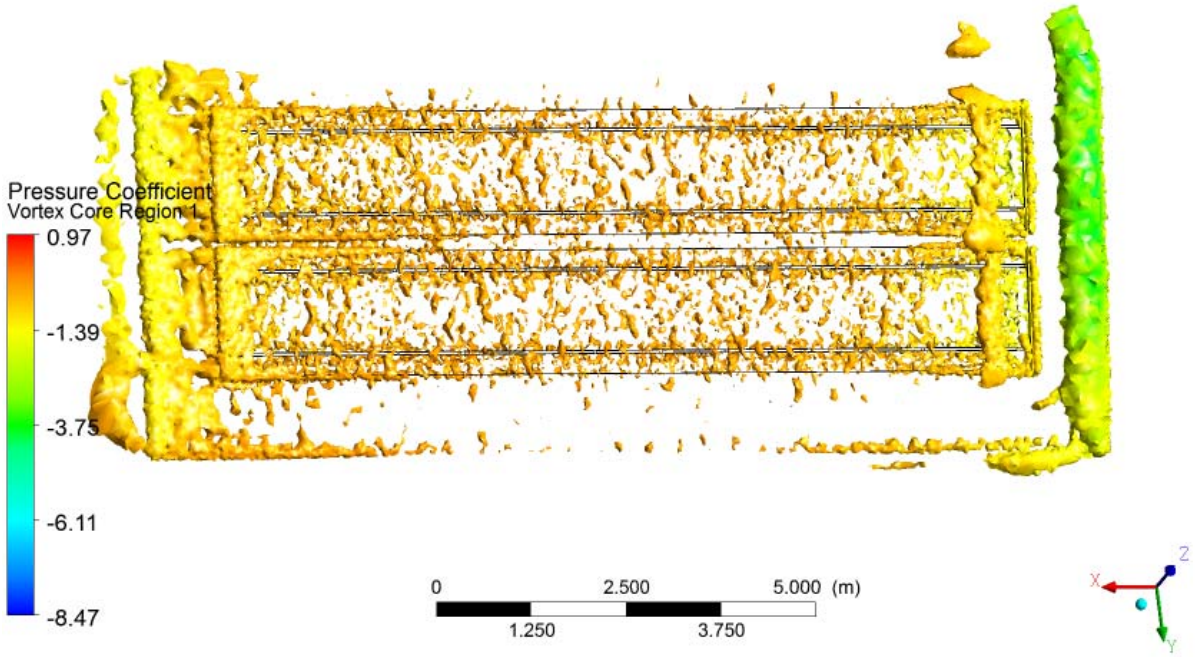


Fig. E. 133. Cp on turbulences above solar panels on one side of the roof, no building contours, S 15º, WD 0º

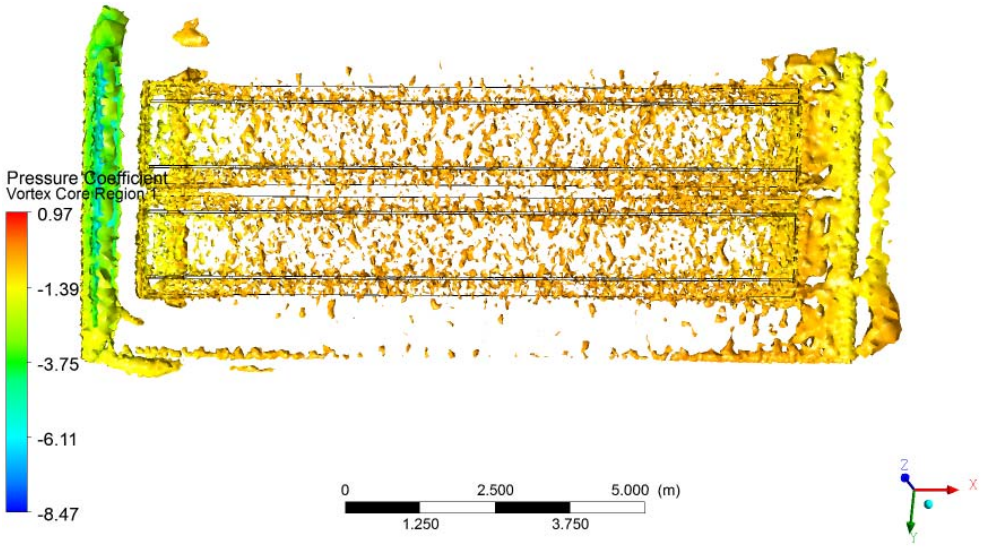


Fig. E. 134. Cp on turbulences on bottom of the solar panels on one side of the roof, no building contours, S 15º, WD 0º

1.2.4. Detailed Distribution of Wind Pressure and Speed on Roof Mounted Solar Panels, S8" C3"

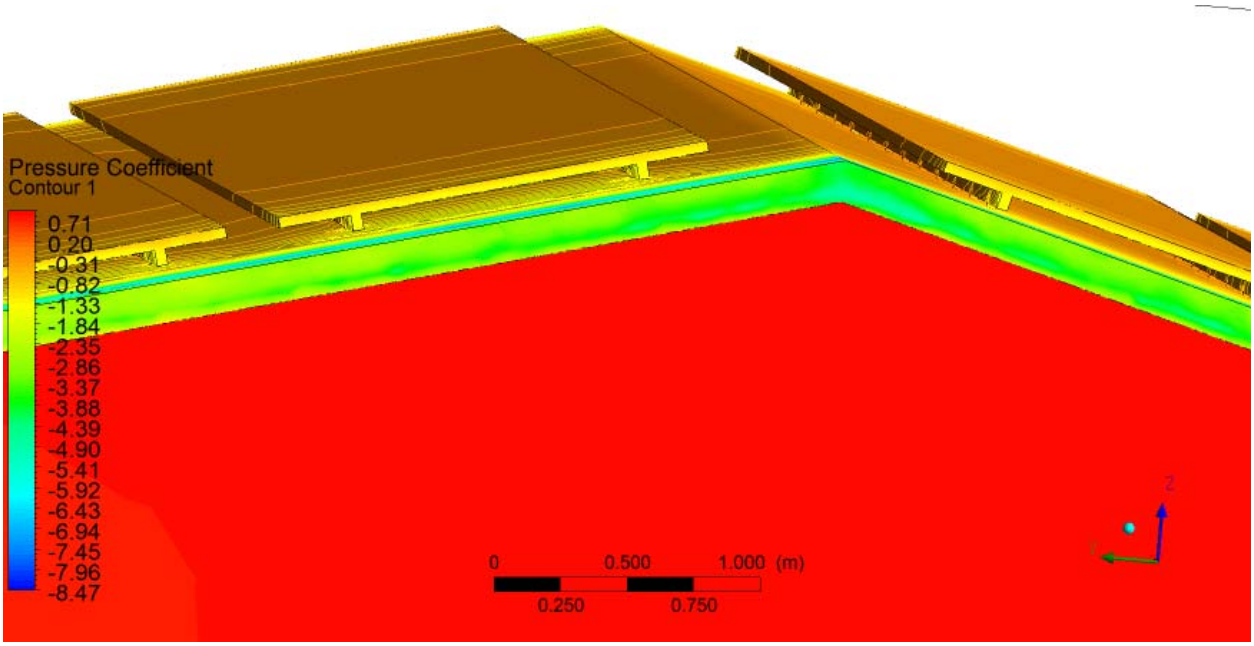


Fig. E. 135. Close view shows space under solar panels and support of the solar panels, WD 0º, WW.

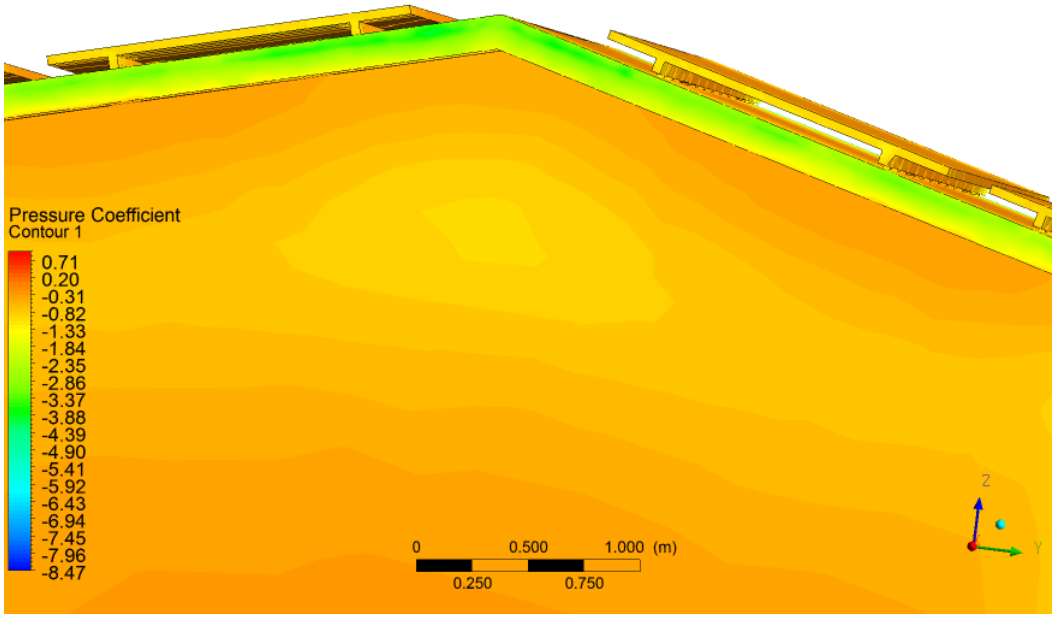


Fig. E. 136. Close view shows space under solar panels and support of the solar panels, WD 0º, LW.

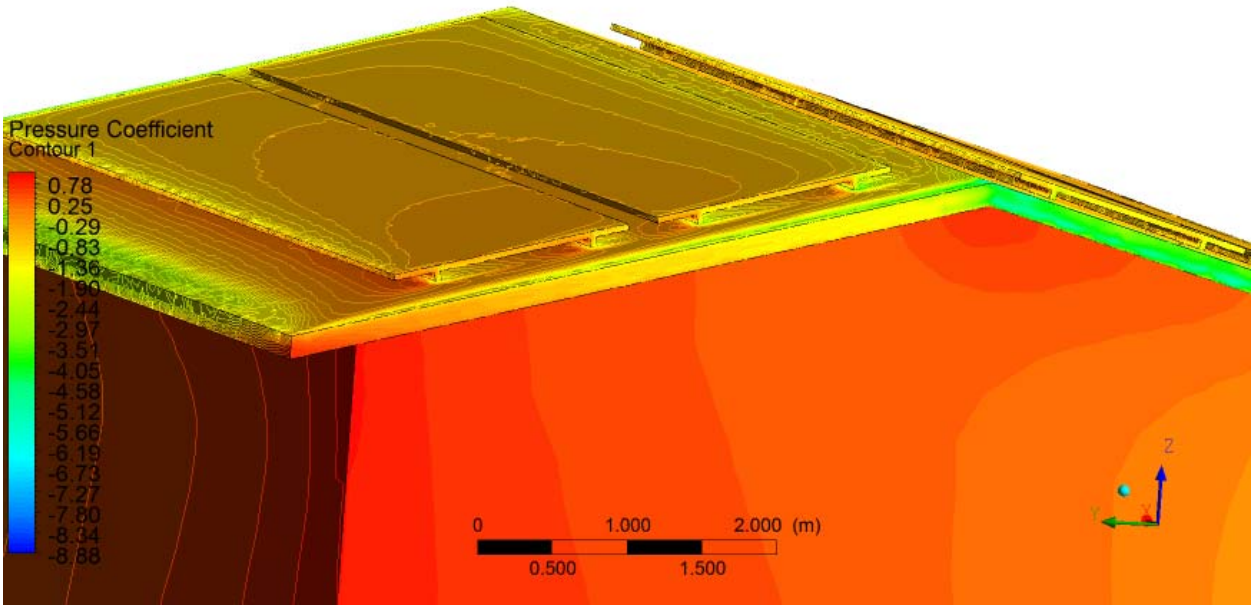


Fig. E. 137. Close view shows separation of solar panels from roof structure, WD 45º, WW

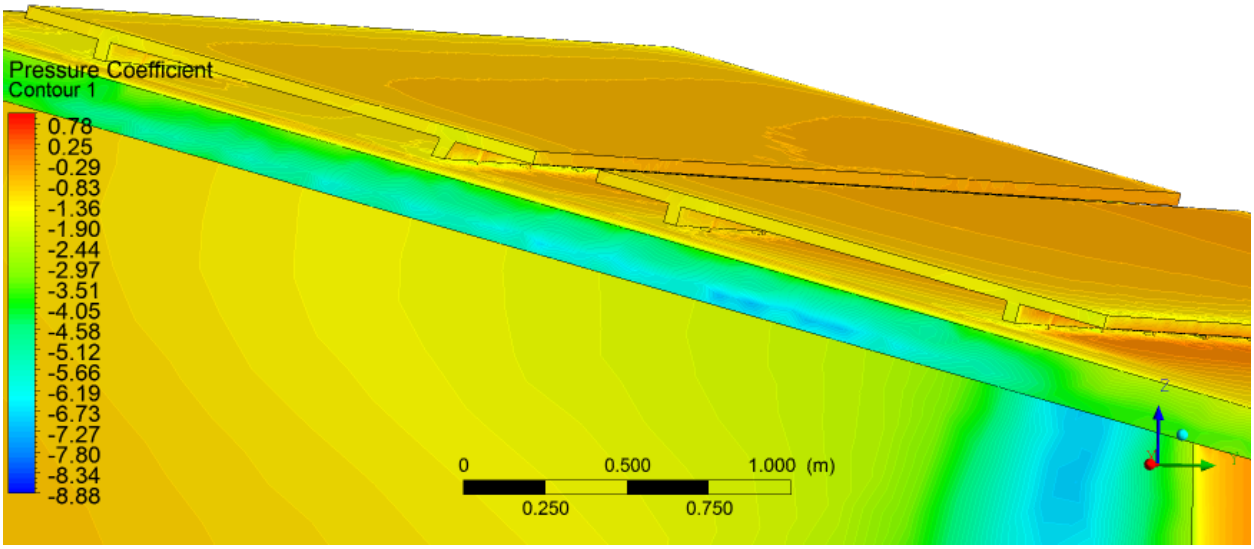


Fig. E. 138. Close view shows separation of solar panels from roof structure, WD 45º, LW

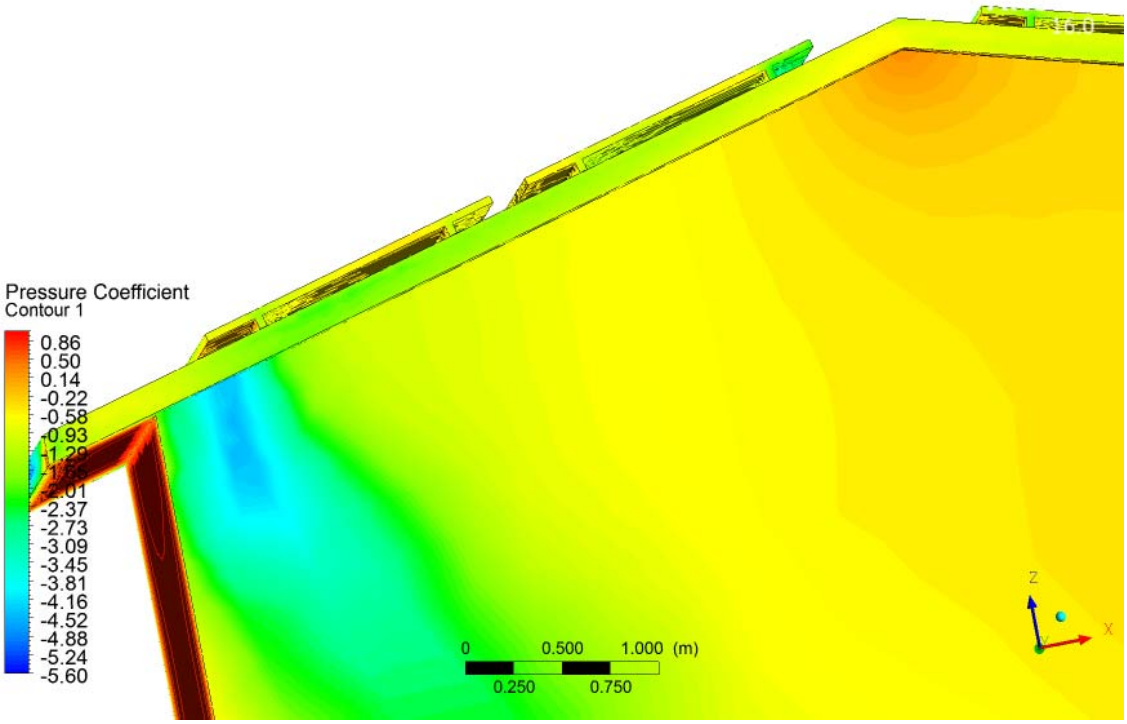


Fig. E. 139. Close view shows space under solar panels and solar panel support, WD 90º, WW

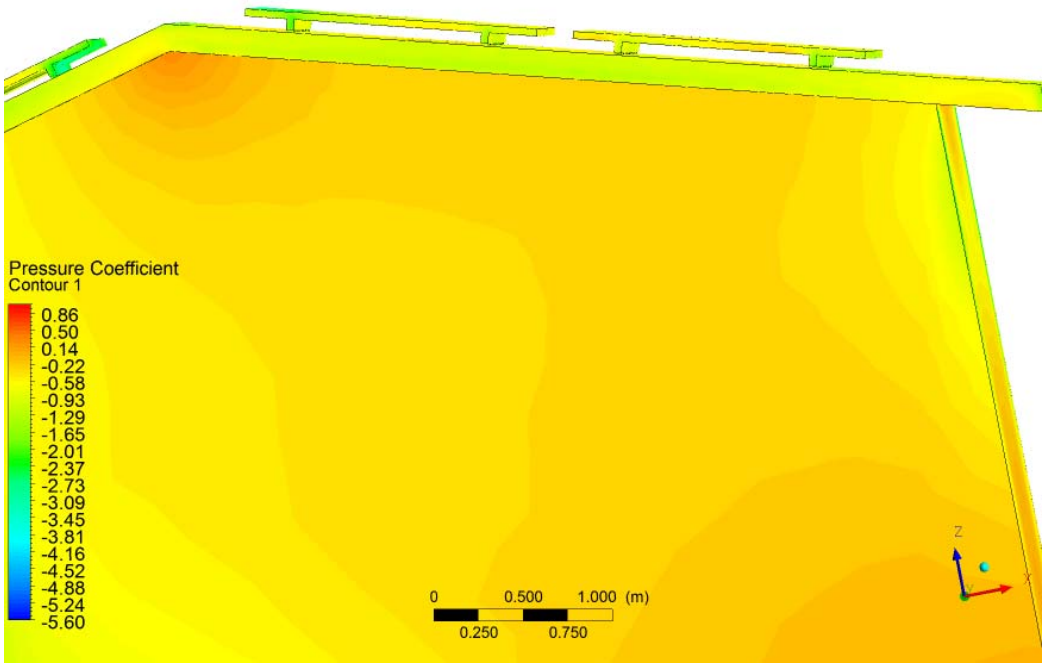


Fig. E. 140. Close view shows space under solar panels and solar panel support, WD 90º, LW

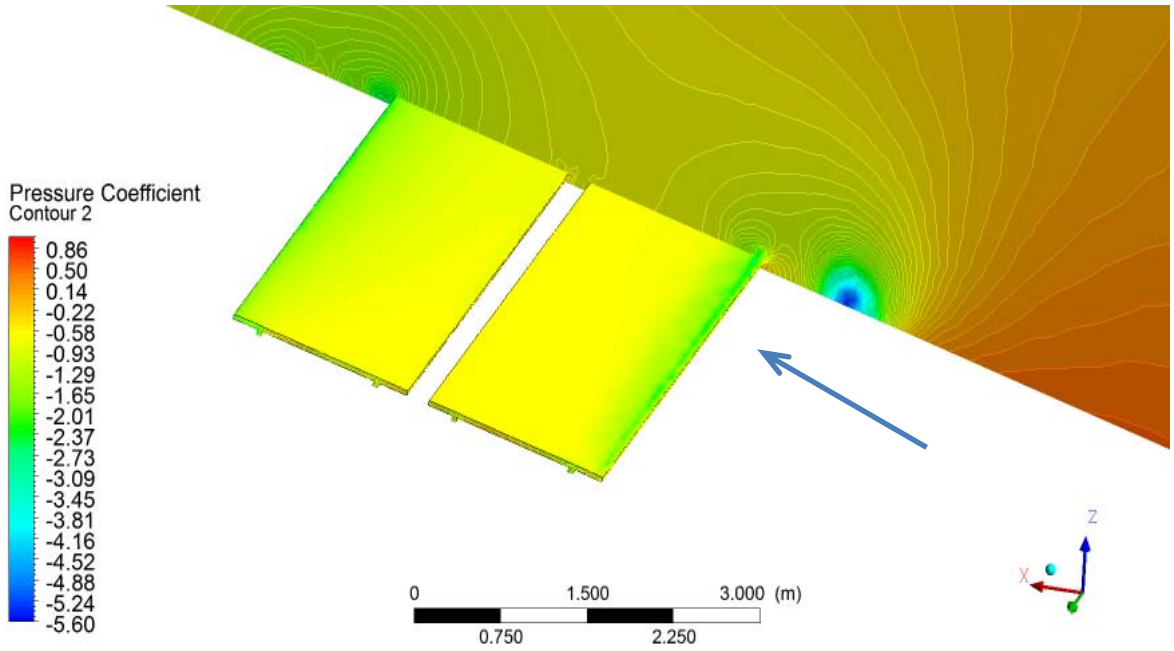


Fig. E. 141. Cp on a perpendicular plan on top of panels, Close up WD 90º, WW

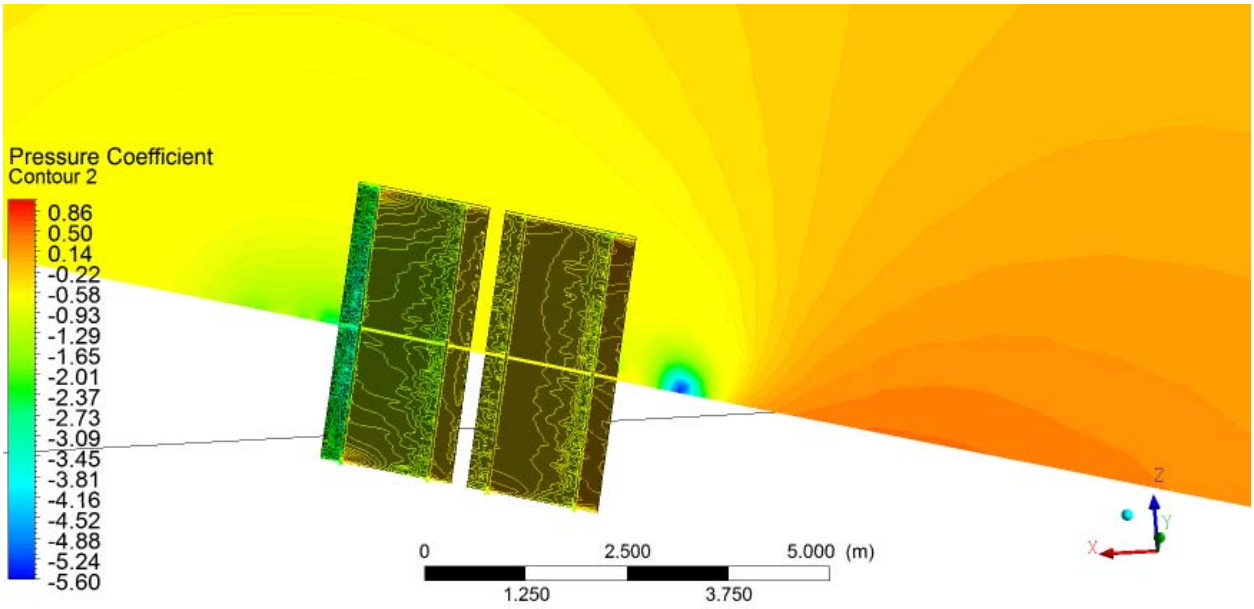


Fig. E. 142. Cp on a perpendicular plan and on bottom of panels, WD 90º, WW

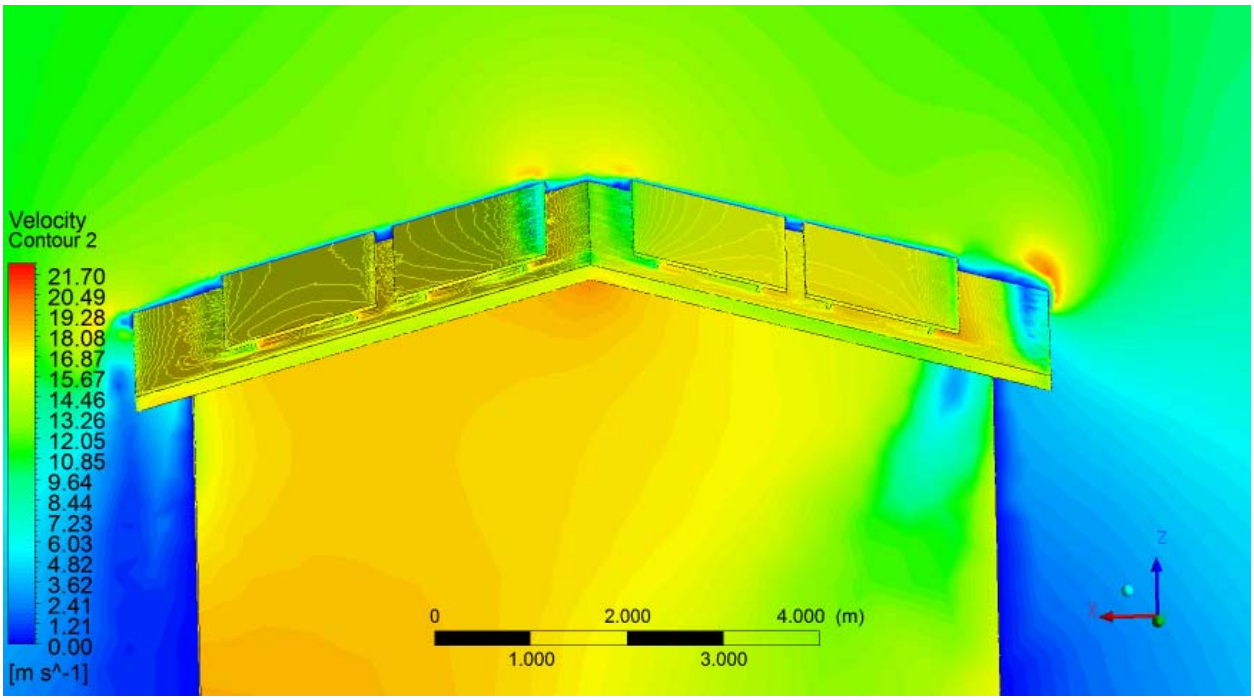


Fig. E. 143. Velocity distribution on a perpendicular plan to the ridge of the building, WD 90º, WW

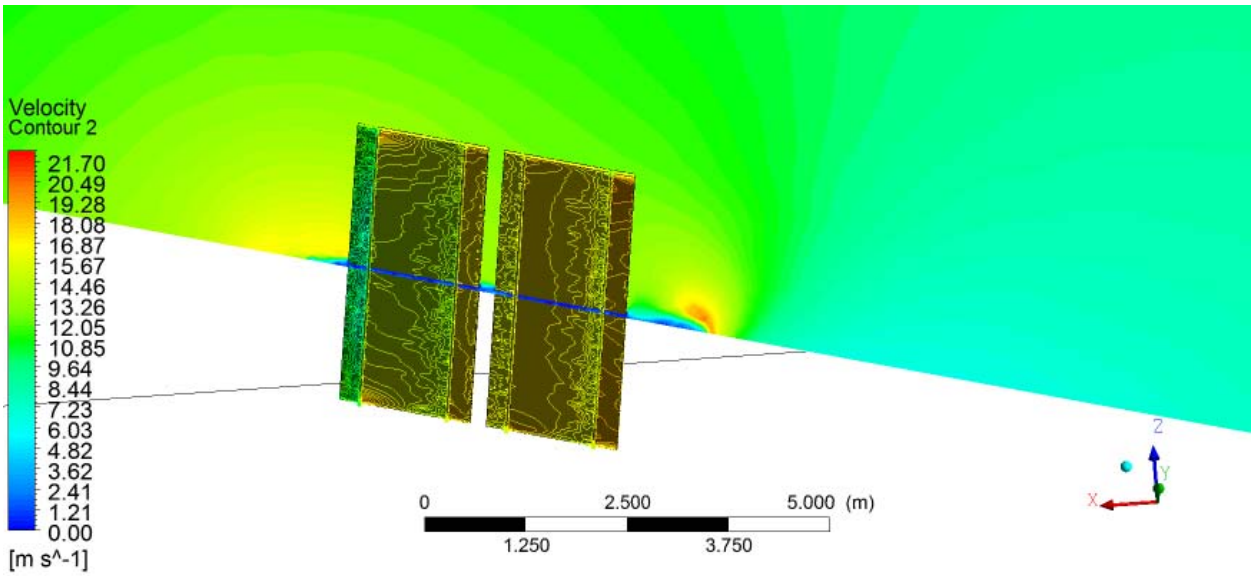


Fig. E. 144. Velocity distribution bottom of panels and a perpendicular plan to the building ridge, WD 90º, WW

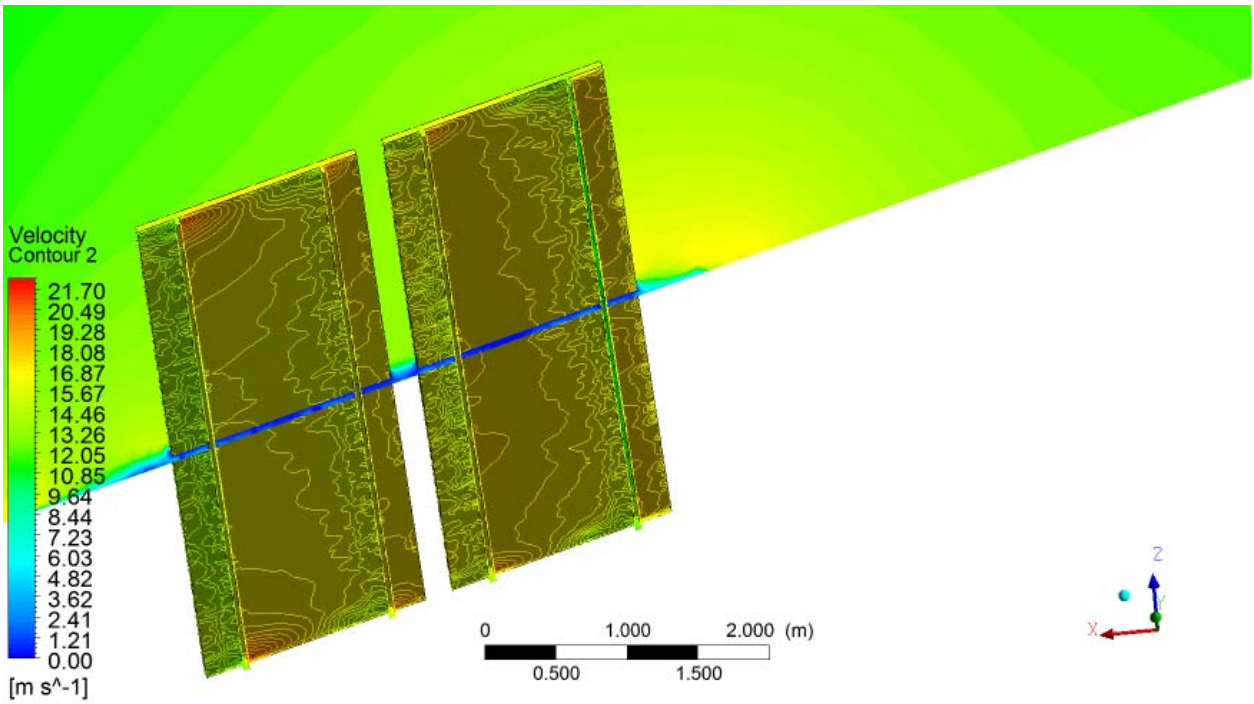


Fig. E. 145. Velocity distribution bottom of panels and a perpendicular plan to the building ridge, WD 90º, LW

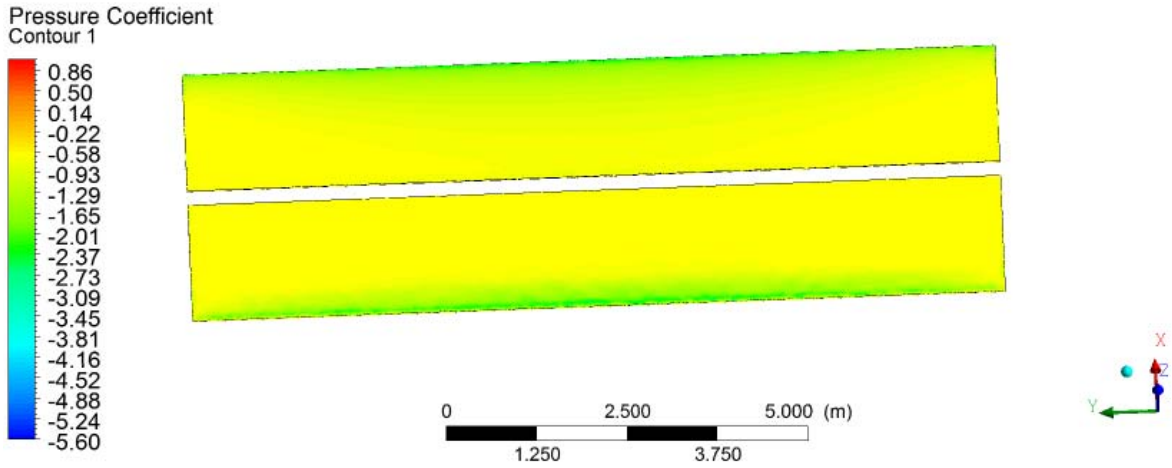


Fig. E. 146. Cp on a perpendicular plan on top of panels, Close up WD 90º, WW

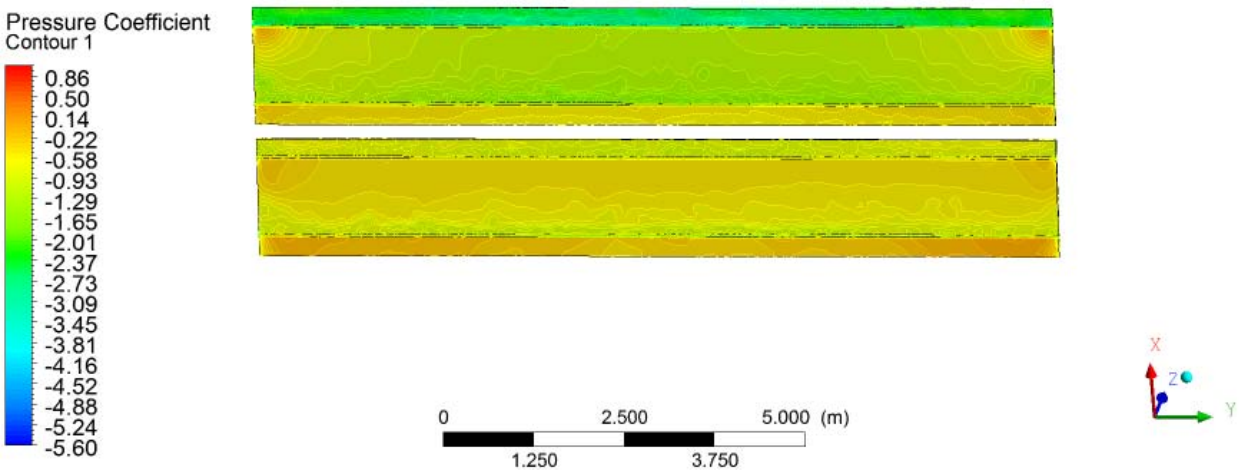


Fig. E. 147. Cp on a perpendicular plan on bottom of panels, Close up WD 90º, WW

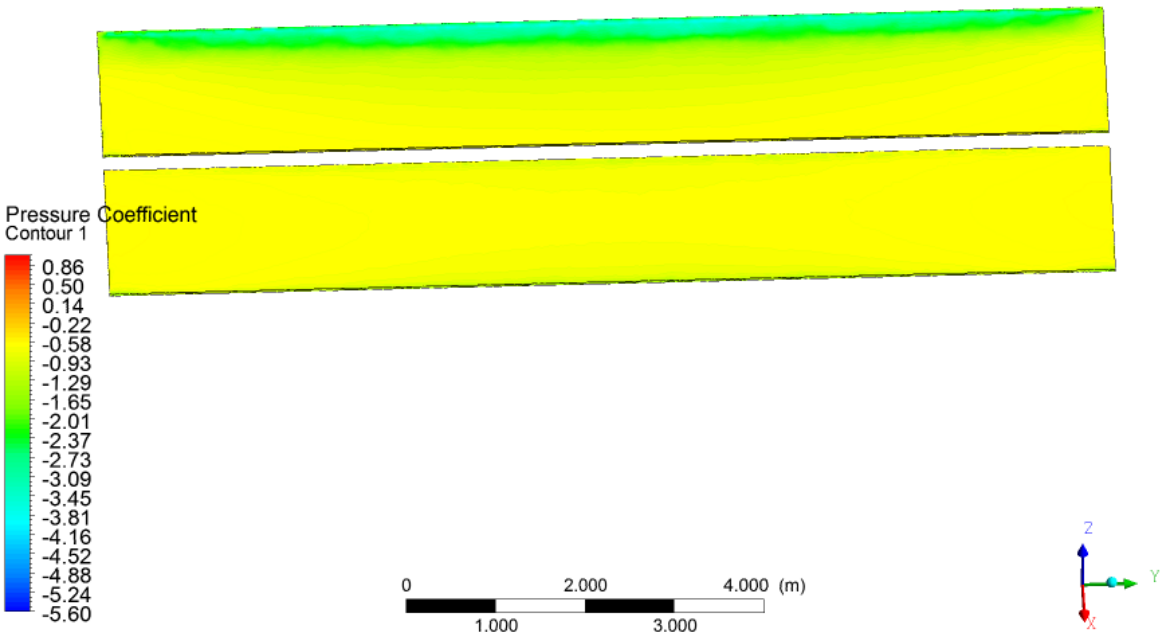


Fig. E. 148. Cp on top of panels, WD 90º, LW

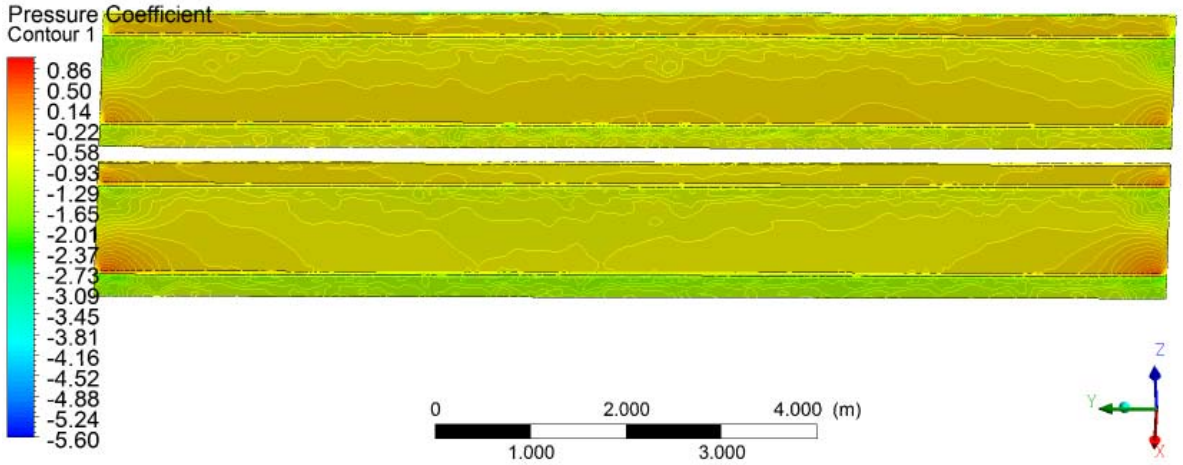


Fig. E. 149. Cp on bottom of panels, WD 90º, LW

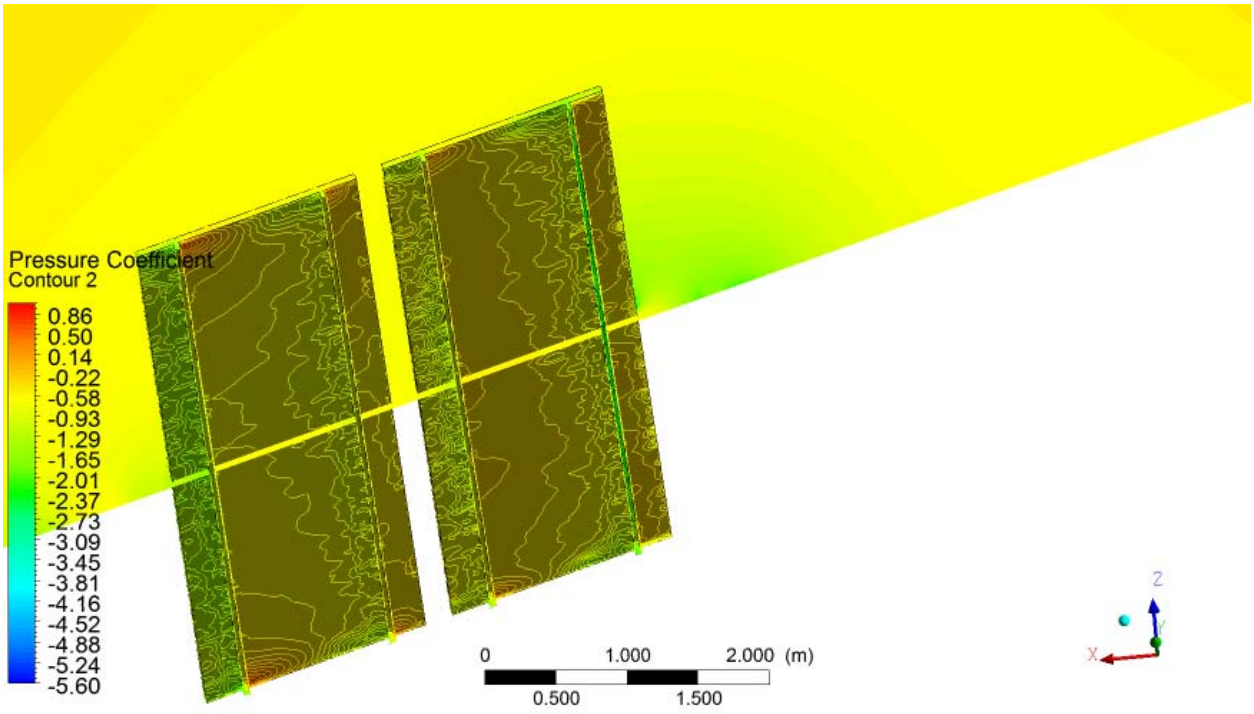


Fig. E. 150. Cp on a perpendicular plane under panels, WD 90º, LW

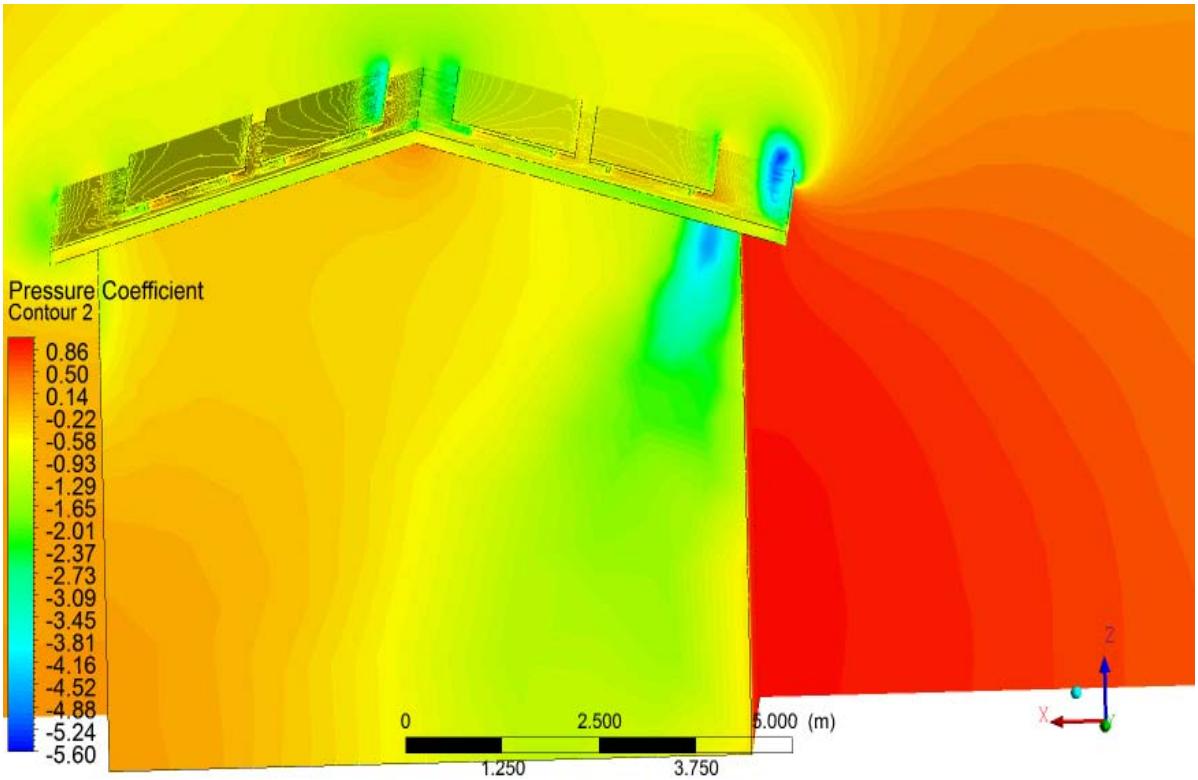


Fig. E. 151. Cp on a perpendicular plane on ridge of the house, WD 90º

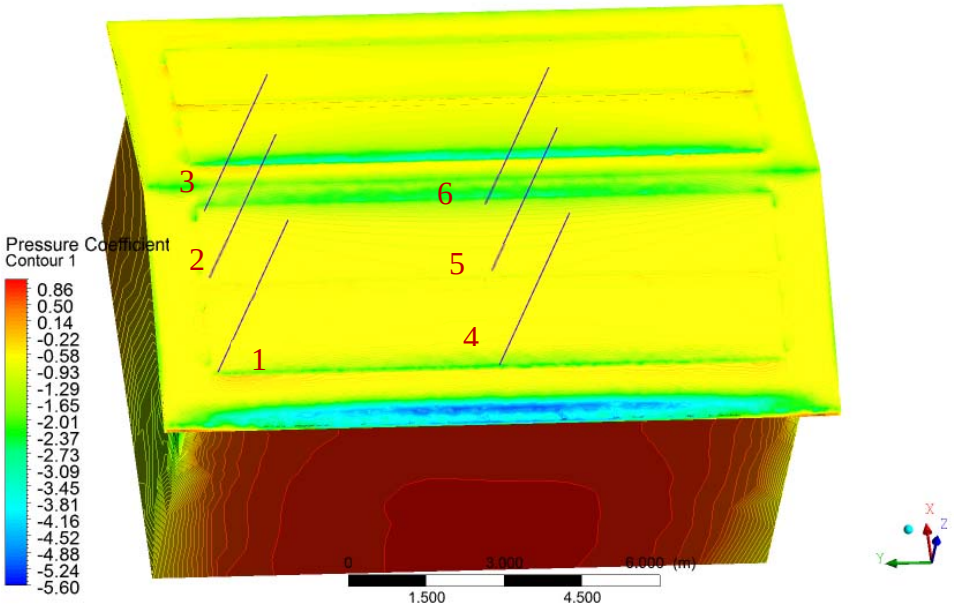


Fig. E. 152. Lines used to draw velocity and pressure changes, WD 90º

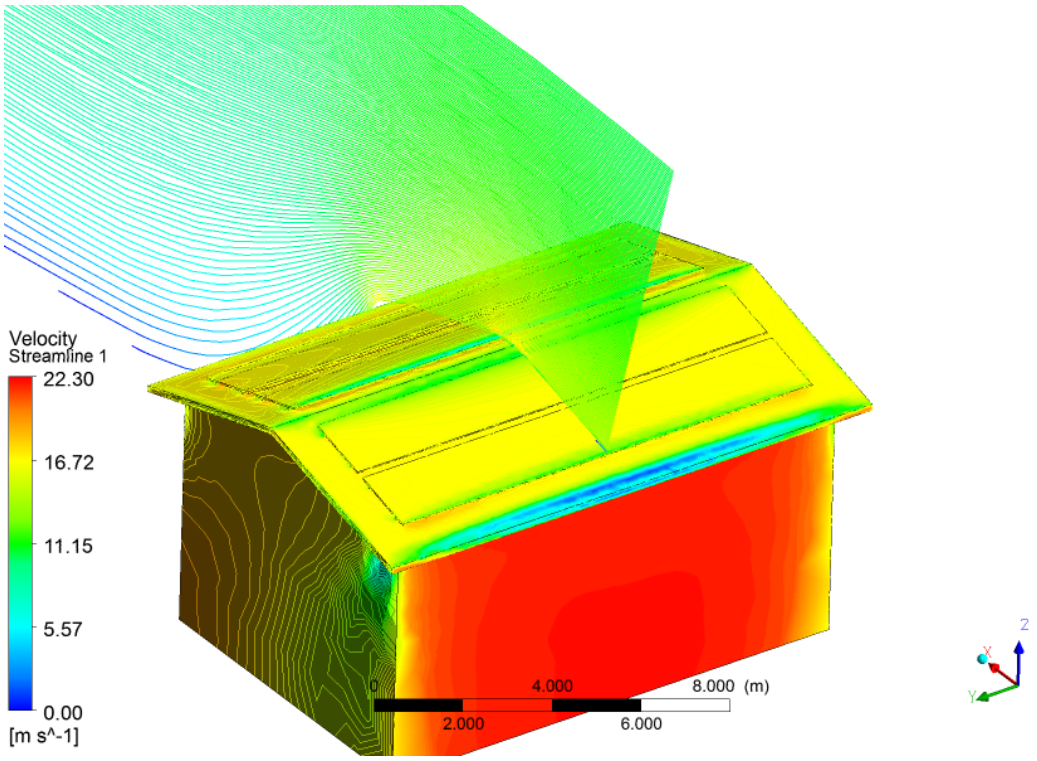


Fig. E. 153. Velocity stream lines at middle cross section plane , WD 90º

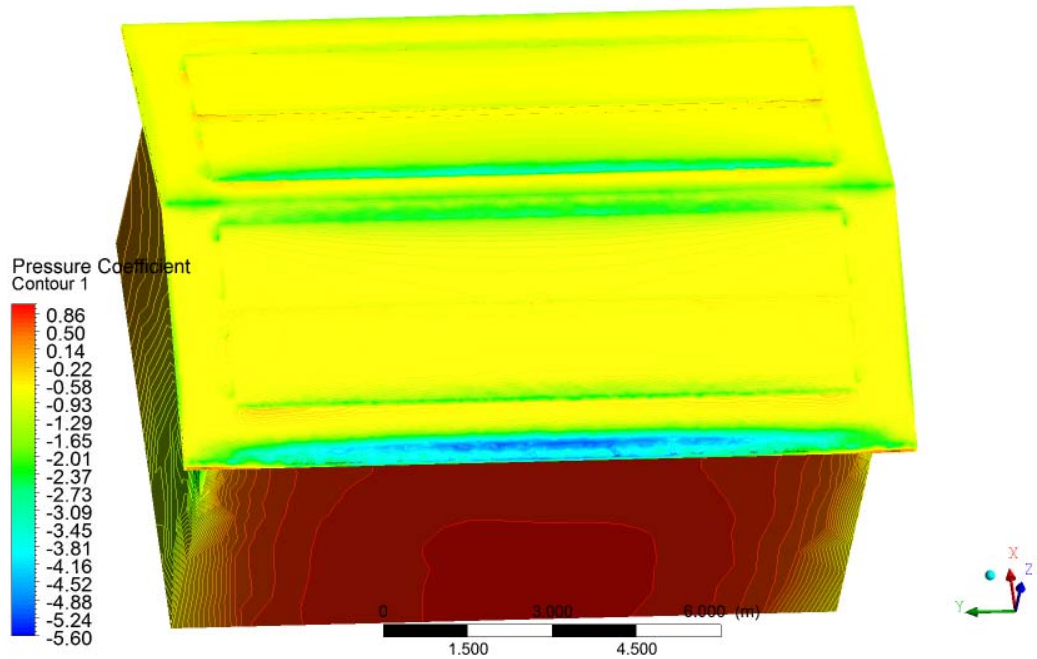


Fig. E. 154. Cp contour whole building, WD 90º, WW

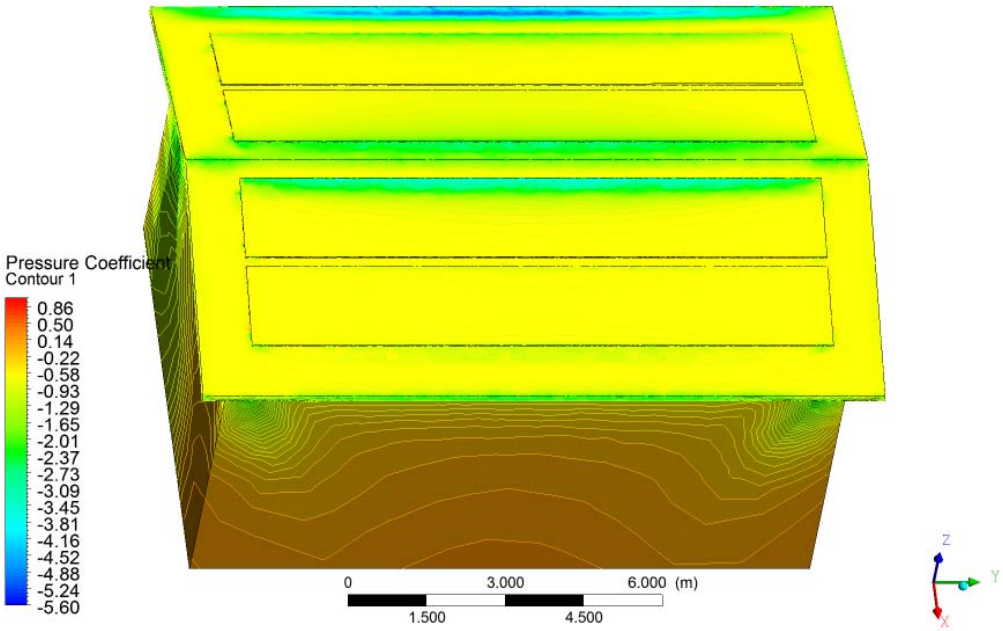


Fig. E. 155. Cp contour whole building, perspective view, WD 90º, LW

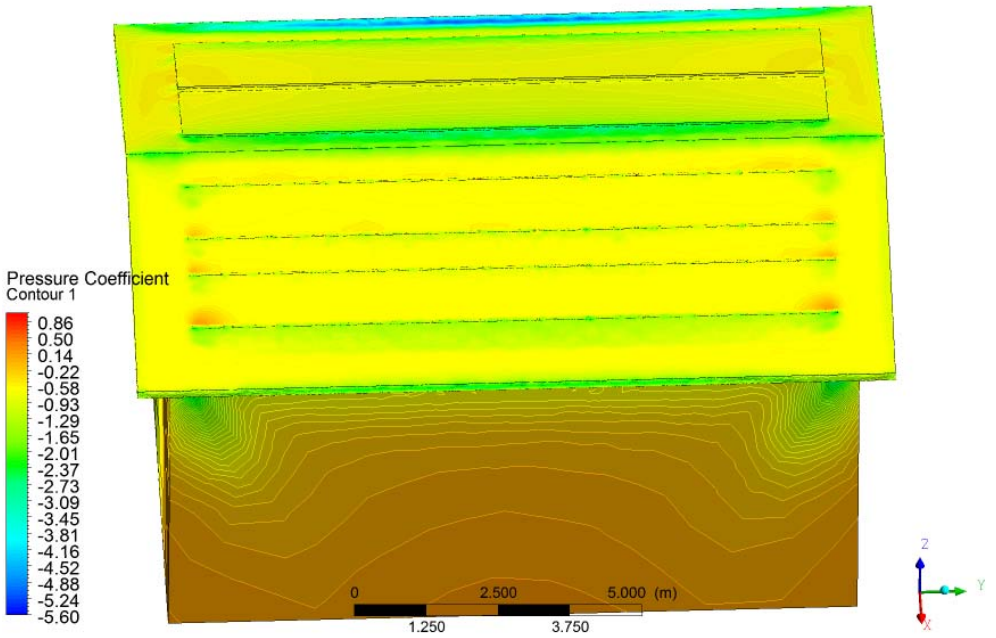


Fig. E. 156. Cp contour whole building, perspective view, roof under panels, WD 90º, LW

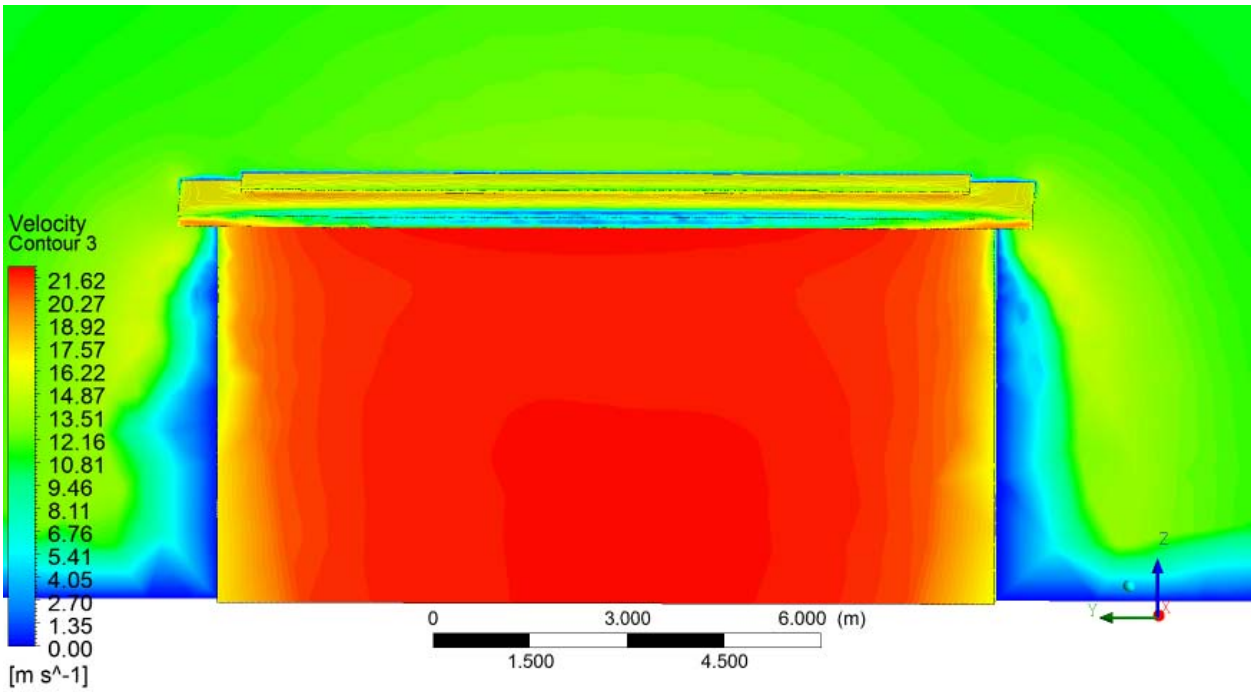


Fig. E. 157. Velocity on a perpendicular longitudinal plane with the house, WD 90º, WW

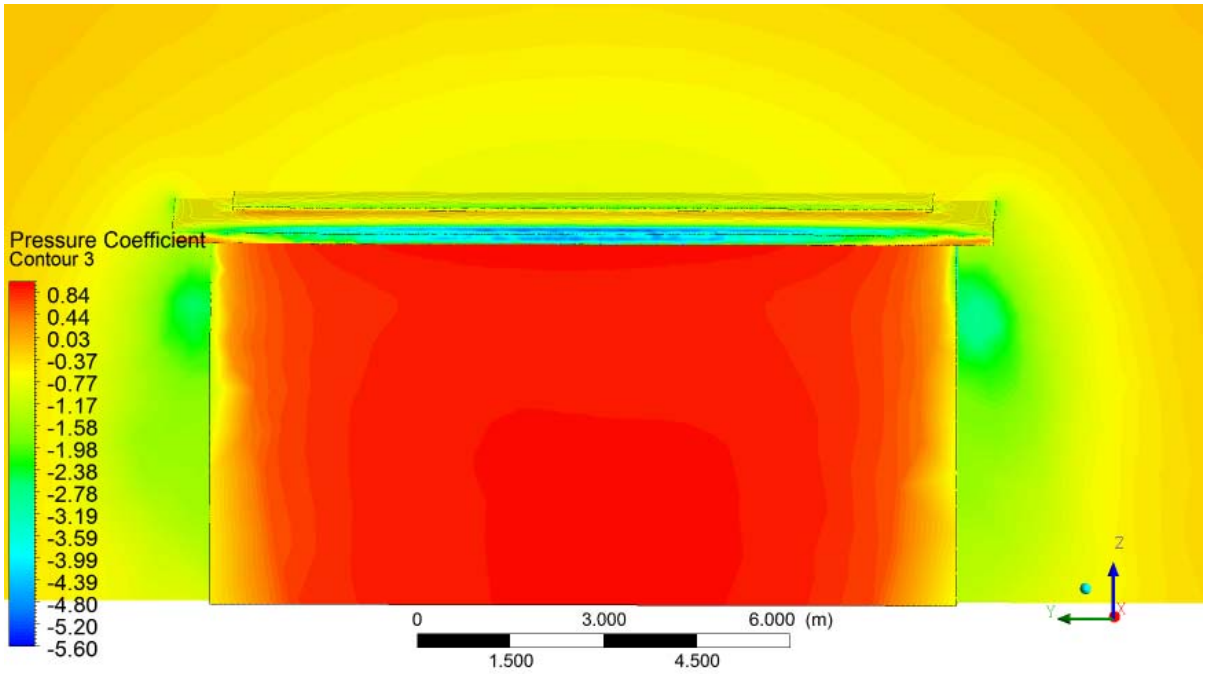


Fig. E. 158. Cp on a perpendicular longitudinal plane with the house, WD 90º, WW

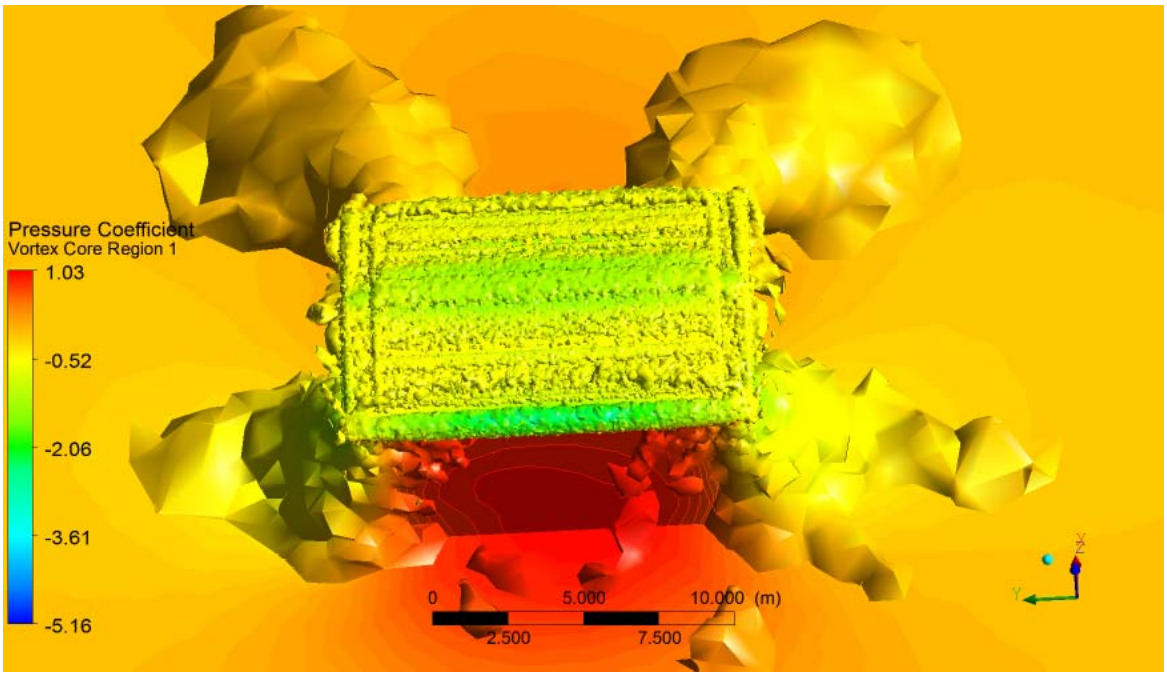


Fig. E. 159. Turbulence distribution on roof and on the building structure, with building contours, WD 90º, WW

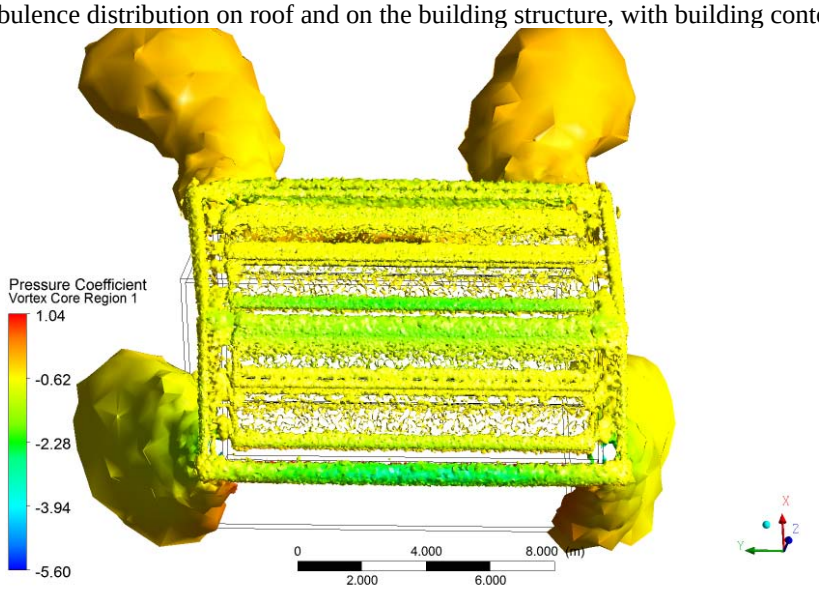


Fig. E. 160. Turbulence distribution on roof and building structure, with No building contours, WD 90º , WW

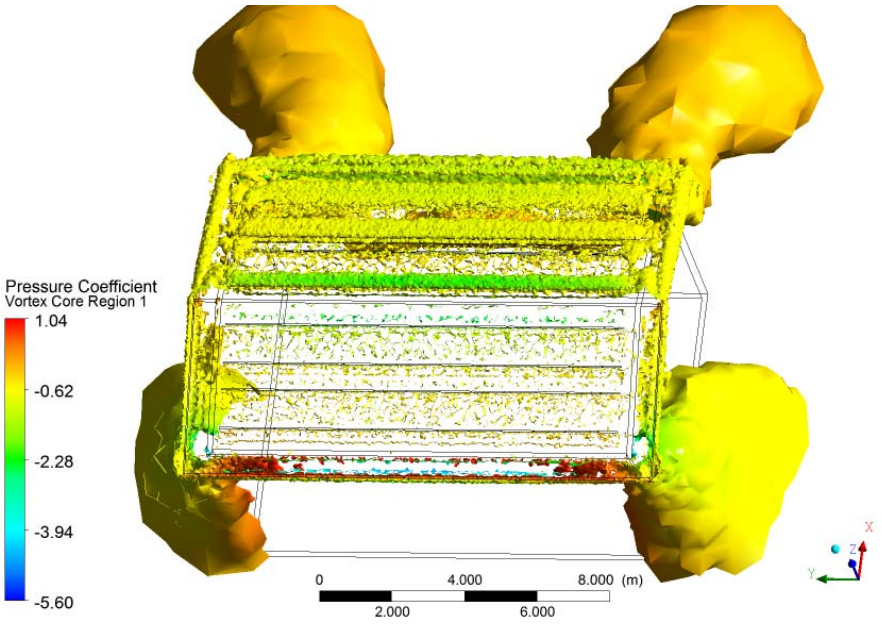


Fig. E. 161. Turbulence distribution on roof under panels and building structure, with No building contours, WW

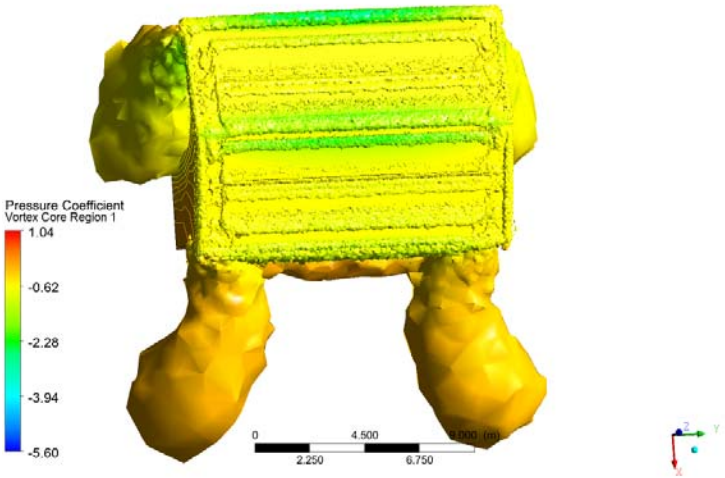


Fig. E. 162. Turbulence distribution on roof and on the building structure, with building contours, WD 90º, LW

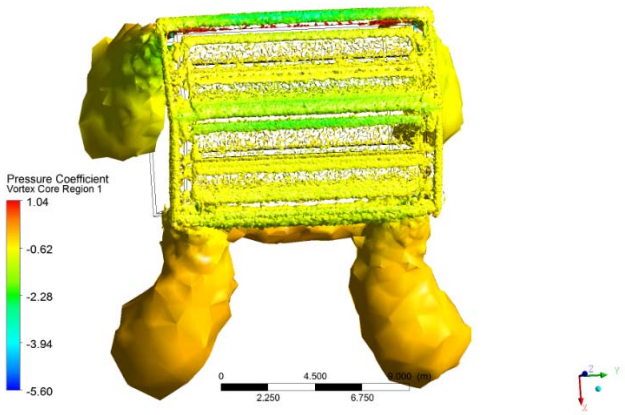


Fig. E. 163. Turbulence distribution on roof and building structure, with No building contours, WD 90º , LW

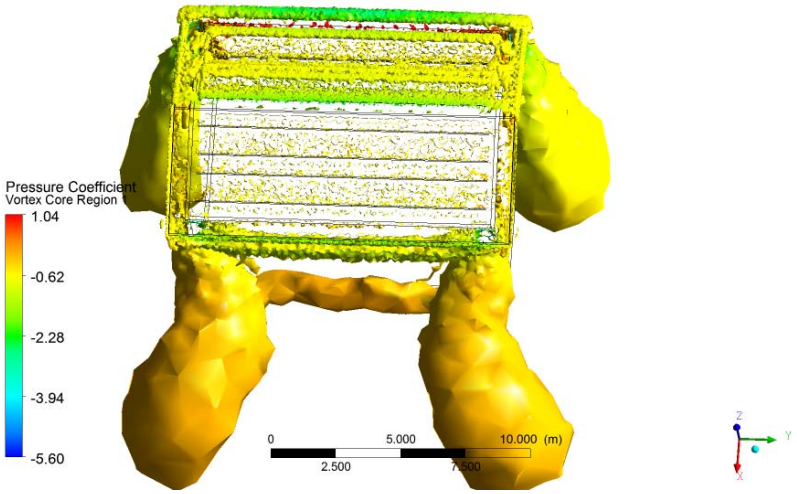


Fig. E. 164. Turbulence distribution on roof under panels and building structure, with No building contours, LW

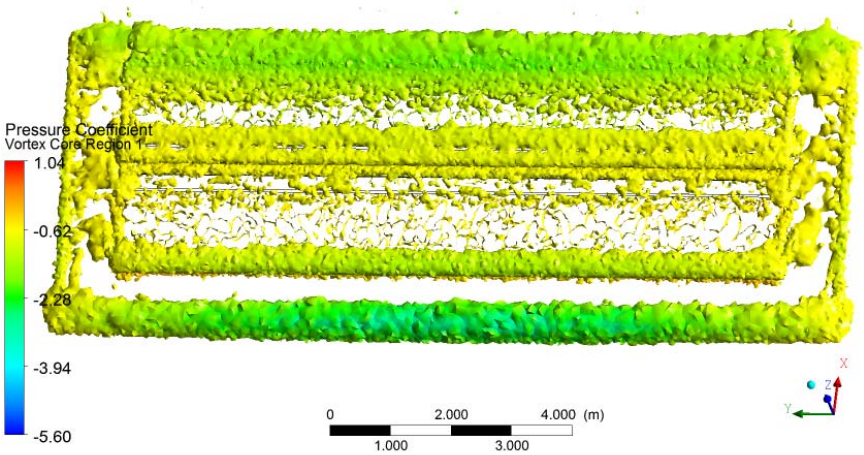


Fig. E. 165. Turbulence distribution, on top of the panels, No building contours shown, WD 90º, WW

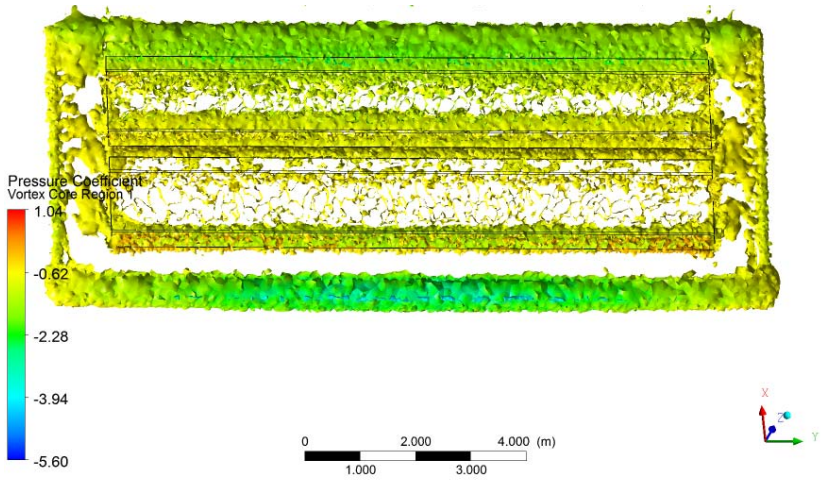


Fig. E. 166. Turbulence distribution, on bottom of the panels, No building contours shown, WD 90º, WW

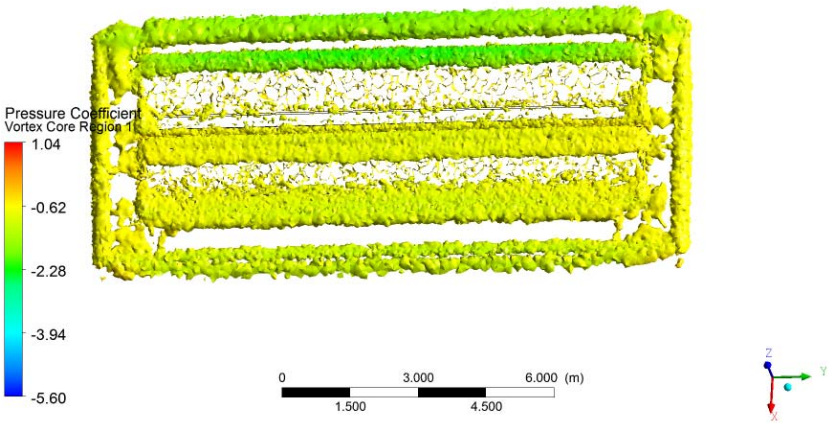


Fig. E. 167. Turbulence distribution, on top of the panels, No building contours shown, WD 90º, LW

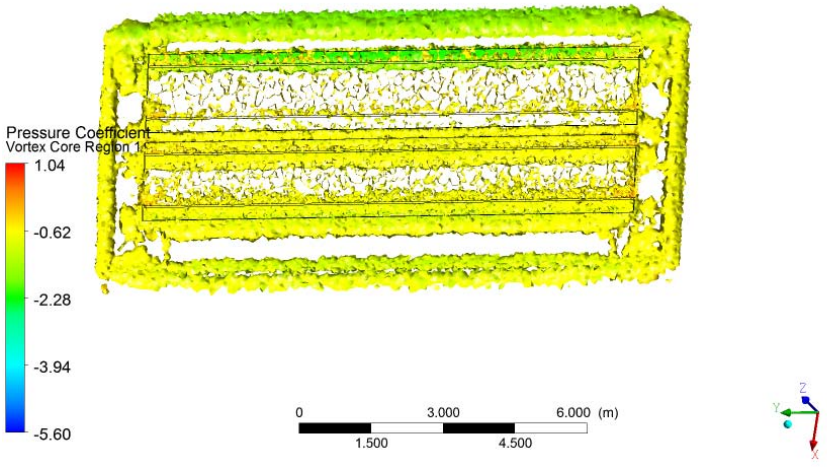


Fig. E. 168. Turbulence distribution, on bottom of the panels, No contours shown, WD 90º, LW

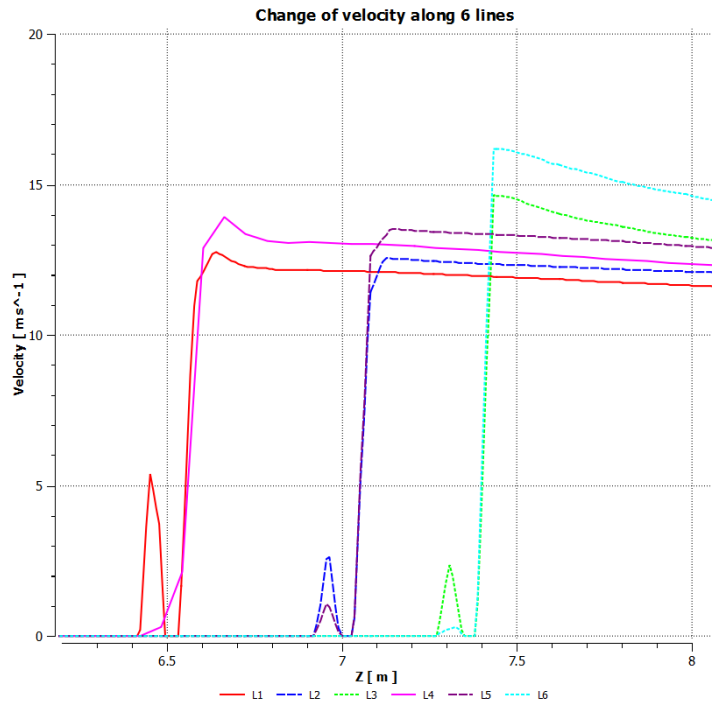


Fig. E. 169. Velocity changes between panels, and above roof, all lines.

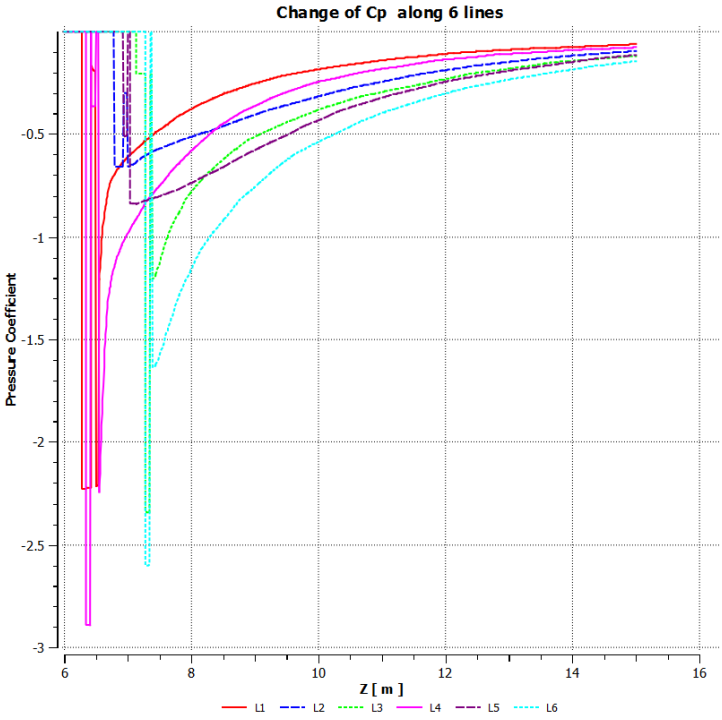
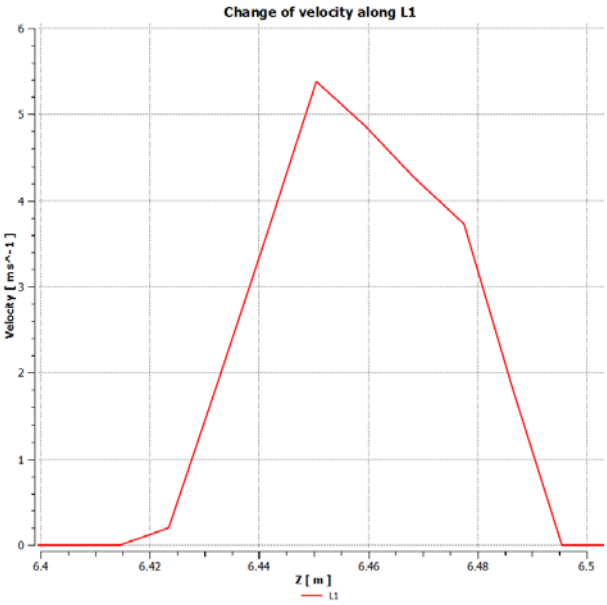
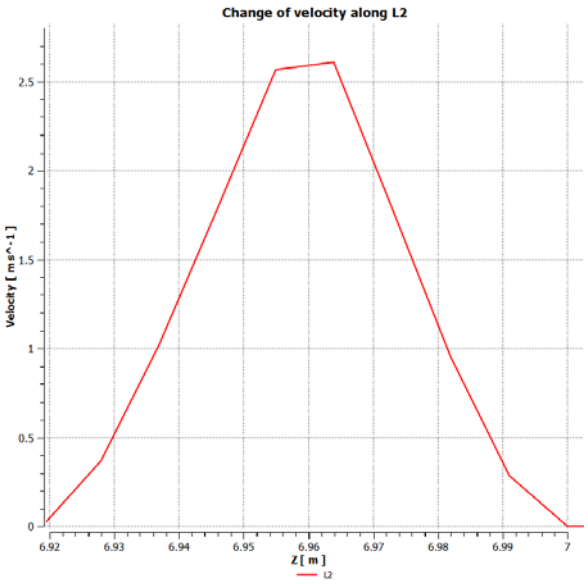
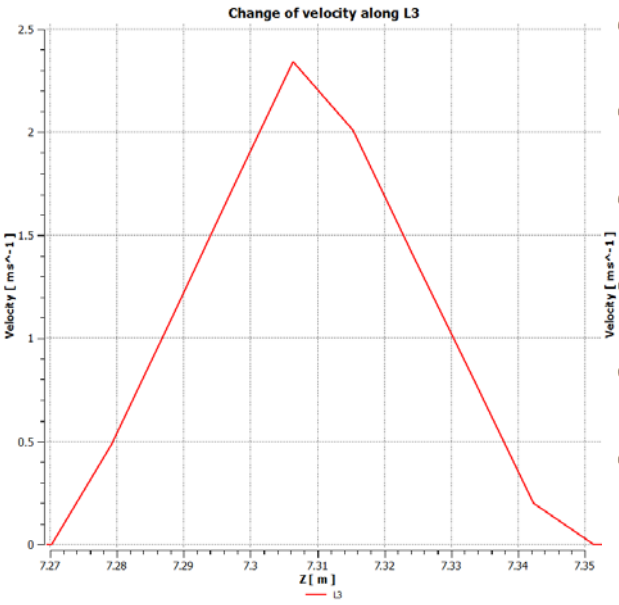
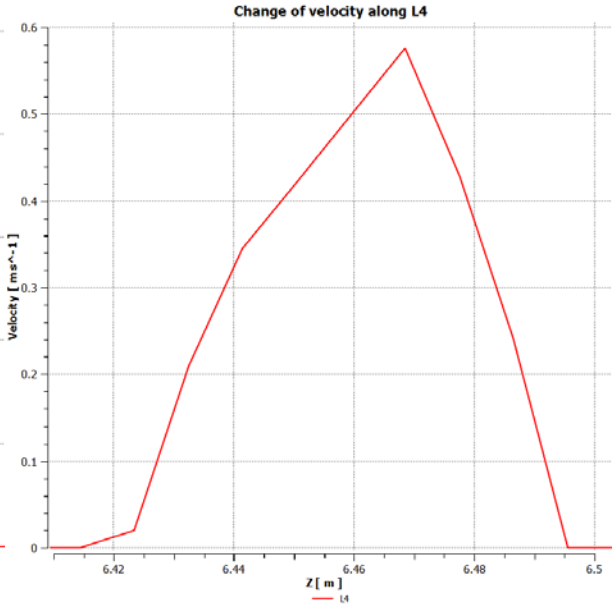


Fig. E. 170. Cp changes between panels, and above roof, all lines.


Change of velocity along L1
Velocity [ms^-1]
Z [m]
L1


Change of velocity along L2
Velocity [ms^-1]
Z [m]
L2


Change of velocity along L3
Velocity [ms^-1]
Z [m]
L3


Change of velocity along L4
Velocity [ms^-1]
Z [m]
L4

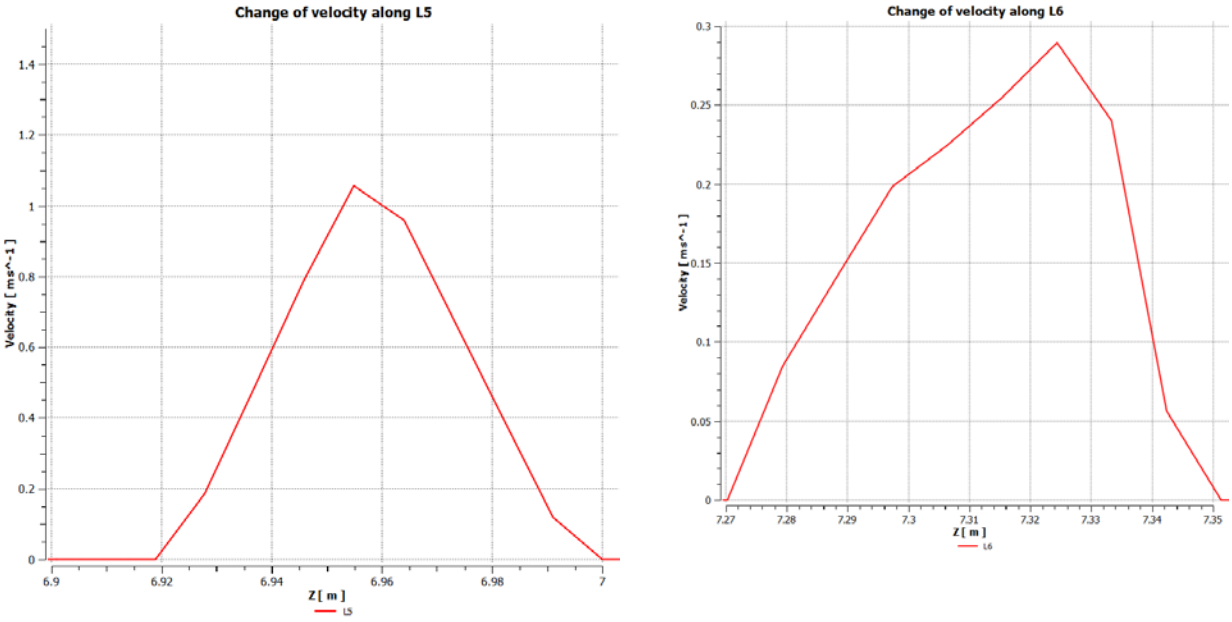
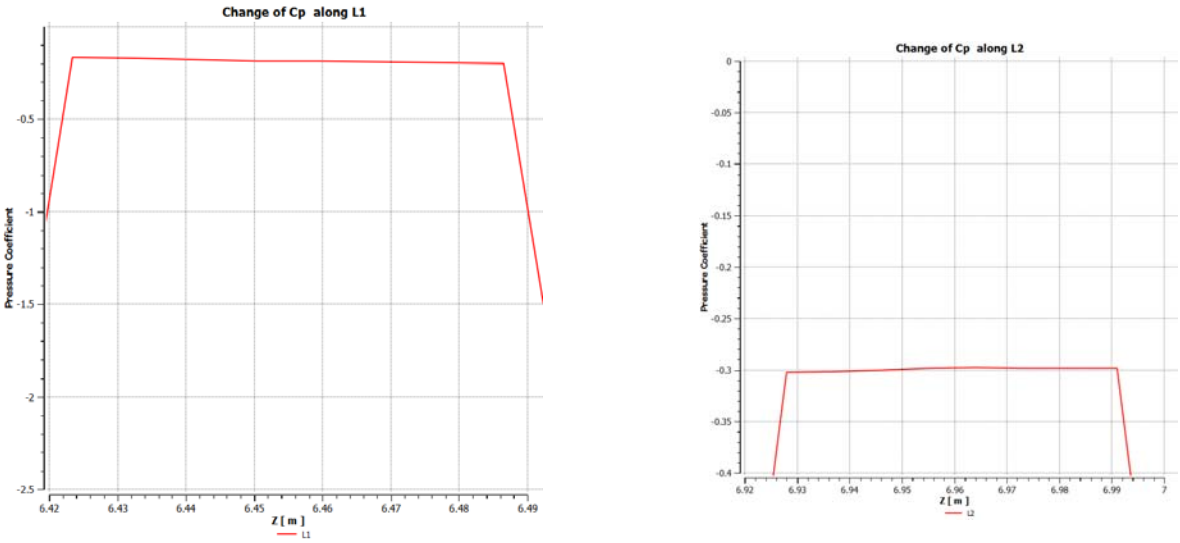


Fig. E. 171. Velocity changes between panels, all lines separated.



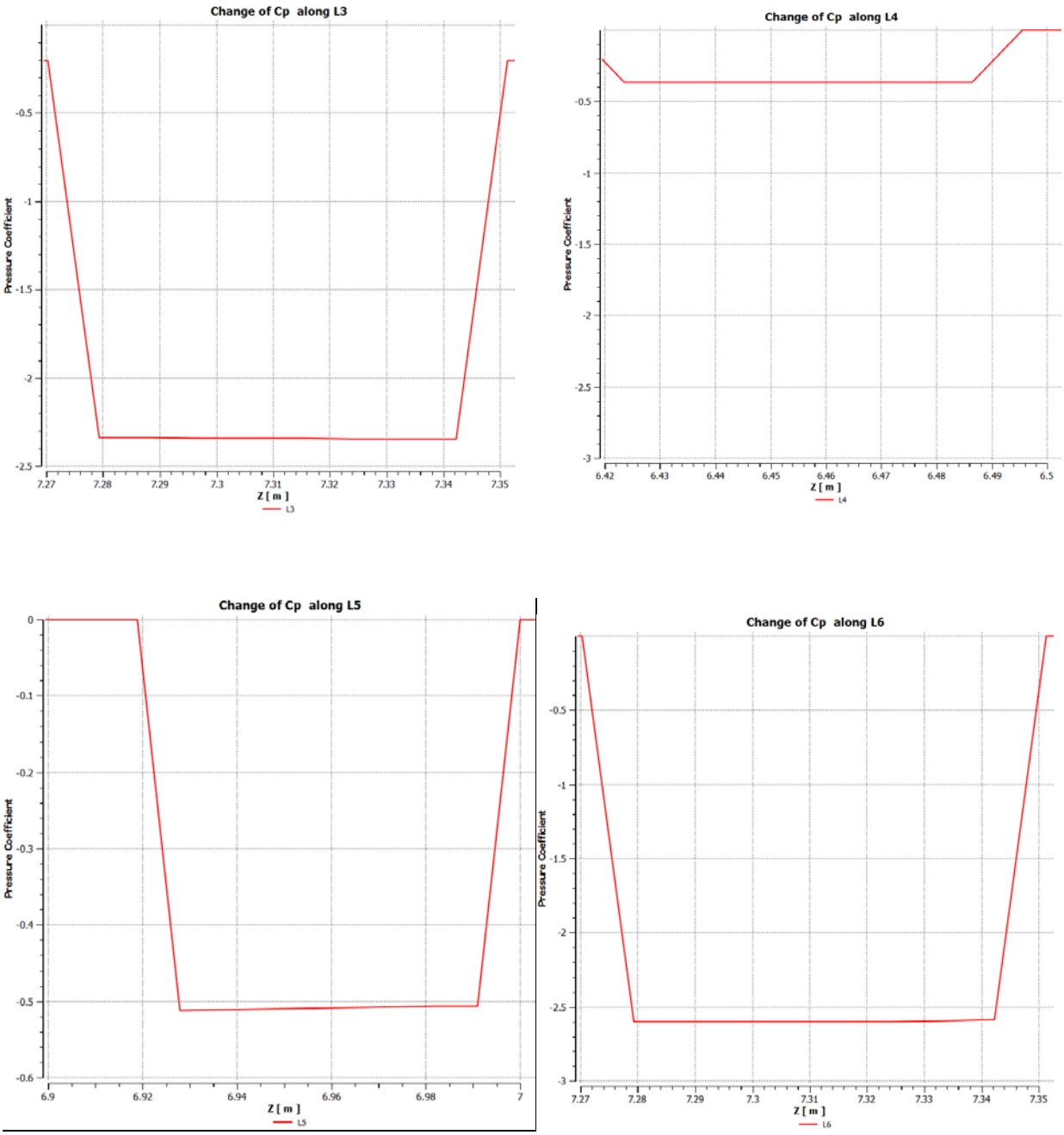


Fig. E. 172. Cp changes between panels, all lines separated.

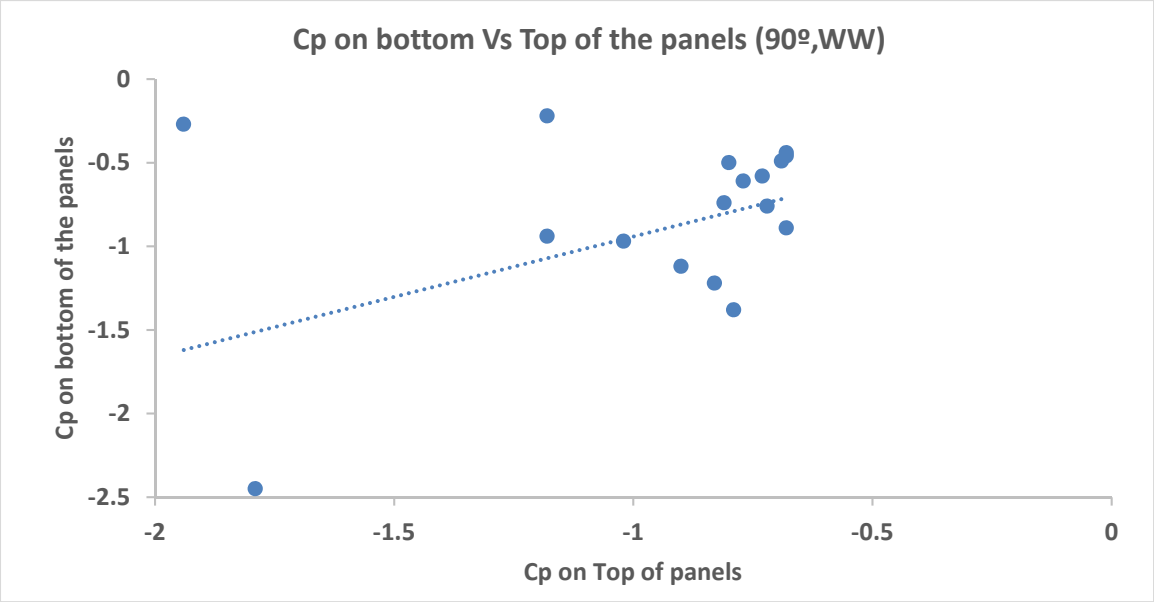


Fig. E. 173. Correlation between Cp on top and bottom of panels surfaces, WW, WD 90º

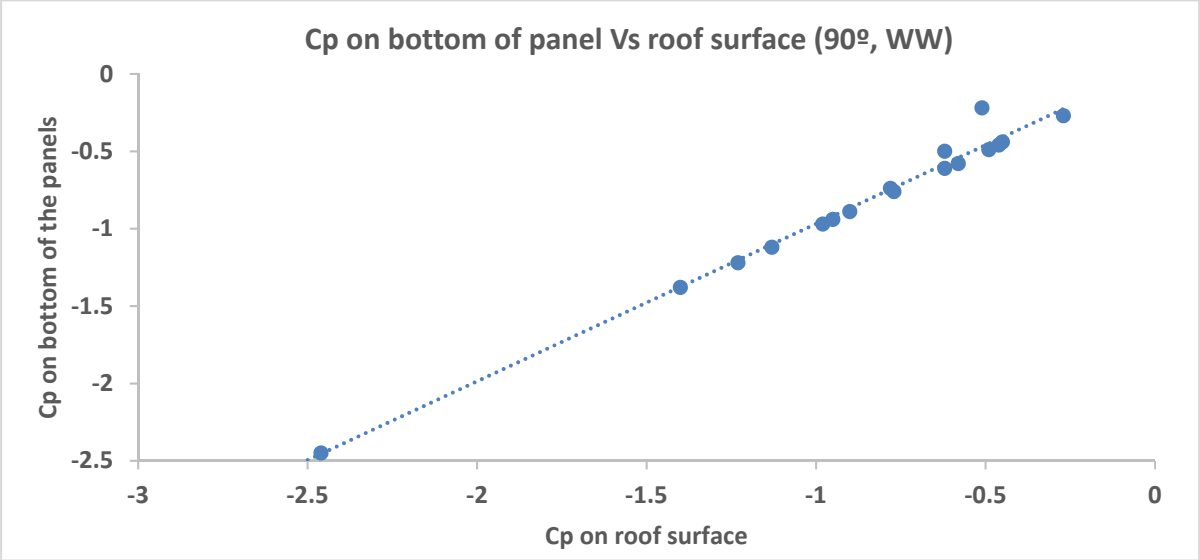


Fig. E. 174. Correlation between Cp on bottom of panels and roof surfaces, WW, WD 90º

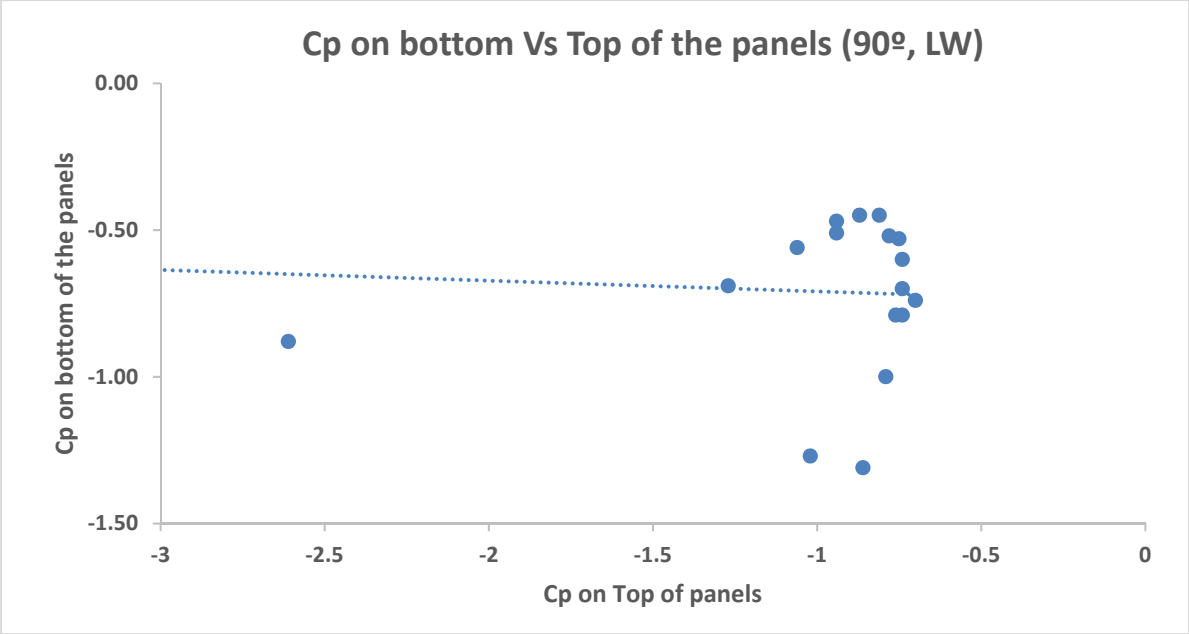


Fig. E. 175. Correlation between Cp on top and bottom of panels surfaces, LW, WD 90º

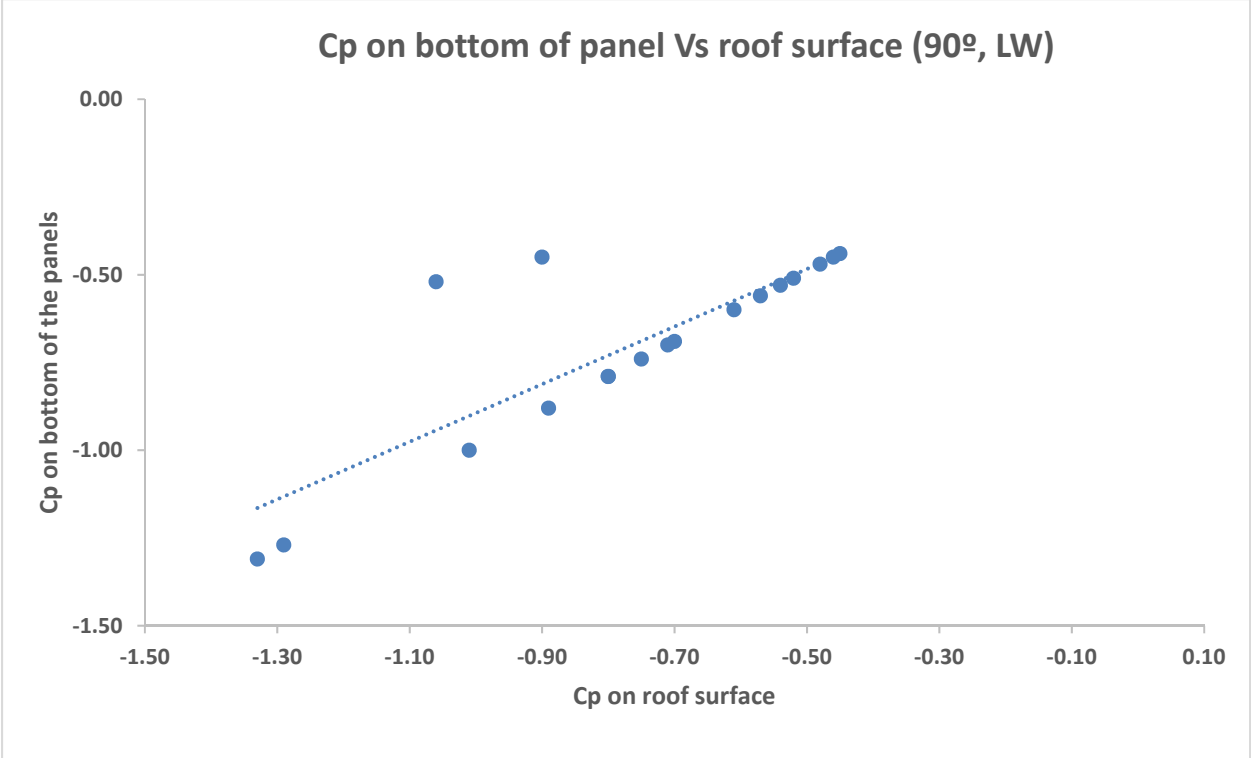


Fig. E. 176. Correlation between Cp on bottom of panels and roof surfaces, LW, WD 90º

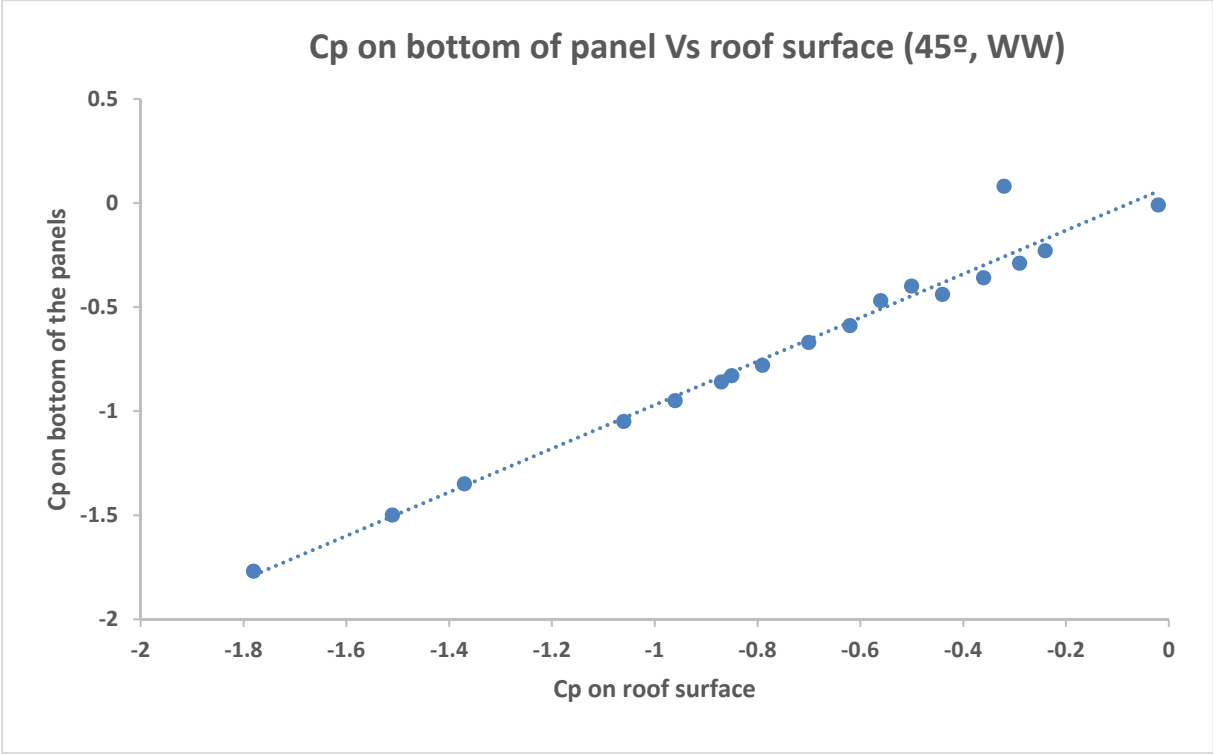


Fig. E. 177. Correlation between Cp on bottom of panels and roof surfaces, WW, WD 45º

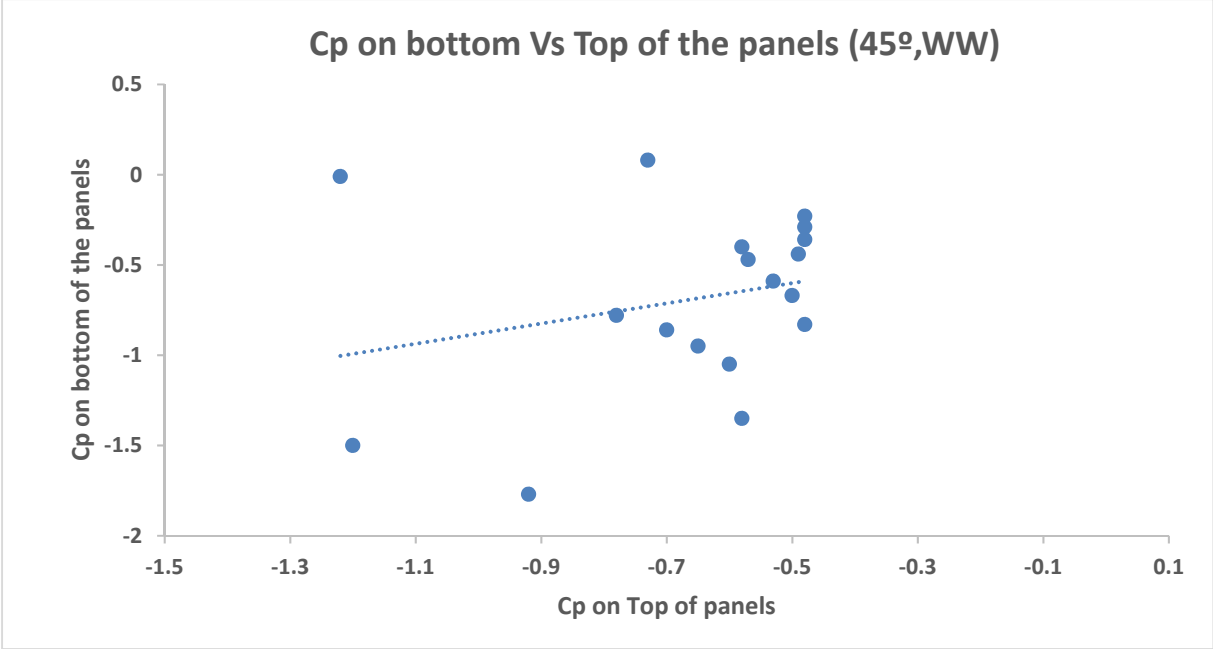


Fig. E. 178. Correlation between Cp on top and bottom of panels surfaces, WW, WD 45º

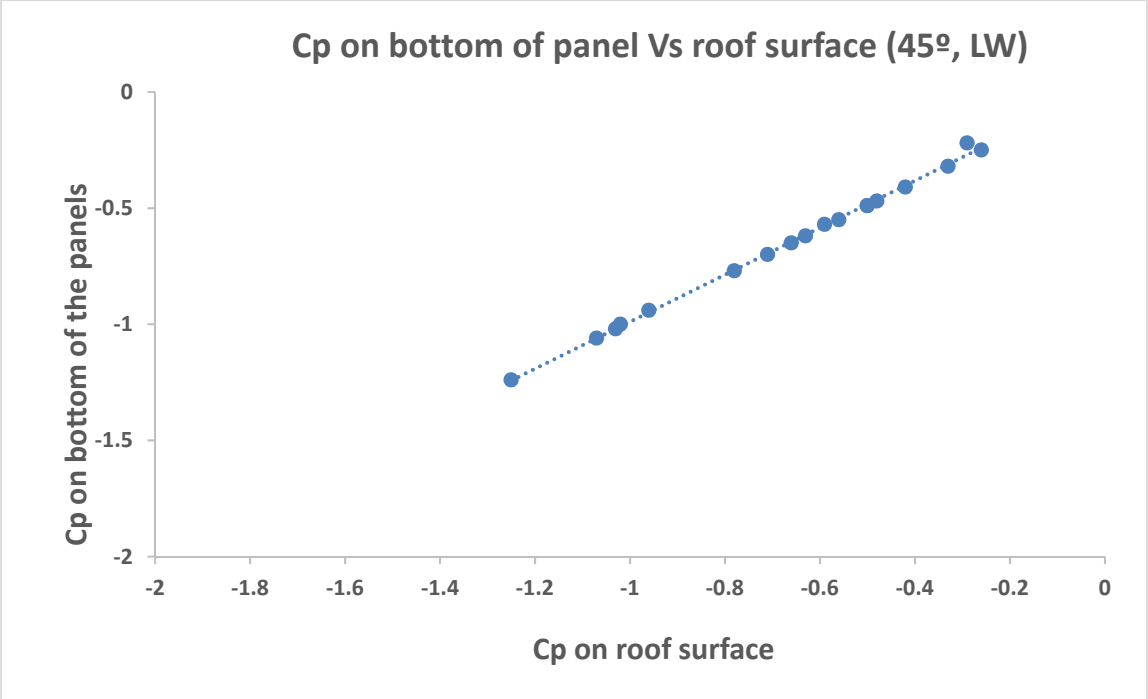


Fig. E. 179. Correlation between Cp on bottom of panels and roof surfaces, LW, WD 45º

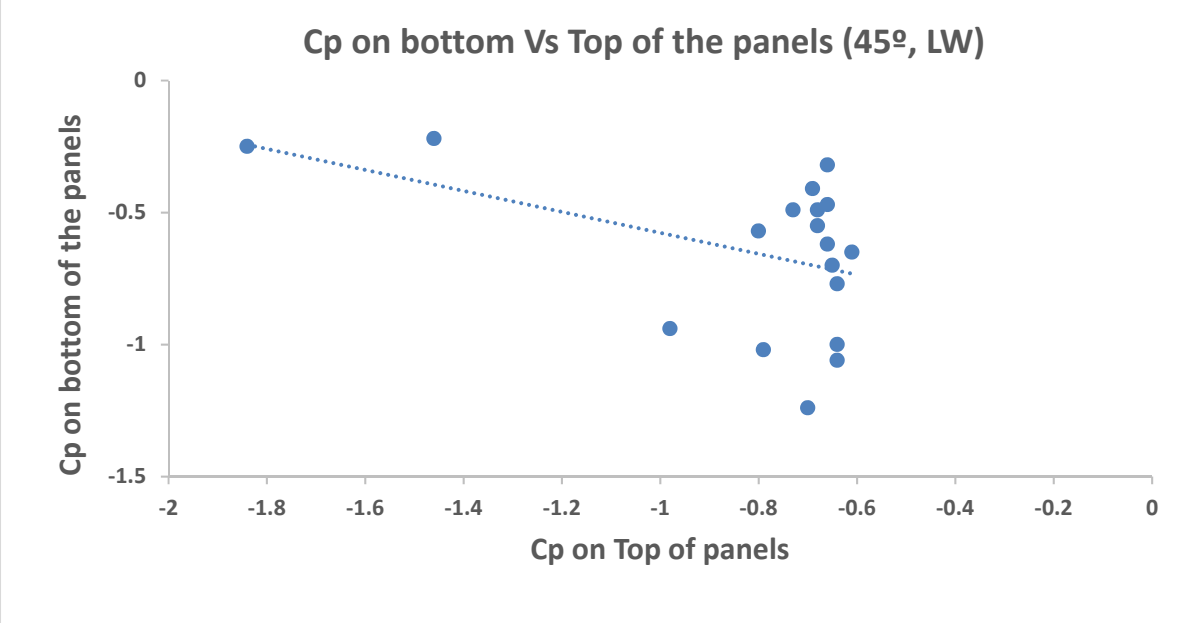


Fig. E. 180. Correlation between Cp on top and bottom of panels surfaces, LW, WD 45º

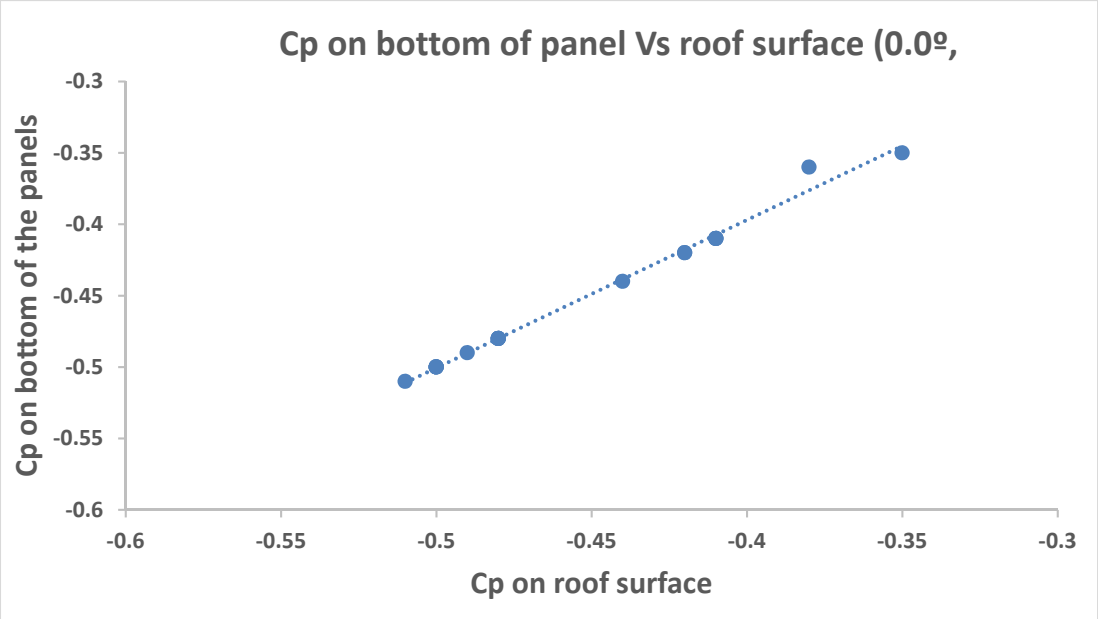


Fig. E. 181. Correlation between Cp on roof surface and bottom of panels, WD 0º

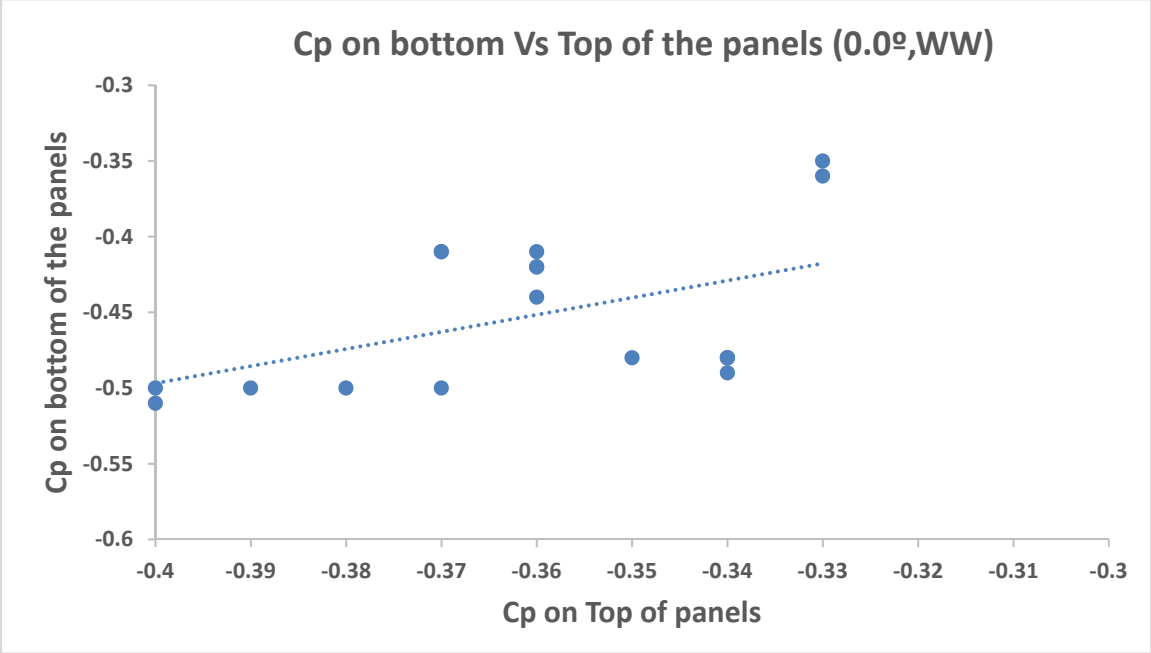


Fig. E. 182. Correlation between Cp on top and bottom of panels surfaces, LW, WD 0º

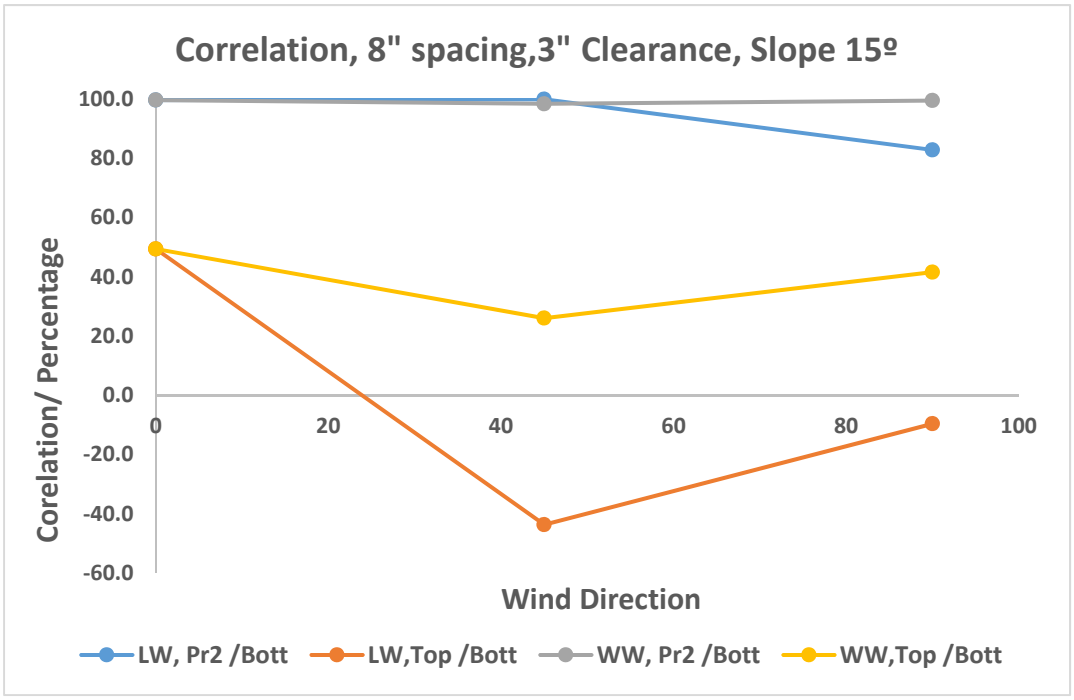


Fig. E. 183. Correlation between Cp on top, bottom of panels and roof surface under the panels with wind directions.

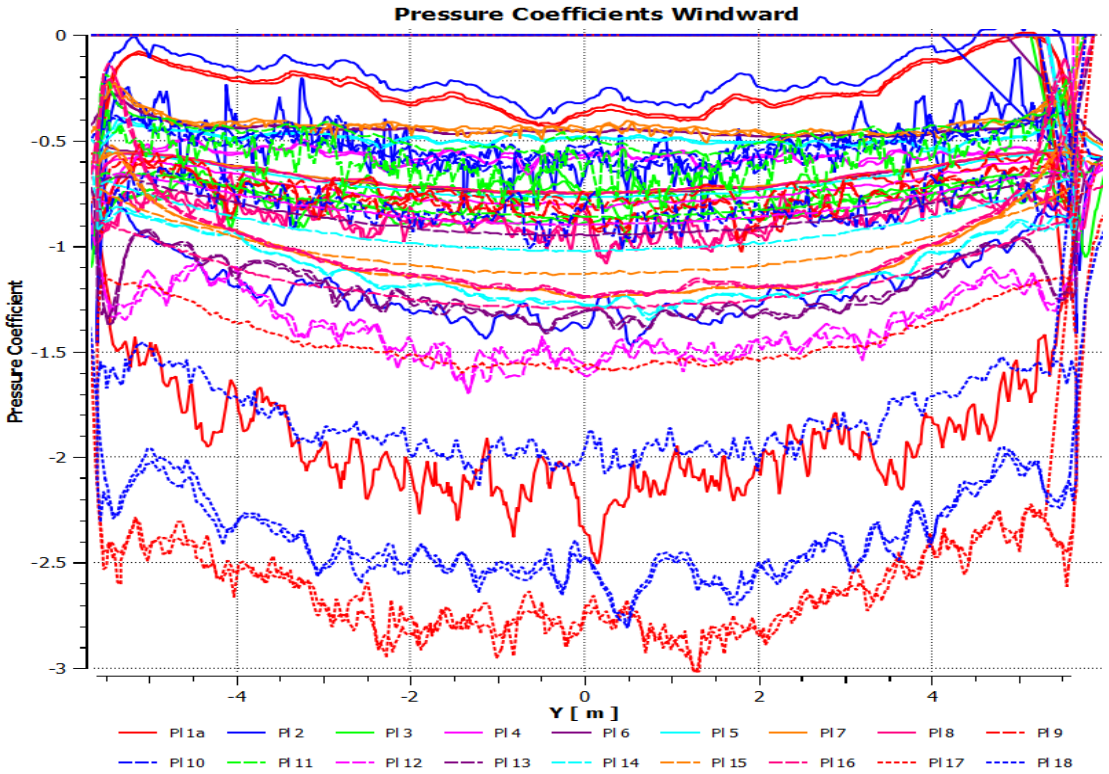


Fig. E. 184. All Cp charts, WW, WD 90º

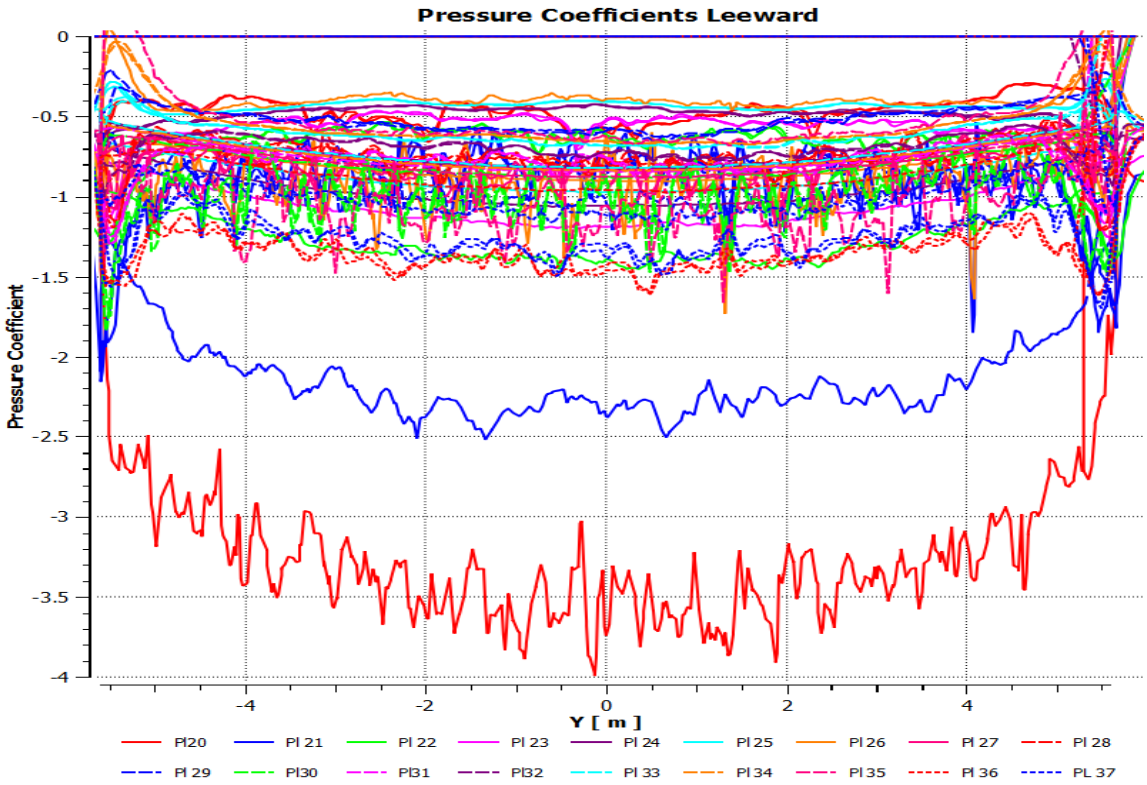


Fig. E. 185. All Cp charts, LW, WD 90º

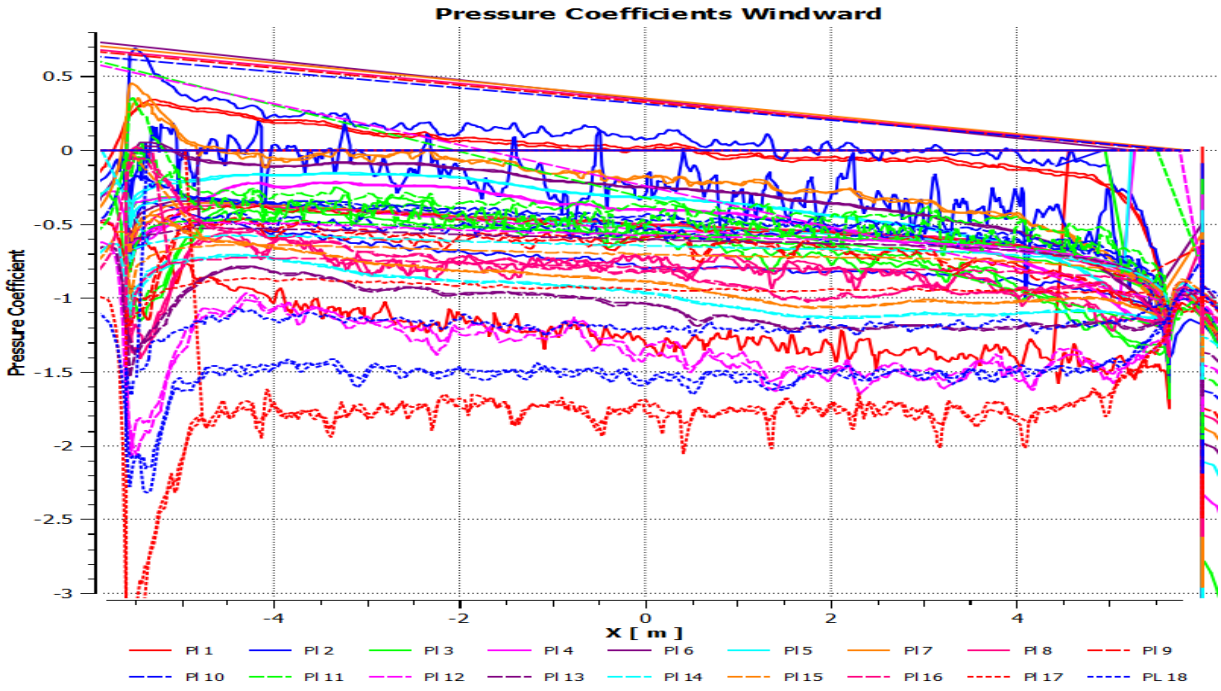


Fig. E. 186. All Cp charts, WW, WD 45º

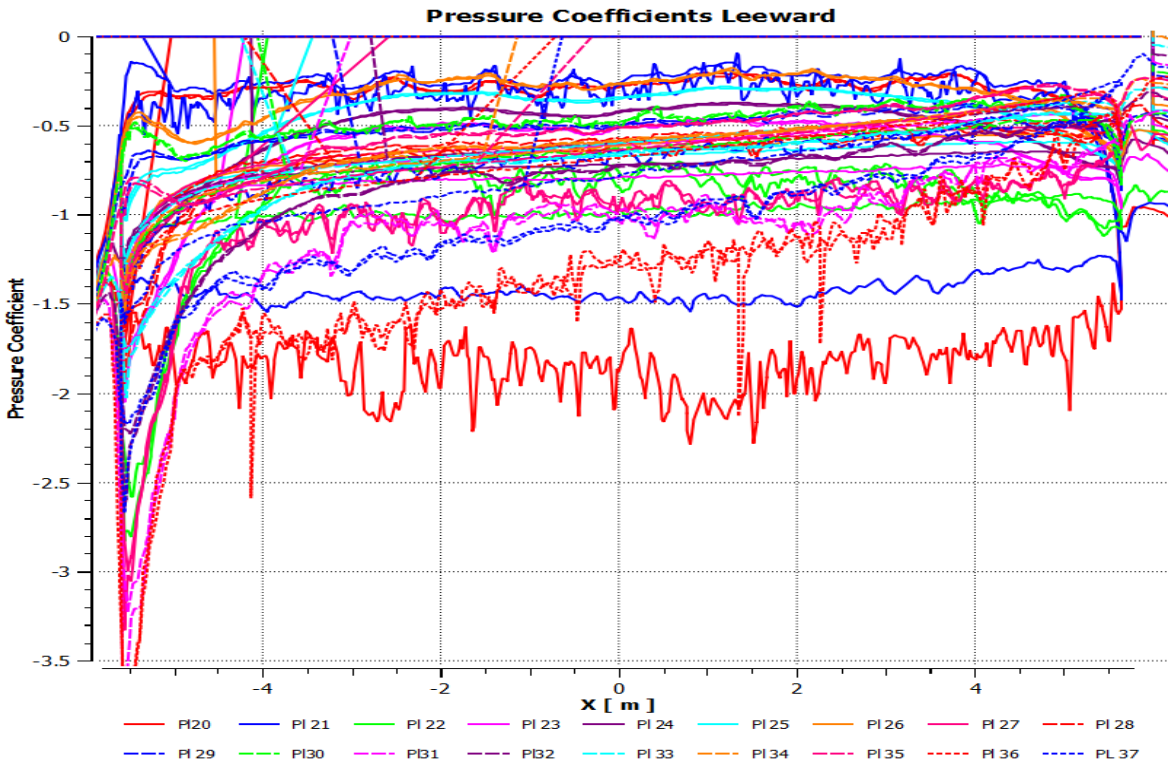


Fig. E. 187. All Cp charts, LW, WD 45º

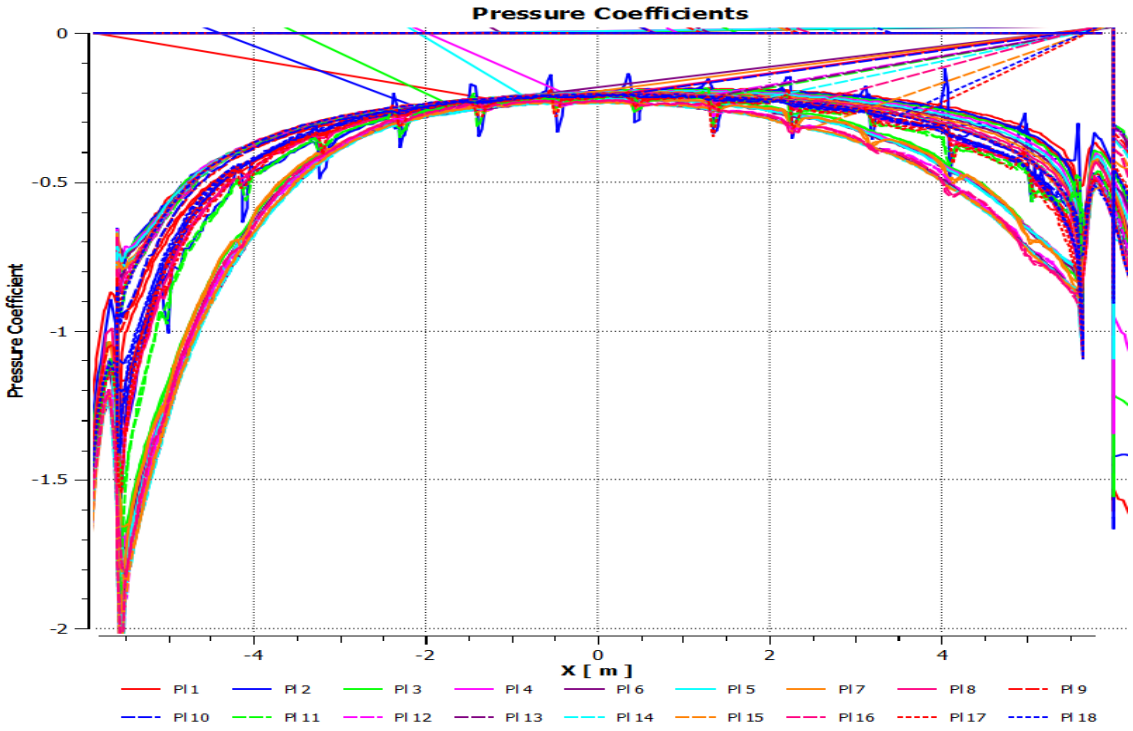


Fig. E. 188. All Cp charts, WD 0º

1.2.5. Integration of Cp on The Three Surfaces and the Resultant of CP on Roof Mounted Solar Panels in Comparison with Bare Roof, S8"C3"

Tabulated results of the integration,

Table E. 11. Cp on bare roof Vs. roof under solar panels and solar panels surfaces, Slope 15º, 45º, WW

Polylines	Cp (SP)	Pr2	Cp Bott	Diff	Ttl Cp	Ttl/Brf
Pl1A	-1.22	-0.02	-0.01	-1.21	-1.23	2.32
Pl2	-0.73	-0.32	0.08	-0.81	-1.13	2.22
Pl3	-0.53	-0.62	-0.59	0.06	-0.56	1.10
Pl4	-0.49	-0.44	-0.44	-0.05	-0.49	0.96
Pl5	-0.48	-0.36	-0.36	-0.12	-0.48	0.94
Pl6	-0.48	-0.29	-0.29	-0.19	-0.48	0.96
Pl7	-0.48	-0.24	-0.23	-0.25	-0.49	0.98
Pl8	-0.48	-0.85	-0.83	0.35	-0.5	1.00
Pl9	-0.5	-0.70	-0.67	0.17	-0.53	1.04
Pl10	-0.57	-0.56	-0.47	-0.10	-0.66	1.29
Pl11	-0.58	-0.50	-0.40	-0.18	-0.68	1.31
Pl12	-0.58	-1.37	-1.35	0.77	-0.6	1.11
Pl13	-0.6	-1.06	-1.05	0.45	-0.61	1.09
Pl14	-0.65	-0.96	-0.95	0.30	-0.66	1.12
Pl15	-0.7	-0.87	-0.86	0.16	-0.71	1.16
Pl16	-0.78	-0.79	-0.78	0.00	-0.79	1.34
Pl17	-0.92	-1.78	-1.77	0.85	-0.93	1.58
Pl18	-1.2	-1.51	-1.50	0.30	-1.21	1.98
Cp	-0.67	-0.74	-0.69	0.03	-0.71	1.27
SDT	0.23	0.47	0.50	0.49	0.25	0.44
Cov	0.35	0.64	0.72	17.77	0.36	0.34

Table E. 12. Cp on bare roof Vs. Top of Panels, Slope 15º, 45º, WW

Polylines	Cp Bare roof	Cp (SP)	Cp (SP/BRf)
Pl1A	-0.53	-1.22	2.30
Pl2	-0.51	-0.73	1.43
Pl3	-0.51	-0.53	1.04
Pl4	-0.51	-0.49	0.96
Pl5	-0.51	-0.48	0.94
Pl6	-0.5	-0.48	0.96
Pl7	-0.5	-0.48	0.96
Pl8	-0.5	-0.48	0.96
Pl9	-0.51	-0.5	0.98
Pl10	-0.51	-0.57	1.12

Pl11	-0.52	-0.58	1.12
Pl12	-0.54	-0.58	1.07
Pl13	-0.56	-0.6	1.07
Pl14	-0.59	-0.65	1.10
Pl15	-0.61	-0.7	1.15
Pl16	-0.65	-0.78	1.20
Pl17	-0.7	-0.92	1.31
Pl18	-0.75	-1.2	1.60
Cp	-0.56	-0.67	1.20
SDT	0.08	0.23	0.33
Cov	0.13	0.35	0.28

Table E. 13. Cp on bare roof Vs. roof under solar panels and solar panels surfaces, Slope 15º, WD 45º, LW

Polylines	Cp (SP)	Pr2	Cp Bott	Diff	Ttl Cp	Ttl/Brf
Pl20a	-1.84	-0.26	-0.25	-1.59	-1.85	2.08
Pl21	-1.46	-0.29	-0.22	-1.24	-1.53	1.89
Pl22	-0.98	-0.96	-0.94	-0.04	-1	1.35
Pl23	-0.8	-0.59	-0.57	-0.23	-0.82	1.21
Pl24	-0.73	-0.5	-0.49	-0.24	-0.74	1.16
Pl25	-0.69	-0.42	-0.41	-0.28	-0.7	1.13
Pl26	-0.66	-0.33	-0.32	-0.34	-0.67	1.10
Pl27	-0.64	-1.02	-1.00	0.36	-0.66	1.10
Pl28	-0.61	-0.66	-0.65	0.04	-0.62	1.04
Pl29	-0.68	-0.50	-0.49	-0.19	-0.69	1.17
Pl30	-0.66	-0.48	-0.47	-0.19	-0.67	1.15
Pl31	-0.64	-1.07	-1.06	0.42	-0.65	1.12
Pl32	-0.64	-0.78	-0.77	0.13	-0.65	1.13
Pl33	-0.65	-0.71	-0.70	0.05	-0.66	1.16
Pl34	-0.66	-0.63	-0.62	-0.04	-0.67	1.20
Pl35	-0.68	-0.56	-0.55	-0.13	-0.69	1.25
Pl36	-0.7	-1.25	-1.24	0.54	-0.71	1.31
Pl37	-0.79	-1.03	-1.02	0.23	-0.8	1.43
Cp	-0.81	-0.67	-0.65	-0.15	-0.82	1.28
SDT	0.33	0.29	0.30	0.53	0.33	0.28
Cov	0.40	0.44	0.45	3.46	0.41	0.22

Table E. 14. Cp bare roof Vs. Top of Panels, Slope 15º, WD 45º, LW

Polylines	Bare Roof	Cp (SP)	Cp (SP/BRf)
Pl20A	-0.89	-1.84	2.07
Pl21	-0.81	-1.46	1.80
Pl22	-0.74	-0.98	1.32
Pl23	-0.68	-0.8	1.18
Pl24	-0.64	-0.73	1.14
Pl25	-0.62	-0.69	1.11

Pl26	-0.61	-0.66	1.08
Pl27	-0.60	-0.64	1.07
Pl28	-0.60	-0.61	1.03
Pl29	-0.59	-0.68	1.15
Pl30	-0.59	-0.66	1.13
Pl31	-0.58	-0.64	1.10
Pl32	-0.58	-0.64	1.11
Pl33	-0.57	-0.65	1.14
Pl34	-0.56	-0.66	1.18
Pl35	-0.55	-0.68	1.24
Pl36	-0.54	-0.7	1.30
Pl37	-0.56	-0.79	1.41
Cp	-0.63	-0.81	1.25
SDT	0.10	0.33	0.27
Cov	0.15	0.40	0.22

Table E. 15. Cp on bare roof Vs. roof under solar panels and solar panels surfaces, Slope 15º, WD 90º, WW

Polylines	Cp (SP)	Pr2	Cp Bott	Diff	Ttl Cp	Ttl/Brf
Pl1A	-1.94	-0.27	-0.27	-1.67	-1.94	1.41
Pl2	-1.18	-0.51	-0.22	-0.96	-1.47	1.79
Pl3	-0.81	-0.78	-0.74	-0.07	-0.85	1.39
Pl4	-0.73	-0.58	-0.58	-0.15	-0.73	1.35
Pl5	-0.69	-0.49	-0.49	-0.20	-0.69	1.30
Pl6	-0.68	-0.46	-0.46	-0.22	-0.68	1.28
Pl7	-0.68	-0.45	-0.44	-0.24	-0.69	1.21
Pl8	-0.68	-0.90	-0.89	0.21	-0.69	1.28
Pl9	-0.72	-0.77	-0.76	0.04	-0.73	1.28
Pl10	-0.8	-0.62	-0.50	-0.30	-0.92	1.53
Pl11	-0.77	-0.62	-0.61	-0.16	-0.78	1.24
Pl12	-0.79	-1.40	-1.38	0.59	-0.81	1.23
Pl13	-0.83	-1.23	-1.22	0.39	-0.84	1.18
Pl14	-0.9	-1.13	-1.12	0.22	-0.91	1.18
Pl15	-1.02	-0.98	-0.97	-0.05	-1.03	1.23
Pl16	-1.18	-0.95	-0.94	-0.24	-1.19	1.68
Pl17	-1.43	-2.65	-2.63	1.20	-1.45	2.04
Pl18	-1.79	-2.46	-2.45	0.66	-1.8	2.34
Cp	-0.98	-0.96	-0.93	-0.05	-1.01	1.40
SDT	0.38	0.65	0.67	0.62	0.40	0.32
Cov	0.39	0.68	0.72	11.70	0.39	0.23

Table E. 16. Cp bare roof Vs top of panels, Slope 15º, WD 90º, WW

Polylines	Cp Bare roof	Cp (SP)	Cp (SP/BRf)
Pl1A	-1.38	-1.94	1.41
Pl2	-0.82	-1.18	1.44
Pl3	-0.61	-0.81	1.33
Pl4	-0.54	-0.73	1.35
Pl5	-0.53	-0.69	1.30
Pl6	-0.53	-0.68	1.28
Pl7	-0.57	-0.68	1.19
Pl8	-0.54	-0.68	1.26
Pl9	-0.57	-0.72	1.26
Pl10	-0.60	-0.8	1.33
Pl11	-0.63	-0.77	1.22
Pl12	-0.66	-0.79	1.20
Pl13	-0.71	-0.83	1.17
Pl14	-0.77	-0.9	1.17
Pl15	-0.84	-1.02	1.21
Pl16	-0.80	-1.18	1.48
Pl17	-0.92	-1.43	1.55
Pl18	-0.96	-1.79	1.86
Cp	-0.72	-0.98	1.36
SDT	0.22	0.38	0.17
Cov	0.30	0.39	0.13

Table E. 17. Cp on bare roof Vs. roof under solar panels and solar panels surfaces, Slope 15º, WD 90º, LW

Polylines	Cp (SP)	Pr2	Cp Bott	Diff	Ttl Cp	Ttl/Brf
Pl20	-3.28	-0.45	-0.44	-2.84	-3.29	2.99
Pl21	-2.61	-0.89	-0.88	-1.73	-2.62	2.67
Pl22	-1.27	-0.70	-0.69	-0.58	-1.28	1.42
Pl23	-1.06	-0.57	-0.56	-0.50	-1.07	1.26
Pl24	-0.94	-0.48	-0.47	-0.47	-0.95	1.23
Pl25	-0.87	-0.46	-0.45	-0.42	-0.88	1.22
Pl26	-0.81	-0.9	-0.45	-0.36	-1.26	1.85
Pl27	-0.74	-0.8	-0.79	0.05	-0.75	1.14
Pl28	-0.7	-0.75	-0.74	0.04	-0.71	1.11
Pl29	-0.94	-0.52	-0.51	-0.43	-0.95	1.53
Pl30	-0.79	-1.01	-1.00	0.21	-0.8	1.31
Pl31	-0.76	-0.80	-0.79	0.03	-0.77	1.33
Pl32	-0.74	-0.71	-0.70	-0.04	-0.75	1.34
Pl33	-0.74	-0.61	-0.60	-0.14	-0.75	1.36
Pl34	-0.75	-0.54	-0.53	-0.22	-0.76	1.43
Pl35	-0.78	-1.06	-0.52	-0.26	-1.32	2.54
Pl36	-0.86	-1.33	-1.31	0.45	-0.88	1.80
Pl37	-1.02	-1.29	-1.27	0.25	-1.04	2.17
Cp	-1.09	-0.77	-0.71	-0.39	-1.16	1.65

SDT	0.11	0.28	0.28	0.29	0.19	0.41
Cov	0.10	0.36	0.40	0.76	0.16	0.25

Table E. 18. Cp bare roof Vs top of panels, Slope 15º, WD 90º, LW

Polylines	Bare Roof	Cp (SP)	Cp (SP/BRf)
Pl20	-1.10	-3.28	2.98
Pl21	-0.98	-2.61	2.66
Pl22	-0.90	-1.27	1.41
Pl23	-0.85	-1.06	1.25
Pl24	-0.77	-0.94	1.22
Pl25	-0.72	-0.87	1.21
Pl26	-0.68	-0.81	1.19
Pl27	-0.66	-0.74	1.12
Pl28	-0.64	-0.7	1.09
Pl29	-0.62	-0.94	1.52
Pl30	-0.61	-0.79	1.30
Pl31	-0.58	-0.76	1.31
Pl32	-0.56	-0.74	1.32
Pl33	-0.55	-0.74	1.35
Pl34	-0.53	-0.75	1.42
Pl35	-0.52	-0.78	1.50
Pl36	-0.49	-0.86	1.76
Pl37	-0.48	-1.02	2.13
Cp	-0.68	-1.09	1.38
SDT	0.11	0.11	0.27
Cov	0.16	0.10	0.19

Table E. 19. Cp on bare roof Vs. roof under solar panels and solar panels surfaces, Slope 15º, 0º

Polylines	Cp (SP)	Pr2	Cp Bott	Diff	Ttl Cp	Ttl/Brf
Pl1A	-0.33	-0.35	-0.35	0.02	-0.33	0.75
Pl2	-0.33	-0.38	-0.36	0.03	-0.35	0.78
Pl3	-0.34	-0.48	-0.48	0.14	-0.34	0.74
Pl4	-0.34	-0.49	-0.49	0.15	-0.34	0.72
Pl5	-0.34	-0.48	-0.48	0.14	-0.34	0.71
Pl6	-0.35	-0.48	-0.48	0.13	-0.35	0.71
Pl7	-0.34	-0.48	-0.48	0.14	-0.34	0.69
Pl8	-0.36	-0.42	-0.42	0.06	-0.36	0.73
Pl9	-0.37	-0.41	-0.41	0.04	-0.37	0.74
Pl10	-0.37	-0.41	-0.41	0.04	-0.37	0.73
Pl11	-0.36	-0.44	-0.44	0.08	-0.36	0.71
Pl12	-0.37	-0.5	-0.5	0.13	-0.37	0.73
Pl13	-0.38	-0.5	-0.5	0.12	-0.38	0.75
Pl14	-0.39	-0.5	-0.5	0.11	-0.39	0.76

Pl15	-0.4	-0.51	-0.51	0.11	-0.4	0.77
Pl16	-0.4	-0.5	-0.5	0.10	-0.4	0.77
Pl17	-0.36	-0.42	-0.42	0.06	-0.36	0.69
Pl18	-0.36	-0.41	-0.41	0.05	-0.36	0.69
Cp	-0.36	-0.45	-0.45	0.09	-0.36	0.73
SDT	0.02	0.05	0.05	0.04	0.02	0.03
Cov	0.06	0.11	0.11	0.48	0.06	0.04

Table E. 20. Cp bare roof Vs. Top of Solar Panels, Slope 15º, WD 0º

Polylines	Cp Bare roof	Cp (SP)	Cp (SP/BRf)
Pl1A	-0.44	-0.33	0.75
Pl2	-0.45	-0.33	0.73
Pl3	-0.46	-0.34	0.74
Pl4	-0.47	-0.34	0.72
Pl5	-0.48	-0.34	0.71
Pl6	-0.49	-0.35	0.71
Pl7	-0.49	-0.34	0.69
Pl8	-0.49	-0.36	0.73
Pl9	-0.5	-0.37	0.74
Pl10	-0.51	-0.37	0.73
Pl11	-0.51	-0.36	0.71
Pl12	-0.51	-0.37	0.73
Pl13	-0.51	-0.38	0.75
Pl14	-0.51	-0.39	0.76
Pl15	-0.52	-0.4	0.77
Pl16	-0.52	-0.4	0.77
Pl17	-0.52	-0.36	0.69
Pl18	-0.52	-0.36	0.69
Cp	-0.49	-0.36	0.73
SDT	0.03	0.02	0.03
Cov	0.05	0.06	0.03

1.3. 8” Spacing, 10” Clearance

1.3.1. Wind direction 45º,

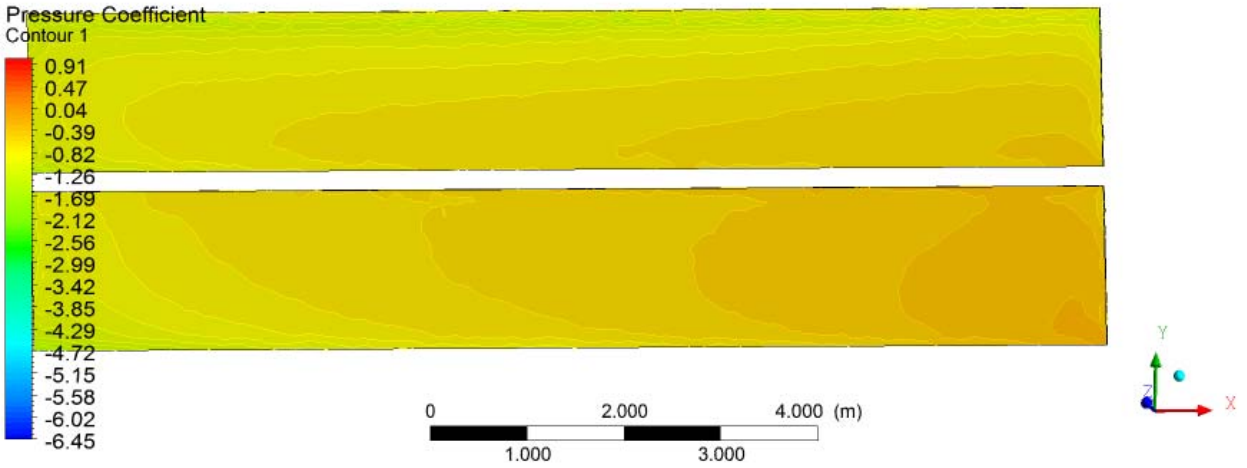


Fig. E. 189. Cp on top of the solar panels, WW, WD 45º

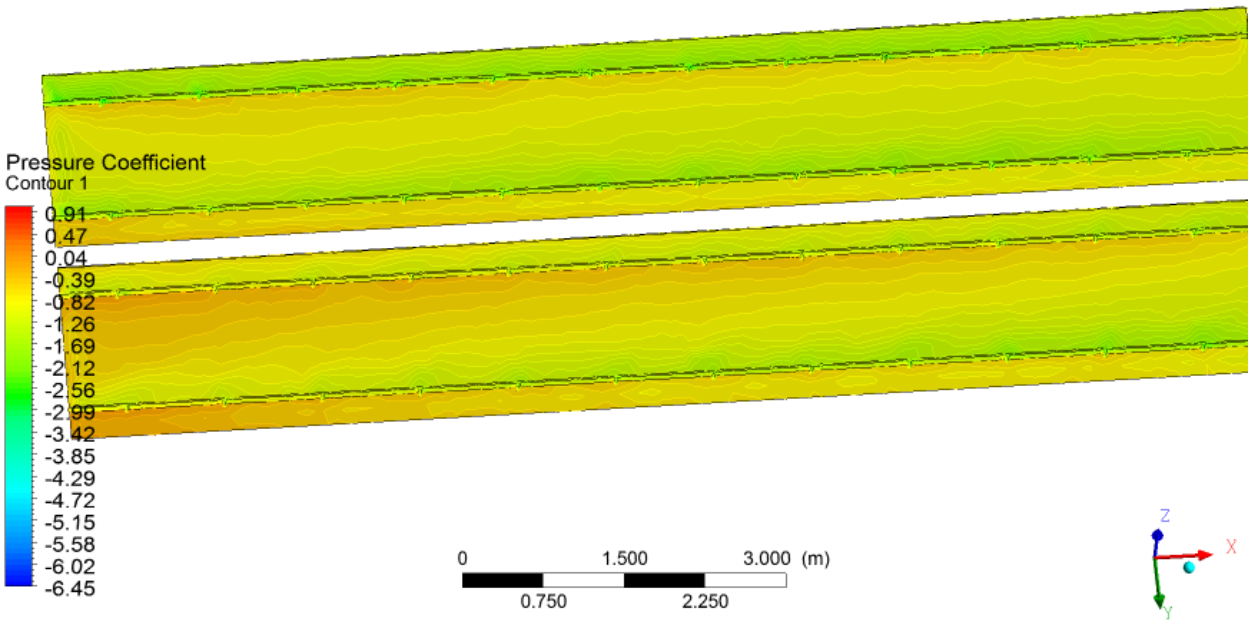


Fig. E. 190. Cp on bottom of the solar panels, WW, WD 45º

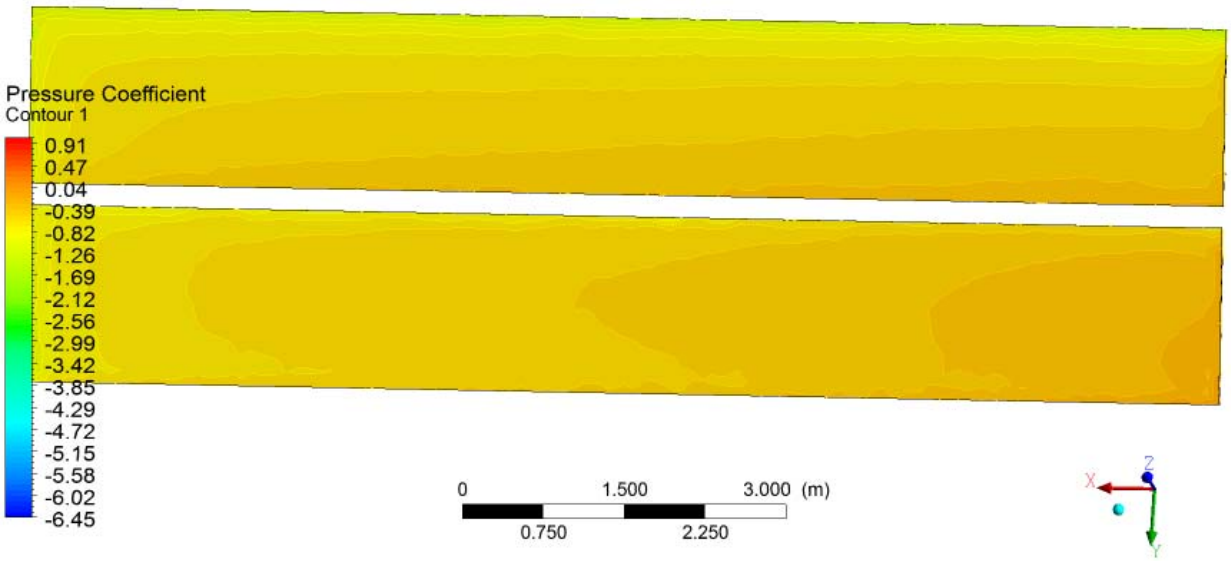


Fig. E. 191. Cp on top of the solar panels, LW, WD 45º

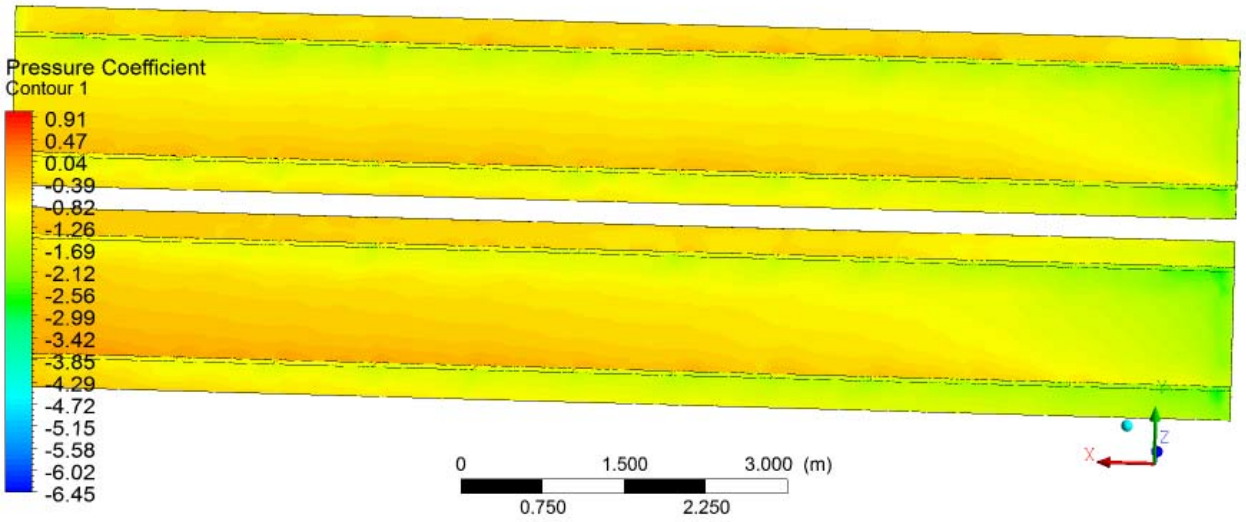


Fig. E. 192. Cp on bottom of the solar panels, LW, WD 45º

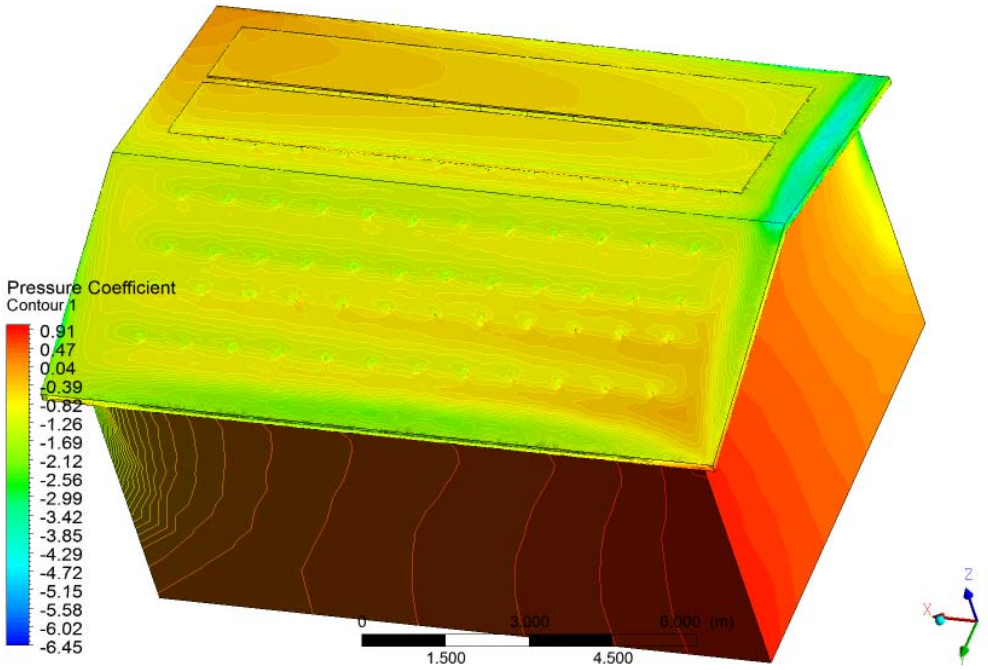


Fig. E. 193. Cp on roof under the solar panels, cut off solar panels, WW, WD 45º

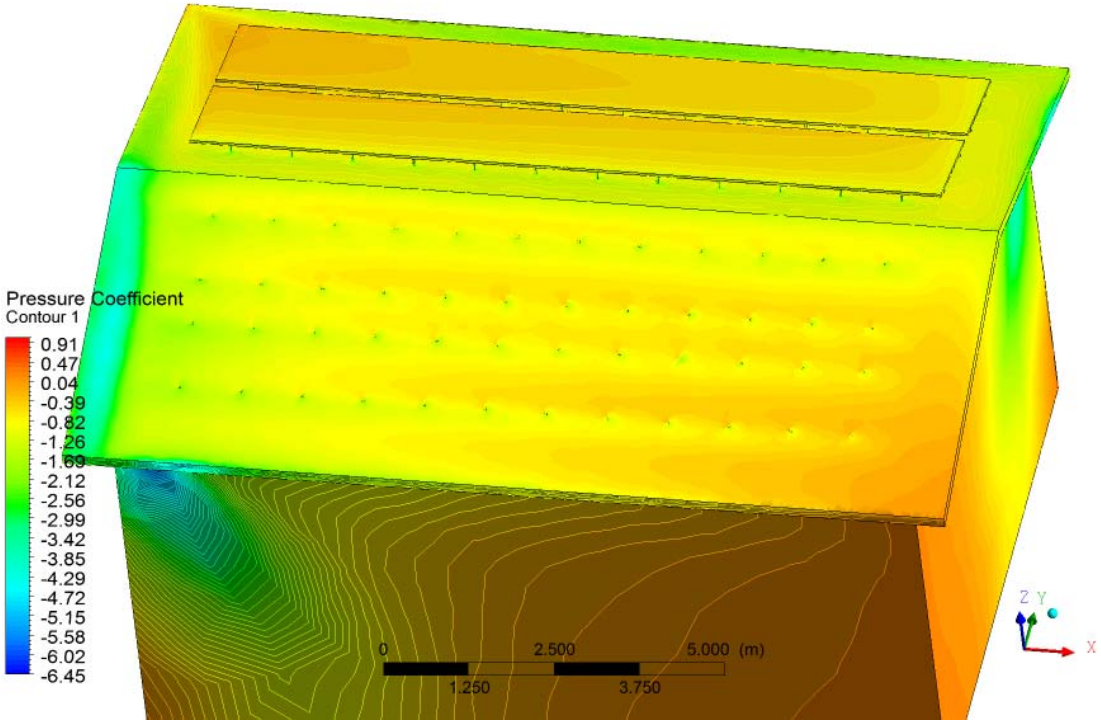


Fig. E. 194. Cp on roof under the solar panels, cut off solar panels, LW, WD 45º

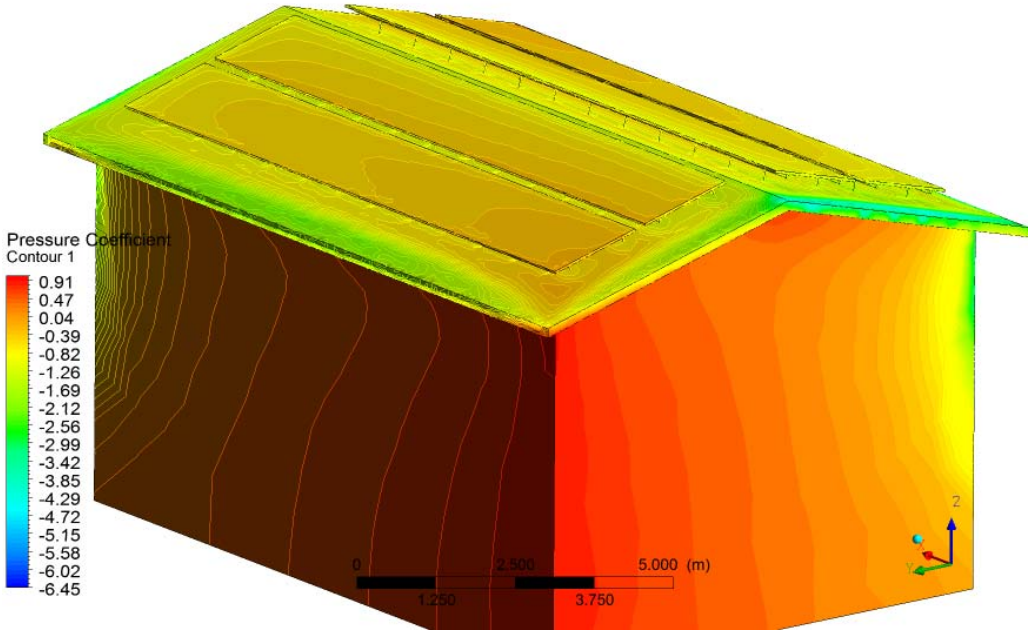


Fig. E. 195. Pressure coefficient on building surfaces with solar panels, WD 45º, WW

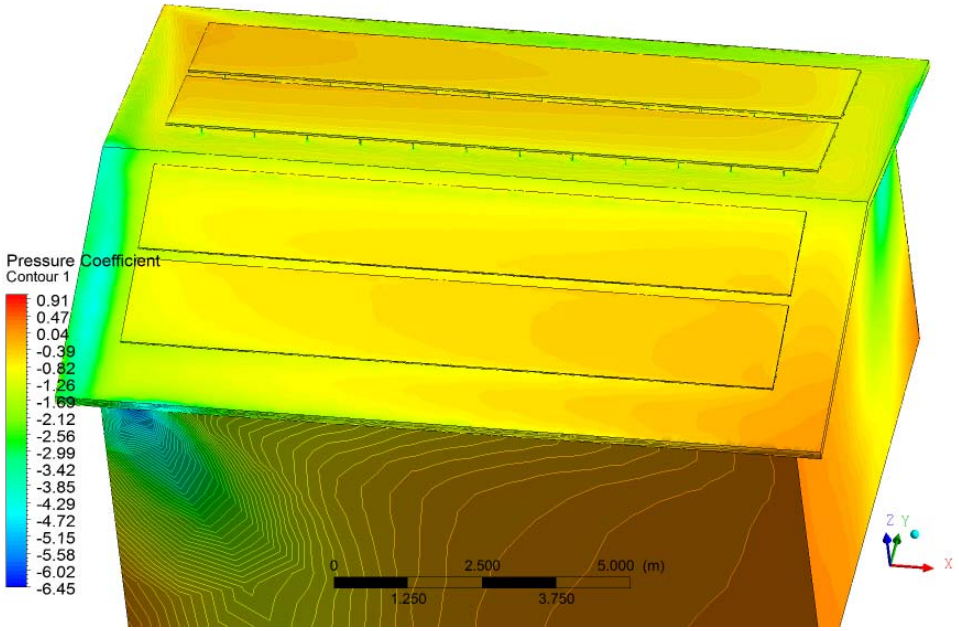


Fig. E. 196. Pressure coefficient on building surfaces with solar panels, WD 45º, LW

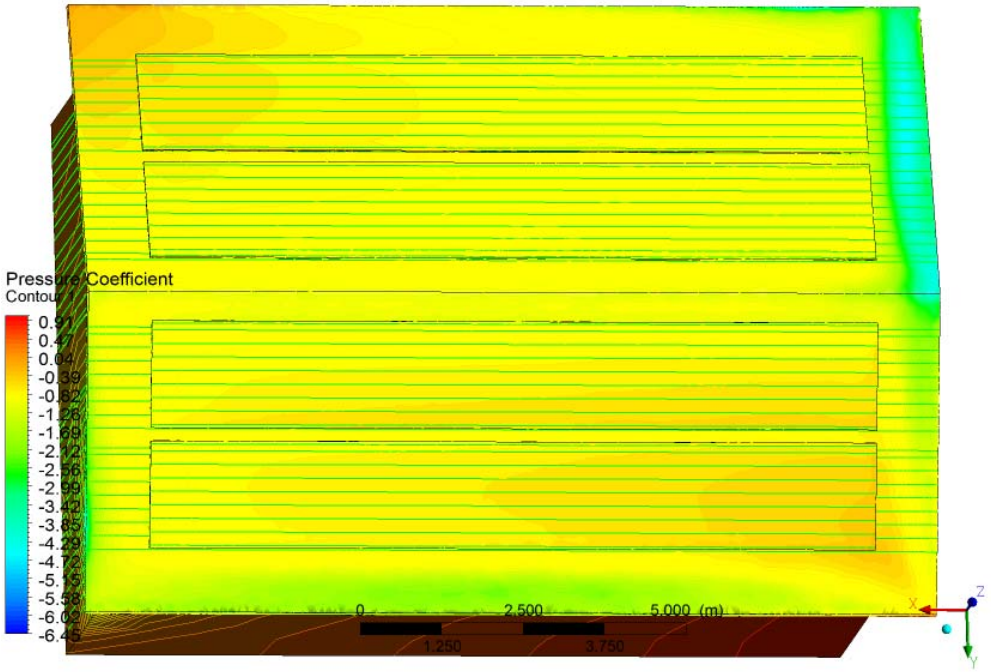


Fig. E. 197. Pressure coefficient on roof, plines, , WD 45º

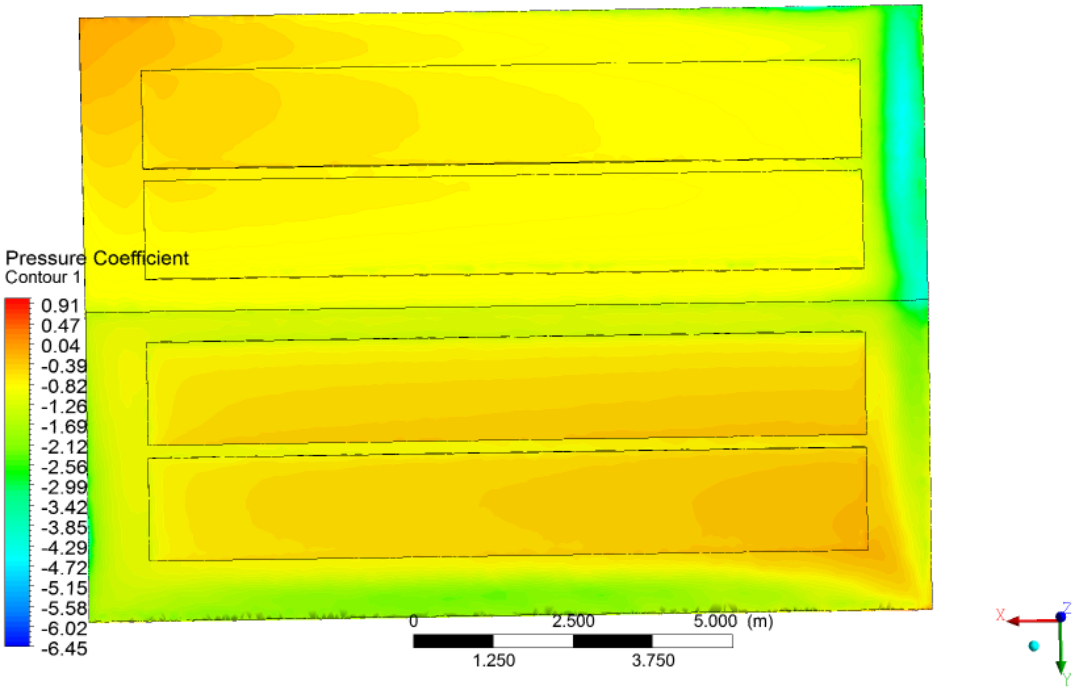


Fig. E. 198. Pressure coefficient on roof, top view, WD 45º

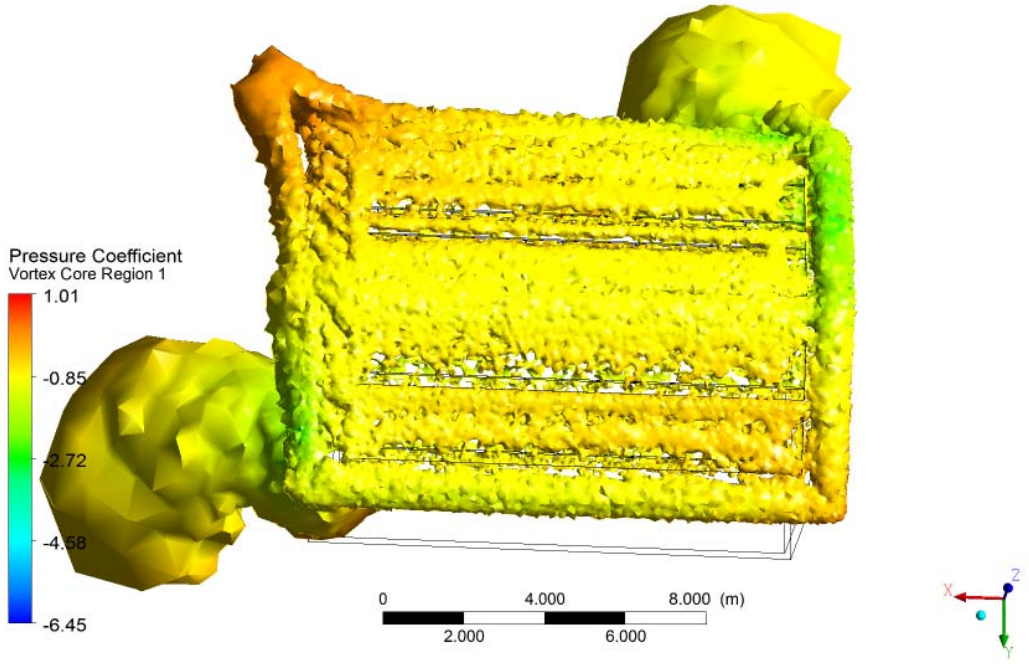


Fig. E. 199. Turbulence distribution, with CP on roof and top of panels, WW, WD 45º

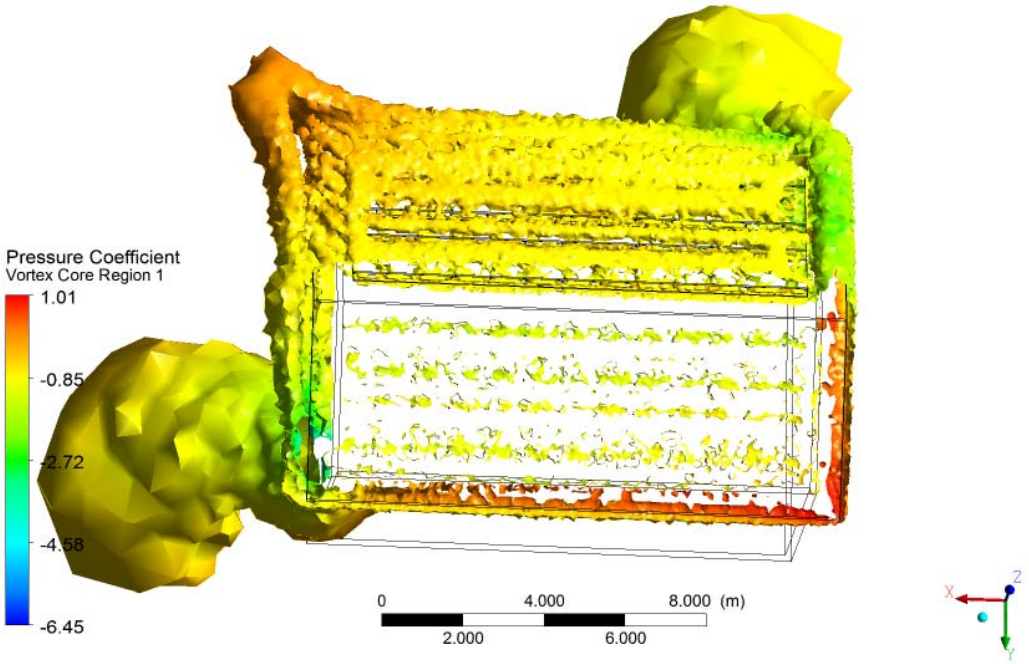


Fig. E. 200. Turbulence distribution, with CP on roof under panels WW and LW with panels, WD 45º

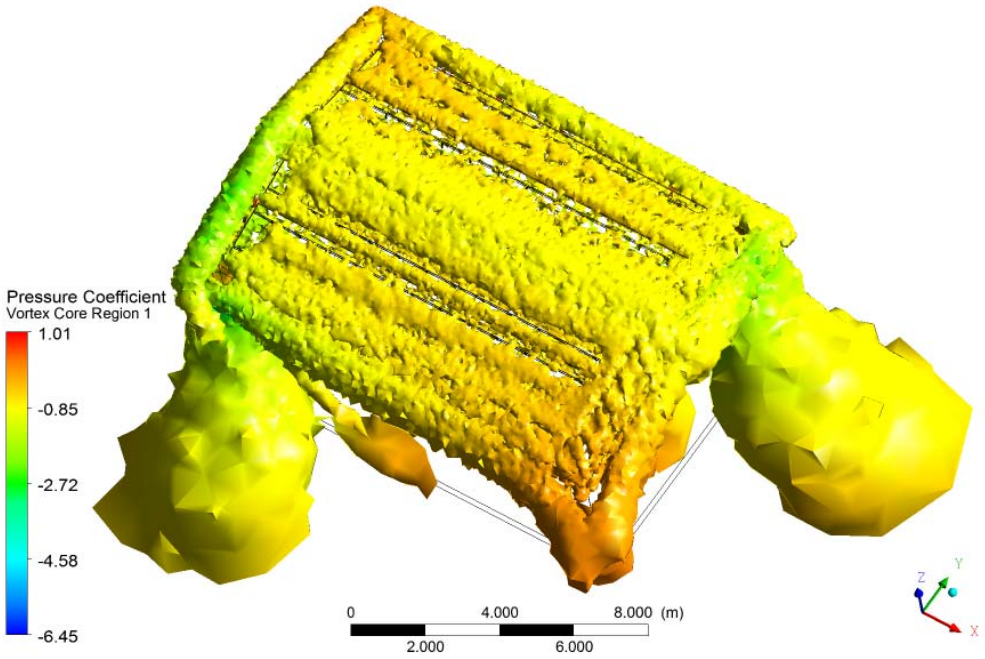


Fig. E. 201. Turbulence distribution, with CP on roof and top of panels, LW, WD 45º

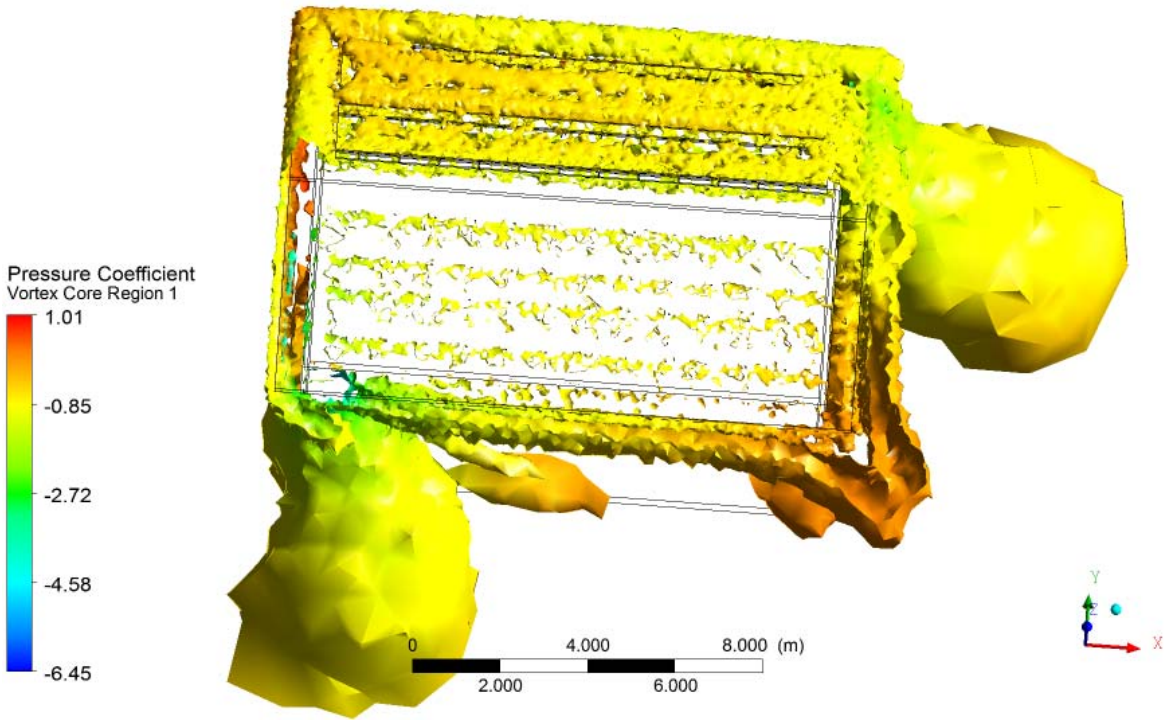


Fig. E. 202. Turbulence distribution, with CP on roof under panels LW and WW with panels, WD 45º

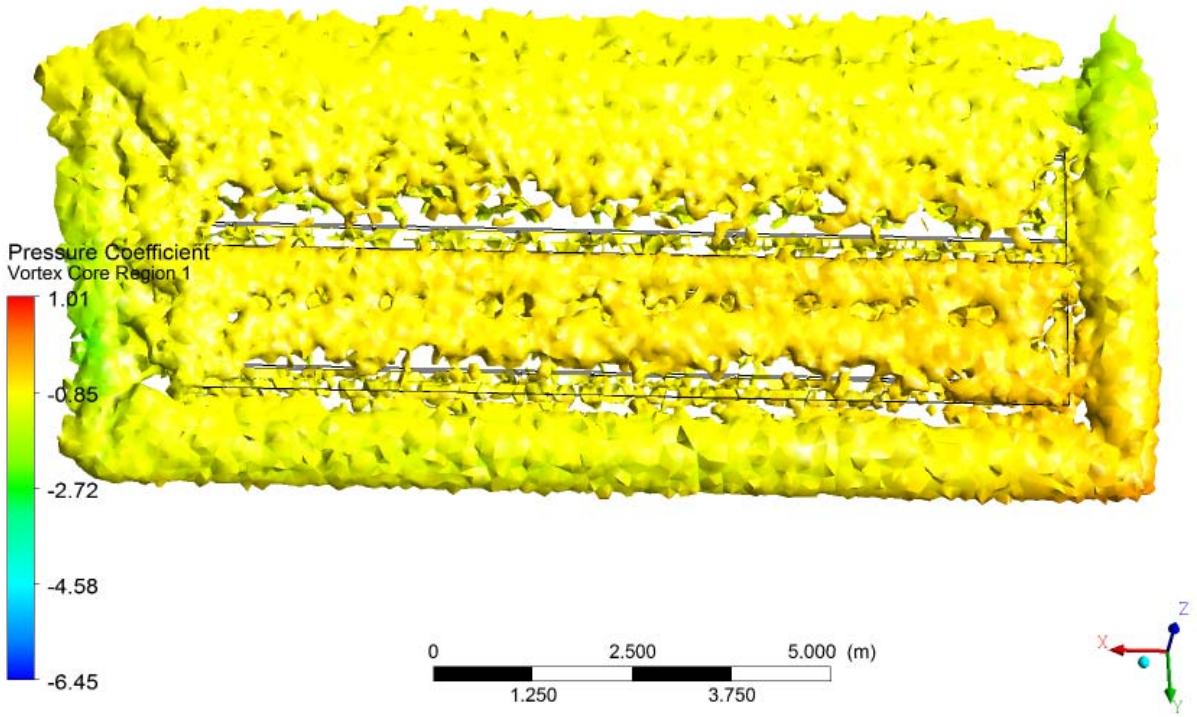


Fig. E. 203. Turbulence distribution, with CP on top of panels, WW, WD 45º

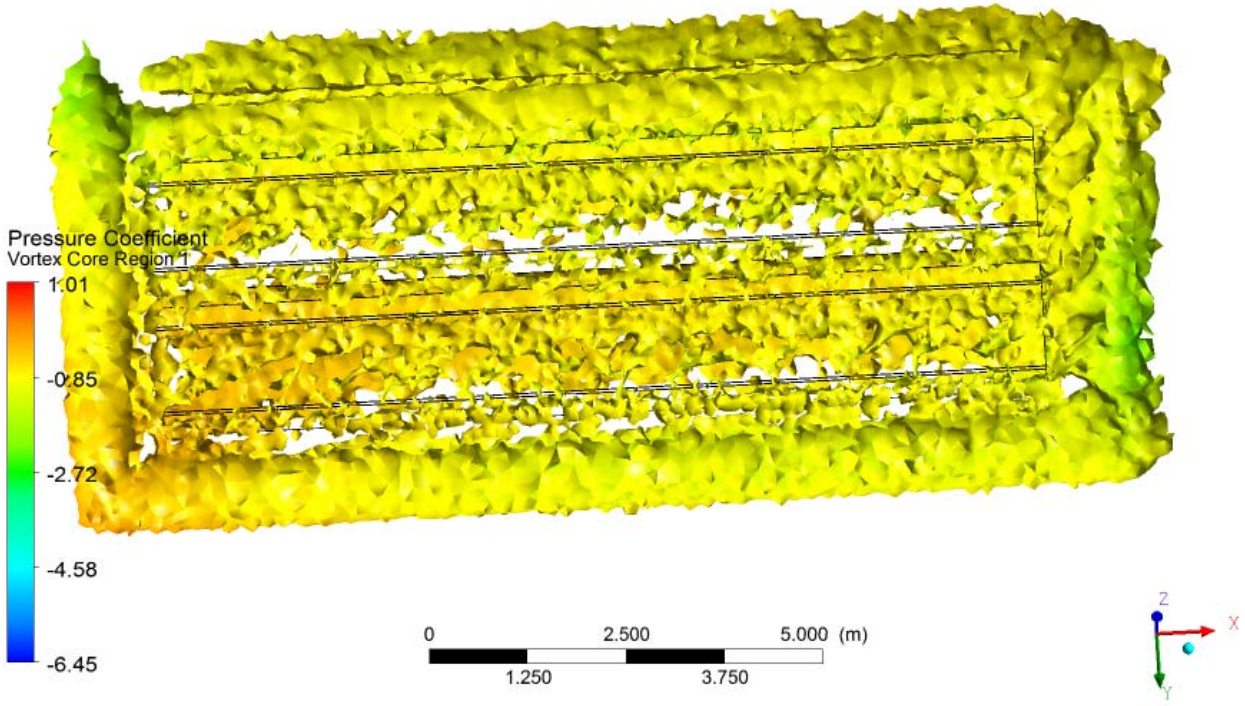


Fig. E. 204. Turbulence distribution, with CP on bottom of panels, WW, WD 45º

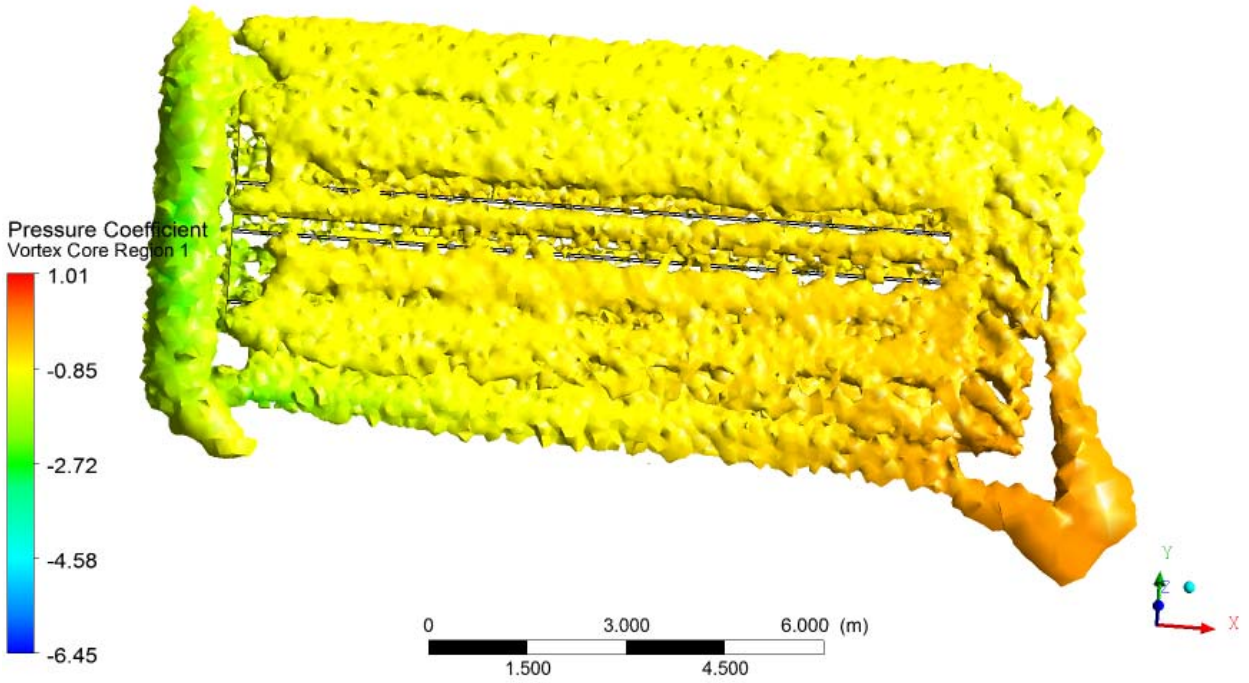


Fig. E. 205. Turbulence distribution, with CP on top of panels, LW, , WD 45º

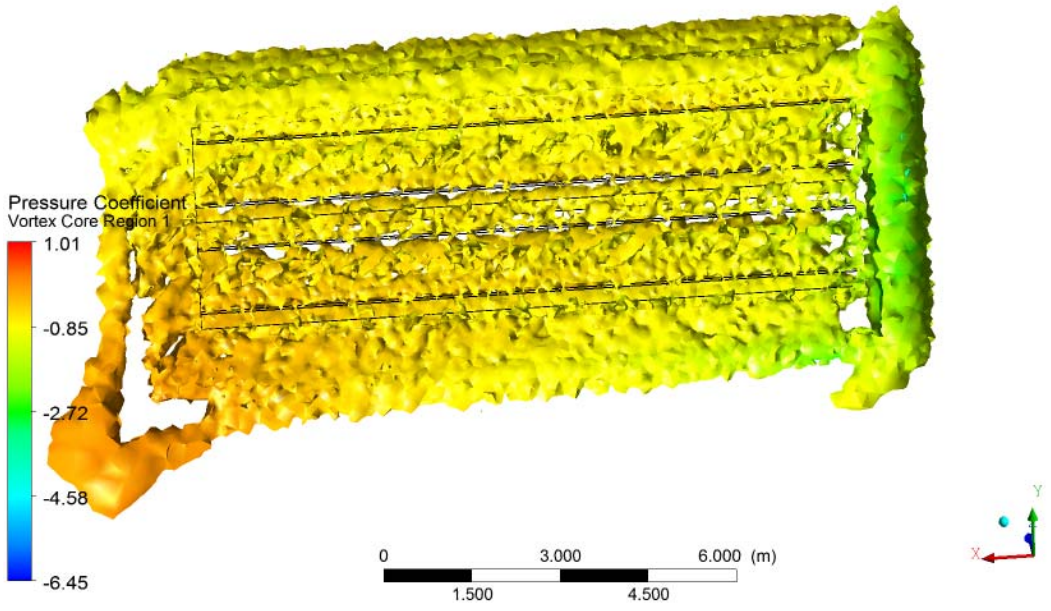


Fig. E. 206. Turbulence distribution, with CP on bottom of panels, LW, WD 45º

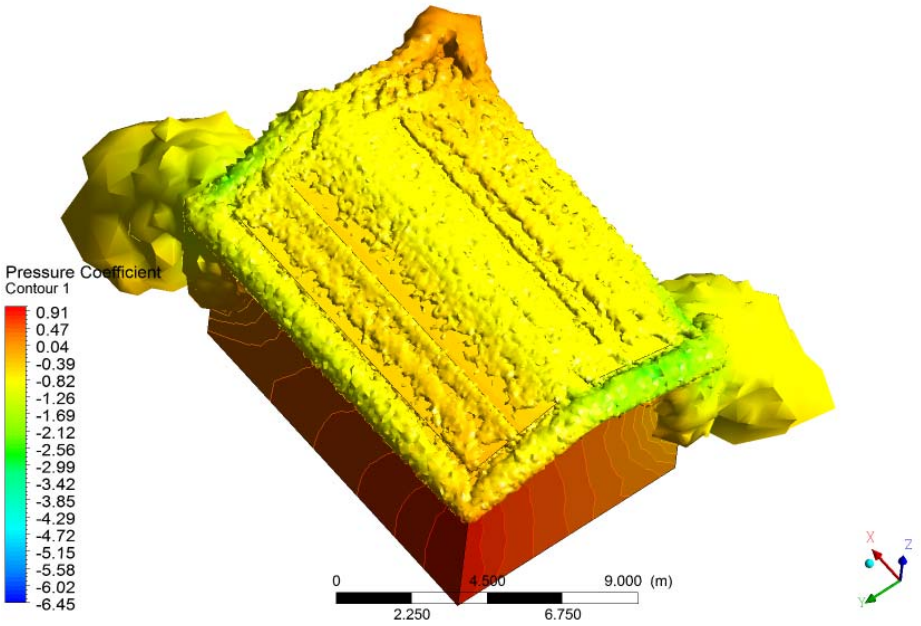


Fig. E. 207. Turbulence distribution, with CP on whole building and panels, WW, WD 45º

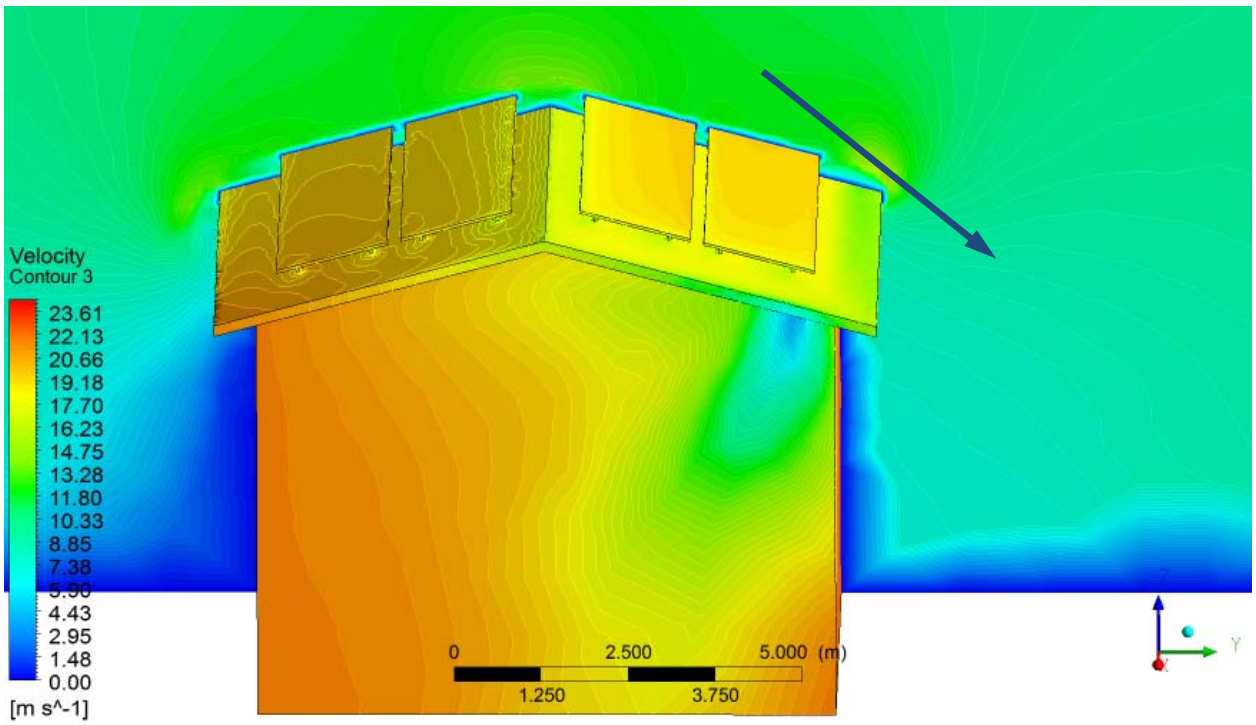


Fig. E. 208. Velocity distribution on a perpendicular plane to building ridge, WD 45º

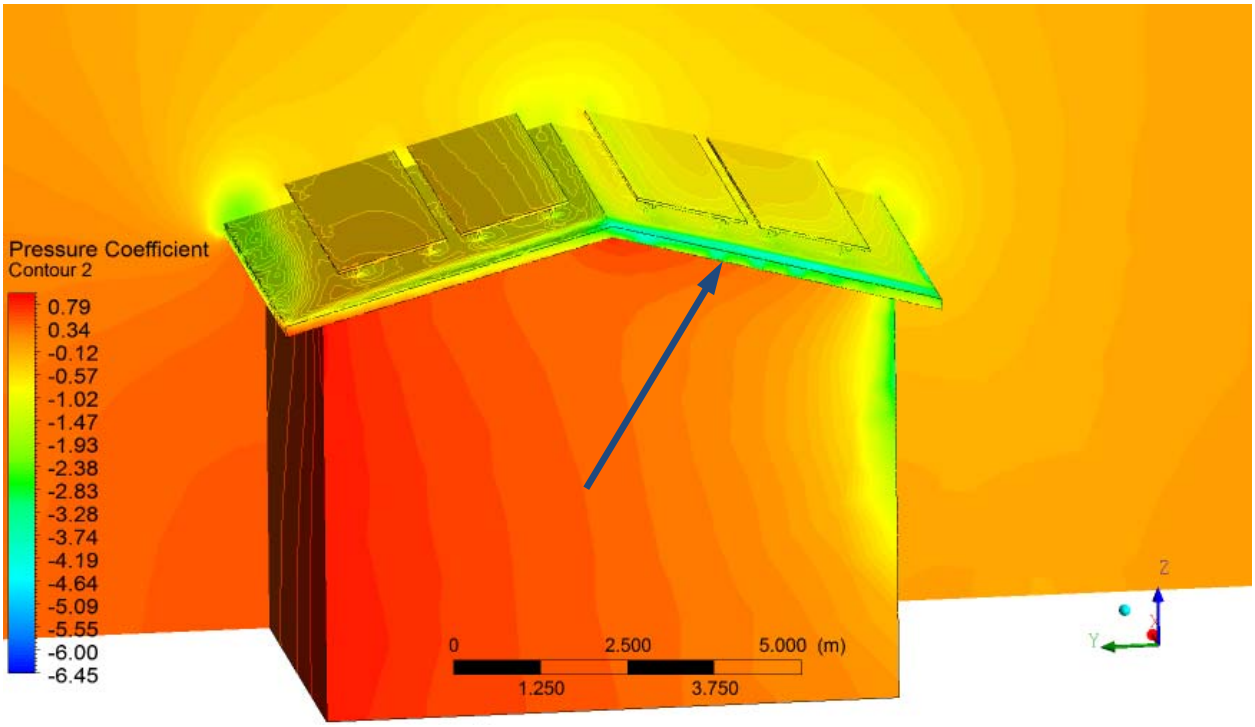


Fig. E. 209. Cp distribution on a perpendicular plane to building ridge, WD 45º

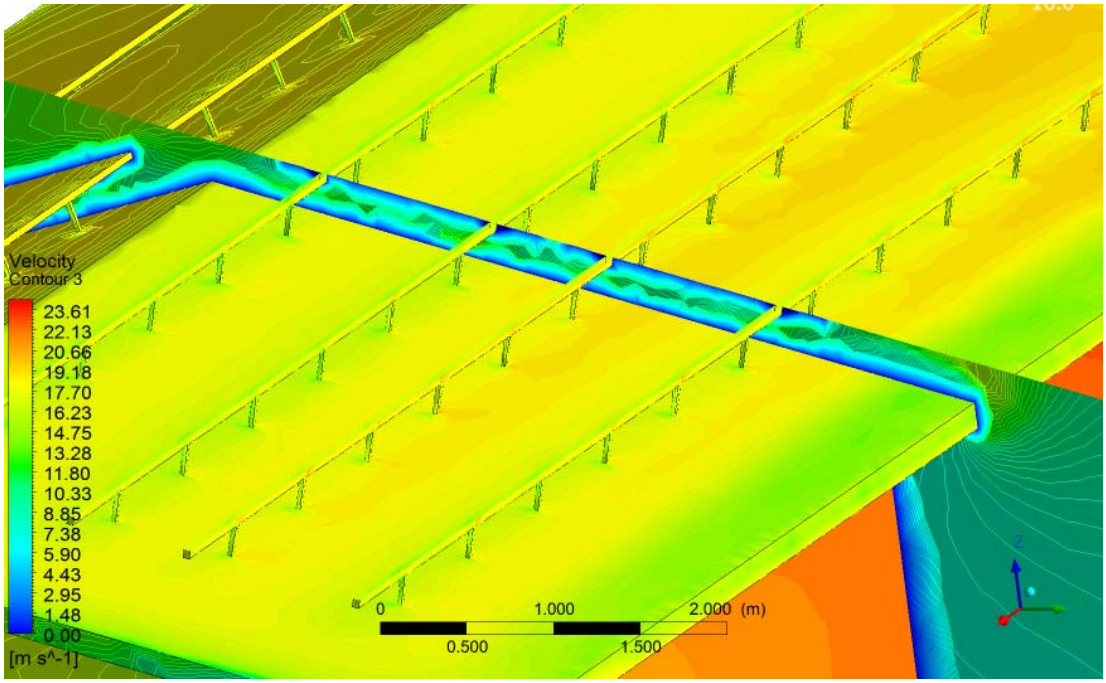


Fig. E. 210. Velocity distribution on a perpendicular plane to building ridge between panels and roof, WD 45º, WW

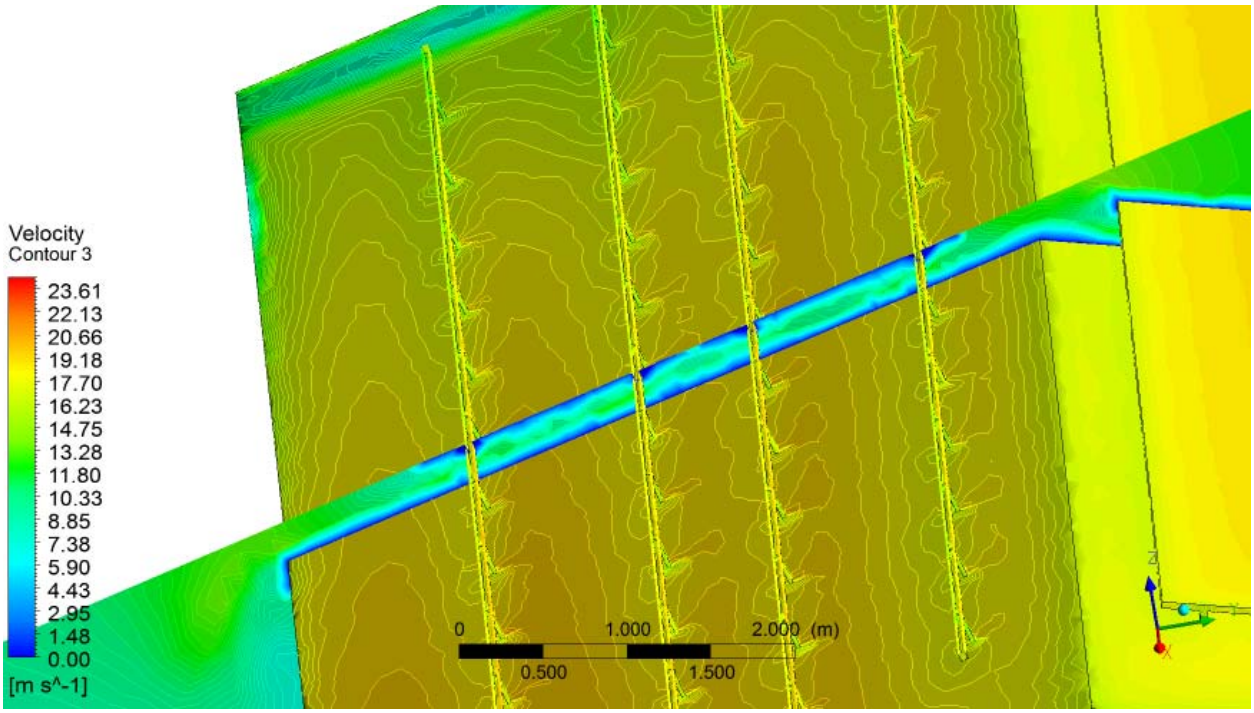


Fig. E. 211. Velocity distribution on a perpendicular plane to building ridge between panels and roof, WD 45º, WW

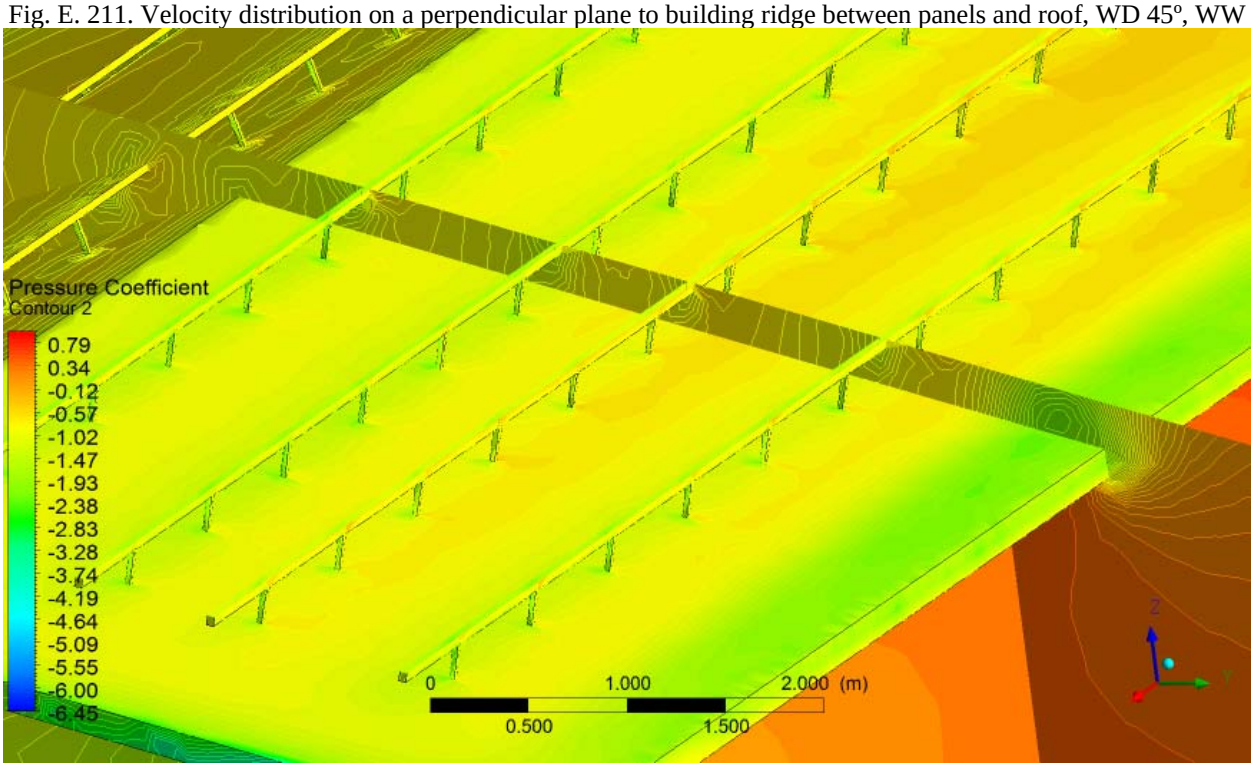


Fig. E. 212. Cp distribution on a perpendicular plane to building ridge between panels and roof, WD 45º, WW

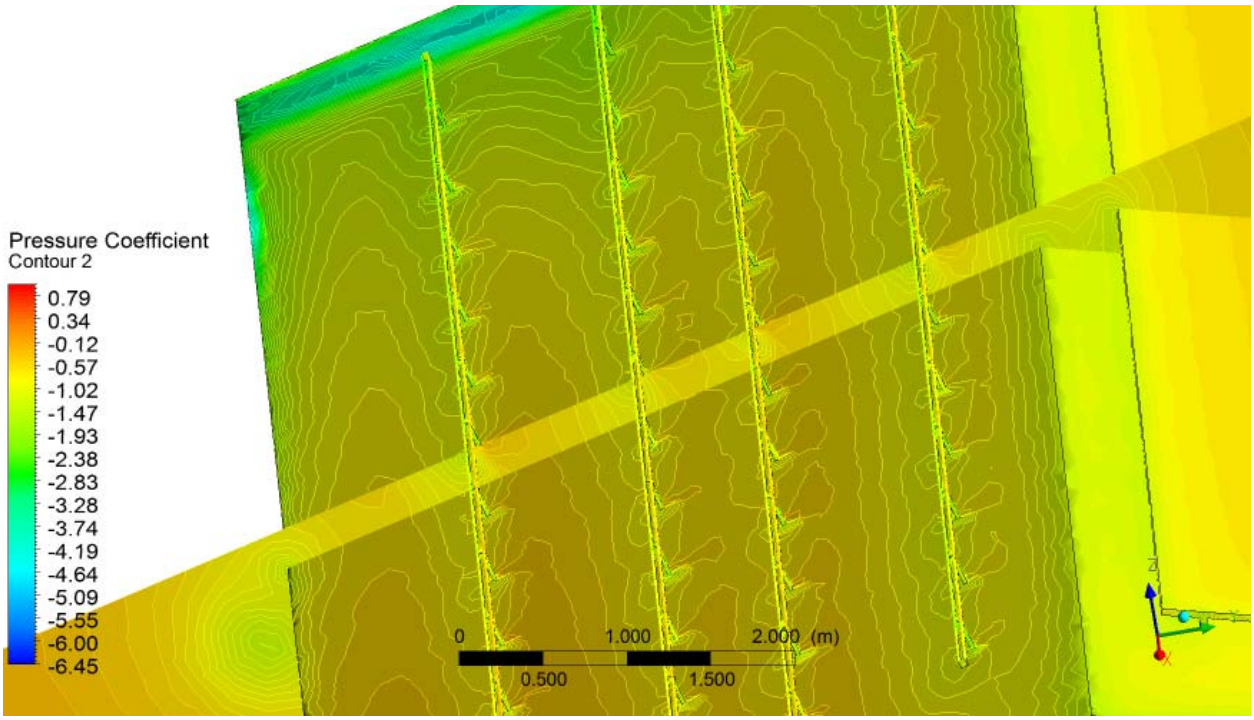


Fig. E. 213. Cp distribution on a perpendicular plane to building ridge between panels and roof, WD 45º, LW

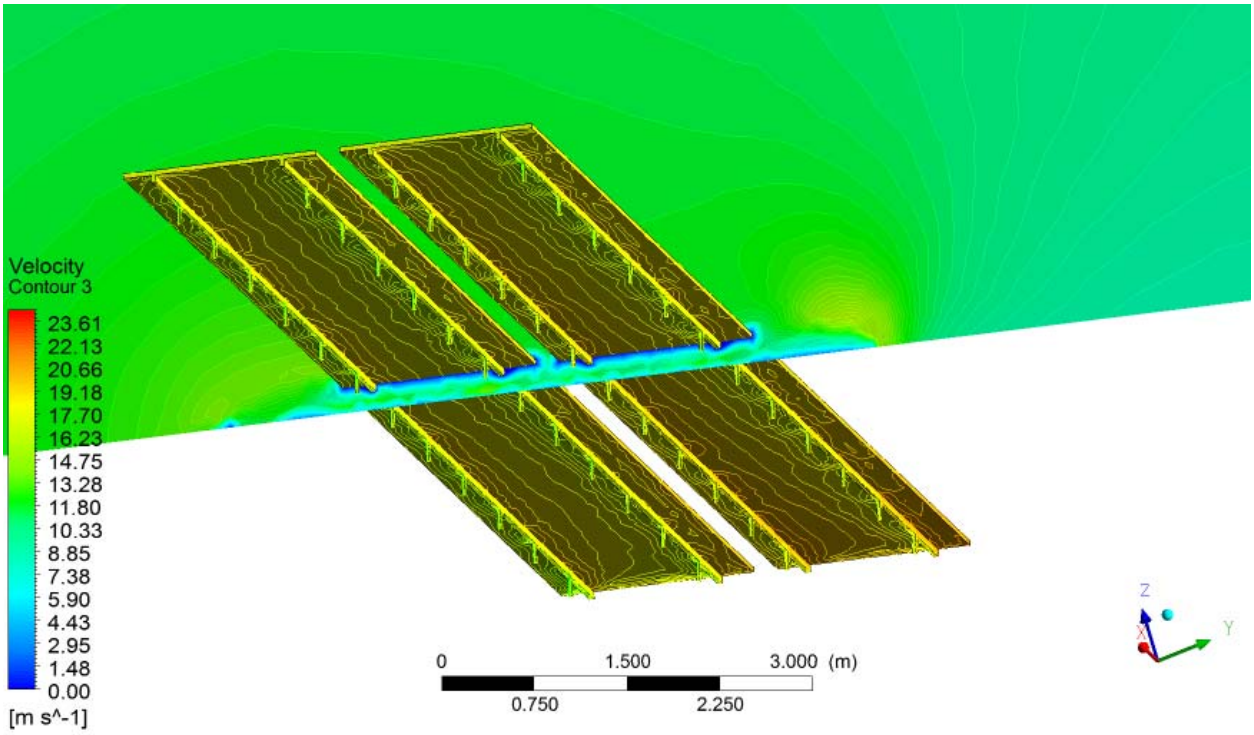


Fig. E. 214. Velocity distribution on bottom of panels and a perpendicular plane to building ridge, WD 45º, WW

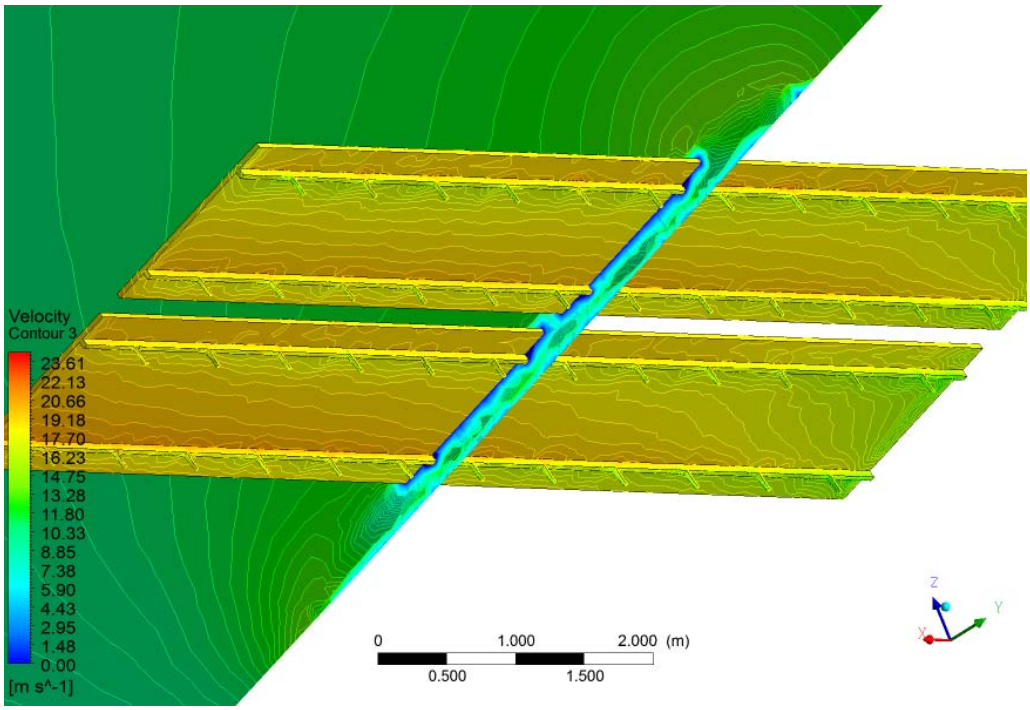


Fig. E. 215. Velocity distribution on bottom of panels and a perpendicular plane to building ridge, WD 45º, LW

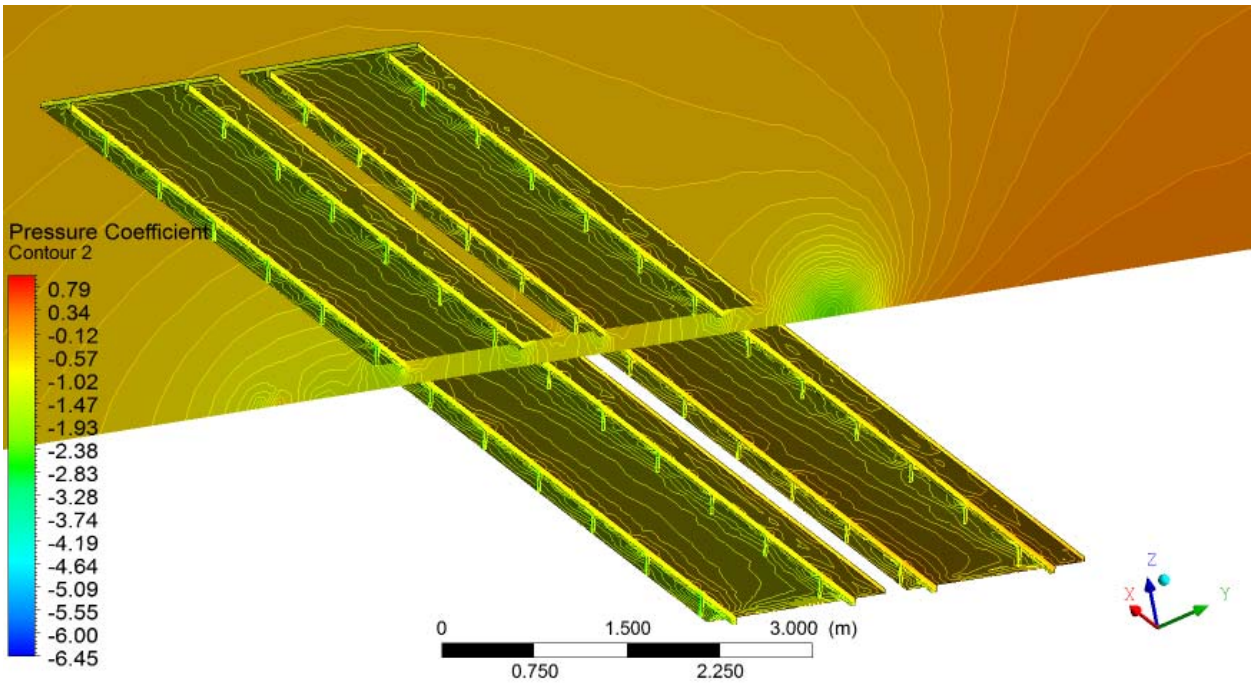


Fig. E. 216. Cp distribution on bottom of panels and a perpendicular plane to building ridge, WD 45º, WW

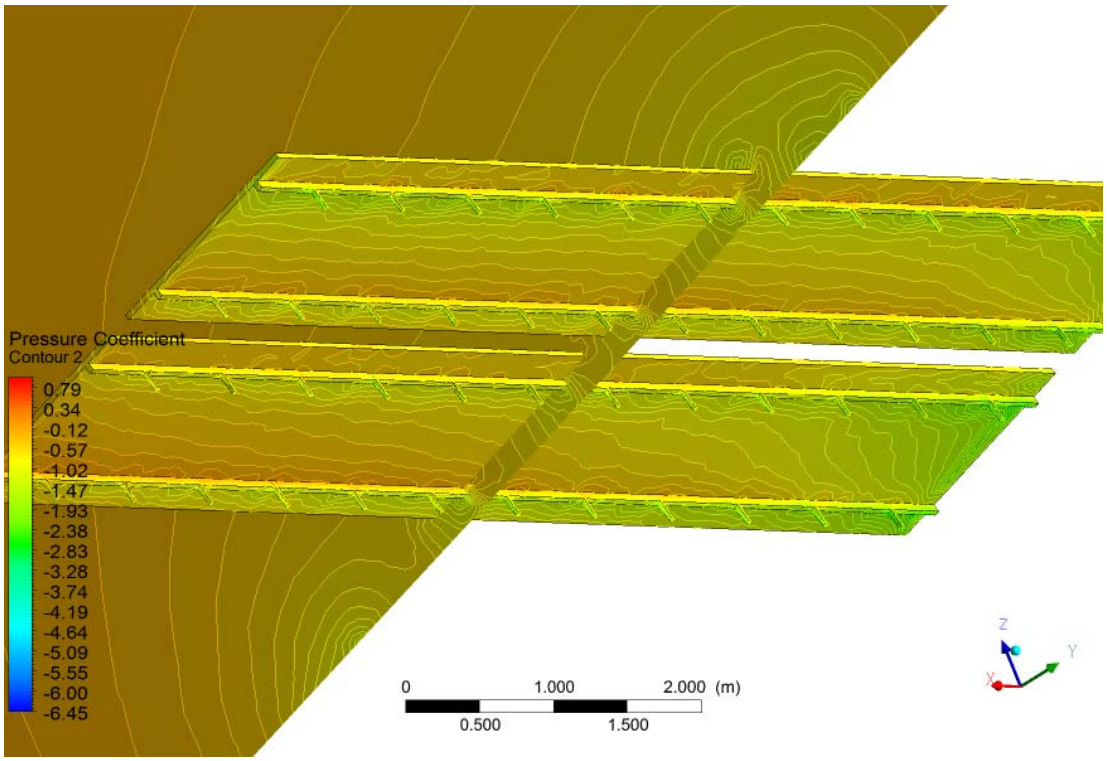


Fig. E. 217. Cp distribution on bottom of panels and a perpendicular plane to building ridge, WD 45º, LW

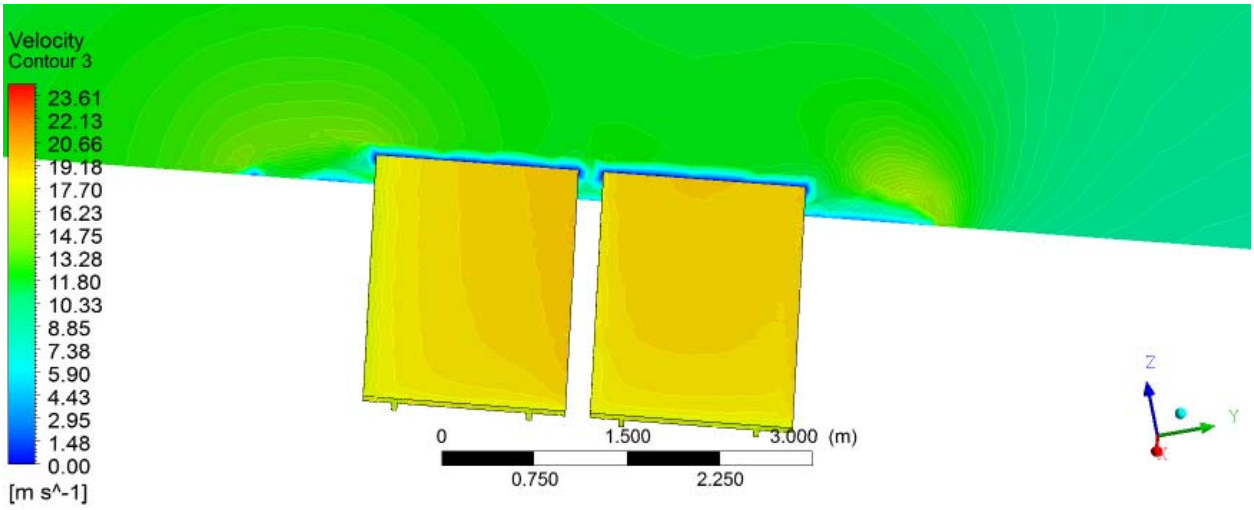


Fig. E. 218. Velocity distribution on top of panels and a perpendicular plane to building ridge, WD 45º, WW

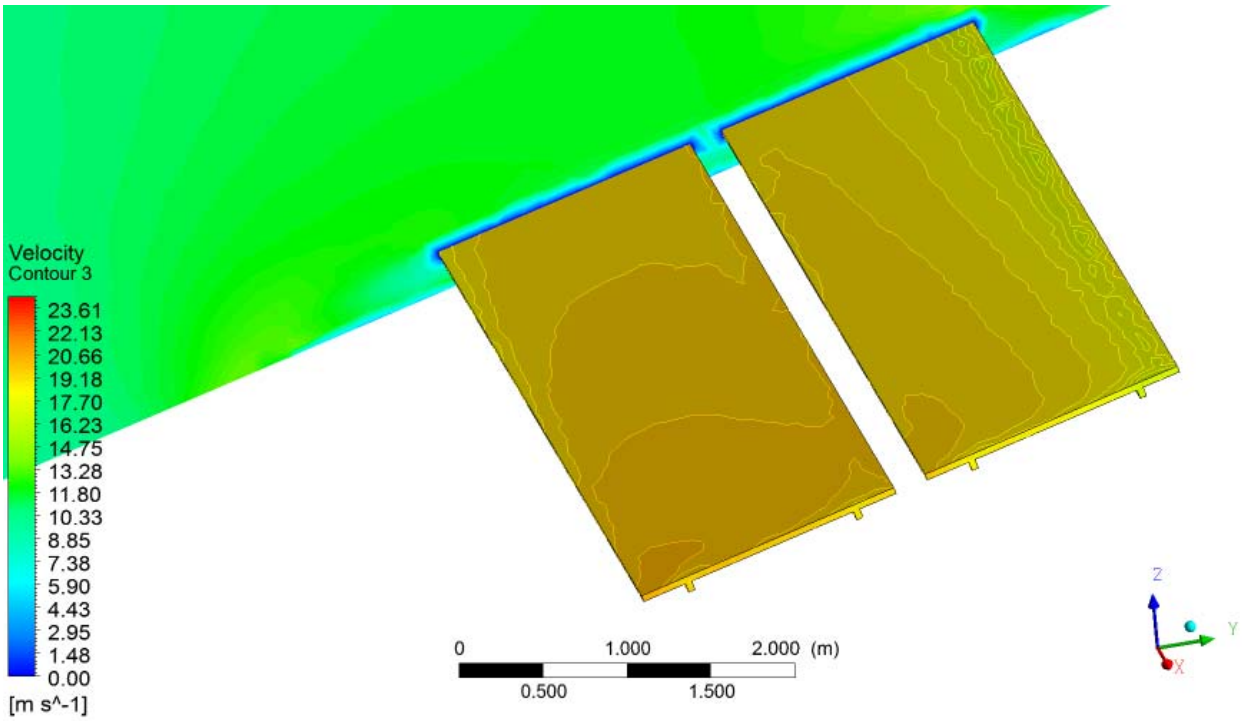


Fig. E. 219. Velocity distribution on top of panels and a perpendicular plane to building ridge, WD 45º, LW

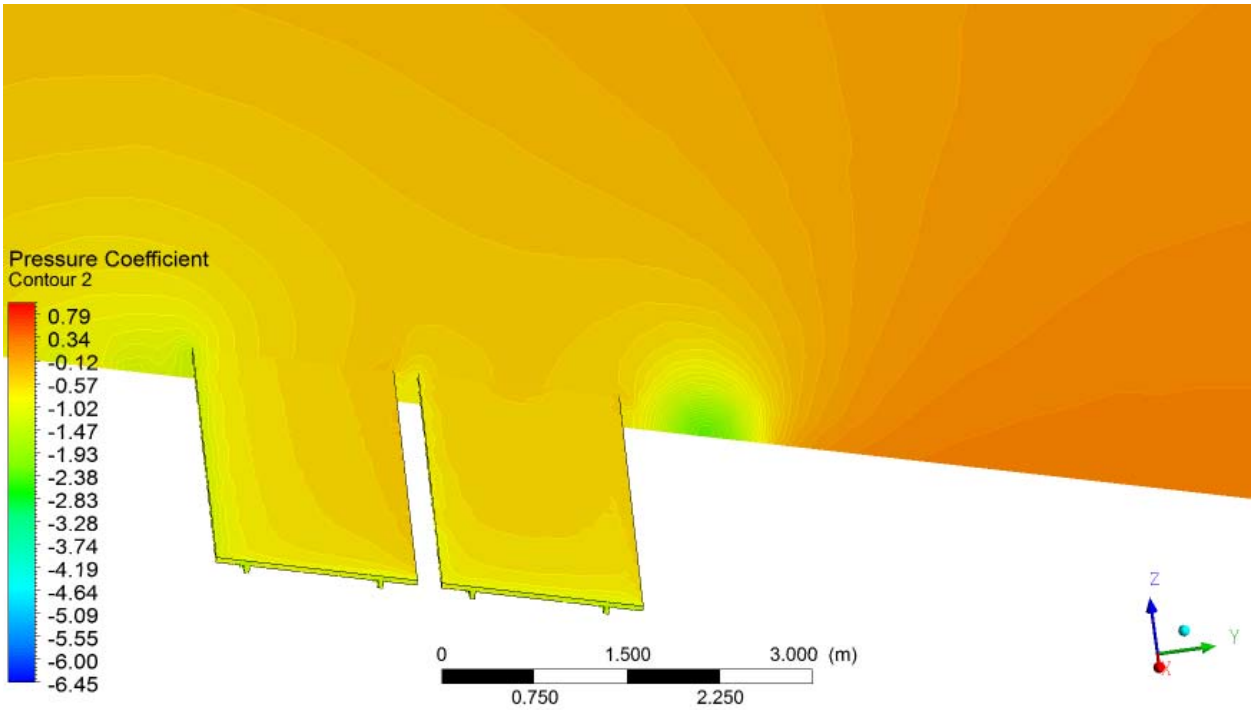


Fig. E. 220. Cp distribution on top of panels and a perpendicular plane to building ridge, WD 45º, WW

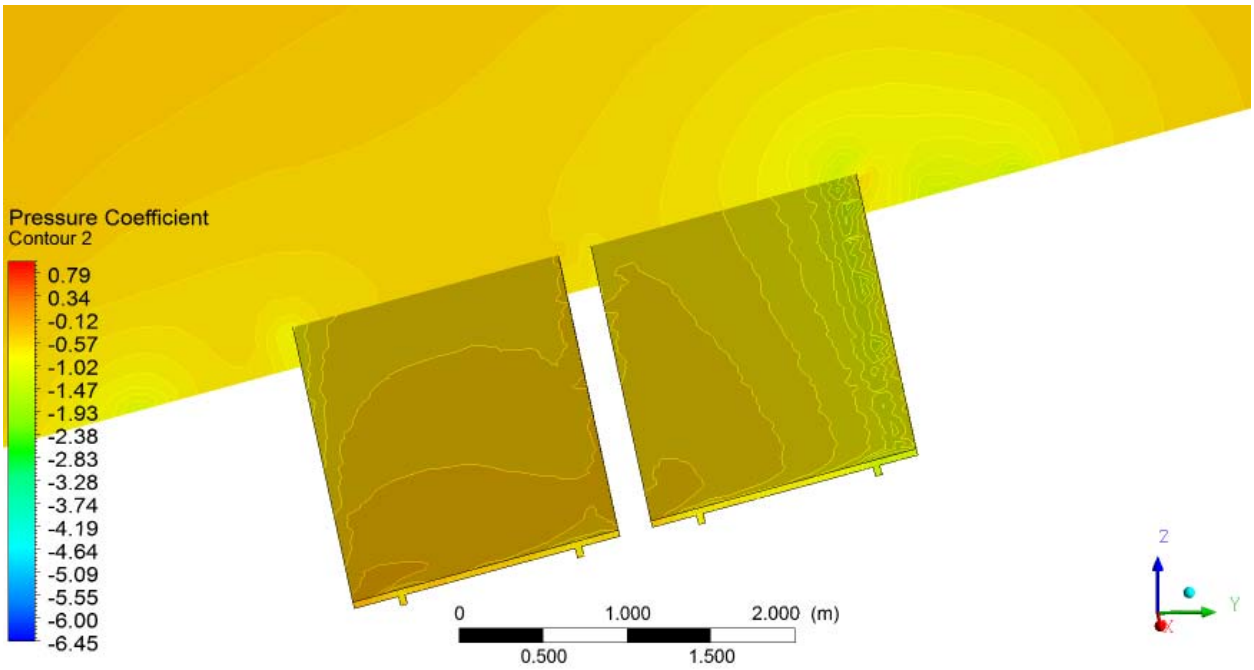


Fig. E. 221. Cp distribution on top of panels and a perpendicular plane to building ridge, WD 45º, LW

1.3.2. WIND DIRECTION 90º

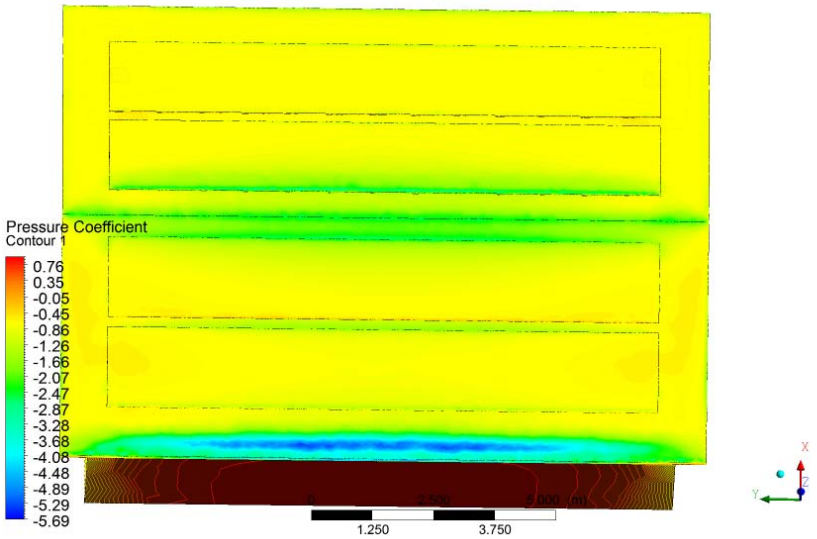


Fig. E. 222. CP on roof with solar panels, S 15º, WW, WD 90º

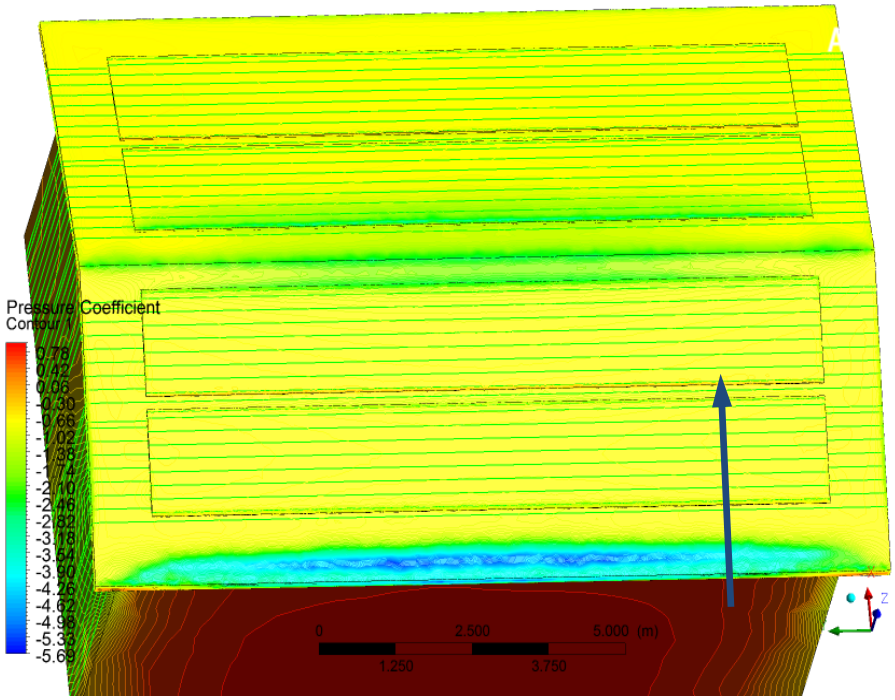


Fig. E. 223.Cp on top of solar panels with plines, S 15º, WW, WD 90º

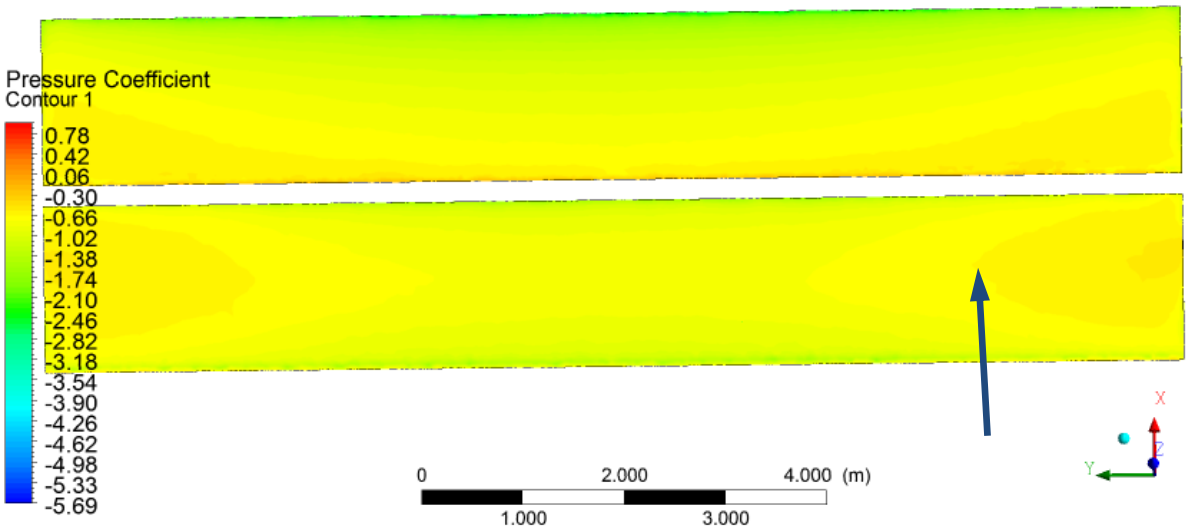


Fig. E. 224. Cp on top of solar panels, S 15º, WW, WD 90º

1.3.3. WIND DIRECTION 0º

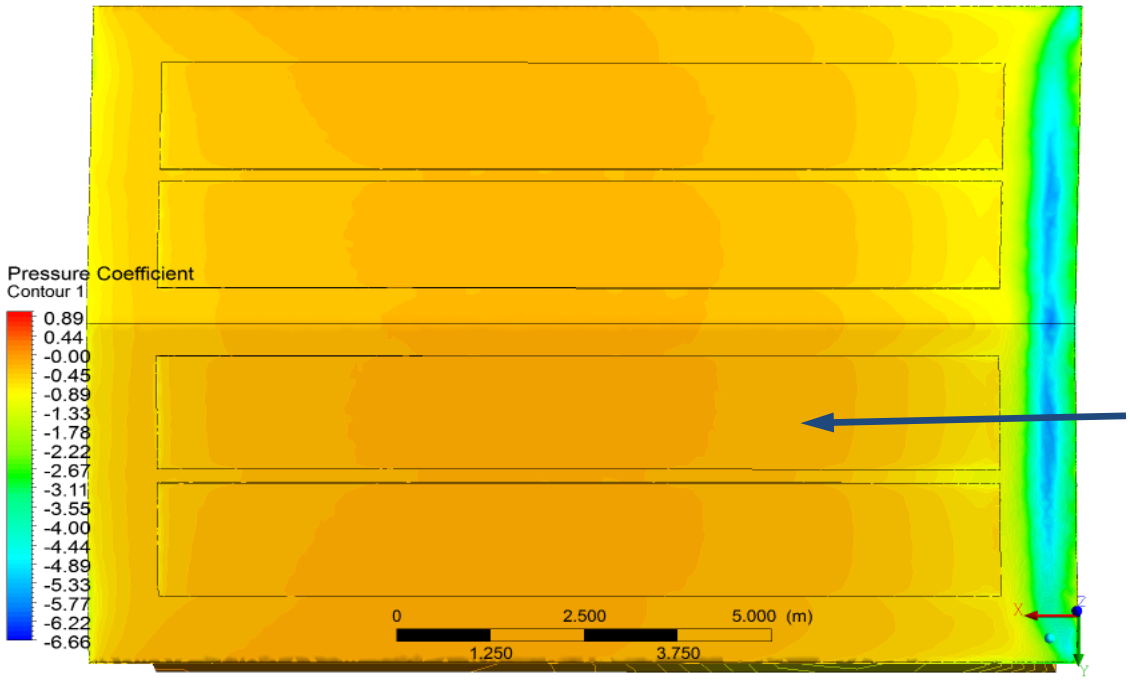


Fig. E. 225. Cp on roof with solar panels, top view, S 15º, WD 0º

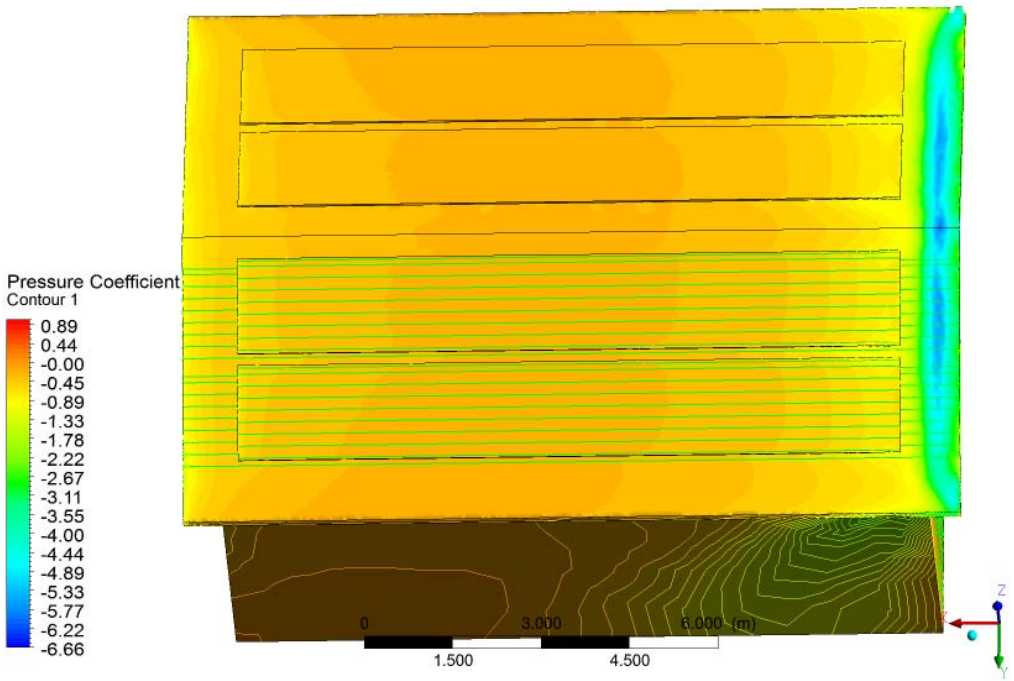


Fig. E. 226. Cp on roof with solar panels and Plines S 15º, WD 0º

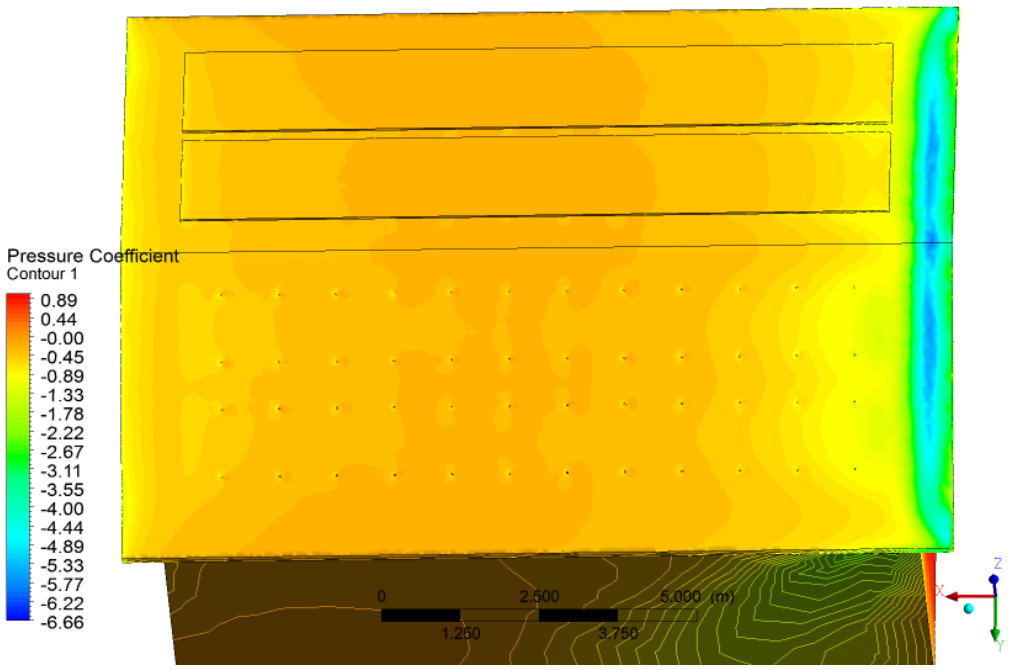


Fig. E. 227. Cp on roof under solar panels on one side and on solar panels on the other side, S 15º, WD 0º

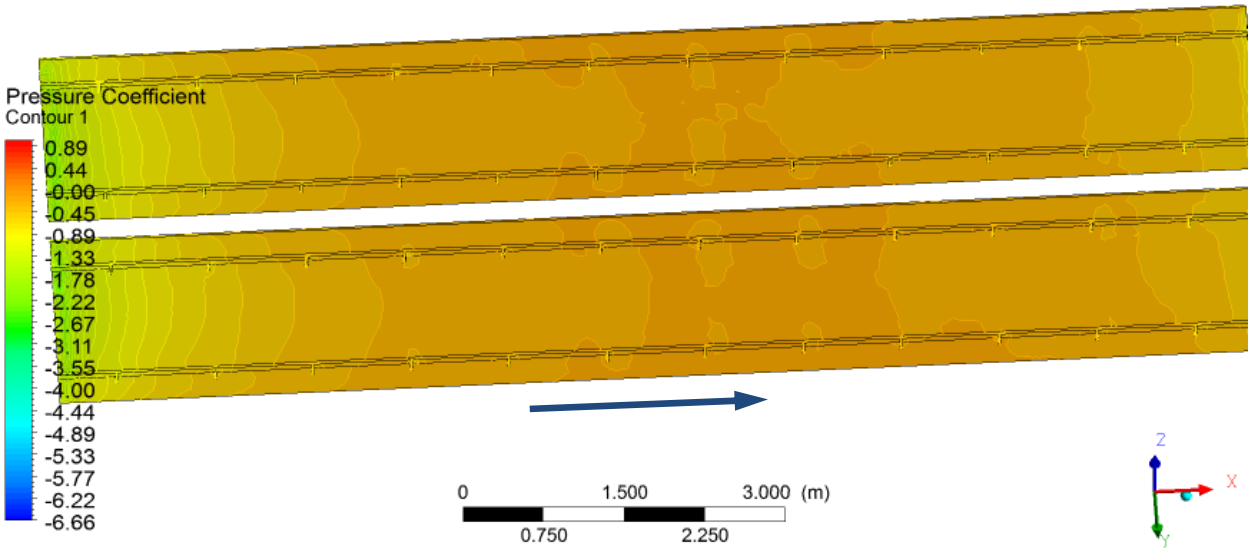


Fig. E. 228. Cp, on bottom of solar panels, S 15º, WD 0º

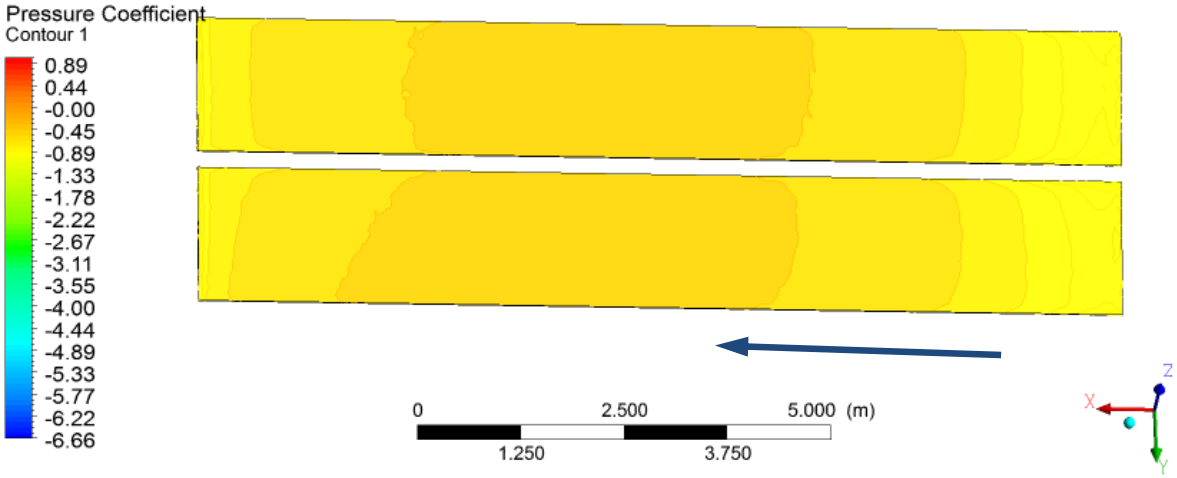


Fig. E. 229. Cp on top of solar panels, S 15º, WD 0º

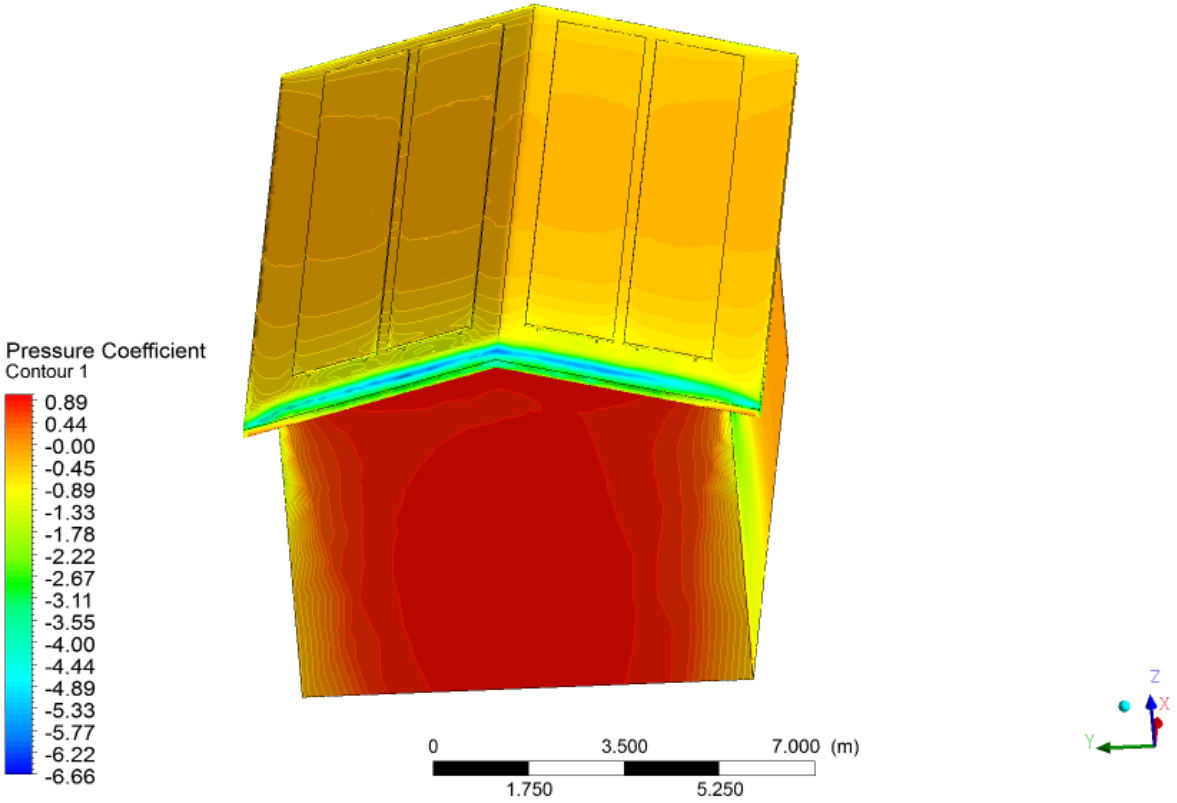


Fig. E. 230. Cp on building with the solar panels, S 15º, WD 0º, WW

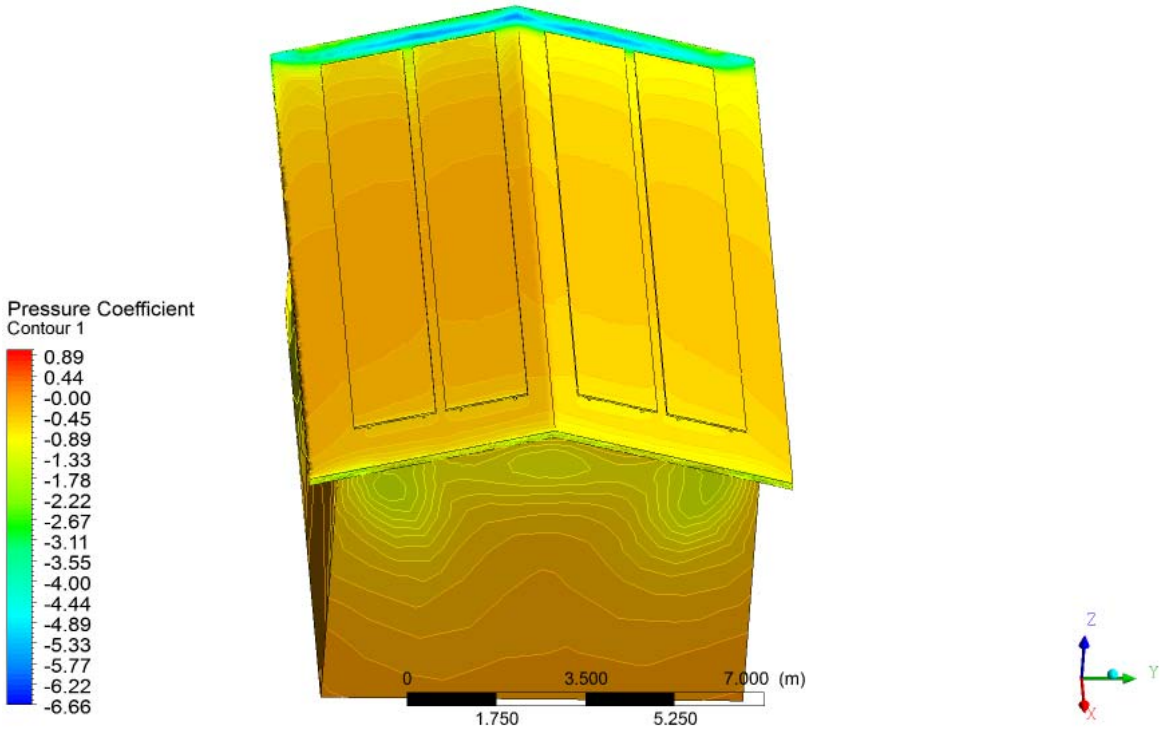


Fig. E. 231. Cp on building with the solar panels, S 15º, WD 0º, LW

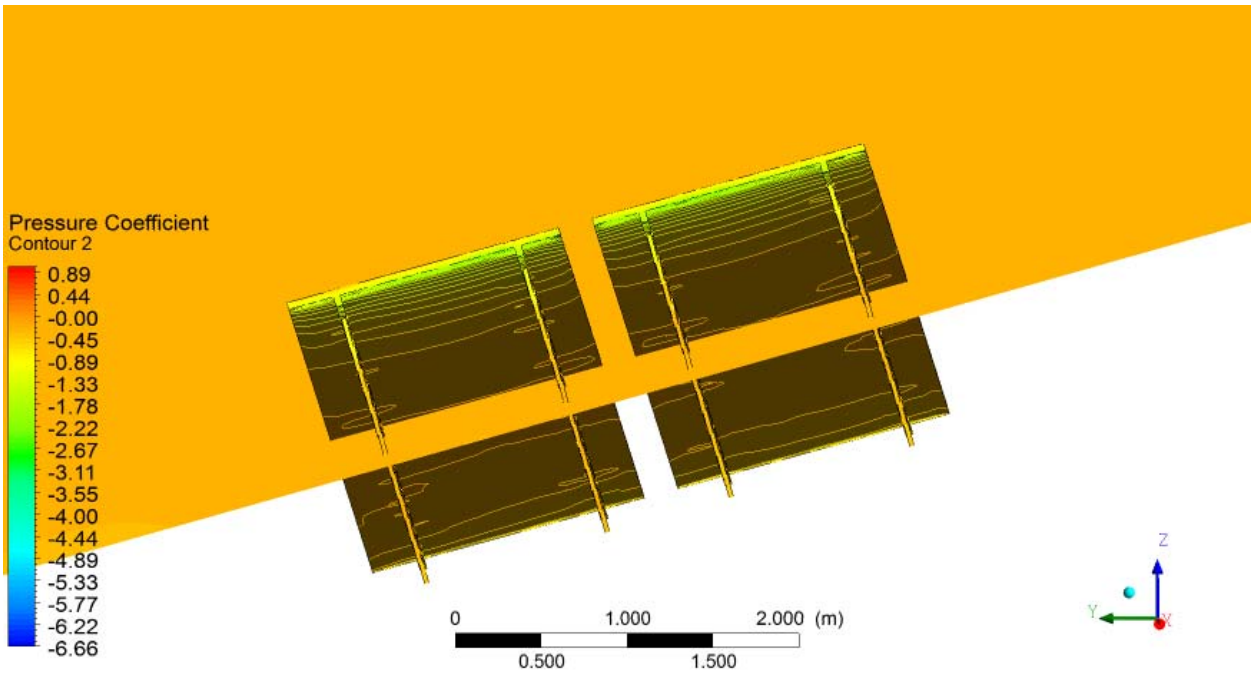


Fig. E. 232. Cp on a perpendicular plane and on bottom of panels, WD 0º, WW

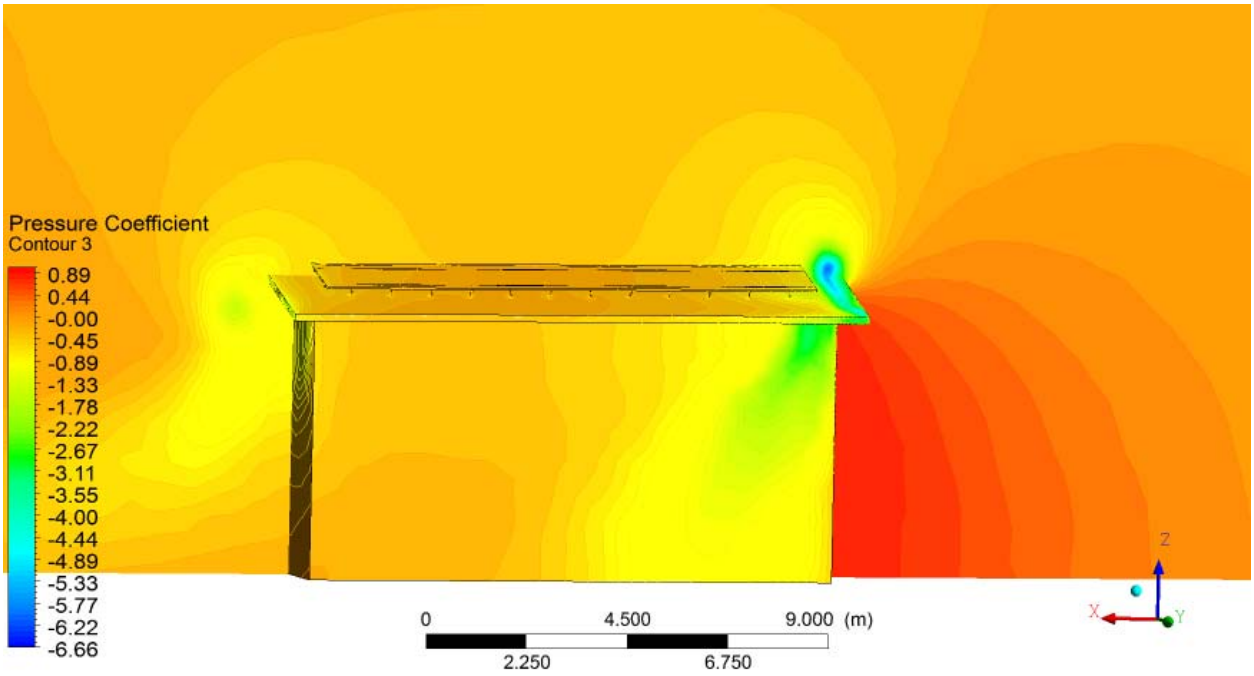


Fig. E. 233. Cp distribution on a plane parallel to the ridge of the building, WD 0º, WW

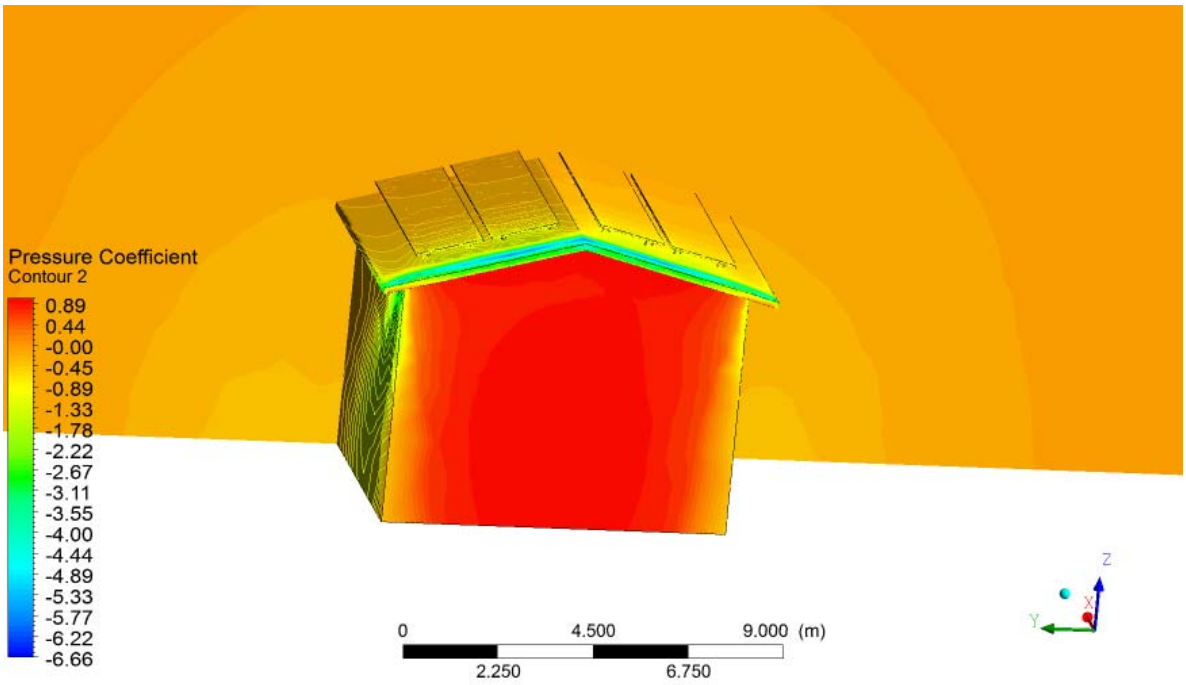


Fig. E. 234. Cp distribution on a plane parallel to the ridge of the building, WD 0º, WW, distant view

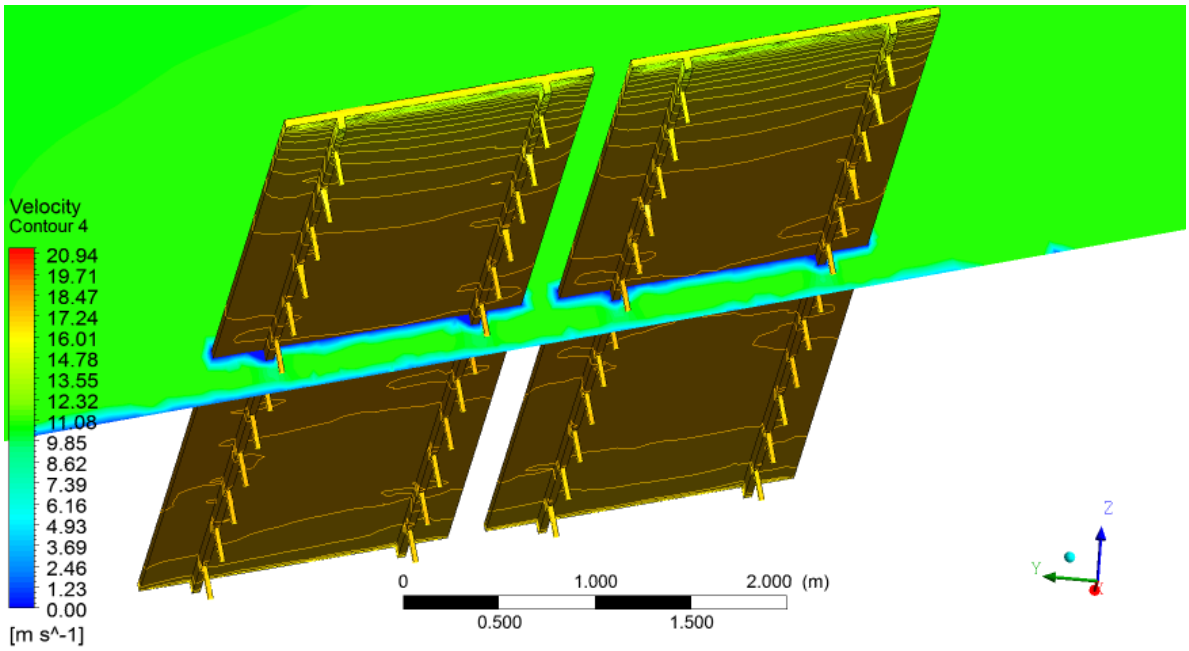


Fig. E. 235. Velocity distribution bottom of panels and a perpendicular plane to the building ridge, WD 0º

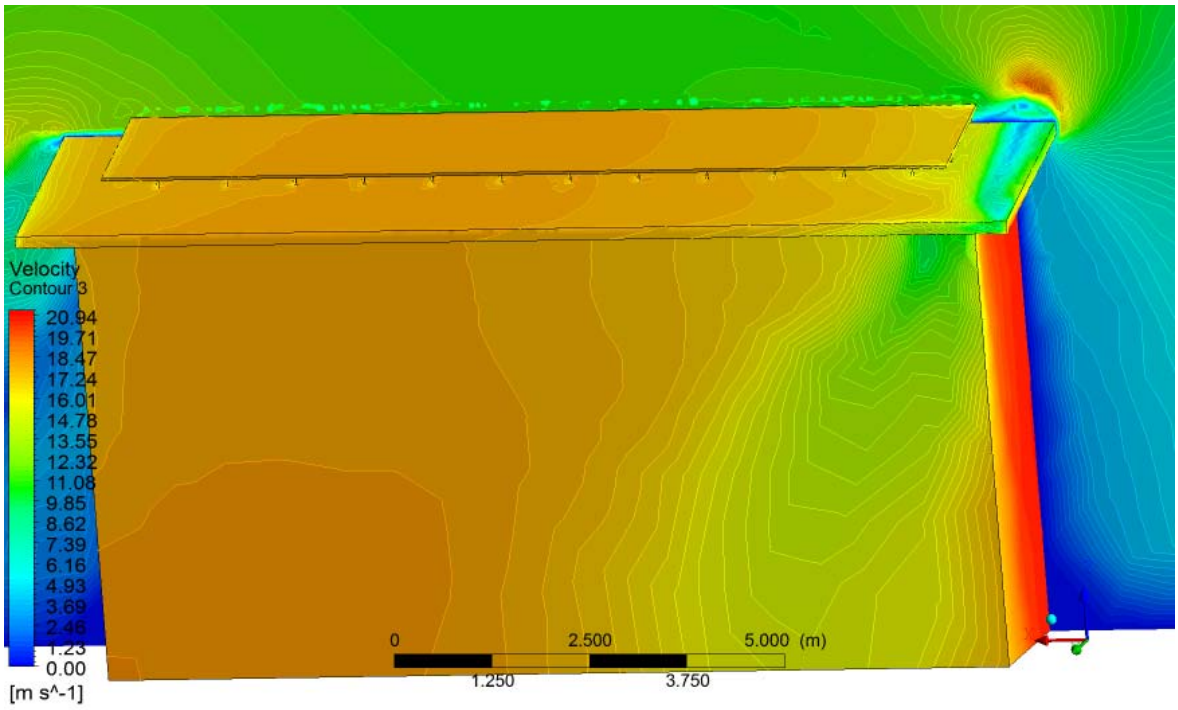


Fig. E. 236. Velocity distribution on a plane parallel to the ridge of the building, WD 0º, WW

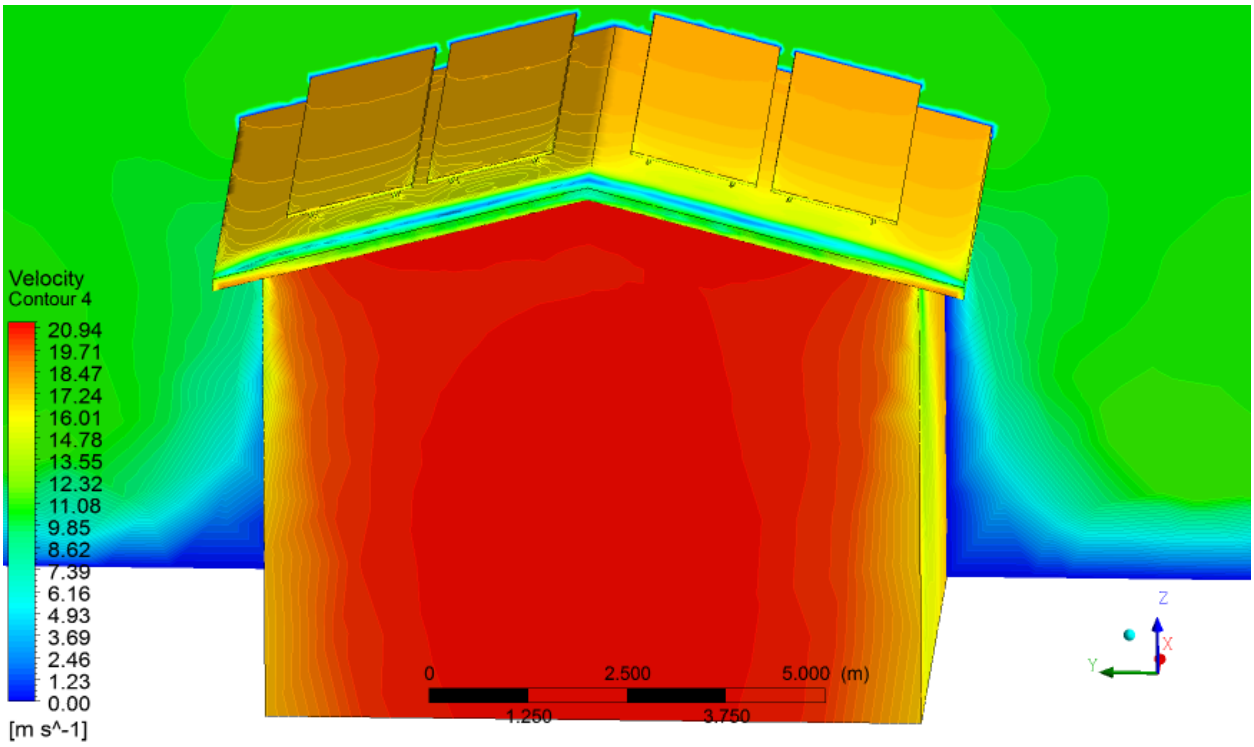


Fig. E. 237. Velocity distribution on a perpendicular plane to the ridge of the building, WD 0º, WW

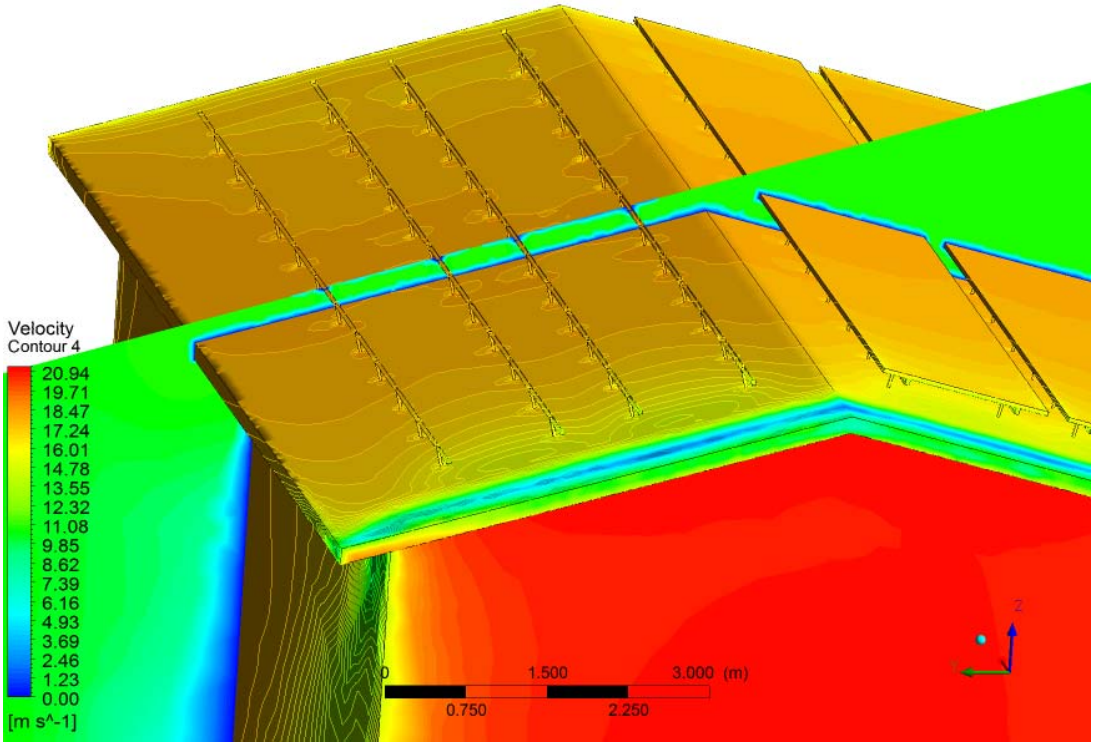


Fig. E. 238. Velocity distribution on a perpendicular plane to the building ridge, between roof and panels, WD 0º

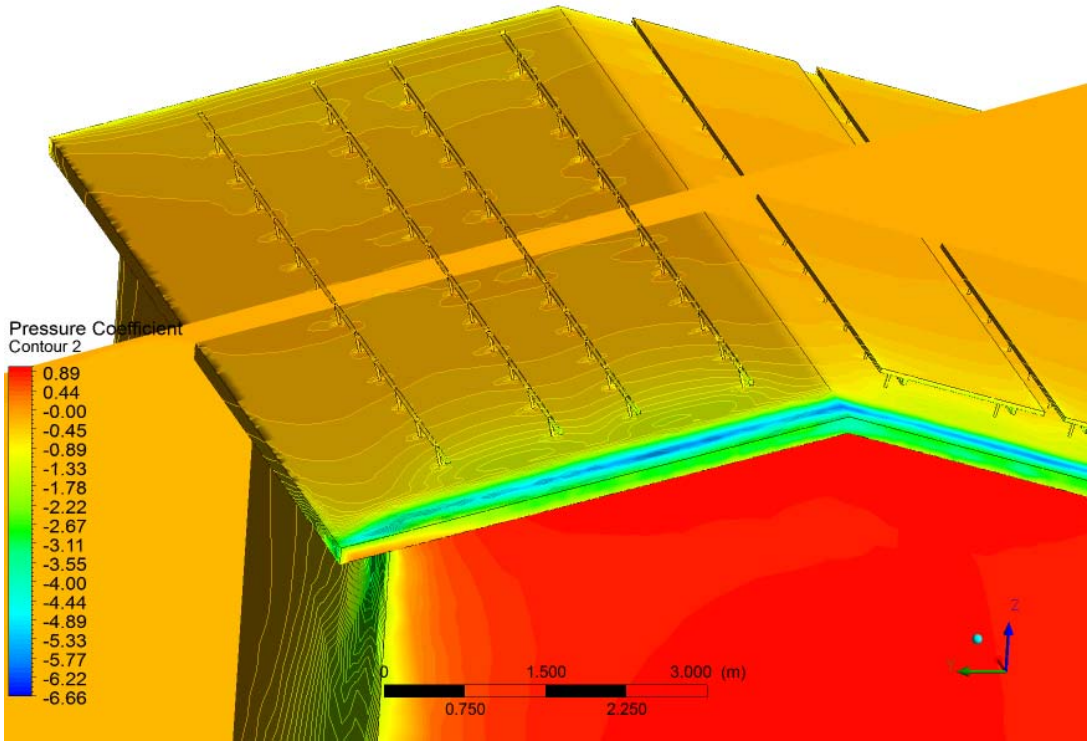


Fig. E. 239. Cp distribution on a perpendicular plane to the building ridge, between roof and panels, WD 0º

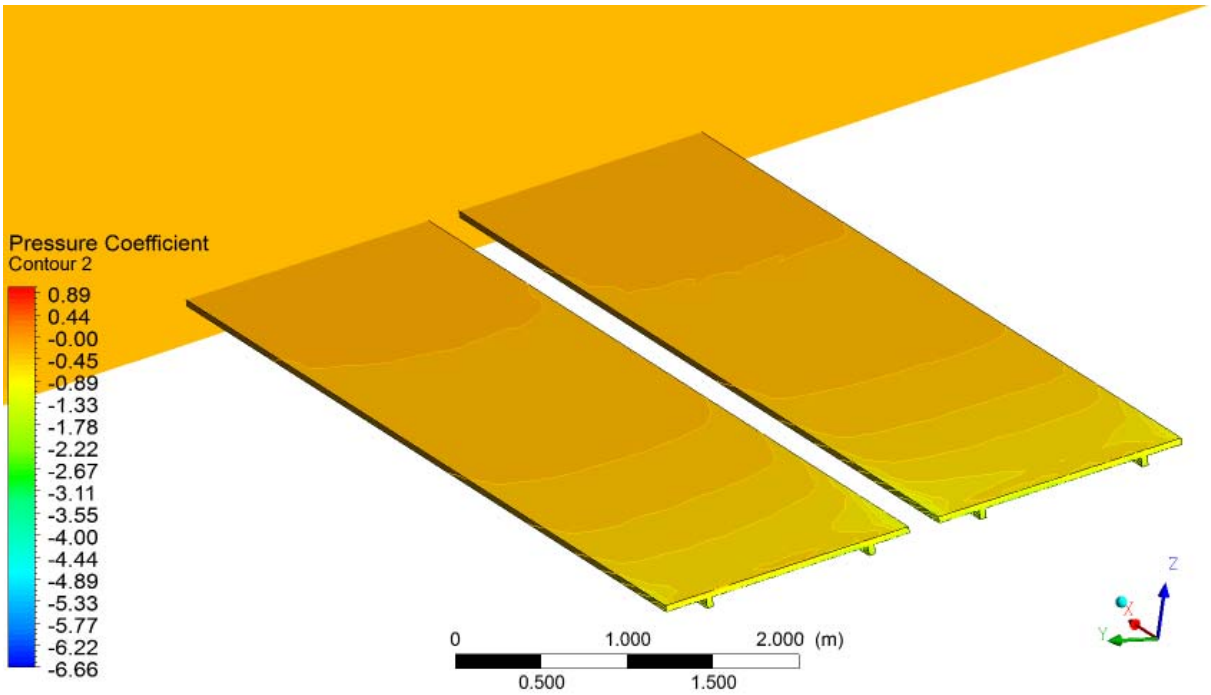


Fig. E. 240. Cp distribution on a perpendicular plane to the building ridge, above the panels, WD 0º

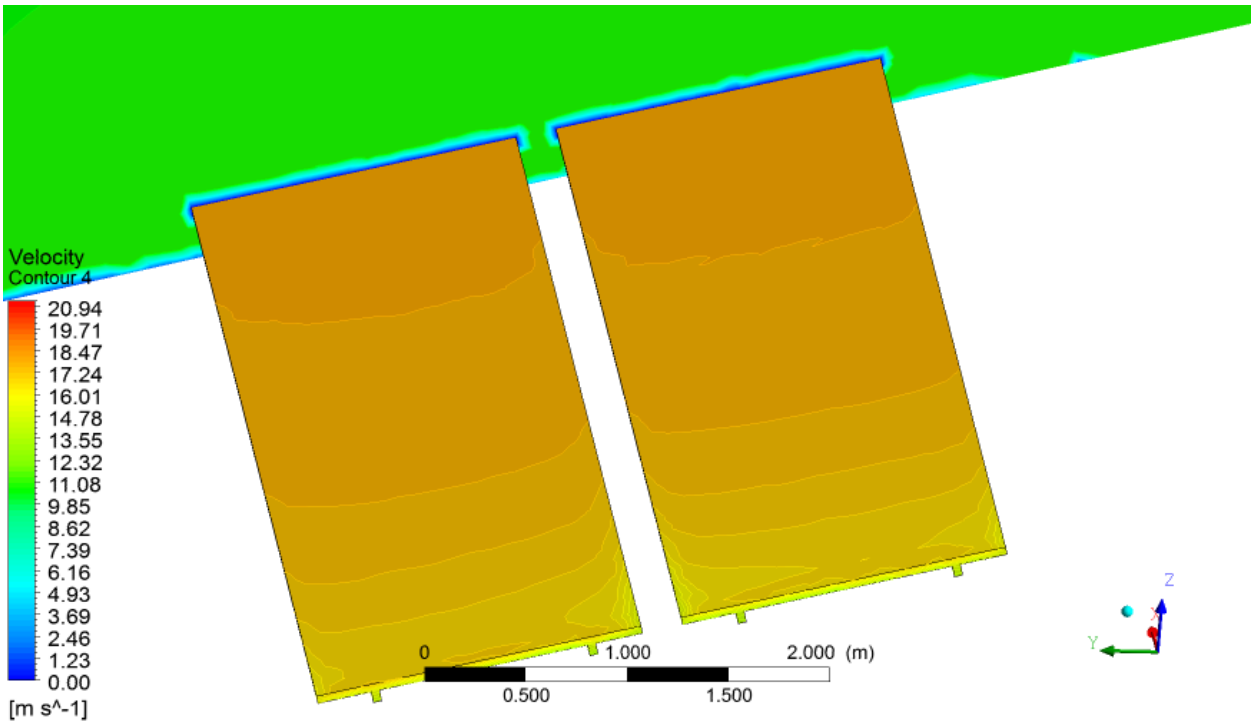


Fig. E. 241. Velocity distribution on a perpendicular plane to the building ridge, above the panels, WD 0º

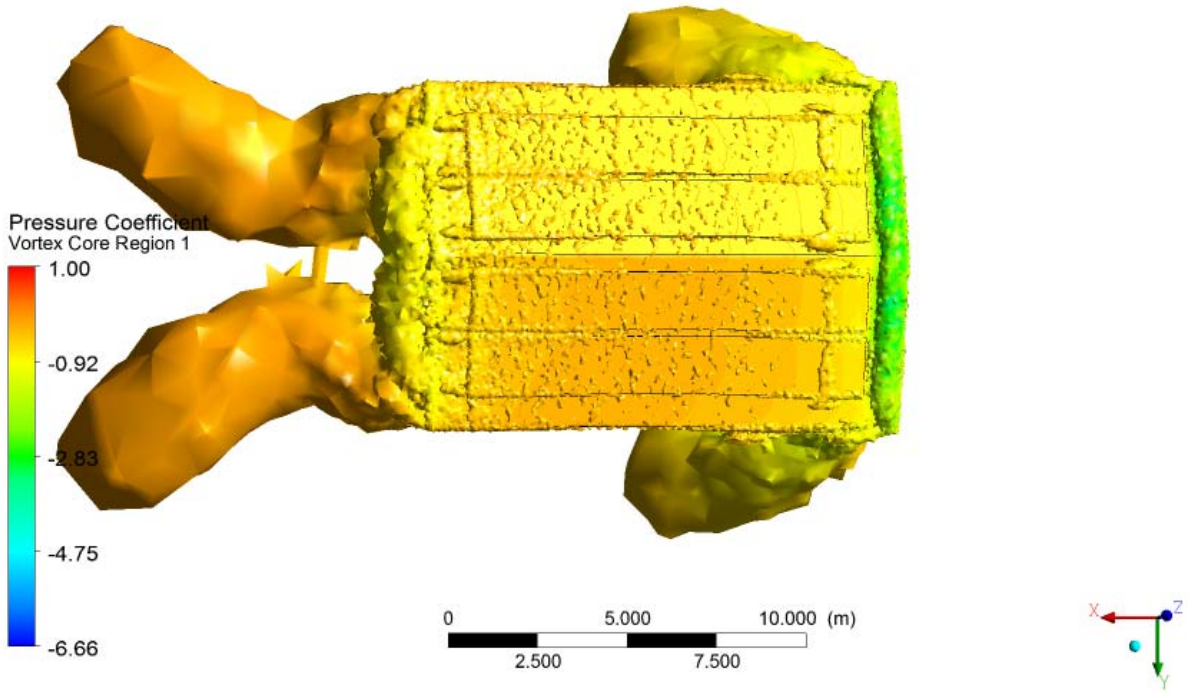


Fig. E. 242. Turbulence distribution, with CP, top view, building contours are shown, WW, S 15º, WD 0º

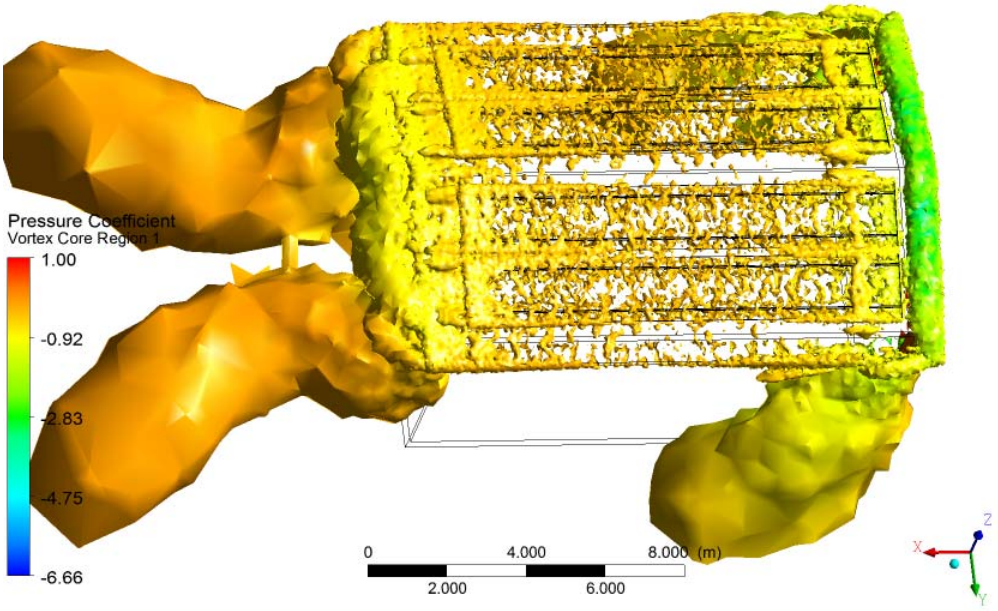


Fig. E. 243. Turbulence distribution, with CP, top view no building contours are shown, LW, S 15º, WD 0º

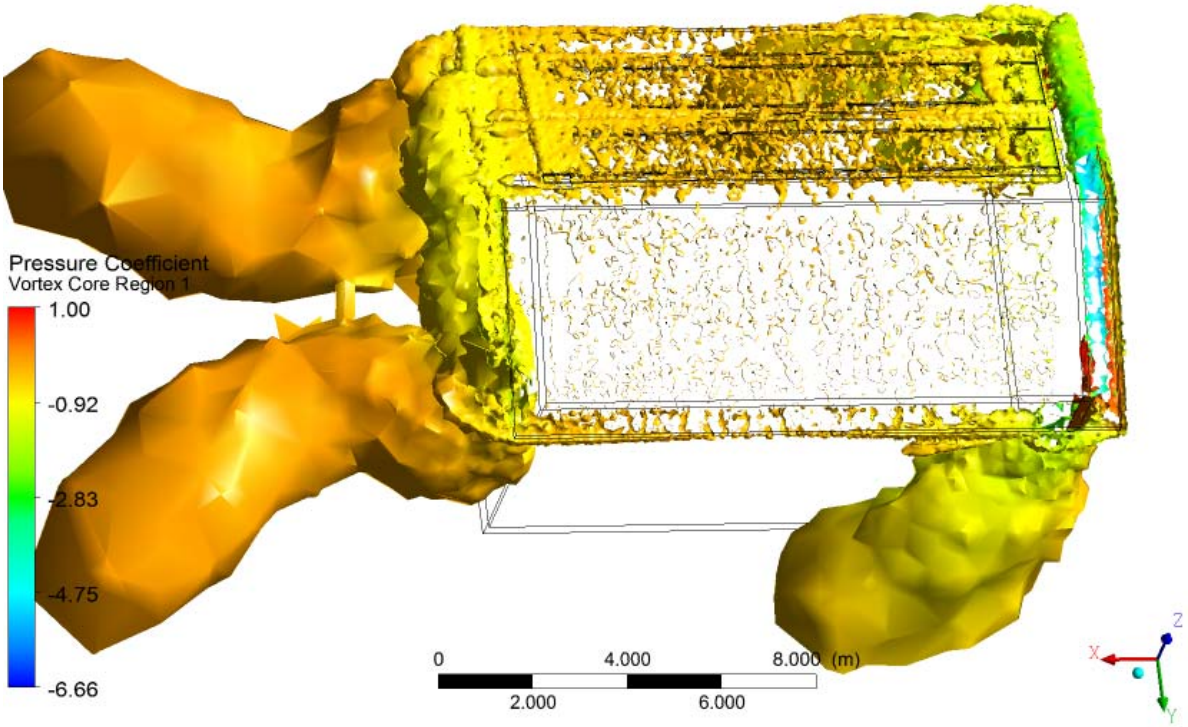


Fig. E. 244. Turbulence distribution, with CP on top of solar panels on one side and on roof under solar panels on the other side, top view no building contours are shown, S 15º, WD 0º

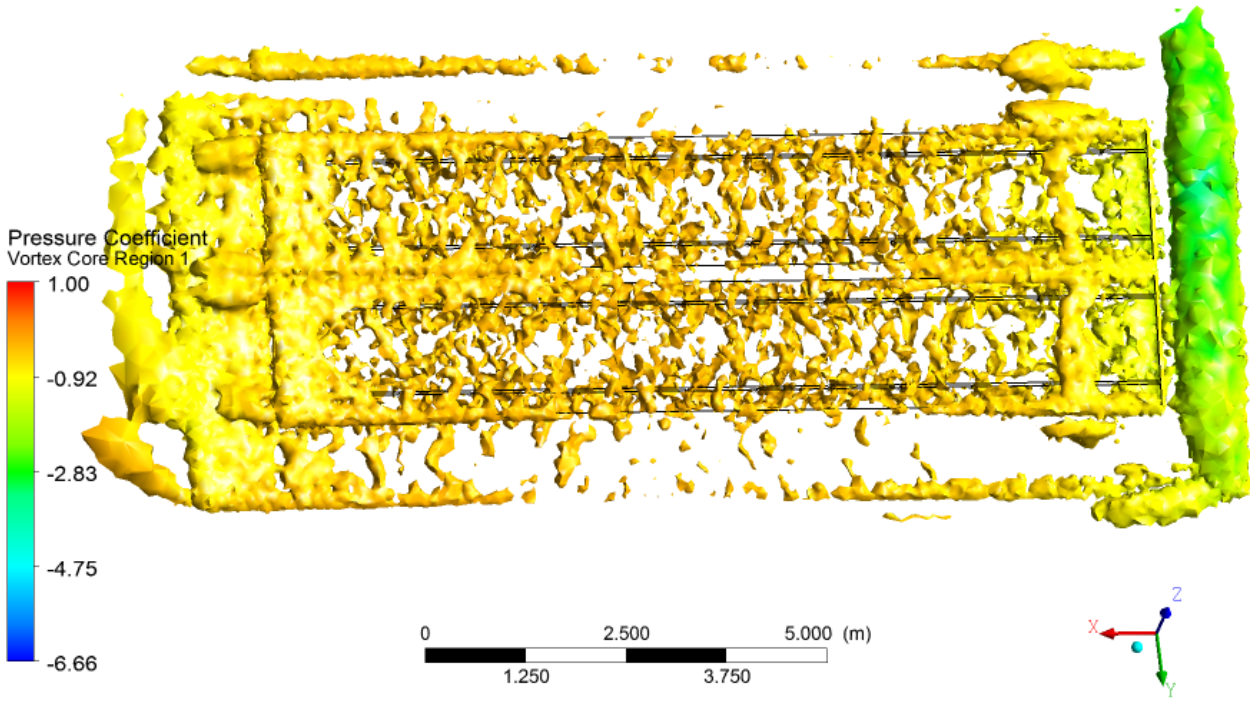


Fig. E. 245. Cp on turbulences on top of solar panels on one side of the roof, no building contours, S 15º, WD 0º

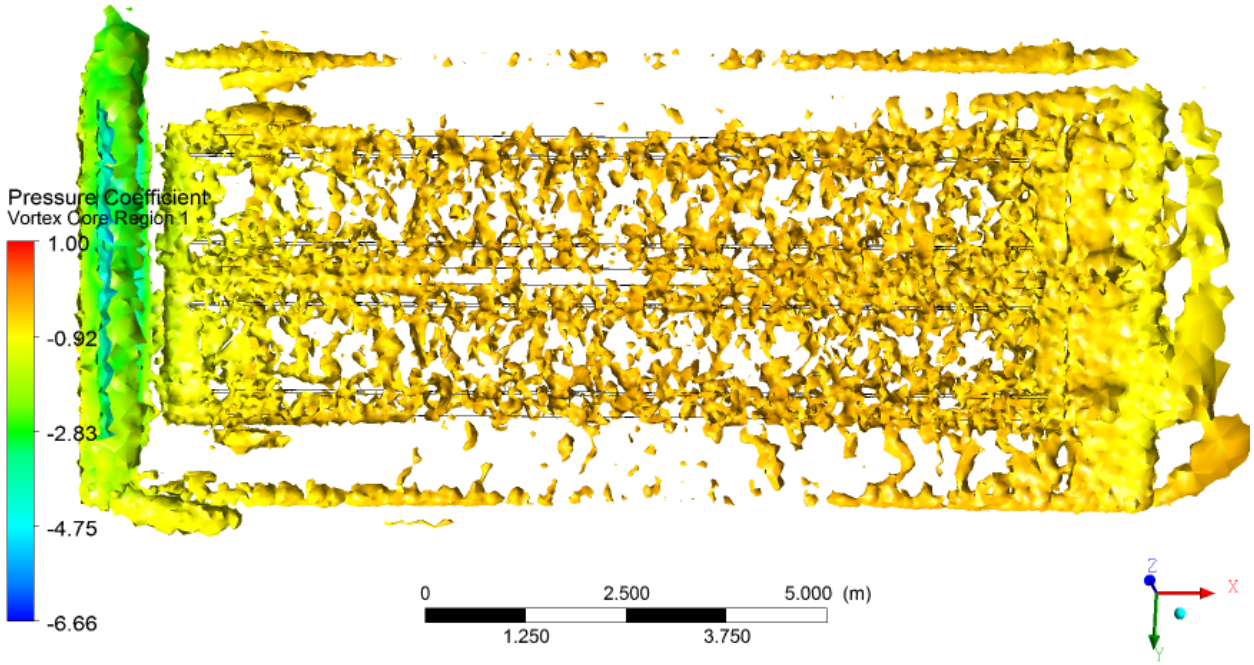


Fig. E. 246. Cp on turbulences on bottom of the solar panels on one side of the roof, no building contours, S 15º, WD 0º

1.3.4. Detailed Distribution of Wind Pressure and speed on Roof Mounted Solar Panels in Comparison with Bare Roof, S8"C10"

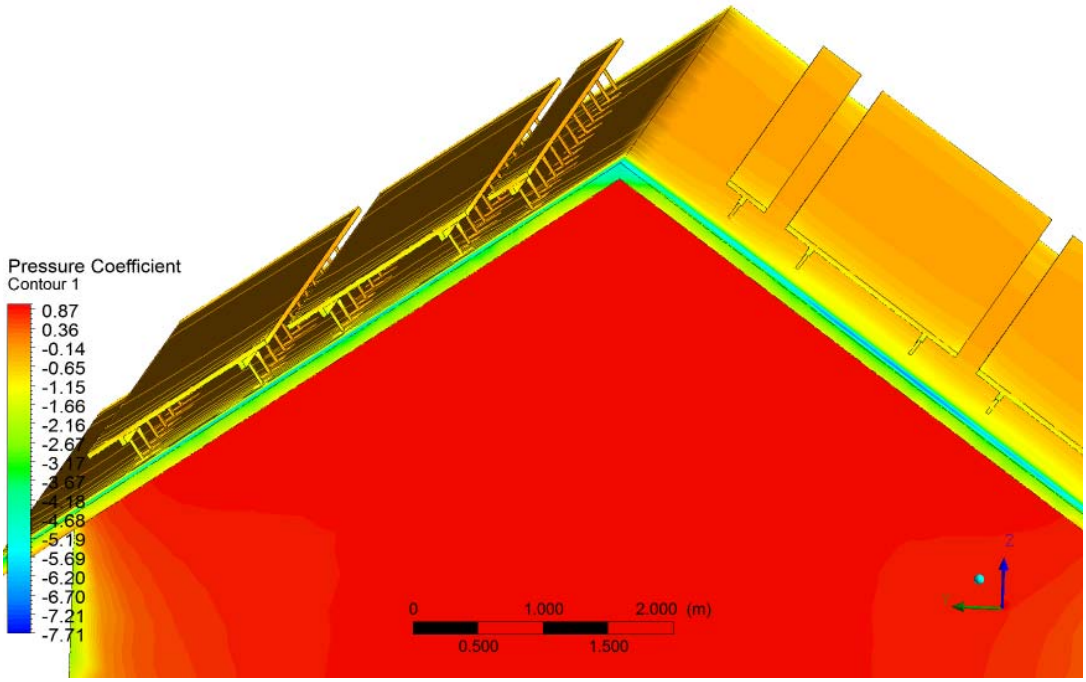


Fig. E. 247. Cp of a close view shows panel supports, WD 0º, LW

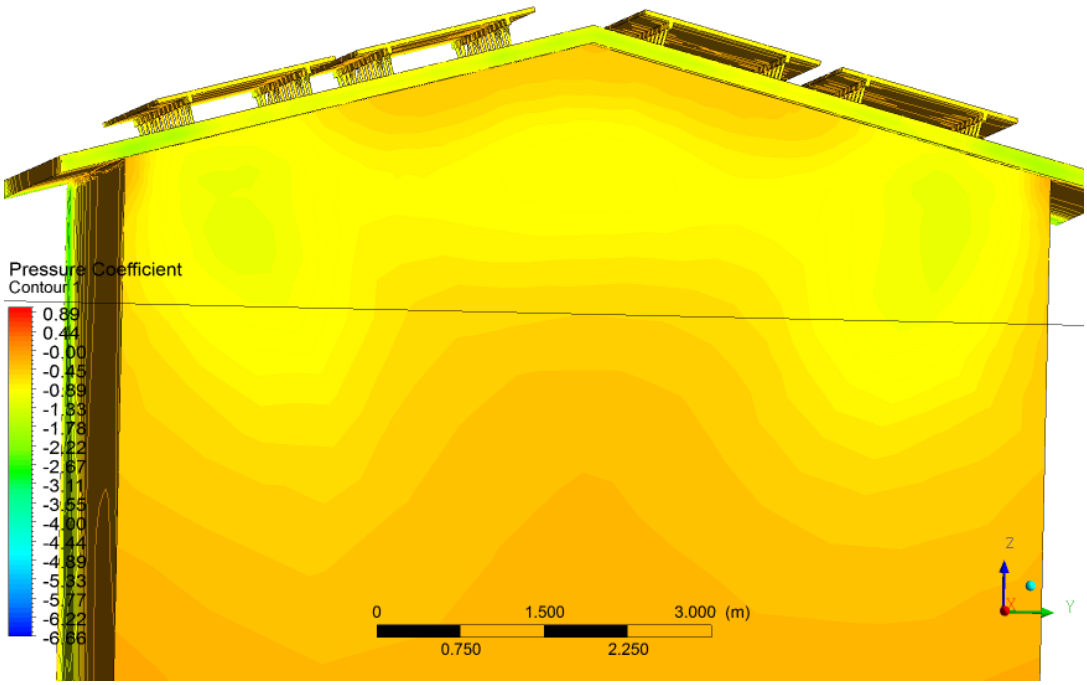


Fig. E. 248. Cp of a close view shows panel supports, WD 0º, LW

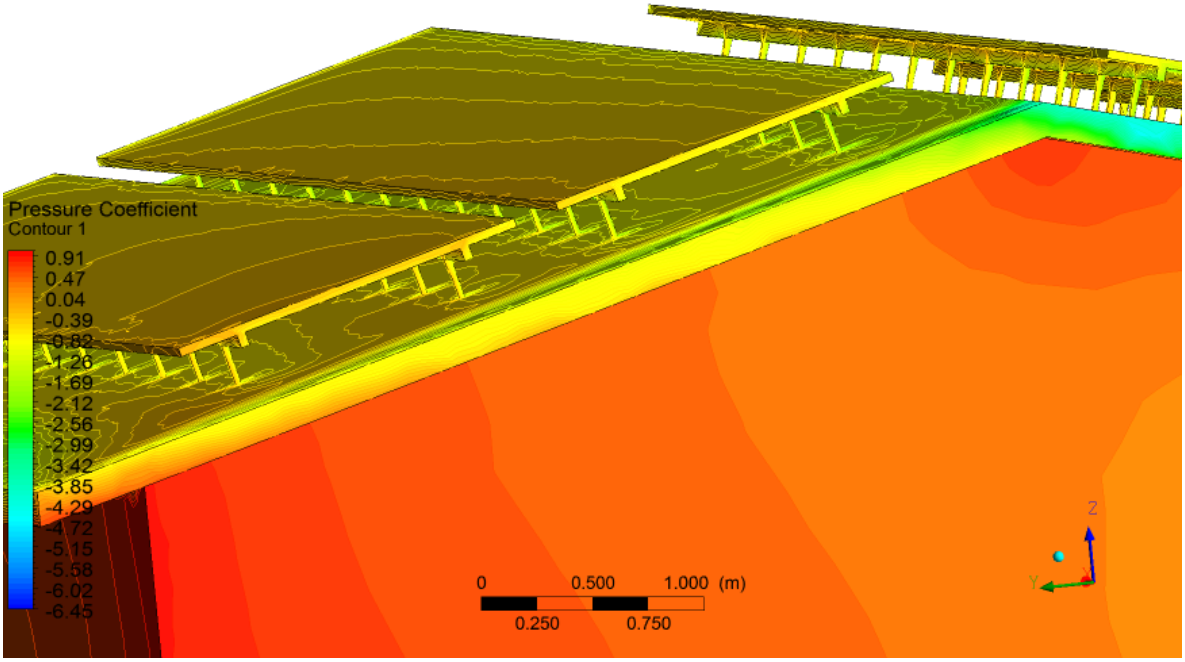


Fig. E. 249. Cp of a close view shows panel supports, WD 45º, WW

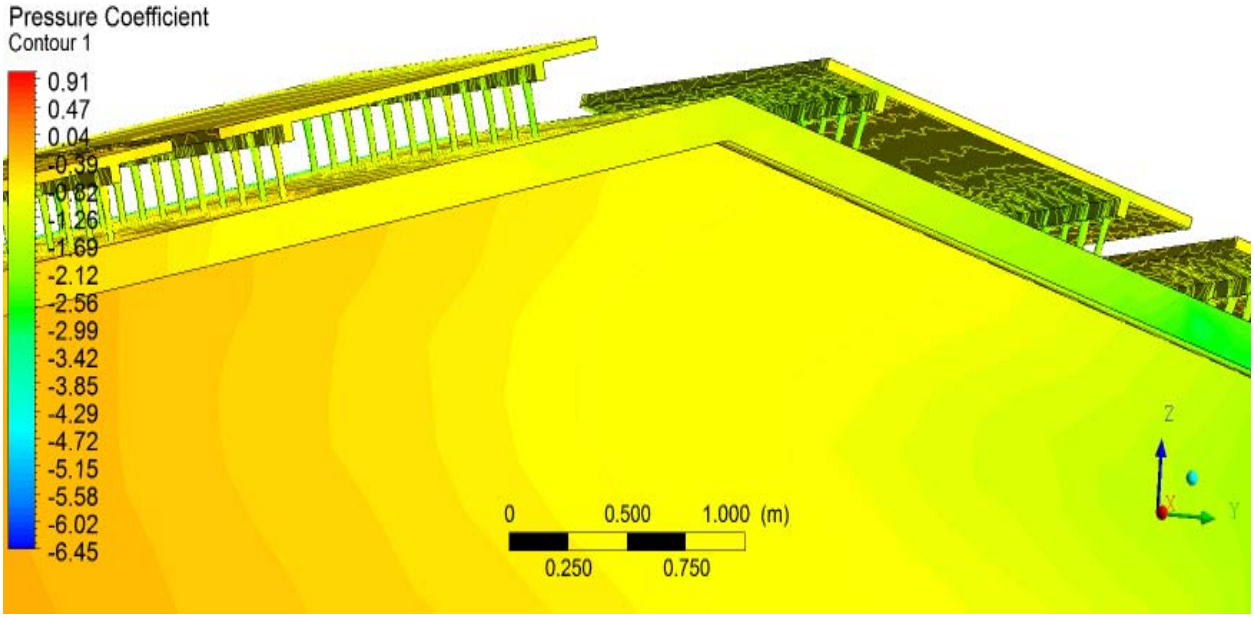


Fig. E. 250. Cp of a close view shows panel supports, WD 45º, LW

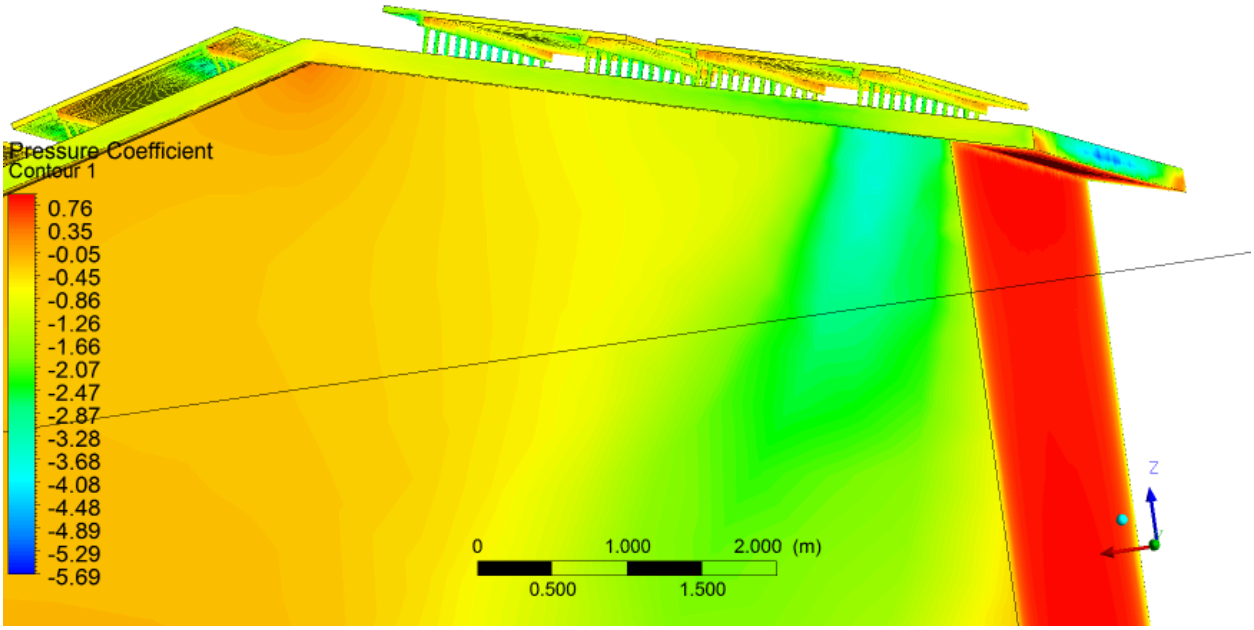


Fig. E. 251. Cp of a close view shows panel supports, WD 90º, WW

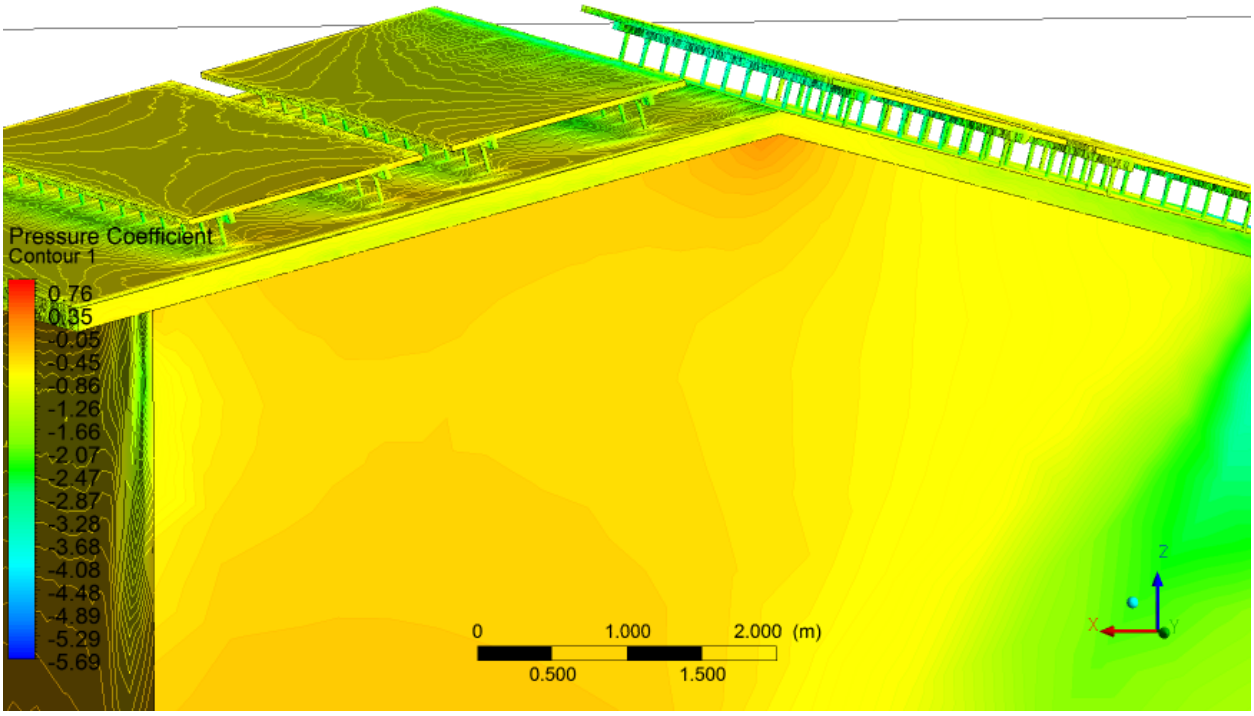


Fig. E. 252. Cp of a close view shows panel supports, WD 90º, LW

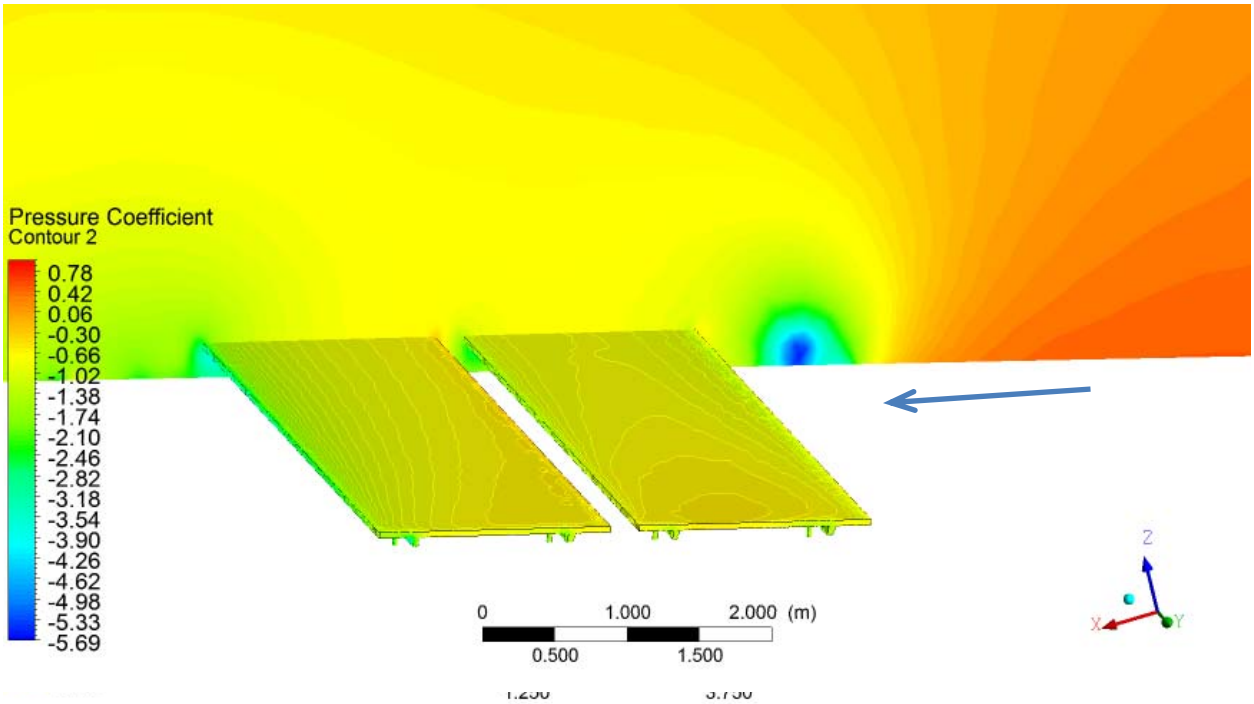


Fig. E. 253. Cp on a perpendicular plane and on top of panels, WD 90º, WW

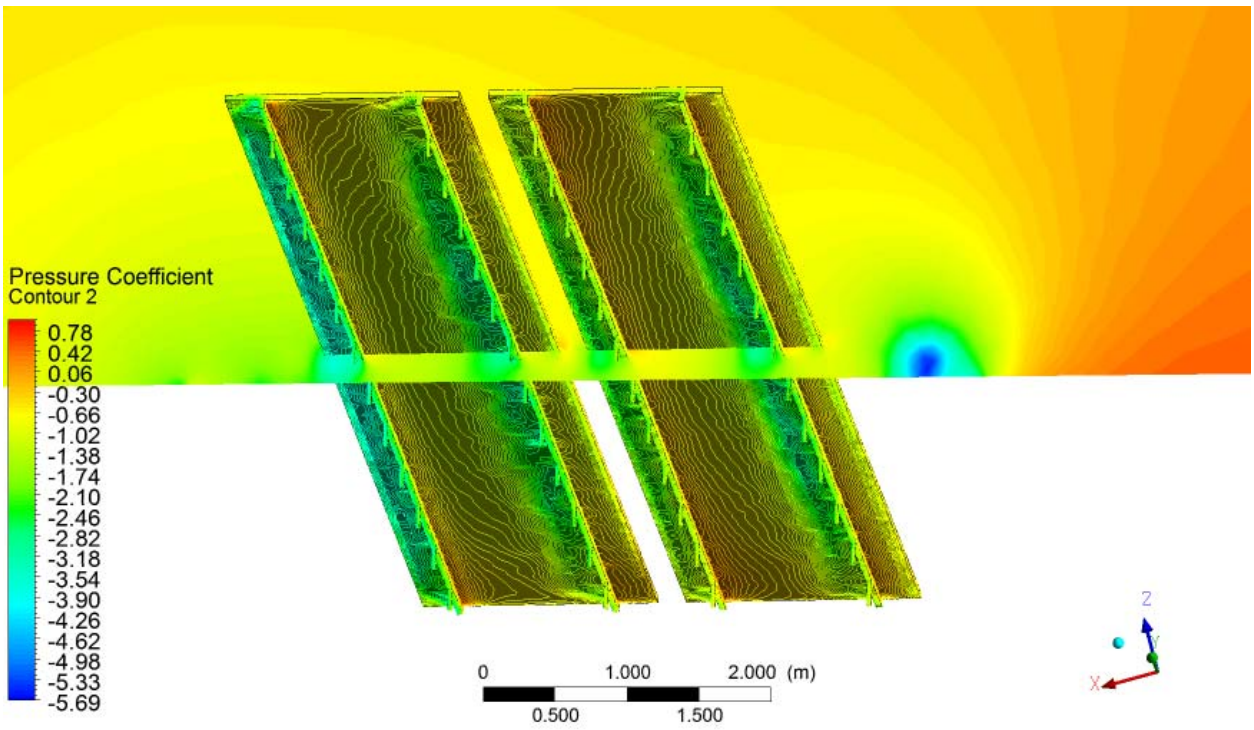


Fig. E. 254. Cp on a perpendicular plane and bottom of panels, WD 90º, WW

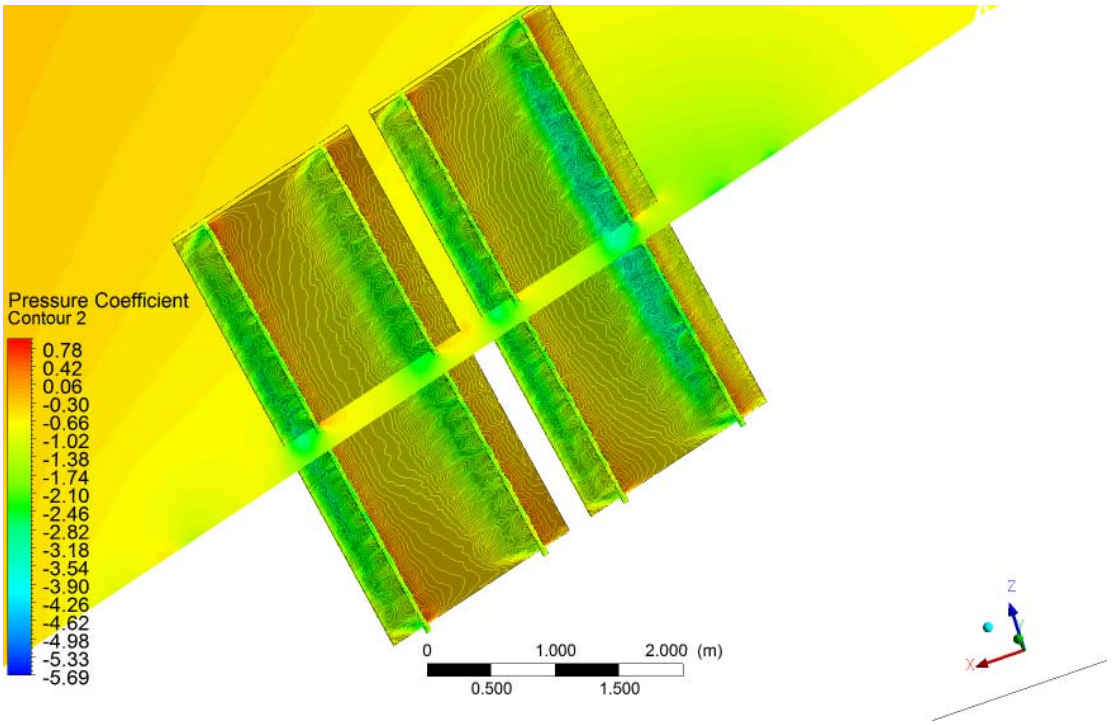


Fig. E. 255. Cp on a perpendicular plane and bottom of panels, WD 90º, LW

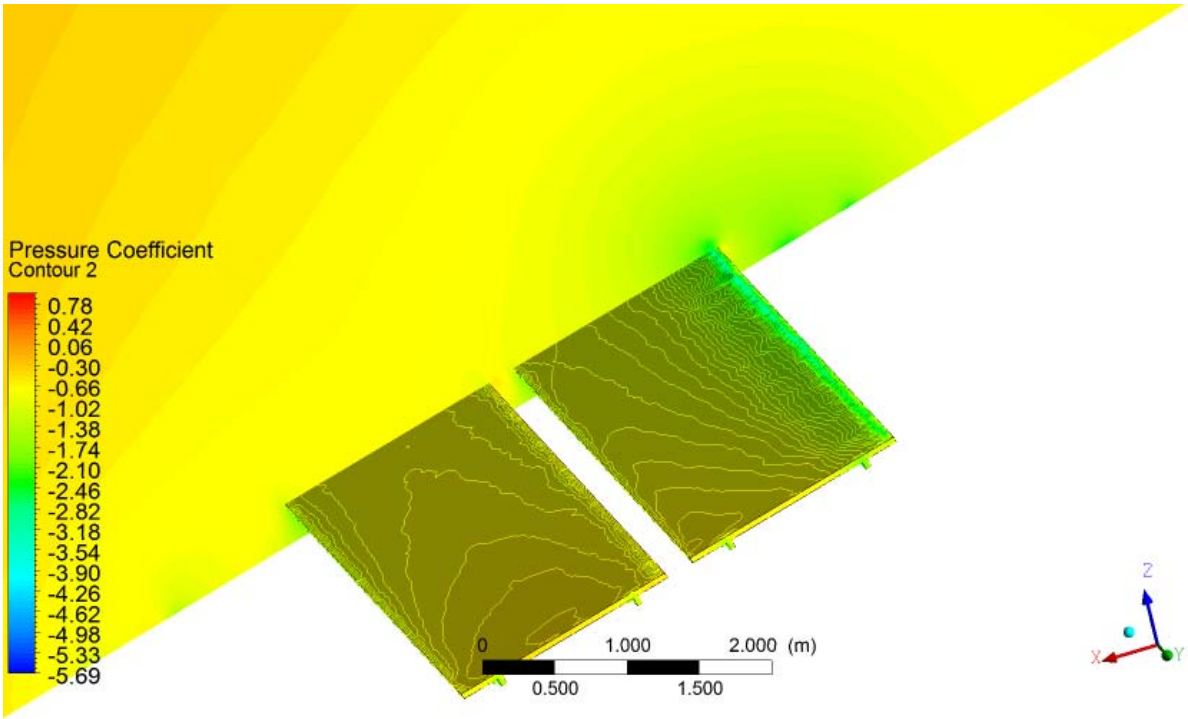


Fig. E. 256. Cp on a perpendicular plane and on top of panels, WD 90º, LW

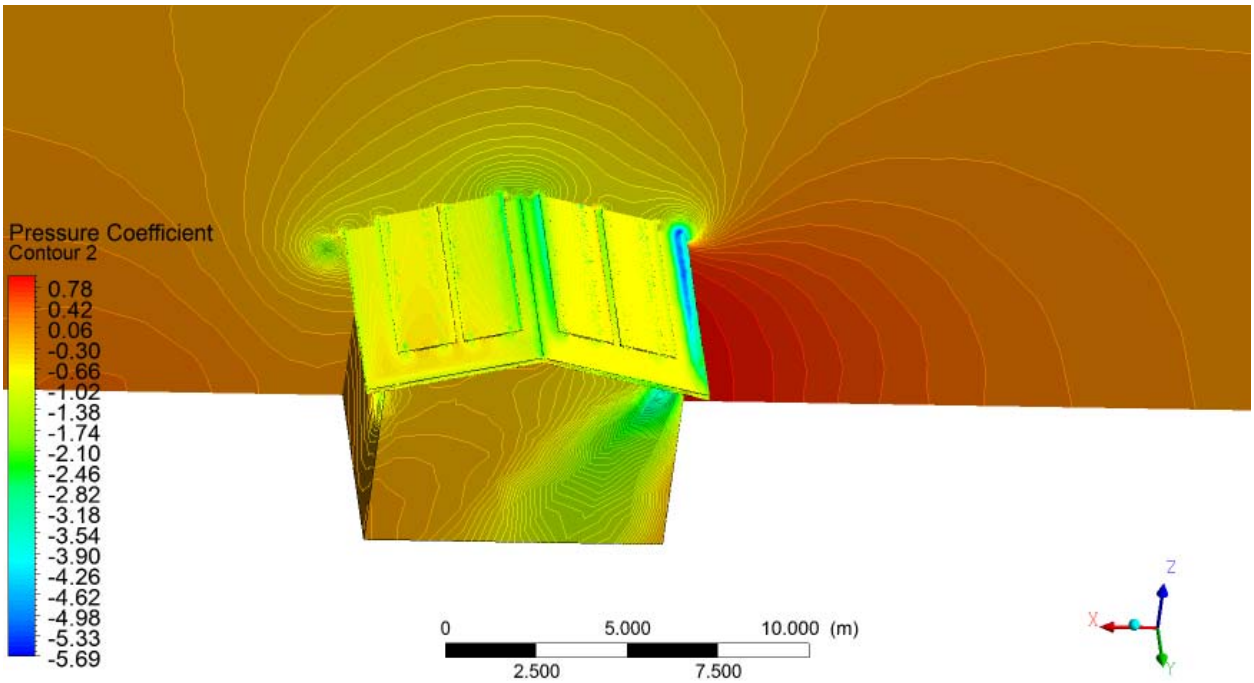


Fig. E. 257. Cp on a perpendicular plane on ridge of the building, WD 90º

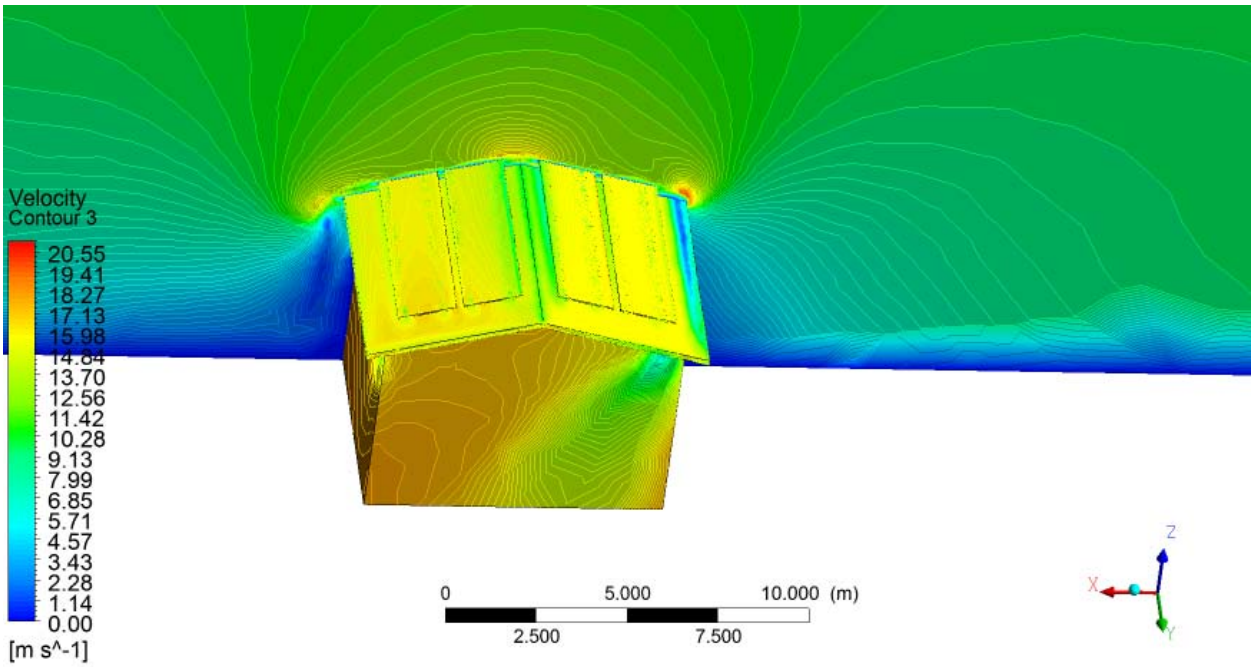


Fig. E. 258.Velocity distribution on a perpendicular plane to the ridge of the building, WD 90º

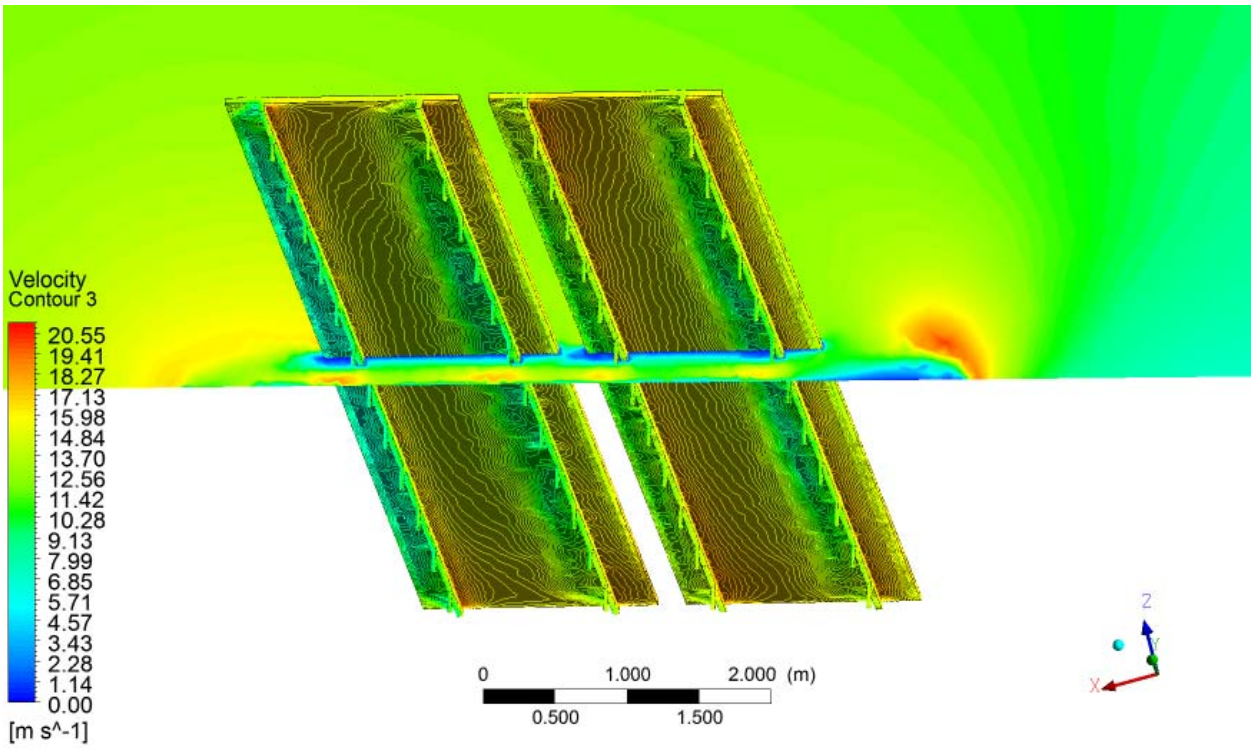


Fig. E. 259. Velocity distribution on bottom of panels and a perpendicular plane to building ridge, WD 90º, WW

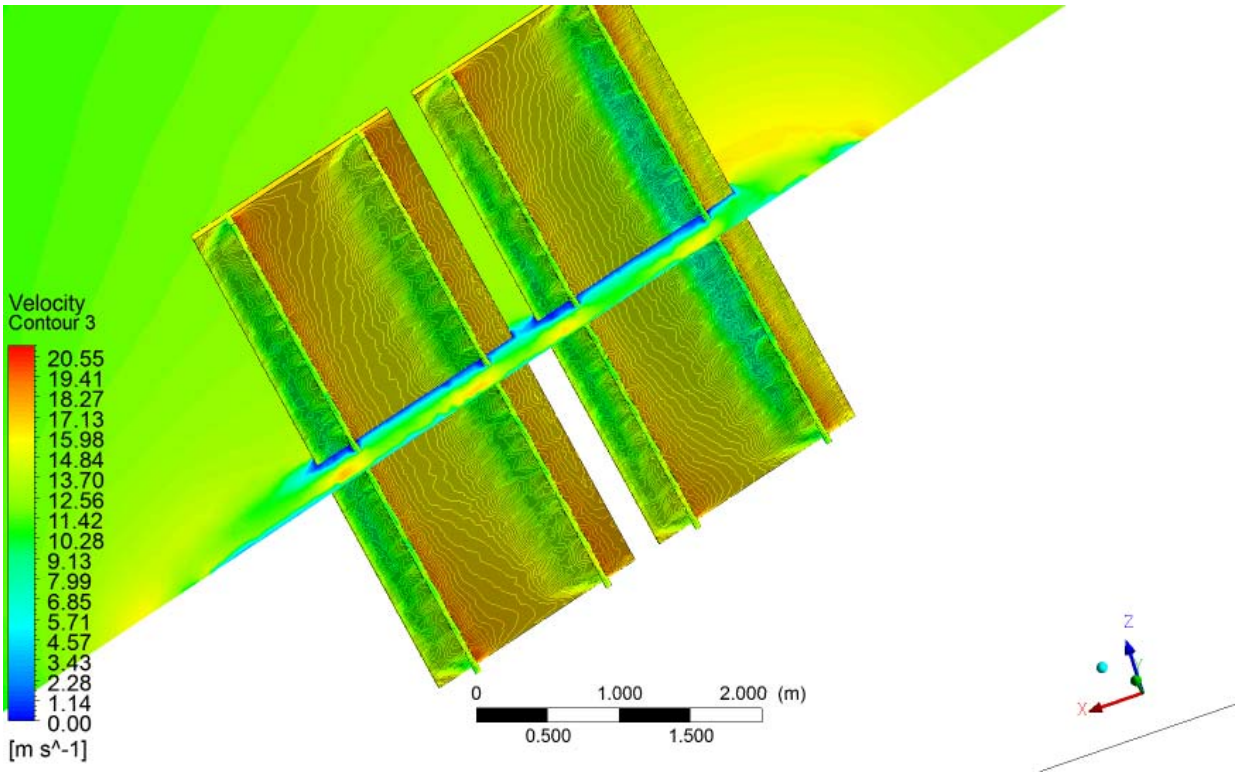


Fig. E. 260. Velocity distribution on bottom of panels and a perpendicular plane to building ridge, WD 90º, LW

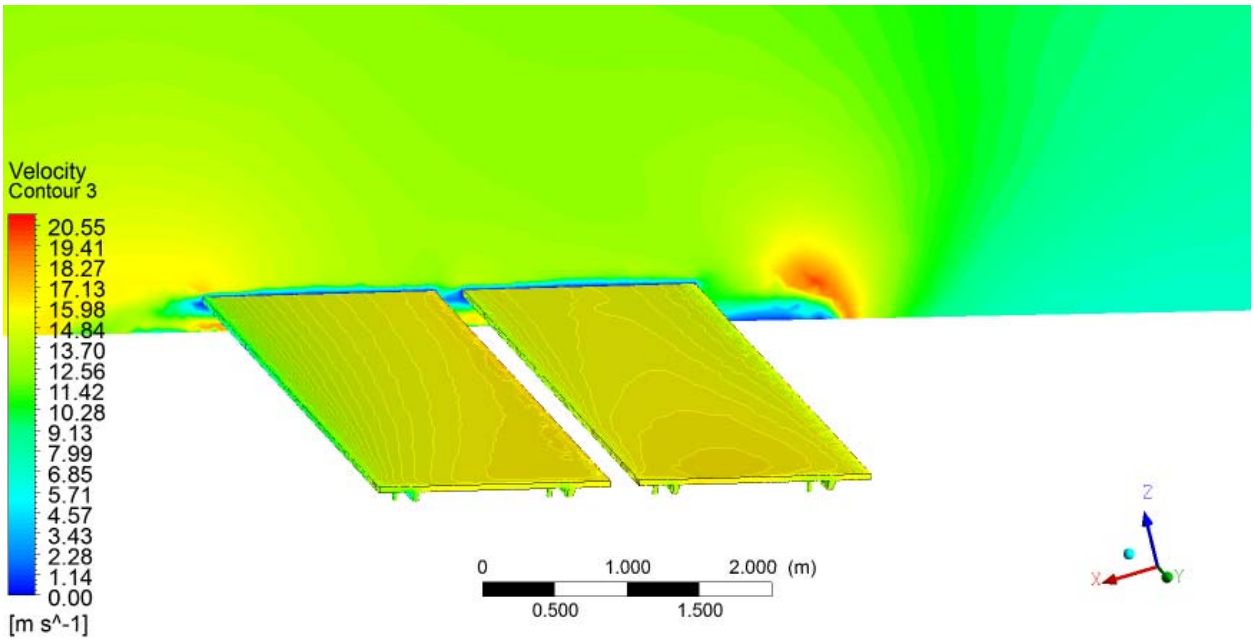


Fig. E. 261. Velocity distribution on top of panels and a perpendicular plane to building ridge, WD 90º, WW

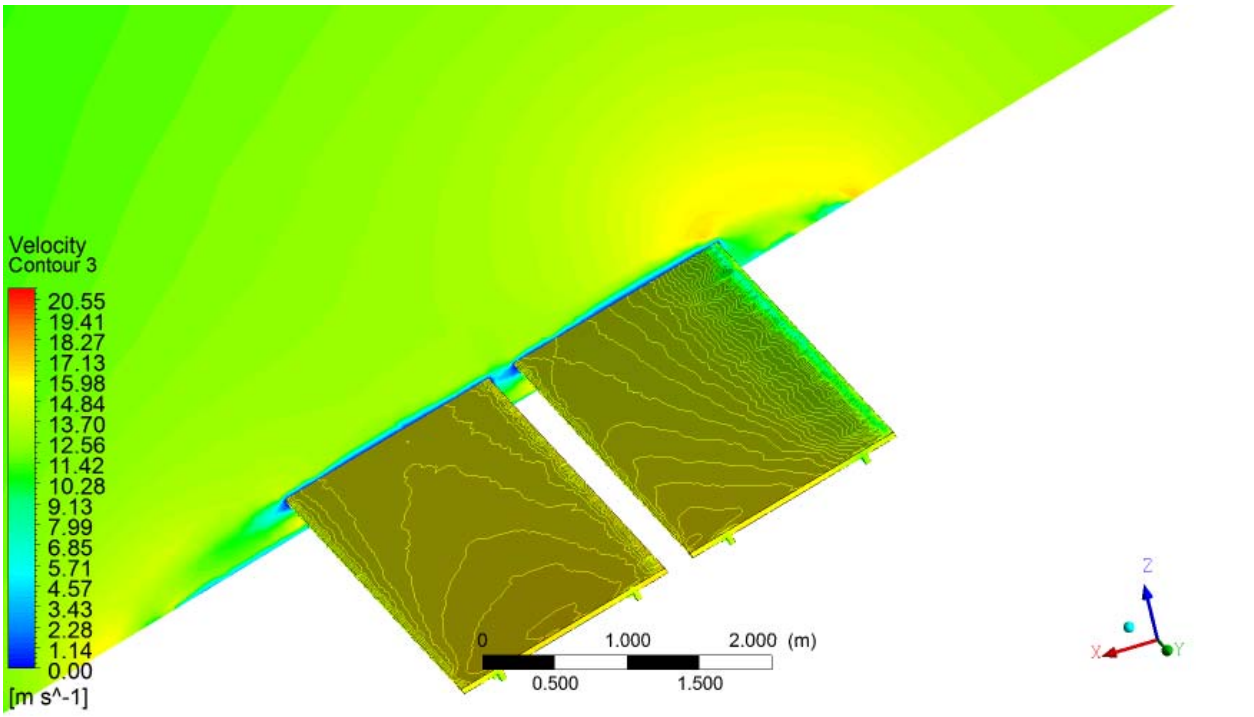


Fig. E. 262. Velocity distribution on top of panels and a perpendicular plane to building ridge, WD 90º, LW

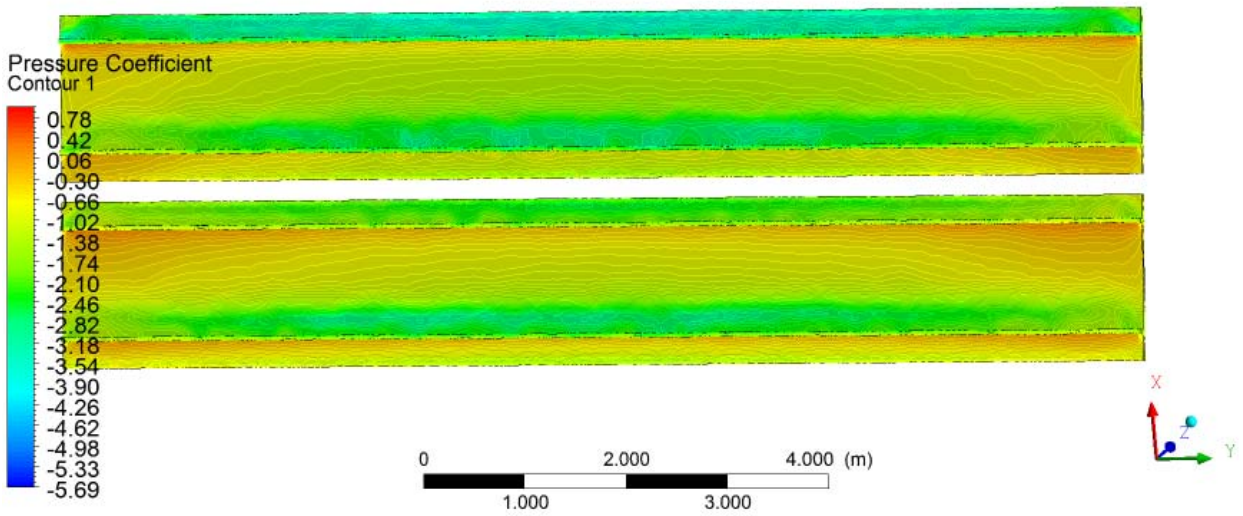


Fig. E. 263. Cp on a perpendicular plane on bottom of panels, Close up WD 90º, WW

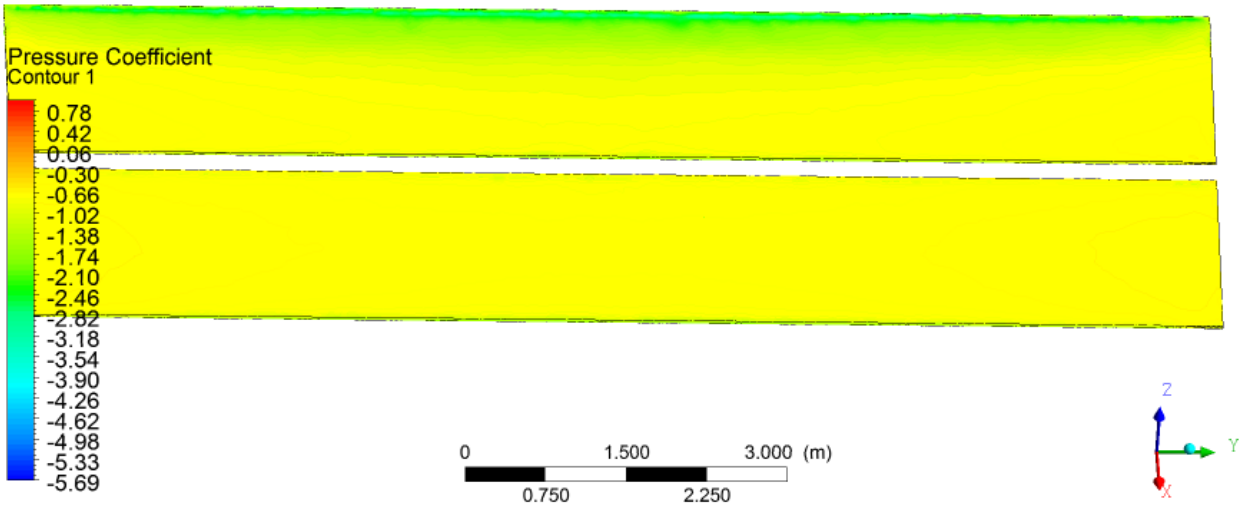


Fig. E. 264. Cp on top of panels, WD 90º, LW

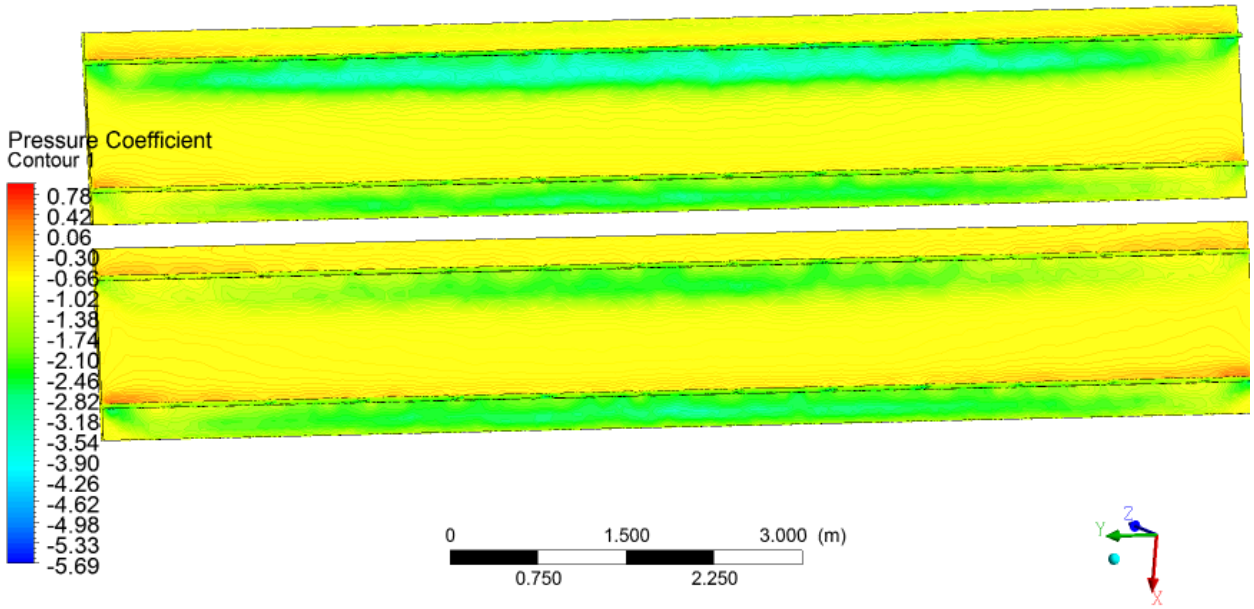


Fig. E. 265. Cp on bottom of panels, WD 90º, LW

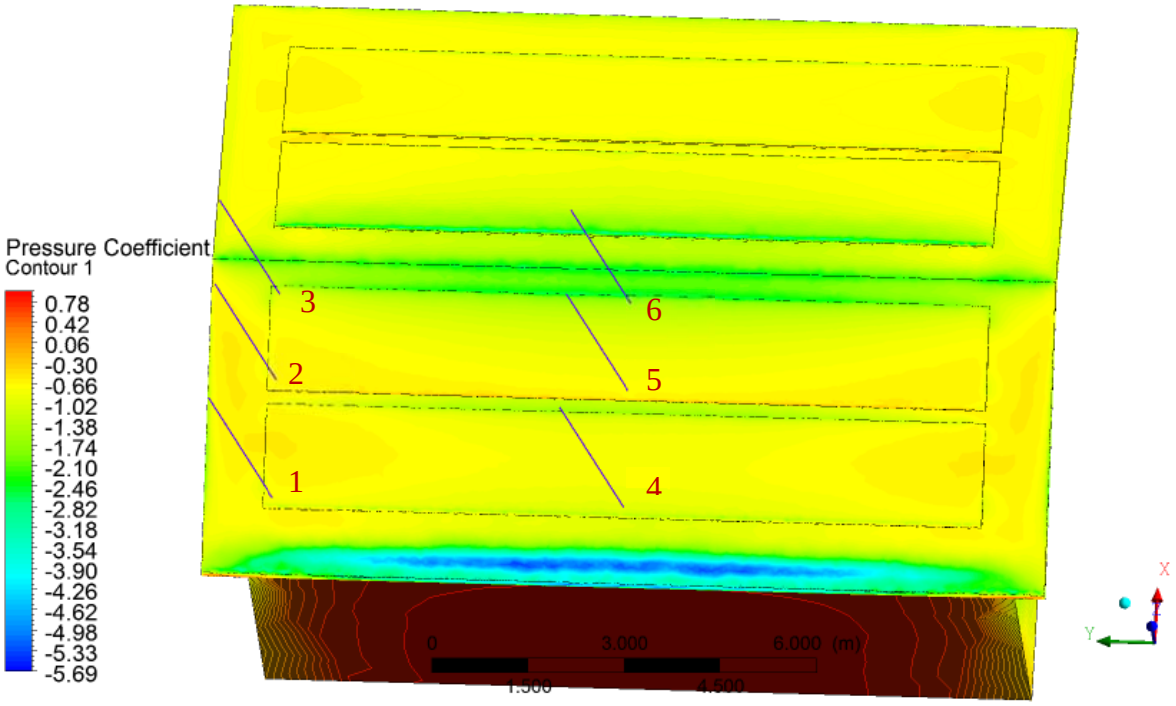


Fig. E. 266. Lines used to draw velocity and pressure changes, WD 90º

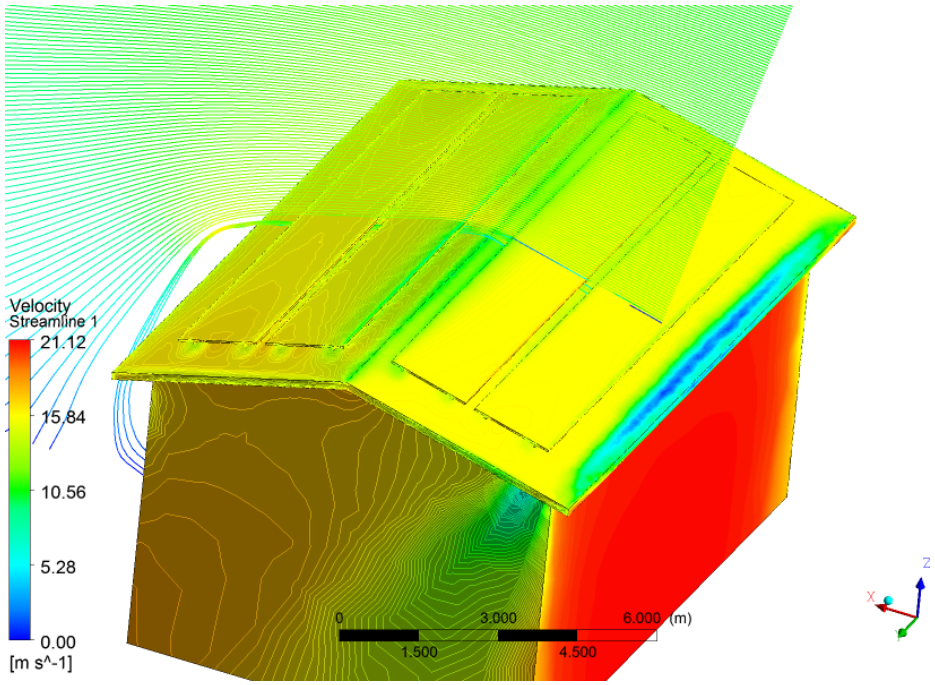


Fig. E. 267. Velocity stream lines at middle cross section plane, WD 90º

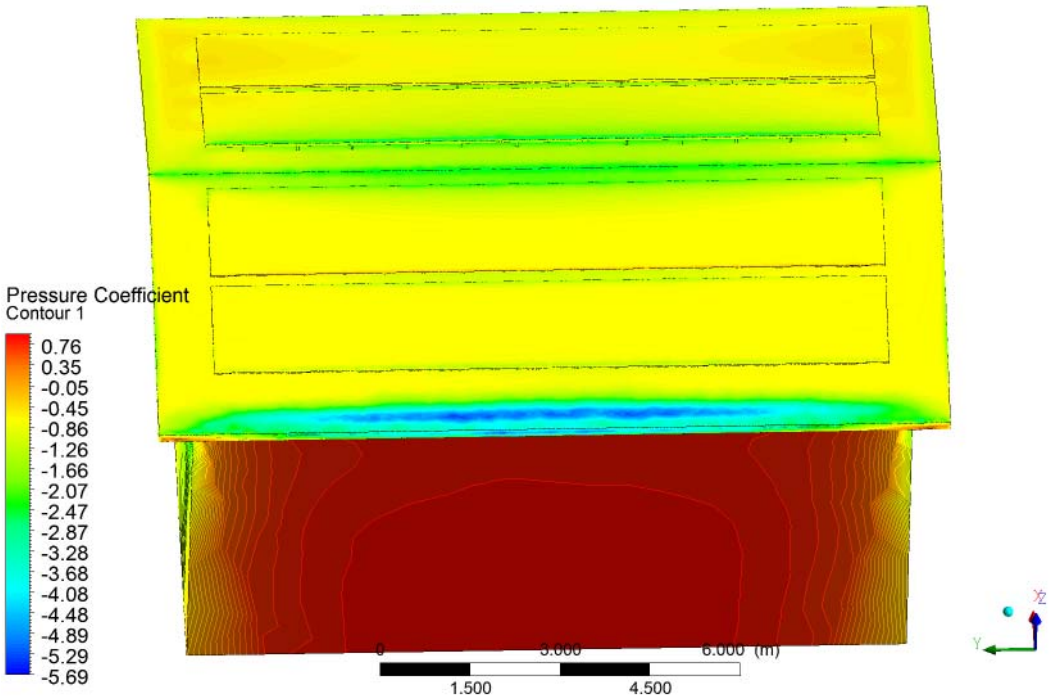


Fig. E. 268. Cp contour whole building, WD 90º, WW

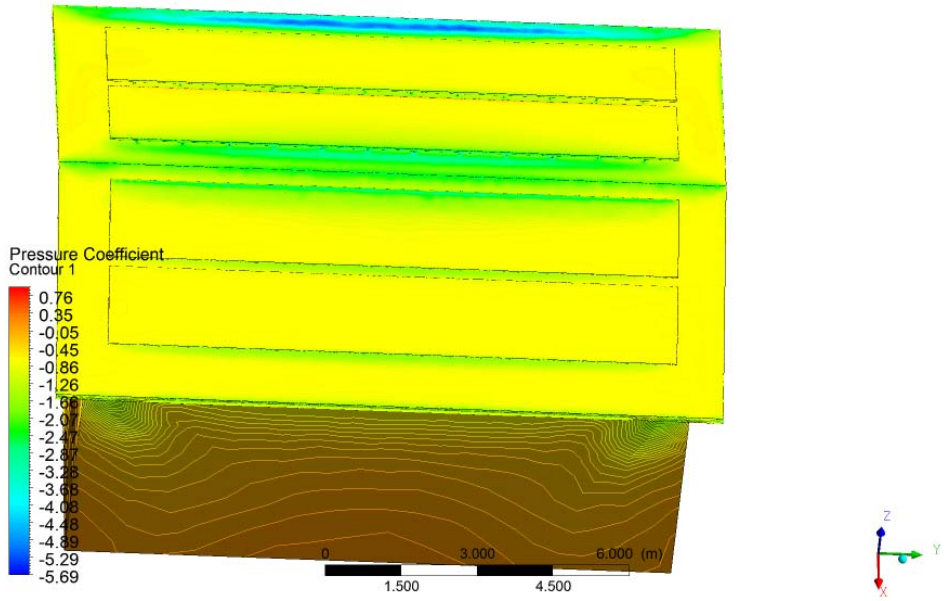


Fig. E. 269. Cp contour whole building, perspective view, WD 90º, LW

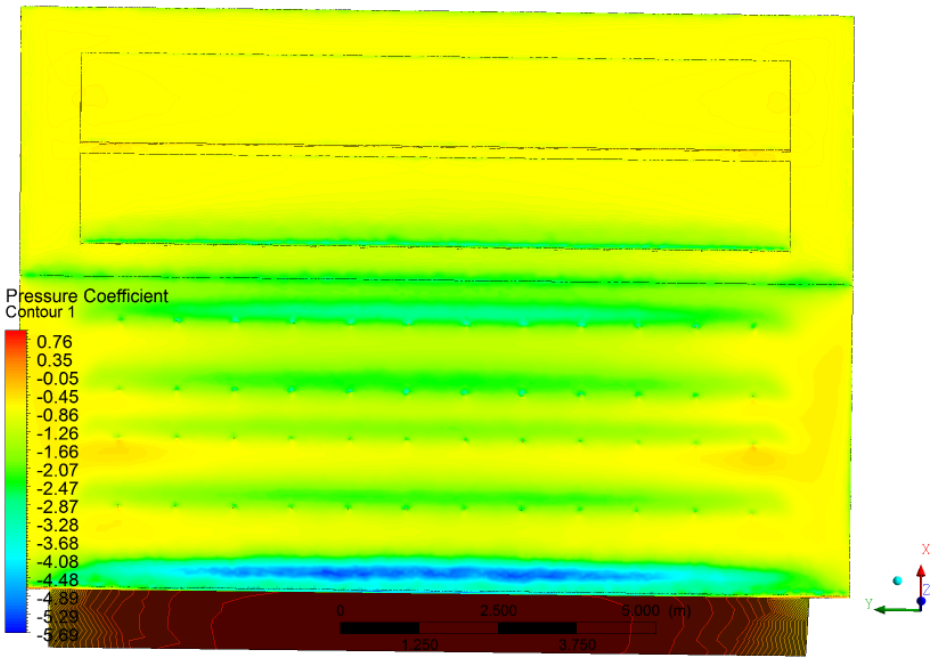


Fig. E. 270. Cp contour, roof under panels, WD 90º, WW

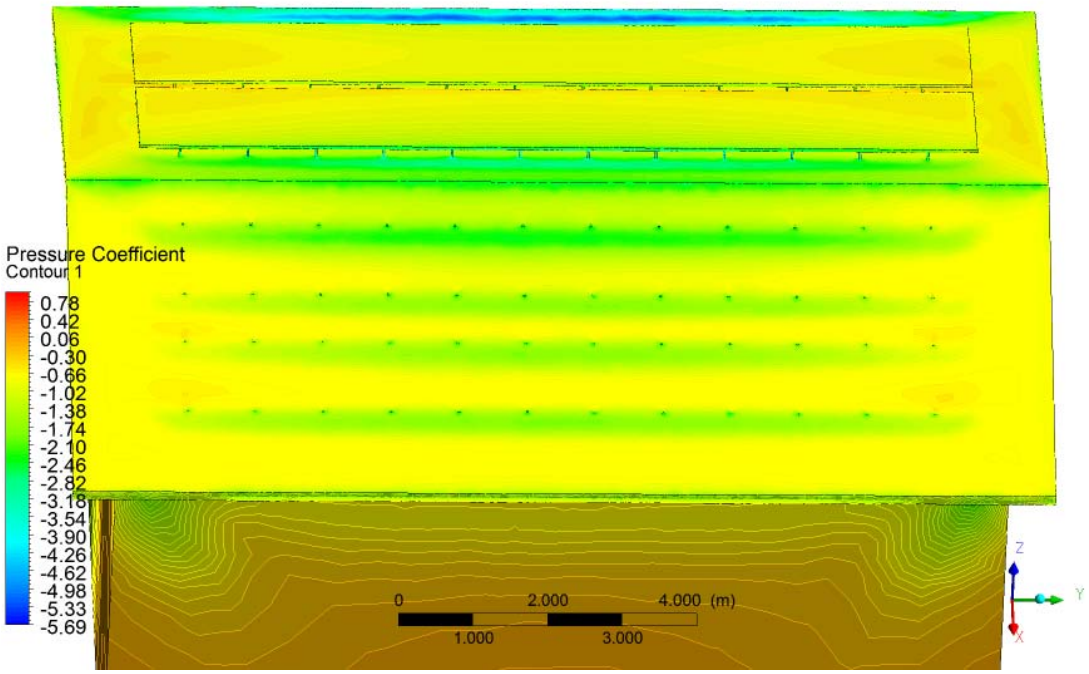


Fig. E. 271. Cp contour, roof under panels, WD 90º, LW

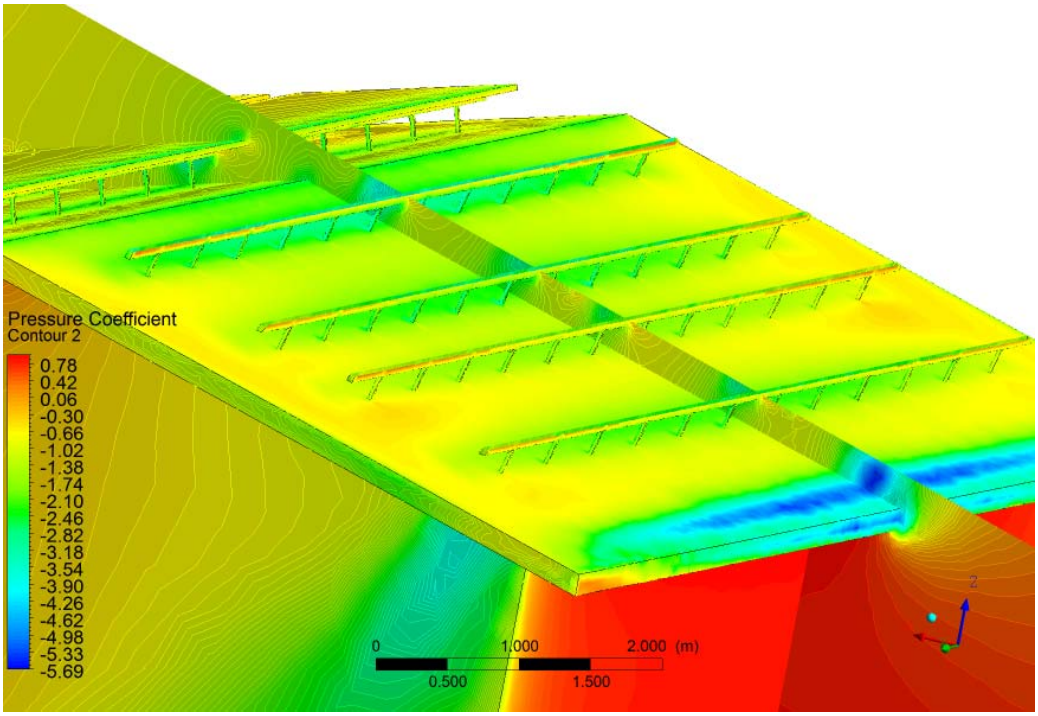


Fig. E. 272. Cp distribution between roof and bottom of panels, WD 90º, WW

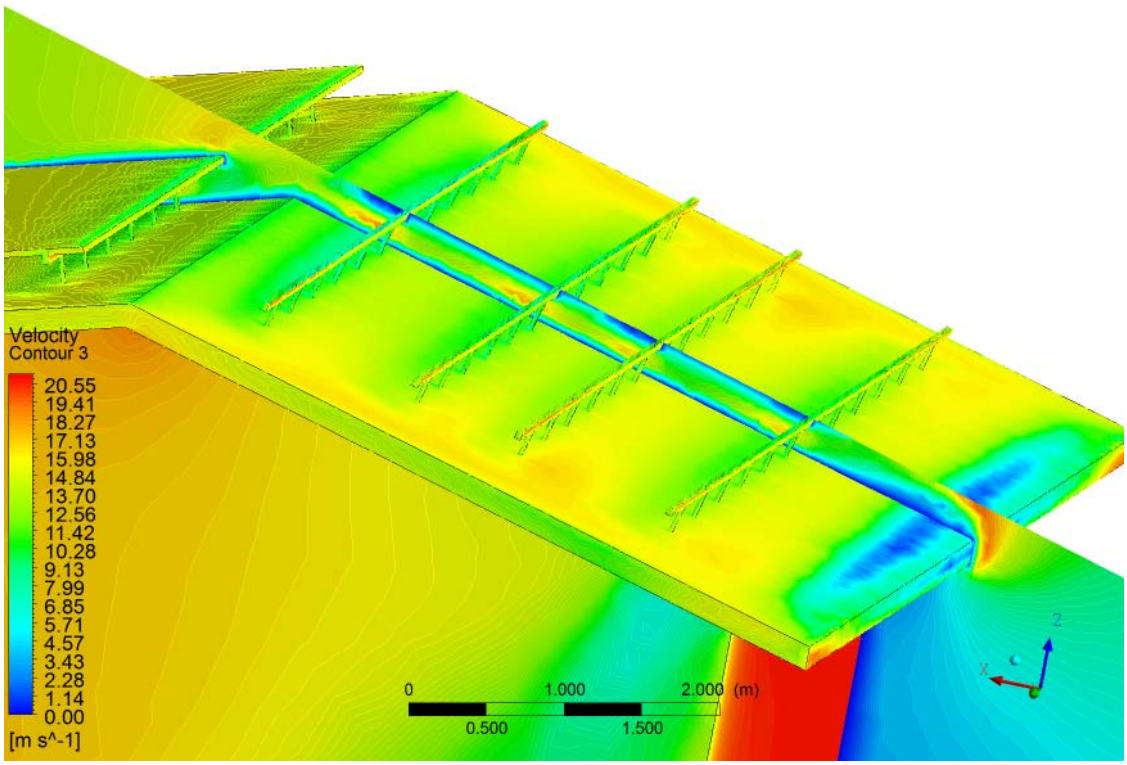


Fig. E. 273. Velocity distribution between roof and bottom of panels, WD 90º, WW

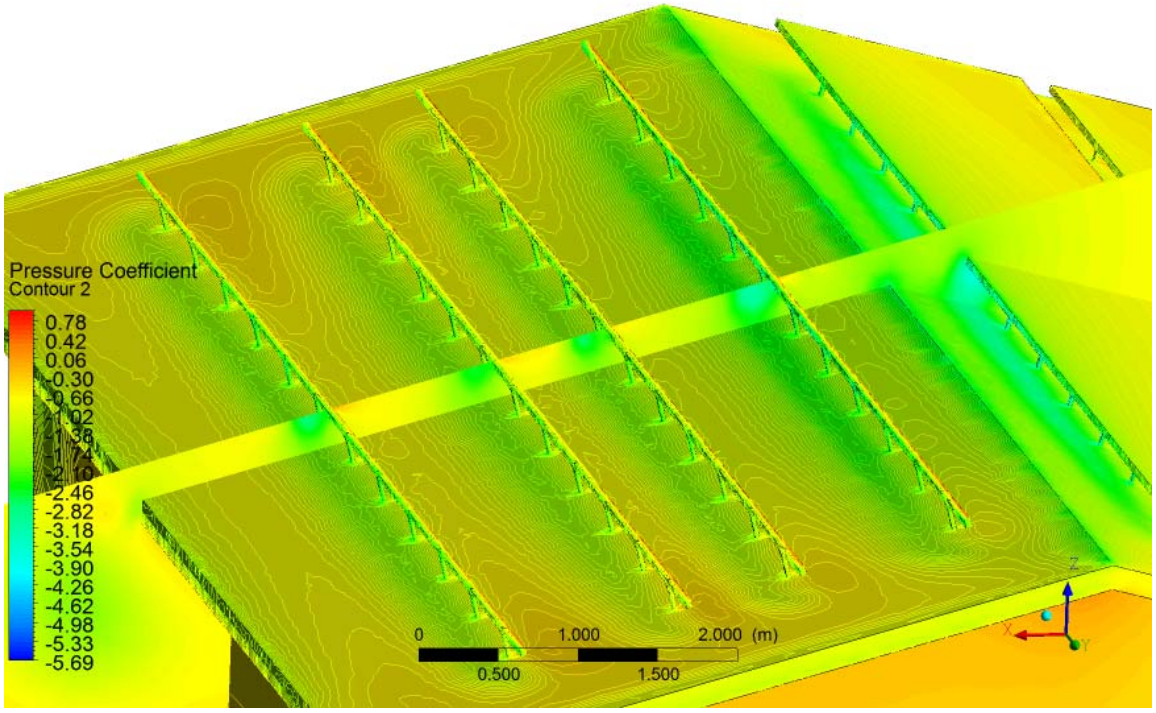


Fig. E. 274. Cp distribution between roof and bottom of panels, WD 90º, LW

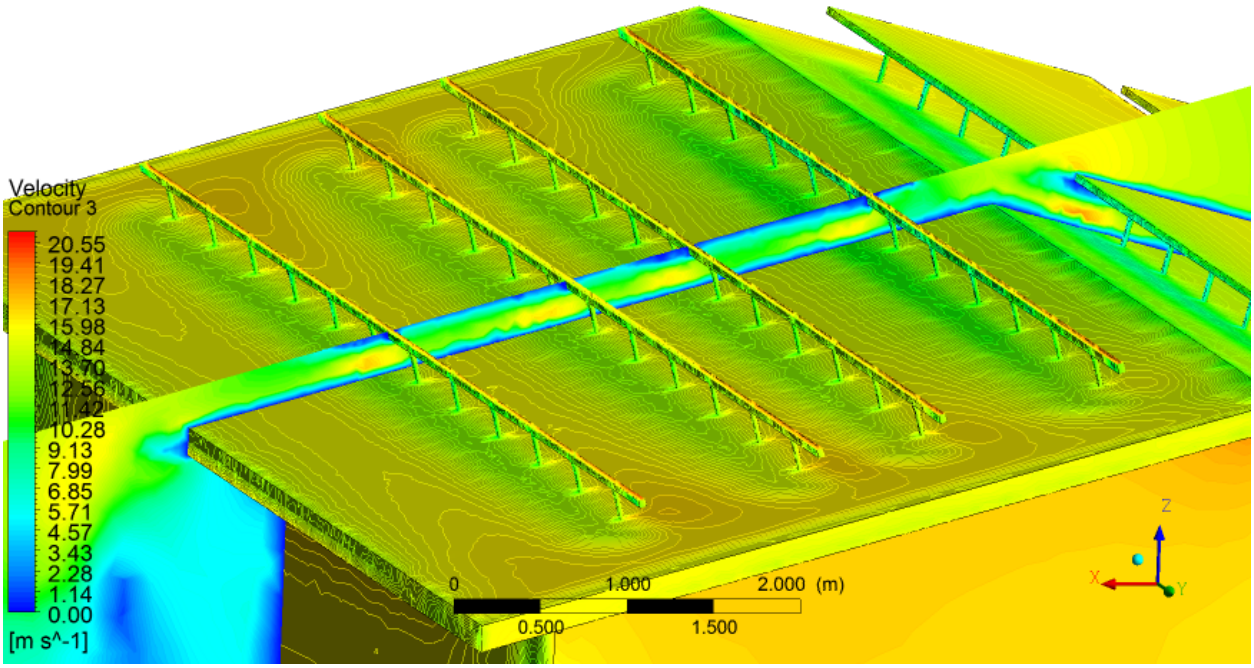


Fig. E. 275. Velocity distribution between roof and bottom of panels, WD 90º, LW

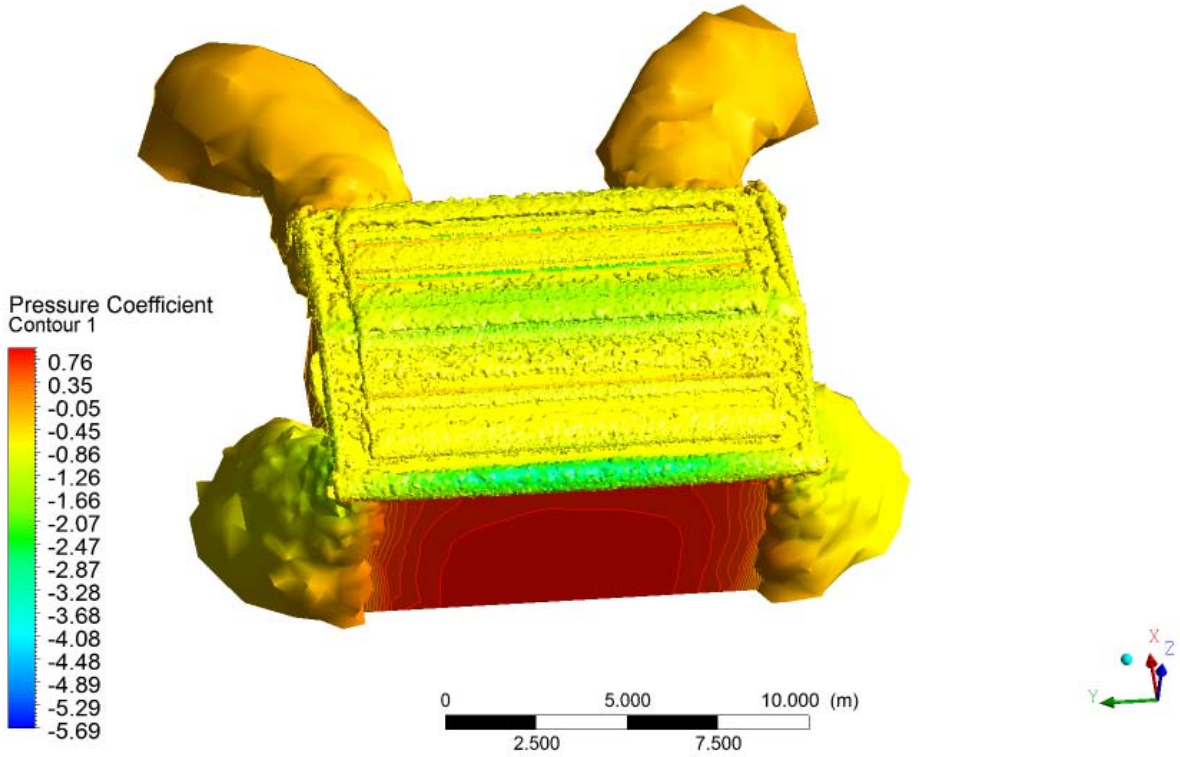


Fig. E. 276. Turbulence distribution on roof and on the building structure, with building contours, WD 90º, WW

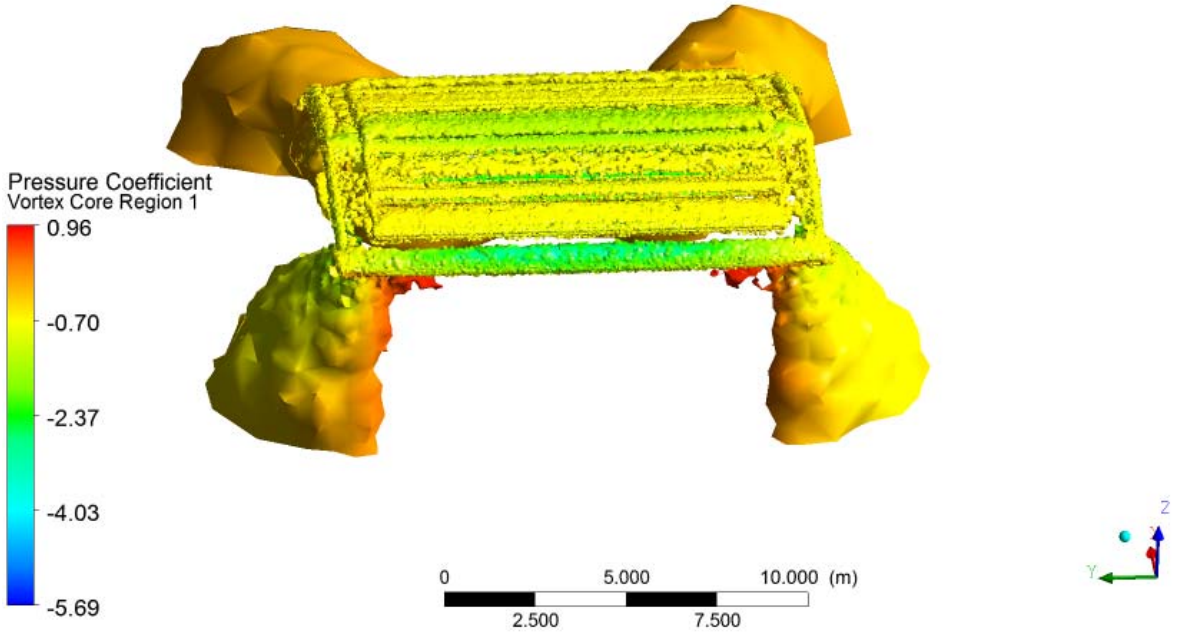


Fig. E. 277. Turbulence distribution on roof and building structure, with No building contours, WD 90° , WW

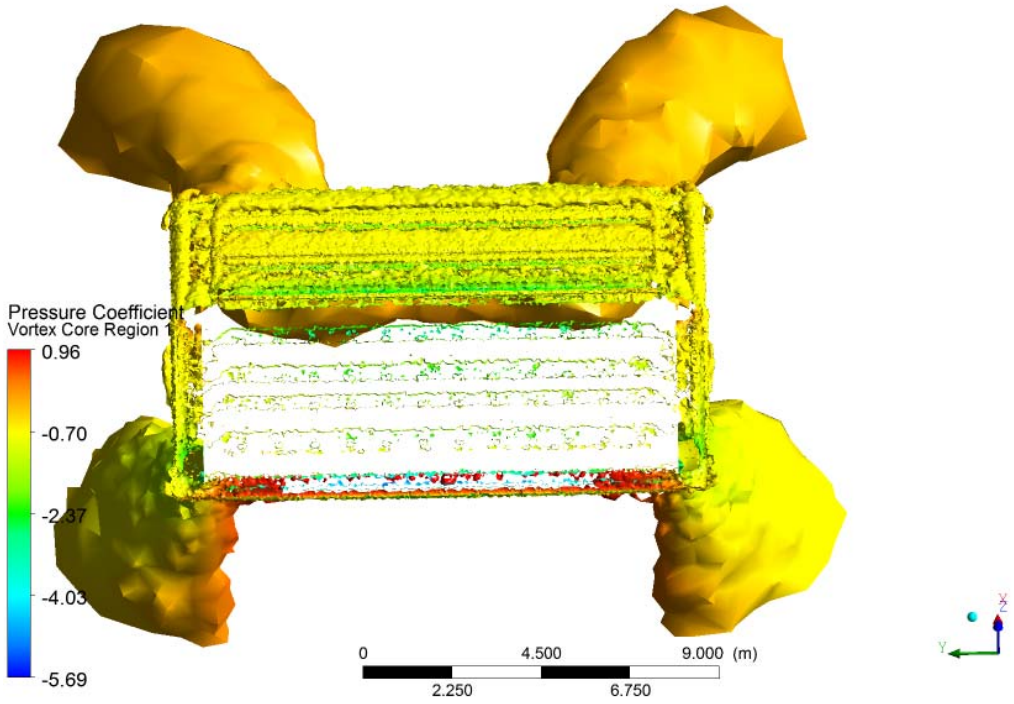


Fig. E. 278. Turbulence distribution on roof under panels and building structure, with No building contours, WW

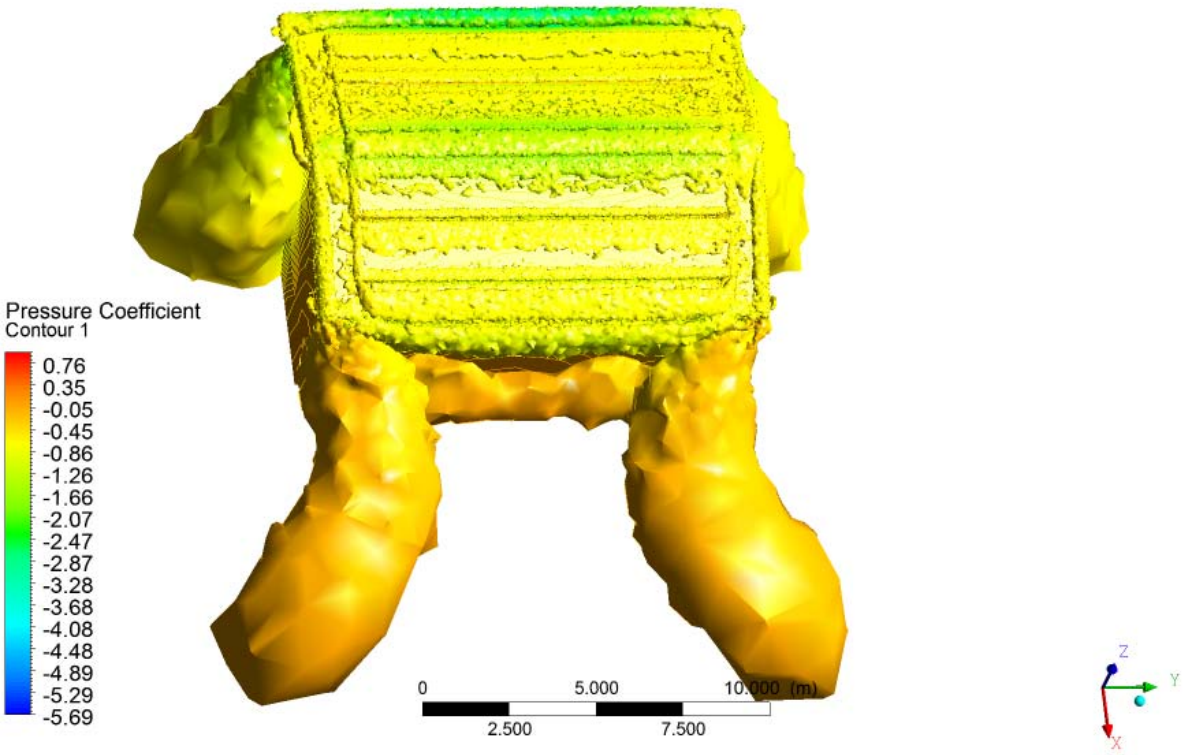


Fig. E. 279. Turbulence distribution on roof and on the building structure, with building contours, WD 90º, LW

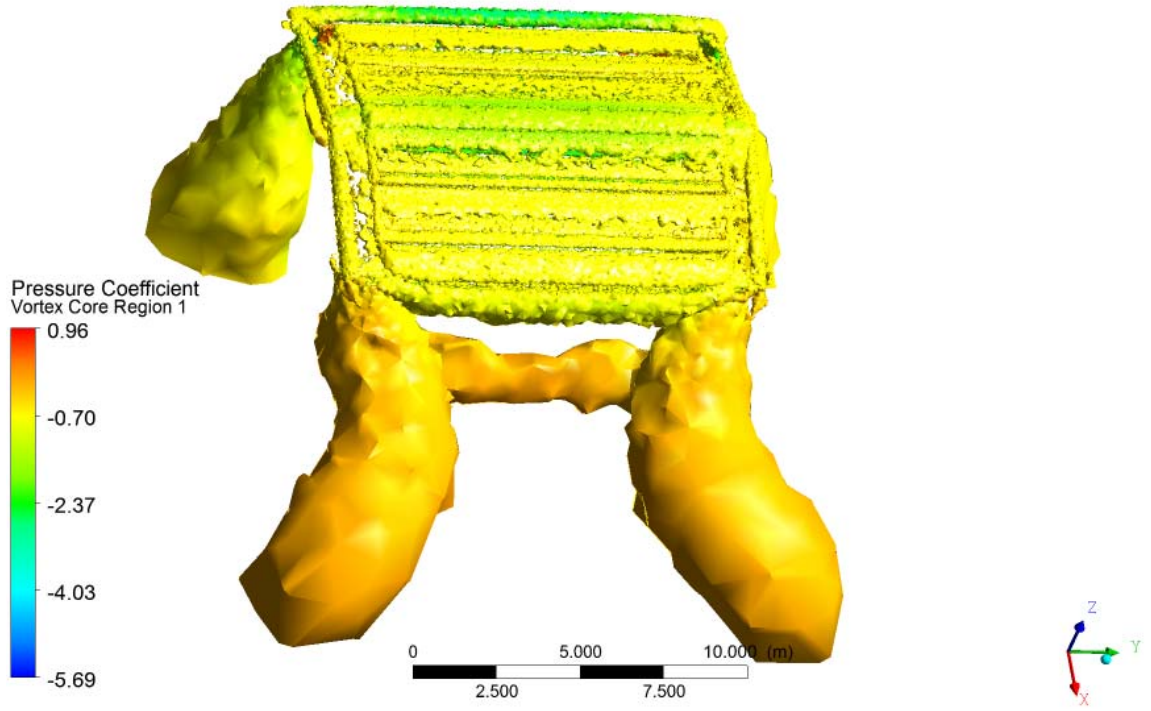


Fig. E. 280. Turbulence distribution on roof and building structure, with No building contours, WD 90º , LW

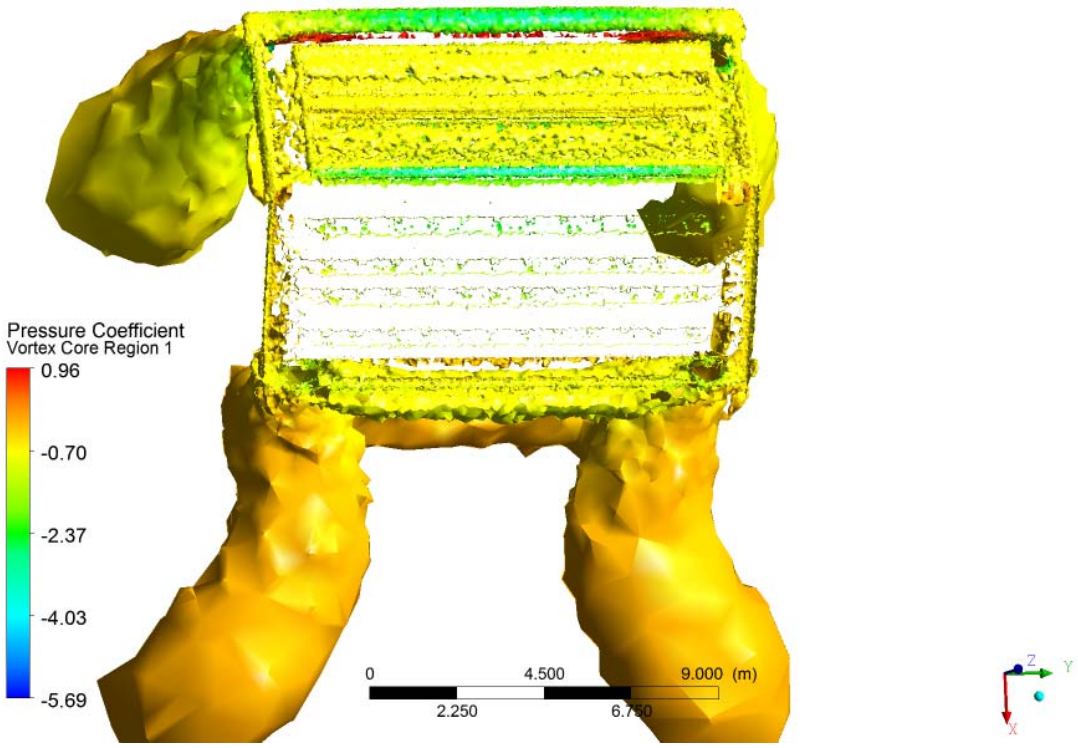


Fig. E. 281. Turbulence distribution on roof under panels and building structure, with No building contours, LW

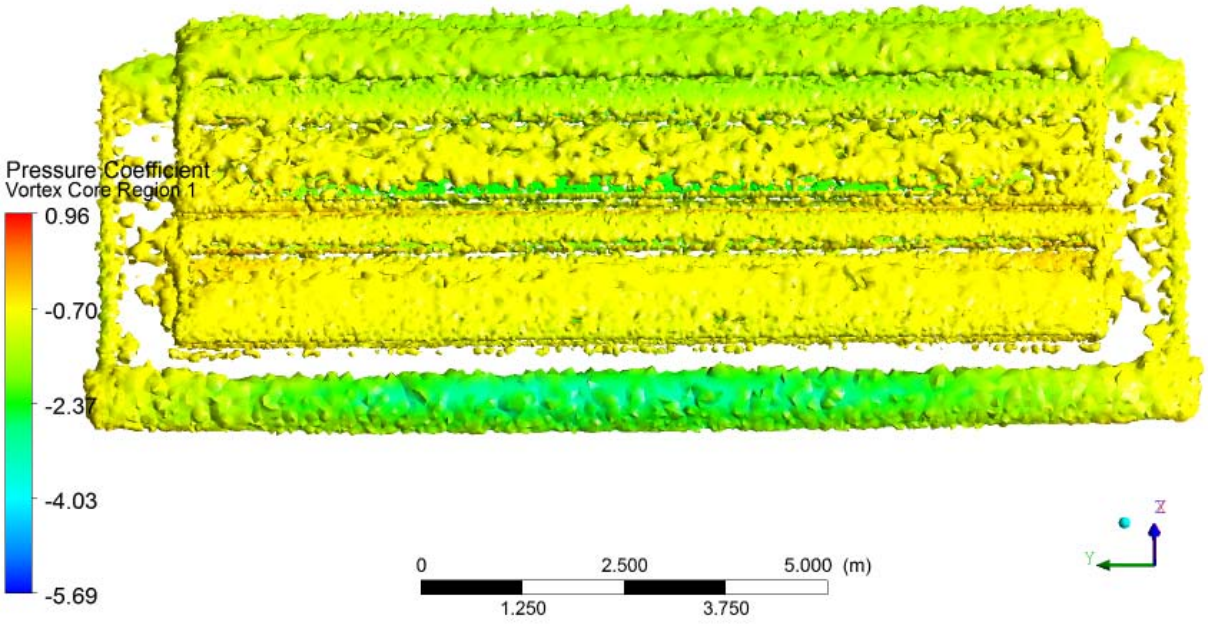


Fig. E. 282. Turbulence distribution, on top of the panels, No building contours shown, WD 90º, WW

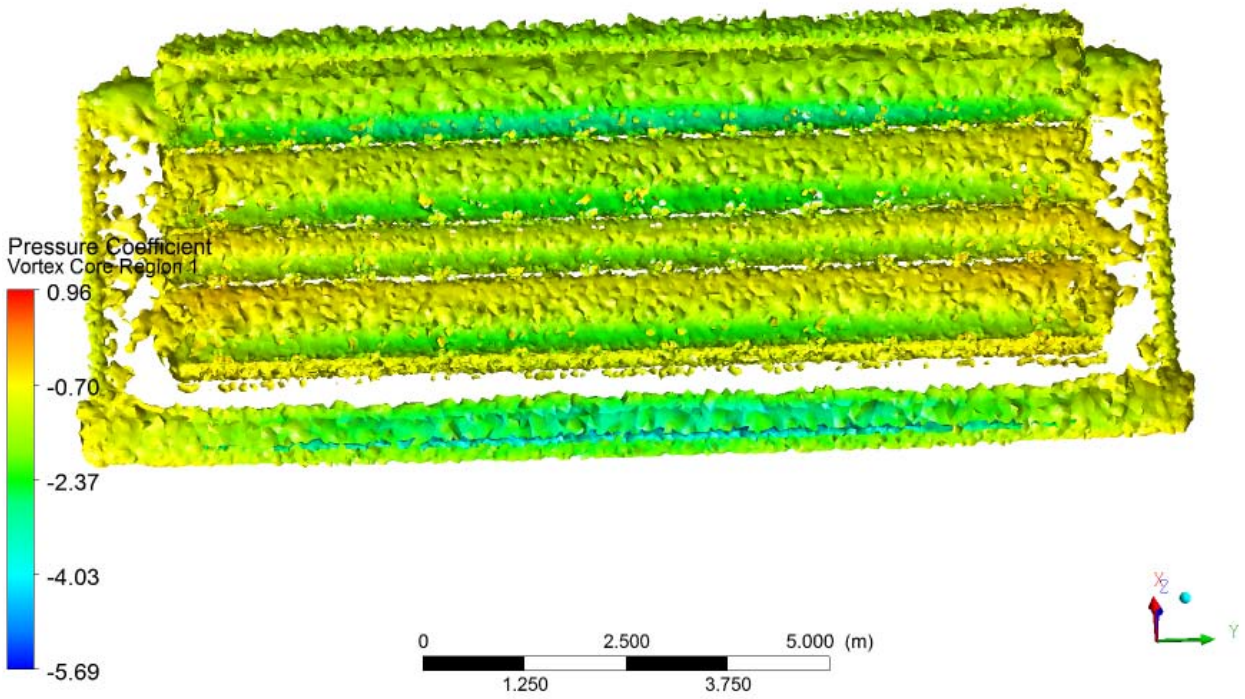


Fig. E. 283. Turbulence distribution, on bottom of the panels, No building contours shown, WD 90º, WW

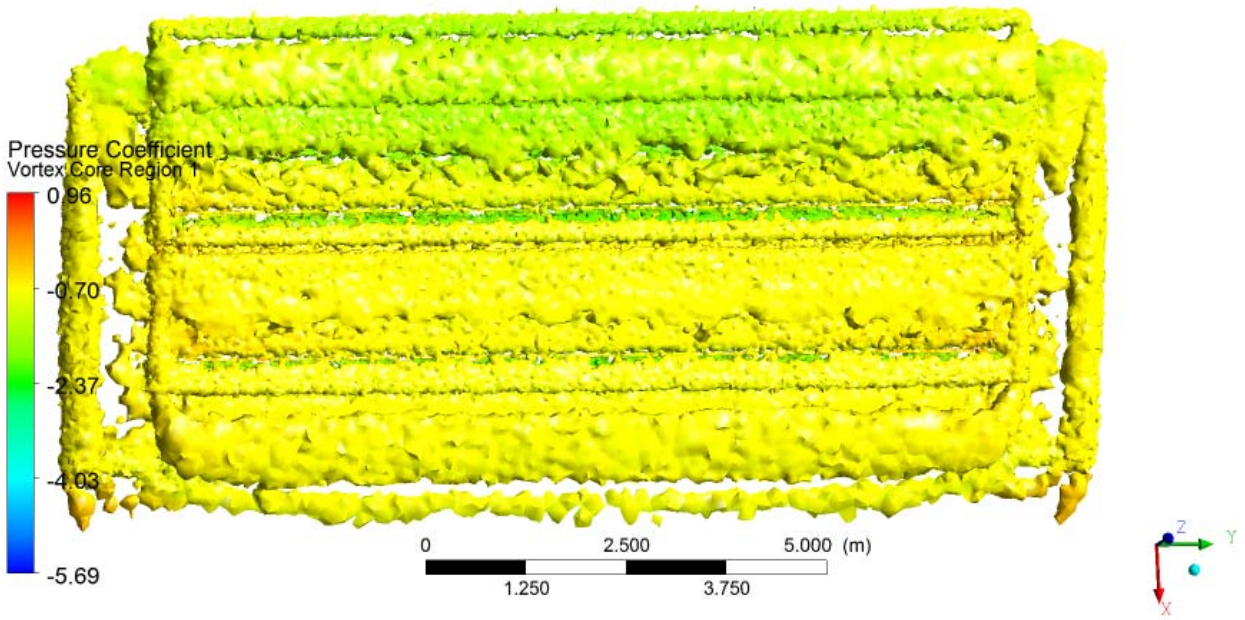


Fig. E. 284. Turbulence distribution, on top of the panels, No building contours shown, WD 90º, LW

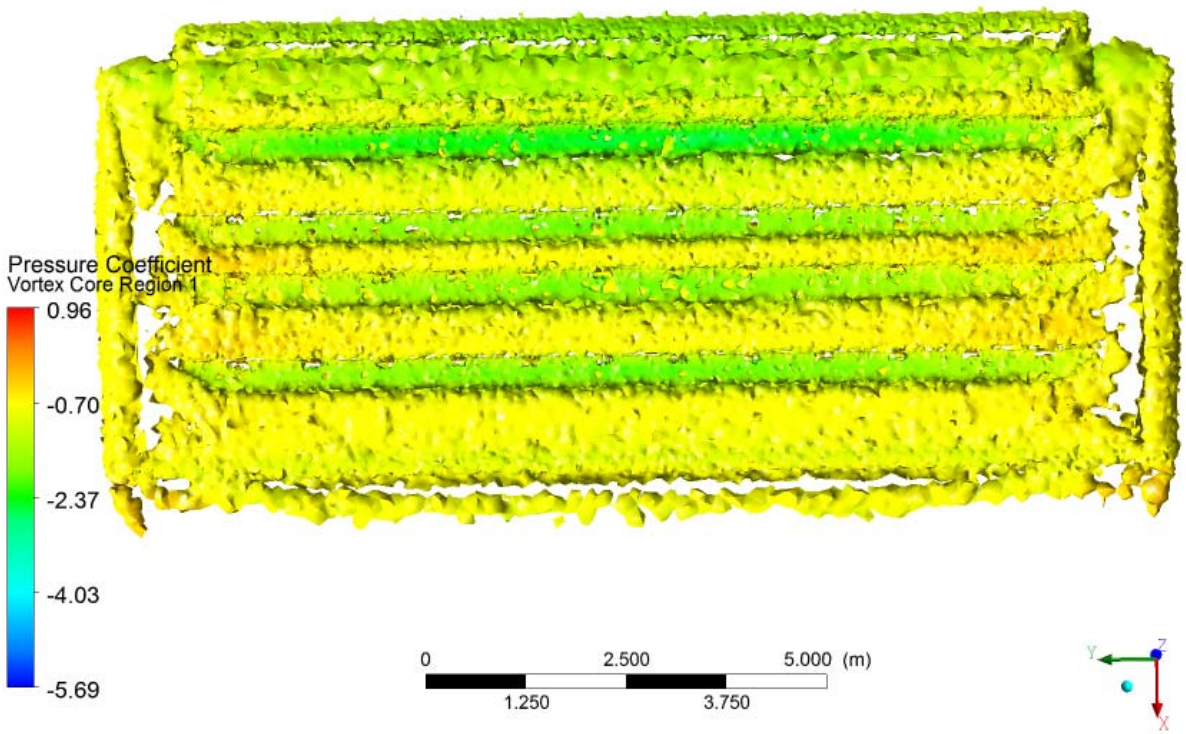


Fig. E. 285. Turbulence distribution, on bottom of the panels, No contours shown, WD 90º, LW

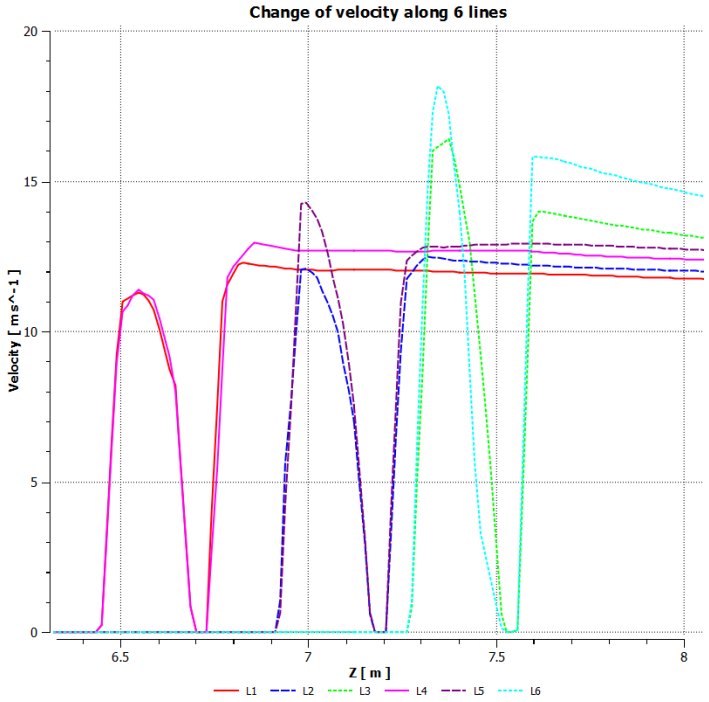


Fig. E. 286. Velocity changes between panels, and above roof, all lines, WD 90º, WW.

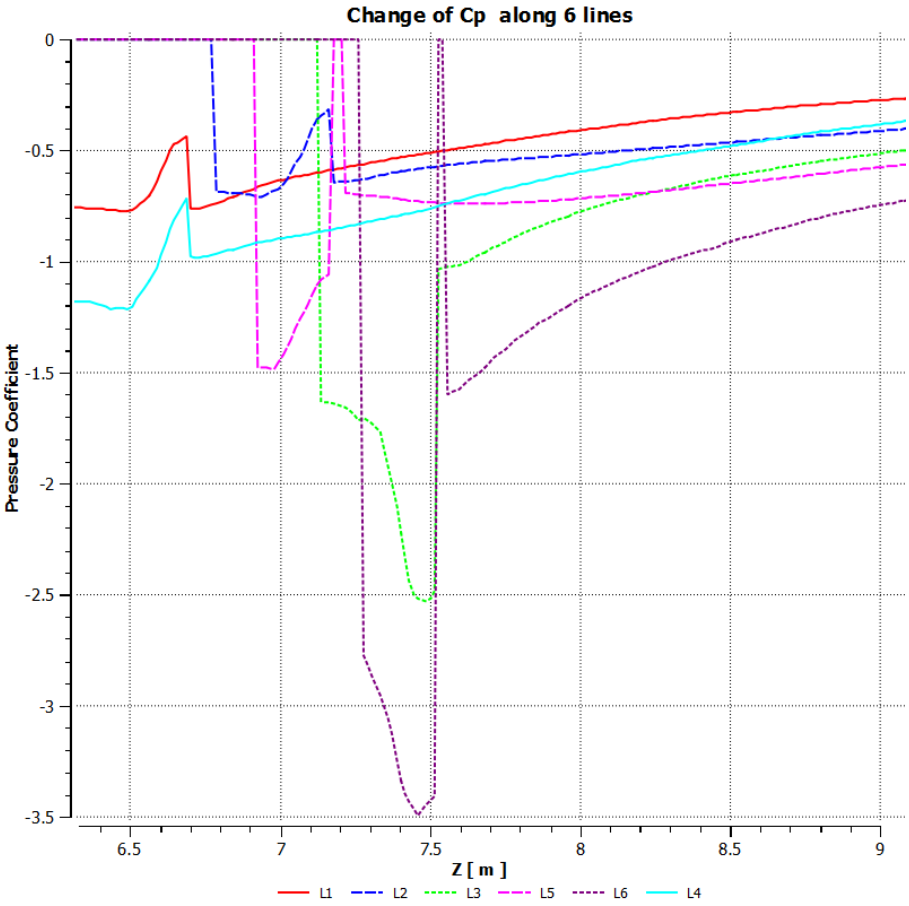
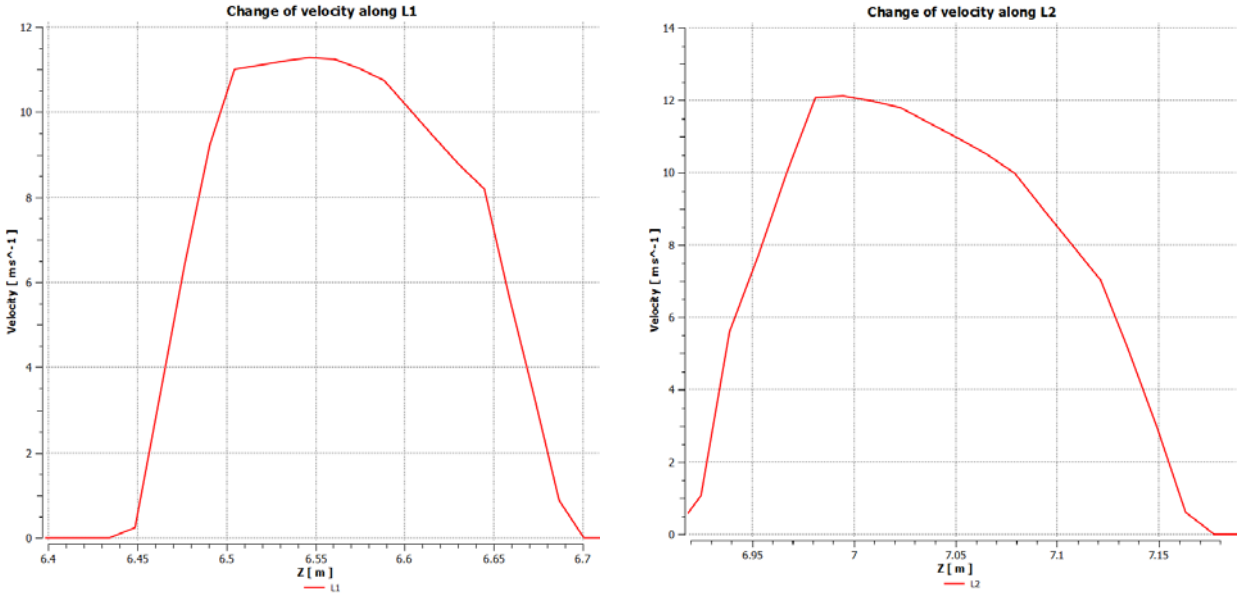


Fig. E. 287. Cp changes between panels, and above roof, all lines, WD 90º, WW



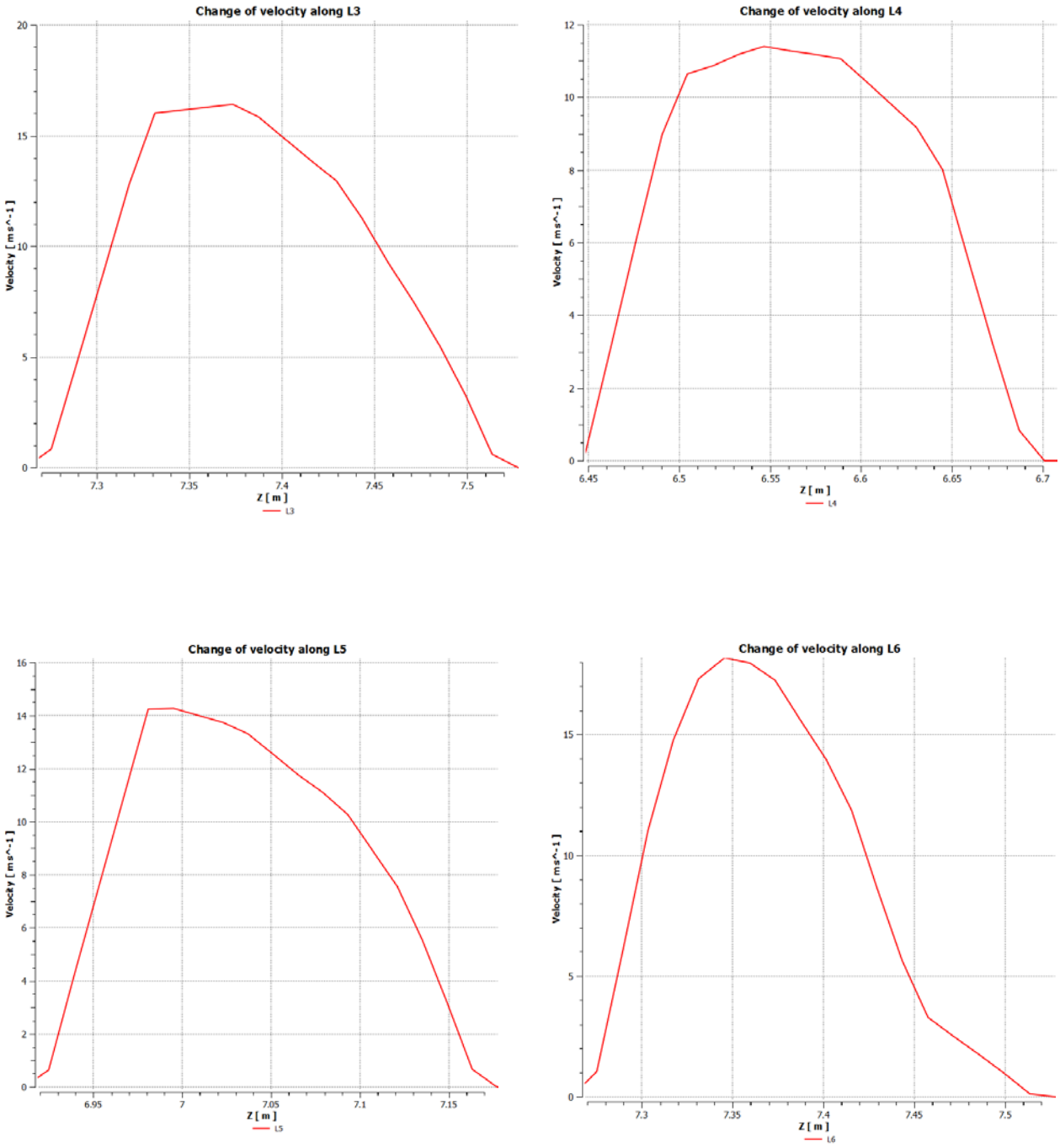
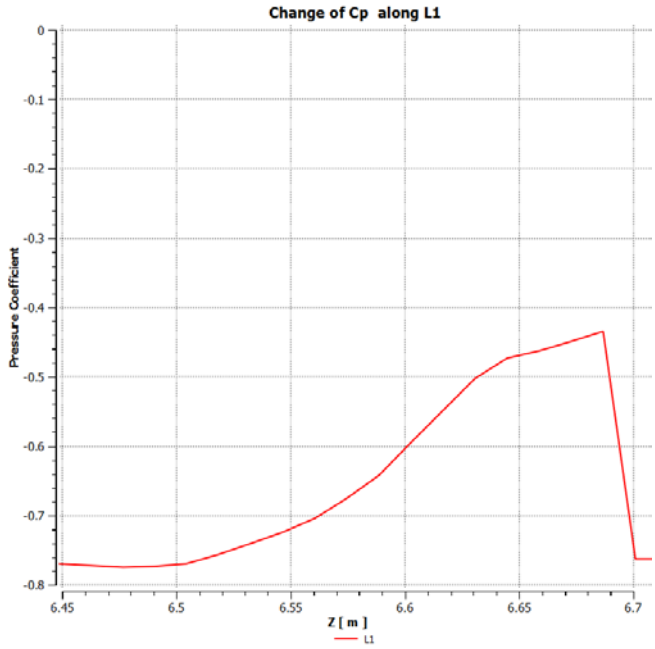
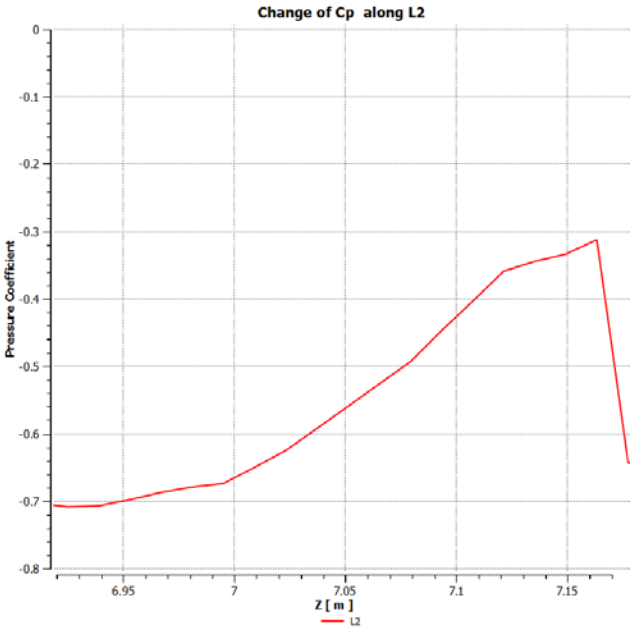
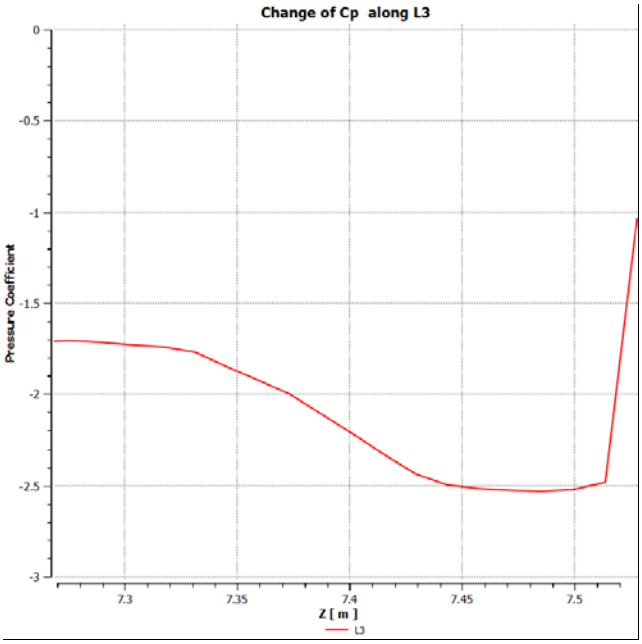
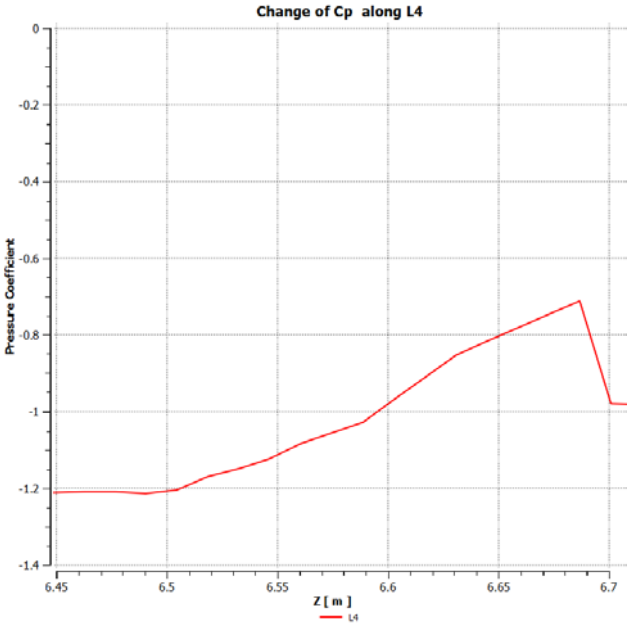


Fig. E. 288. Velocity changes in the cavity between panels and roof, all lines separated. WD 90º, WW


Change of Cp along L1
Pressure Coefficient
0
-0.1
-0.2
-0.3
-0.4
-0.5
-0.6
-0.7
-0.8
6.45
6.5
6.55
6.6
6.65
6.7
Z [m]
L1


Change of Cp along L2
Pressure Coefficient
0
-0.1
-0.2
-0.3
-0.4
-0.5
-0.6
-0.7
-0.8
6.95
7
7.05
7.1
7.15
Z [m]
L2


Change of Cp along L3
Pressure Coefficient
0
-0.5
-1
-1.5
-2
-2.5
-3
7.3
7.35
7.4
7.45
7.5
Z [m]
L3


Change of Cp along L4
Pressure Coefficient
0
-0.2
-0.4
-0.6
-0.8
-1
-1.2
-1.4
6.45
6.5
6.55
6.6
6.65
6.7
Z [m]
L4

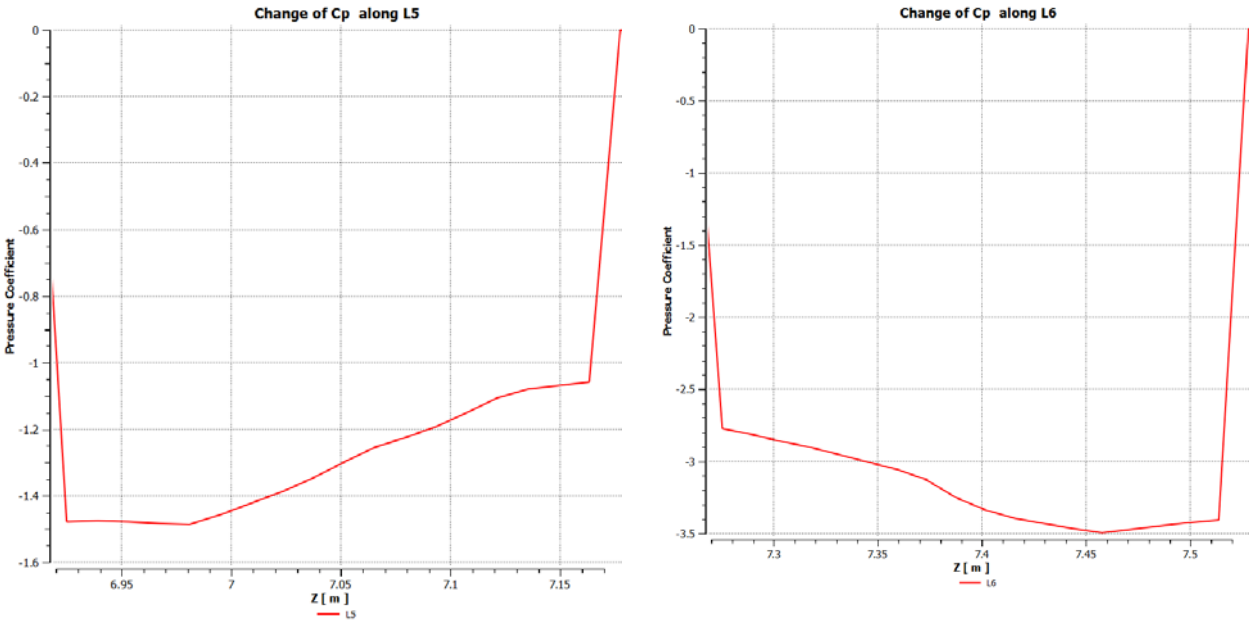


Fig. E. 289. Cp changes between panels, all lines separated, WD 90º, WW

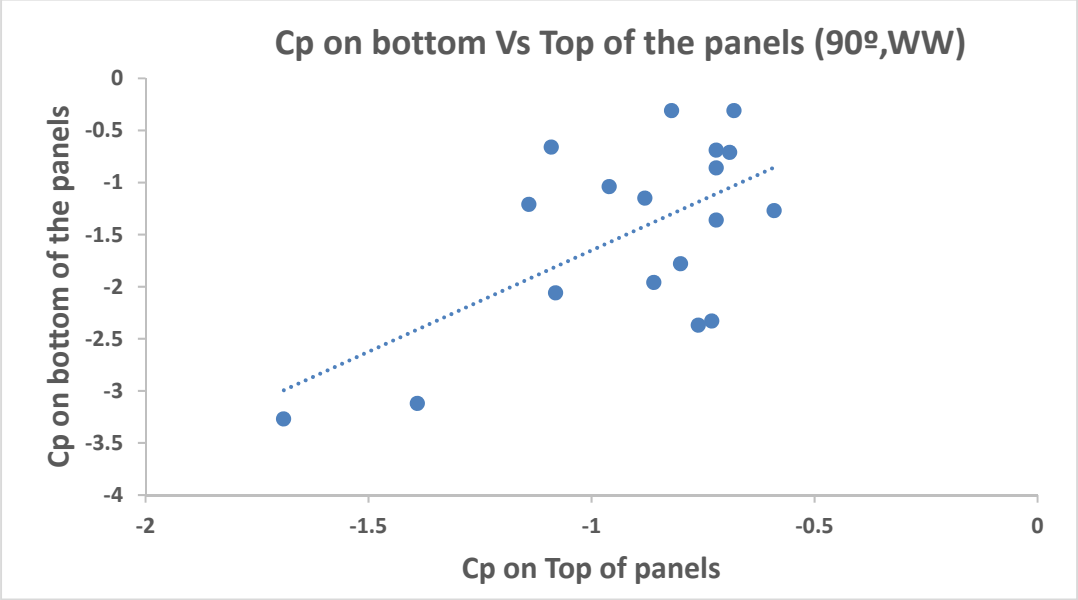


Fig. E. 290. Correlation between Cp on top and bottom of panels surfaces, WW, WD 90º

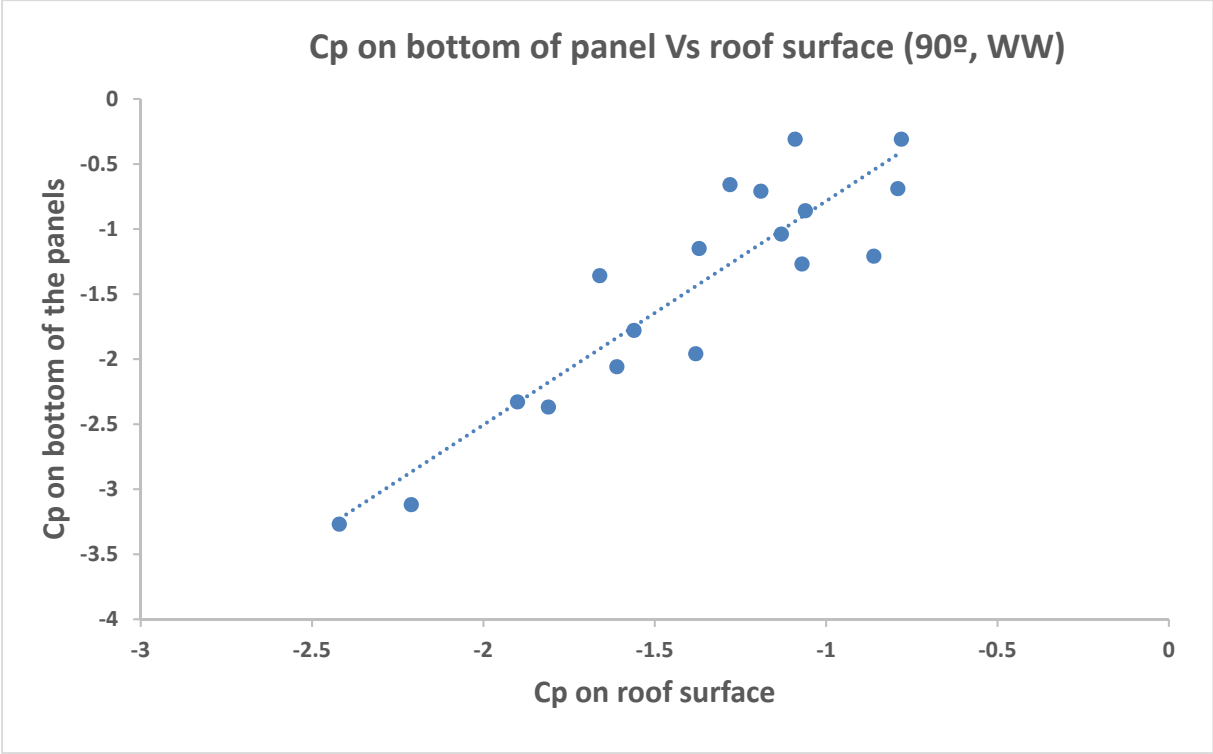


Fig. E. 291. Correlation between Cp on bottom of panels and roof surfaces, WW, WD 90º

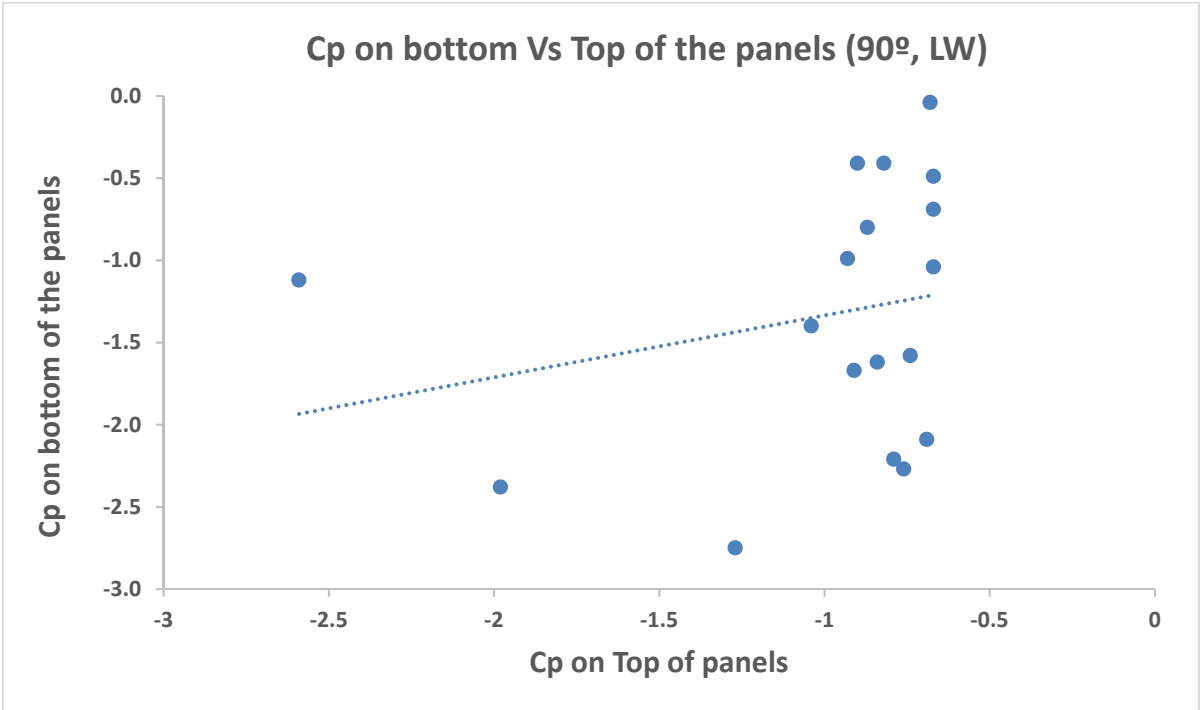


Fig. E. 292. Correlation between Cp on top and bottom of panels surfaces, LW, WD 90º

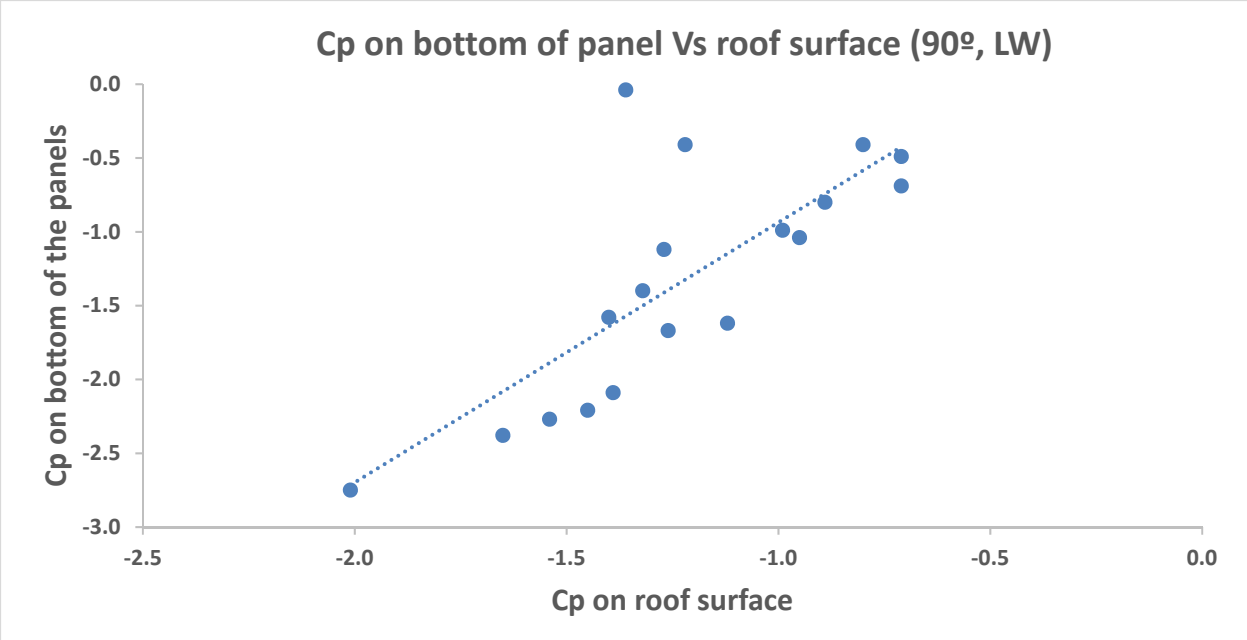


Fig. E. 293. Correlation between Cp on bottom of panels and roof surfaces, LW, WD 90º

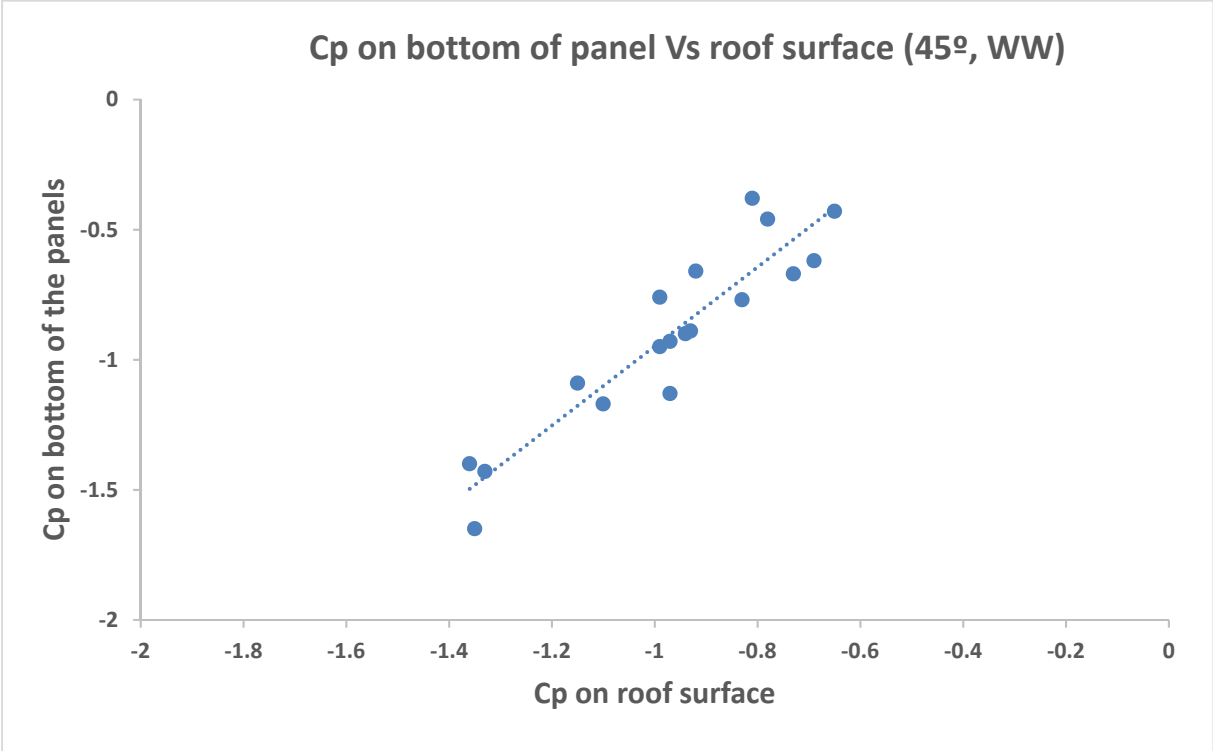


Fig. E. 294. Correlation between Cp on bottom of panels and roof surfaces, WW, WD 45º

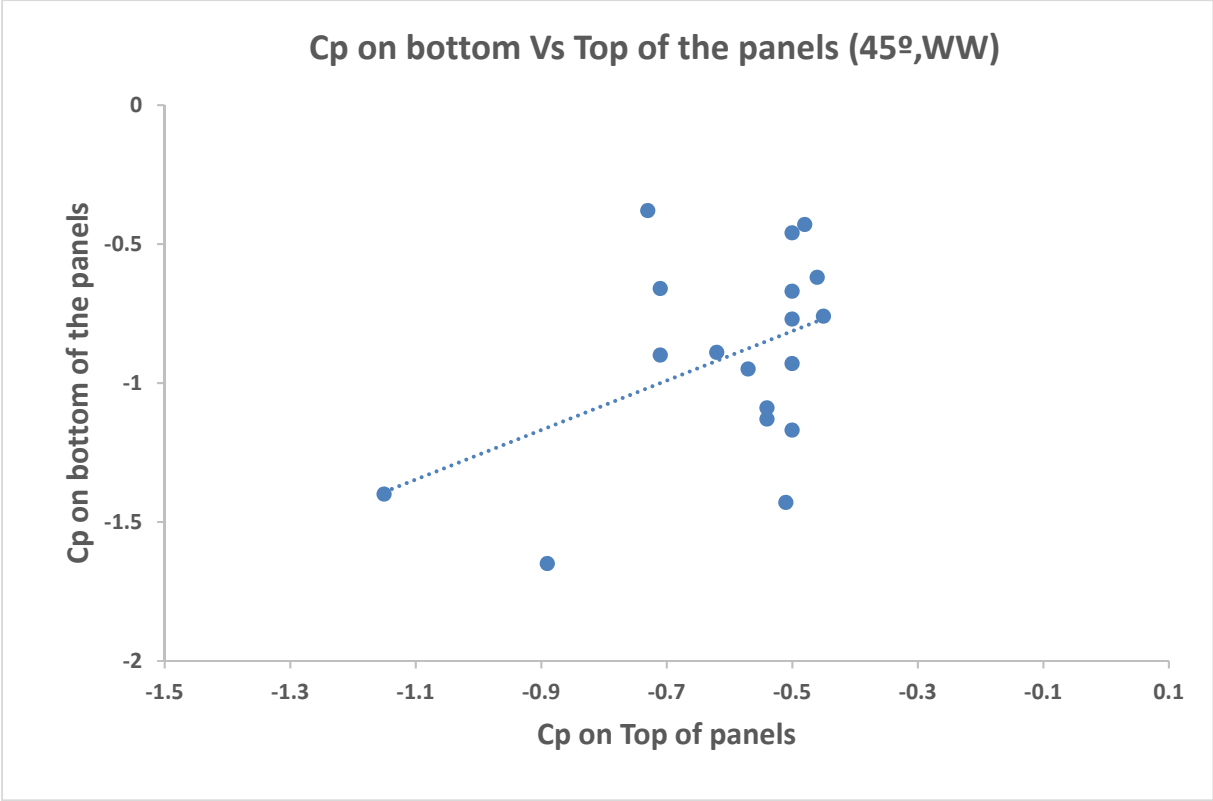


Fig. E. 295. Correlation between Cp on top and bottom of panels surfaces, WW, WD 45º

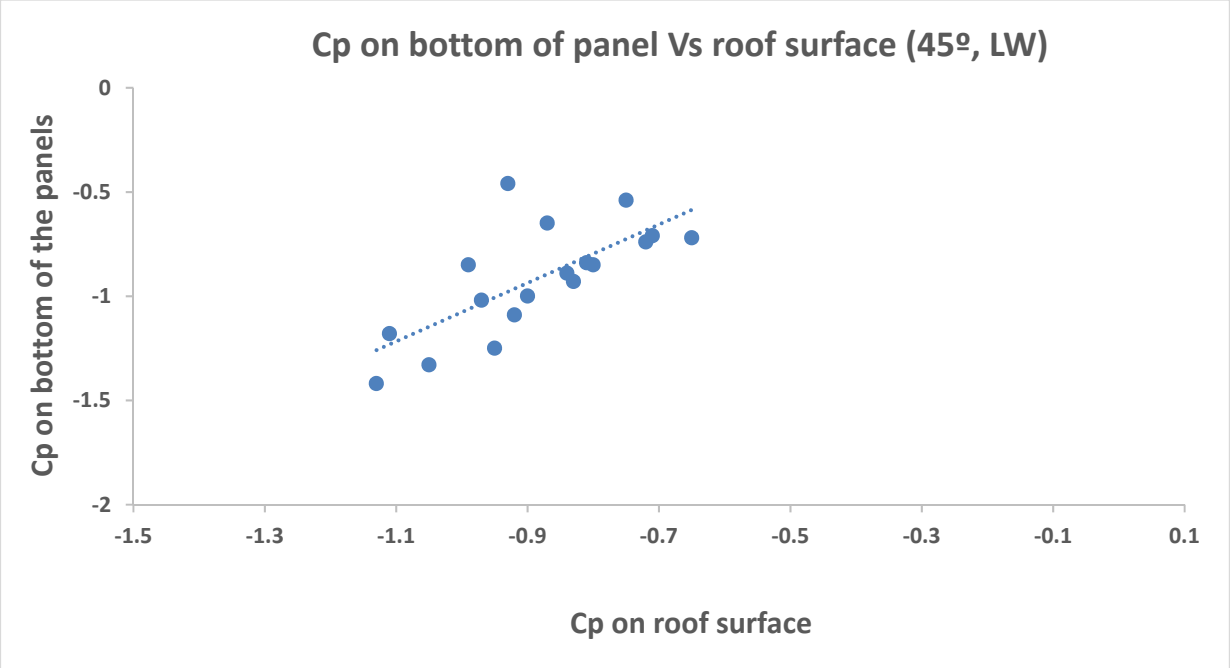


Fig. E. 296. Correlation between Cp on bottom of panels and roof surfaces, LW, WD 45º

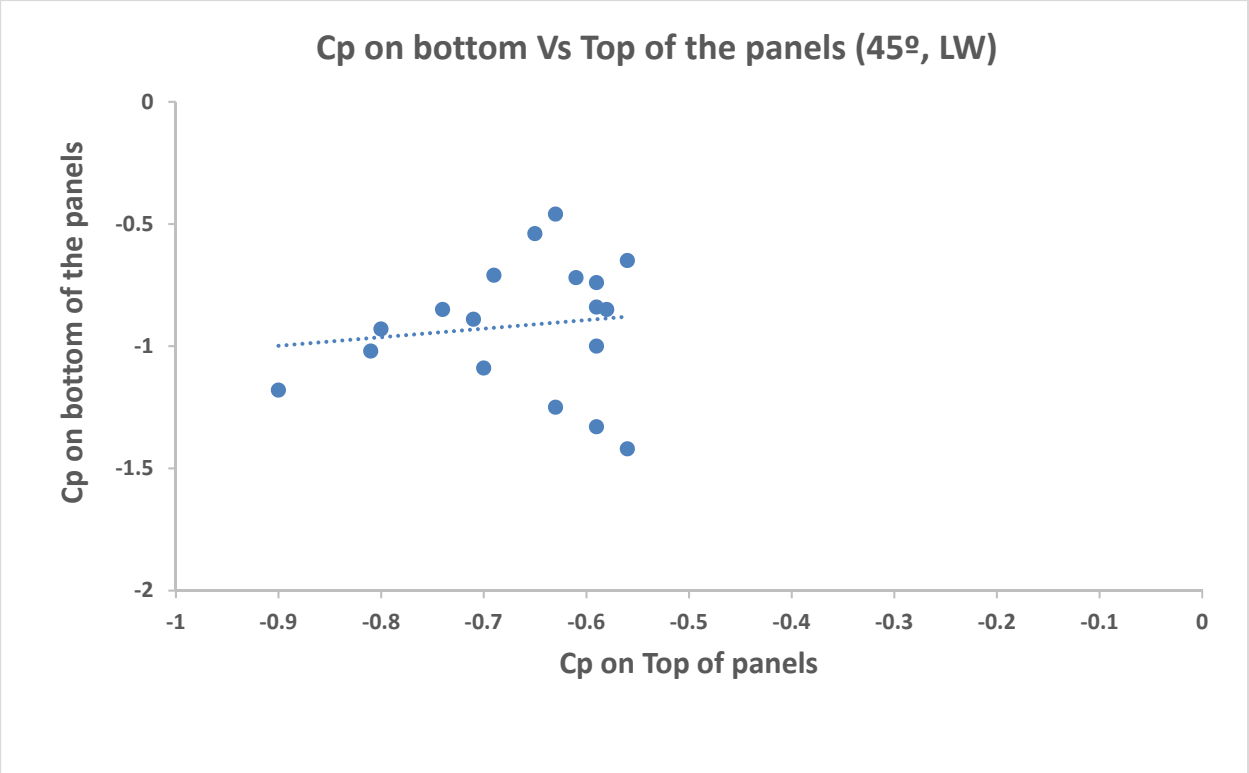


Fig. E. 297. Correlation between Cp on top and bottom of panels surfaces, LW, WD 45º

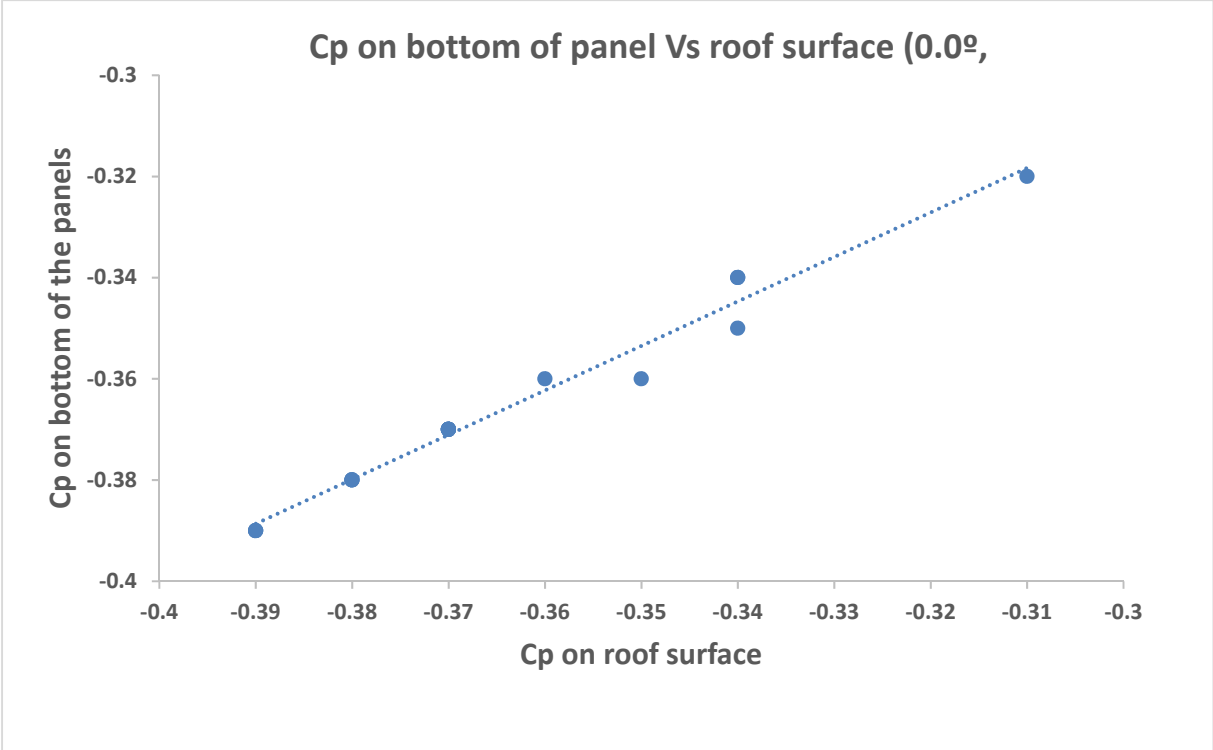


Fig. E. 298. Correlation between Cp on roof surface and bottom of panels, WD 0º

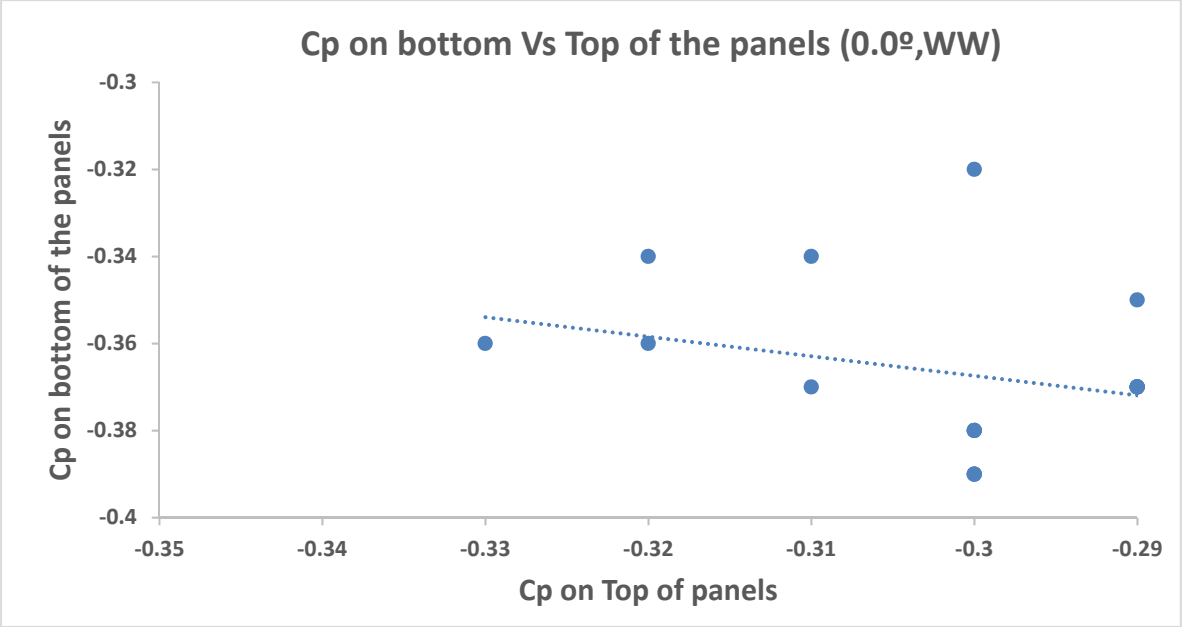


Fig. E. 299. Correlation between Cp on top and bottom of panels surfaces, LW, WD 0º



Fig. E. 300. Correlation between Cp on top, bottom of panels and roof surface, with wind directions.

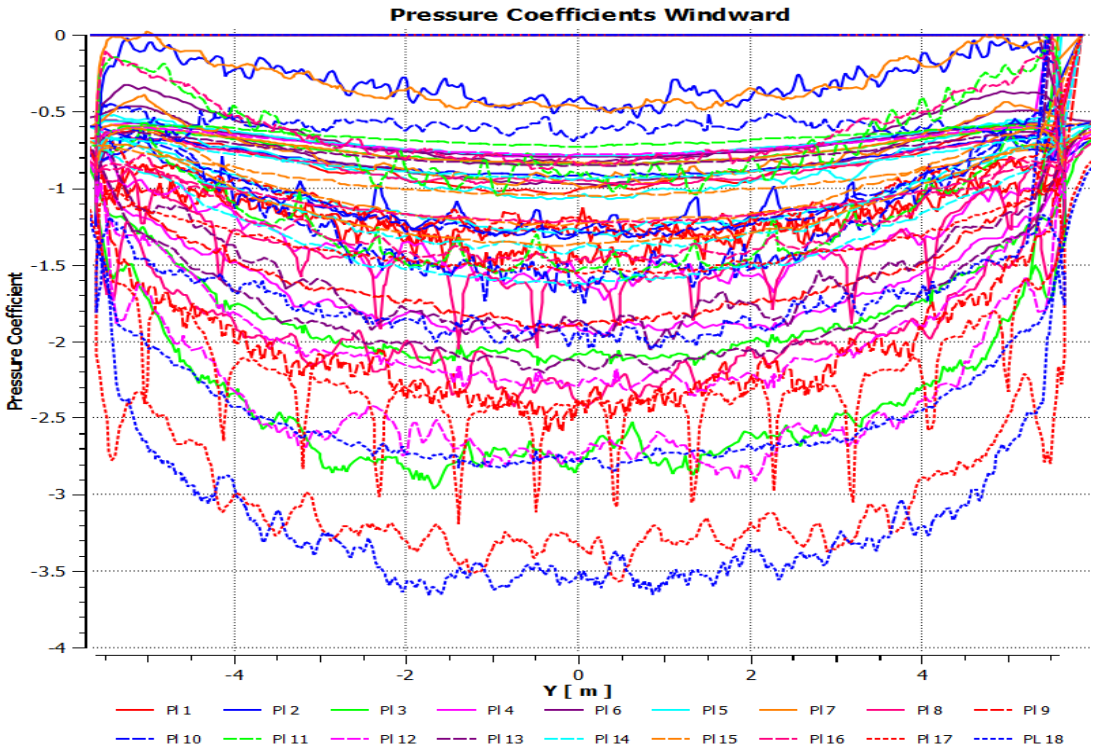


Fig. E. 301. All Cp charts, WW, WD 90º

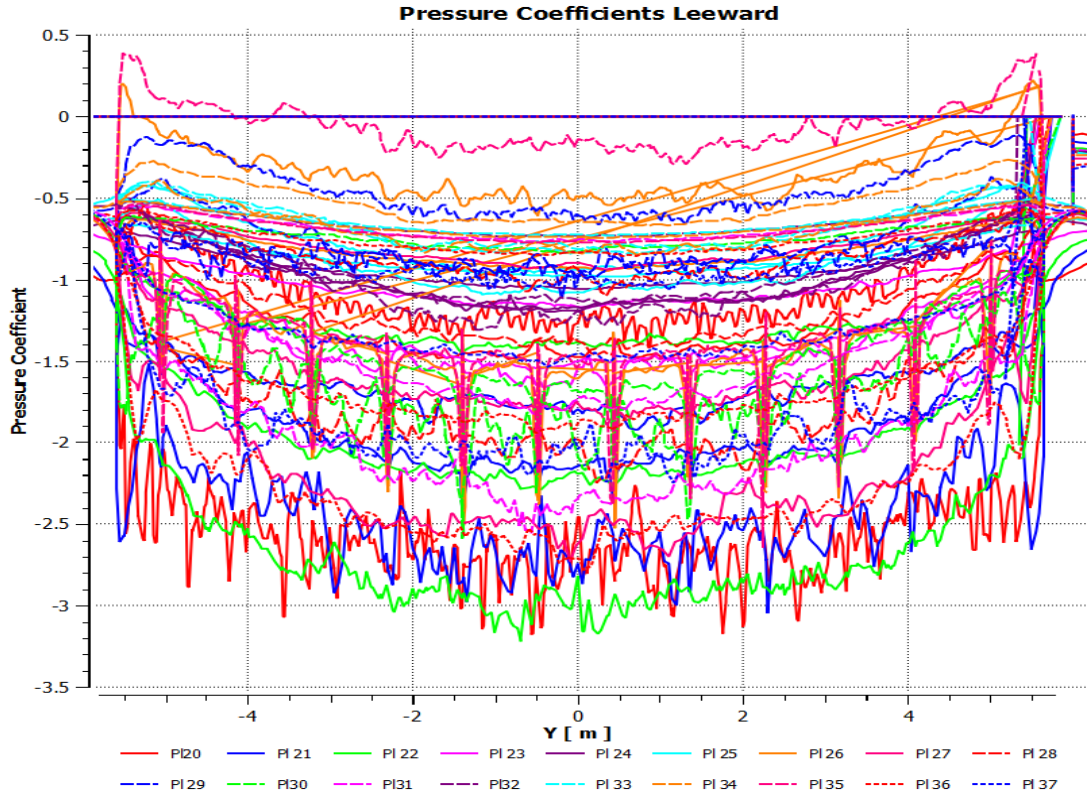


Fig. E. 302. All Cp charts, LW, WD 90º

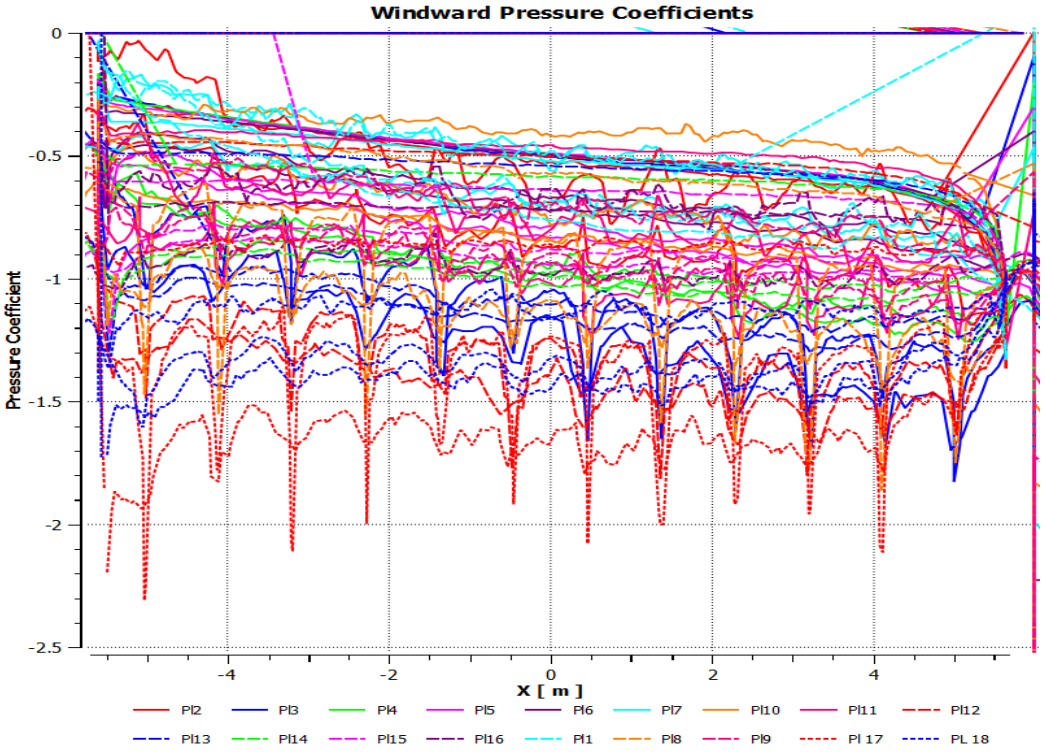


Fig. E. 303. All Cp charts, WW, WD 45º

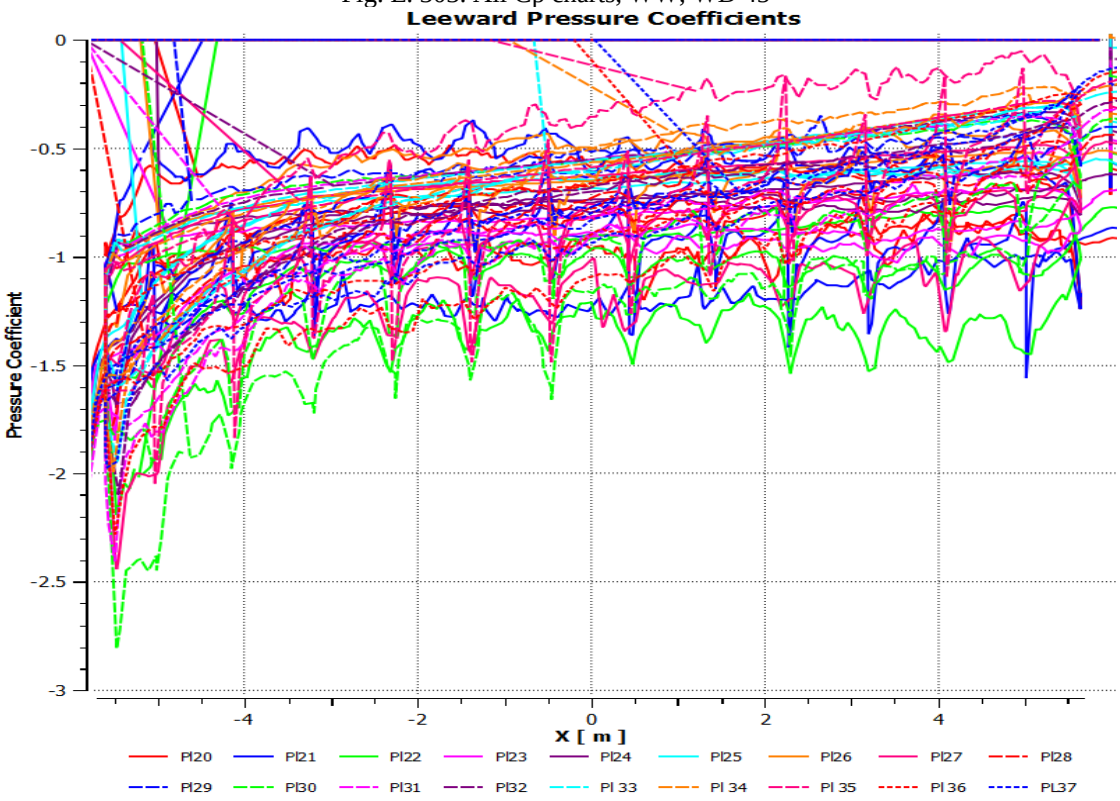


Fig. E. 304. All Cp charts, LW, WD 45º

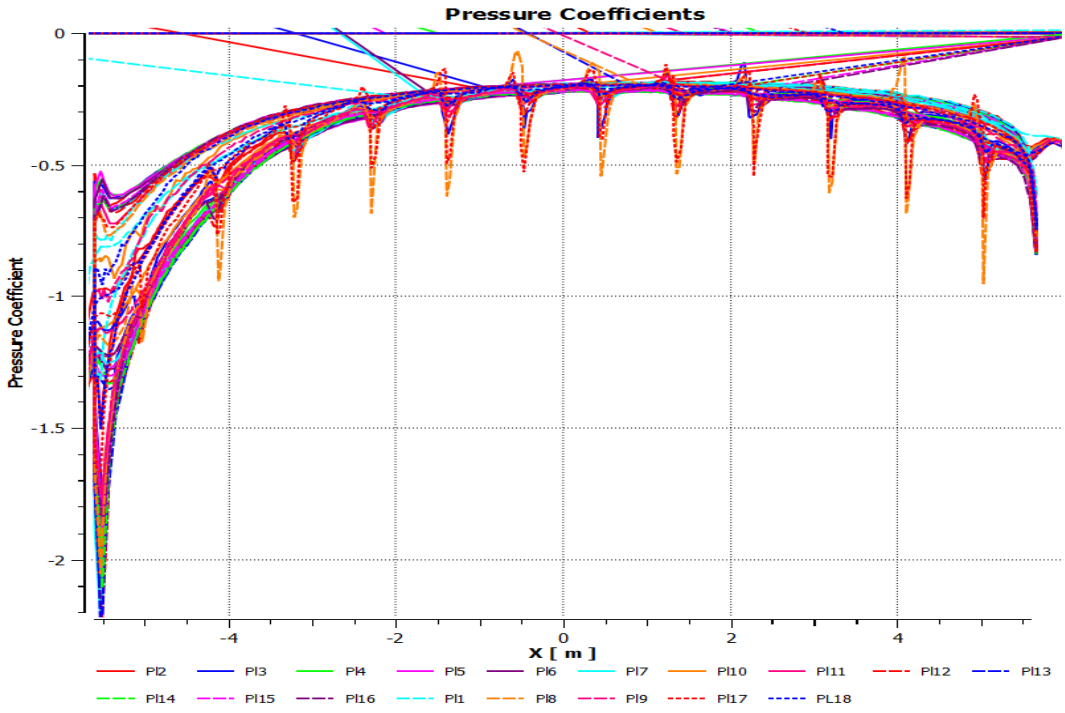


Fig. E. 305. All Cp charts, WD 0º

1.3.5. Integration of Cp on The Three Surfaces and Resultant Cp of Roof Mounted Solar Panels in Comparison with Bare Roof,S8"C10"

Tabulated results of the integration,

Table E. 21. Cp on bare roof Vs. roof under solar panels and solar panels surfaces, Slope 15º, 45º, WW

Polylines	Cp (SP)	Pr2	Cp Bott	Diff	Ttl Cp	Ttl/Brf
Pl1A	-0.46	-0.69	-0.62	0.16	-0.53	1.00
Pl2	-0.5	-0.78	-0.46	-0.04	-0.82	1.61
Pl3	-0.5	-1.1	-1.17	0.67	-0.43	0.84
Pl4	-0.5	-0.97	-0.93	0.43	-0.54	1.06
Pl5	-0.5	-0.83	-0.77	0.27	-0.56	1.10
Pl6	-0.5	-0.73	-0.67	0.17	-0.56	1.12
Pl7	-0.48	-0.65	-0.43	-0.05	-0.7	1.40
Pl8	-0.54	-0.97	-1.13	0.59	-0.38	0.76
Pl9	-0.71	-0.94	-0.90	0.19	-0.75	1.47
Pl10	-0.73	-0.81	-0.38	-0.35	-1.16	2.27
Pl11	-0.45	-0.99	-0.76	0.31	-0.68	1.31
Pl12	-0.51	-1.33	-1.43	0.92	-0.41	0.76
Pl13	-0.54	-1.15	-1.09	0.55	-0.6	1.07

Pl14	-0.57	-0.99	-0.95	0.38	-0.61	1.03
Pl15	-0.62	-0.93	-0.89	0.27	-0.66	1.08
Pl16	-0.71	-0.92	-0.66	-0.05	-0.97	1.64
Pl17	-0.89	-1.35	-1.65	0.76	-0.59	1.00
Pl18	-1.15	-1.36	-1.40	0.25	-1.11	1.82
Cp	-0.60	-0.97	-0.91	0.30	-0.67	1.20
SDT	0.18	0.22	0.36	0.32	0.22	0.40
Cov	0.30	0.22	0.39	1.06	0.33	0.33

Table E. 22. Cp on bare roof Vs top of solar panels, Slope 15º, 45º, WW

Pl1A	-0.53	-0.46	0.87
Pl2	-0.51	-0.5	0.98
Pl3	-0.51	-0.5	0.98
Pl4	-0.51	-0.5	0.98
Pl5	-0.51	-0.5	0.98
Pl6	-0.5	-0.5	1.00
Pl7	-0.5	-0.48	0.96
Pl8	-0.5	-0.54	1.08
Pl9	-0.51	-0.71	1.39
Pl10	-0.51	-0.73	1.43
Pl11	-0.52	-0.45	0.87
Pl12	-0.54	-0.51	0.94
Pl13	-0.56	-0.54	0.96
Pl14	-0.59	-0.57	0.97
Pl15	-0.61	-0.62	1.02
Pl16	-0.65	-0.71	1.09
Pl17	-0.7	-0.89	1.27
Pl18	-0.75	-1.15	1.53
Cp	-0.56	-0.60	1.08
SDT	0.08	0.18	0.20
Cov	0.13	0.30	0.18
Pl1A	-0.53	-0.46	0.87

Table E. 23. Cp bare roof Vs. roof under solar panels and solar panel surfaces, Slope 15º, WD 45º, LW

Polylines	Cp (SP)	Pr2	Cp Bott	Diff	Ttl Cp	Ttl/Brf
Pl20a	-0.58	-0.99	-0.85	0.27	-0.72	0.81
Pl21	-0.56	-1.13	-1.42	0.86	-0.27	0.33
Pl22	-0.9	-1.11	-1.18	0.28	-0.83	1.12
Pl23	-0.81	-0.97	-1.02	0.21	-0.76	1.12
Pl24	-0.74	-0.8	-0.85	0.11	-0.69	1.08
Pl25	-0.69	-0.71	-0.71	0.02	-0.69	1.11
Pl26	-0.65	-0.75	-0.54	-0.11	-0.86	1.41
Pl27	-0.63	-0.95	-1.25	0.62	-0.33	0.55
Pl28	-0.71	-0.84	-0.89	0.18	-0.66	1.11

Pl29	-0.56	-0.87	-0.65	0.09	-0.78	1.32
Pl30	-0.59	-1.05	-1.33	0.74	-0.31	0.53
Pl31	-0.59	-0.90	-1.00	0.41	-0.49	0.84
Pl32	-0.59	-0.81	-0.84	0.25	-0.56	0.97
Pl33	-0.59	-0.72	-0.74	0.15	-0.57	1.00
Pl34	-0.61	-0.65	-0.72	0.11	-0.54	0.96
Pl35	-0.63	-0.93	-0.46	-0.17	-1.1	2.00
Pl36	-0.7	-0.92	-1.09	0.39	-0.53	0.98
Pl37	-0.8	-0.83	-0.93	0.13	-0.7	1.25
Cp	-0.66	-0.89	-0.92	0.25	-0.63	1.03
SDT	0.10	0.14	0.27	0.27	0.21	0.37
Cov	0.15	0.15	0.29	1.08	0.33	0.36

Table E. 24. Cp bare roof Vs top of panels, Slope 15º, WD 45º, LW

Polylines	Bare Roof	Cp (SP)	Cp (SP/BRf)
Pl20A	-0.89	-0.58	0.65
Pl21	-0.81	-0.56	0.69
Pl22	-0.74	-0.9	1.22
Pl23	-0.68	-0.81	1.19
Pl24	-0.64	-0.74	1.16
Pl25	-0.62	-0.69	1.11
Pl26	-0.61	-0.65	1.07
Pl27	-0.60	-0.63	1.05
Pl28	-0.60	-0.71	1.19
Pl29	-0.59	-0.56	0.95
Pl30	-0.59	-0.59	1.01
Pl31	-0.58	-0.59	1.02
Pl32	-0.58	-0.59	1.03
Pl33	-0.57	-0.59	1.04
Pl34	-0.56	-0.61	1.09
Pl35	-0.55	-0.63	1.15
Pl36	-0.54	-0.7	1.30
Pl37	-0.56	-0.8	1.43
Cp	-0.63	-0.66	1.07
SDT	0.10	0.10	0.19
Cov	0.15	0.15	0.17

Table E. 25. Cp on bare roof Vs. roof under solar panels and solar panel surfaces, Slope 15º, WD 90º, WW

Polylines	Cp (SP)	Pr2	Cp Bott	Diff	Ttl Cp	Ttl/Brf
Pl1A	-1.14	-0.86	-1.21	0.07	-0.79	0.57
Pl2	-0.82	-1.09	-0.31	-0.51	-1.6	1.95
Pl3	-0.76	-1.81	-2.37	1.61	-0.2	0.33
Pl4	-0.72	-1.66	-1.36	0.64	-1.02	1.89
Pl5	-0.72	-1.06	-0.86	0.14	-0.92	1.74
Pl6	-0.72	-0.79	-0.69	-0.03	-0.82	1.55
Pl7	-0.68	-0.78	-0.31	-0.37	-1.15	2.02
Pl8	-0.86	-1.38	-1.96	1.10	-0.28	0.52
Pl9	-1.08	-1.61	-2.06	0.98	-0.63	1.11
Pl10	-0.59	-1.07	-1.27	0.68	-0.39	0.65
Pl11	-0.69	-1.19	-0.71	0.02	-1.17	1.86
Pl12	-0.73	-1.90	-2.33	1.60	-0.3	0.45
Pl13	-0.8	-1.56	-1.78	0.98	-0.58	0.82
Pl14	-0.88	-1.37	-1.15	0.27	-1.1	1.43
Pl15	-0.96	-1.13	-1.04	0.08	-1.05	1.25
Pl16	-1.09	-1.28	-0.66	-0.43	-1.71	2.41
Pl17	-1.39	-2.21	-3.12	1.73	-0.48	0.68
Pl18	-1.69	-2.42	-3.27	1.58	-0.84	1.09
Cp	-0.91	-1.40	-1.47	0.56	-0.84	1.16
SDT	0.28	0.47	0.89	0.75	0.43	0.64
Cov	0.31	0.34	0.61	1.34	0.52	0.55

Table E. 26. Cp bare roof Vs top of panels, Slope 15º, WD 90º, WW

Polylines	Cp Bare roof	Cp (SP)	Cp (SP/BRf)
Pl1A	-1.38	-1.14	0.83
Pl2	-0.82	-0.82	1.00
Pl3	-0.61	-0.76	1.25
Pl4	-0.54	-0.72	1.33
Pl5	-0.53	-0.72	1.36
Pl6	-0.53	-0.72	1.36
Pl7	-0.57	-0.68	1.19
Pl8	-0.54	-0.86	1.59
Pl9	-0.57	-1.08	1.89
Pl10	-0.60	-0.59	0.98
Pl11	-0.63	-0.69	1.10
Pl12	-0.66	-0.73	1.11
Pl13	-0.71	-0.8	1.13
Pl14	-0.77	-0.88	1.14
Pl15	-0.84	-0.96	1.14
Pl16	-0.80	-1.09	1.36
Pl17	-0.92	-1.39	1.51
Pl18	-0.96	-1.69	1.76

Cp	-0.72	-0.91	1.26
SDT	0.22	0.28	0.28
Cov	0.30	0.31	0.22

Table E. 27. Cp bare roofs Vs. roof under solar panels and solar panel surfaces, Slope 15º, WD 90º, LW

Polylines	Cp (SP)	Pr2	Cp Bott	Diff	Ttl Cp	Ttl/Brf
Pl20	-2.59	-1.27	-1.12	-1.47	-2.74	2.49
Pl21	-1.98	-1.65	-2.38	0.40	-1.25	1.28
Pl22	-1.27	-2.01	-2.75	1.48	-0.53	0.59
Pl23	-1.04	-1.32	-1.4	0.36	-0.96	1.13
Pl24	-0.93	-0.99	-0.99	0.06	-0.93	1.21
Pl25	-0.87	-0.89	-0.8	-0.07	-0.96	1.33
Pl26	-0.82	-1.22	-0.41	-0.41	-1.63	2.40
Pl27	-0.79	-1.45	-2.21	1.42	-0.03	0.05
Pl28	-0.84	-1.12	-1.62	0.78	-0.34	0.53
Pl29	-0.9	-0.80	-0.41	-0.49	-1.29	2.08
Pl30	-0.74	-1.40	-1.58	0.84	-0.56	0.92
Pl31	-0.69	-1.39	-2.09	1.40	0.01	-0.02
Pl32	-0.67	-0.95	-1.04	0.37	-0.58	1.04
Pl33	-0.67	-0.71	-0.69	0.02	-0.69	1.25
Pl34	-0.67	-0.71	-0.49	-0.18	-0.89	1.68
Pl35	-0.68	-1.36	-0.04	-0.64	-2	3.85
Pl36	-0.76	-1.54	-2.27	1.51	-0.03	0.06
Pl37	-0.91	-1.26	-1.67	0.76	-0.5	1.04
Cp	-0.80	-1.14	-1.18	0.38	-0.76	1.24
SDT	0.12	0.28	0.71	0.71	0.58	1.00
Cov	0.14	0.25	0.60	1.86	0.76	0.81

Table E. 28. Cp bare roof Vs top of panels, Slope 15º, WD 90º, LW

Polylines	Bare Roof	Cp (SP)	Cp (SP/BRf)
Pl20	-1.10	-2.59	2.35
Pl21	-0.98	-1.98	2.02
Pl22	-0.90	-1.27	1.41
Pl23	-0.85	-1.04	1.22
Pl24	-0.77	-0.93	1.21
Pl25	-0.72	-0.87	1.21
Pl26	-0.68	-0.82	1.21
Pl27	-0.66	-0.79	1.20
Pl28	-0.64	-0.84	1.31
Pl29	-0.62	-0.9	1.45
Pl30	-0.61	-0.74	1.21
Pl31	-0.58	-0.69	1.19
Pl32	-0.56	-0.67	1.20

Pl33	-0.55	-0.67	1.22
Pl34	-0.53	-0.67	1.26
Pl35	-0.52	-0.68	1.31
Pl36	-0.49	-0.76	1.55
Pl37	-0.48	-0.91	1.90
Cp	-0.68	-0.80	1.31
SDT	0.11	0.12	0.19
Cov	0.16	0.14	0.15

Table E. 29. Cp on bare roofs Vs. roof under solar panels and solar panel surfaces, Slope 15º, WD 0º

Polylines	Cp (SP)	Pr2	Cp Bott	Diff	Ttl Cp	Ttl/Brf
Pl1A	-0.3	-0.31	-0.32	0.02	-0.29	0.66
Pl2	-0.29	-0.34	-0.35	0.06	-0.28	0.62
Pl3	-0.29	-0.37	-0.37	0.08	-0.29	0.63
Pl4	-0.29	-0.37	-0.37	0.08	-0.29	0.62
Pl5	-0.29	-0.37	-0.37	0.08	-0.29	0.60
Pl6	-0.29	-0.37	-0.37	0.08	-0.29	0.59
Pl7	-0.29	-0.37	-0.37	0.08	-0.29	0.59
Pl8	-0.31	-0.37	-0.37	0.06	-0.31	0.63
Pl9	-0.32	-0.36	-0.36	0.04	-0.32	0.64
Pl10	-0.33	-0.35	-0.36	0.03	-0.32	0.63
Pl11	-0.3	-0.39	-0.39	0.09	-0.3	0.59
Pl12	-0.3	-0.39	-0.39	0.09	-0.3	0.59
Pl13	-0.3	-0.39	-0.39	0.09	-0.3	0.59
Pl14	-0.3	-0.38	-0.38	0.08	-0.3	0.59
Pl15	-0.3	-0.38	-0.38	0.08	-0.3	0.58
Pl16	-0.3	-0.38	-0.38	0.08	-0.3	0.58
Pl17	-0.31	-0.34	-0.34	0.03	-0.31	0.60
Pl18	-0.32	-0.34	-0.34	0.02	-0.32	0.62
Cp	-0.30	-0.37	-0.37	0.07	-0.30	0.61
SDT	0.01	0.02	0.02	0.03	0.01	0.02
Cov	0.04	0.06	0.05	0.39	0.04	0.04

Table E. 30.Cp bare roof Vs top of solar panels, Slope 15º, WD 0º

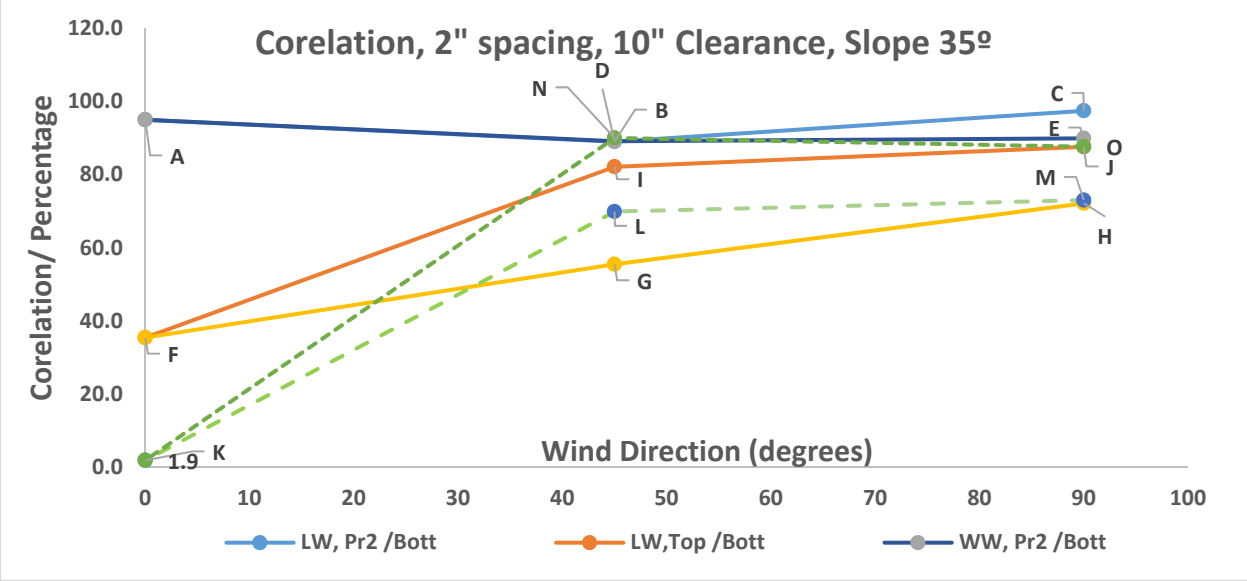
	Cp Bare roof	Cp (SP)	Cp (SP/BRf)
Pl1A	-0.44	-0.3	0.68
Pl2	-0.45	-0.29	0.64
Pl3	-0.46	-0.29	0.63
Pl4	-0.47	-0.29	0.62
Pl5	-0.48	-0.29	0.60
Pl6	-0.49	-0.29	0.59

Pl7	-0.49	-0.29	0.59
Pl8	-0.49	-0.31	0.63
Pl9	-0.5	-0.32	0.64
Pl10	-0.51	-0.33	0.65
Pl11	-0.51	-0.3	0.59
Pl12	-0.51	-0.3	0.59
Pl13	-0.51	-0.3	0.59
Pl14	-0.51	-0.3	0.59
Pl15	-0.52	-0.3	0.58
Pl16	-0.52	-0.3	0.58
Pl17	-0.52	-0.31	0.60
Pl8	-0.52	-0.32	0.62
Cp	-0.49	-0.30	0.61
SDT	0.03	0.01	0.03
Cov	0.05	0.04	0.05

APPENDIX F

Chapter 6, Correlations

F.1. Correlations between pressure coefficients on top, bottom of the panels and roof surface, 2” spacing, 10” clearance, 35º roof slope and roof without solar panels



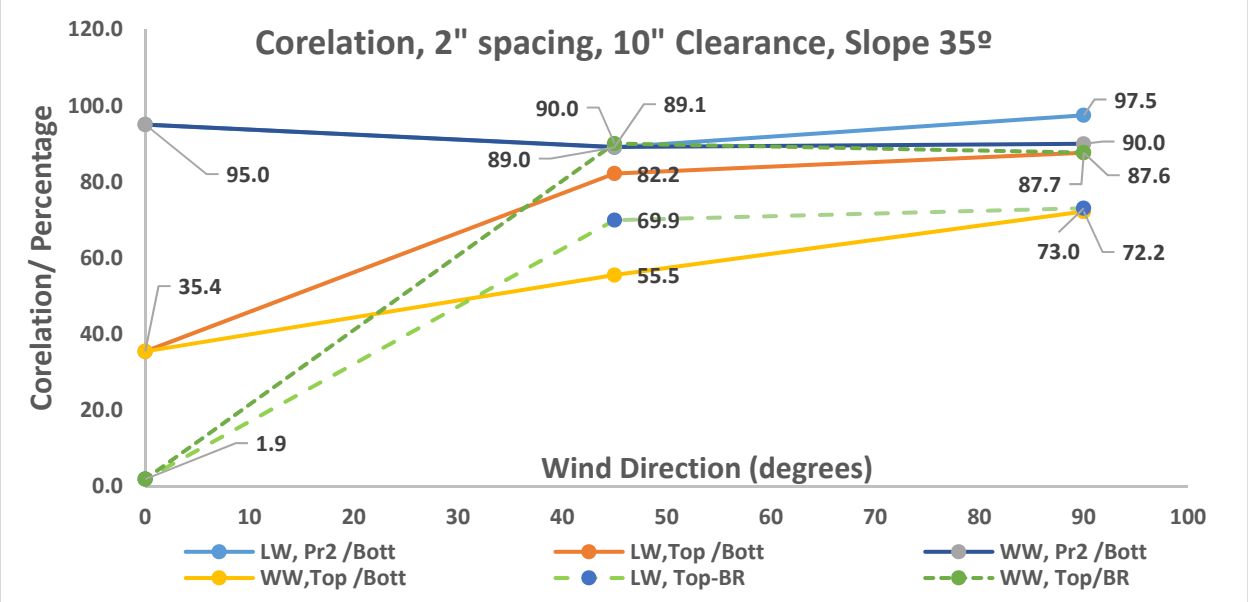


Fig. F. 1. Correlation between pressure coefficient of the surfaces, 2" spacing, 10" clearance, slope 35º

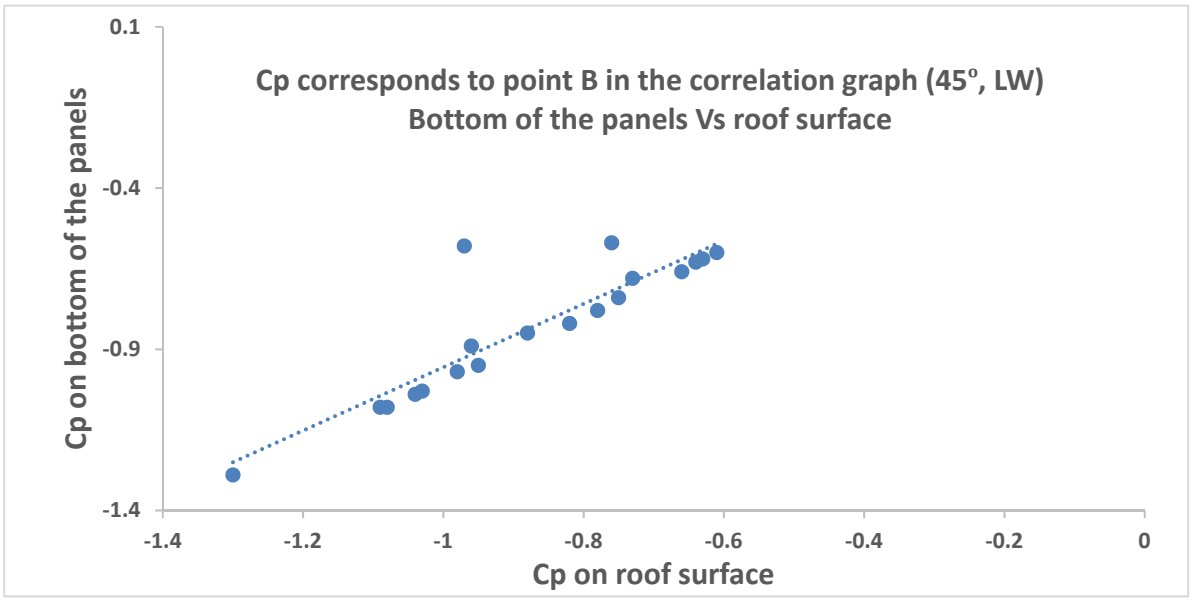
Table F. 1. Cp on top and bottom surfaces of solar panels, clearance 10", spacing 2"

Leeward 90º wind direction				windward 90º wind direction			
Polylines	Cp Top of panels	Cp roof under panels	Cp Bottom of panels	Polylines	Cp Top of panels	Cp roof under panels	Cp Bottom of panels
Pl17	-1.6	-2.68	-3.11	Pl1A	-0.1	-0.15	-0.33
Pl18	-2.29	-2.60	-3.04	Pl2	-0.08	-0.27	-0.02
Pl19	-1.23	-2.36	-2.49	Pl3	-0.1	-1.06	-0.97
Pl20	-0.98	-2.24	-2.29	Pl4	-0.12	-0.82	-0.52
Pl21	-0.88	-1.93	-2.22	Pl5	-0.15	-0.47	-0.24
Pl22	-0.78	-1.65	-1.82	Pl6	-0.23	-0.3	0.11
Pl23	-0.71	-1.52	-1.54	Pl7	-0.55	-0.73	-1.24
Pl24	-0.69	-1.62	-1.76	Pl8	-0.14	-1.01	-0.97
Pl25	-0.85	-1.54	-1.74	Pl9	-0.26	-0.92	-0.76
Pl26	-0.64	-1.56	-1.52	Pl10	-0.34	-1.15	-1.07
Pl27	-0.48	-1.38	-1.56	Pl11	-0.42	-1.00	-0.79
Pl28	-0.48	-1.01	-1.36	Pl12	-0.52	-0.83	-0.64
Pl29	-0.48	-0.75	-0.92	Pl13	-0.66	-0.65	-0.45
Pl30	-0.48	-0.66	-0.64	Pl14	-1.4	-1.39	-1.62
Pl31	-0.5	-1.00	-1.25	Pl15	-1.03	-1.47	-1.47
Pl32	-0.68	-0.65	-1.11	Pl16	-1.23	-1.50	-1.36

Leeward 45º wind direction				Wind ward 45º wind direction				0º wind direction			
Polylines	Cp Top	Cp roof under panels	Cp bottom of panels	Polylines	Cp Top	Cp roof under panels	Cp bottom of panels	Polylines	Cp Top	Cp roof under panels	Cp bottom of panels
Pl20a	-1.19	-1.3	-1.29	Pl1A	-0.3	-0.15	-0.29	Pl1A	-0.35	-0.36	-0.37
Pl21	-1.13	-1.09	-1.08	Pl2	-0.17	-0.21	0.07	Pl2	-0.34	-0.36	-0.38
Pl22	-1.03	-1.04	-1.04	Pl3	-0.29	-0.65	-0.59	Pl3	-0.34	-0.39	-0.41
Pl23	-0.99	-1.03	-1.03	Pl4	-0.18	-0.49	-0.31	Pl4	-0.34	-0.41	-0.41
Pl24	-0.78	-1.08	-1.08	Pl5	-0.2	-0.33	-0.24	Pl5	-0.34	-0.41	-0.41
Pl25	-0.71	-0.95	-0.95	Pl6	-0.21	-0.33	-0.06	Pl6	-0.34	-0.42	-0.42
Pl26	-0.66	-0.78	-0.78	Pl7	-0.23	-0.34	0.15	Pl7	-0.36	-0.43	-0.43
Pl27	-0.63	-0.66	-0.66	Pl8	-0.45	-0.65	-0.56	Pl8	-0.38	-0.43	-0.43
Pl28	-0.62	-0.76	-0.57	Pl9	-0.15	-0.68	-0.72	Pl9	-0.38	-0.43	-0.43
Pl29	-0.6	-0.73	-0.68	Pl10	-0.25	-0.61	-0.40	Pl10	-0.35	-0.43	-0.43
Pl30	-0.6	-0.64	-0.63	Pl11	-0.29	-0.97	-0.88	Pl11	-0.35	-0.43	-0.43
Pl31	-0.68	-0.61	-0.60	Pl12	-0.33	-0.75	-0.55	Pl12	-0.35	-0.44	-0.44
Pl32	-0.69	-0.98	-0.97	Pl13	-0.39	-0.55	-0.48	Pl13	-0.35	-0.44	-0.44
Pl33	-0.68	-0.82	-0.82	Pl14	-0.46	-0.48	-0.36	Pl14	-0.35	-0.44	-0.44
Pl34	-0.68	-0.75	-0.74	Pl15	-0.52	-0.50	-0.23	Pl15	-0.35	-0.42	-0.42
Pl35	-0.68	-0.63	-0.62	Pl16	-0.79	-0.89	-0.98	Pl16	-0.36	-0.42	-0.42
Pl36	-0.69	-0.97	-0.58	Pl17	-0.52	-1.00	-0.91	Pl17	-0.37	-0.39	-0.42
Pl37	-0.71	-0.96	-0.89	Pl18	-0.72	-0.92	-0.68	Pl18	-0.35	-0.40	-0.41
Pl38a	-0.73	-0.88	-0.85	Pl19a	-0.84	-0.92	-0.70	Pl19a	-0.35	-0.39	-0.40

Every point in Fig F.1 represents a correlation value of a pair of series corresponding to the Cp on 2 surfaces, of the top or bottom of the panels, roof surface, and roof without solar panels surface. Each of those series of points is illustrated in one of the following figures, from F.2 to F.11, which depict one series as function of the other series of the pair. A linear trend line is added to the points. Pressure coefficients of the 35º inclined roof without solar panels for 90º, 45º, and 0º wind directions are listed in Table F.1.

As shown in the first graph in Fig. F.2, the Cp points of the bottom of the panels and roof surfaces on the leeward side of the roof are distributed along and very close to a straight line, which is reflected by the high correlation factor of 0.89. The second graph in Fig. F.2 displays the Cp points for the top and bottom of the panels on the same leeward side. The last points are distributed close to a straight line (correlation 0.82), but are not as close along the line as the cavity surfaces. However, Fig. F.16 shows that the Cp points for the top of the panels and roof without solar panels surfaces on the leeward side of the roof are distributed much farther from a straight line than the other 2 pairs represented in Fig. F.2. Some points in Fig. F.3 align with a line nearly perpendicular to the trend line, which all reflected in a correlation factor of 0.70, much lower than the other 2 pairs in Figs. F.2 and F.3.



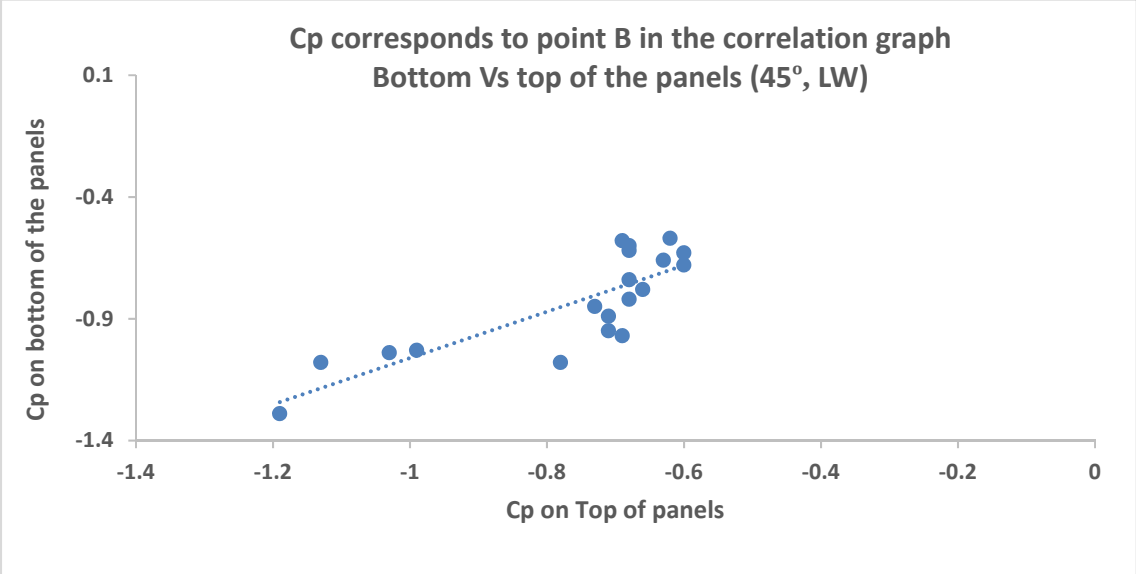


Fig. F. 2. Cp as a function of one surface Cp on the other, 2" spacing, 10" clearance, slope 35º, wind direction 45º, leeward

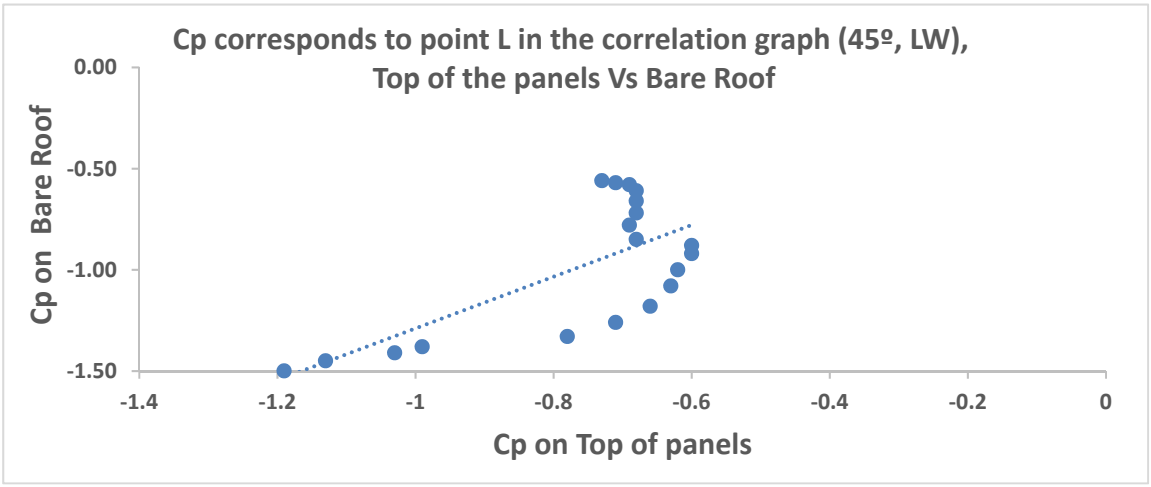
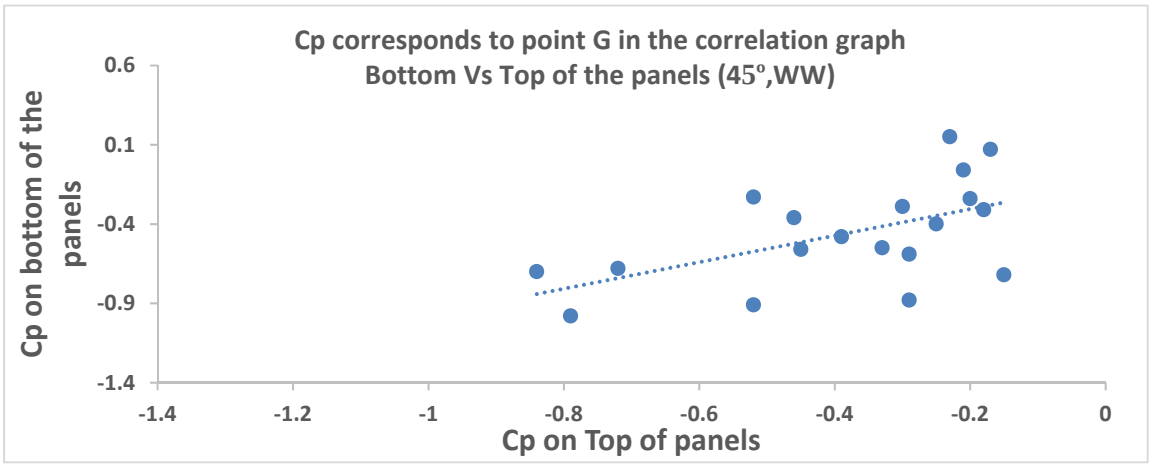


Fig. F. 3. Cp as a function of one surface Cp on the other, 2" spacing, 10" clearance, slope 35º, wind direction 45º, leeward

In Figure F.4, the Cp points for the bottom of the panels and the roof surfaces on windward side of the roof are distributed very close to a straight line, which is reflected by the high correlation factor of 0.89. Similarly, Fig. F.18, which represents the Cp points of top of the panels and roof without solar panels surfaces on the windward side of the roof, shows that those points are

distributed close to a straight line. These similar distributions indicate similar correlation factors, which is the case because the points in Fig. F.5 have a 0.90 correlation factor.

However, the distribution of Cp points for the top and bottom of the panel surfaces on the windward side (Fig. F.4, second graph), shows very scattered points around a positive slope of the straight trend line, which is translated in much lower correlation, i.e., 0.5F.



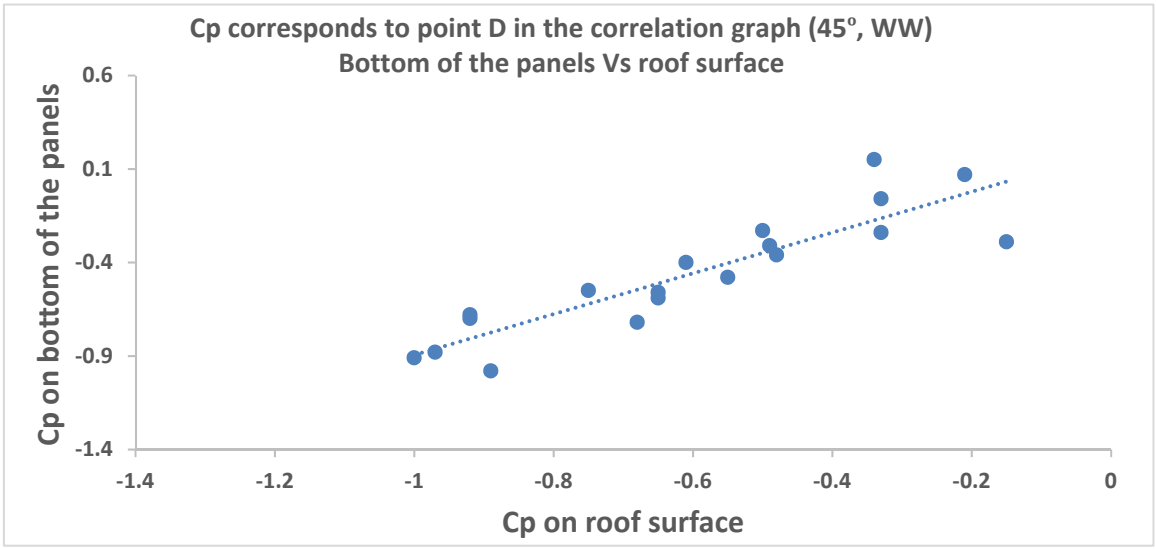


Fig. F. 4. Cp as a function of one surface Cp on the other, 2" spacing, 10" clearance, slope 35º, wind direction 45º, windward

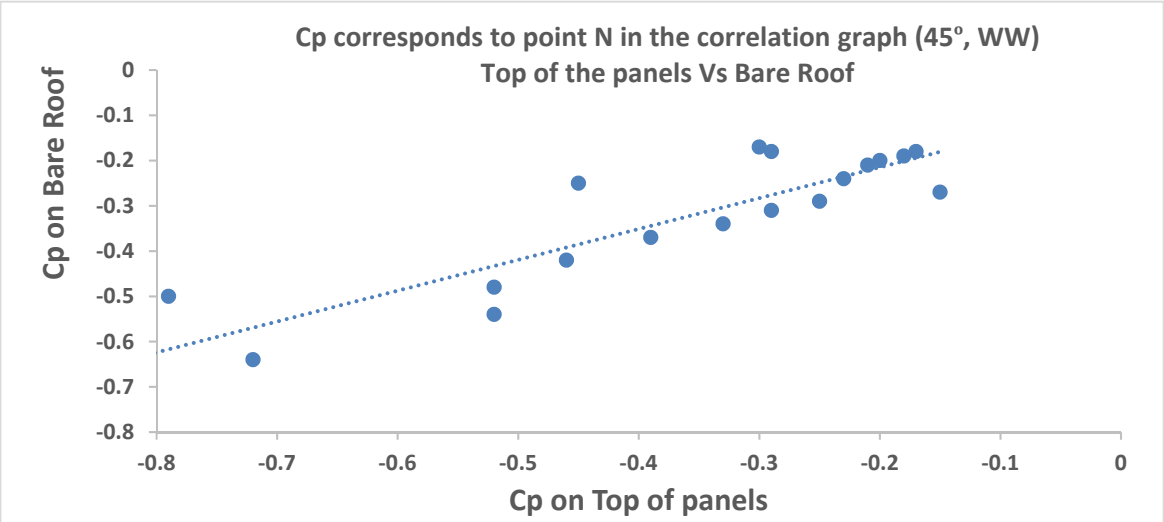


Fig. F. 5. Cp as a function of one surface Cp of the other, 2" spacing, 10" clearance, slope 35º, wind direction 45º, windward

For the 90 wind direction on the leeward side of the roof, Fig. F.6 depicts the Cp points at the bottom of the panels and at the roof surface, where the points are distributed extremely close to a straight line, (correlation of 0.98), while the Cp points located on the top and bottom of the panels on the same leeward side are distributed slightly farther from a straight line (correlation of 0.88). On the other hand, Fig. F.7 shows the distribution of the Cp points of the top of the panels and the roof without solar panels surfaces on the leeward side of the roof. The points are distributed a little more scattered around a straight line than the other 2 pairs presented in Fig.

F.6. The last scattered points have a lower correlation (0.73) than the other 2 pairs in Figs. F.6 and F.7.

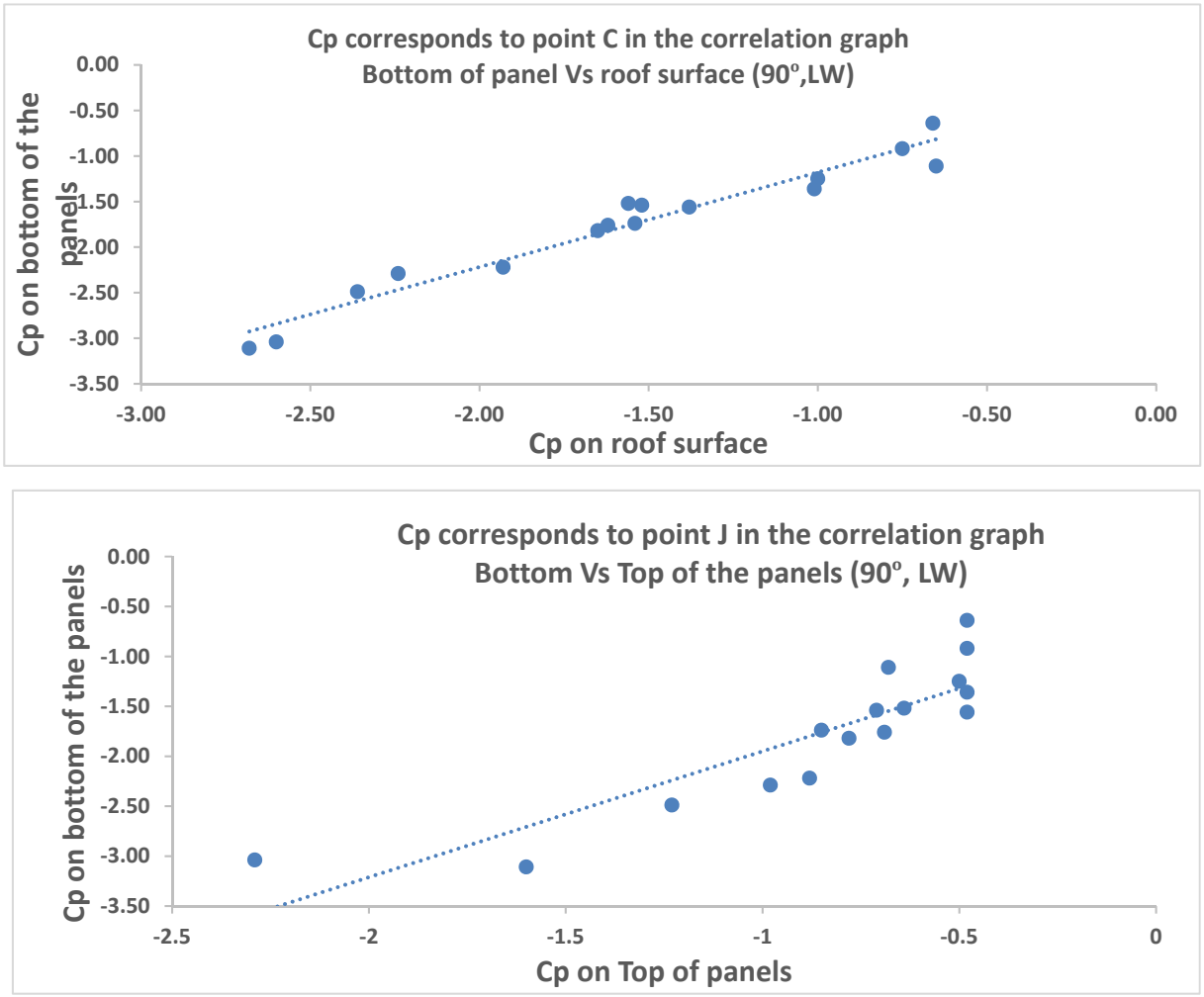


Fig. F. 6. Cp as a function of one surface Cp on the other, 2" spacing, 10" clearance, slope 35°, wind direction 90°, leeward

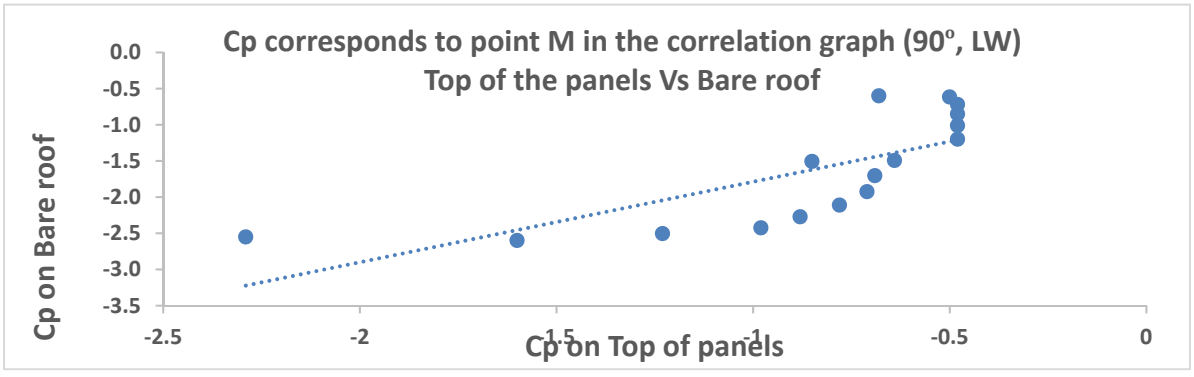


Fig. F. 7. Cp as a function of one surface Cp of the other, 2" spacing, 10" clearance, slope 35°, wind direction 90°, leeward

On the windward side of the roof and for the same wind direction of 90º, the distribution of the Cp points on the bottom of the panels and on the roof surfaces is close to a straight line, but more scattered than for the leeward side, which is translated by a lower correlation factor (0.90, Fig. F.8). However, the distribution of Cp points on the top and bottom of the panel surfaces on the windward side is much more scattered (0.72 correlation) around a straight line than the same surfaces on the leeward side (Fig. F.8).

Nonetheless, the distribution of Cp points of the top of the panels and the roof without solar panels surfaces on the windward side of the roof depict more alignment with a straight line than those surfaces on the leeward side, and more than the top and bottom of the panels on the windward side. That is demonstrated in the higher correlation of 0.88 (Fig. F.9).

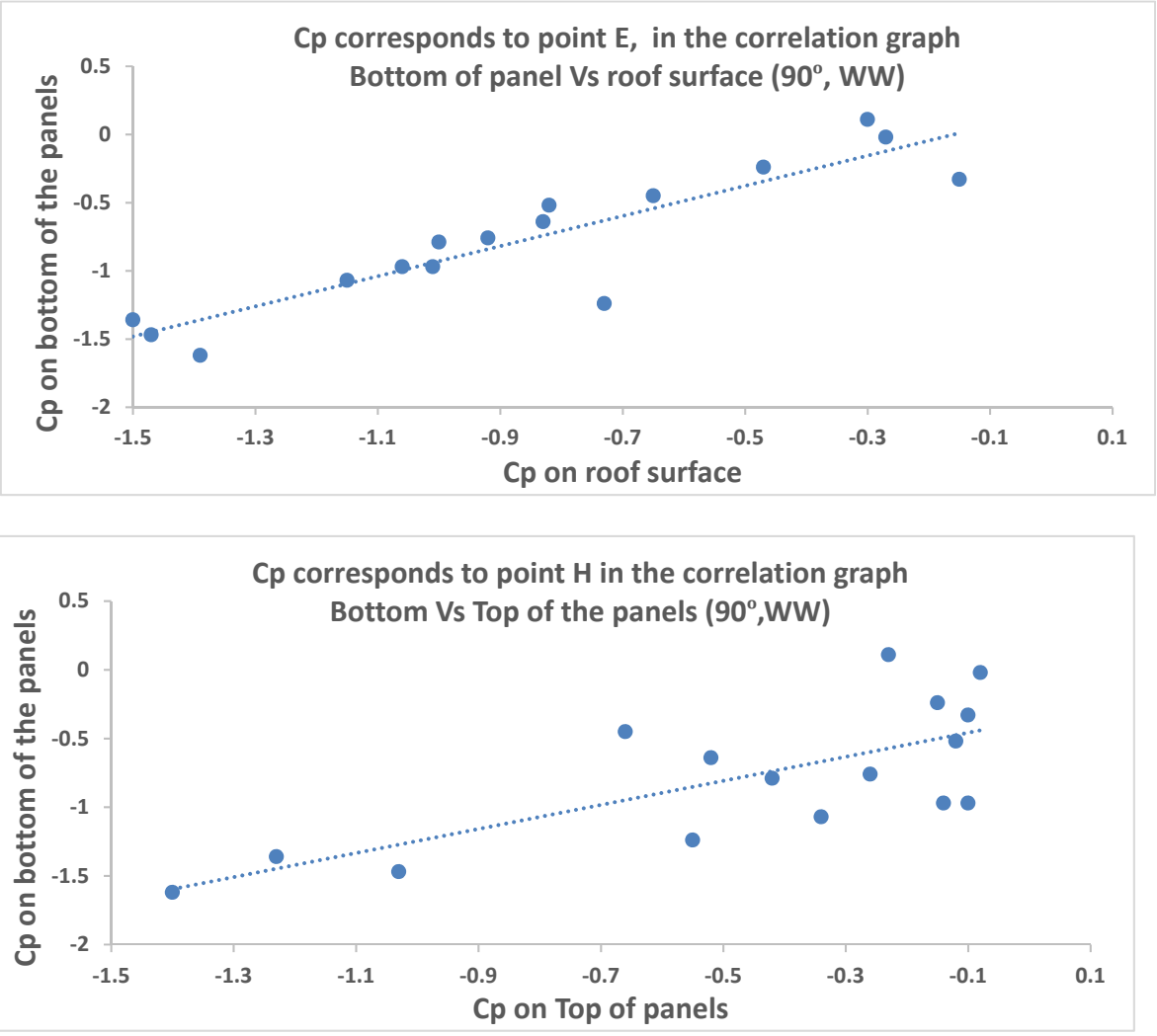


Fig. F. 8. Cp as a function of one surface Cp of the other, 2" spacing, 10" clearance, slope 35º, wind direction 90º, windward

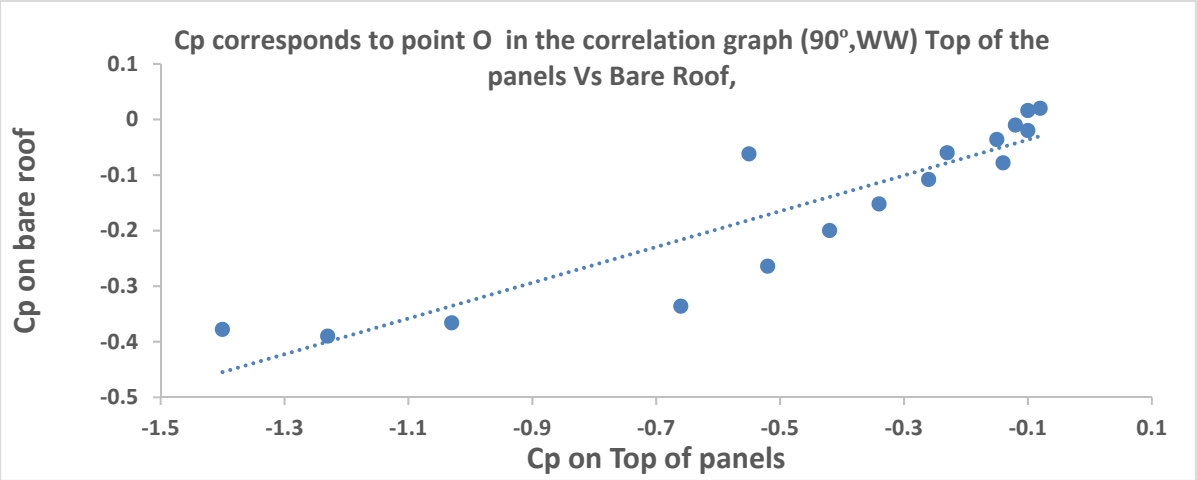


Fig. F. 9. Cp as a function of one surface Cp of the other, 2" spacing, 10" clearance, slope 35º, wind direction 90º, windward

The distribution of the Cp points for the bottom of the panels and the roof surfaces for the 0º wind direction is very close to a straight line. That indicates a very high correlation factor (0.95, Fig. F.10, first graph).

However, the distribution of the Cp points for the top and bottom panel surfaces is very scattered and perpendicular to a straight line (0.35 correlation), as seen in the second graph in Fig. F.10.

As well, the Cp points for the top of the panels and the roof without solar panels surfaces are much more scattered, and all points are distributed nearly perpendicular to a straight line (Fig. F.11). That is reflected by the 0.02 correlation factor in Fig. F.11.

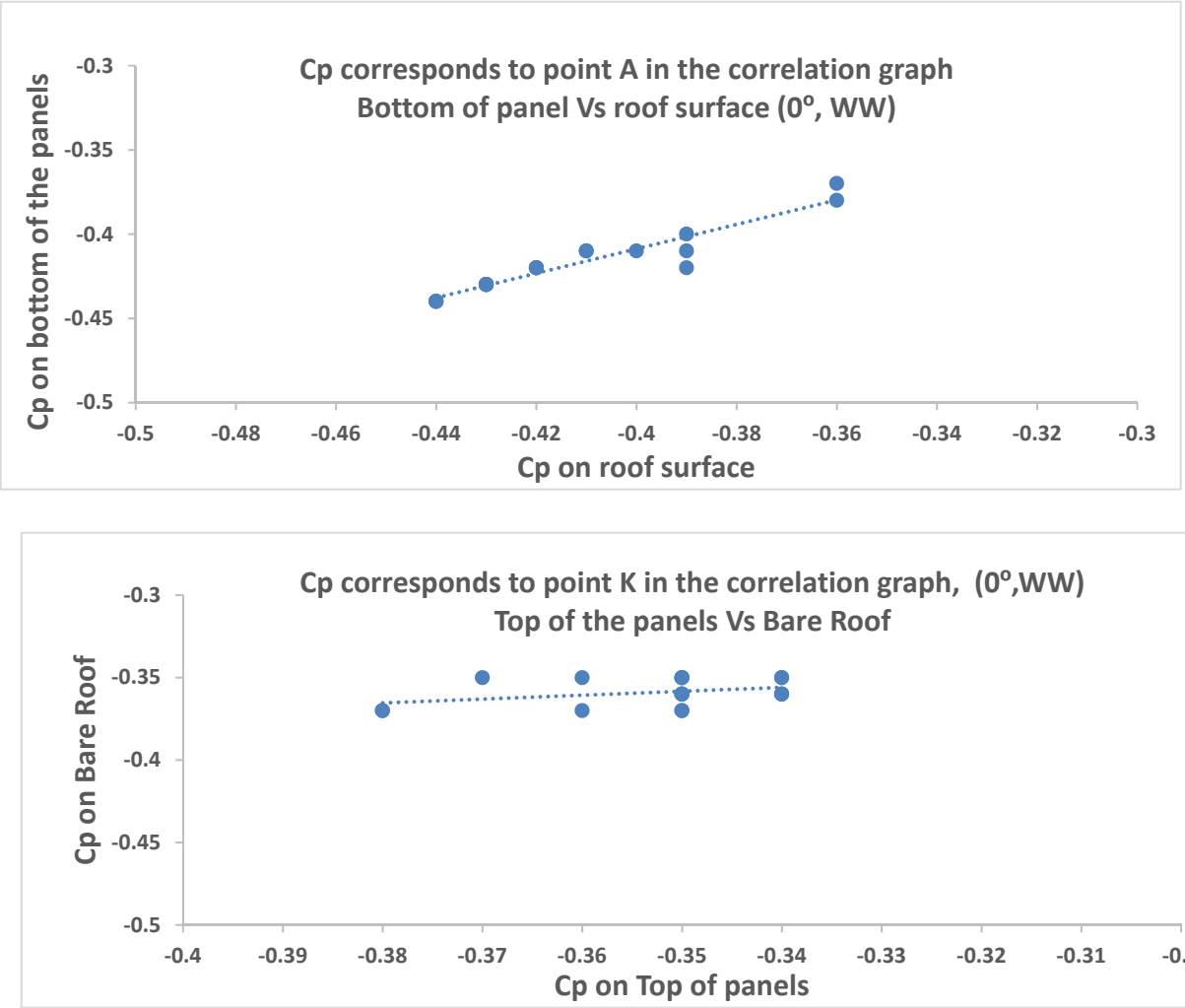


Fig. F. 10. Cp as a function of one surface Cp on the other, 2" spacing, 10" clearance, slope 35°, wind direction 0°

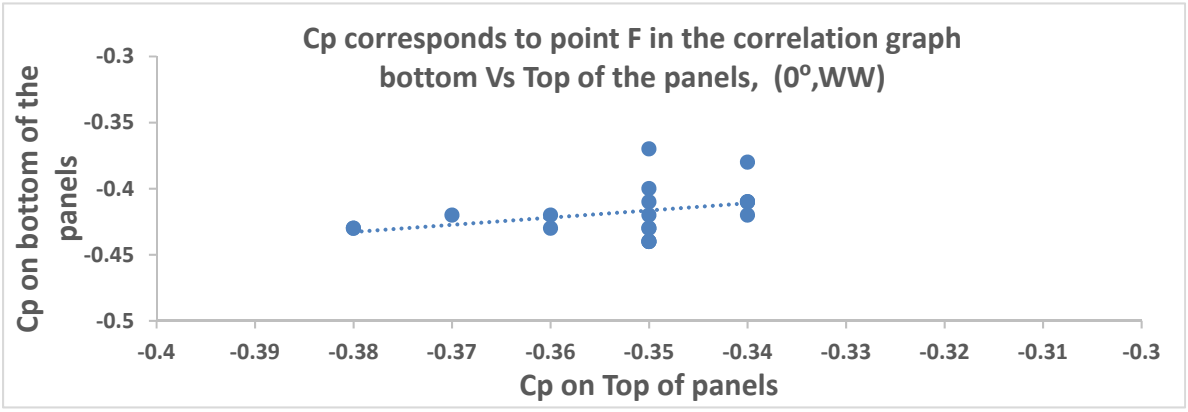
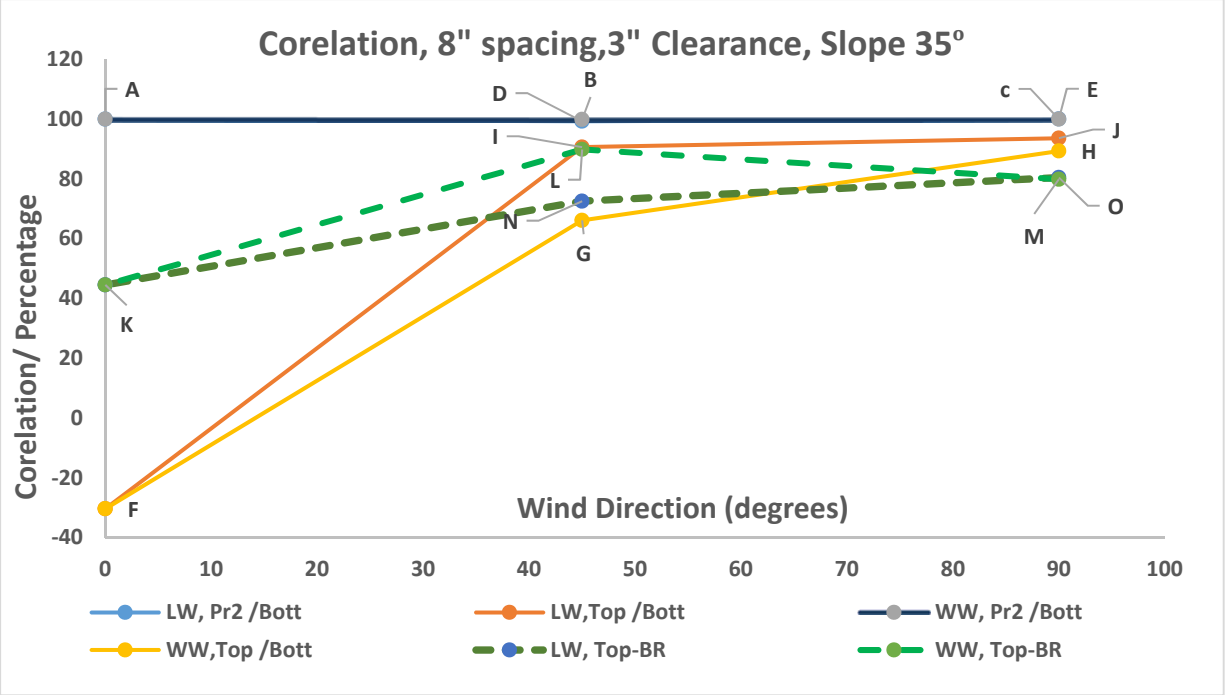


Fig. F. 11. Cp as a function of one surface Cp on the other, 2" spacing, 10" clearance, slope 35°, wind direction 0°

F.2. Correlations between pressure coefficients on top, bottom of the panels, and roof

surface, 8” spacing, 3” clearance, 35º roof slope, and roof without solar panels



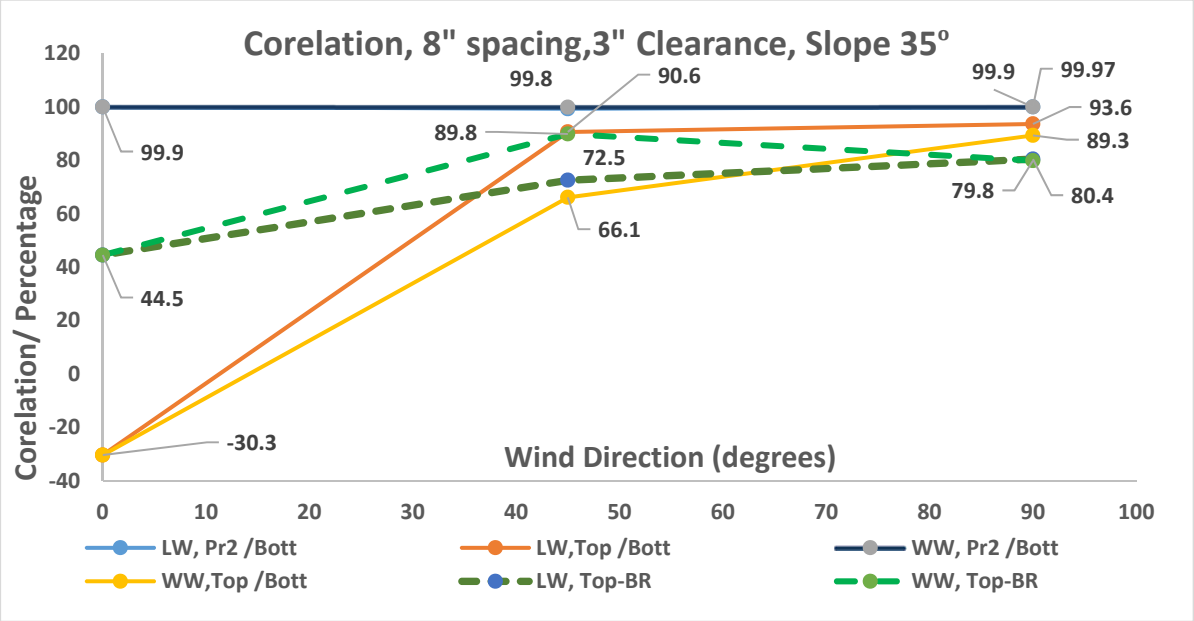


Fig. F. 12. Correlation between pressure coefficients of the surfaces, 8" spacing, 3" clearance, slope 35º

Table F. 2. Cp on top and bottom surfaces of solar panels, clearance 3", spacing 8"

Leeward 90º wind direction				windward 90º wind direction				Leeward 45º wind direction			
Polylines	Cp Top of panels	Cp roof under panels	Cp Bottom of panels	Polylines	Cp Top of panels	Cp roof under panels	Cp Bottom o f panels	Polylines	Cp Top	Cp roof without panels	Cp Bottom of panels
Pl20	-2.77	-4.00	-3.96	Pl1A	-0.62	-0.54	-0.52	Pl20a	-1.64	-1.86	-1.76
Pl21	-2.02	-1.86	-1.76	Pl2	-0.33	-0.1	-0.13	Pl21	-1.37	-1.45	-1.44
Pl22	-1.83	-1.73	-1.72	Pl3	-0.2	-0.21	-0.19	Pl22	-1.23	-1.18	-1.18
Pl23	-1.2	-1.29	-1.27	Pl4	-0.2	-0.1	-0.09	Pl23	-0.83	-0.97	-0.92
Pl24	-1.08	-1.12	-1.11	Pl5	-0.21	-0.05	-0.05	Pl24	-0.76	-0.96	-1.06
Pl25	-0.96	-1.02	-1.01	Pl6	-0.24	-0.03	-0.03	Pl25	-0.7	-0.87	-0.86
Pl26	-0.84	-0.91	-0.9	Pl7	-0.27	-0.42	-0.38	Pl26	-0.66	-0.77	-0.76
Pl27	-0.75	-0.8	-0.79	Pl8	-0.36	-0.21	-0.17	Pl27	-0.63	-0.64	-0.64
Pl28	-0.66	-0.77	-0.77	Pl9	-0.39	-0.44	-0.43	Pl28	-0.58	-0.87	-0.89
Pl29	-0.58	-0.66	-0.65	Pl10	-0.47	-0.68	-0.66	Pl29	-0.54	-0.56	-0.58
Pl30	-0.69	-0.40	-0.39	Pl11	-0.55	-0.62	-0.62	Pl30	-0.45	-0.64	-0.58
Pl31	-0.55	-0.61	-0.60	Pl12	-0.65	-0.57	-0.57	Pl31	-0.6	-0.73	-0.80
Pl32	-0.5	-0.50	-0.49	Pl13	-0.74	-0.56	-0.56	Pl32	-0.6	-0.68	-0.68
Pl33	-0.48	-0.43	-0.43	Pl14	-0.88	-1.20	-1.15	Pl33	-0.6	-0.60	-0.60
Pl34	-0.47	-0.37	-0.36	Pl15	-1.37	-0.88	-0.84	Pl34	-0.6	-0.48	-0.48
Pl35	-0.48	-0.98	-0.99	Pl16	-1.44	-1.00	-0.89	Pl35	-0.61	-1.08	-1.09
Pl36a	-0.53	-0.76	-0.75	Pl17a	-2.01	-2.75	-2.69	Pl36a	-0.68	-0.77	-0.80

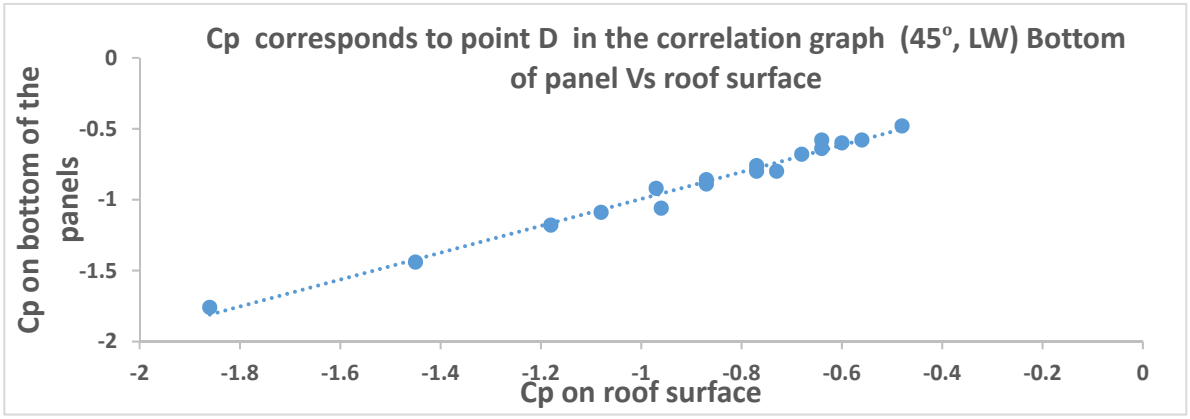
Windward 45º wind direction				0º wind direction			
Polylines	Cp Top	Cp roof under panels	Cp bottom of panels	Polylines	Cp Top	Cp roof under panels	Cp bottom of panels
Pl1A	-0.65	0.2	0.23	Pl1A	-0.36	-0.34	-0.34
Pl2	-0.28	0.22	0.24	Pl2	-0.36	-0.35	-0.35
Pl3	-0.24	-0.31	-0.28	Pl3	-0.36	-0.43	-0.43
Pl4	-0.24	-0.26	-0.26	Pl4	-0.36	-0.43	-0.43
Pl5	-0.25	-0.31	-0.31	Pl5	-0.36	-0.43	-0.43
Pl6	-0.25	-0.36	-0.36	Pl6	-0.36	-0.43	-0.43
Pl7	-0.26	-0.49	-0.49	Pl7	-0.37	-0.46	-0.46
Pl8	-0.32	-0.25	-0.25	Pl8	-0.35	-0.5	-0.5
Pl9	-0.34	-0.22	-0.17	Pl9	-0.36	-0.48	-0.48
Pl10	-0.36	-0.94	-0.82	Pl10	-0.35	-0.58	-0.57
Pl11	-0.4	-0.70	-0.69	Pl11	-0.35	-0.58	-0.57
Pl12	-0.45	-0.61	-0.60	Pl12	-0.35	-0.58	-0.57
Pl13	-0.54	-0.55	-0.54	Pl13	-0.35	-0.57	-0.57
Pl14	-0.63	-1.07	-1.06	Pl14	-0.35	-0.42	-0.42
Pl15	-0.85	-0.68	-0.65	Pl15	-0.35	-0.37	-0.37
Pl16	-0.98	-0.67	-0.62	Pl16	-0.35	-0.37	-0.37
Pl17a	-1.28	-1.95	-1.93	Pl17a	-0.35	-0.37	-0.37

Figure F.12 demonstrates the correlation graphs for the pairs of series listed in Table F.2 above and are represented in Figures F.13 to F.22, which illustrate the distribution of Cp values on one surface vs. the Cps of the compared pairs of surfaces, along with a trend line of the series. However, the Cps for the 35º inclined roof without solar panels for the 90º, 45º, and 0º wind directions, which are listed in Table F.1, are not repeated in Table F.2 because they are identical.

Every point in Fig F.12 represents the correlation factor of 2 series of pressure coefficients on a pair of the 4 surfaces, top or bottom of the panels, roof surface under panels, and roof without solar panels surface without any panel.

For the wind direction of 45º, Fig. F.13 shows the Cp points for the bottom of for panels and for roof surfaces on leeward side of the roof. The Cp points are almost aligned with a straight line, which indicates a very high correlation factor of 0.99. However, the Cp points for the top and bottom of the panels on the same leeward side are distributed a little farther from a straight line, with a correlation of 0.91. As well, Fig. F.14 shows the Cp points for the top of the panels and the roof without solar panels surfaces on the leeward side of the roof. These points are distributed much farther from a straight line (correlation of 0.73) than the other 2 pairs represented in Fig. F.13. Moreover, some of the Cp points in Fig. F.14 are scattered

perpendicular to a straight line.



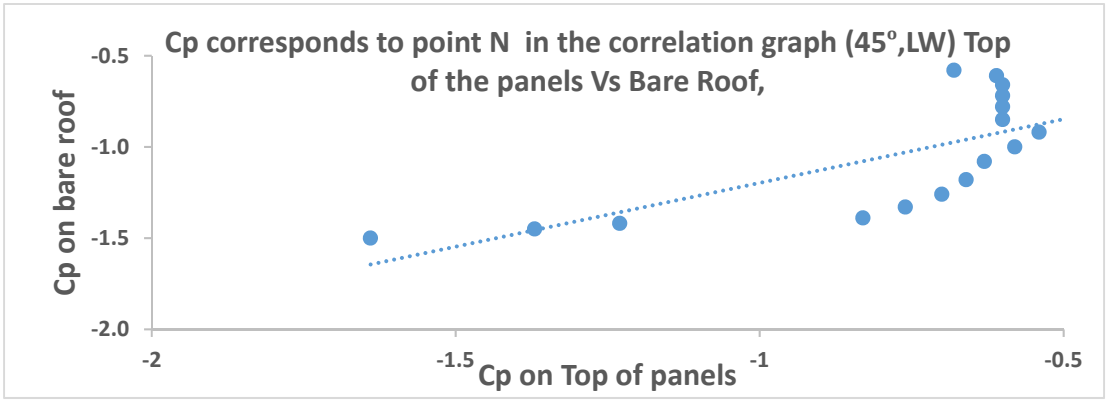


Fig. F. 13. Cp as a function of one surface Cp of the other, 8" spacing, 3" clearance, slope 35º, wind direction 45º

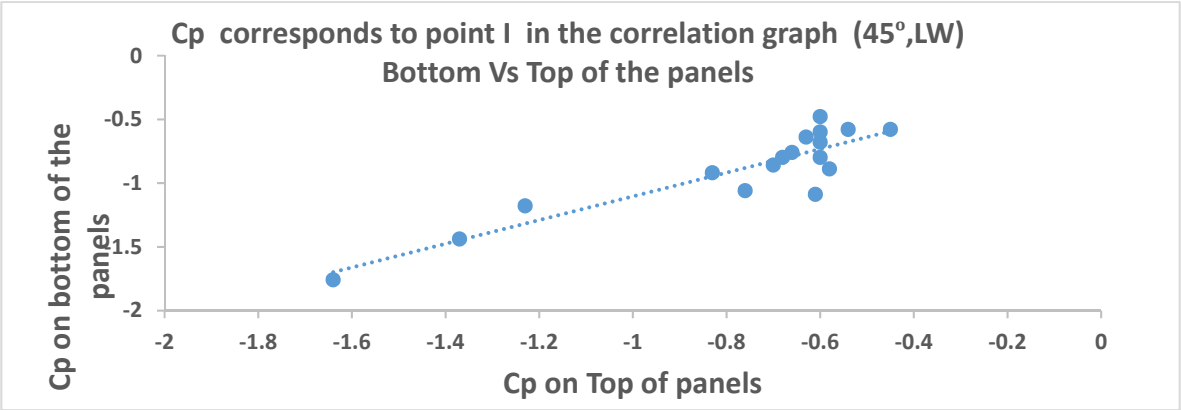
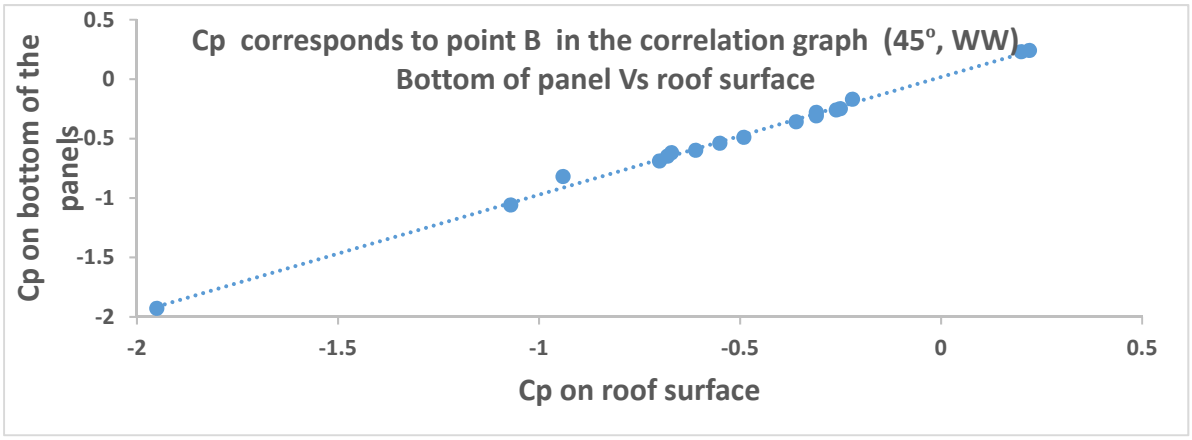


Fig. F. 14. Cp as a function of one surface Cp of the other, 8" spacing, 3" clearance, slope 35º, wind direction 45º, leeward

On the windward side and for same wind direction (45º), the Cp points for the bottom of the panels and the roof surfaces on the windward side of the roof are distributed almost in a straight line, and those points are closest to a straight line than any other pairs of surfaces on the leeward and windward surfaces for the 45º wind direction. This distribution corresponds to a 0.99 correlation factor (Fig. F.15). However, the distribution of Cp points for the top and bottom of the panel surfaces on the windward side is very scattered (0.66 correlation) around a straight line, as shown in Fig. F.15. Also, Fig. F.16 shows the Cp points for the top of the panels and the roof without solar panels surfaces on the windward side of the roof. The points are slightly scattered (0.90 correlation factor) around a straight line, closer than the points of the top and bottom of the panels, but farther than the points of the cavity surfaces.



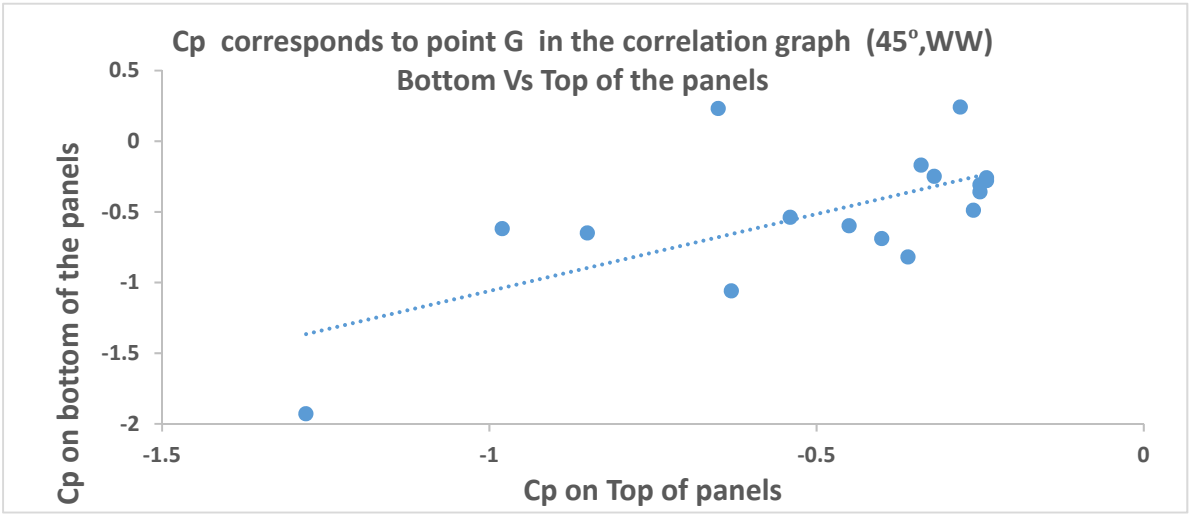


Fig. F. 15. Cp as a function of one surface Cp on the other, 8" spacing, 3" clearance, slope 35°, wind direction 45°, windward

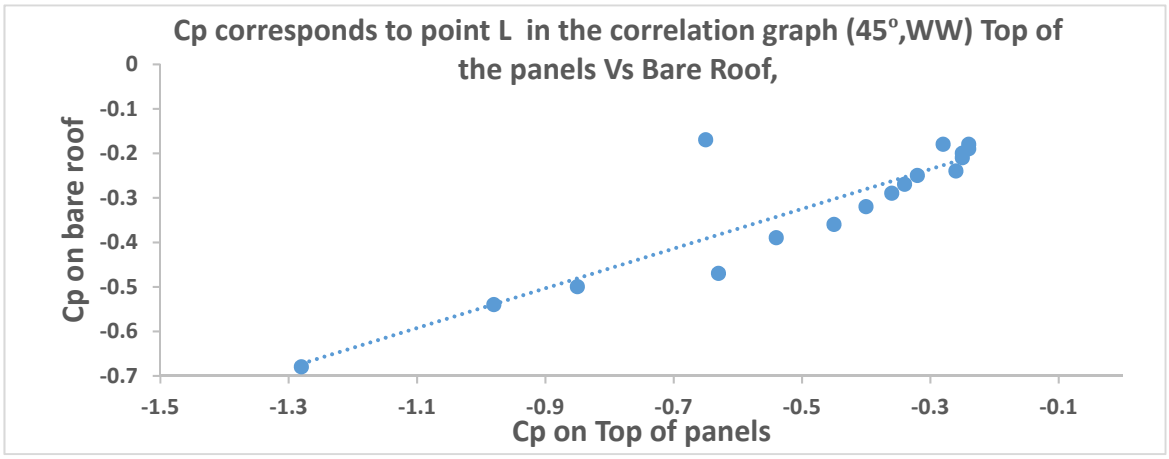
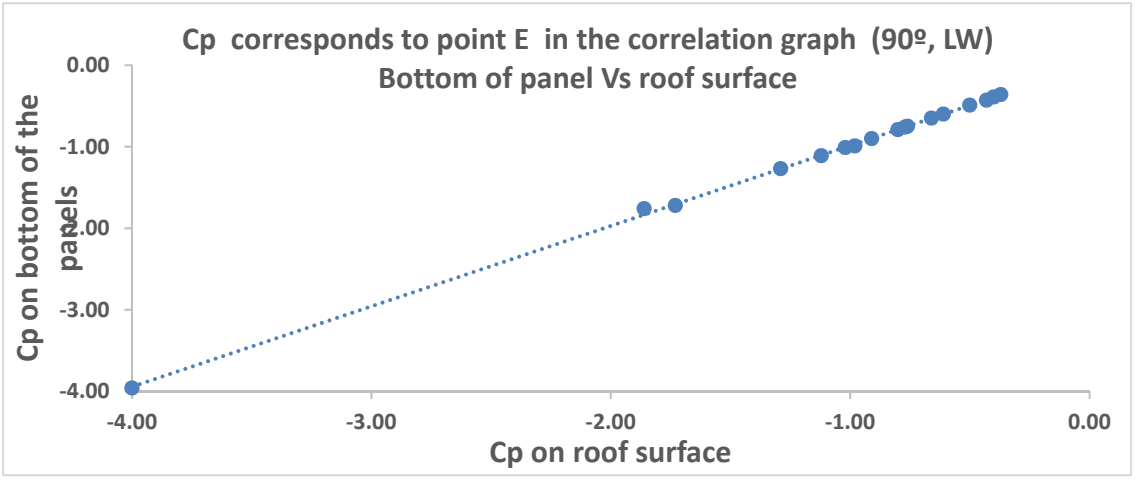


Fig. F. 16. Cp as a function of one surface Cp on the other, 8" spacing, 3" clearance, slope 35°, wind direction 45°, windward

For the wind direction 90º on the leeward side of the roof, the Cp points for the bottom of the panels and the roof surface are distributed nearly on a straight line (correlation of 0.99), while the Cp points for the top and bottom of the panels on the leeward side are distributed slightly farther from a straight line (correlation of 0.94).

For comparison, Fig. F.18 shows the distribution of the Cp points for the top of the panels and the roof without solar panels surfaces on the leeward side of the roof, which are distributed a little more scattered around a straight line than the other 2 pairs represented in Fig. F.17, and their correlation is 0.80.



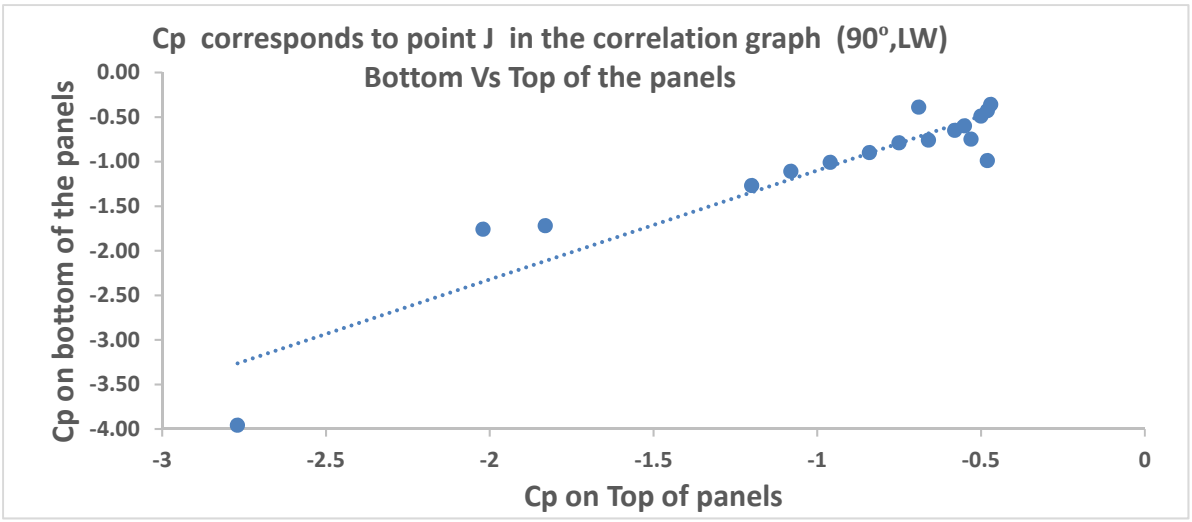


Fig. F. 17. Cp as a function of one surface Cp on the other, 8" spacing, 3" clearance, slope 35º, wind direction 90º, leeward

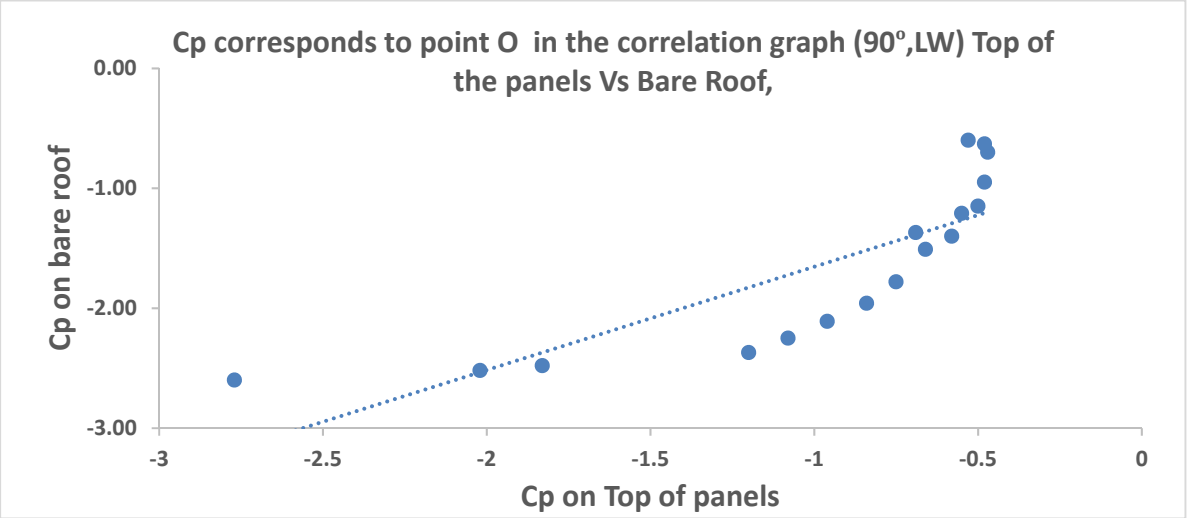


Fig. F. 18. Cp as a function of one surface Cp on the other, 8" spacing, 3" clearance, slope 35º, wind direction 90º, leeward

For same wind direction of 90º on the windward side of the roof, the first graph in Fig. F.19 represents the distribution of Cp points for the bottom of the panels and the roof surfaces, which are distributed close to a straight line. Those aligned points indicate a very high correlation factor (0.99), which might be a result of identical pressures at the bottom of the panels and the roof surfaces. However, the distribution of Cp points of the top and bottom of the panel surfaces on the windward side is slightly scattered (0.89 correlation) around a straight line, as shown in the second graph of Fig. F.19.

Fig. F.20 shows the distribution of Cp points for the top of the panels and the roof without solar panels surfaces on the windward side of the roof. The last two series of points are distributed close

to a straight line, but more scattered than other 2 pairs of surfaces in Fig. F.32 (top and bottom of panels and cavity surfaces), with a correlation factor of 0.80.

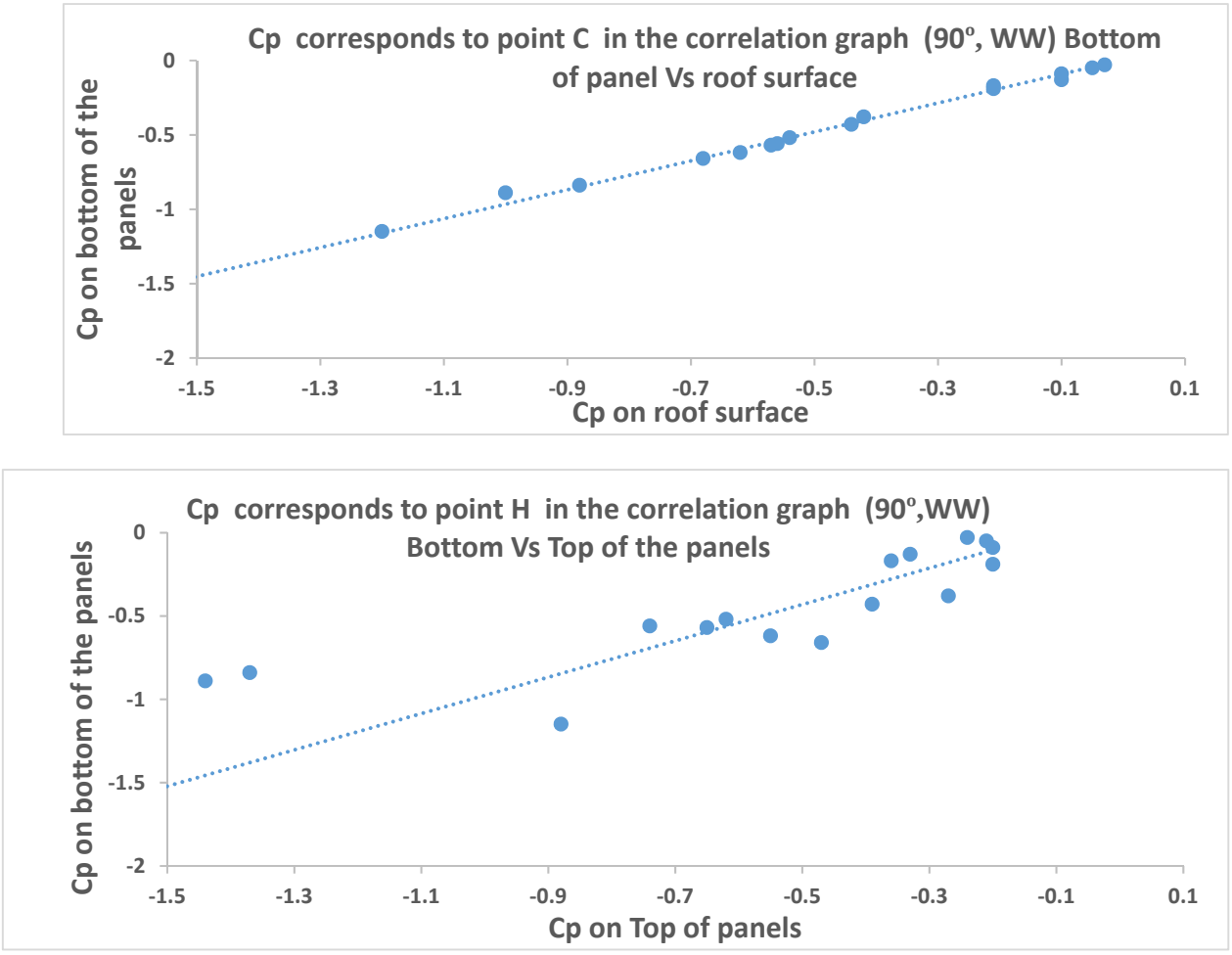


Fig. F. 19. Cp as a function of one surface Cp on the other, 8" spacing, 3" clearance, slope 35°, wind direction 90°, windward

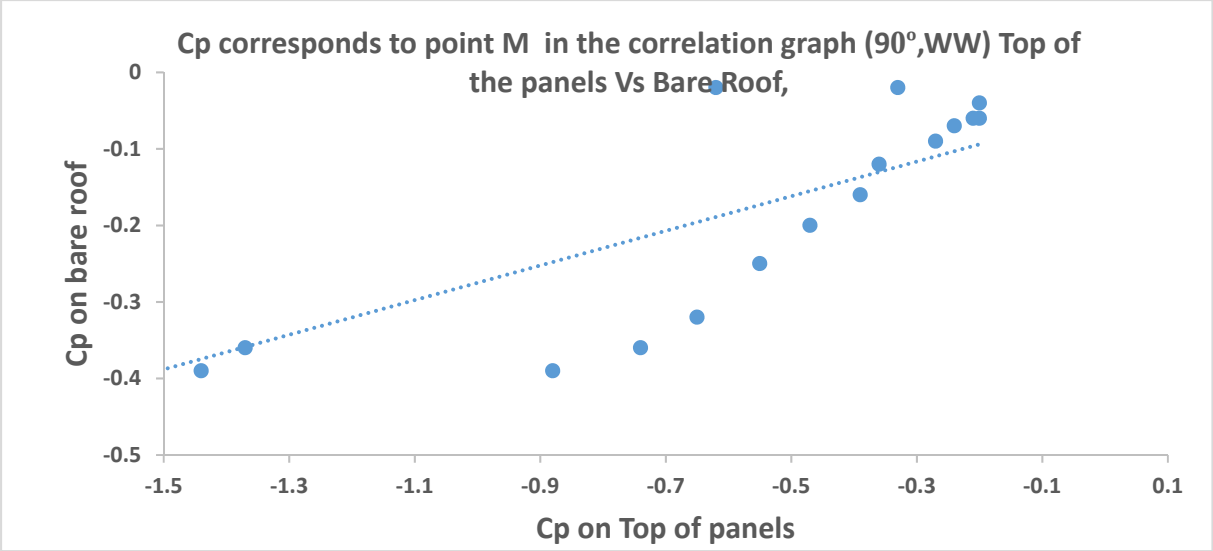
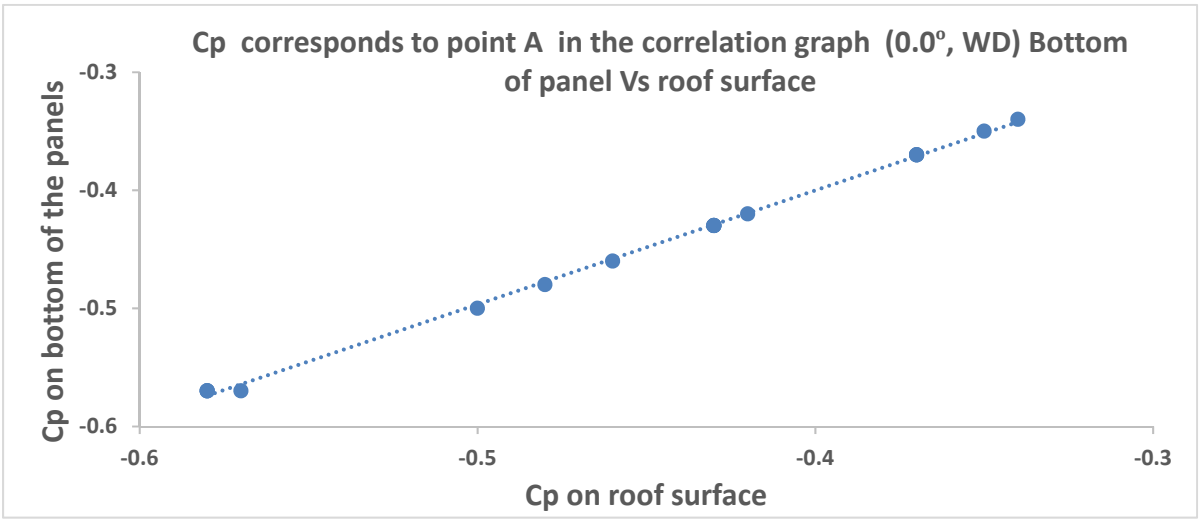


Fig. F. 20. Cp as a function of one surface Cp on the other, 8" spacing, 3" clearance, slope 35º, wind direction 90º, windward

For the 0º wind direction, the first graph in Fig. F.21 represents the distribution of Cp points for the bottom of the panels and the roof surfaces on the windward side of the roof, which depicts the points as very much distributed on a straight line, which indicates a very high correlation factor (0.99), which might be a result of identical pressures at the bottom of the panels and the roof surfaces.

In contrast, the distribution of Cp points for the top and bottom of the panel surfaces on the windward side is quite scattered around a straight line, and some of those points are perpendicular to a straight line. Those 2 series are negatively related, (-0.30 correlation), as shown in the second graph of Fig. F.21. These negative correlation factors mean that there are not much of proportional changes to the two functions, and that the two functions sometimes have different change trends. The more frequent the opposite changes, the lower the correlation factors. The slight opposite changes depicted in the slight negative slope of the trend line for the points for the top and bottom of the panels are represented in the first graph of Fig. F.21. However, the Cp points of the top of the panels and the roof without solar panels surfaces on windward side of the roof (Fig. F.22) are very scattered (0.45 correlation). The trend line in the last distribution has a very slight positive slope, and the points are spread out on and outside a straight line.



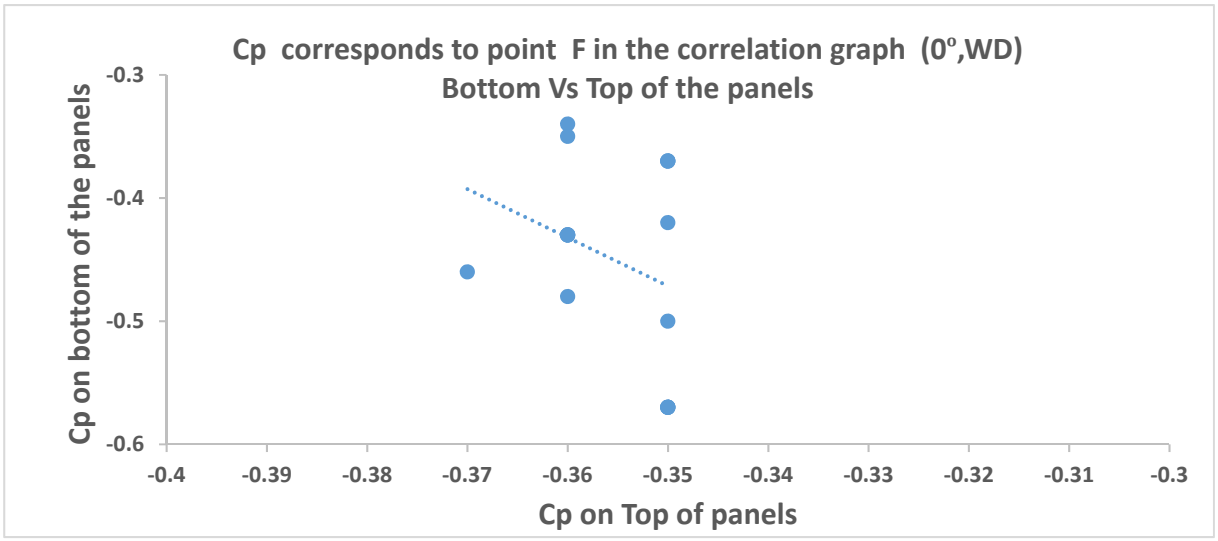


Fig. F. 21. Cp as a function of one surface Cp on the other, 8" spacing, 3" clearance, slope 35°, wind direction

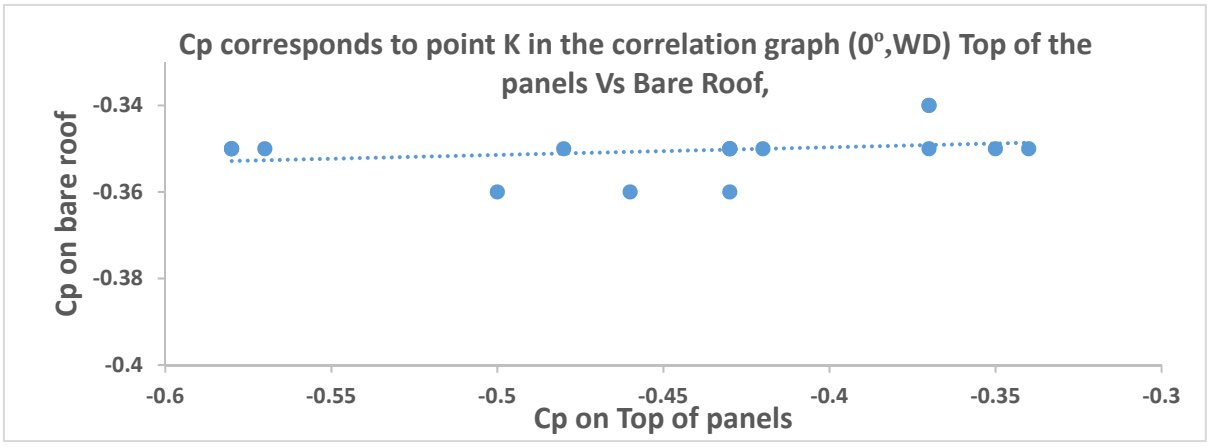
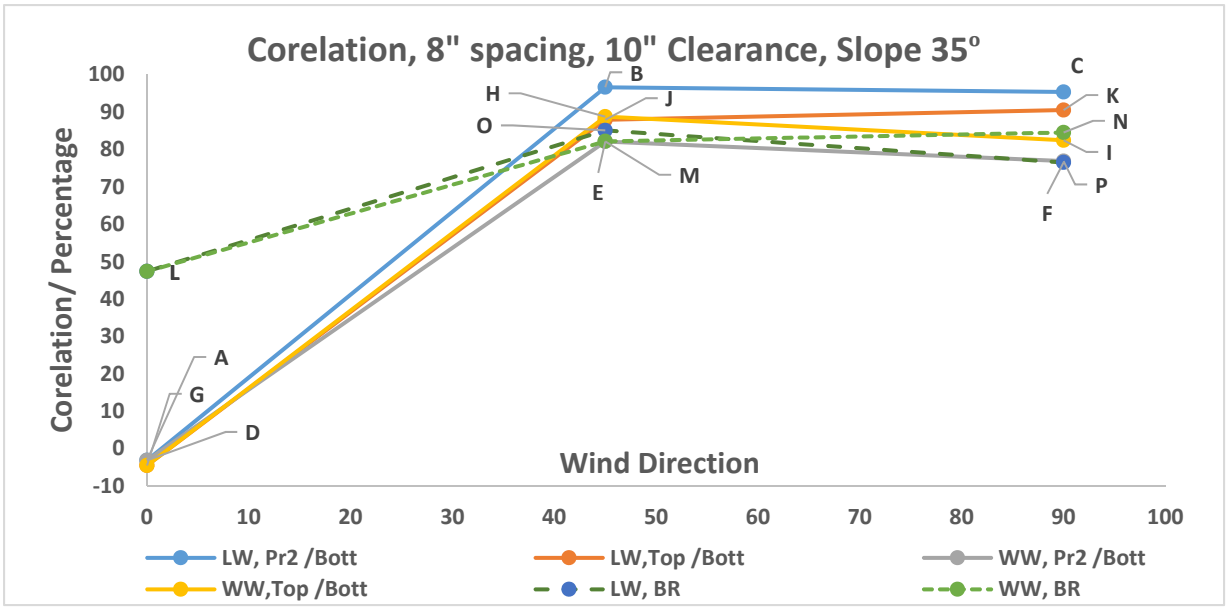


Fig. F. 22. Cp as a function of one surface Cp on the other, 8" spacing, 3" clearance, slope 35°, wind direction 0°,

F.3. Correlations between pressure coefficients on top, bottom of the panels and roof surface, 8" spacing, 10" clearance, 35º roof slope and roof without solar panels



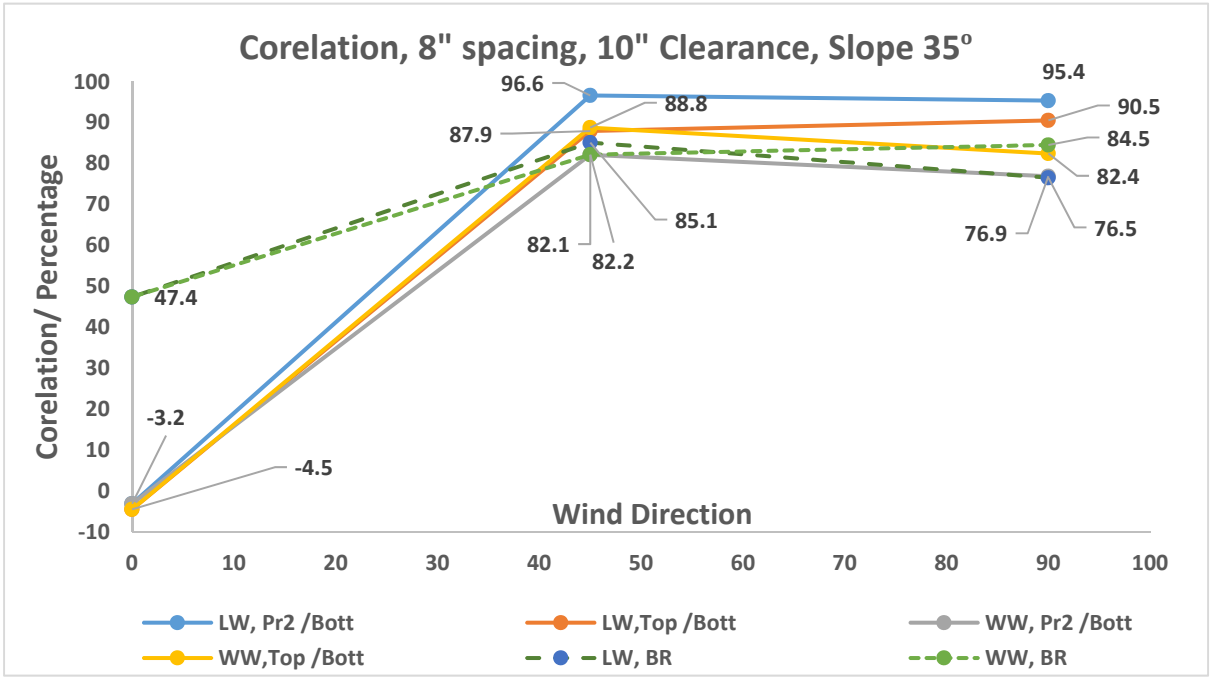


Fig. F. 23. Cp as a function of one surface Cp on the other, 8" spacing, 3" Clearance, Slope 35º, wind direction 0º

Table F. 3. Cp on top and bottom surfaces of solar panels, clearance 10", spacing 8"

Leeward 90º wind direction				windward 90º wind direction			
Polylines	Cp (SP)	roof under panels	Cp bottom of panels	Polylines	Cp (SP)	roof under panels	Cp bottom of panels
Pl17a	-2.53	-3.6	-3.7	Pl1A	-0.12	-0.23	-0.23
Pl18	-2.5	-2.43	-2.94	Pl2	-0.09	-0.86	0.04
Pl19	-1.29	-2.4	-2.38	Pl3	-0.11	-0.73	-0.85
Pl20	-1.05	-2.33	-2.32	Pl4	-0.14	-0.32	-0.35
Pl21	-0.97	-2.29	-2.27	Pl5	-0.18	-0.18	-0.14
Pl22	-0.85	-1.63	-1.45	Pl6	-0.23	-0.57	0.15
Pl23	-0.78	-1.19	-1.09	Pl7	-0.54	-0.57	-1.04
Pl24	-0.74	-1.05	-1.30	Pl8	-0.18	-0.62	-0.61
Pl25	-0.84	-1.19	-1.28	Pl9	-0.25	-1.22	-0.79
Pl26	-0.52	-0.83	-0.48	Pl10	-0.36	-1.11	-1.23
Pl27	-0.52	-0.79	-1.20	Pl11	-0.47	-0.75	-0.75
Pl28	-0.48	-0.91	-0.90	Pl12	-0.6	-0.59	-0.55
Pl29	-0.45	-0.58	-0.50	Pl13	-0.78	-1.12	-0.18
Pl30	-0.42	-0.38	-0.30	Pl14	-1.11	-1.45	-2.04
Pl31	-0.42	-0.41	-1.22	Pl15	-0.98	-1.82	-1.10
Pl32	-0.58	-0.87	-0.95	Pl16A	-2.15	-2.23	-2.70
Cp	-0.93	-1.43	-1.52	Cp	-0.52	-0.90	-0.77
SDT	0.67	0.92	0.95	SDT	0.54	0.57	0.75
Cov	0.71	0.64	0.63	Cov	1.04	0.63	0.98

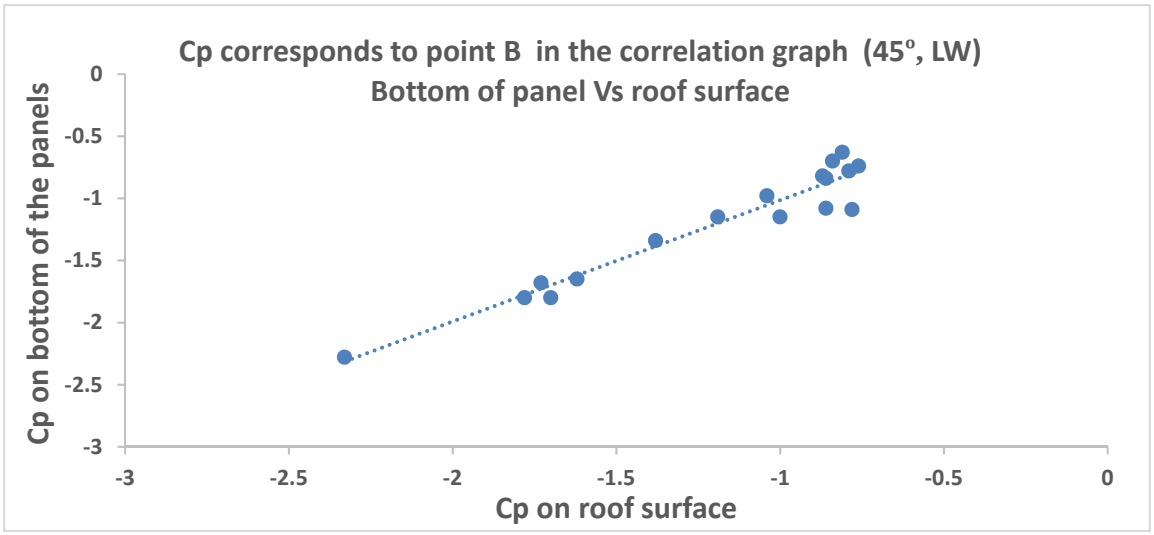
Leeward 45º wind direction				Windward 45º wind direction				0º wind direction			
Polylines	Cp (SP)	roof under panels	Cp bottom of panels	Polylines	Cp (SP)	roof under panels	Cp bottom of panels	Polylines	Cp (SP)	roof under panels	Cp bottom of panels
Pl20a	-1.6	-2.33	-2.28	Pl1A	-0.17	-0.27	-0.23	Pl1A	-0.34	-0.43	-0.36
Pl21	-1.48	-1.78	-1.8	Pl2	-0.2	-0.52	-0.18	Pl2	-0.31	-0.43	-0.43
Pl22	-1.53	-1.7	-1.8	Pl3	-0.2	-0.46	-0.51	Pl3	-0.31	-0.43	-0.43
Pl23	-0.97	-1.73	-1.68	Pl4	-0.2	-0.36	-0.37	Pl4	-0.31	-0.43	-0.43
Pl24	-0.75	-1.62	-1.65	Pl5	-0.21	-0.29	-0.29	Pl5	-0.31	-0.43	-0.43
Pl25	-0.73	-1.38	-1.34	Pl6	-0.23	-0.5	-0.15	Pl6	-0.32	0.40	-0.43
Pl26	-0.69	-1.19	-1.15	Pl7	-0.39	-0.53	-0.57	Pl7	-0.36	-0.40	-0.40
Pl27	-0.66	-1.04	-0.98	Pl8	-0.16	-0.59	-0.38	Pl8	-0.36	-0.41	-0.40
Pl28	-0.66	-1.00	-1.15	Pl9	-0.26	-0.90	-0.38	Pl9	-0.33	-0.43	-0.41
Pl29	-0.77	-0.87	-0.82	Pl10	-0.32	-0.80	-0.88	Pl10	-0.31	-0.41	-0.41
Pl30	-0.52	-0.84	-0.70	Pl11	-0.38	-0.70	-0.71	Pl11	-0.3	-0.43	-0.41
Pl31	-0.51	-0.86	-1.08	Pl12	-0.45	-0.62	-0.62	Pl12	-0.31	-0.43	-0.43
Pl32	-0.51	-0.86	-0.84	Pl13	-0.54	-0.98	-0.48	Pl13	-0.31	-0.33	-0.43
Pl33	-0.5	-0.79	-0.78	Pl14	-0.9	-0.98	-1.02	Pl14	-0.32	-0.32	-0.34
Pl34	-0.5	-0.76	-0.74	Pl15	-0.58	-0.97	-0.84	Pl15	-0.31	-0.33	-0.33
Pl35	-0.51	-0.78	-1.09	Pl16	-0.89	-1.15	-0.87	Pl16	-0.31	-0.33	-0.33
Pl36	-0.5	-0.81	-0.63	Pl17	-1.2	-1.43	-1.70	Pl17a	-0.31	-0.31	-0.31
Cp	-0.79	-1.20	-1.21	Cp	-0.43	-0.71	-0.60	Cp	-0.32	-0.35	-0.39
SDT	0.38	0.47	0.48	SDT	0.31	0.32	0.39	SDT	0.02	0.20	0.04

Cov	0.48	0.40	0.40	Cov	0.71	0.45	0.65	Cov	0.06	0.57	0.11

Figure F.23 demonstrates the correlation graphs for the pairs of series listed in Table F.5 above, and represented in Figures F.24 to F.33, which illustrate the distribution of Cp values of one surface vs. the Cps on the compared surface of the 2 pairs of surfaces, along with the trend line.

The Cps of the 35º inclined roof without solar panels for the 90º, 45º, and 0º wind directions, which are listed in Table F.2, are not repeated in Table F.4 because they are identical. Every point in Fig F.36 represents the correlation of pressure coefficients on one pair of the 4 surfaces, top or bottom of the panels, roof surface under panels, and roof without solar panels surface without any panel. Detailed graphic representations in Figures F.24 to F.33 illustrate the distribution of Cp values on one surface as a function of the other, along with the trend lines.

For the wind direction 45º on the leeward side of the roof, Fig. F.24 illustrates the Cp points of the bottom of the panels and the roof surfaces, which are distributed very close to a straight line, which is seen in the high correlation factor of 0.97. However, the Cp points for the top and bottom of the panels on the leeward side are distributed a little farther from a straight line, with a correlation of 0.88. Also, Fig. F.25 shows the Cp points for the top of the panels and the roof without solar panels surfaces on the leeward side of the roof. The points in Fig. F.38 are distributed a little farther from a straight line (correlation of 0.85) than the other 2 pairs represented in Fig. F.24.



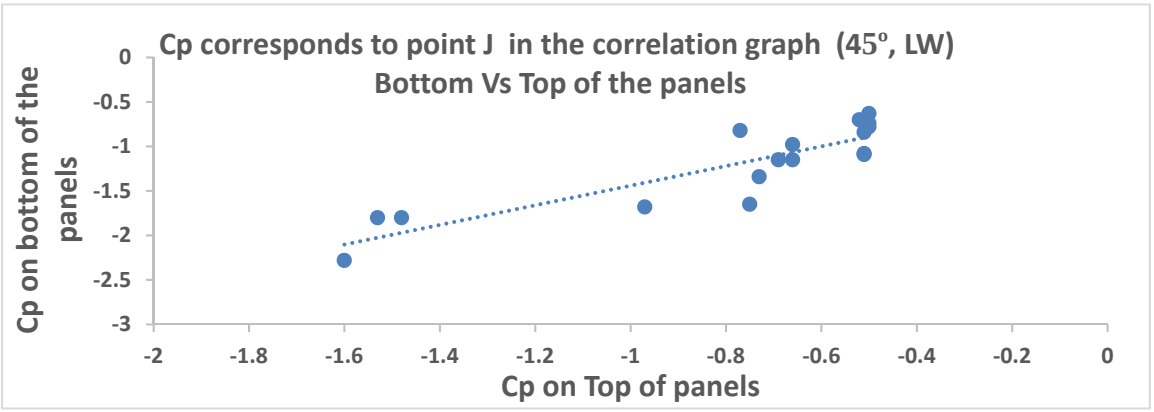


Fig. F. 24. Cp as a function of one surface Cp of the other, 8" spacing, 3" clearance, slope 35°, wind direction 45°, leeward

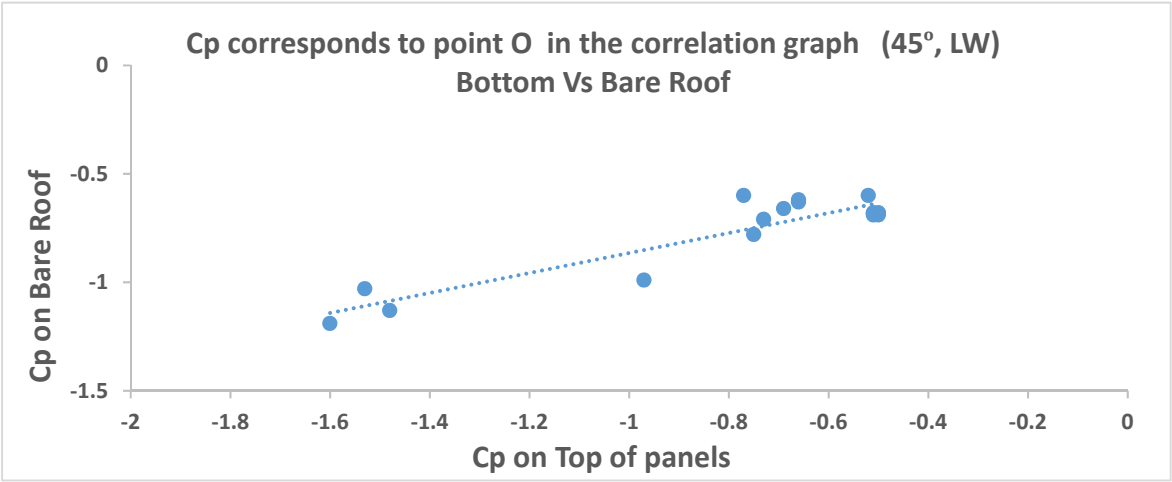


Fig. F. 25. Cp as a function of one surface Cp of the other, 8" spacing, 3" clearance, slope 35°, wind direction 45°, leeward

In Figure F.26, the Cp points for the the bottom of the panels and the roof surfaces on the windward side of the roof are distributed somewhat close to a straight line, but those points are farther from a straight line than the pairs of similar surfaces on the leeward side for the 45º wind direction. This distribution corresponds to a 0.82 correlation factor. However, the distribution of Cp points of the top and bottom of the panel surfaces on the windward side is closer to a straight line (0.89 correlation), as shown in Fig. F.26. Also, Fig. F.27 shows the Cp points of the top of the panels and the roof without solar panels surfaces on the windward side of the roof, which are similarly scattered (0.82 correlation factor) around a straight line like the points of the cavity surfaces, but slightly farther than the points for the top and bottom of the panel surfaces.

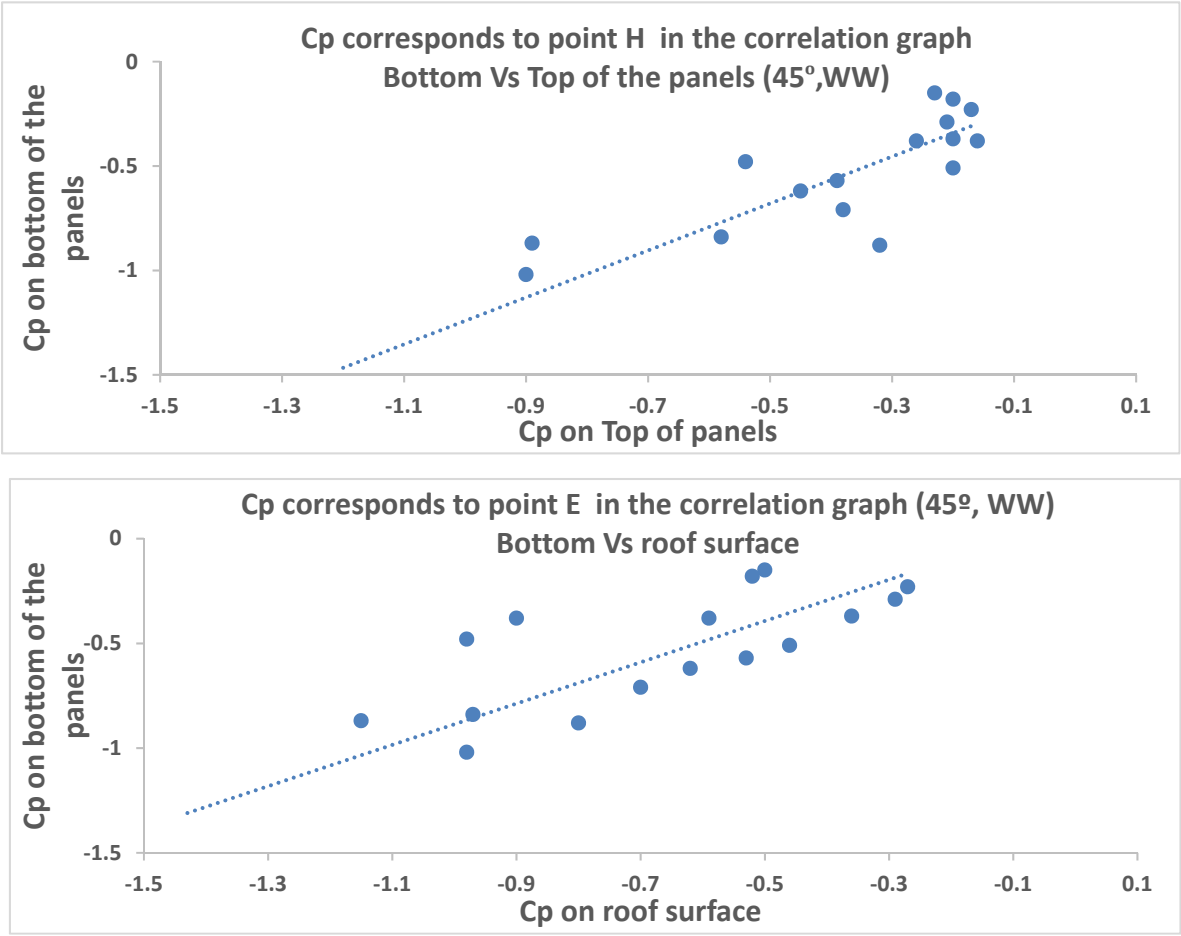


Fig. F. 26. Cp as a function of one surface Cp on the other, 8" spacing, 3" clearance, slope 35º, wind direction 45º, windward

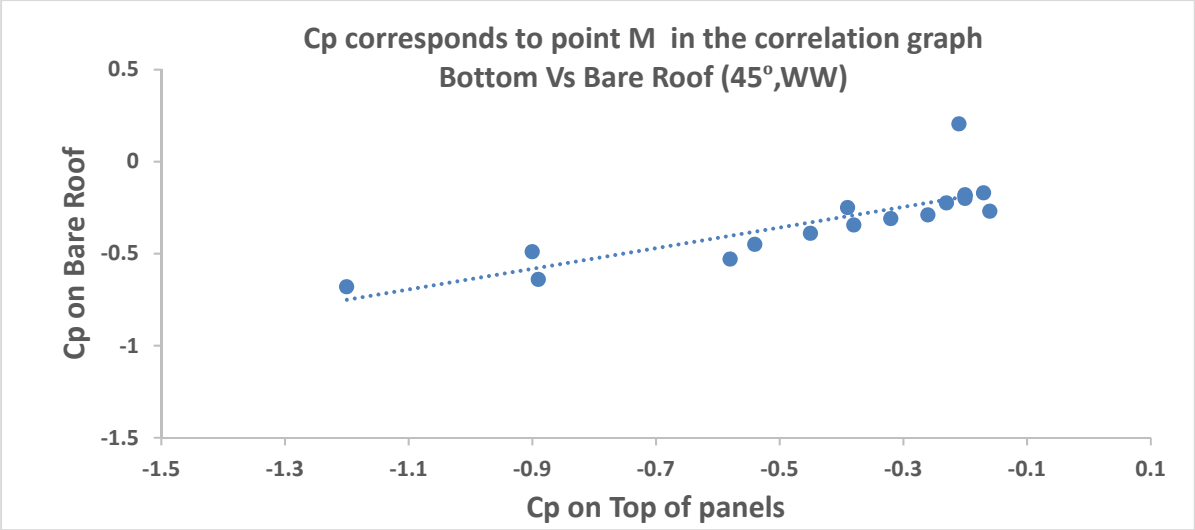
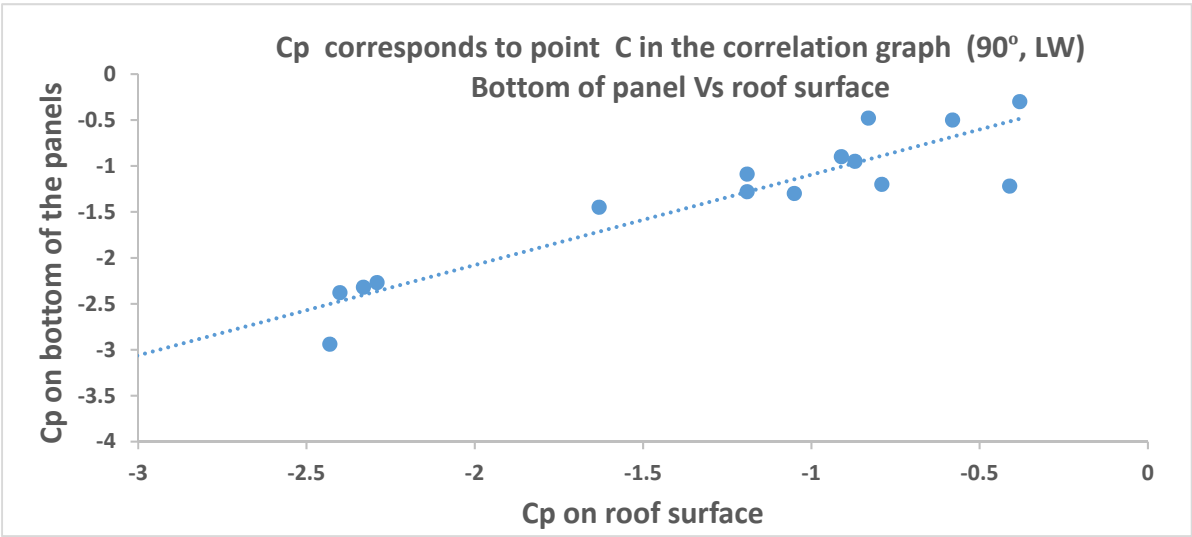


Fig. F. 27. Cp as a function of one surface Cp on the other, 8" spacing, 3" clearance, slope 35º, wind direction 45º, windward

For the 90º wind direction, Fig. F.28 shows that the Cp points for the bottom of the panels and the roof surface on the leeward side of the roof are distributed very close to a straight line, (correlation of 0.95), while the Cp points for the top and bottom of the panels on the same leeward side are distributed slightly farther from a straight line (correlation of 0.91).

Also, Fig. F.29 shows the distribution of Cp points for the top of the panels and the roof without solar panels surfaces on the leeward side. The points are a little more scattered around a straight line than the other 2 pairs represented in Fig. F.28, and their correlation is 0.77.



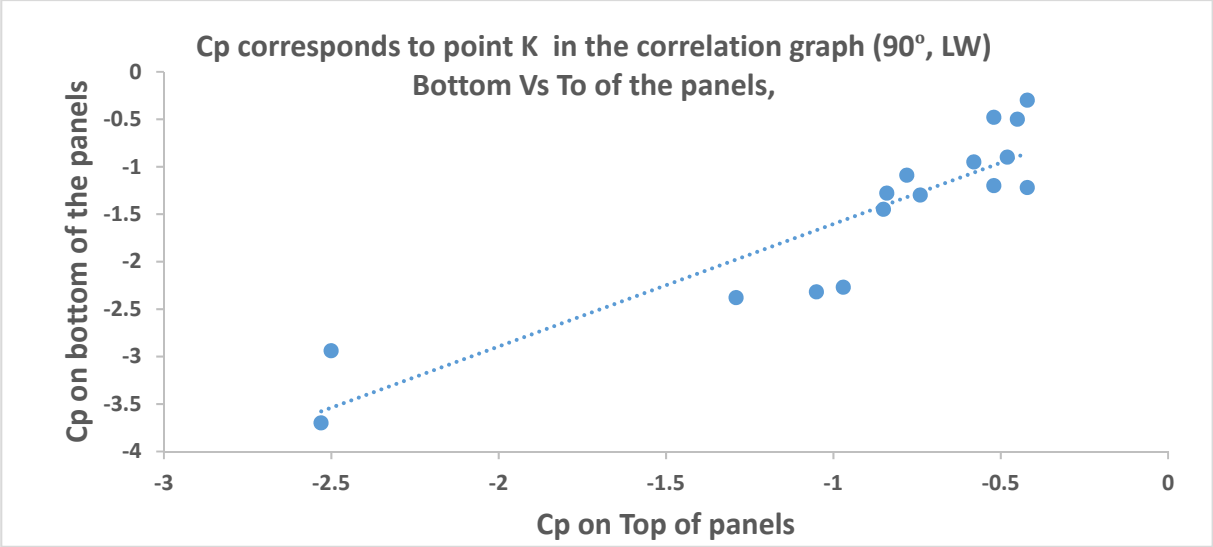


Fig. F. 28. Cp as a function of one surface Cp on the other, 8" spacing, 3" clearance, slope 35º, wind direction 90º, leeward

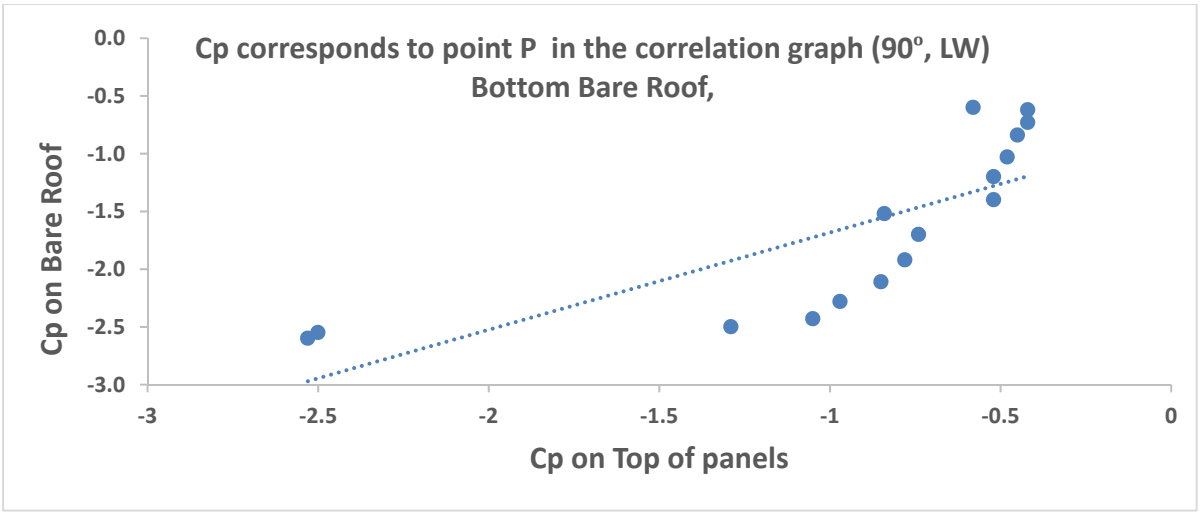


Fig. F. 29. Cp as a function of one surface Cp on the other, 8" spacing, 3" clearance, slope 35º, wind direction 90º, leeward

The first graph in Figure F.30 represents the distribution of Cp points for the bottom of the panels and the roof surfaces on the windward side of the roof, which are slightly scattered around a straight line. Those points indicate a moderate correlation factor of 0.77. However, the distribution of Cp points for the top and bottom of the panel surfaces on the windward side is a little less scattered (0.82 correlation) around a straight line, as shown in the second graph in Fig. F.30. On the other hand, Fig. F.31 shows the distribution of Cp points for the top of the panels and the roof without solar panels surfaces on the windward side of the roof. The last two series of points are

distributed a little closer to a straight line than the other 2 series, and the correlation factor is 0.85 for the top of the panels and the roof without solar panels.

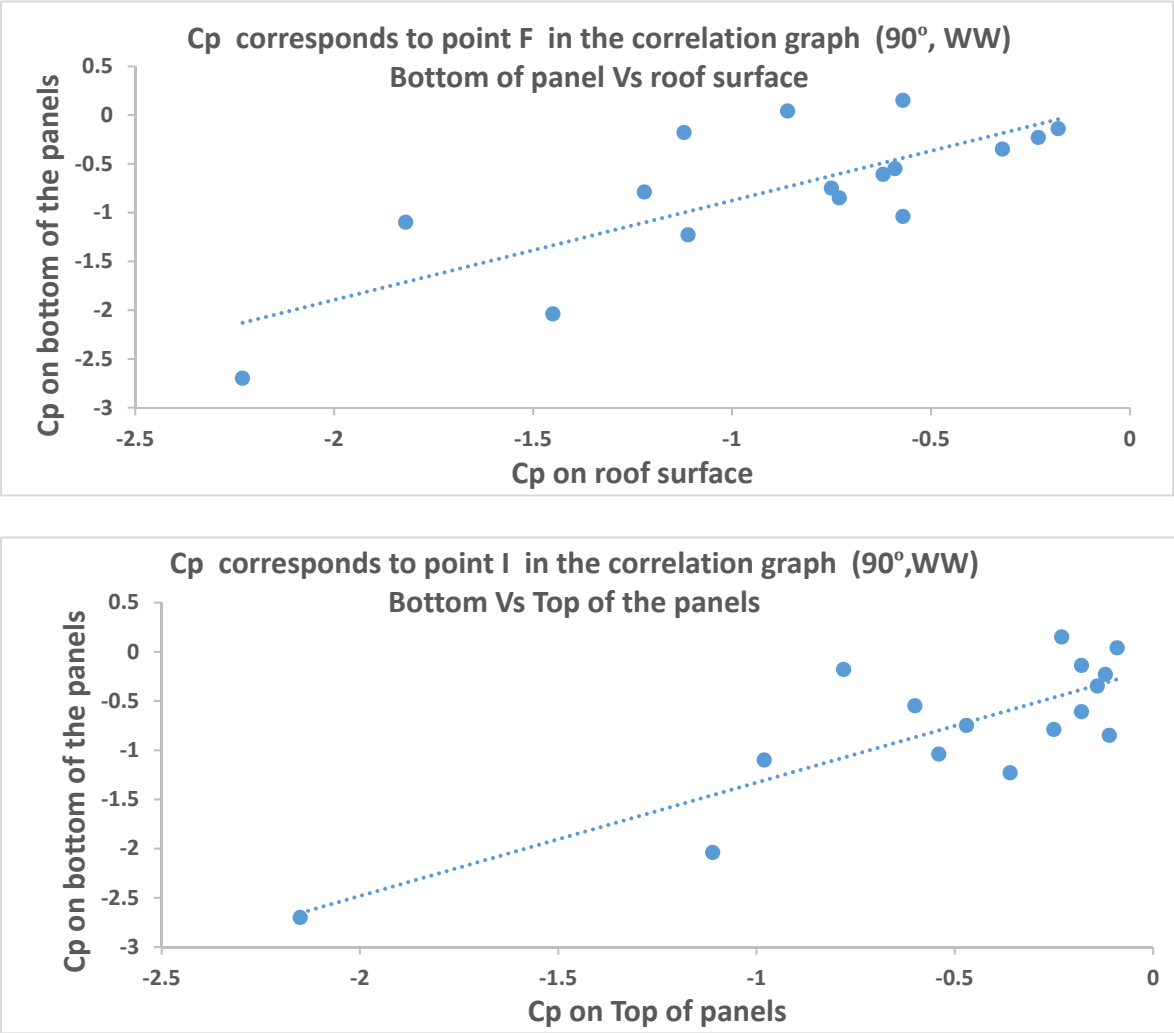


Fig. F. 30. Cp as a function of one surface Cp on the other, 8" spacing, 3" clearance, slope 35°, wind direction 90°, windward

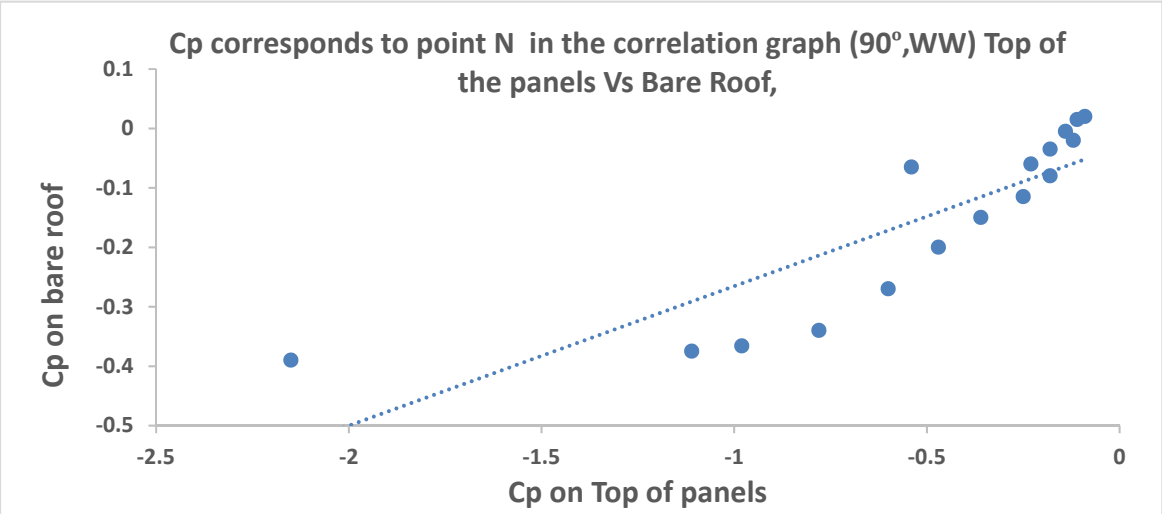
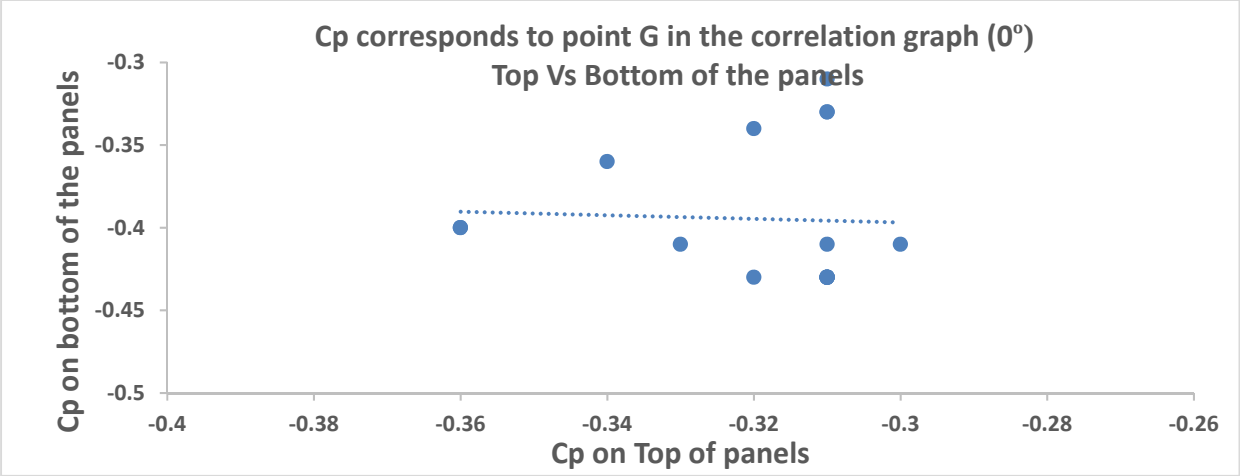


Fig. F. 31. Cp as a function of one surface Cp on the other, 8" spacing, 3" clearance, slope 35º, wind direction 90º, windward

For the wind direction of 0º, Figure F.33 shows the graphs representing the distribution of Cp points of the bottom of the panels and the roof surfaces, where it depicts points very much scattered from a straight line, which indicates a very low correlation factor (-03). The trend line is almost horizontal in this case. Similarly, the distribution of Cp points for the top and bottom of the panel surfaces for the 0º wind direction is very much scattered around a straight line, and the trend line is negatively sloped (-0.04 correlation), as shown in the first graph in Fig. F.33. The slight negative correlation factors mean that there are no proportional changes of the two functions, and that the two functions sometimes have slightly different change trends.

Fig. F.34 shows a small correlation of 0.45 between the Cp points for the top of the panels and the roof without solar panels surfaces for the 0º wind direction. The trend line in the last distribution has a slight positive slope, and the points are spread around a straight line.



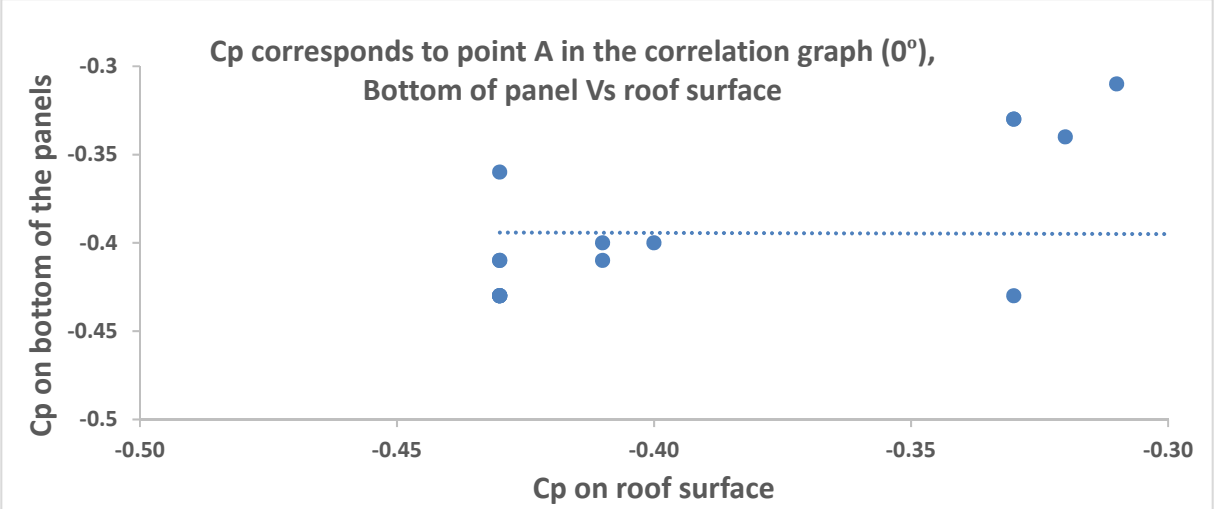


Fig. F. 32. Cp as a function of one surface Cp on the other, 8" spacing, 3" clearance, slope 35°, wind direction 0°

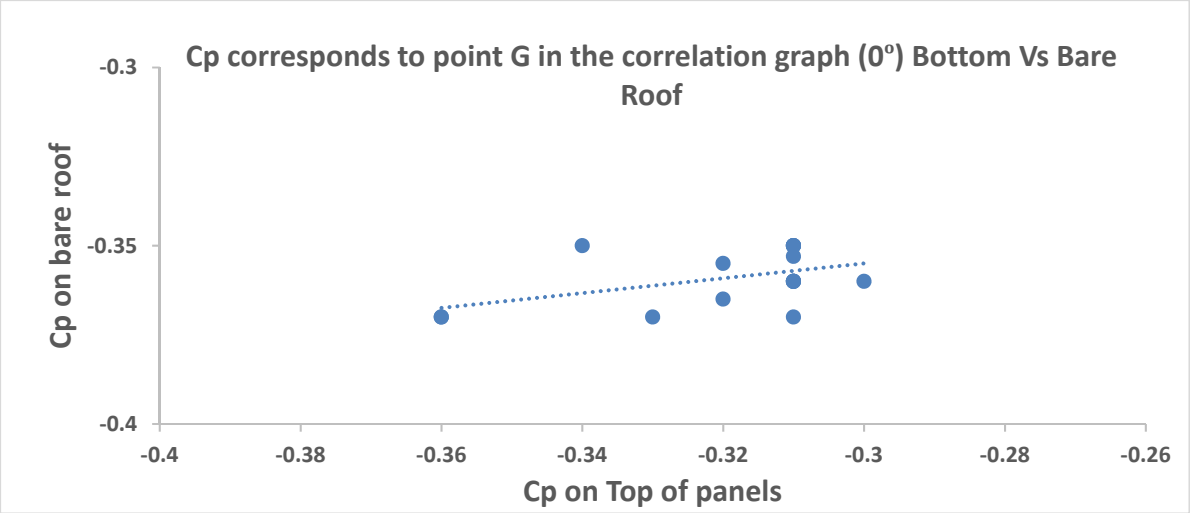


Fig. F. 33. Cp as a function of one surface Cp on the other, 8" spacing, 3" clearance, slope 35º, wind direction 0º

F.4. Correlation between pressure coefficients on top and bottom surfaces of roof tiles/pavers

Habtea et al. (2017) studied the effects of wind on the ridge, hip and perimeter roof tiles installed with a cavity underneath. In the last study the wind effects on hip tiles T1 and T2 on one hip, and T3and T4 on another hip, are shown in Figure F.34.

In this figure, the wind direction 135º corresponds to 45º in this thesis, and wind direction 90º and 180º in Fig. F.1. correspond to 90º and 0º respectively, for T1 and T2, while they correspond to 0º and 90º respectively for T3 and T4.

The correlation charts are derived in Fig. F.35, and tabulated in Table F.4, based on the data presented in Fig. F.34.

For both sets of tiles, (T1,T2) and (T3, T4), there is high correlation in wind direction 135º, and no correlation in the wind directions 0º and 90º.

This trend is derived directly from full-scale experimental results, and the evolution of the correlation between the upper surface and the cavity pressures resemble the correlation between the corresponding surfaces on top and bottom of the solar panels in this thesis, with some differences.

The reasons of those differences, are that Habtea et al. (2017) did the experiment on a hip roof, uses only two points on each side of the hip roof and used locations at the perimeter of the hip roof.

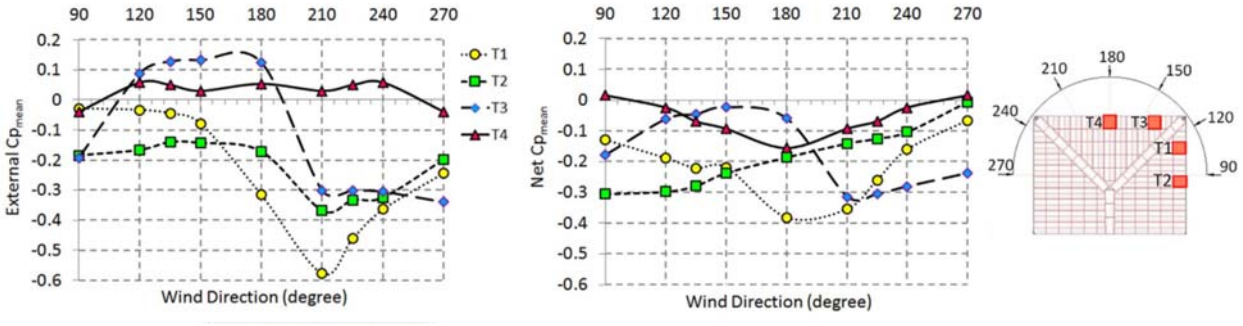


Fig. F. 34. External and net C_{pmean} on the hip tiles on the hip roof (Habte et al., 2017)

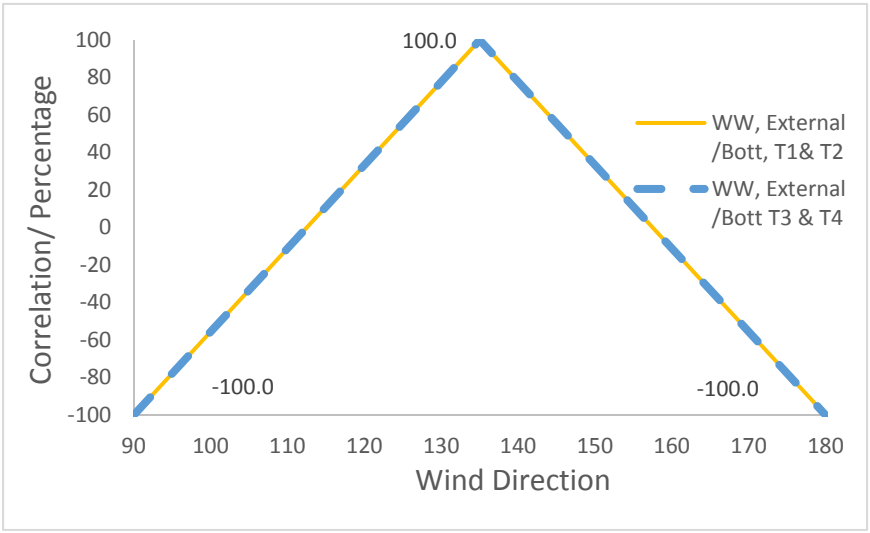


Fig. F. 35. Correlation between Cp on top surface of the tiles and in the cavity Cp under tiles of a hip roof, for roof slope 18.5º (Drawn based on Habte et al., 2017)

Fig. F.35. shows different trends from those in the tiles installed on gable roofs, (which might be represented by E1 and E2 points in the same study), where E1 and E2 are installed on the long side of the hip roof, which resemble the gable roof geometry.

The derived values from Fig. F.34. of Habte et al. (2017) are based on the equation

$$external\ Cp - Bottom\ Cp = Net\ pressure\ on\ tile$$

Table F. 4. Derived Cp values from Fig. 1.6 of Habte et al. (2017)

Wind speed direction (degrees)	Hip tile's designation	Top surface Cp	Net pressure Cp	Cavity Cp
90	T1	-0.03	-0.12	0.09
90	T2	-0.18	-0.3	0.12
90	T3	-0.19	-0.18	-0.01
90	T4	-0.04	0.1	-0.14
135	T1	-0.04	-0.22	0.18
135	T2	-0.14	-0.28	0.14
135	T3	0.13	-0.04	0.17
135	T4	0.05	-0.08	0.13
180	T1	-0.32	-0.38	0.06
180	T2	-0.17	-0.19	0.02
180	T3	0.12	-0.05	0.17
180	T4	0.04	-0.17	0.21

F.5. External pressure on gable roofs as per ASCE 7-10

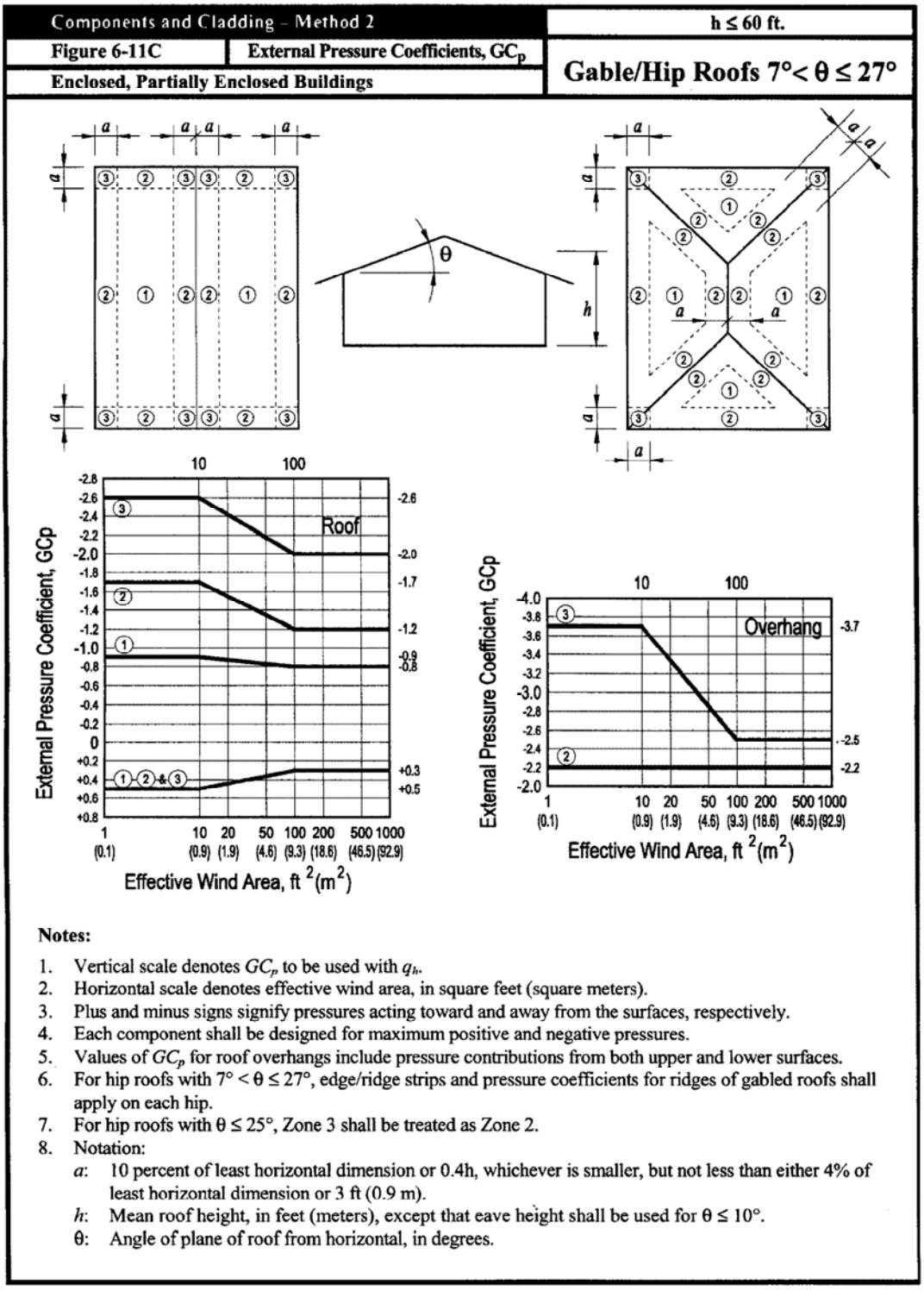


Fig. F. 36. External pressure-gust coefficients, GCp, on single-span gabled and hipped roofs, 7°< slope ≤ 27° for the design of structural components and cladding (ASCE 7-10).

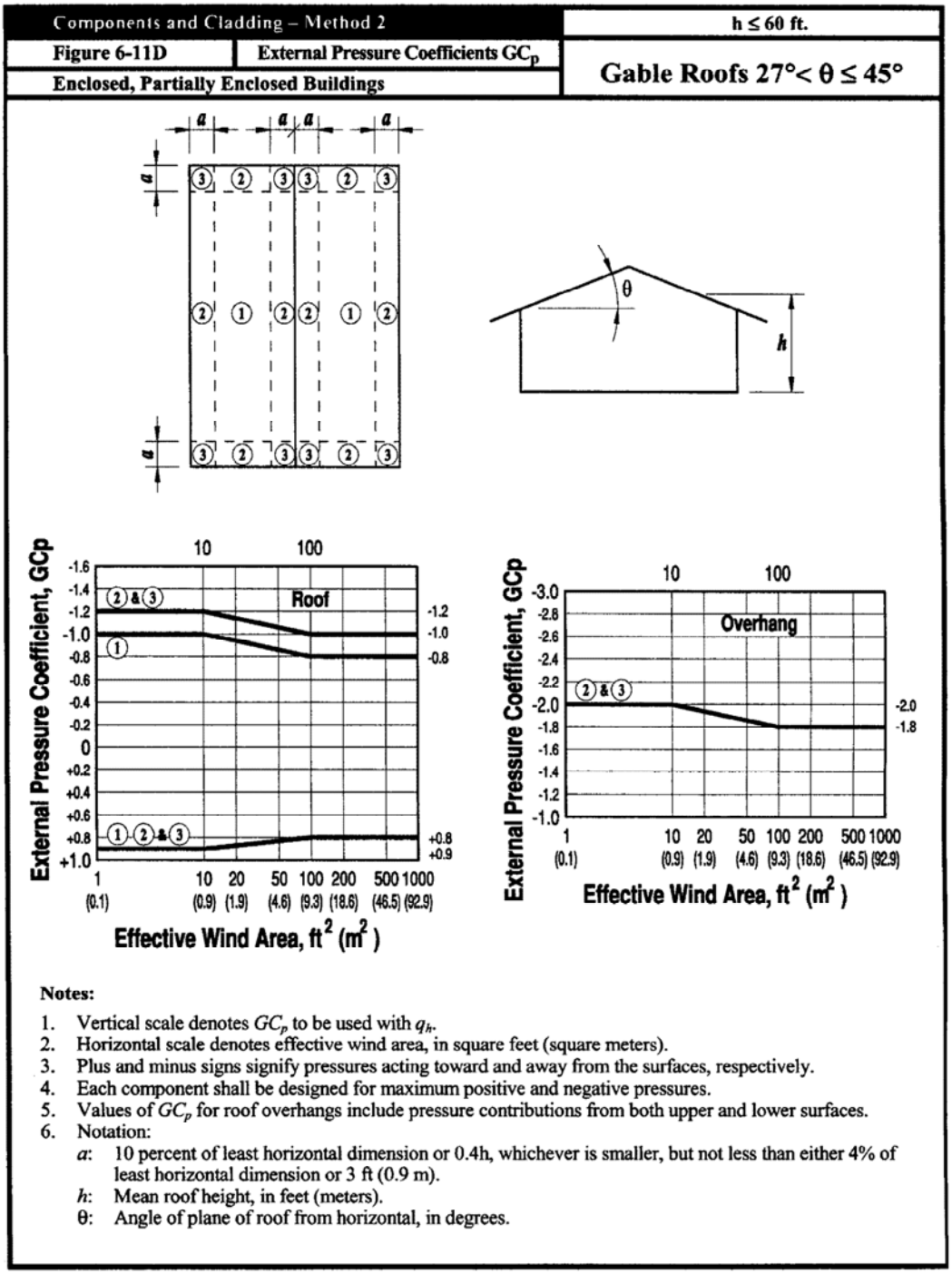


Fig. F. 37. External pressure-gust coefficients, GCp, on single-span gabled and hipped roofs, 27°< slope ≤ 45° for the design of structural components and cladding (ASCE 7-10).